ISSN 2307-8960 (online)

World Journal of *Clinical Cases*

World J Clin Cases 2022 June 16; 10(17): 5518-5933

Published by Baishideng Publishing Group Inc

World Journal of Clinical Cases

Contents Thrice Monthly Volume 10 Number 17 June 16, 2022

MINIREVIEWS

5518 Occult hepatitis B — the result of the host immune response interaction with different genomic expressions of the virus

Gherlan GS

5531 Pulmonary complications of portal hypertension: The overlooked decompensation

Craciun R, Mocan T, Procopet B, Nemes A, Tefas C, Sparchez M, Mocan LP, Sparchez Z

5541 Ethical review of off-label drugs during the COVID-19 pandemic

Li QY, Lv Y, An ZY, Dai NN, Hong X, Zhang Y, Liang LJ

ORIGINAL ARTICLE

Case Control Study

5551 Gut peptide changes in patients with obstructive jaundice undergoing biliary drainage: A prospective case control study

Pavić T, Pelajić S, Blažević N, Kralj D, Milošević M, Mikolasevic I, Lerotic I, Hrabar D

Retrospective Cohort Study

5566 Longitudinal assessment of liver stiffness by transient elastography for chronic hepatitis C patients

Mezina A, Krishnan A, Woreta TA, Rubenstein KB, Watson E, Chen PH, Rodriguez-Watson C

Retrospective Study

5577 Clinical evaluation of prone position ventilation in the treatment of acute respiratory distress syndrome induced by sepsis

Xia WH, Yang CL, Chen Z, Ouyang CH, Ouyang GQ, Li QG

5586 Three-dimensional arterial spin labeling and diffusion kurtosis imaging in evaluating perfusion and infarct area size in acute cerebral ischemia

Jiang YY, Zhong ZL, Zuo M

5595 Intrathecal methotrexate in combination with systemic chemotherapy in glioblastoma patients with leptomeningeal dissemination: A retrospective analysis

Kang X, Chen F, Yang SB, Wang YL, Qian ZH, Li Y, Lin H, Li P, Peng YC, Wang XM, Li WB

5606 Hepatic epithelioid hemangioendothelioma: Clinical characteristics, diagnosis, treatment, and prognosis

Zhao M, Yin F

5620 Difference between type 2 gastroesophageal varices and isolated fundic varices in clinical profiles and portosystemic collaterals

Song YH, Xiang HY, Si KK, Wang ZH, Zhang Y, Liu C, Xu KS, Li X

World Journal of Clinical Cases

Thrice Monthly Volume 10 Number 17 June 16, 2022

Contents

5634 Assessment of incidental focal colorectal uptake by analysis of fluorine-18 fluorodeoxyglucose positron emission tomography parameters

Lee H, Hwang KH, Kwon KA

Observational Study

5646 "Zero ischemia" laparoscopic partial nephrectomy by high-power GreenLight laser enucleation for renal carcinoma: A single-center experience

Zhang XM, Xu JD, Lv JM, Pan XW, Cao JW, Chu J, Cui XG

5655 High Eckardt score and previous treatment were associated with poor postperoral endoscopic myotomy pain control: A retrospective study

Chen WN, Xu YL, Zhang XG

5667 Higher volume growth rate is associated with development of worrisome features in patients with branch duct-intraductal papillary mucinous neoplasms

Innocenti T, Danti G, Lynch EN, Dragoni G, Gottin M, Fedeli F, Palatresi D, Biagini MR, Milani S, Miele V, Galli A

Prospective Study

5680 Application of a new anatomic hook-rod-pedicle screw system in young patients with lumbar spondylolysis: A pilot study

Li DM, Li YC, Jiang W, Peng BG

META-ANALYSIS

5690 Systematic review of Yougui pills combined with levothyroxine sodium in the treatment of hypothyroidism

Liu XP, Zhou YN, Tan CE

CASE REPORT

5702 Allogeneic stem cell transplantation-A curative treatment for paroxysmal nocturnal hemoglobinuria with PIGT mutation: A case report

Schenone L, Notarantonio AB, Latger-Cannard V, Fremeaux-Bacchi V, De Carvalho-Bittencourt M, Rubio MT, Muller M, D'Aveni M

5708 Gray zone lymphoma effectively treated with cyclophosphamide, doxorubicin, vincristine, prednisolone, and rituximab chemotherapy: A case report

Hojo N, Nagasaki M, Mihara Y

5717 Diagnosis of spontaneous isolated superior mesenteric artery dissection with ultrasound: A case report

Zhang Y, Zhou JY, Liu J, Bai C

5723 Adrenocorticotropic hormone-secreting pancreatic neuroendocrine carcinoma with multiple organ infections and widespread thrombosis: A case report

Yoshihara A, Nishihama K, Inoue C, Okano Y, Eguchi K, Tanaka S, Maki K, Fridman D'Alessandro V, Takeshita A, Yasuma T, Uemura M, Suzuki T, Gabazza EC, Yano Y

5732 Management of the palato-radicular groove with a periodontal regenerative procedure and prosthodontic treatment: A case report

Ling DH, Shi WP, Wang YH, Lai DP, Zhang YZ

World Journal of Clinical Cases

Thrice Monthly Volume 10 Number 17 June 16, 2022

Contents

5741 Combined thoracic paravertebral block and interscalene brachial plexus block for modified radical mastectomy: A case report

Hu ZT, Sun G, Wang ST, Li K

5748 Chondromyxoid fibroma of the cervical spine: A case report

Li C, Li S, Hu W

5756 Preterm neonate with a large congenital hemangioma on maxillofacial site causing thrombocytopenia and heart failure: A case report

Ren N, Jin CS, Zhao XQ, Gao WH, Gao YX, Wang Y, Zhang YF

5764 Simultaneous multiple primary malignancies diagnosed by endoscopic ultrasound-guided fine-needle aspiration: A case report

Yang J, Zeng Y, Zhang JW

5770 Neuroendocrine tumour of the descending part of the duodenum complicated with schwannoma: A case report

Zhang L, Zhang C, Feng SY, Ma PP, Zhang S, Wang QQ

5776 Massive hemothorax following internal jugular vein catheterization under ultrasound guidance: A case report

Kang H, Cho SY, Suk EH, Ju W, Choi JY

5783 Unilateral adrenal tuberculosis whose computed tomography imaging characteristics mimic a malignant tumor: A case report

Liu H, Tang TJ, An ZM, Yu YR

5789 Modified membrane fixation technique in a severe continuous horizontal bone defect: A case report

Wang LH, Ruan Y, Zhao WY, Chen JP, Yang F

5798 Surgical repair of an emergent giant hepatic aneurysm with an abdominal aortic dissection: A case report

Wen X, Yao ZY, Zhang Q, Wei W, Chen XY, Huang B

5805 Heterotopic ossification beneath the upper abdominal incision after radical gastrectomy: Two case reports

Zhang X, Xia PT, Ma YC, Dai Y, Wang YL

5810 Non-alcoholic Wernicke encephalopathy in an esophageal cancer patient receiving radiotherapy: A case report

Zhang Y, Wang L, Jiang J, Chen WY

5816 New approach for the treatment of vertical root fracture of teeth: A case report and review of literature

Zhong X, Yan P, Fan W

5825 Ultrasound-guided microwave ablation as a palliative treatment for mycosis fungoides eyelid involvement: A case report

Chen YW, Yang HZ, Zhao SS, Zhang Z, Chen ZM, Feng HH, An MH, Wang KK, Duan R, Chen BD

5833 Pulp revascularization on an adult mandibular right second premolar: A case report

Yang YQ, Wu BL, Zeng JK, Jiang C, Chen M

World Journal of Clinical Cases

Thrice Monthly Volume 10 Number 17 June 16, 2022

Contents

5841 Barrett's esophagus in a patient with bulimia nervosa: A case report

Gouda A, El-Kassas M

5846 Spontaneous gallbladder perforation and colon fistula in hypertriglyceridemia-related severe acute pancreatitis: A case report

Wang QP, Chen YJ, Sun MX, Dai JY, Cao J, Xu Q, Zhang GN, Zhang SY

5854 Beware of gastric tube in esophagectomy after gastric radiotherapy: A case report

Yurttas C, Wichmann D, Gani C, Bongers MN, Singer S, Thiel C, Koenigsrainer A, Thiel K

5861 Transition from minimal change disease to focal segmental glomerulosclerosis related to occupational exposure: A case report

Tang L, Cai Z, Wang SX, Zhao WJ

5869 Lung adenocarcinoma metastasis to paranasal sinus: A case report

Li WJ, Xue HX, You JQ, Chao CJ

5877 Follicular lymphoma presenting like marginal zone lymphoma: A case report

Peng HY, Xiu YJ, Chen WH, Gu QL, Du X

5884 Primary renal small cell carcinoma: A case report

Xie K, Li XY, Liao BJ, Wu SC, Chen WM

5893 Gitelman syndrome: A case report

Chen SY, Jie N

5899 High-frame-rate contrast-enhanced ultrasound findings of liver metastasis of duodenal gastrointestinal stromal tumor: A case report and literature review

Chen JH, Huang Y

5910 Tumor-like disorder of the brachial plexus region in a patient with hemophilia: A case report

Guo EQ, Yang XD, Lu HR

5916 Response to dacomitinib in advanced non-small-cell lung cancer harboring the rare delE709_T710insD mutation: A case report

Xu F, Xia ML, Pan HY, Pan JW, Shen YH

5923 Loss of human epidermal receptor-2 in human epidermal receptor-2+ breast cancer after neoadjuvant treatment: A case report

Yu J, Li NL

LETTER TO THE EDITOR

5929 Repetitive transcranial magnetic stimulation for post-traumatic stress disorder: Lights and shadows

Concerto C, Lanza G, Fisicaro F, Pennisi M, Rodolico A, Torrisi G, Bella R, Aguglia E

World Journal of Clinical Cases

Thrice Monthly Volume 10 Number 17 June 16, 2022

Contents

ABOUT COVER

Editorial Board Member of *World Journal of Clinical Cases*, Raden Andri Primadhi, MD, PhD, Assistant Professor, Surgeon, Department of Orthopaedics and Traumatology, Universitas Padjadjaran Medical School, Hasan Sadikin Hospital, Bandung 40161, Indonesia. randri@unpad.ac.id

AIMS AND SCOPE

The primary aim of *World Journal of Clinical Cases* (*WJCC*, *World J Clin Cases*) is to provide scholars and readers from various fields of clinical medicine with a platform to publish high-quality clinical research articles and communicate their research findings online.

WJCC mainly publishes articles reporting research results and findings obtained in the field of clinical medicine and covering a wide range of topics, including case control studies, retrospective cohort studies, retrospective studies, clinical trials studies, observational studies, prospective studies, randomized controlled trials, randomized clinical trials, systematic reviews, meta-analysis, and case reports.

INDEXING/ABSTRACTING

The *WJCC* is now abstracted and indexed in Science Citation Index Expanded (SCIE, also known as SciSearch®), Journal Citation Reports/Science Edition, Current Contents®/Clinical Medicine, PubMed, PubMed Central, Scopus, Reference Citation Analysis, China National Knowledge Infrastructure, China Science and Technology Journal Database, and Superstar Journals Database. The 2022 Edition of Journal Citation Reports® cites the 2021 impact factor (IF) for *WJCC* as 1.534; IF without journal self cites: 1.491; 5-year IF: 1.599; Journal Citation Indicator: 0.28; Ranking: 135 among 172 journals in medicine, general and internal; and Quartile category: Q4. The *WJCC*'s CiteScore for 2021 is 1.2 and Scopus CiteScore rank 2021: General Medicine is 443/826.

RESPONSIBLE EDITORS FOR THIS ISSUE

Production Editor: *Hua-Ge Yu*; **Production Department Director:** *Xiang Li*; **Editorial Office Director:** *Jin-Lei Wang*.

NAME OF JOURNAL
World Journal of Clinical Cases

ISSN
ISSN 2307-8960 (online)

LAUNCH DATE
April 16, 2013

FREQUENCY
Thrice Monthly

EDITORS-IN-CHIEF
Bao-Gan Peng, Jerzy Tadeusz Chudek, George Kontogeorgos, Maurizio Serati, Ja Hyeon Ku

EDITORIAL BOARD MEMBERS
https://www.wjgnet.com/2307-8960/editorialboard.htm

PUBLICATION DATE
June 16, 2022

COPYRIGHT
© 2022 Baishideng Publishing Group Inc

INSTRUCTIONS TO AUTHORS
https://www.wjgnet.com/bpg/gerinfo/204

GUIDELINES FOR ETHICS DOCUMENTS
https://www.wjgnet.com/bpg/GerInfo/287

GUIDELINES FOR NON-NATIVE SPEAKERS OF ENGLISH
https://www.wjgnet.com/bpg/gerinfo/240

PUBLICATION ETHICS
https://www.wjgnet.com/bpg/GerInfo/288

PUBLICATION MISCONDUCT
https://www.wjgnet.com/bpg/gerinfo/208

ARTICLE PROCESSING CHARGE
https://www.wjgnet.com/bpg/gerinfo/242

STEPS FOR SUBMITTING MANUSCRIPTS
https://www.wjgnet.com/bpg/GerInfo/239

ONLINE SUBMISSION
https://www.f6publishing.com

© 2022 Baishideng Publishing Group Inc. All rights reserved. 7041 Koll Center Parkway, Suite 160, Pleasanton, CA 94566, USA

E-mail: bpgoffice@wjgnet.com https://www.wjgnet.com

World Journal of Clinical Cases

Submit a Manuscript: https://www.f6publishing.com

World J Clin Cases 2022 June 16; 10(17): 5518-5530

DOI: 10.12998/wjcc.v10.i17.5518

ISSN 2307-8960 (online)

MINIREVIEWS

Occult hepatitis B — the result of the host immune response interaction with different genomic expressions of the virus

George Sebastian Gherlan

Specialty type: Infectious diseases

Provenance and peer review: Invited article; Externally peer reviewed.

Peer-review model: Single blind

Peer-review report's scientific quality classification

Grade A (Excellent): 0
Grade B (Very good): B
Grade C (Good): C
Grade D (Fair): D
Grade E (Poor): E

P-Reviewer: Gerlich W, Germany; Lee GH, Singapore; Mrzljak A, Croatia

Received: January 5, 2022
Peer-review started: January 5, 2022
First decision: January 27, 2022
Revised: January 30, 2022
Accepted: April 4, 2022
Article in press: April 4, 2022
Published online: June 16, 2022

George Sebastian Gherlan, Department of Infectious Diseases, "Carol Davila" University of Medicine and Pharmacy, Bucharest 030303, Romania

George Sebastian Gherlan, Department of Infectious Diseases, "Dr. Victor Babes" Hospital of Infectious and Tropical Diseases, Bucharest 030303, Romania

Corresponding author: George Sebastian Gherlan, MD, PhD, Lecturer, Department of Infectious Diseases, "Carol Davila" University of Medicine and Pharmacy, 281 Mihai Bravu Street, Bucharest 030303, Romania. george.gherlan@umfcd.ro

Abstract

With over 40 years of history, occult hepatitis B infection (OBI) continues to remain an important and challenging public health problem. Defined as the presence of replication-competent hepatitis B virus (HBV) DNA (*i.e.*, episomal HBV covalently closed circular DNA) in the liver and/or HBV DNA in the blood of people who test negative for hepatitis B surface antigen (HBsAg) in currently available assays, OBI is currently diagnosed using polymerase chain reaction (PCR) and real-time PCR assays. However, all efforts should be made to exclude a false negative HBsAg in order to completely follow the definition of OBI. In recent years, significant advances have been made in understanding the HBV lifecycle and the molecular mechanisms that lead to the persistence of the virus in the occult form. These factors are mainly related to the host immune system and, to a smaller proportion, to the virus. Both innate and adaptive immune responses are important in HBV infection management, and epigenetic changes driven by host mechanisms (acetylation, methylation, and microRNA implication) are added to such actions. Although greater genetic variability in the *S* gene of HBV isolated from OBIs was found compared with overt infection, the mechanisms of OBI are not mainly viral mutations.

Key Words: Hepatitis B virus; Occult hepatitis B; Covalently closed circular DNA; Epigenetic factors; Immune factors; MicroRNA

©The Author(s) 2022. Published by Baishideng Publishing Group Inc. All rights reserved.

Core Tip: Every year, our knowledge of occult hepatitis B infection becomes richer with new information. This review is an up-to-date analysis of the viral and host factors that interact and lead to an occult form of hepatitis B virus infection. The latest discoveries in microRNA involvement, epigenetic mechanisms, immune system factors, and viral variants have been included for a comprehensive understanding of this challenging problem. We emphasize that occult hepatitis B infection is not only and not primarily a virus-driven condition; host immune and epigenetic mechanisms are also its important determinants.

Citation: Gherlan GS. Occult hepatitis B — the result of the host immune response interaction with different genomic expressions of the virus. *World J Clin Cases* 2022; 10(17): 5518-5530
URL: https://www.wjgnet.com/2307-8960/full/v10/i17/5518.htm
DOI: https://dx.doi.org/10.12998/wjcc.v10.i17.5518

INTRODUCTION

More than 40 years from its first description in the late 1970s[1], occult hepatitis B virus (HBV) infection (OBI) continues to be one of the most challenging topics in the field of viral hepatitis. OBI represents an important public health problem because of its many implications.

Since the introduction of hepatitis B surface antigen (HBsAg) testing in the routine screening of blood donors in the early 1970s, the incidence of transfusion-transmitted hepatitis has been dramatically reduced; however, it did not eliminate this unwanted event, and neither associating alanine aminotransferase level measurement nor anti HBc testing did. The majority of transmissions is attributable to occult hepatitis B. HBV remains the most frequent transfusion-transmitted viral infection[2].

OBI may also be the cause of HBV transmission in organ transplants or can represent a problem in patients receiving immunosuppressive therapy for various conditions, chemotherapy, or anti-CD-20 therapy because of the risk of reactivation.

The persistence of OBI may lead to the development of liver cirrhosis and, eventually, to hepatocellular carcinoma (HCC)[3]. OBI can be one of the possible causes of cryptogenic liver disease.

In people co-infected with hepatitis C virus (HCV) who have OBI, curing HCV with current direct-acting antiviral medication can lead to HBV reactivation, although this happens rarely in patients with OBI, mostly in those with overt HBV infection[4]. The risk of HBV reactivation is also documented in human immunodeficiency virus (HIV) co-infected patients, especially after withdrawal of antiretrovirals that are also active on HBV[5].

SOURCES AND SELECTION CRITERIA

We searched PubMed for studies published in English between January 1979 (when the first reference to OBI was considered to be found) and December 2019. We initially used the following search terms in combination with the term "HBV" or "hepatitis B": "lifecycle," "persistence," "natural history," "guidelines," "cccDNA," "integrated DNA," "immunity," "immune system," "innate immunity," "adaptive immunity," "pathogenesis," "physiopathology," and then with "OBI HBV" or "Occult hepatitis" + "HBV": "definition," "cccDNA," "mutations," "HBV variants," "immune system," "innate immunity," "adaptive immunity," "physiopathology," "pathogenesis," "mechanism," "viral factors," "host factors," "epigenetics," "miRNA."

We prioritized studies performed in humans, chimpanzees, or humanized chimeric mice, when available, but we also included those performed in other animal models, such as woodchucks and mice or *in vitro* primary hepatocytes or cell lines. We looked into the most recent sources first, but if data from older sources were still available, we also cited such data. For the best quality of clinical evidence, we prioritized guidelines, technical reviews, or high-quality prospective observational studies or their meta-analyses, when available.

DEFINITION OF OCCULT HEPATITIS B INFECTION

Over time, several definitions have been proposed for OBI.

The first article considered to refer to occult B hepatitis, although it did not identify it by this specific term, dates back to 1979. It retrospectively analyzed sera from 128 donors from 1971 to 1977, who were chosen because their blood recipients developed clinically recognizable posttransfusion hepatitis. "The detection of hepatitis B core antibody (anti-HBc) alone in nine of 29 implicated donors with HBV markers, suggests that some HBsAg-negative donors implicated in the transmission of hepatitis B may

be low-level carriers potentially detectable using tests for anti-HBc. However, the total absence of HBV markers in many implicated donors probably indicates that such donors did not transmit HBV infection" was one of that study's[1] conclusion, and today, we know that their assumptions were not completely correct, although they identified an important category of patients. When we refer to that study, we have to keep in mind that it was a retrospective study; furthermore, the sensitivity of the serological tests used at that time was low, and molecular biology testing was not available.

The definition that resulted from the first Taormina workshop on occult hepatitis B was as follows: "Presence of HBV DNA in the liver (with detectable or undetectable HBV DNA in the serum) of individuals testing HBsAg negative by currently available assays"[6]. The revision made 10 years later in the re-edited workshop was only slightly different: "the presence of replication-competent HBV DNA [*i.e.*, episomal HBV covalently closed circular DNA (cccDNA)] in the liver and/or HBV DNA in the blood of people who test negative for HBsAg by currently available assays"; the latter emphasizes the importance of the fact that HBV DNA should be competent to replicate[7]. There is another change of optics between the two workshops; in the first one, patients with *S* gene mutations that make HBsAg not detectable by usual commercially available detection assays but with HBV DNA levels comparable to those of the overt infections were called false OBIs[6], whereas in the 2018 workshop, these patients were considered a subset of OBI.

OBI can be seropositive when either the anti-HBc and/or the hepatitis B surface antibody (anti-HBs) is positive (without prior hepatitis B vaccination) or seronegative and when both anti-HBc and anti-HBs are negative. Up to 20% of OBI are seronegative[3,8].

The latest issue of the Asian Pacific Association for the Study of the Liver clinical practice guidelines on the management of hepatitis B[8] and the latest European Association for the Study of the Liver clinical practice guidelines on the management of hepatitis B virus infection[9] recognize occult hepatitis B as a particular form of evolution of HBV infection, characterized by the absence of secreted HBsAg and the presence of HBV DNA either in the liver or in the blood of the patient. American Association for the Study of Liver Diseases (AASLD) guidelines identify a category of patients who test positive for anti-HBc antibodies but negative for HBsAg and, among them, a sub-category of patients who may or may not be HBV DNA positive - these groups may be at risk for reactivation or for developing HCC; however, AASLD guidelines do not define the category specifically as OBI[10].

TYPES OF OBIS

According to the 2019 Taormina workshop[7], OBIs can be categorized mainly into seropositive and seronegative. The seropositive status may be achieved either after the resolution of acute hepatitis (which is the case in more than 95% of immune-competent adults) or after a chronic HBV infection (with or without liver injury), either spontaneously or after antiviral treatment (that with actual substances rarely achieves this functional cure). In these cases, we have to ensure that the most sensitive HBsAg kits are used to rule out false OBIs. HBV DNA can be found intermittently in the blood of these patients, usually at levels below 200 IU/mL[3,7]. The seronegative status may be the consequence of an OBI that progressively lost anti-HBc and anti-HBs antibodies or might be negative from the beginning (a situation called primary occult infection and demonstrated in woodchucks infected with small amounts of viral particles[11]).

A special category of OBI is represented by HBV genetic variants in which the HBs antigen is not recognized by available assays. The main cause of this situation is a mutation in the *S*-gene (S-escape mutants), but a mutation in the *S*-gene promoter or a splice variant can also be considered[7]. This type of OBI is mainly seropositive; in a study regarding this issue, out of 99 patients with OBI and mutant HBV variants, only 3 patients were seronegative[3]. At the previous Taormina workshop, this type of OBI was considered false[6]. HBV DNA can have levels comparable with those of the overt HBV infection in this subtype of OBI, except in the one with splice variants, in which HBV DNA levels are low or undetectable[7]. The above pathways to OBI are summarized in Figure 1.

The term "functional cure" refers to OBIs in which HBsAg is not detectable as a result of the immune system's action and not because of the situations in which HBsAg is present, mutant, and not detected by conventional commercially available assays.

HEPATITIS B VIRUS LIFECYCLE AND PERSISTENCE

HBV is a member of the Hepadnaviridae family, and its complete HBV virion consists of an outer envelope, an inner nucleocapsid, and a 3.2 kb partially double-stranded DNA, known as relaxed circular DNA (RC-DNA), which is covalently connected with the DNA polymerase. The HBV genome contains four overlapping open reading frames, namely, preS1/S2/S, pre-core/core, polymerase, and X domains, which encode seven viral proteins[12]. Of these proteins, four are of major importance: (1) The viral polymerase, that has a role in viral replication and packaging; (2) The small (S), medium (M), and large (L) surface antigens, polypeptides that constitute the HBsAg, that is part of the viral envelope and

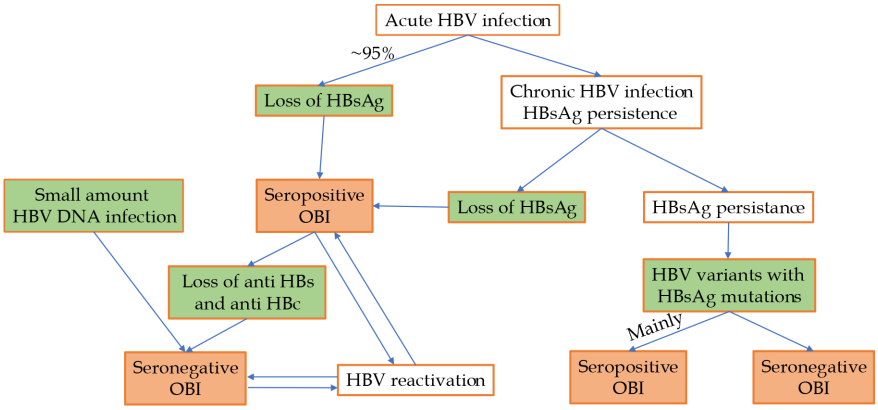

DOI: 10.12998/wjcc.v10.i17.5518 **Copyright** ©The Author(s) 2022.

Figure 1 Pathways to different occult hepatitis B infection types. OBI: Occult hepatitis B infection; HBV: Hepatitis B virus; HBsAg: Hepatitis B surface antigen.

play a major role in viral entry; (3) HBV core protein (HBc), part of the viral capsid (that play a role in viral replication and packaging); and (4) The X protein (HBx), which has various functions, one of them being the regulation of viral genome transcription. HBx functions may vary with the stage of the HBV infection[12-14].

HBV virions bind initially to hepatocytes by interacting with heparan sulfate proteoglycans for virus docking and subsequently with the recently discovered functional receptor - sodium taurocholate co-transporting polypeptide[13,15]. After endocytosis, the nucleocapsid is released in the cytoplasm and transported to the nucleus, where RC-DNA is released and converted (some say repaired) by host factors into cccDNA[12,14]. When RC-DNA is not completely converted to cccDNA, the aberrant double-stranded linear DNA of HBV can be used for viral integrations into the host genome[16]. The chromatinized cccDNA, which results after a complex multiple-step process, is a mini-chromosome that serves as a template for the pregenomic RNA and subgenomic RNA transcripts, encoding all viral proteins[12-14,17]. The pregenomic RNA is the template for the generation of the progeny HBV RC-DNA, and for this to occur, it has to interact with its own translation products, HBV polymerase, and the core protein, thus forming the nucleocapsid; the latter matures through complex processes and can either be enveloped to form HBV virions or can be re-imported into the nucleus to be converted into cccDNA from its RC-DNA in order to maintain a stable pool of cccDNA[12,14,17]. HBs-coated mature nucleocapsids containing RC-DNA are released from infected cells *via* host cellular multivesicular body function[14,18] and can infect other hepatocytes. Other sub-viral particles, such as HBsAg, which can be produced in excess, are released by similar pathways as subviral noninfectious HBsAg particles[13,14,18].

After exposure to HBV, over 95% of immune-competent adults can eliminate HBsAg and HBV DNA from circulation, in many cases with HBs and HBe antigen seroconversion (loss of these antigens with the appearance of corresponding antibodies); despite this, HBV DNA can persist in the liver in the form of cccDNA or be integrated in the genome for years or a lifetime. This is called a functional cure and is a type of OBI. By contrast, infections in newborns with HBeAg expressing HBV strains lead to chronic overt infections in over 90% of cases.

The persistence of viable HBV virus particles is maintained through cccDNA or genomic material persistence (integrated HBV DNA fragments). We should keep in mind that laboratory techniques that are used to characterize HBV persistence are not perfect; they lack sensitivity, they may fail in recognizing HBsAg mutant variants, and they cannot distinguish the origin of HBsAg - whether it is from cccDNA or integrated HBV DNA.

HOST IMMUNE RESPONSE TO HBV

Both innate and adaptive immune responses are important in the course of HBV infection.

Innate immunity represents the first line in host defense, playing an important role in the resolution of a viral infection either through its direct activity or by initiating and regulating adaptive immunity. HBV, similar to many other pathogens, is recognized through germline-encoded pattern recognition receptors that are present either on the cell surface or within some intracellular compartments. The activation of these receptors normally triggers the recruitment of different types of adaptor molecules that eventually activate the signaling pathways of nuclear factor-kb and interferon (IFN) regulatory factors. Finally, this leads to the production of interferon-stimulated genes (ISGs) and different inflammatory cytokines, interferons (type I/III IFNs), and chemokines[19,20]. Studies on experimentally

infected chimpanzees and human patients with acute infection showed that HBV does not induce type I/III IFNs and also does not significantly increase ISGs, suggesting that the receptors are unable to recognize HBV or that HBV can actively block these pathways[21,22]. In vitro studies (on HBV-infected cultures of human hepatocytes) or studies on liver specimens collected by biopsy from patients with chronic HBV infection showed similar results - ISG levels are not increased compared with those of the controls[23,24]. Therefore, the term stealth virus was coined for HBV[22,23].

Natural killer (NK) cells are also important parts of the innate immune system, and they normally provide a rapid response when viral invasion is recognized. Their activity also seems to be impaired in HBV-infected hosts, and the mechanisms that could be involved include the reduction of the expression of NK group receptors 2D (NKG2D) and 2B4 (NKG2B4) (activating receptors), which consequently reduces NK cells' capacity to produce INFs and mediate cytotoxicity; the suppression of the expression of the major complexes of histocompatibility class I-related molecules A and B; and the increased expression of T cell immunoglobulin- and mucin-domain-containing molecule-3 in circulating NKs[25,26].

Nevertheless, the innate immune system eventually responds to the presence of HBV through both its components (circulating and intra-hepatic) and its cells; macrophages, monocytes, NK cells, dendritic cells (DC), myeloid-derived suppressor cells, and innate lymphoid cells start producing different signals that will lead to the activation of the adaptive immune system[27]. The adaptive immune system acts mainly through specially developed subsets of T and B cells that are created to recognize and destroy HBV-infected hepatocytes. Prolonged exposure to viral components, such as HBsAg, HBeAg, and HBxAg, leads to immune system exhaustion and downregulation of host response[28].

Regulatory T cells (Tregs) normally play an immune suppressive role by suppressing DCs, NK cells, CD4 cells, and CD8 T cells[27,29]. They perform their role by producing immunosuppressive mediators, IL-10 and TGF-β, and through direct contact[27]. During acute HBV infection, Tregs protect the liver from exceedingly severe immune-mediated liver damage[30]. On the other hand, the same Tregs seem to play a role in promoting chronic infection, as they are found in larger amounts in patients with chronic hepatitis B than in those with acute hepatitis B or HBe-negative HBV infection (formerly inactive carriers).

CD4 T cells play a central role in HBV infection management by manifesting their functions, including the activation of innate immune cells, B cells, and cytotoxic T cells. They promote antibody production and generate signals to attract neutrophiles at the site of infection[31]. CD4 T cells also contribute to the selection and maintenance of HBV-specific CD8 T cells[32]. On the other hand, besides the above-mentioned functions, CD4 T cells are involved in the pathogenesis of HBV chronic infection by producing and promoting inflammation and fibrosis[27]. CD8 T cells are the actual effectors that perform viral clearance by inhibiting viral replication and contributing to the apoptosis of infected liver cells. In patients who achieve a functional cure, a polyclonal and multi-specific HBV CD8 T cell response can be identified, whereas in those with chronic hepatitis B, CD8 T cells display a narrow spectrum of epitopes and a consequently weak response[27,33,34].

B cells are essentially seen as cells that produce antibodies and elements that can differentiate into plasma cells, providing long-term immunity. Lately, a new function of B cells has been identified - the regulatory function. This B subtype is called B regulatory cells (Bregs). Bregs produce IL-10, a mediator that serves as a downregulatory agent for other immune cells and promotes immune tolerance[35]. In HBV-infected patients, Bregs are considered to promote viral replication and liver fibrosis. They could also be responsible for HBV flares by suppressing CD8 cells[36]. The antibody production function of B cells is critical for the management of HBV infection; these cells can produce antibodies against different viral proteins, including but not limited to HBsAg, HBcAg, and HBeAg. HBs antibodies are critical for controlling or preventing viral infection. They are produced by B cells stimulated by specific T helper cells (follicular helpers) mainly through IL-21. Impairment of this chain at any of its links leads to persistent HBV infection[31].

Also of interest are human apolipoprotein B mRNA-editing catalytic polypeptide-like enzymes (APOBECs), essential components of our innate immune system, which can inhibit a wide range of viruses using mainly de-amination processes[37]. By exerting their activity, APOBECs can lead to the selection of HBsAg mutants (*e.g.*, G145R), which are not detectable by some commercially available assays[38] and can produce replication-incompetent transcripts (splice variants), which can also elude some HBsAg detection kits[39]. Furthermore, APOBECs can inhibit DNA-RNA hybridization; they can increase susceptibility to nuclease digestion and decrease protein processing, leading to OBI[37,39].

The interaction of viral factors with the immune system of the host can lead to various outcomes, and the following are the five phases of the natural evolution of HBV infection[10,11]: (1) HBeAg-positive chronic infection (immune tolerance); (2) HBeAg-positive chronic hepatitis (immune clearance/chronic hepatitis); (3) HBeAg-negative chronic infection (inactive carriers); (4) HBeAg-negative chronic hepatitis (chronic hepatitis); and (5) HBsAg-negative phase (OBI).

MECHANISMS THAT LEAD TO OBI

In recent years, significant advances have been made in understanding the HBV lifecycle and the molecular mechanisms leading to the persistence of the virus in the occult state. These factors are mainly related to the host immune system and, to a smaller proportion, to the virus[40]. Some external factors can contribute to the appearance of OBI by interfering either with the host immune system or with the lifecycle of HBV. Of these, notable are HIV and HCV co-infections[3,40]. Furthermore, co-infection with Schistosoma mansoni was found to inhibit HBV replication[39,41].

Viral factors

The factors related to HBV that result in OBIs are mainly related to the situation in which HBsAg is not recognized by available kits because of various mutations of the virus.

HBV variants may show different types of mutations:

In the major hydrophilic region (MHR/aminoacids 99-169) of the S protein. G119R, Q129R, T140I, and D144A are the mutations of this region found in one study, affecting mainly the "a" determinant of MHR (aminoacids 124-147), which contains a cluster of B-cells epitopes[42]. P120T and S143L are other mutations associated with OBI[43]. Another study looked even further and differentiated between OBIs in different genotypes. In this case, sM103, sS113, sS114, sG130, sS132, and sK160 appear specific to OBI with genotype B; sD102 and sW165 appear specific to OBI with genotype C; and sT118, sP135, and sS154 appear common to both genotypes[12]. E2 mutations (E2G/A/V/D) can also influence the detection of HBsAg, leading to OBI[12,44].

In the T-cell epitopes. Positions 41, 44, 48, 93, 96, 97, 171, 175, 176, 178, 185, 190, 207, and 213 are affected and may generate immune-escape variants, with some not being recognized even by the host's circulating HBs antibodies. These positions are outside the MHR, in the N-terminal and C-terminal regions of the S domain[40,45].

In the pre S1/S2 genomic region. The following pre-S1 mutations were found in one study: F25L, A28T, K57T, del 57-99, P65L, S78N, P89T, N98NK, N98NT, N98I, G102R; the following were found for pre S2: del 9-22, A11T, P36Q, and P54Q[42]. Mutations in this genomic region can affect antigenicity, immunogenicity, cell elimination, and/or expression of HBsAg, leading to the failure of its detection or reducing or even inhibiting the replication and/or secretion of virions and thus having a negative effect on HBsAg detection[46].

In virus regulatory elements. Gene promoter regions are essential sites in DNA recognized by proteins for the downstream processes of replication and transcription. Alterations in these regions can lead to the down- or upregulation of the respective genes[40]. One study showed that a 129 bp in-frame deletion in the S promoter region is associated with reduced levels of middle and small surface protein transcripts, resulting in a marked reduction in the expression of the two proteins. In infections with these mutants, a large amount of surface proteins accumulates inside the hepatocytes[47].

In the core protein. Generally, studies have focused on the mutations occurring in the S and pre-S regions, but at least two studies have shown that core protein mutations can also lead to occult HBV infection. The W62R mutation in the core protein significantly reduces HBcAg and HBeAg production during HBV replication, potentially contributing to the occurrence of OBI[48,49].

Mutations that affect the posttranslational production of virus envelope proteins. For example, N-glycosylation in the position N146 of the S domain in wild-type virus may lead to an escape variant[50].

Mutations that appear as a consequence of treatment with nucleotide/nucleoside analogs and may affect both viral polymerase and S protein[51]. Lamivudine-associated polymerase gene mutations M204I and L180M/M204I, corresponding to sI195M and sW196S in HBsAg, have been shown to be associated with reduced binding to HBs antibodies, and these mutants may not be correctly identified by HBsAg detection kits[39].

Although a greater genetic variability in the *S* gene of HBV isolated from OBIs was found compared with overt infection, it has also been proven that the majority of OBI patients are not infected with mutant variants, suggesting that the mechanisms of OBI are not mainly viral mutations[40]. MHR variants and, generally, *S* gene mutants may escape anti-HBs antibodies and may not be recognized by available kits, thus representing a serious health problem because they could infect even vaccinated persons[39]. The same mutants are implicated in reinfections following liver transplantation, despite correct Hepatitis B Immune Globulin (HBIG) prophylaxis. Stopping HBIG administration after the procedure allows the mutant HBV to revert into the wild type, suggesting that HBIG may favor the selection of MHR mutants[52]. In patients who present the reactivation of HBV infection from OBI during or after immunosuppressive therapy, the heterogeneity of reactivated HBV has been reported to be significantly lower than that from HBsAg-positive carriers, suggesting that OBI individuals are infected with HBV populations of low genomic heterogeneity in their liver[53].

RNA alternative splicing is an important posttranscriptional mechanism that enables single genes to produce multiple proteins. RNA splicing contributes to mRNA and protein diversities. It regulates gene expressions, providing an important causative relationship link between genetic variation and disease [54,55]. Splicing has been shown to have a significant effect on gene expression in HBV, and its implication in the occurrence of OBI has been claimed. A G-to-A mutation at position 458 of the surface gene altered the splicing of the *S* gene mRNA because nucleotide 458 is close to the 5′ splice site of *S*

gene mRNA. The mutation prevents the splicing of the pre-S2/S mRNA from positions 458 to 1305, and the two analyzed patients did not express pre-S2/S mRNA and HBsAg[56]. Another group found another mutation mechanism based on splicing, which is specific to genotype D. They describe an evolutionary branch in which the acceptor site at nucleotide 202 and the donor site at nucleotide 2986 are involved in a splice event, resulting in the loss of the spacer region from the viral polymerase gene while retaining the original reading frame. As a result, polymerase functions are not affected, but the expression of the small, middle, and large surface proteins is. Reduced HBsAg expression in the infection with HBV with this mutation leads to OBI[57].

Despite all the above arguments, it is important to note that most OBI patients are not infected with specific mutants. Mutant populations, especially pre-S/S variants, can be found in people with overt infections. Occult HBV genotypes are more often perfectly able to replicate, and their heterogeneity is similar to those from overt infections. In vitro studies have shown that HBV taken from the host's environment is going back to the wild type, being able to normally synthesize proteins and replicate. A similar situation is described above regarding post-liver transplantation from OBI donor reactivation of HBV in its wild type[40,51,52].

Host factors

Immune host factors: The first evidence, though indirect, that the host immune system is important in OBI is the possibility of HBV infection reactivation in patients subjected to immune suppression, regardless of the possible virus mutations.

A long-term follow-up study has shown that cytotoxic-T lymphocyte (CTL) response following an acute HBV infection persists for decades after serological recovery. CTL response is directly correlated with the presence of HBV DNA in the serum of these patients[58]. Therefore, it is possible to hypothesize that during the occult phase of the infection, HBV can still synthesize very small amounts of antigens that are not detectible by available kits but are sufficient to maintain an HBV-specific T cell response. This assumption is confirmed by the findings showing that, apart from HBV cccDNA molecules, all viral HBV transcripts (including the pregenomic RNA) can also be detected and quantified in the livers of OBI individuals[40,58]. Some other studies have reported similar vigorous T cell responses in OBI[59,60]. The presence or absence of serologic HBV markers defined two profiles of HBV-specific T-cell responses in occult infection. Anti-HBc-positive patients showed a T-cell response typical of protective memory, with robust *in vitro* expansion and IFN-γ production by HBV-specific T cells, suggesting that this condition represents a resolved infection with immune-mediated virus control. By contrast, HBV-specific T cells in anti-HBc-negative patients did not readily expand and produce interferon-gamma in vitro, suggesting the possibility of less complete maturation of protective memory[60]. It has been demonstrated that clearance of more than 90% of intrahepatic HBV DNA does not require lysis of HBV-infected hepatocytes, suggesting that some noncytolytic immune responses are critical in the clearance of acute HBV infection. It has also been shown that even HBV cccDNA is susceptible to these noncytolytic mechanisms. A noncytolytic HBsAg-specific T-cell response has been suggested as the potential mechanism for occult HBV infections associated with very low and undetectable levels of HBsAg[39].

One study that examined cytokine expression in OBI compared with chronic HBV hepatitis found that interleukin 2, interleukin 4, and IFN-β responses were low in both situations. The authors also found that significantly lower levels of the soluble form of the anti-apoptotic regulator Fas (sFas) were detected in occult HBV infection than in chronic HBV infection (P = 0.01)[61]. As a marker of apoptotic inhibition, decreased sFas during occult HBV infection would indicate that apoptosis occurs at higher rates in occult compared with chronic HBV infection and, therefore, may contribute to HBsAg clearance and HBV replication downregulation. Another study showed that reduced expression of CXCL12, a chemokine that modulates apoptosis, may play a role in occult HBV infection[62]. Increased apoptosis may thus play a role in the occurrence of OBI[39,61,62]. A more recent study found that in patients with OBI and chronic HCV infections compared with monoinfected (HCV) patients and healthy donors, the levels of TNF-α, IL-10, IL-6, IL-4, and IL-2 were increased[63]. Vitamin D3 and vitamin D receptor (VDR) regulate several cytokines and are important determinants of anti-HBV response. They also modulate HBV loads and HBV protein expression[64,65]. The polymorphisms in the T/T allele of exon 9 of VDR are possibly associated with OBI, and VDR and its functional polymorphisms are likely to be related to the occurrence of OBI in some patients[66].

With regard to antibodies, one study found that positive anti-HBs (≥ 10 mIU/mL) were more frequent in HBsAgNx [ARCHITECT HBsAg NEXT (sensitivity 0.005 IU/mL)]- negative than in HBsAgNx-positive nucleic acid testing yield samples (P = 0.0014), while there was no significant difference for the HBsAgNx-negative *vs* HBsAgNx-positive OBI samples (P = 0.0748)[42]. HBsAgNx is a "supersensitive" assay and its use in this study has been shown to improve HBsAg detection with 22.6% as compared to standard tests[42]. The masking of HBsAg by anti-HBs has been proposed as one reason for the lack of detection of OBI even if anti-HBs is undetectable[67]. Data from the first study[42] suggest that anti-HBs levels over 300 mIU/mL may affect the detection of samples with extremely low viral loads (median viral load: 4.42 IU/mL) and that the detection of such samples would require at least a 20000-fold excess of HBsAg to reach the detection limit of the HBsAgNx assay. Whether anti-HBs might be a consequence of vaccination in these cases or produced as a normal response to the immunogenic

stimulus could be the subject of another discussion.

The physiological function of apolipoprotein B mRNA-editing enzyme catalytic polypeptides is cytidine deamination[68]. The expression of APOBEC3G in cells replicating HBV resulted in a 50-fold reduction in HBV DNA levels. Both deamination-dependent and deamination-independent mechanisms of inhibition of HBV replication have been reported for APOBECs[69]. Both mechanisms have also been implicated in the APOBEC-induced inhibition of HBV replication[70]. APOBEC deamination-dependent activity may lead to HBsAg mutants, as mentioned above[38,39]. IFN-alpha can upregulate APOBEC3A in HBV-infected cells in which HBV core protein mediates the interaction of APOBEC3A with HBV cccDNA, resulting in cytidine deamination, apurinic/apyrimidinic site formation, and, finally, cccDNA degradation[70]. Deamination-independent processes of APOBECs lead to decreased HBV DNA production and to a decrease in HBV protein synthesis[37,38].

Epigenetic host factors: Some of the mechanisms that control HBV transcription or replication can be influenced in some cases by the modification of gene expression rather than by the alteration of the DNA sequence itself. This is called epigenetic modification. Epigenetic modifications can alter the expression pattern of a gene without changing its nucleotide sequence. Many studies have revealed that epigenetic mechanisms are important for the occurrence of OBI[39,71,72].

HBV cccDNA minichromosomes are located in the nucleus of infected hepatocytes and can be associated with histones, such as H1, H2A, H2B, H3, and H4[72], or non-histone proteins (HBV core proteins)[73]. The acetylation status of cccDNA-bound histones H3 and H4 regulates HBV replication, while the recruitment of histone deacetylase 1 correlates with low HBV replication[74]. In the presence of histone deacetylase inhibitors (valproic acid or trichostatin A), high HBV transcript levels and increased HBV replication are correlated with an increase in acetylated histones bound to cccDNA[74]. IFN-α can inhibit cccDNA-based RNA transcription by inducing the hypoacetylation of cccDNA-bound histones. This mechanism could be implicated not only in OBI but also in an active epigenetic long-term control of cccDNA activity after IFN-α therapy[75,76].

Along with histones, HBx protein can be recruited to cccDNA, and an HBx mutant has been shown to induce rapid hypoacetylation of histones, thus reducing HBV pregenomic RNA and HBV regulation[77,78].

Besides acetylation, methylation is another epigenetic mechanism considered to be involved in OBI occurrence. Cytosine-guanine dinucleotide (CpG) methylation in a gene promoter region rich in CpGs (CpG island) acts like a switch, silencing the gene[79]. It was already demonstrated a long time ago that HBV DNA integrated into the host genome is methylated, leading to the loss of HBV core protein in PLC/PRF/5. Methylation of HBV DNA is an epigenetic mechanism that modifies HBV proteins, interferes HBV replication, and impairs HBV virion production, possibly leading to occult HBV infection[80]. Methylation of CpG island 2 in the HBV genome is frequently detected in occult HBV infection[81]. Hypermethylated HBV DNA sequences are often found in HCC patients with occult HBV infection[82].

Emerging data suggest that microRNAs (miRNAs) play vital roles in the occurrence and development of HBV infection, particularly in OBI occurrence. MiR-199a-3p and miR-210 were found to efficiently reduce HBsAg expression, and quantification of HBV DNA by real-time PCR showed that both miRNAs suppressed viral replication[83]. In another study, miR-125a-5p was found to interact with the viral sequence and to suppress HBsAg expression and release[84]. MiR-141 was identified to repress HBV expression, and synthetic miR-141 could also significantly suppress HBV expression and replication by targeting peroxisome proliferator-activated receptor alpha[85]. In a more recent study, miRNAs, including hsa-miR-25-3p, -486-5p, -92a-3p, and -1-3p, showed the ability to distinguish OBI from healthy controls efficiently, with an area under the curve value of 0.874, 0.776, 0.886, and 0.807, respectively. In total, 32 differentially expressed miRNAs were identified between OBI and the healthy controls by miRNA sequencing[86]. Compared with the case of the healthy controls, plasma miR-451a and miR-340-3p were significantly upregulated in OBI, making the authors propose these markers for distinguishing OBI from healthy donors[86].

The above depicted mechanisms that may lead to OBI are summarized in Figure 2.

CONCLUSION

OBI remains one of the most challenging problems in the hepatology field. It is a public health problem and a subject that needs further research in the future. OBI is currently diagnosed using PCR and real-time PCR assays. However, all efforts should be made to exclude false negative HBsAg, and new standardized methods must be developed to correctly identify OBI. Some of the studies mentioned above have found different markers (especially in the miRNA field) that could be used in the future for this purpose. Facts regarding OBI have become clearer in recent years; the factors that determine this outcome are now better understood, with host factors (immune or epigenetic) being identified as seemingly the main contributors. Viral factors are important but account for only a minority of OBIs. Some external factors can contribute to the appearance of OBI by interfering either with the host immune system or with the lifecycle of HBV. Of these, HIV and HCV co-infections are notable. Co-

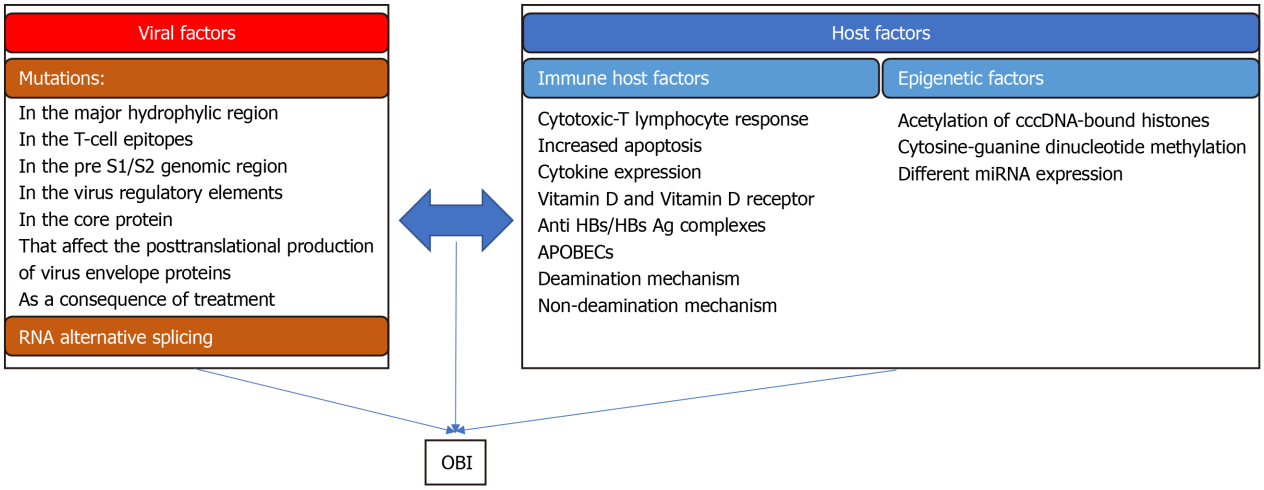

DOI: 10.12998/wjcc.v10.i17.5518 **Copyright** ©The Author(s) 2022.

Figure 2 Mechanisms that produce occult hepatitis B infection. APOBECs: Apolipoprotein B mRNA-editing catalytic polypeptide-like enzymes; OBI: Occult hepatitis B infection; HBsAg: Hepatitis B surface antigen; cccDNA: Covalently closed circular DNA; miRNA: MicroRNAs.

infection with Schistosoma mansoni was also found to inhibit HBV replication. Future research in this domain and increased awareness regarding this topic must be encouraged, as this particular form of evolution of HBV infection is still far from being completely understood and controlled.

FOOTNOTES

Author contributions: Gherlan GS reviewed the literature, wrote the paper and elaborated the figures.

Conflict-of-interest statement: Gherlan GS has no conflict of interest to declare.

Open-Access: This article is an open-access article that was selected by an in-house editor and fully peer-reviewed by external reviewers. It is distributed in accordance with the Creative Commons Attribution NonCommercial (CC BY-NC 4.0) license, which permits others to distribute, remix, adapt, build upon this work non-commercially, and license their derivative works on different terms, provided the original work is properly cited and the use is non-commercial. See: https://creativecommons.org/Licenses/by-nc/4.0/

Country/Territory of origin: Romania

ORCID number: George Sebastian Gherlan 0000-0003-3994-5020.

S-Editor: Gong ZM
L-Editor: A
P-Editor: Gong ZM

REFERENCES

1 **Tabor E**, Hoofnagle JH, Smallwood LA, Drucker JA, Pineda-Tamondong GC, Ni LY, Greenwalt TJ, Barker LF, Gerety RJ. Studies of donors who transmit posttransfusion hepatitis. *Transfusion* 1979; **19**: 725-731 [PMID: 230620 DOI: 10.1046/j.1537-2995.1979.19680104098.x]
2 **Niederhauser C**, Mansouri Taleghani B, Graziani M, Stolz M, Tinguely C, Schneider P. Blood donor screening: how to decrease the risk of transfusion-transmitted hepatitis B virus? *Swiss Med Wkly* 2008; **138**: 134-141 [PMID: 18330733]
3 **Makvandi M**. Update on occult hepatitis B virus infection. *World J Gastroenterol* 2016; **22**: 8720-8734 [PMID: 27818588 DOI: 10.3748/wjg.v22.i39.8720]
4 **Mücke MM**, Backus LI, Mücke VT, Coppola N, Preda CM, Yeh ML, Tang LSY, Belperio PS, Wilson EM, Yu ML, Zeuzem S, Herrmann E, Vermehren J. Hepatitis B virus reactivation during direct-acting antiviral therapy for hepatitis C: a systematic review and meta-analysis. *Lancet Gastroenterol Hepatol* 2018; **3**: 172-180 [PMID: 29371017 DOI: 10.1016/S2468-1253(18)30002-5]
5 **Puoti M**, Torti C, Bruno R, Filice G, Carosi G. Natural history of chronic hepatitis B in co-infected patients. *J Hepatol* 2006; **44**: S65-S70 [PMID: 16338021 DOI: 10.1016/j.jhep.2005.11.015]
6 **Raimondo G**, Allain JP, Brunetto MR, Buendia MA, Chen DS, Colombo M, Craxì A, Donato F, Ferrari C, Gaeta GB, Gerlich WH, Levrero M, Locarnini S, Michalak T, Mondelli MU, Pawlotsky JM, Pollicino T, Prati D, Puoti M, Samuel D,

Shouval D, Smedile A, Squadrito G, Trépo C, Villa E, Will H, Zanetti AR, Zoulim F. Statements from the Taormina expert meeting on occult hepatitis B virus infection. *J Hepatol* 2008; **49**: 652-657 [PMID: 18715666 DOI: 10.1016/j.jhep.2008.07.014]

7 **Raimondo G**, Locarnini S, Pollicino T, Levrero M, Zoulim F, Lok AS; Taormina Workshop on Occult HBV Infection Faculty Members. Update of the statements on biology and clinical impact of occult hepatitis B virus infection. *J Hepatol* 2019; **71**: 397-408 [PMID: 31004683 DOI: 10.1016/j.jhep.2019.03.034]

8 **Sarin SK**, Kumar M, Lau GK, Abbas Z, Chan HL, Chen CJ, Chen DS, Chen HL, Chen PJ, Chien RN, Dokmeci AK, Gane E, Hou JL, Jafri W, Jia J, Kim JH, Lai CL, Lee HC, Lim SG, Liu CJ, Locarnini S, Al Mahtab M, Mohamed R, Omata M, Park J, Piratvisuth T, Sharma BC, Sollano J, Wang FS, Wei L, Yuen MF, Zheng SS, Kao JH. Asian-Pacific clinical practice guidelines on the management of hepatitis B: a 2015 update. *Hepatol Int* 2016; **10**: 1-98 [PMID: 26563120 DOI: 10.1007/s12072-015-9675-4]

9 **European Association for the Study of the Liver**. EASL 2017 Clinical Practice Guidelines on the management of hepatitis B virus infection. *J Hepatol* 2017; **67**: 370-398 [PMID: 28427875 DOI: 10.1016/j.jhep.2017.03.021]

10 **Terrault NA**, Lok ASF, McMahon BJ, Chang KM, Hwang JP, Jonas MM, Brown RS Jr, Bzowej NH, Wong JB. Update on prevention, diagnosis, and treatment of chronic hepatitis B: AASLD 2018 hepatitis B guidance. *Hepatology* 2018; **67**: 1560-1599 [PMID: 29405329 DOI: 10.1002/hep.29800]

11 **Mulrooney-Cousins PM**, Michalak TI. Asymptomatic Hepadnaviral Persistence and Its Consequences in the Woodchuck Model of Occult Hepatitis B Virus Infection. *J Clin Transl Hepatol* 2015; **3**: 211-219 [PMID: 26623268 DOI: 10.14218/JCTH.2015.00020]

12 **Wang J**, Zhang P, Zeng J, Du P, Zheng X, Ye X, Zhu W, Fu Y, Candotti D, Allain JP, Li C, Li T. Occurrence of occult hepatitis B virus infection associated with envelope protein mutations according to anti-HBs carriage in blood donors. *Int J Infect Dis* 2020; **92**: 38-45 [PMID: 31877352 DOI: 10.1016/j.ijid.2019.12.026]

13 **Wei L**, Ploss A. Mechanism of Hepatitis B Virus cccDNA Formation. *Viruses* 2021; **13** [PMID: 34452329 DOI: 10.3390/v13081463]

14 **Shi Y**, Zheng M. Hepatitis B virus persistence and reactivation. *BMJ* 2020; **370**: m2200 [PMID: 32873599 DOI: 10.1136/bmj.m2200]

15 **Selzer L**, Zlotnick A. Assembly and Release of Hepatitis B Virus. *Cold Spring Harb Perspect Med* 2015; **5** [PMID: 26552701 DOI: 10.1101/cshperspect.a021394]

16 **Yan H**, Zhong G, Xu G, He W, Jing Z, Gao Z, Huang Y, Qi Y, Peng B, Wang H, Fu L, Song M, Chen P, Gao W, Ren B, Sun Y, Cai T, Feng X, Sui J, Li W. Sodium taurocholate cotransporting polypeptide is a functional receptor for human hepatitis B and D virus. *Elife* 2012; **1**: e00049 [PMID: 23150796 DOI: 10.7554/eLife.00049]

17 **Tuttleman JS**, Pourcel C, Summers J. Formation of the pool of covalently closed circular viral DNA in hepadnavirus-infected cells. *Cell* 1986; **47**: 451-460 [PMID: 3768961 DOI: 10.1016/0092-8674(86)90602-1]

18 **Nassal M**. HBV cccDNA: viral persistence reservoir and key obstacle for a cure of chronic hepatitis B. *Gut* 2015; **64**: 1972-1984 [PMID: 26048673 DOI: 10.1136/gutjnl-2015-309809]

19 **Seeger C**, Mason WS. Molecular biology of hepatitis B virus infection. *Virology* 2015; **479-480**: 672-686 [PMID: 25759099 DOI: 10.1016/j.virol.2015.02.031]

20 **Shin EC**, Sung PS, Park SH. Immune responses and immunopathology in acute and chronic viral hepatitis. *Nat Rev Immunol* 2016; **16**: 509-523 [PMID: 27374637 DOI: 10.1038/nri.2016.69]

21 **Dandri M**, Bertoletti A, Lütgehetmann M. Innate immunity in hepatitis B and D virus infection: consequences for viral persistence, inflammation, and T cell recognition. *Semin Immunopathol* 2021; **43**: 535-548 [PMID: 34019142 DOI: 10.1007/s00281-021-00864-x]

22 **Dunn C**, Peppa D, Khanna P, Nebbia G, Jones M, Brendish N, Lascar RM, Brown D, Gilson RJ, Tedder RJ, Dusheiko GM, Jacobs M, Klenerman P, Maini MK. Temporal analysis of early immune responses in patients with acute hepatitis B virus infection. *Gastroenterology* 2009; **137**: 1289-1300 [PMID: 19591831 DOI: 10.1053/j.gastro.2009.06.054]

23 **Wieland SF**, Chisari FV. Stealth and cunning: hepatitis B and hepatitis C viruses. *J Virol* 2005; **79**: 9369-9380 [PMID: 16014900 DOI: 10.1128/JVI.79.15.9369-9380.2005]

24 **Mutz P**, Metz P, Lempp FA, Bender S, Qu B, Schöneweis K, Seitz S, Tu T, Restuccia A, Frankish J, Dächert C, Schusser B, Koschny R, Polychronidis G, Schemmer P, Hoffmann K, Baumert TF, Binder M, Urban S, Bartenschlager R. HBV Bypasses the Innate Immune Response and Does Not Protect HCV From Antiviral Activity of Interferon. *Gastroenterology* 2018; **154**: 1791-1804.e22 [PMID: 29410097 DOI: 10.1053/j.gastro.2018.01.044]

25 **Sun C**, Fu B, Gao Y, Liao X, Sun R, Tian Z, Wei H. TGF-β1 down-regulation of NKG2D/DAP10 and 2B4/SAP expression on human NK cells contributes to HBV persistence. *PLoS Pathog* 2012; **8**: e1002594 [PMID: 22438812 DOI: 10.1371/journal.ppat.1002594]

26 **Wu J**, Zhang XJ, Shi KQ, Chen YP, Ren YF, Song YJ, Li G, Xue YF, Fang YX, Deng ZJ, Xu X, Gao J, Tang KF. Hepatitis B surface antigen inhibits MICA and MICB expression *via* induction of cellular miRNAs in hepatocellular carcinoma cells. *Carcinogenesis* 2014; **35**: 155-163 [PMID: 23917076 DOI: 10.1093/carcin/bgt268]

27 **Ju Y**, Hou N, Meng J, Wang X, Zhang X, Zhao D, Liu Y, Zhu F, Zhang L, Sun W, Liang X, Gao L, Ma C. T cell immunoglobulin- and mucin-domain-containing molecule-3 (Tim-3) mediates natural killer cell suppression in chronic hepatitis B. *J Hepatol* 2010; **52**: 322-329 [PMID: 20133006 DOI: 10.1016/j.jhep.2009.12.005]

28 **Khanam A**, Chua JV, Kottilil S. Immunopathology of Chronic Hepatitis B Infection: Role of Innate and Adaptive Immune Response in Disease Progression. *Int J Mol Sci* 2021; **22** [PMID: 34071064 DOI: 10.3390/ijms22115497]

29 **Bertoletti A**, Kennedy PT. The immune tolerant phase of chronic HBV infection: new perspectives on an old concept. *Cell Mol Immunol* 2015; **12**: 258-263 [PMID: 25176526 DOI: 10.1038/cmi.2014.79]

30 **Gol-Ara M**, Jadidi-Niaragh F, Sadria R, Azizi G, Mirshafiey A. The role of different subsets of regulatory T cells in immunopathogenesis of rheumatoid arthritis. *Arthritis* 2012; **2012**: 805875 [PMID: 23133752 DOI: 10.1155/2012/805875]

31 **Stross L**, Günther J, Gasteiger G, Asen T, Graf S, Aichler M, Esposito I, Busch DH, Knolle P, Sparwasser T, Protzer U. Foxp3+ regulatory T cells protect the liver from immune damage and compromise virus control during acute experimental hepatitis B virus infection in mice. *Hepatology* 2012; **56**: 873-883 [PMID: 22487943 DOI: 10.1002/hep.25765]

32 **Wang X**, Dong Q, Li Q, Li Y, Zhao D, Sun J, Fu J, Meng F, Lin H, Luan J, Liu B, Wang M, Wang FS, He F, Tang L. Dysregulated Response of Follicular Helper T Cells to Hepatitis B Surface Antigen Promotes HBV Persistence in Mice and Associates With Outcomes of Patients. *Gastroenterology* 2018; **154**: 2222-2236 [PMID: 29544722 DOI: 10.1053/j.gastro.2018.03.021]

33 **Thimme R**, Wieland S, Steiger C, Ghrayeb J, Reimann KA, Purcell RH, Chisari FV. CD8(+) T cells mediate viral clearance and disease pathogenesis during acute hepatitis B virus infection. *J Virol* 2003; **77**: 68-76 [PMID: 12477811 DOI: 10.1128/jvi.77.1.68-76.2003]

34 **Bertoletti A**, Ferrari C, Fiaccadori F, Penna A, Margolskee R, Schlicht HJ, Fowler P, Guilhot S, Chisari FV. HLA class I-restricted human cytotoxic T cells recognize endogenously synthesized hepatitis B virus nucleocapsid antigen. *Proc Natl Acad Sci USA* 1991; **88**: 10445-10449 [PMID: 1660137 DOI: 10.1073/pnas.88.23.10445]

35 **Vazquez MI**, Catalan-Dibene J, Zlotnik A. B cells responses and cytokine production are regulated by their immune microenvironment. *Cytokine* 2015; **74**: 318-326 [PMID: 25742773 DOI: 10.1016/j.cyto.2015.02.007]

36 **Alatrakchi N**. Bregs in Chronic HBV: Is It Time for Bragging Rights? *Dig Dis Sci* 2015; **60**: 1115-1117 [PMID: 25686744 DOI: 10.1007/s10620-015-3584-1]

37 **Sadeghpour S**, Khodaee S, Rahnama M, Rahimi H, Ebrahimi D. Human APOBEC3 Variations and Viral Infection. *Viruses* 2021; **13** [PMID: 34372572 DOI: 10.3390/v13071366]

38 **Komatsu H**, Inui A, Umetsu S, Tsunoda T, Sogo T, Konishi Y, Fujisawa T. Evaluation of the G145R Mutant of the Hepatitis B Virus as a Minor Strain in Mother-to-Child Transmission. *PLoS One* 2016; **11**: e0165674 [PMID: 27812178 DOI: 10.1371/journal.pone.0165674]

39 **Samal J**, Kandpal M, Vivekanandan P. Molecular mechanisms underlying occult hepatitis B virus infection. *Clin Microbiol Rev* 2012; **25**: 142-163 [PMID: 22232374 DOI: 10.1128/CMR.00018-11]

40 **Raimondo G**, Pollicino T. Occult HBV Infection. In: Liaw YF, Zoulim F. (eds) Hepatitis B Virus in Human Diseases. Molecular and Translational Medicine. Humana Press, Cham. 2016: 277-301

41 **McClary H**, Koch R, Chisari FV, Guidotti LG. Inhibition of hepatitis B virus replication during schistosoma mansoni infection in transgenic mice. *J Exp Med* 2000; **192**: 289-294 [PMID: 10899915 DOI: 10.1084/jem.192.2.289]

42 **Kuhns MC**, Holzmayer V, Anderson M, McNamara AL, Sauleda S, Mbanya D, Duong PT, Dung NTT, Cloherty GA. Molecular and Serological Characterization of Hepatitis B Virus (HBV)-Positive Samples with Very Low or Undetectable Levels of HBV Surface Antigen. *Viruses* 2021; **13** [PMID: 34696483 DOI: 10.3390/v13102053]

43 **Elkady A**, Iijima S, Aboulfotuh S, Mostafa Ali E, Sayed D, Abdel-Aziz NM, Ali AM, Murakami S, Isogawa M, Tanaka Y. Characteristics of escape mutations from occult hepatitis B virus infected patients with hematological malignancies in South Egypt. *World J Hepatol* 2017; **9**: 477-486 [PMID: 28396718 DOI: 10.4254/wjh.v9.i9.477]

44 **Wang H**, Liao F, Xie J, Gao W, Wang M, Huang J, Xu R, Liao Q, Shan Z, Zheng Y, Rong X, Li C, Fu Y. E2 Site Mutations in S Protein Strongly Affect Hepatitis B Surface Antigen Detection in the Occult Hepatitis B Virus. *Front Microbiol* 2021; **12**: 664833 [PMID: 34867835 DOI: 10.3389/fmicb.2021.664833]

45 **Lazarevic I**, Banko A, Miljanovic D, Cupic M. Immune-Escape Hepatitis B Virus Mutations Associated with Viral Reactivation upon Immunosuppression. *Viruses* 2019; **11** [PMID: 31450544 DOI: 10.3390/v11090778]

46 **Zhu HL**, Li X, Li J, Zhang ZH. Genetic variation of occult hepatitis B virus infection. *World J Gastroenterol* 2016; **22**: 3531-3546 [PMID: 27053845 DOI: 10.3748/wjg.v22.i13.3531]

47 **Xu Z**, Yen TS. Intracellular retention of surface protein by a hepatitis B virus mutant that releases virion particles. *J Virol* 1996; **70**: 133-140 [PMID: 8523517 DOI: 10.1128/JVI.70.1.133-140.1996]

48 **Chen J**, Liu B, Tang X, Zheng X, Lu J, Zhang L, Wang W, Candotti D, Fu Y, Allain JP, Li C, Li L, Li T. Role of core protein mutations in the development of occult HBV infection. *J Hepatol* 2021; **74**: 1303-1314 [PMID: 33453326 DOI: 10.1016/j.jhep.2020.12.023]

49 **Quarleri J**. Core promoter: a critical region where the hepatitis B virus makes decisions. *World J Gastroenterol* 2014; **20**: 425-435 [PMID: 24574711 DOI: 10.3748/wjg.v20.i2.425]

50 **El Chaar M**, Candotti D, Crowther RA, Allain JP. Impact of hepatitis B virus surface protein mutations on the diagnosis of occult hepatitis B virus infection. *Hepatology* 2010; **52**: 1600-1610 [PMID: 20815025 DOI: 10.1002/hep.23886]

51 **Pollicino T**, Cacciola I, Saffioti F, Raimondo G. Hepatitis B virus PreS/S gene variants: pathobiology and clinical implications. *J Hepatol* 2014; **61**: 408-417 [PMID: 24801416 DOI: 10.1016/j.jhep.2014.04.041]

52 **Ghany MG**, Ayola B, Villamil FG, Gish RG, Rojter S, Vierling JM, Lok AS. Hepatitis B virus S mutants in liver transplant recipients who were reinfected despite hepatitis B immune globulin prophylaxis. *Hepatology* 1998; **27**: 213-222 [PMID: 9425940 DOI: 10.1002/hep.510270133]

53 **Inuzuka T**, Ueda Y, Morimura H, Fujii Y, Umeda M, Kou T, Osaki Y, Uemoto S, Chiba T, Marusawa H. Reactivation from occult HBV carrier status is characterized by low genetic heterogeneity with the wild-type or G1896A variant prevalence. *J Hepatol* 2014; **61**: 492-501 [PMID: 24798622 DOI: 10.1016/j.jhep.2014.04.033]

54 **Li YI**, van de Geijn B, Raj A, Knowles DA, Petti AA, Golan D, Gilad Y, Pritchard JK. RNA splicing is a primary link between genetic variation and disease. *Science* 2016; **352**: 600-604 [PMID: 27126046 DOI: 10.1126/science.aad9417]

55 **Kelemen O**, Convertini P, Zhang Z, Wen Y, Shen M, Falaleeva M, Stamm S. Function of alternative splicing. *Gene* 2013; **514**: 1-30 [PMID: 22909801 DOI: 10.1016/j.gene.2012.07.083]

56 **Hass M**, Hannoun C, Kalinina T, Sommer G, Manegold C, Günther S. Functional analysis of hepatitis B virus reactivating in hepatitis B surface antigen-negative individuals. *Hepatology* 2005; **42**: 93-103 [PMID: 15962285 DOI: 10.1002/hep.20748]

57 **van Hemert FJ**, Zaaijer HL, Berkhout B, Lukashov VV. Occult hepatitis B infection: an evolutionary scenario. *Virol J* 2008; **5**: 146 [PMID: 19077239 DOI: 10.1186/1743-422X-5-146]

58 **Rehermann B**, Ferrari C, Pasquinelli C, Chisari FV. The hepatitis B virus persists for decades after patients' recovery from acute viral hepatitis despite active maintenance of a cytotoxic T-lymphocyte response. *Nat Med* 1996; **2**: 1104-1108 [PMID: 8837608 DOI: 10.1038/nm1096-1104]

59 **Bes M**, Vargas V, Piron M, Casamitjana N, Esteban JI, Vilanova N, Pinacho A, Quer J, Puig L, Guardia J, Sauleda S. T cell

responses and viral variability in blood donation candidates with occult hepatitis B infection. *J Hepatol* 2012; **56**: 765-774 [PMID: 22173156 DOI: 10.1016/j.jhep.2011.11.011]

60 **Zerbini A**, Pilli M, Boni C, Fisicaro P, Penna A, Di Vincenzo P, Giuberti T, Orlandini A, Raffa G, Pollicino T, Raimondo G, Ferrari C, Missale G. The characteristics of the cell-mediated immune response identify different profiles of occult hepatitis B virus infection. *Gastroenterology* 2008; **134**: 1470-1481 [PMID: 18355815 DOI: 10.1053/j.gastro.2008.02.017]

61 **Martin CM**, Welge JA, Shire NJ, Shata MT, Sherman KE, Blackard JT. Cytokine expression during chronic versus occult hepatitis B virus infection in HIV co-infected individuals. *Cytokine* 2009; **47**: 194-198 [PMID: 19625194 DOI: 10.1016/j.cyto.2009.06.005]

62 **Hassanshahi G**, Arababadi MK, Khoramdelazad H, Yaghini N, Zarandi ER. Assessment of CXCL12 (SDF-1α) polymorphisms and its serum level in posttransfusion occult HBV-infected patients in Southeastern Iran. *Arch Med Res* 2010; **41**: 338-342 [PMID: 20851290 DOI: 10.1016/j.arcmed.2010.07.001]

63 **Ribeiro CRA**, de Almeida NAA, Martinelli KG, Pires MA, Mello CEB, Barros JJ, de Paula VS. Cytokine profile during occult hepatitis B virus infection in chronic hepatitis C patients. *Virol J* 2021; **18**: 15 [PMID: 33435966 DOI: 10.1186/s12985-021-01487-2]

64 **Kong J**, Grando SA, Li YC. Regulation of IL-1 family cytokines IL-1alpha, IL-1 receptor antagonist, and IL-18 by 1,25-dihydroxyvitamin D3 in primary keratinocytes. *J Immunol* 2006; **176**: 3780-3787 [PMID: 16517748 DOI: 10.4049/jimmunol.176.6.3780]

65 **Huang YW**, Liao YT, Chen W, Chen CL, Hu JT, Liu CJ, Lai MY, Chen PJ, Chen DS, Yang SS, Kao JH. Vitamin D receptor gene polymorphisms and distinct clinical phenotypes of hepatitis B carriers in Taiwan. *Genes Immun* 2010; **11**: 87-93 [PMID: 19693091 DOI: 10.1038/gene.2009.65]

66 **Arababadi MK**, Pourfathollah AA, Jafarzadeh A, Hassanshahi G, Rezvani ME. Association of exon 9 but not intron 8 VDR polymorphisms with occult HBV infection in south-eastern Iranian patients. *J Gastroenterol Hepatol* 2010; **25**: 90-93 [PMID: 19793172 DOI: 10.1111/j.1440-1746.2009.05950.x]

67 **Gerlich WH**, Glebe D, Schüttler CG. Hepatitis B viral safety of blood donations: New gaps identified. *Ann Blood* 2018; **3**: 38 [DOI: 10.21037/aob.2018.09.03]

68 **Navaratnam N**, Morrison JR, Bhattacharya S, Patel D, Funahashi T, Giannoni F, Teng BB, Davidson NO, Scott J. The p27 catalytic subunit of the apolipoprotein B mRNA editing enzyme is a cytidine deaminase. *J Biol Chem* 1993; **268**: 20709-20712 [PMID: 8407891]

69 **Turelli P**, Mangeat B, Jost S, Vianin S, Trono D. Inhibition of hepatitis B virus replication by APOBEC3G. *Science* 2004; **303**: 1829 [PMID: 15031497 DOI: 10.1126/science.1092066]

70 **Bonvin M**, Greeve J. Hepatitis B: modern concepts in pathogenesis--APOBEC3 cytidine deaminases as effectors in innate immunity against the hepatitis B virus. *Curr Opin Infect Dis* 2008; **21**: 298-303 [PMID: 18448976 DOI: 10.1097/QCO.0b013e3282fe1bb2]

71 **Levrero M**, Pollicino T, Petersen J, Belloni L, Raimondo G, Dandri M. Control of cccDNA function in hepatitis B virus infection. *J Hepatol* 2009; **51**: 581-592 [PMID: 19616338 DOI: 10.1016/j.jhep.2009.05.022]

72 **Zhang X**, Hou J, Lu M. Regulation of hepatitis B virus replication by epigenetic mechanisms and microRNAs. *Front Genet* 2013; **4**: 202 [PMID: 24133502 DOI: 10.3389/fgene.2013.00202]

73 **Bock CT**, Schwinn S, Locarnini S, Fyfe J, Manns MP, Trautwein C, Zentgraf H. Structural organization of the hepatitis B virus minichromosome. *J Mol Biol* 2001; **307**: 183-196 [PMID: 11243813 DOI: 10.1006/jmbi.2000.4481]

74 **Pollicino T**, Belloni L, Raffa G, Pediconi N, Squadrito G, Raimondo G, Levrero M. Hepatitis B virus replication is regulated by the acetylation status of hepatitis B virus cccDNA-bound H3 and H4 histones. *Gastroenterology* 2006; **130**: 823-837 [PMID: 16530522 DOI: 10.1053/j.gastro.2006.01.001]

75 **Belloni L**, Allweiss L, Guerrieri F, Pediconi N, Volz T, Pollicino T, Petersen J, Raimondo G, Dandri M, Levrero M. IFN-α inhibits HBV transcription and replication in cell culture and in humanized mice by targeting the epigenetic regulation of the nuclear cccDNA minichromosome. *J Clin Invest* 2012; **122**: 529-537 [PMID: 22251702 DOI: 10.1172/JCI58847]

76 **Dandri M**. Epigenetic modulation in chronic hepatitis B virus infection. *Semin Immunopathol* 2020; **42**: 173-185 [PMID: 32185454 DOI: 10.1007/s00281-020-00780-6]

77 **Belloni L**, Pollicino T, De Nicola F, Guerrieri F, Raffa G, Fanciulli M, Raimondo G, Levrero M. Nuclear HBx binds the HBV minichromosome and modifies the epigenetic regulation of cccDNA function. *Proc Natl Acad Sci USA* 2009; **106**: 19975-19979 [PMID: 19906987 DOI: 10.1073/pnas.0908365106]

78 **Gong Q**, Chen S, Guo J, Sun H, Zheng G, Liu Q, Ren H, He S. Chromosome remodeling related to hepatitis B virus replication in HepG2 cells. *DNA Cell Biol* 2011; **30**: 347-354 [PMID: 21345131 DOI: 10.1089/dna.2010.1172]

79 **Portela A**, Esteller M. Epigenetic modifications and human disease. *Nat Biotechnol* 2010; **28**: 1057-1068 [PMID: 20944598 DOI: 10.1038/nbt.1685]

80 **Miller RH**, Robinson WS. Integrated hepatitis B virus DNA sequences specifying the major viral core polypeptide are methylated in PLC/PRF/5 cells. *Proc Natl Acad Sci USA* 1983; **80**: 2534-2538 [PMID: 6302693 DOI: 10.1073/pnas.80.9.2534]

81 **Vivekanandan P**, Thomas D, Torbenson M. Hepatitis B viral DNA is methylated in liver tissues. *J Viral Hepat* 2008; **15**: 103-107 [PMID: 18184192 DOI: 10.1111/j.1365-2893.2007.00905.x]

82 **Kaur P**, Paliwal A, Durantel D, Hainaut P, Scoazec JY, Zoulim F, Chemin I, Herceg Z. DNA methylation of hepatitis B virus (HBV) genome associated with the development of hepatocellular carcinoma and occult HBV infection. *J Infect Dis* 2010; **202**: 700-704 [PMID: 20653444 DOI: 10.1086/655398]

83 **Zhang GL**, Li YX, Zheng SQ, Liu M, Li X, Tang H. Suppression of hepatitis B virus replication by microRNA-199a-3p and microRNA-210. *Antiviral Res* 2010; **88**: 169-175 [PMID: 20728471 DOI: 10.1016/j.antiviral.2010.08.008]

84 **Potenza N**, Papa U, Mosca N, Zerbini F, Nobile V, Russo A. Human microRNA hsa-miR-125a-5p interferes with expression of hepatitis B virus surface antigen. *Nucleic Acids Res* 2011; **39**: 5157-5163 [PMID: 21317190 DOI: 10.1093/nar/gkr067]

85 **Hu W**, Wang X, Ding X, Li Y, Zhang X, Xie P, Yang J, Wang S. MicroRNA-141 represses HBV replication by targeting PPARA. *PLoS One* 2012; **7**: e34165 [PMID: 22479552 DOI: 10.1371/journal.pone.0034165]

86 **Hao QQ**, Wang QH, Xia W, Qian HZ. Circulating miRNA expression profile and bioinformatics analysis in patients with occult hepatitis B virus infection. *J Med Virol* 2020; **92**: 191-200 [PMID: 31513283 DOI: 10.1002/jmv.25594]

World Journal of Clinical Cases

Submit a Manuscript: https://www.f6publishing.com

World J Clin Cases 2022 June 16; 10(17): 5531-5540

DOI: 10.12998/wjcc.v10.i17.5531

ISSN 2307-8960 (online)

MINIREVIEWS

Pulmonary complications of portal hypertension: The overlooked decompensation

Rares Craciun, Tudor Mocan, Bogdan Procopet, Andrada Nemes, Cristian Tefas, Mihaela Sparchez, Lavinia-Patricia Mocan, Zeno Sparchez

Specialty type: Medicine, research and experimental

Provenance and peer review: Invited article; Externally peer reviewed.

Peer-review model: Single blind

Peer-review report's scientific quality classification

Grade A (Excellent): 0
Grade B (Very good): B, B
Grade C (Good): C
Grade D (Fair): 0
Grade E (Poor): 0

P-Reviewer: Chen J, China; Elshimi E, Egypt; Xing HC, China

Received: January 16, 2022
Peer-review started: January 16, 2022
First decision: February 7, 2022
Revised: February 22, 2022
Accepted: April 9, 2022
Article in press: April 9, 2022
Published online: June 16, 2022

Rares Craciun, Tudor Mocan, Bogdan Procopet, Cristian Tefas, Zeno Sparchez, 3rd Medical Clinic, Department of Internal Medicine, "Iuliu Hatieganu" University of Medicine and Pharmacy, Cluj-Napoca 400162, Romania

Rares Craciun, Tudor Mocan, Bogdan Procopet, Cristian Tefas, Zeno Sparchez, Gastroenterology Clinic, "Prof. Dr. O. Fodor" Regional Institute of Gastroenterology and Hepatology, Cluj-Napoca 400162, Romania

Andrada Nemes, Intensiv Care Unit I, Cluj County Emergency Hosptial, Cluj-Napoca 400006, Romania

Mihaela Sparchez, 2nd Paediatric Clinic, "Iuliu Hatieganu" University of Medicine and Pharmacy, Cluj-Napoca 400126, Please enter the state or province, Romania

Lavinia-Patricia Mocan, Department of Histology, "Iuliu Hatieganu" University of Medicine and Pharmacy, Cluj-Napoca 400349, Romania

Corresponding author: Tudor Mocan, MD, PhD, Doctor, Senior Researcher, 3rd Medical Clinic, Department of Internal Medicine, "Iuliu Hatieganu" University of Medicine and Pharmacy, 19-21 Croitorilor Street, Cluj-Napoca 400162, Romania. mocan_tudor@yahoo.com

Abstract

The systemic nature of cirrhosis and portal hypertension has long been recognized, and the amount of data characterizing the interplay between each system is becoming ever so complex. Lung involvement was among the first described associated entities in cirrhosis, with reports dating back to the late nineteenth century. However, it appears that throughout the years, interest in the pulmonary complications of portal hypertension has generally faded, especially in contrast to other decompensating events, as expertise in this field has primarily been concentrated in highly experienced tertiary care facilities and liver transplantation centers. Despite affecting up to 10%-15% of patients with advanced liver disease and having a proven prognostic impact, hepato-pulmonary syndrome, porto-pulmonary hypertension, and hepatic hydrothorax are frequently misdiagnosed, mistreated, or misinterpreted. This lack of precision might adversely impact patient care, referral to expert centers, and, ultimately, liver disease-related mortality and successful transplantation odds. The present minireview aims to increase awareness of the pulmonary complications of chronic liver disease by providing a brief overview of each of the three entities. The paper

focuses on the essential theoretical aspects, addressing the most critical knowledge gaps on the one hand and, on the other hand, critically discussing one key issue for each complication.

Key Words: Hepato-pulmonary syndrome; Porto-pulmonary hypertension; Hepatic hydrothorax; Cirrhosis; Portal hypertension; Advanced liver disease

©The Author(s) 2022. Published by Baishideng Publishing Group Inc. All rights reserved.

Core Tip: There is an increasing interest in the systemic involvement associated with chronic liver disease and portal hypertension. There are three main pulmonary complications of chronic liver disease: Hepato-pulmonary syndrome, porto-pulmonary hypertension, and hepatic hydrothorax. Despite being recognized for over a century, these entities are relatively understudied, forming a niche that typically becomes the appanage of tertiary care facilities and liver transplantation centers. This minireview aims to shed light on one hot topic for each entity with direct implications for day-to-day clinical practice.

Citation: Craciun R, Mocan T, Procopet B, Nemes A, Tefas C, Sparchez M, Mocan LP, Sparchez Z. Pulmonary complications of portal hypertension: The overlooked decompensation. *World J Clin Cases* 2022; 10(17): 5531-5540
URL: https://www.wjgnet.com/2307-8960/full/v10/i17/5531.htm
DOI: https://dx.doi.org/10.12998/wjcc.v10.i17.5531

INTRODUCTION

The systemic nature of cirrhosis is becoming increasingly evident, expanding well beyond liver function and direct Newtonian complications of portal hypertension (PHT). Disease severity ranges from advanced chronic liver disease (ACLD) with mild portal hypertension, to decompensated disease and a late decompensation stage, with significant, progressive hemodynamic impairment[1]. Systemic involvement includes individual organ dysfunctions accompanying classical events (such as the hepato-renal syndrome in ascites or hepatic encephalopathy in variceal bleeding), longstanding slowly progressive entities (sarcopenia), or the ultimate multi organic storm: acute-on-chronic liver failure.

The kidneys, brain, heart, and lungs are closely intertwined with liver function and consecutive vascular alterations. However, while kidney dysfunction and hepatic encephalopathy represent common clinical issues that are regularly recognized, treated, and studied by hepatologists across the board, pulmonary involvement is typically overlooked and examined only in expert settings and liver transplantation units, despite their relatively high prevalence. Lung involvement in liver disease consists of three major entities: Hepato-pulmonary syndrome (HPS), porto-pulmonary hypertension (PoPH), and hepatic hydrothorax (HH). All three conditions have distinct pathophysiology, which is in close correlation to the adapted homeostasis of ACLD. The current minireview aims to shed light on the three complications in a structured manner, from definitions to summarizing the main research themes, and, ultimately to expand on one under-discussed clinical issue for each entity.

HEPATOPULMONARY SYNDROME - THE UNRECOGNIZED DECOMPENSATION

Definition and diagnostic criteria

Hepatopulmonary syndrome is defined by the presence of two key elements encountered in a patient with cirrhosis, portal hypertension, or congenital portosystemic shunts: abnormal arterial oxygenation and the presence of intrapulmonary vascular dilations (IPVDs) in the absence of underlying lung disease. The complete diagnostic criteria are depicted in Figure 1.

Context and a brief history

Lung involvement in cirrhosis has long been recognized, as cyanosis and finger clubbing were among the earliest clinical signs associated with longstanding liver disease, with reports dating back to the late 19th century by Austrian physician and researcher M. Fluckinger[2]. Yet, almost one hundred years had passed before the term "Hepatopulmonary Syndrome" was first coined by Timothy Kennedy and Ronald Knudson in 1977 in an illustrative case report and literature review[3]. In their paper, the authors attempt to crayon the basic clinical profile of "a syndrome characterized by hypoxemia aggravated by exercise, orthodeoxia, hypocapnia, and evidence of hyperdynamic circulation" in patients with cirrhosis and no underlying pulmonary disease. They suggest that HPS might be

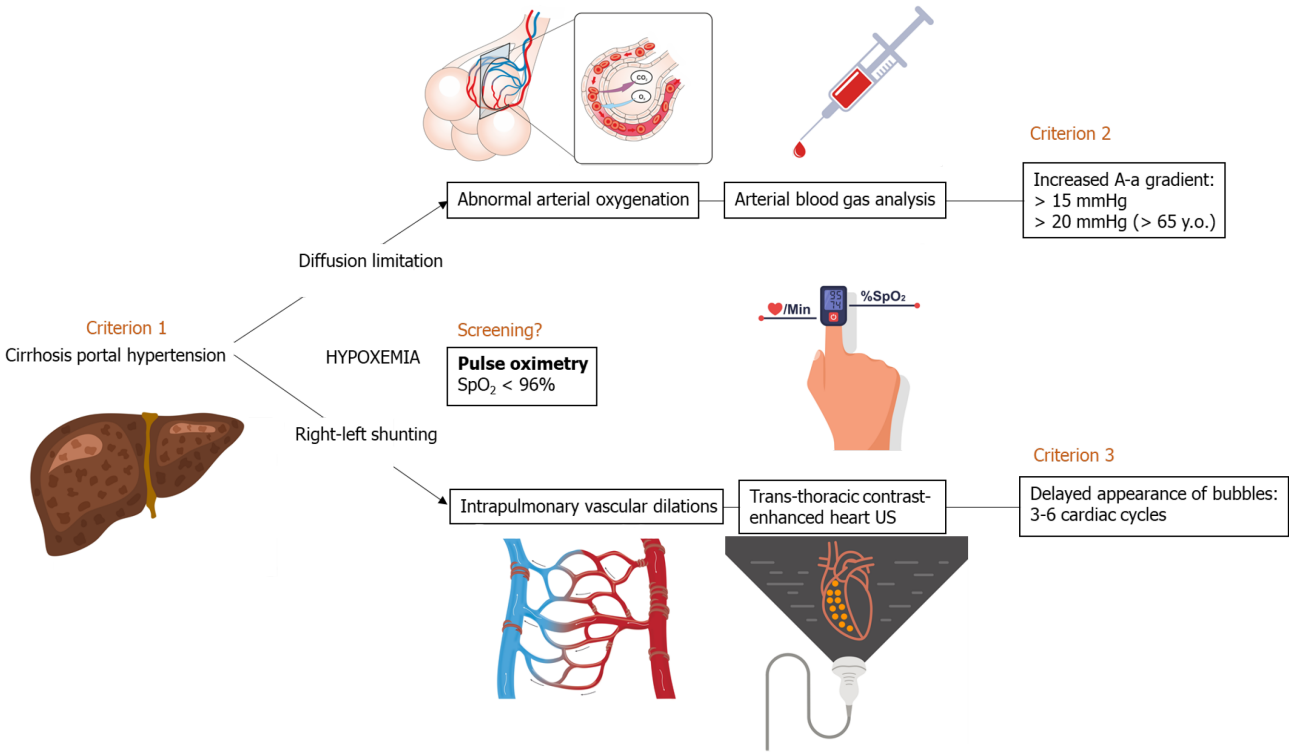

DOI: 10.12998/wjcc.v10.i17.5531 **Copyright** ©The Author(s) 2022.

Figure 1 Pathophysiology and diagnostic criteria of the hepatopulmonary syndrome. A-a: Alveolo-arterial; US: Ultrasonography.

determined by the "presence of a shunt or shunt-like mechanism consisting of low-resistance vascular communication within the lung," suggesting a common pathophysiological pathway with hepatorenal syndrome. In the subsequent years, along with the emergence of liver transplantation (LT) as a definite curative solution for patients with cirrhosis and the lack of therapeutic solutions for HPS, research has begun on the impact of HPS on pre-and post-LT outcomes. Initially regarded as an absolute contraindication, evidence has shown the resolution of HPS post-LT. In 1997, Michael J. Krowka and his Mayo Clinic team suggested that HPS might even be considered as a primary indication for LT[4], paving the way towards MELD exceptions in 2006[5], with favorable outcomes recently reported both in the United States[6] and Europe[7]. Since, most of the research has been split between basic science (typically on portal hypertension animal models) and LT, disregarding the largest proportion of patients with ACLD not on LT waitlist.

Current treatment strategies

According to the most recent guidelines on the diagnosis and management of HPS and PoPH, the therapeutic options for HPS are extremely limited[8]. Currently, there is no effective pharmacological therapy approved for HPS, although there have been some tentative attempts with methylene blue, somatostatin, pentoxifylline, propranolol, antibiotics, sorafenib, or garlic with modest or null effects[9]. Although the evidence is primarily anecdotal, there appears to be little or no benefit in alleviating portal pressure by transjugular intrahepatic portosystemic shunt (TIPS) placement[10,11]. Therefore, the only valid strategies are supportive oxygen therapy to maintain O_2 saturations above 88% and consideration for LT as the sole definite curative solution with excellent long-term results[7,8].

The (non)diagnostic challenge

HPS is theoretically encountered in up to one-third of the patients listed for LT, according to current estimates. The reported prevalence of HPS is highly heterogeneous, ranging between 5 and 32%, depending on the diagnostic criteria[12]. However, these estimates raise some concerns. All the figures are reported on LT candidates, theoretically skewing the estimates towards the more severe liver disease spectrum. On the other hand, it appears that the presence of HPS does not correlate with liver disease severity[13], which should support the presumption that HPS is also frequently encountered in patients not currently enlisted for LT. Yet, there seems to be little to no evidence of HPS in the literature beyond the realm of LT. Still, the main issue is not the inexact prevalence of HPS among patients with ACLD, but rather its implications of being under- or misdiagnosed. HPS appears to double the risk for waitlist mortality compared to non-HPS candidates[13], which might bear increasing relevance given the scarcity of therapeutic options.

In this light, one key question arises: Is HPS hiding in plain sight? The available evidence seems to point towards an affirmative response. A US-based study group has evaluated the rate of HPS diagnosis in a sizeable cirrhotic cohort, which included over 40000 patients from 28 medical centers, of which only two were LT centers. Moreover, using the available medical records, the authors have also analyzed whether the patients were correctly diagnosed, having both contrast-enhanced trans-thoracic heart ultrasonography with evidence of delayed shunting and abnormal arterial oxygenation (A-a gradient exceeding 15 mmHg). The results were in stark contrast with prior estimates. Of the 42749 unique patients, only 194 (0.45%) had a diagnosis of HPS. Furthermore, few met the current diagnostic criteria among these patients, as only 54% of them had evidence of delayed shunting, and 26% had documented abnormal oxygenation. Thus, only 41 patients ultimately fulfilled the criteria of HPS (22.5% of the patients initially diagnosed, and less than 0.1% of the entire cohort)[14]. The findings support the conclusion that HPS is grossly underdiagnosed outside LT centers, and, even when suspected, the diagnostic workup tends to be incomplete. This reflects a critical knowledge gap between transplantation hepatologists and their peers who work in non-LT centers and might provide sufficient ground to increase the visibility, education, and, not least, active screening for HPS.

Screening for HPS using pulse oximetry is highly convenient, as it takes less than 10 s to perform and is typically included within the regular clinical examination. However, screening for HPS appears to be less straightforward. In theory, the direct result of shunting is hypoxemia, which should be easily diagnosed using pulse oximetry and the current practice guidelines recommend a cut-off value of SpO_2 < 96% for further testing[8]. Yet, recent evidence suggests that the area under the receiving operating characteristic (AUROC) curve is only 0.59, which is sub-par for a screening method. Moreover, SpO_2 had a very low sensitivity (28%)[15]. Therefore, the path towards a more accurate HPS diagnosis using an efficient and easy-to-use screening method might face a serious roadblock, and its disentanglement should provide the basis for further research, as both contrast-enhanced heart ultrasonography and arterial blood gas analysis are less than ideal screening tools.

Summing up, our opinion is that beyond exact cut-offs and perfect diagnostic criteria, one must think of HPS each time when facing a patient with portal hypertension, as the silent clinical appearance of this entity is not detached from its proven prognostic significance.

PORTO-PULMONARY HYPERTENSION - THE UNTREATED DECOMPENSATION

Definition and diagnostic criteria

Porto-pulmonary hypertension is a pulmonary vascular complication defined by the presence of pulmonary arterial hypertension (PAH) as a direct consequence of PHT in a patient with no underlying pulmonary disease or left ventricular failure[9]. The gold standard for PoPH diagnosis is cardio-pulmonary hemodynamic assessment *via* right heart catheterization (RHC). The hemodynamic diagnostic triad for PoPH consists of increased mean pulmonary artery pressure (mPAP), due to increased pulmonary vascular resistance (PVR), in the setting of a normal pulmonary artery wedged pressure (PAWP)[8]. The hemodynamic criteria for POPH are depicted in Figure 2.

Given that RHC is an invasive diagnostic method, transthoracic Doppler heart ultrasonography is recommended as a less invasive surrogate method to provide the grounds for further testing[8]. However, its effectiveness as a screening method is disputable, being more accurate at ruling out rather than ruling in PAH[16].

Context and a brief history

The concept of PoPH gained traction in hepatology in the early 1990s, prior reports being few and far between[17]. In the largest available series of patients with PHT and RHC, the reported prevalence of PoPH was 2%[18], although higher figures were reported in patients evaluated for LT, even up to 8.5% [19]. Similar to HPS, clinical research in PoPH is closely tied to LT. In contrast to HPS, though, the relationship between PoPH and LT is multifaceted. On the one hand, an mPAP < 35 mmHg appears to pose no additional risk for LT outcomes and, along with patients with mPAP > 35 mmHg who respond adequately to PAH-specific treatment, can benefit from MELD exceptions. On the other hand, severe PoPH, with mPAP exceeding 45-50 mmHg, is associated with severe postoperative complications and thus, is regarded as an absolute contraindication to LT[8]. Therefore, LT patients with PoPH walk on a tightrope between favorable LT odds if PAH is mild or adequately controlled and extremely low LT probability if PAH is unstable or progressive.

Therapeutic options - the role of PAH-specific treatment

The outcome of patients with PoPH is highly dependent on the therapeutic approach: patients with PoPH and no medical treatment had a dismal 14% 5-year survival[20], while data from the US Registry to Evaluate Early and Long-term Pulmonary Arterial Hypertension Disease Management (REVEAL) has shown that patients with pharmacological-only treatment, who did not benefit from LT had a 40% 5-year survival[21]. The statistics vastly improve for patients who benefited from both medical therapy and liver transplantation, with 5-year survival rates of 81% according to recent data from the large-scale

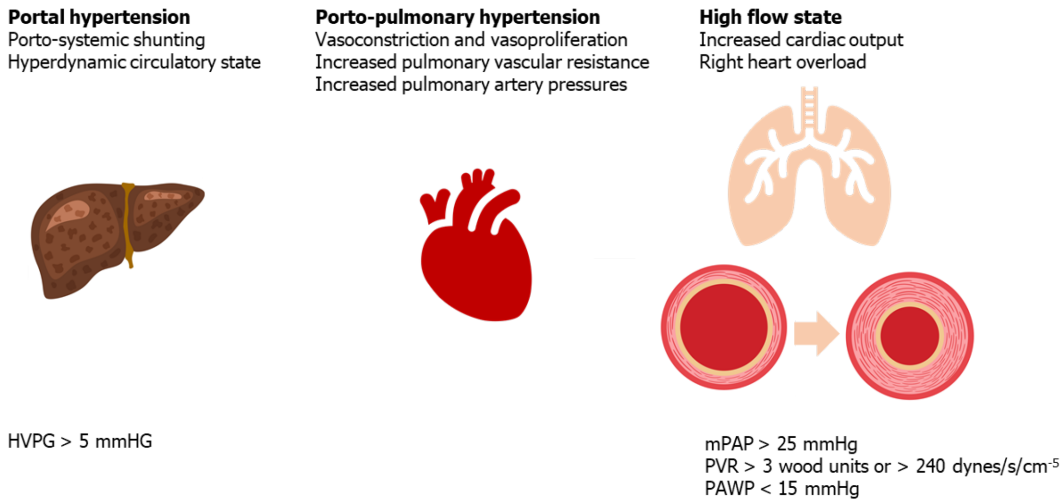

DOI: 10.12998/wjcc.v10.i17.5531 **Copyright** ©The Author(s) 2022.

Figure 2 Hemodynamic definition criteria for porto-pulmonary hypertension. HVPG: Hepatic venous pressure gradient; mPAP: Mean pulmonary artery pressure; PVR: Pulmonary vascular resistance; PAWP: Pulmonary artery wedged pressure.

French PoPH registry[22].

The staples of PoPH pharmacological treatment are phosphodiesterase 5-inhibitors (sildenafil), endothelin receptor antagonists (bosentan, ambrisentan, and macitentan), and prostanoids (epoprostenol, treprostinil, and inhaled iloprost). However, most of their therapeutic prowess is extrapolated from studies on PAH, with available data on PoPH barely exceeding a pooled 100 patients for each drug class, mostly comprised of small, non-controlled studies, typically including patients on LT waiting lists[9]. Yet when and how to treat patients with PoPH remains poorly defined and is largely up to the latitude of the LT center in which the patient is followed.

To this point, the PORTICO study is the only randomized controlled trial published on the pharmacological treatment of PoPH[23]. In this multicentric study, 85 patients were enrolled and randomly assigned to receive either macitentan or placebo. Following a 12-week treatment course, patients receiving macitentan had a 35% decline in PVR, a significant reduction in mPAP (-6.4 mmHg *vs* +0.4 mmHg in the placebo arm), and an improved cardiac index. The rate of adverse events was slightly higher in the active arm (84% *vs* 79% in the placebo arm), but event severity was low, with less than 10% of patients requiring treatment interruption. The second consistent batch of data comes from the French Pulmonary Hypertension Registry[22]. While the prospective design was not controlled and treatment selection was deliberate (non-random), the study's strength resides in the long-term follow-up (up to 10 years), a large number of patients included (n = 637), and the focus on mortality as a major outcome. Most patients were initially treated with oral monotherapy with phosphodiesterase 5-inhibitors (sildenafil or tadalafil) or endothelin receptor antagonists (bosentan, ambrisentan, or macitentan), while some were on double or, exceptionally (n = 5) triple therapy. Regardless of therapeutic regimens, all patients had significant improvements after 4.5 mo in PVR, mPAP, cardiac output, and functional capacity. In most variables, gains were augmented in dual therapy. Overall survival rates at 1, 3, and 5 years were significantly higher for patients who also benefited LT (92% *vs* 84%, 83% *vs* 69%, and 81% *vs* 51%, respectively).

The un/mistreated complication

The evidence appears to be relatively straightforward regarding the efficacy of PAH-specific therapy in PoPH. However, translation to clinical practice seems far from ideal despite proven benefits. Krowka *et al*. have analyzed the PoPH-related data from the REVEAL registry and found that even though patients with PoPH had a worse outcome than PAH etiologies, they were less likely to be on pharmacological therapy. This fact is even more striking given that patients with PoPH were in a worse cardiac functional class and, consequently, had a higher symptom burden[21]. Moreover, a recent prognostic analysis, REVEAL 2.0, designed to redefine the prior risk score, has attributed an additional risk point for patients with PoPH. This marks PoPH as the single most important predictor for high-risk PAH[24]. Another critical aspect is defining the optimal timing for PAH-therapy commencement. Analyzing recently published data from the Spanish REHAP registry, patients with PoPH appear to have a better hemodynamic profile than other patients with PAH, yet have a worse outcome, even when strictly considering PAH-related deaths. Therefore, an educated guess would suggest that the indication for pharmacological treatment commencement should start at a lower PVR or mPAP threshold. Furthermore, data from REHAP further reinforce the significant discrepancy in treatment between POPH and other cases of PAH, as patients with PoPH were both less likely to be treated and more likely

to be on monotherapy rather than combination therapy[25]. A potential explanation might reside in hepatologists' lack of awareness and familiarity with PAH and its corresponding therapeutic options outside large LT centers and a lack of pulmonologist referrals for patients with PHT to provide an adequate, personalized, multidisciplinary approach to care.

HEPATIC HYDROTHORAX - THE HIDDEN LATE DECOMPENSATION

Definition and diagnostic criteria

HH is an uncommon, understudied complication of cirrhosis and portal hypertension, occurring in 5%-15% of patients[26]. It is defined as a transudative pleural effusion, usually larger than 500 mL occurring in a cirrhotic patient in the absence of underlying cardiac, pulmonary, or pleural disease.

Context and a brief history

Morrow first coined the term hepatic hydrothorax in 1958 in an illustrative case report aimed to acknowledge the relationship between the occurrence of a pleural transudate and advanced liver disease[27]. In the subsequent decades, the relatively few papers published in the field have focused on epidemiological data. Yet, some notable attempts to characterize the pathophysiology using radioiodinated albumin and India ink in select cases were published[28]. The exact mechanism through which HH develops is not yet fully known. However, it seems to stem from an imbalance between hydrostatic and osmotic pressures. During inspiration, the negative intrathoracic pressure allows the fluid to pass from the abdomen to the pleural space through minor parietal defects of less than 1 cm, situated in the tendinous part of the diaphragm, more common on the right side[9]. Consequently, 85% of patients develop HH on the right side, while only 2% of cases are bilateral[29].

As opposed to patients with ascites, who can tolerate large volumes of fluid with only mild symptoms, HH can become symptomatic at a buildup of only 500 mL. Clinical manifestations may include cough, shortness of breath, pleuritic chest pain, hypoxemia, and respiratory failure. Most patients have progressive dyspnea and a reduced tolerance for physical effort.

The diagnosis is based on the presence of liver cirrhosis and lack of any primary pleural, cardiac, or pulmonary disease that could account for the buildup of fluid. HH can be complicated by spontaneous bacterial empyema (SBEM), the infection of a preexisting HH that can appear in approximately 15% of patients and should be evaluated through fluid analysis[29]. The work-up includes serum and fluid protein, albumin, lactate dehydrogenase levels, cell count, Gram stain, and culture. Other tests may be required depending on the clinical setting. Pharmacological treatment of HH closely resembles the treatment of ascites. Sodium restriction and diuretics, with a combination of furosemide 40 mg and spironolactone 100 mg daily, are the cornerstones for therapy. If there is a lack of response, the doses may be doubled stepwise every three to five days up to a maximum of 160 mg furosemide and 400 mg spironolactone daily. In uncomplicated HH, the polymorphonuclear cell (PMN) count is low (< 250 cells/mm^3). In contrast, in the setting of SBEM, the PMN count is elevated, with a diagnostic cutoff of > 250 cells/mm^3 if cultures are positive or > 500 cells/mm^3 if cultures are negative. The etiologic agents in most cases are Escherichia coli, Streptococcus, Enterococcus, Klebsiella, or Pseudomonas, which typically respond well to a 7 d to 10 d course of third-generation cephalosporins.

Treatment strategies - evidence beyond diuretics

Akin to patients with other decompensating events, there is a stepwise approach to treating HH beyond diuretics and salt restriction. However, in contrast to other, more established complications of cirrhosis, the quality of evidence is typically low, consisting of single-center, low-volume, and non-controlled data.

Therapeutic thoracocentesis is the next logical step in patients with severe symptoms that diuretics cannot control. However, it appears that the need for repeat thoracocentesis is associated with higher rates of acute-on-chronic liver failure and inpatient mortality compared to patients without HH, possibly related to a higher rate of nosocomial infections[30]. Patients who require thoracentesis every two to three weeks should be considered for alternative treatments. They are at increased risk of having adverse events such as pneumothorax, pleural empyema, purulent soft tissue infection of the chest wall, and air embolism. In addition, large-volume thoracentesis may increase microvascular permeability and cause re-expansion pulmonary edema. The complication rates appear to be significantly higher compared to patients with ascites and repeated paracenteses[31].

Chest tubes should not be placed for HH treatment, as this can result in massive protein and electrolyte depletion, infection, renal failure, and bleeding[32-34].

Local therapeutic options for patients who are refractory to the treatments mentioned above include pleurodesis and thoracoscopic surgery for diaphragmatic repair. However, it should be noted that although control of symptoms and resolution of effusion can be achieved in up to 75% of patients, recurrence rates are high, and a significantly increased prevalence of procedure-related morbidity and mortality hinders this procedure's routine application[35-37].

Another therapeutic option is TIPS placement. Several studies have reported a beneficial effect in patients with HH, with an overall response rate of up to 80%, an average 30 d mortality rate of 18%, and a 1-year survival rate of 52%[33,38-43]. However, TIPS should be avoided in patients older than 60 years, as this seems to correlate inversely with survival rates[38]. Of note, most of the data is relatively old and precedes the covered stent era, which drastically improved shunt patency rates. However, considering the data, it appears sensible that HH is a viable indication for TIPS, especially in patients with concurrent decompensating events, such as ascites or a single episode of variceal bleeding.

Liver transplantation is an excellent definitive therapeutic option for cirrhotic patients with HH and end-stage liver disease. The need for thoracenteses decreases post-transplantation, and the presence of preoperative HH does not seem to have a significant negative influence on postoperative outcomes, with similar long-term survival as in other indications for LT[44,45].

Is hepatic hydrothorax an indicator for late decompensation?

Hepatic hydrothorax is more frequent in patients with higher Child-Pugh scores, potentially serving as a marker of decreased liver function (8%, 26%, and 65% in Child-Pugh class A, B, and C, respectively)[46]. HH seems to be more frequent in patients with cirrhosis and ascites with a recurrent need for paracentesis, higher bilirubin, diabetes, and lack of NSBB therapy[47]. While the MELD score doesn't seem to predict the risk of HH more accurately than the Child-Pugh score, one might consider HH a prognostic indicator itself, akin to other decompensation events such as ascites or variceal bleeding. As previously shown in a study by our group, patients with HH have a significantly higher long-term mortality rate when compared to patients without HH. Their underlying liver disease is more advanced, based on markers of liver function, decompensation, and prognostic scores. Yet, even after matching patients for age and liver function, HH appears to be an independent mortality predictor[48]. HH tends to develop later in the disease course and increases mortality up to four times, especially in patients with MELD scores higher than 16[47,48]. These data are further reinforced by a study that included 3487 patients. Pleural effusion was associated with 30 d, 90 d, 1-year, and 3-year mortalities of 20.1%, 40.2%, 59.1%, and 75.9%, respectively[49]. Considering this, HH might be viewed as an independent risk factor for disease progression. Therefore, it should be taken into account when selecting patients for tertiary care referral or more expensive and less available procedures, such as TIPS or LT, especially in limited-resource settings. Regarding LT, evidence suggests that it can significantly improve survival rates and should be considered whenever possible. Sersté demonstrated a similar time frame of HH resolution and no significant difference in duration of postoperative mechanical ventilation, providing sufficient ground for a similar post LT survival, compared to other indications[45]. Yet, given that patients with HH are typically in a worse shape compared to non-HH patients with otherwise similar characteristics, the question should be raised whether recurrent HH despite optimal therapy could be considered on an individual basis for a non-standard MELD exception[50], similar to HPS and PoPH.

CONCLUSION

All evidence suggests that the pulmonary complications of cirrhosis and portal hypertension are associated with a worse outcome. These conditions might be hiding in the clinical background throughout the ACLD disease course, sometimes requiring an active diagnostic process. Their pathophysiology and therapeutic options often reside outside the interests of most hepatologists, as it appears that the lungs and the liver are separated by a barrier thicker than the diaphragm. Consequently, research and clinical practice barriers should be faced by paying closer attention to these entities in study protocols and day-to d care, aiming to improve diagnosis, therapy, and, ultimately, patient care.

FOOTNOTES

Author contributions: Craciun R, Mocan T, Nemes A, and Tefas C performed the majority of the writing; Mocan LP and Sparchez M prepared the figures; Craciun R and Nemes A performed data acquisition and writing; Sparchez Z and Procopet B provided the input in writing the paper; Craciun R, Sparchez Z, and Procopet B designed the outline and coordinated the writing of the paper.

Conflict-of-interest statement: The authors declare no conflict of interest regarding the contents of the current manuscript.

Open-Access: This article is an open-access article that was selected by an in-house editor and fully peer-reviewed by external reviewers. It is distributed in accordance with the Creative Commons Attribution NonCommercial (CC BY-NC 4.0) license, which permits others to distribute, remix, adapt, build upon this work non-commercially, and license their derivative works on different terms, provided the original work is properly cited and the use is non-commercial. See: https://creativecommons.org/Licenses/by-nc/4.0/

Country/Territory of origin: Romania

ORCID number: Rares Craciun 0000-0002-5872-8630; Tudor Mocan 0000-0001-7785-6403; Bogdan Procopet 0000-0001-8118-1760; Andrada Nemes 0000-0002-0600-6097; Cristian Tefas 0000-0002-8263-7923; Mihaela Sparchez 0000-0001-8620-9160; Lavinia-Patricia Mocan 0000-0003-4957-4390; Zeno Sparchez 0000-0002-3813-1677.

S-Editor: Wang LL
L-Editor: A
P-Editor: Wang LL

REFERENCES

1 **Amico GD**, Morabito A, Amico MD, Pasta L. New concepts on the clinical course and stratification of compensated and decompensated cirrhosis. *Hepatol Int* 2018; **12**: 34-43 [PMID: 28681347 DOI: 10.1007/s12072-017-9808-z]
2 **Fluckinger M**. Vorkommen von trommelschlagelformigen finger- endphalangen ohne chronische veriinderungen an den lungen oder am herzen. *Wiener Medizinische Wochenschrift* 1884; 49: 1457-1458
3 **Kennedy TC**, Knudson RJ. Exercise-aggravated hypoxemia and orthodeoxia in cirrhosis. *Chest* 1977; **72**: 305-309 [PMID: 891282 DOI: 10.1378/chest.72.3.305]
4 **Krowka MJ**, Porayko MK, Plevak DJ, Pappas SC, Steers JL, Krom RA, Wiesner RH. Hepatopulmonary syndrome with progressive hypoxemia as an indication for liver transplantation: case reports and literature review. *Mayo Clin Proc* 1997; **72**: 44-53 [PMID: 9005286 DOI: 10.4065/72.1.44]
5 **Fallon MB**, Mulligan DC, Gish RG, Krowka MJ. Model for end-stage liver disease (MELD) exception for hepatopulmonary syndrome. *Liver Transpl* 2006; **12**: S105-S107 [PMID: 17123282 DOI: 10.1002/Lt.20971]
6 **Goldberg DS**, Krok K, Batra S, Trotter JF, Kawut SM, Fallon MB. Impact of the hepatopulmonary syndrome MELD exception policy on outcomes of patients after liver transplantation: an analysis of the UNOS database. *Gastroenterology* 2014; **146**: 1256-65.e1 [PMID: 24412528 DOI: 10.1053/j.gastro.2014.01.005]
7 **Raevens S**, Rogiers X, Geerts A, Verhelst X, Samuel U, van Rosmalen M, Berlakovich G, Delwaide J, Detry O, Lehner F, Mittler J, Nadalin S, Nevens F, Pirenne J, Saner F, Schneeberger S, Stippel D, Turk JM, Zoltan M, Troisi RI, Van Vlierberghe H, Colle I. Outcome of liver transplantation for hepatopulmonary syndrome: a Eurotransplant experience. *Eur Respir J* 2019; **53** [PMID: 30487203 DOI: 10.1183/13993003.01096-2018]
8 **Krowka MJ**, Fallon MB, Kawut SM, Fuhrmann V, Heimbach JK, Ramsay MAE, Sitbon O, Sokol RJ. International liver transplant society practice guidelines: Diagnosis and management of hepatopulmonary syndrome and portopulmonary hypertension. *Transplantation* 2016; **100**: 1440-1452 [PMID: 27326810 DOI: 10.1097/tp.0000000000001229]
9 **Cartin-Ceba R**, Krowka MJ. Pulmonary Complications of Portal Hypertension. *Clin Liver Dis* 2019; **23**: 683-711 [PMID: 31563218 DOI: 10.1016/j.cld.2019.06.003]
10 **Riegler JL**, Lang KA, Johnson SP, Westerman JH. Transjugular intrahepatic portosystemic shunt improves oxygenation in hepatopulmonary syndrome. *Gastroenterology* 1995; **109**: 978-983 [PMID: 7657128 DOI: 10.1016/0016-5085(95)90409-3]
11 **Corley DA**, Scharshmidt B, Bass N, Sonnenberg K, Gold W, Riegler JL, Lang KA. Lack of efficacy of TIPS for hepatopulmonary syndrome. *Gastroenterology* 1997; **113**: 728-30 [PMID: 9247498 DOI: 10.1053/gast.1997.v113.agast971130728]
12 **Rodríguez-Roisin R**, Krowka MJ. Hepatopulmonary syndrome--a liver-induced lung vascular disorder. *N Engl J Med* 2008; **358**: 2378-2387 [PMID: 18509123 DOI: 10.1056/NEJMra0707185]
13 **Fallon MB**, Krowka MJ, Brown RS, Trotter JF, Zacks S, Roberts KE, Shah VH, Kaplowitz N, Forman L, Wille K, Kawut SM; Pulmonary Vascular Complications of Liver Disease Study Group. Impact of hepatopulmonary syndrome on quality of life and survival in liver transplant candidates. *Gastroenterology* 2008; **135**: 1168-1175 [PMID: 18644373 DOI: 10.1053/j.gastro.2008.06.038]
14 **Bommena S**, Gerkin RD, Agarwal S, Raevens S, Glassberg MK, Fallon MB. Diagnosis of Hepatopulmonary Syndrome in a Large Integrated Health System. *Clin Gastroenterol Hepatol* 2021; **19**: 2370-8 [PMID: 33007510 DOI: 10.1016/j.cgh.2020.09.050]
15 **Forde KA**, Fallon MB, Krowka MJ, Sprys M, Goldberg DS, Krok KL, Patel M, Lin G, Oh JK, Mottram CD, Scanlon PD, Kawut SM. Pulse Oximetry is Insensitive for Detection of Hepatopulmonary Syndrome in Patients evaluated for Liver Transplantation. *Hepatology* 2019; **69**: 270-81 [PMID: 30070715 DOI: 10.1002/hep.30139]
16 **Raevens S**, Colle I, Reyntjens K, Geerts A, Berrevoet F, Rogiers X, Troisi RI, Van Vlierberghe H, De Pauw M. Echocardiography for the detection of portopulmonary hypertension in liver transplant candidates: an analysis of cutoff values. *Liver Transpl* 2013; **19**: 602-610 [PMID: 23584902 DOI: 10.1002/Lt.23649]
17 **Krowka MJ**. Hepatopulmonary Syndrome and Portopulmonary Hypertension: The Pulmonary Vascular Enigmas of Liver Disease. *Clin Liver Dis (Hoboken)* 2020; **15**: S13-S24 [PMID: 32140210 DOI: 10.1002/cld.846]
18 **Hadengue A**, Benhayoun MK, Lebrec D, Benhamou JP. Pulmonary hypertension complicating portal hypertension: prevalence and relation to splanchnic hemodynamics. *Gastroenterology* 1991; **100**: 520-528 [PMID: 1985048 DOI: 10.1016/0016-5085(91)90225-a]
19 **Ramsay MAE**, Simpson BR, Nguyen AT, Ramsay KJ, East C, Klintmalm GB. Severe pulmonary hypertension in liver transplant candidates. *Liver Transplant Surg* 1997; **3**: 494-500 [PMID: 9346791 DOI: 10.1002/Lt.500030503]
20 **Swanson KL**, Wiesner RH, Krowka MJ. Natural history of hepatopulmonary syndrome: Impact of liver transplantation. *Hepatology* 2005; **41**: 1122-1129 [PMID: 15828054 DOI: 10.1002/hep.20658]
21 **Krowka MJ**, Miller DP, Barst RJ, Taichman D, Dweik RA, Badesch DB, McGoon MD. Portopulmonary hypertension: a

report from the US-based REVEAL Registry. *Chest* 2012; **141**: 906-915 [PMID: 21778257 DOI: 10.1378/chest.11-0160]
22 **Savale L**, Guimas M, Ebstein N, Fertin M, Jevnikar M, Renard S, Horeau-Langlard D, Tromeur C, Chabanne C, Prevot G, Chaouat A, Moceri P, Artaud-Macari É, Degano B, Tresorier R, Boissin C, Bouvaist H, Simon AC, Riou M, Favrolt N, Palat S, Bourlier D, Magro P, Cottin V, Bergot E, Lamblin N, Jaïs X, Coilly A, Durand F, Francoz C, Conti F, Hervé P, Simonneau G, Montani D, Duclos-Vallée JC, Samuel D, Humbert M, De Groote P, Sitbon O. Portopulmonary hypertension in the current era of pulmonary hypertension management. *J Hepatol* 2020; **73**: 130-139 [PMID: 32145258 DOI: 10.1016/j.jhep.2020.02.021]
23 **Sitbon O**, Bosch J, Cottreel E, Csonka D, de Groote P, Hoeper MM, Kim NH, Martin N, Savale L, Krowka M. Macitentan for the treatment of portopulmonary hypertension (PORTICO): a multicentre, randomised, double-blind, placebo-controlled, phase 4 trial. *Lancet Respir Med* 2019; **7**: 594-604 [PMID: 31178422 DOI: 10.1016/S2213-2600(19)30091-8]
24 **Benza RL**, Gomberg-Maitland M, Elliott CG, Farber HW, Foreman AJ, Frost AE, McGoon MD, Pasta DJ, Selej M, Burger CD, Frantz RP. Predicting Survival in Patients With Pulmonary Arterial Hypertension: The REVEAL Risk Score Calculator 2.0 and Comparison With ESC/ERS-Based Risk Assessment Strategies. *Chest* 2019; **156**: 323-337 [PMID: 30772387 DOI: 10.1016/j.chest.2019.02.004]
25 **Lazaro Salvador M**, Quezada Loaiza CA, Rodríguez Padial L, Barberá JA, López-Meseguer M, López-Reyes R, Sala-Llinas E, Alcolea S, Blanco I, Escribano-Subías P; REHAP Investigators. Portopulmonary hypertension: prognosis and management in the current treatment era - results from the REHAP registry. *Intern Med J* 2021; **51**: 355-365 [PMID: 31943676 DOI: 10.1111/imj.14751]
26 **Banini BA**, Alwatari Y, Stovall M, Ogden N, Gershman E, Shah RD, Strife BJ, Shojaee S, Sterling RK. Multidisciplinary Management of Hepatic Hydrothorax in 2020: An Evidence-Based Review and Guidance. *Hepatology* 2020; **72**: 1851-1863 [PMID: 32585037 DOI: 10.1002/hep.31434]
27 **Morrow CS**, Kantor M, Armen RN. Hepatic hydrothorax. *Ann Intern Med* 1958; **49**: 193-203 [PMID: 13545745 DOI: 10.7326/0003-4819-49-1-193]
28 **Johnston RF**, Loo RV. Hepatic Hydrothorax: Studies to determine the source of the fluid and report on thirteen cases. *Ann Intern Med* 1964; **61**: 385-401 [PMID: 14218925 DOI: 10.7326/0003-4819-61-3-385]
29 **Lv Y**, Han G, Fan D. Hepatic Hydrothorax. *Ann Hepatol* 2018; **17**: 33-46 [PMID: 29311408 DOI: 10.5604/01.3001.0010.7533]
30 **O'Leary JG**, Rajender Reddy K, Tandon P, Biggins SW, Wong F, Kamath PS, Garcia-Tsao G, Maliakkal B, Lai JC, Fallon M, Vargas HE, Thuluvath P, Subramanian R, Thacker LR, Bajaj JS. Increased Risk of ACLF and Inpatient Mortality in Hospitalized Patients with Cirrhosis and Hepatic Hydrothorax. *Dig Dis Sci* 2021; **66**: 3612-3618 [PMID: 33185787 DOI: 10.1007/s10620-020-06677-6]
31 **Garbuzenko DV**, Arefyev NO. Hepatic hydrothorax: An update and review of the literature. *World J Hepatol* 2017; **9**: 1197-1204 [PMID: 29152039 DOI: 10.4254/wjh.v9.i31.1197]
32 **Gurung P**, Goldblatt M, Huggins JT, Doelken P, Nietert PJ, Sahn SA. Pleural fluid analysis and radiographic, sonographic, and echocardiographic characteristics of hepatic hydrothorax. *Chest* 2011; **140**: 448-453 [PMID: 21273292 DOI: 10.1378/chest.10-2134]
33 **Singh A**, Bajwa A, Shujaat A. Evidence-based review of the management of hepatic hydrothorax. *Respiration* 2013; **86**: 155-173 [PMID: 23571767 DOI: 10.1159/000346996]
34 **Covington MF**, Choudhary G, Avery RJ, Kuo PH. Pitfalls in the Performance and Interpretation of Scintigraphic Imaging for Pleuroperitoneal Shunt. *Clin Nucl Med* 2016; **41**: 858-861 [PMID: 27488430 DOI: 10.1097/RLU.0000000000001326]
35 **Helmy N**, Akl Y, Kaddah S, El Hafiz HA, El Makhzangy H. A case series: Egyptian experience in using chemical pleurodesis as an alternative management in refractory hepatic hydrothorax. *Arch Med Sci* 2010; 6: 336-42 [PMID: 2231768 DOI: 10.5114/aoms.2010.14252]
36 **Ferrante D**, Arguedas MR, Cerfolio RJ, Collins BG, van Leeuwen DJ. Video-assisted thoracoscopic surgery with talc pleurodesis in the management of symptomatic hepatic hydrothorax. *Am J Gastroenterol* 2002; **97**: 3172-3175 [PMID: 12492206 DOI: 10.1111/j.1572-0241.2002.07126.x]
37 **Lee WJ**, Kim HJ, Park JH, Park D Il, Cho YK, Sohn C Il, Jeon WK, Kim BI. Chemical pleurodesis for the management of refractory hepatic hydrothorax in patients with decompensated liver cirrhosis. *Korean J Hepatol* 2011; **17**: 292-298 [DOI: 10.3350/kjhep.2011.17.4.292]
38 **Siegerstetter V**, Deibert P, Ochs A, Olschewski M, Blum HE, Ro M. Treatment of refractory hepatic hydrothorax with transjugular intrahepatic portosystemic shunt: long-term results in 40 patients. *Eur J Gastroenterol Hepatol* 2001; 13: 529-34 [PMID: 11396532 DOI: 10.1097/00042737-200105000-00011]
39 **Gordon FD**, Anastopoulos HT, Crenshaw W, Gilchrist B, McEniff N, Falchuk KR, LoCicero J 3rd, Lewis WD, Jenkins RL, Trey C. The successful treatment of symptomatic, refractory hepatic hydrothorax with transjugular intrahepatic portosystemic shunt. *Hepatology* 1997; **25**: 1366-1369 [PMID: 9185754 DOI: 10.1002/hep.510250611]
40 **Jeffries MA**, Kazanjian S, Wilson M, Punch J, Fontana RJ. Transjugular intrahepatic portosystemic shunts and liver transplantation in patients with refractory hepatic hydrothorax. *Liver Transpl Surg* 1998; **4**: 416-423 [PMID: 9724480 DOI: 10.1002/Lt.500040506]
41 **Chalasani N**, Clark WS, Martin LG, Kamean J, Khan MA, Patel NH, Boyer TD. Determinants of mortality in patients with advanced cirrhosis after transjugular intrahepatic portosystemic shunting. *Gastroenterology* 2000; **118**: 138-144 [PMID: 10611162 DOI: 10.1016/s0016-5085(00)70422-7]
42 **Dhanasekaran R**, West JK, Gonzales PC, Subramanian R, Parekh S, Spivey JR, Martin LG, Kim HS. Transjugular intrahepatic portosystemic shunt for symptomatic refractory hepatic hydrothorax in patients with cirrhosis. *Am J Gastroenterol* 2010; **105**: 635-641 [PMID: 19904245 DOI: 10.1038/ajg.2009.634]
43 **Brooke Spencer E**, Cohen DT, Darcy MD. Safety and efficacy of transjugular intrahepatic portosystemic shunt creation for the treatment of hepatic hydrothorax. *J Vasc Interv Radiol* 2002; 13: 385-90 [PMID: 11932369 DOI: 10.1016/s1051-0443(07)61741-2]
44 **Xiol X**, Tremosa G, Castellote J, Gornals J, Lama C, Lopez C, Figueras J. Liver transplantation in patients with hepatic hydrothorax. *Transpl Int* 2005; **18**: 672-675 [PMID: 15910292 DOI: 10.1111/j.1432-2277.2005.00116.x]

45 **Sersté T**, Moreno C, Francoz C, Razek WA, Paugham C, Belghitti J, Valla D, Moreau R, Durand F. The impact of preoperative hepatic hydrothorax on the outcome of adult liver transplantation. *Eur J Gastroenterol Hepatol* 2010; **22**: 207-212 [PMID: 19779352 DOI: 10.1097/MEG.0b013e3283311140]

46 **Abbasi A**, Bhutto AR, Alam MT, Aurangzaib M, Masroor M. Frequency of Hepatic Hydrothorax and its Association with Child Pugh Class in Liver Cirrhosis Patients. *J Coll Physicians Surg* 2016; **26**: 566-569 [PMID: 27504545 DOI: 10.37575/b/med/0038]

47 **Deleuran T**, Watson H, Vilstrup H, Jepsen P. Risk Factors for Hepatic Hydrothorax in Cirrhosis Patients with Ascites - A Clinical Cohort Study. *Dig Dis Sci* 2021 [PMID: 34191185 DOI: 10.1007/s10620-021-07134-8]

48 **Matei D**, Craciun R, Crisan D, Procopet B, Mocan T, Pasca S, Zaharie R, Popovici B, Sparchez Z. Hepatic Hydrothorax-An Independent Decompensating Event Associated with Long-Term Mortality in Patients with Cirrhosis. *J Clin Med* 2021; **10** [PMID: 34441984 DOI: 10.3390/jcm10163688]

49 **Hung TH**, Tseng CW, Tsai CC, Tseng KC, Hsieh YH. The long-term outcomes of cirrhotic patients with pleural effusion. *Saudi J Gastroenterol* 2018; **24**: 46-51 [PMID: 29451184 DOI: 10.4103/sjg.SJG_336_17]

50 **Raevens S**, Boret M, De Pauw M, Fallon MB, Van Vlierberghe H. Pulmonary Abnormalities in Liver Disease: Relevance to Transplantation and Outcome. *Hepatology* 2021; **74**: 1674-1686 [PMID: 33636019 DOI: 10.1002/hep.31770]

World Journal of Clinical Cases

Submit a Manuscript: https://www.f6publishing.com

World J Clin Cases 2022 June 16; 10(17): 5541-5550

DOI: 10.12998/wjcc.v10.i17.5541

ISSN 2307-8960 (online)

MINIREVIEWS

Ethical review of off-label drugs during the COVID-19 pandemic

Qiu-Yu Li, Ye Lv, Zhuo-Yu An, Ni-Ni Dai, Xue Hong, Yu Zhang, Li-Jun Liang

Specialty type: Medical ethics

Provenance and peer review: Unsolicited article; Externally peer reviewed.

Peer-review model: Single blind

Peer-review report's scientific quality classification

Grade A (Excellent): 0
Grade B (Very good): B, B
Grade C (Good): 0
Grade D (Fair): 0
Grade E (Poor): 0

P-Reviewer: Kumar P, United States; Moretti A, Italy

Received: February 7, 2022
Peer-review started: February 7, 2022
First decision: March 22, 2022
Revised: March 26, 2022
Accepted: April 9, 2022
Article in press: April 9, 2022
Published online: June 16, 2022

Qiu-Yu Li, Ni-Ni Dai, Department of Pulmonary and Critical Care Medicine, Peking University Third Hospital, Beijing 100191, China

Ye Lv, Advanced Institute for Medical Sciences, Dalian Medical University, Dalian 116044, Liaoning Province, China

Zhuo-Yu An, Peking University Institute of Hematology, Peking University People's Hospital, Beijing 100191, China

Xue Hong, Yu Zhang, Li-Jun Liang, Department of Ethics Office, Peking University Third Hospital, Beijing 100191, China

Corresponding author: Qiu-Yu Li, MD, Doctor, Department of Pulmonary and Critical Care Medicine, Peking University Third Hospital, No. 49 Huayuan North Road, Haidian District, Beijing 100191, China. liqiuyu00@bjmu.edu.cn

Abstract

High-quality scientific research is very important in attempting to effectively control the coronavirus disease 2019 (COVID-19) pandemic and ensure people's health and safety. Chloroquine (CQ) and hydroxychloroquine (HCQ) have received much attention. This article comprehensively investigates the ethical review of off-label CQ and HCQ research during the COVID-19 pandemic with regard to strictly abiding by review standards, improving review efficiency, ensuring the rights and interests of subjects and that ethics committees conduct independent reviews, and achieving full ethics supervision of research conducted during an emergency. Research must be both rigorous and prudent to ensure the best outcome, with the maximization of benefits as the core principle. Standardization of the application, implementation and ethical review processes are needed to prevent unnecessary risk.

Key Words: COVID-19; Off-label; Chloroquine; Hydroxychloroquine

©The Author(s) 2022. Published by Baishideng Publishing Group Inc. All rights reserved.

Core Tip: High-quality scientific research is very important in the attempt to effectively control the coronavirus disease 2019 epidemic and ensure people's life health and safety. Chloroquine and hydroxychloroquine have received much attention.

Citation: Li QY, Lv Y, An ZY, Dai NN, Hong X, Zhang Y, Liang LJ. Ethical review of off-label drugs during the COVID-19 pandemic. *World J Clin Cases* 2022; 10(17): 5541-5550
URL: https://www.wjgnet.com/2307-8960/full/v10/i17/5541.htm
DOI: https://dx.doi.org/10.12998/wjcc.v10.i17.5541

INTRODUCTION

High-quality scientific research is very important in attempting to effectively control the coronavirus disease 2019 (COVID-19) pandemic and ensure people's health and safety. Chloroquine (CQ) and hydroxychloroquine (HCQ) have received much attention. This article comprehensively investigates the ethical review of off-label CQ and HCQ research during the COVID-19 pandemic with regard to strictly abiding by review standards, improving review efficiency, ensuring the rights and interests of subjects and that ethics committees conduct independent reviews, and achieving full ethics supervision of research conducted during an emergency.

OFF-LABEL DRUG USE FOR COVID-19

Off-label studies investigate the use of drugs for purposes other than those that are already approved. These studies involve indications, treated populations, usages and dosages that are not included in the label approved by the drug regulatory authority[1]. Although the efficacy of the off-label use of a medication is unconfirmed, such uses may serve as life-saving treatments for patients with rare diseases or new infectious diseases for which there is no cure. In addition, due to the complexity of revising drug labels, such revision usually lags behind clinical practice; therefore, a drug label does not always reflect the cutting-edge use of the medicine in question[2]. At the same time, drug labels also have certain limitations, such as the specified dose. Randomized controlled trials (RCTs) and the consequent label content do not always reflect clinical practice. Off-label medication use is a form of medical exploration that largely meets some clinical needs. At present, foreign academic circles refer to this kind of expanded research as "drug reuse or relocation". There have been a large number of successful cases of drug reuse or relocation based on knowledge of the mechanisms of action of existing drugs. However, the use of medication beyond the scope of the instructions cannot be regarded as safe simply because the on-label use was deemed safe. The investigation of off-label medication use must be rigorous and prudent, with the maximization of patients' interests as the core principle. It is important to standardize the application, implementation and ethical review processes to prevent causing problems. Given that SARS-CoV-2 is a new pathogen, there is not yet a specific drug that can be used to treat COVID-19. The drugs recommended in diagnosis and treatment plans include interferon, lopinavir/ritonavir, ribavirin, and phosphoric acid. The treatment of COVID-19 with CQ and arbidol is considered off-label use; therefore, clinical trials need to be carried out to provide clinical evidence of their efficacy. Research has focused on the use of HCQ/CQ.

POTENTIAL EFFECTIVENESS OF HCQ/CQ FOR COVID-19

On February 4, 2020, an article published in "Cell Research" mentioned that remdesivir and CQ showed good inhibitory effects on SARS-CoV-2 in vitro, and the half maximal effective concentration (EC50) of remdesivir was 0.77 μmol/L, while that of CQ was 1.13 μmmol/L[3]. Although the effects of CQ are slightly weaker than those of remdesivir based on this index, its advantages are still obvious because it is a well-known drug that has been used for decades. Subsequently, HCQ, which is a CQ derivative, has also attracted attention. On March 20, 2020, French scientist Didier Raoult published an article suggesting that the combination of HCQ and azithromycin is effective for the treatment of COVID-19. The open clinical trial included a total of 20 patients. The article pointed out that the use of HCQ was related to a decrease in or the disappearance of the viral load, and the addition of azithromycin enhanced the therapeutic effect[4]. Although the sample of this trial was small and it was not a randomized double-blind trial, this result still stimulated research on HCQ. Although there is no systematic clinical evidence that HCQ and CQ are effective, it is undoubtedly very tempting to believe that established drugs have good treatment effects. On March 28, 2020, the United States FDA authorized the use of CQ and HCQ for the treatment of COVID-19. On April 3, 2020, the COVID-19 international working group comprising 80 clinical experts from 20 countries jointly issued interim guidance for the treatment of COVID-19, and HCQ/CQ was the only drug recommended by the group. On June 1, 2020, ClinicalTrials.gov had 203 registered COVID-19 trials related to HCQ, 60 of which focused on prevention. This article pertains to the currently ongoing clinical trials for CQ and HCQ (Table 1).

Table 1 Clinical trials of chloroquine and hydroxychloroquine use for coronavirus disease 2019

NCT Number	Population's age	Intervention	Control	Outcome measures
NCT04362332	18-110 yr	CQ or HCQ	Standard supportive care	Composite endpoint with disease progression defined as a NEWS2 score within 14 d or resulting in admission to the Intensive/Medium Care unit or resulting in death within 14 d | Side effects
NCT04303507	16 yr and older	CQ or HCQ	Placebo	Number of symptomatic COVID-19 infections | COVID-19 symptom severity | Number of asymptomatic cases of COVID-19 | Number of symptomatic acute respiratory illnesses | Severity of symptomatic acute respiratory illnesses
NCT04360759	18 yr and older	CQ or HCQ	Placebo	Event-free survival at 28 d postrandomization between the experimental group and standard of care group | Incidence of serious adverse events | Incidence of adverse events of special interest related to the investigational product at time of hospitalization | Premature discontinuation of treatment | Time from treatment initiation to death, ARDS (PF/SF ratio < 300), or mechanical ventilation | Proportion with moderate and severe ARDS | Duration of hospitalization and ICU stay for survivors | Incidence of COVID-19 in household contacts
NCT04420247	18 yr and older	CQ or HCQ	Standard care	World Health Organization (WHO) 9-levels scale (from 0-8) | WHO 9-levels scale (from 0-8) | Mortality | Ventilation-free days | Duration of mechanical ventilation | National Early Warning Score (NEWS) | ICU Length of Stay | Hospital Length of Stay | Acute Kidney Disease incidence | Percentage of patients needing dialysis | Mean C Reactive Protein Levels | Mean Leucocytes Levels | Mean Lymphocyte Levels
NCT04351191	20-50 yr	HCQ Sulfate Regular dose, HCQ Sulfate Loading Dose or CQ	Placebo	RT–PCR results | Progression of symptoms | Mortality
NCT04447534	18 yr older	CQ	Zinc	Number of patients with negative PCR
NCT04346667	20-50 yr	HCQ Sulfate Regular dose, HCQ Sulfate Loading Dose or CQ	Placebo	RT–PCR tests | Progression of symptoms | Development of Symptoms | Adverse events
NCT04341727	18 yr older	HCQ Sulfate or Azithromycin	CQ Sulfate	Hours to recovery | Time to fever resolution
NCT04346329	18 yr older	HCQ	Placebo	Adverse effects | Immune score | COVID-19 prevention | Clinical response
NCT04371406	18-75 yr	HCQ and Azithromycin	Dietary Supplement: Azinc	Rate of patients with the occurrence of an unfavorable outcome between randomization and day 14 | Primary outcome of ancillary virological study: The evolution of viral load between day 0 and day 14 | The all-cause mortality rate at day 14 | The all-cause mortality rate at day 28 | Rate of patients with the occurrence of an unfavorable outcome between randomization and day 28 | The rate of use of mechanical ventilation at day 14 | The rate of use of mechanical ventilation at day 28 | The Intensive Care Unit admission rate at day 14 | The Intensive Care Unit admission rate at day 28 | Number of days of hospitalization for any cause between day 0 and day 14 | Number of days of hospitalization for any cause between day 0 and day 28 | The time to resolution of all COVID symptoms at day 14 | The time to resolution of all COVID symptoms at day 28 | The rate of use of oxygen therapy at day 14 | The rate of use of oxygen therapy at day 28 | The rate of use of secondary antibiotic therapy (after day 2) at day 14 | The rate of use of secondary antibiotic therapy (after day 2) at day 28 | Clinical status at day 14 | Clinical status at day 28 | Number of serious adverse events at day 14 | Number of serious adverse events at day 28 | Number of adverse events at day 14 | Number of adverse events at day 28 | The rate of patients with treatment withdrawal | Ancillary virological study: The rate of patients with a negative viral load at day 8 | Ancillary virological study: The rate of patients with a negative viral load at day 14
NCT04340544	18-99 yr	HCQ	Placebo	Difference in the time to resolution of clinical signs and symptoms of mild COVID-19 treated with HCQ or placebo as assessed by daily self-assessment | Difference between HCQ- and placebo-treated patients on an ordinal outcome scale until day 28 (death, admission to intensive care, hospitalization, continuing disease, recovered) | All-cause mortality within 28 d
NCT04342221	18-99 yr	HCQ	Placebo	Effect of HCQ on in *vivo* viral clearance
NCT04330144	18-99 yr	HCQ	No intervention	The rate of COVID-19
NCT04384380	20-79 yr	HCQ	No intervention	Time to a negative RT–PCR test | Virological assessment | Number of

				participants with treatment-related adverse events as assessed by the CTCAE v.4.0
NCT04374903	18 yr and older	HCQ and azithromycin	HCQ	Time to Clinical improvement (TTCI) | Clinical failure defined as death or the need for intubation and mechanical ventilation | Adverse effects | QT interval prolongation | Failure to continue assigned therapy | Time to viral clearance
NCT04347512	18 yr and older	HCQ and azithromycin	Placebo	The rate of patients reaching a significant hypoxemia, in each arm.
NCT04391127	16-90 yr	HCQ or Ivermectin	Placebo	Mean days of hospital stay | The rate of respiratory deterioration, the requirement of invasive mechanical ventilation or death | Mean oxygenation index delta | Mean time to viral PCR negativity
NCT04363866	18 yr and older	HCQ	Placebo	Clinical status at Day 5 assessed by a 6-Point Ordinal Scale | Number of participants with detectable SARS-CoV-2 virus from day 0 to day 28 and at day 5 | Toxicity of the study drug assessed by the incidence of adverse events
NCT04443725	18-65 yr	HCQ	Standard treatment	Virological cure
NCT04344951	18-90 yr	CQ	Standard treatment	50% reduction in the symptom score for patients with lower respiratory tract infections | Lack of progression for patients with upper respiratory tract infections | Comparison of the primary endpoint with respective patients not receiving the treatment | Serious respiratory failure until Day 14. This was compared with respective patients not receiving the treatment | Frequency of AEs and SAEs
NCT04359095	18 yr and older	HCQ or Lopinavir/Ritonavir Pill or Azithromycin	Standard treatment	Mortality | Number of participants with treatment-related severe adverse events as assessed by the NCORP Guidance for Collection of Adverse Events Related to COVID-19 Infection | Time to death | Number of participants transferred to the intensive care unit (ICU) | Number of participants that need mechanical ventilation support with endotracheal intubation | Number of participants cured as assessed by nasopharyngeal swabs, oropharyngeal swabs, and blood aspiration for COVID-19 (RT–PCR) without clinical symptoms and normal chest X ray | Number of participants with any adverse event related to treatment as assessed by the NCORP Guidance for Collection of Adverse Events Related to COVID-19 Infection
NCT04321278	18 yr and older	HCQ + azithromycin	HCQ	Evaluation of clinical status | All-cause mortality | Number of days free from mechanical ventilation | Duration of mechanical ventilation | Duration of hospitalization | Other secondary infections | Time from the start of treatment to death | Medium- and long-term outcomes of SARS-CoV-2 infection on morbimortality, daily life activities, mental health, and quality of life | Assessment of whether the tested therapies may be affected by leucocyte phenotype
NCT04316377	18 yr and older	HCQ	No intervention	Rate of decline in SARS-CoV-2 viral load | Change in National Early Warning Score scores | Admission to the intensive care unit | In-hospital mortality | Duration of hospital admission | Mortality at 30 and 90 d | Clinical status | Change in C-reactive protein concentrations | Change in alanine aminotransferase concentrations | Change in aspartate aminotransferase concentrations | Change in bilirubin concentrations | Change in the estimated glomerular filtration rate | Change in cardiac troponin concentrations | Change in natriuretic peptide concentrations
NCT04331470	15-100 yr	Levamisole Pill + Budesonide+Formoterol inhaler	Lopinavir/Ritonavir + HCQ	Clear chest CT-scan | PCR test | Physical status of the patient
NCT04325893	18 yr and older	HCQ	Placebo	Number of deaths from any cause, or the need for intubation and mechanical ventilation during the 14 d following inclusion and the start of treatment | Number of deaths from any cause, or the need for intubation and mechanical ventilation during the 28 d following inclusion and the start of treatment | Clinical evolution on the WHO Ordinal Scale for Clinical Improvement for COVID-19 between day 0 and day 14 | Clinical evolution on the WHO Ordinal Scale for Clinical Improvement for COVID-19 between day 0 and day 28 | Number of all-cause mortalities at day 14 | Number of all-cause mortalities at day 28 | Rate of positive SARS-CoV-2 RT–PCR nasopharyngeal samples at day 5 | Rate of positive SARS-CoV-2 RT–PCR nasopharyngeal samples at day 10 | The rate of venous thromboembolic events at day 28, documented and confirmed by an adjudication committee | Number of all-cause mortalities at day 28 in patients aged 75 yr and older | Clinical evolution on the WHO OSCI scale for COVID-19 between day 0 and day 28 for patients aged 75 yr or older | Rate of severe adverse events at day 28 | Number of all-cause mortalities at day 14 in patients aged 75 yr and older
NCT04353037	50-75 yr	HCQ	Placebo	Sub Study 1: Patients | Sub Study 2: Health Care Workers | Sub Study

				1: Patients: Rate of secondary infection of coinhabitants | Sub Study 1: Patients: Adverse Events | Sub Study 1: Patients: Negative for COVID-19 | Sub Study 2: Health Care Workers: Number of shifts missed | Sub Study 2: Health Care Workers: Rate of adverse events | Sub Study 2: Health Care Workers: Rate of hospitalization
NCT04351724	18-99 yr	CQ or HCQ	Placebo	Sustained improvement (> 48 h) of one point on the WHO scale | Time to improvement on the WHO scale | Mean change in the ranking on an ordinal scale from baseline | Time to discharge or a National Early Warning Score (NEWS) (maintained for 24 h), whichever occurs first | Change from baseline in the National Early Warning Score (NEWS) | Oxygenation-free days | Incidence of new oxygen use during the trial | Duration of oxygen use during the trial | Ventilator-free days until day 29 | Incidence of new mechanical ventilation use during the trial | Duration of mechanical ventilation use during the trial | Viral load/viral clearance | Duration of hospitalization | Mortality | Obesity – mortality | Obesity - duration of hospitalization | Obesity - ICU admission | Obesity - new oxygen use | Drug–drug interactions with lopinavir/ritonavir | Renin Angiotensin System (RAS) fingerprint
NCT04359316	18 yr and older	HCQ	Azithromycin	Time to clinical improvement | Mortality | SpO_2 improvement | Incidence of new mechanical ventilation use | Duration of hospitalization | Cumulative incidence of serious adverse events
NCT04334148	18 yr and older	HCQ	Placebo oral tablet	Number of participants with clinical COVID-19 infection | Number of participants with COVID-19 viral shedding | Safety as measured by the number of adverse events

CQ: Chloroquine; HCQ: Hydroxychloroquine; COVID-19: Coronavirus disease 2019; SARS-CoV2: Severe acute respiratory syndrome coronavirus 2.

However, as more standardized clinical trials were published, doubts about the efficacy of CQ/HCQ began to increase. On April 14, 2020, a multicenter open-label randomized clinical trial conducted at Ruijin Hospital showed that HCQ did not improve the rate of negative conversion of SARS-CoV-2 nucleic acid tests. This was the first clinical trial in which CQ/HCQ was shown to be ineffective[5]. On May 7, 2020, the New England Journal of Medicine (NEJM) published an important observational study reporting the clinical efficacy of HCQ for the treatment of COVID-19. Our team also confirmed this conclusion[6]. The conclusion was that there was no obvious effect[7]. Since then, more scholars have warned that HCQ/CQ has serious side effects[8,9]. This article reviews the published RCTs related to CQ and HCQ (Table 2).

ETHICAL CHALLENGES FOR HCQ/CQ OFF-LABEL USE FOR COVID-19

The results of existing clinical trials show that there are still some problems with the methodologies. For example, the controlled trials did not use randomization. The populations were not generally representative (the subjects of some trials were young), and the combined dose was too low to thoroughly explore the effectiveness of the drug; however, adverse events, such as cardiotoxicity, have occurred with high doses and drug combinations. Therefore, a well-designed clinical trial to clarify the safety and effectiveness of HCQ/CQ and to guide the development of drugs for the treatment of COVID-19 is needed. Simultaneously, obtaining ethical approval before conducting clinical trials is very important.

We found that many clinical trials lacked a solid ethical basis in the ethical review of studies involving the treatment of COVID-19 with HCQ/CQ during the pandemic.

ETHICAL RECOMMENDATIONS FOR CONDUCTING CLINICAL TRIALS WITH HCQ/CQ FOR COVID-19

In addition to applying for standardized ethical review and adhering to the "Key Guidelines on the Ethical Acceptability of COVID-19 Human Challenge Tests" issued by the WHO, postmarketing studies of clinical drugs initiated by researchers need to consider the following.

Paying attention to the scientific basis of the research

Scientificity is essential to the effectiveness of clinical research results. To research the off-label use of CQ and HCQ, it is necessary to carefully study the instructions for these drugs, obtain and consider the latest supplementary instructions for their use, and design the research plan accordingly.

Table 2 Published randomized controlled trials related to chloroquine and hydroxychloroquine use for coronavirus disease 2019

DOI		Number of subjects	Patients' age (mean ± SD)	Basic diseases (%)	Treatment plan
10.3785/j.issn.1008-9292.2020.03.03	Experimental group	15	50.5 ± 3.8	40.00%	Routine treatment + oral HCQ sulfate days 1-5, 400 mg QD
	Control group	15	46.7 ± 3.6	33.30%	Routine treatment
10.1101/2020.03.22.20040758	Experimental group	31	45.2 ± 14.7	NA	Standard treatment + oral HCQ sulfate days 1-5, 200 mg bid
	Control group	31	44.1 ± 16.1	NA	Standard treatment
10.1101/2020.04.10.20060558	Experimental group	75	48.0 ± 14.1	37.30%	Standard care + oral HCQ sulfate days 1-3, 1200 mg QD; Day 4 – 800 mg QD
	Control group	75	44.1 ± 15.0	22.70%	Standard care
10.1101/2020.04.10.20060699	Experimental group	84	59 ± 48-67	NA	Standard care + oral HCQ sulfate day 1 - 600 mg QD
	Control group	97	63 ± 53-68	NA	Standard care

Routine treatment includes bed rest, oxygen inhalation, symptomatic support treatment, the use of antiviral drugs recommended in the "diagnosis and treatment plan", if necessary, antibiotics, *etc*. Standard treatments include oxygen therapy, antiviral drugs, antibiotics and immunoglobulins, with or without corticosteroids. The minimum requirements for standard care include intravenous infusion, oxygen supply, regular laboratory tests and severe acute respiratory syndrome coronavirus 2 tests, hemodynamic monitoring and intensive care, and the provision of symptomatic drugs. HCQ: Hydroxychloroquine; NA: Not available.

Research design

When considering using CQ and HCQ to treat COVID-19, it is necessary to fully consider the indications, usages, dosages, precautions, adverse reactions, contraindications, drug interactions and possible risks. In view of the above considerations, researchers should refine their plans and measurements, clarify the specific indicators, and, for the long-term follow-up of the clinical responses, develop medical countermeasures. At the same time, in accordance with the scientific requirements, a gold standard for evaluating interventions involving CQ and HCQ needs to be established, and alternative research designs, such as adaptive designs and stepwise designs, should be explored. Before using alternative research designs, the advantages and disadvantages must be carefully evaluated to minimize the risk to the subjects.

Sample size and estimation method

The sample sizes needed in studies of CQ and HCQ are uncertain. According to the developing trends of the pandemic, it is necessary to recruit a large numbers of clinical research subjects; research should not be wasted due to an insufficient sample size. At present, countries are gradually gaining control over the pandemic, and it is also important to ensure that there are enough subjects in CQ and HCQ trials to prevent the unnecessary exposure of subjects to risk.

Criteria for patient inclusion, exclusion and early withdrawal

When determining patients for inclusion, it is important to consider that CQ should be used with caution in patients with the following conditions: Liver and kidney insufficiency, heart disease, severe multitype erythema, hematoporphyria, psoriasis, and psychosis. Other considerations include the following: (1) "Providers should be careful when applying it for patients with liver disease"; (2) "It is particularly dangerous for patients with porphyria"; (3) "Patients lacking glucose 6-phosphate dehydrogenase are at great risk of hemolysis"; (4) "Children are particularly sensitive to the toxicity of this drug"; and (5) "It can aggravate the onset of psoriasis or promote the recurrence of psoriasis". The clinical precautions needed when using HCQ are clear: "All patients should undergo ophthalmological and ECG examinations" and "Patients with the following conditions should increase their frequency of eye examinations": (1) Patients with a daily dose exceeding the ideal body weight of 6.5 mg/kg (using the absolute body weight as a dosing guide can cause overdosing in obese patients); (2) Patients with renal insufficiency; (3) Patients with a cumulative dose exceeding 200 g; and (4) Patients with adverse reactions". In addition, precautions in the "elderly" population should be fully considered with regard to patient exclusion or as early withdrawal criteria to prevent their incorrect inclusion. At the same time, there must be a withdrawal standard that takes into account the rapid progression of the disease and sudden changes in each stage to protect the safety and rights of the subjects to the greatest extent. All

patients who meet the criteria should enter the selection process for screening. Selected patients must strictly abide by a program's selection and exclusion criteria. Criteria that are too loose will lead to the inclusion of patients who are not suited for the program. Criteria that are too strict actually added new exclusion criteria and eventually led to so-called "super selection". There will be bias in both cases. To ensure the speed and quality of patient selection, although it is possible to mobilize more doctors to recommend patients, it is best to focus on a few doctors who understand the plan and are available at any time. It is important for these doctors to ask for clarification when there is a paradox in the exclusion criteria. When seeking clarification, the PI of a unit should be contacted before the inspector. If there is a period of uncertainty regarding the inclusion of a patient in a trial, the treatment of the patient's condition should be the primary focus, and the diagnosis and treatment should not be delayed due to selection. In the event of serious adverse reactions such as cardiotoxicity, subjects should be considered for early withdrawal. We should also pay attention to people with rare diseases where off-label drugs for COVID-19 might lead to severe complications, such as patients with neuromuscular diseases[10].

Evaluation indicators and standards

It is important to distinguish among mild, severe, slowly developing, and urgent symptoms of COVID-19 to determine the status of the subjects and the specific timing and conditions indicating the use of CQ and HCQ. For example, patients with mild COVID-19 should receive the medication at the beginning of the diagnostic process; when hospitalized, patients with severe COVID-19 should receive it before intubation; and patients experiencing a life-threatening emergency should receive it after intubation. In the above situation, the corresponding evaluation index should be set after the medication is administered. The main evaluation index used for patients with mild COVID-19 is the cure rate or the rate of conversion from severe COVID-19; the main evaluation indicator for critical patients is the case fatality rate. In emergencies, the clinical recovery time can be used as a surrogate endpoint. At the same time, the dosage of a patient's medication at each stage, the rate of ventilator use after drug treatment, and whether drug treatment was combined with other medications should be considered important evaluation indicators. It is necessary to compare the evaluation indicators among patients with various symptoms who have and have not been treated with CQ and HCQ to comprehensively determine the benefits of the medications.

Assessing risks and potential benefits, and fully informing subjects of the risks of participating in the research

We need to reasonably evaluate and anticipate the risks and benefits of the research. The expected benefits should be greater than the risks, and the subjects should be fully informed of the risks involved in the research. Appropriate strategies should be adopted as much as possible to minimize the risks to patients. It is important to identify the possible risks and symptoms of adverse events in each stage of the process related to treatment with CQ and HCQ to formulate targeted risk mitigation measures to carefully control and reduce the risks.

There are clinical trials reporting that taking high doses of CQ and HCQ carries the risk of clinical arrhythmia. According to the reports, a total of 81 subjects participated in a randomized double-blind HCQ trial for the treatment of COVID-19 in Brazil. Approximately half of the patients took 450 mg twice a day for 5 consecutive days, while the other half took 600 mg a day (high-dose group). On the third day of the trial, some patients in the high-dose group experienced severe arrhythmia, and 11 people died; the investigator had to terminate the trial as soon as possible[11]. In addition, there have been studies showing that the combination of HCQ or CQ with azithromycin can cause cardiac safety issues; one such study was an analysis of HCQ use in more than 950000 patients from 6 countries. The results showed that the current HCQ recommended dose for rheumatoid arthritis is safe; when azithromycin is used at the same time, the QT interval may be prolonged or even torsade de pointes tachycardia, resulting in sudden death. This suggests that caution should be used when combining medications. Current reports show that SARS-CoV-2 may affect the heart muscle and cause myocarditis. Individual autopsy reports suggest that the myocardium is infiltrated by interstitial mononuclear inflammatory cells, indicating that the heart tissue is infected. Severe myocarditis with decreased myocardial contractile function has also been reported in COVID-19 patients. Studies of cardiac biomarkers have also shown that the incidence of cardiac damage in hospitalized patients is high. COVID-19-induced electrolyte disorders (such as hypokalemia and hypomagnesemia) should not be understated, as they can explain why COVID-19 patients are at high risk for ventricular arrhythmias when treated with HCQ. The cytokine storm can also have a prolonging effect on the QT interval[12].

However, there are major uncertainties about the pathogenesis of COVID-19. Despite our efforts to reduce risks, serious harm may still occur. Therefore, subjects should be provided with high-quality supportive care (including necessary intensive care), long-term follow-up (to detect any lasting injury), and adequate compensation for any injury that occurs to fully protect their rights and interests.

STRENGTHENING CONSULTATION AMONG STAKEHOLDERS

Clinical research should focus on consulting with and soliciting the opinions of stakeholders (subjects, researchers, ethics committee members, *etc*.). For example, when researching the off-label use of CQ and HCQ, it is necessary to ask the CQ and HCQ drug manufacturers for the latest supplementary instructions regarding their use. Research-related risks and potential benefits should be presented in a transparent manner to participants; the opinions of subjects, people interested in the research and relevant experts should be incorporated; and the acceptability of the clinical research to the public and the acceptance of the off-label use of CQ/HCQ by the research subjects should be comprehensively considered. At the same time, consultations with local and international researchers, ethics committee members, decision makers, and other relevant experts should also be conducted.

Promoting research coordination

Coordinated research is intended to ensure that clinical research-related public health benefits are achieved with the greatest possible safety and efficiency. Therefore, research should be coordinated with public health agencies to prevent unduly compromising the local public health response to COVID-19. Research should also be fully supervised by the relevant authorities (including the World Health Organization when appropriate), and adequate communication and coordination with regulatory agencies should be ensured to maximize safety. During early coordination with regulatory agencies, attention should also be paid to the data and results regarding research on the off-label use of CQ and HCQ.

Paying attention to the qualifications of the research team

The research team is the main group involved in conducting drug trials. With regards to drug research conducted during a pandemic, the clinical qualifications, scientific research ability and industry influence of the team members determine the effectiveness of the research.

In terms of personnel qualifications, the main investigator should have clinical experience in the use of CQ, HCQ, *etc*. The research team members should have the appropriate qualifications and clinical research experience and should have received training on drug clinical trial quality management practices and infectious disease protective measures. In addition, a certain number of clinically experienced pharmacists and nursing staff should participate.

In terms of the division of responsibilities, the main researchers should adequately delegate the responsibilities and coordinate the research team, and reasonably allocate the time and energy needed for the clinical research and clinical treatment, including designing the research plan, obtaining informed consent, screening patients for enrollment, acquiring clinical specimens, collecting data in the field, filling in case report forms, performing the statistical analysis, *etc*. All processes should be carried out by the specific personnel responsible. The China national medical aid team in Hubei can be considered as an example. The clinical trial is led by the academician, and the vice president is directly responsible for the trial. The chief physician of the Department of Respiratory Medicine and Critical Care implements the specific treatments and monitors changes in the patients' conditions, and the clinical pharmacology trial institution conducts the trial. With regard to data management and analysis, the entire team has a comprehensive relevant professional background, and there is a clear division of labor and a mechanism to ensure smooth communication and collaboration.

Respecting the subjects' choices

In addition to referring to the criteria for the inclusion, exclusion and withdrawal of subjects specified in the study design, the selection of subjects should also follow the principle of fairness. The principle of fairness is one of the four basic principles of medical ethics. Fairness in research plays an important role in maintaining trust in the relationship between the public and medical researchers. During a pandemic, the principle of fairness is particularly important.

Researchers, sponsors and ethics committees need to ensure that the risks and benefits to subjects are fairly balanced. During a sudden infectious disease pandemic, potentially effective interventional clinical research may be limited. Therefore, researchers should recruit subjects fairly and pay special attention to the inclusion or exclusion of subjects from special groups (such as medical personnel with confirmed infections). There should be sufficient and reasonable rationale behind the selection of subjects. Equity is also reflected in the fact that the subjects should have equal access to the results of the research, and the subjects' welfare should be ensured after the trial.

EXPERT REVIEW

Clinical trials related to SARS-CoV-2 should be included in an independent review category, in addition to or in combination with local ethical review standards, similar to other types of research. Such trials may be controversial or involve higher risks and levels of uncertainty. An independent ethical review committee should include members with relevant scientific knowledge and relevant knowledge of

clinical trial ethics. In all cases, the review process should involve a high level of the necessary knowledge and should be carried out quickly to improve the efficiency of the review process while strictly abiding by the review standards.

At the same time, the researchers and the ethics committee should regularly negotiate, whether before or during the research, and pay special attention to new data (especially data related to risks). In addition, the ethics committee should supervise the entire process of the clinical research and conduct a follow-up review. During the implementation of the trial protocol, the review and approval of important documents, the review of protocol violations, and the review of serious adverse events, it is important to pay close attention to the safety of the subjects. With regard to the subjects involved in the trials of the off-label use of CQ and HCQ, unanticipated adverse events and violations of ethical principles harmed the subjects. The research team should submit research progress reports during each phase with links to key reports, and the overall research process should conform to the requirements in the ethical approval documents with regard to follow-up frequency. A summary report should be submitted after the end of the project.

OBTAINING THE INFORMED CONSENT OF SUBJECTS

Adhering to the priority of patients' rights is the core principle of ethical review and the fundamental manifestation of medical ethics. It is a basic principle that cannot be neglected, regardless of the circumstances. In the case of a pandemic, the ethical review of research on the off-label use of CQ and HCQ still needs to prioritize the rights and interests of subjects and guarantee that subjects give their informed consent.

First, fully informed consent requires the explanation of the involved risks and possible benefits. Subjects should receive an explanation of the in vitro test results and possible positive effects of CQ and HCQ and an explanation of the adverse reactions and possible side effects, such as digestive tract symptoms, cardiovascular symptoms and ocular discomfort. The possibility of lifelong adverse consequences should be explained. Any application for exemption from the need to obtain informed consent or explain the risks due to inconvenience, a shortage of researchers, an increased opportunity for infection, or the lack of personal protective equipment needed when entering isolation wards are not in line with the principles of ethical review. In addition, due to the contagious nature of the disease, there are additional challenges related to the work environment and sanitation with regards to the signing of the informed consent form for off-label CQ and HCQ trials. The research team needs to comply with the principles of ethical review and obtain fully informed consent. For example, during the pandemic, researchers in Wuhan sent WeChat messages that contained the informed consent form signed by the patient and the electrocardiogram (ECG) results from mobile phones in the contaminated area to mobile phones in the clean area. Consent for participation for mechanically ventilated and sedated subjects who lack the capacity to sign the informed consent form can be obtained from their legal representative. No emotional rhetoric should be used under any circumstances to pressure or deceive subjects. Patients should be given sufficient time to consider their participation in a clinical research trial, and their decision regarding their participation in the trial should be respected.

CONCLUSION

Research must be both rigorous and prudent to ensure the best outcome, with the maximization of benefits as the core principle. Standardization of the application, implementation and ethical review processes are needed to prevent unnecessary risk.

FOOTNOTES

Author contributions: Li QY and Lv Y contributed equally to this paper; Li QY and Ye L reviewed the literature and contributed to manuscript drafting and revising; An ZY, Dai NN, Hong X, Zhang Y and Liang LJ contributed to making a revision to the manuscript; Li QY also contributed to conceptualization, methodology, and funding acquisition; and All authors issued final approval for the version to be submitted.

Supported by National Natural Science Foundation of China, No. 81900641; Peking University Health Center for Combating the Pandemic Programs, No. BMU 2021MX020, and No. BMU 2022MX008.

Conflict-of-interest statement: There is no conflict of interests to declare.

Open-Access: This article is an open-access article that was selected by an in-house editor and fully peer-reviewed by external reviewers. It is distributed in accordance with the Creative Commons Attribution Non Commercial (CC BY-NC 4.0) license, which permits others to distribute, remix, adapt, build upon this work non-commercially, and license

their derivative works on different terms, provided the original work is properly cited and the use is non-commercial. See: https://creativecommons.org/Licenses/by-nc/4.0/

Country/Territory of origin: China

ORCID number: Qiu-Yu Li 0000-0002-8707-5229; Ye Lv 0000-0001-7920-074X; Zhuo-Yu An 0000-0003-0976-160X; Ni-Ni Dai 0000-0003-0429-1645; Yu Zhang 0000-0002-9734-4779; Li-Jun Liang 0000-0003-0919-246X.

S-Editor: Ma YJ
L-Editor: A
P-Editor: Ma YJ

REFERENCES

1 ASHP statement on the use of medications for unlabeled uses. *Am J Hosp Pharm* 1992; **49**: 2006-2008 [PMID: 1442846 DOI: 10.1093/ajhp/49.8.2006]
2 **Shojaei A**, Salari P. COVID-19 and off label use of drugs: an ethical viewpoint. *Daru* 2020; **28**: 789-793 [PMID: 32385829 DOI: 10.1007/s40199-020-00351-y]
3 **Wang M**, Cao R, Zhang L, Yang X, Liu J, Xu M, Shi Z, Hu Z, Zhong W, Xiao G. Remdesivir and chloroquine effectively inhibit the recently emerged novel coronavirus (2019-nCoV) in vitro. *Cell Res* 2020; **30**: 269-271 [PMID: 32020029 DOI: 10.1038/s41422-020-0282-0]
4 **Gautret P**, Lagier JC, Parola P, Hoang VT, Meddeb L, Mailhe M, Doudier B, Courjon J, Giordanengo V, Vieira VE, Tissot Dupont H, Honoré S, Colson P, Chabrière E, La Scola B, Rolain JM, Brouqui P, Raoult D. Hydroxychloroquine and azithromycin as a treatment of COVID-19: results of an open-label non-randomized clinical trial. *Int J Antimicrob Agents* 2020; **56**: 105949 [PMID: 32205204 DOI: 10.1016/j.ijantimicag.2020.105949]
5 **Tang W**, Cao Z, Han M, Wang Z, Chen J, Sun W, Wu Y, Xiao W, Liu S, Chen E, Chen W, Wang X, Yang J, Lin J, Zhao Q, Yan Y, Xie Z, Li D, Yang Y, Liu L, Qu J, Ning G, Shi G, Xie Q. Hydroxychloroquine in patients with mainly mild to moderate coronavirus disease 2019: open label, randomised controlled trial. *BMJ* 2020; **369**: m1849 [PMID: 32409561 DOI: 10.1136/bmj.m1849]
6 **Li Q**, Cui C, Xu F, Zhao J, Li N, Li H, Wang T, Zhang H, Liu N, Wei Y, Niu X, Xu Y, Dong J, Yao X, Wang X, Chen Y, Song C, Qiao J, Liu D, Shen N. Evaluation of the efficacy and safety of hydroxychloroquine in comparison with chloroquine in moderate and severe patients with COVID-19. *Sci China Life Sci* 2021; **64**: 660-663 [PMID: 33471276 DOI: 10.1007/s11427-020-1871-4]
7 **Geleris J**, Sun Y, Platt J, Zucker J, Baldwin M, Hripcsak G, Labella A, Manson DK, Kubin C, Barr RG, Sobieszczyk ME, Schluger NW. Observational Study of Hydroxychloroquine in Hospitalized Patients with Covid-19. *N Engl J Med* 2020; **382**: 2411-2418 [PMID: 32379955 DOI: 10.1056/NEJMoa2012410]
8 **Borba MGS**, Val FFA, Sampaio VS, Alexandre MAA, Melo GC, Brito M, Mourão MPG, Brito-Sousa JD, Baía-da-Silva D, Guerra MVF, Hajjar LA, Pinto RC, Balieiro AAS, Pacheco AGF, Santos JDO Jr, Naveca FG, Xavier MS, Siqueira AM, Schwarzbold A, Croda J, Nogueira ML, Romero GAS, Bassat Q, Fontes CJ, Albuquerque BC, Daniel-Ribeiro CT, Monteiro WM, Lacerda MVG; CloroCovid-19 Team. Effect of High vs Low Doses of Chloroquine Diphosphate as Adjunctive Therapy for Patients Hospitalized With Severe Acute Respiratory Syndrome Coronavirus 2 (SARS-CoV-2) Infection: A Randomized Clinical Trial. *JAMA Netw Open* 2020; **3**: e208857 [PMID: 32330277 DOI: 10.1001/jamanetworkopen.2020.8857]
9 **Chorin E**, Dai M, Shulman E, Wadhwani L, Bar-Cohen R, Barbhaiya C, Aizer A, Holmes D, Bernstein S, Spinelli M, Park DS, Chinitz LA, Jankelson L. The QT interval in patients with COVID-19 treated with hydroxychloroquine and azithromycin. *Nat Med* 2020; **26**: 808-809 [PMID: 32488217 DOI: 10.1038/s41591-020-0888-2]
10 **Liguori S**, Moretti A, Paoletta M, Gimigliano F, Iolascon G. Rehabilitation of Neuromuscular Diseases During COVID-19: Pitfalls and Opportunities. *Front Neurol* 2021; **12**: 626319 [PMID: 33679588 DOI: 10.3389/fneur.2021.626319]
11 **Huang M**, Li M, Xiao F, Pang P, Liang J, Tang T, Liu S, Chen B, Shu J, You Y, Li Y, Tang M, Zhou J, Jiang G, Xiang J, Hong W, He S, Wang Z, Feng J, Lin C, Ye Y, Wu Z, Zhong B, Sun R, Hong Z, Liu J, Chen H, Wang X, Li Z, Pei D, Tian L, Xia J, Jiang S, Zhong N, Shan H. Preliminary evidence from a multicenter prospective observational study of the safety and efficacy of chloroquine for the treatment of COVID-19. *Natl Sci Rev* 2020; **7**: 1428-1436 [PMID: 34676087 DOI: 10.1093/nsr/nwaa113]
12 **Madjid M**, Safavi-Naeini P, Solomon SD, Vardeny O. Potential Effects of Coronaviruses on the Cardiovascular System: A Review. *JAMA Cardiol* 2020; **5**: 831-840 [PMID: 32219363 DOI: 10.1001/jamacardio.2020.1286]

World Journal of Clinical Cases

Submit a Manuscript: https://www.f6publishing.com

World J Clin Cases 2022 June 16; 10(17): 5551-5565

DOI: 10.12998/wjcc.v10.i17.5551

ISSN 2307-8960 (online)

ORIGINAL ARTICLE

Case Control Study

Gut peptide changes in patients with obstructive jaundice undergoing biliary drainage: A prospective case control study

Tajana Pavić, Stipe Pelajić, Nina Blažević, Dominik Kralj, Milan Milošević, Ivana Mikolasevic, Ivan Lerotic, Davor Hrabar

Specialty type: Gastroenterology and hepatology

Provenance and peer review: Invited article; Externally peer reviewed.

Peer-review model: Single blind

Peer-review report's scientific quality classification
Grade A (Excellent): 0
Grade B (Very good): 0
Grade C (Good): C, C
Grade D (Fair): 0
Grade E (Poor): 0

P-Reviewer: Abdalla MMI, Malaysia; Tan X, China

Received: December 10, 2021
Peer-review started: December 10, 2021
First decision: January 8, 2022
Revised: January 20, 2022
Accepted: April 9, 2022
Article in press: April 9, 2022
Published online: June 16, 2022

Tajana Pavić, Stipe Pelajić, Nina Blažević, Dominik Kralj, Ivan Lerotic, Davor Hrabar, Department of Gastroenterology and Hepatology, University Hospital Center Sestre Milosrdnice, Zagreb 10000, Croatia

Milan Milošević, Andrija Stampar School of Public Health WHO Collaborative Centre for Occupational Health, University of Zagreb, School of Medicine, Zagreb 10000, Croatia

Ivana Mikolasevic, Department of Gastroenterology, University Hospital Center Rijeka, Rijeka 51000, Croatia

Corresponding author: Tajana Pavić, MD, PhD, Assistant Professor, Department of Gastroenterology and Hepatology, University Hospital Center Sestre Milosrdnice, Vinogradska cesta 29, Zagreb 10000, Croatia. tajana.pavic@gmail.com

Abstract

BACKGROUND

Biliary obstruction is a relatively common condition that affects approximately 5 in 1000 people annually. Malnutrition is very common in patients with biliary obstruction and since it is associated with significant morbidity and mortality, it is important to identify factors and mechanisms involved in its development.

AIM

To determine the influence of obstructive jaundice on the hormones controlling appetite and nutritive status.

METHODS

This was a prospective case control study performed in a tertiary center in Zagreb, Croatia. Patients with biliary obstruction undergoing internal biliary drainage from September 2012 until August 2013 were enrolled. After excluding patients who developed procedure related complications or were lost in the follow-up, out of initial 73 patients, 55 patients were included in the analysis, including 34 with benign and 21 with malignant disease. Meanwhile, 40 non-jaundiced controls were also included. Appetite, nutritional status, and serum ghrelin, cholecystokinin (CCK), interleukin 6 (IL-6), and tumor necrosis factor α (TNF-α) were determined at admission, 48 h and 28 d after internal biliary drainage. Chi square test was used for categorical variables. Continuous variables were analysed for normality by Kolmogorov–Smirnov test and relevant non-parametric (Mann-

Whitney, Kruskal-Wallis, and Friedman) or parametric (*t*-test and analysis of variance) tests were used.

RESULTS

Patients with obstructive jaundice were significantly malnourished compared to controls, regardless of disease etiology. Plasma ghrelin and CCK levels were significantly higher in patients with obstructive jaundice. Serum bilirubin concentrations were negatively correlated with ghrelin levels and positively correlated with TNF-α, but had no correlation with CCK concentrations. After internal biliary drainage, a significant improvement of nutritional status was observed although serum concentrations of ghrelin, IL-6, and TNF-α remained significantly elevated even 28 d after the procedure. CCK levels in patients without malnutrition remained elevated 28 d after the procedure, but in patients with malnutrition, CCK levels decreased to levels comparable with those in the control group. We have not established any correlation between appetite and serum levels of ghrelin, CCK, IL-6, and TNF-α before and after biliary drainage.

CONCLUSION

Possible abnormalities in ghrelin and CCK regulation may be associated with the development of malnutrition during the inflammatory response in patients with biliary obstruction.

Key Words: Ghrelin; Cholecystokinin; Biliary obstruction; Malnutrition

©The Author(s) 2022. Published by Baishideng Publishing Group Inc. All rights reserved.

Core Tip: Biliary obstruction is a common condition with subsequent malnutrition that contributes to patient's high morbidity and mortality. Therefore, it is important to better understand the interaction of hormonal and inflammatory parameters on nutritional status. We conducted a case control study to determine the influence of obstructive jaundice on the hormones controlling appetite and nutritional status and showed that patients with obstructive jaundice had worse nutritional status compared to controls, regardless of disease etiology. Plasma ghrelin and cholecystokinin levels were significantly higher in patients with obstructive jaundice, which may be associated with the development of malnutrition during the inflammatory response.

Citation: Pavić T, Pelajić S, Blažević N, Kralj D, Milošević M, Mikolasevic I, Lerotic I, Hrabar D. Gut peptide changes in patients with obstructive jaundice undergoing biliary drainage: A prospective case control study. *World J Clin Cases* 2022; 10(17): 5551-5565

URL: https://www.wjgnet.com/2307-8960/full/v10/i17/5551.htm

DOI: https://dx.doi.org/10.12998/wjcc.v10.i17.5551

INTRODUCTION

Biliary obstruction is a relatively common condition that affects approximately 5 in 1000 people annually[1]. It can be caused by a variety of malignant and benign conditions[2-4]. Regardless of the underlying pathology, the blockage of bile ducts causes accumulation of bilirubin and bile salts in the blood and can lead to complications such as acute cholangitis, sepsis, liver dysfunction, renal failure, and cardiovascular impairment[1,3]. Malnutrition is common in patients with biliary obstruction with the prevalence of malnutrition in this population being up to 80% according to some studies[5-7]. Since malnutrition is associated with significant morbidity and mortality[8-10], it is important to identify factors and mechanisms involved in development of malnutrition in patients with biliary obstruction.

Tumor necrosis factor α (TNF-α) and interleukin 6 (IL-6) are inflammatory cytokines associated with negative energy balance and cachexia[11,12]. Previous studies have found increased levels of both TNF-α and IL-6 in patients with biliary obstruction[1,2,5]. Cholecystokinin (CCK) is a gut derived hormone that inhibits food intake in humans[13,14]. CCK regulates gallbladder and small intestinal motility through CCK1-1 receptor (CCK-1R) found in various locations throughout the digestive system[15]. A study by Padillo *et al*[4] found that increased CCK concentration can be predictive of malnutrition in patients with biliary obstruction. Ghrelin is a 28 amino acid peptide hormone produced mostly by X/A cells found in the neck to the base of the oxyntic gland in the gastric fundus. It is the only known peripherally produced hormone with central orexigenic effect to date[16] and it exhibits a functional antagonism with CCK[14,17,18]. It also has anti-inflammatory effects and studies have shown that it can antagonize the effects of TNF-α and IL-6 by limiting the activation of NF-κB signaling[19,20]. The few studies performed so far have not given us clear answers about factors that regulate appetite and

nutritional status of patients before and after resolution of biliary obstruction. Food intake and energy homeostasis are tightly linked by a complex system of nervous structures and humoral factors that form the brain-gut axis[21]. In biologically important signaling systems, multiple repetitive components are often encountered in order to be able to compensate in the event of failure of some parts of the signaling network[22]. Food intake is one of the vital functions, so it is not surprising that there are a multitude of regulatory molecules networked by complex interactions. Moreover, many of the primary regulatory molecules controlling body weight are deployed at multiple physiological levels, as an example of evolutionary adjustment[22]. CCK was the first intestinal hormone to be shown to reduce appetite in humans[23]. This was followed by the discovery of a multitude of peptides from the stomach and intestines that have a similar effect, but to date the only known peripheral peptide with central action that stimulates appetite is ghrelin[24]. Many researchers believe that the example of ghrelin illustrates the importance of the functional interdependence of the stomach and hypothalamus and that it is one of the missing links in understanding the regulation of energy balance, growth, and the functioning of the digestive system[24]. There is evidence to support a functional antagonism of ghrelin and CCK on food intake, but their exact interaction in specific clinical situations has not yet been proven[25]. Since the presence of bile in the duodenum is an important modulator of postprandial CCK secretion, the aim of this study was to examine the effect of biliary obstruction and consequent decreased bile acid content in the duodenum on serum CCK concentration and its influence on ghrelin, CCK, TNF-α, and IL-6, as well as nutritional parameters and appetite.

MATERIALS AND METHODS

Participants

We recruited 73 patients with biliary obstruction who underwent biliary drainage *via* endoscopic retrograde cholangiopancreatography (ERCP) at University Hospital Center Sestre Milosrdnice from September 2012 until December 2013 and 40 sex and age matched healthy controls. The inclusion criteria were bilirubin levels > 35 μmol/L and intrahepatic and/or extrahepatic biliary dilation on transabdominal ultrasound. Patients who developed complications such as acute pancreatitis, acute cholangitis, or biliary sepsis as well as patients with other conditions that are known to lead to malnutrition or inadequate oral intake were excluded from the study. The study was approved by the ethics committees of University Hospital Center Sestre Milosrdnice and University of Zagreb School of Medicine.

Study design and protocol

This was a prospective case control study carried out at the University Hospital Center Sestre Milosrdnice, Zagreb, Croatia. After obtaining informed consent, patients had blood drawn for laboratory studies including complete blood count, C-reactive protein (CRP), sedimentation rate, liver enzymes, bilirubin, creatinine, blood glucose, electrolytes, calcium, amylase in blood and urine, protein electrophoresis, and lipid status and coagulation parameters. As a standard pre-ERCP procedure, esophagogastroduodenoscopy (EGD) was performed and biopsies for *Helicobacter pylori* (*H. pylori*) were taken. On the day of the procedure, after 10 h of fasting, anthropometric measurements were obtained, including mass, height, body mass index (BMI), and body fat percentage. Nutritional risk screening 2002 scoring (NRS 2002) was performed[26,27]. Blood samples for concentration of CRP, CCK, TNF–α, and IL-6 measurements were drawn. Pain and appetite were assessed using validated visual analog scales. ERCP was performed in intravenous anesthesia and obstruction was managed depending on underlying pathology either by stone extraction or biliary stent implantation. Nutritive assessment, laboratory studies and hormone levels were obtained 48 h and 28 d after successful biliary drainage. Patients at high nutritional risk received oral nutritional supplements (720-880 kcal/d) for 28 d or more. After a follow-up period of 6 mo, all the available patients were clinically reassessed. Healthy controls underwent the same initial laboratory studies and anthropometric measurement, but without EGD, so the testing for *H. pylori* was done using stool antigen test.

Biochemical measurements

Ten milliliters of venous blood were collected in chilled test tubes with ethylenediaminetetraacetic acid and 1000 units of aprotinin per milliliter of blood. Plasma was separated by centrifugation (1000 revolutions per min, 15 min, 4 °C) within 30 min of collection and stored at -70 °C until thawed for analysis.

CCK was measured quantitatively by enzyme-linked immunosorbent assay method using a commercial CCK kit (Cusabio). It is an *in vitro* quantitative assay that uses antibodies specific for human CCK in a double sandwich technique. Cross-reactivity with other similar molecules has not been found. The minimal detectable level was 20 pg/mL.

Ghrelin concentration was measured by radioimmunoassay technique using a commercial kit (DIAsource ImmunoAssays, South Africa) that uses 125I-labeled recombinant ghrelin as a tracer and a polyclonal antibody raised in rabbits against the C-terminal end of human ghrelin. No cross-reactivity with any relevant molecules such as insulin and growth hormone has been found. The measuring range

for ghrelin using this method was 200-6400 pg/mL.

IL-6 concentration was determined by electrochemiluminescence immunoassay using a commercial kit (Roche Diagnostics GmbH, D-68305 Mannheim, Germany) and Roche Cobas e411 automatic analyzer. The method uses IL-6 specific monoclonal antibodies labeled with biotin and ruthenium that produce chemiluminesence when exposed to electrodes. The measuring range is 1.5-5000 pg/mL.

TNF-α was measured by chemiluminescence immunoassay using a commercially available kit (IMMULITE 1000 System, Siemens Medical). It is a quantitative assay that uses TNF-α antibodies as a solid phase and alkaline phosphatase as a reagent and substrate for chemiluminescent enzyme. The measuring range for this method is 1.7-1000 pg/mL.

For the patients who underwent EGD and had standard biopsies taken, presence of *H. pylori* infection was assessed histologically after Giemsa staining. Patients taking proton pump inhibitors (PPI) and healthy controls were tested for *H. pylori* antigen in stool using a commercially available test (Diaquick, Dialab) after at least 2 wk of PPI therapy cessation.

Other routine blood tests were performed using the automatic analyzer AU 2700 (Beckman 40 Coulter International, South Africa) and Beckman Coulter HmX automatic hematologic analyzer.

Statistical analysis

Analysis of test power for analysis of variance (ANOVA) (3 repeated measurements) with the following parameters: Test power of 90%, α significance level of 0.05, and sample size effect of 0.2 with an assumed correlation between measurements of 0.5, estimated the total sample size to be 55. Additional analysis for the independent *t*-test (difference between test and control groups), under the same conditions, found that the control group should consist of 40 healthy subjects. After testing for normality by Kolmogorov-Smirnov test, relevant parametric and nonparametric tests were used. Quantitative data are expressed as the arithmetic mean and their standard deviation if they were normally distributed, or as medians with interquartile ranges if they did not fit a normal distribution. Continuous variables were compared by Mann-Whitney and Kruskal-Wallis tests. Differences in quantitative values between measurements were analyzed using repeated measurement ANOVA and Friedman's test. Logistic regression was used to make a multivariate model for the impact of clinical features, inflammatory predictors, as well as ghrelin and CCK concentrations on appetite and nutritional status. P values < 0.05 were considered significant. The statistical analyses were done using G*Power for windows version 3.1.2. and MedCalc for windows version 11.3.1.

RESULTS

Clinical characteristics

We initially enrolled 73 patients with biliary obstruction out of which 55 were included in the final analysis, as well as 40 healthy sex and age matched controls. Reasons for exclusion of the 18 patients were inadequate biliary drainage in six patients, postprocedural pancreatitis in five patients, loss to follow-up in six, and one patient underwent a liver transplant during the study period in one (Figure 1). Patients with biliary obstruction were further divided into two groups based on etiology of the obstruction; 65% had benign and 57% malignant biliary obstruction. Various clinical characteristics were compared among the groups, and the results are summarized in Table 1. Compared to the control group, patients with biliary obstruction had worse nutritional parameters, as expected, but there was no significant difference in appetite levels (P = 0.641). Patients with malignant biliary obstruction were on average older, and had longer duration of symptoms and worse nutritional parameters compared to those with benign etiology. There was no difference in appetite, pain levels, or prevalence of *H. pylori* colonization (P = 0.834), while smoking was far more prevalent in patients with benign etiology of obstruction (P = 0.001).

Laboratory parameters

Table 2 presents measured laboratory parameters and their comparison between the groups. In patients with biliary obstruction all inflammatory markers (CRP, IL-6, and TNF-α), except leukocyte count, were significantly higher compared to controls. Patients with biliary obstruction also had significantly higher levels of ghrelin and CCK. Regarding etiology, there was no significant difference for most of the measured laboratory parameters between the two groups, except CRP levels which were higher in patients with benign etiology, while bilirubin levels were higher in patients with malignant etiology. There was also no significant difference regarding ghrelin or CCK levels.

The intensity of biliary obstruction was negatively correlated to ghrelin (r = -0.424; P = 0.001), and positively correlated to TNF-α (r = 0.486, P < 0.001), loss of body weight, and nutritional risk. There was no correlation between the intensity of biliary obstruction and CCK levels and appetite. We did not observe a correlation between duration of biliary obstruction and tested hormones, inflammatory markers, and appetite. We also did not observe the effect of *H. pylori* colonization on the concentrations of appetite-regulating hormones (ghrelin: τb = - 0.152, P = 0.267, CCK: τb = 0.136, P = 0.323), but appetite levels correlated positively with *H. pylori* colonization (τb = 0.356, P = 0.008). Of all the inflammatory

Table 1 Clinical characteristics of the participants

		Benign etiology (*n* = 34)	Malignant etiology (*n* = 21)	Control (*n* = 40)	*P* value
Gender	Female	12 (35%)	9 (43%)	13 (32%)	
	Male	22 (65%)	12 (57%)	27 (68%)	
Age (yr)	Median (Q1-Q3)	55.0 (43.0-67.0)	66.0 (60.5-83.0)	55.0 (43.0-67.0)	
	Min-max	33-84	55-88	39-90	
Biliary obstruction etiology	Biliary stones	28 (82%)			
	Chronic pancreatitis	5 (15%)			
	Stenosing papillitis	1 (3%)			
	Tumor of pancreatic head		15 (72%)		
	Malignant lymphadenopathy		4 (19%)		
	Cholangiocarcinoma		2 (9%)		
Duration of biliary obstruction (d)		10.0 (5.0-20.2)	14.0 (10.0-21.0)	NA	0.045[1]
Body weight (kg)		80.5 (73.5-92.0)	61.0 (46.0-75.8)	72.5 (63.0-75.4)	0.04[1]
BMI (kg/m^2)		26.9 (23.7-28.7)	21.8 (17.0-24.0)	25.8 (22.9-27.9)	0.001[1]
Weight loss (%)		3.8 (0.0-7.6)	12.0 (8.1-18.0)	0.0 (0.0-0.0)	0.002[2]
Body fat (%)		24.0 (22.0-25.3)	19.0 (13.0-24.0)	29.5 (27.0-32.0)	< 0.001[2]
NRS 2002		2.5 (0.0-3.3)	4.0 (3.5-5.0)	0.0 (0.0-0.0)	< 0.001[2]
NRS 2002	< 3	17 (50%)	2 (9.5%)	38 (95%)	< 0.001[2]
	≥ 3	17 (50%)	19 (90.5%)	2 (5%)	
Appetite (VAS)		4.0 (2.8-6.3)	3.0 (2.0-6.0)	4.0 (2.0-5.0)	0.641[2]
Pain (VAS)		0.0 (0.0-1.3)	1.0 (0.0-2.5)	0.0 (0.0-0.0)	0.001[2]
Helicobacter pylori infection		12 (35.2%)	8 (38.1%)	3 (7.5%)	0.005[2]
Smoking		15 (44.1%)	0 (0%)	7 (17.5%)	< 0.001[2]

[1]Mann-Whitney U test (comparison between benign and malignant groups).
[2]Kruskal-Wallis test (comparison between all three groups).
Values are presented as median (Q1-Q3) for continuous and as *n* (%) for categorical variables. BMI: Body mass index; NRS: Nutritional risk screening; VAS: Visual Analogue Scale; NA: Not available.

markers, only TNF-α showed a positive correlation in the case of colonization with *H. pylori* (τb = 0.396, *P* = 0.003).

General characteristics and ghrelin, CCK, inflammatory markers, appetite, and nutritional status

There was a positive correlation between age and CCK levels (*r* = 0.354, *P* = 0.008), while no effect was observed for ghrelin (*r* = -0.104, *P* = 0.451). Also, there was no statistically significant correlation between age and tested inflammatory markers (IL-6: *r* = 0.230, *P* = 0.091; TNF-α: *r* = 0.180, *P* = 0.189; CRP: *r* = -0.105, *P* = 0.444). As expected, age was associated with higher nutritional risk measured by NRS 2002 (*r* = 0.454, *P* = 0.001), greater loss of body weight (*r* = 0.304, *P* = 0.024), lower fat percentage (*r* = -0.309, *P* = 0.022), and lower albumin levels (*r* = -0.346, *P* = 0.010).

A negative correlation between ghrelin and CRP levels was observed (*r* = -0.37, *P* = 0.005), while no significant correlation was found between CCK levels and all tested inflammatory markers.

We found that the concentrations of tested humoral parameters were sex-dependent-male gender was associated with higher ghrelin levels (τb = -0.100, *P* = 0.467), and higher concentrations of IL-6 (τb = -0.371, *P* = 0.005), TNF-α (τb = -0.341, *P* = 0.011), and CRP (τb = -0.502, *P* = 0.001).

Smoking had no effect on the concentration of any of the appetite-regulating hormones, but lower concentrations of TNF-α were observed in smokers (τb = -0.379, *P* = 0.004). Interestingly, a lower percentage of weight loss was also registered in smokers (τb = -0.521, *P* < 0.001). Since there were no smokers in the group of patients with malignant biliary obstruction, a subanalysis was performed only for patients with benign etiology, which confirmed that the percentage of weight loss was significantly

Table 2 Etiology of biliary obstruction and various humoral parameters, median (25%-75%)

Parameter	Benign etiology (*n* = 34)	Malignant etiology (*n* = 21)	*P* value[1]	Controls (*n* = 40)	*P* value[2]
CRP (mg/L)	13.1 (6.6-19.6)	6.3 (2.9-11.3)	0.001	2.3 (0.9-3.4)	< 0.001
ES (mm/h)	25 (13.0-31.5)	25 (12.0-41.0)	NS	6.5 (4-13.2)	< 0.001
Leukocytes (× 10^9)	6.7 (4.9-8.9)	6.7 (3.9-7.0)	NS	5.9 (5.5-7.2)	NS
Hemoglobin (g/L)	141 (123.8-147.0)	125 (113.5-134.5)	0.002	140 (135.0-156.5)	< 0.001
Thrombocytes (× 10^9)	220 (197.2-248.3)	178 (113.5-289.5)	NS	241 (188.5-289)	0.042
Bilirubin (mmol/L)	85.3 (51.9-183.3)	270 (145-359.8)	< 0.001	12.1 (10.7-14.0)	< 0.001
AST (U/L)	123 (84.0-212.3)	155.0 (78.0-186.0)	NS	19.0 (18.0-23.8)	< 0.001
ALT (U/L)	337.5 (84.8-547.5)	232 (114-355.5)	NS	16.0 (14.0-21.8)	< 0.001
GGT (U/L)	448 (333.8-602.8)	396.0 (243.5-892.5)	NS	18.0 (16.0-25.8)	< 0.001
ALP (U/L)	287.5 (261.8-418.5)	281.0 (243.5-434.0)	NS	83.5 (63.5-94.3)	< 0.001
Blood glucose (mmol/L)	5.8 (5.2-6.7)	6.7 (6.3-7.6)	0.006	5.3 (4.8-5.6)	< 0.001
Creatinine (mmol/L)	89.0 (82.0-110.5)	105.0 (80.5-123.5)	NS	84.5 (76.0-104.0)	0.032
Calcium (mmol/L)	2.3 (2.2-2.5)	2.4 (2.3-2.4)	NS	2.4 (2.3-2.4)	NS
LDH (U/L)	187.5 (152.8-213.5)	196.0 (175.0-232.5)	NS	158.0 (147.3-188.0)	0.004
Cholesterol (U/L)	5.2 (4.9-6.8)	5.4 (4.7-8.4)	NS	6.0 (5.5-6.6)	0.033
Triglycerides (mmol/L)	1.9 (1.1-2.3)	2.4 (1.9-3.1)	0.005	1.3 (1.1-1.6)	< 0.001
Albumin (g/L)	37.8 (32.9-41.0)	36.0 (33.1-39.3)	NS	43.0 (42.0-44.1)	< 0.001
Ghrelin (pg/mL)	1449.5 (1124.5-2398.8)	1646.0 (1010.0-4179.0)	NS	533.5 (368.5-931.5)	< 0.001
CCK (pg/mL)	291.7 (160.9-411.7)	191.0 (142.6-218.5)	NS	153.1 (72.3-262.4)	< 0.001
IL-6 (pg/mL)	7.0 (5.0-18.3)	9.0 (80-11.0)	NS	2.5 (2.0-4.0)	< 0.001
TNF-α (pg/mL)	11.0 (8.0-12.0)	12.0 (10.5-14.5)	NS	6.0 (5.0-7.0)	< 0.001

[1]Mann-Whitney U test (comparison between benign and malignant groups).
[2]Kruskal-Wallis test (comparison between all three groups).
Values are presented as median (Q1-Q3). AST: Aspartate aminotransferase; ALT: Alanine aminotransferase; ALP: Alkaline phosphatase; CRP: C-reactive protein; CCK: Cholecystokinin; ES: Erythrocyte sedimentation rate; GGT: Gamma-glutamyl transferase; LDH: Lactate dehydrogenase; NS: Not significant; IL-6: Interleukin 6; TNF-α: Tumor necrosis factor α.

higher in non-smokers (median 6.3% *vs*. 1.9%, $P = 0.047$).

Ghrelin and CCK concentrations did not differ significantly between malnourished patients and those with normal nutritional status, but significantly higher CCK levels were observed in malnourished patients compared to the control group ($P = 0.017$). Again, TNF-α levels were significantly increased in patients with a high nutritional risk compared to those with normal nutritional status ($P = 0.001$), although both groups had higher TNF-α levels compared to the control group, as stated earlier. Furthermore, the correlation of inflammatory markers and appetite-regulating hormones with various nutritional parameters was analyzed and the results are summarized in Table 3. The data shows that patients with a higher concentrations of TNF-α experienced significantly higher weight loss. Interestingly, patients with higher BMI and adipose tissue values had significantly higher serum CRP concentrations. Likewise, a positive correlation of BMI and adipose tissue was observed with serum IL-6 and CCK concentrations, while a negative correlation existed with serum ghrelin concentration. Again, we could not establish a significant correlation between the levels of tested inflammatory and hormonal markers and appetite, but a negative correlation was observed between appetite and pain level ($r = -0.306$, $P = 0.023$).

Effects of biliary drainage

The tested parameters were repeated after successful biliary drainage and differences across multiple measurements are summarized in Table 4.

As expected, biliary drainage had a positive effect on the reduction of all cholestatic parameters. CRP levels increased significantly 48 h after biliary drainage and resolved to lower than initial values after 28 d. IL-6, TNF-α, and ghrelin concentrations did not significantly change after biliary drainage. CCK

Table 3 Correlation of inflammatory markers and appetite regulating hormones with various nutritional parameters

Spearman's correlation coefficient		CRP (mg/L)	IL-6 (pg/mL)	TNF-α (pg/mL)	Ghrelin (pg/mL)	CCK (pg/mL)
Weight loss (%)	rho	-0.21	0.263	0.438	0.12	0.242
	P	0.124	0.052	0.001	0.385	0.075
BMI (kg/m^2)	rho	0.638	0.31	0.024	-0.342	0.411
	P	0.001	0.021	0.861	0.011	0.002
NRS2002	rho	-0.236	0.193	0.355	-0.057	0.142
	P	0.083	0.157	0.008	0.682	0.302
Adipose tissue (%)	rho	0.313	0.136	0.069	-0.348	0.289
	P	0.02	0.324	0.617	0.009	0.033
Albumin (g/L)	rho	0.002	-0.384	-0.461	-0.024	-0.026
	P	0.987	0.004	0.001	0.861	0.848
Cholesterol (U/L)	rho	-0.162	0.054	-0.212	0.209	0.355
	P	0.238	0.696	0.121	0.125	0.008
Apetite (VAS)	rho	0.047	0.039	0.037	0.027	-0.121
	P	0.733	0.776	0.786	0.847	0.379

CRP: C-reactive protein; IL-6: Interleukin 6; TNF-α: Tumor necrosis factor α; CCK: Cholecystokinin; BMI: Body mass index; NRS: Nutritional risk screening; VAS: Visual analog scale.

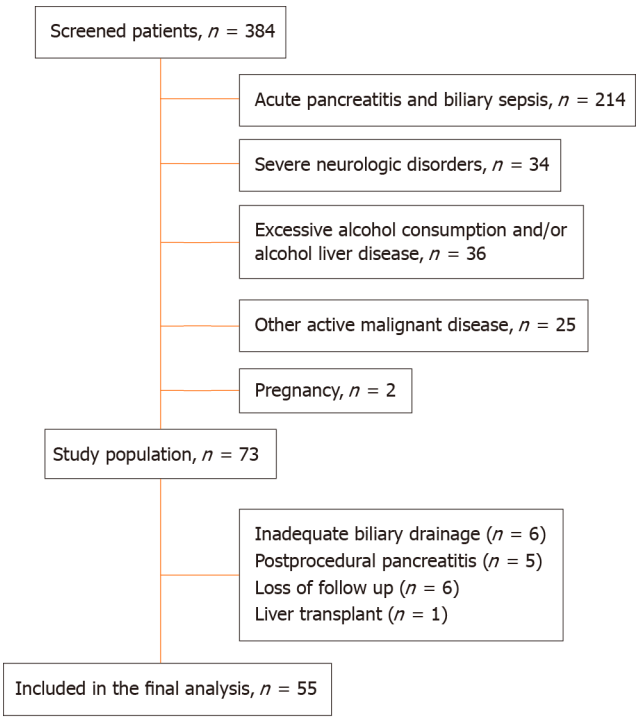

DOI: 10.12998/wjcc.v10.i17.5551 **Copyright** ©The Author(s) 2022.

Figure 1 Study enrollment flowchart.

concentration showed significant dynamics, 48 h after biliary drainage it increased, but after 28 d it dropped to a value which was significantly higher than initial measurement, but lower than the one 48 h after intervention (Figure 2). There was significant improvement in appetite after biliary drainage as well as in relevant nutritional parameters.

Ghrelin levels remained elevated in both patients with and without nutritional risk even 28 d after resolution of biliary obstruction ($P < 0.001$). CCK concentrations also did not show a difference between malnourished patients and those with normal nutritional status, but significantly higher CCK concen-

Table 4 Effects of biliary drainage

	During biliary obstruction (*n* = 55)	48 h after drainage (*n* = 55)	28 d after drainage (*n* = 55)	*P* value[1]
Bilirubin (mmol/L)	145 (63.9-230.7)	88.5 (38.75-190.5)	25 (18.85-38.7)	< 0.001
ALT (U/L)	133 (78-194)	91.5 (63.75-144.25)	30 (23-46.5)	< 0.001
GGT (U/L)	278 (103-421)	194 (103.25-267.25)	36 (28-64)	< 0.001
ALP (U/L)	448 (288.5-612.5)	382.5 (184-606.5)	85 (61-111)	< 0.001
AST (U/L)	284 (260.5-382)	281.5 (231.75-429.25)	123 (103.5-166)	< 0.001
CRP (mg/L)	10.0 (5.8-14.1)	17.9 (5.9-26.8)	8.3 (2.5-17.3)	0.009
IL-6 (pg/mL)	9 (6-13)	11 (7-22)	9 (5-21.5)	0.332
TNF-α (pg/mL)	11 (8.5-13)	10 (9-12)	10 (8-12.5)	0.088
Ghrelin (pg/mL)	1549 (1079.5-2400.5)	1648.5 (1137.25-2767)	1612 (891.5-2962)	0.552
Cholecystokinin (pg/mL)	213.0 (161.0-380.7)	266.0 (203.0-400.5)	235.0 (158.0-433.0)	0.03
Albumin (g/L)	37.1 (33.0-40.8)	35.0 (32.4 -38.0)	38.0 (35.0-42.0)	< 0.001
Appetite (VAS)	4 (2-6)	6 (4-8)	7 (6-9)	< 0.001
BMI (kg/m^2)	24.5 (21.3-28.2)	24.4 (20.6-27.9)	24.9 (21.2-26.8)	< 0.001
Body fat (%)	23 (17-25)	23 (17-24)	23 (19-25)	0.002
NRS 2002	3.0 (2.0-4.0)	3.5 (2.0-4.0)	0.0 (0.0-4.0)	< 0.001

[1]Friedman test across three observations.

Values are presented as median (Q1-Q3); ALT: Alanine aminotransferase; GGT: Gamma-glutamyl transferase; ALP: Alkaline phosphatase; AST: Aspartate aminotransferase; CRP: C-reactive protein; IL-6: Interleukin 6; TNF-α: Tumor necrosis factor α; VAS: Visual analog scale; BMI: Body mass index; NRS: Nutritional risk screening.

trations were now observed in both patient groups compared to the controls. IL-6 and TNF-α concentrations were significantly higher in the serum of malnourished patients, while there were no longer significant differences in TNF-α concentration between the control group and patients with normal nutritional status (Figure 3).

Multivariate analysis

Predictive factors associated with higher nutritional risk were increased TNF-α at the initial measurement [odds ratio (OR): 2.03, 95% confidence interval (CI)] and increased IL-6 and TNF-α concentrations 48 h after biliary drainage (OR: 1.88, 95%CI: 1.12-3.15 and OR: 5.01, 95%CI: 1.19-21.12, respectively). Higher concentration of CCK 28 d after successful biliary drainage significantly reduced the chance of nutritional risk by 1.01 times. The regression model for predicting the influence of ghrelin, CCK, and serum inflammatory markers on appetite did not show statistical significance during the biliary obstruction and 28 d after its resolution. However, 48 h after resolution of the obstruction, higher IL-6 concentration (OR: 1.07, 95%CI: 1.00-1.14, P = 0.043) increased the chance of having better appetite, while higher CCK concentration (OR: 0.99, 95%CI: 0.99-1.00, P = 0.032) and leukocyte count (OR: 0.62, 95%CI: 0.38-0.99, P = 0.045) decreased that chance.

Follow-up

During the follow-up period of 6 mo, eight patients with malignant biliary obstruction died-the cause of death was pneumonia in one patient and pulmonary embolism in three, one patient died within 7 d after hepatectomy, and for three patients the cause of death was unknown. The remaining 47 patients were clinically stable. Patients who died at the time of the initial measurement had greater loss in body weight, lower appetite, higher NRS 2002 scores, and higher concentrations of TNF-α and CRP, and 28 d after biliary drainage, they also had worse NRS 2002 scores and appetite levels, reported higher pain levels, and had higher concentrations of TNF-α and IL-6, as well as lower CCK and albumin concentrations. In a sub-group analysis, in patients with malignant etiology higher concentrations of TNF-α (P = 0.018) and IL-6 (P = 0.003) in initial measurement and after 28 d were significantly correlated with death. We observed significant dynamics in CCK levels across the measurements in the surviving group (P = 0.003), while no changes have been noted for the group with a negative outcome. There were no significant changes in ghrelin levels regardless of the outcome. TNF-α (P = 0.004) levels were higher at initial measurement in the group with a negative clinical outcome, while IL-6 levels did not significantly

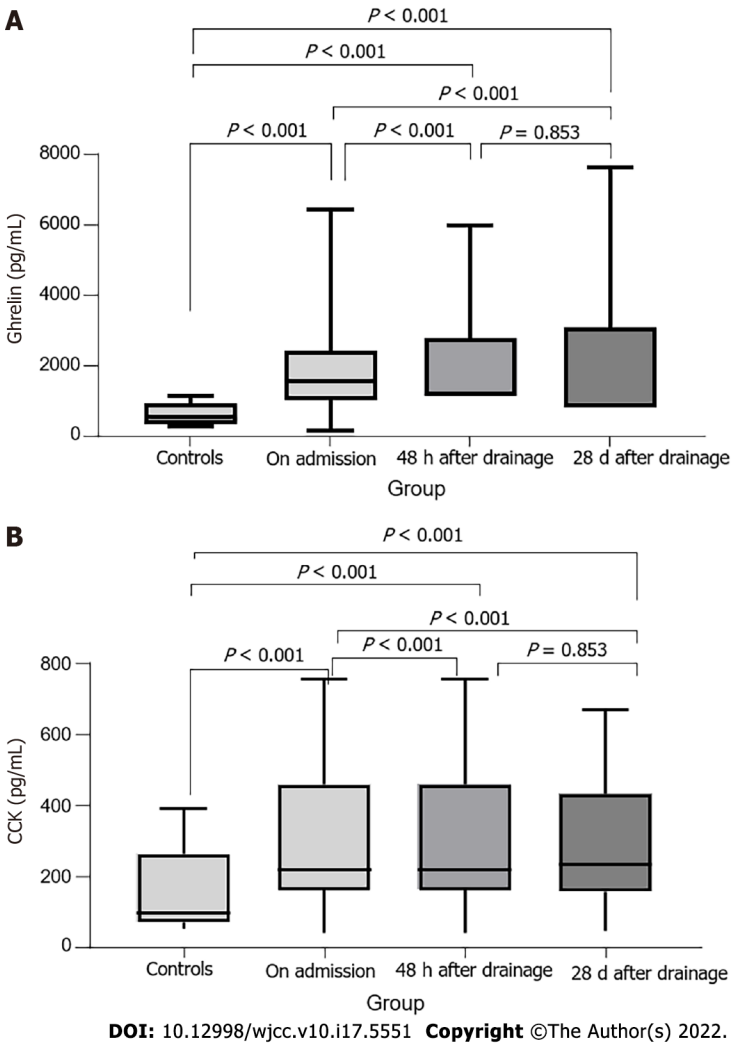

DOI: 10.12998/wjcc.v10.i17.5551 **Copyright** ©The Author(s) 2022.

Figure 2 Appetite regulating hormone dynamics in biliary obstruction. A: Ghrelin levels during and after resolution of biliary obstruction compared to those of the control group; B: Cholecystokinin levels during and after resolution of biliary obstruction compared to those of the control group. CCK: Cholecystokinin.

differ. The percentage of body fat was higher in surviving patients, and it also showed a significant increase across the measurements ($P < 0.001$), while there was no significant dynamic in deceased patients. Surviving patients had better appetite, although both groups showed a significant increase in appetite across measurements.

DISCUSSION

Our results confirmed observations made in previous studies[1,2,4,5] that patients with biliary obstruction, and especially those with malignant etiology, generally have worse nutritional indicators compared to healthy controls. To the best of our knowledge, this is the first study to prove elevated ghrelin concentrations in patients with biliary obstruction. At the same time, CCK concentrations were significantly elevated in malnourished patients compared to controls. There was a positive correlation of CCK with BMI and percentage of body fat, while the same parameters correlated negatively with ghrelin. These results are in accordance with studies suggesting that ghrelin is a clinical marker of catabolism, since elevated ghrelin levels are found in serum of patients with cachexia associated with malignant diseases and chronic kidney failure[28]. Our results also support the theory that circulating ghrelin reflects changes in body weight over a longer period of time and that it could be an adiposity signal[29-31]. Contrary to expectations, in the correlation analysis we found a negative association of biliary obstruction severity with ghrelin concentrations, while no association was found with serum CCK concentration. This confirms the results of Koop and associates that a chronic decrease in the amount of bile in the duodenum does not have an effect on serum CCK concentration[32]. However, in a study by Padillo *et al*[4], which had a similar design to our study, serum bilirubin showed a clear correlation to CCK concentration. Different findings could be partially explained by higher inclusion criterion regarding bilirubin values (> 85 μmol/L compared to > 35μmol/L in our study); their study

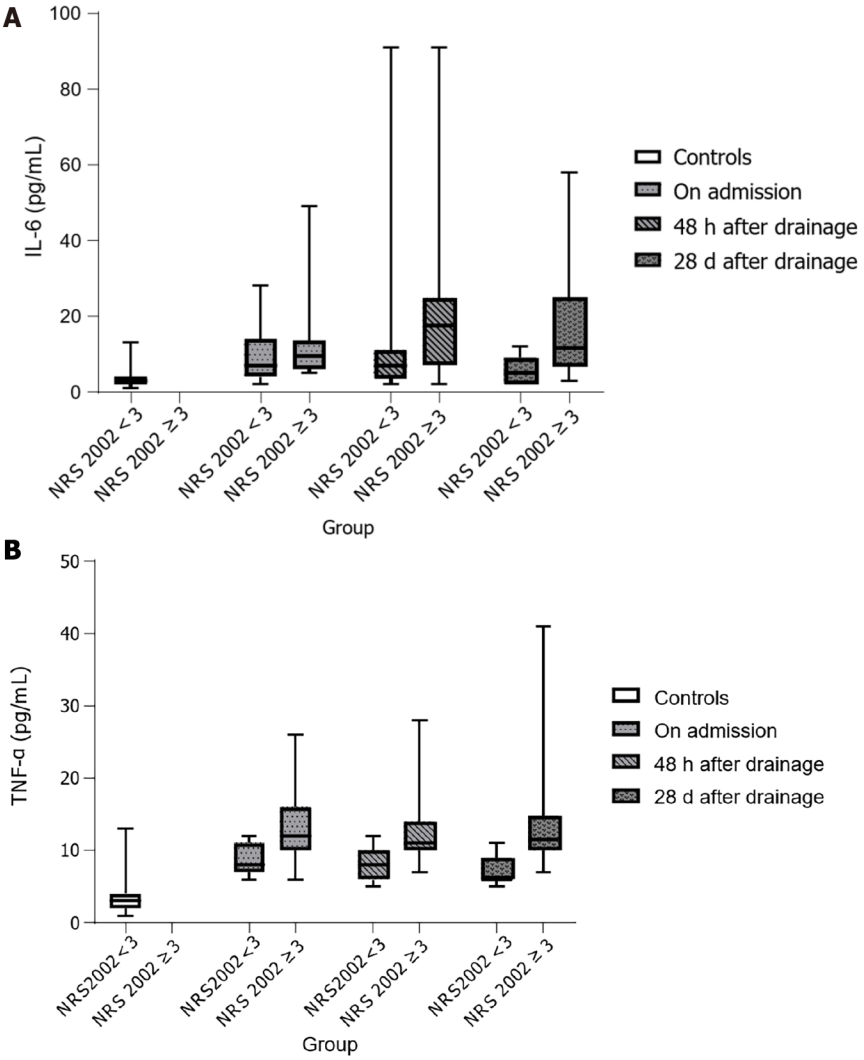

DOI: 10.12998/wjcc.v10.i17.5551 **Copyright** ©The Author(s) 2022.

Figure 3 Differences in inflammatory marker changes depending on nutritional risk. A: Interleukin 6 levels during and after biliary obstruction depending on nutritional status; B: Tumor necrosis factor α levels during and after biliary obstruction depending on nutritional status. TNF-α: Tumor necrosis factor α; NRS: Nutritional risk screening.

also had a higher proportion of patients with pancreatic malignancies who had significantly higher bilirubin concentrations. Our results did show a tendency toward positive correlation between CCK and bilirubin, but this was only borderline significant, so these inconsistent findings might be due to a small sample size along with high variations among subjects.

All tested inflammatory markers, including IL-6, TNF-α, and CRP, were significantly elevated in patients with biliary obstruction. When comparing the etiology of the obstruction, only CRP values were significantly elevated in patients with benign biliary obstruction (P = 0.001), while there was no difference in TNF-α or IL-6 concentrations. However, TNF-α showed a positive correlation with both biliary obstruction severity and nutritional risk. Furthermore, TNF-α proved to be a prognostic factor of malnutrition in a binary logistic model. Interestingly, CRP correlated positively with body mass index and body fat, while simultaneously having a negative correlation with ghrelin. This is another indirect proof of ghrelin as a marker of catabolism and signal of changes in the amount of adipose tissue.

We have not established any significant correlation between appetite and appetite regulating hormones or inflammatory markers. The only two parameters for which we found correlation with appetite were pain level and *H. pylori* colonization. Appetite expectedly correlated negatively with pain intensity. Interestingly, although *H. pylori* colonization was more prevalent among subjects with biliary obstruction compared to the control group, *H. pylori* colonization was associated with better appetite. *H. pylori* colonization did not show correlation with ghrelin concentration. Most studies suggest that *H. pylori* colonization negatively affects ghrelin production and that *H. pylori* eradication leads to an increase in ghrelin levels, appetite and BMI[33-35]. However, a clear mechanism of these effects is not yet understood[36].

Our study showed a positive correlation between age and CCK concentration, but not for ghrelin. We have also found that patients older than 65 years had significantly higher CCK levels, while there was

no difference in ghrelin, IL-6, or TNF-α concentrations. These results are in accordance with previous studies[12,37,38] and indicate that CCK is a potential mediator of anorexia of aging. Appetite level was not significantly different regarding the age of subjects, but older patients had significantly worse nutritional parameters, including loss of body weight, albumin concentration, and percentage of body fat. However, BMI did not significantly differ between older and younger patients, which confirms that it is not a precise tool and should only be used in context with other nutritional parameters[7].

All relevant nutritional parameters expectedly showed significant improvement after resolution of biliary obstruction. Regarding inflammatory factors, only CRP concentration showed significant changes after biliary drainage (first increasing and then decreasing to lower than initial values). A possible explanation for these results is transient asymptomatic bacteremia after ERCP, which, according to some studies, may occur in up to 27% of therapeutic procedures[39,40]. It is important to note that patients who had clinical complications after the procedure were excluded from the analysis. Although IL-6 and TNF-α concentrations did not show significant changes, their concentrations after biliary drainage were higher in malnourished patients and patients with malignant obstruction. Previous studies done in patients with malignant obstruction also have not found significant changes after biliary drainage in IL-6 and TNF-α levels, even after a prolonged follow-up[41,42]. One of the possible explanations for this phenomenon can be found in the study of Rosen *et al*[43] in which they investigated biliary concentration of IL-6 and TNF-α in patients undergoing ERCP; these cytokines have been shown to be sensitive markers of subclinical biliary infection. One can assume that aside from the tumor role in activation of acute-phase reactants, the increased levels of TNF-α and IL-6 might be a host response to contamination and biliary tree infection after loss of Oddi sphincter control due to biliary sphincterotomy.

After resolution of biliary obstruction, both ghrelin and CCK levels were not significantly different between malnourished and patients with normal nutritional status. Higher ghrelin levels persisted after biliary drainage, without changing significantly between the measurements. Ghrelin levels also did not significantly differ regarding the etiology of the obstruction. Contrary to ghrelin, we observed a significant increase in CCK concentration 48 h after intervention, followed by a significant decrease after 28 d. The increase in CCK concentration might be explained by a transient postprocedural bacteremia [40] and subsequent lipopolysaccharide and IL-1 production, which are known stimulators for CCK secretion[44]. Furthermore, we showed that patients with malignant obstruction who died had lower CCK levels initially, and a more pronounced decrease in CCK levels after 28 d compared to patients who survived. The same dynamic was also observed for malnourished patients. Both malnourished and deceased patients had higher IL-6 and TNF-α levels both initially and after 28 d. There is evidence in animal models that prolonged IL-6 secretion leads to a decrease in IL-1 activity through increased secretion of soluble IL-1R[44]. We hypothesize that in patients with advanced malignant disease and malnourishment prolonged inflammation, secretion of IL-6 and TNF-α leads to suppression of CCK secretion, possibly through lower IL-1 activity[44], but this requires further studies. Logistic regression model also showed that higher CCK levels after 28 d reduce chances of malnutrition. Although there was no significant difference in appetite level between the control group and patients with biliary obstruction, we observed a significant increase in appetite levels after a successful biliary drainage. During biliary obstruction and 28 d after its resolution, ghrelin and CCK levels were not predictive of appetite levels. However, higher CCK levels 48 h after biliary drainage were predictive of decreased appetite.

Among other investigated parameters, higher loss of body weight, malnutrition, lower appetite, and lower CRP concentration and higher concentration of TNF-α in serum were associated with negative clinical outcome after 6 mo. Factors correlating with negative outcome after biliary obstruction resolution were higher values of IL-6 and TNF-α, as well as lower CCK concentration, poorer appetite and lower albumin concentrations. This confirms previous findings of lower albumin concentration as a predictor of mortality in hospitalized patients[8].

Ghrelin can have an anti-inflammatory effect by inhibiting the expression of IL-6 and TNF-α in humans[45]. High ghrelin levels possibly represent a compensatory mechanism due to persistent inflammation considering that, along with ghrelin, both TNF-α and IL-6 levels were elevated 28 d after resolution of biliary obstruction. We have demonstrated a correlation between TNF-α and weight loss, as well as increased TNF-α levels in malnourished patients, which is in accordance with previous studies suggesting that TNF-α and IL-6 are mediators of cachexia and increased catabolism[12,46]. Increased plasma ghrelin concentration could therefore reflect a compensatory mechanism for negative energy balance. The fact that appetite level was not increased despite increased plasma ghrelin concentration could suggest ghrelin resistance. Moreover, the increase in appetite after biliary drainage, despite increased TNF-α and IL-6 levels, suggests the existence of additional factors of appetite regulation. Des-acyl ghrelin is a ghrelin isoform that does not activate growth hormone secretagogue receptor-1a, and was previously thought to be a byproduct of ghrelin degradation, but recent research indicates it is a distinct hormone with a wide variety of biological activity. It has been extensively studied in feeding disorders, obesity, and cardiovascular diseases[16,25,47-49]. Although specific pathways are not yet understood, studies suggested that des-acyl ghrelin might exhibit opposite effects to those that of acylated ghrelin in peripheral tissues[16,47,50,51], so measuring des-acyl ghrelin concentration and its relation to acylated ghrelin in future studies might lead to better interpretation of the

results.

Previous research indicated functional antagonism between ghrelin and CCK regarding food intake [52], but their interaction on secretion of both peptides is not well understood. An animal study showed that intraduodenal ghrelin infusion increases CCK concentration[52], and human research indicated that CCK can suppress ghrelin secretion[14,17]. Nonetheless, in our study group, both high CCK and ghrelin concentrations persisted. A previous study showed that application of ghrelin after CCK infusion does not induce feeding and *vice versa*, and CCK application after ghrelin infusion does not reduce food intake[53]. This suggests that the efficacy of ghrelin and CCK signaling depends on their mutual balance. Disruption of that balance, such as that being able to be seen in patients with biliary obstruction, can lead to dysfunction in appetite regulation which, according to our results, can be restored, but through some other mechanisms. This shows that changes in concentrations of appetite regulating hormones and inflammatory factors play only a small part in feeding regulation. More studies are needed to gain a better grasp of underlying mechanisms involved in this complex process.

Limitations of the study

The overall small sample size was a constraint in this study. Despite the initial power analysis, we have observed some differences between patients with malignant and benign etiology of biliary obstruction, but the separate subgroup analysis of the effects of biliary drainage could not be performed due to the lack of power. Unacylated ghrelin was not measured due to the biochemical reagent being unavailable at the time of the study. Since we had very limited data on CCK and ghrelin changes in this specific population, we have decided to increase a follow-up period bearing in mind the results of the only available study (6 d, Padillo *et al*[5]), but our results have shown that even a period of 28 d follow-up was too short to observe the complete dynamics of these hormones following a resolution of biliary obstruction.

CONCLUSION

Patients with biliary obstruction have higher plasma concentrations of ghrelin, as well as increased concentrations of TNF-α, IL-6, and CRP and worse nutritional status. Resolution of biliary obstruction *via* endoscopic drainage leads to improvement in nutritional status and appetite, but levels of ghrelin and CCK remain increased even 28 d after drainage. Biliary drainage has no effect on the dynamics of TNF-α and IL-6 concentrations, with higher levels noted in patients with malignant disease. Concentration of CCK is higher in patients with biliary obstruction and worse nutritional status. Appetite does not correlate with ghrelin, CCK, IL-6, or TNF-α serum concentrations before or after resolution of biliary obstruction. In patients with malignant obstruction, negative clinical outcome after 6 mo is associated with greater loss of body weight, lower appetite levels, and higher TNF-α concentrations.

ARTICLE HIGHLIGHTS

Research background

The basic assumption of this study is based on the observation from everyday clinical practice that obstructive jaundice has a negative effect on the nutritional status of patients regardless of the obstruction etiology. Nutritional parameters play an important role in the treatment outcome of these patients.

Research motivation

Given the conflicting results of a very small number of studies determining the concentrations of appetite-regulating hormones in patients with biliary obstruction and their changes after cholestasis resolution, we considered that it is of scientific interest to investigate key mediators regulating the appetite and nutritional status of patients before and after biliary obstruction resolution.

Research objectives

The research objectives were to determine the levels of ghrelin, cholecystokinin and inflammatory markers in patients with obstructive jaundice, and to analyze their effect on appetite and nutritional status; to investigate the influence of the severity, duration and etiology of biliary obstruction, *Helicobacter pylori* infection and general characteristics of patients on the concentrations of hormones and inflammatory markers and the impact of endoscopic internal biliary drainage on the investigated parameters.

Research methods

This was a prospective case control study performed in a tertiary center in Zagreb, Croatia. Fifty-five

patients (34 with benign and 21 with malignant disease) with biliary obstruction undergoing internal biliary drainage, along with 40 healthy controls, were enrolled. Appetite, nutritional status, serum ghrelin, cholecystokinin (CCK), interleukin 6 (IL-6), and tumor necrosis factor α (TNF-α) were determined at admission, 48 h and 28 d after internal biliary drainage. Chi square test was used for categorical variables. Continuous variables were analyzed for normality by Kolmogorov–Smirnov test and relevant non-parametric (Mann-Whitney, Kruskal-Wallis, and Friedman) or parametric (t-test and ANOVA) tests were used.

Research results

Plasma ghrelin, IL-6, TNF-α, and C-reactive protein (CRP) were significantly higher in patients with obstructive jaundice. An increase in CCK was observed only in malnourished patients with obstructive jaundice. TNF-α was a predictive factor for malnutrition in obstructive jaundice. After internal biliary drainage, a significant improvement of nutritional status was observed in spite of the fact that concentrations of ghrelin, CCK, IL-6, and TNF-α remained significantly elevated even 28 d after procedure. We have not established any correlation between appetite and serum levels of ghrelin, CCK, IL-6, and TNF-α before and after biliary drainage. Malnutrition, lower appetite, lower serum CRP and higher TNF-α in patients with obstructive jaundice were associated with long-term mortality.

Research conclusions

The efficacy of ghrelin and CCK signaling depends on their mutual balance. Disruption of that balance, such as it that be able to be seen in patients with biliary obstruction, can lead to dysfunction in appetite regulation which, according to our results, can be restored, but through some other mechanisms. This shows that changes in concentrations of appetite regulating hormones and inflammatory factors play only a small part in feeding regulation.

Research perspectives

Changes in the concentration of appetite-regulating hormones and inflammatory markers are only a part of the feeding regulation process, which will certainly continue to be the subject of numerous future studies due to its complexity.

FOOTNOTES

Author contributions: Pavić T contributed to study design and conception and collected the data; Pelajić S, Blažević N, Kralj D, and Mikolasevic I wrote the draft of the manuscript and contributed to data interpretation; Milošević M performed statistical analysis; Lerotic I collected the data; Hrabar D served as scientific advisor and guided the study.

Institutional review board statement: The study was reviewed and approved by the University Hospital Center Sestre Milosrdnice Ethics Committee, No. EP-15584/10.

Conflict-of-interest statement: The authors declare that there is no conflict of interest to disclose.

Data sharing statement: Technical appendix, statistical code, and dataset available from the corresponding author at tajana.pavic@gmail.com.

Open-Access: This article is an open-access article that was selected by an in-house editor and fully peer-reviewed by external reviewers. It is distributed in accordance with the Creative Commons Attribution NonCommercial (CC BY-NC 4.0) license, which permits others to distribute, remix, adapt, build upon this work non-commercially, and license their derivative works on different terms, provided the original work is properly cited and the use is non-commercial. See: https://creativecommons.org/Licenses/by-nc/4.0/

Country/Territory of origin: Croatia

ORCID number: Tajana Pavić 0000-0002-0370-5001; Stipe Pelajić 0000-0001-9668-5064; Nina Blažević 0000-0001-6657-8268; Dominik Kralj 0000-0001-6503-6870; Milan Milošević 0000-0001-9008-7645; Ivana Mikolasevic 0000-0001-9676-0642; Ivan Lerotic 0000-0003-3067-7226; Davor Hrabar 0000-0001-9129-3897.

S-Editor: Guo XR
L-Editor: Wang TQ
P-Editor: Yu HG

REFERENCES

1 **Pavlidis ET**, Pavlidis TE. Pathophysiological consequences of obstructive jaundice and perioperative management.

Hepatobiliary Pancreat Dis Int 2018; **17**: 17-21 [PMID: 29428098 DOI: 10.1016/j.hbpd.2018.01.008]
2 **Boulay BR**, Birg A. Malignant biliary obstruction: From palliation to treatment. *World J Gastrointest Oncol* 2016; **8**: 498-508 [PMID: 27326319 DOI: 10.4251/wjgo.v8.i6.498]
3 **Gondal B**, Aronsohn A. A Systematic Approach to Patients with Jaundice. *Semin Intervent Radiol* 2016; **33**: 253-258 [PMID: 27904243 DOI: 10.1055/s-0036-1592331]
4 **Padillo FJ**, Andicoberry B, Muntane J, Lozano JM, Miño G, Sitges-Serra A, Pera-Madrazo C. Factors predicting nutritional derangements in patients with obstructive jaundice: multivariate analysis. *World J Surg* 2001; **25**: 413-418 [PMID: 11344390 DOI: 10.1007/s002680020043]
5 **Padillo FJ**, Andicoberry B, Pera-Madrazo C, Sitges-Serra A. Anorexia and malnutrition in patients with obstructive jaundice. *Nutrition* 2002; **18**: 987-990 [PMID: 12431722 DOI: 10.1016/s0899-9007(02)00982-6]
6 **La Torre M**, Ziparo V, Nigri G, Cavallini M, Balducci G, Ramacciato G. Malnutrition and pancreatic surgery: prevalence and outcomes. *J Surg Oncol* 2013; **107**: 702-708 [PMID: 23280557 DOI: 10.1002/jso.23304]
7 **Pavic T**, Ljubicic N, Stojsavljevic S, Krznaric Z. Nutritional screening model in tertiary medical unit in Croatia. *Ann Nutr Metab* 2012; **61**: 65-69 [PMID: 22831958 DOI: 10.1159/000338967]
8 **Dixon JM**, Armstrong CP, Duffy SW, Davies GC. Factors affecting morbidity and mortality after surgery for obstructive jaundice: a review of 373 patients. *Gut* 1983; **24**: 845-852 [PMID: 6604001 DOI: 10.1136/gut.24.9.845]
9 **Goldwasser P**, Feldman J. Association of serum albumin and mortality risk. *J Clin Epidemiol* 1997; **50**: 693-703 [PMID: 9250267 DOI: 10.1016/s0895-4356(97)00015-2]
10 **Norman K**, Pichard C, Lochs H, Pirlich M. Prognostic impact of disease-related malnutrition. *Clin Nutr* 2008; **27**: 5-15 [PMID: 18061312 DOI: 10.1016/j.clnu.2007.10.007]
11 **Langhans W**, Hrupka B. Interleukins and tumor necrosis factor as inhibitors of food intake. *Neuropeptides* 1999; **33**: 415-424 [PMID: 10657519 DOI: 10.1054/npep.1999.0048]
12 **Patel HJ**, Patel BM. TNF-α and cancer cachexia: Molecular insights and clinical implications. *Life Sci* 2017; **170**: 56-63 [PMID: 27919820 DOI: 10.1016/j.lfs.2016.11.033]
13 **Di Francesco V**, Fantin F, Omizzolo F, Residori L, Bissoli L, Bosello O, Zamboni M. The anorexia of aging. *Dig Dis* 2007; **25**: 129-137 [PMID: 17468548 DOI: 10.1159/000099477]
14 **Degen L**, Drewe J, Piccoli F, Gräni K, Oesch S, Bunea R, D'Amato M, Beglinger C. Effect of CCK-1 receptor blockade on ghrelin and PYY secretion in men. *Am J Physiol Regul Integr Comp Physiol* 2007; **292**: R1391-R1399 [PMID: 17138722 DOI: 10.1152/ajpregu.00734.2006]
15 **Wang HH**, Portincasa P, Wang DQ. Update on the Molecular Mechanisms Underlying the Effect of Cholecystokinin and Cholecystokinin-1 Receptor on the Formation of Cholesterol Gallstones. *Curr Med Chem* 2019; **26**: 3407-3423 [PMID: 28625150 DOI: 10.2174/0929867324666170619104801]
16 **Yanagi S**, Sato T, Kangawa K, Nakazato M. The Homeostatic Force of Ghrelin. *Cell Metab* 2018; **27**: 786-804 [PMID: 29576534 DOI: 10.1016/j.cmet.2018.02.008]
17 **Brennan IM**, Otto B, Feltrin KL, Meyer JH, Horowitz M, Feinle-Bisset C. Intravenous CCK-8, but not GLP-1, suppresses ghrelin and stimulates PYY release in healthy men. *Peptides* 2007; **28**: 607-611 [PMID: 17129639 DOI: 10.1016/j.peptides.2006.10.014]
18 **Steinert RE**, Feinle-Bisset C, Asarian L, Horowitz M, Beglinger C, Geary N. Ghrelin, CCK, GLP-1, and PYY(3-36): Secretory Controls and Physiological Roles in Eating and Glycemia in Health, Obesity, and After RYGB. *Physiol Rev* 2017; **97**: 411-463 [PMID: 28003328 DOI: 10.1152/physrev.00031.2014]
19 **Qu R**, Chen X, Hu J, Fu Y, Peng J, Li Y, Chen J, Li P, Liu L, Cao J, Wang W, Qiu C, Guo L, Vasilev K, Zhou G, Li W, Zhao Y. Ghrelin protects against contact dermatitis and psoriasiform skin inflammation by antagonizing TNF-α/NF-κB signaling pathways. *Sci Rep* 2019; **9**: 1348 [PMID: 30718736 DOI: 10.1038/s41598-018-38174-2]
20 **Himmerich H**, Sheldrick AJ. TNF-alpha and ghrelin: opposite effects on immune system, metabolism and mental health. *Protein Pept Lett* 2010; **17**: 186-196 [PMID: 20214644 DOI: 10.2174/092986610790225941]
21 **Ellacott KL**, Halatchev IG, Cone RD. Interactions between gut peptides and the central melanocortin system in the egulation of energy homeostasis. *Peptides* 2006; **27**: 340-9 [PMID: 16309792 DOI: 10.1016/j.peptides.2005.02.031]
22 **Meyer-Gerspach AC**, Häfliger S, Meili J, Doody A, Rehfeld JF, Drewe J, Beglinger C, Wölnerhanssen B. Effect of L-Tryptophan and L-Leucine on Gut Hormone Secretion, Appetite Feelings and Gastric Emptying Rates in Lean and Non-Diabetic Obese Participants: A Randomized, Double-Blind, Parallel-Group Trial. *PLoS One* 2016; **11**: e0166758 [PMID: 27875537 DOI: 10.1371/journal.pone.0166758]
23 **Pi-Sunyer X**, Kissileff HR, Thornton J, Smith GP. C-terminal octapeptide of cholecystokinin decreases food intake in obese men. *Physiol Behav* 1982; **29**: 627-630 [PMID: 6294699 DOI: 10.1016/0031-9384(82)90230-x]
24 **Wren AM**, Bloom SR. Gut hormones and appetite control. *Gastroenterology* 2007; **132**: 2116-2130 [PMID: 17498507 DOI: 10.1053/j.gastro.2007.03.048]
25 **Wisser AS**, Habbel P, Wiedenmann B, Klapp BF, Mönnikes H, Kobelt P. Interactions of gastrointestinal peptides: ghrelin and its anorexigenic antagonists. *Int J Pept* 2010; **2010** [PMID: 20798884 DOI: 10.1155/2010/817457]
26 **Padillo F**, Rodríguez Mf, Hervas A, Miño G, Sitges-Serra A, Pera-Madrazo C. Nutritional assessment of patients with benign and malignant obstructions of the biliary tract. *Rev Esp Enferm Dig* 1999; **91**: 622-629 [PMID: 10502710]
27 **Kondrup J**, Allison SP, Elia M, Vellas B, Plauth M; Educational and Clinical Practice Committee, European Society of Parenteral and Enteral Nutrition (ESPEN). ESPEN guidelines for nutrition screening 2002. *Clin Nutr* 2003; **22**: 415-421 [PMID: 12880610 DOI: 10.1016/s0261-5614(03)00098-0]
28 **Inui A**. Ghrelin: an orexigenic and somatotrophic signal from the stomach. *Nat Rev Neurosci* 2001; **2**: 551-560 [PMID: 11483998 DOI: 10.1038/35086018]
29 **Al Massadi O**, López M, Tschöp M, Diéguez C, Nogueiras R. Current Understanding of the Hypothalamic Ghrelin Pathways Inducing Appetite and Adiposity. *Trends Neurosci* 2017; **40**: 167-180 [PMID: 28108113 DOI: 10.1016/j.tins.2016.12.003]
30 **Ma X**, Lin L, Yue J, Wu CS, Guo CA, Wang R, Yu KJ, Devaraj S, Murano P, Chen Z, Sun Y. Suppression of Ghrelin

Exacerbates HFCS-Induced Adiposity and Insulin Resistance. *Int J Mol Sci* 2017; **18** [PMID: 28629187 DOI: 10.3390/ijms18061302]

31 **Mihalache L**, Gherasim A, Niţă O, Ungureanu MC, Pădureanu SS, Gavril RS, Arhire LI. Effects of ghrelin in energy balance and body weight homeostasis. *Hormones (Athens)* 2016; **15**: 186-196 [PMID: 27376422 DOI: 10.14310/horm.2002.1672]

32 **Koop I**, Koop H, Gerhardt C, Schafmayer A, Arnold R. Do bile acids exert a negative feedback control of cholecystokinin release? *Scand J Gastroenterol* 1989; **24**: 315-320 [PMID: 2734590 DOI: 10.3109/00365528909093053]

33 **Testerman TL**, Morris J. Beyond the stomach: an updated view of Helicobacter pylori pathogenesis, diagnosis, and treatment. *World J Gastroenterol* 2014; **20**: 12781-12808 [PMID: 25278678 DOI: 10.3748/wjg.v20.i36.12781]

34 **Jeffery PL**, McGuckin MA, Linden SK. Endocrine impact of Helicobacter pylori: focus on ghrelin and ghrelin o-acyltransferase. *World J Gastroenterol* 2011; **17**: 1249-1260 [PMID: 21455323 DOI: 10.3748/wjg.v17.i10.1249]

35 **Cindoruk M**, Yetkin I, Deger SM, Karakan T, Kan E, Unal S. Influence of H pylori on plasma ghrelin in patients without atrophic gastritis. *World J Gastroenterol* 2007; **13**: 1595-1598 [PMID: 17461454 DOI: 10.3748/wjg.v13.i10.1595]

36 **Boltin D**, Niv Y. Ghrelin, Helicobacter pylori and body mass: is there an association? *Isr Med Assoc J* 2012; **14**: 130-132 [PMID: 22693798]

37 **Moss C**, Dhillo WS, Frost G, Hickson M. Gastrointestinal hormones: the regulation of appetite and the anorexia of ageing. *J Hum Nutr Diet* 2012; **25**: 3-15 [PMID: 22118060 DOI: 10.1111/j.1365-277X.2011.01211.x]

38 **Akimoto S**, Miyasaka K. Age-associated changes of appetite-regulating peptides. *Geriatr Gerontol Int* 2010; **10** Suppl 1: S107-S119 [PMID: 20590826 DOI: 10.1111/j.1447-0594.2010.00587.x]

39 **Kullman E**, Borch K, Lindström E, Anséhn S, Ihse I, Anderberg B. Bacteremia following diagnostic and therapeutic ERCP. *Gastrointest Endosc* 1992; **38**: 444-449 [PMID: 1511819 DOI: 10.1016/s0016-5107(92)70474-x]

40 **Kovaleva J**, Peters FT, van der Mei HC, Degener JE. Transmission of infection by flexible gastrointestinal endoscopy and bronchoscopy. *Clin Microbiol Rev* 2013; **26**: 231-254 [PMID: 23554415 DOI: 10.1128/CMR.00085-12]

41 **Ballinger AB**, Woolley JA, Ahmed M, Mulcahy H, Alstead EM, Landon J, Clark ML, Farthing MJ. Persistent systemic inflammatory response after stent insertion in patients with malignant bile duct obstruction. *Gut* 1998; **42**: 555-559 [PMID: 9616320 DOI: 10.1136/gut.42.4.555]

42 **Kimmings AN**, van Deventer SJ, Obertop H, Rauws EA, Huibregtse K, Gouma DJ. Endotoxin, cytokines, and endotoxin binding proteins in obstructive jaundice and after preoperative biliary drainage. *Gut* 2000; **46**: 725-731 [PMID: 10764720 DOI: 10.1136/gut.46.5.725]

43 **Rosen HR**, Winkle PJ, Kendall BJ, Diehl DL. Biliary interleukin-6 and tumor necrosis factor-alpha in patients undergoing endoscopic retrograde cholangiopancreatography. *Dig Dis Sci* 1997; **42**: 1290-1294 [PMID: 9201097 DOI: 10.1023/a:1018822628096]

44 **Cross-Mellor SK**, Kent WD, Ossenkopp KP, Kavaliers M. Differential effects of lipopolysaccharide and cholecystokinin on sucrose intake and palatability. *Am J Physiol* 1999; **277**: R705-R715 [PMID: 10484487 DOI: 10.1152/ajpregu.1999.277.3.R705]

45 **Hattori N**. Expression, regulation and biological actions of growth hormone (GH) and ghrelin in the immune system. *Growth Horm IGF Res* 2009; **19**: 187-197 [PMID: 19144554 DOI: 10.1016/j.ghir.2008.12.001]

46 **Ryan AM**, Power DG, Daly L, Cushen SJ, Ní Bhuachalla Ē, Prado CM. Cancer-associated malnutrition, cachexia and sarcopenia: the skeleton in the hospital closet 40 years later. *Proc Nutr Soc* 2016; **75**: 199-211 [PMID: 26786393 DOI: 10.1017/S002966511500419X]

47 **Nishida T**, Tsubouchi H, Hamada T, Imamura N, Hiyoshi M, Yano K, Kangawa K, Nakazato M, Nanashima A. Plasma desacyl ghrelin-to-acyl ghrelin ratio is a predictor of postoperative complications and prognosis after pancreaticoduodenectomy. *Oncol Lett* 2019; **18**: 4974-4983 [PMID: 31612009 DOI: 10.3892/ol.2019.10821]

48 **Cardoso AL**, Fernandes A, Aguilar-Pimentel JA, de Angelis MH, Guedes JR, Brito MA, Ortolano S, Pani G, Athanasopoulou S, Gonos ES, Schosserer M, Grillari J, Peterson P, Tuna BG, Dogan S, Meyer A, van Os R, Trendelenburg AU. Towards frailty biomarkers: Candidates from genes and pathways regulated in aging and age-related diseases. *Ageing Res Rev* 2018; **47**: 214-277 [PMID: 30071357 DOI: 10.1016/j.arr.2018.07.004]

49 **Stark R**, Santos VV, Geenen B, Cabral A, Dinan T, Bayliss JA, Lockie SH, Reichenbach A, Lemus MB, Perello M, Spencer SJ, Kozicz T, Andrews ZB. Des-Acyl Ghrelin and Ghrelin O-Acyltransferase Regulate Hypothalamic-Pituitary-Adrenal Axis Activation and Anxiety in Response to Acute Stress. *Endocrinology* 2016; **157**: 3946-3957 [PMID: 27490185 DOI: 10.1210/en.2016-1306]

50 **Stengel A**, Goebel M, Wang L, Taché Y. Ghrelin, des-acyl ghrelin and nesfatin-1 in gastric X/A-like cells: role as regulators of food intake and body weight. *Peptides* 2010; **31**: 357-369 [PMID: 19944123 DOI: 10.1016/j.peptides.2009.11.019]

51 **Müller TD**, Nogueiras R, Andermann ML, Andrews ZB, Anker SD, Argente J, Batterham RL, Benoit SC, Bowers CY, Broglio F, Casanueva FF, D'Alessio D, Depoortere I, Geliebter A, Ghigo E, Cole PA, Cowley M, Cummings DE, Dagher A, Diano S, Dickson SL, Diéguez C, Granata R, Grill HJ, Grove K, Habegger KM, Heppner K, Heiman ML, Holsen L, Holst B, Inui A, Jansson JO, Kirchner H, Korbonits M, Laferrère B, LeRoux CW, Lopez M, Morin S, Nakazato M, Nass R, Perez-Tilve D, Pfluger PT, Schwartz TW, Seeley RJ, Sleeman M, Sun Y, Sussel L, Tong J, Thorner MO, van der Lely AJ, van der Ploeg LH, Zigman JM, Kojima M, Kangawa K, Smith RG, Horvath T, Tschöp MH. Ghrelin. *Mol Metab* 2015; **4**: 437-460 [PMID: 26042199 DOI: 10.1016/j.molmet.2015.03.005]

52 **Stengel A**, Taché Y. Interaction between gastric and upper small intestinal hormones in the regulation of hunger and satiety: ghrelin and cholecystokinin take the central stage. *Curr Protein Pept Sci* 2011; **12**: 293-304 [PMID: 21428875 DOI: 10.2174/138920311795906673]

53 **Date Y**, Toshinai K, Koda S, Miyazato M, Shimbara T, Tsuruta T, Niijima A, Kangawa K, Nakazato M. Peripheral interaction of ghrelin with cholecystokinin on feeding regulation. *Endocrinology* 2005; **146**: 3518-3525 [PMID: 15890776 DOI: 10.1210/en.2004-1240]

World Journal of Clinical Cases

Submit a Manuscript: https://www.f6publishing.com

World J Clin Cases 2022 June 16; 10(17): 5566-5576

DOI: 10.12998/wjcc.v10.i17.5566

ISSN 2307-8960 (online)

ORIGINAL ARTICLE

Retrospective Cohort Study

Longitudinal assessment of liver stiffness by transient elastography for chronic hepatitis C patients

Anya Mezina, Arunkumar Krishnan, Tinsay A Woreta, Kevin B Rubenstein, Eric Watson, Po-Hung Chen, Carla Rodriguez-Watson

Specialty type: Gastroenterology and hepatology

Provenance and peer review: Invited article; Externally peer reviewed.

Peer-review model: Single blind

Peer-review report's scientific quality classification

Grade A (Excellent): 0
Grade B (Very good): B
Grade C (Good): 0
Grade D (Fair): 0
Grade E (Poor): 0

P-Reviewer: Kishida Y

Received: August 10, 2021
Peer-review started: August 10, 2021
First decision: November 17, 2021
Revised: December 16, 2021
Accepted: April 21, 2022
Article in press: April 21, 2022
Published online: June 16, 2022

Anya Mezina, Department of Medicine, Johns Hopkins School of Medicine, Baltimore, MD 21287, United States

Arunkumar Krishnan, Tinsay A Woreta, Po-Hung Chen, Division of Gastroenterology and Hepatology, Johns Hopkins School of Medicine, Baltimore, MD 21231, United States

Kevin B Rubenstein, Eric Watson, Carla Rodriguez-Watson, Mid-Atlantic Permanente Research Institute, Kaiser Permanente Mid-Atlantic States, Rockville 20852, United States

Carla Rodriguez-Watson, Department of Health Policy and Management, Bloomberg School of Public Health, Johns Hopkins University, Baltimore, MD 21287, United States

Carla Rodriguez-Watson, Innovation in Medical Evidence Development and Surveillance (IMEDS) Program, Reagan-Udall Foundation for the FDA, Washington, 20036, United States

Corresponding author: Carla Rodriguez-Watson, PhD, Senior Researcher, Mid-Atlantic Permanente Research Institute, Kaiser Permanente Mid-Atlantic States, 2101 E Jefferson Street, Rockville 20852, United States. crodriguezwatson@reaganudall.org

Abstract

BACKGROUND

Liver fibrosis is a common pathway of liver injury and is a feature of most chronic liver diseases. Fibrosis progression varies markedly in patients with hepatitis C virus (HCV). Liver stiffness has been recommended as a parameter of fibrosis progression/regression in patients with HCV.

AIM

To investigate changes in liver stiffness measured by transient elastography (TE) in a large, racially diverse cohort of United States patients with chronic hepatitis C (CHC).

METHODS

We evaluated the differences in liver stiffness between patients treated with direct-acting antiviral (DAA) therapy and untreated patients. Patients had ≥ 2 TE measurements and no prior DAA exposure. We used linear regression to measure the change in liver stiffness between first and last TE in response to treatment, controlling for age, sex, race, diabetes, smoking status, human immunodeficiency

virus status, baseline alanine aminotransferase, and baseline liver stiffness. Separate regression models analyzed the change in liver stiffness as measured by kPa, stratified by cirrhosis status.

RESULTS

Of 813 patients, 419 (52%) initiated DAA treatment. Baseline liver stiffness was 12 kPa in 127 (16%). Median time between first and last TE was 11.7 and 12.7 mo among treated and untreated patients, respectively. There was no significant change in liver stiffness observed over time in either the group initiating DAA treatment (0.016 kPa/month; CI: -0.051, 0.084) or in the untreated group (0.001 kPa/mo; CI: -0.090, 0.092), controlling for covariates. A higher baseline kPa score was independently associated with decreased liver stiffness.

CONCLUSION

DAA treatment was not associated with a differential change in liver stiffness over time in patients with CHC compared to untreated patients.

Key Words: Chronic hepatitis C; Liver stiffness; Cirrhosis; Transient elastography; Direct-acting antiviral therapy

©The Author(s) 2022. Published by Baishideng Publishing Group Inc. All rights reserved.

Core Tip: We evaluated changes in liver stiffness measured by transient elastography (TE) in a large, racially diverse cohort of United States patients with chronic hepatitis C (CHC). We retrospectively evaluated differences in liver stiffness between patients treated with direct-acting antiviral (DAA) therapy and untreated patients. Our study shows a higher baseline kPa score was independently associated with decreased liver stiffness, and that differences in liver stiffness may be observed on serial TE measurements in patients with higher baseline scores, irrespective of treatment effect. DAA treatment was not associated with a differential change in liver stiffness over time in patients with CHC compared to untreated patients.

Citation: Mezina A, Krishnan A, Woreta TA, Rubenstein KB, Watson E, Chen PH, Rodriguez-Watson C. Longitudinal assessment of liver stiffness by transient elastography for chronic hepatitis C patients. *World J Clin Cases* 2022; 10(17): 5566-5576

URL: https://www.wjgnet.com/2307-8960/full/v10/i17/5566.htm

DOI: https://dx.doi.org/10.12998/wjcc.v10.i17.5566

INTRODUCTION

Chronic hepatitis C (CHC) infection, affecting an estimated 71.1 million people worldwide, is a major cause of liver cirrhosis [1,2]. The degree of liver fibrosis is a chief determinant of complications related to end-stage liver disease and is associated with the risk of hepatic decompensation, hepatocellular carcinoma, and mortality[3]. The level of CHC-related hepatic fibrosis is detected through histology by the meta-analysis of histological data in viral hepatitis (METAVIR) scoring system (F0 indicating no fibrosis to F4 indicating cirrhosis)[4]. The temporal evolution of fibrosis in patients with CHC is non-linear, with variable progression observed between different stages of disease specified by METAVIR fibrosis scores[5]. The degree of progression of liver fibrosis is further influenced by variables including age, gender, alcohol consumption, insulin resistance, high body mass index, and co-infection with hepatitis B virus (HBV) or human immunodeficiency virus (HIV)[6-9]. Histological assessment of the liver is considered the optimal approach to evaluate changes in fibrosis over time and remains the gold standard for the diagnosis of cirrhosis[10]. However, reliance on liver biopsy is limited by the intra- and interobserver variability of fibrosis scoring, the sampling variability, and finally, the potential for complications from an invasive procedure, which renders serial histopathological assessments impractical in routine clinical care[11-13].

Transient elastography (TE) has become a widely used, noninvasive ultrasound-based technique to measure liver stiffness and accurately assess severe fibrosis and cirrhosis without the morbidity and mortality associated with liver biopsy. TE is validated in patients with CHC with 89% sensitivity and 91% specificity for the diagnosis of cirrhosis[14]. Achieving sustained virological response (SVR) after treatment of CHC has been shown to reduce the rate of liver fibrosis progression and even partially reverse fibrosis as assessed by histology as well as TE[15-17]. Eradication of HCV is associated with a reduction in all-cause and liver-related mortality and a lower risk of progression to cirrhosis[15,18,19]. However, despite achieving SVR, some patients will develop progressively higher liver stiffness measurements over time, and up to 60% of those with cirrhosis at the time of treatment with direct-

acting antiviral agents (DAA) will continue to exhibit liver stiffness measurements in the cirrhotic range, increasing the risk for hepatic decompensation and adverse clinical outcomes[20-22]. Due to the broad implementation of guideline-directed treatment of CHC, understanding the factors leading to differential changes in liver stiffness will be integral to refining clinical decisions regarding management and surveillance for complications of end-stage liver disease[17,23]. Many studies utilizing TE to evaluate longitudinal changes in liver stiffness have been limited to the duration of DAA therapy or the 12-24 wk post-treatment when SVR is ascertained[24,25-27]. Other studies with long-term follow-up periods have been conducted outside of the United States and may not reflect the same racially diverse patient population and genotypic distribution of HCV, limiting the generalizability of findings[22,28].

The American Gastroenterological Association has recognized the need for large, long-term investigations of outcomes in patients with CHC treated with DAA therapy and indicated that current evidence is insufficient to recommend a universal policy of noninvasive testing of liver fibrosis in successfully treated patients[14,29]. To address this need, we performed a longitudinal, retrospective observational study investigating changes in liver stiffness measured by TE in a racially diverse cohort of United States patients with CHC.

MATERIALS AND METHODS

Study design: We conducted a longitudinal retrospective study of patients with confirmed CHC infection seen at Johns Hopkins Health System (JHHS) and Kaiser Permanente Mid-Atlantic States (KPMAS) between April 1, 2014 and March 31, 2018. JHHS is an academic health system primarily serving Baltimore, MD, and the surrounding area. KPMAS is an integrated healthcare system serving more than 750000 members in a region that includes the District of Columbia, Maryland, and Virginia. The Institutional Review Board approved the study at JHHS and KPMAS.

Study population: Patients at JHHS were identified by querying the electronic health record (EHR) system for the International Classification of Disease, Ninth (ICD-9), or Tenth Revision (ICD-10) diagnosis codes for hepatitis C viral (HCV) infection or a positive HCV RNA test. At KPMAS, HCV patients were identified by positive HCV RNA, HCV genotype, ≥ 2 refills of interferon-based HCV therapy within 1 year, or positive HCV antibody test plus ≥ 1 HCV-coded visit. Included patients were at least 18 years of age, treatment naïve to DAA at the time of the first liver stiffness measurement, and had at least two liver stiffness measurements. Patients were excluded if the date of the first liver stiffness measurement was more than 30 d before the date on which our HCV definition is met. We reason that liver stiffness measurements performed fewer than 30 d before HCV recognition was likely due to clinically suspected HCV, but those performed more than 30 d before were due to other chronic liver conditions. We further excluded any patients found to have an undetectable HCV viral load within 180 d prior to the first liver stiffness measurement indicating clearance of HCV infection. The baseline was defined as the date of the first liver stiffness measurement. Treatment was defined by pharmacy dispensation dates in the EHR. Only those patients initiating treatment between the date of the first and last TE were included in the treatment group. TE results and biochemical, clinical, and demographic characteristics were extracted from the EHR. We collected data on the following: age, sex, race, diabetes, chronic kidney disease (CKD), body mass index (BMI), smoking status, alcohol consumption, HIV status, HBV status, hepatocellular carcinoma, aspartate aminotransferase (AST), alanine aminotransferase (ALT), HCV RNA viral load, bilirubin, platelet count, and TE results. The most proximal laboratory and clinical data were collected from a window that spanned 180 days prior to the baseline TE scan and up to 30 d after.

Liver stiffness measurements: Liver stiffness measurements were obtained using transient elastography (Fibroscan 502, Echosens, Paris, France) by trained operators at JHHS and KPMAS. Participants were instructed to fast for a minimum of 2 h prior to testing. The liver stiffness measurement was considered reliable only if a minimum of 10 successful acquisitions were obtained, with an interquartile range ≤ 30% of the median liver stiffness measurement and success rate ≥ 60%. The success rate was calculated as the ratio of the number of successful acquisitions over the total number of acquisitions. The result was reported as a median of liver stiffness expressed in kilopascals (kPa).

Statistical analysis: All statistical analyses were conducted using R version 3.6.0, Stata version 14 (StataCorp LP., College Station, TX, United States), and SAS version 9.4 (SAS Institute Inc., Cary, NC, United States). Descriptive statistics were computed, including counts and percentages for categorical variables, and either means and standard deviations, medians with quartiles, or medians with minimum and maximum values for continuous variables. A *t*-test was used to compare mean baseline liver stiffness measurements (kPa) between treatment groups. We used multivariable linear regression models to assess the association between treatment and the difference in liver stiffness measurements between first and last TE, adjusting for baseline kPa, and the covariates mentioned above. We included an interaction term between time and treatment to directly compare the change in kPa between treated and untreated subjects. This model can be considered equivalent to one with only the last TE

measurement as the outcome, provided that baseline kPa (also referred to as first TE measurement) is included along with all of the same covariates[30]. The analysis was further stratified by baseline cirrhosis status (kPa ≥ 12). A *P* value < 0.05 was considered statistically significant.

Sensitivity analysis: We found that some patients had two liver stiffness measurements obtained in rapid succession within 7 d of one another. We chose to omit patients with only two measurements taken within 7 d because differences in liver stiffness during a brief time interval are likely to reflect measurement error rather than meaningful physiological changes in the liver. Therefore, as a sensitivity analysis, we repeated all analyses, including patients with liver stiffness measurements taken within 7 d of one another. We will describe results, both including and excluding pairs of liver stiffness measurements taken within 7 d, to assess whether these data impact our conclusions.

RESULTS

Of 813 patients, 84% were at least 50 years of age, 79% were Black, 79% were current or former smokers, 37% were coinfected with HIV, 3% were coinfected with HBV, 19% had diabetes, and 52% initiated treatment with a DAA (Table 1). The median (Q1, Q3) time between first and last liver stiffness measurement was 11.73 (7.41, 17.87) months among those initiating treatment and 12.68 (8.71, 16.94) months among those who were untreated (Table 2). 22% (*n* = 91) of treated subjects had a kPa score ≥ 12, compared with 9% (*n* = 36) of untreated patients. The mean (SD) baseline liver stiffness among treated patients was 10.69 (9.48) kPa, significantly higher compared to the mean (SD) of 7.32 (6.10) kPa among untreated patients (*P* < 0.001). The HCV genotype was genotype 1 in 60% of patients (comprising 91% of patients with known HCV genotype); however, HCV genotype data are not included elsewhere in our analyses because of missing data in 34% of patients. Additionally, due to missing data regarding sustained virologic response (SVR) rates in treated patients, alcohol consumption, and body mass index, these variables were also excluded from the analyses. We also omitted 38 patients (4.7%) who did not have an ALT result up to 180 d before the first liver stiffness measurement, as well as 3 patients (0.4%) with unknown race and 2 patients (0.2%) with unknown smoking status. After excluding these 43 total patients with incomplete information, 770 total patients were included in the regression models. In the multivariable linear regression model examining the change in kPa as the dependent variable, the baseline kPa score was independently associated with a reduction in liver stiffness between the first and last TE (-0.557 kPa; CI: -0.699, -0.415), controlling for age, race (Black, White, or other), sex, HIV status, smoking status, baseline ALT score, and treatment status (Table 3). We observed no significant change in liver stiffness over time among patients who were treated (0.016 kPa/mo; CI: -0.051, 0.084) or untreated (0.001 kPa/mo; CI: -0.090, 0.092); as such, there was no significant difference in the change in liver stiffness among treated patients compared to untreated patients (0.015 kPa/mo, CI: -0.106, 0.136). The difference in the kPa score between the first and last TE, stratified by treatment status, is shown in Figure 1. Next, the analysis was stratified to examine the association of these covariates with liver stiffness in patients with cirrhosis (kPa ≥ 12, *n* = 119) as well as non-cirrhotic patients (kPa < 12, *n* = 651). There was not a significant effect of DAA treatment on the change in liver stiffness over time in either cohort, and the difference in liver stiffness between treated and untreated patients was similar. A higher baseline kPa was an independent predictor of a reduction in liver stiffness measurement in both groups. Among patients without cirrhosis, age ≥ 50 was independently associated with increased liver stiffness (0.949 kPa; CI: 0.336, 1.563).

Sensitivity analysis results: We repeated the analyses described above with the inclusion of patients who had two liver stiffness measurements obtained within 7 d (*n* = 7). We did not observe a significant change over time in liver stiffness in the treated (0.017 kPa/mo; CI: -0.051, 0.086) or untreated patients (-0.027 kPa/mo; CI: -0.120, 0.066), and the rate of change was not different when comparing treated and untreated patients. Results stratified by cirrhosis status (kPa < 12 and kPa ≥ 12) were similar to the original analysis (Supplementary Table 1 and Supplementary Figure 1). Estimates for all other covariates yielded qualitatively comparable results to the main analysis.

DISCUSSION

The widespread application of TE as a noninvasive tool to estimate liver stiffness in patients with CHC has raised important questions regarding the clinical benefit of repeating TE following DAA treatment and the evolution of fibrosis on post-treatment measurements. Our retrospective longitudinal cohort study employed TE to investigate changes in liver stiffness over time in a large, racially diverse patient population with CHC infection and assess treatment response.

In our multivariable regression models, we compared the rate of change of liver stiffness over time between DAA-treated and untreated subjects, controlling for race, age, gender, diabetes, smoking status, HIV co-infection, baseline ALT, and baseline kPa that may be independently associated with liver

Table 1 Demographic and clinical variables in patients with chronic hepatitis C stratified by treatment status (*n* = 813)

Variables	HCV treated (*n* = 419 (51.5%)]	HCV untreated [*n* = 394 (48.5%)]
Age (yr) [mean (SD)]	56.54 (8.26)	56.14 (9.02)
Male sex [*n* (%)]	285 (68.02)	234 (59.39)
Race [*n* (%)]		
Black	339 (80.91)	303 (77.49)
Other	18 (4.30)	20 (5.12)
White	62 (14.80)	68 (17.39)
Smoking history		
Non-smoker	70 (16.71)	98 (25.00)
Current smoker	216 (51.55)	183 (46.68)
Former smoker	133 (31.74)	111 (28.32)
Co-infections [*n* (%)]		
HIV	184 (43.91)	113 (28.68)
HBV	9 (2.15)	15 (3.81)
HCV RNA at baseline, IU/mL [median (Q1, Q3)]	2220000 (803000, 6606934)	2340000 (693015, 5924209)
Biochemistry		
AST, IU/L, mean (SD)	57.91 (44.75)	46.38 (31.13)
ALT, IU/L, mean (SD)	56.63 (51.54)	51.52 (59.04)
Bilirubin < 2 mg/dL [*n* (%)]	393 (97.52)	359 (98.09)
Platelets, K/uL, median (Q1, Q3)	196.00 (155.50, 238.00)	209.00 (170.50, 255.00)
Hepatocellular carcinoma [*n* (%)]	4 (0.95)	2 (0.51)
Baseline diabetes [*n* (%)]	82 (19.57)	73 (18.53)
Baseline chronic kidney disease [*n* (%)]	41 (9.79)	26 (6.60)

HCV: Hepatitis C virus; AST: Aspartate aminotransferase; ALT: Alanine aminotransferase; HBV: Hepatitis B virus; HIV: human immunodeficiency virus.

Table 2 Transient elastography characteristics in patients with chronic hepatitis C according to treatment status

Variables	HCV treated (*n* = 419)	HCV untreated (*n* = 394)
Baseline liver stiffness (kPa) [mean (SD); range]	10.69 (9.48); 1.30-75.00	7.32 (6.10); 0.00-75.00
Change in kPa score [mean (SD)]	-2.78 (7.10)	0.51 (5.14)
Months between first and last TE [median (Q1, Q3)]	11.73 (7.41, 17.87)	12.68 (8.71, 16.94)
Months between first TE and DAA start [median (Q1, Q3)]	1.64 (0.95, 3.84)	–
Months between DAA end and last TE [median (Q1, Q3)]	4.17 (3.07, 10.96)	–

DAA: Direct-acting antiviral therapy; kPa: kilopascals; TE: Transient elastography

fibrosis. Interestingly, estimated liver stiffness as measured in kPa did not improve over a median of 11.7 mo among patients treated with DAA therapy. There was no significant difference in the change in liver stiffness between treated and untreated patients when stratifying patients based on underlying cirrhosis. Patients with longer times between TE measurements did not exhibit more pronounced differences in liver stiffness.

Our findings were unexpected due to abundant clinical evidence that initiation of antiviral treatment is associated with rapid improvement in liver stiffness scores as well as long-term attenuation of liver fibrosis in patients who achieve SVR[17]. It is possible that our study was underpowered to detect a

Table 3 Variables associated with the change in liver stiffness measurements in patients with chronic hepatitis C stratified by baseline kilopascals score

	All patients (*n* = 770)			Baseline kPa < 12 (*n* = 651)			Baseline kPa ≥ 12 (*n* = 119)		
Variables	**Effect estimate**	**95%CI**	***P***	**Effect estimate**	**95%CI**	***P* value**	**Effect estimate**	**95%CI**	***P* value**
Antiviral treatment effect	-1.821	(-3.452, -0.191)	0.029	-1.487	(-2.820, -0.154)	0.029	-2.071	(-7.477, 3.335)	0.453
Baseline kPa	-0.557	(-0.699, -0.415)	< 0.001	-0.677	(-0.875, -0.480)	< 0.001	-0.600	(-0.818, -0.383)	< 0.001
Black race[1]	-0.797	(-1.775, 0.181)	0.110	-0.654	(-1.362, 0.054)	0.070	-2.747	(-7.304, 1.810)	0.237
Other race[1]	-0.497	(-1.901, 0.907)	0.488	-0.687	(-1.893, 0.520)	0.264	1.071	(-6.423, 8.566)	0.779
Age ≥ 50[2]	0.663	(-0.165, 1.490)	0.117	0.949	(0.336, 1.563)	0.002	-0.204	(-4.089, 3.682)	0.918
Female gender	-0.210	(-0.843, 0.424)	0.517	-0.269	(-0.772, 0.235)	0.295	0.383	(-3.330, 4.096)	0.840
Diabetes	0.758	(-0.189, 1.705)	0.117	0.751	(-0.097, 1.599)	0.082	1.721	(-2.034, 5.475)	0.369
Current smoker	0.617	(-0.390, 1.624)	0.230	0.199	(-0.467, 0.865)	0.558	2.266	(-3.371, 7.903)	0.431
Former smoker	-0.258	(-1.155, 0.638)	0.572	-0.236	(-0.867, 0.395)	0.464	-0.554	(-6.741, 5.633)	0.861
HIV co-infected	0.468	(-0.230, 1.166)	0.189	0.254	(-0.286, 0.794)	0.356	2.040	(-1.292, 5.372)	0.230
Baseline ALT (per 10 units)	0.023	(-0.043, 0.089)	0.499	0.018	(-0.039, 0.075)	0.532	0.060	(-0.250, 0.370)	0.705
Time between first and last TE (untreated group) (mo)	0.001	(-0.090, 0.092)	0.975	-0.012	(-0.103, 0.078)	0.787	0.129	(-0.229, 0.488)	0.480
Time between first and last TE (treated group) (mo)[3]	0.016	(-0.051, 0.084)	0.634	0.008	(-0.044, 0.059)	0.772	0.004	(-0.215, 0.223)	0.972
Interaction of treatment and time	0.015	(-0.106, 0.136)	0.807	0.020	(-0.086, 0.126)	0.711	-0.125	(-0.523, 0.273)	0.537
Intercept	4.146	(2.365, 5.927)	< 0.001	4.781	(2.478, 7.084)	< 0.001	5.852	(-0.994, 12.698)	0.094

kPa: kilopascals; ALT: Alanine aminotransferase; TE: Transient elastography; HIV: Human immunodeficiency virus;
[1]Effect of race estimated relative to white race as a reference.
[2]Reference ages 18-49.
[3]Estimated effect of time between first and last TE (treated group) is not directly included as a covariate in the model. Estimates for this row are derived from the antiviral treatment, time between first and last TE, and interaction terms.

change in liver stiffness during a median follow-up time period of 4.2 mo after treatment. Since liver stiffness measurements were not always available at the initiation of DAA therapy, the effect of treatment may have been underestimated due to the inclusion of a median of 1.6 mo of untreated time in the treated group. Our study may have been underpowered to detect a modest effect of treatment on cirrhosis regression, as the analysis subsumed only 119 patients with cirrhosis at baseline. The apparent lack of improvement in hepatic stiffness among treated patients may be due to continued liver injury from other, potentially modifiable causes, including non-alcoholic fatty liver disease, alcohol use and drug use, which were not fully captured in our dataset. Despite successful treatment, a subset of patients cured of CHC, particularly those with advanced fibrosis at baseline, will exhibit a progression of liver fibrosis and are at risk of developing adverse liver-related outcomes[21,31]. Although we did not capture clinical data indicative of portal hypertension or decompensated cirrhosis in our study population, it has been postulated that decompensated cirrhosis represents an irreversible threshold that precludes regression to a noncirrhotic state[31,32].

In all analyses, higher baseline liver stiffness was independently associated with a reduction in kPa measurements between first and last TE, which is consistent with results from other investigations. In one systematic review and meta-analysis by Singh *et al*[17] of studies examining liver stiffness measurements after antiviral therapy, a greater absolute decrease in stiffness over time was observed

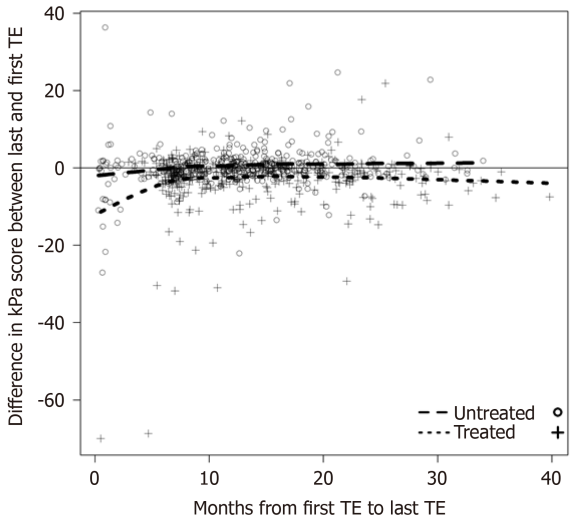

DOI: 10.12998/wjcc.v10.i17.5566 **Copyright** ©The Author(s) 2022.

Figure 1 Change in liver stiffness between first and last transient elastography measurement in patients with chronic hepatitis C infection. Scatter plot illustrating the difference in liver stiffness (kPa) between the first and last transient elastography measurement for patients who were treated (*n* = 405) and not treated (*n* = 365) with direct-acting antiviral therapy for chronic hepatitis C infection during the study period. Circles correspond to values for individual patients. kPa: Kilopascals; TE: Transient elastography.

among studies that included a larger proportion of patients with advanced fibrosis and cirrhosis at baseline. We found that antiviral treatment status was associated with a decline in kPa when analyzing the entire study population as well as patients without baseline cirrhosis. However, this estimated effect of treatment was independent of time, therefore, this does not represent the incremental decrease in stiffness that may be expected in successfully treated patients, and may instead reflect another confounder in our population. We cannot rule out the possibility that this observed decline in kPa is an artifact of regression towards the mean[33,34]. If there is random variability in the measurement of liver stiffness, then misclassifying patients with cirrhosis based on high baseline liver stiffness may result in observed declines in subsequent stiffness measurements that do not reflect a biological change in the liver[34,35]. We further found that treated patients have significantly higher baseline liver stiffness than untreated patients on average, which may make this effect stronger in the treated group than the untreated group. We included baseline kPa in our models to mitigate the impact of regression to the mean on the change over time in liver stiffness, but we cannot be certain that we have entirely accounted for this effect[35].

Based on our eligibility criteria, we identified 7 subjects who underwent serial TE measurements within 7 d or fewer. We performed a sensitivity analysis to investigate a potential bias introduced by our decision to exclude these subjects from the main analysis, based on the hypothesis that changes in liver stiffness observed in a short time period would be more likely to reflect measurement error than changes in inflammation or fibrosis due to DAA treatment. The sensitivity analysis demonstrated that DAA treatment did not significantly change liver stiffness when comparing treated *vs* untreated patients.

We found that age ≥ 50 was independently associated with increased liver stiffness, consistent with the natural history of fibrosis progression in CHC infection[36]. Baseline pre-treatment ALT levels were not predictive of a change in liver stiffness. However, other reports have identified a positive relationship between elevated ALT levels and improvement in liver stiffness over time as measured by TE, which may be partially due to a decline in necroinflammation[25,37].

Limitations of our study include missing data regarding SVR rates in patients initiating treatment with DAA. Although reported SVR rates are greater than 95% with DAA combinations, this approximation may dilute the effect of treatment on liver stiffness measurements in our study[38]. We were unable to assess the relationship between DAA treatment and liver-related outcomes in our cohort as these data were not collected as part of our study, however, achieving SVR has been demonstrated to lower the risk of liver-related morbidity and mortality[19,36,37].

The results from our study contribute to the clinical evidence regarding the real-world utility of post-treatment evaluation for fibrosis regression using TE[14,39]. We found that differences in liver stiffness may be observed on serial TE measurements in patients with higher baseline scores, irrespective of treatment effect, which suggests that false positive results on TE are not uncommon in clinical practice. The Baveno VI Consensus criteria includes a weak recommendation for obtaining two fasting TE measurements for patients undergoing screening for compensated advanced chronic liver disease[40]. Since liver stiffness measurements may be taken into account by both clinicians and patients as part of the decision to pursue a liver biopsy for definitive histopathologic assessment, and may impact clinical

management with respect to variceal bleeding surveillance, we advocate that a repeat confirmatory TE measurement should be considered for patients with an elevated kPa without other clinical or radiographic signs of advanced fibrosis.

CONCLUSION

Our study underscores the imperfect characteristics of TE for the assessment of liver fibrosis and cirrhosis, compared with the gold standard metrics of hepatic venous pressure gradient measurement and liver histopathology, despite the impetus to avoid invasive testing as part of routine clinical care of patients with CHC[41]. Ultimately, the question remains whether a decline in liver stiffness measurements after successful treatment with DAA is correlated with a reduced risk of liver-related complications, particularly among patients with advanced liver disease at baseline. Further long-term prospective studies must be performed to better understand the clinical utility of obtaining TE measurements in patients with CHC who have achieved SVR and to evaluate liver fibrosis progression in diverse populations, with incorporation of histological, hemodynamic, and clinical data on liver-related outcomes.

ARTICLE HIGHLIGHTS

Research background

Liver fibrosis is a common pathway of liver injury and is a feature of most chronic liver diseases. Fibrosis progression varies markedly in patients with hepatitis C virus (HCV), and the severity of liver fibrosis is associated with the prognosis of liver disease. Liver stiffness has been recommended as a parameter of fibrosis progression/regression in patients with HCV.

Research motivation

To investigate the changes in liver stiffness measured by transient elastography (TE) in a large, racially diverse cohort of U.S. patients with chronic hepatitis C (CHC).

Research objectives

We evaluated the differences in liver stiffness between patients treated with direct-acting antiviral (DAA) therapy and untreated patients. In addition, we performed a longitudinal, retrospective observational study investigating changes in liver stiffness measured by TE in a racially diverse cohort of United States patients with CHC.

Research methods

We conducted a longitudinal retrospective study of patients with confirmed CHC infection seen at Johns Hopkins Health System (JHHS) and Kaiser Permanente Mid-Atlantic States (KPMAS). Patients had ≥ 2 TE measurements and no prior DAA exposure. We used linear regression to measure the change in liver stiffness between first and last TE in response to treatment, controlling for age, sex, race, diabetes, smoking status, HIV status, baseline ALT, and baseline liver stiffness.

Research results

Of 813 patients, 84% were at least 50 years of age, 79% were Black, 79% were current or former smokers, 37% were coinfected with HIV, 3% were coinfected with HBV, 19% had diabetes, and 52% initiated treatment with a DAA. The median time between first and last TE was 11.7 and 12.7 mo among treated and untreated patients, respectively. There was no significant change in liver stiffness observed over time in either the group initiating DAA treatment (0.016 kPa/month; CI: -0.051, 0.084) or in the untreated group (0.001 kPa/month; CI: -0.090, 0.092), controlling for covariates. A higher baseline kPa score was independently associated with decreased liver stiffness.

Research conclusions

DAA treatment was not associated with a differential change in liver stiffness over time, as measured by TE, in patients with CHC compared to untreated patients. Our study underscores the imperfect characteristics of any single noninvasive test for assessing liver fibrosis, which continues to be compared to the gold standard of liver biopsy and histopathology, despite the impetus to avoid invasive testing for CHC infection in clinical practice.

Research perspectives

Direct-acting antiviral therapy was not associated with a differential change in liver stiffness over time in patients with CHC compared to untreated patients. Further longitudinal prospective studies are

needed to evaluate the clinical utility of obtaining TE measurements in patients with CHC who have achieved sustained virologic response and assess liver fibrosis progression in diverse populations.

FOOTNOTES

Author contributions: Tinsay A Woreta and Po-Hung Chen conceptualized the study; Anya Mezina, Tinsay A Woreta and Po-Hung Chen investigated the study; Anya Mezina, Tinsay A Woreta, Kevin B Rubenstein Po-Hung Chen and Carla Rodriguez-Watson did the methodology; Anya Mezina did the writing - original draft; Arunkumar Krishnan, Tinsay A Woreta, Kevin B Rubenstein Po-Hung Chen and Carla Rodriguez-Watson did the writing-review and editing; Kevin B Rubenstein did the software and visualization; Tinsay A Woreta and Eric Watson did the data curation; Arunkumar Krishnan did the validation.

Supported by the National Center for Advancing Translational Sciences, No. 5KL2TR001077-05 (to Po-Hung Chen).

Institutional review board statement: The study was reviewed and approved for publication by the Institutional Review Board of Johns Hopkins Medicine and Kaiser Permanente Mid-Atlantic States.

Informed consent statement: The need for informed consent was waived due to the retrospective nature of the study.

Conflict-of-interest statement: All the Authors have no conflict of interest related to the manuscript.

Data sharing statement: No additional data are available.

Open-Access: This article is an open-access article that was selected by an in-house editor and fully peer-reviewed by external reviewers. It is distributed in accordance with the Creative Commons Attribution NonCommercial (CC BY-NC 4.0) license, which permits others to distribute, remix, adapt, build upon this work non-commercially, and license their derivative works on different terms, provided the original work is properly cited and the use is non-commercial. See: https://creativecommons.org/Licenses/by-nc/4.0/

Country/Territory of origin: United States

ORCID number: Anya Mezina 0000-0002-1515-4358; Arunkumar Krishnan 0000-0002-9452-7377; Tinsay A Woreta 0000-0001-7292-4518; Kevin B Rubenstein 0000-0003-3516-5932; Eric Watson 0000-0002-1917-2748; Po-Hung Chen 0000-0002-9865-1009; Carla Rodriguez-Watson 0000-0003-4898-1613.

S-Editor: Xing YX
L-Editor: A
P-Editor: Xing YX

REFERENCES

1 **Perz JF**, Armstrong GL, Farrington LA, Hutin YJ, Bell BP. The contributions of hepatitis B virus and hepatitis C virus infections to cirrhosis and primary liver cancer worldwide. *J Hepatol* 2006; **45**: 529-538 [PMID: 16879891 DOI: 10.1016/j.jhep.2006.05.013]
2 **Polaris Observatory HCV Collaborators**. Global prevalence and genotype distribution of hepatitis C virus infection in 2015: a modelling study. *Lancet Gastroenterol Hepatol* 2017; **2**: 161-176 [PMID: 28404132 DOI: 10.1016/S2468-1253(16)30181-9]
3 **Singh S**, Fujii LL, Murad MH, Wang Z, Asrani SK, Ehman RL, Kamath PS, Talwalkar JA. Liver stiffness is associated with risk of decompensation, liver cancer, and death in patients with chronic liver diseases: a systematic review and meta-analysis. *Clin Gastroenterol Hepatol* 2013; **11**: 1573-84.e1 [PMID: 23954643 DOI: 10.1016/j.cgh.2013.07.034]
4 **Bedossa P**, Poynard T. An algorithm for the grading of activity in chronic hepatitis C. The METAVIR Cooperative Study Group. *Hepatology* 1996; **24**: 289-293 [PMID: 8690394 DOI: 10.1002/hep.510240201]
5 **Thein HH**, Yi Q, Dore GJ, Krahn MD. Estimation of stage-specific fibrosis progression rates in chronic hepatitis C virus infection: a meta-analysis and meta-regression. *Hepatology* 2008; **48**: 418-431 [PMID: 18563841 DOI: 10.1002/hep.22375]
6 **Marcellin P**, Asselah T, Boyer N. Fibrosis and disease progression in hepatitis C. *Hepatology* 2002; **36**: S47-S56 [PMID: 12407576 DOI: 10.1053/jhep.2002.36993]
7 **Hoefs JC**, Shiffman ML, Goodman ZD, Kleiner DE, Dienstag JL, Stoddard AM; HALT-C Trial Group. Rate of progression of hepatic fibrosis in patients with chronic hepatitis C: results from the HALT-C Trial. *Gastroenterology* 2011; **141**: 900-908.e1 [PMID: 21699796 DOI: 10.1053/j.gastro.2011.06.007]
8 **Konerman MA**, Mehta SH, Sutcliffe CG, Vu T, Higgins Y, Torbenson MS, Moore RD, Thomas DL, Sulkowski MS. Fibrosis progression in human immunodeficiency virus/hepatitis C virus coinfected adults: prospective analysis of 435 liver biopsy pairs. *Hepatology* 2014; **59**: 767-775 [PMID: 24436062 DOI: 10.1002/hep.26741]
9 **Patel S**, Jinjuvadia R, Patel R, Liangpunsakul S. Insulin Resistance is Associated With Significant Liver Fibrosis in Chronic Hepatitis C Patients: A Systemic Review and Meta-Analysis. *J Clin Gastroenterol* 2016; **50**: 80-84 [PMID: 26302498 DOI: 10.1097/MCG.0000000000000400]

10 **McHutchison J**, Poynard T, Afdhal N. Fibrosis as an end point for clinical trials in liver disease: a report of the international fibrosis group. *Clin Gastroenterol Hepatol* 2006; **4**: 1214-1220 [PMID: 16979947 DOI: 10.1016/j.cgh.2006.07.006]

11 **Maharaj B**, Maharaj RJ, Leary WP, Cooppan RM, Naran AD, Pirie D, Pudifin DJ. Sampling variability and its influence on the diagnostic yield of percutaneous needle biopsy of the liver. *Lancet* 1986; **1**: 523-525 [PMID: 2869260 DOI: 10.1016/s0140-6736(86)90883-4]

12 **Regev A**, Berho M, Jeffers LJ, Milikowski C, Molina EG, Pyrsopoulos NT, Feng ZZ, Reddy KR, Schiff ER. Sampling error and intraobserver variation in liver biopsy in patients with chronic HCV infection. *Am J Gastroenterol* 2002; **97**: 2614-2618 [PMID: 12385448 DOI: 10.1111/j.1572-0241.2002.06038.x]

13 **Colloredo G**, Guido M, Sonzogni A, Leandro G. Impact of liver biopsy size on histological evaluation of chronic viral hepatitis: the smaller the sample, the milder the disease. *J Hepatol* 2003; **39**: 239-244 [PMID: 12873821 DOI: 10.1016/s0168-8278(03)00191-0]

14 **Lim JK**, Flamm SL, Singh S, Falck-Ytter YT; Clinical Guidelines Committee of the American Gastroenterological Association. American Gastroenterological Association Institute Guideline on the Role of Elastography in the Evaluation of Liver Fibrosis. *Gastroenterology* 2017; **152**: 1536-1543 [PMID: 28442119 DOI: 10.1053/j.gastro.2017.03.017]

15 **Poynard T**, McHutchison J, Manns M, Trepo C, Lindsay K, Goodman Z, Ling MH, Albrecht J. Impact of pegylated interferon alfa-2b and ribavirin on liver fibrosis in patients with chronic hepatitis C. *Gastroenterology* 2002; **122**: 1303-1313 [PMID: 11984517 DOI: 10.1053/gast.2002.33023]

16 **D'Ambrosio R**, Aghemo A, Fraquelli M, Rumi MG, Donato MF, Paradis V, Bedossa P, Colombo M. The diagnostic accuracy of Fibroscan for cirrhosis is influenced by liver morphometry in HCV patients with a sustained virological response. *J Hepatol* 2013; **59**: 251-256 [PMID: 23528378 DOI: 10.1016/j.jhep.2013.03.013]

17 **Singh S**, Facciorusso A, Loomba R, Falck-Ytter YT. Magnitude and Kinetics of Decrease in Liver Stiffness After Antiviral Therapy in Patients With Chronic Hepatitis C: A Systematic Review and Meta-analysis. *Clin Gastroenterol Hepatol* 2018; **16**: 27-38.e4 [PMID: 28479504 DOI: 10.1016/j.cgh.2017.04.038]

18 **Singal AG**, Volk ML, Jensen D, Di Bisceglie AM, Schoenfeld PS. A sustained viral response is associated with reduced liver-related morbidity and mortality in patients with hepatitis C virus. *Clin Gastroenterol Hepatol* 2010; **8**: 280-288, 288.e1 [PMID: 19948249 DOI: 10.1016/j.cgh.2009.11.018]

19 **Backus LI**, Boothroyd DB, Phillips BR, Belperio P, Halloran J, Mole LA. A sustained virologic response reduces risk of all-cause mortality in patients with hepatitis C. *Clin Gastroenterol Hepatol* 2011; **9**: 509-516.e1 [PMID: 21397729 DOI: 10.1016/j.cgh.2011.03.004]

20 **Chekuri S**, Nickerson J, Bichoupan K, Sefcik R, Doobay K, Chang S, DelBello D, Harty A, Dieterich DT, Perumalswami PV, Branch AD. Liver Stiffness Decreases Rapidly in Response to Successful Hepatitis C Treatment and Then Plateaus. *PLoS One* 2016; **11**: e0159413 [PMID: 27442255 DOI: 10.1371/journal.pone.0159413]

21 **van der Meer AJ**, Feld JJ, Hofer H, Almasio PL, Calvaruso V, Fernández-Rodríguez CM, Aleman S, Ganne-Carrié N, D'Ambrosio R, Pol S, Trapero-Marugan M, Maan R, Moreno-Otero R, Mallet V, Hultcrantz R, Weiland O, Rutter K, Di Marco V, Alonso S, Bruno S, Colombo M, de Knegt RJ, Veldt BJ, Hansen BE, Janssen HLA. Risk of cirrhosis-related complications in patients with advanced fibrosis following hepatitis C virus eradication. *J Hepatol* 2017; **66**: 485-493 [PMID: 27780714 DOI: 10.1016/j.jhep.2016.10.017]

22 **Pietsch V**, Deterding K, Attia D, Ringe KI, Heidrich B, Cornberg M, Gebel M, Manns MP, Wedemeyer H, Potthoff A. Long-term changes in liver elasticity in hepatitis C virus-infected patients with sustained virologic response after treatment with direct-acting antivirals. *United European Gastroenterol J* 2018; **6**: 1188-1198 [PMID: 30288281 DOI: 10.1177/2050640618786067]

23 **AASLD-IDSA**. HCV testing and linkage to care. Recommendations for testing, managing, and treating hepatitis C. [cited 2018 Nov 21] Available from: https://www.hcvguidelines.org/evaluate/when-whom

24 **Bernuth S**, Yagmur E, Schuppan D, Sprinzl MF, Zimmermann A, Schad A, Kittner JM, Weyer V, Knapstein J, Schattenberg JM, Wörns MA, Galle PR, Zimmermann T. Early changes in dynamic biomarkers of liver fibrosis in hepatitis C virus-infected patients treated with sofosbuvir. *Dig Liver Dis* 2016; **48**: 291-297 [PMID: 26514736 DOI: 10.1016/j.dld.2015.09.015]

25 **Sporea I**, Lupușoru R, Mare R, Popescu A, Gheorghe L, Iacob S, Șirli R. Dynamics of liver stiffness values by means of transient elastography in patients with HCV liver cirrhosis undergoing interferon free treatment. *J Gastrointestin Liver Dis* 2017; **26**: 145-150 [PMID: 28617884 DOI: 10.15403/jgld.2014.1121.262.dyn]

26 **Knop V**, Hoppe D, Welzel T, Vermehren J, Herrmann E, Vermehren A, Friedrich-Rust M, Sarrazin C, Zeuzem S, Welker MW. Regression of fibrosis and portal hypertension in HCV-associated cirrhosis and sustained virologic response after interferon-free antiviral therapy. *J Viral Hepat* 2016; **23**: 994-1002 [PMID: 27500382 DOI: 10.1111/jvh.12578]

27 **Elsharkawy A**, Alem SA, Fouad R, El Raziky M, El Akel W, Abdo M, Tantawi O, AbdAllah M, Bourliere M, Esmat G. Changes in liver stiffness measurements and fibrosis scores following sofosbuvir based treatment regimens without interferon. *J Gastroenterol Hepatol* 2017; **32**: 1624-1630 [PMID: 28177543 DOI: 10.1111/jgh.13758]

28 **Bachofner JA**, Valli PV, Kröger A, Bergamin I, Künzler P, Baserga A, Braun D, Seifert B, Moncsek A, Fehr J, Semela D, Magenta L, Müllhaupt B, Terziroli Beretta-Piccoli B, Mertens JC. Direct antiviral agent treatment of chronic hepatitis C results in rapid regression of transient elastography and fibrosis markers fibrosis-4 score and aspartate aminotransferase-platelet ratio index. *Liver Int* 2017; **37**: 369-376 [PMID: 27678216 DOI: 10.1111/liv.13256]

29 **Jacobson IM**, Lim JK, Fried MW. American Gastroenterological Association Institute Clinical Practice Update-Expert Review: Care of Patients Who Have Achieved a Sustained Virologic Response After Antiviral Therapy for Chronic Hepatitis C Infection. *Gastroenterology* 2017; **152**: 1578-1587 [PMID: 28344022 DOI: 10.1053/j.gastro.2017.03.018]

30 **Garcia-Tsao G**. Regression of HCV cirrhosis: Time will tell. *Hepatology* 2018; **67**: 1651-1653 [PMID: 29222930 DOI: 10.1002/hep.29720]

31 **Labarga P**, Fernandez-Montero JV, de Mendoza C, Barreiro P, Pinilla J, Soriano V. Liver fibrosis progression despite HCV cure with antiviral therapy in HIV-HCV-coinfected patients. *Antivir Ther* 2015; **20**: 329-334 [PMID: 25372299 DOI: 10.3851/IMP2909]

32 Garcia-Tsao G. Regression of HCV cirrhosis: Time will tell. *Hepatology* 2018; **67**: 1651-1653 [PMID: 29222930 DOI: 10.1002/hep.29720]

33 **Joy KP**, Agha AK. Seasonal effects of administration of melatonin and 5-methoxytryptophol on ovarian activity in the catfish Heteropneustes fossilis (Bloch). *J Pineal Res* 1991; **10**: 65-70 [PMID: 2056435 DOI: 10.1002/hep.23744]

34 **Fleminger S**. Statistical notes. Regression towards the mean. *BMJ* 1994; **309**: 539 [PMID: 8086922]

35 **Barnett AG**, van der Pols JC, Dobson AJ. Regression to the mean: what it is and how to deal with it. *Int J Epidemiol* 2005; **34**: 215-220 [PMID: 15333621 DOI: 10.1093/ije/dyh299]

36 **Lingala S**, Ghany MG. Natural History of Hepatitis C. *Gastroenterol Clin North Am* 2015; **44**: 717-734 [PMID: 26600216 DOI: 10.1016/j.gtc.2015.07.003]

37 **Martinez SM**, Foucher J, Combis JM, Métivier S, Brunetto M, Capron D, Bourlière M, Bronowicki JP, Dao T, Maynard-Muet M, Lucidarme D, Merrouche W, Forns X, de Lédinghen V. Longitudinal liver stiffness assessment in patients with chronic hepatitis C undergoing antiviral therapy. *PLoS One* 2012; **7**: e47715 [PMID: 23082200 DOI: 10.1371/journal.pone.0047715]

38 **Nahon P**, Bourcier V, Layese R, Audureau E, Cagnot C, Marcellin P, Guyader D, Fontaine H, Larrey D, De Lédinghen V, Ouzan D, Zoulim F, Roulot D, Tran A, Bronowicki JP, Zarski JP, Leroy V, Riachi G, Calès P, Péron JM, Alric L, Bourlière M, Mathurin P, Dharancy S, Blanc JF, Abergel A, Serfaty L, Mallat A, Grangé JD, Attali P, Bacq Y, Wartelle C, Dao T, Benhamou Y, Pilette C, Silvain C, Christidis C, Capron D, Bernard-Chabert B, Zucman D, Di Martino V, Thibaut V, Salmon D, Ziol M, Sutton A, Pol S, Roudot-Thoraval F; ANRS CO12 CirVir Group. Eradication of Hepatitis C Virus Infection in Patients With Cirrhosis Reduces Risk of Liver and Non-Liver Complications. *Gastroenterology* 2017; **152**: 142-156.e2 [PMID: 27641509 DOI: 10.1053/j.gastro.2016.09.009]

39 **Cheng PN**, Chiu HC, Chiu YC, Chen SC, Chen Y. Comparison of FIB-4 and transient elastography in evaluating liver fibrosis of chronic hepatitis C subjects in community. *PLoS One* 2018; **13**: e0206947 [PMID: 30403744 DOI: 10.1371/journal.pone.0206947]

40 **de Franchis R**; Baveno VI Faculty. Expanding consensus in portal hypertension: Report of the Baveno VI Consensus Workshop: Stratifying risk and individualizing care for portal hypertension. *J Hepatol* 2015; **63**: 743-752 [PMID: 26047908 DOI: 10.1016/j.jhep.2015.05.022]

41 **Castera L**, Pinzani M, Bosch J. Non invasive evaluation of portal hypertension using transient elastography. *J Hepatol* 2012; **56**: 696-703 [PMID: 21767510 DOI: 10.1016/j.jhep.2011.07.005]

World Journal of Clinical Cases

Submit a Manuscript: https://www.f6publishing.com

World J Clin Cases 2022 June 16; 10(17): 5577-5585

DOI: 10.12998/wjcc.v10.i17.5577

ISSN 2307-8960 (online)

ORIGINAL ARTICLE

Retrospective Study

Clinical evaluation of prone position ventilation in the treatment of acute respiratory distress syndrome induced by sepsis

Wen-Han Xia, Chun-Li Yang, Zhi Chen, Cheng-Hong Ouyang, Guo-Quan Ouyang, Qiu-Gen Li

Specialty type: Respiratory System

Provenance and peer review: Unsolicited article; Externally peer reviewed.

Peer-review model: Single blind

Peer-review report's scientific quality classification

Grade A (Excellent): 0
Grade B (Very good): B
Grade C (Good): C
Grade D (Fair): 0
Grade E (Poor): 0

P-Reviewer: Aguiar P, Spain; Rombach M, Germany

Received: January 10, 2022
Peer-review started: January 10, 2022
First decision: February 14, 2022
Revised: February 26, 2022
Accepted: April 3, 2022
Article in press: April 3, 2022
Published online: June 16, 2022

Wen-Han Xia, Chun-Li Yang, Cheng-Hong Ouyang, Department of Intensive Care Unit, Jiangxi Provincial People's Hospital Affiliated to Nanchang University, Nanchang 330006, Jiangxi Province, China

Zhi Chen, Department of Emergency, Jiangxi Provincial People's Hospital Affiliated to Nanchang University, Nanchang 330006, Jiangxi Province, China

Guo-Quan Ouyang, Qiu-Gen Li, Department of Respiratory Medicine, Jiangxi Provincial People's Hospital Affiliated to Nanchang University, Nanchang 330006, Jiangxi Province, China

Corresponding author: Qiu-Gen Li, MM, Chief Physician, Department of Respiratory Medicine, Jiangxi Provincial People's Hospital Affiliated to Nanchang University, No. 92 Aiguo Road, Nanchang 330006, Jiangxi Province, China. liqiugen1976@163.com

Abstract

BACKGROUND

Acute respiratory distress syndrome (ARDS) is an acute, diffuse, inflammatory lung injury. Previous studies have shown prone position ventilation (PPV) to be associated with improvement in oxygenation. However, its role in patients with ARDS caused by sepsis remains unknown.

AIM

To analyze the clinical effects of PPV in patients with ARDS caused by sepsis.

METHODS

One hundred and two patients with ARDS were identified and divided into a control group (n = 55) and a PPV treatment group (n = 47). Outcomes included oxygenation index, lung compliance (Cst) and platform pressure (Pplat), which were compared between the two groups after ventilation. Other outcomes included heart rate (HR), mean arterial pressure (MAP), central venous pressure (CVP), left ventricular ejection fraction (LVEF), the length of mechanical ventilation time and intensive care unit (ICU) stay, and levels of C-reactive protein (CRP), procalcitonin (PCT), and interleukin-6 (IL-6) after ventilation. Finally, mortality rate was also compared between the two groups.

RESULTS

On the first day after ventilation, the oxygenation index and Cst were higher and

Pplat level was lower in the PPV group than in the conventional treatment group ($P < 0.05$). There were no significant differences in oxygenation index, Cst, and Pplat levels between the two groups on the 2nd, 4th, and 7th day after ventilation ($P > 0.05$). There were no significant differences in HR, MAP, CVP, LVEF, duration of mechanical ventilation and ICU stay, and the levels of CRP, PCT, and IL-6 between the two groups on the first day after ventilation (all $P > 0.05$). The mortality rates on days 28 and 90 in the PPV and control groups were 12.77% and 29.09%, and 25.53% and 45.45%, respectively ($P < 0.05$).

CONCLUSION

PPV may improve respiratory mechanics indices and may also have mortality benefit in patients with ARDS caused by sepsis. Finally, PPV was not shown to cause any adverse effects on hemodynamics and inflammation indices.

Key Words: Acute respiratory distress syndrome; Sepsis; Prone position; Supine position; Mechanical ventilation; Hemodynamics

©The Author(s) 2022. Published by Baishideng Publishing Group Inc. All rights reserved.

Core Tip: Acute respiratory distress syndrome (ARDS) is an acute, short-onset, diffuse, inflammatory lung injury disease. Previous studies have reported on the benefits of the prone position over the supine position in terms of mechanical ventilation and oxygenation; however, this has not been addressed in patients with ARDS caused by sepsis. Herein, we retrospectively reviewed the data of 106 patients who underwent mechanical ventilation for ARDS caused by sepsis. We found that mechanical ventilation in the prone position was associated with reduced mortality with no adverse effects on inflammatory and hemodynamic indices.

Citation: Xia WH, Yang CL, Chen Z, Ouyang CH, Ouyang GQ, Li QG. Clinical evaluation of prone position ventilation in the treatment of acute respiratory distress syndrome induced by sepsis. *World J Clin Cases* 2022; 10(17): 5577-5585

URL: https://www.wjgnet.com/2307-8960/full/v10/i17/5577.htm

DOI: https://dx.doi.org/10.12998/wjcc.v10.i17.5577

INTRODUCTION

Acute respiratory distress syndrome (ARDS) is an acute and diffuse inflammatory lung injury disease. It is usually caused by a variety of internal and external pathogenic factors, such as severe infection, trauma, and shock. Clinical manifestation may include respiratory failure, refractory hypoxemia, and respiratory distress, which can cause severe damage to the respiratory system[1,2]. Mechanical ventilation is an important clinical intervention for ARDS that improves bodily oxygenation, thus improving survival rate. A lung-protective ventilation strategy has been proposed based on the clinical pathophysiology of ARDS. This strategy mainly involves limiting tidal volume and airway pressure during mechanical ventilation to avoid lung over-inflation while allowing for the partial pressure of carbon dioxide to rise within a certain range. In addition, a higher level of positive end-expiratory pressure is used to improve lung compliance, suggesting that the lung recruitment strategy should be included in the lung-protective ventilation strategy. However, during the clinical application of mechanical ventilation, it was observed that different positioning influenced the effect of the intervention. Prone position ventilation improves oxygenation by changing the patient's position and is an important auxiliary method of mechanical ventilation[3-5]. However, few studies have evaluated the effect of prone position mechanical ventilation in patients with ARDS caused by sepsis, which limits its use in clinical practice. To this end, this study retrospectively analyzed the clinical data of patients with ARDS caused by sepsis treated with mechanical ventilation in the prone position and explored the effect of the intervention in this position.

MATERIALS AND METHODS

Baseline data

A retrospective analysis was performed using a sample of 102 patients who were treated with mechanical ventilation for ARDS caused by sepsis in the Intensive Care Unit (ICU) of our hospital from

January 2016 to January 2020. All enrolled patients received a lung-protective ventilation treatment strategy. The patients were divided into a control group (n = 55) (undergoing routine treatment) and prone position ventilation treatment group (n = 47) based on their positions during mechanical ventilation. The inclusion criteria were as follows: (1) all patients were diagnosed with ARDS after clinical examination; this diagnosis met the 2012 Berlin Criteria[6] and was caused by sepsis; and (2) the ICU admission time ≥ 24 h. The exclusion criteria were as follows: incidence of (1) pregnancy or lactation; (2) multiple rib fractures; (3) clavicle, spine, and facial fractures; (4) intracranial hypertension; (5) severe cerebral edema; and (6) hemodynamic instability.

Research methods

Patients in the control group were treated with mechanical ventilation in the supine position combined with the lung-protective ventilation strategy while patients in the prone position ventilation treatment group were treated with prone position ventilation combined with the lung-protective ventilation strategy. The mechanical ventilation methods also included sedative and analgesic treatment with fentanyl and midazolam in both groups; patients in the prone position ventilation treatment group received this treatment only after the airway secretions were completely cleared according to the prone position protocol. The Ramsay score was calculated if the patient was beyond 4 or 5 points on the scale. A healthcare provider with extensive clinical experience stood by the patient's head to prevent movement in the central venous line and artificial airway. Two healthcare providers stood on both sides of the patient. When the tubes were properly placed, the patient was required to lean to one side in the lateral decubitus position, and the posture was changed to a prone position. Soft pillows were placed at the chest, ilium, and knees to help minimize the abdominal pressure. Subsequently, for patients with tracheal intubation, the head was tilted to one side, and for those who underwent tracheotomy, the head was placed in the middle with the arms of the patient naturally extended and placed on either side. The ventilation mode remained unchanged in the prone position, with the patient required to remain in the prone position for more than 16 h every day. It was necessary to turn the patient back to a supine position urgently if a large amount of sputum in the airway could not cleared or in cases of hemodynamic instability. Heart rate (HR), mean arterial pressure (MAP), and central venous pressure (CVP) measurements were required for hemodynamic monitoring of arterial and central venous catheterization. A Philips IntelliVue MP40 multifunctional monitor (Royal Philips, Netherlands) was selected to monitor various indicators, and color Doppler echocardiography was performed to assess the left ventricular ejection fraction (LVEF).

Observation items

Baseline characteristics, including age, sex, acute physiological and chronic health score (score), sequential organ failure score, and number of comorbid illnesses of the patients in the two groups were compared. Next, we compared respiratory mechanical indices, such as aerobic fitness index, lung compliance (Cst), and platform pressure (Pplat) between the two groups on days 1, 2, 4, and 7 after ventilation. We also compared hemodynamic indices between the groups, including HR, MAP, CVP, and LVEF, one day after ventilation. Clinical outcomes were also assessed between the two groups, including duration of mechanical ventilation and ICU stay of the patients. We also compared laboratory assessments between the two groups including levels of C-reactive protein (CRP), procalcitonin (PCT), and interleukin-6 (IL-6) on the first day after ventilation. Finally, the mortality rate was compared between the two groups on days 28 and 90.

Statistical analysis

All statistical analyses were performed using SPSS 22.0 software. Continuous variables were summarized as means and standard deviations and compared between groups using a t-test. Categorical variables were reported as percentages, and compared between the two groups using the χ^2 test. Statistical significance was set at $P > 0.05$.

RESULTS

Comparison of baseline characteristics of patients between the two groups

We did not observe any significant differences in baseline characteristics between the two groups ($P > 0.05$) (Table 1).

Comparison of respiratory mechanical indices of patients between the two groups on days 1, 2, 4 and 7 after ventilation

On the first day after ventilation, the oxygenation index and Cst in the routine treatment group were lower and the Pplat level was higher than that of the prone position ventilation group ($P < 0.05$). There were no significant differences in oxygenation index, Cst, and Pplat levels between the two groups on the 2nd, 4th and 7th day after ventilation ($P > 0.05$) (Table 2).

Table 1 Comparison of general data of patients between the two groups, *n* (%)

Group	Sex		Age (yr)	Acute physiological and chronic health score (score)	Sequential organ failure score (score)	Number of basic illnesses					
	Female	Male				1 type	2 type	3 type	4 type	5 type	6 type
Conventional treatment group (n = 55)	15 (27.27)	40 (72.73)	53.82 ± 16.08	27.71 ± 4.55	11.76 ± 3.15	5 (9.09)	11 (20.00)	17 (30.91)	14 (25.45)	5 (9.09)	3 (5.45)
Prone position ventilation treatment group (n = 47)	14 (29.79)	33 (70.21)	53.15 ± 14.16	28.28 ± 4.49	10.57 ± 3.01	5 (10.64)	14 (29.79)	19 (40.43)	4 (8.5)	4 (8.51)	1 (2.13)
χ^2 / t value	0.079		0.222	0.634	1.941	6.551					
P value	0.779		0.825	0.527	0.055	0.256					

Comparison of hemodynamic indicators of patients between the two groups on the first day after ventilation

There were no significant differences in HR, MAP, CVP, and LVEF on the first day after ventilation between the two groups (P > 0.05) (Table 3).

Comparison of mechanical ventilation time and ICU stay of patients between the two groups

There were no significant differences in duration of mechanical ventilation or length of ICU stay between the two groups (P > 0.05) (Table 4).

Comparison of the levels of inflammatory factors in patients of each group on the first day after ventilation

There were no significant differences in the levels of CRP, PCT, and IL-6 between the two groups on the first day after ventilation (P > 0.05) (Table 5).

Comparison of day 28 and day 90 mortality in each group

The mortality on the 28th and 90th days was higher in the control group than in the prone position ventilation treatment group (P < 0.05) (Table 6).

DISCUSSION

ARDS is a hypoxic, progressive, and acute respiratory failure caused by indirect or direct factors. Patients may experience dyspnea and tachypnea. Arterial blood gas analysis in patients with this condition shows that all indicators fail to reach the normal level, and hypoxemia is often difficult to treat. Therefore, close attention should be paid to the correction of hypoxemia in the clinical intervention for ARDS. Symptomatic intervention using ventilation treatment with auxiliary ventilation instruments such as ventilators is common in clinical practice[7-9]. ARDS is also characterized by lung injury caused by the action of local alveolar inflammatory factors on the alveoli and capillaries, resulting in increased lung permeability, exudation of substances such as plasma protein into the alveolar cavity and mesenchyme and leading ultimately to dyspnea[10,11]. Therefore, correction of dyspnea is particularly important in ARDS treatment.

Mechanical ventilation treatment for patients can improve lung volume; however, if used improperly, it can lead to excessive expansion of lung tissue, repeated opening and closing of the alveoli, and subsequently, ventilator-associated lung injury[12,13]. Patients are usually in the supine position for ventilation using a ventilator. In the supine position, under the influence of gravity, the blood flow may remain distributed on the dorsal side, and the proportion of ventilated blood flow becomes imbalanced. Thus, the supine position may be ineffective for ventilation in patients with severe lung consolidation in gravity-dependent parts[14,15]. In a study by Walter *et al*[16], prone position ventilation for patients with ARDS resulted in significant improvement in lung compliance, shortening of mechanical ventilation time, and improvement in oxygenation. Therefore, Walter *et al*[16] believed that prone position ventilation could be effective for oxygenation capacity and hypoxia. In this study, on the first day after ventilation, the oxygenation index and Cst level in the prone position ventilation treatment group were higher than those in the control group. The prone position ventilation treatment group had a lower Pplat level compared to the control group (P < 0.05). From our results, it can be inferred that the prone position may have improved oxygenation by the following mechanisms: (1) the volume of the lung tissue is reduced as it is compressed by the heart; (2) the ventilation/blood flow ratio is further improved in the prone position as compared to that in the supine position, thus significantly reducing

Table 2 Differences in respiratory mechanics indices of patients in each group before and after ventilation

Group	Oxygenation index				Cst (mL/cmH_2O)				Pplat (cmH_2O)			
	Day 1	Day 2	Day 4	Day 7	Day 1	Day 2	Day 4	Day 7	Day 1	Day 2	Day 4	Day 7
Routine treatment group (n = 55)	85.31 ± 25.69	198.33 ± 42.81	254.86 ± 49.56	308.03 ± 57.47	24.09 ± 2.87	36.06 ± 3.62	36.38 ± 3.75	36.45 ± 3.82	25.32 ± 1.06	21.96 ± 0.79	21.80 ± 0.72	21.73 ± 0.65
Prone position ventilation treatment group (n = 47)	129.34 ± 40.02	205.23 ± 41.81	255.50 ± 54.54	320.81 ± 66.15	29.80 ± 3.52	36.24 ± 3.65	36.42 ± 3.72	36.55 ± 3.90	22.01 ± 0.82	21.90 ± 0.75	21.76 ± 0.68	21.70 ± 0.61
t value	6.704	0.820	0.062	1.044	9.024	0.249	0.054	0.131	17.410	0.391	0.287	0.239
P value	0.001	0.414	0.951	0.299	0.001	0.804	0.957	0.896	0.001	0.696	0.775	0.812

Cst: Lung compliance; Pplat: Platform pressure.

pulmonary shunting; and (3) when the gravitational intrapleural pressure gradient is changed, the gravity-dependence of pulmonary edema fluid is redistributed. Furthermore, during prone position ventilation treatment, the curvature of the dorsal diaphragm is significantly reduced compared with that of the ventral diaphragm, which is affected by tension. When the posture of the patient changes, the pressure-forming direction of the abdominal contents also change correspondingly. In the supine position, the pressure from the abdominal contents mainly acts on the dorsal diaphragm, thus counteracting the pressure of the ipsilateral diaphragm and keeping the diaphragm position unchanged[17,18]. In the prone position, the pressure acting on the dorsal diaphragm is reduced. Subsequently, the diaphragm position changes, leading to an increase in the functional residual air volume, redistribution of the air in the lungs along with the blood flow, and improvement in the ventilatory blood perfusion ratio in line with bodily requirement; thus, it is effective for the oxygenation capacity and hypoxia[19]. Prone position ventilation may also impact hemodynamics[20]. However, the findings of the present study showed that there were no significant changes in the hemodynamic indicators and inflammatory factor levels on the first day after ventilation in either group. In this study, the 28- and 90-day mortality were lower in the prone position ventilation group than in the control group ($P < 0.05$). Analysis of the results of the study reveal that the development of prone position ventilation therapy can reduce patient mortality. When patients' oxygenation capacity is improved, conditions such as hypoxemia and respiratory failure are also significantly improved, leading to a reduced disease mortality rate.

Prone position ventilation can reduce the regional heterogeneity of lung ventilation and optimize the regional distribution of transpulmonary pressure in the lung, thus improving gas exchange and reducing the risk of mechanical lung injury[21]. The multicenter PROSEVA trial found that the prone position significantly improved survival and shortened mechanical ventilation time compared with the supine position[22]. Unlike many previous trials, the PROSEVA trial included only patients with moderate or severe ARDS (PaO_2/FiO_2 < 150 mmHg), using prone position early in the treatment process, requiring patients to maintain a prone position for at least 16 h a day, customizing a rehabilitation plan for the patient, and using low tidal volume ventilation, which are potential necessary conditions for achieving the final therapeutic effect 3[23]. Therefore, most recommendations now require patients with severe ARDS to be treated in the prone position for a long time[24].

Table 3 Differences in hemodynamic indices of patients in each group on the first day after ventilation

Group	HR (time/min)	MAP (mmHg)	CVP (cmH_2O)	LVEF (%)
Conventional treatment group (n = 55)	95.60 ± 10.31	89.11 ± 5.67	8.87 ± 1.92	44.32 ± 1.35
Prone position ventilation treatment group (n = 47)	97.82 ± 12.51	90.50 ± 5.72	9.17 ± 2.32	44.30 ± 1.30
t value	0.983	1.229	0.715	0.076
P value	0.328	0.222	0.477	0.940

HR: Heart rate; MAP: mean arterial pressure; CVP: Central venous pressure; LVEF: Left ventricular ejection fraction.

Table 4 Differences in mechanical ventilation time and intensive care unit stay in patients in each group (d)

Group	Mechanical ventilation time	ICU hospitalization
Conventional treatment group (n = 55)	24.38 ± 7.95	30.02 ± 9.75
Prone position ventilation treatment group (n = 47)	23.88 ± 7.02	28.45 ± 8.23
t value	0.334	0.870
P value	0.739	0.386

ICU: Intensive care unit.

Table 5 Differences in inflammatory factors (ug/L) in patients of each group before and after ventilation

Group	CRP (mg/L)	PCT (ug/L)	IL-6 (ug/L)
Conventional treatment group (n = 55)	12.92 ± 1.06	20.85 ± 2.21	76.29 ± 3.75
Prone position ventilation treatment group (n = 47)	12.80 ± 1.01	20.80 ± 2.25	76.25 ± 2.26
t value	0.582	0.113	0.064
P value	0.562	0.910	0.949

CRP: C-reactive protein; PCT: Procalcitonin; IL-6: Interleukin-6.

Table 6 Difference in death rate on day 28 and day 90 for patients in each group, n (%)

Group	Day 28 mortality	Day 90 mortality
Conventional treatment group (n = 55)	16 (29.09)	25 (45.45)
Prone position ventilation treatment group (n = 47)	6 (12.77)	12 (25.53)
χ^2 value	3.993	4.352
P value	0.046	0.037

CONCLUSION

Prone position ventilation in patients with ARDS caused by sepsis can improve respiratory mechanics and reduce patient mortality on the first day after ventilation and does not cause significant fluctuations in patients' hemodynamic indicators and inflammatory factor levels, thus playing an important role in ARDS treatment.

ARTICLE HIGHLIGHTS

Research background

Previous studies have shown prone position ventilation (PPV) to be associated with improvement in oxygenation. However, its role in patients with acute respiratory distress syndrome (ARDS) caused by sepsis remains unknown.

Research motivation

This study analyzed the clinical effects of PPV in patients with ARDS caused by sepsis.

Research objectives

The study aimed to investigate whether PPV treatment can significantly improve patients' heart rate (HR), mean arterial pressure (MAP), central venous pressure (CVP), left ventricular ejection fraction (LVEF), mechanical ventilation time and intensive care unit (ICU)stay. And reduced post-ventilation C-reactive protein (CRP), procalcitonin (PCT) and interleukin-6 (IL-6) Levels and mortality.

Research methods

All enrolled patients received a lung-protective ventilation treatment strategy. The patients were divided into a control group (n = 55) (undergoing routine treatment) and prone position ventilation treatment group (n = 47) based on their positions during mechanical ventilation. Patients in the control group were treated with mechanical ventilation in the supine position combined with the lung-protective ventilation strategy while patients in the prone position ventilation treatment group were treated with prone position ventilation combined with the lung-protective ventilation strategy. HR, MAP, and CVP measurements were required for hemodynamic monitoring of arterial and central venous catheterization. The length of mechanical ventilation time and ICU stay, and levels of CRP, PCT, and IL-6 after ventilation. Finally, mortality rate was also compared between the two groups.

Research results

On the first day after ventilation, the oxygenation index and Cst were higher and Pplat level was lower in the PPV group than in the conventional treatment group. There were no significant differences in oxygenation index, Cst, and Pplat levels between the two groups on the 2nd, 4th, and 7th day after ventilation. There were no significant differences in HR, MAP, CVP, LVEF, duration of mechanical ventilation and ICU stay, and the levels of CRP, PCT, and IL-6 between the two groups on the first day after ventilation. There were significant differences on days 28 and 90 mortality in the PPV and control groups.

Research conclusions

Finally, PPV was not shown to cause any adverse effects on hemodynamics and inflammation indices.

Research perspectives

We will continue to investigate the improvement effect of prone position ventilation on other pulmonary function diseases.

FOOTNOTES

Author contributions: Xia WH and Li QG designed this retrospective study, Xia WH and Yang CL wrote the manuscript; Xia WH, Yang CL, Chen Z, Ouyang CH and Ouyang GQ were responsible for sorting the data.

Supported by Science and Technology Plan of Jiangxi Provincial Health Commission, No. 202130095.

Institutional review board statement: The study was reviewed and approved by the ethics committee of Jiangxi Provincial People's Hospital Affiliated to Nanchang University Institutional Review Board (Approval No. 2016ED13).

Informed consent statement: All study participants, or their legal guardian, provided informed written consent prior to study enrollment.

Conflict-of-interest statement: The authors have nothing to disclose.

Data sharing statement: No additional data are available.

Open-Access: This article is an open-access article that was selected by an in-house editor and fully peer-reviewed by external reviewers. It is distributed in accordance with the Creative Commons Attribution NonCommercial (CC BY-

NC 4.0) license, which permits others to distribute, remix, adapt, build upon this work non-commercially, and license their derivative works on different terms, provided the original work is properly cited and the use is non-commercial. See: https://creativecommons.org/Licenses/by-nc/4.0/

Country/Territory of origin: China

ORCID number: Wen-Han Xia 0000-0001-5742-8591; Chun-Li Yang 0000-0001-6858-6587; Zhi Chen 0000-0002-9467-9151; Cheng-Hong Ouyang 0000-0002-7389-2527; Guo-Quan Ouyang 0000-0002-5359-1479; Qiu-Gen Li 0000-0001-9151-5453.

S-Editor: Wang JL
L-Editor: A
P-Editor: Wang JL

REFERENCES

1 **Thompson BT**, Chambers RC, Liu KD. Acute Respiratory Distress Syndrome. *N Engl J Med* 2017; **377**: 562-572 [PMID: 28792873 DOI: 10.1056/NEJMra1608077]
2 **Nanchal RS**, Truwit JD. Recent advances in understanding and treating acute respiratory distress syndrome. *F1000Res* 2018; **7** [PMID: 30210781 DOI: 10.12688/f1000research.15493.1]
3 **Fan E**, Brodie D, Slutsky AS. Acute Respiratory Distress Syndrome: Advances in Diagnosis and Treatment. *JAMA* 2018; **319**: 698-710 [PMID: 29466596 DOI: 10.1001/jama.2017.21907]
4 **Mauri T**, Lazzeri M, Bellani G, Zanella A, Grasselli G. Respiratory mechanics to understand ARDS and guide mechanical ventilation. *Physiol Meas* 2017; **38**: R280-H303 [PMID: 28967868 DOI: 10.1088/1361-6579/aa9052]
5 **Tobin M**, Manthous C. Mechanical Ventilation. *Am J Respir Crit Care Med* 2017; **196**: P3-P4 [PMID: 28707967 DOI: 10.1164/rccm.1962P3]
6 **ARDS Definition Task Force**. , Ranieri VM, Rubenfeld GD, Thompson BT, Ferguson ND, Caldwell E, Fan E, Camporota L, Slutsky AS. Acute respiratory distress syndrome: the Berlin Definition. *JAMA* 2012; **307**: 2526-2533 [PMID: 22797452 DOI: 10.1001/jama.2012.5669]
7 **Saguil A**, Fargo MV. Acute Respiratory Distress Syndrome: Diagnosis and Management. *Am Fam Physician* 2020; **101**: 730-738 [PMID: 32538594]
8 **Pelosi P**, Brazzi L, Gattinoni L. Prone position in acute respiratory distress syndrome. *Eur Respir J* 2002; **20**: 1017-1028 [PMID: 12412699 DOI: 10.1183/09031936.02.00401702]
9 **Gattinoni L**, Marini JJ, Collino F, Maiolo G, Rapetti F, Tonetti T, Vasques F, Quintel M. The future of mechanical ventilation: lessons from the present and the past. *Crit Care* 2017; **21**: 183 [PMID: 28701178 DOI: 10.1186/s13054-017-1750-x]
10 **Spieth PM**, Güldner A, Gama de Abreu M. [Acute respiratory distress syndrome : Basic principles and treatment]. *Anaesthesist* 2017; **66**: 539-552 [PMID: 28677019 DOI: 10.1007/s00101-017-0337-x]
11 **Yehya N**, Hodgson CL, Amato MBP, Richard JC, Brochard LJ, Mercat A, Goligher EC. Response to Ventilator Adjustments for Predicting Acute Respiratory Distress Syndrome Mortality. Driving Pressure versus Oxygenation. *Ann Am Thorac Soc* 2021; **18**: 857-864 [PMID: 33112644 DOI: 10.1513/AnnalsATS.202007-862OC]
12 **Pham T**, Brochard LJ, Slutsky AS. Mechanical Ventilation: State of the Art. *Mayo Clin Proc* 2017; **92**: 1382-1400 [PMID: 28870355 DOI: 10.1016/j.mayocp.2017.05.004]
13 **Grübler MR**, Wigger O, Berger D, Blöchlinger S. Basic concepts of heart-lung interactions during mechanical ventilation. *Swiss Med Wkly* 2017; **147**: w14491 [PMID: 28944931 DOI: 10.4414/smw.2017.14491]
14 **Wang L**, Li X, Yang Z, Tang X, Yuan Q, Deng L, Sun X. Semi-recumbent position versus supine position for the prevention of ventilator-associated pneumonia in adults requiring mechanical ventilation. *Cochrane Database Syst Rev* 2016; CD009946 [PMID: 26743945 DOI: 10.1002/14651858.CD009946.pub2]
15 **Xin Y**, Cereda M, Hamedani H, Martin KT, Tustison NJ, Pourfathi M, Kadlecek S, Siddiqui S, Amzajerdian F, Connell M, Abate N, Kajanaku A, Duncan I, Gee JC, Rizi RR. Positional Therapy and Regional Pulmonary Ventilation. *Anesthesiology* 2020; **133**: 1093-1105 [PMID: 32773690 DOI: 10.1097/ALN.0000000000003509]
16 **Walter JM**, Corbridge TC, Singer BD. Invasive Mechanical Ventilation. *South Med J* 2018; **111**: 746-753 [PMID: 30512128 DOI: 10.14423/SMJ.0000000000000905]
17 **Katz S**, Arish N, Rokach A, Zaltzman Y, Marcus EL. The effect of body position on pulmonary function: a systematic review. *BMC Pulm Med* 2018; **18**: 159 [PMID: 30305051 DOI: 10.1186/s12890-018-0723-4]
18 **Yamada Y**, Yamada M, Yokoyama Y, Tanabe A, Matsuoka S, Niijima Y, Narita K, Nakahara T, Murata M, Fukunaga K, Chubachi S, Jinzaki M. Differences in Lung and Lobe Volumes between Supine and Standing Positions Scanned with Conventional and Newly Developed 320-Detector-Row Upright CT: Intra-Individual Comparison. *Respiration* 2020; **99**: 598-605 [PMID: 32640453 DOI: 10.1159/000507265]
19 **Smith LJ**, Macleod KA, Collier GJ, Horn FC, Sheridan H, Aldag I, Taylor CJ, Cunningham S, Wild JM, Horsley A. Supine posture changes lung volumes and increases ventilation heterogeneity in cystic fibrosis. *PLoS One* 2017; **12**: e0188275 [PMID: 29176899 DOI: 10.1371/journal.pone.0188275]
20 **Munshi L**, Del Sorbo L, Adhikari NKJ, Hodgson CL, Wunsch H, Meade MO, Uleryk E, Mancebo J, Pesenti A, Ranieri VM, Fan E. Prone Position for Acute Respiratory Distress Syndrome. A Systematic Review and Meta-Analysis. *Ann Am Thorac Soc* 2017; **14**: S280-S288 [PMID: 29068269 DOI: 10.1513/AnnalsATS.201704-343OT]
21 **Gattinoni L**, Busana M, Giosa L, Macrì MM, Quintel M. Prone Positioning in Acute Respiratory Distress Syndrome.

Semin Respir Crit Care Med 2019; **40**: 94-100 [PMID: 31060091 DOI: 10.1055/s-0039-1685180]

22 **Guérin C**, Reignier J, Richard JC, Beuret P, Gacouin A, Boulain T, Mercier E, Badet M, Mercat A, Baudin O, Clavel M, Chatellier D, Jaber S, Rosselli S, Mancebo J, Sirodot M, Hilbert G, Bengler C, Richecoeur J, Gainnier M, Bayle F, Bourdin G, Leray V, Girard R, Baboi L, Ayzac L; PROSEVA Study Group. Prone positioning in severe acute respiratory distress syndrome. *N Engl J Med* 2013; **368**: 2159-2168 [PMID: 23688302 DOI: 10.1056/NEJMoa1214103]

23 **Beitler JR**, Shaefi S, Montesi SB, Devlin A, Loring SH, Talmor D, Malhotra A. Prone positioning reduces mortality from acute respiratory distress syndrome in the low tidal volume era: a meta-analysis. *Intensive Care Med* 2014; **40**: 332-341 [PMID: 24435203 DOI: 10.1007/s00134-013-3194-3]

24 **Fan E**, Del Sorbo L, Goligher EC, Hodgson CL, Munshi L, Walkey AJ, Adhikari NKJ, Amato MBP, Branson R, Brower RG, Ferguson ND, Gajic O, Gattinoni L, Hess D, Mancebo J, Meade MO, McAuley DF, Pesenti A, Ranieri VM, Rubenfeld GD, Rubin E, Seckel M, Slutsky AS, Talmor D, Thompson BT, Wunsch H, Uleryk E, Brozek J, Brochard LJ; American Thoracic Society, European Society of Intensive Care Medicine, and Society of Critical Care Medicine. An Official American Thoracic Society/European Society of Intensive Care Medicine/Society of Critical Care Medicine Clinical Practice Guideline: Mechanical Ventilation in Adult Patients with Acute Respiratory Distress Syndrome. *Am J Respir Crit Care Med* 2017; **195**: 1253-1263 [PMID: 28459336 DOI: 10.1164/rccm.201703-0548ST]

World Journal of Clinical Cases

Submit a Manuscript: https://www.f6publishing.com

World J Clin Cases 2022 June 16; 10(17): 5586-5594

DOI: 10.12998/wjcc.v10.i17.5586

ISSN 2307-8960 (online)

ORIGINAL ARTICLE

Retrospective Study

Three-dimensional arterial spin labeling and diffusion kurtosis imaging in evaluating perfusion and infarct area size in acute cerebral ischemia

Yan-Yan Jiang, Zhi-Lin Zhong, Min Zuo

Specialty type: Radiology, nuclear medicine and medical imaging

Provenance and peer review: Unsolicited article; Externally peer reviewed.

Peer-review model: Single blind

Peer-review report's scientific quality classification

Grade A (Excellent): 0
Grade B (Very good): B
Grade C (Good): C
Grade D (Fair): 0
Grade E (Poor): 0

P-Reviewer: Cvijic M, Slovenia; Narain R, Canada

Received: January 6, 2022
Peer-review started: January 6, 2022
First decision: February 14, 2022
Revised: March 1, 2022
Accepted: April 9, 2022
Article in press: April 9, 2022
Published online: June 16, 2022

Yan-Yan Jiang, Department of Magnetic Resonance, Wuhan Asia General Hospital, Wuhan 430056, Hubei Province, China

Zhi-Lin Zhong, Department of Radiology, Wuhan Yaxin General Hospital, Wuhan 430056, Hubei Province, China

Min Zuo, Department of Radiology, Wuhan Hanyang Hospital, Wuhan University of Science and Technology, Wuhan 430050, Hubei Province, China

Corresponding author: Min Zuo, BM BCh, Associate Chief Physician, Department of Radiology, Wuhan Hanyang Hospital, Wuhan University of Science and Technology, No. 53 Moohu Road, Anyang District, Wuhan 430050, Hubei Province, China. ypzm0518@163.com

Abstract

BACKGROUND

Early thrombolytic therapy is crucial to treat acute cerebral infarction, especially since the onset of thrombolytic therapy takes 1-6 h. Therefore, early diagnosis and evaluation of cerebral infarction is important.

AIM

To investigate the diagnostic value of magnetic resonance multi-delay three-dimensional arterial spin labeling (3DASL) and diffusion kurtosis imaging (DKI) in evaluating the perfusion and infarct area size in patients with acute cerebral ischemia.

METHODS

Eighty-four patients who experienced acute cerebral ischemia from March 2019 to February 2021 were included. All patients in the acute stage underwent magnetic resonance-based examination, and the data were processed by the system's own software. The apparent diffusion coefficient (ADC), average diffusion coefficient (MD), axial diffusion (AD), radial diffusion (RD), average kurtosis (MK), radial kurtosis (fairly RK), axial kurtosis (AK), and perfusion parameters post-labeling delays (PLD) in the focal area and its corresponding area were compared. The correlation between the lesion area of cerebral infarction under MK and MD and T2-weighted imaging (T2WI) was analyzed.

RESULTS

The DKI parameters of focal and control areas in the study subjects were compared. The ADC, MD, AD, and RD values in the lesion area were significantly lower than those in the control area. The MK, RK, and AK values in the lesion area were significantly higher than those in the control area. The MK/MD value in the infarct lesions was used to determine the matching situation. MK/MD < 5 mm was considered matching and MK/MD ≥ 5 mm was considered mismatching. PLD1.5s and PLD2.5s perfusion parameters in the central, peripheral, and control areas of the infarct lesions in MK/MD-matched and -unmatched patients were not significantly different. PLD1.5s and PLD2.5s perfusion parameter values in the central area of the infarct lesions in MK/MD-matched and -unmatched patients were significantly lower than those in peripheral and control areas. The MK and MD maps showed a lesion area of 20.08 ± 5.74 cm^2 and 22.09 ± 5.58 cm^2, respectively. T2WI showed a lesion area of 19.76 ± 5.02 cm^2. There were no significant differences in the cerebral infarction lesion areas measured using the three methods. MK, MD, and T2WI showed a good correlation.

CONCLUSION

DKI parameters showed significant difference between the focal and control areas in patients with acute ischemic cerebral infarction. 3DASL can effectively determine the changes in perfusion levels in the lesion area. There was a high correlation between the area of the infarct lesions diagnosed by DKI and T2WI.

Key Words: Magnetic resonance; Multi-delay 3D arterial spin labeling; Diffusion kurtosis imaging; Acute ischemic cerebral infarction; Perfusion; Nerve function

©The Author(s) 2022. Published by Baishideng Publishing Group Inc. All rights reserved.

Core Tip: Through the analysis and research of patients in the hospital, we have concluded that diffusion kurtosis imaging (DKI) parameters show that there is a significant difference between the lesions of patients with acute ischemic cerebral infarction and the control area. Three-dimensional arterial spin labeling can effectively determine the changes in the perfusion level of the diseased area. The infarct size diagnosed by DKI is highly correlated with T2-weighted imaging.

Citation: Jiang YY, Zhong ZL, Zuo M. Three-dimensional arterial spin labeling and diffusion kurtosis imaging in evaluating perfusion and infarct area size in acute cerebral ischemia. *World J Clin Cases* 2022; 10(17): 5586-5594
URL: https://www.wjgnet.com/2307-8960/full/v10/i17/5586.htm
DOI: https://dx.doi.org/10.12998/wjcc.v10.i17.5586

INTRODUCTION

Cerebral infarction mainly occurs in geriatric patients, and it is a common clinical cerebrovascular disease with high disability and fatality rates. Therefore, it can severely affect patients' quality of life and health. Clinical practice has demonstrated that early and effective thrombolytic therapy can significantly improve the prognosis of patients with acute cerebral infarction, and that treatment options vary according to the severity of the infarction[1]. Therefore, it is important to explore effective methods for the accurate diagnosis of cerebral infarction to improve the treatment modalities and prognosis.

Magnetic resonance imaging (MRI) has important advantages in the diagnosis of central nervous system diseases due to its high soft tissue resolution. Multi-delay three-dimensional arterial spin labeling (3DASL) can accurately evaluate cerebral blood flow (CBF). Diffusion kurtosis imaging (DKI) is a clinical imaging method used to describe the non-Gaussian diffusion of water molecules in tissues; it can accurately reflect the complexity and heterogeneity of neural tissue microstructure by quantifying the diffusion characteristics of water molecules[2,3]. Our study aimed to investigate the diagnostic value of magnetic resonance multi-delay 3DASL and DKI in evaluating the perfusion and infarct area size in patients with acute cerebral ischemia.

MATERIALS AND METHODS

Baseline data

A total of 84 patients who experienced acute cerebral ischemia from March 2019 to February 2021 in our hospital were selected. The inclusion criteria were as follows: Patients (1) Aged 57–82 years; (2) diagnosed with unilateral acute ischemic cerebral infarction (diagnostic criteria of the Fourth National Academic Conference on Cerebrovascular Diseases in 1996)[4]; (3) with dizziness, vomiting, limb numbness, and headache as the main clinical manifestations; (4) who were hospitalized within 24 h of the onset of the disease and who underwent MRI; and (5) who provided informed consent before the relevant examination. The exclusion criteria were as follows: Patients with (1) Cerebrovascular hemorrhagic diseases (hypertensive cerebral hemorrhage, aneurysm, arterial malformation); (2) intracranial tumors; (3) a history of craniotomy; (4) a history of acute myocardial infarction and had an implanted pacemaker placed less than 3 mo previously; (5) cochlear implants and other such complications; (6) mental illness and hyperthyroidism; and (7) a history of drug allergy. The study tender and related materials was implemented after the decision of the medical ethics committee.

MRI and data collection

A 3DASL scan was performed using our MRI scanner (1.5 T, 8-channel cranial coil) from the cranial top to the lower margin of the foramen magnum. Conventional transverse T1-weighted imaging, T2-weighted imaging (T2WI), and coronal fat-suppressed (FS) + fluid-attenuated inversion recovery imaging were performed. The 3DASL sequence adopted 3D spiral fast spin echo technology. The scanning parameters were as follows: echo time (TE), 10.5 ms; repetition time (TR), 4548 ms; labeling delay time, 1.5; layer thickness, 4 mm; and post-labeling delay (PLD), 1525. The CBF values of PLD1.5s and PLD2.5s were obtained.

The DKI sequence scanning parameters were as follows: TR, 6000 ms; layer thickness, 5 mm; TE, minimum; layer spacing, 1.5 mm; field of vision, 240 mm × 240 mm; matrix, 96 × 130; diffusion direction, 15; and B = 0, 1000, and 2000 s/mm^2. The images obtained were analyzed by the supporting software for the following DKI parameters: apparent diffusion coefficient (ADC), axial tensor (AD), mean diffusion coefficient (MD), radial tensor (RD), mean kurtosis (MK), radial kurtosis (RK), and axial kurtosis (AK).

Image and data processing

The original data were processed using a GEMR processing workstation. Two imaging physicians with a senior professional title in our hospital agreed to select the infarction area, abnormal ASL perfusion area, mismatching area, and corresponding contralateral normal brain tissue as regions of interest (ROIs). The CBF value of each ROI area and the ADC value were measured and calculated.

Statistical analysis

In this study, the DKI parameters, CBF values under PLD1.5s and PLD2.5s, and other measurement indices were consistent with the approximate normal distribution or the normal distribution by a normal distribution test, and they are expressed as mean ± SD. The *t*-test was used for group comparisons. The Statistical Package for the Social Sciences (version 21.0; IBM, Armonk, NY) was used for data analysis. The inspection level was $\alpha = 0.05$.

RESULTS

Comparison of baseline data between the joint and control groups

The age, body mass index, and time from onset to admission of the study subjects were 57-82 (average, 68.8 ± 5.8) years, 23.8 ± 2.1 kg/m^2, and 9-24 (average, 14.2 ± 4.0) h, respectively. The study subjects included 48 males and 36 females. A total of 27 and 30 patients smoked and consumed alcohol, respectively. Moreover, 29, 15, 16, and 34 patients had hypertension, diabetes, coronary heart disease, and hyperlipidemia, respectively. The National Institutes of Health Stroke Scale (NIHSS) score within 24 h after admission ranged from 11–18 points, and the average NIHSS score was 14.8 ± 2.2 points.

Comparison of DKI parameters between the lesion and control areas

The DKI parameters of the focal and control areas in the study subjects were compared. The ADC, MD, AD, and RD values in the lesion area were significantly lower than those in the control areas ($P < 0.05$). The MK, RK, and AK values in the lesion area were significantly higher than those in the control area ($P < 0.05$) (Table 1).

Comparison of perfusion parameters between the lesion and control areas under different PLDs

The CBF values of the focal area of the study subjects at PLD1.5s and PLD2.5s were significantly lower than that of the control area ($P < 0.05$). The results are presented in Table 2 and Figure 1.

Table 1 Comparison of diffusion kurtosis imaging parameters between the lesion and control areas (mean ± SD)

Indexes	The lesion area (*n* = 84)	The control area (*n* = 84)	*t* value	*P* value
ADC	576.3 ± 94.2	756.0 ± 102.1	-11.856	0.000
MD	0.651 ± 0.150	0.847 ± 0.167	-8.003	0.000
AD	0.830 ± 0.167	1.305 ± 0.204	-16.513	0.000
RD	0.531 ± 0.093	0.644 ± 0.122	-6.751	0.000
AK	1.281 ± 0.224	0.760 ± 0.115	18.964	0.000
MK	1.256 ± 0.241	0.922 ± 0.207	9.636	0.000
RK	1.328 ± 0.304	0.987 ± 0.185	8.782	0.000

ADC: Apparent diffusion coefficient; MD: Average diffusion coefficient; AD: Axial diffusion; RD: Radial diffusion; AK: Axial kurtosis; MK: Average kurtosis; RK: Radial kurtosis.

Table 2 Comparison of cerebral blood flow values between the lesion area and control area under different parameters of different delay time after labeling (mean ± SD, mL/100 g/min)

Groups	*n*	PLD1.5s	PLD2.5s
Focal area	84	22.64 ± 5.81	14.03 ± 3.91
Control area	84	34.51 ± 7.03	37.58 ± 7.76
t value		-11.929	-24.839
P value		0.000	0.000

PLD: Perfusion parameters post-labeling delays.

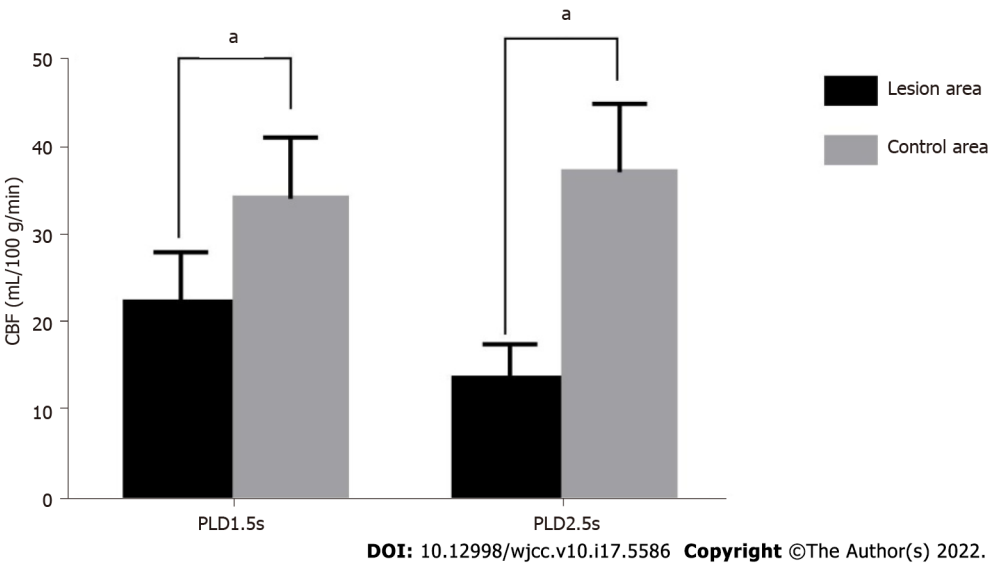

DOI: 10.12998/wjcc.v10.i17.5586 **Copyright** ©The Author(s) 2022.

Figure 1 Histogram of cerebral blood flow values of the lesion and control areas under parameters of different delay time after labeling 1.5 s and 2.5 s. [a]*P* < 0.05 *vs* control areas. CBF: Cerebral blood flow; PLD: Parameters of different delay time.

Comparison of PLD1.5s perfusion parameters of MK/MD-matched and -unmatched infarct lesions

The MK/MD value in the infarct lesions was used to determine the matching situation. MK/MD < 5 mm was considered matching, whereas MK/MD ≥ 5 mm was considered mismatching. The PLD1.5s perfusion parameters in the central, peripheral, and control areas of the infarct lesions in MK/MD-matched and -unmatched patients were not significantly different ($P > 0.05$). The PLD1.5s perfusion parameter values in the central area of infarct lesions in MK/MD-matched and -unmatched lesions were significantly lower than those in peripheral and control areas ($P < 0.05$) (Table 3).

Table 3 Comparison of parameters of different delay time after labeling 1.5s perfusion parameters of average kurtosis/average diffusion coefficient-matched and unmatched infarct lesions (mean ± SD, mL/100 g/min)

Lesion area	MK/MD unmatched (*n* = 48)	MK/MD matched (*n* = 36)	*t* value	*P* value
Central are	16.33 ± 4.75	17.50 ± 4.82	-1.110	0.270
Peripheral area	26.95 ± 5.30[a,d]	28.03 ± 5.47[a,d]	-0.912	0.365
Unmatched area	25.73 ± 5.54[a,d]	-		
Matched area	34.60 ± 6.95[d]	34.12 ± 6.85[d]	0.315	0.753
F value	29.064	28.551		
P value	0.000	0.000		

[a]$P < 0.05$ *vs* the control area.
[d]$P < 0.05$ *vs* the central area.
MK: Average kurtosis; MD: Average diffusion coefficient.

Comparison of PLD2.5s perfusion parameters of MK/MD-matched and -unmatched infarct lesions

The PLD2.5s perfusion parameters in the central, peripheral, and control areas of the infarct lesions in MK/MD-matched and -unmatched patients were not significantly different ($P > 0.05$). The values of the PLD2.5s perfusion parameters in the central area of infarct lesions in MK/MD-matched and -unmatched patients were significantly lower than those in peripheral and control areas ($P < 0.05$) (Table 4).

Results of low perfusion area measurement

The MK map showed an infarct area of 20.08 ± 5.74 cm^2, and the MD map showed an area of 22.09 ± 5.58 cm^2 in the study subjects. T2WI showed a lesion area of 19.76 ± 5.02 cm^2. There were no significant differences in the cerebral infarction areas measured using these three methods (F = 2.094, $P = 0.227$). MK, MD, and T2WI showed a good correlation ($r = 0.617$, $r = 0.620$, $P < 0.05$) (Figure 2A and B).

Case introduction

A 67-year-old male patient was admitted to the hospital due to dizziness, vomiting, and limb dysfunction for 12 h (Figure 3).

DISCUSSION

The traditional method used for clinical diagnosis of cerebral infarction relies on computed tomography (CT), which evaluates the absorption of different types of radiation by different tissues. However, some studies[5-7] have suggested that CT diagnosis and evaluation of cerebral infarction often cannot be performed within 6 h of onset, thus affecting the treatment.

DKI technology analyzes the motion of water molecules in tissues in a non-Gaussian distribution, which is closer to the real motion characteristics of water molecules, and is an extension of magnetic resonance diffusion tensor imaging and magnetic resonance diffusion-weighted imaging[8,9]. In our study, the ADC, MD, AD, and RD values in the lesion area were significantly lower than those in the control group, whereas the MK, RK, and AK values were significantly higher than those in the control group. DKI was more prone to uneven signals due to the large variation in DKI parameters when taken soon after the cerebral infarction occurred, suggesting that DKI has a higher sensitivity in differentiating ischemic brain injuries and can be used as an indicator of complexity and heterogeneity of the changes in the microenvironment inside the cerebral infarction tissue. The movement of water molecules in brain tissue is restricted by the cell membrane, organelles, axons, and myelin sheath; therefore, water molecules in brain tissue cannot show the ideal normal distribution diffusion movement because of restricted movement. Therefore, DKI is more sensitive to pathological changes in brain tissue after ischemia than DWI and DTI, and it is conducive for a more comprehensive analysis of the microstructural changes in cerebral infarction[10-12].

3DASL technology is a type of perfusion imaging with total brain volume coverage and can be used to determine the appropriate treatment method for stroke. In this study, the CBF values of the focal area in the study subjects at PLD1.5s and PLD2.5s were significantly lower than that of the control area. 3DASL is a non-invasive and quantitative diagnostic method, which can accurately evaluate blood flow in the entire brain, determine the blood flow status of the local infarction area, quantitatively analyze blood flow velocity, and evaluate the establishment of collateral circulation, which is of crucial significance for the formulation of a treatment plan and the evaluation of its curative effect[13-15].

Table 4 Comparison of parameters of different delay time after labeling 2.5s perfusion parameters of average kurtosis/average diffusion coefficient-matched and unmatched infarct lesions (mean ± SD, mL/100 g/min)

Lesion area	MK/MD unmatched (*n* = 48)	MK/MD matched (*n* = 36)	*t* value	*P* value
Central area	11.50 ± 3.89	12.28 ± 4.03	-0.896	0.373
Peripheral area	25.84 ± 6.03[a,d]	26.71 ± 5.94[a,d]	-0.659	0.512
Unmatched area	21.76 ± 5.20[a,d]	-		
Control area	37.85 ± 7.54	38.90 ± 7.41[d]	-0.636	0.526
F value	41.025	43.008		
P value	0.000	0.000		

[a]$P < 0.05$ *vs* the control area.
[d]$P < 0.05$ *vs* the central area.
MK: Average kurtosis; MD: Average diffusion coefficient.

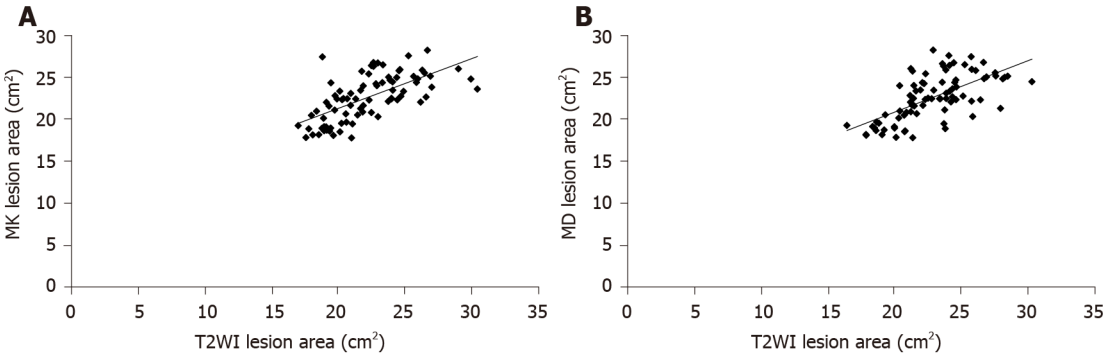

DOI: 10.12998/wjcc.v10.i17.5586 **Copyright** ©The Author(s) 2022.

Figure 2 Correlation between the average kurtosis, the average diffusion coefficient, and the area of cerebral infarction on T2-weighted imaging. A: Correlation between the average kurtosis and the area of cerebral infarction; B: Correlation between the average diffusion coefficient and the area of cerebral infarction. MD: Average diffusion coefficient; MK: Average kurtosis; T2WI: T2-weighted imaging.

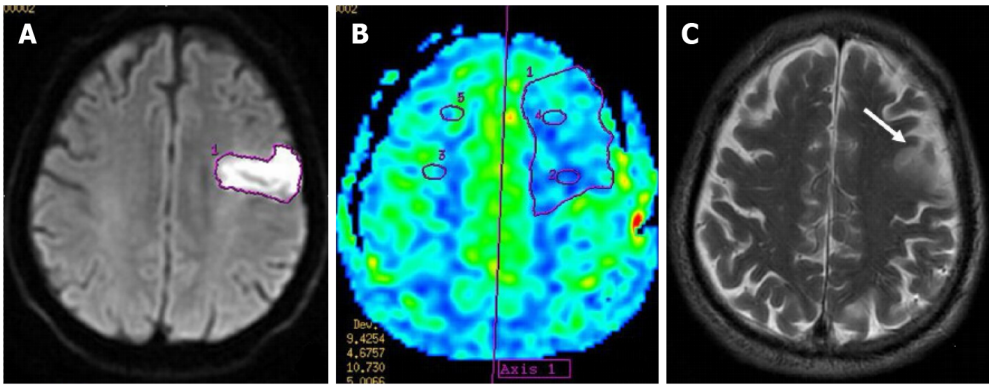

DOI: 10.12998/wjcc.v10.i17.5586 **Copyright** ©The Author(s) 2022.

Figure 3 A 67-year-old male patient was admitted to the hospital due to dizziness, vomiting, and limb dysfunction for 12 h. Magnetic resonance imaging examination was performed within 4 h after admission, and the patient was diagnosed with acute cerebral infarction in the left frontal lobe. A: The diffusion-weighted imaging image and the focal area of cerebral infarction showing high signal performance; B: The color map of cerebral perfusion, showing significant hypoperfusion in the infarct lesion area; C: T2-weighted imaging, with the infarct area indicated by the white arrow showing high signal intensity (Arrow).

The comparison of the PLD1.5s and PLD2.5s perfusion parameters between the two groups showed that the values of the PLD1.5s perfusion parameters in the central area of infarct lesions in MK/MD-matched and -unmatched patients were significantly lower than those in the peripheral and control areas. 3DASL, as a whole-brain non-invasive volume perfusion evaluation technology, can provide quantitative and accurate whole-brain blood perfusion information and help in the precise and early

diagnosis and treatment of stroke. Moreover, the selection of the PLD is important for the analysis of ASL results. PLD1.5s showed the perfusion behavior and the compensatory ability of rapid collateral circulation and PLD2.5s showed the perfusion result. The results of this study also suggested that 3DASL can effectively evaluate and determine the infarct area[16].

The results of the low perfusion area measurement indicated that MK, MD, and T2WI showed no significant differences in the measurement of the area of cerebral infarction lesions in the study subjects, suggesting that these three modalities showed good correlation. The MK and MD values are dependent on the complexity of the tissue microstructure in the ROI and are the most representative parameters of DKI, which can show the degree of limited diffusion of water molecules and the complexity of tissue microstructure. The more complex the structure, the more evident the limited diffusion of water molecules and the larger the MK and MD values[17-20]; whereas there was a significant increase in CBF value on T2WI of the cerebral infarction area, which was closely correlated with MK, MD, and T2WI.

CONCLUSION

In conclusion, the difference in DKI parameters between the focal and control areas in patients with acute ischemic cerebral infarction is significant, which is important for the diagnosis of infarction. 3DASL can effectively determine the changes in perfusion levels in the lesion area. There was a high correlation between the area of the infarct lesions diagnosed by DKI and T2WI.

ARTICLE HIGHLIGHTS

Research background

Early thrombolytic therapy is crucial to treat acute cerebral infarction, especially since the onset of thrombolytic therapy takes 1–6 h. Therefore, early diagnosis and evaluation of cerebral infarction is important.

Research motivation

This study explored the methods for assessing perfusion and infarct size in patients with acute cerebral ischemia.

Research objectives

The study aimed to investigate the diagnostic value of magnetic resonance multi-delay three-dimensional arterial spin labeling (3DASL) and diffusion kurtosis imaging (DKI) in evaluating the perfusion and infarct area size in acute cerebral ischemia patients.

Research methods

Eighty-four patients who experienced acute cerebral ischemia from March 2019 to February 2021 were included.

Research results

The apparent diffusion coefficient, average diffusion coefficient (MD), axial diffusion, and radial diffusion values in the lesion area were significantly lower than those in the control area. The average kurtosis (MK), radial kurtosis, and axial kurtosis values in the lesion area were significantly higher than those in the control area. parameters post-labeling delays (PLD) 1.5s and PLD2.5s perfusion parameters in the central, peripheral, and control areas of the infarct lesions in MK/MD-matched and -unmatched patients were not significantly different. PLD1.5s and PLD2.5s perfusion parameter values in the central area of the infarct lesions in MK/MD-matched and -unmatched patients were significantly lower than those in peripheral and control areas. There were no significant differences in the cerebral infarction lesion areas measured using the three methods.

Research conclusions

DKI parameters showed significant difference between the focal and control areas in patients with acute ischemic cerebral infarction. 3DASL can effectively determine the changes in perfusion levels in the lesion area. There was a high correlation between the area of the infarct lesions diagnosed by DKI and T2-weighted imaging.

Research perspectives

3DASL and DKI have broader application value in assessing perfusion and infarct size in patients with acute cerebral ischemia.

FOOTNOTES

Author contributions: Jiang YY and Zhong ZL contributed equally to this study, and should be regarded as co-first authors, Jiang YY and Zhong ZL designed the study and collected the data; Zuo M drafted the manuscript, Zuo M and Jiang YY analyzed and interpreted data.

Institutional review board statement: This study was approved by the Wuhan Yaxin General Hospital Ethics Committee.

Informed consent statement: All study participants, or their legal guardian, provided informed written consent prior to study enrollment.

Conflict-of-interest statement: The authors declare that there are no conflicts of interest.

Data sharing statement: No additional data are available.

Open-Access: This article is an open-access article that was selected by an in-house editor and fully peer-reviewed by external reviewers. It is distributed in accordance with the Creative Commons Attribution NonCommercial (CC BY-NC 4.0) license, which permits others to distribute, remix, adapt, build upon this work non-commercially, and license their derivative works on different terms, provided the original work is properly cited and the use is non-commercial. See: https://creativecommons.org/Licenses/by-nc/4.0/

Country/Territory of origin: China

ORCID number: Yan-Yan Jiang 0000-0001-7831-6775; Zhi-Lin Zhong 0000-0002-9215-3578; Min Zuo 0000-0001-7205-1462.

S-Editor: Wang JL
L-Editor: A
P-Editor: Wang JL

REFERENCES

1 **Zhu LH**, Zhang ZP, Wang FN, Cheng QH, Guo G. Diffusion kurtosis imaging of microstructural changes in brain tissue affected by acute ischemic stroke in different locations. *Neural Regen Res* 2019; **14**: 272-279 [PMID: 30531010 DOI: 10.4103/1673-5374.244791]
2 **Yang Z**, Rong Y, Cao Z, Wu Y, Zhao X, Xie Q, Luo M, Liu Y. Microstructural and Cerebral Blood Flow Abnormalities in Subjective Cognitive Decline Plus: Diffusional Kurtosis Imaging and Three-Dimensional Arterial Spin Labeling Study. *Front Aging Neurosci* 2021; **13**: 625843 [PMID: 33597860 DOI: 10.3389/fnagi.2021.625843]
3 **Mao C**, Fu Y, Ye X, Wu A, Yan Z. [Study of 3D-pcASL in differentiation of acute cerebral infarction and acute encephalitis]. *Zhonghua Yi Xue Za Zhi* 2015; **95**: 1846-1848 [PMID: 26712404]
4 **Frank L**, Burigk L, Lehmbecker A, Wohlsein P, Schütter A, Meyerhoff N, Tipold A, Nessler J. Meningioma and associated cerebral infarction in three dogs. *BMC Vet Res* 2020; **16**: 177 [PMID: 32503537 DOI: 10.1186/s12917-020-02388-2]
5 **Kong LM**, Zeng JY, Zheng WB, Shen ZW, Wu RH. Effects of Acute Alcohol Consumption on the Human Brain: Diffusional Kurtosis Imaging and Arterial Spin-Labeling Study. *AJNR Am J Neuroradiol* 2019; **40**: 641-647 [PMID: 30872417 DOI: 10.3174/ajnr.A5992]
6 **Zhou IY**, Guo Y, Igarashi T, Wang Y, Mandeville E, Chan ST, Wen L, Vangel M, Lo EH, Ji X, Sun PZ. Fast diffusion kurtosis imaging (DKI) with Inherent COrrelation-based Normalization (ICON) enhances automatic segmentation of heterogeneous diffusion MRI lesion in acute stroke. *NMR Biomed* 2016; **29**: 1670-1677 [PMID: 27696558 DOI: 10.1002/nbm.3617]
7 **Sun PZ**, Wang Y, Mandeville E, Chan ST, Lo EH, Ji X. Validation of fast diffusion kurtosis MRI for imaging acute ischemia in a rodent model of stroke. *NMR Biomed* 2014; **27**: 1413-1418 [PMID: 25208309 DOI: 10.1002/nbm.3188]
8 **Lu D**, Jiang Y, Ji Y, Zhou IY, Mandeville E, Lo EH, Wang X, Sun PZ. JOURNAL CLUB: Evaluation of Diffusion Kurtosis Imaging of Stroke Lesion With Hemodynamic and Metabolic MRI in a Rodent Model of Acute Stroke. *AJR Am J Roentgenol* 2018; **210**: 720-727 [PMID: 29470156 DOI: 10.2214/AJR.17.19134]
9 **Arab A**, Ruda-Kucerova J, Minsterova A, Drazanova E, Szabó N, Starcuk Z Jr, Rektorova I, Khairnar A. Diffusion Kurtosis Imaging Detects Microstructural Changes in a Methamphetamine-Induced Mouse Model of Parkinson's Disease. *Neurotox Res* 2019; **36**: 724-735 [PMID: 31209787 DOI: 10.1007/s12640-019-00068-0]
10 **Tan ZR**, Zhang C, Tian FF. Spectrum of clinical features and neuroimaging findings in acute cerebral infarction patients with unusual ipsilateral motor impairment- a series of 22 cases. *BMC Neurol* 2019; **19**: 279 [PMID: 31718589 DOI: 10.1186/s12883-019-1516-y]
11 **Suman G**, Rusin JA, Lebel RM, Hu HH. Multidelay Arterial Spin Labeling MRI in the Assessment of Cerebral Blood Flow: Preliminary Clinical Experience in Pediatrics. *Pediatr Neurol* 2020; **103**: 79-83 [PMID: 31570299 DOI: 10.1016/j.pediatrneurol.2019.08.005]
12 **Qu Y**, Zhou L, Jiang J, Quan G, Wei X. Combination of three-dimensional arterial spin labeling and stretched-exponential model in grading of gliomas. *Medicine (Baltimore)* 2019; **98**: e16012 [PMID: 31232933 DOI: 10.1097/MD.0000000000016012]

13 **Tortora D**, Severino M, Rossi A. Arterial spin labeling perfusion in neonates. *Semin Fetal Neonatal Med* 2020; **25**: 101130 [PMID: 32591228 DOI: 10.1016/j.siny.2020.101130]

14 **Uetani H**, Kitajima M, Sugahara T, Muto Y, Hirai K, Kuroki Y, Nakaura T, Tateishi M, Yamashita Y. Perfusion abnormality on three-dimensional arterial spin labeling in patients with acute encephalopathy with biphasic seizures and late reduced diffusion. *J Neurol Sci* 2020; **408**: 116558 [PMID: 31715327 DOI: 10.1016/j.jns.2019.116558]

15 **Aoike S**, Sugimori H, Fujima N, Suzuki Y, Shimizu Y, Suwa A, Ishizaka K, Kudo K. Three-dimensional Pseudo-continuous Arterial Spin-labeling Using Turbo-spin Echo with Pseudo-steady State Readout: A Comparison with Other Major Readout Methods. *Magn Reson Med Sci* 2019; **18**: 170-177 [PMID: 30318501 DOI: 10.2463/mrms.tn.2018-0031]

16 **Shinohara Y**, Kato A, Kuya K, Okuda K, Sakamoto M, Kowa H, Ogawa T. Perfusion MR Imaging Using a 3D Pulsed Continuous Arterial Spin-Labeling Method for Acute Cerebral Infarction Classified as Branch Atheromatous Disease Involving the Lenticulostriate Artery Territory. *AJNR Am J Neuroradiol* 2017; **38**: 1550-1554 [PMID: 28596191 DOI: 10.3174/ajnr.A5247]

17 **Wei Y**, Wu L, Wang Y, Liu J, Miao P, Wang K, Wang C, Cheng J. Disrupted Regional Cerebral Blood Flow and Functional Connectivity in Pontine Infarction: A Longitudinal MRI Study. *Front Aging Neurosci* 2020; **12**: 577899 [PMID: 33328960 DOI: 10.3389/fnagi.2020.577899]

18 **Wang C**, Miao P, Liu J, Wei S, Guo Y, Li Z, Zheng D, Cheng J. Cerebral blood flow features in chronic subcortical stroke: Lesion location-dependent study. *Brain Res* 2019; **1706**: 177-183 [PMID: 30419222 DOI: 10.1016/j.brainres.2018.11.009]

19 **Lin L**, Chen X, Jiang R, Zhong T, Du X, Xu G, Duan Q, Xue Y. Differentiation between vestibular schwannomas and meningiomas with atypical appearance using diffusion kurtosis imaging and three-dimensional arterial spin labeling imaging. *Eur J Radiol* 2018; **109**: 13-18 [PMID: 30527294 DOI: 10.1016/j.ejrad.2018.10.009]

20 **Hoehn M**, Küstermann E, Blunk J, Wiedermann D, Trapp T, Wecker S, Föcking M, Arnold H, Hescheler J, Fleischmann BK, Schwindt W, Bührle C. Monitoring of implanted stem cell migration in vivo: a highly resolved *in vivo* magnetic resonance imaging investigation of experimental stroke in rat. *Proc Natl Acad Sci U S A* 2002; **99**: 16267-16272 [PMID: 12444255 DOI: 10.1073/pnas.242435499]

World Journal of Clinical Cases

Submit a Manuscript: https://www.f6publishing.com

World J Clin Cases 2022 June 16; 10(17): 5595-5605

DOI: 10.12998/wjcc.v10.i17.5595

ISSN 2307-8960 (online)

ORIGINAL ARTICLE

Retrospective Study

Intrathecal methotrexate in combination with systemic chemotherapy in glioblastoma patients with leptomeningeal dissemination: A retrospective analysis

Xun Kang, Feng Chen, Shou-Bo Yang, Ya-Li Wang, Zeng-Hui Qian, Yan Li, Hao Lin, Parker Li, Yi-Chen Peng, Xiao-Min Wang, Wen-Bin Li

Specialty type: Oncology

Provenance and peer review: Unsolicited article; Externally peer reviewed.

Peer-review model: Single blind

Peer-review report's scientific quality classification

Grade A (Excellent): 0
Grade B (Very good): 0
Grade C (Good): C, C, C
Grade D (Fair): 0
Grade E (Poor): 0

P-Reviewer: Ata F, Qatar; Lang F, United States

Received: November 23, 2021
Peer-review started: November 23, 2021
First decision: January 22, 2022
Revised: January 30, 2022
Accepted: April 3, 2022
Article in press: April 3, 2022
Published online: June 16, 2022

Xun Kang, Feng Chen, Shou-Bo Yang, Ya-Li Wang, Hao Lin, Yi-Chen Peng, Xiao-Min Wang, Wen-Bin Li, Department of Neuro-oncology, Cancer Center, Beijing Tiantan Hospital, Capital Medical University, Beijing 100070, China

Zeng-Hui Qian, Department of Neurosurgery, Beijing Tiantan Hsopital, Capital Medical University, Beijing 100070, China

Yan Li, Department of Oncology, Beijing Shijitan Hospital, Capital Medical University, Beijing 100038, China

Parker Li, Clinical Medicine, Shanghai Jiao Tong University School of Medicine, Shanghai 200240, China

Corresponding author: Wen-Bin Li, Doctor, MD, Chief Doctor, Professor, Department of Neuro-oncology, Cancer Center, Beijing Tiantan Hospital, Capital Medical University, No. 119 South Fourth Ring West Road, Fengtai District, Beijing 100070, China. liwenbin@ccmu.edu.cn

Abstract

BACKGROUND

Glioblastoma (GBM) is one of the most common and aggressive primary malignant brain tumors with severe symptoms and a poor prognosis. Leptomeningeal dissemination (LMD) is a serious complication of GBM that often results in dire outcomes. There is currently no effective treatment.

AIM

To estimate the clinical outcomes of combination therapy in GBM patients with LMD

METHODS

A retrospective analysis was conducted using data collected from GBM patients diagnosed with LMD from January 2012 to December 2019 at our institution. All these patients had received at least one cycle of a combination therapy consisting of intrathecal methotrexate (MTX) and systemic chemotherapy. Clinical and pathological data were analyzed to explore the outcome of GBM patients with LMD and to determine the most effective treatment.

RESULTS
Twenty-six patients were enrolled in this study. The median time from GBM diagnosis to LMD development was 9.3 mo (range: 2-59 mo). The median overall survival of LMD patients from diagnosis to after receiving systemic chemotherapy in combination with intrathecal MTX was 10.5 mo (range: 2-59 mo). In the Cox univariate analysis, gross resection of tumor (P = 0.022), Karnofsky performance status (KPS) > 60 (P = 0.002), and Ommaya reservoir implant (P < 0.001) were correlated with survival. Multivariate analysis showed that KPS > 60 (P = 0.037) and Ommaya reservoir implant (P = 0.014) were positive factors correlated with survival. Myelotoxicity and gastrointestinal reactions were the common toxicities of this combination therapy. According to Common Terminology Criteria of Adverse Events 4.03, most of the patients presented with toxicity less than grade 3.

CONCLUSION
Intrathecal MTX administration combined with systemic chemotherapy is a potentially effective treatment for patients with GBM and LMD, with mild treatment-related side effects.

Key Words: Glioma; Glioblastoma; Leptomeningeal dissemination; Intrathecal methotrexate; Chemotherapy

©The Author(s) 2022. Published by Baishideng Publishing Group Inc. All rights reserved.

Core Tip: Glioblastoma (GBM) patients with leptomeningeal dissemination (LMD) have severe symptoms and poor prognosis. We investigated the use of intrathecal methotrexate in combination with systemic chemotherapy in terms of effectivity and patient outcome. We showed the potential effectivity of this treatment and that KPS > 60, gross resection of the brain tumor, and the Ommaya reservoir implantation are positive prognostic factors for patients with LMD. We believe that our study gives evidence systemetic treatment is potentially effective in GBM patients with LMD.

Citation: Kang X, Chen F, Yang SB, Wang YL, Qian ZH, Li Y, Lin H, Li P, Peng YC, Wang XM, Li WB. Intrathecal methotrexate in combination with systemic chemotherapy in glioblastoma patients with leptomeningeal dissemination: A retrospective analysis. *World J Clin Cases* 2022; 10(17): 5595-5605
URL: https://www.wjgnet.com/2307-8960/full/v10/i17/5595.htm
DOI: https://dx.doi.org/10.12998/wjcc.v10.i17.5595

INTRODUCTION

Glioblastoma (GBM) is one of the most malignant brain tumors with a median overall survival (OS) of 14.6 mo despite treatment with surgery, radiotherapy, and temozolomide (TMZ)[1,2]. The survival time for patients with GBM was shown to increase after treatment with a combination of tumor-treating fields, but only to 20.9 mo[3]. Leptomeningeal dissemination (LMD) occurs when glioma cells invade the cerebrospinal fluid (CSF) and the leptomeninges. GBM patients with LMD often showed a worse prognosis than those with progression of parenchymal disease and had a median survival of 2-5 mo[4-6]. LMD was initially considered a rare complication of gliomas, but the incidence seems to be higher than the estimated rate of 4%, reaching 25% in postmortem neuropathological studies[4,7,8]. Recent studies indicated that LMD incidence is increasing, possibly due to the improvement in survival rates and survival time of GBM patients[9,10]. Diagnosis of LMD involves either only enhanced magnetic resonance imaging (MRI) or MRI along with positive morphology of CSF cells.

Intrathecal injection of methotrexate (MTX) is a potentially effective method for treating glioma with LMD. Our team found that MTX can inhibit the growth of GBM cells by downregulating the Ras/MAPK/Myc/CD47 signaling pathway[11]. However, an intrathecal injection of MTX was insufficient because it is ineffective on tumor cells in the brain parenchyma. Thus, a combined systemic treatment is needed. TMZ and its combination regimen with etoposide combined with a platinum chemotherapy regimen are optional systemic treatments. We used intrathecal MTX in combination with systemic chemotherapy as a treatment regimen for patients with LMD. This study aimed to estimate the clinical outcomes of combination therapy in GBM patients with LMD.

MATERIALS AND METHODS

This study was approved by the Medical Ethics Committee of Beijing Tiantan Hospital, Capital Medical University. Between January 2012 and December 2019, intrathecal MTX in combination with systemic chemotherapy was administered to 26 patients with GBM with LMD in our institution. The patient cohort had a median age of 43 years (range: 18-61 years). Their GBM diagnosis was confirmed by specialized neuropathologists according to the 2016 World Health Organization classification of brain tumors.

Diagnosis of LMD was performed as explained above. Concomitant chemoradiotherapy followed by adjuvant TMZ chemotherapy was administered according to standard protocols[1,2].

Data on sex, date of birth, date of initial glioma diagnosis, date of LMD diagnosis, Karnofsky Performance Status (KPS) score at LMD diagnosis, molecular pathologic analysis, initial and subsequent LMD treatments, first CSF results after LMD diagnosis, hematological toxicity of treatment, and date of death or last follow-up were collected for each patient.

Treatment plan

Each treatment cycle lasted for 28 d. MTX was intrathecally injected 2-3 times during each cycle, with a single dose of 10 mg once a week. A TMZ regimen was the first choice until after 6 cycles of TMZ systemic chemotherapy had been completed. A dose of 150-200 mg/m^2/d TMZ was administered over 5 d every 28 d. An etoposide and carboplatin (EC) regimen was used in patients in whom the previous TMZ regimen failed in less than 6 mo. Carboplatin AUC5 was administered once every 28 d, and etoposide was administered at 100 mg/m^2/d, for 3 d every 28 d. A TMZ and cisplatin (TP) combinatorial regimen was used in patients whose previous TMZ regimen had failed for over 6 mo. Cisplatin was administered at 30 mg/m^2/d, 3 d every 28 d, and TMZ was administered at 150-200 mg/m^2/d, 5 d every 28 d. Bevacizumab (BEV) was administered to patients with severe brain edema after they showed poor reactions to conventional brain edema treatment. BEV was administered at 5 mg/kg, 1 day every 28 d. Chemotherapy dosage and interval were adjusted according to chemotherapy principles. Either only MRI or MRI along with CSF morphology was reviewed every 2 mo. If the treatments were evaluated as effective, then patients would continue for no more than 8 cycles. If the treatment was ineffective, then the patient was changed to another combined chemotherapy regimen. This process was carried on until either the tumor progressed, the patients gave up treatment, or the patient died.

Statistical analysis

The time from patients' initial GBM diagnosis to their death, time from GBM diagnosis to LMD diagnosis, time from LMD diagnosis to death or last follow-up, and OS (recorded until January 1, 2021) were evaluated using the Kaplan–Meier method. The comparison between patients' characteristics was assessed using a log-rank test. Univariate Cox regression models were applied to assess the effect of the covariates of interest on the time-to-event endpoint. A P value of < 0.05 was considered significant for all analyses. All computations were carried out in SPSS 23.0.

RESULTS

Twenty-six patients with GBM developed LMD and were treated at our institution.

Patients' characteristics before LMD diagnosis

Among the 26 patients included in the analysis, 16 (61.5%) were men and 10 (38.5%) were women, with a median age of 43 years (range: 16-61 years). Most patients had supratentorial primary tumor locations; only two had infratentorial tumors (in the cerebellum). Total gross resection was carried out for 7 patients' tumors (26.9%). Eighteen tumors (69.2%) that were within 1 cm of the ventricular system or that had infiltrated the ventricular system were opened during the initial surgery. Tumor samples from all patients were sent for molecular pathology tests, namely immunohistochemistry or next-generation sequencing. The patterns of treatment after GBM diagnosis and before LMD diagnosis are provided in Table 1.

Patients' characteristics at the time of LMD diagnosis

Twenty-six of these LMD patients had 4 types of clinical symptoms: headache (46.2%), backache (15.4%), lower extremity weakness (11.5%), and visual changes (3.8%). Only 6 patients (23.1%) were asymptomatic upon diagnosis, needing diagnosis to be made through routine examination. With the progress of the disease, most patients appeared to have intracranial hypertension syndrome, severe headache, progressive cognitive impairment, cranial nerve damage, ataxia, and other symptoms of brain and spinal cord injury. The details are presented in Table 2.

Table 1 Clinical characteristics of the patients at the time of glioblastoma diagnosis

Variable	N (%)
Patient	26 (100)
Age at GBM diagnosis: median (range)	43 (18-61)
Sex	
Female	10 (38.5)
Male	16 (61.5)
Location	
Infratentorial (cerebellum)	2 (7.7)
Supratentorial	24 (92.3)
Extent of resection of GBM at diagnosis	
Gross total	7 (26.9)
Non-gross total	19 (73.1)
Communicating with the ventricle at time of GBM diagnosis[a]	
Yes	18 (69.2)
No	8 (30.8)
Concurrent radiation + TMZ after GBM diagnosis	
Yes	26 (100)
No	0 (0)
Adjuvant TMZ cycles for GBM: Median (range)	7 (1-20)
< 7	15 (57.7)
≥ 7	11 (42.3)
Molecular pathology, positive test[b]	
MGMT methylation	5 (19.2)
IDH1 mutation	1 (3.8)
TERT C228T mutation	8 (30.8)

[a]The tumor was within 1 cm of the ventricular system or the ventricular system was open during the operation.
[b]Positive test for immunohistochemistry or NextGen sequencing.
GBM: Glioblastoma; TMZ: Temozolomide; IDH: Isocitrate dehydrogenase; LMD: Leptomeningeal dissemination; MGMT: O6-methylguanine-DNA methyltransferase; TERT: Telomerase reverse transcriptase.

The median time from GBM surgery to diagnosis of LMD was 9.4 mo (range: 0.7–41.4 mo). One patient (3.8%) was diagnosed with LMD (spinal cord metastasis) at the time of initial GBM diagnosis, and the remaining 25 patients were diagnosed after surgery.

All 26 patients had positive MRI findings. Leptomeningeal tumor enhancement was found in the brain around the contours of the gyri and sulci or in multiple nodular deposits in the subarachnoid space, cerebellar folia, and the cortical surface. When these are observed in the spinal cord as linear or nodular enhancements along the surface, a conclusive diagnosis of LMD can be made.

All 26 patients underwent a single lumbar puncture for CSF analysis. Only half these samples (13, 50%) were positive for malignant cells in the cytologic examination. Twenty-one patients (80.8%) had total CSF protein levels over the normal range.

For both the convenience of intrathecal chemotherapy and to avoid lumbar puncture-related metastasis, 20 patients (76.9%) accepted an Ommaya reservoir implant. According to the chemotherapy plan mentioned above, 5 patients used TMZ as systemic chemotherapy, 8 accepted TMZ+DDP (TP), and 13 were treated with vp-16 + CBP (EC). The median number of chemotherapy cycles was 4 (range: 1-8). Four patients changed their systemic chemotherapy plan after first-line failure. One patient accepted vemurafenib therapy because of a BRAF mutation.

Toxicity

The significant treatment-related side effects were gastrointestinal toxicity and myelotoxicity. According

Table 2 Patients' characteristics at the time of the leptomeningeal disease diagnosis

Variable	N (%)
Patient	26 (100)
Time from GBM diagnosis to develop of LMD (months)	
Median (range)	9.3 (0.7-41.4)
KPS at LMD diagnosis	
≤ 60	12 (46.2)
> 60	14 (53.8)
Common presenting symptoms	
Headache	12 (46.2)
None	6 (23.1)
Backache	4 (15.4)
Lower extremity weakness	3 (11.5)
Visual changes	1 (3.8)
MRI positive characteristics	
Subarachnoid and ventricular Spinal cord	10 (38.5)16 (61.5)
CSF cytology for malignant cells	
Yes	13 (50)
No	13 (50)
The content of total protein in the CSF (mg/fL)[a]	
Median (range)	149.2 (21.6-1600.3)
15-45	2 (7.7)
> 45	21 (80.8)
Ommaya reservoir implant	
Yes	20 (76.9)
No	6 (23.1)
Intrathecal injection chemotherapy	
MTX	26 (100)
Systemic chemotherapy	
TMZ	5 (19.2)
TMZ + DDP	8 (30.8)
vp-16 + CBP	13 (50)
Bevacizumab	
Yes	8 (28.6)
No	18 (71.4)
Cycles of intrathecal injection and systemic chemotherapy	
Median (range)	4 (1-8)
< 4	13 (50)
≥ 4	13 (50)
Gastrointestinal toxicity (grade)[b]	
1	17 (65.4)
2	7 (26.9)
3	2 (7.7)

Myelotoxicity	
< 3	19 (73.1)
3-4	7 (26.9)

[a]Three patients CSF protein dates were lost. The tumors were within 1 cm of the ventricular system, or the ventricular system was open during the operation.
[b]Toxicity was determined by grading standard for toxic and side effects of chemotherapy drugs.
GBM: Glioblastoma; CSF: Cerebral spinal fluid; LMD: Leptomeningeal disease; KPS: Karnofsky performance status; MTX: Methotrexate; DDP: Cisplatin; CBP: Carboplatin; MRI: Magnetic resonance imaging.

to the Common Terminology Criteria of Adverse Events version 4.03, 24 patients (92.3%) had grade 1-2 gastrointestinal side effects, whereas 19 patients (73.1%) had grade 1-2 myelotoxicity.

Survival

At the last follow-up, 6 patients were still alive. The median OS for all patients from the date of GBM diagnosis was 27.8 mo. The median survival time from diagnosis of GBM to LMD was 9.4 mo (range: 2-59 mo). The median survival from the diagnosis of LMD was 10.5 mo (Figure 1A). Ten patients showed improvement in neurological symptoms and imaging. The image of a typical case is shown in Figure 2. Eight patients had stable disease, whereas treatment was not effective in the remaining 8 patients.

Univariate analysis showed that the median OS from the diagnosis of LMD was significantly different between those with KPS > 60 and KPS ≤ 60 (16 mo *vs* 9 mo, $P = 0.002$), Ommaya reservoir implant or no implant (15 mo *vs* 6 mo, $P < 0.001$), and gross total resection of the tumor or not [median 24.7, 95%CI (15.1, 34.3) *vs* 10.9, 95%CI (8.0, 13.7), $P = 0.022$] (Figure 1B-D). MGMT methylation ($P = 0.187$), communicating with the ventricle at time of GBM diagnosis ($P = 0.778$), total protein in CSF ($P = 0.321$), and BEV use ($P = 0.085$) had no significant outcome association (Table 3).

Multivariate analysis showed that OS from diagnosis of LMD was positively associated with KPS > 60 ($P = 0.037$) and the Ommaya reservoir implant ($P = 0.014$) (Table 4).

DISCUSSION

LMD in patients with GBM is a serious complication with adverse outcomes. There is no consensus on the treatment for LDM. Disease progression or treatment-related complications, such as intrathecal treatment leading to bleeding and infection after ventricular-abdominal shunt, can sometimes lead to fatal results[6,12]. Considering the multifocal nature of LMD, surgical treatment is not appropriate. Palliative radiotherapy is the most used treatment that can relieve symptoms and slightly improve survival[13,14]. Completed clinical trials have explored the application of a variety of single-use intrathecal chemotherapeutics, including topotecan, MTX, and cytarabine. Although the safety evaluation is satisfactory, none of the single-use drugs have been shown to significantly improve the survival rate of LMD patients[15]. Most intrathecal drugs are single use for LMD patients[A1]; Scott *et al* [16] reported that concurrent intrathecal MTX and liposomal cytarabine for solid tumors that developed LMD showed a median non-GBM OS of 30.2 wk, thereby demonstrating a possible strategy of multidrug intrathecal chemotherapy. Single-use BEV or BEV in combination with irinotecan showed inconsistent clinical benefits[4,17,18]. Targeted therapy can be used in selected cases with sensitive mutations, but it is not widely used due to the insufficient detection or the low sensitivity of glioma mutations[19-21]. Although Chimeric Antigen Receptor T-Cell Immunotherapy therapy for IDH wild-type MGMT-methylated GBM combined with LMD has shown encouraging effects and no related side effects[22], it is difficult to find a suitable target. An immunosuppressive microenvironment and subsequent toxicity limits immunotherapy.

Chemotherapy is one of the main treatment methods for brain tumors. Multiple chemotherapeutic regimens have been investigated, both single or combination treatments (TMZ, lomustine, irinotecan, and BEV)[4,17]. No significant effect was achieved with the intrathecal injection chemotherapy of different drugs (MTX or cytarabine)[5,23]. Based on our team's previous research on the use of MTX in the treatment of gliomas and on the combined therapeutic effect of chemotherapy on recurrent gliomas, we combined an intrathecal MTX injection with systemic chemotherapy. The results showed that the current OS improved compared to that obtained in previous studies[4-6]. To the best of our knowledge, this clinical study has the largest number of patients receiving treatment for GBM and LMD by intrathecal MTX combined with systemic chemotherapy showing good clinical research conclusions.

Previous studies have shown that MGMT promoter methylation status can be used as an indicator for prognosis in newly diagnosed GBM patients. It was also proposed as a risk factor of LMD development in glioma patients[24]. The suspected mechanisms include the increase in the survival of patients subjected to MGMT methylation treatment. MGMT status has no correlation with OS for GBM after

Table 3 Univariate Cox regression models from diagnosis of leptomeningeal disease to death according to treatment

Covariate	χ^2	*P* value
Sex	< 0.001	0.99
Extent of resection of GBM at diagnosis	5.236	0.022
Communicating with the ventricle at time of GBM diagnosis	0.08	0.778
MGMT methylation	1.743	0.187
TERT C228T mutation	0.811	0.368
Adjuvant TMZ cycles for GBM	0.153	0.695
Bevacizumab	2.963	0.085
KPS at the time of LMD diagnosis	9.192	0.002
Total protein in the CSF	0.986	0.321
Ommaya reservoir implant	12.701	< 0.001
CSF cytology	3.28	0.07

GBM: Glioblastoma; CSF: Cerebral spinal fluid; LMD: Leptomeningeal disease; KPS: Karnofsky performance status; MTX: Methotrexate; DDP: Cisplatin; CBP: Carboplatin; MRI: Magnetic resonance imaging; TERT: Telomerase reverse transcriptase; MGMT: O6-methylguanine-DNA methyltransferase; TMZ: Temozolomide.

Table 4 Multivariate Cox regression models from diagnosis of leptomeningeal disease to death according to treatment

Covariate	HR (95%CI)	*P* value
Extent of resection of GBM at diagnosis	0.485 (0.126, 1.871)	0.293
KPS at the time of LMD diagnosis	0.338 (0.122, 0.935)	0.037
Ommaya reservoir implant	0.212 (0.062, 0.729)	0.014

GBM: Glioblastoma; LMD: Leptomeningeal disease; KPS: Karnofsky performance status.

LMD diagnosis. Therefore, for patients diagnosed with LMD, MGMT methylation status should not determine whether TMZ treatment should be used.

BEV has been suggested to promote the development of LMD[18], but available data remain conflicting. Considering the high cost of the BEV and the fact that BEV was not approved by the FDA in China until this year, all the patients in this cohort did not use BEV when GBM was first diagnosed. We only used BEV in patients with severe brain edema and in those who did not respond to conventional dehydration treatment. The results showed that the use of BEV had a negative effect on the OS of patients with LMD but had a favorable effect on relieving intracranial hypertension.

Some studies have shown that ventricular opening during surgery or tumor invasion of the ventricle system may be one of the main factors causing LMD[7,25]. In our study, 18 patients with LMD (69.2%) showed communication with the ventricle at GBM diagnosis, and this result is consistent with what was obtained in other studies. When it comes to the relationship between ventricular opening and OS of LMD patients, there was no significant difference between the two groups, possibly due to the small sample sizes. Further verification is needed.

Ommaya reservoir implants have been widely used to treat LDM in different cancers. It can avoid the injury caused by a lumbar puncture and reduce the corresponding risks. In this study, Ommaya reservoir implant was a positive factor for the OS of LMD patients. In addition to intrathecal MTX administration, we also used the Ommaya reservoir as a simple device for external ventricular drainage at the end stage of the disease, which can sometimes alleviate the symptoms of intracranial hypertension.

In this study, the MRI [A2] abnormalities of the brain and spinal cord were used to diagnose LMD. However, only 13 patients had positive results on a CSF morphological examination. Generally, the CSF morphology test should be combined with another test result, and with CSF flow cytometry if necessary. Considering that our CSF morphology result is a single lumbar puncture test before an intrathecal MTX injection, the presence of false negatives is possible.

The CSF protein content is a clinical characteristic of patients with brain tumors. Of [A3] 23 patients, 21 showed increased levels of CSF proteins in this study, and the protein content of CSF decreased in

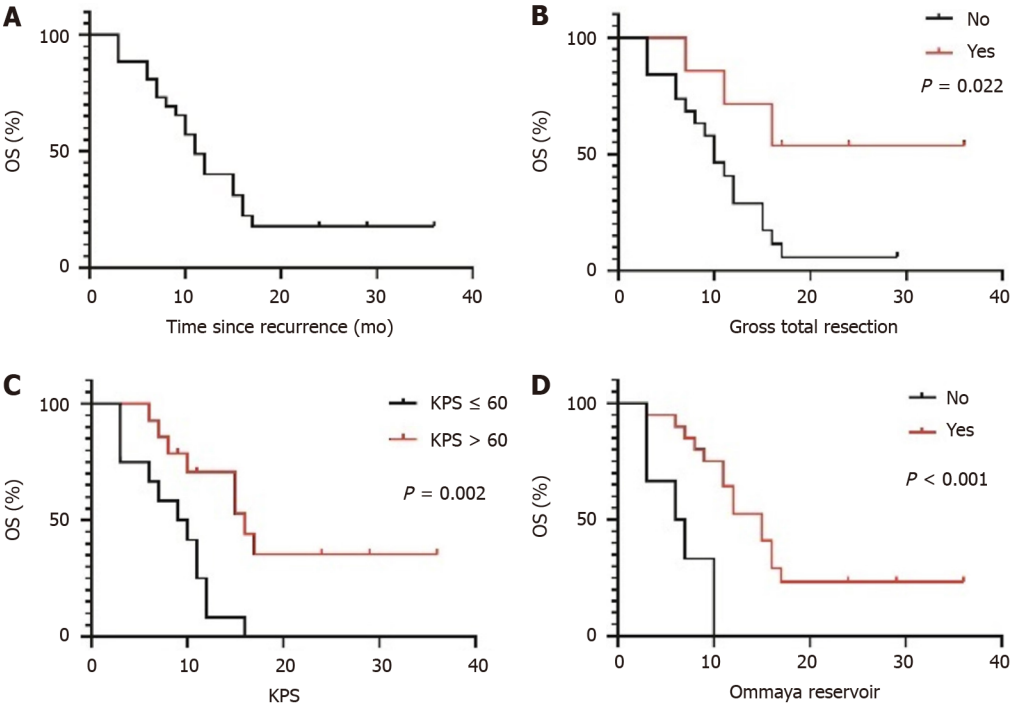

DOI: 10.12998/wjcc.v10.i17.5595 **Copyright** ©The Author(s) 2022.

Figure 1 Kaplan-Meier survival curve from leptomeningeal dissemination diagnosis according to treatment. A: Overall survival (OS) of all leptomeningeal dissemination (LMD) patients; B: OS of patients with gross total resection of the tumor or not [median 24.7, 95%CI (15.1, 34.3) *vs* 10.9, 95%CI (8.0, 13.7), $P = 0.022$]; C: Difference between KPS > 60 and KPS ≤ 60 (16 mo and 9 mo, respectively, $P = 0.002$); D: Difference between Ommaya reservoir implant or not (15 mo *vs* 6 mo, $P < 0.001$).

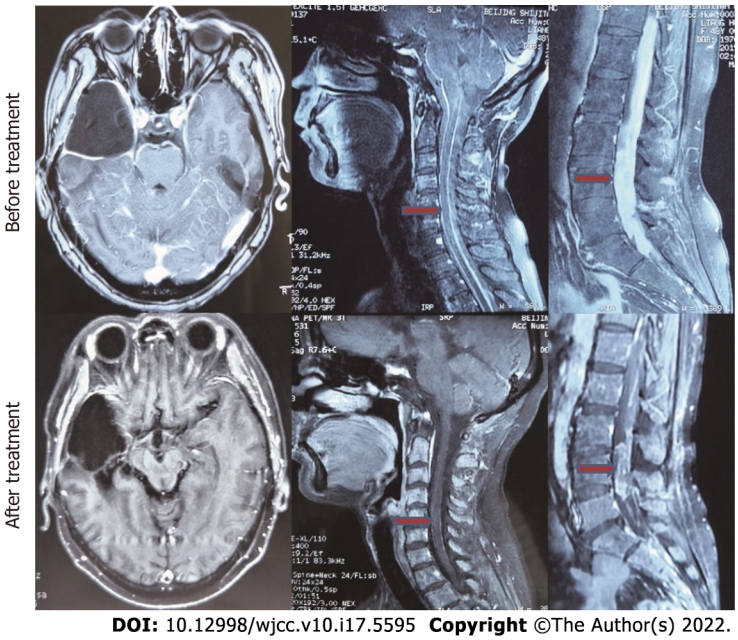

DOI: 10.12998/wjcc.v10.i17.5595 **Copyright** ©The Author(s) 2022.

Figure 2 Magnetic resonance imaging scans (T1 + gadolinium) of a patient before (upper panel) and after 4 cycles of vp-16 + CBP chemotherapy combination with methotrexate intrathecal injection (lower panel). The lesion in the right temporal lobe was stable after surgery. The multiple lesions in the cervical (middle column, red arrows) and lumbar (right column, red arrows) spine went into remission.

effectively treated patients. Therefore, we supposed that CSF protein content can be used as a marker for disease diagnosis and as a treatment efficiency evaluator.

Our results showed that total resection of the brain tumor at initial diagnosis and KPS ≥ 60 at the time of LMD diagnosis are good prognostic factors, and this conclusion is similar to that obtained in other studies[4].

In the study, some patients showed improvement in clinical symptoms, and partial remission was observed with imaging. Considering the lack of a unified evaluation standard, it is impossible to evaluate the curative effect. Therefore, this study only takes OS as the main endpoint and evaluation standard of the curative effect.

Limitations

Firstly, this is a single-center retrospective study with a small sample size. Secondly, it is a single-arm study that lacks a control group. Nevertheless, this retrospective study aimed to preliminarily evaluate the efficacy and safety of intrathecal MTX in combination with systemic chemotherapy in GBM patients with LMD. Promising outcomes have been obtained. Based on this result, a prospective study of combination therapy in GBM patients with LMD is ongoing.

CONCLUSION

LMD is a lethal outcome among patients with glioma and is showing an increasing incidence rate. It remarkably reduces patients' OS. Intrathecal MTX combined with systemic chemotherapy is a potentially effective therapy for GBM patients with LMD. KPS > 60, gross resection of the brain tumor, and the Ommaya reservoir implant are positive prognostic factors for patients with LMD.

ARTICLE HIGHLIGHTS

Research background

Glioblastoma (GBM) is one of the most common and aggressive primary malignant brain tumors with severe symptoms and a poor prognosis. Leptomeningeal dissemination (LMD) is a serious complication of GBM that often results in dire outcomes. There is currently no effective treatment.

Research motivation

Looking for a potential effective methods in GBM patients with LMD.

Research objectives

To estimate the clinical outcomes of intrathecal MTX combination with systemic therapy in GBM patients with LMD.

Research methods

A retrospective analysis was conducted using data collected from GBM patients diagnosed with LMD from January 2012 to December 2019 at our institution. Clinical and pathological data were analyzed to explore the clinical outcome of GBM patients with LMD.

Research results

Twenty-six patients were enrolled in this study. The median time from GBM diagnosis to LMD development was 9.3 mo (range: 2-59 mo). The median overall survival of LMD patients from diagnosis to after receiving systemic chemotherapy in combination with intrathecal MTX was 10.5 mo (range: 2-59 mo). In the Cox univariate analysis, gross resection of tumor (P = 0.022), Karnofsky Performance Status (KPS) > 60 (P = 0.002), and Ommaya reservoir implant (P < 0.001) were correlated with survival. Multivariate analysis showed that KPS > 60 (P = 0.037) and Ommaya reservoir implant (P = 0.014) were positive factors correlated with survival. Myelotoxicity and gastrointestinal reactions were the common toxicities of this combination therapy. According to Common Terminology Criteria of Adverse Events 4.03, most of the patients presented with toxicity less than grade 3.

Research conclusions

Intrathecal MTX administration combined with systemic chemotherapy is a potentially effective treatment for patients with GBM and LMD, with mild treatment-related side effects.

Research perspectives

This retrospective study aimed to preliminarily evaluate the efficacy and safety of intrathecal MTX in combination with systemic chemotherapy in GBM patients with LMD. Promising outcomes have been obtained. Based on this result, a prospective study of combination therapy in GBM patients with LMD is ongoing.

ACKNOWLEDGEMENTS

The authors sincerely thank all the patients and their families for their participation in the present study.

FOOTNOTES

Author contributions: Kang X and Li WB designed and performed this study; Chen F, Qian ZH, Li Y, and Li P contributed to the patient recruitment and collected the data; Yang SB, Lin H, Wang XM, and Wang YL performed the statistical analysis; Peng YC helped with the manuscript write-up; all authors read and approved the final manuscript.

Supported by Special Research Project of Capital Health Development 2016, No. 2020-2-2048.

Institutional review board statement: This study was carried out in accordance with the Declaration of Helsinki on experimentations involving human subjects and was approved by the Medical Ethics Committee of Beijing Tiantan Hospital, Capital Medical University.

Informed consent statement: Patients were not required to give informed consent to the study because the analysis used anonymous clinical data that were obtained after each patient agreed to treatment by written consent. For full disclosure, the details of the study are published on the home page of Fukushima Medical University.

Conflict-of-interest statement: The authors declare no potential conflicts of interest with respect to the research, authorship, and/or publication of this article.

Data sharing statement: All data generated or analyzed during this study are included in this published article.

Open-Access: This article is an open-access article that was selected by an in-house editor and fully peer-reviewed by external reviewers. It is distributed in accordance with the Creative Commons Attribution NonCommercial (CC BY-NC 4.0) license, which permits others to distribute, remix, adapt, build upon this work non-commercially, and license their derivative works on different terms, provided the original work is properly cited and the use is non-commercial. See: https://creativecommons.org/Licenses/by-nc/4.0/

Country/Territory of origin: China

ORCID number: Xun Kang 0000-0002-8940-8402; Feng Chen 0000-0003-4819-2518; Shou-Bo Yang 0000-0003-1126-5461; Ya-Li Wang 0000-0003-2258-584X; Zeng-Hui Qian 0000-0002-9713-1028; Yan Li 0000-0001-9688-0257; Hao Lin 0000-0003-0807-8462; Parker Li 0000-0002-4660-7321; Yi-Chen Peng 0000-0003-0358-5422; Xiao-Min Wang 0000-0002-0516-5061; Wen-Bin Li 0000-0001-7638-4395.

S-Editor: Liu JH
L-Editor: A
P-Editor: Liu JH

REFERENCES

1 **Stupp R**, Mason WP, van den Bent MJ, Weller M, Fisher B, Taphoorn MJ, Belanger K, Brandes AA, Marosi C, Bogdahn U, Curschmann J, Janzer RC, Ludwin SK, Gorlia T, Allgeier A, Lacombe D, Cairncross JG, Eisenhauer E, Mirimanoff RO; European Organisation for Research and Treatment of Cancer Brain Tumor and Radiotherapy Groups; National Cancer Institute of Canada Clinical Trials Group. Radiotherapy plus concomitant and adjuvant temozolomide for glioblastoma. *N Engl J Med* 2005; **352**: 987-996 [PMID: 15758009 DOI: 10.1056/NEJMoa043330]

2 **Stupp R**, Hegi ME, Gilbert MR, Chakravarti A. Chemoradiotherapy in malignant glioma: standard of care and future directions. *J Clin Oncol* 2007; **25**: 4127-4136 [PMID: 17827463 DOI: 10.1200/JCO.2007.11.8554]

3 **Stupp R**, Taillibert S, Kanner A, Read W, Steinberg D, Lhermitte B, Toms S, Idbaih A, Ahluwalia MS, Fink K, Di Meco F, Lieberman F, Zhu JJ, Stragliotto G, Tran D, Brem S, Hottinger A, Kirson ED, Lavy-Shahaf G, Weinberg U, Kim CY, Paek SH, Nicholas G, Bruna J, Hirte H, Weller M, Palti Y, Hegi ME, Ram Z. Effect of Tumor-Treating Fields Plus Maintenance Temozolomide *vs* Maintenance Temozolomide Alone on Survival in Patients With Glioblastoma: A Randomized Clinical Trial. *JAMA* 2017; **318**: 2306-2316 [PMID: 29260225 DOI: 10.1001/jama.2017.18718]

4 **Mandel JJ**, Yust-Katz S, Cachia D, Wu J, Liu D, de Groot JF, Yung AW, Gilbert MR. Leptomeningeal dissemination in glioblastoma; an inspection of risk factors, treatment, and outcomes at a single institution. *J Neurooncol* 2014; **120**: 597-605 [PMID: 25168214 DOI: 10.1007/s11060-014-1592-1]

5 **Noh JH**, Lee MH, Kim WS, Lim DH, Kim ST, Kong DS, Nam DH, Lee JI, Seol HJ. Optimal treatment of leptomeningeal spread in glioblastoma: analysis of risk factors and outcome. *Acta Neurochir (Wien)* 2015; **157**: 569-576 [PMID: 25663100 DOI: 10.1007/s00701-015-2344-5]

6 **Autran D**, Barrie M, Matta M, Monserrat C, Campello C, Petrirena G, Boucard C, Padovani L, Loundou A, Appay R,

Graillon T, Dufour H, Figarella-Branger D, Chinot O, Tabouret E. Leptomeningeal Gliomatosis: A Single Institution Study of 31 Patients. *Anticancer Res* 2019; **39**: 1035-1041 [PMID: 30711992 DOI: 10.21873/anticanres.13210]

7 **Alatakis S**, Malham GM, Thien C. Spinal leptomeningeal metastasis from cerebral glioblastoma multiforme presenting with radicular pain: case report and literature review. *Surg Neurol* 2001; **56**: 33-7; discussion 37 [PMID: 11546569 DOI: 10.1016/s0090-3019(01)00459-1]

8 **Krause Molle Z**, Gierga K, Turowski B, Steiger HJ, Cornelius JF, Rapp M, Sabel M, Kamp MA. 5-ALA-Induced Fluorescence in Leptomeningeal Dissemination of Spinal Malignant Glioma. *World Neurosurg* 2018; **110**: 345-348 [PMID: 29066318 DOI: 10.1016/j.wneu.2017.10.069]

9 **Narayana A**, Golfinos JG, Fischer I, Raza S, Kelly P, Parker E, Knopp EA, Medabalmi P, Zagzag D, Eagan P, Gruber ML. Feasibility of using bevacizumab with radiation therapy and temozolomide in newly diagnosed high-grade glioma. *Int J Radiat Oncol Biol Phys* 2008; **72**: 383-389 [PMID: 18793954 DOI: 10.1016/j.ijrobp.2008.05.062]

10 **de Groot JF**, Fuller G, Kumar AJ, Piao Y, Eterovic K, Ji Y, Conrad CA. Tumor invasion after treatment of glioblastoma with bevacizumab: radiographic and pathologic correlation in humans and mice. *Neuro Oncol* 2010; **12**: 233-242 [PMID: 20167811 DOI: 10.1093/neuonc/nop027]

11 **Bai Y**, Zhong XS, Li WB. Glioblastoma progression is inhibited by methotrexate *via* RAS/MEK/ERK/MYC/CD47 signaling pathways. *Electron J Metab Nutr Cancer* 2018; **5**: 144-150

12 **Saito R**, Kumabe T, Jokura H, Yoshimoto T. Fatal hemorrhage after radiochemotherapy for leptomeningeal dissemination of glioma: report of two cases. *Surg Neurol* 2002; **57**: 46-48 [PMID: 11834277 DOI: 10.1016/s0090-3019(01)00605-x]

13 **Karaca M**, Andrieu MN, Hicsonmez A, Guney Y, Kurtman C. Cases of glioblastoma multiforme metastasizing to spinal cord. *Neurol India* 2006; **54**: 428-430 [PMID: 17114859 DOI: 10.4103/0028-3886.28122]

14 **Fiorentino A**, Caivano R, Chiumento C, Cozzolino M, Fusco V. Radiotherapy and bevacizumab for intramedullary and leptomenigeal metastatic glioblastoma: a case report and review of the literature. *Int J Neurosci* 2012; **122**: 691-694 [PMID: 22720749 DOI: 10.3109/00207454.2012.704456]

15 **Birzu C**, Tran S, Bielle F, Touat M, Mokhtari K, Younan N, Psimaras D, Hoang-Xuan K, Sanson M, Delattre JY, Idbaih A. Leptomeningeal Spread in Glioblastoma: Diagnostic and Therapeutic Challenges. *Oncologist* 2020; **25**: e1763-e1776 [PMID: 33394574 DOI: 10.1634/theoncologist.2020-0258]

16 **Scott BJ**, van Vugt VA, Rush T, Brown T, Chen CC, Carter BS, Schwab R, Fanta P, Helsten T, Bazhenova L, Parker B, Pingle S, Saria MG, Brown BD, Piccioni DE, Kesari S. Concurrent intrathecal methotrexate and liposomal cytarabine for leptomeningeal metastasis from solid tumors: a retrospective cohort study. *J Neurooncol* 2014; **119**: 361-368 [PMID: 24942463 DOI: 10.1007/s11060-014-1486-2]

17 **Burger MC**, Zeiner PS, Jahnke K, Wagner M, Mittelbronn M, Steinbach JP. Addition of Anti-Angiogenetic Therapy with Bevacizumab to Chemo- and Radiotherapy for Leptomeningeal Metastases in Primary Brain Tumors. *PLoS One* 2016; **11**: e0155315 [PMID: 27253224 DOI: 10.1371/journal.pone.0155315]

18 **Ruff MW**, Kizilbash SH. Glioblastoma with bilateral extraocular muscle infiltration preceded by evidence of vascular tropism. *J Clin Neurosci* 2019; **61**: 277-278 [PMID: 30472340 DOI: 10.1016/j.jocn.2018.11.017]

19 **Leaver KE**, Zhang N, Ziskin JL, Vogel H, Recht L, Thomas RP. Response of metastatic glioma to vemurafenib. *Neurooncol Pract* 2016; **3**: 268-271 [PMID: 31386052 DOI: 10.1093/nop/npv054]

20 **Burger MC**, Ronellenfitsch MW, Lorenz NI, Wagner M, Voss M, Capper D, Tzaridis T, Herrlinger U, Steinbach JP, Stoffels G, Langen KJ, Brandts C, Senft C, Harter PN, Bähr O. Dabrafenib in patients with recurrent, BRAF V600E mutated malignant glioma and leptomeningeal disease. *Oncol Rep* 2017; **38**: 3291-3296 [PMID: 29039591 DOI: 10.3892/or.2017.6013]

21 **Woo PYM**, Lam TC, Pu JKS, Li LF, Leung RCY, Ho JMK, Zhung JTF, Wong B, Chan TSK, Loong HHF, Ng HK. Regression of *BRAF* ^{V600E} mutant adult glioblastoma after primary combined BRAF-MEK inhibitor targeted therapy: a report of two cases. *Oncotarget* 2019; **10**: 3818-3826 [PMID: 31217909]

22 **Brown CE**, Alizadeh D, Starr R, Weng L, Wagner JR, Naranjo A, Ostberg JR, Blanchard MS, Kilpatrick J, Simpson J, Kurien A, Priceman SJ, Wang X, Harshbarger TL, D'Apuzzo M, Ressler JA, Jensen MC, Barish ME, Chen M, Portnow J, Forman SJ, Badie B. Regression of Glioblastoma after Chimeric Antigen Receptor T-Cell Therapy. *N Engl J Med* 2016; **375**: 2561-2569 [PMID: 28029927 DOI: 10.1056/NEJMoa1610497]

23 **Zhao KH**, Zhang C, Bai Y, Li Y, Kang X, Chen JX, Yao K, Jiang T, Zhong XS, Li WB. Antiglioma effects of cytarabine on leptomeningeal metastasis of high-grade glioma by targeting the PI3K/Akt/mTOR pathway. *Drug Des Devel Ther* 2017; **11**: 1905-1915 [PMID: 28721010 DOI: 10.2147/DDDT.S135711]

24 **Brandes AA**, Tosoni A, Franceschi E, Sotti G, Frezza G, Amistà P, Morandi L, Spagnolli F, Ermani M. Recurrence pattern after temozolomide concomitant with and adjuvant to radiotherapy in newly diagnosed patients with glioblastoma: correlation With MGMT promoter methylation status. *J Clin Oncol* 2009; **27**: 1275-1279 [PMID: 19188675 DOI: 10.1200/JCO.2008.19.4969]

25 **Grabb PA**, Albright AL, Pang D. Dissemination of supratentorial malignant gliomas *via* the cerebrospinal fluid in children. *Neurosurgery* 1992; **30**: 64-71 [PMID: 1738457 DOI: 10.1227/00006123-199201000-00012]

World Journal of Clinical Cases

Submit a Manuscript: https://www.f6publishing.com

World J Clin Cases 2022 June 16; 10(17): 5606-5619

DOI: 10.12998/wjcc.v10.i17.5606

ISSN 2307-8960 (online)

ORIGINAL ARTICLE

Retrospective Study

Hepatic epithelioid hemangioendothelioma: Clinical characteristics, diagnosis, treatment, and prognosis

Man Zhao, Fei Yin

Specialty type: Gastroenterology and hepatology

Provenance and peer review: Unsolicited article; Externally peer reviewed.

Peer-review model: Single blind

Peer-review report's scientific quality classification

Grade A (Excellent): 0
Grade B (Very good): B
Grade C (Good): C, C
Grade D (Fair): 0
Grade E (Poor): 0

P-Reviewer: Garbuzenko DV, Russia; Yu EYW, Netherlands

Received: December 1, 2021
Peer-review started: December 1, 2021
First decision: January 12, 2022
Revised: January 23, 2022
Accepted: April 15, 2022
Article in press: April 15, 2022
Published online: June 16, 2022

Man Zhao, Fei Yin, Department of Gastroenterology, The Fourth Hospital of Hebei Medical University, Shijiazhuang 050000, Hebei Province, China

Corresponding author: Fei Yin, PhD, Chief Physician, Department of Gastroenterology, The Fourth Hospital of Hebei Medical University, No. 12 Jiankang Road, Shijiazhuang 050000, Hebei Province. China. yinfei_4y@sina.com

Abstract

BACKGROUND

Hepatic epithelioid hemangioendothelioma (HEHE) is a rare hepatic vascular tumor with unpredictable malignant potential. The etiology, characteristics, diagnosis, treatment, and prognosis of HEHE are not well-understood, and large-scale retrospective studies are required to understand better this disease.

AIM

To determine the characteristics of HEHE and identify its optimal treatments and prognostic factors.

METHODS

The clinical data of two patients diagnosed with HEHE at the Fourth Hospital of Hebei Medical University and 258 previously reported cases retrieved from the China National Knowledge Infrastructure and PubMed databases between 1996 and 2021 were combined and summarized. All cases were pathologically identified as HEHE. Information such as clinical features, laboratory examination findings, imaging findings, pathological characteristics, treatment, and survival periods was reviewed. Kaplan-Meir curves were used for survival analysis. Prognostic factors were identified by Cox regression analysis.

RESULTS

HEHE primarily affected middle-aged women. The typical manifestations included epigastric pain, hepatosplenomegaly, inappetence, distension, weight loss, and fatigue. Tumor markers were expressed normally. The incidence of extrahepatic metastasis was 34.5% at the time of diagnosis. The most common sites of extrahepatic involvement were the lungs (22.3%), lymph nodes (5.6%), peritoneum (3.6%), bones (6.6%), and spleen (5.1%). Furthermore, "capsular retraction", "target sign", and "lollipop sign" were the characteristic features of HEHE on imaging. The immunohistochemical profile for HEHE (expression of vascular markers, such as factor VIII-related antigen, CD31, and CD34; expression

levels of D2-40) can facilitate and ensure an accurate diagnosis. The management options for patients with HEHE include liver resection (29.7%), liver transplantation (16.1%), palliative treatments (12.7%), transhepatic arterial chemotherapy and embolization (TACE, 10.2%), chemotherapy (11.0%), antiangiogenic therapy (15.3%), and other treatments (5.1%); the mean survival time was 158.6, 147.3, 4.2, 90.8, 71.4, 83.1, and 55.0 mo, respectively. The survival time of patients who underwent surgical treatment was longer than that of patients who did not. TACE and antiangiogenic therapy tended to prolong survival compared with other nonsurgical treatments. The 1-, 5-, and 10-year survival rates were 82%, 71%, and 64%, respectively. Multivariate analysis showed that liver function (P = 0.045), intrahepatic metastasis (P = 0.029), and treatment (P = 0.045) were independent prognostic factors. The presence of extrahepatic metastases was not an independent risk factor for poor prognosis (P = 0.558).

CONCLUSION

The clinical course of HEHE is rare and variable, and patients with intrahepatic metastases and liver dysfunction may have a poorer prognosis than those without. Surgical intervention, whether liver resection or transplantation, might be warranted regardless of extrahepatic metastasis. For patients without the option for surgery, clinicians should consider the use of TACE with antiangiogenic drugs in the treatment of HEHE.

Key Words: Hepatic epithelioid hemangioendothelioma; Clinical characteristics; Diagnosis; Treatment; Prognosis

©The Author(s) 2022. Published by Baishideng Publishing Group Inc. All rights reserved.

Core Tip: Hepatic epithelioid hemangioendothelioma (HEHE) is a rare hepatic vascular tumor with unpredictable malignant potential. Patients with intrahepatic metastases and liver dysfunction may have a poorer prognosis than those without. Surgical intervention, whether liver resection or transplantation, might be warranted regardless of extrahepatic metastasis. However, the therapeutic strategy for patients without the option for surgery is particularly controversial. Our experience highlights the efficacy of transhepatic arterial chemotherapy and embolization and antiangiogenic therapy in the management of HEHE.

Citation: Zhao M, Yin F. Hepatic epithelioid hemangioendothelioma: Clinical characteristics, diagnosis, treatment, and prognosis. *World J Clin Cases* 2022; 10(17): 5606-5619
URL: https://www.wjgnet.com/2307-8960/full/v10/i17/5606.htm
DOI: https://dx.doi.org/10.12998/wjcc.v10.i17.5606

INTRODUCTION

Hepatic epithelioid hemangioendothelioma (HEHE) is a rare neoplasm of vascular origin[1]. The natural course of this neoplasm is variable, ranging from long-term survival without treatment to a rapidly progressive course with a fatal outcome[2]. The etiology, characteristics, diagnosis, treatment, and prognosis of HEHE are not well-understood, and large-scale retrospective studies are required to understand better this disease.

MATERIALS AND METHODS

The clinical data of two patients diagnosed with HEHE at the Fourth Hospital of Hebei Medical University and previously reported cases retrieved from the literature were combined and summarized.

Data search

We searched PubMed and China National Knowledge Infrastructure databases from January 1996 through December 2021 using search terms including "HEHE" and "epithelioid hemangioendothelioma of liver". The references of related studies and reviews were also retrieved, if necessary.

Study inclusion and exclusion criteria

The studies that met the following criteria were included: (1) Tumor tissues obtained by liver biopsy or

surgery were pathologically identified as HEHE; (2) accurate clinical statistical indicators were provided in the studies; and (3) articles were published in English or Chinese.

The exclusion criteria were: (1) Epithelioid hemangioendothelioma from other sites with liver metastasis; (2) duplicate publications; (3) studies without sufficient data; and (4) care reports, meeting abstracts, meta-analyses, and reviews.

Data extraction

We reviewed all titles and abstracts to identify potentially relevant articles. Two investigators reviewed all potentially relevant full texts for inclusion, with disagreements resolved through discussion and consensus. We used standardized data extraction forms to collect the following information: First author's name, geographical region and year of publication, study design, inclusion/exclusion criteria, size of the patient cohort, and clinical statistical indicators (age, sex, etiology, clinical features, laboratory tests, radiographic findings, pathological features, treatment, and survival).

Statistical analysis

Statistical analyses were performed using SPSS 26.0 (Armonk, NY, United States). Distributions of patients' characteristics (age, sex, clinical features, laboratory tests, radiographic findings, pathological features, treatment, and survival) were explored and summarized using descriptive statistics. Survival analysis was performed using the Kaplan-Meier method. The differences between the survival curves were compared using the log-rank test. Multivariate Cox hazard regression analysis was performed on the factors shown to be significant in the univariate analysis. All tests were two-sided, and P values ≤ 0.05 were considered significant.

RESULTS

Two cases diagnosed with HEHE at The Fourth Hospital of Hebei Medical University

Case one: A 53-year-old female patient was admitted to the hospital because of intermittent right upper abdominal pain for > 10 d. Initial liver function tests indicated increased levels of alanine transaminase and alkaline phosphatase. Tumor markers were normal. Computed tomography (CT) revealed two round low-density nodules in the right lobe of the liver. The peripheral rims of the nodules were enhanced using a contrast medium, giving the appearance of cancer metastases, but no tumors were found elsewhere (Figure 1). The preliminary diagnosis for the preoperative liver biopsy was HEHE. The patient subsequently underwent segmental hepatectomy of segments VIII and VI. Immunohistochemically, the tumor cells expressed CD34, vimentin, factor VIII-related antigen (FVIII-RAg), smooth muscle actin (SMA), S-100, and Ki-67 (Figure 2). Based on these histological and immunohistochemical findings, the tumor was pathologically diagnosed as HEHE, which was consistent with the preoperative biopsy results. After 4 years postoperatively, the patient was in good health and had no recurrence.

Case two: A 35-year-old woman was referred to our institution for the management of incidentally discovered nodules in the liver without symptoms. Laboratory examination findings were normal. CT showed multiple hypodense hepatic nodular formations, all of which were slightly enhanced in the arterial phase (Figure 3A). Immunohistochemical staining of the tumor tissue obtained *via* laparoscopic liver biopsy revealed tumor cells that were positive for CD34, factor VIII-related antigen (FVIII-RAg), SMA, CD68, and vimentin and negative for alpha fetoprotein (AFP), Cal, Me, cytokeratin, and S100. The final pathological diagnosis was HEHE, and the patient was diagnosed with unresectable hepatic disease with no distant metastases. Liver transplantation (LT) was recommended, but the patient refused due to personal reasons. Transhepatic arterial chemotherapy and embolization (TACE) was performed using 1 g of fluorine glycosides, 10 mg of epirubicin, and 10 mL of lipiodol. Unfortunately, repeat CT indicated that the number of lesions had increased (Figure 3B). A decision was then made to change the treatment to interferon (IFN)-α2b with a dose of 3 MU being administered every alternate day. The patient underwent clinical evaluation and laboratory tests every 3 wk and abdominal CT scans every 3.0 mo. As shown in Figure 3C-F, an evaluation of the tumor response using serial CT revealed a favorable response with a decrease in the number of lesions, which finally disappeared 18.0 mo after the initiation of treatment with IFN-α2b.The patient remained tumor-free after 7 years and currently maintains a functional state of health.

Literature results

A total of 2166 related studies were eliminated according to the inclusion and exclusion criteria, and 170 studies with 258 cases were finally included (Supplementary material) after quality evaluation. Reasons for exclusion at time of review are detailed in Figure 4. The total number of cases was 260, including the two confirmed cases from the Fourth Hospital of Hebei Medical University.

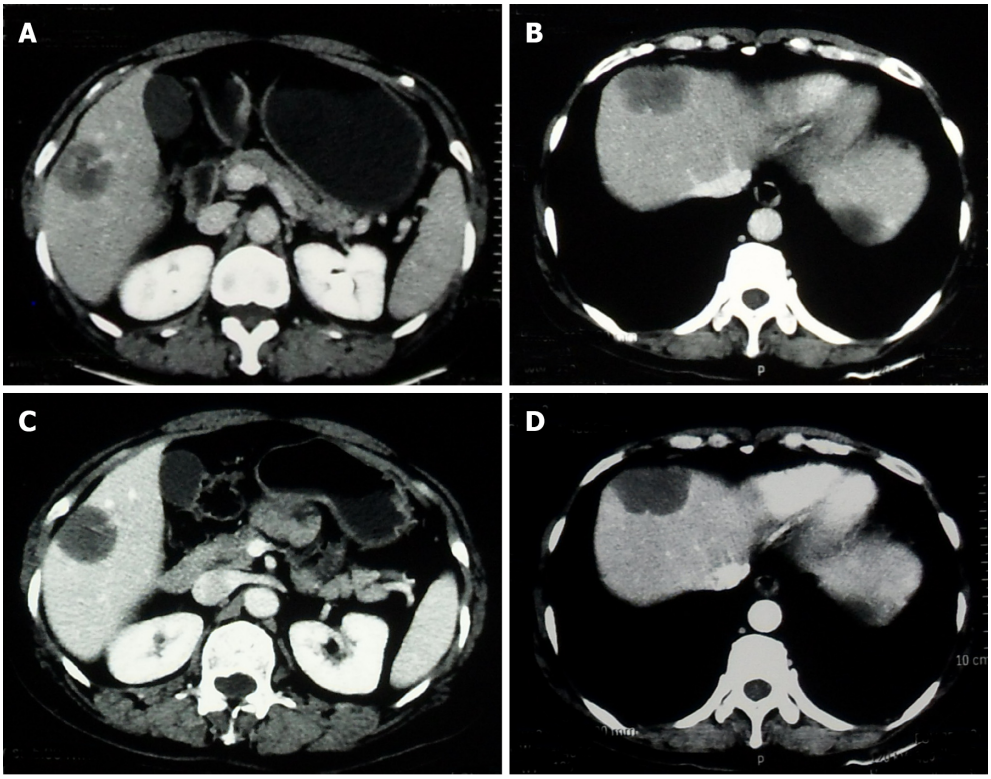

DOI: 10.12998/wjcc.v10.i17.5606 **Copyright** ©The Author(s) 2022.

Figure 1 Abdominal computed tomography of case one. A and B: Computed tomography (CT) showed two round low-density nodules in the right lobe of the liver; C and D: Contrast-enhanced CT showed that the peripheral rim of the nodules was enhanced.

Demographics

Among the patients with HEHE, 171 of 260 patients were women (65.8%), and the male-to-female ratio was 2.0:3.8. The mean age was 44.4 years (range: 3-84 years). Further, 27 patients had a history of viral hepatitis, including 2 cases of hepatitis A, 22 cases of hepatitis B, and 3 cases of hepatitis C. Four patients had a history of long-term oral contraceptive use, one patient had a silicone breast implant, and one patient was pregnant.

Clinical features

The clinical manifestations were variable and nonspecific, and 27.2% of the patients were incidentally discovered without symptoms. Among symptomatic patients, the typical manifestations included epigastric pain (39.0%), hepatosplenomegaly (15.4%), inappetence (13.4%), distension (12.2%), weight loss (10.6%), and fatigue (10.2%) in addition to other manifestations like epigastric discomfort, hydrothorax, ascites, fever, and jaundice, with 35.0% of the patients with HEHE presenting with two or more symptoms simultaneously (Table 1).

Most of the patients presented with multiple lesions (85.3%). The incidence of extrahepatic metastases was 34.5% at the time of diagnosis. The most common sites of extrahepatic involvement were the lungs (22.3%), lymph nodes (5.6%), peritoneum (3.6%), bones (6.6%), and spleen (5.1%). The involvement of the pleura and omentum was also described, albeit relatively rarely (Table 1).

Laboratory parameters

Approximately 43.3% of the patients had abnormal liver function. The most common changes were increased levels of alanine transaminase (25.5%), aspartate transaminase (25.5%), total bilirubin (15.3%), γ-glutamyl transpeptidase (20.4%), and alkaline phosphatase (27.4%). The levels of the tumor markers AFP, carcinoembryonic antigen (CEA), and carbohydrate antigen 19-9 (CA-199) were mostly normal (Table 1).

Imaging studies

CT was performed in 198 patients. Low-density patterns were the most common abnormal features (98.5%). High-density and heterogeneous mixed-density lesions were observed in 1.5% of the patients with HEHE. Information on enhancement patterns was available for 163 patients. Enhancement was observed in 84.7% of the patients. Most of the lesions were found along the liver periphery, which tended to occur in groups and coalesce over time, forming large, confluent masses (21.2%). Additional findings included calcification (15.2%), capsular retraction (17.2%), "target sign" (20.2%), and "lollipop

Table 1 General features of patients with hepatic epithelioid hemangioendothelioma

General feature	No. of patients	%
Presence of symptoms, *n* = 254		
Asymptomatic	69	27.2
Symptomatic	185	72.8
Epigastric pain	99	39.0
Hepatosplenomegaly	39	15.4
Inappetence	34	13.4
Abdominal distension	31	12.2
Weight loss	27	10.6
Fatigue	26	10.2
Epigastric discomfort	25	9.8
Hydrothorax and ascite	18	7.1
Fever	12	4.7
Jaundice	24	9.4
Thoracalgia and humeral back pain	20	7.9
Nausea and vomiting	10	3.9
Edema	8	3.1
Cough and expectoration	9	3.5
Abdominal mass	2	0.8
Hematemesis and melena	2	0.8
Intrahepatic involvement type, *n* = 197		
Multinodular type (including diffuse type)	168	85.3
Mononodular type	29	14.7
Type of involvement, *n* = 197		
Intrahepatic involvement	129	65.5
Extrahepatic involvement	68	34.5
Lung	44	22.3
Lymph node	11	5.6
Bone	13	6.6
Peritoneum	7	3.6
Spleen	10	5.1
Pleura	4	2.0
Omentum	2	1.0
Liver function, *n* = 157		
Normal	89	56.7
Abnormal	68	43.3
Elevated ALT in U/L	40	25.5
Elevated AST in U/L	40	25.5
Elevated TBIL in μmol/L	24	15.3
Elevated ALP in U/L	43	27.4
Elevated GGT in U/L	32	20.4
Tumor markers		

Elevated AFP in ng/mL	8/171	4.7
Elevated CEA in ng/mL	7/130	5.4
Elevated CA19-9 in U/mL	13/135	9.6
Elevated CA125 in U/mL	14/53	26.4
Plain CT scan, *n* = 198		
Low density lesions	195/198	98.6
High density or uneven density lesions	3/198	1.4
Calcification	30/198	15.2
Capsular retraction	34/198	17.2
Confluent masses	42/198	21.2
Contrast-enhanced CT, *n* = 163		
Tumor edge enhancement	138/163	84.7
Tumor edge without enhancement	25/163	15.3
Target sign	33/163	20.2
Lollipop sign	19/163	11.7
Immunohistopathological markers		
FVIII-RAg	117/118	99.2
CD34	215/218	98.6
CD31	171/173	98.8
Vimentin	94/95	98.9
SMA	12/27	44.4
Desmin	0/13	NA
Hepatocyte	8/58	13.8
CK	38/81	46.9
EMA	6/34	17.6
AFP	0/34	NA
CEA	0/11	NA
S-100	1/33	9.1
D2-40	7/11	63.6
Genetics		
YAP1-TFE3	3/4	75.0
WWTR1-CAMTA1	3/5	60.0

HEHE: Hepatic epithelioid hemangioendothelioma; CT: Computed tomography; AST: Aspartate aminotransferase; ALT: Alanine aminotransferase; CEA: Carcinoembryonic antigen; AFP: Alpha fetoprotein; CK: Cytokeratin; GGT: Gamma-glutamyl transferase; SMA: Smooth muscle actin; EMA: Epithelial membrane antigen; FVIII-RAg: Factor VIII-related antigen; YAP-1: Yes-associated protein 1; TFE3: Transcription factor E3; WWTR1: WW domain-containing transcription regulator 1; CAMTA1: Calmodulin-binding transcription activator 1.

sign" (11.7%) (Figure 5 and Table 1).

Histopathology and genetics

The immunohistochemical factors detected in patients with HEHE were varied. FVIII-RAg (99.2%), CD34 (98.6%), CD31 (98.8%), vimentin (98.9%), and D2-40 (63.6%) were positive in the majority of the patients, whereas cytokeratin (46.9%), SMA (44.4%), hepatocytes (13.8%), epithelial membrane antigen (17.6%), and S-100 (9.1%) were positive only in a small group of patients. Some markers, such as AFP, CEA, and desmin, were consistently negative. Moreover, at the genetic level, 75% of the patients had yes-associated protein 1 (*YAP1*)-transcription factor E3 (*TFE3*) gene fusion, and 60% of the patients had WW domain-containing transcription regulator 1 (*WWTR1*)-calmodulin-binding transcription activator 1 (*CAMTA1*) gene fusion (Table 1).

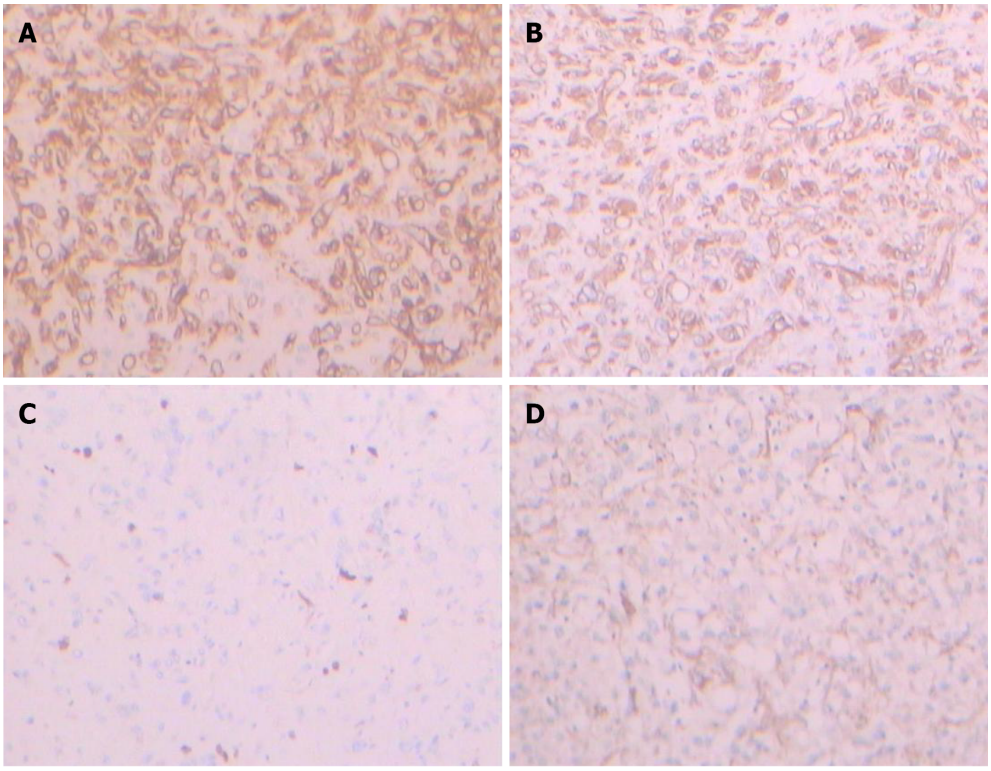

DOI: 10.12998/wjcc.v10.i17.5606 **Copyright** ©The Author(s) 2022.

Figure 2 Immunohistochemical staining of case one. A: Positivity for CD34 in case one (magnification, × 200); B: Positivity for vimentin in case one (magnification, × 200); C: Positivity for Ki-67 in case one (magnification, × 200); D: Positivity for smooth muscle actin in case one (magnification, × 200).

Treatment and survival rates

The management options for patients with HEHE included liver resection (LR), LT, palliative treatments, TACE, chemotherapy, antiangiogenic therapy, and other treatments, such as traditional Chinese medications and radiofrequency ablation. A number of patients (29.7%) underwent LR, and their mean survival time was 158.6 mo. Some patients (16.1%) underwent LT, and their mean survival time was 147.3 mo. Other patients (12.7%) opted for follow-up without any therapy, and their mean survival time was 4.2 mo. Some patients (10.2%) underwent TACE, and their mean survival time was 90.8 mo. Some patients (11.0%) chose chemotherapy, and their mean survival time was 71.4 mo. Additionally, some patients (15.3%) opted for antiangiogenic therapy, and their mean survival time was 83.1 mo. Further, some patients (5.1%) chose other treatments, and their mean survival time was 55.0 mo. For surgically treated patients, the 1-, 5-, and 10-year survival rates were 87%, 87%, and 77%, respectively. However, for patients who underwent nonsurgical treatment, the 1-, 5-, and 10-year survival rates were 78%, 58%, 52%, respectively. Not considering the type of treatment provided, the 1-, 5-, and 10-year survival rates were 82%, 71%, and 64%, respectively. The survival time of patients who underwent surgical treatment was longer than that of patients who did not. Similarly, the survival time of treated patients was longer than that of untreated ones (Table 2).

Prognostic analysis

We collected nine possible factors from other studies that influenced the survival of these patients. Based on univariate analysis, sex, age, AFP, maximum tumor diameter, and symptoms had no significant prognostic value ($P > 0.05$); however, extrahepatic metastasis, liver function, treatment, and intrahepatic metastasis significantly affected the prognosis ($P < 0.05$). Based on multivariate analysis, liver function ($P = 0.045$), intrahepatic metastasis ($P = 0.029$), and treatment ($P = 0.045$) were independent prognostic factors (Figure 6 and Table 3).

DISCUSSION

Epithelioid hemangioendothelioma is a rare tumor of vascular origin with low-to-moderate grade malignant properties. It arises preferentially in the soft tissues, lungs, and bones, and rarely in the liver (with a global incidence of < 1 in 1000000)[3].

Table 2 Treatments and prognosis of patients with hepatic epithelioid hemangioendothelioma

Treatment and outcome, *n* = 118	*n* (%)	Mean survival time in months, mean ± SD
LR	35 (29.7)	158.6 ± 20.5
LT	19 (16.1)	147.3 ± 13.8
Palliative treatment	15 (12.7)	4.2 ± 0.8
TACE	12 (10.2)	90.8 ± 13.4
Chemotherapy	13 (11.0)	71.4 ± 23.5
Other treatments	6 (5.1)	55.0 ± 17.0
Antiangiogenic therapy	18 (15.3)	83.1 ± 9.7

LR: Liver resection; LT: Liver transplantation; TACE: Transhepatic arterial chemotherapy and embolization.

Table 3 Results of univariable and multivariate analysis

Parameter	Univariate analysis		Multivariate analysis	
	HR (95%CI)	*P* value	HR (95%CI)	*P* value
Sex, male/female	1.175 (0.549-2.513)	0.678		
Age, > 45 yr/≤ 45 yr	0.952 (0.447-2.027)	0.898		
Symptoms, symptomatic/asymptomatic	3.047 (0.911-10.185)	0.070		
AFP, elevated/normal	1.261 (0.555-2.863)	0.579		
Liver function, abnormal/normal	2.720 (1.236-5.988)	0.013	2.258 (1.017-5.009)	0.045
Maximum diameter of tumor, ≥ 5 cm/< 5 cm	2.430 (0.856-6.901)	0.096		
Intrahepatic metastasis, yes/no	3.553 (1.228-10.277)	0.019	3.930 (1.152-13.404)	0.029
Extrahepatic metastasis, yes/no	2.328 (1.065-5.089)	0.034		0.558
Treatments, nonsurgical treatment/surgical treatment	2.831 (1.195-6.704)	0.018	2.591 (1.022-6.565)	0.045

HR: Hazard ratio; CI: Confidence interval; AFP: Alpha fetoprotein.

Demographics

HEHE occurs in all age groups, but it primarily affects middle-aged women[4]. The pathogenesis of HEHE remains unclear, and it is speculated that it is related to oral contraceptive use[5], pregnancy and hormone therapy[6], vinyl chloride pollution[7], asbestos[8], colloidal thorium oxide[9], trauma repair [10], and viral hepatitis[11].

Clinical features

The clinical manifestations of HEHE were variable and nonspecific. Approximately half of the patients had abnormal liver function. Tumor markers were normal in most patients. The incidence of extrahepatic metastasis was 34.5% at the time of diagnosis. The most common sites of extrahepatic involvement were the lungs. The radiologic features of HEHE can vary, and it can present in diffuse, multifocal, or solitary nodular forms. The "target sign", "capsule retraction sign", and "lollipop sign" [12,13] support the diagnosis of the disease, but the specificity is not high, and the final diagnosis must rely on pathological examination. Immunohistochemical staining can provide the evidence of endothelial differentiation for the definitive diagnosis of HEHE. Neoplastic cells are positive for endothelial markers (FVIII-RAg, CD31, and CD34)[14]. The lymphatic endothelial marker D2-40 is specifically expressed in 63.6% of epithelioid hemangioendotheliomas. At the genetic level, two specific fusion genes have been identified for HEHE. *WWTR1-CAMTA1* and *YAP1-TFE3* are pathognomonic for the diagnosis. In this study, *WWTR1-CAMTA1* gene fusions were observed in 60% of cases, and *YAP1-TFE3* gene fusions were observed in 75% of cases[15-17].

Treatments and prognosis

A standard treatment for HEHE has not been established owing to its low incidence. The management of patients with HEHE includes LR, LT, palliative treatments, TACE, chemotherapy, antiangiogenic

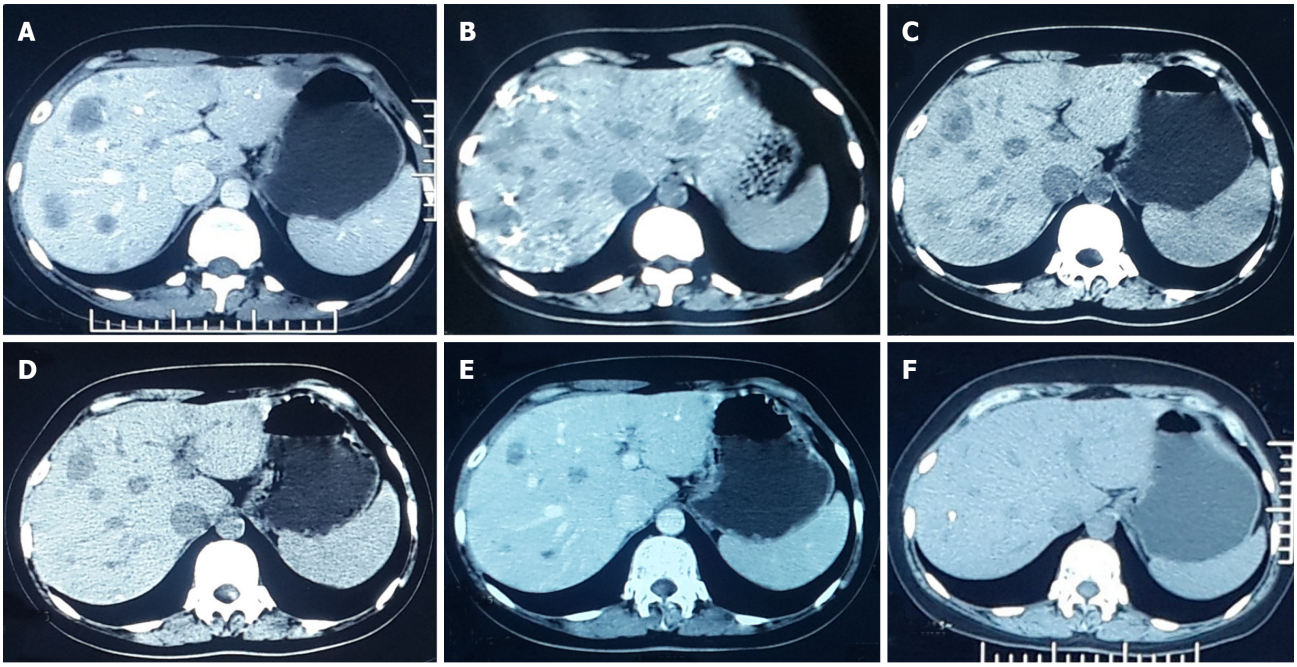

DOI: 10.12998/wjcc.v10.i17.5606 **Copyright** ©The Author(s) 2022.

Figure 3 Abdominal computed tomography of case two. A: Computed tomography showed multiple hypodense hepatic nodular formations, all of which were slightly enhanced during the arterial phase; B: After four cycles of transhepatic arterial chemotherapy and embolization, the number of lesions increased; C-F: After 18 mo of interferon treatment, the lesions were gradually reduced and disappeared.

therapy, and other treatments, such as traditional Chinese medications and radiofrequency ablation.

For localized disease, complete resection of the tumor is preferred to reduce the chances of recurrence. Palliative resection is not suggested because these tumors tend to behave aggressively after LR[18]. In this study, case one had no recurrence 4 years after LR. The mean survival time of patients after LR was better than that after other treatments. The 5-year survival rate after resection was 86% [19]. Radical hepatic resection with negative margins was the best curative approach if feasible and was associated with the best prognosis.

However, in the majority of the patients, oncologic resection is impossible because of the multicentricity of the lesions or anatomic difficulties. LT had been proposed as the treatment of choice in patients with unresectable and diffuse HEHE. In this study, after LT, the mean survival time was lower than that after LR but better than that after other nonsurgical treatments. Notably, unlike other malignant hepatic tumors, limited extrahepatic disease should not be considered as an absolute contraindication to LT as the life expectancy of patients with HEHE is potentially favorable[20]. Zamparelli *et al*[21] described a patient who showed a good outcome following LT despite lung metastasis. The 5-year survival rate after LT was 54%-88% (superior to the overall survival of other indications for LT)[22].

The optimal treatment for patients who do not undergo surgical treatment remains uncertain. There is still controversy about the effectiveness of traditional chemotherapeutic drugs. Doxorubicin, 5-fluorouracil, cyclophosphamide, and platinum are the most commonly used drugs for chemotherapy [23]. In this study, one patient with HEHE who had lung metastasis was treated with adriamycin liposomes and was alive after 9 years[24]. Patients who received chemotherapy had significantly better survival than those who did not receive treatment. However, another study suggested that chemotherapy in patients who do not undergo surgical treatment decreased their 5-year survival rate (43.6%) compared with patients who did not receive treatment (82.9%)[25]. These differences in survival can be explained by the very different levels of HEHE aggressiveness and the diversity of chemotherapy regimens in addition to selection biases resulting from the small sample size of the investigated studies. Hence, the effectiveness of traditional chemotherapy drugs for HEHE warrants further investigation.

In this study, 10.2% of the patients underwent TACE, and their mean survival time was 90.8 mo, which showed a trend of prolonged survival compared with other nonsurgical treatments. In this study, one patient was treated with the combination of TACE and the administration of cisplatin, pirarubicin, and hydroxyamptothecin. This patient survived for 112.0 mo[26]. However, another patient died of hepatic failure 4.0 mo after treatment with TACE[27]. Clinicians should be aware of the potential adverse effects of hepatic decompensation that is induced by TACE, particularly in cases of widespread tumor involvement and poorly preserved hepatic function. TACE may be a valid treatment for patients with HEHE who have advanced hepatic lesions and good liver reserve.

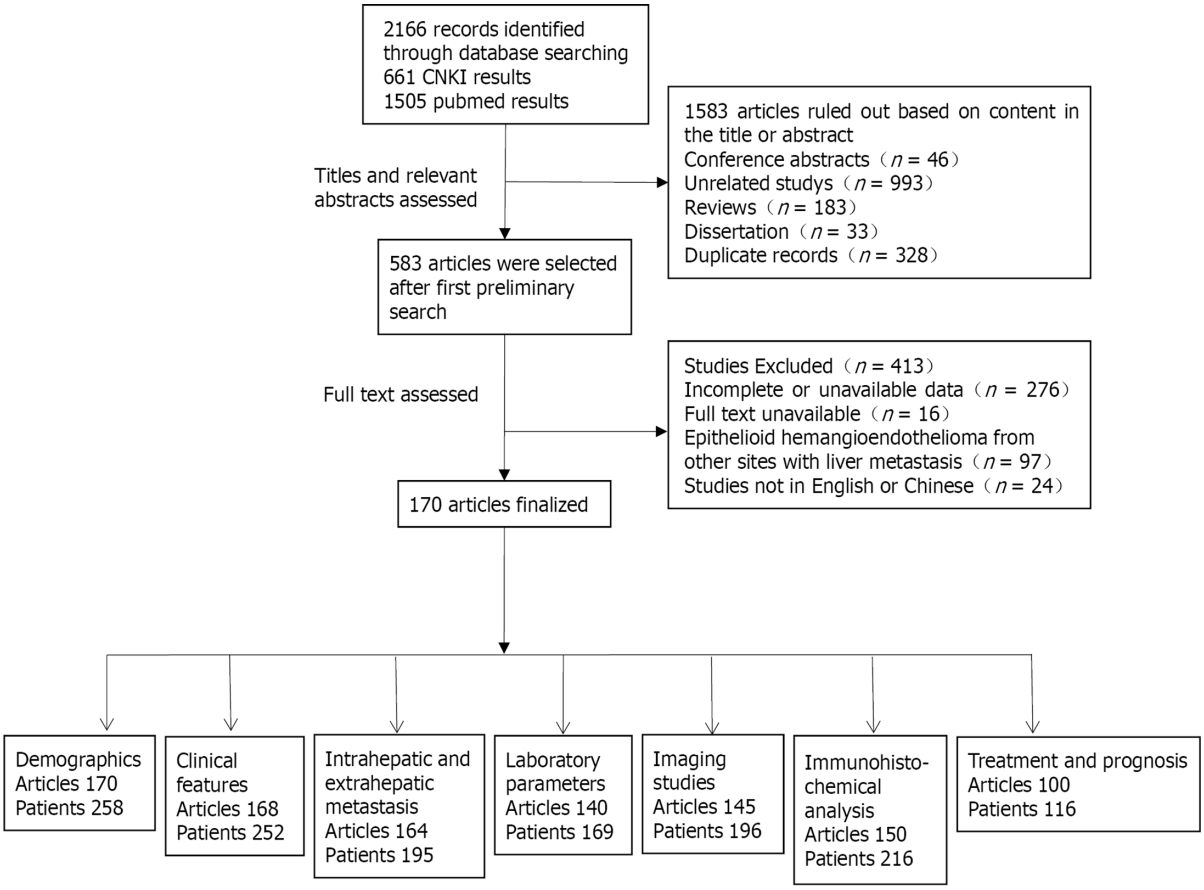

DOI: 10.12998/wjcc.v10.i17.5606 **Copyright** ©The Author(s) 2022.

Figure 4 Search and selection process. CNKI: China National Knowledge Infrastructure.

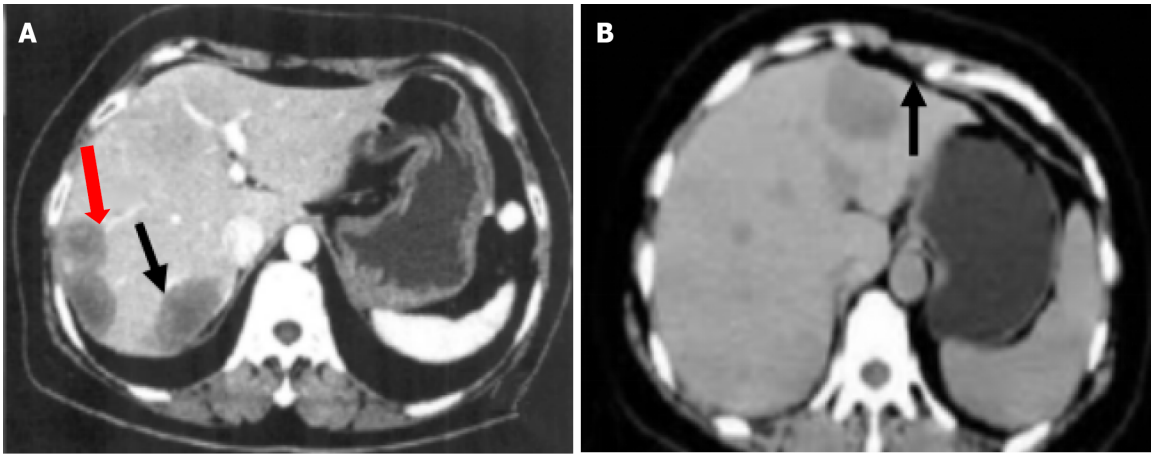

DOI: 10.12998/wjcc.v10.i17.5606 **Copyright** ©The Author(s) 2022.

Figure 5 Abdominal computed tomography of hepatic epithelioid hemangioendothelioma. A: Target sign (black arrow) and lollipop sign (red arrow); B: Capsular retraction (black arrow).

Because HEHE originates from vascular endothelial cells, antiangiogenic drugs, such as IFN, sunitinib, thalidomide, sorafenib, and bevacizumab, have attracted the attention of researchers. In this study, the mean survival time of patients treated with antiangiogenic drugs was similar to that of patients treated with TACE. One patient with pulmonary metastasis was treated with sunitinib for 6 years, which resulted in a substantial regression of extrahepatic disease[28]. The French Sarcoma Group previously reported the outcome of sorafenib treatment in a series of 15 patients with HEHE, and the Eastern Cooperative Oncology Group reported the results of bevacizumab treatment in a series of 7 patients with HEHE. Both studies were phase II trials including patients with advanced, unresectable, metastatic diseases. Both drugs could stabilize the disease up to 10.0 mo in 20%-40% of the patients;

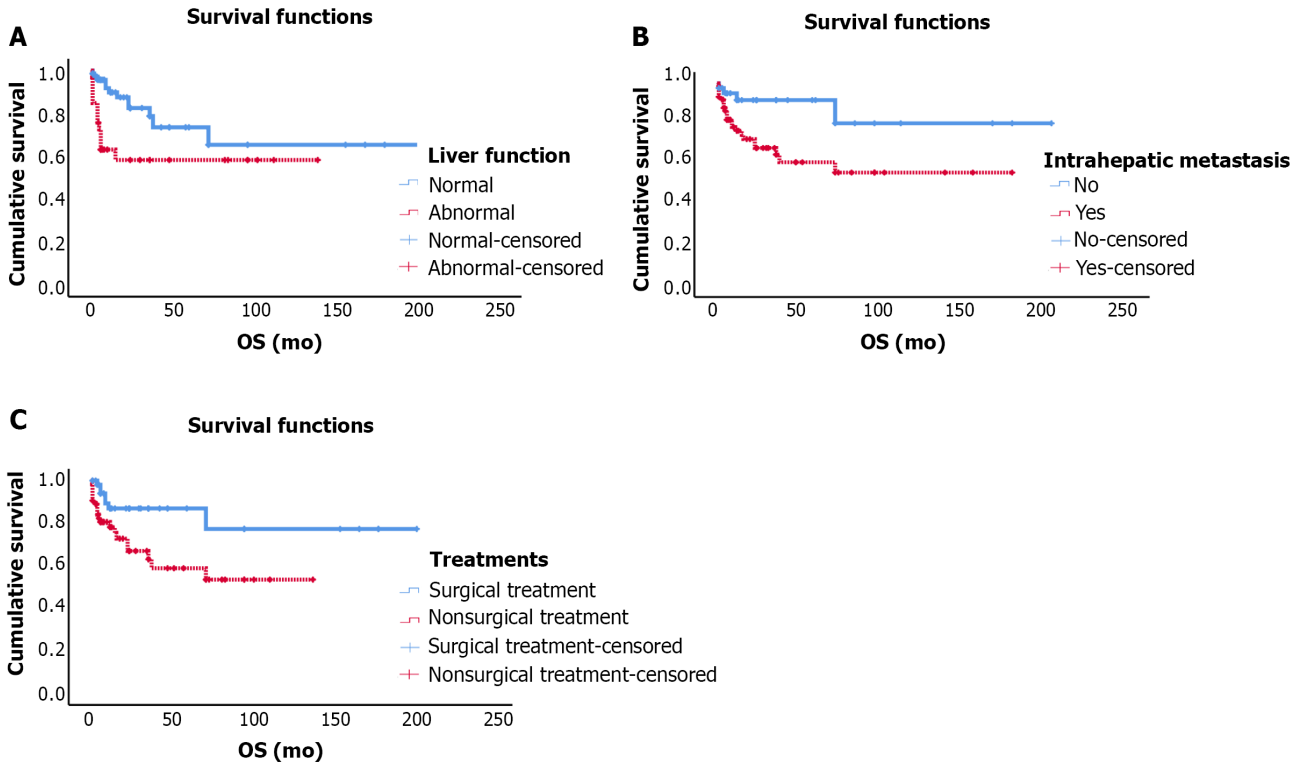

DOI: 10.12998/wjcc.v10.i17.5606 **Copyright** ©The Author(s) 2022.

Figure 6 Overall survival of patients with hepatic epithelioid hemangioendothelioma. A-C: Overall survival according to liver function (A), intrahepatic metastasis (B), and treatment (C). OS: Overall survival.

approximately 10% of the patients showed a partial response up to 6.0 mo[29,30]. IFN therapy for HEHE has also been proposed for tumor reduction and metastasis prevention[31]. IFN has been reported to inhibit cancer cell growth, activate immune cells, inhibit vascularization, and induce cytokines[32,33]. In this study, case two underwent TACE, but the disease was not controlled, and she was subsequently treated with IFN-α2b. The lesion gradually shrank, and the disease was in complete remission for 7 years. TACE can cause ischemia and necrosis of the cancer tissue and control tumor growth. However, hypoxia after treatment can upregulate angiogenic factors, stimulate the proliferation of residual tumor cells, and lead to tumor survival or recurrence[34]. The combination of IFN with TACE can be synergistic for the treatment of HEHE by reducing the stimulation of tumor cells by angiogenic factors and inhibiting tumor angiogenesis. This proved to be an effective, tolerable regimen for a patient with metastatic hepatic hemangioendothelioma. Although LT and LR may be the best options for improved survival, clinicians should consider the use of TACE with antiangiogenic drugs in the treatment of HEHE, particularly in those awaiting LT or nonsurgical candidates.

The clinical course of HEHE is variable, ranging from spontaneous regression and long-term survival without any treatment to a rapidly progressive and deadly course. Makhlouf *et al*[6] reported one patient who was alive after 27 years without any treatment. However, in this study, the mean survival time of untreated patients was only 4.2 mo. Compared with the untreated patients, the survival time of the treated patients was significantly longer. This may be because most of the untreated patients had poor prognostic factors, 53.3% had abnormal liver function, and 60.0% had intrahepatic metastases. Notably, there are some reports of long-term survival in the presence of stable HEHE without any treatment. However, until the reliable identification of patients with nonaggressive stable disease is possible, a wait-and-see approach is not recommended.

The prognosis of HEHE was much better than that of other hepatic malignant tumors. The 1-, 5-, and 10-year survival rates of all patients were 82%, 71%, and 64%, respectively. The prognostic factors of HEHE remain mostly undetermined till date. This study found that patients with intrahepatic metastasis (diffuse type) and liver dysfunction have a poor prognosis. Unlike other liver malignancies, the presence of extrahepatic metastases was not an independent risk factor for poor prognosis. Active treatment should be considered in cases of liver decompensation or radiological evidence of diffuse or progressive disease.

CONCLUSION

The clinical course of HEHE is rare and variable, and patients with intrahepatic metastases and liver dysfunction may have a poorer prognosis than those without. Surgical intervention, whether LR or transplantation, might be warranted regardless of extrahepatic metastasis. For patients without the option for surgery, clinicians should consider the use of TACE with antiangiogenic drugs in the treatment of HEHE.

ARTICLE HIGHLIGHTS

Research background

Hepatic epithelioid hemangioendothelioma (HEHE) is a rare hepatic vascular tumor with unpredictable malignant potential.

Research motivation

The etiology, characteristics, diagnosis, treatment, and prognosis of HEHE are not well-understood, and large-scale retrospective studies are required to better understand this disease.

Research objectives

To determine the characteristics of HEHE and identify its optimal treatments and prognostic factors.

Research methods

The clinical data of two patients diagnosed with HEHE at the Fourth Hospital of Hebei Medical University and 258 previously reported cases retrieved from the China National Knowledge Infrastructure and PubMed databases between 1996 and 2021 were combined and summarized. Information such as clinical features, laboratory examination findings, imaging findings, pathological characteristics, treatment, and survival periods were reviewed. Kaplan-Meir curves were used for survival analysis. Prognostic factors were identified by Cox regression analysis.

Research results

The management options for patients with HEHE included liver resection (LR, 29.7%), liver transplantation (16.1%), palliative treatments (12.7%), transhepatic arterial chemotherapy and embolization (10.2%), chemotherapy (11.0%), antiangiogenic therapy (15.3%), and other treatments (5.1%); the mean survival time was 158.6, 147.3, 4.2, 90.8, 71.4, 83.1, and 55.0 mo, respectively. Multivariate analysis showed that liver function (P = 0.045), intrahepatic metastasis (P = 0.029), and treatment (P = 0.045) were independent prognostic factors.

Research conclusions

The clinical course of HEHE is rare and variable, and patients with intrahepatic metastases and liver dysfunction may have a poorer prognosis than those without. Surgical intervention, whether LR or transplantation, might be warranted regardless of extrahepatic metastasis. For patients without the option for surgery, clinicians should consider the use of transhepatic arterial chemotherapy and embolization with antiangiogenic drugs in the treatment of HEHE.

Research perspectives

Large prospective studies are needed to determine the best nonsurgical treatment options.

FOOTNOTES

Author contributions: Yin F designed the research study; Zhao M and Yin F performed the research, analyzed the data, and wrote the manuscript; all authors have read and approved the final manuscript.

Institutional review board statement: The study was reviewed and approved by the Ethics Committee and Institutional Review Board of The Fourth Hospital of Hebei Medical University.

Conflict-of-interest statement: There are no conflicts of interest to report.

Data sharing statement: The data that support the findings of this study are available from the corresponding author, upon reasonable request.

Open-Access: This article is an open-access article that was selected by an in-house editor and fully peer-reviewed by

external reviewers. It is distributed in accordance with the Creative Commons Attribution NonCommercial (CC BY-NC 4.0) license, which permits others to distribute, remix, adapt, build upon this work non-commercially, and license their derivative works on different terms, provided the original work is properly cited and the use is non-commercial. See: https://creativecommons.org/Licenses/by-nc/4.0/

Country/Territory of origin: China

ORCID number: Man Zhao 0000-0001-7368-1079; Fei Yin 0000-0002-1075-0951.

S-Editor: Chen YL
L-Editor: Wang TQ
P-Editor: Chen YL

REFERENCES

1 **Sardaro A**, Bardoscia L, Petruzzelli MF, Portaluri M. Epithelioid hemangioendothelioma: an overview and update on a rare vascular tumor. *Oncol Rev* 2014; **8**: 259 [PMID: 25992243 DOI: 10.4081/oncol.2014.259]
2 **Ishak KG**, Sesterhenn IA, Goodman ZD, Rabin L, Stromeyer FW. Epithelioid hemangioendothelioma of the liver: a clinicopathologic and follow-up study of 32 cases. *Hum Pathol* 1984; **15**: 839-852 [PMID: 6088383 DOI: 10.1016/s0046-8177(84)80145-8]
3 **Bioulac-Sage P**, Laumonier H, Laurent C, Blanc JF, Balabaud C. Benign and malignant vascular tumors of the liver in adults. *Semin Liver Dis* 2008; **28**: 302-314 [PMID: 18814083 DOI: 10.1055/s-0028-1085098]
4 **Giardino A**, Miller FH, Kalb B, Ramalho M, Martin DR, Rodacki K, Woosley JT, Semelka RC. Hepatic epithelioid hemangioendothelioma: a report from three university centers. *Radiol Bras* 2016; **49**: 288-294 [PMID: 27818541 DOI: 10.1590/0100-3984.2015.0059]
5 **Singhal S**, Jain S, Singla M, Pippal RB, Gondal R, Agarwal A, Kar P. Multifocal epitheloid hemangioendothelioma of liver after long-term oral contraceptive use--a case report and discussion of management difficulties encountered. *J Gastrointest Cancer* 2009; **40**: 59-63 [PMID: 19711203 DOI: 10.1007/s12029-009-9083-x]
6 **Makhlouf HR**, Ishak KG, Goodman ZD. Epithelioid hemangioendothelioma of the liver: a clinicopathologic study of 137 cases. *Cancer* 1999; **85**: 562-582 [PMID: 10091730 DOI: 10.1002/(sici)1097-0142(19990201)85:3<562::aid-cncr7>3.0.co;2-t]
7 **Darras T**, Moisse R, Colette JM. Epithelioid hemangioendothelioma of the liver. *J Belge Radiol* 1988; **71**: 722-723 [PMID: 3243752]
8 **Al-Shraim M**, Mahboub B, Neligan PC, Chamberlain D, Ghazarian D. Primary pleural epithelioid haemangioendothelioma with metastases to the skin. A case report and literature review. *J Clin Pathol* 2005; **58**: 107-109 [PMID: 15623498 DOI: 10.1136/jcp.2004.018937]
9 **Soslow RA**, Yin P, Steinberg CR, Yang GC. Cytopathologic features of hepatic epithelioid hemangioendothelioma. *Diagn Cytopathol* 1997; **17**: 50-53 [PMID: 9218904 DOI: 10.1002/(sici)1097-0339(199707)17:1<50::aid-dc10>3.0.co;2-9]
10 **Terada T**, Nakanuma Y, Hoso M, Kono N, Watanabe K. Hepatic epithelioid hemangioendothelioma in primary biliary cirrhosis. *Gastroenterology* 1989; **97**: 810-811 [PMID: 2753340 DOI: 10.1016/0016-5085(89)90675-6]
11 **Radin DR**, Craig JR, Colletti PM, Ralls PW, Halls JM. Hepatic epithelioid hemangioendothelioma. *Radiology* 1988; **169**: 145-148 [PMID: 3420251 DOI: 10.1148/radiology.169.1.3420251]
12 **Gan LU**, Chang R, Jin H, Yang LI. Typical CT and MRI signs of hepatic epithelioid hemangioendothelioma. *Oncol Lett* 2016; **11**: 1699-1706 [PMID: 26998064 DOI: 10.3892/ol.2016.4149]
13 **Miller WJ**, Dodd GD 3rd, Federle MP, Baron RL. Epithelioid hemangioendothelioma of the liver: imaging findings with pathologic correlation. *AJR Am J Roentgenol* 1992; **159**: 53-57 [PMID: 1302463 DOI: 10.2214/ajr.159.1.1302463]
14 **Azzam RI**, Alshak NS, Pham HP. AIRP best cases in radiologic-pathologic correlation: Hepatic epithelioid hemangioendothelioma. *Radiographics* 2012; **32**: 789-794 [PMID: 22582359 DOI: 10.1148/rg.323115010]
15 **Errani C**, Zhang L, Sung YS, Hajdu M, Singer S, Maki RG, Healey JH, Antonescu CR. A novel WWTR1-CAMTA1 gene fusion is a consistent abnormality in epithelioid hemangioendothelioma of different anatomic sites. Genes Chromosomes Cancer 2011; 50: 644–653 [PMID: 21584898 DOI: 10.1002/gcc.20886]
16 **Kou K**, Chen YG, Zhou JP, Sun XD, Sun DW, Li SX, Lv GY. Hepatic epithelioid hemangioendothelioma: Update on diagnosis and therapy. *World J Clin Cases* 2020; **8**: 3978-3987 [PMID: 33024754 DOI: 10.12998/wjcc.v8.i18.3978]
17 **Lee SJ**, Yang WI, Chung WS, Kim SK. Epithelioid hemangioendotheliomas with TFE3 gene translocations are compossible with CAMTA1 gene rearrangements. *Oncotarget* 2016; **7**: 7480-7488 [PMID: 26840265 DOI: 10.18632/oncotarget.7060]
18 **Penn I**. Hepatic transplantation for primary and metastatic cancers of the liver. *Surgery* 1991; **110**: 726-34; discussion 734 [PMID: 1656538]
19 **Grotz TE**, Nagorney D, Donohue J, Que F, Kendrick M, Farnell M, Harmsen S, Mulligan D, Nguyen J, Rosen C, Reid-Lombardo KM. Hepatic epithelioid haemangioendothelioma: is transplantation the only treatment option? *HPB (Oxford)* 2010; **12**: 546-553 [PMID: 20887322 DOI: 10.1111/j.1477-2574.2010.00213.x]
20 **Lai Q**, Feys E, Karam V, Adam R, Klempnauer J, Oliverius M, Mazzaferro V, Pascher A, Remiszewski P, Isoniemi H, Pirenne J, Foss A, Ericzon BG, Markovic S, Lerut JP; European Liver Intestine Transplant Association (ELITA). Hepatic Epithelioid Hemangioendothelioma and Adult Liver Transplantation: Proposal for a Prognostic Score Based on the Analysis of the ELTR-ELITA Registry. *Transplantation* 2017; **101**: 555-564 [PMID: 28212256 DOI: 10.1097/TP.0000000000001603]

21 **Gigante E**, Lai Q, Lerut JP, Nault JC. Hepatic haemangioendothelioma: A proteiform disease. *Dig Liver Dis* 2020; **52**: 1039-1040 [PMID: 32553702 DOI: 10.1016/j.dld.2020.05.041]

22 **Remiszewski P**, Szczerba E, Kalinowski P, Gierej B, Dudek K, Grodzicki M, Kotulski M, Paluszkiewicz R, Patkowski W, Zieniewicz K, Krawczyk M. Epithelioid hemangioendothelioma of the liver as a rare indication for liver transplantation. *World J Gastroenterol* 2014; **20**: 11333-11339 [PMID: 25170219 DOI: 10.3748/wjg.v20.i32.11333]

23 **Pallotti MC**, Nannini M, Agostinelli C, Leoni S, Scioscio VD, Mandrioli A, Lolli C, Saponara M, Pileri S, Bolondi L, Biasco G, Pantaleo MA. Long-term durable response to lenalidomide in a patient with hepatic epithelioid hemangioendothelioma. *World J Gastroenterol* 2014; **20**: 7049-7054 [PMID: 24944501 DOI: 10.3748/wjg.v20.i22.7049]

24 **Grenader T**, Vernea F, Reinus C, Gabizon A. Malignant epithelioid hemangioendothelioma of the liver successfully treated with pegylated liposomal doxorubicin. *J Clin Oncol* 2011; **29**: e722-e724 [PMID: 21788568 DOI: 10.1200/JCO.2011.35.5891]

25 **Thomas RM**, Aloia TA, Truty MJ, Tseng WH, Choi EA, Curley SA, Vauthey JN, Abdalla EK. Treatment sequencing strategy for hepatic epithelioid haemangioendothelioma. *HPB (Oxford)* 2014; **16**: 677-685 [PMID: 24308564 DOI: 10.1111/hpb.12202]

26 **Li YY**, Liu J. Clinical Analysis of Hepatic Epithelioid Hemangioendothelioma:Five Cases Report. *Zhongguo Zhongliu Zazhi* 2013; **19** (11): 905-908 [DOI: 10.11735/j.issn.1671-170X.2013.11.B019]

27 **Hsu CY**, Liu YC, Li CP, Huang PH, Lin CH, Chao Y. Malignant hepatic epithelioid hemangioendothelioma with high-output heart failure: successful management of heart failure with transcatheter arterial chemoembolization. *Asia Pac J Clin Oncol* 2014; **10**: e118-e121 [PMID: 23384412 DOI: 10.1111/ajco.12056]

28 **Saada E**, Saint Paul MC, Gugenheim J, Follana P, François E. Metastatic hepatic epithelioid hemangio-endothelioma: long-term response to sunitinib malate. *Oncol Res Treat* 2014; **37**: 124-126 [PMID: 24685916 DOI: 10.1159/000360208]

29 **Chevreau C**, Le Cesne A, Ray-Coquard I, Italiano A, Cioffi A, Isambert N, Robin YM, Fournier C, Clisant S, Chaigneau L, Bay JO, Bompas E, Gauthier E, Blay JY, Penel N. Sorafenib in patients with progressive epithelioid hemangioendothelioma: a phase 2 study by the French Sarcoma Group (GSF/GETO). *Cancer* 2013; **119**: 2639-2644 [PMID: 23589078 DOI: 10.1002/cncr.28109]

30 **Agulnik M**, Yarber JL, Okuno SH, von Mehren M, Jovanovic BD, Brockstein BE, Evens AM, Benjamin RS. An open-label, multicenter, phase II study of bevacizumab for the treatment of angiosarcoma and epithelioid hemangioendotheliomas. *Ann Oncol* 2013; **24**: 257-263 [PMID: 22910841 DOI: 10.1093/annonc/mds237]

31 **Kayler LK**, Merion RM, Arenas JD, Magee JC, Campbell DA, Rudich SM, Punch JD. Epithelioid hemangioendothelioma of the liver disseminated to the peritoneum treated with liver transplantation and interferon alpha-2B. *Transplantation* 2002; **74**: 128-130 [PMID: 12134111 DOI: 10.1097/00007890-200207150-00022]

32 **Asmana Ningrum R**. Human interferon alpha-2b: a therapeutic protein for cancer treatment. *Scientifica (Cairo)* 2014; **2014**: 970315 [PMID: 24741445 DOI: 10.1155/2014/970315]

33 **Zhang L**, Tai YT, Ho MZG, Qiu L, Anderson KC. Interferon-alpha-based immunotherapies in the treatment of B cell-derived hematologic neoplasms in today's treat-to-target era. *Exp Hematol Oncol* 2017; **6**: 20 [PMID: 28725493 DOI: 10.1186/s40164-017-0081-6]

34 **Kawaoka T**, Aikata H, Hyogo H, Morio R, Morio K, Hatooka M, Fukuhara T, Kobayashi T, Naeshiro N, Miyaki D, Hiramatsu A, Imamura M, Kawakami Y, Takahashi S, Waki K, Tsuji K, Kohno H, Moriya T, Chayama K. Comparison of hepatic arterial infusion chemotherapy versus sorafenib monotherapy in patients with advanced hepatocellular carcinoma. *J Dig Dis* 2015; **16**: 505-512 [PMID: 26121102 DOI: 10.1111/1751-2980.12267]

World Journal of Clinical Cases

Submit a Manuscript: https://www.f6publishing.com

World J Clin Cases 2022 June 16; 10(17): 5620-5633

DOI: 10.12998/wjcc.v10.i17.5620

ISSN 2307-8960 (online)

ORIGINAL ARTICLE

Retrospective Study

Difference between type 2 gastroesophageal varices and isolated fundic varices in clinical profiles and portosystemic collaterals

Yu-Hu Song, Hong-Yu Xiang, Ke-Ke Si, Ze-Hui Wang, Yu Zhang, Chang Liu, Ke-Shu Xu, Xin Li

Specialty type: Gastroenterology and hepatology

Provenance and peer review: Unsolicited article; Externally peer reviewed.

Peer-review model: Single blind

Peer-review report's scientific quality classification

Grade A (Excellent): 0
Grade B (Very good): B
Grade C (Good): C
Grade D (Fair): 0
Grade E (Poor): 0

P-Reviewer: Kao JT, Taiwan; Yankol Y, United States

Received: December 8, 2021
Peer-review started: December 8, 2021
First decision: March 11, 2022
Revised: March 17, 2022
Accepted: April 9, 2022
Article in press: April 9, 2022
Published online: June 16, 2022

Yu-Hu Song, Hong-Yu Xiang, Ze-Hui Wang, Chang Liu, Ke-Shu Xu, Department of Gastroenterology, Union Hospital, Tongji Medical College, Huazhong University of Science and Technology, Wuhan 430022, Hubei Province, China

Ke-Ke Si, Yu Zhang, Xin Li, Department of Radiology, Union Hospital, Tongji Medical College, Huazhong University of Science and Technology, Wuhan 430022, Hubei Province, China

Ke-Ke Si, Yu Zhang, Hubei Province Key Laboratory of Molecular Imaging, Union Hospital, Tongji Medical College, Huazhong University of Science and Technology, Wuhan 430022, Hubei Province, China

Corresponding author: Xin Li, MD, PhD, Chief Doctor, Professor, Department of Radiology, Union Hospital, Tongji Medical College, Huazhong University of Science and Technology, No. 1277 Jiefang Avenue, Wuhan 430022, Hubei Province, China. lxwsry2014@163.com

Abstract

BACKGROUND

There is significant heterogeneity between gastroesophageal varices (GOV2) and isolated gastric varices (IGV1). The data on the difference between GOV2 and IGV1 are limited.

AIM

To determine the etiology, clinical profiles, endoscopic findings, imaging signs, portosystemic collaterals in patients with GOV2 and IGV1.

METHODS

Medical records of 252 patients with gastric fundal varices were retrospectively collected, and computed tomography images were analyzed.

RESULTS

Significant differences in routine blood examination, Child–Pugh classification and MELD scores were found between GOV2 and IGV1. The incidence of peptic ulcers in patients with IGV1 (26.55%) was higher than that of GOV2 (11.01%), while portal hypertensive gastropathy was more commonly found in patients with GOV2 (22.02%) than in those with IGV1 (3.54%). Typical radiological signs of cirrhotic liver were more commonly observed in patients with GOV2 than in those with IGV1. In patients with GOV2, the main afferent vessels were *via* the left gastric vein (LGV) (97.94%) and short gastric vein (SGV) (39.18%). In patients with

IGV1, the main afferent vessels were *via* the LGV (75.61%), SGV (63.41%) and posterior gastric vein (PGV) (43.90%). In IGV1 patients with pancreatic diseases, spleno-gastromental-superior mesenteric shunt (48.15%) was a major collateral vessel. In patients with fundic varices, the sizes of gastric/esophageal varices were positively correlated with afferent vessels (LGVs and PGVs) and efferent vessels (gastrorenal shunts). The size of the esophageal varices was negatively correlated with gastrorenal shunts in GOV2 patients.

CONCLUSION
Significant heterogeneity in the etiology and vascular changes between GOV2 and IGV1 is useful in making therapeutic decisions.

Key Words: Gastrorenal shunt; Spleno-gastroomental-superior mesenteric shunt; Liver cirrhosis; Pancreatic diseases

©The Author(s) 2022. Published by Baishideng Publishing Group Inc. All rights reserved.

Core Tip: These findings highlight the differences in the etiology, clinical profiles, endoscopic findings, imaging signs, portosystemic collaterals between patients with gastroesophageal varices and patients with isolated gastric varices. Knowledge of the etiology and portosystemic collaterals in our study is helpful in making therapeutic decisions.

Citation: Song YH, Xiang HY, Si KK, Wang ZH, Zhang Y, Liu C, Xu KS, Li X. Difference between type 2 gastroesophageal varices and isolated fundic varices in clinical profiles and portosystemic collaterals. *World J Clin Cases* 2022; 10(17): 5620-5633
URL: https://www.wjgnet.com/2307-8960/full/v10/i17/5620.htm
DOI: https://dx.doi.org/10.12998/wjcc.v10.i17.5620

INTRODUCTION

Gastric varices (GVs) are dilated submucosal veins in the stomach and represent a type of portosystemic shunt[1-4]. GVs are a life-threatening cause of upper gastrointestinal bleeding[2,3,5-8]. According to their location, GVs are classified as gastroesophageal varices (GOVs) and isolated gastric varices (IGVs) [2,9]. GOVs are divided into GOV1 (esophageal varices extending down to the cardia or the lesser curve of the stomach) and GOV2 (esophageal varices and fundic varices)[2,9,10]. IGVs are subdivided into IGV1 (fundic varices) and IGV2 (ectopic varices located anywhere in the stomach, such as in the body, antrum or pylorus)[3,9,10]. This classification, initially described by Sarin *et al*[9], was helpful in understanding the natural history and management of gastric varices[2]. Physiologically, GOV1 are a continuation of esophageal varices, and their vascular alternations and therapeutic strategies are similar to those of esophageal varices[2,10], and will not be further discussed in our study. Since the incidence of IGV2 and the morbidity of IGV2-induced bleeding are much lower than those of IGV1, patients with IGV2 were not enrolled in our research. Our study focused mainly on patients with IGV1 and GOV2, the so-called fundic varices. Obviously, there are some similarities between IGV1 and GOV2. The Sarin classification does not truly describe the heterogeneity in the etiology and vascular alternation. Thus, studies should be performed to determine the etiology, clinical profiles, and imaging signs in patients with GOV2 and IGV1. However, the data are limited. To obtain a better understanding of fundic varices (GOV2 and IGV1), a large sample of patients (119 patients with GOV2, 133 patients with IGV1) was enrolled, and then the etiology, clinical profiles, endoscopic findings, imaging signs, and portosystemic collateral veins in patients with fundic varices were investigated in our study. The data in our study are helpful in making therapeutic decisions.

MATERIALS AND METHODS

Further details are provided in the supplement.

Patient selection

Our retrospective study was performed at Union Hospital of Huazhong University of Science and Technology (Wuhan, China). A total of 252 consecutive patients with gastric fundal varices (GOV2 and IGV1) were enrolled from October 2013 to November 2020. The inclusion criteria were as follows: (1)

Patients with confirmed fundic varices after endoscopic examination; and (2) Stable hemodynamics for at least 5 d. The exclusion criteria were as follows: (1) Patients who received radiologic intervention [transjugular intrahepatic portosystemic shunt (TIPS) or balloon-occluded retrograde transvenous obliteration (BRTO)]; (2) Patients who received endoscopic therapy within 5 years [endoscopic variceal ligation (EVL), endoscopic injection sclerosis (EIS), endoscopic cyanoacrylate glue injection (ECGI)]; (3) Patients who received surgery (surgical portosystemic shunts, devascularization within 5 years); and (4) Patients who had insufficient data for further evaluation. The study was conducted according to the principles of the Declaration of Helsinki, and the protocol was approved by the ethics committee of Tongji Medical College, Huazhong University of Science and Technology (No. 2020-S216) and registered at www.chictr.org.cn (ChiCTR 2100042267).

Data collection

Baseline clinical data were obtained from medical records, and then tabulated into a database. The pertinent data included etiology, age, sex, peripheral blood routine examination, biochemistry, Child–Pugh, MELD, endoscopic findings, imaging signs, and PSCV (computed tomography portal venography).

Imaging technique and imaging analysis

Images were acquired from one of the following CT scanners (Siemens Somatom Definition AS+, Siemens Somatom Definition, and Toshiba Aquilion ONE). Multidetector row CT portal venography (CTPV) was performed after intravenous administration of high-iodine-concentration contrast medium (iodixanol) (320 mg/mL) [Hengrui Medicine Co., Ltd., China]. All images were retrospectively and independently reviewed by two radiologists. First, cirrhotic-related radiological signs were evaluated. We assessed the following signs: the volume of esophageal/gastric varices using the regional growth method [11], the diameter of the main portal vein (1 cm distal to the junction of the splenic vein and superior mesenteric vein), splenic vein and superior mesenteric vein (1 cm proximal to the junction), portal vein thrombosis, cavernous transformation of the portal vein, gallbladder wall thickening (> 3 mm)[12-14], the longest dimension of the spleen on an axial or coronal view and the presence of ascites. Second, afferent veins and efferent veins of gastric fundal varices were determined. Third, we assessed the presence of other PSCVs, such as paraumbilical veins, intrahepatic portosystemic shunts (> 3 mm), and retroperitoneal shunts.

Statistical analysis

Continuous variables were expressed as the mean and standard deviation or median (25^{th}-75^{th} percentiles). Categorical variables are presented as *n* (%). The interobserver agreement between the two radiologists for determining radiological features was determined using kappa (κ) statistics[15-17]. The correlations of categorical or continuous variables were analyzed by Spearman's correlation test. A *P* value less than 0.05 was considered to indicate statistical significance. Statistical analyses were performed using SPSS version 22.0 (IBM Inc., Armonk, NY, United States).

RESULTS

Study population

In this retrospective analysis, 252 consecutive patients with confirmed fundic varices were enrolled, and 30 patients were excluded (Figure 1). A total of 222 enrolled patients had liver cirrhosis (75.68%), pancreatic diseases (17.12%), and other diseases (7.21%) (Supplementary Table 1). Among patients with liver cirrhosis, the etiologies included hepatitis B/C (*n* = 106), alcoholic liver disease (*n* = 7), schistosomiasis (*n* = 9), autoimmune liver diseases (*n* = 11), cardiac cirrhosis (*n* = 1), Wilson diseases (*n* = 1), nonalcoholic fatty liver disease (*n* = 1), Budd-Chiari syndrome (*n* = 1) and cryptogenic cirrhosis (*n* = 31). Based on the Sarin classification, they were divided into the GOV2 group (109 patients) and IGV1 group (113 patients). Both GOV2 and IGV1 were primarily caused by liver cirrhosis (Supplementary Table 1). As shown in Supplementary Table 1, the results revealed that the constituent ratio of underlying diseases in cirrhotic patients with GOV2 was similar to that of IGV1 patients with liver cirrhosis. Importantly, the percentage of pancreatic diseases in the IGV1 group was greater than that in GOV2 patients.

Clinical profiles and endoscopic findings of enrolled patients with fundic varices

Demographic data, laboratory tests (peripheral blood routine examination and biochemistry) and endoscopic findings of enrolled patients were determined, and the results are shown in Table 1. First, demographic data showed that the median age of the patients was 53 years old, and male patients were more frequently affected than female patients. No differences in sex or age were observed between the GOV2 group and IGV1 group. Second, the results of peripheral blood routine examination demonstrated that the values of erythrocytes, leukocytes and platelets were lower in GOV2 patients

Table 1 Demographic characteristics and laboratory tests in different groups of enrolled patients

Variables	Total (222)	GOV2 (109)	IGV1 (113)	*P* value	IGV1 (113)			
					Liver cirrhosis (67)	Pancreatic diseases (38)	Others (8)	*P* value
Gender, *n* (M/F)	128/94	70/39	58/55	0.052	33/34	22/16	3/5	0.497
Age, yr	53.52 ± 12.20	53.00 ± 11.92	54.03 ± 12.51	0.532	55.61 ± 10.75	50.16 ± 14.74	59.13 ± 11.38	0.047
Peripheral blood routine examination								
Erythrocytes (10^{12}/L)	3.32 ± 0.78	3.20 ± 0.73	3.44 ± 0.81	0.022	3.47 ± 0.86	3.33 ± 0.75	3.83 ± 0.62	0.315
Leukocyte (10^9/L)	3.94 (2.56-5.62)	3.28 (2.00-5.32)	4.42 (3.29-5.86)	0.001	3.85 (2.75-5.52)	5.08 (3.79-7.61)	4.50 (4.27-5.86)	0.034
Platelet (10^9/L)	87.50 (57.00-148.75)	70.00 (49.00-137.00)	113.00 (73.00-156.00)	0.001	84.00 (59.00-129.00)	147.00 (96.00-181.00)	117.00 (115.00-187.00)	< 0.001
Biochemistry								
ALT (U/L)	28.00 (18.00-41.00)	28.00 (20.00-39.25)	27.00 (14.00-44.00)	0.403	34.00 (21.00-48.00)	18.00 (10.00-32.00)	12.00 (7.00-23.00)	< 0.001
AST (U/L)	33.00 (22.00-49.00)	35.00 (24.75-51.00)	31.00 (19.00-47.50)	0.095	41.00 (25.00-62.00)	19.00 (15.00-31.00)	20.00 (12.00-24.00)	< 0.001
ALP (U/L)	84.00 (64.00-126.00)	85.00 (67.75-119.25)	82.00 (59.00-128.00)	0.515	92.00 (62.00-139.00)	71.00 (51.00-113.00)	82.00 (49.00-100.00)	0.163
γGT (U/L)	35.00 (19.00-75.00)	36.50 (20.00-75.00)	33.00 (16.00-78.50)	0.523	46.00 (25.00-84.00)	21.00 (11.00-60.00)	19.00 (8.00-23.00)	0.001
T-Bil (μmol/L)	18.20 (13.00-26.00)	19.70 (14.83-29.45)	16.70 (10.65-24.05)	0.003	18.00 (13.00-26.70)	13.90 (9.80-19.40)	12.50 (10.20-16.70)	0.045
Albumin (g/L)	34.73 ± 6.43	33.54 ± 5.87	35.93 ± 6.77	0.007	34.64 ± 7.06	37.54 ± 5.87	39.40 ± 6.09	0.046
INR	1.22 (1.10-1.38)	1.27 (1.14-1.44)	1.18 (1.06-1.31)	0.001	1.22 (1.08-1.39)	1.12 (1.04-1.20)	1.04 (0.99-1.43)	0.021
Cholesterol	3.37 (2.68-4.15)	3.14 (2.54-4.04)	3.64 (2.82-4.35)	0.036	3.55 (2.82-4.27)	3.75 (2.96-4.77)	3.43 (2.30-7.95)	0.607
Child-Pugh classification (A/B/C)	113/70/4	48/49/1	65/21/3	< 0.001	35/14/3	26/7/0	4/0/0	0.467
MELD	10.00 (8.00-11.00)	10.00 (8.00-12.50)	9.00 (7.00-11.00)	0.006	10.00 (8.00-11.00)	8.00 (7.00-9.00)	7.00 (6.50-10.00)	0.007
Endoscopic findings								
Portal hypertensive gastropathy	28/222 (12.61%)	24/109 (22.02%)	4/113 (3.54%)	< 0.001	4/67 (5.97%)	0	0	/
Peptic ulcer	42/222 (18.92%)	12/109 (11.01%)	30/113 (26.55%)	0.003	26/67 (38.81%)	4/38 (10.53%)	0	0.001

Note: Continuous variables were presented as median (25th–75th percentiles) (skewed distribution) or mean ± SD (Gaussian distribution), and categorical variables are presented as count (percentage). Normal ranges: Erythrocytes: 4.3 × 10^{12}/L-5.8 × 10^{12}/L; Leukocyte: 3.5 × 10^9/L-9.5 × 10^9/L; Platelet: 125 × 10^9/L-350 × 10^9/L; Alanine aminotransferase: 5-40 U/L; Aspartate aminotransferase: 8-40 U/L; Alkaline phosphatase: 40-150 U/L; γ-glutamyl transpeptidase: 11-50 U/L; total bilirubin: 5.1-19.0 μmol/L; Albumin: 35-55 g/L; International normalized ratio: 0.80-1.31; cholesterol: < 5.2 mmol/L. GOV2: Gastroesophageal varices; IGV1: Isolated gastric varices; ALT: Alanine aminotransferase; AST: Aspartate aminotransferase; ALP: Alkaline phosphatase; γ-GT: γ-glutamyl transpeptidase; T-BIL: Total bilirubin; INR: International normalized ratio.

than of those in IGV1 patients. Additionally, among patients with IGV1, the values of erythrocytes, leukocytes and platelets were lower in cirrhotic patients than in patients with pancreatic diseases. Third, the biochemical parameters of the enrolled patients were also evaluated. No differences were observed in biomarkers of liver damage (ALT, AST) and cholestasis (ALP, γGT) between GOV2 patients and IGV1 patients. Biomarkers of liver synthetic ability (albumin, INR and cholesterol) in GOV2 patients were inferior to those of IGV1 patients (Table 1). As expected, biomarkers of liver damage, cholestasis and liver synthetic ability in cirrhotic patients with IGV1 were inferior to those of IGV1 patients resulting from pancreatic diseases. Fourth, the Child–Pugh classification and MELD score, the parameters for the prognosis of chronic liver disease, were calculated. The results showed that the

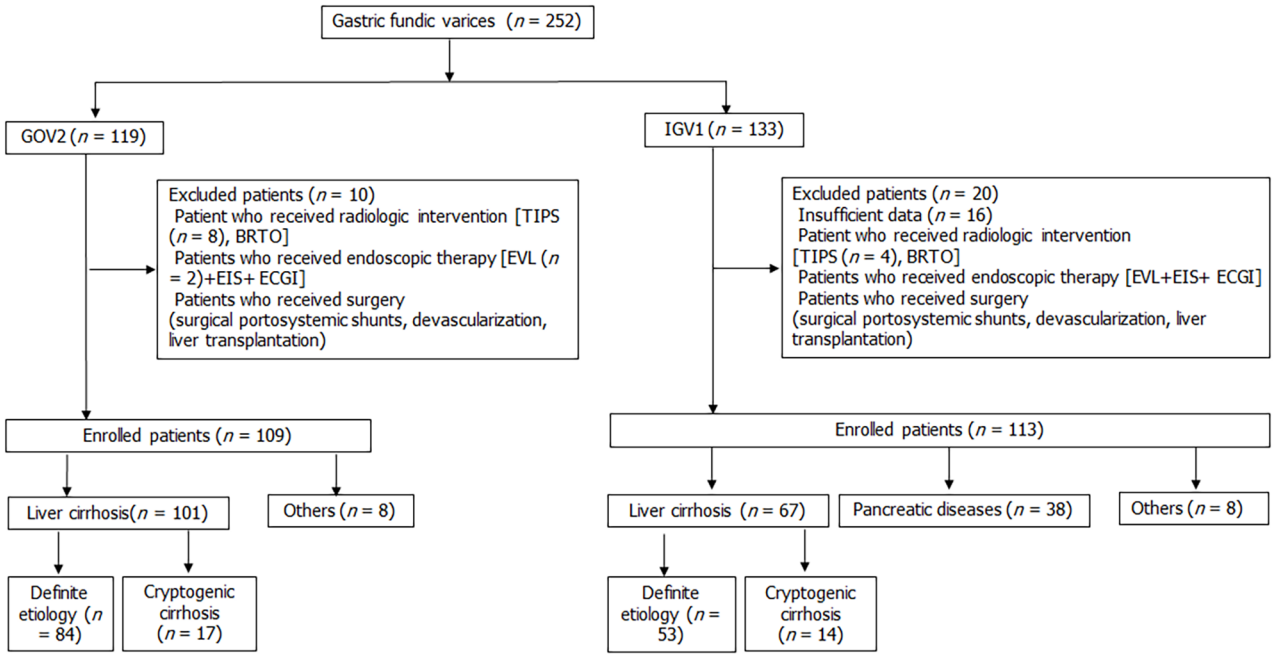

DOI: 10.12998/wjcc.v10.i17.5620 **Copyright** ©The Author(s) 2022.

Figure 1 Flowchart of the patients' enrollment. GOV2: Gastroesophageal varices; IGV1: Isolated gastric varices; TIPS: Transjugular intrahepatic portosystemic shunt; BRTO: Balloon-occluded retrograde transvenous obliteration; EVL: Endoscopic variceal ligation; EIS: Endoscopic injection sclerosis; ECGI: Endoscopic cyanoacrylate glue injection.

percentage of Child–Pugh class A in GOV1 patients was lower than that of IGV2 caused by liver cirrhosis or pancreatic diseases. Moreover, MELD scores in GOV1 patients were higher than those in IGV1 patients. Finally, endoscopic findings were assessed. The incidence of peptic ulcers in patients with IGV1 (26.55%) was higher than that in GOV2 patients (11.01%); portal hypertensive gastropathy (PHG) was more commonly observed in patients with GOV2 (22.02%) than in those with IGV2 (3.54%). Interestingly, in cirrhotic patients, a lower incidence of peptic ulcers and a higher incidence of PHG were found in GOV2 than in IGV1.

Radiological findings and portosystemic collaterals in patients with fundic varices

Radiological signs and portosystemic collateral vessels (PSCVs) were determined in patients with fundic varices using multidetector computed tomography (MDCT). Unfortunately, 43 cases were excluded because the patients had not received contrast CT scans or the image data were not obtained. First, typical radiological signs of liver cirrhosis were evaluated. Our study revealed gallbladder wall thickening in 42.07% of patients, ascites in 44.69% of cases, portal vein thrombosis in 18.99% of cases, and cavernous transformation of the portal vein in 11.73% of cases (Table 2). Importantly, the above radiologic signs were more commonly observed in patients with GOV2 than in those with IGV1. Moreover, the diameters of the main portal vein (PV), splenic vein and superior mesenteric vein (SMV) and the longest dimension of the spleen in the GOV2 group were larger than those in the IGV1 group. The mean volume of GVs in cirrhotic patients with IGV1 (10.00 mL) was larger than that of GOV2 (2.39 mL) patients and IGV1 patients caused by pancreatic diseases (4.12 mL). Second, afferent veins of GVs were reviewed. In patients with GOV2, gastric varices were principally supplied by the left gastric vein (LGV) (97.94%) and short gastric vein (SGV) (39.18%); in patients with IGV1, afferent veins of GVs were LGV (75.61%), SGV (63.41%) and posterior gastric vein (PGV) (43.90%). Third, efferent veins of gastric varices were also investigated. In patients with GOV2, gastric varices were drained by esophageal and para-esophageal varices (100%, data not shown), splenorenal shunts (11.34%) and gastrorenal shunts (21.65%); in patients with IGV1, efferent veins of cirrhotic patients with IGV1 were splenorenal shunts (14.00%) and gastrorenal shunts (78.00%) (Figure 2A and B). Interestingly, in IGV1 patients with pancreatic diseases, the splenogastromental-superior mesenteric shunt (48.15%) was a major collateral vessel due to splenic vein occlusion (Figure 2C). Finally, other PSCVs were assessed. Paraumbilical vein patency was more common in the GOV2 group (38.14%) than the IGV1 group (8.54%) (Table 2). A similar pattern was also observed in retroperitoneal shunts. Obvious intrahepatic portosystemic shunts were infrequent.

Correlations among portosystemic collateral veins in patients with GOV2

To provide useful reference information for the management of gastric varices, the relationship among different PSCVs should be illustrated. First, we determined the correlation between the volumes of

Table 2 Radiological findings and portosystemic collateral vessels in patients with gastric fundic varices

Variables	Total (179)	GOV2 (97)	IGV1 (82)	*P* value	IGV1 (82)			
					Liver cirrhosis (50)	Pancreatic diseases (27)	Others (5)	*P* value
Gallbladder wall thickening[1]	69/164 (42.07%)	51/92 (55.43%)	18/72 (25.00%)	< 0.001	10/46 (21.74%)	7/21 (33.33%)	1/5 (20.00%)	0.678
The longest dimension of spleen (cm)	14.06 (12.44-15.93)	15.74 ± 2.97	13.30 ± 2.25	< 0.001	13.50 ± 2.30	12.90 ± 1.62	13.55 ± 4.91	0.529
Ascites	80/179 (44.69%)	61/97 (62.89%)	19/82 (23.17%)	< 0.001	13/50 (26.00%)	6/27 (22.22%)	0	0.583
Portal vein thrombosis	34/179 (18.99%)	30/97 (30.93%)	4/82 (4.88%)	< 0.001	2/50 (4.00%)	2/27 (7.41%)	0	0.697
Cavernous transformation of portal vein	21/179 (11.73%)	18/97 (18.56%)	3/82 (3.66%)	< 0.001	1/50 (2.00%)	2/27 (7.41%)	0	0.405
The volume of gastric varices (mL)	3.35 (1.62-8.55)	2.39 (1.35-4.81)	5.60 (2.35-15.68)	< 0.001	10.00 (3.14-21.50)	4.12 (2.72-6.35)	1.24 (0.63-8.17)	0.005
The diameter of main portal vein (mm)	14.71 (12.19-16.59)	15.17 (13.44-17.21)	13.65 ± 2.76	< 0.001	13.08 ± 2.40	14.38 ± 3.21	15.14 ± 2.29	0.066
The diameter of splenic vein (mm)	10.14 (8.21-12.38)	11.00 (9.17-13.61)	9.08 ± 2.43	< 0.001	8.92 (7.19-10.67)	8.14 (5.18-10.95)	9.98 (9.42-12.37)	0.312
The diameter of superior mesenteric vein (mm)	11.78 (10.09-13.44)	12.63 (10.77-13.90)	11.06 ± 2.11	< 0.001	11.00 ± 2.02	11.23 ± 2.16	10.73 ± 3.07	0.845
Afferent veins of gastric varices								
Left gastric vein	157/179 (87.71%)	95/97 (97.94%)	62/82 (75.61%)	< 0.001	39/50 (78.00%)	21/27 (77.78%)	2/5 (40.00%)	0.194
Short gastric vein	90/179 (50.28%)	38/97 (39.18%)	52/82 (63.41%)	0.001	30/50 (60.00%)	22/27 (81.48%)	0	0.002
Posterior gastric vein	60/179 (33.52%)	24/97 (24.74%)	36/82 (43.90%)	0.007	25/50 (50.00%)	9/27 (33.33%)	2/5 (40.00%)	0.381
Efferent veins of gastric varices								
Splenorenal shunt	20/179 (11.17%)	11/97 (11.34%)	9/82 (10.98%)	0.939	7/50 (14.00%)	1/27 (3.70%)	1/5 (20.00%)	0.212
Gastrorenal shunt	65/179 (36.31%)	21/97 (21.65%)	44/82 (53.66%)	< 0.001	39/50 (78.00%)	4/27 (14.81%)	1/5 (20.00%)	< 0.001
Other portosystemic collateral vessels								
Spleno-gastroomental-superior mesenteric shunt	17/179 (9.50%)	1/97 (1.03%)	16/82 (19.51%)	< 0.001	3/50 (6.00%)	13/27 (48.15%)	0	< 0.001
Paraumbilical vein patency	44/179 (24.58%)	37/97 (38.14%)	7/82 (8.54%)	< 0.001	7/50 (14.00%)	0	0	/
Intrahepatic portosystemic shunts	7/179 (3.91%)	4/97 (4.12%)	3/82 (3.66%)	1.000	3/50 (6.00%)	0	0	/
Retroperitoneal shunt	52/179 (29.05%)	37/97 (38.14%)	15/82 (18.29%)	0.004	6/50 (12.00%)	8/27 (29.63%)	1/5 (20.00%)	0.131

[1]Indicated 15 of patients with fundic varices had received cholecystectomy.
GOV2: Gastroesophageal varices; IGV1: Isolated gastric varices.

varices and PSCVs. In patients with GOV2, the volume of the gastric varices was positively correlated with afferent veins (the maximum diameter of the LGV and PGV) (Table 3). In addition, the volume of GVs was associated with efferent veins (the maximum diameter of the gastrorenal shunt). Interestingly, the volume of esophageal varices was negatively correlated with the gastrorenal shunt diameter (Table 3), which revealed a negative correlation between the two major divisions of efferent veins. Second, the correlation between afferent veins and efferent veins was evaluated in patients with GOV2. Only a positive correlation between the maximum diameter of the PGV and the maximum diameter of the gastrorenal shunt was found (Table 3). Third, we demonstrated no correlation among gastric varices with other PSCVs (intrahepatic portosystemic shunt, paraumbilical vein patency and retroperitoneal

Table 3 The correlations between afferent/efferent veins and portosystemic collaterals in patients with gastroesophageal varices

Variables		The volume of varices (mL)		The diameter of main portal vein (mm)	Afferent veins			Efferent veins		Other portosystemic collateral vessels		
		The volume of EVs (mL)	The volume of GVs (mL)		Maximum diameter of LGV (mm)	Maximum diameter of PGV (mm)	Maximum diameter of SGV (mm)	Maximum diameter of SRS (mm)	Maximum diameter of GRS (mm)	Intrahepatic portosystemic shunts	Paraumbilical vein patency	Retroperitoneal shunt
Maximum diameter of LGV (mm)	Correlation coefficient	0.411	0.372	0.052	/	0.099	0.307	-0.374	-0.018	0.061	0.081	-0.039
	P value	0.000	0.000	0.632	/	0.654	0.061	0.258	0.940	0.556	0.437	0.711
	n	92	90	88	/	23	38	11	20	95	95	95
Short gastric vein	Correlation coefficient	0.139	0.066	0.013	0.132	-0.038	/	-0.179	0.268	0.046	0.022	0.065
	P value	0.182	0.532	0.903	0.204	0.859	/	0.598	0.241	0.655	0.831	0.524
	n	94	92	90	95	24	38	11	21	97	97	97
Posterior gastric vein	Correlation coefficient	-0.055	0.378	-0.239	0.199	/	0.100	0.298	0.520	0.121	-0.106	0.091
	P value	0.600	0.000	0.023	0.053	/	0.550	0.373	0.016	0.236	0.302	0.377
	n	94	92	90	95	24	38	11	21	97	97	97
Maximum diameter of splenorenal shunt (mm)	Correlation coefficient	0.200	-0.155	-0.533	-0.374	1.000	0.000	/	/	/	-0.418	0.000
	P value	0.580	0.650	0.139	0.258	/	1.000	/	/	/	0.200	1.000
	n	10	11	9	11	2	7	/	1	11	11	11
Maximum diameter of gastrorenal shunt (mm)	Correlation coefficient	-0.518	0.755	-0.434	-0.018	0.745	0.576	/	/	0.332	-0.113	-0.238
	P value	0.023	0.000	0.072	0.940	0.013	0.082	/	/	0.141	0.625	0.298
	n	19	20	18	20	10	10	1	/	21	21	21

The correlations of categorical or continuous variables were analyzed by Spearman correlation test. In determining the maximum diameter of a vessel, isolated saccular dilatation of a vessel in venous ectasia or venous aneurysm was excluded. EVs: Esophageal varices; GVs: Gastric varices; LGV: Left gastric vein; PGV: Posterior gastric vein; SGV: Short gastric vein; SRS: Splenorenal shunt; GRS: Gastrorenal shunt.

shunt) (Table 3). Finally, the results showed no correlation of the main portal vein with afferent/efferent veins of the GV, except for the diameter of the PGV (Table 3).

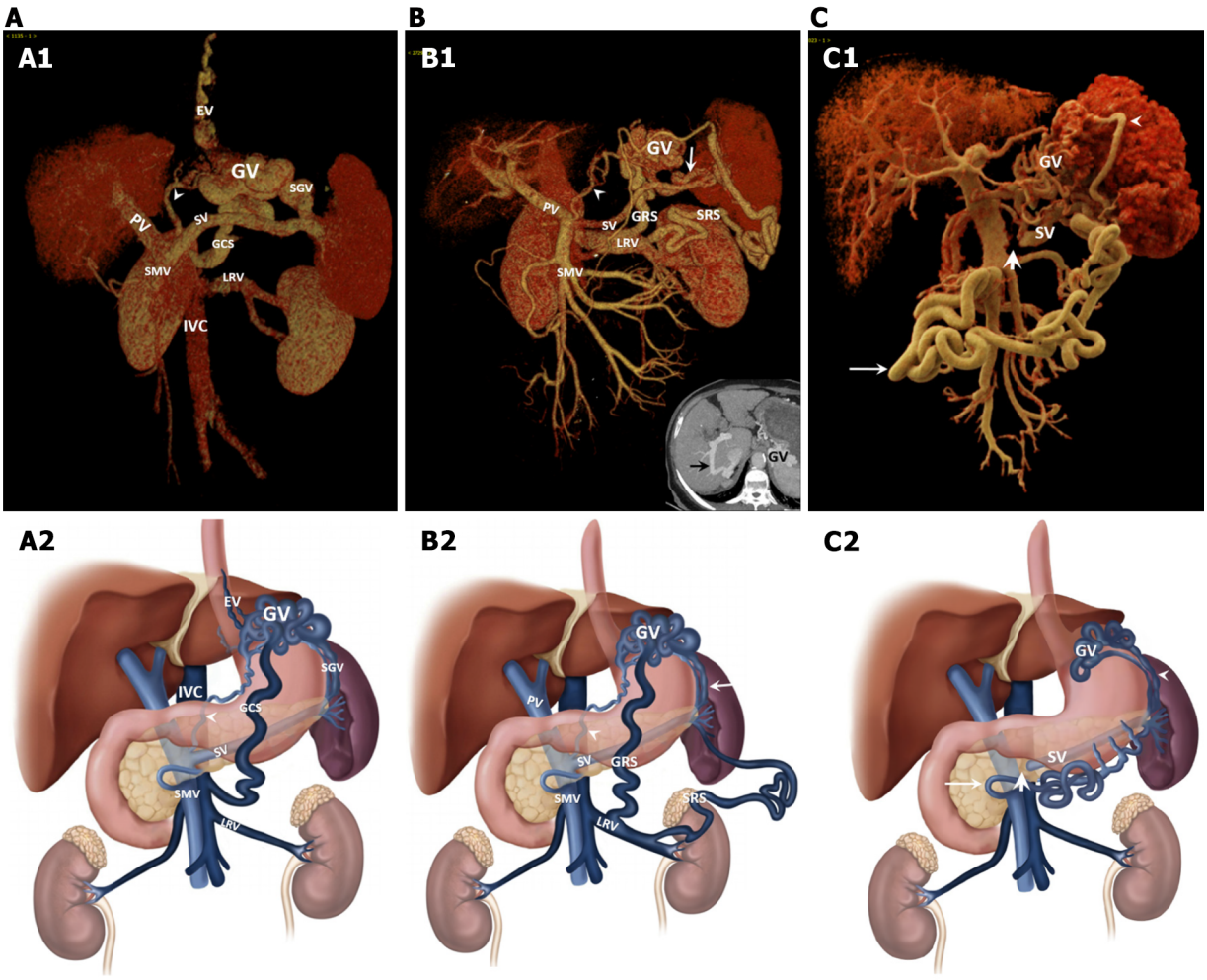

DOI: 10.12998/wjcc.v10.i17.5620 **Copyright** ©The Author(s) 2022.

Figure 2 Computed tomography portal venography of gastric variceal collateral vessels. A: Coronal oblique volume-rendered (VR) computed tomography (CT) portal venogram views (A1) and schematic drawing (A2) illustrated collateral circulation of esophageal varices (GVs) in the patient with gastroesophageal varices (75-years-old male patients with liver cirrhosis). GVs were supplied by left gastric vein (LGV) (arrowhead) and SGV, and drained by gastrocaval shunt (GCS), and esophageal and para-esophageal varices (EVs); B: Coronal oblique VR CT portal venogram views (B1) and schematic drawing (B2) illustrated collateral circulation of GVs in the patient with isolated gastric varices (IGV1) (75-years-old female patients). GVs were supplied by LGV (arrowhead) and SGV (white arrow), and drained by GRS, SRS and intrahepatic portosystemic shunts (black arrow in the MIP image); C: Coronal oblique cinematically rendered reconstruction in CT portal venogram views (C1) and schematic drawing (C2) showing collateral vessels in a 42-years-old male patient with IGV1 caused by pancreatic pseudocyst secondary to pancreatitis. GVs were supplied by SGV (arrowhead), spleno-gastroomental -superior mesenteric shunt (white arrow) was a major collateral vessel due to partial splenic vein occlusion (thick arrow).

Correlations among portosystemic collateral veins in patients with IGV1

The correlations among PSCVs in patients with IGV1 are shown in Table 4. First, the correlations between the volumes of gastric varices and efferent/afferent veins were determined, and the results showed that the volume of gastric varices was positively correlated with afferent veins (the maximum diameter of LGV and posterior gastric vein) and efferent veins (the maximum diameter of gastrorenal shunt). Second, the correlation between afferent veins and efferent veins was evaluated in patients with IGV1. The results revealed a positive correlation between the main afferent vessel (the diameter of gastrorenal shunts (GRS) and efferent veins (LGV, SGV and PGV)) (Table 4). Third, the results showed no correlations between major divisions of efferent/afferent veins and other portosystemic collateral vessels (intrahepatic portosystemic shunt, paraumbilical vein patency and retroperitoneal shunt). Finally, a negative correlation of the main portal vein with efferent veins (the gastrorenal shunt) was observed (Table 4).

DISCUSSION

Although the incidence of bleeding from GVs is relatively low, bleeding is more severe and is associated with higher mortality[2,3,18]. In this study, 222 patients with fundic varices were enrolled, and the

Table 4 The correlations between afferent/efferent veins and portosystemic collaterals in patients with isolated gastric varices

Variables		The volume of gastric varices (mL)	The diameter of main portal vein (mm)	Afferent veins			Efferent veins			Other portosystemic collateral vessels		
				Maximum diameter of LGV (mm)	Maximum diameter of SGV (mm)	Maximum diameter of PGV) (mm)	Maximum diameter of splenorenal shunt (mm)	Maximum diameter of gastrorenal shunt (mm)	Spleno-gastroomental-superior mesenteric shunt	Intrahepatic portosystemic shunts	Paraumbilical vein patency	Retroperitoneal shunt
Maximum diameter of LGV (mm)	Correlation coefficient	0.405	0.241	/	0.167	0.143	0.543	0.366	0.259	-0.211	-0.121	0.153
	P value	0.001	0.065	/	0.291	0.506	0.266	0.036	0.042	0.100	0.350	0.236
	n	59	59	/	42	24	6	33	62	62	62	62
Maximum diameter of SGV (mm)	Correlation coefficient	0.212	0.113	0.167	/	0.328	-0.600	0.421	0.223	0.007	-0.014	0.083
	P value	0.135	0.432	0.291	/	0.215	0.285	0.026	0.111	0.963	0.919	0.559
	n	51	51	42	/	16	5	28	52	52	52	52
Posterior gastric vein	Correlation coefficient	0.047	0.007	0.257	-0.317	/	0.548	-0.091	-0.064	0.220	0.082	0.090
	P value	0.682	0.949	0.044	0.022	/	0.127	0.555	0.571	0.047	0.467	0.422
	n	78	79	62	52	36	9	44	82	82	82	82
Maximum diameter of PGV (mm)	Correlation coefficient	0.667	0.012	0.143	0.328	/	1.000	0.506	0.093	-0.053	-0.111	-0.315
	P value	0.000	0.946	0.506	0.215	/	0.000	0.014	0.588	0.758	0.521	0.061
	n	34	33	24	16	/	3	23	36	36	36	36
Splenorenal shunt	Correlation coefficient	0.175	-0.008	0.093	-0.128	0.102	/	-0.131	0.024	-0.068	0.172	0.036
	P value	0.126	0.945	0.472	0.365	0.555	/	0.395	0.830	0.541	0.122	0.750
	n	78	79	62	52	36	9	44	82	82	82	82
Maximum diameter of Splenorenal shunt (mm)	Correlation coefficient	0.667	-0.083	0.543	-0.600	1.000	/	-0.500	-0.621	/	0.104	-0.414
	P value	0.071	0.831	0.266	0.285	0.000	/	0.667	0.074	/	0.791	0.268
	n	8	9	6	5	3	/	3	9	9	9	9
Gastrorenal shunt	Correlation coefficient	0.173	-0.245	-0.123	-0.148	-0.062	-0.456	/	-0.419	0.177	0.102	-0.141

	P value	0.129	0.029	0.340	0.296	0.718	0.217	/	0.000	0.112	0.364	0.205
	n	78	79	62	52	36	9	44	82	82	82	82
Maximum diameter of gastrorenal shunt (mm)	Correlation coefficient	0.735	-0.242	0.366	0.421	0.506	-0.500	/	0.043	0.018	0.149	-0.037
	P value	0.000	0.123	0.036	0.026	0.014	0.667	/	0.782	0.909	0.333	0.814
	n	44	42	33	28	23	3	/	44	44	44	44
Spleno-gastroomental-superior mesenteric shunt	Correlation coefficient	-0.025	0.314	0.259	0.223	0.093	-0.621	0.043	/	-0.096	-0.150	0.245
	P value	0.826	0.005	0.042	0.111	0.588	0.074	0.782	/	0.391	0.177	0.027
	n	78	79	62	52	36	9	44	/	82	82	82

The correlation of categorical or continuous variables was analyzed by Spearman correlation test. In determining the maximum diameter of a vessel, isolated saccular dilatation of a vessel in venous ectasia or venous aneurysm was excluded. LGV: Left gastric vein; SGV: Short gastric veins; PGV: Posterior gastric vein.

etiology, clinical profiles, imaging signs, and PSCVs were determined in patients with IGV1 and GOV2. The primary cause of fundic varices was liver cirrhosis. Left-side portal hypertension (LSPH) occurs as a result of narrowing and obstruction of the splenic vein secondary to pancreatitis, pancreatic cancer, and pancreatic pseudocysts, which usually results in the formation of isolated fundal varices[19]. Gastric varices were frequently supplied by LGVs, SGVs and PGVs; major efferent veins included esophageal varices, gastrorenal shunts, and splenorenal shunts. These findings were consistent with previous studies[1,3,4,20-22].

Obviously, there is substantial heterogeneity between IGV1 and GOV2. Liver cirrhosis is a major cause of GOV2, and the major etiologies of IGV1 include liver cirrhosis and pancreatic diseases. Cytopenia was frequently observed in patients with GOV2 compared with IGV1, which revealed that hypersplenism occurred more commonly in patients with GOV2. The constituent ratio of underlying diseases contributed to the difference in routine blood examination. In addition, cirrhotic patients with GOV2 had higher rates of hypersplenism than cirrhotic patients with IGV1. Simultaneously, abnormal liver function was more commonly observed in patients with GOV2. Normal liver function was observed in most of the patients with LSPH. The discrepancy between GOV2 and IGV1 was attributed to the constituent ratio of underlying diseases. Interestingly, PHG was more commonly observed in patients with GOV2 than in IGV1 patients. PHG, a complication of portal hypertension, is associated with portal venous pressure[23-25]. Patients with IGV1 have large gastrorenal shunts, so portal venous pressure in patients with IGV1 was lower than that in patients with GOV2[23,25]. In addition, the degree of liver dysfunction was correlated with the severity of PHG in cirrhotic patients[24]. High portal venous pressure and liver dysfunction resulted in a higher incidence of PHG in patients with GOV2. Interestingly, the incidence of peptic ulcers in patients with IGV1 was higher than that in GOV2 patients; HP infection, the use of NSAIDs, gastric mucosal blood flow, gastric mucosal barrier, epithelial renewal, and mucosa defense mechanisms are involved in ulcer formation. In patients with IGV1, gastrorenal shunts increased gastric submucosal shunting of blood away from the gastric mucosa,

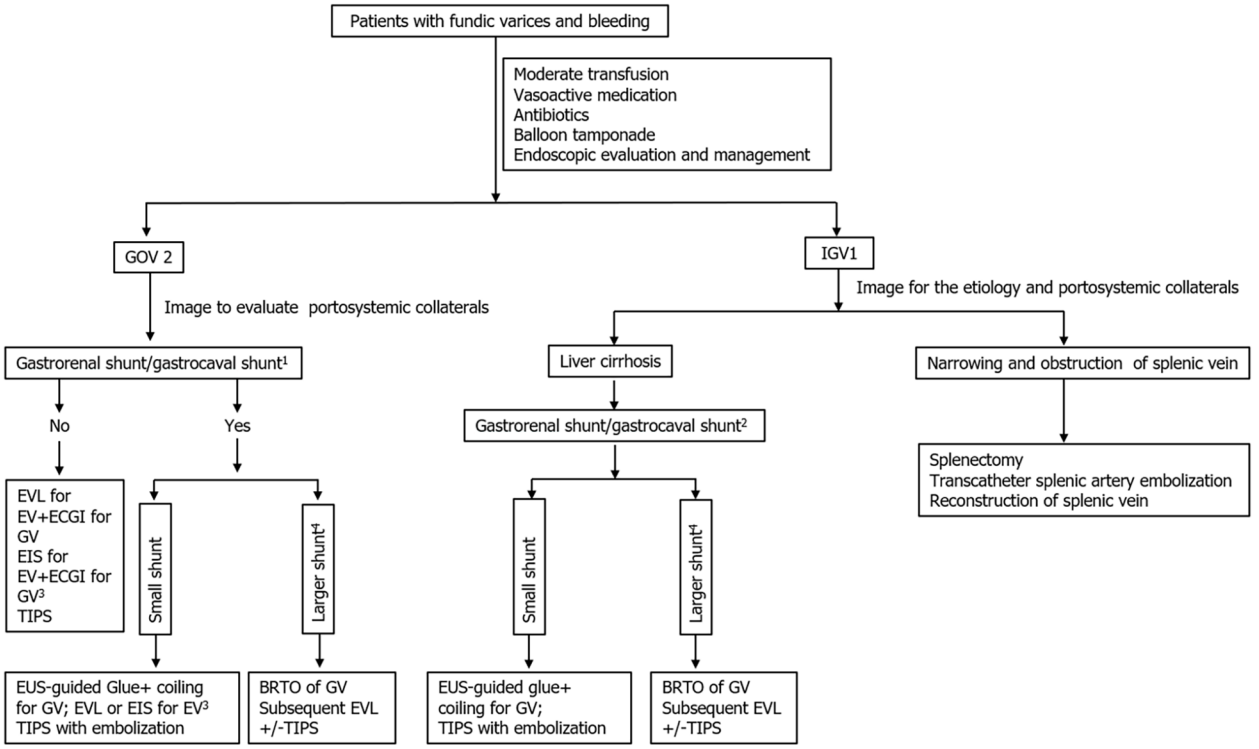

DOI: 10.12998/wjcc.v10.i17.5620 **Copyright** ©The Author(s) 2022.

Figure 3 treatment algorithm for gastric fundic varices. [1]Gastro-renal shunt or gastrocaval shunt occurred frequently in gastroesophageal varices patients with small size of esophageal varices; [2]Gastro-renal shunt or gastrocaval shunt were mainly found in isolated gastric varices patients caused by liver cirrhosis; [3]Endoscopic injection sclerosis should be performed when the size of esophageal varices is larger than 2 cm; [4]Balloon-occluded retrograde transvenous obliteration should be considered in the patients with large gastrorenal shunts or gastrocaval shunt. GOV2: Gastroesophageal varices; IGV1: Isolated gastric varices; EVL: Endoscopic variceal ligation; EV: Esophageal varices; ECGI: Endoscopic cyanoacrylate glue injection; GV: Gastric varices; TIPS: Transjugular intrahepatic portosystemic shunt; EUS: Endoscopic ultrasound; EIS: Endoscopic injection sclerosis; BRTO: Balloon-occluded retrograde transvenous obliteration.

leading to reduced perfusion and accelerated ulcer formation[26,27].

Typical CT features of liver cirrhosis include morphologic changes of the liver, portal vein enlargement, portal venous thrombosis, cavernous transformation, splenomegaly, regenerative nodule, PSCVs, and ascites. Typical radiological signs were more commonly observed in patients with GOV2 than in those with IGV1. In addition to the constituent ratio of underlying diseases, the distinction between cirrhotic patients with GOV2 and IGV1 contributed to the differences in radiological signs. The afferents to GVs come from the LVG, SGV and PGV; GVs enter systemic veins through esophageal and paraesophageal varices, gastrorenal shunts, splenorenal shunts, *etc*. In patients with IGV1 caused by pancreatic diseases, fundic varices were supplied by SGV and PGV. More importantly, we first found that the splenogastromental-superior mesenteric shunt is a major collateral vessel.

We first found that the size of varices was positively correlated with efferent/afferent vessels in patients with GOV2 or IGV1; in patients with GOV2, the size of esophageal varices was negatively correlated with gastrorenal shunt. When patients have gastrorenal shunts or gastrocaval shunts, endoscopic glue injection might result in distal systemic thromboembolic events, such as pulmonary embolism, acute kidney injury, obliteration of splenic or portal vein[3,4]. Thus, it is important to determine whether patients with gastric fundal varices have gastrorenal shunts. Our study showed that gastric varices drain mainly into the inferior vena cava *via* gastrorenal shunts or direct gastrocaval shunts in IGV1 caused by liver cirrhosis. Importantly, our research revealed that the size of esophageal varices was negatively correlated with the gastrorenal shunt diameter in patients with GOV2. This result indicated that gastrorenal shunts probably occurred in GOV2 patients with small esophageal varices. All these results indicated that gastrorenal shunts or gastrocaval shunts occurred frequently in GOV2 patients with small esophageal varices and IGV1 patients with liver cirrhosis. Thus, endoscopic glue injection should not be performed in these patients (Figure 3). For patients with large shunts, cardiofundal GVs with lower portal pressures reduced the efficacy of TIPS in bleeding control. Additionally, a large GRS or gastrocaval shunt increased the risks of TIPS (hepatic encephalopathy and hepatic ischemia)[3]. BRTO with subsequent EVL/EIS or TIPS should be considered for the management of gastric varices in these patients (Figure 3). For patients with small shunts, endoscopic ultrasound-guided glue coil placement and glue injection and TIPS with embolization are preferred strategies (Figure 3). In IGV patients with splenic vein obstruction, splenectomy and transcatheter splenic artery embolization are good therapeutic choices (Figure 3). In addition, the correlation of PSCVs

with clinical profiles was determined in fundic varices; unfortunately, no correlation was found between PSCVs and clinical profiles (Supplementary Tables 2 and 3).

Our study had several limitations. First, it was a single center retrospective study, not a prospective, randomized, multicenter study. Second, the hepatic venous pressure gradient (HVPG) was not determined in our study. Fortunately, HVPG measurement is a valuable method to evaluate the severity of portal hypertension, predict outcomes, and guide therapeutic decisions. Our conclusions are reliable without HVPG measurement because clinical profiles and imaging findings are our research priorities. Finally, follow-up data could not be provided since the retrospective study involved a 7-year span.

CONCLUSION

These findings highlight the differences in the etiology, clinical profiles, endoscopic findings, imaging signs, and portosystemic collaterals between patients with GOV2 and patients with IGV1. Our study would be helpful in making therapeutic decisions. Further studies should be performed to confirm our conclusion based on large samples, and follow-up data should be provided based on the development of suitable therapeutic strategies in the future.

ARTICLE HIGHLIGHTS

Research background

There is significant heterogeneity between gastroesophageal varices (GOV2) and isolated gastric varices (IGV1). The data on the difference between GOV2 and IGV1 are limited.

Research motivation

The Sarin classification does not truly describe the heterogeneity in the etiology and vascular alternation. Thus, studies should be performed to determine the etiology, clinical profiles, and imaging signs in patients with GOV2 and IGV1.

Research objectives

The Sarin classification does not truly describe the heterogeneity in the etiology To obtain a better understanding of fundic varices (GOV2 and IGV1), a large sample of patients (119 patients with GOV2, 133 patients with IGV1) was enrolled, and then the etiology, clinical profiles, endoscopic findings, imaging signs, and portosystemic collateral veins in patients with fundic varices were investigated in our study. The data in our study are helpful in making therapeutic decisions.

Research methods

The authors retrospectively collected the medical records of 252 patients with gastric fundal varices, and analyzed computed tomography images.

Research results

Significant differences in the etiology, blood routine examination, liver function, the incidence of peptic ulcer and the morbidity of portal hypertensive gastropathy were found between GOV2 and IGV1. Typical radiological signs of liver cirrhosis were more commonly observed in patients with GOV2 compared with IGV1. Spleno-gastroomental-superior mesenteric shunt was a major collateral vessel of IGV1 patients caused by the obstruction of the splenic vein. Gastro-renal shunt or gastrocaval shunt occurred in GOV2 patients with small size of esophageal varices and IGV1 patients caused by liver cirrhosis

Research conclusions

These findings highlight the differences in the etiology, clinical profiles, endoscopic findings, imaging signs, portosystemic collaterals between patients with GOV2 and patients with IGV1. Knowledge of the etiology and portosystemic collaterals in our study is helpful in making therapeutic decisions.

Research perspectives

A multicenter study should be performed to determine the differences in the etiology, clinical profiles, endoscopic findings, imaging signs, portosystemic collaterals between patients with GOV2 and patients with IGV1. A prospective RCT study should be performed to determine therapeutic interventions for patients with GOV2 or IGV1.

ACKNOWLEDGEMENTS

We thank Mr. Hai-Tao Shang and Tao Bai (Union Hospital, Tongji Medical College, Huazhong University of Science and Technology) for helpful suggestions in statistical analysis.

FOOTNOTES

Author contributions: Li X and Xiang HY contributed equally to this work; Song YH designed the study; Li X, Xiang HY, Si KK, Wang ZH and Song YH performed the research and collected data; Xiang HY, Li X and Song YH wrote the paper; Li X, Xiang HY, Si KK, Wang ZH, Liu C, Song YH, Xu KS, Song YH analyzed the data, reviewed the chart; Xiang HY, Si KK, Wang ZH, Liu C and Song YH performed statistical analysis.

Supported by National Natural Science Foundation of China, No. 82070631.

Institutional review board statement: The study was conducted according to the principles of the Declaration of Helsinki, and the protocol was approved by the ethics committee of Tongji Medical College, Huazhong University of Science and Technology (No. 2020-S216) and registered at www.chictr.org.cn (ChiCTR 2100042267).

Informed consent statement: The requirement for informed consent was waived because of retrospective study.

Conflict-of-interest statement: All authors have nothing to disclose

Data sharing statement: All authors had access to the study data and reviewed and approved the final manuscript.

Open-Access: This article is an open-access article that was selected by an in-house editor and fully peer-reviewed by external reviewers. It is distributed in accordance with the Creative Commons Attribution NonCommercial (CC BY-NC 4.0) license, which permits others to distribute, remix, adapt, build upon this work non-commercially, and license their derivative works on different terms, provided the original work is properly cited and the use is non-commercial. See: https://creativecommons.org/Licenses/by-nc/4.0/

Country/Territory of origin: China

ORCID number: Yu-Hu Song 0000-0003- 1952-654X; Hong-Yu Xiang 0000-0003-4336-5774; Ke-Ke Si 0000-0002-0834-2684; Ze-Hui Wang 0000-0001-5767-7459; Yu Zhang 0000-0003-0562-4544; Chang Liu 0000-0002-5124-8917; Ke-Shu Xu 0000-0003-2792-3094; Xin Li 0000-0002-7381-1352.

S-Editor: Ma YJ
L-Editor: A
P-Editor: Ma YJ

REFERENCES

1 **Sharma M**, Rameshbabu CS. Collateral pathways in portal hypertension. *J Clin Exp Hepatol* 2012; **2**: 338-352 [PMID: 25755456 DOI: 10.1016/j.jceh.2012.08.001]
2 **Garcia-Pagán JC**, Barrufet M, Cardenas A, Escorsell A. Management of gastric varices. *Clin Gastroenterol Hepatol* 2014; **12**: 919-28.e1; quiz e51 [PMID: 23899955 DOI: 10.1016/j.cgh.2013.07.015]
3 **Henry Z**, Patel K, Patton H, Saad W. AGA Clinical Practice Update on Management of Bleeding Gastric Varices: Expert Review. *Clin Gastroenterol Hepatol* 2021; **19**: 1098-1107.e1 [PMID: 33493693 DOI: 10.1016/j.cgh.2021.01.027]
4 **Philips CA**, Ahamed R, Rajesh S, George T, Mohanan M, Augustine P. Beyond the scope and the glue: update on evaluation and management of gastric varices. *BMC Gastroenterol* 2020; **20**: 361 [PMID: 33126847 DOI: 10.1186/s12876-020-01513-7]
5 **Tripathi D**, Ferguson JW, Therapondos G, Plevris JN, Hayes PC. Review article: recent advances in the management of bleeding gastric varices. *Aliment Pharmacol Ther* 2006; **24**: 1-17 [PMID: 16803599 DOI: 10.1111/j.1365-2036.2006.02965.x]
6 **Mishra SR**, Sharma BC, Kumar A, Sarin SK. Primary prophylaxis of gastric variceal bleeding comparing cyanoacrylate injection and beta-blockers: a randomized controlled trial. *J Hepatol* 2011; **54**: 1161-1167 [PMID: 21145834 DOI: 10.1016/j.jhep.2010.09.031]
7 **Garcia-Tsao G**, Sanyal AJ, Grace ND, Carey W; Practice Guidelines Committee of the American Association for the Study of Liver Diseases; Practice Parameters Committee of the American College of Gastroenterology. Prevention and management of gastroesophageal varices and variceal hemorrhage in cirrhosis. *Hepatology* 2007; **46**: 922-938 [PMID: 17879356 DOI: 10.1002/hep.21907]
8 **Garcia-Tsao G**, Abraldes JG, Berzigotti A, Bosch J. Portal hypertensive bleeding in cirrhosis: Risk stratification, diagnosis, and management: 2016 practice guidance by the American Association for the study of liver diseases. *Hepatology* 2017; **65**: 310-335 [PMID: 27786365 DOI: 10.1002/hep.28906]
9 **Sarin SK**, Lahoti D, Saxena SP, Murthy NS, Makwana UK. Prevalence, classification and natural history of gastric varices:

a long-term follow-up study in 568 portal hypertension patients. *Hepatology* 1992; **16**: 1343-1349 [PMID: 1446890 DOI: 10.1002/hep.1840160607]

10 **Ryan BM**, Stockbrugger RW, Ryan JM. A pathophysiologic, gastroenterologic, and radiologic approach to the management of gastric varices. *Gastroenterology* 2004; **126**: 1175-1189 [PMID: 15057756 DOI: 10.1053/j.gastro.2004.01.058]

11 **Ahmed R**, Kiyosue H, Maruno M, Matsumoto S, Mori H. Coexistence of "extra-gastric afferent-efferent direct connection" with gastric varices: CT evaluation and clinical significance. *Abdom Radiol (NY)* 2019; **44**: 2699-2707 [PMID: 31030246 DOI: 10.1007/s00261-019-02033-z]

12 **Kan X**, Ye J, Rong X, Lu Z, Li X, Wang Y, Yang L, Xu K, Song Y, Hou X. Diagnostic performance of Contrast-enhanced CT in Pyrrolizidine Alkaloids-induced Hepatic Sinusoidal Obstructive Syndrome. *Sci Rep* 2016; **6**: 37998 [PMID: 27897243 DOI: 10.1038/srep37998]

13 **Yang XQ**, Ye J, Li X, Li Q, Song YH. Pyrrolizidine alkaloids-induced hepatic sinusoidal obstruction syndrome: Pathogenesis, clinical manifestations, diagnosis, treatment, and outcomes. *World J Gastroenterol* 2019; **25**: 3753-3763 [PMID: 31391770 DOI: 10.3748/wjg.v25.i28.3753]

14 **Liu F**, Rong X, Guo H, Xu D, Liu C, Meng L, Yang X, Guo T, Kan X, Song Y. Clinical characteristics, CT signs, and pathological findings of Pyrrolizidine alkaloids-induced sinusoidal obstructive syndrome: a retrospective study. *BMC Gastroenterol* 2020; **20**: 30 [PMID: 32019495 DOI: 10.1186/s12876-020-1180-0]

15 **Li X**, Yang X, Xu D, Li Q, Kong X, Lu Z, Bai T, Xu K, Ye J, Song Y. Magnetic Resonance Imaging Findings in Patients With Pyrrolizidine Alkaloid-Induced Hepatic Sinusoidal Obstruction Syndrome. *Clin Gastroenterol Hepatol* 2017; **15**: 955-957 [PMID: 28126425 DOI: 10.1016/j.cgh.2017.01.009]

16 **Guo T**, Li X, Yang X, Kong X, Liu H, Bai T, Xu K, Ye J, Song Y. Gadoxetic Acid-Enhanced Hepatobiliary-Phase Magnetic Resonance Imaging for Pyrrolizidine Alkaloid-Induced Hepatic Sinusoidal Obstruction Syndrome and Association with Liver Function. *Sci Rep* 2019; **9**: 1231 [PMID: 30718698 DOI: 10.1038/s41598-018-37775-1]

17 **Lei P**, Zhang L, Han P, Zheng C, Tong Q, Shang H, Yang F, Hu Y, Li X, Song Y. Liver injury in patients with COVID-19: clinical profiles, CT findings, the correlation of the severity with liver injury. *Hepatol Int* 2020; **14**: 733-742 [PMID: 32886333 DOI: 10.1007/s12072-020-10087-1]

18 **Mishra SR**, Chander Sharma B, Kumar A, Sarin SK. Endoscopic cyanoacrylate injection *vs* beta-blocker for secondary prophylaxis of gastric variceal bleed: a randomised controlled trial. *Gut* 2010; **59**: 729-735 [PMID: 20551457 DOI: 10.1136/gut.2009.192039]

19 **Köklü S**, Coban S, Yüksel O, Arhan M. Left-sided portal hypertension. *Dig Dis Sci* 2007; **52**: 1141-1149 [PMID: 17385040 DOI: 10.1007/s10620-006-9307-x]

20 **Zhao LQ**, He W, Ji M, Liu P, Li P. 64-row multidetector computed tomography portal venography of gastric variceal collateral circulation. *World J Gastroenterol* 2010; **16**: 1003-1007 [PMID: 20180241 DOI: 10.3748/wjg.v16.i8.1003]

21 **Moubarak E**, Bouvier A, Boursier J, Lebigot J, Ridereau-Zins C, Thouveny F, Willoteaux S, Aubé C. Portosystemic collateral vessels in liver cirrhosis: a three-dimensional MDCT pictorial review. *Abdom Imaging* 2012; **37**: 746-766 [PMID: 22002160 DOI: 10.1007/s00261-011-9811-0]

22 **Nardelli S**, Riggio O, Gioia S, Puzzono M, Pelle G, Ridola L. Spontaneous porto-systemic shunts in liver cirrhosis: Clinical and therapeutical aspects. *World J Gastroenterol* 2020; **26**: 1726-1732 [PMID: 32351289 DOI: 10.3748/wjg.v26.i15.1726]

23 **Watanabe K**, Kimura K, Matsutani S, Ohto M, Okuda K. Portal hemodynamics in patients with gastric varices. A study in 230 patients with esophageal and/or gastric varices using portal vein catheterization. *Gastroenterology* 1988; **95**: 434-440 [PMID: 3391371 DOI: 10.1016/0016-5085]

24 **Bayraktar Y**, Balkanci F, Uzunalimoglu B, Gokoz A, Koseoglu T, Batman F, Gurakar A, Van Thiel DH, Kayhan B. Is portal hypertension due to liver cirrhosis a major factor in the development of portal hypertensive gastropathy? *Am J Gastroenterol* 1996; **91**: 554-558 [PMID: 8633508]

25 **Iwao T**, Toyonaga A, Oho K, Sakai T, Tayama C, Masumoto H, Sato M, Nakahara K, Tanikawa K. Portal-hypertensive gastropathy develops less in patients with cirrhosis and fundal varices. *J Hepatol* 1997; **26**: 1235-1241 [PMID: 9210609 DOI: 10.1016/s0168-8278]

26 **Saad RJ**, Chey WD. Peptic ulcer disease in patients with chronic liver disease: looking beyond bugs and drugs. *Gastrointest Endosc* 2005; **62**: 357-359 [PMID: 16111951 DOI: 10.1016/j.gie.2005.06.003]

27 **Venkatesh PG**, Parasa S, Njei B, Sanaka MR, Navaneethan U. Increased mortality with peptic ulcer bleeding in patients with both compensated and decompensated cirrhosis. *Gastrointest Endosc* 2014; **79**: 605-14.e3 [PMID: 24119507 DOI: 10.1016/j.gie.2013.08.026]

World Journal of Clinical Cases

Submit a Manuscript: https://www.f6publishing.com

World J Clin Cases 2022 June 16; 10(17): 5634-5645

DOI: 10.12998/wjcc.v10.i17.5634

ISSN 2307-8960 (online)

ORIGINAL ARTICLE

Retrospective Study

Assessment of incidental focal colorectal uptake by analysis of fluorine-18 fluorodeoxyglucose positron emission tomography parameters

Haejun Lee, Kyung-Hoon Hwang, Kwang An Kwon

Specialty type: Radiology, nuclear medicine and medical imaging

Provenance and peer review: Unsolicited article; Externally peer reviewed.

Peer-review model: Single blind

Peer-review report's scientific quality classification

Grade A (Excellent): 0
Grade B (Very good): B, B
Grade C (Good): C
Grade D (Fair): 0
Grade E (Poor): 0

P-Reviewer: Liu Z, China; Tsujinaka S, Japan

Received: December 27, 2021
Peer-review started: December 27, 2021
First decision: January 25, 2022
Revised: February 11, 2022
Accepted: April 9, 2022
Article in press: April 29, 2022
Published online: June 16, 2022

Haejun Lee, Kyung-Hoon Hwang, Department of Nuclear Medicine, Gachon University College of Medicine, Gil Medical Center, Incheon 21565, South Korea

Kwang An Kwon, Department of Gastroenterology, Gachon University College of Medicine, Gil Medical Center, Incheon 21565, South Korea

Corresponding author: Kyung-Hoon Hwang, MD, PhD, Professor, Department of Nuclear Medicine, Gachon University College of Medicine, Gil Medical Center, 21, Namdong-daero 774 beon-gil, Namdong-gu, Incheon 21565, South Korea. forrest88@hanmail.net

Abstract

BACKGROUND

Colon and rectal cancers are among the top five cancers worldwide in terms of their incidence and mortality rates. As the treatment options for cure include surgery even in specific advanced-stage cases, the early detection of lesions is important for applying active treatment methods. Fluorine-18 fluorodeoxyglucose (F-18 FDG) positron emission tomography/computed tomography (PET/CT) is an established imaging study for many types of cancers; however, physiologic uptake in the gastrointestinal tract is a frequent finding and may interfere with lesion identification. Nevertheless, as unexpectedly observed focal colorectal F-18 FDG uptake may harbor malignant lesions, further examination must not be avoided.

AIM

To assess the clinical implications of unexpected focal colorectal F-18 FDG uptake by analyzing FDG PET parameters.

METHODS

A total of 15143 F-18 FDG PET/CT scans performed at our hospital between January 2016 and September 2021 were retrospectively reviewed to identify incidentally observed focal colorectal FDG uptake. Finally, 83 regions showing focal colorectal FDG uptake with final histopathological reports from 80 patients (45 men and 35 women with mean ages of 66.9 ± 10.7 years and 63.7 ± 15.3 years, respectively) were eligible for inclusion in the present study. Each focal hypermetabolic colorectal region was classified as malignant, premalignant, or benign according to the histopathological report. PET parameters such as

maximum and peak standardized uptake value (SUVmax and SUVpeak), metabolic tumor volume (MTV), mean SUV of the metabolic tumor volume (mSUVmtv), and total lesion glycolysis (TLG) were measured or calculated for the corresponding hypermetabolic regions. Parametric and non-parametric statistical comparisons of these parameters were performed among the three groups. Receiver operating characteristic curves were plotted to identify cut-off values.

RESULTS

The detection rate of incidental focal colorectal uptake was 0.53% (80/15,143). Of the 83 regions with unexpected focal colorectal hypermetabolism, 28.9% (24/83) were malignant, 32.5% (27/83) were premalignant, and 38.6% (32/83) were benign. Overall, 61.4% of the regions had malignant or premalignant lesions. SUVmax, SUVpeak, and mSUVmtv differentiated malignant and/or premalignant lesions from benign lesions with statistical significance ($P < 0.05$). mSUVmtv3.5 differentiated malignant from benign lesions, with the largest area under the curve (AUC) of 0.792 and a cut-off of 4.9. SUVmax showed the largest AUC of 0.758 with a cut-off value of 7.5 for distinguishing between premalignant and benign lesions. Overall, SUVmax with a cut-off value of 7.6 (AUC: 0.770, 95% confidence interval (CI): 0.668-0.872; sensitivity, 0.686; specificity, 0.688) was a superior parameter for distinguishing between malignant/premalignant and benign lesions or physiologic uptake. No parameters differentiated malignant from premalignant lesions. Moderate or weak positive correlations were observed between the long diameter of the malignant lesions and PET parameters such as SUVpeak and some mSUVmtv.

CONCLUSION

Approximately two-thirds (61.4%) of incidental focal hypermetabolic colorectal regions were malignant/premalignant lesions, for which SUVmax was an independent diagnostic parameter. Unexpected suspicious focal colorectal FDG uptake should not be avoided and consideration for further evaluation is strongly recommended not to miss the two-thirds.

Key Words: Colorectal; Incidental; Fluorine-18 fluorodeoxyglucose; Positron emission tomography/computed tomography; Standardized uptake value

©The Author(s) 2022. Published by Baishideng Publishing Group Inc. All rights reserved.

Core Tip: Although intestinal fluorine-18 fluorodeoxyglucose (F-18 FDG) uptake is not a rare finding on F-18 FDG positron emission tomography/computed tomography, focal colorectal uptake may harbor malignant lesions. Therefore, it is important to differentiate between malignant/premalignant and benign lesions. The present study compared PET parameters such as standardized uptake value (SUV), metabolic tumor volume, mean SUV of metabolic tumor volume, and total lesion glycolysis among the malignant, premalignant, and benign incidental focal hypermetabolism to evaluate the implications of unexpectedly observed focal colorectal FDG uptake.

Citation: Lee H, Hwang KH, Kwon KA. Assessment of incidental focal colorectal uptake by analysis of fluorine-18 fluorodeoxyglucose positron emission tomography parameters. *World J Clin Cases* 2022; 10(17): 5634-5645
URL: https://www.wjgnet.com/2307-8960/full/v10/i17/5634.htm
DOI: https://dx.doi.org/10.12998/wjcc.v10.i17.5634

INTRODUCTION

According to the Global Cancer Observatory, the worldwide estimated age-standardized incidence and mortality rates of colorectal cancer for both sexes and all ages in 2020 were 19.5 (4th) and 9.0 (3rd), respectively[1,2], placing the disease among the top five leading cancers.

Like many other cancers, the treatment options for colorectal cancer include local or systemic treatments; however, surgery may be useful for cure in selected colorectal cancer patients with a limited number of small metastatic lesions (stage IV). Even in cases with large or many metastases, surgery may still be considered if the lesions shrink after neoadjuvant chemotherapy. In this way, more active treatment method could be a choice for colorectal cancer than for other cancers, and an improvement in overall survival may be expected through the early detection of lesions.

Fluorine-18 fluorodeoxyglucose (F-18 FDG) positron emission tomography/computed tomography (PET/CT) is an established imaging modality used for the diagnosis, treatment response, and follow-up of many types of cancers. Physiologic gastrointestinal FDG uptake is well known, particularly in the

colon and rectum, and diffusely or segmentally increased intestinal F-18 FDG uptake (hypermetabolism) is often observed as normal physiologic uptake[3-7]. This may obscure and interfere with the detection of true lesions. Despite this pitfall, FDG PET/CT may help detect lesions that are malignant or harbor a risk of malignancy, which appear as incidentally visualized focal FDG uptake in the intestines [8-10]. This retrospective study aimed to identify the implications of unexpectedly observed focal colorectal hypermetabolism on F-18 FDG PET/CT performed for purposes other than colorectal concerns by comparing PET parameters among histopathologically confirmed malignant, premalignant, and benign focal hypermetabolism.

MATERIALS AND METHODS

Patients

To identify incidental focal colorectal hypermetabolic lesions, we retrospectively reviewed 15,143 F-18 FDG PET/CT scans performed at our hospital between January 2016 and September 2021. After excluding the scans of patients with current or prior colorectal malignancies or without histopathological reports (gold standard) of the corresponding hypermetabolic regions, 80 patients (45 men and 35 women with mean age 66.9 ± 10.7 years and 63.7 ± 15.3 years, respectively) with 83 regions of focal colorectal FDG uptake and their final histopathological reports were eligible for this study.

F-18 FDG PET/CT imaging

To acquire images of F-18 FDG PET/CT with optimal image quality, all patients fasted for 4-6 h and their blood glucose levels were checked. The examination was rescheduled in cases with blood glucose levels ≥ 11 mmol/L (200 mg/dL). Scanning was performed 60 min after the intravenous injection of 185 MBq F-18 FDG. Images from the skull base to the upper thigh were acquired using a dedicated PET/CT scanner (Biograph mCT 128, Siemens Healthcare GmbH, Erlangen, Germany). Emission scans were acquired using the step-and-shoot method for 3 min per bed. CT scans were performed using the continuous spiral mode with CareDose4D and CARE kV activated to reduce patient radiation exposure and acquire individually optimized images. No contrast material was used for the CT scans. Both PET and CT images were reconstructed using the iterative reconstruction method and the final fused PET/CT images were generated on a dedicated image acquisition workstation provided with the PET/CT device.

Analyses of the F-18 FDG PET/CT images and histopathological reports

Two nuclear medicine physicians, one with over 20 years of experience, reviewed the PET/CT images. When a region of focal abnormal FDG uptake by the colon and/or rectum was identified, the patient's medical records were reviewed to obtain a histopathological report of the corresponding location, if available. The hypermetabolic regions revealed by the final histopathological reports, as well as on PET/CT, were categorized as malignant, premalignant, or benign. For these, semi-quantitative standardized uptake value (SUV) was measured as maximum (SUVmax) and peak (SUVpeak). In addition, the metabolic tumor volume (MTV) was measured, which provided information on both the volume and the mean SUV of the volume. When measuring the MTV, different volumes of interest can be applied using different settings of the SUV threshold. This study used several SUV thresholds, ranging from 2 to 5 in increments of 0.5, to obtain multiple MTVs and the mean SUV of each MTV with specific SUV threshold # (MTV# and mSUVmtv#, respectively). Finally, the total lesion glycolysis (TLG) # was calculated by multiplying the volume from the MTV# by the mSUVmtv#. All imaging analyses were performed using a dedicated PET/CT workstation equipped with SyngoMMWP (Siemens Healthcare GmbH, Erlangen, Germany). The measured and calculated PET parameters were compared among the malignant, premalignant, malignant/premalignant, and benign lesions, and receiver operating characteristic (ROC) curve analysis was performed to identify the cut-off values. Additionally, the correlations between PET parameters and tumor size (long diameter) were evaluated.

Statistics

Both parametric (Student's *t*-test) and non-parametric (such as Mann–Whitney U test) methods were used to compare SUVmax, SUVpeak, MTV#, mSUVmtv#, and TLG# among the categorized lesions, and to correlate the parameters and size of malignant tumors. ROC curves were plotted and the areas under the curves (AUCs) were calculated to determine the optimal cut-off values to distinguish malignant and/or premalignant from benign lesions. Statistical analysis was performed using SPSS for Windows, version 16.0 (SPSS, Inc., Chicago, IL, United States). Statistical significance was set at $P < 0.05$.

Ethics

This retrospective study was approved by the Institutional Review Board of our hospital (IRB no. GAIRB2020-297), and the requirement for informed consent was waived. The study was conducted in accordance with the 1964 Declaration of Helsinki and later amendments.

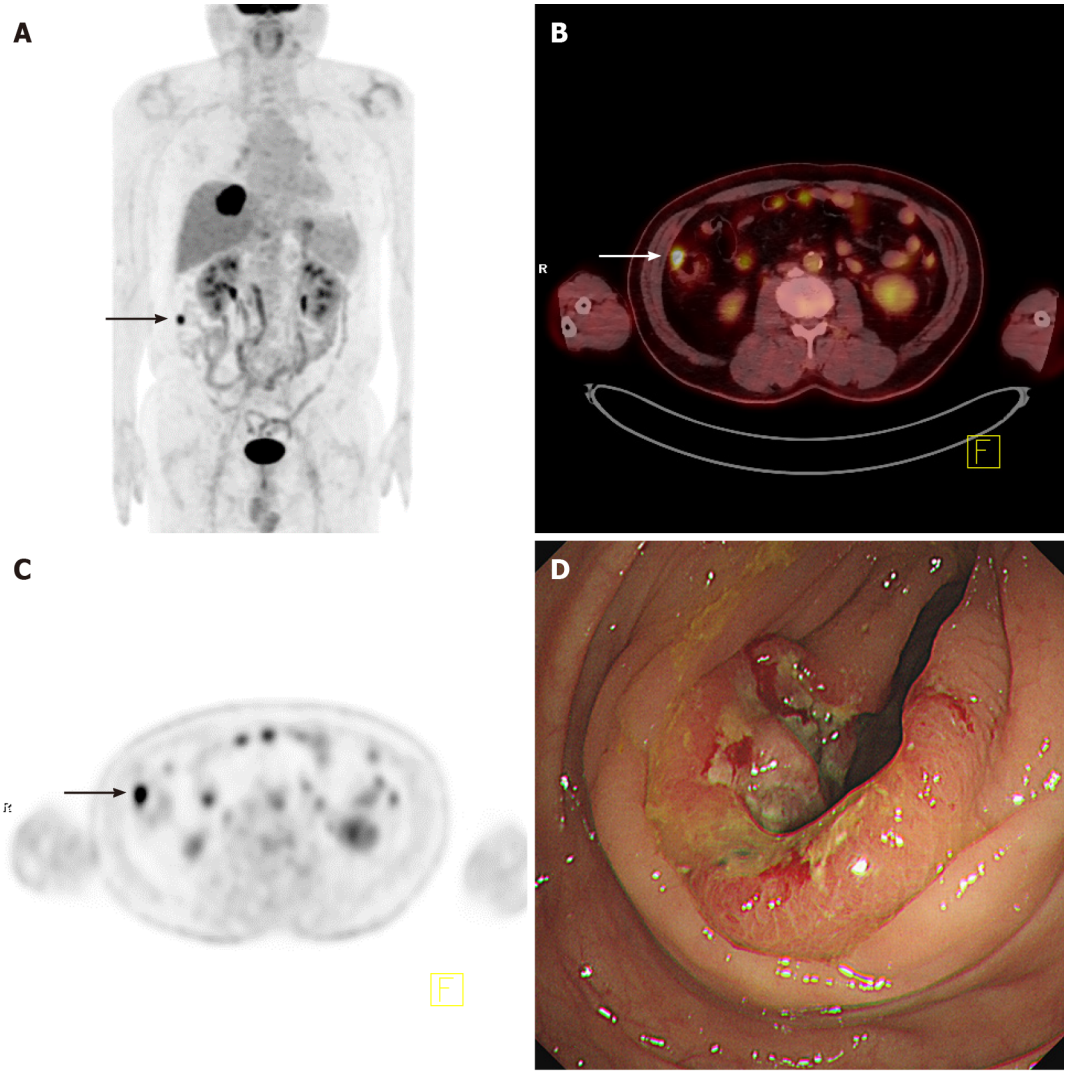

DOI: 10.12998/wjcc.v10.i17.5634 **Copyright** ©The Author(s) 2022.

Figure 1 A case with malignant incidental focal ascending colon fluorine-18 fluorodeoxyglucose uptake. A: Focal uptake (black arrow) in the right abdomen on the maximum intensity projection (MIP) image of a 67-year-old man diagnosed with intrahepatic cholangiocarcinoma; B and C: Axial images of fused positron emission tomography/computed tomography (B, white arrow) and positron emission tomography only (C, black arrow) indicating focal uptake of the MIP image (maximum standardized uptake value 9.0); D: Visualization of the lesion by colonoscopy. The lesion was histopathologically diagnosed as an adenocarcinoma of the ascending colon.

RESULTS

The demographic and clinical characteristics of the 80 patients classified by histopathological reports are shown in Table 1. The detection rate of incidental focal colorectal uptake was 0.53% (80/15,143). Among the 83 eligible regions of focal colorectal hypermetabolism, 24 were diagnosed as malignant lesions, 27 were premalignant, and the remaining 32 were benign. In terms of malignant lesions, they were 28.9% (24/83) of the focal hypermetabolic regions, consisting of 23 cases of adenocarcinoma and one case of neuroendocrine tumor. Premalignant lesions included tubular (77.8%, 21/27), villous (7.4%, 2/27), and tubulovillous (14.8%, 4/27) adenomas. The benign group comprised patients with inflammation or physiologic uptake with no remarkable mucosal abnormalities on colonoscopy. Overall, 61.4% (51/83) of the regions had malignant or premalignant lesions.

Comparisons of PET parameters and cut-offs

The five PET parameters considered in this study (SUVmax, SUVpeak, MTV#, mSUVmtv#, and TLG#) were compared among malignant, premalignant, malignant/premalignant, and benign lesions. Table 2 shows representative examples of these comparisons. SUVmax, SUVpeak, and all mSUVmtv# differed significantly between malignant and benign, premalignant and benign, and malignant/premalignant and benign lesions, while no parameters showed significant differences between malignant and premalignant lesions. Figure 1 shows an example of incidental focal ascending colon uptake, which was diagnosed as adenocarcinoma in a patient with a known intrahepatic cholangiocarcinoma. Figure 2

Table 1 Demographic and clinical characteristics of patients with incidental focal hypermetabolism in the colon and/or rectum (*n* = 80)

Nature of incidental focal hypermetabolism	Characteristics	Men	Women	Total, %
Malignant	Subjects (*n*)	16	8	24
(lesions, *n* = 24)	Age (yr, mean ± SD)	70.1 ± 11.5	72.5 ± 14.1	71 ± 12.1
	Primary malignancy (*n*)			
	Lung	5	0	5 (20.8)
	Stomach	5	0	5 (20.8)
	Breast	0	3	3 (12.5)
	Prostate	1	0	1 (4.2)
	Lymphoma	0	1	1 (4.2)
	Hepatobiliary	2	1	3 (12.5)
	Other	3	3	6 (25.0)
Premalignant	Subjects (*n*)	20	6	26
(lesions, *n* = 27)	Age (yr, mean ± SD)	67.9 ± 6.4	68.8 ± 18.7	68.1 ± 10.1
	Primary malignancy (*n*)			
	Lung	10	1	11 (42.3)
	Stomach	4	1	5 (19.2)
	Breast	0	0	0 (0.0)
	Prostate	2	0	2 (7.7)
	Lymphoma	1	1	2 (7.7)
	Hepatobiliary	2	2	4 (15.4)
	Other	1	1	2 (7.7)
Malignant/	Subjects (*n*)	36	14	50
Premalignant	Age (yr, mean ± SD)	68.9 ± 8.94	70.9 ± 15.7	69.4 ± 11.1
(lesions, *n* = 51)	Primary malignancy (*n*)			
	Lung	15	1	16 (32.0)
	Stomach	9	1	10 (20.0)
	Breast	0	3	3 (6.0)
	Prostate	3	0	3 (6.0)
	Lymphoma	1	2	3 (6.0)
	Hepatobiliary	4	3	7 (14.0)
	Other	4	4	8 (16.0)
Benign	Subjects (*n*)	9	21	30
(lesions, *n* = 32)	Age (yr, mean ± SD)	58.9 ± 13.9	58.9 ± 13.3	58.9 ± 13.3
	Primary malignancy (n)			
	Lung	3	2	5 (16.7)
	Stomach	3	5	8 (26.7)
	Breast	0	4	4 (13.3)
	Prostate	1	0	1 (3.3)
	Lymphoma	0	1	1 (3.3)
	Hepatobiliary	2	2	4 (13.3)
	Other	0	7	7 (23.3)

yr: Year; SD: Standard deviation.

Table 2 Comparisons of positron emission tomography parameters among malignant, premalignant, malignant/premalignant, and benign lesions

	Malignant (*n* = 24)	Premalignant (*n* = 27)	*P* value
mean SUVmax ± SD	12.8 ± 7.6	10.5 ± 4.7	> 0.05
mean SUVpeak ± SD	9.7 ± 6.1	7.9 ± 4.0	> 0.05
	Malignant (*n*=24)	Benign (*n*=32)	*P* value
mean SUVmax ± SD	12.8 ± 7.6	7.2 ± 3.4	< 0.05
mean SUVpeak ± SD	9.7 ± 6.1	5.6 ± 2.7	< 0.05
mean mSUVmtv3.5 ± SD	6.1 ± 1.8	4.7 ± 0.8	< 0.05
	Premalignant (*n*=27)	Benign (*n*=32)	*P* value
mean SUVmax ± SD	10.5 ± 4.7	7.2 ± 3.4	< 0.05
mean SUVpeak ± SD	7.9 ± 4.0	5.6 ± 2.7	< 0.05
mean mSUVmtv4.5 ± SD	6.5 ± 1.5	5.5 ± 0.9	< 0.05
	Malignant/premalignant (*n* = 51)	Benign (*n* = 32)	*P* value
mean SUVmax ± SD	11.6 ± 6.3	7.2 ± 3.4	< 0.05
mean SUVpeak ± SD	8.8 ± 5.1	5.6 ± 2.7	< 0.05
mean mSUVmtv3.5 ± SD	5.9 ± 1.6	4.7 ± 0.8	< 0.05

SUV: Standardized uptake value; mSUVmtv#: mean SUV of metabolic tumor volume segmented by SUV threshold #; SD: Standard deviation.

shows a patient with incidental focal rectal uptake (A and B) diagnosed as villous adenoma and a case of proximal ascending colon uptake (C and D) with no remarkable mucosal lesion revealed on colonoscopy.

ROC curves were plotted, and cut-offs were determined for malignant, premalignant, and malignant/premalignant lesions. The AUC, cut-off, 95% confidence interval (CI), sensitivity, and specificity of each parameter are shown in Table 3. An AUC of 0.792 was calculated for mSUVmtv3.5 and a cut-off of 4.9 (CI, 0.671-0.914; sensitivity, 0.667; specificity, 0.656) differentiated malignant from benign lesions. An AUC of 0.758 was calculated for SUVmax, with a cut-off of 7.5 (CI, 0.634-0.882; sensitivity, 0.704; specificity, 0.688) distinguishing between premalignant and benign lesions. Likewise, an AUC 0.770 for SUVmax and a cut-off of 7.6 (CI, 0.668-0.872; sensitivity, 0.686; specificity, 0.688) differentiated malignant/premalignant from benign lesions. Figure 3 shows the ROC curves for SUVmax and mSUVmtv3.5 for malignant/premalignant lesions.

Correlation between PET parameters and tumor size

The long diameters of the malignant lesions were determined histopathologically after surgery, with an average of 32.8 ± 23.3 mm. Using the parametric method (Pearson correlation), SUVpeak was moderately positively correlated with tumor size, with a correlation coefficient (*r*) of 0.511. The mSUVmtv# (# = 2, 2.5, 3, 3.5, and 4) also showed moderate positive correlations. Using non-parametric methods, mSUVmtv# (# = 2, 2.5, and 3, Spearman's rho, *r* = 0.457 - 0.522) and mSUVmtv2 (Kendall's tau, *r* = 0.349) showed moderate or weak positive correlations.

DISCUSSION

Non-malignant intestinal FDG uptake occurs under several conditions, including inflammation[11-14] and the use of medications such as metformin[15-18]. This uptake may be diffuse, intense, and cover a large portion of the intestine. In such cases, it is not easy to identify obscured or hidden lesions. However, the presence of focal FDG uptake in the intestine suggests the need for further evaluation for malignant lesions.

The SUV is a representative semi-quantitative parameter for PET/CT. A high SUV could be more suggestive of malignancy than a benign lesion or physiologic uptake and might be associated with

Table 3 Area under the curve and cut-off values of positron emission tomography parameters distinguishing malignant or/and premalignant from benign lesions

	Parameter	AUC	Cut-off	Confidence interval	Sensitivity	Specificity
Malignant	SUVmax	0.784	7.6	0.659 - 0.909	0.708	0.688
	SUVpeak	0.767	5.9	0.640 - 0.894	0.708	0.656
	mSUVmtv5	0.773	6.0	0.632 - 0.914	0.696	0.680
	mSUVmtv4.5	0.778	5.6	0.647 - 0.909	0.667	0.667
	mSUVmtv4	0.784	5.3	0.657 - 0.911	0.667	0.677
	mSUVmtv3.5	0.792	4.9	0.671 - 0.914	0.667	0.656
	mSUVmtv3	0.786	4.5	0.664 - 0.909	0.667	0.656
	mSUVmtv2.5	0.775	4.1	0.649 - 0.902	0.625	0.656
	mSUVmtv2	0.722	3.8	0.588 - 0.856	0.625	0.625
Premalignant	SUVmax	0.758	7.5	0.634 - 0.882	0.704	0.688
	SUVpeak	0.719	6.0	0.586 - 0.853	0.667	0.366
	mSUVmtv5	0.694	6.0	0.547 - 0.841	0.667	0.680
	mSUVmtv4.5	0.747	5.6	0.617 - 0.877	0.667	0.667
	mSUVmtv4	0.741	5.3	0.612 - 0.870	0.667	0.677
	mSUVmtv3.5	0.736	4.9	0.609 - 0.864	0.667	0.656
	mSUVmtv3	0.722	4.5	0.591 - 0.852	0.667	0.656
	mSUVmtv2.5	0.718	4.1	0.588 - 0.848	0.667	0.656
	mSUVmtv2	0.668	3.7	0.531 - 0.806	0.593	0.594
Malignant/	SUVmax	0.770	7.6	0.668 - 0.872	0.686	0.688
Premalignant	SUVpeak	0.742	6.0	0.635 - 0.848	0.647	0.656
	mSUVmtv5	0.730	6.0	0.613 - 0.847	0.680	0.680
	mSUVmtv4.5	0.761	5.6	0.656 - 0.867	0.667	0.667
	mSUVmtv4	0.761	5.2	0.656 - 0.866	0.686	0.677
	mSUVmtv3.5	0.763	4.9	0.658 - 0.867	0.667	0.656
	mSUVmtv3	0.752	4.5	0.645 - 0.859	0.667	0.656
	mSUVmtv2.5	0.745	4.1	0.636 - 0.854	0.647	0.656
	mSUVmtv2	0.694	3.7	0.577 - 0.810	0.588	0.594

SUV: Standardized uptake value; mSUVmtv#: mean SUV of metabolic tumor volume segmented by SUV threshold #; AUC: Area under the curve.

advanced disease or poor prognosis/overall survival in various cancers[19-25]. The present study assessed the clinical significance of incidental focal colorectal uptake by analyzing FDG PET parameters.

The detection rate of unexpected focal colorectal uptake in this study was 0.53% (80/15,143), consistent with the range of 0.5% - 3.3% reported by other studies[26-31]. A meta-analysis reported that a pooled prevalence of focal colorectal incidentalomas of 3.6%[32]. Of the 83 eligible lesions in this study, 51 (61.4%) were malignant (28.9%, 24/83) or premalignant (32.5%, 27/83). The remaining 32 (38.6%) were benign lesions or physiologic uptake. The proportion of premalignant lesions was slightly larger than that of malignant lesions, consistent with other studies[33,34]. The rate (61.4%, 51/83) of malignant/premalignant lesions was also comparable to that in other studies[32] and colonoscopy was recommended for further evaluation of focal hypermetabolism[35].

SUVmax, SUVpeak, and all mSUVmtv# differentiated malignant and premalignant lesions from benign lesions and physiologic uptake. According to the AUC curves, mSUVmtv3.5, with an AUC of 0.792 and a cut-off of 4.9, showed the best performance in distinguishing between malignant and benign lesions. Other mSUVmtv#s were also useful in identifying malignant lesions; however, as the # of mSUVmtv# approached extreme values (2 or 5, for instance), the boundaries of the visible MTV segmentations tended to be smaller or larger than the actual visible tumor boundaries. Thus, they might not have accurately reflected the MTV and, therefore, mSUVmtv. Practically, SUVmax, which is the

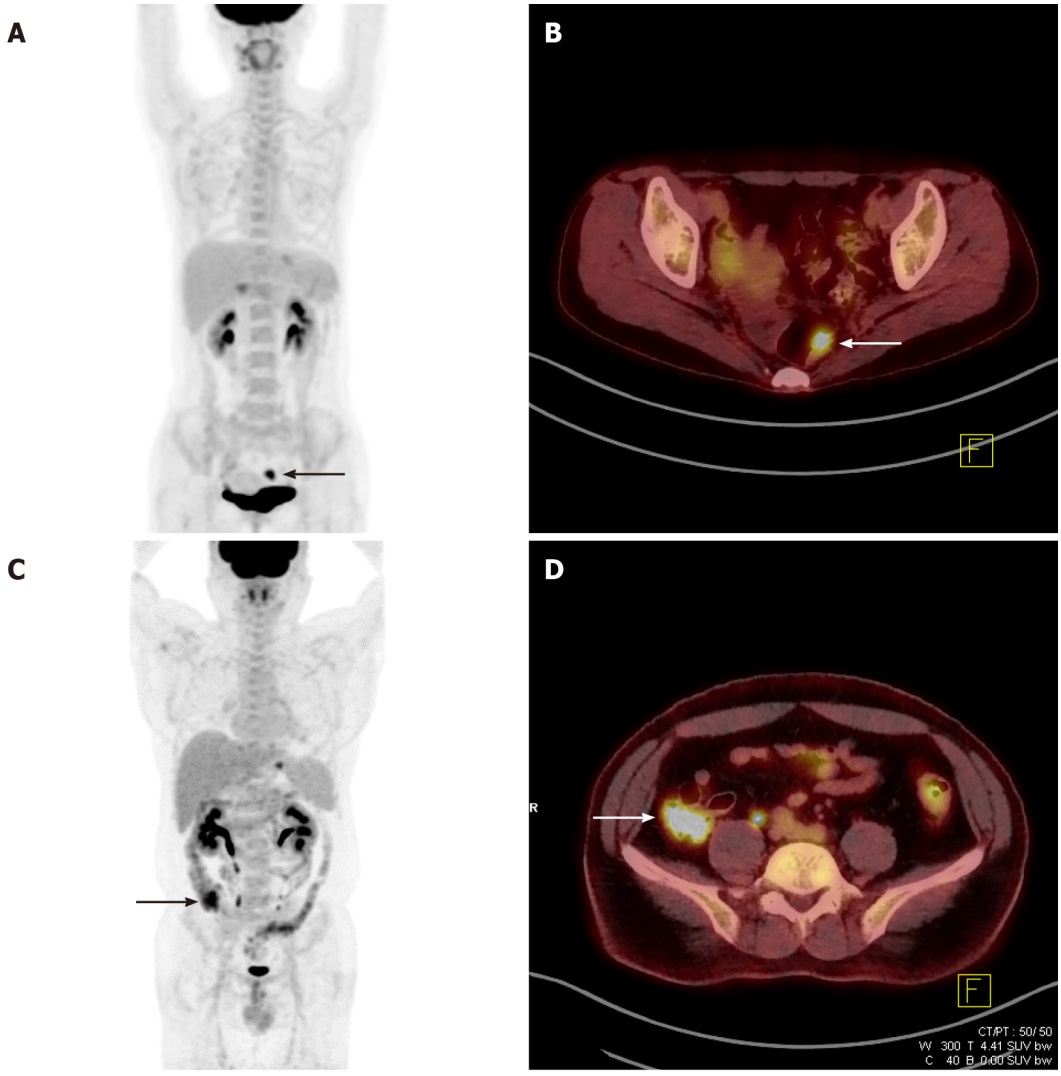

DOI: 10.12998/wjcc.v10.i17.5634 **Copyright** ©The Author(s) 2022.

Figure 2 Cases with premalignant and benign incidental focal colorectal fluorine-18 fluorodeoxyglucose uptake. A: Focal uptake (black arrow) in the lower abdomen on the maximum intensity projection (MIP) image of a 41-year-old woman diagnosed with stomach cancer; B: Axial view showing a hypermetabolic rectal lesion (white arrow, SUVmax 10.1) diagnosed as rectal villous adenoma; C: Focal uptake (black arrow) in the right lower abdomen on the MIP image of a 42-year-old man diagnosed with stomach cancer; D: Axial view showing hypermetabolism (white arrow, maximum standardized uptake value 8.6) with a final colonoscopy report of "No remarkable mucosal lesion".

most used among these parameters in the clinical setting, showed a similar AUC (0.784) and higher sensitivity and specificity, suggesting that it could replace mSUVmtv3.5. If the SUVmax is used as a determining factor, 7.6 would be the optimal cut-off. As shown in Table 3, the cut-offs for malignant lesions are similar to those for premalignant lesions, in which the malignant lesions are hardly distinguishable from premalignant lesions using the cut-offs derived in this study. None of the parameters involved in this study could distinguish them by statistical comparisons ($P > 0.05$). Other studies have shown inconsistent results[33,34], and some studies reported that even the SUVs of malignant lesions were not distinguishable from those of non-pathologic FDG uptake[27,28]. MTV and TLG were not useful for differentiating malignant and premalignant lesions from benign lesions. Both parameters showed better results than the SUVmax in other studies[36]. By combining malignant and premalignant lesions into one group, SUVmax (AUC 0.770, cut-off 7.6) was superior in distinguishing this group from benign focal colorectal hypermetabolism.

Among the 24 malignant lesions, regardless of the tumor type, 18 (75.0%) were located in the distal colon/rectum, and of the 27 premalignant lesions, 16 (59.3%) were in the proximal colon. Different genetic mechanisms play roles in cancer development in the distal or proximal colon[37-39] and different frequent locations were suggested in various studies[40-42]. Moreover, the distribution of colorectal cancer appears to vary by country, region, race, sex, and age[43-46]. Although the results of these studies are not always consistent, patient characteristics should be taken into account while interpreting PET/CT images. None of the parameters in this study differed significantly between the proximal and distal colon/rectum for malignant, premalignant, and malignant/premalignant lesions.

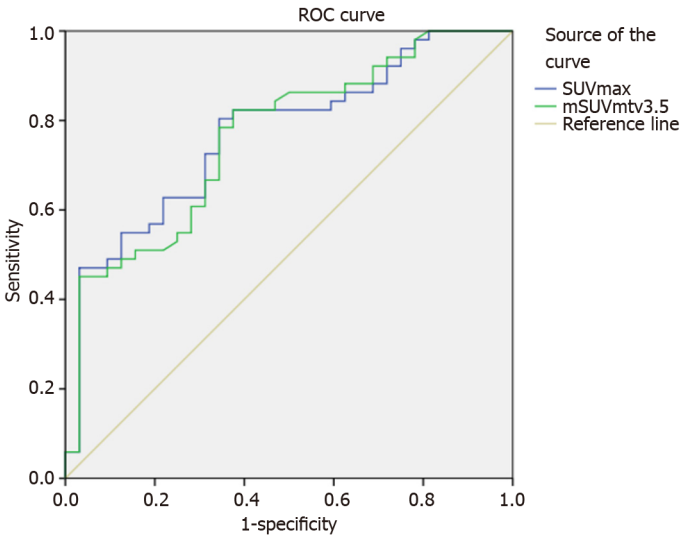

DOI: 10.12998/wjcc.v10.i17.5634 **Copyright** ©The Author(s) 2022.

Figure 3 Receiver operating characteristic curves. Receiver operating characteristic (ROC) curves of the maximum standardized uptake value (SUV) and mean SUV of metabolic tumor volume 3.5 of malignant/premalignant lesions. The values of area under the curve are 0.770 and 0.763 and the cut-offs are 7.6 [confidence interval (CI) 0.668-0.0.872, sensitivity 0.686, specificity 0.688] and 4.9 (CI 0.658-0.867, sensitivity 0.667, specificity 0.656), respectively.

The long diameter of the malignant lesions was moderately to weakly positively correlated with several PET parameters (SUVpeak and a few mSUVmtv#); however, its clinical significance was unclear. In addition, SUVmax, which significantly distinguished malignant/premalignant from benign lesions, did not show any statistically significant correlations (P = 0.055).

This study was conducted retrospectively at a single institution. The incidental focal colorectal hypermetabolism discovered with the naked eye may have missed non/Less-FDG-avid pathologic lesions; therefore, there was a selection bias. For the same reason, the incidence of malignancy may be higher than that in the general population. As this study did not include focal hypermetabolism without histopathological reports, the results of this study might not be the same if there were pathological reports for all focal hypermetabolism. Despite these limitations, given the high frequency of malignant/premalignant lesions and statistically significant PET parameters, incidental focal colorectal FDG uptake has clinical significance; thus, the consideration of further assessment such as colonoscopy should not be avoided.

CONCLUSION

Approximately two-thirds (61.4%) of the incidentally observed focal hypermetabolic colorectal regions were malignant or premalignant. Although the role of FDG PET parameters in colorectal cancer remains controversial, the results of this study showed that SUVmax was an independent diagnostic parameter for malignant/premalignant lesions. Therefore, any unexpected suspicious focal colorectal FDG uptake requires attention, and further evaluation is strongly recommended not to miss the two-thirds.

ARTICLE HIGHLIGHTS

Research background

Intestinal fluorine-18 fluorodeoxyglucose (F-18 FDG) uptake is often observed on positron emission tomography/computed tomography (PET/CT). However, unexpectedly observed focal colorectal hypermetabolism might harbor a risk of malignancy; thus, distinguishing malignant from benign tumors is critical.

Research motivation

As with other cancers, early lesion detection is critical in colorectal cancer. As surgery may still be the treatment of choice for cure in selected patients with advanced colorectal cancer, the importance of early detection of lesions is even greater.

Research objectives

To assess the implications of focal colorectal F-18 FDG uptake by analyzing FDG PET parameters.

Research methods

This study included 83 focal colorectal hypermetabolic regions from 80 patients. Each region was classified as malignant, premalignant, or benign according to the histopathological report. PET parameters such as maximum and peak standardized uptake values (SUVmax and SUVpeak), metabolic tumor volume (MTV), mean SUV of metabolic tumor volume (mSUVmtv), and total lesion glycolysis (TLG) of F-18 FDG PET/CT were measured and calculated for the regions, and compared among malignant, premalignant, malignant/premalignant, and benign hypermetabolic regions. Receiver operating characteristic (ROC) curves were plotted to determine the cut-off values for these parameters.

Research results

Of the 83 incidentally observed focal colorectal hypermetabolic regions on F-18 FDG PET-CT, 61.4% (51/83) were malignant/premalignant lesions confirmed by histopathological reports of the corresponding locations. SUVmax, SUVpeak, and mSUVmtv can be used to differentiate malignant and premalignant lesions from benign lesions. SUVmax, with an AUC of 0.770 and a cut-off of 7.6 (confidence interval: 0.668–0.872, sensitivity 0.686, specificity 0.688) was the superior FDG PET parameter in distinguishing malignant and premalignant from benign lesions.

Research conclusions

Approximately two-thirds (61.4%) of the incidental focal hypermetabolic colorectal regions were malignant/premalignant. SUVmax was demonstrated as an independent diagnostic parameter for the lesions. Unexpected suspicious focal colorectal FDG uptake should not be avoided and further evaluation is required.

Research perspectives

Controversies and debates regarding the parameters assessed in this study remain ongoing. Further studies with larger numbers of subjects are warranted.

FOOTNOTES

Author contributions: Lee H and Hwang KH contributed to this work; Lee H and Hwang KH designed the research study; Lee H, Kwon KA and Hwang KH performed the research; Lee H contributed analytic tools; Lee H, Kwon KA and Hwang KH analyzed the data and wrote the manuscript; and all authors have read and approved the final manuscript.

Institutional review board statement: The study was reviewed and approved by the Institutional Review Board at our institution. The requirement for informed consent was waived.

Conflict-of-interest statement: The authors have no potential conflicts of interest to disclose.

Data sharing statement: Technical appendix, statistical code, and dataset available from the corresponding author at [forrest88@hanmail.net]. Informed consent for data sharing was waived because of the retrospective nature of the study and this retrospective study was approved by the Institutional Review Board of our hospital (IRB No. GAIRB2020-297).

Open-Access: This article is an open-access article that was selected by an in-house editor and fully peer-reviewed by external reviewers. It is distributed in accordance with the Creative Commons Attribution NonCommercial (CC BY-NC 4.0) license, which permits others to distribute, remix, adapt, build upon this work non-commercially, and license their derivative works on different terms, provided the original work is properly cited and the use is non-commercial. See: https://creativecommons.org/Licenses/by-nc/4.0/

Country/Territory of origin: South Korea

ORCID number: Haejun Lee 0000-0002-6284-2903; Kyung-Hoon Hwang 0000-0002-9988-1906; Kwang An Kwon 0000-0002-2947-2111.

S-Editor: Liu JH
L-Editor: A
P-Editor: Liu JH

REFERENCES

1 Estimated age-standardized incidence and mortality rates (World) in 2020. Available from: https://gco.iarc.fr/today/online-analysis-multi-bars?v=2020&mode=cancer&mode_population=countries&population=900&populations=900&key=asr&sex=0&cancer=39&type=0&statistic=5&prevalence=0&population_group=0&ages_group%5B%5D=0&ages_group%5B%5D=17&nb_items=10&group_cancer=1&include_nmsc=1&include_nmsc_other=1&type_multiple=%257B%2522inc%2522%253Atrue%252C%2522mort%2522%253Atrue%252C%2522prev%2522%253Afalse%257D&orientation=horizontal&type_sort=0&type_nb_items=%257B%2522top%2522%253Atrue%252C%2522bottom%2522%253Afalse%257D

2 **Sung H**, Ferlay J, Siegel RL, Laversanne M, Soerjomataram I, Jemal A, Bray F. Global Cancer Statistics 2020: GLOBOCAN Estimates of Incidence and Mortality Worldwide for 36 Cancers in 185 Countries. *CA Cancer J Clin* 2021; **71**: 209-249 [PMID: 33538338 DOI: 10.3322/caac.21660]

3 **Prabhakar HB**, Sahani DV, Fischman AJ, Mueller PR, Blake MA. Bowel hot spots at PET-CT. *Radiographics* 2007; **27**: 145-159 [PMID: 17235004 DOI: 10.1148/rg.271065080]

4 **Ahmad Sarji S**. Physiological uptake in FDG PET simulating disease. *Biomed Imaging Interv J* 2006; **2**: e59 [PMID: 21614339 DOI: 10.2349/biij.2.4.e59]

5 **Zukotynski K**, Kim CK. Abdomen: normal variations and benign conditions resulting in uptake on FDG-PET/CT. *PET Clin* 2014; **9**: 169-183 [PMID: 25030280 DOI: 10.1016/j.cpet.2013.10.008]

6 **Shammas A**, Lim R, Charron M. Pediatric FDG PET/CT: physiologic uptake, normal variants, and benign conditions. *Radiographics* 2009; **29**: 1467-1486 [PMID: 19755606 DOI: 10.1148/rg.295085247]

7 **Engel H**, Steinert H, Buck A, Berthold T, Huch Böni RA, von Schulthess GK. Whole-body PET: physiological and artifactual fluorodeoxyglucose accumulations. *J Nucl Med* 1996; **37**: 441-446 [PMID: 8772641]

8 **Sone Y**, Sobajima A, Kawachi T, Kohara S, Kato K, Naganawa S. Ability of 18-fludeoxyglucose positron emission tomography/CT to detect incidental cancer. *Br J Radiol* 2014; **87**: 20140030 [PMID: 25117626 DOI: 10.1259/bjr.20140030]

9 **Wu GZ**, Sun D, Chen JY, Qiu JM, Kong Y. [Clinical diagnostic value of (18)F-FDG PET-CT in incidental finding of focal hypermetabolism focus in the colon and rectum]. *Zhonghua Wei Chang Wai Ke Za Zhi* 2013; **16**: 555-560 [PMID: 23801210]

10 **Salazar Andía G**, Prieto Soriano A, Ortega Candil A, Cabrera Martín MN, González Roiz C, Ortiz Zapata JJ, Cardona Arboniés J, Lapeña Gutiérrez L, Carreras Delgado JL. Clinical relevance of incidental finding of focal uptakes in the colon during 18F-FDG PET/CT studies in oncology patients without known colorectal carcinoma and evaluation of the impact on management. *Rev Esp Med Nucl Imagen Mol* 2012; **31**: 15-21 [PMID: 21640441 DOI: 10.1016/j.remn.2011.03.014]

11 **Ahn BC**, Lee SW, Lee J. Intense accumulation of F-18 FDG in colonic wall in adult onset still disease with pseudomembranous colitis. *Clin Nucl Med* 2008; **33**: 806-808 [PMID: 18936623 DOI: 10.1097/RLU.0b013e318187eec4]

12 **Kjaer ASL**, Ribberholt I, Thomsen K, Ibsen PH, Markova E, Graff J. ^{18}F-FDG PET/CT Findings in Cytomegalovirus Colitis. *Diagnostics (Basel)* 2018; **9** [PMID: 30587768 DOI: 10.3390/diagnostics9010003]

13 **Parbo P**, Stribolt K, Rittig CS, Gormsen LC. Active ulcerative colitis diagnosed by (18)F-FDG PET/CT in an anti-TNF alpha treated patient with no visible luminal lesions on colonoscopy. *Int J Colorectal Dis* 2014; **29**: 643-644 [PMID: 24531694 DOI: 10.1007/s00384-014-1840-z]

14 **Hannah A**, Scott AM, Akhurst T, Berlangieri S, Bishop J, McKay WJ. Abnormal colonic accumulation of fluorine-18-FDG in pseudomembranous colitis. *J Nucl Med* 1996; **37**: 1683-1685 [PMID: 8862310]

15 **Bevilacqua T**, Greene GS. Diffuse bowel uptake of 18F-FDG on PET/CT examination of a patient with diabetes treated with metformin. *BMJ Case Rep* 2014; **2014** [PMID: 24700035 DOI: 10.1136/bcr-2013-202058]

16 **Bahler L**, Stroek K, Hoekstra JB, Verberne HJ, Holleman F. Metformin-related colonic glucose uptake; potential role for increasing glucose disposal? *Diabetes Res Clin Pract* 2016; **114**: 55-63 [PMID: 27103370 DOI: 10.1016/j.diabres.2016.02.009]

17 **Lee SH**, Jin S, Lee HS, Ryu JS, Lee JJ. Metformin discontinuation less than 72 h is suboptimal for F-18 FDG PET/CT interpretation of the bowel. *Ann Nucl Med* 2016; **30**: 629-636 [PMID: 27392947 DOI: 10.1007/s12149-016-1106-7]

18 **Bybel B**, Greenberg ID, Paterson J, Ducharme J, Leslie WD. Increased F-18 FDG intestinal uptake in diabetic patients on metformin: a matched case-control analysis. *Clin Nucl Med* 2011; **36**: 452-456 [PMID: 21552023 DOI: 10.1097/RLU.0b013e318217399e]

19 **Cheng NM**, Hsieh CE, Liao CT, Ng SH, Wang HM, Fang YD, Chou WC, Lin CY, Yen TC. Prognostic Value of Tumor Heterogeneity and SUVmax of Pretreatment 18F-FDG PET/CT for Salivary Gland Carcinoma With High-Risk Histology. *Clin Nucl Med* 2019; **44**: 351-358 [PMID: 30932974 DOI: 10.1097/RLU.0000000000002530]

20 **Chin AL**, Kumar KA, Guo HH, Maxim PG, Wakelee H, Neal JW, Diehn M, Loo BW Jr, Gensheimer MF. Prognostic Value of Pretreatment FDG-PET Parameters in High-dose Image-guided Radiotherapy for Oligometastatic Non-Small-cell Lung Cancer. *Clin Lung Cancer* 2018; **19**: e581-e588 [PMID: 29759331 DOI: 10.1016/j.cllc.2018.04.003]

21 **Kwon SY**, Choi EK, Kong EJ, Chong A, Ha JM, Chun KA, Cho IH, Bom HS, Min JJ, Kim J, Song HC, O JH, Kim SH. Prognostic value of preoperative 18F-FDG PET/CT in papillary thyroid cancer patients with a high metastatic lymph node ratio: a multicenter retrospective cohort study. *Nucl Med Commun* 2017; **38**: 402-406 [PMID: 28306621 DOI: 10.1097/MNM.0000000000000657]

22 **Özgü E**, Öz M, Yıldız Y, Özgü BS, Erkaya S, Güngör T. Prognostic value of 18F-FDG PET/CT for identifying high- and low-risk endometrial cancer patients. *Ginekol Pol* 2016; **87**: 493-497 [PMID: 27504941 DOI: 10.5603/GP.2016.0032]

23 **Bahri H**, Laurence L, Edeline J, Leghzali H, Devillers A, Raoul JL, Cuggia M, Mesbah H, Clement B, Boucher E, Garin E. High prognostic value of 18F-FDG PET for metastatic gastroenteropancreatic neuroendocrine tumors: a long-term evaluation. *J Nucl Med* 2014; **55**: 1786-1790 [PMID: 25286923 DOI: 10.2967/jnumed.114.144386]

24 **Fuglø HM**, Jørgensen SM, Loft A, Hovgaard D, Petersen MM. The diagnostic and prognostic value of ^{18}F-FDG PET/CT in the initial assessment of high-grade bone and soft tissue sarcoma. A retrospective study of 89 patients. *Eur J Nucl Med Mol Imaging* 2012; **39**: 1416-1424 [PMID: 22699526 DOI: 10.1007/s00259-012-2159-z]

25 **Groheux D**, Giacchetti S, Moretti JL, Porcher R, Espié M, Lehmann-Che J, de Roquancourt A, Hamy AS, Cuvier C, Vercellino L, Hindié E. Correlation of high 18F-FDG uptake to clinical, pathological and biological prognostic factors in breast cancer. *Eur J Nucl Med Mol Imaging* 2011; **38**: 426-435 [PMID: 21057787 DOI: 10.1007/s00259-010-1640-9]

26 **Treglia G**, Calcagni ML, Rufini V, Leccisotti L, Meduri GM, Spitilli MG, Dambra DP, De Gaetano AM, Giordano A. Clinical significance of incidental focal colorectal (18)F-fluorodeoxyglucose uptake: our experience and a review of the literature. *Colorectal Dis* 2012; **14**: 174-180 [PMID: 21689289 DOI: 10.1111/j.1463-1318.2011.02588.x]

27 **Kei PL**, Vikram R, Yeung HW, Stroehlein JR, Macapinlac HA. Incidental finding of focal FDG uptake in the bowel during PET/CT: CT features and correlation with histopathologic results. *AJR Am J Roentgenol* 2010; **194**: W401-W406 [PMID: 20410385 DOI: 10.2214/AJR.09.3703]

28 **Weston BR**, Iyer RB, Qiao W, Lee JH, Bresalier RS, Ross WA. Ability of integrated positron emission and computed tomography to detect significant colonic pathology: the experience of a tertiary cancer center. *Cancer* 2010; **116**: 1454-1461 [PMID: 20143447 DOI: 10.1002/cncr.24885]

29 **van Hoeij FB**, Keijsers RG, Loffeld BC, Dun G, Stadhouders PH, Weusten BL. Incidental colonic focal FDG uptake on PET/CT: can the maximum standardized uptake value (SUVmax) guide us in the timing of colonoscopy? *Eur J Nucl Med Mol Imaging* 2015; **42**: 66-71 [PMID: 25139518 DOI: 10.1007/s00259-014-2887-3]

30 **Peng J**, He Y, Xu J, Sheng J, Cai S, Zhang Z. Detection of incidental colorectal tumours with 18F-labelled 2-fluoro-2-deoxyglucose positron emission tomography/computed tomography scans: results of a prospective study. *Colorectal Dis* 2011; **13**: e374-e378 [PMID: 21831098 DOI: 10.1111/j.1463-1318.2011.02727.x]

31 **Oh JR**, Min JJ, Song HC, Chong A, Kim GE, Choi C, Seo JH, Bom HS. A stepwise approach using metabolic volume and SUVmax to differentiate malignancy and dysplasia from benign colonic uptakes on 18F-FDG PET/CT. *Clin Nucl Med* 2012; **37**: e134-e140 [PMID: 22614211 DOI: 10.1097/RLU.0b013e318239245d]

32 **Treglia G**, Taralli S, Salsano M, Muoio B, Sadeghi R, Giovanella L. Prevalence and malignancy risk of focal colorectal incidental uptake detected by (18)F-FDG-PET or PET/CT: a meta-analysis. *Radiol Oncol* 2014; **48**: 99-104 [PMID: 24991198 DOI: 10.2478/raon-2013-0035]

33 **Seivert M**, Plomteux O, Colard A, Leclercq P, Gauthier D, Houbiers G, Dupont P, Demoulin JC, Fontaine F, Namur G, Witvrouw N, Bastens B. Endoscopic findings in case of incidental colonic uptake in PET-CT how to improve PET-CT specificity? *Acta Gastroenterol Belg* 2014; **77**: 413-417 [PMID: 25682631]

34 **Purandare NC**, Gawade SK, Puranik AD, Agrawal A, Shah S, Rangarajan V. Etiology and significance of incidentally detected focal colonic uptake on FDG PET/CT. *Indian J Radiol Imaging* 2012; **22**: 260-266 [PMID: 23833416 DOI: 10.4103/0971-3026.111476]

35 **Roh SH**, Jung SA, Kim SE, Kim HI, Lee MJ, Tae CH, Choi JY, Shim KN, Jung HK, Kim TH, Yoo K, Moon IH, Kim BS. The Clinical Meaning of Benign Colon Uptake in (18)F-FDG PET: Comparison with Colonoscopic Findings. *Clin Endosc* 2012; **45**: 145-150 [PMID: 22866255 DOI: 10.5946/ce.2012.45.2.145]

36 **Suzuki Y**, Okabayashi K, Hasegawa H, Tsuruta M, Shigeta K, Murakami K, Kitagawa Y. Metabolic Tumor Volume and Total Lesion Glycolysis in PET/CT Correlate With the Pathological Findings of Colorectal Cancer and Allow Its Accurate Staging. *Clin Nucl Med* 2016; **41**: 761-765 [PMID: 27556789 DOI: 10.1097/RLU.0000000000001332]

37 **Bufill JA**. Colorectal cancer: evidence for distinct genetic categories based on proximal or distal tumor location. *Ann Intern Med* 1990; **113**: 779-788 [PMID: 2240880 DOI: 10.7326/0003-4819-113-10-779]

38 **Fearon ER**, Vogelstein B. A genetic model for colorectal tumorigenesis. *Cell* 1990; **61**: 759-767 [PMID: 2188735 DOI: 10.1016/0092-8674(90)90186-i]

39 **Beart RW**, Melton LJ 3rd, Maruta M, Dockerty MB, Frydenberg HB, O'Fallon WM. Trends in right and left-sided colon cancer. *Dis Colon Rectum* 1983; **26**: 393-398 [PMID: 6851801 DOI: 10.1007/BF02553382]

40 **Siegel RL**, Miller KD, Fedewa SA, Ahnen DJ, Meester RGS, Barzi A, Jemal A. Colorectal cancer statistics, 2017. *CA Cancer J Clin* 2017; **67**: 177-193 [PMID: 28248415 DOI: 10.3322/caac.21395]

41 **Shmidt E**, Nehra V, Lowe V, Oxentenko AS. Clinical significance of incidental [18 F]FDG uptake in the gastrointestinal tract on PET/CT imaging: a retrospective cohort study. *BMC Gastroenterol* 2016; **16**: 125 [PMID: 27716085 DOI: 10.1186/s12876-016-0545-x]

42 **Golfam F**, Golfam P, Neghabi Z. Frequency of all types of colorectal tumors in the patients referred to selected hospitals in tehran. *Iran Red Crescent Med J* 2013; **15**: 473-476 [PMID: 24349744 DOI: 10.5812/ircmj.4026]

43 **Qing SH**, Rao KY, Jiang HY, Wexner SD. Racial differences in the anatomical distribution of colorectal cancer: a study of differences between American and Chinese patients. *World J Gastroenterol* 2003; **9**: 721-725 [PMID: 12679919 DOI: 10.3748/wjg.v9.i4.721]

44 **Thomas CR Jr**, Jarosz R, Evans N. Racial differences in the anatomical distribution of colon cancer. *Arch Surg* 1992; **127**: 1241-1245 [PMID: 1417493 DOI: 10.1001/archsurg.1992.01420100107018]

45 **Kim SE**, Paik HY, Yoon H, Lee JE, Kim N, Sung MK. Sex- and gender-specific disparities in colorectal cancer risk. *World J Gastroenterol* 2015; **21**: 5167-5175 [PMID: 25954090 DOI: 10.3748/wjg.v21.i17.5167]

46 **Schmuck R**, Gerken M, Teegen EM, Krebs I, Klinkhammer-Schalke M, Aigner F, Pratschke J, Rau B, Benz S. Gender comparison of clinical, histopathological, therapeutic and outcome factors in 185,967 colon cancer patients. *Langenbecks Arch Surg* 2020; **405**: 71-80 [PMID: 32002628 DOI: 10.1007/s00423-019-01850-6]

World Journal of Clinical Cases

Submit a Manuscript: https://www.f6publishing.com

World J Clin Cases 2022 June 16; 10(17): 5646-5654

DOI: 10.12998/wjcc.v10.i17.5646

ISSN 2307-8960 (online)

ORIGINAL ARTICLE

Observational Study

"Zero ischemia" laparoscopic partial nephrectomy by high-power GreenLight laser enucleation for renal carcinoma: A single-center experience

Xiang-Min Zhang, Ji-Dong Xu, Jian-Min Lv, Xiu-Wu Pan, Jian-Wei Cao, Jian Chu, Xin-Gang Cui

Specialty type: Surgery

Provenance and peer review: Unsolicited article; Externally peer reviewed.

Peer-review model: Single blind

Peer-review report's scientific quality classification

Grade A (Excellent): 0
Grade B (Very good): B
Grade C (Good): 0
Grade D (Fair): 0
Grade E (Poor): 0

P-Reviewer: Salimi M, Iran

Received: November 4, 2021
Peer-review started: November 4, 2021
First decision: March 3, 2022
Revised: March 16, 2022
Accepted: April 9, 2022
Article in press: April 9, 2022
Published online: June 16, 2022

Xiang-Min Zhang, Xiu-Wu Pan, Jian-Wei Cao, Xin-Gang Cui, Department of Urology, Xinhua Hospital, Shanghai Jiaotong University, School of Medicine, Shanghai 200092, China

Xiang-Min Zhang, Jian Chu, Department of Urology, Shanghai Baoshan Luodian Hospital, Shanghai 201908, China

Ji-Dong Xu, Department of Urology, Gongli Hospital of The Second Military Medical University, Shanghai 200135, China

Jian-Min Lv, Department of Urology, Shanghai The Seventh People's Hospital, Shanghai 200137, China

Corresponding author: Xin-Gang Cui, MD, PhD, Chief Doctor, Professor, Research Scientist, Department of Urology, Xinhua Hospital, Shanghai Jiaotong University, School of Medicine, No. 1665 Kongjiang Road, Shanghai 200092, China. cuixingang@xinhuamed.com.cn

Abstract

BACKGROUND

Laparoscopic partial nephrectomy has been widely used in renal cell carcinoma treatment. The efficacy of GreenLight laser on Laparoscopic partial nephrectomy is still unknown.

AIM

To present the first series of laparoscopic partial nephrectomy (LPN) by GreenLight laser enucleation without renal artery clamping. Due to the excellent coagulation and hemostatic properties of the laser, laser-assisted LPN (LLPN) makes it possible to perform a "zero ischemia" resection.

METHODS

Fifteen patients with T1a exogenous renal tumors who received high-power GreenLight laser non-ischemic LPN in our hospital were retrospectively analyzed. All clinical information, surgical and post-operative data, complications, pathological and functional outcomes were analyzed.

RESULTS

Surgery was successfully completed in all patients, and no open or radical

nephrectomy was performed. The renal artery was not clamped, leading to no ischemic time. No blood transfusions were required, the average hemoglobin level ranged from 96.0 to 132.0 g/L and no postoperative complications occurred. The mean operation time was 104.3 ± 8.2 min. The postoperative removal of negative pressure drainage time ranged from 5.0 to 7.0 d, and the mean postoperative hospital stay was 6.5 ± 0.7 d. No serious complications occurred. Postoperative pathological results showed clear cell carcinoma in 12 patients, papillary renal cell carcinoma in 2 patients, and hamartoma in 1 patient. The mean creatinine level was 75.0 ± 0.8 μmol/L (range 61.0-90.4 μmol/L) at 1 mo after surgery, and there were no statistically significant differences compared with pre-operation ($P > 0.05$). The glomerular filtration rate ranged from 45.1 to 60.8 mL/min, with an average of 54.0 ± 5.0 mL/min, and these levels were not significantly different from those before surgery ($P > 0.05$).

CONCLUSION

GreenLight laser has extraordinary cutting and sealing advantages when used for small renal tumors (exogenous tumors of stage T1a) during LPN. However, use of this technique can lead to the generation of excessive smoke.

Key Words: GreenLight laser; Zero ischemia; Partial nephrectomy; Laparoscopy; Renal tumor

©The Author(s) 2022. Published by Baishideng Publishing Group Inc. All rights reserved.

Core Tip: GreenLight laser has extraordinary cutting and sealing advantages when applied to exogenous T1a tumors during laparoscopic partial nephrectomy; GreenLight reduced the substantial sutures; GreenLight could lead to excessive smoke.

Citation: Zhang XM, Xu JD, Lv JM, Pan XW, Cao JW, Chu J, Cui XG. "Zero ischemia" laparoscopic partial nephrectomy by high-power GreenLight laser enucleation for renal carcinoma: A single-center experience. *World J Clin Cases* 2022; 10(17): 5646-5654

URL: https://www.wjgnet.com/2307-8960/full/v10/i17/5646.htm

DOI: https://dx.doi.org/10.12998/wjcc.v10.i17.5646

INTRODUCTION

Kidney cancer is a common tumor, accounting for 2%-3% of all carcinomas, and is one of the top 10 cancers worldwide[1]. Recent years have witnessed a consistent increase in the incidence rate in most countries[2]. To date, surgical therapy is still the primary treatment, especially in patients with a small renal mass (SRM), although surveillance is under study. Recent guidelines indicate that, as far as possible, all patients with tumors < 7 cm should receive nephron-sparing surgery (NSS). The disease-specific prognosis is similar between radical nephrectomy and partial nephrectomy (PN), with the benefit of better protection of kidney function in PN patients[3]. Thus, a critical target of NSS is to preserve the maximum amount of kidney parenchyma, with minimum warm ischemia time (WIT). Hilar clamping has been standard practice in previous decades to achieve the lowest blood loss. However, blockage of the renal blood supply results in WIT, and even renal function damage[4]. Bleeding is still the most frequent complication of NSS, with a risk of transfusion in up to 5% of patients [5]. Optimization of Renal cell carcinoma surgical treatment has received increased research interest. Over the years, progress has been made in reducing the risk of bleeding and the complications of WIT. From open to laparoscopic partial nephrectomy (LPN), therapy has recently changed to robot auxiliary partial nephrectomy[6]. Patients receiving laparoscopic surgery had lower intraoperative blood loss than those receiving the open surgery, and postoperative complications did not increase[7]. However, LPN prolonged WIT as the procedure is challenging even for experienced surgeons with critical time scales[8]. Thus, various techniques to reduce or eliminate WIT surgery have been used, including specific kidney artery block, targeted kidney blood flow or renal parenchyma clamping, laser-assisted minimal invasive partial nephrectomy (MIPN), MIPN auxiliary radio frequency, MIPN auxiliary water jet, and sequential preset kidney suture[9]. Although these techniques are not widely accepted, their applications are being increasingly investigated.

The initial GreenLight laser used potassium titanoxate phosphate, which produced a green visible light beam at 532 nm with a short penetration depth of 0.8 mm. GreenLight is selectively absorbed by hemoglobin rather than water within the tissue. The laser works by photoselective vaporization of tissues. This was followed by the development of a high-power 120W (GreenLight HPS) laser and,

finally, the development of an 180W GreenLight accelerated performance system (XPS) laser with a Moxy fiber. The power of the laser and the laser beam area is increased by 50%, and the energy density at the laser point is similar, thus maintaining similar safety to the previous 120W system[10]. However, the GreenLight laser was widely used in transurethral resection of the prostate (TURP) for lower urinary tract symptoms associated with benign prostate enlargement, which led to the introduction of less invasive treatments. Although there have been animal experiments and pre-clinical investigations on GreenLight laser for NSS[11,12], the safety and feasibility of this technique in human NSS is unclear.

As different types of lasers have been tested, the purpose of this study was to demonstrate the feasibility of GreenLight (high-power 80-100W) laser-assisted LPN (LLPN). When oncology results and actual care standards match, tumor excision ability and the pathological report after laser excision are important.

MATERIALS AND METHODS

Patients

From February 2021 to June 2021, 15 patients with localized exogenous kidney tumors were retrospectively analyzed. All patients received GreenLight laser surgery for NSS at the Gongli Hospital of Second Military Medical University. The surgical procedure and ethics were authorized by the Scientific Research Review Board of Gongli Hospital of Second Military Medical University. According to the results of imaging data, both the diagnosis of SRM and the surgical decision were made. To assess the complexity of the intervention, all patients were evaluated according to PADUA and R.E.N.A.L scores[6,13]. In the present study, only patients with a single lesion were included, with a maximum renal mass of 4 cm. Patients with centrally located tumors and with a single functional kidney were excluded. Ten males and 5 females, aged 47.0-74.0 years, with an average age of 58.6 ± 9.2 years were included. The tumor diameter ranged from 2.0 to 3.8 cm (3.0 ± 0.56 cm), 8 tumors on the left side and 7 on the right side, 14 on the dorsal side, and 1 on the ventral side. The preoperative glomerular filtration rate (GFR) on the diseased side was 44.6-67.3 mL/min (56.3 ± 6.8 mL/min). The preoperative hemoglobin level was 119.0-156.0 g/L, with an average value of 135.4 ± 10.8 g/L. All patients had exogenous renal space-occupying lesions on physical examination, and were diagnosed with renal carcinoma by renal artery enhanced CT examination before surgery. The R.E.N.A.L scores ranged from 4.0 to 6.0 (4.9 ± 0.8). One case was complicated with hypertension, one with coronary heart disease, and two with diabetes.

GreenLight laser for zero-ischemic LLPN

The targeted kidney SRMs were removed by zero-ischemic LLPN under the 180W XPS green laser system with a wavelength of 532 nm. The left foot set for the steam power of 80-100W, created a continuous launch mode. The hemostatic power of the right foot was 30-35W, and this was the simulated pulse emission mode. A Green laser fiber with active cooling cap technology was used. Retroperitoneal and transabdominal LPN was selected depending on the location and size of the patient's tumor. The patient was placed in the lateral decubitus position under general anesthesia, and the lumbar bridge was elevated.

We applied continuous waves during the entire procedure. To perform laparoscopy, a flexible laser fiber with a beam of light was placed in the laparoscopic instrument. The procedure was conducted laparoscopically *via* retroperitoneal access. All procedures were performed by the same experienced surgeon. Small incisions were made in the 12th subcostal area of the posterior axillary line, the subcostal arch of the anterior axillary line, and 2 cm above the iliac crest of the mid-axillary line. The extra-peritoneal fat was removed, the lateral cone fascia was opened, and the renal artery was separated along the dorsal side of the kidney for reserve (Figure 1A). In the transabdominal approach, trocars were placed 3 cm above the umbilicus at the lateral margin of the rectus abdominis, 2 cm below the costal margin at the midline of the clavicle, and 3 cm above the internal anterior superior iliac spine. The lateral peritoneum at the para-colonic sulcus was opened to move the intestine downward. Dissociated along the pedicle direction, the renal vein was observed, separated and exposed, and the renal artery on the deep surface of the renal vein for reserve (no dissociation of the renal artery on the superficial surface of the tumor due to the small size of the tumor in 2 patients). Depending on the location of the tumor, the surrounding area was fully isolated and the renal tumor was completely exposed (Figure 1B). The laser fiber was inserted into the trocar through the green laser hand (Figure 1C and D), the fiber was connected to normal saline to wash the strips, the initial green laser steam power was set at 80W, and the hemostasis power was set at 35W (Figure 1E). The renal parenchyma was cut with 80W power (Figure 1F and G) at the height of one optical fiber head from the edge of the tumor approximately 3 mm from the renal parenchyma. When vaporizing, interference due to smoke was reduced by high pressure flushing of the optical fiber, and the tumor was pushed and stripped by the aspirator. In the case of intraoperative bleeding, the hemostatic power was used to seal the bleeding point (the power can be increased for large blood vessel bleeding), and the power was gradually increased to 80-100W according to the status of the evaporated kidney tissue. Progression was gradual until the tumor was

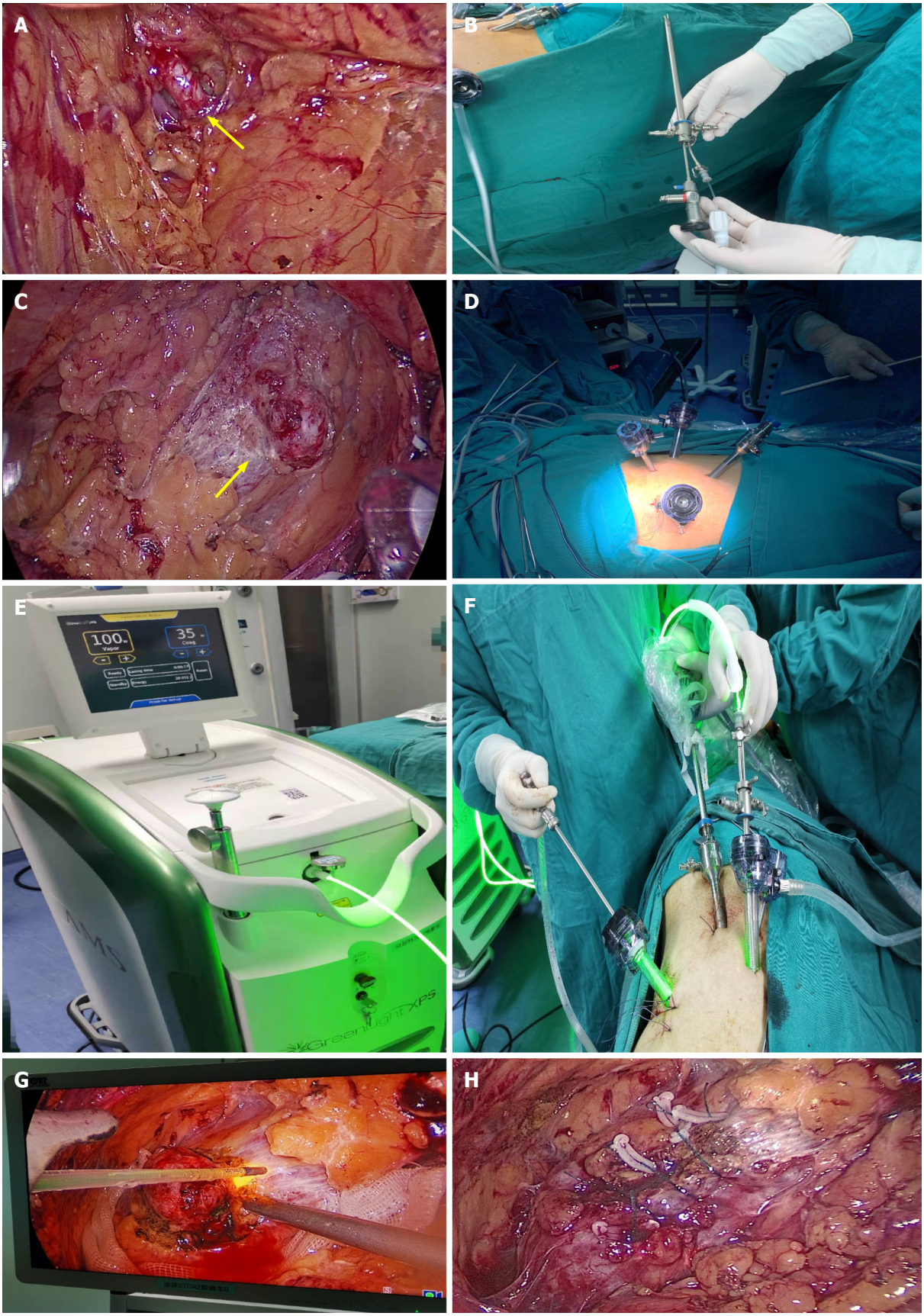
A
B
C
D
E
F
G
H

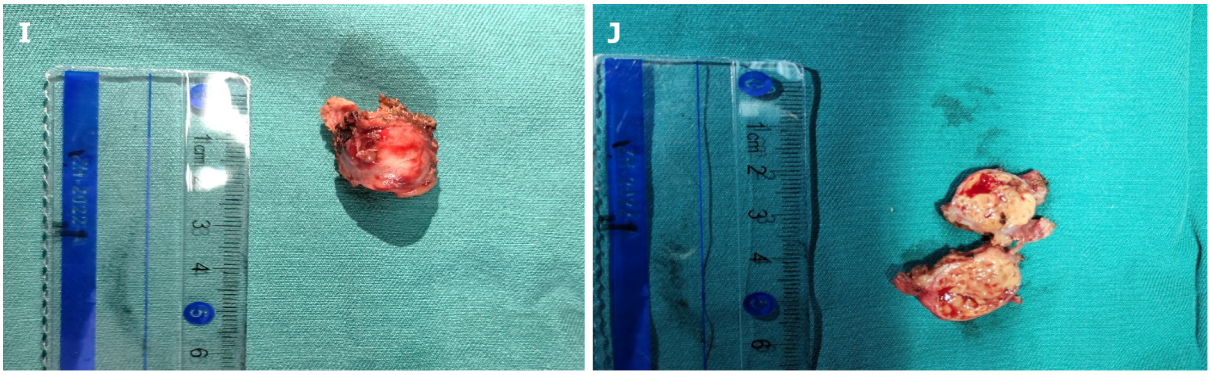

DOI: 10.12998/wjcc.v10.i17.5646 **Copyright** ©The Author(s) 2022.

Figure 1 "Zero ischemia" laparoscopic partial nephrectomy assisted by high-power side-emission green laser. A: Free renal artery for standby; B: Renal tumor; C: Green laser hand parts embedded in the optical fiber; D: Trocar for green laser hand placement; E: The initial green laser vaporization power was 80W and hemostasis power was 35W; F: Process of tumor resection by green laser; G: *In vivo* view of green laser resection of tumor; H: Complete suture of kidney wounds; I and J: Complete resection and appearance of the tumor specimen.

completely removed. The wound surface of the inner medulla and outer cortex of the kidney were continuously sutured with 1-3 Layers of barb sutures (Figure 1H). The specimen bag was placed, the surgical area was flushed, the wound was checked for no active bleeding, a drainage tube was placed, the specimen was removed (Figure 1I and J) and the incision was sutured. All specimens were placed in formalin and histologically examined by pathologists. Drainage was inserted by default. Postoperative treatment was in accordance with our standard surgical procedures. The patients were followed up for 6 mo. The clinical manifestations and imaging findings were used to determine recurrence after surgery.

Statistical analysis

GraphPad Prism 7.00 was used for statistical analysis. The mean ± SD (numerical range) was used for statistical description of the data. The paired *t*-test was used for comparisons between preoperative and postoperative measurement data. The difference was considered statistically significant if the *P* value was less than 0.05.

RESULTS

Operation overview

Due to severe intraoperative bleeding, one patient underwent laparoscopic scissors rapid resection, and suturing to stop the bleeding. None of the patients were converted to open surgery or radical nephrectomy. The operative time ranged from 90.0 to 120.0 min, with an average time of 104.3 ± 8.2 min. The postoperative hemoglobin level was 96.0-132.0 g/L (114.9 ± 11.2 g/L), which was statistically significant compared with that before surgery ($P < 0.05$). The postoperative hemoglobin level decreased and ranged from 12.0 to 25.0 g/L. The average drainage time was 5.7 ± 0.7 d (5.0-7.0 d). The postoperative hospital stay ranged from 5.0 to 8.0 d (6.7 ± 0.7 d). No serious complications occurred in these patients. One patient had hypertension, one patient had coronary heart disease, and two patients had diabetes. One month after the operation, the creatinine was 61.0-90.4 μmol/L (75.0 ± 8.5 μmol/L), which was not significant compared with that before surgery ($P > 0.05$). The GFR on the affected side was evaluated one month after surgery, and the average value was 54.0 ± 5.0 mL/min. There was no significant difference between preoperative and preoperative levels ($P > 0.05$). No tumor recurrence or metastasis was observed during the short-term follow-up period.

DISCUSSION

It is standard procedure to perform laparoscopic surgery for the removal of renal tumors and SRMs, with renal artery clamping and WIT. However, the difficulty and requirements of LPN lead to longer WIT, compared with the open method. Moreover, WIT deserves more attention in the case of pre-damaged organs or a single kidney[8]. More recently, robot-assisted LPN has emerged as an alternative to LPN. Compared with laparoscopic surgery, the ischemia time during robotic surgery is significantly shortened, thereby reducing the risk of renal dysfunction[14]. Current studies have shown that renal artery clamping for more than 30 min can cause irreversible renal function damage[15]. Recently, Thompson *et al*[16] proposed that as long as the blood supply to the kidney is blocked, kidney damage

will gradually increase every minute. These findings present a significant challenge to urologists in how best to preserve renal function in patients with early renal tumors. Therefore, a complete unblocked nephrectomy of the renal artery is necessary. This technique was first reported by Marshall *et al*[17] and Abaza *et al*[18] in 2000. Surgeons performed PN without blood vessel clamping in patients with SRMs using hemostasis devices such as double-click electro-coagulation[18]. It seems that decreasing WIT could be a favorable modifiable risk factor to avoid postoperative kidney dysfunction. Thus, we attempted to investigate the safety and feasibility of the GreenLight laser, and to reduce or prevent WIT in renal laparoscopic surgery.

The application of a laser during kidney surgery remains uncertain in the experimental or preclinical stage, although it has been widely used and extensively investigated in other medical areas. As the laser's efficacy depends on the wavelength and the proportion of water in the tissue, its efficacy must be determined. The feasibility of using lasers in kidney procedures has been shown previously[19-21]. Kyriazis *et al*[19] first reported 2 cases of unblocked thulium laser-assisted robotic PN with no obvious intraoperative or postoperative complications, and the pathological results showed a negative surgical margin. Boris *et al*[22] successfully carried out green laser partial zero ischemia nephrectomy in pigs, and the results showed that the green laser effectively stop bleeding within a very short time, with a tissue penetration rate of only 0.8 mm. The GreenLight laser applied in the present study at 532 nm, was preferentially absorbed by oxyhemoglobin (absorption coefficient 102/cm), but not by rinsing (absorption coefficient 104/cm). The increased energy absorbed from hemoglobin caused the tissue to vaporize, leading to physical separation of the tissue. In addition, it resulted in thermally-induced coagulation of superficial blood vessels; thus, an almost blood-free area was produced for surgery. The 532 nm wavelength has a small penetration depth (1-2 mm) leading to less charring[15,23,24]. Thus, GreenLight laser vaporization is considered an effective alternative for TURP. Based on this, we attempted to demonstrate the balance between laser energy and NSS.

In this study involving 15 patients, no obvious complications such as urine leakage and bleeding occurred during the perioperative period. The postoperative follow-up examination indicated that no patient had positive surgical margins or postoperative local recurrence, and there were no significant statistical differences between preoperative and postoperative serum creatinine levels. LPN is safe, feasible, and beneficial for maximum preservation of renal function in patients. To our knowledge, this is the first report on GreenLight LLPN to date. Moreover, all the tumors were removed without WIT, which protected kidney function. However, one of the major limitations of surgery was the excessive accumulation of smoke during vaporization of tissue. We attempted to reduce this by rinsing, but visibility was not improved. Favorable visibility could be obtained by using one of the trocars as a fume hood. However, this was not the best option as better visibility could not be acquired from suction alone. In addition, it appears that undefined resection margins and positive resection margins are an issue on histopathological examination. Nevertheless, this should be validated in further large-cohort studies. All patients with unclear or positive surgical margins were followed up and no tumor recurrence has been observed.

CONCLUSION

The potential efficacy of laser-assisted LPN without WIT has been witnessed for over a decade[25], but until now this technical option has been considered experimental. In this retrospective study, which consisted of the first series of patients to date, we showed the strengths and main problems of GreenLight (80-100W) LLPN. However, this technique is mainly limited to single cases with a small tumor volume and superficial locations. The number of cases in the present study was small; thus, further clinical trials are required to determine whether this technique should be promoted.

ARTICLE HIGHLIGHTS

Research background

Laparoscopic partial nephrectomy has been widely used in renal cell carcinoma treatment. The efficacy of GreenLight laser on Laparoscopic partial nephrectomy is still unknown. To present the first series of laparoscopic partial nephrectomy (LPN) by GreenLight laser (KTP) enucleation without renal artery clamping. Due to the excellent coagulation and hemostatic properties of the laser, laser-assisted LPN (LLPN) makes it possible to perform a “zero ischemia” resection.

Research motivation

To date, surgical therapy is still the primary treatment, especially in patients with a small renal mass, although surveillance is under study. Recent guidelines indicate that, as far as possible, all patients with tumors < 7 cm should receive nephron-sparing surgery (NSS). The disease-specific prognosis is similar between radical nephrectomy and partial nephrectomy (PN), with the benefit of better protection of

kidney function in PN patients. Thus, a critical target of NSS is to preserve the maximum amount of kidney parenchyma, with minimum warm ischemia time (WIT). Hilar clamping has been standard practice in previous decades to achieve the lowest blood loss. However, blockage of the renal blood supply results in WIT, and even renal function damage. Bleeding is still the most frequent complication of NSS, with a risk of transfusion in up to 5% of patients.

Research objectives

To present the first series of LPN by GreenLight laser enucleation without renal artery clamping. Due to the excellent coagulation and hemostatic properties of the laser, LLPN makes it possible to perform a "zero ischemia" resection.

Research methods

Fifteen patients with T1a exogenous renal tumors who received high-power GreenLight laser non-ischemic LPN in our hospital were retrospectively analyzed. All clinical information, surgical and post-operative data, complications, pathological and functional outcomes were analyzed.

Research results

Surgery was successfully completed in all patients, and no open or radical nephrectomy was performed. The renal artery was not clamped, leading to no ischemic time. No blood transfusions were required, the average hemoglobin level ranged from 96.0 to 132.0 g/L and no postoperative complications occurred. The mean operation time was 104.3 ± 8.2 min. The postoperative removal of negative pressure drainage time ranged from 5.0 to 7.0 d, and the mean postoperative hospital stay was 6.5 ± 0.7 d. No serious complications occurred. Postoperative pathological results showed clear cell carcinoma in 12 patients, papillary renal cell carcinoma in 2 patients, and hamartoma in 1 patient. The mean creatinine level was 75.0 ± 0.8 μmol/L (range 61.0-90.4 μmol/L) at 1 mo after surgery, and there were no statistically significant differences compared with pre-operation ($P > 0.05$). The glomerular filtration rate ranged from 45.1 to 60.8 mL/min, with an average of 54.0 ± 5.0 mL/min, and these levels were not significantly different from those before surgery ($P > 0.05$).

Research conclusions

GreenLight laser has extraordinary cutting and sealing advantages when used for small renal tumors (exogenous tumors of stage T1a) during LPN. However, use of this technique can lead to the generation of excessive smoke.

Research perspectives

GreenLight laser has extraordinary cutting and sealing advantages when applied to exogenous T1a tumors during LPN; GreenLight reduced the substantial sutures; GreenLight could lead to excessive smoke.

FOOTNOTES

Author contributions: Cui XG contributed to conception and design; Zhang XM, Xu JD, Lv JM contributed to acquisition of data; Zhang XM, Xu JD, Lv JM, Pan XW contributed to analysis and interpretation of data; Zhang XM, Lv JM, Cui XG contributed to writing, review, and/or revision of the manuscript; Pan XW, Cao JW, Chu J, Cui XG contributed to administrative, technical, or material support; Cui XG contributed to study supervision; Zhang XM, Xu JD, and Chu J contributed equally to this work and should be considered as co-first authors.

Supported by the Program of Shanghai Academic/Technology Research Leader, No. 19XD1405100; the Clinical Research Plan of SHDC, No. SHDC2020CR4025; Hospital Funded Clinical Research, Xin Hua Hospital Affiliated to Shanghai Jiao Tong University School of Medicine, No. 21XHDB06.

Institutional review board statement: Ethical approval for all research procedures was provided by the Scientific Research Review and Investigation Committee of Gong Li Hospital, Second Military Medical University.

Conflict-of-interest statement: The authors state that there is no potential conflict of interest.

Data sharing statement: All data are available on reasonable request *via* email from the corresponding author.

Open-Access: This article is an open-access article that was selected by an in-house editor and fully peer-reviewed by external reviewers. It is distributed in accordance with the Creative Commons Attribution NonCommercial (CC BY-NC 4.0) license, which permits others to distribute, remix, adapt, build upon this work non-commercially, and license their derivative works on different terms, provided the original work is properly cited and the use is non-commercial. See: https://creativecommons.org/Licenses/by-nc/4.0/

Country/Territory of origin: China

ORCID number: Xiang-Min Zhang 0000-0001-6980-665X; Ji-Dong Xu 0000-0003-1019-9669; Jian-Min Lv 0000-0001-9339-1079; Xiu-Wu Pan 0000-0001-5268-0886; Jian-Wei Cao 0000-0002-6664-7080; Jian Chu 0000-0003-1167-058X; Xin-Gang Cui 0000-0002-3162-2705.

S-Editor: Liu JH
L-Editor: A
P-Editor: Liu JH

REFERENCES

1 **Bray F**, Ferlay J, Soerjomataram I, Siegel RL, Torre LA, Jemal A. Global cancer statistics 2018: GLOBOCAN estimates of incidence and mortality worldwide for 36 cancers in 185 countries. *CA Cancer J Clin* 2018; **68**: 394-424 [PMID: 30207593 DOI: 10.3322/caac.21492]
2 **Jonasch E**, Gao J, Rathmell WK. Renal cell carcinoma. *BMJ* 2014; **349**: g4797 [PMID: 25385470 DOI: 10.1136/bmj.g4797]
3 **MacLennan S**, Imamura M, Lapitan MC, Omar MI, Lam TB, Hilvano-Cabungcal AM, Royle P, Stewart F, MacLennan G, MacLennan SJ, Canfield SE, McClinton S, Griffiths TR, Ljungberg B, N'Dow J; UCAN Systematic Review Reference Group; EAU Renal Cancer Guideline Panel. Systematic review of oncological outcomes following surgical management of localised renal cancer. *Eur Urol* 2012; **61**: 972-993 [PMID: 22405593 DOI: 10.1016/j.eururo.2012.02.039]
4 **Volpe A**, Blute ML, Ficarra V, Gill IS, Kutikov A, Porpiglia F, Rogers C, Touijer KA, Van Poppel H, Thompson RH. Renal Ischemia and Function After Partial Nephrectomy: A Collaborative Review of the Literature. *Eur Urol* 2015; **68**: 61-74 [PMID: 25703575 DOI: 10.1016/j.eururo.2015.01.025]
5 **Gratzke C**, Seitz M, Bayrle F, Schlenker B, Bastian PJ, Haseke N, Bader M, Tilki D, Roosen A, Karl A, Reich O, Khoder WY, Wyler S, Stief CG, Staehler M, Bachmann A. Quality of life and perioperative outcomes after retroperitoneoscopic radical nephrectomy (RN), open RN and nephron-sparing surgery in patients with renal cell carcinoma. *BJU Int* 2009; **104**: 470-475 [PMID: 19239445 DOI: 10.1111/j.1464-410X.2009.08439.x]
6 **Laird A**, Choy KC, Delaney H, Cutress ML, O'Connor KM, Tolley DA, McNeill SA, Stewart GD, Riddick AC. Matched pair analysis of laparoscopic versus open radical nephrectomy for the treatment of T3 renal cell carcinoma. *World J Urol* 2015; **33**: 25-32 [PMID: 24647880 DOI: 10.1007/s00345-014-1280-y]
7 **Gong EM**, Orvieto MA, Zorn KC, Lucioni A, Steinberg GD, Shalhav AL. Comparison of laparoscopic and open partial nephrectomy in clinical T1a renal tumors. *J Endourol* 2008; **22**: 953-957 [PMID: 18363510 DOI: 10.1089/end.2007.0300]
8 **Muramaki M**, Miyake H, Sakai I, Fujisawa M. Prognostic Factors Influencing Postoperative Development of Chronic Kidney Disease in Patients with Small Renal Tumors who Underwent Partial Nephrectomy. *Curr Urol* 2013; **6**: 129-135 [PMID: 24917730 DOI: 10.1159/000343526]
9 **Hou W**, Ji Z. Achieving zero ischemia in minimally invasive partial nephrectomy surgery. *Int J Surg* 2015; **18**: 48-54 [PMID: 25895732 DOI: 10.1016/j.ijsu.2015.04.046]
10 **Gomez-Sancha F**. GreenLight laser vaporization of the prostate: has it come of age? *Curr Opin Urol* 2015; **25**: 40-44 [PMID: 25393270 DOI: 10.1097/MOU.0000000000000124]
11 **Hindley RG**, Barber NJ, Walsh K, Petersen A, Poulsen J, Muir GH. Laparoscopic partial nephrectomy using the potassium titanyl phosphate laser in a porcine model. *Urology* 2006; **67**: 1079-1083 [PMID: 16635508 DOI: 10.1016/j.urology.2005.11.006]
12 **Eret V**, Hora M, Sykora R, Hes O, Urge T, Klecka J, Matejovic M. GreenLight (532 nm) laser partial nephrectomy followed by suturing of collecting system without renal hilar clamping in porcine model. *Urology* 2009; **73**: 1115-1118 [PMID: 18502479 DOI: 10.1016/j.urology.2008.03.011]
13 **Drerup M**, Magdy A, Hager M, Colleselli D, Kunit T, Lusuardi L, Janetschek G, Mitterberger M. Non-ischemic laparoscopic partial nephrectomy using 1318-nm diode laser for small exophytic renal tumors. *BMC Urol* 2018; **18**: 99 [PMID: 30413201 DOI: 10.1186/s12894-018-0405-9]
14 **Benway BM**, Bhayani SB, Rogers CG, Dulabon LM, Patel MN, Lipkin M, Wang AJ, Stifelman MD. Robot assisted partial nephrectomy versus laparoscopic partial nephrectomy for renal tumors: a multi-institutional analysis of perioperative outcomes. *J Urol* 2009; **182**: 866-872 [PMID: 19616229 DOI: 10.1016/j.juro.2009.05.037]
15 **Barber NJ**, Muir GH. High-power KTP laser prostatectomy: the new challenge to transurethral resection of the prostate. *Curr Opin Urol* 2004; **14**: 21-25 [PMID: 15091045 DOI: 10.1097/00042307-200401000-00005]
16 **Thompson RH**, Lane BR, Lohse CM, Leibovich BC, Fergany A, Frank I, Gill IS, Blute ML, Campbell SC. Every minute counts when the renal hilum is clamped during partial nephrectomy. *Eur Urol* 2010; **58**: 340-345 [PMID: 20825756 DOI: 10.1016/j.eururo.2010.05.047]
17 **Marshall FF**. Laparoscopic nephron-sparing surgery for renal tumors. *J Urol* 2002; **168**: 876 [PMID: 12136865]
18 **Abaza R**, Picard J. A novel technique for laparoscopic or robotic partial nephrectomy: feasibility study. *J Endourol* 2008; **22**: 1715-1719 [PMID: 18681808 DOI: 10.1089/end.2007.0433]
19 **Kyriazis I**, Ozsoy M, Kallidonis P, Panagopoulos V, Vasilas M, Liatsikos E. Current evidence on lasers in laparoscopy: partial nephrectomy. *World J Urol* 2015; **33**: 589-594 [PMID: 24989846 DOI: 10.1007/s00345-014-1343-0]
20 **Korhonen AK**, Talja M, Karlsson H, Tuhkanen K. Contact Nd:YAG laser and regional renal hypothermia in partial nephrectomy. *Ann Chir Gynaecol Suppl* 1993; **206**: 59-62 [PMID: 8291872]
21 **Zhou XF**, Ding ZS, Wang JF, Chen X, Fang ZL, Liu NB, Zhang G, Zhao PY. Laparoscopic Partial Nephrectomy by Diode Laser with Highly Selective Clamping of Segmental Renal Arterial. *Chin Med J (Engl)* 2015; **128**: 2262-2264 [PMID:

26265623 DOI: 10.4103/0366-6999.162513]

22 **Boris RS**, Eun D, Bhandari A, Lyall K, Bhandari M, Rogers C, Alassi O, Menon M. Potassium-titanyl-phosphate laser assisted robotic partial nephrectomy in a porcine model: can robotic assistance optimize the power needed for effective cutting and hemostasis? *J Robot Surg* 2007; **1**: 185-189 [PMID: 25484960 DOI: 10.1007/s11701-007-0032-z]

23 **Van Cleynenbreugel B**, Srirangam SJ, Van Poppel H. High-performance system GreenLight laser: indications and outcomes. *Curr Opin Urol* 2009; **19**: 33-37 [PMID: 19057213 DOI: 10.1097/MOU.0b013e328317cab3]

24 **Benejam Gual J**, Servera Ruiz de Velasco A, Hernández Martínez Y, García-Miralles Grávalos R. [Greenlight laser vaporization: Past, present and future? *Arch Esp Urol* 2020; **73**: 675-681 [PMID: 33025912]

25 **Malloy TR**, Schultz RE, Wein AJ, Carpiniello VL. Renal preservation utilizing neodymium:YAG laser. *Urology* 1986; **27**: 99-103 [PMID: 3753808 DOI: 10.1016/0090-4295(86)90363-8]

World Journal of Clinical Cases

Submit a Manuscript: https://www.f6publishing.com

World J Clin Cases 2022 June 16; 10(17): 5655-5666

DOI: 10.12998/wjcc.v10.i17.5655

ISSN 2307-8960 (online)

ORIGINAL ARTICLE

Observational Study

High Eckardt score and previous treatment were associated with poor postperoral endoscopic myotomy pain control: A retrospective study

Wan-Nan Chen, Yao-Lin Xu, Xiao-Guang Zhang

Specialty type: Medicine, research and experimental

Provenance and peer review: Unsolicited article; Externally peer reviewed.

Peer-review model: Single blind

Peer-review report's scientific quality classification

Grade A (Excellent): 0
Grade B (Very good): 0
Grade C (Good): C
Grade D (Fair): D
Grade E (Poor): 0

P-Reviewer: Cascella M, Italy; Pallav K, United States

Received: November 13, 2021
Peer-review started: November 13, 2021
First decision: December 27, 2021
Revised: March 25, 2022
Accepted: April 4, 2022
Article in press: April 4, 2022
Published online: June 16, 2022

Wan-Nan Chen, Xiao-Guang Zhang, Department of Anesthesia, Zhongshan Hospital, Fudan University, Shanghai 200032, China

Yao-Lin Xu, Department of General Surgery, Zhongshan Hospital Fudan University, Shanghai 200032, China

Corresponding author: Xiao-Guang Zhang, MD, Doctor, Department of Anesthesia, Zhongshan Hospital, Fudan University, No. 180 Fenglin Road, Xuhui District, Shanghai 200032, China. zhang.xiaoguang@zs-hospital.sh.cn

Abstract

BACKGROUND

Peroral endoscopic myotomy (POEM) is a safe and effective endoscopic treatment for achalasia. However, postoperative pain management for these patients is often neglected by anesthesiologists because of the short operative time, short hospital stay and the minimally invasive nature of the procedure.

AIM

To assess the pain and sleep quality of achalasia patients receiving the POEM procedure and investigate factors that affect postoperative pain.

METHODS

This observational study included patients with achalasia who underwent POEM at Zhongshan Hospital from December 2017 to March 2018. General anesthesia was performed with endotracheal intubation. The postoperative visual analog scale (VAS), postoperative sleep quality, basic patient information, and surgical parameters were collected. Depending on whether the 12-h post-POEM VAS score was less than 4, patients were divided into two groups, a well-controlled pain group and a poorly controlled pain group. Univariate, multivariate, and stepwise logistic regression analyses were used to investigate risk factors for poor pain control. A prediction model of post-POEM pain risk was established in the form of a nomogram. The calibration curve and receiver operating characteristic curve were used to evaluate the clinical usage of the prediction model. Repeated measures analysis of variance and simple effect analysis were used to verify whether differences in the VAS and sleep scores of the high- and low-risk groups, divided by the model from the raw data, were statistically significant.

RESULTS

A total of 45 eligible patients were included. Multivariate logistic regression and further stepwise logistic regression analysis found that the preoperative Eckardt score [odds ratio (OR): 1.82, 95% confidence interval (CI): 1.17-2.84, $P < 0.001$], previous treatment (OR: 7.59, 95%CI: 1.12-51.23, $P = 0.037$) and the distance between the end of the muscle incision and the cardia (OR: 1.52, 95%CI: 0.79-293.93, $P = 0.072$) were risk factors for post-POEM pain. Repeated measures analysis of variance demonstrated that VAS ($P = 0.0097$) and sleep scores ($P = 0.043$) were higher in the high-risk group, and the interactions between the two main effects were obvious (VAS score: $P = 0.019$, sleep score: $P = 0.035$). Further simple effect analysis found that VAS scores were higher in the high-risk group at 2 h, 6 h and 12 h ($P = 0.005$, $P = 0.019$, $P < 0.001$), and sleep scores were higher in the high-risk group at day 1 ($P = 0.006$).

CONCLUSION

Achalasia patients who underwent POEM experienced serious postoperative pain, which may affect sleep quality. A higher Eckardt score, previous treatment, and a longer distance between the muscle incision ending and the cardia were risk factors for poor post-POEM pain control.

Key Words: Achalasia; Peroral endoscopic myotomy; Anesthesia; Postoperative pain; Sleep quality; Nomogram

©The Author(s) 2022. Published by Baishideng Publishing Group Inc. All rights reserved.

Core Tip: Post-peroral endoscopic myotomy (POEM) pain management has been neglected by anesthesiologists and endoscopists. In the present study, we found that achalasia patients experienced moderate to severe postoperative pain after the POEM procedure. The preoperative Eckardt score, previous treatment, and a longer distance between the muscle incision ending and the cardia were high risk factors for postoperative pain.

Citation: Chen WN, Xu YL, Zhang XG. High Eckardt score and previous treatment were associated with poor postperoral endoscopic myotomy pain control: A retrospective study. *World J Clin Cases* 2022; 10(17): 5655-5666
URL: https://www.wjgnet.com/2307-8960/full/v10/i17/5655.htm
DOI: https://dx.doi.org/10.12998/wjcc.v10.i17.5655

INTRODUCTION

Achalasia is a decrease in esophageal tension and esophageal dilation caused by a reduction in esophageal ganglion cells, disappearance of the thoracic esophagus, and diastolic dysfunction of the lower esophageal sphincter (LES). Clinical symptoms include dysphagia, gastroesophageal reflux, chest pain, weight loss, and anemia[1]. The incidence of achalasia is approximately 1.6/100000, regardless of sex and ethnicity, and is higher in younger patients[2-4].

Noninvasive treatments for achalasia include endoscopic botulinum toxin injection, esophageal stenting, and pneumatic balloon dilation. Invasive treatment can be performed with cardiomyotomy (also known as Heller surgery), which involves permanent surgical cutting of the LES[5,6]. In 2010, peroral endoscopic myotomy (POEM) was introduced as a clinical application by Inoue *et al*[7], and its use has rapidly spread worldwide. POEM surgery is a safe and effective treatment for achalasia, as verified by a large number of clinical studies, and has become a first-line treatment for achalasia[8], replacing Heller surgery and other noninvasive treatments.

Several published studies mainly focused on comparing the postoperative pain of achalasia patients receiving either the POEM procedure or laparoscopic Heller's myelotomy (LMH), but their conclusions were inconsistent[9-13]. Meanwhile, postoperative pain management differs among studies, varying from oral opioids and intravenous nonsteroidal anti-inflammatory drugs to intraoperative nerve block [10-12,14]. There was little general agreement on the postoperative pain management of achalasia patients. Thus, the authors conducted this retrospective study to examine the postoperative pain intensity of achalasia patients receiving the POEM procedure and to investigate possible risk factors for postoperative pain.

MATERIALS AND METHODS

Patient identification and data collection

This study was approved by the Ethics Committee of Zhongshan Hospital at Fudan University, No. B2018-004R. This was a preliminary study for a prospective study conducted at the Department of Anesthesiology within Zhongshan Hospital at Fudan University.

Inclusion criteria: (1) Male or female. Age between 18 and 75 years; (2) With diagnosis of achalasia; (3) Received POEM surgery in Zhongshan Hospital Fudan University from November 2017 to April 2018; (4) Complete anesthesia record and operative report; and (5) Signed informed consent.

Exclusion criteria: (1) Past experience with Heller surgery or POEM surgery; (2) Preoperative chronic pain management; and (3) Cognitive dysfunction or an inability to attend follow-up.

The diagnosis of achalasia was established based on the following: (1) Clinical symptoms; (2) X-ray angiography of the esophagus and sputum; (3) Esophagogastroduodenoscopy; (4) Esophageal manometry; and (5) Chest computed tomography (CT) scan[15].

Measurement

The main results collected were the visual analog scale (VAS) scores at 2 h, 6 h, 12 h, 24 h, and 36 h after surgery. The secondary results collected were sleep quality on the night of surgery and on the night of the first day after surgery. A self-reported sleep questionnaire was used to investigate postoperative sleep quality, which included 6 yes-or-no questions. A score of 1 indicated the best quality sleep, and the highest score of 6 indicated the worst sleep quality. A correlation analysis of postoperative pain scores at each follow-up time with postoperative sleep quality and pain scores with related factors was performed. Related factors included the following: (1) Patient demographic information (sex, age, illness duration, disease grade and previous treatment); and (2) Surgical parameters (surgical time, anesthesia time, tunnel length, length of muscle incision, length between the muscle incision ending and the cardia, and perioperative opioid dose).

POEM surgical procedure

POEM surgery was performed at the endoscopy center of the hospital by endoscopic specialists who had received specialized POEM surgery training. Saline was submucosally injected 10-12 cm above the gastroesophageal junction (GEJ), and the mucosal layer was longitudinally cut to form a mucosal opening to expose the stratum submucosa (Figure 1A). Submucosal injection was performed while the mucosa was separated to form a submucosal tunnel (3-4 cm) to the distal end of the GEJ (Figure 1B). The myometrial incision was performed from the distal end of the mucosal tunnel opening at 2 cm to at least 2 cm to the distal end of the GEJ (Figure 1C). After proper hemostasis, the mucosal opening was closed with a hemostatic clip (Figure 1D). To avoid the occurrence of air-related complications, carbon dioxide inflation was continued throughout the procedure (Figure 2).

Anesthesia method

The procedures were performed on patients under general anesthesia with endotracheal intubation. Patients were maintained on carbohydrate drinks the day before the procedure, and oral intake was withheld for 12 h before the surgery. Esophagoscopy was performed while the patients were awake to clear the esophagus. Rapid sequence induction was employed with propofol (2-2.5 mg/kg), succinylcholine (2 mg/kg) and remifentanil (1 μg/kg). Anesthesia was maintained with desflurane (0.8 MAC), fentanyl 2-4 μg/kg, remifentanil 0.05-0.1 μg/kg *per* min. Cis-atracurium (0.03 mg/kg *per* hour) was used to assist intraoperative mechanical ventilation. The ventilator was set up as follows: Tidal volume 8 mL/kg, respiratory rate 10-12/min, and $etCO_2$ maintained between 35-45 mmHg. A protective ventilation strategy was adopted to maintain the peak airway pressure below 30 mmHg and the plateau airway pressure below 25 mmHg. A certain degree of hypercapnia was considered as acceptable ($etCO_2$ lower than 60 mmHg). Two grams of acetaminophen and 4 mg of ondansetron were given before the end of the operation. After the operation, the awakened patients were sent to the postanesthesia care unit (PACU) with a 25 μg titration of fentanyl to maintain a VAS score < 4 and were sent to the ward after a one-hour observation period. To control postoperative pain, 3 mg of dizocine was given intravenously at 8 pm on the day of the surgery and at 8 am on the first day after surgery.

Adverse events

Although these were quite rare, POEM-related adverse events included postoperative transfer to the intensive care unit, unstable vital signs, readmission, change to open surgery, postoperative invasive operation, delayed mucosal barrier failure, delayed bleeding and transfusion of blood, hydrothorax, pneumothorax, and extended hospital stay (> 5 d) due to functional impairment[16]. Anesthesia-related adverse events included reflux aspiration, delayed awakening time for more than 30 min, reintubation, postoperative nausea and vomiting.

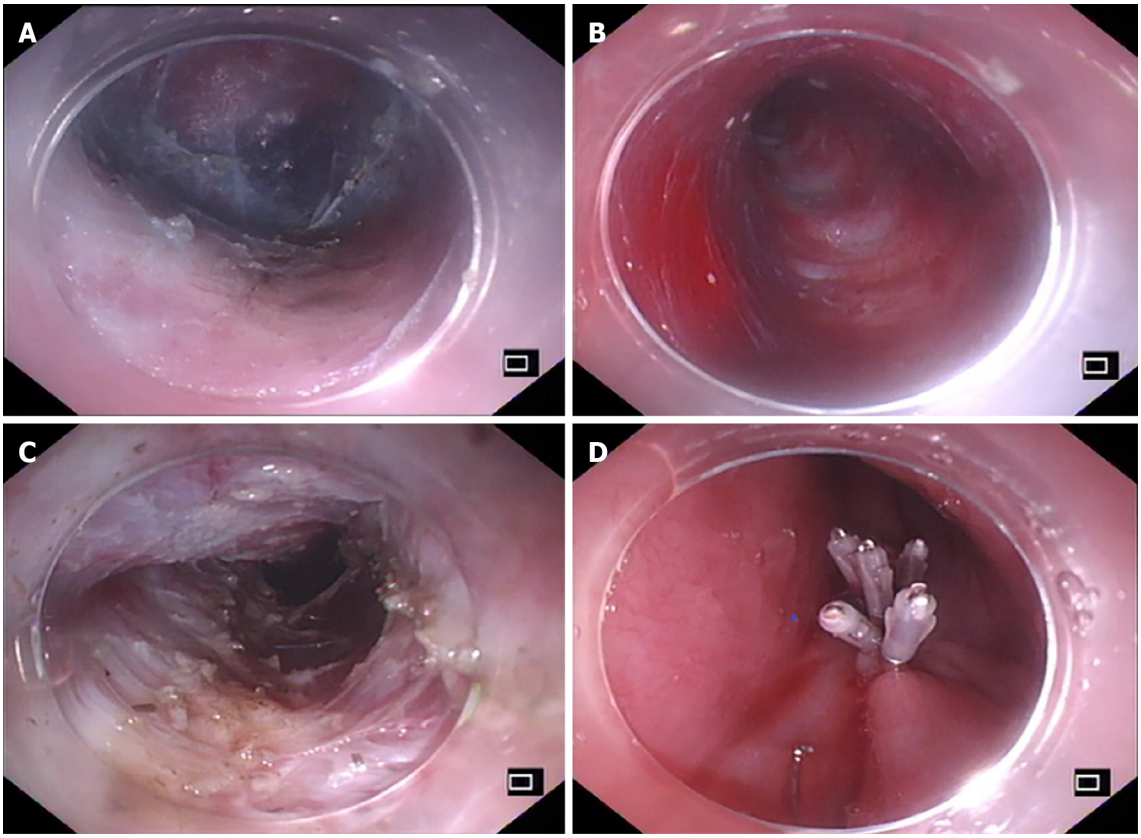

DOI: 10.12998/wjcc.v10.i17.5655 **Copyright** ©The Author(s) 2022.

Figure 1 The peroral endoscopic myotomy procedure. A: The mucosal layer was longitudinally cut to form a mucosal opening to expose the stratum submucosa; B: Submucosal injection was performed while the mucosa was separated to form a submucosal tunnel (3-4 cm) to the distal end of the gastroesophageal junction (GEJ); C: The myometrial incision was performed from the distal end of the mucosal tunnel opening at 2 cm to at least 2 cm to the distal end of the GEJ; D: After proper hemostasis, the mucosal opening was closed with a hemostatic clip.

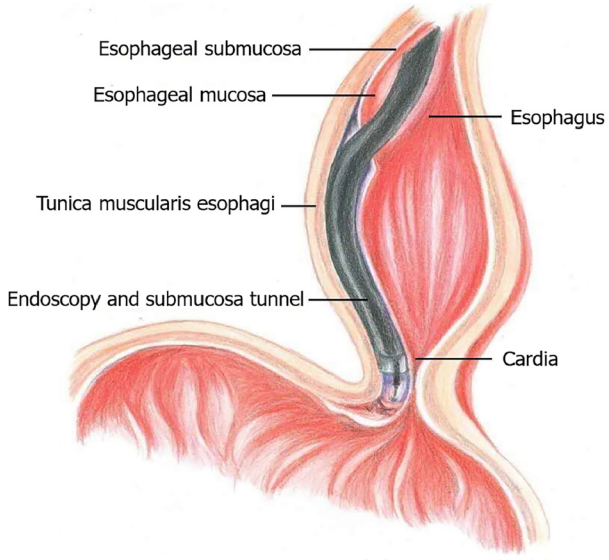

DOI: 10.12998/wjcc.v10.i17.5655 **Copyright** ©The Author(s) 2022.

Figure 2 Illustration of the main peroral endoscopic myotomy procedure.

Statistical analysis

The data were expressed as numerical values and percentages, and continuous data were expressed using the mean ± SD. All patients were divided into groups according to the 12-h postoperative VAS score; the poorly controlled pain group had a VAS score greater than or equal to 4, and the well-controlled pain group had a VAS score less than 4. Student's t test or the Wilcoxon rank sum test was

used to compare quantitative variables, and the chi-square test or Fisher's exact test was used for qualitative variables. Univariate, multivariate, and stepwise logistic regression analyses were used to determine risk factors for poor pain control. The nomogram was formed by the optimal model fitted by logistic regression analysis. The area under the receiver operating characteristic curve (AUC) of the model was evaluated. Repeated measures analysis and of variance and simple effect analysis were used to verify whether the differences in the VAS and sleep scores between the high- and low-risk groups, divided by the model from the raw data, were statistically significant. *P* values over 0.05 were considered as statistically significant. The test was two-sided. All analyses were performed using RStudio software version 1.3.1093.

RESULTS

Patient basic information and surgical parameters

The flowchart of patient selection is summarized in Figure 3. Forty-five patients were enrolled with a mean age of 43.2 ± 15.7 years, including 24 males and 21 females. The average duration of symptoms was 6.0 ± 6.3 years, with an average preoperative Eckardt score of 7.6 ± 2.1 and esophageal dilation of 42.9 ± 10.7 cm. Ten (22.2%) patients had a past history of treatment (Table 1).

With regard to the surgical procedure, the mean surgery and anesthesia times were 61.3 ± 18.8 min and 74.1 ± 21.0 min, respectively. The average submucosal tunnel length, myotomy length, and distance between the muscle incision ending and the cardia were 12.7 ± 1.2 cm, 10.7 ± 1.1 cm, and 2.1 ± 0.3 cm, respectively. Thirty-seven patients (82.2%) were administered 100 μg fentanyl during the surgery, and 8 patients (17.8%) were given 150 μg fentanyl. The total intraoperative remifentanil dose was 265.5 ± 90.8 μg. No patient received fentanyl in the PACU (Table 1).

Risk factors for poor post-POEM pain control

A 12-h postoperative VAS score ≥ 4 was defined as poor post-POEM pain control. As shown in Table 1, patients with poorly controlled postoperative pain had prolonged symptom duration (VAS ≥ 4 *vs* VAS < 4, 7.5 years *vs* 4.1 years, $P = 0.019$), a higher preoperative Eckardt score (VAS ≥ 4 *vs* VAS < 4, 8.4 *vs* 6.7, $P = 0.013$), and a larger esophageal diameter (VAS ≥ 4 *vs* VAS < 4, 46.3 mm *vs* 39 mm, $P = 0.022$). Further univariate logistic regression analyses demonstrated that the preoperative Eckardt score ($P = 0.011$) and preoperative esophageal dilatation ($P = 0.028$) were potential risk factors for poor pain control. Multivariate logistic regression analysis and further stepwise logistic regression were used to exclude the internal effects of the participants, and the optimal fitted model for the risk of poor pain control was constructed. We found that the preoperative Eckardt score (OR: 1.82, 95%CI: 1.17-2.84, $P < 0.001$), previous treatment (OR: 7.59, 95%CI: 1.12-51.23, $P = 0.037$) and the distance between the muscle incision ending and the cardia (OR: 1.52, 95%CI: 0.79-293.93, $P = 0.072$) were risk factors and were included in the model for predicting postoperative pain (Table 2).

Nomogram construction and verification

We further built a nomogram, as shown in Figure 4, to illustrate and visualize the relationship between the potential risk factors and postoperative pain. To calculate the risk for postoperative pain, each parameter was assigned a point vertically corresponding to the "points" axis, and the sum of the points was plotted on the "total points" axis. The risk of poor post-POEM pain control is the value on the "Risk of poor pain control" axis at the vertical position from the corresponding point on the "Total Points" axis. To evaluate the effect of the nomogram, we used the raw data for internal verification to obtain the calibration and receiver operating characteristic curve (ROC) curves. The calibration curve demonstrated good agreement between the predicted value and the actual value (Figure 5A). The ROC curve reflected a good classification ability, with an AUC value of 0.822 and an optimal cutoff of 0.730 (Figure 5B).

Validation of the model using the VAS and sleep scores

Patients were then divided into high- and low-risk groups according to the calculated cutoff from the ROC curve. To investigate whether postoperative VAS and sleep scores differed between the groups, a repeated measures analysis of variance was conducted, and we found that patients in the high-risk group had higher VAS ($P = 0.0097$) and sleep scores ($P = 0.043$) (Table 3). A further simple effect analysis found that VAS scores were higher in the high-risk group at 2 h, 6 h and 12 h ($P = 0.005$, $P = 0.019$, $P < 0.001$), and sleep scores were higher in the high-risk group at day 1 ($P = 0.006$) (Table 4). Line charts of the VAS and sleep scores of the two groups are presented to visually represent the trend in their variation (Figure 6).

Table 1 Basic characteristics according to the visual analog scale at 12 h after surgery (mean ± SD)

	Total	VAS < 4	VAS ≥ 4	*P* value
Sex (%)				
Female	21 (46.7)	8 (38.1)	13 (54.2)	0.44
Male	24 (53.3)	13 (61.9)	11 (45.8)	
Age	43.2 ± 15.7	45.0 ± 18.0	41.5 ± 13.6	0.60
Symptom duration (yr)	6.0 ± 6.3	4.1 ± 4.9	7.5 ± 7.0	0.019
Eckardt score	7.6 ± 2.1	6.7 ± 2.2	8.4 ± 1.6	0.013
Esophageal diameter (mm)	42.9 ± 10.7	39.0 ± 10.0	46.3 ± 10.4	0.022
Esophageal dilatation classification (%)				
I	20 (44.4)	13 (61.9)	7 (29.2)	0.088
II	21 (46.7)	7 (33.3)	14 (58.3)	
III	4 (8.9)	1 (4.8)	3 (12.5)	
Previous treatment (%)				
No	35 (77.8)	19 (90.5)	16 (66.7)	0.078
Yes	10 (22.2)	2 (9.5)	8 (33.3)	
Operative time (min)	61.3 ± 18.8	58.8 ± 16.9	63.5 ± 20.4	0.46
Anesthesia time (min)	74.1 ± 21.0	72.1 ± 17.5	75.8 ± 23.9	0.73
Tunnel length (cm)	12.7 ± 1.2	12.6 ± 0.6	12.8 ± 1.5	0.56
Myotomy length (cm)	10.7 ± 1.1	10.6 ± 0.7	10.8 ± 1.4	0.35
Distance from muscle incision ending to cardia (cm)	2.1 ± 0.3	2.0 ± 0.2	2.2 ± 0.4	0.22
Fentanyl dosage (ug) (%)				
100	37 (82.2)	16 (76.2)	21 (87.5)	0.44
150	8 (17.8)	5 (23.8)	3 (12.5)	
Remifentanil dosage (ug)	265.5 ± 90.8	264.8 ± 85.3	266.1 ± 97.2	1.0

VAS: Visual analog scale.

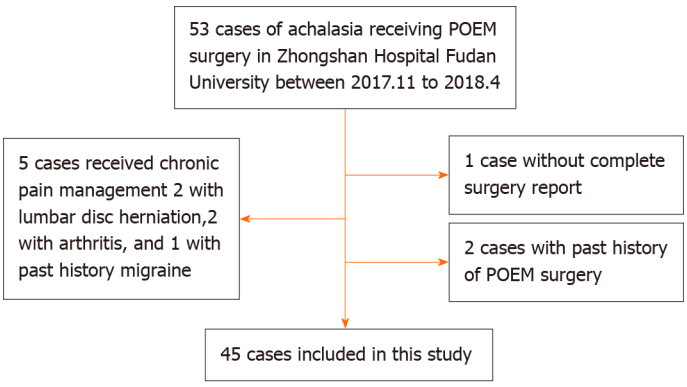

DOI: 10.12998/wjcc.v10.i17.5655 **Copyright** ©The Author(s) 2022.

Figure 3 Flowchart of patient selection. POEM: Peroral endoscopic myotomy.

DISCUSSION

Postoperative pain management of achalasia patients who undergo the POEM procedure is often neglected by anesthesiologists due to the short operative time and minimally invasive nature of the POEM procedure. In this retrospective study, we included 45 achalasia patients who received POEM at our medical center, evaluated their postoperative pain intensity and sleep quality, and explored factors

Table 2 Univariate and multivariate logistic regression analyses of poor pain control, defined as those whose 12-h visual analog scale score was greater than 3

Parameter	Univariate		Multivariate	
	OR (95%CI)	*P* value	OR (95%CI)	*P* value
Sex	0.52 (0.16-1.71)	0.283		
Age	0.99 (0.95-1.02)	0.45		
Duration	1.12 (0.98-1.27)	0.091		
Eckardt Score	1.64 (1.12-2.40)	0.011	1.82 (1.17-2.84)	< 0.001
Esophageal diameter	1.07 (1.01-1.14)	0.028		
Esophageal dilatation classification	3.71 (1.02-13.51)	0.046		
	5.57 (0.48-64.09)	0.17		
Previous treatment	4.75 (0.88-25.65)	0.07	7.59 (1.12-51.23)	0.037
Operative time	1.01 (0.98-1.05)	0.40		
Anesthesia time	1.01 (0.98-1.04)	0.55		
Tunnel length	1.18 (0.69-2.01)	0.54		
Myotomy length	1.20 (0.69-2.09)	0.52		
Distance from muscle incision ending to cardia	4.00 (0.41-39.00)	0.23	1.52 (0.79-293.93)	0.072
Fentanyl dosage	0.46 (0.095-2.20)	0.33		
Remifentanil dosage	1.00 (0.99-1.01)	0.96		

Table 3 Repeated measures analysis of variance of visual analog scale and sleep scores

		F value	*P* value
VAS	Groups	7.33	0.0097
	Time	226.47	< 0.001
	Groups: Time	3.03	0.019
Sleep score	Groups	4.35	0.043
	Time	138.57	< 0.001
	Groups: Time	4.72	0.035

VAS: Visual analog scale.

associated with post-POEM pain. Our results demonstrated that patients with postoperative VAS scores (12 h after surgery) greater than or equal to 4 had longer symptom durations, higher preoperative Eckardt scores, and larger esophageal diameters. The Eckardt score, previous treatment for achalasia, and the distance between the muscle incision ending and the cardia were associated with poor postoperative pain control and were further included in the model for predicting postoperative pain. Patients in the high-risk group had higher VAS and sleep scores.

POEM has been proven to be a safe and effective endoscopic procedure for treating achalasia[16,17]. Previous studies on anesthesia management in POEM procedures have mostly focused on intraoperative anesthesia, reflux aspiration, and anesthesia-related complications[18-20]. Tanaka *et al*[18] administered remifentanil during surgery, and patients complained of postoperative upper abdominal pain. Twenty of the twenty-eight enrolled patients received diclofenac sodium turunda within 24 h after surgery, among whom 3 patients were given additional pentazocine. Nishihara *et al*[20] also delivered remifentanil during surgery but did not report any information about postoperative pain. Another retrospective study of 12 patients performed by Misra *et al*[21] revealed that patients had mild to moderate pain after POEM. These patients received fentanyl, hydromorphone, morphine, acetaminophen, oxycodone, and ketorolac as postoperative analgesia; however, there were no records on opioid use during surgery. Thus, the present study is the first retrospective study incorporating complete anesthesia management data and medical records to evaluate postoperative pain intensity and investigate potential risk factors among achalasia patients who underwent POEM.

Table 4 Simple effect analysis of variance of visual analog scale and sleep scores

		F value	*P* value
VAS	Risk (2 h)	8.34	0.005
	Risk (6 h)	5.71	0.019
	Risk (12 h)	12.91	< 0.001
	Risk (24 h)	1.42	0.24
	Risk (36 h)	0.69	0.41
Sleep score	Risk (day 1)	8.05	0.006
	Risk (day 2)	0.80	0.375

VAS: Visual analog scale.

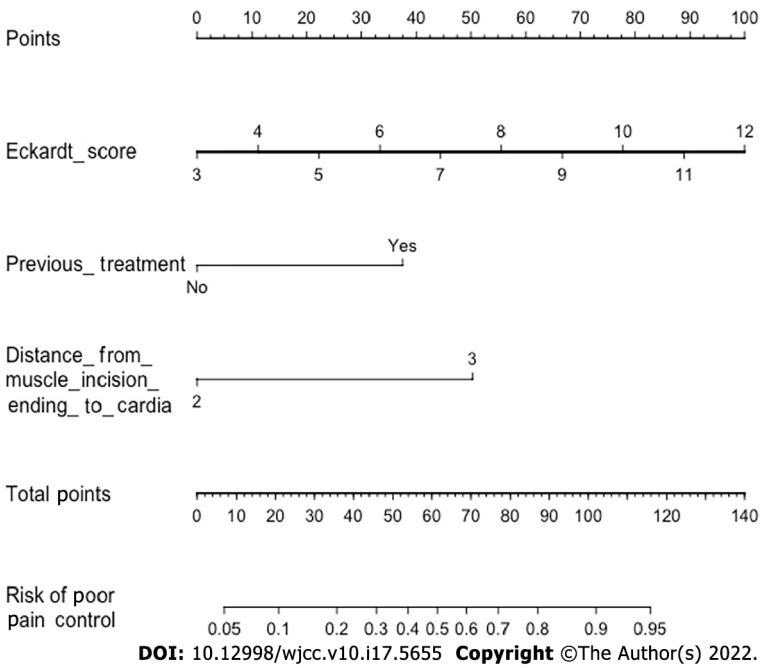

DOI: 10.12998/wjcc.v10.i17.5655 **Copyright** ©The Author(s) 2022.

Figure 4 The nomogram was constructed from 3 parameters (Table 2). To calculate a patient's risk for poor pain control, defined as a visual analog scale score greater than or equal to 4 at 12 h after peroral endoscopic myotomy (POEM), each parameter was assigned a point by its vertical correspondence to the "points" axis, and the sum of the points was plotted on the "total points" axis. The risk for poor post-POEM pain control is the value on the "Risk of poor pain control" axis at a vertical position from the corresponding point on the "Total Points" axis.

No patient complained of pain during the telephone follow-up on the 28th day after surgery, suggesting that POEM may not lead to chronic pain. This result was consistent with previous research conducted by Misra *et al*[21], which revealed that postoperative pain associated with the POEM procedure seldom lasts for months.

A comparison of the baseline characteristics between groups demonstrated that patients who suffered from postoperative pain had longer symptom durations, higher Eckardt scores and larger esophageal diameters, *i.e.*, more severe cases. Further stepwise logistic regression analyses showed that a higher Eckardt score and previous treatment for achalasia were associated with poor postoperative pain control (VAS ≥ 4 at 12 h after surgery). Patients with higher Eckardt scores had worse symptoms of achalasia and were also more likely to have relapsed or intractable achalasia, resulting in increased surgical difficulty and greater surgical wounds, which may contribute to severe postoperative pain. Interestingly, we also found that the 12-h postoperative VAS score was associated with the distance between the muscle incision ending and the cardia; the longer the distance, the more severe the pain. However, there was no significant difference between the VAS < 4 and VAS ≥ 4 groups in terms of surgical parameters. The suggestion for the range of submucosal tunnels was from 10-12 cm above the GEJ to 3-4 cm below the GEJ[7]. Previous studies showed that patients with shorter tunnels (10.7 ± 1.4 cm) had fewer complications than those with longer tunnels (13.1 ± 0.8 cm)[22]. Meanwhile, the range of myotomy is still controversial. It was suggested that excess myotomy was unnecessary, while

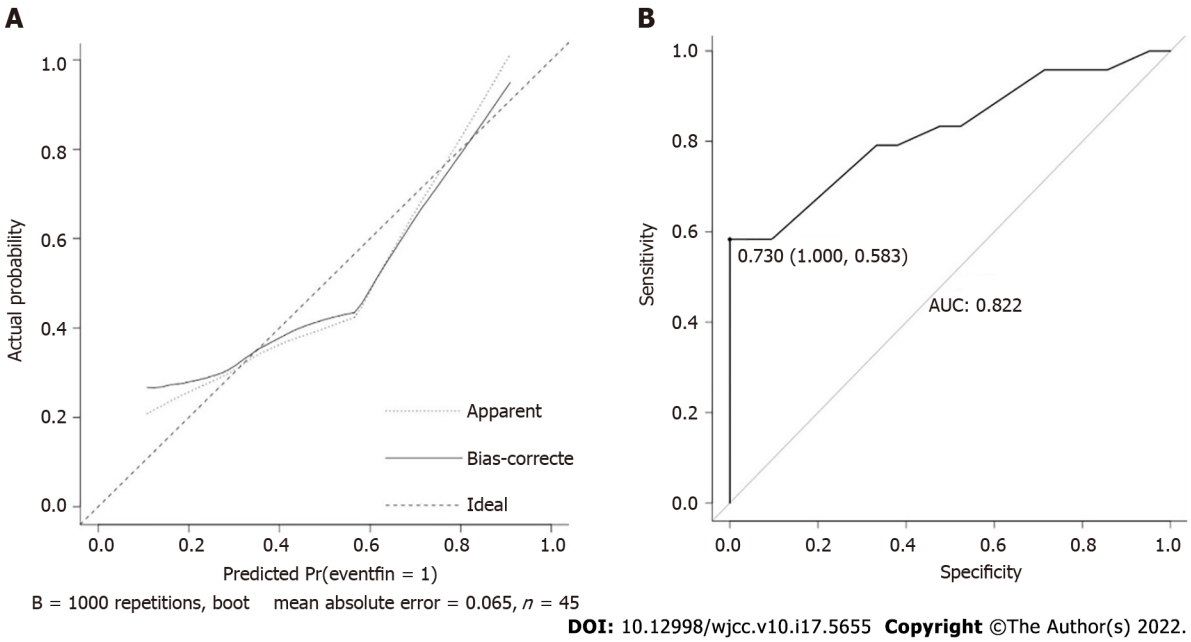

DOI: 10.12998/wjcc.v10.i17.5655 **Copyright** ©The Author(s) 2022.

Figure 5 Calibration plots and receiver operating characteristic curve of the nomogram for prediction. A: The calibration plot is the comparison between predicted and actual outcomes. The dashed line is a reference line, indicating where an ideal nomogram would lie; B: Receiver operating characteristic curve of the nomogram with an area under the receiver operating characteristic curve of 0.822 and an optimal cutoff of 0.730.

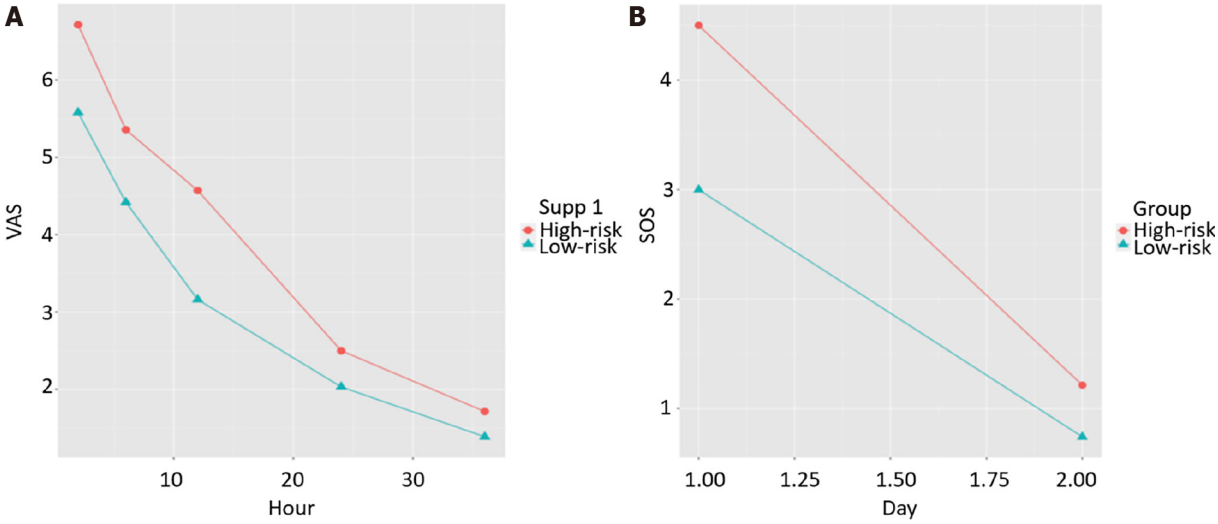

DOI: 10.12998/wjcc.v10.i17.5655 **Copyright** ©The Author(s) 2022.

Figure 6 Line charts of the means of the high- and low-risk groups, divided from the raw data, by the nomogram over time. A: Line chart of the visual analog scale; B: Line chart of the sleep score. VAS: Visual analog scale.

insufficient myotomy may lead to recurrence. A muscle incision ending within 3 cm of the cardia was recommended. However, commonly used endoscopic markers of the gastric side are inaccurate, particularly in patients who have received previous treatment, such as balloon dilation or Botox injection of the LES[23]. Thus, anesthesiologists and endoscopists should pay attention to not only the surgical procedure itself but also the severity of achalasia.

With the small number of patients enrolled in this study, meaningful conclusions are still limited to some degree. This was an observational study performed during the early stage of an randomized controlled trial (RCT), and we will further explore the optimal approach to postoperative analgesia in patients who underwent POEM surgery in the RCT study and will cooperate with endoscopists to explore the effect of the POEM modus operandi (intrapleural tunnel length and myotomy position) on postoperative pain.

In summary, achalasia patients who underwent the POEM procedure experienced moderate to severe postoperative pain that required pain management. Patients with higher preoperative Eckardt scores, previous treatments, and longer distances between the muscle incision ending and the cardia may have

a higher risk for postoperative pain.

CONCLUSION

Achalasia patients receiving POEM surgery experienced moderate to severe postoperative pain, which affected their sleep quality. Patients with higher preoperative Eckardt scores, previous treatments, and longer distances between the muscle incision ending and the cardia have a higher risk for poor postoperative pain control. Anesthetists and endoscopists should pay more attention to the severity of achalasia than to the POEM procedure itself when evaluating the risk for post-POEM pain.

ARTICLE HIGHLIGHTS

Research background

Postoperative pain management for peroral endoscopic myotomy (POEM) is often neglected by anesthesiologists because of the short operative time, short hospital stay and the minimally invasive nature of the procedure.

Research motivation

The authors conducted this retrospective study to examine the postoperative pain intensity of achalasia patients receiving the POEM procedure and to investigate possible risk factors for postoperative pain.

Research objectives

To achieve better postoperative pain management.

Research methods

We included patients with achalasia who underwent POEM at Zhongshan Hospital from December 2017 to March 2018. The postoperative visual analog scale, postoperative sleep quality, basic patient information, and surgical parameters were collected.

Research results

The preoperative Eckardt score [odds ratio (OR): 1.82, 95% confidence interval (CI): 1.17-2.84, $P < 0.001$], previous treatment (OR: 7.59, 95%CI: 1.12-51.23, $P = 0.037$) and the distance between the end of the muscle incision and the cardia (OR: 1.52, 95%CI: 0.79-293.93, $P = 0.072$) were risk factors for post-POEM pain.

Research conclusions

Achalasia patients who underwent POEM experienced serious postoperative pain, which may affect sleep quality. A higher Eckardt score, previous treatment, and a longer distance between the muscle incision ending and the cardia were risk factors for poor post-POEM pain control.

Research perspectives

We will further explore the optimal approach to postoperative analgesia in patients who underwent POEM surgery in the randomized controlled trial study and will cooperate with endoscopists to explore the effect of the POEM modus operandi (intrapleural tunnel length and myotomy position) on postoperative pain.

FOOTNOTES

Author contributions: Chen WN and Xu YL contributed equally to this work; Chen WN designed the research; Chen WN and Zhang XG managed the clinical process; Xu YL collected clinical data; Chen WN and Xu YL wrote the manuscript; Zhang XG revised the manuscript.

Institutional review board statement: The study was reviewed and approved by the Ethics Committee of Zhongshan Hospital affiliated with Fudan University, No. B2018-004R.

Conflict-of-interest statement: There are no conflicts of interest related to this study.

Data sharing statement: Technical appendix, statistical code, and dataset available from the corresponding author at zhang.xiaoguang@zs-hospital.sh.cn.

STROBE statement: The authors have read the STROBE Statement—checklist of items, and the manuscript was prepared and revised according to the STROBE Statement—checklist of items.

Open-Access: This article is an open-access article that was selected by an in-house editor and fully peer-reviewed by external reviewers. It is distributed in accordance with the Creative Commons Attribution NonCommercial (CC BY-NC 4.0) license, which permits others to distribute, remix, adapt, build upon this work non-commercially, and license their derivative works on different terms, provided the original work is properly cited and the use is non-commercial. See: https://creativecommons.org/Licenses/by-nc/4.0/

Country/Territory of origin: China

ORCID number: Wan-Nan Chen 0000-0003-1236-2386; Yao-Lin Xu 0000-0002-0971-518X; Xiao-Guang Zhang 0000-0002-4636-792X.

S-Editor: Fan JR
L-Editor: A
P-Editor: Yu HG

REFERENCES

1 **Winter H**, Shukla R, Elshaer M, Riaz AA. Current management of achalasia—a review. *Br J Med Pract* 2015; **8**: a810
2 **O'Neill OM**, Johnston BT, Coleman HG. Achalasia: a review of clinical diagnosis, epidemiology, treatment and outcomes. *World J Gastroenterol* 2013; **19**: 5806-5812 [PMID: 24124325 DOI: 10.3748/wjg.v19.i35.5806]
3 **Sadowski DC**, Ackah F, Jiang B, Svenson LW. Achalasia: incidence, prevalence and survival. A population-based study. *Neurogastroenterol Motil* 2010; **22**: e256-e261 [PMID: 20465592 DOI: 10.1111/j.1365-2982.2010.01511.x]
4 **Francis DL**, Katzka DA. Achalasia: update on the disease and its treatment. *Gastroenterology* 2010; **139**: 369-374 [PMID: 20600038 DOI: 10.1053/j.gastro.2010.06.024]
5 **Campos GM**, Vittinghoff E, Rabl C, Takata M, Gadenstätter M, Lin F, Ciovica R. Endoscopic and surgical treatments for achalasia: a systematic review and meta-analysis. *Ann Surg* 2009; **249**: 45-57 [PMID: 19106675 DOI: 10.1097/SLA.0b013e31818e43ab]
6 **Boeckxstaens GE**, Annese V, des Varannes SB, Chaussade S, Costantini M, Cuttitta A, Elizalde JI, Fumagalli U, Gaudric M, Rohof WO, Smout AJ, Tack J, Zwinderman AH, Zaninotto G, Busch OR; European Achalasia Trial Investigators. Pneumatic dilation versus laparoscopic Heller's myotomy for idiopathic achalasia. *N Engl J Med* 2011; **364**: 1807-1816 [PMID: 21561346 DOI: 10.1056/NEJMoa1010502]
7 **Inoue H**, Minami H, Kobayashi Y, Sato Y, Kaga M, Suzuki M, Satodate H, Odaka N, Itoh H, Kudo S. Peroral endoscopic myotomy (POEM) for esophageal achalasia. *Endoscopy* 2010; **42**: 265-271 [PMID: 20354937 DOI: 10.1055/s-0029-1244080]
8 **Pasricha PJ**, Hawari R, Ahmed I, Chen J, Cotton PB, Hawes RH, Kalloo AN, Kantsevoy SV, Gostout CJ. Submucosal endoscopic esophageal myotomy: a novel experimental approach for the treatment of achalasia. *Endoscopy* 2007; **39**: 761-764 [PMID: 17703382 DOI: 10.1055/s-2007-966764]
9 **Murata H**, Ichinomiya T, Hara T. Anesthesia for peroral endoscopic myotomy in Japan. *Curr Opin Anaesthesiol* 2019; **32**: 511-516 [PMID: 30994477 DOI: 10.1097/ACO.0000000000000742]
10 **Hungness ES**, Teitelbaum EN, Santos BF, Arafat FO, Pandolfino JE, Kahrilas PJ, Soper NJ. Comparison of perioperative outcomes between peroral esophageal myotomy (POEM) and laparoscopic Heller myotomy. *J Gastrointest Surg* 2013; **17**: 228-235 [PMID: 23054897 DOI: 10.1007/s11605-012-2030-3]
11 **Docimo S Jr**, Mathew A, Shope AJ, Winder JS, Haluck RS, Pauli EM. Reduced postoperative pain scores and narcotic use favor per-oral endoscopic myotomy over laparoscopic Heller myotomy. *Surg Endosc* 2017; **31**: 795-800 [PMID: 27338580 DOI: 10.1007/s00464-016-5034-3]
12 **Ujiki MB**, Yetasook AK, Zapf M, Linn JG, Carbray JM, Denham W. Peroral endoscopic myotomy: A short-term comparison with the standard laparoscopic approach. *Surgery* 2013; **154**: 893-7; discussion 897 [PMID: 24074429 DOI: 10.1016/j.surg.2013.04.042]
13 **Talukdar R**, Inoue H, Nageshwar Reddy D. Efficacy of peroral endoscopic myotomy (POEM) in the treatment of achalasia: a systematic review and meta-analysis. *Surg Endosc* 2015; **29**: 3030-3046 [PMID: 25539695 DOI: 10.1007/s00464-014-4040-6]
14 **Elmunzer BJ**, Lewis BR, Miller KF, Wolf BJ, Zeiler L, Gutman DA, Elias P, Tansel A, Moran RA, Bolin ED. Paravertebral anesthetic nerve block for pain control after peroral endoscopic myotomy. *Tech Innov Gastrointest Endosc* 2021; **23**: 297-303 [PMID: 34870251 DOI: 10.1016/j.tige.2021.06.006]
15 **Vaezi MF**, Pandolfino JE, Vela MF. ACG clinical guideline: diagnosis and management of achalasia. *Am J Gastroenterol* 2013; **108**: 1238-49; quiz 1250 [PMID: 23877351 DOI: 10.1038/ajg.2013.196]
16 **Zhang XC**, Li QL, Xu MD, Chen SY, Zhong YS, Zhang YQ, Chen WF, Ma LL, Qin WZ, Hu JW, Cai MY, Yao LQ, Zhou PH. Major perioperative adverse events of peroral endoscopic myotomy: a systematic 5-year analysis. *Endoscopy* 2016; **48**: 967-978 [PMID: 27448052 DOI: 10.1055/s-0042-110397]
17 **Li QL**, Wu QN, Zhang XC, Xu MD, Zhang W, Chen SY, Zhong YS, Zhang YQ, Chen WF, Qin WZ, Hu JW, Cai MY, Yao LQ, Zhou PH. Outcomes of per-oral endoscopic myotomy for treatment of esophageal achalasia with a median follow-up of 49 months. *Gastrointest Endosc* 2018; **87**: 1405-1412.e3 [PMID: 29108981 DOI: 10.1016/j.gie.2017.10.031]

18 **Tanaka E**, Murata H, Minami H, Sumikawa K. Anesthetic management of peroral endoscopic myotomy for esophageal achalasia: a retrospective case series. *J Anesth* 2014; **28**: 456-459 [PMID: 24185834 DOI: 10.1007/s00540-013-1735-0]

19 **Löser B**, Werner YB, Punke MA, Saugel B, Haas S, Reuter DA, Mann O, Duprée A, Schachschal G, Rösch T, Petzoldt M. Anesthetic considerations for patients with esophageal achalasia undergoing peroral endoscopic myotomy: a retrospective case series review. *Can J Anaesth* 2017; **64**: 480-488 [PMID: 28116675 DOI: 10.1007/s12630-017-0820-5]

20 **Nishihara Y**, Yoshida T, Ooi M, Obata N, Izuta S, Mizobuchi S. Anesthetic management and associated complications of peroral endoscopic myotomy: A case series. *World J Gastrointest Endosc* 2018; **10**: 193-199 [PMID: 30283602 DOI: 10.4253/wjge.v10.i9.193]

21 **Misra L**, Fukami N, Nikolic K, Trentman TL. Peroral endoscopic myotomy: procedural complications and pain management for the perioperative clinician. *Med Devices (Auckl)* 2017; **10**: 53-59 [PMID: 28260955 DOI: 10.2147/MDER.S115632]

22 **Ma XB**, Linghu EQ, Wang NJ, Wang XD, Du H, Meng JY, Wang HB, Zhu J, Tang P, Huang QY, Zhao XW, Chai GQ, Kong JY, Qiu XY. Application of peroral endoscopic myotomy with short tunnel for Ling IIc type achalasia. *Chin J Laparoscopic Sur* 2014; **7**: 271-274 [DOI: 10.1007/s00464-018-6414-7]

23 **Grimes KL**, Inoue H, Onimaru M, Ikeda H, Tansawet A, Bechara R, Tanaka S. Double-scope per oral endoscopic myotomy (POEM): a prospective randomized controlled trial. *Surg Endosc* 2016; **30**: 1344-1351 [PMID: 26173548 DOI: 10.1007/s00464-015-4396-2]

World Journal of Clinical Cases

Submit a Manuscript: https://www.f6publishing.com

World J Clin Cases 2022 June 16; 10(17): 5667-5679

DOI: 10.12998/wjcc.v10.i17.5667

ISSN 2307-8960 (online)

ORIGINAL ARTICLE

Observational Study

Higher volume growth rate is associated with development of worrisome features in patients with branch duct-intraductal papillary mucinous neoplasms

Tommaso Innocenti, Ginevra Danti, Erica Nicola Lynch, Gabriele Dragoni, Matteo Gottin, Filippo Fedeli, Daniele Palatresi, Maria Rosa Biagini, Stefano Milani, Vittorio Miele, Andrea Galli

Specialty type: Gastroenterology and hepatology

Provenance and peer review: Unsolicited article; Externally peer reviewed.

Peer-review model: Single blind

Peer-review report's scientific quality classification

Grade A (Excellent): 0
Grade B (Very good): B
Grade C (Good): 0
Grade D (Fair): D, D
Grade E (Poor): 0

P-Reviewer: Jin ZD, China; Kang KJ, South Korea

Received: December 21, 2021
Peer-review started: December 21, 2021
First decision: March 10, 2022
Revised: March 18, 2022
Accepted: April 9, 2022
Article in press: April 9, 2022
Published online: June 16, 2022

Tommaso Innocenti, Erica Nicola Lynch, Gabriele Dragoni, Matteo Gottin, Maria Rosa Biagini, Stefano Milani, Andrea Galli, Gastroenterology Research Unit, Department of Experimental and Clinical Biomedical Sciences "Mario Serio", University of Florence, Florence 50134, Italy

Ginevra Danti, Filippo Fedeli, Daniele Palatresi, Vittorio Miele, Emergency Radiology Unit, Department of Services, Careggi University Hospital, Florence 50134, Italy

Gabriele Dragoni, Department of Medical Biotechnologies, University of Siena, Siena 53100, Italy

Corresponding author: Andrea Galli, MD, PhD, Full Professor, Gastroenterology Research Unit, Department of Experimental and Clinical Biomedical Sciences "Mario Serio", University of Florence, Viale G.B. Morgagni, 50, Florence 50134, Italy. a.galli@dfc.unifi.it

Abstract

BACKGROUND

Branch duct-intraductal papillary mucinous neoplasms (BD-IPMNs) are the most common pancreatic cystic tumours and have a low risk of malignant transformation. Current guidelines only evaluate cyst diameter as an important risk factor but it is not always easy to measure, especially when comparing different methods. On the other side, cyst volume is a new parameter with low inter-observer variability and is highly reproducible over time.

AIM

To assess both diameter and volume growth rate of BD-IPMNs and evaluate their correlation with the development of malignant characteristics.

METHODS

Computed tomography scans and magnetic resonance imaging exams were retrospectively reviewed. The diameter was measured on three planes, while the volume was calculated by segmentation: The volume of the entire cyst was determined by manually drawing a region of interest along the edge of the neoplasm on each consecutive slice covering the whole lesion; therefore, a three-dimensional volume of interest was finally obtained with the calculated value expressed in cm^3. Changes in size over time were measured. The development of

worrisome features was evaluated.

RESULTS

We evaluated exams of 98 patients across a 40.5-mo median follow-up time. Ten patients developed worrisome features. Cysts at baseline were significantly larger in patients who developed worrisome features (diameters P = 0.0035, P = 0.00652, P = 0.00424; volume P = 0.00222). Volume growth rate was significantly higher in patients who developed worrisome features (1.12 cm^3/year *vs* 0 cm^3/year, P = 0.0001); diameter growth rate was higher as well, but the difference did not always reach statistical significance. Volume but not diameter growth rate in the first year of follow-up was higher in patients who developed worrisome features (0.46 cm^3/year *vs* 0 cm^3/year, P = 0.00634).

CONCLUSION

The measurement of baseline volume and its variation over time is a reliable tool for the follow-up of BD-IPMNs. Volume measurement could be a better tool than diameter measurement to predict the development of worrisome features.

Key Words: Intraductal papillary mucinous neoplasms; Cyst; Volume; Growth; Worrisome features; Malignancies

©The Author(s) 2022. Published by Baishideng Publishing Group Inc. All rights reserved.

Core Tip: Branch duct-intraductal papillary mucinous neoplasms (BD-IPMNs) are the most common pancreatic cystic tumours. Size is the most important risk factor in patients with BD-IPMNs. A high diameter growth-rate is associated with malignancy as well. In our study, we demonstrated that volume is associated with the development of worrisome features and that a higher volume growth-rate can lead to a higher risk of worrisome features. Moreover, in our cohort, volume growth-rate in the first year of follow-up predicted the development of worrisome features. Based on these data, measuring volume could be a better tool than the diameter to predict early BD-IPMNs malignant transformation.

Citation: Innocenti T, Danti G, Lynch EN, Dragoni G, Gottin M, Fedeli F, Palatresi D, Biagini MR, Milani S, Miele V, Galli A. Higher volume growth rate is associated with development of worrisome features in patients with branch duct-intraductal papillary mucinous neoplasms. *World J Clin Cases* 2022; 10(17): 5667-5679
URL: https://www.wjgnet.com/2307-8960/full/v10/i17/5667.htm
DOI: https://dx.doi.org/10.12998/wjcc.v10.i17.5667

INTRODUCTION

Pancreatic intraductal papillary mucinous neoplasms (IPMN), in their branch-duct form (BD-IPMN) are the most frequent cystic tumours of the exocrine pancreas and harbour a low risk of malignant transformation[1,2]. For this reason, it is essential to stratify the risk of malignancy in order to plan the most appropriate follow-up for each patient.

The current guidelines suggest an individual risk-based screening with computed tomography (CT) scan, magnetic resonance imaging (MRI) or endoscopic ultrasound (EUS)[3-5]. Cyst diameter growth rate is one of the parameters that is associated with the development of malignant features in patients with BD-IPMN[6,7]. However, only the International Guidelines by Tanaka *et al*[4] consider the cyst diameter growth rate as a worrisome feature. Recently, a nomogram based on cyst size, pancreatic duct size, presence of mural nodule, serum carbohydrate antigen (CA) 19.9 and carcinoembryonic antigen (CEA) was constructed to predict malignancy in BD-IPMNs[8]. However, none of the current guidelines take into account the volume of the cysts and its evolution over time, although it has recently been shown that this is a highly reproducible parameter with low inter-observer variability[9]. To date, there are no studies investigating the correlation between cyst volume growth rate and the risk of malignant degeneration in patients with BD-IPMN.

In light of the lack of agreement between current guidelines, we believe it would be useful to implement the available evidence regarding the risk factors for malignancy of pancreatic BD-IPMN. Moreover, assessing cyst volume growth rate may enable the identification of patients who would benefit from a close follow-up, distinguishing them from those for whom it would be more useful to delay check-ups over time or even interrupt them for cost-effective reasons.

In this study, we assess the growth rate (both diameter and volume) of low-risk BD-IPMNs and evaluate its correlation with the development of malignant characteristics. Moreover, we aim to evaluate the possible superiority of measuring cyst volume instead of cyst diameters in predicting poor outcomes.

MATERIALS AND METHODS

Study design and patient enrolment

We designed a single-centre, retrospective study at our tertiary referral centre. In accordance with the ethical standards as laid down in the 1964 Declaration of Helsinki and its later amendments, we evaluated data of 148 patients who were referred to our pancreatic disease outpatient clinic (Gastroenterology Unit, Careggi University Hospital, Florence, Italy) for regular IPMN follow-up. We searched in the digital clinical records using a free text entry ("IPMN" or "intraductal papillary mucinous neoplasms" or "pancreatic cyst" and "branch-duct" or "BD") into a 10-years-period (between July 2011 and July 2021). The study was approved by the local Ethical Committee of Careggi University Hospital on July 13th 2021 (protocol number: 20256_oss).

We included all adult patients with a known BD-IPMN who had at least two contrast-enhanced MRI studies or CT scans at our centre and a 12-mo minimum follow-up time. For patients who had multifocal BD-IPMN, the largest cyst was considered. Exclusion criteria were paediatric age (< 18 years), prior history of pancreatic cancer or surgery, history of acute or chronic pancreatitis, patients with worrisome features or high-risk stigmata (mentioned later) at first imaging study and patients who had their imaging studies in other clinical centres or for whom radiological study images were unavailable.

IPMN were defined as a grape-like cluster of small cysts originating from a branch of the pancreatic duct, a multilocular cyst with finger-like projections or a single, lobulated cyst communicating with the main pancreatic duct (MPD)[6,10]. Mucinous fluid at fine-needle aspiration and cyst fluid cytology consistent with IPMN were additional criteria.

Worrisome features and high-risk stigmata were defined as in the 2017 Fukuoka guidelines (Figure 1). Worrisome features include cyst of ≥ 3 cm, enhancing mural nodule < 5 mm, thickened enhanced cyst walls, MPD size of 5-9 mm, abrupt change in the MPD calibre with distal pancreatic atrophy, lymphadenopathy, an elevated serum level of CA19.9 and a rapid rate of cyst growth > 5 mm/2 years. High-risk stigmata include obstructive jaundice in a patient with a cystic lesion of the pancreatic head, enhanced mural nodule ≥ 5 mm and MPD size ≥ 10 mm[4].

For each patient we collected demographic and clinical data including sex, age at start of follow-up, smoking habits, familial history, diabetes history and follow-up duration (in months). When possible, we collected biochemical data including serum CA19.9 and CEA. Serum CA19.9 was considered high if > 37 IU/L, as reported in a recent update by Ciprani *et al*[11]. When available, we also collected data regarding EUS examination including cyst dimension (two largest diameters) and (if FNA was performed) cyst fluid CEA, amylases and cytology characteristics.

Radiological protocol

All CT investigations were carried out on a 128-slice CT scanner (Brilliance iCT, Philips Medical Systems, Netherlands). Patients were scanned in the supine position with cranio-caudal breath-hold scans. All patients underwent non-contrast and contrast-enhanced CT scanning with a slice thickness of 2-3 mm. Iodinated contrast medium (iopromide 370 mg I/mL - Ultravist®, Bayer Schering, Berlin) was injected into the antecubital vein at a flow rate of 3-4 mL/s using an automatic injector, immediately followed by a saline flush. The dose of the contrast medium was administered according to the patient's body weight [mL/kg body weight: 80-100 mL (< 80 kg) or 100-120 mL (> 80 kg)]. Contrast-enhanced CT images were acquired during the arterial (30-35 s), portal venous (80-90 s) and late phase (> 180 s).

All MRI examinations were carried out on a 1.5 Tesla MRI scanner (MAGNETOM Aera, Siemens, Germany). MRI protocol for IPMN included: T2-weighted Turbo Spin Echo (TSE) or Single Shot TSE sequence acquired in axial and coronal planes; T1-weighted gradient echo (GRE) in-phase and out-of-phase sequence acquired in the axial plane; diffusion weighted imaging (DWI) (b value = 0; 100; 500; 800) acquired in the axial plane and ADC map; cholangiographic sequences, that is T2-weighted Single Shot TSE 2D (radial) fat-sat sequences and T2-weighted volume (3D) TSE fat-sat sequences (with maximum intensity projection reconstructions). The dynamic study was obtained during the intravenous administration of gadolinium chelates contrast agents (gadoteridol 279.3 mg/mL - Prohance®, Bracco Diagnostics Inc., Germany; 0.2 mL/kg of body weight) at a rate of 2-3 mL/s followed by saline injection with a triphasic technique: pancreatic (35-45 s), portal venous (80-90 s), and late phase (> 180 s). The dynamic study was performed with T1-weighted volume GRE sequences (3D), with selective fat saturation acquired in the axial plane. The slice thickness necessarily included the entire biliary tree and pancreatic ductal system. Figure 2 and Figure 3 report examples of our patients' CT and MRI images.

Worrisome features[4]

Cyst largest diameter ≥ 3 cm
Enhancing mural nodule < 5 mm
Thickened enhanced cyst walls
MPD size of 5-9 mm
Abrupt change in the MPD calibre with distal pancreatic atrophy
Lymphadenopathy
Elevated serum level of CA19.9
Cyst growth > 5 mm/2 yr

High risk stigmata[4]

Obstructive jaundice in a patient with a cystic lesion of the pancreatic head
Enhanced mural nodule ≥ 5 mm
MPD size ≥ 10 mm

DOI: 10.12998/wjcc.v10.i17.5667 **Copyright** ©The Author(s) 2022.

Figure 1 Worrisome features and high-risk stigmata.

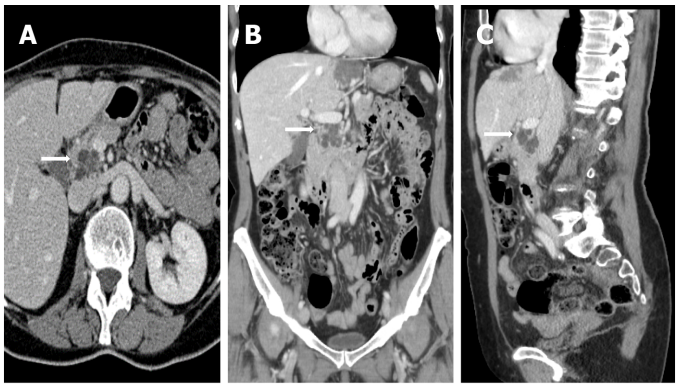

DOI: 10.12998/wjcc.v10.i17.5667 **Copyright** ©The Author(s) 2022.

Figure 2 Contrast-enhanced computed tomography images (Brilliance iCT, Philips Medical Systems) of intraductal papillary mucinous neoplasms of the pancreatic head in the three planes of space. A: Axial view; B: Coronal view; and C: Sagittal view. The arrows indicate the location of the cyst.

Lesions were measured on both CT and MRI images along the three major diameters (antero-posterior, latero-lateral, cranio-caudal). Volume measurement was obtained by manual segmentation with 3D Slicer software version 4.10.2 (available at https://slicer.org). Manual segmentation is a widely validated and reliable method for volume measurement in both abdominal radiology and in other fields of research[12-15]. The volume of the entire cyst was determined by manually drawing a region of interest along the edge of the neoplasm on each consecutive slice covering the whole lesion. Therefore, a three-dimensional (3D) volume of interest was finally obtained with the calculated value expressed in cm^3. More particularly, the tumour contours were individually outlined slice-by-slice by two radiologists (at least 5 years of experience) and then reviewed by a senior radiologist (more than 10 years of experience). Any disagreement between the readers was discussed until a final consensus was generated. An example of segmentation is reported in Figure 4.

Statistical analysis

All statistical analyses were performed using SPSS Statistics version 26.0 (IBM, Armonk, NY, United States). Continuous variables were expressed as medians and interquartile ranges (IQR) while categorical variables were presented as percentages. Descriptive statistics was used to compare the characteristics of patients who developed worrisome features or high-risk stigmata with that of patients who did not: continuous variables were compared using the Mann-Whitney *U*-test while categorical variables were compared with a Yate's χ^2 test or a Fisher's exact test (depending on the sample size). A two-sided P value < 0.05 was considered as significant.

Outcomes

The primary outcomes of our study were to assess the volume growth rate of BD-IPMNs without worrisome features or high-risk stigmata at baseline and to evaluate if a higher volume growth rate correlates with the development of worrisome features or high-risk stigmata. The secondary outcomes

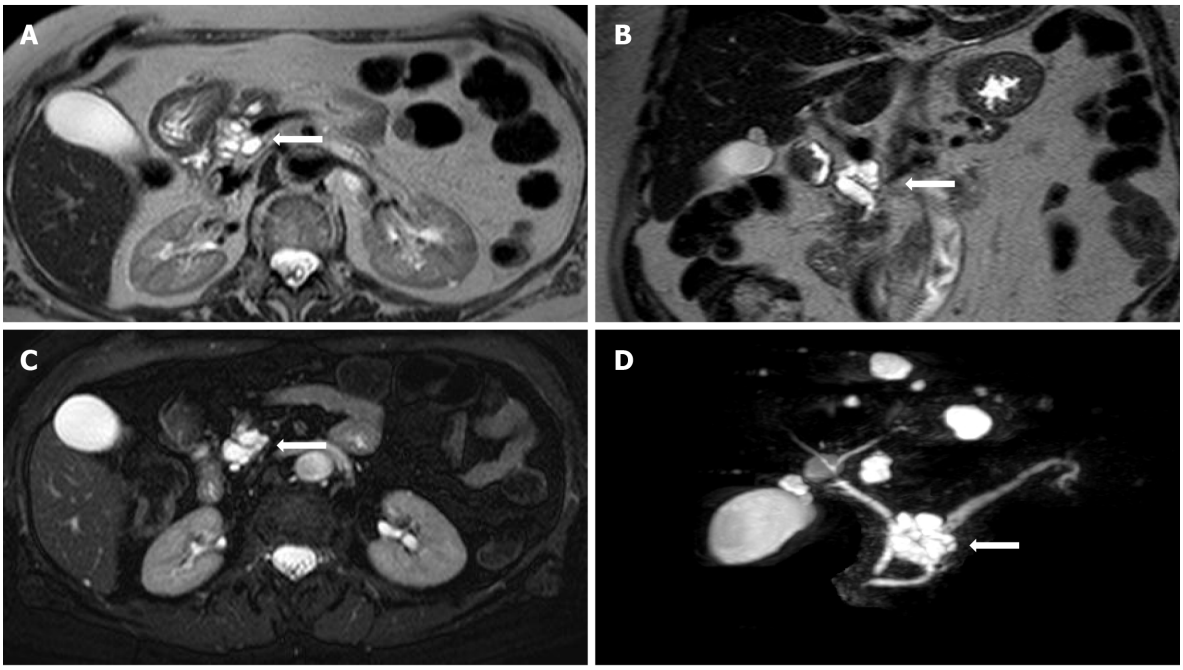

DOI: 10.12998/wjcc.v10.i17.5667 **Copyright** ©The Author(s) 2022.

Figure 3 Non-contrast-enhanced magnetic resonance images of intraductal papillary mucinous neoplasms. A: T2-weighted Turbo Spin Echo (TSE) axial image; B: T2-weighted TSE coronal image; C: T2-weighted TSE fat-sat axial image; and D: T2-weighted TSE volume (3D) TSE fat-sat sequences (with MIP reconstructions). The arrows indicate the location of the cyst.

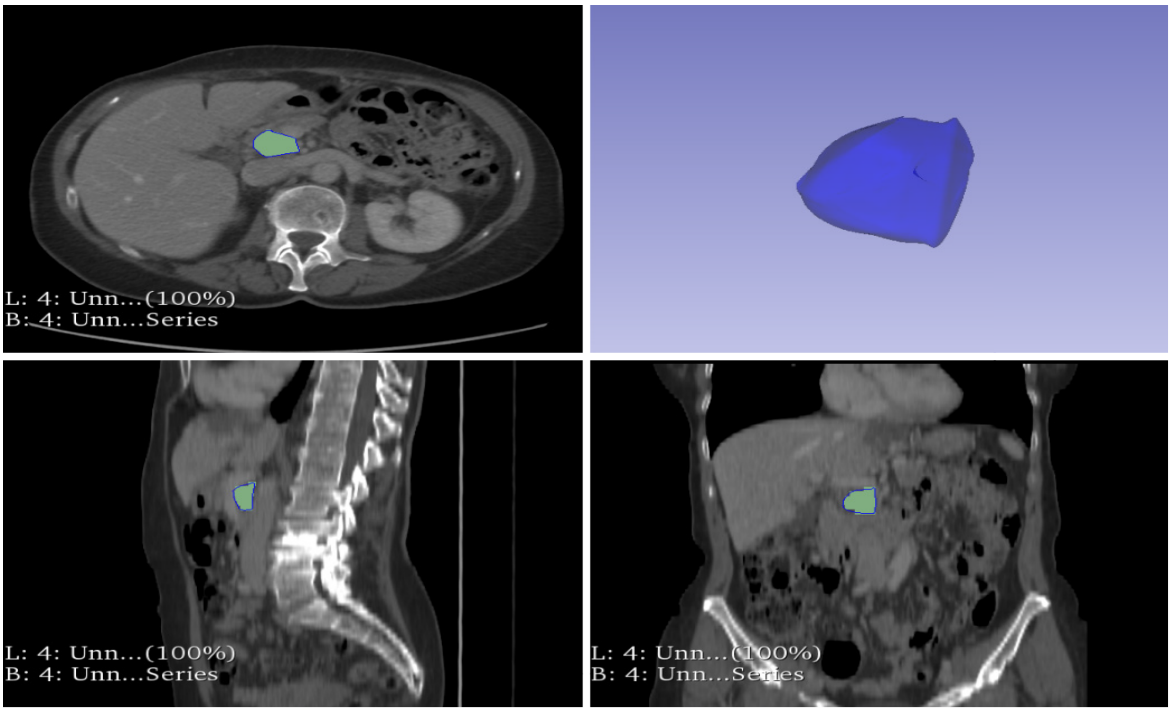

Segment	Number of voxels (voxels)	Volume (mm^3)	Volume (cm^3)
4: Unnamed Series_roi_label_thresholded	3165	7823.64	7.82364

DOI: 10.12998/wjcc.v10.i17.5667 **Copyright** ©The Author(s) 2022.

Figure 4 Segmentation of intraductal papillary mucinous neoplasms in a portal venous phase contrast-enhanced computed tomography images using the 3D Slicer software. The volume of the entire cyst was determined by manually drawing a region of interest along the edge of the neoplasm on each consecutive slice covering the whole lesion.

were the following: (1) To evaluate the impact of measuring volume dimension *vs* flat dimension (axial, coronal and longitudinal diameters); (2) To evaluate the impact of measuring volume growth rate *vs* diameter growth rate; and (3) To test the ability of first-year volume growth rate to predict the development of worrisome features or high-risk stigmata.

RESULTS

Study population

Overall, 148 patients were identified. Five patients had worrisome features or high-risk stigmata at baseline and were excluded from the study. An additional 45 patients were excluded as they had unsatisfactory or incomplete follow-up information. Therefore, a total of 98 patients were included in our study. Baseline and demographic characteristics of the patients and cysts are reported in Table 1.

After a 40.5-mo median follow-up (IQR 24-72), 10 patients (10.2%) developed worrisome features: 6 patients had cysts larger diameter > 3 cm; 3 patients had increased serum CA19.9 (> 37 IU/L); 1 patient had MPD ≥ 5 mm. No patients developed high-risk stigmata. Baseline cyst dimensions, both diameter and volume, were the only patient baseline characteristics which were significantly associated with the development of worrisome features (Table 2). Two of the patients who developed worrisome features underwent surgical resection. They both had a pancreaticoduodenectomy and their main characteristics are resumed in Table 3.

Cyst dimension and growth rate

Baseline median cyst sizes were 9 mm (IQR 6-15) × 10 mm (IQR 6.75-16) × 10 mm (IQR 6-16). Measurements are intended to be sagittal (antero-posterior) × transversal (latero-lateral) × coronal (cranio-caudal). Baseline cyst volume was 0.54 cm^3 (IQR 0.17-1.65). Cysts at baseline were significantly larger in patients who developed worrisome features, as reported in Table 4. Cyst sizes and growth after follow-up are resumed in Tables 5-7. Particularly, at the end of the follow-up, patients who developed worrisome features had a median cyst volume of 10.17 cm^3 (IQR 2.72-19.36), with a median growth of 4.01 cm^3 (IQR 0.83-13.87). Both volume and cyst volume growth were significantly higher in patients who developed worrisome features (P = 0.0005 and P < 0.00001, respectively). Indeed, in patients who developed worrisome features, cyst volume grew faster than in patients who did not (1.12 cm^3/year, IQR 0.28-2.65 *vs* 0 cm^3/year, IQR -0.02-0.17, P = 0.0001). Diameter size also grew more in patients who developed worrisome features but this growth was not always significant across all three measurement planes.

First-year prediction of worrisome features

Seventy-four patients had at least 3 follow-up timepoints, of which at least two were 12 mo apart and another one later in time. In this subgroup of patients, followed for a median time of 56.5 mo (IQR 30-80.25), 10 developed worrisome features. The first-year volume growth rate was higher in patients who developed worrisome features (P = 0.00634). The first-year diameter growth rate was also higher in patients with worrisome features at the end of follow-up but differences with patients who did not end up with worrisome features were not always significant. Data regarding this group of patients are reported in Table 8.

DISCUSSION

Pancreatic cystic neoplasms are often detected incidentally in patients who undergo abdomen CT scans or MRI for various indications[16-18]. IPMNs are the most frequently diagnosed pancreatic cystic neoplasms[1] and they come in several variants: main duct IPMN or type 1 (MD-IPMN), branch duct IPMN or type 2 (BD-IPMN), and mixed type[19]. IPMNs have a malignancy progression cumulative risk of 7%-24% in 10 years and percentages vary on an individual risk basis[2]. In particular, MD-IPMN may reach a malignancy risk of 60%, while in BD-IPMN the risk remains lower than 25% in both surgical and non-surgical series[20-22].

Current guidelines agree on surgically treating MD-IPMN and MT-IPMN and monitoring most BD-IPMN (CT scan, MRI, EUS)[3-5]. BD-IPMN follow-up may vary on the basis of some radiological characteristics of the cysts and on clinical and biochemical parameters. In particular, International Guidelines outlined some "high-risk stigmata" and "worrisome features"[4]. The former guide the physician to a surgical approach, while the latter require a tighter follow-up.

As already mentioned, the baseline characteristic which is considered most important by the scientific community is the dimension of the cyst of larger diameter and only the International Guidelines by Tanaka *et al*[4] include the cyst diameter growth rate as a worrisome feature. What is more, it is not always easy to identify which is the larger diameter especially when comparing different methods such as CT scan, MRI and EUS. In this study, we tried to find a new parameter that is easy to use and that

Table 1 Baseline and demographic characteristics of patients and cysts

Characteristics		*n* = 98
Males (%)		33 (33.7)
Females (%)		65 (66.3)
Median age at diagnosis (IQR)		69 (63-75)
Familial history (%)		9 (9.2)
History of diabetes (%)		16 (16.3)
Diabetes onset during follow-up (%)		0 (0.0)
Median follow-up [mo (IQR)]		40.5 (24-72)
Former smokers (%)		14 (14.3)
Active smokers (%)		8 (8.1)
Never smoked (%)		76 (77.6)
Multifocal		57 (58.2)
Largest cyst localization	Head (%)	44 (44.9)
	Isthmus/body (%)	40 (40.8)
	Tail (%)	14 (14.3)
Median cyst size	a [mm (IQR)]	9 (6-15)
	b [mm (IQR)]	10 (6.75-16)
	c [mm (IQR)]	10 (6-16)
	Volume [cm^3 (IQR)]	0.54 (0.17-1.65)
EUS		19 (19.4)
Median time to EUS (IQR)		6 (0-31.5)
FNA (%)		9 (47.4)
Cyst fluid amylases [IU/L (IQR)], *n* = 5		289 (69.25-1725.25)
Cyst fluid CEA [IU/L (IQR)], *n* = 6		166 (8.55-24062.75)
Serum CA19.9 [IU/L (IQR)], *n* = 25		25.2 (6.1-58.7)
Serum CEA [IU/L (IQR)], *n* = 22		2.15 (1.27-2.92)

CA19.9: Carbohydrate antigen 19.9; CEA: Carcinoembriogenic antigen; EUS: Endoscopic ultrasound; FNA: Fine needle aspiration; IQR: Interquartile range; IU: International units; a: Sagittal (antero-posterior); b: Transversal (latero-lateral); c: Coronal (cranio-caudal).

brings more information about the evolutionary potential of BD-IPMNs: we identified it in the volume of the cysts. Cyst volume is a parameter with high reproducibility and low inter-observer variability[9] and in our opinion may allow the diagnostician to overcome some issues related to the flat measurement of the cyst.

In this study, we assess the diameter and volume growth rate of BD-IPMNs and evaluate its correlation with the development of worrisome features. We reviewed both CT and MRI images: many previous studies confirmed that diagnostic performance of contrast-enhanced CT and MRI is comparable without significant differences[23-25]. We retrospectively analysed the evolution of BD-IPMNs of 98 patients, who were referred to our tertiary referral centre for pancreatic diseases. Worrisome features appeared in 10.8% of patients, while no-one had high-risk stigmata, over a median 40.5-mo follow-up time. These data are in line with the current literature[26,27].

In our cohort, patients who developed worrisome features had larger cysts at baseline. In this group, cysts were significantly larger if we considered both diameters (for all diameters, $P = 0.0035$, $P = 0.00652$, $P = 0.00424$, respectively) and volume ($P = 0.00222$). Patients who developed worrisome features had a median baseline cyst volume of 5.8 cm^3 and a final cyst volume of 10.17 cm^3. These findings are in line with a previous study in which CT and MRI techniques were used to measure IPMNs volume: a volume > 10 cm^3 was associated with malignancy[28]. However, this study did not assess volume changes over time but only a spot volume measurement.

Table 2 Baseline and demographic characteristics of patients and cysts: subgroups

		Non-worrisome features (*n* = 88)	Worrisome features (*n* = 10)	*P* value
Males (%)		31 (35.2)	2 (20.0)	0.540234
Females (%)		57 (64.8)	8 (80.0)	0.540234
Median age at diagnosis (IQR)		70 (63.5-74.75)	67 (59.75-76.25)	0.58232
Familial history (%)		8 (9.1)	1 (10.0)	0.628786
History of diabetes (%)		14 (15.9)	2 (20.0)	0.904665
Diabetes onset during follow-up (%)		0 (0.0)	0 (0.0)	-
Median follow-up [mo (IQR)]		37.5 (23.25-71)	69.5 (46.5-94)	0.01828
Former smokers (%)		11 (12.5)	3 (30.0)	0.306885
Active smokers (%)		8 (9.1)	0 (0.0)	0.738111
Never smoked (%)		69 (78.4)	7 (70.0)	0.83833
Multifocal		52 (59.1)	5 (50.0)	0.830551
Largest cyst localization	Head (%)	39 (44.3)	5 (50.0)	0.994538
	Isthmus/body (%)	35 (39.8)	5 (50.0)	0.776364
	Tail (%)	14 (15.9)	0 (0.0)	0.746616
Median cyst size	a [mm (IQR)]	9 (6-13)	19 (11.25-21.25)	0.0035
	b [mm (IQR)]	10 (6-15)	18 (10.75-20.75)	0.00652
	c [mm (IQR)]	9.5 (6-15)	22.5 (12-27.65)	0.00424
EUS		14 (15.9)	5 (50.0)	0.030618
Median time to EUS (IQR)		3 (0-18.25)	29 (5.5-69.5)	0.22628
Serum CA19.9 [IU/L (IQR)], *n* = 25		6.2 (5.6-24.2)	23.8 (6.2-37.9)	0.1556
Serum CEA [IU/L (IQR)], *n* = 22		2.15 (1.28-2.93)	2.15 (1.55-2.75)	0.93624

IQR: Interquartile range; a: Sagittal (antero-posterior); b: Transversal (latero-lateral); c: Coronal (cranio-caudal).

Table 3 Patients who underwent surgery

	Sex, age	Final cyst volume (cm^3)	Growth rate (cm^3/yr)	MPD (mm)	Location	CA19.9 (IU/L)	Time to surgery (mo)	Histopathology
Patient A	F, 68	28.73	33.91	< 5	Isthmus	33.2	85	LGD
Patient B	F, 74	14.70	24.27	< 5	Head	22.5	65	LGD

CA19.9: Carbohydrate antigen 19.9; F: Female; LGD: Low-grade dysplasia; MPD: Main pancreatic duct.

In the group of patients who developed worrisome features, diameter growth rate was significantly higher if we considered latero-lateral and cranio-caudal diameters (1.55 mm/year *vs* 0.0 mm/year, P = 0.0394, and 1.96 mm/year *vs* 0.0 mm/year, P = 0.00152, respectively), but not antero-posterior diameters (0.63 mm/year *vs* 0.0 mm/year, P = 0.14156). In a recent study by Kolb *et al*[7], 188 patients were followed-up for a median 55-mo period and 12 out of all patients developed worrisome features. They measured cysts diameter on both the axial and coronal plans on X and Y axis and cyst growth rate was higher in patients who developed worrisome features (axial X 2.84 mm/year *vs* 0.23 mm/year, P < 0.001; axial Y 1.02 mm/year *vs* 0.02 mm/year, P = 0.033; coronal X 1.21 mm/year *vs* 0.19 mm/year, P = 0.001, coronal Y 1.56 mm/year *vs* 0.00 mm/year, P < 0.001). The larger population and the longer median follow-up period may have contributed to improving statistical significance in their work. A similar result was obtained in a previous surgical cohort (4.1 mm/year *vs* 1.0 mm/year, P = 0.001)[6].

The peculiarity of our work was the measurement of cyst volume over time. In our cohort, total growth and growth rate were significantly higher in patients who developed worrisome features if compared to patients who did not (P < 0.00001 and P = 0.0001, respectively). To our knowledge, this is

Table 4 Baseline cysts size

	All (*n* = 98)	Non-worrisome features (*n* = 88)	Worrisome features (*n* = 10)	*P* value
a [mm (IQR)]	9 (6-15)	9 (6-13)	19 (11.25-21.25)	0.0035
b [mm (IQR)]	10 (6.75-16)	10 (6-15)	18 (10.75-20.75)	0.00652
c [mm (IQR)]	10 (6-16)	9.5 (6-15)	22.5 (12-27.65)	0.00424
volume [cm^3 (IQR)]	0.54 (0.17-1.65)	0.45 (0.15-1.28)	5.28 (1.10-6.30)	0.00222

IQR: Interquartile range; a: Sagittal (antero-posterior); b: Transversal (latero-lateral); c: Coronal (cranio-caudal).

Table 5 Final cysts size

	All (*n* = 98)	Non-worrisome features (*n* = 88)	Worrisome features (*n* = 10)	*P* value
a [mm (IQR)]	9 (6-16)	9 (6-13.75)	23 (13.5-27.5)	0.00288
b [mm (IQR)]	12 (7-18)	11 (7-16.75)	28 (19.25-37.5)	0.00054
c [mm (IQR)]	11 (7-18)	10.5 (6.25-16)	29 (15.75-38.75)	0.0003
volume [cm^3 (IQR)]	0.58 (1.76-2.02)	0.52 (0.17-1.63)	10.17 (2.72-19.36)	0.0005

IQR: Interquartile range; a: Sagittal (antero-posterior); b: Transversal (latero-lateral); c: Coronal (cranio-caudal).

Table 6 Total cysts growth

	All (*n* = 98)	Non-worrisome features (*n* = 88)	Worrisome features (*n* = 10)	*P* value
a [mm (IQR)]	0 (-0.25-2)	0 (-0.75-1.75)	2 (-0.5-8.75)	0.0601
b [mm (IQR)]	0 (0-3)	0 (0-2)	10 (-0.25-14.25)	0.01016
c [mm (IQR)]	0 (0-3)	0 (-1-2)	5 (3.25-14)	0.00008
Volume [cm^3 (IQR)]	0.02 (-0.01-0.70)	0 (-0.03-0.24)	4.01 (0.83-13.87)	< 0.00001
Volume increased (%)	28 (28.6)	18 (20.4)	10 (100.0)	< 0.00001
Volume unchanged or reduced (%)	70 (71.4)	70 (79.6)	0 (0.0)	< 0.00001

IQR: Interquartile range; a: Sagittal (antero-posterior); b: Transversal (latero-lateral); c: Coronal (cranio-caudal).

Table 7 Yearly cysts growth rate

	All (*n* = 98)	Non-worrisome features (*n* = 88)	Worrisome features (*n* = 10)	*P* value
a [mm/yr (IQR)]	0 (-0.04-0.73)	0 (-0.11-0.6)	0.63 (-0.11-1.275)	0.14156
b [mm/yr (IQR)]	0 (0-1.33)	0 (0-1.09)	1.55 (-0.53-3.52)	0.0394
c [mm/yr (IQR)]	0 (0-0.99)	0 (-0.29-0.71)	1.96 (0.64-2.47)	0.00152
Volume [cm^3/yr (IQR)]	0 (-0.01-0.27)	0 (-0.02-0.17)	1.12 (0.28-2.65)	0.0001

a: Sagittal (antero-posterior); b: Transversal (latero-lateral); c: Coronal (cranio-caudal). IQR: Interquartile range.

the first study in which baseline volume and particularly volume total growth and growth rate are correlated with development of worrisome features in patients with BD-IPMN.

Beyond the raw data of annual growth, we set out to identify a parameter that allows the early prediction of development of worrisome features in the medium-long term: we found out that patients who developed worrisome features had a higher first-year cyst volume growth if compared with patients who did not (0.46 cm^3/year *vs* 0.0 cm^3/year, $P = 0.00634$). These data are notable if we consider that the diameter growth rate was not significantly different between the two groups, except for the cranio-caudal one ($P = 0.22628$, $P = 0.64552$, $P = 0.00932$). To our knowledge, this is a unique result as

Table 8 First-year cysts growth and development of worrisome features

	All (*n* = 74)	Non-worrisome features (*n* = 64)	Worrisome features (*n* = 10)	*P* value
a [mm (IQR)]	0 (0-0.56)	0 (0-0.5)	0.47 (-0.11-1.1)	0.22628
b [mm (IQR)]	0 (0-1.13)	0 (0-0.14)	0.4 (-1.12-2.81)	0.64552
c [mm (IQR)]	0 (0-0.94)	0 (0-0.74)	1.4 (0-2.47)	0.00932
Volume [cm^3 (IQR)]	0 (-0.02-0.18)	0 (-0.04-0.08)	0.46 (0-1.62)	0.00634
Volume increased (%)	35 (47.3)	28 (43.7)	7 (70.0)	0.227942
Volume unchanged or reduced (%)	39 (52.7)	36 (56.3)	3 (30.0)	0.227942

a: Sagittal (antero-posterior); b: Transversal (latero-lateral); c: Coronal (cranio-caudal). IQR: Interquartile range.

this is the first study to prove that cyst volume growth in the first year predicts development of worrisome features in patients with BD-IPMN without worrisome features at baseline. This could be an important tool to add to the current knowledge to improve the management of low-risk IPMNs.

In summary, as opposed to diameter growth, the cyst volume growth (total, annual and first-year growth) was consistently greater in patients who developed worrisome features. The diameter growth rate was also significantly correlated in some cases, but not of all diameters at once, and not always of the largest diameter. Therefore, the flat growth rate could be misinterpreted if it is not the largest diameter that grows, or when the cysts have an irregular shape which is hard to measure in a reproducible way. The volume measurement could overcome these issues. In fact, the volume has a unique size instead of diameters that are virtually endless. For these reasons, volume measurement could be more comparable than diameters. Recently, Pandey *et al*[9] demonstrated that measurement of volume is feasible and reproducible and can be considered as an alternative to diameter measurement. In their work, they used both a manual and a semiautomatic technique of measurement while we used a manual technique.

This study has some limitations. First, the retrospective design could not allow us to set pre-determined timepoints of imaging follow-up. We solved this problem by assessing growth rate rather than the total growth. Moreover, we could not assess the presence of atypia or dysplasia as histology was not available for our patients unless they underwent surgery. Third, we could not carry out a proper statistical analysis involving the characteristics of the cyst fluid as FNA was not routinely performed in our patients. However, our study was meant to search for characteristics that predict the development of worrisome features so clinical, radiological and biochemical parameters were sufficient for our purposes. Finally, since BD-IPMNs grow very slowly[29,30], a possible criticism could be addressed to the length of our cohort follow-up median time (40.5 mo *vs* 55 mo in the study by Kolb *et al* [7]). It must be said that small increases in diameter can result in bigger volume variations so a shorter follow-up is justified. Indeed, the first-year volume growth was superior to diameter growth in predicting the development of worrisome features in our cohort. Anyway, a prospective extension of our study is ongoing to confirm our results.

CONCLUSION

Our study confirms that BD-IPMN higher cyst growth rate is associated with a higher risk of developing worrisome features. Moreover, we proved that cyst volume growth rate is also related to the emergence of worrisome features and that the cyst volume increase in the first year of follow-up is an early predictor of the development of worrisome features. More specifically, our data show that in the first year of follow-up, volume measurement is more accurate than diameter alone for risk stratification. This suggests that measuring cyst volume routinely could be a useful tool to monitor low-risk IPMNs. Further studies, comprehensive of a larger pool of patients and a longer follow-up time are needed to corroborate these data and to understand whether our findings could influence routine clinical practice.

ARTICLE HIGHLIGHTS

Research background

Branch duct-intraductal papillary mucinous neoplasms (BD-IPMNs) are the most common pancreatic cystic tumours. Cyst diameter growth rate is one of the parameters that current guidelines take into account to predict the development of malignant features in patients with BD-IPMN. However, to date,

there are no studies investigating the correlation between cyst volume growth rate and the risk of BD-IPMNs malignant degeneration.

Research motivation

The optimal surveillance protocol for BD-IPMNs has not been established as there is lack of agreement on when follow-up should be intensified or interrupted mainly due to the slow growth rate of BD-IPMNs. We propose a more precise tool for the measurement of BD-IPMNs which allows an early prediction of the development of worrisome features.

Research objectives

The primary objective of our research was to assess the volume growth rate of BD-IPMNs without worrisome features or high-risk stigmata at baseline and to evaluate its correlation with the development of worrisome features or high-risk stigmata during follow-up. We also aimed to evaluate the impact of measuring volume *vs* diameter growth rate and to test the ability of first-year volume growth rate to predict the development of worrisome features or high-risk stigmata.

Research methods

We measured diameter in CT-scans and MRI on three planes, while we calculated the volume by manual segmentation: the volume of the cyst was determined by drawing a region of interest along the edge of the neoplasm on each consecutive slice covering the whole lesion; therefore, a three-dimensional volume of interest was finally obtained with the calculated value expressed in cm^3. Changes in size over time and development of worrisome features or high-risk stigmata were measured.

Research results

Ninety-eight patients were evaluated across a 40.5-mo median follow-up time, of which 10 developed worrisome features, while none developed high-risk stigmata. Baseline volume was larger, and volume and first-year volume growth rate were higher in patients who developed worrisome features than in patients who did not. Baseline diameter was larger in patients who developed worrisome features. Diameter growth rate was higher as well but the difference did not always reach statistical significance.

Research conclusions

The measurement of baseline volume and of its variation over time is a reliable tool for the follow-up of BD-IPMNs. Particularly, in the first year of BD-IPMNs follow-up, volume measurement is more accurate than diameter alone for risk stratification.

Research perspectives

We suggest that measuring cyst volume routinely could be a useful tool to monitor low-risk IPMNs. Larger cohorts of patients and a longer follow-up time are needed to corroborate these data and to understand whether our findings could influence routine clinical practice.

FOOTNOTES

Author contributions: Innocenti T designed the study and drafted the initial manuscript; Innocenti T, Danti G, Lynch EN and Gottin M participated in the acquisition, analysis and interpretation of the data; Danti G, Fedeli F and Palatresi D participated in the acquisition and segmentation of the CT and MRI images and provided important contribution to analysis and interpretation of the data; Biagini MR, Milani S, Miele V and Galli A revised the article critically for important intellectual content; Lynch EN provided English language revision as a native speaker; Galli A cooperated to set the study design, revised the statistical analysis and was the guarantor of the study; All authors approved the final version of the article.

Institutional review board statement: The study was approved by the local Ethical Committee of Careggi University Hospital on July 13th 2021 (protocol number: 20256_oss).

Informed consent statement: All study participants provided informed written consent about personal and medical data collection prior to study enrolment.

Conflict-of-interest statement: The Authors declare no conflict of interest and no financial interests in any products mentioned in this paper.

Data sharing statement: No additional data are available.

STROBE statement: The authors have read the STROBE Statement—checklist of items, and the manuscript was prepared and revised according to the STROBE Statement—checklist of items.

Open-Access: This article is an open-access article that was selected by an in-house editor and fully peer-reviewed by

external reviewers. It is distributed in accordance with the Creative Commons Attribution NonCommercial (CC BY-NC 4.0) license, which permits others to distribute, remix, adapt, build upon this work non-commercially, and license their derivative works on different terms, provided the original work is properly cited and the use is non-commercial. See: https://creativecommons.org/Licenses/by-nc/4.0/

Country/Territory of origin: Italy

ORCID number: Tommaso Innocenti 0000-0002-2154-0490; Ginevra Danti 0000-0002-7109-8119; Erica Nicola Lynch 0000-0002-2638-2559; Gabriele Dragoni 0000-0001-5752-5113; Matteo Gottin 0000-0002-9292-7078; Filippo Fedeli 0000-0002-7918-9912; Daniele Palatresi 0000-0003-0452-7232; Maria Rosa Biagini 0000-0003-4840-6731; Stefano Milani 0000-0002-1337-9107; Vittorio Miele 0000-0002-7848-1567; Andrea Galli 0000-0001-5416-6290.

Corresponding Author's Membership in Professional Societies: Società Italiana Di Gastroenterologia Ed Endoscopia Digestiva.

S-Editor: Gong ZM
L-Editor: Filipodia
P-Editor: Gong ZM

REFERENCES

1 **Nagtegaal ID**, Odze RD, Klimstra D, Paradis V, Rugge M, Schirmacher P, Washington KM, Carneiro F, Cree IA; WHO Classification of Tumours Editorial Board. The 2019 WHO classification of tumours of the digestive system. *Histopathology* 2020; **76**: 182-188 [PMID: 31433515 DOI: 10.1111/his.13975]
2 **Choi SH**, Park SH, Kim KW, Lee JY, Lee SS. Progression of Unresected Intraductal Papillary Mucinous Neoplasms of the Pancreas to Cancer: A Systematic Review and Meta-analysis. *Clin Gastroenterol Hepatol* 2017; **15**: 1509-1520.e4 [PMID: 28342950 DOI: 10.1016/j.cgh.2017.03.020]
3 **Vege SS**, Ziring B, Jain R, Moayyedi P; Clinical Guidelines Committee; American Gastroenterology Association. American gastroenterological association institute guideline on the diagnosis and management of asymptomatic neoplastic pancreatic cysts. *Gastroenterology* 2015; **148**: 819-822; quize12 [PMID: 25805375 DOI: 10.1053/j.gastro.2015.01.015]
4 **Tanaka M**, Fernández-Del Castillo C, Kamisawa T, Jang JY, Levy P, Ohtsuka T, Salvia R, Shimizu Y, Tada M, Wolfgang CL. Revisions of international consensus Fukuoka guidelines for the management of IPMN of the pancreas. *Pancreatology* 2017; **17**: 738-753 [PMID: 28735806 DOI: 10.1016/j.pan.2017.07.007]
5 **European Study Group on Cystic Tumours of the Pancreas**. European evidence-based guidelines on pancreatic cystic neoplasms. *Gut* 2018; **67**: 789-804 [PMID: 29574408 DOI: 10.1136/gutjnl-2018-316027]
6 **Kang MJ**, Jang JY, Kim SJ, Lee KB, Ryu JK, Kim YT, Yoon YB, Kim SW. Cyst growth rate predicts malignancy in patients with branch duct intraductal papillary mucinous neoplasms. *Clin Gastroenterol Hepatol* 2011; **9**: 87-93 [PMID: 20851216 DOI: 10.1016/j.cgh.2010.09.008]
7 **Kolb JM**, Argiriadi P, Lee K, Liu X, Bagiella E, Gupta S, Lucas AL, Kim MK, Kumta NA, Nagula S, Sarpel U, DiMaio CJ. Higher Growth Rate of Branch Duct Intraductal Papillary Mucinous Neoplasms Associates With Worrisome Features. *Clin Gastroenterol Hepatol* 2018; **16**: 1481-1487 [PMID: 29535058 DOI: 10.1016/j.cgh.2018.02.050]
8 **Jang JY**, Park T, Lee S, Kim Y, Lee SY, Kim SW, Kim SC, Song KB, Yamamoto M, Hatori T, Hirono S, Satoi S, Fujii T, Hirano S, Hashimoto Y, Shimizu Y, Choi DW, Choi SH, Heo JS, Motoi F, Matsumoto I, Lee WJ, Kang CM, Han HS, Yoon YS, Sho M, Nagano H, Honda G, Kim SG, Yu HC, Chung JC, Nagakawa Y, Seo HI, Yamaue H. Proposed Nomogram Predicting the Individual Risk of Malignancy in the Patients With Branch Duct Type Intraductal Papillary Mucinous Neoplasms of the Pancreas. *Ann Surg* 2017; **266**: 1062-1068 [PMID: 27607098 DOI: 10.1097/SLA.0000000000001985]
9 **Pandey P**, Pandey A, Varzaneh FN, Ghasabeh MA, Fouladi D, Khoshpouri P, Shao N, Zarghampour M, Hruban RH, Canto M, O'Broin-Lennon AM, Kamel IR. Are pancreatic IPMN volumes measured on MRI images more reproducible than diameters? *Eur Radiol* 2018; **28**: 2790-2800 [PMID: 29404774 DOI: 10.1007/s00330-017-5268-z]
10 **Kim SY**, Lee JM, Kim SH, Shin KS, Kim YJ, An SK, Han CJ, Han JK, Choi BI. Macrocystic neoplasms of the pancreas: CT differentiation of serous oligocystic adenoma from mucinous cystadenoma and intraductal papillary mucinous tumor. *AJR Am J Roentgenol* 2006; **187**: 1192-1198 [PMID: 17056905 DOI: 10.2214/AJR.05.0337]
11 **Ciprani D**, Morales-Oyarvide V, Qadan M, Hank T, Weniger M, Harrison JM, Rodrigues C, Horick NK, Mino-Kenudson M, Ferrone CR, Warshaw AL, Lillemoe KD, Fernández-Del Castillo C. An elevated CA 19-9 is associated with invasive cancer and worse survival in IPMN. *Pancreatology* 2020; **20**: 729-735 [PMID: 32332003 DOI: 10.1016/j.pan.2020.04.002]
12 **Zhang X**, Zhong L, Zhang B, Zhang L, Du H, Lu L, Zhang S, Yang W, Feng Q. The effects of volume of interest delineation on MRI-based radiomics analysis: evaluation with two disease groups. *Cancer Imaging* 2019; **19**: 89 [PMID: 31864421 DOI: 10.1186/s40644-019-0276-7]
13 **Granata V**, Fusco R, Barretta ML, Picone C, Avallone A, Belli A, Patrone R, Ferrante M, Cozzi D, Grassi R, Izzo F, Petrillo A. Radiomics in hepatic metastasis by colorectal cancer. *Infect Agent Cancer* 2021; **16**: 39 [PMID: 34078424 DOI: 10.1186/s13027-021-00379-y]
14 **Nazari M**, Shiri I, Zaidi H. Radiomics-based machine learning model to predict risk of death within 5-years in clear cell renal cell carcinoma patients. *Comput Biol Med* 2021; **129**: 104135 [PMID: 33254045 DOI: 10.1016/j.compbiomed.2020.104135]
15 **Sepehri S**, Tankyevych O, Iantsen A, Visvikis D, Hatt M, Cheze Le Rest C. Accurate Tumor Delineation *vs.* Rough

Volume of Interest Analysis for ^{18}F-FDG PET/CT Radiomics-Based Prognostic Modeling inNon-Small Cell Lung Cancer. *Front Oncol* 2021; **11**: 726865 [PMID: 34733779 DOI: 10.3389/fonc.2021.726865]

16 **Laffan TA**, Horton KM, Klein AP, Berlanstein B, Siegelman SS, Kawamoto S, Johnson PT, Fishman EK, Hruban RH. Prevalence of unsuspected pancreatic cysts on MDCT. *AJR Am J Roentgenol* 2008; **191**: 802-807 [PMID: 18716113 DOI: 10.2214/AJR.07.3340]

17 **Lee KS**, Sekhar A, Rofsky NM, Pedrosa I. Prevalence of incidental pancreatic cysts in the adult population on MR imaging. *Am J Gastroenterol* 2010; **105**: 2079-2084 [PMID: 20354507 DOI: 10.1038/ajg.2010.122]

18 **Pezzilli R**, Buscarini E, Pollini T, Bonamini D, Marchegiani G, Crippa S, Belfiori G, Sperti C, Moletta L, Pozza G, De Nucci G, Manes G, Mandelli ED, Casadei R, Ricci C, Alicante S, Vattiato C, Carrara S, Di Leo M, Fabbri C, Giovanelli S, Barresi L, Tacelli M, Mirante VG, Conigliaro R, Antonini F, Macarri G, Frulloni L, De Marchi G, Sassatelli R, Cecinato P, Del Vecchio Blanco G, Galli A, Pezzullo A, Fantin A, Graffeo M, Frego M, Stillittano D, Monica F, Germanà B, Capurso G, Quartini M, Veneroni L, Cannizzaro R, Falconi M. Epidemiology, clinical features and diagnostic work-up of cystic neoplasms of the pancreas: Interim analysis of the prospective PANCY survey. *Dig Liver Dis* 2020; **52**: 547-554 [PMID: 32122771 DOI: 10.1016/j.dld.2020.02.003]

19 **Klibansky DA**, Reid-Lombardo KM, Gordon SR, Gardner TB. The clinical relevance of the increasing incidence of intraductal papillary mucinous neoplasm. *Clin Gastroenterol Hepatol* 2012; **10**: 555-558 [PMID: 22210438 DOI: 10.1016/j.cgh.2011.12.029]

20 **Perri G**, Marchegiani G, Frigerio I, Dervenis CG, Conlon KC, Bassi C, Salvia R. Management of Pancreatic Cystic Lesions. *Dig Surg* 2020; **37**: 1-9 [PMID: 30636253 DOI: 10.1159/000496509]

21 **Pergolini I**, Sahora K, Ferrone CR, Morales-Oyarvide V, Wolpin BM, Mucci LA, Brugge WR, Mino-Kenudson M, Patino M, Sahani DV, Warshaw AL, Lillemoe KD, Fernández-Del Castillo C. Long-term Risk of Pancreatic Malignancy in Patients With Branch Duct Intraductal Papillary Mucinous Neoplasm in a Referral Center. *Gastroenterology* 2017; **153**: 1284-1294.e1 [PMID: 28739282 DOI: 10.1053/j.gastro.2017.07.019]

22 **Crippa S**, Capurso G, Cammà C, Fave GD, Castillo CF, Falconi M. Risk of pancreatic malignancy and mortality in branch-duct IPMNs undergoing surveillance: A systematic review and meta-analysis. *Dig Liver Dis* 2016; **48**: 473-479 [PMID: 26965783 DOI: 10.1016/j.dld.2016.02.003]

23 **Choi SY**, Kim JH, Yu MH, Eun HW, Lee HK, Han JK. Diagnostic performance and imaging features for predicting the malignant potential of intraductal papillary mucinous neoplasm of the pancreas: a comparison of EUS, contrast-enhanced CT and MRI. *Abdom Radiol (NY)* 2017; **42**: 1449-1458 [PMID: 28144718 DOI: 10.1007/s00261-017-1053-3]

24 **Liu H**, Cui Y, Shao J, Shao Z, Su F, Li Y. The diagnostic role of CT, MRI/MRCP, PET/CT, EUS and DWI in the differentiation of benign and malignant IPMN: A meta-analysis. *Clin Imaging* 2021; **72**: 183-193 [PMID: 33321460 DOI: 10.1016/j.clinimag.2020.11.018]

25 **Huynh T**, Ali K, Vyas S, Dezsi K, Strickland D, Basinski T, Chen DT, Jiang K, Centeno B, Malafa M, Klapman JB, Hodul PJ, Jeong D, Permuth JB. Comparison of imaging modalities for measuring the diameter of intraductal papillary mucinous neoplasms of the pancreas. *Pancreatology* 2020; **20**: 448-453 [PMID: 32113936 DOI: 10.1016/j.pan.2020.02.013]

26 **Canto MI**, Almario JA, Schulick RD, Yeo CJ, Klein A, Blackford A, Shin EJ, Sanyal A, Yenokyan G, Lennon AM, Kamel IR, Fishman EK, Wolfgang C, Weiss M, Hruban RH, Goggins M. Risk of Neoplastic Progression in Individuals at High Risk for Pancreatic Cancer Undergoing Long-term Surveillance. *Gastroenterology* 2018; **155**: 740-751.e2 [PMID: 29803839 DOI: 10.1053/j.gastro.2018.05.035]

27 **Ciprani D**, Weniger M, Qadan M, Hank T, Horick NK, Harrison JM, Marchegiani G, Andrianello S, Pandharipande PV, Ferrone CR, Lillemoe KD, Warshaw AL, Bassi C, Salvia R, Fernández-Del Castillo C. Risk of malignancy in small pancreatic cysts decreases over time. *Pancreatology* 2020; **20**: 1213-1217 [PMID: 32819844 DOI: 10.1016/j.pan.2020.08.003]

28 **Murayama S**, Kimura W, Hirai I, Takasu N, Takeshita A, Moriya T. Volumetric and morphological analysis of intraductal papillary mucinous neoplasm of the pancreas using computed tomography and magnetic resonance imaging. *Pancreas* 2011; **40**: 876-882 [PMID: 21747312 DOI: 10.1097/MPA.0b013e31821fdcff]

29 **Crippa S**, Bassi C, Salvia R, Malleo G, Marchegiani G, Rebours V, Levy P, Partelli S, Suleiman SL, Banks PA, Ahmed N, Chari ST, Fernández-Del Castillo C, Falconi M. Low progression of intraductal papillary mucinous neoplasms with worrisome features and high-risk stigmata undergoing non-operative management: a mid-term follow-up analysis. *Gut* 2017; **66**: 495-506 [PMID: 26743012 DOI: 10.1136/gutjnl-2015-310162]

30 **Lee BS**, Nguyen AK, Tekeste TF, Chang K, Girgis A, Adeyemo M, Hanna MS, Yao JF, Kwok KK, Giap AQ, Hunt GC, Chaya CT, Kao KT, Attam R, Ko A, Pio JR, Tovar S, Lim BS. Long-term follow-up of branch-duct intraductal papillary mucinous neoplasms with No change in first 5 Years of diagnosis. *Pancreatology* 2021; **21**: 144-154 [PMID: 33309223 DOI: 10.1016/j.pan.2020.10.040]

World Journal of Clinical Cases

Submit a Manuscript: https://www.f6publishing.com

World J Clin Cases 2022 June 16; 10(17): 5680-5689

DOI: 10.12998/wjcc.v10.i17.5680

ISSN 2307-8960 (online)

ORIGINAL ARTICLE

Prospective Study

Application of a new anatomic hook-rod-pedicle screw system in young patients with lumbar spondylolysis: A pilot study

Duan-Ming Li, Yong-Chao Li, Wei Jiang, Bao-Gan Peng

Specialty type: Orthopedics

Provenance and peer review: Unsolicited article; Externally peer reviewed.

Peer-review model: Single blind

Peer-review report's scientific quality classification

Grade A (Excellent): 0
Grade B (Very good): B, B
Grade C (Good): 0
Grade D (Fair): 0
Grade E (Poor): 0

P-Reviewer: Augustin G, Croatia; Nanda SN, India

Received: October 23, 2021
Peer-review started: October 23, 2021
First decision: January 22, 2022
Revised: March 28, 2022
Accepted: April 20, 2022
Article in press: April 20, 2022
Published online: June 16, 2022

Duan-Ming Li, Yong-Chao Li, Bao-Gan Peng, Department of Orthopaedics, The Third Medical Center of PLA General Hospital, Beijing 100039, China

Wei Jiang, Department of Anesthesiology, The Third Medical Center of PLA General Hospital, Beijing 100039, China

Corresponding author: Bao-Gan Peng, MD, PhD, Department of Orthopaedics, The Third Medical Center of PLA General Hospital, No. 69 Yongding Road, Beijing 100039, China. pengbaogan76611@163.com

Abstract

BACKGROUND

The pedicle screw-laminar hook system has strong fixation and is conducive to bone graft fusion for lumbar spondylolysis. However, the current pedicle screw-laminar hook fixation system is not specifically designed for lumbar spondylolysis.

AIM

To investigate the clinical effects of a new anatomical hook-rod-pedicle screw system in the treatment of lumbar spondylolysis in young adults.

METHODS

We designed a new anatomic hook-rod-pedicle screw system for young patients with lumbar spondylolysis. The isthmus and the corresponding pedicle screw entry point were exposed through the intermuscular approach. Autogenous iliac bone graft was obtained to bridge the isthmus defect, and then the anatomic hook-rod-pedicle screw system was used to fix the isthmus in 15 young patients.

RESULTS

At 24 mo follow-up, the visual analogue scale score of low back pain decreased from 6.73 ± 0.88 to 0.73 ± 0.59, and the Oswestry disability index score decreased from 58.20 ± 8.99 to 7.87 ± 4.97. Computed tomography showed bilateral isthmic bone healing in 14 cases and unilateral isthmic bone healing in 1 case. Magnetic resonance imaging showed that the lumbar disc signal of diseased segment and adjacent segments had no change compared with that before surgery. The pain visual analogue scale score of the donor site was 0.20 ± 0.41 at the last follow-up. According to the Modified Macnab score, the excellent and good rate was 100%.

CONCLUSION
The application of this new anatomical hook-rod-pedicle screw system to treat young patients with lumbar spondylolysis has the advantages of less trauma, a simple operation and satisfactory clinical effects.

Key Words: Lumbar spondylolysis; Hook-rod-pedicle screw system; Internal fixation; Bone healing

©The Author(s) 2022. Published by Baishideng Publishing Group Inc. All rights reserved.

Core Tip: Lumbar spondylolysis is one of the common causes of low back pain in adolescents. The main indication for surgical repair of lumbar spondylolysis is that low back pain is not relieved after at least 6 mo of non-surgical treatment. Application of isthmus debridement, bone grafting and a new anatomical hook-rod-pedicle screw system fixation in young patients with lumbar spondylolysis has the advantages of less trauma, a simple operation and satisfactory curative effect.

Citation: Li DM, Li YC, Jiang W, Peng BG. Application of a new anatomic hook-rod-pedicle screw system in young patients with lumbar spondylolysis: A pilot study. *World J Clin Cases* 2022; 10(17): 5680-5689
URL: https://www.wjgnet.com/2307-8960/full/v10/i17/5680.htm
DOI: https://dx.doi.org/10.12998/wjcc.v10.i17.5680

INTRODUCTION

Spondylolysis is a bony defect in the pars interarticularis of a vertebra, which can be complete or incomplete, bilateral or unilateral and more commonly complete bilateral (Figure 1)[1-3]. It is often asymptomatic but quite common in young people and adolescents with low back pain[4,5]. These patients are usually treated conservatively with analgesics, lumbar orthoses, limitation of movement and physical therapy, and surgery is performed only when the pain persists[6,7]. For this young group of patients, spinal surgeons have paid more and more attention to how to minimize the impact on the range of motion of the spine and prevent the adjacent segments from producing excessive mechanical stress[8,9], so as to turn their attention to repairing the pars interarticularis, bone grafting and restoring the stability of the posterior arch[10,11]. Because the most common lesion of spondylolysis is acquired pseudarthrosis, bone grafting combined with internal fixation is a treatment that does not require arthrodesis. There are multiple reports on direct pars repair techniques in the literature[12-15]. Two common methods are: (1) Direct repair using a lamina/pars compression screw through the isthmic defect; and (2) Compression of the isthmic defect using a set of pedicle screw, rod and laminar hook assembly within the same segment.

More and more surgeons repair lumbar isthmus defects with bone grafting and the pedicle screw-laminar hook system to treat young patients with lumbar spondylolysis because of its firm fixation and good clinical effect[16-18]. However, the pedicle screw-laminar hook systems currently in use are not specifically designed for the treatment of lumbar spondylolysis. It has some disadvantages, such as incomplete matching between hook and lamina, difficulty in installation between rod and pedicle screw and large trauma. Complete exposure of the lamina is usually required, resulting in excessive paraspinal soft tissue dissection. To this end, we designed a new anatomical hook-rod-pedicle screw system for lumbar spondylolysis and observed its clinical efficacy.

MATERIALS AND METHODS

Patient selection

From April 2017 to July 2018, 15 men with an average age of 22 (18-30 years) participated in the study. There were 11 cases of single segment, including L4 (1 case) and L5 (10 cases) and 4 cases of double segments, including L3 and L5 (1 case) and L4 and L5 (3 cases). All cases were bilateral isthmus defects. Inclusion criteria were: (1) The patient presented with severe low back pain and limited lumbar function but no radiating pain (sciatica) in the lower extremities; (2) Computed tomography (CT) of the lumbar spine showed spondylolysis but no spina bifida or missing lamina, and dynamic lumbar radiographs showed no lumbar instability and spondylolisthesis; (3) At isthmic defect and adjacent levels, there was no disc degeneration on magnetic resonance imaging (MRI); (4) Conservative treatment, such as restriction of movement, oral anti-inflammatory analgesics and physiotherapy for 3-6 mo, did not relieve symptoms; and (5) Positive diagnosis test (low back pain disappeared after injection of small

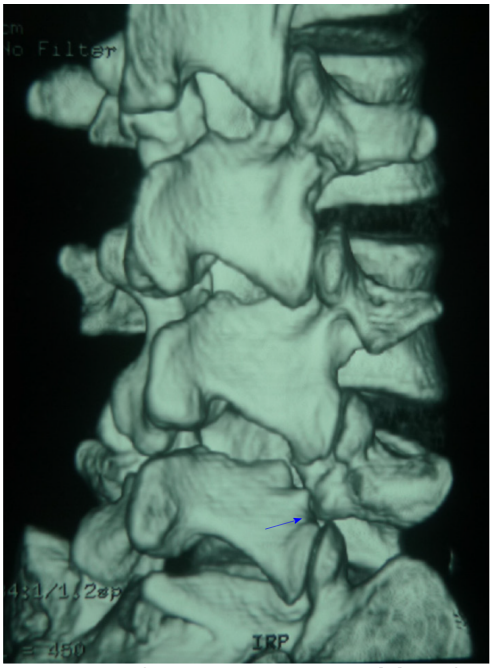

DOI: 10.12998/wjcc.v10.i17.5680 **Copyright** ©The Author(s) 2022.

Figure 1 Three-dimensional computed tomography scan showed L5 isthmus fracture (blue arrow).

dose local anesthetics into the isthmus defect site). Exclusion criteria were metabolic diseases or chronic inflammatory diseases, such as arthrolithiasis, rheumatoid arthritis or ankylosing spondylitis. Physical examination revealed limited lumbar motion, tenderness above and/or adjacent spinous processes and normal motor, sensory and tendon reflexes in both lower extremities.

The study was approved by the ethical review committee from The Third Medical Centre of Chinese PLA General Hospital, and the study was in accordance with the Helsinki Declaration. All patients gave informed written consent.

Surgical procedure

The patient was placed prone on the operating table under general endotracheal anesthesia, carefully cushioning all pressure points and keeping the neck in a neutral position. A midline incision was made, cutting the skin to the deep fascia layer. The deep fascia was cut longitudinally 1.5 cm outside the midline. The longissimus-multifidus muscle interval was bluntly dissected with a finger to avoid unnecessary tissue damage (Figure 2). Through the intermuscular approach, the isthmic defect site and the insertion point of the pedicle screw were exposed, and the fibrous tissue at the defect area was removed. A high-speed burr was used to debride sclerotic surfaces until bleeding bone surface was seen in the fractured pars. Gross motion was noted in the fissure area of the isthmus. Care was taken not to injure the facet joint capsule. Then a universal multiaxial pedicle screw was inserted into the corresponding vertebral body. Autogenous bone graft was obtained from the posterior superior iliac crest and implanted into the isthmus defect site, and the donor area of the posterior superior iliac crest was filled with allogeneic bone. After releasing the lower edge of the lamina with the ligamentum flavum stripper, the middle part of the hook rod was clamped with the rod holding forceps, and the hook could easily hook the lower edge of the lamina. The rod end of the anatomical hook was connected with the multiaxial pedicle screw. The construct was then loaded with compression force and tightened.

The contralateral anatomical hook-rod-pedicle screw was installed in the same way. After the installation of both sides, there was no loosening of the hook-rod-pedicle screw system and no movement of bone graft. Then the wound was rinsed with saline, the drainage tube was placed, and the incision was closed layer by layer. The average intraoperative blood loss was 40 mL (28-56 mL). On the second day after the operation, the drainage tube was pulled out, and the patient put on a lumbar brace and got out of bed for low back muscle function exercise. Three months after the operation, the brace can be removed for normal activity and exercise.

Clinical and radiologic assessments

The visual analog scale (VAS) score (in the range of 0 = no pain to 10 = worst pain) was used to evaluate the severity of back pain and donor area pain. The Oswestry disability index (ODI) was used for functional assessment. The measures were recorded preoperatively and 3, 6, 12 and 24 mo after surgery. Functional status was qualified as "excellent," "good," "fair" and "poor" according to the Modified Macnab criteria[19] and recorded at 3, 6, 12 and 24 mo postoperatively.

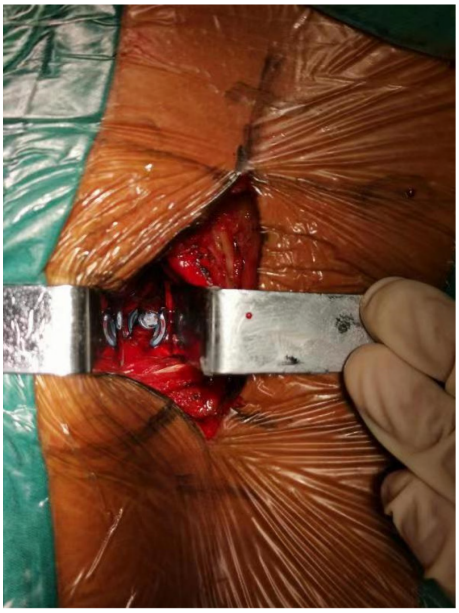

DOI: 10.12998/wjcc.v10.i17.5680 **Copyright** ©The Author(s) 2022.

Figure 2 Exposure *via* longissimus-multifidus muscle interval.

Lumbar plain radiographs, CT and MRI were re-examined at 3, 6, 12 and 24 mo after operation. Lumbar plain radiographs were used to evaluate whether the internal fixation was loose and broken. CT was used to evaluate the fusion of the isthmic fracture and the osteogenesis of the iliac crest donor site. MRI was used to evaluate the degeneration of the intervertebral disc in the corresponding segment of lumbar spondylolysis.

Statistical analysis

Data were expressed as the mean ± standard error of the mean. Statistical analyses were carried out using SPSS 22.0 (IBM Corporation, Armonk, NY, United States). The VAS score and ODI before and after operation were compared using the paired *t*-test. The significance level was set to 0.05.

RESULTS

During the follow-up period of 24 mo, no patient developed sciatica or motor or sensory disturbance. The VAS score of low back pain and ODI score at 3, 6, 12 and 24 mo postoperatively significantly improved compared with those before surgery ($P < 0.05$, Table 1). At 24 mo after operation, the VAS score of low back pain decreased from 6.73 ± 0.88 preoperatively to 0.73 ± 0.59 postoperatively, and the ODI score decreased from 58.20 ± 8.99 preoperatively to 7.87 ± 4.97 postoperatively (Table 1). CT showed bilateral isthmus bone fusion in 14 cases and unilateral isthmus bone fusion in 1 case. The signs of intervertebral discs in diseased and adjacent segments had no change on MRI. The VAS score of donor site pain was 0.20 ± 0.41. Allogeneic bone filling in the bone donor site showed osteogenesis (Figure 3). According to the Modified Macnab standard, the excellent and good rate of operation was 100% at 24 mo follow-up (Table 2). A typical case was shown in Figure 4.

DISCUSSION

Lumbar spondylolysis is one of the common causes of low back pain in adolescents[4]. The incidence rate is 3%-10% in adolescents and 6% in adults[20,21]. More than 80% of lumbar spondylolysis appears in L4 and L5[4]. Patients with lumbar spondylolysis mostly like sports or engage in sports, dancing and other industries. The specific cause of spondylolysis may be stress fractures caused by long-term fatigue on the basis of isthmic dysplasia. For the treatment of symptomatic lumbar spondylolysis in adolescents, active measures should be taken to avoid further problems such as intervertebral disc degeneration, herniation, lumbar instability or spondylolisthesis. If early diagnosis of lumbar spondylolysis is made in adolescents, measures such as wearing a lumbosacral brace and restricting movement will most likely result in isthmic healing[7], but those who do not heal should be actively treated by surgery. The main indication for surgical repair of lumbar spondylolysis is that low back pain is not relieved after at least 6 mo of non-surgical treatment, including activity modification, bracing and

Table 1 Visual analog scale and Oswestry disability index scores at each time point

Measure	Baseline	3 mo	6 mo	12 mo	24 mo
Back pain VAS	6.73 ± 0.88	2.20 ± 0.86[a]	1.47 ± 0.92[a]	1.13 ± 0.64[a]	0.73 ± 0.59[a]
ODI	58.20 ± 8.99	21.73 ± 6.24[a]	16.40 ± 4.55[a]	12.13 ± 3.72[a]	7.87 ± 4.97[a]
Donor area VAS	-	1.93 ± 0.96	0.67 ± 0.82	0.40 ± 0.51	0.20 ± 0.41

[a]$P < 0.05$ *vs* the baseline values. VAS: Visual analog scale; ODI: Oswestry disability index.

Table 2 Modified Macnab rating at different time points

Postoperative time	Excellent	Good	Fair	Poor
3 mo	5 (33)	7 (47)	3 (20)	0
6 mo	6 (40)	8 (53)	1 (7)	0
12 mo	8 (53)	7 (47)	0	0
24 mo	10 (67)	5 (33)	0	0

Data are presented as *n* (%).

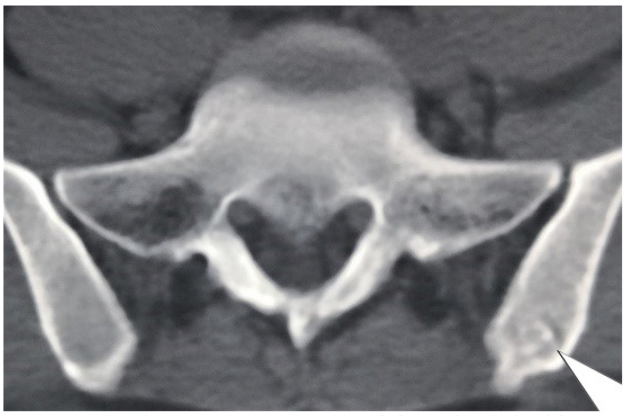

DOI: 10.12998/wjcc.v10.i17.5680 **Copyright** ©The Author(s) 2022.

Figure 3 The donor site of iliac crest was filled with allogeneic bone, which resulted in osteogenesis (white arrow).

physical therapy. Aggravation of pain, deterioration of neurological symptoms and progressive listhesis also are indications for surgical consideration. In the present study, our patient group, due to severe low back pain, failure of conservative treatment for more than 3 mo, isthmus dissection, osteosclerosis and nonunion, needed surgical treatment.

There are many surgical methods for lumbar spondylolysis. In 1968, Kimura[22] described an isolated bone graft that directly repaired the isthmus defect without internal fixation and retained segmental activity but required a postoperative cast and long bed rest. Later, Scott[23] proposed the use of wire under the lamina and transverse processes, which has been improved by several authors over the years [24,25]. In 1970, Buck[26] first used screw internal fixation and bone grafting to repair defects directly, and subsequently other approaches with special constructs and temporary fixations were reported[27, 28]. There were also posterolateral bone graft fusion, cross-segmental pedicle screw fixation and other methods. Patients with spondylolisthesis or disc herniation can be treated with pedicle screw fixation and interbody fusion[29].

The treatment of young patients with lumbar spondylolysis with isthmus debridement, bone grafting and pedicle screw laminar hook fixation has achieved satisfactory results[16-18], which proves that the pedicle screw-laminar hook system has strong fixation and is conducive to bone graft fusion. It is an intrasegmental fixation and does not affect the lumbar interbody movement and the kinematics of the adjacent segment. Studies[30-32] have reached a consensus that the lumbar intramuscular approach can reduce the dissection of paravertebral muscles, reduce the denervation of paravertebral muscles, preserve the structure of muscle ligament complex, reduce postoperative pain and recover quickly. However, the current pedicle screw-laminar hook fixation system is not specifically designed for lumbar

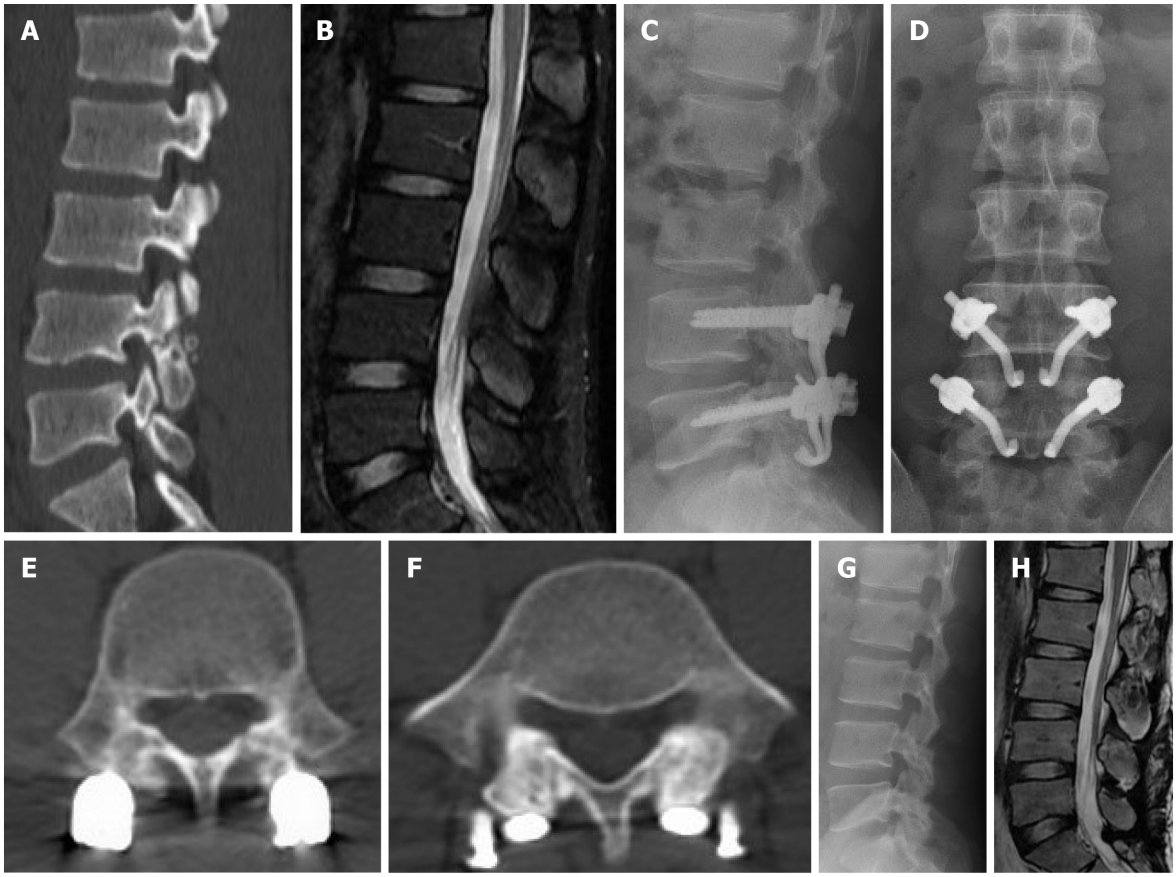

DOI: 10.12998/wjcc.v10.i17.5680 **Copyright** ©The Author(s) 2022.

Figure 4 Typical case. A 21-yr-old male patient had recurrent low back pain for more than 2 yr. A: Two-dimensional computed tomography scan showed lumbar spondylolysis at bilateral L4 and L5 levels; B: Lumbar magnetic resonance imaging showed normal signals of all lumbar intervertebral discs; C: Lateral radiograph after lumbar surgery; D: Anteroposterior radiograph of lumbar spine after operation; E: Computed tomography scan of the lumbar spine at 6 mo after lumbar operation showed the healing of the bone graft in the L4 isthmus; F: Computed tomography scan of the lumbar spine at 6 mo after lumbar operation showed the healing of the bone graft in the L5 isthmus; G: 12 mo after the operation the lateral radiograph showed that the internal fixation had been removed; H: 12 mo after the operation, magnetic resonance imaging showed that the signals of all lumbar intervertebral discs were normal.

spondylolysis but mainly for the correction of scoliosis. Before the hook is installed, the muscles around the spinous process and lamina need to be separated, resulting in severe tissue damage. At the same time, the installation of the system is difficult because the lamina, hook and pedicle screw are not on the same plane.

To solve these problems, we designed a new anatomical hook-rod instrument (Figure 5), which combined with pedicle screw to form anatomical hook-rod-pedicle screw system. The system can be installed by the intermuscular approach, which has the advantages of less trauma and convenient operation. At the same time, the system is firmly fixed, which is favorable for bone graft fusion. According to the anatomy of the lumbar spine, the spinous process is at a certain angle with the lamina, the lamina is inclined backward and upward, and the lower edge of lamina and the tail of pedicle screw are at a certain angle with the sagittal plane. According to the above anatomical features, the hook and the rod are inclined in these three directions. The hook is completely matched with the lamina, which is conducive to the installation of the hook at the lower edge of the lamina, and the rod is easy to connect with the universal pedicle screw. Of course, the angles of L4 and L5 are different. We have designed a series of hook-rods with different angles, which are convenient for operation. Of course, in terms of our new implant design, the fundamental principle of this system is only slightly novel compared with the traditional segmental pedicle screw rod and hook. However, according to our literature review, the design of this implant is unique so far.

In this study, 15 cases of young patients with lumbar spondylolysis were treated with isthmus repair, bone grafting and anatomical hook-rod-pedicle screw fixation and achieved satisfactory results. At the same time, the injury was small, and the operation was simple and convenient. However, in all 15 patients with lumbar spondylolysis who underwent repair of the isthmic defect, 1 patient with L5 bilateral isthmic defect had no bone healing on one side. Most of the isthmus defects occurred in preschool, and a few occurred in adulthood. Isthmus rupture will no longer occur in adulthood. After the occurrence of lumbar isthmus defect, the defect usually does not heal spontaneously. In this way, the broken ends of bone on both sides of the defect will atrophy and harden. In this case, nonunion after

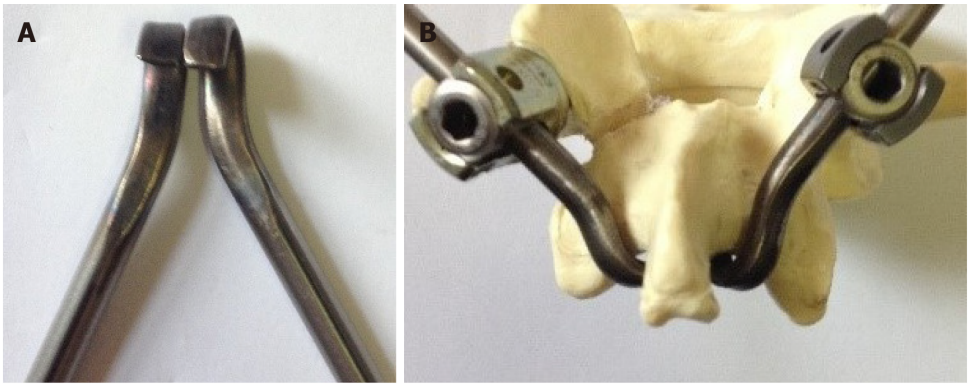

DOI: 10.12998/wjcc.v10.i17.5680 **Copyright** ©The Author(s) 2022.

Figure 5 Anatomical hook-rod instrument. A: Physical picture of anatomical hook; B: The hook was completely matched with the lamina, and the rod was connected with the pedicle screw.

repair of the isthmus defect is a common complication. Because this is an intrasegmental fixation, the implant usually does not need to be removed. If unilateral nonunion occurs, the implant must not be removed.

Autologous iliac bone graft is the "gold standard" in bone grafting[33], and pain in the iliac bone donor area is a common complication after iliac bone removal[34]. There are many reasons for postoperative pain in the donor area, such as bone defect, adhesion, osteoporosis and cutaneous nerve injury in the donor area. A bone block with cortex and cancellous bone is taken from the posterior superior iliac spine and can be trimmed to a suitable size to meet the needs of bone grafting in the isthmus. To solve the problem of donor site pain, we used the allogeneic bone with tissue-engineered human bone morphogenetic proteins to fill the defect area of posterior superior iliac spine. Allogeneic bone contains bone morphogenetic proteins, which can induce new bone formation and promote bone growth. During the follow-up, bone growth was found in the defect of the posterior superior iliac spine, as shown in (Figure 3), and the pain in the bone donor area disappeared.

The application of isthmus debridement, bone grafting and anatomical hook-rod-pedicle screw system fixation in young patients with lumbar spondylolysis has the advantages of less trauma, a simple operation and satisfactory curative effect. However, it is not suitable for the cases of lumbar spondylolysis with spondylolisthesis. In addition, it is also not suitable for the cases with missing lamina, bone dysplasia and lumbar disc degenerative diseases. This new hook-rod-pedicle screw system is undergoing biomechanical testing and has been patented in China (Patent No.: ZL201721043286.7). This is a small sample observation study, and further large sample and prospective studies are needed to prove the superiority and reliability of the system.

CONCLUSION

Compared with the use of the traditional instrument, the application of this new anatomical hook-rod-pedicle screw system to treat young patients with lumbar spondylolysis has the advantages of less trauma, a simple operation and satisfactory clinical effects.

ARTICLE HIGHLIGHTS

Research background

The pedicle screw-laminar hook system has strong fixation and is conducive to bone graft fusion for lumbar spondylolysis. However, the current pedicle screw-laminar hook fixation system is not specifically designed for lumbar spondylolysis.

Research motivation

The pedicle screw-laminar hook system currently in use is not specifically designed for the treatment of lumbar spondylolysis. It has some disadvantages, such as incomplete matching between hook and lamina, difficulty in installation between rod and pedicle screw and large trauma. Complete exposure of the lamina is usually required, resulting in excessive paraspinal soft tissue dissection.

Research objectives

To investigate the clinical effects of a new anatomical hook-rod-pedicle screw system in the treatment of lumbar spondylolysis in young adults.

Research methods

We designed a new anatomic hook-rod-pedicle screw system for young patients with lumbar spondylolysis. The isthmus and the corresponding pedicle screw entry point were exposed through the intermuscular approach. Autogenous iliac bone graft was obtained to bridge the isthmus defect, and then the anatomic hook-rod-pedicle screw system was used to fix the isthmus in 15 young patients.

Research results

At 24 mo follow-up, the visual analogue scale score of low back pain decreased from 6.73 ± 0.88 to 0.73 ± 0.59, and the Oswestry disability index score decreased from 58.20 ± 8.99 to 7.87 ± 4.97. Computed tomography showed bilateral isthmic bone healing in 14 cases and unilateral isthmic bone healing in 1 case. Magnetic resonance imaging showed that the lumbar disc signal of the diseased segment and adjacent segments had no change compared with that before surgery. The pain visual analogue scale score of the donor site was 0.20 ± 0.41 at the last follow-up. According to the Modified Macnab score, the excellent and good rate was 100%.

Research conclusions

The application of this new anatomical hook-rod-pedicle screw system to treat young patients with lumbar spondylolysis has the advantages of less trauma, a simple operation and satisfactory clinical effects.

Research perspectives

The new anatomical hook-rod-pedicle screw system should be evaluated in a large sample multicenter randomized controlled study.

FOOTNOTES

Author contributions: Li DM and Jiang W designed the study; Peng BG wrote the manuscript text; Li DM and Peng BG performed the surgical operations; Li DM and Li YC contributed to critical revision; Peng BG and Jiang W contributed equally to this work; All authors reviewed the manuscript and approved the final version.

Institutional review board statement: All procedures performed in studies involving human participants were in accordance with the ethical standards of the institutional and/or national research committee and with the 1964 Helsinki declaration and its later amendments or comparable ethical standards. This study was approved by the ethics committee of The Third Medical Centre of Chinese PLA General Hospital.

Informed consent statement: Informed written consent was obtained from the patients for publication of this manuscript and any accompanying images.

Conflict-of-interest statement: The authors declare that they have no financial or other conflicts of interest in relation to this research and its publication.

Data sharing statement: The datasets used and/or analyzed during the current study are available from the corresponding author on reasonable request.

CONSORT 2010 statement: The authors have read the CONSORT 2010 Statement, and the manuscript was prepared and revised according to the CONSORT 2010 Statement.

Open-Access: This article is an open-access article that was selected by an in-house editor and fully peer-reviewed by external reviewers. It is distributed in accordance with the Creative Commons Attribution NonCommercial (CC BY-NC 4.0) license, which permits others to distribute, remix, adapt, build upon this work non-commercially, and license their derivative works on different terms, provided the original work is properly cited and the use is non-commercial. See: https://creativecommons.org/Licenses/by-nc/4.0/

Country/Territory of origin: China

ORCID number: Duan-Ming Li 0000-0002-9753-1355; Yong-Chao Li 0000-0002-4460-9702; Wei Jiang 0000-0002-0680-2456; Bao-Gan Peng 0000-0003-1667-4125.

S-Editor: Gong ZM
L-Editor: Filipodia

P-Editor: Gong ZM

REFERENCES

1 **Farfan HF**, Osteria V, Lamy C. The mechanical etiology of spondylolysis and spondylolisthesis. *Clin Orthop Relat Res* 1976; 40-55 [PMID: 1277685 DOI: 10.1097/00003086-197606000-00005]
2 **Wiltse LL**, Newman PH, Macnab I. Classification of spondylolisis and spondylolisthesis. *Clin Orthop Relat Res* 1976; 23-29 [PMID: 1277669 DOI: 10.1097/00003086-197606000-00003]
3 **Chen MR**, Moore TA, Cooperman DR, Lee MJ. Anatomic variability of 120 L5 spondylolytic defects. *Global Spine J* 2013; **3**: 243-248 [PMID: 24436876 DOI: 10.1055/s-0033-1356765]
4 **Hensinger RN**. Spondylolysis and spondylolisthesis in children and adolescents. *J Bone Joint Surg Am* 1989; **71**: 1098-1107 [PMID: 2668295 DOI: 10.2106/00004623-198971070-00020]
5 **Nachemson A**. Repair of the spondylolisthetic defect and intertransverse fusion for young patients. *Clin Orthop Relat Res* 1976; 101-105 [PMID: 776482 DOI: 10.1097/00003086-197606000-00013]
6 **Blanda J**, Bethem D, Moats W, Lew M. Defects of pars interarticularis in athletes: a protocol for nonoperative treatment. *J Spinal Disord* 1993; **6**: 406-411 [PMID: 8274809 DOI: 10.1097/00002517-199306050-00007]
7 **Steiner ME**, Micheli LJ. Treatment of symptomatic spondylolysis and spondylolisthesis with the modified Boston brace. *Spine (Phila Pa 1976)* 1985; **10**: 937-943 [PMID: 3914087 DOI: 10.1097/00007632-198512000-00013]
8 **Lee CK**. Accelerated degeneration of the segment adjacent to a lumbar fusion. *Spine (Phila Pa 1976)* 1988; **13**: 375-377 [PMID: 3388124 DOI: 10.1097/00007632-198803000-00029]
9 **Yang SW**, Langrana NA, Lee CK. Biomechanics of lumbosacral spinal fusion in combined compression-torsion loads. *Spine (Phila Pa 1976)* 1986; **11**: 937-941 [PMID: 3824071 DOI: 10.1097/00007632-198611000-00014]
10 **Cyron BM**, Hutton WC. The fatigue strength of the lumbar neural arch in spondylolysis. *J Bone Joint Surg Br* 1978; **60-B**: 234-238 [PMID: 659472 DOI: 10.1302/0301-620X.60B2.659472]
11 **Green TP**, Allvey JC, Adams MA. Spondylolysis. Bending of the inferior articular processes of lumbar vertebrae during simulated spinal movements. *Spine (Phila Pa 1976)* 1994; **19**: 2683-2691 [PMID: 7899964 DOI: 10.1097/00007632-199412000-00016]
12 **Hefti F**, Seelig W, Morscher E. Repair of lumbar spondylolysis with a hook-screw. *Int Orthop* 1992; **16**: 81-85 [PMID: 1572778 DOI: 10.1007/BF00182992]
13 **Pavlovcic V**. Surgical treatment of spondylolysis and spondylolisthesis with a hook screw. *Int Orthop* 1994; **18**: 6-9 [PMID: 8021074 DOI: 10.1007/BF00180169]
14 **Ohmori K**, Suzuki K, Ishida Y. Translamino-pedicular screw fixation with bone grafting for symptomatic isthmic lumbar spondylolysis. *Neurosurgery* 1992; **30**: 379-384 [PMID: 1620301 DOI: 10.1097/00006123-199203000-00011]
15 **Gillet P**, Petit M. Direct repair of spondylolysis without spondylolisthesis, using a rod-screw construct and bone grafting of the pars defect. *Spine (Phila Pa 1976)* 1999; **24**: 1252-1256 [PMID: 10382254 DOI: 10.1097/00007632-199906150-00014]
16 **Tokuhashi Y**, Matsuzaki H. Repair of defects in spondylolysis by segmental pedicular screw hook fixation. A preliminary report. *Spine (Phila Pa 1976)* 1996; **21**: 2041-2045 [PMID: 8883209 DOI: 10.1097/00007632-199609010-00023]
17 **Roca J**, Iborra M, Cavanilles-Walker JM, Albertí G. Direct repair of spondylolysis using a new pedicle screw hook fixation: clinical and CT-assessed study: an analysis of 19 patients. *J Spinal Disord Tech* 2005; **18** Suppl: S82-S89 [PMID: 15699811 DOI: 10.1097/01.bsd.0000123425.12852.3c]
18 **Debusscher F**, Troussel S. Direct repair of defects in lumbar spondylolysis with a new pedicle screw hook fixation: clinical, functional and Ct-assessed study. *Eur Spine J* 2007; **16**: 1650-1658 [PMID: 17520298 DOI: 10.1007/s00586-007-0392-0]
19 **He L**, Ni J, Wu B, Yue J, Cao G, Guo Y, Yang L. Coblation annuloplasty in cervical discogenic pain without radiculopathy. *Wideochir Inne Tech Maloinwazyjne* 2020; **15**: 305-312 [PMID: 32489491 DOI: 10.5114/wiitm.2019.89394]
20 **Rajasekaran S**, Kamath V, Avadhani A. Bucks fusion. *Eur Spine J* 2010; **19**: 343-344 [PMID: 20130927 DOI: 10.1007/s00586-010-1308-y]
21 **Smith JA**, Hu SS. Management of spondylolysis and spondylolisthesis in the pediatric and adolescent population. *Orthop Clin North Am* 1999; **30**: 487-499, ix [PMID: 10393770 DOI: 10.1016/S0030-5898(05)70101-2]
22 **Kimura M**. [My method of filing the lesion with spongy bone in spondylolysis and spondylolistesis]. *Seikei Geka* 1968; **19**: 285-296 [PMID: 5693611]
23 **Askar Z**, Wardlaw D, Koti M. Scott wiring for direct repair of lumbar spondylolysis. *Spine (Phila Pa 1976)* 2003; **28**: 354-357 [PMID: 12590209 DOI: 10.1097/01.BRS.0000048496.55167.22]
24 **Hambly MF**, Wiltse LL. A modification of the Scott wiring technique. *Spine (Phila Pa 1976)* 1994; **19**: 354-356 [PMID: 8171371 DOI: 10.1097/00007632-199402000-00018]
25 **Johnson GV**, Thompson AG. The Scott wiring technique for direct repair of lumbar spondylolysis. *J Bone Joint Surg Br* 1992; **74**: 426-430 [PMID: 1587895 DOI: 10.1302/0301-620X.74B3.1587895]
26 **Buck JE**. Direct repair of the defect in spondylolisthesis. Preliminary report. *J Bone Joint Surg Br* 1970; **52**: 432-437 [PMID: 4916960 DOI: 10.1302/0301-620X.52B3.432]
27 **Morscher E**, Gerber B, Fasel J. Surgical treatment of spondylolisthesis by bone grafting and direct stabilization of spondylolysis by means of a hook screw. *Arch Orthop Trauma Surg* 1984; **103**: 175-178 [PMID: 6497607 DOI: 10.1007/BF00435550]
28 **Louis R**. [Pars interarticularis reconstruction of spondylolysis using plates and screws with grafting without arthrodesis. Apropos of 78 cases]. *Rev Chir Orthop Reparatrice Appar Mot* 1988; **74**: 549-557 [PMID: 3070652]
29 **Zhang S**, Ye C, Lai Q, Yu X, Liu X, Nie T, Zhan H, Dai M, Zhang B. Double-level lumbar spondylolysis and

spondylolisthesis: A retrospective study. *J Orthop Surg Res* 2018; **13**: 55 [PMID: 29548343 DOI: 10.1186/s13018-018-0723-3]

30 **Vialle R**, Wicart P, Drain O, Dubousset J, Court C. The Wiltse paraspinal approach to the lumbar spine revisited: an anatomic study. *Clin Orthop Relat Res* 2006; **445**: 175-180 [PMID: 16456311 DOI: 10.1097/01.blo.0000203466.20314.2a]

31 **Suk KS**, Lee HM, Kim NH, Ha JW. Unilateral versus bilateral pedicle screw fixation in lumbar spinal fusion. *Spine (Phila Pa 1976)* 2000; **25**: 1843-1847 [PMID: 10888955 DOI: 10.1097/00007632-200007150-00017]

32 **Whitecloud TS 3rd**, Roesch WW, Ricciardi JE. Transforaminal interbody fusion versus anterior-posterior interbody fusion of the lumbar spine: a financial analysis. *J Spinal Disord* 2001; **14**: 100-103 [PMID: 11285420 DOI: 10.1097/00002517-200104000-00002]

33 **Dhawan A**, Kuklo TR, Polly DW Jr. Analysis of iliac crest bone grafting process measures. *Am J Orthop (Belle Mead NJ)* 2006; **35**: 322-326 [PMID: 16927657]

34 **Delawi D**, Dhert WJ, Castelein RM, Verbout AJ, Oner FC. The incidence of donor site pain after bone graft harvesting from the posterior iliac crest may be overestimated: a study on spine fracture patients. *Spine (Phila Pa 1976)* 2007; **32**: 1865-1868 [PMID: 17762294 DOI: 10.1097/BRS.0b013e318107674e]

World Journal of Clinical Cases

Submit a Manuscript: https://www.f6publishing.com

World J Clin Cases 2022 June 16; 10(17): 5690-5701

DOI: 10.12998/wjcc.v10.i17.5690

ISSN 2307-8960 (online)

META-ANALYSIS

Systematic review of Yougui pills combined with levothyroxine sodium in the treatment of hypothyroidism

Xiao-Pei Liu, Ya-Nan Zhou, Cong-E Tan

Specialty type: Integrative and complementary medicine

Provenance and peer review: Unsolicited article; Externally peer reviewed.

Peer-review model: Single blind

Peer-review report's scientific quality classification

Grade A (Excellent): A
Grade B (Very good): B
Grade C (Good): C
Grade D (Fair): 0
Grade E (Poor): 0

P-Reviewer: Ciccone MM, Italy; Hegazy AA, Egypt; Trkulja V, Croatia

Received: October 27, 2021
Peer-review started: October 27, 2021
First decision: February 14, 2022
Revised: March 10, 2022
Accepted: April 21, 2022
Article in press: April 21, 2022
Published online: June 16, 2022

Xiao-Pei Liu, Ya-Nan Zhou, Cong-E Tan, School of Basic Medicine, Shaanxi University of Chinese Medicine, Xianyang 712046, Shaanxi Province, China

Corresponding author: Cong-E Tan, PhD, School of Basic Medicine, Shaanxi University of Chinese Medicine, Xixian Avenue, Xixian New District, Xianyang 712046, Shaanxi Province, China. tanzime@163.com

Abstract

BACKGROUND

Yougui pills have long been used to treat hypothyroidism, usually in combination with levothyroxine sodium in clinical treatment, while their clinical efficacy and safety are still controversial when compared to levothyroxine treatment alone.

AIM

To explore the clinical efficacy and safety of Yougui pills combined with levothyroxine sodium in the treatment of hypothyroidism.

METHODS

This meta-analysis was performed in accordance with the PRISMA guidelines. Randomized controlled trials on Yougui pills in the treatment of hypothyroidism published from 2008 to May 2021 were searched in a total of 8 databases (4 databases in Chinese and 4 databases in English). The quality of the included studies was evaluated according to the Cochrane risk assessment tool. Weighted mean difference (WMD) was used for continuous variables, and relative risk (RR) was used for binary variables. Data were extracted, and the meta-analysis was conducted with the statistical software of Stata15.0 and RevMan5.0.

RESULTS

A total of 140 articles were retrieved, and 9 of them were finally included, with a total sample size of 936 cases. The main meta-analysis results are as follows: (1) The group of Yougui pills combined with levothyroxine sodium had a significantly higher overall response rate than the group of levothyroxine sodium (RR = 1.20, 95%CI 1.12, 1.28, $P < 0.00001$); (2) Yougui pills combined with levothyroxine sodium achieved significantly better efficacy than levothyroxine sodium alone in alleviating adverse symptoms [standard mean difference (SMD) = -1.10, 95%CI: -1.37, -0.84, $P < 0.00001$]; (3) The level of thyrotropin stimulating hormone in the group of Yougui pills combined with levothyroxine sodium was significantly lower than in the control group of levothyroxine sodium (WMD = -1.38, 95%CI: -2.10, -0.67, $P = 0.00001$); (4) The level of free triiodothyronine in the

group of Yougui pills combined with levothyroxine sodium was higher than that in the control group of levothyroxine sodium (WMD = 0.41, 95%CI: 0.03, 0.79, P = 0.03); (5) The level of free thyroxine in the group of Yougui pills combined with levothyroxine sodium was significantly higher than that in the control group of levothyroxine sodium (SMD = 0.83, 95%CI: 0.44, 1.22, $P \leq$ 0.0001); and (6) The adverse reactions in the group of Yougui pills combined with levothyroxine sodium were significantly less than those in the control group of levothyroxine sodium (RR = 0.33, 95%CI: 0.20, -0.53, P < 0.00001).

CONCLUSION

In the treatment of hypothyroidism, the combination of Yougui pills with levothyroxine sodium may be better than levothyroxine sodium treatment alone.

Key Words: Yougui pills; Levothyroxine sodium; Hypothyroidism; Systematic review

©The Author(s) 2022. Published by Baishideng Publishing Group Inc. All rights reserved.

Core Tip: The combined treatment of Yougui pills and levothyroxine sodium can effectively reduce or eliminate the adverse reactions caused by the use of hormones, increase the secretion of hormones in serum and thus significantly improve the clinical symptoms of hypothyroidism. We recommended the use of levothyroxine sodium in combination with Yougui pills in patients with hypothyroidism.

Citation: Liu XP, Zhou YN, Tan CE. Systematic review of Yougui pills combined with levothyroxine sodium in the treatment of hypothyroidism. *World J Clin Cases* 2022; 10(17): 5690-5701
URL: https://www.wjgnet.com/2307-8960/full/v10/i17/5690.htm
DOI: https://dx.doi.org/10.12998/wjcc.v10.i17.5690

INTRODUCTION

Hypothyroidism is a condition characterized by impaired metabolism and multisystem function as a result of decreased thyroid hormone synthesis and secretion, insufficient tissue utilization or insufficient biological effects[1,2]. Hypothyroidism is more common in women, with the highest incidence between 30-years-old and 50-years-old, and the incidence of hypothyroidism is rising year by year due to excessive iodine intake, the fast pace of life, pollution of the living environment, *etc.* Hypothyroidism is characterized by low metabolism, which is accompanied by associated symptoms, including fatigue, hypothermia, delayed response time, memory loss, unresponsiveness, irregular menstruation, mucosal edema, *etc* and may lead to further complications such as osteoporosis, anemia and hyperlipidemia. Hypothyroidism is related to cardiovascular diseases, including atrial fibrillation, coronary heart disease, pericardial effusion and a variety of nonspecific electrocardiogram abnormalities[3,4].

Currently, the treatment of hypothyroidism in Western medicine is mainly based on thyroid hormone replacement therapy, which has a high recurrence rate after withdrawal and prolonged treatment duration, and clinical symptoms are difficult to improve quickly. Excessive doses are likely to induce hyperthyroidism or abnormal bone metabolism. Some patients have poor tolerance with side effects such as insomnia, rapid heart rate or tachycardia and arrhythmia, and in the elderly and patients with heart diseases, angina pectoris or myocardial infarction can be induced[5-7]. Considering the limitations of Western medicine treatment, the combined use of traditional Chinese medicine (TCM) and Western medicine may bring better efficacy and safety.

Hypothyroidism is classified as a "gall disease" in TCM, and its etiology is related to emotions, dietary injuries and congenital endowments. TCM treatment advocates warming the spleen yang and the kidney yang as the fundamental methods to improve the functions of the various organs of the body. Yougui pills are derived from Jingyue Quanshu written by the Ming Dynasty physician Zhang Jing-Yue, and the whole prescription consists of ten herbs: rehmannia, yam, cornel, wolfberry, antler gum, dodder, eucommia, angelica, cinnamon and aconite. The main effect is to warm the kidney yang, replenish vital essence, nourish the bone marrow and treat the deficiency of kidney yang and the syndrome of declining vital gate fire. Modern pharmacology shows that Yougui pills have the effects of resisting yang deficiency, regulating the endocrine system, protecting the central nervous system, enhancing the body's immunity and affecting bone metabolism[8,9]. Studies have shown that Yougui pills can be used in combination with Western medicine to produce a synergistic effect, reduce the dosage and hormone usage duration, reduce or eliminate adverse reactions caused by hormone treatment and significantly improve the therapeutic effect of patients[10,11].

Due to the small sample size of previous studies, the value of Yougui pills combined with levothyroxine sodium for hypothyroidism remains unclear. This study compared the efficacy and safety of Yougui pills combined with levothyroxine sodium and levothyroxine sodium alone in the treatment of hypothyroidism using the meta-analysis method to provide more evidence-based medical evidence and evaluate the value of Yougui pills in hypothyroidism.

MATERIALS AND METHODS

Inclusion and exclusion criteria

Inclusion criteria: (1) The study type was randomized controlled trial (RCT); (2) The research subjects all met the syndrome differentiation of kidney yang deficiency/spleen-kidney yang deficiency in TCM[12] and the diagnostic criteria of hypothyroidism in the Guidelines for the Diagnosis and Treatment of Thyroid Diseases in China[13]; (3) Intervention measures: Yougui pills combined with levothyroxine sodium were used in the experimental group, whereas levothyroxine sodium was used in the control group. The course of treatment was clear, with explicit efficacy evaluation criteria. There were no restrictions on the use of the blind method, and the language of publication could be either Chinese or English; and (4) Endpoints: the overall response rate (defined as the disappearance or improvement of symptoms and signs after treatment, recovery of thyroid function and other related indicators[10,11]), thyrotropin (TSH), serum levels of free triiodothyronine (FT3), free thyroxine (FT4), TCM symptom scores and safety indicators (adverse reactions after medication). Exclusion criteria: (1) Case reports, case series, letters, comments and review articles; (2) Articles whose data cannot be extracted; (3) Pure abstract papers; (4) Animal or *in vitro* studies; and (5) Duplicate and irrelevant data.

Data sources and retrieval strategies

Two research reviewers independently conducted a literature search in a total of 8 databases: China National Knowledge Internet, China Academic Journals Database (Wanfang Database), Chinese Science and Technology Journals Database (VIP Database), China Biomedical Literature Database, PubMed, Embase, Cochrane Library and Web of Science. The retrieval time was set from 2008 to May 25, 2021. The Chinese search terms included (Yougui pills) and (hypothyroidism). The English search terms included Yougui pill, you gui wan, you-gui-wan, ygw herbal preparation hypothyroidism, hypothyroidisms and thyroid-stimulating hormone deficiency; and the English PubMed search strategy is shown in Table 1. There were no age, gender or racial restrictions, but the search language was limited to Chinese and English. According to the difference of each database, the subject words were combined with free words or keywords to conduct the retrieval.

Quality evaluation

Literature screening, data extraction and quality evaluation were carried out independently by the two authors. Any differences would be resolved through discussion until reaching a consensus. If disagreement persisted, an evidence-based medicine expert would be consulted for a discussion to reach a consensus. The literature quality evaluation was based on the risk of bias assessment tool on RCT (1) in the Cochrane Handbook 5.1.0[14], and the evaluation included the following aspects: (1) Generation of random sequence; (2) Allocation concealment; (3) Whether the blind method was implemented for the subjects and relevant test personnel; (4) Blind evaluation of effect indicators; (5) Incomplete result data; (6) Selective reporting of results; and (7) Other sources of bias. The evaluation results were represented by the terms "high risk," "unclear" and "low risk."

Statistical analysis

Meta-analysis was performed using Stata 15.0 and RevMan5.0 software. Weighted mean difference was used for continuous variables. In order to eliminate the influence of the dimension, FT4 and TCM syndrome scores in this study were expressed as standard mean difference (SMD) and 95%CI. Binary variables were represented by relative risk (RR) and its 95%CI. The heterogeneity test was performed among the studies. When $P \geq 0.1$ and $I^2 < 50\%$, the heterogeneity was regarded as low, and the fixed-effect model was adopted. Whereas, when $P < 0.1$ and $I^2 > 50\%$, the heterogeneity was considered to exist, and then subgroup analysis and sensitivity analysis were adopted to explore the source of heterogeneity. Furthermore, if the source of heterogeneity could not be determined, a random-effect model was used to conduct a meta-analysis of the literature. Begg's and Egger's tests, as well as funnel plots, were used to assess the publication bias of the included studies. $P < 0.05$ indicated the presence of publication bias, whereas $P > 0.05$ indicated no publication bias.

Table 1 Search strategies in PubMed

ID	Query
#1	"you gui wan" [MESH]
#2	("you gui wan" [Title/Abstract]) OR (you-gui-wan [Title/Abstract]) OR (ygw herbal preparation [Title/Abstract]) OR (yougui pill [Title/Abstract])
#3	#1 OR #2
#4	"hypothyroidism"[MESH]
#5	(((((((hypothyroidism [Title/Abstract]) OR (hypothyroidisms [Title/Abstract])) OR (thyroid-stimulating hormone deficiency [Title/Abstract])) OR (thyroid-stimulating, hormone deficiencies [Title/Abstract])) OR (thyroid stimulating hormone deficiency [Title/Abstract])) OR (thyroid-stimulating hormone deficiencies [Title/Abstract])) OR (tsh deficiency [Title/Abstract])) OR (tsh deficiencies [Title/Abstract])
#6	#4 OR #5
#7	#3 AND #6

RESULTS

Literature retrieval results

A total of 140 pieces of related literature were initially screened, and 9 randomized controlled studies (RCTs)[15-23] including a total of 936 patients were eventually included for meta-analysis through gradual repeated selection. The literature screening flowchart is shown in Figure 1.

Basic characteristics of the included literature

The included studies were single-center RCTs in China, published from 2008 to May 2021. Those articles with incomplete data or that could not be included in statistical analysis, such as duplicates, reviews, conference abstracts, animal experiments and studies involving people with hypothyroidism and other diseases were all excluded, as well as those studies in which the experimental group used Yougui pills combined with levothyroxine sodium and also other drugs or therapies. Finally, 9 RCTs were included [15-23], and the detailed data of the included studies are shown in Table 2.

Quality evaluation of included literature

Revman 5.3 was employed to assess the risk of bias in the included studies as shown in Figure 2A. All 24 studies in Figure 2B are RCTs. The judgment basis for quality evaluation of the 9 articles[15-23] is shown in Table 3.

Efficacy and safety

Overall response rate: A total of 8 articles[15-21,23] reported the overall response rate, and the combined effect size was (RR = 1.20, 95%CI: 1.12, 1.28, $P < 0.00001$. The overall response rate of the Yougui pills combined with the levothyroxine sodium group was significantly higher than that of the levothyroxine sodium group, without significant heterogeneity ($I^2 = 0\%$) (Figure 3A).

TSH: TSH levels were concerned in 8 articles[15,17-23], and the effect sizes were combined using the random-effect model. The results showed that in the treatment of hypothyroidism, the level of TSH in the group of Yougui pills combined with levothyroxine sodium was significantly lower than in the control group of levothyroxine sodium (MD = -1.05, 95%CI: -1.85, -0.25, $P = 0.010$), and the combined result was highly heterogeneous ($I^2 = 92\%$) (Figure 3B). The sensitivity analysis was performed by excluding each study one by one, and it was found that a study by Zhang[17] was the main source of heterogeneity. After removing this study (MD = -0.62, 95%CI: -0.94, -0.31, $P = 0.0001$), the heterogeneity of the combined results was acceptable ($I^2 = 3\%$), suggesting that this study had no effect on the original conclusions and that the combined results were stable.

FT3: Seven articles[15,17,19-23] reported FT3, thereby combining the effect sizes through the random-effect model. The results showed that when compared with the levothyroxine sodium group Yougui pills combined with levothyroxine sodium in the treatment of hypothyroidism could increase the FT3 levels (MD = 0.53, 95%CI: 0.37, 0.69, $P < 0.00001$), with high heterogeneity ($I^2 = 81\%$) (Figure 3C). By removing each study one at a time for the sensitivity analysis, it was found that the study by Li *et al*[18] was the main source of heterogeneity. When this study was excluded (MD = 0.65, 95%CI: 0.48, 0.82, $P < 0.00001$), the heterogeneity of the combined results was acceptable ($I^2 = 19\%$), and the original conclusion was not changed, suggesting that the results were robust.

FT4: FT4 was reported in 7 articles[15,17,19-23]. By adopting the random-effect model to combine the effect sizes, the results demonstrated that, when compared with the levothyroxine sodium group, the Yougui pills combined with levothyroxine sodium could significantly increase the FT4 levels in the

Table 2 Basic characteristics table

Ref.	Intervention measure	Control measure	Average age (yr)		Duration of treatment/ follow-up (wk)
			Experimental group	Control group	
Zhang *et al*[15], 2008	Yougui pills + levothyroxine sodium	Levothyroxine sodium	53	55	8
Li *et al*[16], 2012	Yougui pills + levothyroxine sodium	Levothyroxine sodium	68.1 ± 5.3	66.7 ± 5.1	12
Zhang *et al*[17], 2015	Yougui pills + levothyroxine sodium	Levothyroxine sodium	42.7 ± 3.6	42.7 ± 3.6	
Li *et al*[18], 2016	Yougui pills + levothyroxine sodium	Levothyroxine sodium	40.2 ± 9.4	40.2 ± 9.4	
Wang *et al*[19], 2016	Yougui pills + levothyroxine sodium	Levothyroxine sodium	40.12 ± 9.50	40.57 ± 9.53	12
Jiang *et al*[20], 2017	Yougui pills + levothyroxine sodium	Levothyroxine sodium	40.9 ± 5.6	40.8 ± 5.8	12
Liu *et al*[21], 2017	Yougui pills + levothyroxine sodium	Levothyroxine sodium	37.98 ± 13.83	38.88 ± 12.10	8
Chen *et al*[22], 2018	Yougui pills + levothyroxine sodium	Levothyroxine sodium	40.88 ± 5.12	40.95 ± 5.62	12
Shi *et al*[23], 2018	Yougui pills + levothyroxine sodium	Levothyroxine sodium	44.6 ± 12.4	45.1 ± 11.9	12

Table 3 Methodological quality evaluation of included literature

Ref.	Randomization method	Blind method	Concealment	Integrity of result data	Selective reporting of results	Other bias
Zhang *et al*[15], 2008	Just mentioned random	Not mentioned	Unclear	Complete data	Low risk	Unclear
Li *et al*[16], 2012	Random number table	Not mentioned	Unclear	Complete data	Low risk	Unclear
Zhang *et al*[17], 2015	Not mentioned	Not mentioned	Unclear	Complete data	Low risk	Unclear
Li *et al*[18], 2016	Just mentioned random	Not mentioned	Unclear	Complete data	Low risk	Unclear
Wang *et al*[19], 2016	Just mentioned random	Not mentioned	Unclear	Complete data	Low risk	Unclear
Jiang *et al*[20], 2017	Random number table	Double blind	Unclear	Complete data	Low risk	Unclear
Liu *et al*[21], 2017	Not mentioned	Not mentioned	Unclear	Complete data	Low risk	Unclear
Chen *et al*[22], 2018	Not mentioned	Double blind	Unclear	Complete data	Unclear	Unclear
Shi *et al*[23], 2018	Random number table	Not mentioned	Unclear	Complete data	Unclear	Unclear

treatment of hypothyroidism (SMD = 0.83, 95%CI: 0.44,1.22, $P < 0.0001$], and the combined results were highly heterogeneous ($I^2 = 80\%$) (Figure 3D). The sensitivity analysis was carried out by removing each study one at a time, and two studies by Li *et al*[18] and Shi *et al*[23]were discovered to be the main sources of heterogeneity. After removing these two studies (SMD = 0.78, 95%CI: 0.57, 0.99, $P < 0.0001$], the heterogeneity of the combined results was acceptable ($I^2 = 35\%$), without changing the original conclusion, suggesting that the results were robust.

TCM symptom scores: Three articles[18,20,21] adopted the TCM symptom scores (unresponsiveness, edema, chills, lethargy, *etc*) to evaluate the curative effect. Yougui pills combined with levothyroxine sodium were significantly superior to the control group of levothyroxine sodium in reducing syndrome scores, with a combined effect size of (SMD = -1.10, 95%CI: -1.37, -0.84, $P < 0.00001$], and there was no significant heterogeneity in the combined results ($I^2 = 0\%$) (Figure 3E).

Adverse reactions: Two articles[19,21] involved adverse reactions after medication, and the combined effect size was (RR = 0.33, 95%CI: 0.20, -0.53, $P < 0.00001$. The adverse reactions (dry mouth, hyperhidrosis, insomnia and irritability) were significantly lower in the Yougui pills combined with levothyroxine sodium group than in the levothyroxine sodium group, and there was no significant heterogeneity in the combined results ($I^2 = 0\%$) (Figure 3F).

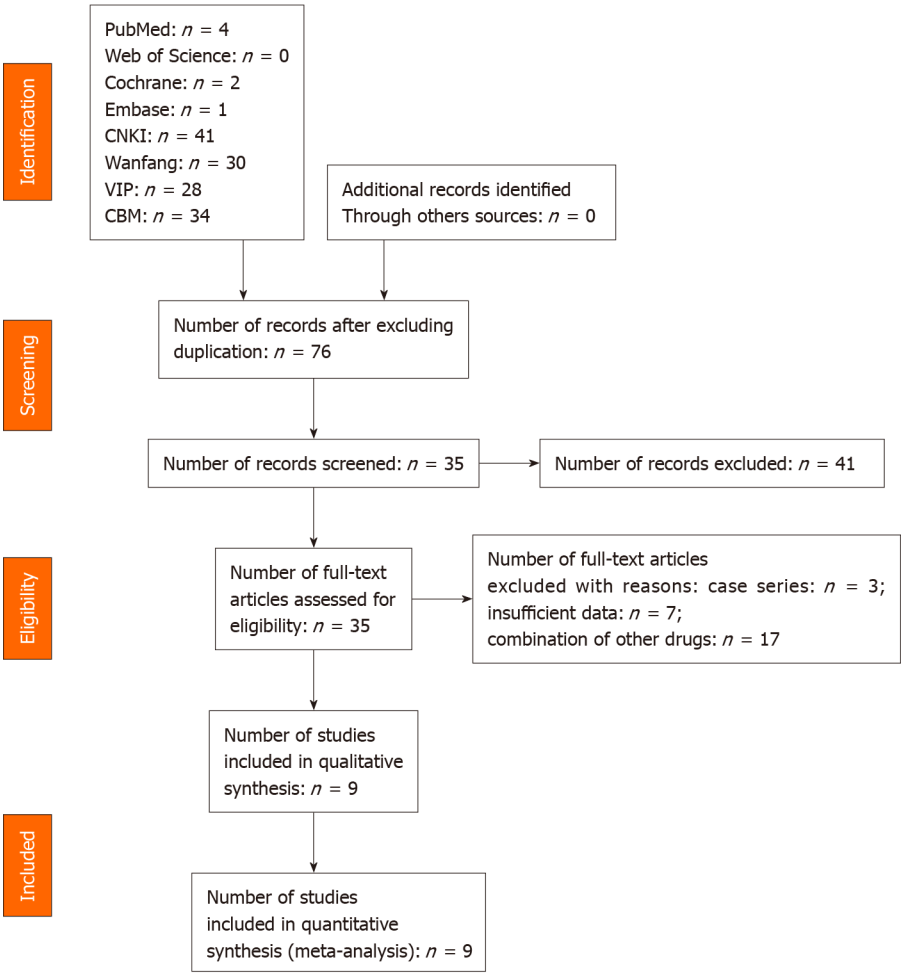

DOI: 10.12998/wjcc.v10.i17.5690 **Copyright** ©The Author(s) 2022.

Figure 1 Literature screening flowchart. CNKI: China National Knowledge Internet; VIP: Chinese Science and Technology Journals Database; CBM: China Biomedical Literature Database.

Publication bias: A funnel plot of total efficacy was drawn using Stata 15.0 and further tested by Begg's and Egger's tests. The funnel chart appears to be symmetrical, suggesting less possibility of publication bias. The Begg's and Egger's tests were adopted to quantitatively analyze the total clinical efficacy of the included studies, and the results showed Begg's Test $P = 0.711$ and Egger's Test $P = 0.506$, indicating that there was no publication bias (Figures 4 and 5).

DISCUSSION

Studies have shown that the combination of Yougui pills and Western medicine can produce a synergistic effect, reduce the dosage and duration of hormone usage and reduce or eliminate the adverse reactions caused by hormone usage. However, the value of Yougui pills combined with levothyroxine sodium for hypothyroidism is unclear at present. The main findings of this study were as follows: (1) The group of Yougui pills combined with levothyroxine sodium had a significantly higher overall response rate than the group of levothyroxine sodium; (2) Yougui pills combined with levothyroxine sodium could significantly improve the adverse symptoms; (3) Yougui pills combined with levothyroxine sodium could significantly increase the levels of FT3 and FT4 and reduce TSH; and (4) When compared to the levothyroxine sodium group, the combination of Yougui pills with levothyroxine sodium could minimize the incidence of adverse reactions significantly. The available evidence shows that Yougui pills combined with levothyroxine sodium are superior to levothyroxine sodium alone in terms of improving the effective rate, reducing adverse reactions and improving clinical symptoms and thyroid function in the treatment of hypothyroidism. It is believed that when Yougui pills are taken with levothyroxine sodium in a treatment plan, Yougui pills can increase the clinical efficacy of levothyroxine sodium and decrease its adverse effects. Therefore, we recommend combining Yougui pills with levothyroxine sodium to treat hypothyroidism.

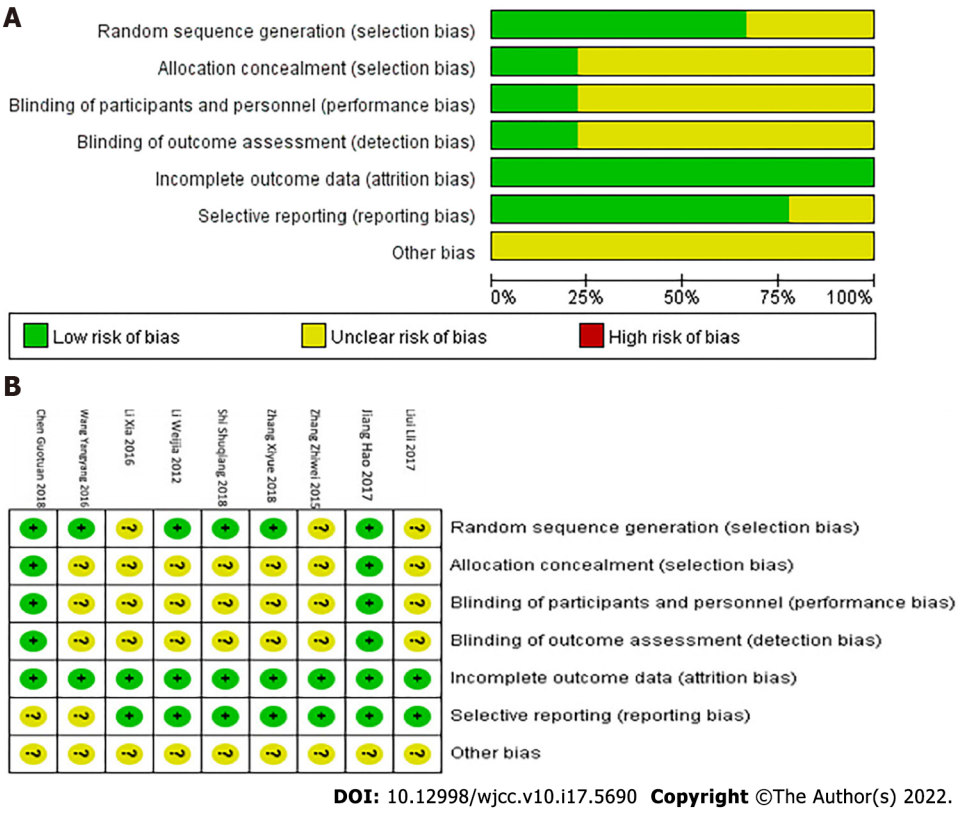

DOI: 10.12998/wjcc.v10.i17.5690 **Copyright** ©The Author(s) 2022.

Figure 2 Cochrane risk of bias. A: Cochrane's risk of bias percentile graph; B: Cochrane's risk of bias summary graph.

According to TCM, the mechanism by which Yougui pills taken with levothyroxine sodium can effectively treat hypothyroidism is due to hypothyroidism belonging to the category of consumptive or edema diseases. The medical pathogenesis is the deficiency of kidney yang, the loss of warmth and nourishment of visceral organs, the decline of qi function and even the overflowing of water; kidney yang is the root of yang qi, equivalent to the energy system of the human body, which is just as important to nature as the sun. As a classic TCM prescription for warming and invigorating the kidney and yang, Yougui pills, from the famous physician Zhang Jingyue's Jingyue Quanshu, are based on warming yang medicines, which are compatible yin-tonifying products in yang-reinforcing medicines and "seeking yang from yin"[24], and its efficacy in the treatment of hypothyroidism has been fully clinically verified.

Modern pharmacological studies of Yougui pills suggest that the mechanism of its curative effect involves the regulation of multiple systems such as nerves, immunity and endocrine. The hypothalamic-pituitary-thyroid axis is an essential branch of the neuroendocrine regulatory circuit that plays a role in thyroid hormone synthesis and release. Studies have verified that deficiency of kidney yang can cause dysfunction of the thalamus-pituitary-thyroid axis[25] and insufficient thyroid hormone secretion[26]. Yougui pills have a dynamic regulatory effect on the function of the pituitary-thyroid axis in rats with kidney-yang deficiency. The blood thyroid hormone level of rats significantly changed following the administration of Yougui pills[27].

Chen *et al*[28] used thyroid hormone content as an indicator to study the effect of Yougui pills on the hypothalamic-pituitary-thyroid axis in rats with kidney-yang deficiency, and the experiment showed that the regulating effect of Yougui pills on kidney-yang deficiency syndrome was slow and required a process of dose-effect accumulation. Wu[29] observed that giving Yougui capsules to elderly patients with kidney-yang deficiency significantly increased the level of thyroxine stimulation, which was inversely proportional to the degree of kidney-yang deficiency. The lower the degree of kidney-yang deficiency, the faster the increase in hormone levels.

In the current study, Yougui pills combined with levothyroxine sodium significantly increased FT3 and FT4 while decreasing TSH. Meanwhile, the total treatment efficiency and symptom improvement are better than those of levothyroxine sodium alone. Therefore, we believe that Yougui pills combined with levothyroxine sodium can effectively increase the secretion of hormone secreted in serum, which is conducive to the normal performance of thyroid function as well as significantly improving the metabolic function of tissue cells in the whole body, promoting thyroid microcirculation and restoring the function of the remaining thyroid tissue.

Any medication used to treat disease and restore normal body function carries the risk of causing damage to the body. TCM has typical characteristics of safety and fewer adverse reactions. Two articles

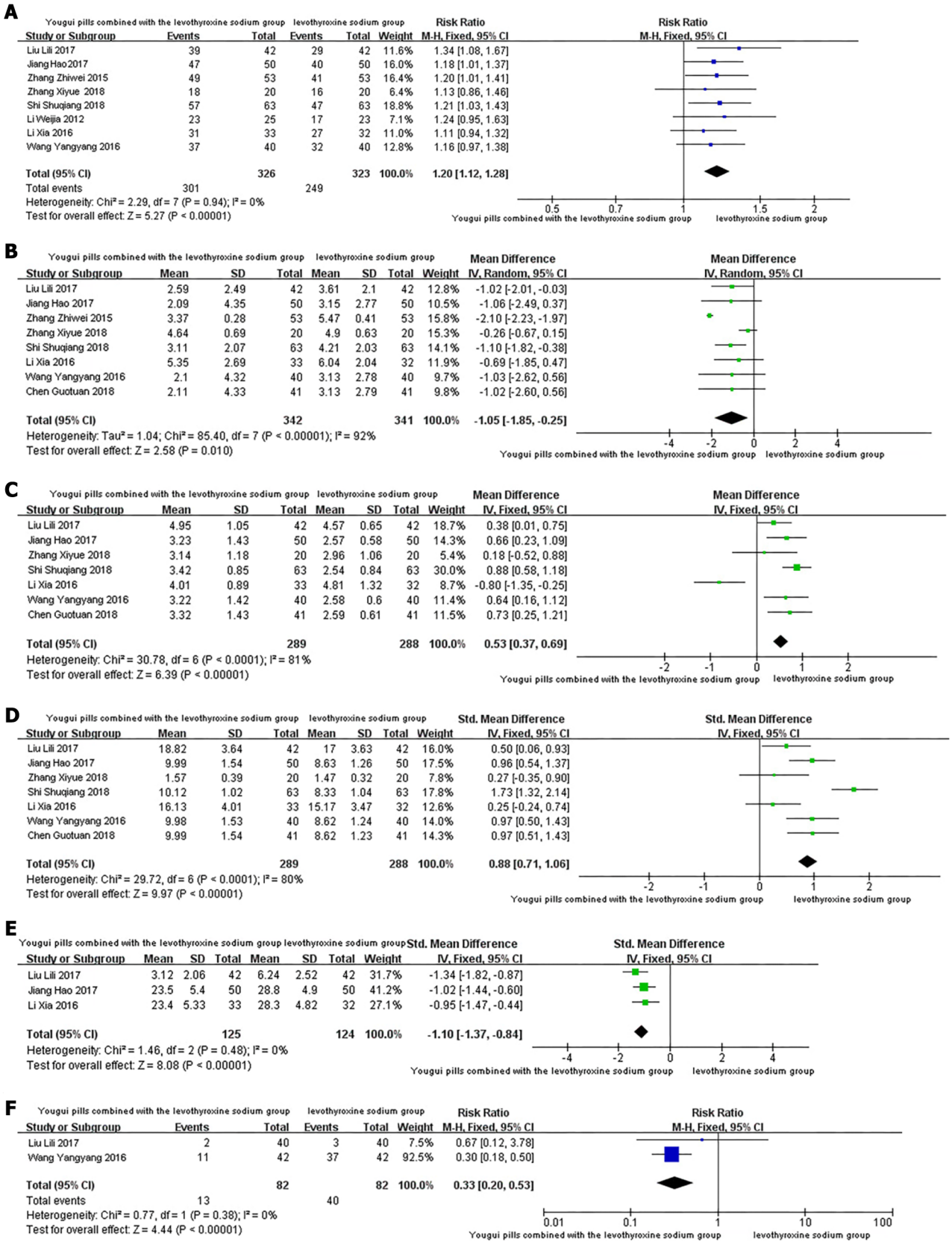

DOI: 10.12998/wjcc.v10.i17.5690 **Copyright** ©The Author(s) 2022.

Figure 3 Forest plot. A: Overall response rate; B: Thyrotropin levels; C: Free triiodothyronine levels; D: Free thyroxine levels; E: Scored clinical symptoms; F: Adverse reactions.

in this study reported adverse reactions, and the meta-analysis results showed that the Yougui pills combined with levothyroxine sodium group had significantly fewer adverse reactions (dry mouth, hyperhidrosis, insomnia, irritability) than the levothyroxine sodium group. Considering the limited

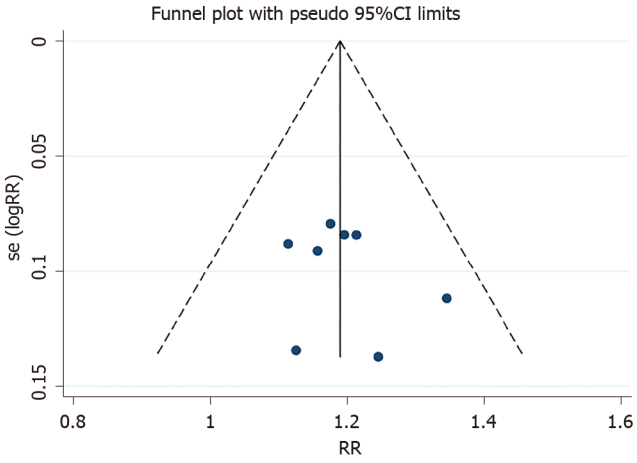

DOI: 10.12998/wjcc.v10.i17.5690 **Copyright** ©The Author(s) 2022.

Figure 4 Total effective funnel chart. RR: Relative risk.

```
Note: default data input format (theta, se_theta) assumed.

Tests for Publication Bias

Begg's Test

  adj. Kendall's Score (P-Q) =       4
        Std. Dev. of Score =    8.08
         Number of Studies =       8
                        z  =    0.49
                  Pr > |z| =   0.621
                        z  =    0.37 (continuity corrected)
                  Pr > |z| =   0.711 (continuity corrected)

Egger's test
```

Std_Eff	Coef.	Std. Err.	t	P>|t|	[95% Conf.	Interval]
slope	1.10032	.1279936	8.60	0.000	.7871312	1.413509
bias	.9491348	1.342963	0.71	0.506	-2.336978	4.235248

DOI: 10.12998/wjcc.v10.i17.5690 **Copyright** ©The Author(s) 2022.

Figure 5 Begg's and Egger's tests of total effective.

sample size, Yougui pills combined with levothyroxine sodium may have some rare adverse reactions. Therefore, attention should be paid to adverse drug reactions in clinical application, early detection and treatment to ensure the drug safety of patients.

This study has the following limitations: (1) The quality of the included literature is generally low; (2) There is a certain degree of heterogeneity among different studies; (3) The sample size of the included studies is relatively small, and larger sample studies are needed to provide more precise conclusions; (4) Grey literature was not retrieved; and (5) All included RCTs were open-label, with no treatment control, in which patients were treated with levothyroxine + T preparation alone. Therefore, all patients and investigators are aware of the prescribed treatment, and knowledge of the treatment also affects thyroid hormone and TSH levels. Effect estimates in such "no treatment controlled" trials are usually much larger than in double-blind (placebo-controlled) trials. The aforementioned factors may have a certain influence on the research results. To further validate the results of this study, further multicenter and large-sample studies should be conducted in accordance with RCT research guidelines.

CONCLUSION

Yougui pills in combination with levothyroxine sodium may be more effective than levothyroxine sodium alone in the treatment of hypothyroidism. The combined treatment can effectively reduce or eliminate the adverse reactions caused by the use of hormones, increase the secretion of hormones in serum and thus significantly improve the clinical symptoms of hypothyroidism. In conclusion, we

recommend using levothyroxine sodium in combination with Yougui pills. Although due to the low quality and heterogeneity of the included literature, the findings of this study need to be confirmed by high-quality RCT studies.

ARTICLE HIGHLIGHTS

Research background

Yougui pills are a classic ancient prescription of Ming Dynasty in China, which has been widely used in combination with levothyroxine sodium in the treatment of hypothyroidism. However, the level of evidence in clinical reports is inconsistent, and the credibility is poor. Thus, we conducted this meta-analysis to further confirm the efficacy and safety of Yougui pills and provide higher level evidence.

Research motivation

By strict study selection and quality evaluation, a total of 9 studies were included for further analysis to evaluate the clinical efficacy and safety. The results of this meta-analysis could help in rational drug use, the scientific research work and the government's health care decisions.

Research objectives

We aimed to find the latest and most reasonable treatment plan for the specific clinical problems of hypothyroidism patients. Further, we collected and summarized the homogenous data of the original study of Yougui pills combined with levothyroxine sodium in the treatment of hypothyroidism.

Research methods

We conducted this meta-analysis to evaluate the clinical efficacy and safety of Yougui pill combined with levothyroxine sodium in the treatment of hypothyroidism. Meta-analysis could combine clinical trial data of multiple small samples to improve the statistical efficiency of the original results and solve the inconsistency of research results. The results from strict meta-analysis have advantage in sample size, coverage, reliability and representativeness.

Research results

Compared with pure levothyroxine sodium, Yougui pills combined with levothyroxine sodium could effectively reduce or eliminate the adverse reactions caused by taking hormone, improve serum hormone secretion and significantly improve the clinical symptoms of hypothyroidism. However, this meta-analysis is still limited by relatively low quality and relatively high heterogeneity. Thus, this conclusion needs to be further verified by randomized controlled trial studies.

Research conclusions

With the aid of modern scientific research means and systematic evaluation meta-analysis in evidence-based medicine, the rationality and scientific nature of the combined use of traditional Chinese medicine (TCM) Yougui pill and Western medicine levothyroxine sodium was studied.

Research perspectives

Improving the quality of the original literature is necessary to strengthen the standardization of TCM syndrome diagnosis methods, and high-quality randomized controlled trials of TCM are necessary to evaluate TCM syndromes. The Endocrine Society should develop uniform testing methods to ensure consistency among units and references in China, which would help in enhancing academic exchange among different regions. Although Chinese herbal medicines are generally safe and have relatively few adverse reactions and the mechanisms of adverse effects caused by Chinese medicine are still unclear, we should still pay attention to adverse events in clinical practice and investigate the mechanisms in scientific studies.

ACKNOWLEDGEMENTS

We would like to thank all authors of the included primary studies.

FOOTNOTES

Author contributions: Tan CE and Liu XP conceptualized and designed the protocol, drafted the initial manuscript and reviewed the manuscript; Liu XP and Zhou YN defined the concepts and search items and performed the data extraction process as well as methodological appraisal of the studies; Zhou YN and Tan CE planned the data

extraction and statistical analysis; Liu XP and Tan CE provided critical insights; All authors have approved and contributed to the final written manuscript.

Supported by the National Natural Science Foundation of China, No. 81973754; Shaanxi University of Traditional Chinese Medicine Innovation Team Project, No. 2019-QN06.

Conflict-of-interest statement: The authors deny any conflict of interest.

PRISMA 2009 Checklist statement: The authors have read the PRISMA 2009 Checklist, and the manuscript was prepared and revised according to the PRISMA 2009 Checklist.

Open-Access: This article is an open-access article that was selected by an in-house editor and fully peer-reviewed by external reviewers. It is distributed in accordance with the Creative Commons Attribution NonCommercial (CC BY-NC 4.0) license, which permits others to distribute, remix, adapt, build upon this work non-commercially, and license their derivative works on different terms, provided the original work is properly cited and the use is non-commercial. See: https://creativecommons.org/Licenses/by-nc/4.0/

Country/Territory of origin: China

ORCID number: Xiao-Pei Liu 0000-0002-7688-2279; Ya-Nan Zhou 0000-0001-5322-0371; Cong-E Tan 0000-0002-6467-5723.

S-Editor: Zhang H
L-Editor: Filipodia CL
P-Editor: Zhang H

REFERENCES

1 **Chen J**. Clinical Endocrinology. Shanghai: Shanghai Science and Technology Press, 2011
2 **Wang Q**, Wang Y. Analysis of the effect of levothyroxine sodium in the treatment of hypothyroidism. *Xiandai Yiyao Weisheng* 2017; **33**: 1358-1360 [DOI: 10.3969/j.issn.1009-5519.2017.09.025]
3 **Hak AE**, Pols HA, Visser TJ, Drexhage HA, Hofman A, Witteman JC. Subclinical hypothyroidism is an independent risk factor for atherosclerosis and myocardial infarction in elderly women: the Rotterdam Study. *Ann Intern Med* 2000; **132**: 270-278 [PMID: 10681281 DOI: 10.7326/0003-4819-132-4-200002150-00004]
4 **Zeng P**, Cao J, Liao M. Intervention study on elderly patients with subclinical hypothyroidism and mild cognitive impairment in Ganzhou City. *Qiqihar Yixue Yuan Xuebao* 2020; **41**: 2556-2557 [DOI: 10.3969/j.issn.1002-1256.2020.20.017]
5 **Lu Z**, Zhong N. Internal Medicine. Beijing: People's Medical Publishing House, 2008
6 **Pucci E**, Chiovato L, Pinchera A. Thyroid and lipid metabolism. *Int J Obes Relat Metab Disord* 2000; **24** Suppl 2: S109-S112 [PMID: 10997623 DOI: 10.1038/sj.ijo.0801292]
7 **Glueck CJ**, Streicher P. Cardiovascular and medical ramifications of treatment of subclinical hypothyroidism. *Curr Atheroscler Rep* 2003; **5**: 73-77 [PMID: 12562546 DOI: 10.1007/s11883-003-0071-5]
8 **Wu P**, Zhou X. Research on alternative treatment of hypothyroidism after thyroidectomy. *Shiyong Yaowu Yu Linchuang* 2015; **18**: 1329-1331 [DOI: 10.14053/j.cnki.ppcr.201511015]
9 **Wu Z**, Bian H, Guo Y, Jiang Y, Xie Z, Yang G. Analysis of related causes of hypothyroidism after partial thyroidectomy. *Zhongguo Putong Waike Zazhi* 2003; **12**: 366-368 [DOI: 10.3969/j.issn.1005-6947.2003.05.016]
10 **Zhang M**, Ni Q. Progress in the treatment of hypothyroidism with traditional Chinese medicine. *Beijing Zhongyi Yao* 2018; **37**: 851-854 [DOI: 10.16025/j.1674-1307.2018.09.015]
11 **Liu Y**. The effect of combined Chinese and Western medicine treatment on hypothyroidism. *Zhongwai Yixue Yanjiu* 2018; **16**: 135-136 [DOI: 10.14033/j.cnki.cfmr.2018.5.069]
12 **Medicine SAoTC**. Standards for the diagnosis and efficacy of diseases and syndromes in traditional Chinese medicine. Nanjing: Nanjing University Press, 1994
13 **Shan Z**. Guide to "Guidelines for Diagnosis and Treatment of Thyroid Diseases in China". *Zhognguo Shiyong Neike Zazhi* 2008; **28**: 260
14 **Higgins JP**, Altman DG, Gøtzsche PC, Jüni P, Moher D, Oxman AD, Savovic J, Schulz KF, Weeks L, Sterne JA; Cochrane Bias Methods Group; Cochrane Statistical Methods Group. The Cochrane Collaboration's tool for assessing risk of bias in randomised trials. *BMJ* 2011; **343**: d5928 [PMID: 22008217 DOI: 10.1136/bmj.d5928]
15 **Zhang X**, Zuo X. Clinical observation of Yougui pill combined with low-dose Youjiale in the treatment of hypothyroidism. *Hubei Zhongyi Yao Zazhi* 2008; 23-24
16 **Li W**, Wang Y. Yougui pill combined with low-dose thyroxine in the treatment of 25 cases of senile hypothyroidism. *Zhongyi Zazhi* 2012; **53**: 1055-1056
17 **Zhang Z**. Observation on the effect of combined treatment of 53 cases of hypothyroidism with Youlejia and Yougui Pills. *Medical Aesthetics and Cosmetology* 2015; **3**: 614-615
18 **Li X**, Lou J, Chen Y, Wu C, Jiang M. Clinical Observation on the Treatment of Primary Hypothyroidism (Kidney Yin and Yang Deficiency Syndrome) with Yougui Pills. *Yatai Chuantong Yiyao* 2016; **12**: 118-119 [DOI: 10.11954/ytctyy.201603056]
19 **Wang Y**, Zhu W. Clinical observation of Yougui pill combined with levothyroxine sodium tablets in the treatment of

hypothyroidism. *Xin Zhongyi* 2016; **48**: 90-92 [DOI: 10.13457/j.cnki.jncm.2016.08.038]

20 **Jiang M**, Wang R, Wang F, Li S. The clinical effects of Yougui Pills combined with levothyroxine sodium tablets in the treatment of hypothyroidism. *Zhongguo Yiyao Daobao* 2017; **14**: 165-168

21 **Liu L**. Observation on the clinical efficacy of the method of warming the kidney and yang in the treatment of hypothyroidism. Thesis, Guangzhou University of Traditional Chinese Medicine. 2017

22 **Chen G**. Clinical effects of Yougui Pills combined with levothyroxine sodium tablets in the treatment of hypothyroidism. *Linchuang Yiyao Wenxian Dianzi Zazhi* 2018; **5**: 55 [DOI: 10.16281/j.cnki.jocml.2018.23.044]

23 **Shi S**, Du Z. Study on the clinical effect of Yougui Pill plus or minus combined with levothyroxine sodium in the treatment of hypothyroidism. *Zhongguo Heli Yongyao Tansuo* 2018; **15**: 23-26 [DOI: 10.3969/j.issn.2096-3327.2018.11.007]

24 **Xie M**, Zhou R. Prescriptions. Beijing: People's Medical Publishing House, 2014

25 **Zhou X**, Jia X, Li M. Clinical effect of Yougui pill in the treatment of TPOAb-positive subclinical hypothyroidism. *Zhongguo Jihua Shengyu Xue Zazhi* 2019; **27**: 457-460 [DOI: 10.3969/j.issn.1004-8189.2019.04.011]

26 **Li F**, Zhang Y, Li Y, Chu Y, Wang F, Li H. Modern research progress in pharmacology of Yougui Pills. *J Tradit Chin Med* 2017; **45**: 108-112 [DOI: 10.19664/j.cnki.1002-2392.2017.03.034]

27 **Zhai X**, Huang Y, Shi J, Jia T, Lou Y, Dong Q. Regulation of Morinda officinalis on hypothalamic-pituitary-thyroid axis in rats with kidney-yang deficiency. *Zhong Cheng Yao* 2017; **39**: 233-237 [DOI: 10.3969/j.issn.1001-1528.2017.02.001]

28 **Chen L**, Wang X, Ma N, Liao C, Liu J, Lai B, Huang M, Chen S. Dynamic effects of Yougui Pill on hypothalamic-pituitary-thyroid axis in rats with kidney-yang deficiency. *Guangdong Yixue Yuan Xuebao* 2016; **32**: 771-774 [DOI: 10.16809/j.cnki.1006-8783.2016071201]

29 **Wu T**. Effect of Yougui Capsule on Hypothalamus-Pituitary-Thyroid Axis Function in Elderly Men with Kidney Yang Deficiency. Thesis, Shandong University of Traditional Chinese Medicine. 2015

World Journal of Clinical Cases

Submit a Manuscript: https://www.f6publishing.com

World J Clin Cases 2022 June 16; 10(17): 5702-5707

DOI: 10.12998/wjcc.v10.i17.5702

ISSN 2307-8960 (online)

CASE REPORT

Allogeneic stem cell transplantation-A curative treatment for paroxysmal nocturnal hemoglobinuria with PIGT mutation: A case report

Laurence Schenone, Anne-Béatrice Notarantonio, Véronique Latger-Cannard, Veronique Fremeaux-Bacchi, Marcelo De Carvalho-Bittencourt, Marie-Thérèse Rubio, Marc Muller, Maud D'Aveni

Specialty type: Hematology

Provenance and peer review: Unsolicited article; Externally peer reviewed.

Peer-review model: Single blind

Peer-review report's scientific quality classification

Grade A (Excellent): A
Grade B (Very good): 0
Grade C (Good): 0
Grade D (Fair): 0
Grade E (Poor): 0

P-Reviewer: Saito M, Japan

Received: November 16, 2021
Peer-review started: November 16, 2021
First decision: February 14, 2022
Revised: February 24, 2022
Accepted: April 2, 2022
Article in press: April 2, 2022
Published online: June 16, 2022

Laurence Schenone, Marie-Thérèse Rubio, Maud D'Aveni, Department of Hematology, CHRU de Nancy, Nancy F-54000, France

Laurence Schenone, Marc Muller, Genetic Laboratory, CHRU de Nancy, Nancy F-54000, France

Anne-Béatrice Notarantonio, Maud D'Aveni, IMoPA, CNRS 7365, University of Lorraine, Nancy F-54000, France

Véronique Latger-Cannard, Hematology Laboratory, Cytometry Platform, CHRU de Nancy, Nancy F-54000, France

Veronique Fremeaux-Bacchi, Immunology Laboratory, Hôpital Européen George Pompidou, Paris 75015, France

Marcelo De Carvalho-Bittencourt, Immunology Laboratory, CHRU de Nancy, Nancy F-54000, France

Corresponding author: Maud D'Aveni, MD, PhD, Doctor, Department of Hematology, CHRU Nancy, Allée du Morvan, Nancy F-54000, France. m.daveni-piney@chru-nancy.fr

Abstract

BACKGROUND

Patients with paroxysmal nocturnal hemoglobinuria (PNH) have a clonal population of blood cells deficient in glycosylphosphatidylinositol-anchored (GPI-anchored) proteins, most of the time resulting from a mutation in the X-linked gene PIGA. We report a patient with PNH resulting from a rare biallelic PIGT mutation on chromosome 20.

CASE SUMMARY

A 47-year-old man was referred to our hospital for febrile pancytopenia. The patient reported a history of recurrent urticaria and arthralgia and he presented during 3 mo recurrent acute dermo-hypodermitis and aseptic meningitidis. Based on clinical cases published with PIGT-PNH, with clinically typical PNH and autoinflammatory symptoms, we treated our patients with repeated infusions of eculizumab to decrease autoinflammatory symptoms and then we performed an allogeneic stem cell transplantation (allo-SCT) with a mismatched unrelated

donor. Our patient experienced no acute Graft *vs* Host disease (GvHD) and a moderate chronic GvHD and is now considered cured at 24 mo after allo-SCT.

CONCLUSION
This case report suggests that allo-SCT should be considered to cure PIGT-PNH patients.

Key Words: Paroxysmal nocturnal hemoglobinuria; Allogeneic stem cell transplantation; PIGT mutation; Recurrent meningitidis; Autoinflammatory symptoms; Case report

©The Author(s) 2022. Published by Baishideng Publishing Group Inc. All rights reserved.

Core Tip: Paroxysmal nocturnal hemoglobinuria with autoinflammatory symptoms has been described in 4 cases with PIG-T mutations (PIGT-PNH entity). We report the fifth case in the world. For the first time we treated him with an allogeneic hematopoietic stem cell transplantation (allo-SCT) after repeated infusions of eculizumab to decrease autoinflammatory symptoms. Allo-SCT was performed with a mismatched unrelated donor and no excess of alloreactivity or toxicity was observed. We think that this new case report with a review of literature will help physicians to have a focus on PIGT-PNH. It suggests that allogeneic SCT should be considered as a curative treatment option for this disease.

Citation: Schenone L, Notarantonio AB, Latger-Cannard V, Fremeaux-Bacchi V, De Carvalho-Bittencourt M, Rubio MT, Muller M, D'Aveni M. Allogeneic stem cell transplantation-A curative treatment for paroxysmal nocturnal hemoglobinuria with PIGT mutation: A case report. *World J Clin Cases* 2022; 10(17): 5702-5707
URL: https://www.wjgnet.com/2307-8960/full/v10/i17/5702.htm
DOI: https://dx.doi.org/10.12998/wjcc.v10.i17.5702

INTRODUCTION

Paroxysmal nocturnal hemoglobinuria (PNH) is an acquired hematopoietic stem cell (HSC) disorder. Deficient HSCs give rise to a clonal population of blood cells deficient in proteins anchored with glycosylphosphatidylinositol (GPI-anchored), a glycolipid moiety that secures 100 different proteins to the cell surface[1]. In 2019, 4 patients with typical PNH and autoinflammatory symptoms, including recurrent aseptic meningitis, were found to have a germline point mutation in one *PIGT* allele, with the other *PIGT* allele being removed by somatic deletion of a 20q region implicated in hematological malignancies. Analyses of patient leukocytes revealed free GPI expressed on the cell surface, triggering autoinflammation through increased IL-1β secretion, activation of the lectin pathway of complement and production of C5b-9 complexes[2]. Therefore, eculizumab treatment abrogates not only intravascular hemolysis but also autoinflammation. We report the fifth case of PIGT-PNH and the first time that allogeneic hematopoietic stem cell transplantation has been applied as treatment. This procedure was readily feasible with no excess alloreactivity or toxicity.

CASE PRESENTATION

Chief complaints

A 47-year-old man was referred to our hospital for pancytopenia with PNH cloning and meningitidis and urticaria.

History of present illness

Upon admission to our hospital, he presented with fever, sudden brownish urine and altered consciousness with mild pancytopenia (hemoglobin 93 g/L, platelets 137.109/L and leukocytes 2.109/L).

History of past illness

The patient reported a history of recurrent urticaria and arthralgia since he was 30-years-old. Three months and one month prior, he was hospitalized for acute dermohypodermitis with pancytopenia and no documented microbiologic agent. He was successfully treated with piperacillin and tazobactam for 14 d.

Personal and family history

No special family history was reported.

Physical examination

Examination revealed urticaria and symptoms of meningitis including headache and stiff neck. His meningitis symptoms were resolved at 3 d after initiation of meropenem. During hospitalization, he experienced 4 episodes of aseptic meningitis and general fatigue, arthralgia and urticaria preceded each episode. He recovered quickly within 3 d from the last episode of meningitis with corticosteroids and without antibiotics. The patient developed severe chronic hemolysis after the first meningitidis episode.

Laboratory examinations

C reactive protein levels were mildly elevated at 20 mg/L. Examination of lumbar cerebrospinal fluid showed 307 polymorphonuclear leukocytes/mm^3. No bacteria, fungi, viruses or mycobacteria were identified, nor were autoantibodies. A biopsy from one urticarial lesion revealed mixed inflammatory (neutrophils and monocytes) infiltrate. Flow cytometric analysis of both erythrocytes and granulocytes indicated deficiency of GPI-anchored proteins (Figure 1); complement system dosing showed a normal CH50 Level. Factor H and Factor I plasma concentrations and anti-Factor H antibodies were also normal. Examination of cellular morphology based on bone marrow aspiration revealed multilineage dysplasia with no excess blasts (< 2%). Medullar cytogenetic analysis detected a 20q deletion in the karyotype, and Sanger sequencing highlighted a deletion of 4 nucleotides (NM_015937.6:c.766_769del) in exon 6 (p. Lys256ThrfsTer38) leading to a frameshift and a premature stop codon. This mutation was found in the heterozygous state in both T lymphocytes and in the negative cellular fraction, suggesting a constitutional anomaly. These results were confirmed using another sample consisting of DNA extracted from fibroblast culture cells collected after skin biopsy. This finding is reported only once in the ClinVar database (RCV000735856.1). According to the CGH array, we detected a large somatic deletion of 18 Mb from 20q11.21 to 20q13.13, an area including the entire PIGT gene. This 20q deletion associated with heterozygous constitutional mutation of PIGT leads to biallelic inactivation of the gene (Figure 2).

Imaging examinations

Cerebral magnetic resonance imaging results were normal.

FINAL DIAGNOSIS

PIGT-PNH.

TREATMENT

All the patient's symptoms, including urticaria, arthralgia, headache/meningitidis and hemolysis, completely disappeared after eculizumab was administered regularly. Finally, after 8 mo on eculizumab treatment, the pancytopenia worsened (hemoglobin 90 g/L, platelets 67.10^9/L and leukocytes 1.10^9/L), and the patient presented a sepsis secondary to a catheter-related bacteriemia of staphylococcus epidermidis resistant to methicillin. Bone marrow tests revealed 8% blast. We decided to transplant the patient because of the episode of severe infection and bone marrow smear results. The decision of transplantation was difficult, because in common PNH caused by mutation of PIGA, there is a high risk of developing GVHD, especially in patients older than 40-years-old with no sibling donors. No data were available about transplantation in PNH caused by mutation of PIGT, and our patient had no sibling or matched unrelated donors. However, recent retrospective studies demonstrated promising results with HLA-mismatched/haploidentical hematopoietic stem cell transplantation after reduced intensity conditioning and GVHD prophylaxis with post-Transplant cyclophosphamide in refractory severe aplastic anemia patients. Moreover, inflammatory symptoms in our patient were totally controlled by eculizumab. We hypothesized that it could be a good time for transplantation. Therefore, allogeneic hematopoietic stem cell transplantation with peripheral blood stem cells from an HLA-mismatched unrelated donor was carried out after a reduced-intensity conditioning regimen consisting of thiotepa (5 mg/m^2 at day -7), a total fludarabine dose of 150 mg/m^2 (30 mg/m^2 from day -5 to day -1), and total intravenous (i.v.) busulfan 6.4 mg/kg (3.2 mg/kg/d on days -4 and -3). Graft *vs* host disease (GvHD) prophylaxis consisted of posttransplant cyclophosphamide (50 mg/kg/j on days +3 and +4), cyclosporine A (starting on day +5 at 3 mg/kg/day) as a continuous i.v. infusion, and i.v. MMF (starting on day +5 at 15 mg/kg every 12 h). A dose of 6×10^6 CD34$^+$/kg body weight was infused.

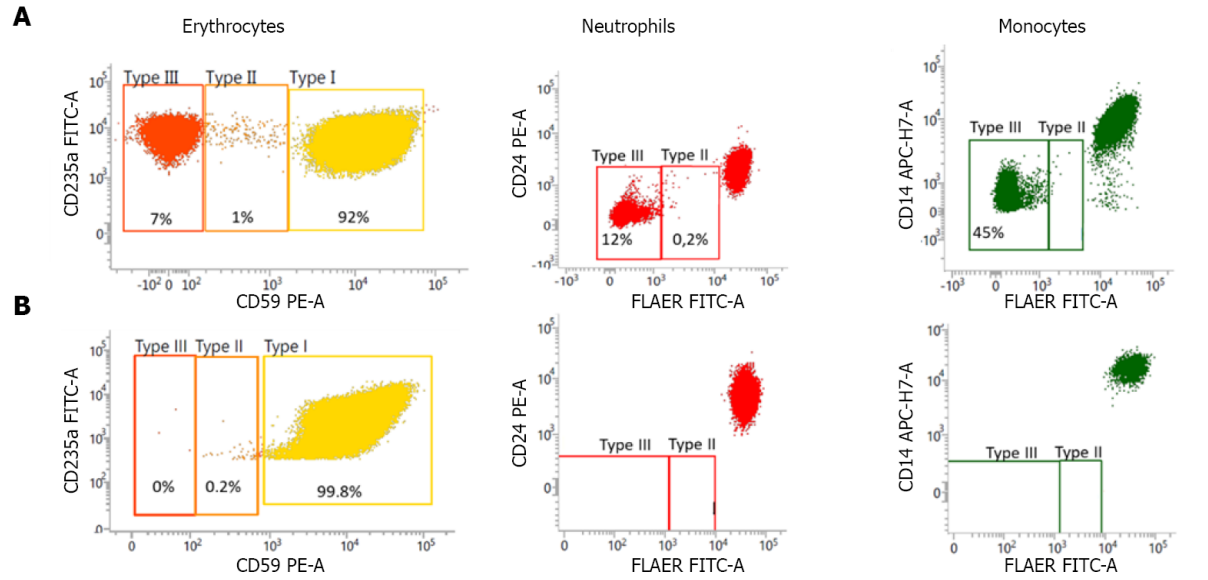

DOI: 10.12998/wjcc.v10.i17.5702 **Copyright** ©The Author(s) 2022.

Figure 1 Expression of GPI-anchored proteins in patient peripheral blood cells before and after allo-HSCT. A: Before transplantation: expression of (left) CD59 on red cells, (center) CD24/FLAER on neutrophils, and (right) CD14/FLAER on monocytes. There is a mosaic of cells with normal expression of GPI-anchored proteins and cells with reduced (type II) or completely lacking expression (type III) of GPI-anchored proteins; B: After transplantation, CD59 was expressed on 99.8% of red cells (left), CD24/FLAER on 100% of neutrophils (center) and CD14/FLAER on 100% of monocytes (right).

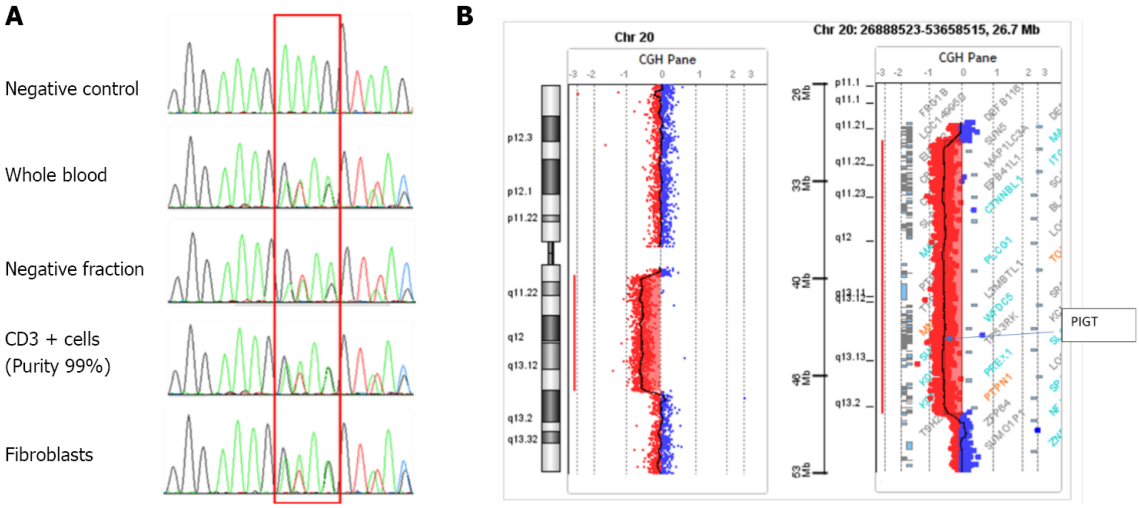

DOI: 10.12998/wjcc.v10.i17.5702 **Copyright** ©The Author(s) 2022.

Figure 2 Genetic analysis. A: Genetic sequencing. Cell sorting was performed on blood samples (*Robosep, Easy sep CD3 whole blood positive selection* kit®). The positive fraction consisted of a T lymphocyte population (purity: 99%), and the negative fraction included B lymphocytes, natural killers, monocytes and polymorphonuclear cells. DNA was extracted from these two fractions using a Qiagen DNA minikit®. The entire *PIGT* gene was sequenced by the Sanger method *(Big Dye Terminator v3.1, Life Technologies*) using primers for each exon; B: CGH array (*Agilent, Sure Print G3 Human CGH Microarray 4x180K*) performed on DNA extracted from bone marrow samples highlights a large somatic deletion of 18 Mb from 20q11.21 to 20q13.13, removing the entire *PIGT* gene.

OUTCOME AND FOLLOW-UP

We observed rapid myeloid engraftment, with a time for neutrophils > 0.5 × 10^9/L and platelet recovery (> 20.10^9/L) of 15 d and 16 d, respectively. Chimerism was complete donor at 1, 3, 12 and 18 mo posttransplant. No acute GvHD was observed. Six months after transplantation, he developed moderate chronic hepatic and skin GvHD that improved by enhancing the calcineurin inhibitor and starting 1 mg/kg/d corticosteroid therapy. At the time of writing, at 24 mo after transplantation, chronic GvHD is in complete remission with no immunosuppressant.

DISCUSSION

PNH is a clonal disorder involving blood cells deficient in glycosylphosphatidylinositol-anchored (GPI-anchored) proteins[1,3], which is often caused by a deficient initial step in GPI anchor synthesis, as catalyzed by the GPI-GlcNAc transferase encoded by the X-chromosomal gene *PIGA*[4-6]. However, 22 *PIG* genes participate in the biosynthesis and protein attachment of GPI[7,8]. The *PIGT* gene on chromosome 20, at position 20q13.12 with 12 exons, encodes phosphatidylinositol-glycan biosynthesis class T protein (PIG-T), a subunit of the heteropentameric GPI transamidase complex that facilitates attachment of GPI anchors to proteins[9]. Four cases of PHN with recurrent inflammatory symptoms have been reported[2] with PIGT defects and successfully treated with eculizumab. In 2013, PNH due to 2 mutation events was reported: a germline splice site mutation and a somatic deletion in *PIGT* (c.1401-2A>G), as identified by next-generation sequencing[10]. In 2018, a second patient with long-term severe urticaria and joint pain before developing PNH harbored similar mutations in *PIGT* (c.250G>T) and exhibited recurrent aseptic meningitis in addition to inflammatory symptoms[11]. Both cases clearly improved with eculizumab treatment. In 2019, 2 additional patients with PHN and inflammatory symptoms were reported: one had chronic lymphocytic leukemia, and the other carried the *JAK2*-V617F mutation. Both patients harbored germline mutations in one *PIGT* allele (one patient with c.761_764delGAAA and the other with c.197delA) associated with somatic deletions, including the entire *PIGT* gene in the second allele without *PIGA* gene abnormalities[2]. In known cases of PHN with *PIGT* disruption, one of the *PIGT* alleles is removed due to a somatic deletion of varying size, including the common deleted region (CDR) of 1.9 Mb, which is close to the centromeric region, often described in myeloid malignancies with 20q deletion. Based on a family segregation study, *PIGT* haploinsufficiency is not sufficient for the development of autoinflammatory symptoms. In our case, the development of MDS with 20q deletion was an indispensable additional abnormality resulting in biallelic inactivation of *PIGT*, explaining the PNH. If mutations in both *PIGA* and *PIGT* can induce PNH, recurrent inflammatory symptoms, including meningitis, are in particular found with *PIGT* mutations. Therefore, some authors have proposed creating a new entity named PIGT-PHN[2]. In PNH-PIGT syndrome, cytokine dosing suggests that increased free GPI might over activate NLRP3 inflammasomes in mononuclear cells with strong IL-1β and IL-18 responses. IL-18 is produced by activated inflammasomes[12,13] and is also produced during clinical GvHD. NLRP3 is known to play a role in enhancing GvHD[14]. Our case report is the fifth published case of PIGT-PNH. Among 4 patients previously described, 3 patients were partially controlled with corticosteroids, colchicine, diphenhydramine, cromoglycin, azathioprine, mycophenolate mofetil, dapsone, anakinra and canakinumab. Only eculizumab treatment abrogates autoinflammation for one patient. We confirm that eculizumab is the best treatment to abrogate intravascular hemolysis and autoinflammation. Because we know that complement activation and inflammatory dysregulation before allo-SCT might be associated to a higher incidence of severe acute GvHD in patients, our main concern was about the toxicity of this procedure. We report fort the first time that allogeneic hematopoietic stem cell transplantation is a readily feasible procedure with no excess alloreactivity or toxicity.

CONCLUSION

Allogeneic stem cell transplantation has not been reported for treating PIGT-PNH, yet this therapy addresses the concern regarding a high risk of alloreactivity and toxicity in patients with activated NLRP3 inflammasomes in mononuclear cells. Our case is the first to be successfully treated with allo-SCT, and no toxicity (especially GvHD) was observed.

ACKNOWLEDGEMENTS

We thank the patient for his full consent.

FOOTNOTES

Author contributions: D'Aveni M provided the concept and design and reviewed and revised the manuscript; Schenone L wrote the manuscript; Schenone L, Notarantonio AB, Latger-Cannard V, Fremeaux-Bacchi V, De Carvalho-Bittencourt M and Muller M performed the analysis; Detrait M, Rubio MT, D'Aveni M took care of the patient; Rubio MT and Muller M revised the manuscript.

Informed consent statement: Informed written consent was obtained from the patient.

Conflict-of-interest statement: The authors declare no competing financial interests.

CARE Checklist (2016) statement: The authors have read the CARE Checklist (2016), and the manuscript was prepared and revised according to the CARE Checklist (2016).

Open-Access: This article is an open-access article that was selected by an in-house editor and fully peer-reviewed by external reviewers. It is distributed in accordance with the Creative Commons Attribution NonCommercial (CC BY-NC 4.0) license, which permits others to distribute, remix, adapt, build upon this work non-commercially, and license their derivative works on different terms, provided the original work is properly cited and the use is non-commercial. See: https://creativecommons.org/Licenses/by-nc/4.0/

Country/Territory of origin: France

ORCID number: Laurence Schenone 0000-0002-6006-4917; Anne-Béatrice Notarantonio 0000-0002-7939-9477; Véronique Latger-Cannard 0000-0002-2831-1850; Veronique Fremeaux-Bacchi 0000-0002-4865-8528; Marcelo De Carvalho-Bittencourt 0000-0002-2698-2458; Marie-Thérèse Rubio 0000-0003-3732-5442; Marc Muller 0000-0002-7190-7684; Maud D'Aveni 0000-0002-5909-2742.

S-Editor: Wu YXJ
L-Editor: Filipodia
P-Editor: Wu YXJ

REFERENCES

1 **Brodsky RA**. Advances in the diagnosis and therapy of paroxysmal nocturnal hemoglobinuria. *Blood Rev* 2008; **22**: 65-74 [PMID: 18063459 DOI: 10.1016/j.blre.2007.10.002]
2 **Höchsmann B**, Murakami Y, Osato M, Knaus A, Kawamoto M, Inoue N, Hirata T, Murata S, Anliker M, Eggermann T, Jäger M, Floettmann R, Höllein A, Murase S, Ueda Y, Nishimura JI, Kanakura Y, Kohara N, Schrezenmeier H, Krawitz PM, Kinoshita T. Complement and inflammasome overactivation mediates paroxysmal nocturnal hemoglobinuria with autoinflammation. *J Clin Invest* 2019; **129**: 5123-5136 [PMID: 31430258 DOI: 10.1172/JCI123501]
3 **Bessler M**, Mason P, Hillmen P, Luzzatto L. Somatic mutations and cellular selection in paroxysmal nocturnal haemoglobinuria. *Lancet* 1994; **343**: 951-953 [PMID: 7909012 DOI: 10.1016/s0140-6736(94)90068-x]
4 **Takahashi M**, Takeda J, Hirose S, Hyman R, Inoue N, Miyata T, Ueda E, Kitani T, Medof ME, Kinoshita T. Deficient biosynthesis of N-acetylglucosaminyl-phosphatidylinositol, the first intermediate of glycosyl phosphatidylinositol anchor biosynthesis, in cell lines established from patients with paroxysmal nocturnal hemoglobinuria. *J Exp Med* 1993; **177**: 517-521 [PMID: 8426120 DOI: 10.1084/jem.177.2.517]
5 **Takeda J**, Miyata T, Kawagoe K, Iida Y, Endo Y, Fujita T, Takahashi M, Kitani T, Kinoshita T. Deficiency of the GPI anchor caused by a somatic mutation of the PIG-A gene in paroxysmal nocturnal hemoglobinuria. *Cell* 1993; **73**: 703-711 [PMID: 8500164 DOI: 10.1016/0092-8674(93)90250-t]
6 **Miyata T**, Takeda J, Iida Y, Yamada N, Inoue N, Takahashi M, Maeda K, Kitani T, Kinoshita T. The cloning of PIG-A, a component in the early step of GPI-anchor biosynthesis. *Science* 1993; **259**: 1318-1320 [PMID: 7680492 DOI: 10.1126/science.7680492]
7 **Wang K**, Li M, Hakonarson H. ANNOVAR: functional annotation of genetic variants from high-throughput sequencing data. *Nucleic Acids Res* 2010; **38**: e164 [PMID: 20601685 DOI: 10.1093/nar/gkq603]
8 **Kinoshita T**, Fujita M, Maeda Y. Biosynthesis, remodelling and functions of mammalian GPI-anchored proteins: recent progress. *J Biochem* 2008; **144**: 287-294 [PMID: 18635593 DOI: 10.1093/jb/mvn090]
9 **Ohishi K**, Inoue N, Kinoshita T. PIG-S and PIG-T, essential for GPI anchor attachment to proteins, form a complex with GAA1 and GPI8. *EMBO J* 2001; **20**: 4088-4098 [PMID: 11483512 DOI: 10.1093/emboj/20.15.4088]
10 **Krawitz PM**, Höchsmann B, Murakami Y, Teubner B, Krüger U, Klopocki E, Neitzel H, Hoellein A, Schneider C, Parkhomchuk D, Hecht J, Robinson PN, Mundlos S, Kinoshita T, Schrezenmeier H. A case of paroxysmal nocturnal hemoglobinuria caused by a germline mutation and a somatic mutation in PIGT. *Blood* 2013; **122**: 1312-1315 [PMID: 23733340 DOI: 10.1182/blood-2013-01-481499]
11 **Kawamoto M**, Murakami Y, Kinoshita T, Kohara N. Recurrent aseptic meningitis with *PIGT* mutations: a novel pathogenesis of recurrent meningitis successfully treated by eculizumab. *BMJ Case Rep* 2018; **2018** [PMID: 30262533 DOI: 10.1136/bcr-2018-225910]
12 **Barker BR**, Taxman DJ, Ting JP. Cross-regulation between the IL-1β/IL-18 processing inflammasome and other inflammatory cytokines. *Curr Opin Immunol* 2011; **23**: 591-597 [PMID: 21839623 DOI: 10.1016/j.coi.2011.07.005]
13 **Dinarello CA**. Immunological and inflammatory functions of the interleukin-1 family. *Annu Rev Immunol* 2009; **27**: 519-550 [PMID: 19302047 DOI: 10.1146/annurev.immunol.021908.132612]
14 **Koehn BH**, Apostolova P, Haverkamp JM, Miller JS, McCullar V, Tolar J, Munn DH, Murphy WJ, Brickey WJ, Serody JS, Gabrilovich DI, Bronte V, Murray PJ, Ting JP, Zeiser R, Blazar BR. GVHD-associated, inflammasome-mediated loss of function in adoptively transferred myeloid-derived suppressor cells. *Blood* 2015; **126**: 1621-1628 [PMID: 26265697 DOI: 10.1182/blood-2015-03-634691]

World Journal of Clinical Cases

Submit a Manuscript: https://www.f6publishing.com

World J Clin Cases 2022 June 16; 10(17): 5708-5716

DOI: 10.12998/wjcc.v10.i17.5708

ISSN 2307-8960 (online)

CASE REPORT

Gray zone lymphoma effectively treated with cyclophosphamide, doxorubicin, vincristine, prednisolone, and rituximab chemotherapy: A case report

Nobumasa Hojo, Makoto Nagasaki, Yasuha Mihara

Specialty type: Hematology

Provenance and peer review: Unsolicited article; Externally peer reviewed.

Peer-review model: Single blind

Peer-review report's scientific quality classification

Grade A (Excellent): 0
Grade B (Very good): 0
Grade C (Good): C
Grade D (Fair): D
Grade E (Poor): 0

P-Reviewer: Chuang SS, Taiwan; Pan H, China

Received: December 11, 2021
Peer-review started: December 11, 2021
First decision: February 8, 2022
Revised: March 8, 2022
Accepted: April 3, 2022
Article in press: April 3, 2022
Published online: June 16, 2022

Nobumasa Hojo, Department of General Medicine, National Hospital Organization Hamada Medical Center, Hamada City 697-8511, Shimane, Japan

Makoto Nagasaki, Department of Pathology, National Hospital Organization Hamada Medical Center, Hamada City 697-8511, Shimane, Japan

Yasuha Mihara, Clinical Resident, National Hospital Organization Hamada Medical Center, Hamada City 697-8511, Shimane, Japan

Corresponding author: Nobumasa Hojo, MD, PhD, Chief Physician, Department of General Medicine, National Hospital Organization Hamada Medical Center, Asai-cho 777-12, Hamada City 697-8511, Shimane, Japan. hojo.nobumasa.qw@mail.hosp.go.jp

Abstract

BACKGROUND

B-cell lymphoma, unclassifiable, with features intermediate between diffuse large B-cell lymphoma and classical Hodgkin lymphoma (BCLu-DLBCL/cHL), also referred to as gray zone lymphoma (GZL), is known to share features with cHL and DLBCL. However, GZL is often difficult to diagnose. There is no consensus regarding the optimal therapeutic regimen. Most reported cases of GZL have been in Caucasian and Hispanic individuals, and its incidence is lower in African-American and Asian populations, including the Japanese population.

CASE SUMMARY

A 69-year-old female presented at our hospital with a growing mass on the right side of her neck. An elastic, soft mass measuring 9 cm × 6 cm was palpable in the right cervical region. Laboratory analyses showed pancytopenia, increased serum lactate dehydrogenase levels, and markedly increased levels of soluble interleukin-2 receptor. Enhanced computed tomography (CT) and fluorodeoxy-glucose positron emission tomography (PET)/CT revealed multiple lesions throughout her body. She was diagnosed with GZL based on the characteristic pathological findings, the immunophenotype [CD20+, PAX5+, OCT2+/BOB1 (focal+), CD30+, CD15-], and the strong positive expression of neoplastic programmed cell death protein ligand 1 (PD-L1) in her lymphoma cells. The lymphoma was stage IV according to the Lugano classification and high-risk according to the International Prognostic Index for aggressive non-Hodgkin

lymphoma. The patient received cyclophosphamide, doxorubicin, vincristine, prednisolone, and rituximab (R-CHOP) chemotherapy because the tumor cells were CD20+. She has remained in complete remission for 3 years.

CONCLUSION
GZL was diagnosed based on histopathology and immunophenotyping with ancillary PD-L1 positivity. R-CHOP chemotherapy was an effective treatment.

Key Words: Classical Hodgkin lymphoma; Diffuse large B-cell lymphoma; Gray zone lymphoma; Programmed cell death protein ligand 1; R-CHOP; Case report

©The Author(s) 2022. Published by Baishideng Publishing Group Inc. All rights reserved.

Core Tip: The incidence of B-cell lymphoma, unclassifiable, with features intermediate between diffuse large B-cell lymphoma and classical Hodgkin lymphoma (BCLu-DLBCL/cHL), also known as gray zone lymphoma (GZL), is low in Asian populations. A patient presented with right-sided cervical lymph node enlargement. The patient was diagnosed based on the characteristic pathological findings, the immunophenotype [CD20+, PAX5+, OCT2+/BOB1 (focal+), CD30+, CD15-], and the strong positive expression of neoplastic programmed cell death protein ligand 1 in her lymphoma cells. There is no consensus regarding the optimal therapeutic regimen for GZL. The addition of rituximab to the chemotherapy regimen should be considered if the tumor cells are CD20+. The patient was successfully treated with the cyclophosphamide, doxorubicin, vincristine, prednisolone, and rituximab regimen and has remained in complete remission for 3 years.

Citation: Hojo N, Nagasaki M, Mihara Y. Gray zone lymphoma effectively treated with cyclophosphamide, doxorubicin, vincristine, prednisolone, and rituximab chemotherapy: A case report. *World J Clin Cases* 2022; 10(17): 5708-5716
URL: https://www.wjgnet.com/2307-8960/full/v10/i17/5708.htm
DOI: https://dx.doi.org/10.12998/wjcc.v10.i17.5708

INTRODUCTION

B-cell lymphoma, unclassifiable, with features intermediate between diffuse large B-cell lymphoma and classical Hodgkin lymphoma (BCLu-DLBCL/cHL), also referred to as GZL, was first recognized in the World Health Organization (WHO) classification of lymphoid neoplasms in 2008[1,2]. The recognition of the disease as a distinct pathological and clinical entity has increased, although its diagnosis remains complex[3]. The diagnostic category was formally included in the WHO classification, which defined the histological and immunophenotypic criteria. In general, GZL tends to have a more aggressive clinical course and is associated with poorer outcomes than either cHL or primary mediastinal large B-cell lymphoma (PMBL). The application of rituximab chemotherapy appears to be beneficial for improving GZL patient outcomes [4,5].

Here, we report the case of a patient with GZL, which is rare in Asian populations[6-9], who was successfully treated with cyclophosphamide, doxorubicin, vincristine, prednisolone, and rituximab (R-CHOP) chemotherapy.

CASE PRESENTATION

Chief complaints

A 69-year-old female presented at the surgical outpatient department of our hospital with a growing mass on the right side of her neck.

History of present illness

The patient was admitted to the hospital for further examination and treatment. The patient had no B symptoms, such as fever, night sweats, or weight loss.

History of past illness

The patient had a past medical history of subarachnoid hemorrhage resulting in the impairment of

higher cognitive functions at 61 years of age.

Personal and family history

There was no personal history of tobacco or alcohol consumption or any other family medical history.

Physical examination

Anemia was suspected based on the color of the palpebral conjunctiva. An elastic, soft mass measuring 9 cm × 6 cm was palpable in the right cervical region. Other superficial lymph nodes and the liver and spleen were not palpable. An increased bleeding tendency was not observed.

Laboratory examinations

Laboratory analyses showed pancytopenia (white blood cells, 1500/μL; red blood cells, 371 × 10^4/μL; hemoglobin, 10.7 g/dL; mean corpuscular volume, 87.3 fL; and platelets, 5.0 × 10^4/μL), increased serum lactate dehydrogenase levels (451 U/L; reference value 124–222 U/L), and markedly increased levels of soluble interleukin-2 receptor (6220 U/mL; reference value 145–519 U/mL).

Imaging examinations

Enhanced CT (Figure 1) and fluorodeoxyglucose PET /CT (Figure 2) revealed multiple lesions throughout the patient's body, including the right neck.

MULTIDISCIPLINARY EXPERT CONSULTATION

Makoto Nagasaki, MD, PhD, Chief of Clinical Laboratory, Department of Pathology, National Hospital Organization Hamada Medical Center

A bone marrow biopsy was obtained from the iliac crest. Fine-needle biopsies were obtained from the right cervical mass (supraclavicular lymph node). Pathological examinations were performed using immunohistochemical (IHC) studies and outsourced flow cytometry (FCM). IHC staining and Epstein–Barr virus (EBV)-encoded small RNA in situ hybridization (EBER-ISH) were performed using standard methods with an automated immunostainer (Ventana Benchmark Ultra, Tucson, AZ, United States). Antibodies against the following markers were used: CD20 (L26, Ventana), CD3 (GV6, Ventana), CD30 (BerH2, Ventana), CD15 (MMA, Ventana), PAX5 (DAKO-Pax5, Dako, Agilent Technologies, Inc., Santa Clara, CA, USA), CD45 (PD7/26,2B11, Nichirei Biosciences, Tokyo, Japan), OCT2 (Oct-207, Leica Biosystems, Wetzlar, Germany), BOB1 (TG14, Leica), CD79a (JCB117, Nichirei), MUM1 (MUM1p, Dako), and ALK (ALK1, Dako). Appropriate positive controls were used for IHC staining. The immunostaining of programmed cell death protein ligand 1 (PD-L1) (clone SP142, Ventana OptiView, Roche) was outsourced.

Histopathological analysis of the iliac crest biopsy revealed hemophagocytosis without bone marrow infiltration. Supraclavicular lymph nodes were infiltrated by large, atypical, and pleomorphic cells (Figure 3). These cells showed sheet-like proliferation and were scattered among the inflammatory cells [small lymphocytes (CD3+ T-cells) and histiocytes]. These large, atypical cells, including Hodgkin and Reed-Sternberg cells or lacunar-like cells, were immunohistochemically positive for CD20, CD79a, CD30, CD45, OCT2, BOB1 (focally), PAX5, and MUM1 but negative for CD15 and ALK. EBV was not detected by EBER-ISH (some of the results are shown in Figure 4). CD20 and PAX5 expression levels were strong, and CD30 expression levels were variable (weak to strong). Nearly 50% of the lymphoma cells were MUM1-positive. As shown in Figure 5, PD-L1 expression (clone SP142) was found in > 75% of the tumor cells (neoplastic PD-L1). Clonal expression of surface and cytoplasmic light chains (sIg and cyIg, respectively) was not detected by FCM (sIg, kappa 12.5%, lambda 12.9%; cyIg, kappa 13.2%, lambda 11.9%). On the other hand, immunoglobulin heavy chain gene rearrangement was detected (data not shown).

FINAL DIAGNOSIS

The patient was diagnosed with stage IV GZL according to the Lugano classification, the International Prognostic Index 4 (high-risk lymphoma) for aggressive non-Hodgkin lymphoma, and the International Prognostic Score 4 for Hodgkin lymphoma.

TREATMENT

The patient was initially treated with a reduced dose (60% of the scheduled dose) of CHOP chemotherapy to prevent tumor lysis syndrome, and it was initially unclear whether the tumor cells

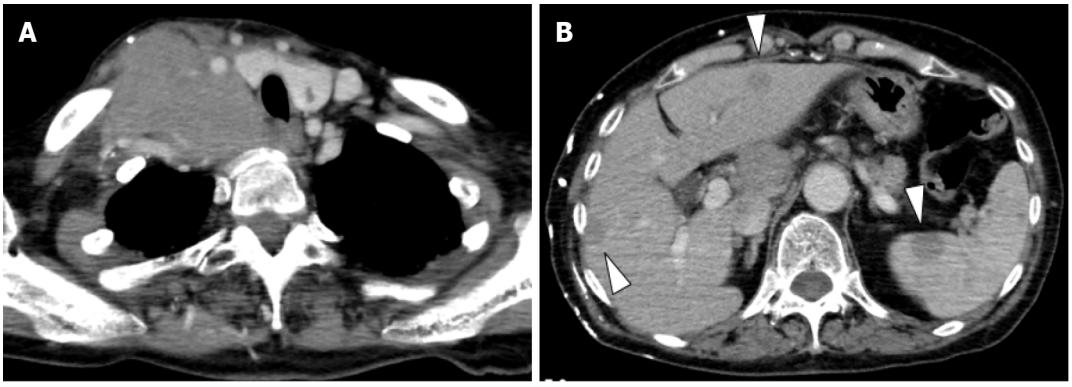

DOI: 10.12998/wjcc.v10.i17.5708 **Copyright** ©The Author(s) 2022.

Figure 1 Enhanced computed tomography showing a right cervical mass (A) and multiple low-density lesions in the liver and spleen (B).

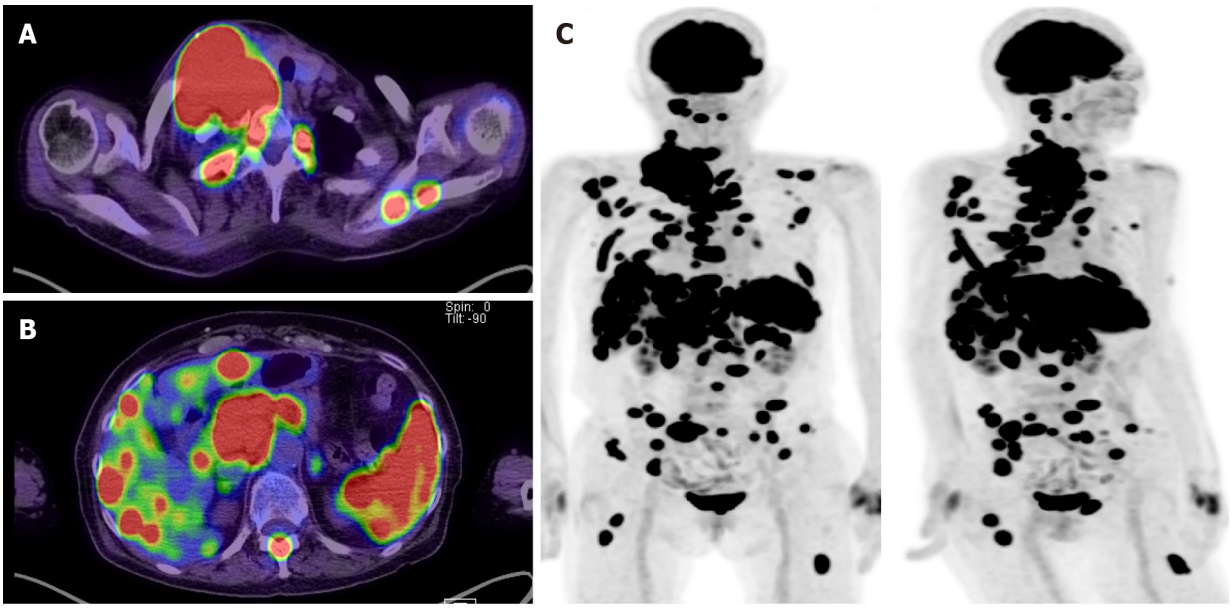

DOI: 10.12998/wjcc.v10.i17.5708 **Copyright** ©The Author(s) 2022.

Figure 2 Fluorodeoxyglucose positron emission tomography/computed tomography revealed multiple lesions throughout the patient's body. A: Abnormal lymph node enlargement in the right neck, right clavicular region, and anterior mediastinum; B: Abnormal lymph node enlargement around the hepatic portal region, pancreatic head, and paraaortic region. Multiple nodular lesions in the liver and spleen; C: Multiple bone lesions in the left skull, thoracic and lumbar vertebrae, bilateral ribs, right clavicle, bilateral scapulae, lower end of the sternum, sacrum, bilateral ilia, left pubis, and bilateral femora.

were CD20-positive. Subsequently, five cycles of R-CHOP chemotherapy were administered at standard doses.

OUTCOME AND FOLLOW-UP

The patient achieved complete remission and has remained in complete remission for 3 years since the last chemotherapy session.

DISCUSSION

GZL is known to share features with cHL and DLBCL; however, it is often difficult to diagnose[10]. The differential diagnosis of the present case included DLBCL [common DLBCL with CD30 expression and anaplastic variant DLBCL (avDLBCL)], T-cell/histiocyte-rich large B-cell lymphoma (THRLBCL), PMBL, and cHL.

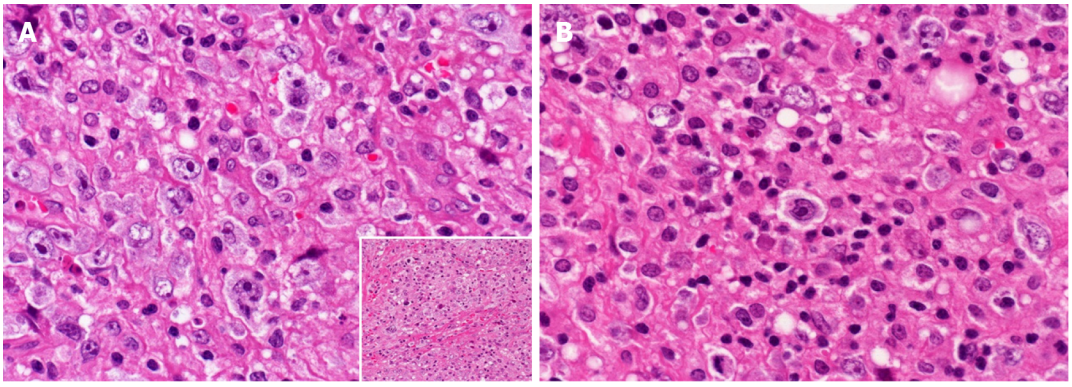

DOI: 10.12998/wjcc.v10.i17.5708 **Copyright** ©The Author(s) 2022.

Figure 3 Large lymphoma cells in the biopsied right supraclavicular lymph node. A: Sheet-like growth of atypical and pleomorphic cells and centroblastic cells (× 400). Inset: Fibrosis around the sheets of lymphoma cells (× 20); B: Large, atypical cells with some retracted pale cytoplasm scattered among the inflammatory cells (× 400).

Regarding the clinical manifestations, the patient had an elastic, soft mass in the right cervical region. Enhanced CT and fluorodeoxyglucose PET/CT revealed abnormal lymph node enlargement in the right neck, right clavicular region, and anterior mediastinum. Multiple lesions in the lymph nodes throughout the body, including the liver, spleen, and multiple bones, were also found. DLBCL involves nodal or extranodal lesions in any location, including the liver, spleen, and bone marrow[11]. THRLBCL mainly involves the lymph nodes, but bone marrow, liver, and spleen involvement is frequently found [12]. CHL also involves the liver, spleen, and bone marrow[13]. PMBL usually lacks bone marrow lesions[14]. Therefore, PMBL was excluded from the differential diagnosis. The most common presentation of GZL is a large anterior mediastinal mass, with or without the involvement of supraclavicular lymph nodes. The tumor may spread directly to the lung, and spread to the liver, spleen, and bone marrow can also be observed[5].

Pathologically, the distribution of large, atypical cells, including centroblastic cells and lacunar-like cells, varied from sheet-like to scattered (with predominantly sheet-like proliferation). Except for the moderate expression of MUM1, the immunophenotype of the tumor cells [positive for CD30 (variable expression) and CD20 (diffuse, strong expression), and negative for CD15] was compatible with the diagnosis of consensus-confirmed GZL but not with cHL[10]. The Lymphoma Study Association has proposed a classification system for GZL with four subcategories based on the morphological and phenotypical spectrum[15]. According to this classification system, the patient's tumor was categorized into the transitional group of cHL-like GZL and large B-cell lymphoma-like GZL. The FCM analysis of the same pathologic specimen did not detect clonal sIg and cyIg expression, although CD20+ B-cells represented a minor population in the gated fraction. Kappa or lambda Ig expression in large tumor cells cannot be estimated by IHC due to background staining. Strong nuclear expression of OCT2 was present in > 50% of the cells; on the other hand, most of the cells were weak to faintly positive for BOB1 (Figure 4E and F), with strong expression observed in only 7.5% (Figure 4E and F, inserted). As previously reported, positive evaluation of OCT2 and BOB1 was based on at least 30% of large tumor cells[16-18], and in one study, strong staining intensity was also a condition[17]. Thus, we interpreted the focal positive BOB1 expression as abnormal in the present case. The focal expression of BOB1 and lack of detectable clonal expression of sIg and cyIg in the FCM analysis were possibly related to abnormal regulation of immunoglobulin expression, similar to cHL but not ordinal DLBCL. The findings were not compatible with the diagnosis of THRLBCL due to the presence of a sheet-like growth area and the positive expression of CD30. Because the primary site of the tumor was not considered to be the mediastinum, PMBL was not considered. Because large tumor cells did not display a sinusoidal growth pattern, the diagnosis of avDLBCL was incompatible.

Recently, neoplastic PD-L1 has been found to be a useful marker of GZL[17-20], enabling researchers to differentiate GZL from nodal avDLBCL[18]. We detected abundant PD-L1-positive (clone SP142) large lymphoma cells (75%) without an EBV association (EBER-ISH negative). Tanaka *et al*[20] reported PD-L1 IHC expression (30% cut off) in 77% of GZL cases (10/13). Sakakibara *et al*[21] reviewed PD-L1 expression (clone SP142) and found it to be useful for the diagnosis of GZL (Nodal DLBCL, EBV-negative 0/275 (0%); Nodal GZL, EBV-negative 3/3 (100%); Nodal avDLBCL, EBV-negative 0/11 (0%). Considering these findings, we diagnosed this patient with nodal GZL.

GZL can be divided into mediastinal GZL (MGZL) and nonmediastinal GZL (NMGZL) depending on the presence or absence of mediastinal lesions, and there are several clinical differences between these two subtypes. It has been reported that patients with MGZL more commonly have bulky disease than patients with NMGZL. Patients with NMGZL are typically significantly older, have a higher likelihood of bone marrow involvement, more often have extranodal disease sites, and present much more

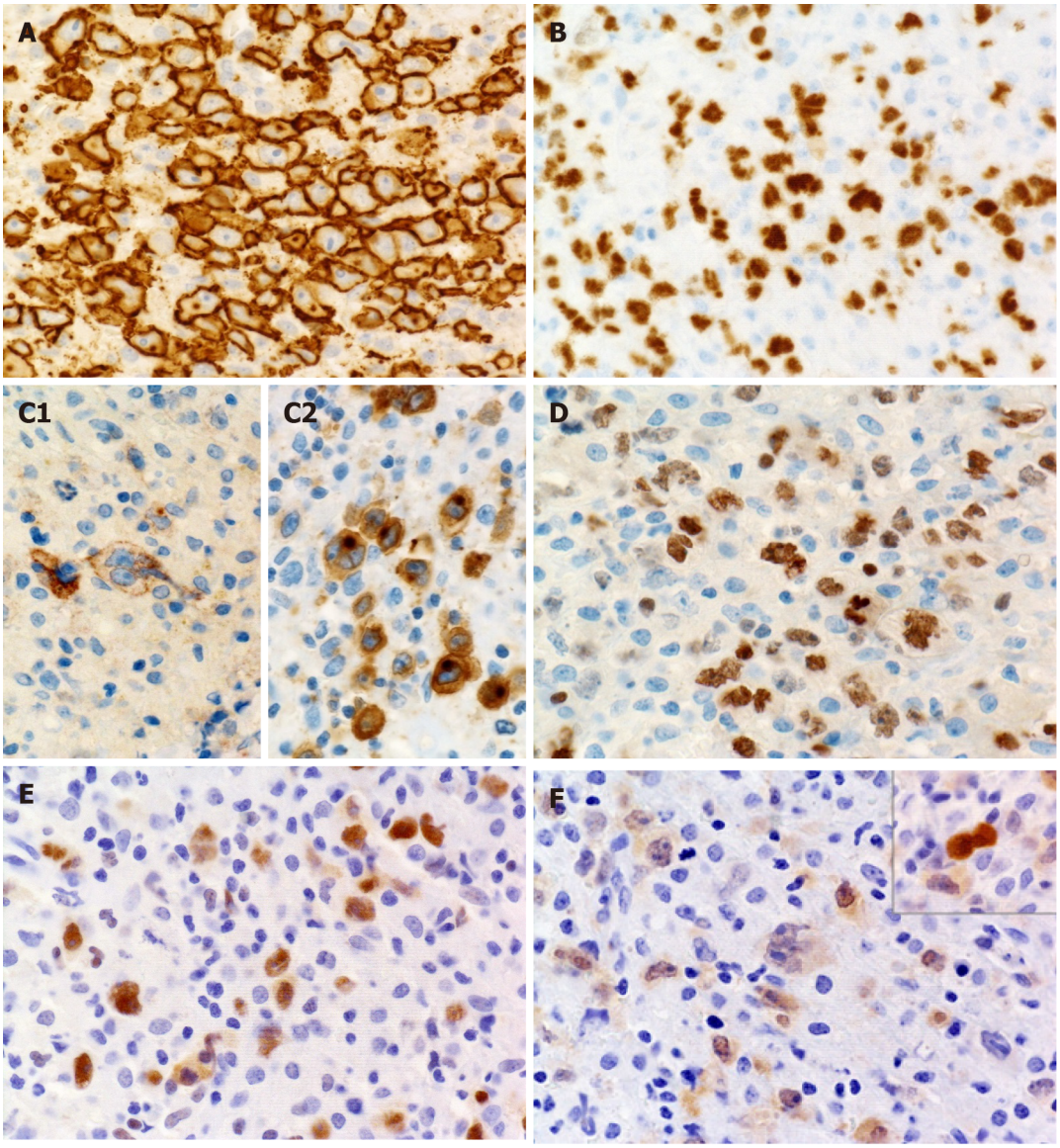

DOI: 10.12998/wjcc.v10.i17.5708 **Copyright** ©The Author(s) 2022.

Figure 4 Immunohistochemical staining of lymphoma cells. A: The cells were strongly and uniformly positive for CD20 (× 400); B: Strongly positive for PAX5 (× 400); C: Variably positive for CD30 [weakly positive (C1) or moderately to strongly positive (C2)] (× 400); D: Moderately to strongly positive for MUM1 (× 400); E: OCT2 was strongly positive for large atypical cells (80%); F: BOB1 strongly positive large atypical cells (inserted) were found in small numbers (< 10%).

commonly with advanced-stage disease[5]. The patient in this case was elderly, had bone marrow involvement, and was diagnosed with advanced-stage disease; therefore, the patient's clinical manifestations were similar to those of NMGZL.

Most reported cases of GZL have been in Caucasian and Hispanic individuals, and its incidence is lower in African-American and Asian populations, including the Japanese population[6,7]. Therefore, reporting cases of rare diseases is important, especially when these diseases occur in regions where they are usually not prevalent. This practice aids in investigating the factors underlying the epidemiology of the disease.

According to the National Comprehensive Cancer Network guidelines, aggressive large B-cell lymphoma treatment regimens are preferred for GZL, though there is no consensus regarding the optimal regimen. If the tumor cells are CD20+, the addition of rituximab to the chemotherapy regimen should be considered[22]. R-CHOP or dose-adjusted etoposide, prednisolone, vincristine, cyclophosphamide, doxorubicin, and rituximab (DA-EPOCH-R) regimens are recommended[23-25].

Recently, brentuximab vedotin, an anti-CD30 antibody, has been used to treat Hodgkin lymphoma and CD30-positive lymphoma[9,26,27]. Pembrolizumab, an anti-PD-L1 monoclonal antibody, is also used for patients with refractory GZL[28]. If the response to the abovementioned chemotherapy regimens is poor, tandem high-dose chemotherapy supported by autologous stem cell transplantations and consolidative radiotherapy can be considered[29]. In this case, the tumor cells were CD20+, and the patient was initially treated with one cycle of CHOP followed by five cycles of R-CHOP chemotherapy.

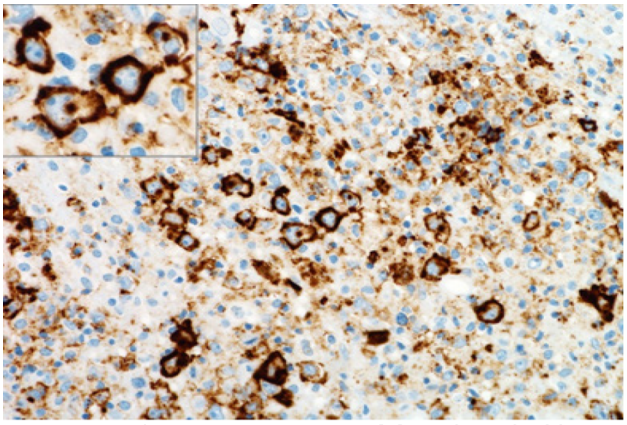

DOI: 10.12998/wjcc.v10.i17.5708 **Copyright** ©The Author(s) 2022.

Figure 5 Programmed cell death protein ligand 1 expression by lymphoma cells. Scattered large lymphoma cells, but not nonlymphoma cells, were strongly positive for programmed cell death protein ligand 1 (clone SP142) (× 200). Insert: Positive staining of the large lymphoma cell membrane was observed (× 400).

She has remained in complete remission for 3 years. These regimens can also be considered for treating recurrent disease.

CONCLUSION

GZL was diagnosed based on histopathology and immunophenotyping with ancillary PD-L1 positivity. R-CHOP chemotherapy was an effective treatment.

FOOTNOTES

Author contributions: Hojo N and Mihara Y were the patient's doctors in charge, reviewed the literature and contributed to manuscript drafting; Nagasaki M was the patient's pathologist, made the pathological diagnosis, reviewed the literature and contributed to manuscript drafting; and All authors issued final approval for this version to be submitted.

Informed consent statement: Written informed consent was obtained from the patient for the publication of this study and any accompanying images.

Conflict-of-interest statement: The authors declare that have no conflicts of interest.

CARE Checklist (2016) statement: The authors have read the CARE Checklist (2016), and the manuscript was prepared and revised according to the CARE Checklist (2016).

Open-Access: This article is an open-access article that was selected by an in-house editor and fully peer-reviewed by external reviewers. It is distributed in accordance with the Creative Commons Attribution NonCommercial (CC BY-NC 4.0) license, which permits others to distribute, remix, adapt, build upon this work non-commercially, and license their derivative works on different terms, provided the original work is properly cited and the use is non-commercial. See: https://creativecommons.org/Licenses/by-nc/4.0/

Country/Territory of origin: Japan

ORCID number: Nobumasa Hojo 0000-0003-0880-0101; Makoto Nagasaki 0000-0002-1344-2364; Yasuha Mihara 0000-0001-8579-3748.

S-Editor: Ma YJ
L-Editor: A
P-Editor: Ma YJ

REFERENCES

1 **Swerdlow SH**, Campo E, Harris NL, Jaffe E, Pileri S, Stein H, Thiele J. WHO classification of tumours of haematopoietic and lymphoid tissues. 4th ed. Lyon: International Agency for Research on Cancer, 2008: 267-268

2 **Campo E**, Swerdlow SH, Harris NL, Pileri S, Stein H, Jaffe ES. The 2008 WHO classification of lymphoid neoplasms and beyond: evolving concepts and practical applications. *Blood* 2011; **117**: 5019-5032 [PMID: 21300984 DOI: 10.1182/blood-2011-01-293050]

3 **Magyari F**, Barna S, Miltényi Z, Rajnai H, Csomor J, Udvardy M, Illés Á, Váróczy L. Histopathological difficulties in an adolescent lymphoma patient. *Pathol Oncol Res* 2015; **21**: 213-217 [PMID: 24985032 DOI: 10.1007/s12253-014-9810-x]

4 **Swerdlow SH**, Campo E, Harris NL, Jaffe E, Pileri S, Stein H, Thiele J. WHO classification of tumours of haematopoietic and lymphoid tissues. Revised 4th ed. Lyon: International Agency for Research on Cancer, 2008: 342-344

5 **Evens AM**, Kanakry JA, Sehn LH, Kritharis A, Feldman T, Kroll A, Gascoyne RD, Abramson JS, Petrich AM, Hernandez-Ilizaliturri FJ, Al-Mansour Z, Adeimy C, Hemminger J, Bartlett NL, Mato A, Caimi PF, Advani RH, Klein AK, Nabhan C, Smith SM, Fabregas JC, Lossos IS, Press OW, Fenske TS, Friedberg JW, Vose JM, Blum KA. Gray zone lymphoma with features intermediate between classical Hodgkin lymphoma and diffuse large B-cell lymphoma: characteristics, outcomes, and prognostication among a large multicenter cohort. *Am J Hematol* 2015; **90**: 778-783 [PMID: 26044261 DOI: 10.1002/ajh.24082]

6 **Iwaki N**, Sato Y, Kurokawa T, Maeda Y, Ohno K, Takeuchi M, Takata K, Orita Y, Nakao S, Yoshino T. B-cell lymphoma, unclassifiable, with features intermediate between diffuse large B-cell lymphoma and classical Hodgkin lymphoma without mediastinal disease: mimicking nodular sclerosis classical Hodgkin lymphoma. *Med Mol Morphol* 2013; **46**: 172-176 [PMID: 23512149 DOI: 10.1007/s00795-013-0038-8]

7 **Shi F**, Zhou Q, Gao Y, Cui XQ, Chang H. Primary splenic B-cell lymphoma, unclassifiable, with features intermediate between diffuse large B-cell lymphoma and classical Hodgkin lymphoma: A case report. *Oncol Lett* 2016; **12**: 1925-1928 [PMID: 27602118 DOI: 10.3892/ol.2016.4840]

8 **Ebisawa K**, Koya J, Shinozaki-Ushiku A, Nakamura F, Kurokawa M. Paraneoplastic limbic encephalitis in B cell lymphoma unclassifiable with features intermediate between diffuse large B cell lymphoma and classical Hodgkin lymphoma. *Ann Hematol* 2016; **95**: 1011-1012 [PMID: 26984106 DOI: 10.1007/s00277-016-2625-y]

9 **Mallipudi RM**, Alquran L, Shenoy VA, Leslie LA, Conti JA. A Rare Case of Grey Zone Lymphoma Successfully Treated with Brentuximab Vedotin and R-CHP Chemotherapy. *Case Rep Oncol Med* 2019; **2019**: 4121234 [PMID: 31110830 DOI: 10.1155/2019/4121234]

10 **Pilichowska M**, Pittaluga S, Ferry JA, Hemminger J, Chang H, Kanakry JA, Sehn LH, Feldman T, Abramson JS, Kritharis A, Hernandez-Ilizaliturri FJ, Lossos IS, Press OW, Fenske TS, Friedberg JW, Vose JM, Blum KA, Jagadeesh D, Woda B, Gupta GK, Gascoyne RD, Jaffe ES, Evens AM. Clinicopathologic consensus study of gray zone lymphoma with features intermediate between DLBCL and classical HL. *Blood Adv* 2017; **1**: 2600-2609 [PMID: 29296913 DOI: 10.1182/bloodadvances.2017009472]

11 **Sehn LH**, Scott DW, Chhanabhai M, Berry B, Ruskova A, Berkahn L, Connors JM, Gascoyne RD. Impact of concordant and discordant bone marrow involvement on outcome in diffuse large B-cell lymphoma treated with R-CHOP. *J Clin Oncol* 2011; **29**: 1452-1457 [PMID: 21383296 DOI: 10.1200/JCO.2010.33.3419]

12 **Abramson JS**. T-cell/histiocyte-rich B-cell lymphoma: biology, diagnosis, and management. *Oncologist* 2006; **11**: 384-392 [PMID: 16614234 DOI: 10.1634/theoncologist.11-4-384]

13 **Shimabukuro-Vornhagen A**, Haverkamp H, Engert A, Balleisen L, Majunke P, Heil G, Eich HT, Stein H, Diehl V, Josting A. Lymphocyte-rich classical Hodgkin's lymphoma: clinical presentation and treatment outcome in 100 patients treated within German Hodgkin's Study Group trials. *J Clin Oncol* 2005; **23**: 5739-5745 [PMID: 16009944 DOI: 10.1200/JCO.2005.17.970]

14 **Barth TF**, Leithäuser F, Joos S, Bentz M, Möller P. Mediastinal (thymic) large B-cell lymphoma: where do we stand? *Lancet Oncol* 2002; **3**: 229-234 [PMID: 12067685 DOI: 10.1016/s1470-2045(02)00714-3]

15 **Sarkozy C**, Copie-Bergman C, Damotte D, Ben-Neriah S, Burroni B, Cornillon J, Lemal R, Golfier C, Fabiani B, Chassagne-Clément C, Parrens M, Herbaux C, Xerri L, Bossard C, Laurent C, Cheminant M, Cartron G, Cabecadas J, Molina T, Salles G, Steidl C, Ghesquières H, Mottok A, Traverse-Glehen A. Gray-zone Lymphoma Between cHL and Large B-Cell Lymphoma: A Histopathologic Series From the LYSA. *Am J Surg Pathol* 2019; **43**: 341-351 [PMID: 30540571 DOI: 10.1097/PAS.0000000000001198]

16 **Gualco G**, Natkunam Y, Bacchi CE. The spectrum of B-cell lymphoma, unclassifiable, with features intermediate between diffuse large B-cell lymphoma and classical Hodgkin lymphoma: a description of 10 cases. *Mod Pathol* 2012; **25**: 661-674 [PMID: 22222636 DOI: 10.1038/modpathol.2011.200]

17 **O'Malley DP**, Fedoriw Y, Weiss LM. Distinguishing Classical Hodgkin Lymphoma, Gray Zone Lymphoma, and Large B-cell Lymphoma: A Proposed Scoring System. *Appl Immunohistochem Mol Morphol* 2016; **24**: 535-540 [PMID: 26447896 DOI: 10.1097/PAI.0000000000000236]

18 **Megahed NA**, Kohno K, Sakakibara A, Eladl AE, Elsayed AA, Wu CC, Suzuki Y, Takahara T, Kato S, Nakamura S, Satou A, Asano N. Anaplastic variant of diffuse large B-cell lymphoma: Reappraisal as a nodal disease with sinusoidal involvement. *Pathol Int* 2019; **69**: 697-705 [PMID: 31872533 DOI: 10.1111/pin.12871]

19 **Kohno K**, Suzuki Y, Harada T, Sakai A, Takeuchi Y, Inagaki Y, Megahed NA, Takahara T, Satou A, Sakakibara A, Nakamura S. Nodal diffuse large B-cell lymphoma with neoplastic PD-L1 positivity, but without EBV association: Three cases highlighting an aspect of gray zone lymphoma. *Pathol Int* 2020; **70**: 695-697 [PMID: 32623805 DOI: 10.1111/pin.12982]

20 **Tanaka Y**, Maeshima AM, Nomoto J, Makita S, Fukuhara S, Munakata W, Maruyama D, Tobinai K, Kobayashi Y. Expression pattern of PD-L1 and PD-L2 in classical Hodgkin lymphoma, primary mediastinal large B-cell lymphoma, and gray zone lymphoma. *Eur J Haematol* 2018; **100**: 511-517 [PMID: 29377256 DOI: 10.1111/ejh.13033]

21 **Sakakibara A**, Kohno K, Ishikawa E, Suzuki Y, Tsuyuki Y, Shimada S, Shimada K, Satou A, Takahara T, Ohashi A, Takahashi E, Kato S, Nakamura S, Asano N. Diagnostic utility of programmed cell death ligand 1 (clone SP142)

immunohistochemistry for malignant lymphoma and lymphoproliferative disorders: A brief review. *J Clin Exp Hematop* 2021; **61**: 182-191 [PMID: 34511582 DOI: 10.3960/jslrt.21003]

22 **NCCN Guidelines for Patients**. Diffuse large b-cell lymphoma, grey zone lymphoma (intermediate between DLBCL and classical HL). Version 2. Plymouth Meeting, PA: NCCN, 2018

23 **Kritharis A**, Pilichowska M, Evens AM. How I manage patients with grey zone lymphoma. *Br J Haematol* 2016; **174**: 345-350 [PMID: 27301470 DOI: 10.1111/bjh.14174]

24 **Chihara D**, Westin JR, Miranda RN, Cheah CY, Oki Y, Turturro F, Romaguera JE, Neelapu SS, Nastoupil LJ, Fayad LE, Rodriguez MA, Fowler NH, Orlowski RZ, Wang M, Hagemeister FB, Medeiros LJ, Fanale MA. Dose adjusted-EPOCH-R and mediastinal disease may improve outcomes for patients with gray-zone lymphoma. *Br J Haematol* 2017; **179**: 503-506 [PMID: 27378601 DOI: 10.1111/bjh.14226]

25 **Simon Z**, Virga B, Pinczés L, Méhes G, Miltényi Z, Barna S, Szabó R, Illés Á. Transition Between Diffuse Large B-Cell Lymphoma and Classical Hodgkin Lymphoma- Our Histopathological and Clinical Experience With Patients With Intermediate Lymphoma. *Pathol Oncol Res* 2021; **27**: 625529 [PMID: 34257590 DOI: 10.3389/pore.2021.625529]

26 **Terao T**, Yuda J, Yamauchi N, Guo YM, Shimada K, Sugano M, Ishii G, Minami Y. Brentuximab vedotin maintenance after autologous stem cell transplantation for refractory gray zone lymphoma with long-term remission. *Mol Clin Oncol* 2021; **14**: 125 [PMID: 33936598 DOI: 10.3892/mco.2021.2287]

27 **Svoboda J**, Bair SM, Landsburg DJ, Dwivedy Nasta S, Nagle SJ, Barta SK, Khan N, Filicko-O'Hara J, Gaballa S, Strelec L, Chong E, Mitnick S, Waite TS, King C, Ballard H, Youngman M, Gerson J, Plastaras JP, Maity A, Bogusz AM, Hung SS, Nakamura H, Nejati R, Steidl C, Lim M, Ruella M, Schuster SJ. Brentuximab vedotin in combination with rituximab, cyclophosphamide, doxorubicin, and prednisone as frontline treatment for patients with CD30-positive B-cell lymphomas. *Haematologica* 2021; **106**: 1705-1713 [PMID: 32414850 DOI: 10.3324/haematol.2019.238675]

28 **Rosales YMZ**, Mesquita JL, Garcia YDO, Paz FRF, Campos NCB, de Vasconcelos Leitão JP, Filho FDR, Filho RVAO, Lemes RPG, Duarte FB. Use of checkpoint inhibitors in gray zone lymphoma. *Hematol Oncol Stem Cell Ther* 2020 [PMID: 32589932 DOI: 10.1016/j.hemonc.2020.06.001]

29 **Takaishi K**, Muto T, Mimura N, Takiguchi J, Nagao Y, Oshima-Hasegawa N, Tsukamoto S, Takeda Y, Mitsukawa S, Takeuchi M, Ohwada C, Ota S, Iseki T, Nakaseko C, Sakaida E. Long-term complete remission following tandem autologous stem cell transplantation and consolidative radiotherapy for refractory mediastinal gray-zone lymphoma. *Int J Hematol* 2018; **108**: 452-455 [PMID: 29786758 DOI: 10.1007/s12185-018-2471-x]

World Journal of Clinical Cases

Submit a Manuscript: https://www.f6publishing.com

World J Clin Cases 2022 June 16; 10(17): 5717-5722

DOI: 10.12998/wjcc.v10.i17.5717

ISSN 2307-8960 (online)

CASE REPORT

Diagnosis of spontaneous isolated superior mesenteric artery dissection with ultrasound: A case report

Yi Zhang, Jiang-Ying Zhou, Jian Liu, Chen Bai

Specialty type: Radiology, nuclear medicine and medical imaging

Provenance and peer review: Unsolicited article; Externally peer reviewed.

Peer-review model: Single blind

Peer-review report's scientific quality classification

Grade A (Excellent): 0
Grade B (Very good): B
Grade C (Good): 0
Grade D (Fair): 0
Grade E (Poor): 0

P-Reviewer: Ghannam WM, Egypt

Received: October 21, 2021
Peer-review started: October 21, 2021
First decision: March 7, 2022
Revised: March 16, 2022
Accepted: April 15, 2022
Article in press: April 15, 2022
Published online: June 16, 2022

Yi Zhang, Jiang-Ying Zhou, Jian Liu, Department of Ultrasound, The First Affiliated Hospital of Chengdu Medical College, Chengdu 610599, Sichuan Province, China

Chen Bai, Department of Radiology, The First Affiliated Hospital of Chengdu Medical College, Chengdu 610599, Sichuan Province, China

Corresponding author: Jian Liu, PhD, Department of Ultrasound, The First Affiliated Hospital of Chengdu Medical College, No. 278 Baoguang Avenue Middle Section, Xindu District, Chengdu 610599, Sichuan Province, China. liujiansh@126.com

Abstract

BACKGROUND

Spontaneous isolated superior mesenteric artery dissection (SISMAD) is a rare disease that originates from the superior mesenteric artery, without the presence of aortic and other arterial dissections. Most cases are diagnosed using contrast-enhanced computed tomography (CECT), whereas the application of ultrasound is less common.

CASE SUMMARY

Here, we report a case of SISMAD with sudden epigastric pain that worsened as the main symptom after eating. The patient had a long history of hypertension with unknown blood pressure control but no history of smoking or alcohol consumption. This case was initially diagnosed using ultrasound and the results were later confirmed by CECT. After admission, the patient fasted, followed by parenteral nutrition support and fluid supplementation to maintain electrolyte and acid–base balance. Metoprolol succinate sustained-release tablets and aspirin were given as nonoperative treatments. After 1 wk, the symptoms improved, and the patient was discharged. During telephone follow-up, the patient did not develop similar symptoms.

CONCLUSION

Whether ultrasound can be used as a routine and noninvasive imaging method for the diagnosis of SISMAD needs further exploration.

Key Words: Abdominal pain; Ultrasound; Spontaneous isolated superior mesenteric artery dissection; Color doppler; Diagnosis; Case report

©The Author(s) 2022. Published by Baishideng Publishing Group Inc. All rights reserved.

Core tip: Spontaneous isolated superior mesenteric artery dissection is a rare disease. Contrast-enhanced computed tomography (CECT) is often the preferred diagnostic method for this disease. The initial diagnosis of this disease by ultrasound is rarely reported. Compared to CECT, ultrasound is a convenient, rapid, noninvasive, inexpensive and feasible bedside imaging method, which can be used to diagnose superior mesenteric artery dissection.

Citation: Zhang Y, Zhou JY, Liu J, Bai C. Diagnosis of spontaneous isolated superior mesenteric artery dissection with ultrasound: A case report. *World J Clin Cases* 2022; 10(17): 5717-5722
URL: https://www.wjgnet.com/2307-8960/full/v10/i17/5717.htm
DOI: https://dx.doi.org/10.12998/wjcc.v10.i17.5717

INTRODUCTION

Spontaneous isolated superior mesenteric artery dissection (SISMAD), first reported in 1947, is a dissection disease arising from the superior mesenteric artery, without aortic and other arterial dissections[1].

Clinical manifestations of SISMAD are atypical. The most common symptoms include sudden persistent or paroxysmal severe abdominal pain, accompanied by other gastrointestinal symptoms. Also, some of the patients are asymptomatic. In addition, clinical and physical examinations reveal no specificity, and no laboratory indicators for SISMAD are currently available[2,3]. SISMAD may directly lead to intestinal ischemic necrosis and arterial rupture, which endangers the life of patients if not treated in a timely manner[4,5]. At present, the diagnosis of SISMAD is mainly dependent on imaging examinations, and contrast-enhanced computed tomography (CECT) and computed tomography angiography (CTA) are most commonly used[6,7]. Ultrasound is rarely used to diagnose SIDSMA. Here, we reported an ultrasound-confirmed SISMAD case without dissecting aneurysm or thrombosis, suggesting that ultrasound could be used in the diagnosis of SISMAD.

CASE PRESENTATION

Chief complaints

A 64-year-old Chinese Han female patient was admitted to the First Affiliated Hospital of Chengdu Medical College on April 27, 2020, due to intermittent pain in the upper abdomen.

History of present illness

Epigastric pain became worse after eating for 3 d.

History of past illness

She had a history of hypertension for > 10 years and was on antihypertensive medication, but her blood pressure control was unknown. The patient received a cardiac pacemaker implant 2 years ago, and was given dabigatran ester (capsules 110 mg bid) as long-term anticoagulant therapy after surgery. She underwent cholecystectomy in the First Affiliated Hospital of Chengdu Medical College due to calculous cholecystitis on March 21, 2019.

Personal and family history

The patient did not have any history of smoking or alcohol consumption.

Physical examination

The blood pressure was 170/110 mmHg at admission.

Laboratory examinations

No other obvious abnormalities were detected based on physical examination and laboratory tests.

Imaging examinations

Abdominal ultrasound was routinely performed since the patient had superior abdominal pain. However, no obvious abnormalities in the liver, pancreas and spleen were observed. Strip echoes were found in the lumen about 1.6 cm from the opening of the superior mesenteric artery distal to the main trunk of the superior mesenteric artery with stripped intima. The arterial lumen was divided into true and false lumen by the exfoliated intima. Ventral false lumen had a large diameter, while that of the

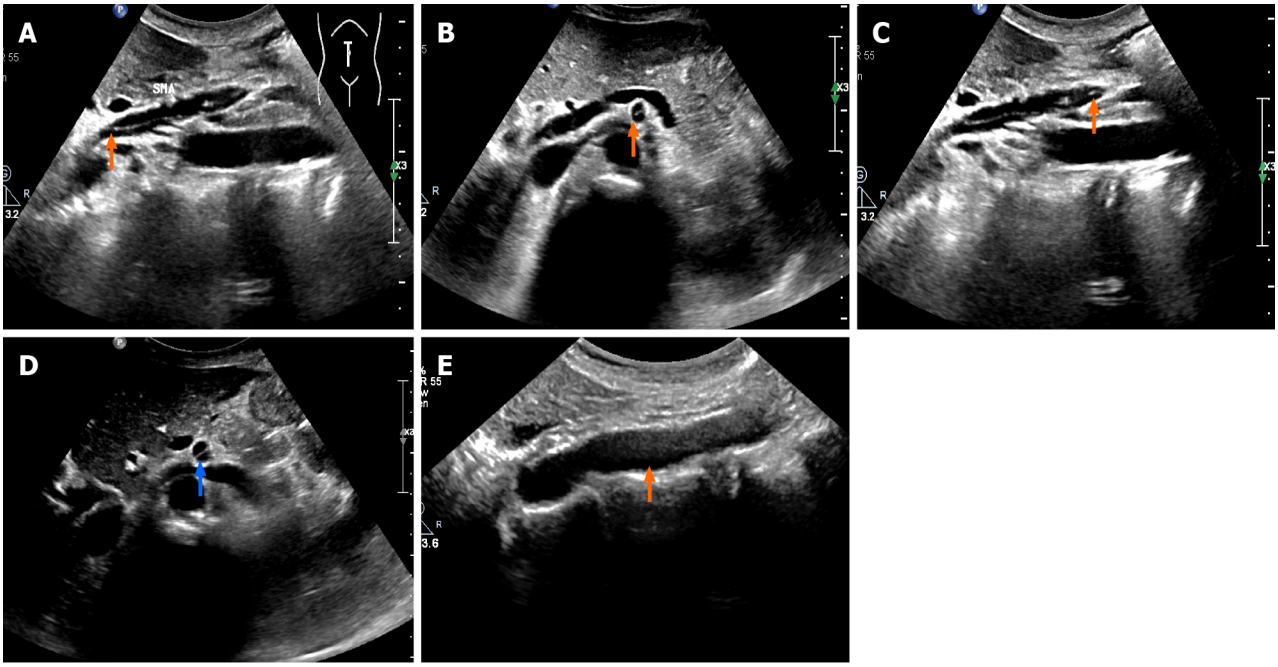

DOI: 10.12998/wjcc.v10.i17.5717 **Copyright** ©The Author(s) 2022.

Figure 1 Gray-scale ultrasound showed the superior mesenteric artery dissection and abdominal aorta. A: Ultrasonic longitudinal view demonstrated the opening of superior mesenteric artery dissection (SISMAD) (orange arrow); B: Transverse view demonstrated the opening of SISMAD (orange arrow); C: Ultrasonic longitudinal view showed the distal end of SISMAD (orange arrow); D: Transverse view showed the distal end of SISMAD (blue arrow); E: No abnormal echo was observed in the abdominal aortic lumen (orange arrow).

dorsal true lumen was small. Lumen sonopenetrability was normal, and no thrombosis was detected. Proximal to the exfoliated intima, a 3-mm wide rupture was observed (Figure 1). Color Doppler imaging showed blood flow passing through the incision. The blood flow in the ventral lumen was dark, while colored blood flow signals were observed in the dorsal lumen. Pulse Doppler was used to assess blood flow velocity in the true lumen (Figure 2).

FINAL DIAGNOSIS

Ultrasonography of the abdominal aorta showed no shed intimal echo (Figure 1), suggesting isolated superior mesenteric artery dissection, which was later confirmed by CECT (Figure 3).

TREATMENT

After admission, the patient fasted, followed by parenteral nutrition support and fluid supplementation to maintain electrolyte and acid–base balance. Metoprolol succinate sustained-release tablets (47.5 mg/d) were given to lower blood pressure, and aspirin (100 mg/d) was given as an antiplatelet treatment.

OUTCOME AND FOLLOW-UP

After 1 wk, the symptoms improved, and the patient was discharged. During telephone follow-up at 1, 3 and 6 mo after discharge, the patient did not experience similar symptoms and did not visit any local medical facility for imaging re-examination.

DISCUSSION

Currently, the most commonly used imaging methods for the diagnosis of SISMAD are CTA and CECT [8], and only a few diagnosed cases have been confirmed by ultrasound[9-12]. In this case report, ordinary grayscale ultrasound could detect the start and end points of the intimal exfoliation in the

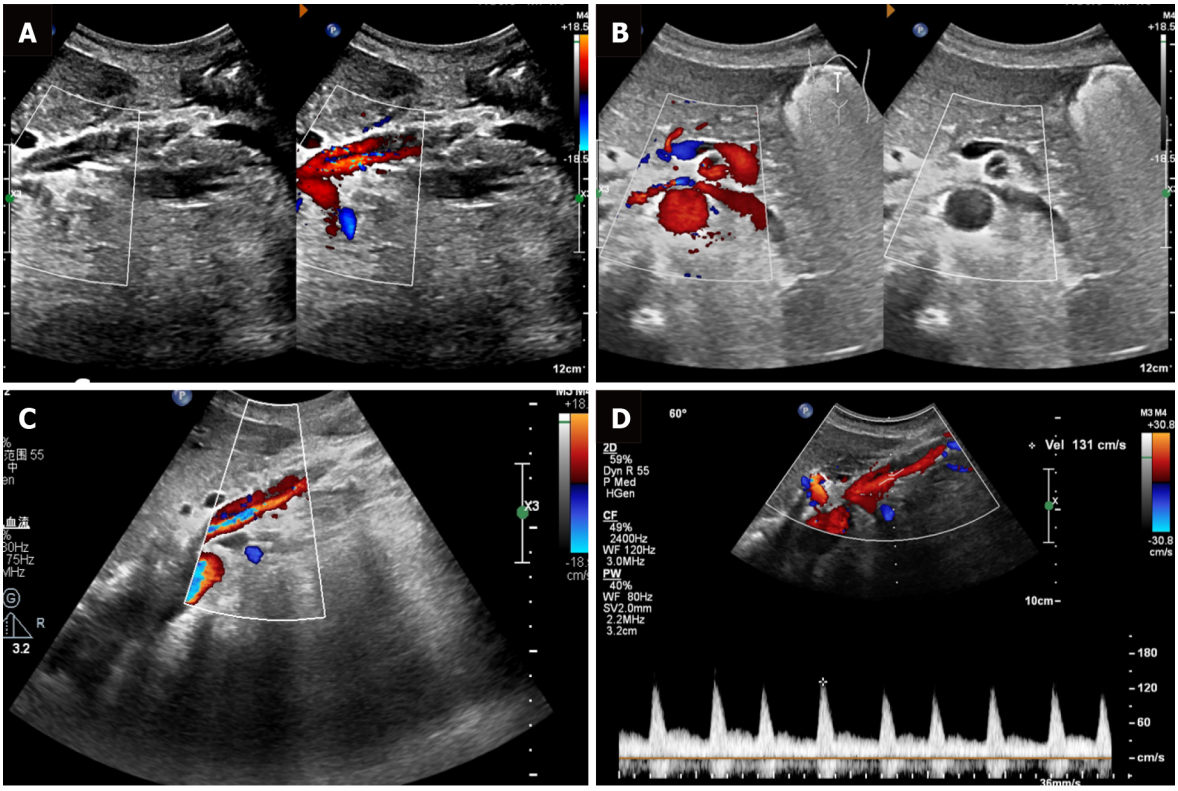

DOI: 10.12998/wjcc.v10.i17.5717 **Copyright** ©The Author(s) 2022.

Figure 2 Doppler ultrasound showed the blood flow of the superior mesenteric artery dissection. A: Ultrasonic longitudinal view showed the flow at the opening of the superior mesenteric artery dissection (SISMAD); B: Ultrasonic transverse view showed the flow at the opening of the SISMAD; C: Color Doppler flow imaging showed the true and false lumens of the SISMAD; D: True lumen velocity of superior mesenteric artery dissection was measured by spectral Doppler.

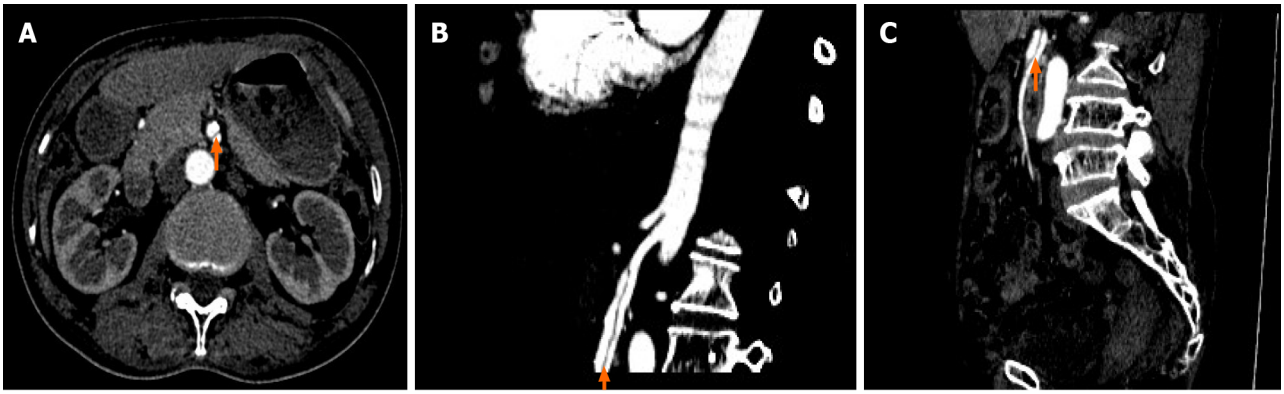

DOI: 10.12998/wjcc.v10.i17.5717 **Copyright** ©The Author(s) 2022.

Figure 3 Contrast enhanced computed tomography (CECT) showed superior mesenteric artery dissection. A: Cross-sectional view of the superior mesenteric artery dissection (SISMAD) (orange arrow) on CECT; B: Sagittal view of proximal SISMAD on CECT (orange arrow); C: Sagittal view of distal SISMAD on CECT (orange arrow).

superior mesenteric artery, the location and number of ruptures, and whether there was thrombus in the lumen. Color Doppler ultrasonography was used to investigate the blood flow through the rupture sites, the blood flow velocity in the true and false lumen, and the filling defect areas caused by thrombus in real time. Yun *et al*[13] classified SISMAD into types I, II (IIa and IIb) and III. In this case, a rupture was detected about 1.6 cm from the opening of the superior mesenteric artery, while its distal end was closed. No thrombosis was detected in either the true or false lumen, and the ultrasound finding was in line with a type IIa SISMAD.

Isolated superior mesenteric artery dissection is a rare disease with unknown etiology. It has been reported that male sex, smoking, atherosclerosis, hypertension, hyperlipidemia, cystic necrosis of the middle artery, and Asian ethnicity might be related to the pathogenesis of SISMAD[14-16]. Among these, hypertension plays a crucial role in the development of arterial dissection. In our case, the patient

had a history of hypertension for > 10 years. Furthermore, SISMAD was a rare acute abdomen with no specific clinical manifestations. The primary symptoms were sudden and severe abdominal pains, mainly epigastric pain[17,18]. Our patient had intermittent pain in the upper abdomen without any specific positive signs. Currently, conservative treatment, endovascular surgery, interventional radiology, and open surgery are therapeutic modalities for patients with SISMAD, but there are no clear recommendations for the treatment of SISMAD[15,16,19,20]. According to current guidelines, SISMAD treatment strategies are designed to control clinical symptoms and prevent complications such as intestinal necrosis. Most studies recommend initial treatment based on clinical presentation at admission. If SISMAD is found accidentally during CTA in other settings, the patient can be carefully observed and treated conservatively[6,21]. Asymptomatic patients receiving conservative treatments do not need secondary interventions[22]. In symptomatic SISMAD patients, EVT may be performed before mesenteric ischemia progresses if clinical symptoms persist. The reconstruction of SMA was significantly improved after EVT, especially for patients with Yun's IIb phenotype[23].

Although CTA or CECT could clearly display and classify the type of superior mesenteric artery dissection, especially small distal branch vessels, there was an issue of contrast agent allergy as patients received a large radiation dose[24]. Ultrasound was simple and easy to perform, radiation free, and repeatable, and could clearly observe the echoes of exfoliated intima, the positions of the rupture and the thrombosis, and hemodynamic changes could be displayed using Doppler ultrasound. Also, bedside examination could be performed when necessary[12,25]. It has also been suggested that early transition to ultrasound imaging exam should be considered in the follow-up of SISMAD patients, which may help to reduce radiation, contrast, and associated costs[17].

CONCLUSION

This case report suggests that ultrasound is a noninvasive examination method for routine screening of SISMAD, which could provide a clinical management basis for the diagnosis and treatment of the disease.

FOOTNOTES

Author contributions: Zhang Y conceived and supervised the study; Zhang Y and Liu J designed experiments; Zhang Y and Bai C performed experiments; Zhang Y, Zhou JY and Bai C analyzed data; Zhang Y wrote the manuscript; Zhang Y and Liu J made manuscript revisions; All authors reviewed the results and approved the final version of the manuscript.

Informed consent statement: Informed consent was obtained from the patient for the publication of the imaging data and other clinical information. The patient understood that her identity would not be disclosed.

Conflict-of-interest statement: The authors have no potential conflicts of interest to disclose.

CARE Checklist (2016) statement: The authors read the CARE Checklist (2016), and the manuscript was prepared and revised according to the CARE Checklist (2016).

Open-Access: This article is an open-access article that was selected by an in-house editor and fully peer-reviewed by external reviewers. It is distributed in accordance with the Creative Commons Attribution NonCommercial (CC BY-NC 4.0) license, which permits others to distribute, remix, adapt, build upon this work non-commercially, and license their derivative works on different terms, provided the original work is properly cited and the use is non-commercial. See: https://creativecommons.org/Licenses/by-nc/4.0/

Country/Territory of origin: China

ORCID number: Yi Zhang 0000-0002-8627-2327; Jiang-Ying Zhou 0000-0002-5236-3861; Jian Liu 0000-0003-2295-8933; Chen Bai 0000-0003-0611-2786.

S-Editor: Liu JH
L-Editor: Kerr C
P-Editor: Liu JH

REFERENCES

1 **Bauersfeld SR**. Dissecting aneurysm of the aorta; a presentation of 15 cases and a review of the recent literature. *Ann Intern Med* 1947; **26**: 873-889 [PMID: 20242656 DOI: 10.7326/0003-4819-26-6-873]

2 **Xu L**, Shao J, Zhang D, Qiu C, Wang J, Li K, Fang L, Zhang X, Lei J, Lai Z, Ma J, Yu Y, Yu X, Du F, Qi W, Chen J, Liu B. Long-term outcomes of conservative treatment and endovascular treatment in patients with symptomatic spontaneous isolated superior mesenteric artery dissection: a single-center experience. *BMC Cardiovasc Disord* 2020; **20**: 256 [PMID: 32471346 DOI: 10.1186/s12872-020-01532-y]

3 **Tanaka Y**, Yoshimuta T, Kimura K, Iino K, Tamura Y, Sakata K, Hayashi K, Takemura H, Yamagishi M, Kawashiri MA. Clinical characteristics of spontaneous isolated visceral artery dissection. *J Vasc Surg* 2018; **67**: 1127-1133 [PMID: 29056349 DOI: 10.1016/j.jvs.2017.08.054]

4 **Kim H**, Park H, Park SJ, Park BW, Hwang JC, Seo YW, Cho HR. Outcomes of Spontaneous Isolated Superior Mesenteric Artery Dissection Without Antithrombotic Use. *Eur J Vasc Endovasc Surg* 2018; **55**: 132-137 [PMID: 29229279 DOI: 10.1016/j.ejvs.2017.11.002]

5 **Karaolanis G**, Antonopoulos C, Tsilimigras DI, Moris D, Moulakakis K. Spontaneous isolated superior mesenteric artery dissection: Systematic review and meta-analysis. *Vascular* 2019; **27**: 324-337 [PMID: 30621507 DOI: 10.1177/1708538118818625]

6 **Kimura Y**, Kato T, Nagao K, Izumi T, Haruna T, Ueyama K, Inada T, Inoko M. Outcomes and Radiographic Findings of Isolated Spontaneous Superior Mesenteric Artery Dissection. *Eur J Vasc Endovasc Surg* 2017; **53**: 276-281 [PMID: 28012909 DOI: 10.1016/j.ejvs.2016.11.012]

7 **Tomita K**, Obara H, Sekimoto Y, Matsubara K, Watada S, Fujimura N, Shibutani S, Nagasaki K, Hayashi S, Harada H, Asami A, Uchida N, Kakefuda T, Kitagawa Y. Evolution of Computed Tomographic Characteristics of Spontaneous Isolated Superior Mesenteric Artery Dissection During Conservative Management. *Circ J* 2016; **80**: 1452-1459 [PMID: 27118619 DOI: 10.1253/circj.CJ-15-1369]

8 **Nath A**, Yewale S, Kousha M. Spontaneous Isolated Superior Mesenteric Artery Dissection. *Case Rep Gastroenterol* 2016; **10**: 775-780 [PMID: 28203123 DOI: 10.1159/000448879]

9 **Ishimura M**, Hayashi R, Shimotsuka H, Ogawa K, Iuchi K. A case of isolated superior mesenteric artery dissection evaluated clinical course by ultrasonography. *ChoonpaIgaku* 2008; **35**: 191-195 [DOI: 10.3179/jjmu.35.191]

10 **Davis CB**, Kendall JL. Emergency bedside ultrasound diagnosis of superior mesenteric artery dissection complicating acute aortic dissection. *J Emerg Med* 2013; **45**: 894-896 [PMID: 23932465 DOI: 10.1016/j.jemermed.2013.04.025]

11 **Huang CY**, Sun JT, Lien WC. Early Detection of Superior Mesenteric Artery Dissection by Ultrasound: Two Case Reports. *J Med Ultrasound* 2019; **27**: 47-49 [PMID: 31031536 DOI: 10.4103/JMU.JMU_81_18]

12 **Bao S**, Wang T, Jin X, Zhang S, Qi H, Dong D, Mou X, Zhang X, Li C. Diagnostic value of color Doppler sonography for spontaneous isolated superior mesenteric artery dissection. *Exp Ther Med* 2019; **17**: 3489-3494 [PMID: 30988728 DOI: 10.3892/etm.2019.7399]

13 **Yun WS**, Kim YW, Park KB, Cho SK, Do YS, Lee KB, Kim DI, Kim DK. Clinical and angiographic follow-up of spontaneous isolated superior mesenteric artery dissection. *Eur J Vasc Endovasc Surg* 2009; **37**: 572-577 [PMID: 19208448 DOI: 10.1016/j.ejvs.2008.12.010]

14 **Shiraki H**, Kasamoto M, Yasutomi M, Kaji S, Akutsu K, Furukawa Y, Shimizu W, Inoue N. Clinical Features of Spontaneous Isolated Dissection of Abdominal Visceral Arteries. *J Clin Med Res* 2020; **12**: 13-17 [PMID: 32010417 DOI: 10.14740/jocmr3916]

15 **Luan JY**, Guan X, Li X, Wang CM, Li TR, Zhang L, Han JT. Isolated superior mesenteric artery dissection in China. *J Vasc Surg* 2016; **63**: 530-536 [PMID: 26597665 DOI: 10.1016/j.jvs.2015.09.047]

16 **Kim YW**. Current Understandings of Spontaneous Isolated Superior Mesenteric Artery Dissection. *Vasc Specialist Int* 2016; **32**: 37-43 [PMID: 27386450 DOI: 10.5758/vsi.2016.32.2.37]

17 **Zettervall SL**, Karthaus EG, Soden PA, Buck DB, Ultee KH, Schermerhorn ML, Wyers MC. Clinical presentation, management, follow-up, and outcomes of isolated celiac and superior mesenteric artery dissections. *J Vasc Surg* 2017; **65**: 91-98 [PMID: 27773728 DOI: 10.1016/j.jvs.2016.08.080]

18 **DeCarlo C**, Ganguli S, Borges JC, Schainfeld RM, Mintz AJ, Mintz J, Jaff MR, Weinberg I. Presentation, treatment, and outcomes in patients with spontaneous isolated celiac and superior mesenteric artery dissection. *Vasc Med* 2017; **22**: 505-511 [PMID: 28901215 DOI: 10.1177/1358863X17729770]

19 **Takahashi B**, Nakayama Y, Shiroma S, Ido K. Three Case Report of Spontaneous Isolated Dissection of the Superior Mesenteric Artery-With an Algorithm Proposed for the Management. *Ann Vasc Dis* 2015; **8**: 120-123 [PMID: 26131035 DOI: 10.3400/avd.cr.15-00013]

20 **Acosta S**, Gonçalves FB. Management of Spontaneous Isolated Mesenteric Artery Dissection: A Systematic Review. *Scand J Surg* 2021; **110**: 130-138 [PMID: 33724090 DOI: 10.1177/14574969211000546]

21 **Qiu C**, He Y, Li D, Shang T, Wang X, Wu Z, Zhang H. Mid-Term Results of Endovascular Treatment for Spontaneous Isolated Dissection of the Superior Mesenteric Artery. *Eur J Vasc Endovasc Surg* 2019; **58**: 88-95 [PMID: 31160187 DOI: 10.1016/j.ejvs.2018.11.013]

22 **Wang J**, He Y, Zhao J, Yuan D, Xu H, Ma Y, Huang B, Yang Y, Bian H, Wang Z. Systematic review and meta-analysis of current evidence in spontaneous isolated celiac and superior mesenteric artery dissection. *J Vasc Surg* 2018; **68**: 1228-1240.e9 [PMID: 30126785 DOI: 10.1016/j.jvs.2018.05.014]

23 **Yu SH**, Hii IH, Wu IH. Comparison of Superior Mesenteric Artery Remodeling and Clinical Outcomes between Conservative or Endovascular Treatment in Spontaneous Isolated Superior Mesenteric Artery Dissection. *J Clin Med* 2022; **11** [PMID: 35054159 DOI: 10.3390/jcm11020465]

24 **Mandlik V**, Prantl L, Schreyer AG. Contrast Media Extravasation in CT and MRI - A Literature Review and Strategies for Therapy. *Rofo* 2019; **191**: 25-32 [PMID: 29913522 DOI: 10.1055/a-0628-7095]

25 **Czihal M**, Lottspeich C, Hoffmann U. Ultrasound imaging in the diagnosis of large vessel vasculitis. *Vasa* 2017; **46**: 241-253 [PMID: 28332442 DOI: 10.1024/0301-1526/a000625]

World Journal of Clinical Cases

Submit a Manuscript: https://www.f6publishing.com

World J Clin Cases 2022 June 16; 10(17): 5723-5731

DOI: 10.12998/wjcc.v10.i17.5723

ISSN 2307-8960 (online)

CASE REPORT

Adrenocorticotropic hormone-secreting pancreatic neuroendocrine carcinoma with multiple organ infections and widespread thrombosis: A case report

Akihiro Yoshihara, Kota Nishihama, Chisa Inoue, Yuko Okano, Kazuhito Eguchi, Soichiro Tanaka, Kanako Maki, Valeria Fridman D'Alessandro, Atsuro Takeshita, Taro Yasuma, Mei Uemura, Toshinari Suzuki, Esteban C Gabazza, Yutaka Yano

Specialty type: Endocrinology and metabolism

Provenance and peer review: Unsolicited article; Externally peer reviewed.

Peer-review model: Single blind

Peer-review report's scientific quality classification
Grade A (Excellent): A, A
Grade B (Very good): B
Grade C (Good): 0
Grade D (Fair): 0
Grade E (Poor): 0

P-Reviewer: Anoshkin K, Russia; Hu HG, China; Sharaf M, Syria

Received: October 23, 2021
Peer-review started: October 23, 2021
First decision: December 17, 2021
Revised: December 20, 2022
Accepted: April 9, 2022
Article in press: April 9, 2022
Published online: June 16, 2022

Akihiro Yoshihara, Department of Diabetes and Endocrinology, Japan Community Health care Organization Yokkaichi Hazu Medical Center, Yokkaichi 510-0016, Mie, Japan

Kota Nishihama, Chisa Inoue, Yuko Okano, Kazuhito Eguchi, Soichiro Tanaka, Kanako Maki, Mei Uemura, Toshinari Suzuki, Yutaka Yano, Department of Diabetes, Metabolism, and Endocrinology, Mie University, Tsu 514-8507, Mie, Japan

Valeria Fridman D'Alessandro, Department of Immunology, Mie University, Tsu 514-8507, Mie, Japan

Atsuro Takeshita, Department of Immunology, Faculty and Graduate School of Medicine, Mie University, Tsu 514-8507, Mie, Japan

Taro Yasuma, Department of Immunology and Department of Diabetes, Metabolism, and Endocrinology, Mie University, Tsu 514-8507, Mie, Japan

Esteban C Gabazza, Department of Immunology, Mie University School of Medicine, Mie University, Tsu 514-8507, Mie, Japan

Corresponding author: Esteban C Gabazza, MD, PhD, Full Professor, Department of Immunology, Mie University School of Medicine, Mie University, Edobashi 2-174, Tsu 514-8507, Mie, Japan. gabazza@doc.medic.mie-u.ac.jp

Abstract

BACKGROUND

Ectopic adrenocorticotropic hormone (ACTH)-secreting neuroendocrine tumors are rare diseases. Patients with ACTH-secreting pancreatic neuroendocrine carcinomas have a poor prognosis. Infections and coagulopathies have been reported as the cause of death. However, detailed clinical descriptions of the morbid complications of ACTH-secreting neuroendocrine carcinomas have not been reported.

CASE SUMMARY

A 78-year-old Japanese woman consulted a medical center due to systemic edema and epigastric discomfort. Laboratory analysis revealed hypercortisolemia with

increased ACTH secretion without diurnal variation in serum cortisol level. An enhanced computed tomography (CT) scan revealed a 3-cm tumor in the pancreatic head. The cytological material from endoscopic ultrasound-guided fine-needle aspiration was compatible with ACTH-secreting pancreatic neuroendocrine carcinoma. The Ki-67 index was 40%. She was transferred to Mie University Hospital for surgical treatment. The patient was diagnosed with urinary tract infection, cytomegalovirus hepatitis, esophageal candidiasis, pulmonary infiltrates suspicious for *Pneumocystis carinii* pneumonia, peripheral deep vein thrombosis, pulmonary embolism, and disseminated intravascular coagulation. The multiple organ infections and thromboses responded well to antimicrobial and anticoagulant therapy. Radioisotope studies disclosed a pancreatic tumor and a metastatic lesion in the liver, whereas somatostatin receptor scintigraphy showed negative findings, suggesting the primary and metastatic tumors were poorly differentiated. A CT scan before admission showed no metastatic liver lesion, suggesting that the pancreatic tumor was rapidly progressing. Instead of surgery, antitumor chemotherapy was indicated. The patient was transferred to another hospital to initiate chemotherapy. However, she died four months later due to the rapidly progressive tumor.

CONCLUSION

ACTH-secreting pancreatic neuroendocrine neoplasm is a rare disease with a very poor prognosis. The clinical course and acute complications of the tumor remain unreported. Here we report the clinical course of a rapidly progressive case of ACTH-secreting pancreatic neuroendocrine tumor that developed infectious complications due to many types of pathogens in multiple organs, widespread thromboses, pulmonary embolism, and disseminated intravascular coagulation.

Key Words: Neuroendocrine tumors; Cushing's syndrome; Ectopic adrenocorticotropic hormone syndrome; Pneumocystis pneumonia; Pulmonary embolism; Infections; Case report

©The Author(s) 2022. Published by Baishideng Publishing Group Inc. All rights reserved.

Core Tip: Adrenocorticotropic hormone (ACTH)-secreting pancreatic neuroendocrine tumor is a rare malignant disease with a poor prognosis. The condition is frequently associated with infectious and thrombotic complications. However, the detailed clinical course and acute complications of the tumor remain unreported. Herein, we report a rare case of ACTH-secreting pancreatic neuroendocrine tumor associated with infections due to multiple pathogens in several organs and systemic coagulopathies. The infectious and thrombotic complications responded well to antibiotics, antiviral and antifungal drugs, and anticoagulants. However, radioisotope studies showed that the tumor was poorly differentiated, rapidly progressive with multiple metastatic lesions in the liver. On this basis, instead of surgical treatment, antitumor chemotherapy was indicated. Unfortunately, the patient died due to systemic tumor dissemination.

Citation: Yoshihara A, Nishihama K, Inoue C, Okano Y, Eguchi K, Tanaka S, Maki K, Fridman D'Alessandro V, Takeshita A, Yasuma T, Uemura M, Suzuki T, Gabazza EC, Yano Y. Adrenocorticotropic hormone-secreting pancreatic neuroendocrine carcinoma with multiple organ infections and widespread thrombosis: A case report. *World J Clin Cases* 2022; 10(17): 5723-5731
URL: https://www.wjgnet.com/2307-8960/full/v10/i17/5723.htm
DOI: https://dx.doi.org/10.12998/wjcc.v10.i17.5723

INTRODUCTION

Neuroendocrine tumors or neuroendocrine neoplasms are classified by the World Health Organization into "well-differentiated" and "poorly differentiated" neuroendocrine carcinomas[1]. Ectopic adrenocorticotropic hormone (ACTH)-secreting neuroendocrine tumors account for 9%-18% of Cushing's syndrome cases[2]. Among ectopic ACTH-secreting tumors, pancreatic neuroendocrine (pNE) tumors are rare (4%-16%) but very aggressive tumors[3]. Previous studies have shown that patients with ACTH-secreting pNE neoplasms have a poorer prognosis than patients with insulinoma, gastrinoma, and non-functioning pNE tumors[4]. In addition, pneumocystis pneumonia, pulmonary embolism, and other complications have been reported as causes of death in patients with ACTH-secreting pNE tumors [5-8]. However, previous reports provided no detailed clinical descriptions of the morbid complications of ACTH-secreting pNE tumors. Clinical follow-up with studies using radioisotope scans is also lacking. Here we report the detailed clinical course of a rapidly progressive case of ACTH-secreting pNE tumor

that developed several complications, including multiple organ infections due to many types of pathogens, disseminated intravascular coagulation, and pulmonary thromboembolism. This case study shows that the progressive and aggressive nature of ACTH-secreting pNE tumors gives no truce for treating the disease with more effective therapeutic modalities, including surgical resection.

CASE PRESENTATION

Chief complaints

The chief complaints of the patient were systemic edema and epigastric discomfort.

History of present illness

Two months before admission to our institution, a 78-year-old Japanese woman consulted a medical center due to systemic edema and epigastric discomfort. Laboratory analysis showed no abnormalities. Therefore, close clinical follow-up was suggested. However, blood analysis performed two months later revealed a high hemoglobin A1c (5.5%-7.2%) and decreased potassium concentration (2.7 mEq/L). Screening of potential causes of secondary diabetes mellitus showed high levels of cortisol (80.6 μg/dL) and ACTH (177 pg/mL) in the early morning and increased levels of cortisol (56.2 μg/dL) at midnight. The daily urine cortisol level (6550 μg/day) was also increased. A dexamethasone suppressive test (8 mg) showed no suppression of fasting blood cortisol (118 μg/dL) or ACTH (342 pg/mL). These results suggested the diagnosis of ACTH-dependent hypercortisolism (Table 1). An abdominal computed tomography (CT) scan showed a 3-cm tumor with poor contrast in the pancreatic tail (Figure 1). Cytological findings of endoscopic ultrasound-guided fine-needle aspiration showed cell clusters forming no specific structures with a high nuclear/cytoplasmic ratio, suggesting adenocarcinoma (Figure 2A). However, the immunostaining results showed positivity for chromogranin A, synaptophysin, CD 56, and ACTH (Figure 2B-E) that were compatible with the diagnosis of ACTH-secreting pNE neoplasm. The Ki-67 index was approximately 40% (Figure 2F). The patient was then referred to Mie University Hospital for subsequent examinations and treatment.

History of past illness

There was no remarkable past or family history. She had no history of allergy, excessive alcohol consumption, or smoking.

Physical examination

The clinical findings on admission to Mie University Hospital were as follows: height 157.5 cm, body weight 54 kg, blood pressure 135/79 mmHg, and pulse rate 91 bpm. In addition, the patient presented a "moon-face" with bilateral pitting edema on the lower limbs on physical examination.

Laboratory examinations

Laboratory analysis revealed thrombocytopenia with elevated blood levels of D-dimer, fibrinogen/fibrin degradation products, liver enzymes, cortisol and ACTH, and hypokalemia (Table 1). Brain magnetic resonance imaging (MRI) showed no pituitary tumor. Blood culture was negative, but urine culture was positive for *Escherichia coli* and *Pseudomonas aeruginosa*. Esophageal candidiasis was diagnosed by esophagogastroduodenoscopy. The patient was also positive for Cytomegalovirus antigen (C7-HRP, on day 1, 132/82500 cells) associated with increased levels of liver enzymes (AST 121 U/L, ALT 294 U/L on day 1), and thus Cytomegalovirus hepatitis was diagnosed. Additional laboratory analysis on day 7 revealed an increased level of β-D glucan (48.0 pg/mL), and a chest CT scan on day 9 showed bilateral ground-glass opacity (Figure 3A and B) suspicious for Pneumocystis pneumonia.

Imaging examinations

In addition to laboratory findings of disseminated intravascular coagulation, venous ultrasonography of the lower extremities performed on day 1 revealed deep venous thrombosis in the right popliteal segment of the femoral vein (size not recorded), right soleus vein (5-6 cm), and left posterior tibial vein (4 cm). In addition, pulmonary embolism was pointed out by a radiologist based on a chest CT scan taken on day 9 (Figure 3D and E).

MULTIDISCIPLINARY EXPERT CONSULTATION

Somatostatin receptor scintigraphy with ^{111}In-pentetoreotide performed on day 21 showed no uptake in any organ (Figure 4A). However, an ^{18}F-fluorodeoxyglucose-positron emission tomography (PET) performed on day 29 showed positive uptake in the pancreatic tumor and the liver (S6 segment; Figure 4B and C). Enhanced CT imaging taken before transfer to Mie University Hospital showed no

Table 1 Laboratory data on admission

Blood cell count		RR	Units	Biochemical and immunology		RR	Units	Endocrinology		RR	Units
White blood cell	6530	3300-8600	/μL	Total protein	4.7	6.6-8.1	g/dL	Cortisol	134.2	4.5-21.1	μg/dL
Neutrophils	91.1	37.0-72.0	%	Albumin	2.8	4.1-5.1	g/dL	Cortisol (23:00)[1]	56.2		μg/dL
Lymphocytes	6.0	20.0-50.9	%	BUN	21.3	8.0-20.0	mg/dL	Cortisol (8 mg-DST)[1]	118.0		μg/dL
CD3+CD4+	24.06	40.4-57.4	%	Creatinine	0.67	0.46-0.79	mg/dL	Urine cortisol[1]	6,550	26-187	μg/day
CD4+CD8+	15.46	15.0-30.0	%	Uric acid	2.2	2.6-5.5	mg/dL	ACTH	134.2	4.5-21.1	pg/mL
CD4+/CD8+ ratio	1.56			Na	150	138-145	mEq/L	ACTH (8 mg-DST)[1]	342.0		pg/mL
Monocytes	2.6	4.1-10.6	%	K	2.7	3.6-4.8	mEq/L				
Eosinophils	0.0	0.6-8.3	%	Cl	108	101-108	mEq/L	Tumor Marker		RR	Units
Basophils	0.3	0.0-1.3	%	Ca	7.9	8.8-10.1	mg/dL	CEA	4.8	< 5.2	ng/mL
Red blood cell	489	386-492	× 10^4/μL	P	2.2	2.7-4.6	mg/dL	CA19-9	28.8	< 36.8	U/mL
Hemoglobin	12.5	11.6-14.8	g/dL	AST	121	13-30	U/L	DUPAN-2	47	0-150	U/mL
Hematocrit	37.3	35.1-44.1	%	ALT	294	7-23	U/L	SPAN-1	15	0-30	U/mL
Platelet	37	15.8-34.8	× 10^4/μL	LDH	978	124-222	U/L				
				γ-GTP	226	9-32	U/L	Infection		RR	Units
Coagulation		RR	Units	ALP	514	106-322	U/L	HBsAg	< 0.01	< 0.05	IU/mL
APTT	20.7	< 37.0	Seconds	T-Bil	1.0	0.4-1.5	mg/dL	HBsAb	0.37	< 10.00	IU/mL
PT	11.1	9.8-12.1	Seconds	CRP	0.26	< 0.14	mg/dL	HBcAb	0.03	< 1.00	S/CO
D-dimer	30.19	< 1.00	μg/mL	Total-cholesterol	209	142-248	mg/dL	HCVAb	0.05	< 1.00	S/CO
FDP	80.1	< 5.0	μg/mL	Triglyceride	129	30-117	mg/dL	β-D Glucan	9.2	< 11.0	pg/mL
				HbA1c	7.8	4.9-6.0	%	CMV-antigen (C7-HRP)	132/82500		cells
				Plasma glucose	246	73-109	mg/dL				
				IgG	498	861-1747	mg/dL				
				IgM	169	93-393	mg/dL				
				IgM	104	50-269	mg/dL				

[1]Shows the results at JA Suzuka General Hospital.

8 mg-DST: 8 mg dexamethasone suppressive test, RR: Reference range; ACTH: Adrenocorticotropic hormone; CRP: C-reactive protein; FDP: Fibrin degradation products; CMV: Cytomegalovirus; APTT: Activated partial thromboplastin time; LDH: Lactic acid dehydrogenase; ALP: Alkaline phosphatase; AST: Aspartate transaminase; ALT: alanine aminotransferase PT: Prothrombin time; -GTP: -glutamyl transferase; T-Bil: Total bilirubin; CEA: Carcinoembryonic antigen; HbA1c: Hemoglobin A1c.

tumor in the liver S6 segment (Figure 4D). Gadolinium-ethoxybenzyl-diethylenetriamine pentaacetic acid (Gd-EOB-DTPA)-MRI revealed multiple liver tumors suggesting liver metastases (Figure 4E and F). Based on these findings, surgical intervention was canceled.

FINAL DIAGNOSIS

The patient's final diagnosis was ACTH-secreting pNE tumor with ACTH-dependent hypercortisolism associated with urinary tract infection, Cytomegalovirus hepatitis, esophageal candidiasis, pulmonary infiltrates suspicious for *Pneumocystis carinii* pneumonia, and widespread peripheral deep vein

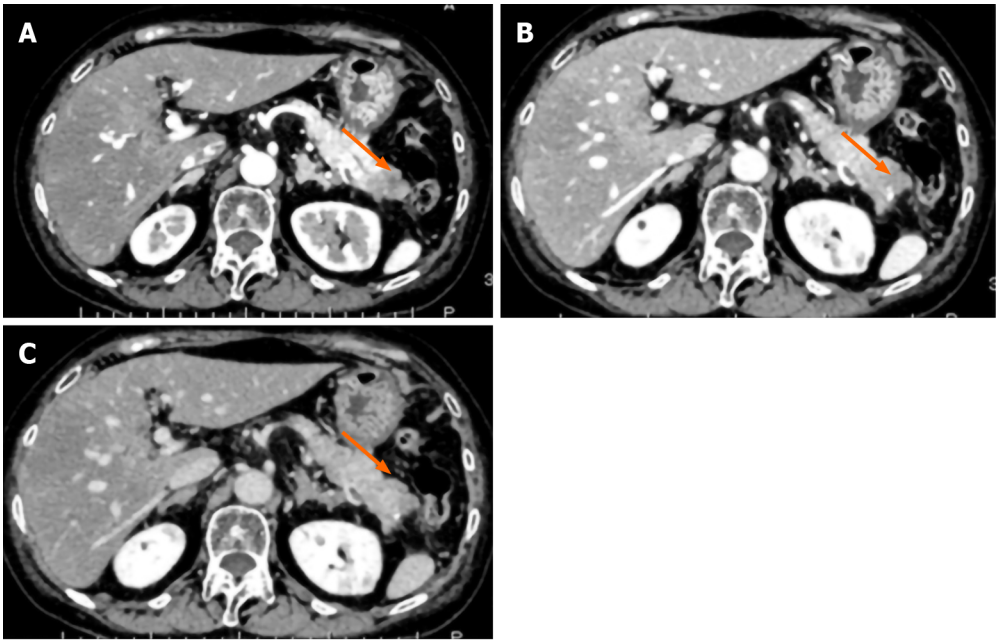

DOI: 10.12998/wjcc.v10.i17.5723 **Copyright** ©The Author(s) 2022.

Figure 1 Contrast-enhanced abdominal computed tomography showing a 3-cm hypovascular lesion in the pancreatic tail. A: Arterial phase; B: Venous phase; C: Equilibrium phase.

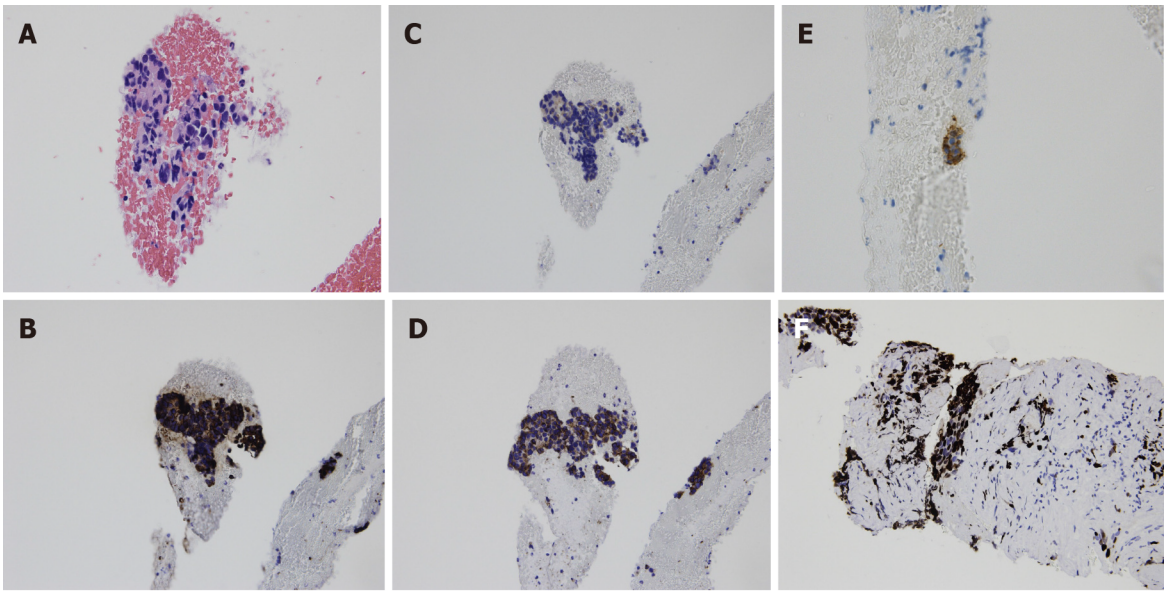

DOI: 10.12998/wjcc.v10.i17.5723 **Copyright** ©The Author(s) 2022.

Figure 2 Cytological images of endoscopic ultrasound-guided fine-needle aspiration showing cell clusters with high nuclear/cytoplasmic ratio. A: Cell clusters show non-specific structure after H-E staining; B: Immunostaining was positive for chromogranin A; C: Synaptophysin; D: CD 56; E: ACTH; and F: The Ki-67 index was approximately 40%.

thromboses, pulmonary embolism, and disseminated intravascular coagulation.

TREATMENT

The pancreas tumor-related hypercortisolism and hypokalemia were treated with metyrapone (1500 to 3000 mg/day), hydrocortisone (60 mg/day), potassium chloride (2400-3600 mg/day) and spironolactone (50 mg/day). Hyperglycemia was treated with multiple daily insulin injections (up to 25 U/day, days 1 to 48) and oral repaglinide (0.75 mg/day). The response to therapy was good with a postprandial blood glucose level of 172 mg/dL, and HbA1c of 5.5% on day 88.

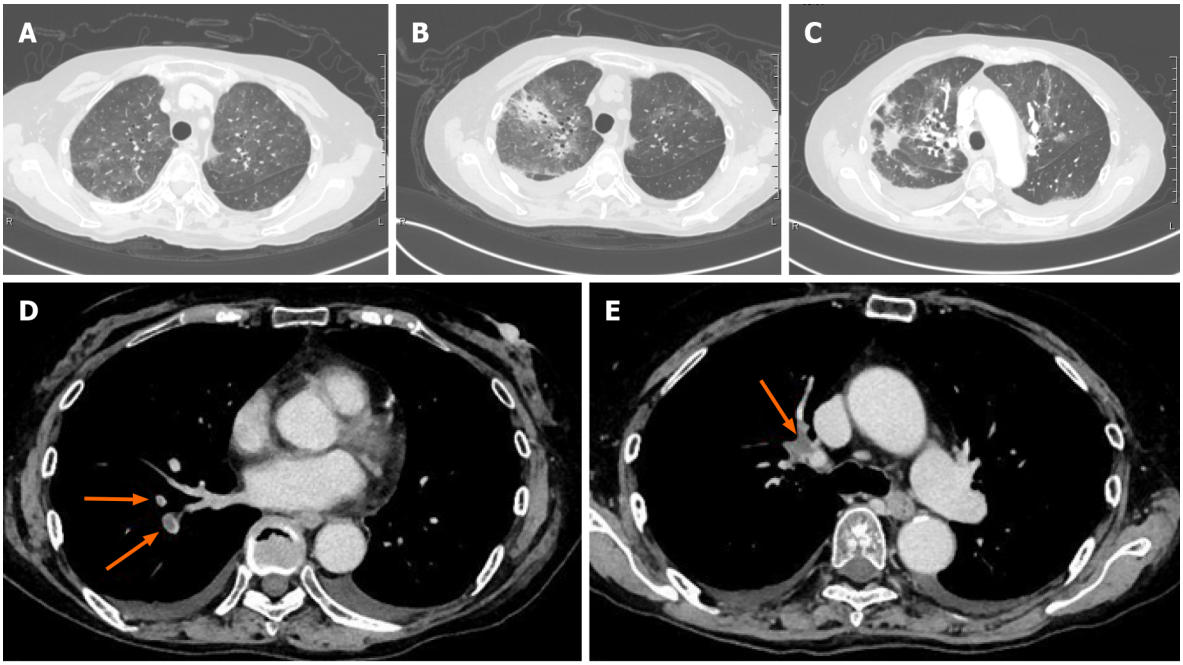

DOI: 10.12998/wjcc.v10.i17.5723 **Copyright** ©The Author(s) 2022.

Figure 3 Representative microphotographs showing hypercortisolemia-related infectious and thrombotic complications. A: Computed tomography revealed bilateral ground-glass opacities (GGO) on day 9; B: The area of GGO was spread, and new patchy consolidations were found in the right lobe on day 19; C: The area of GGO was decreased, and consolidation was observed in the sub-pleural regions suggesting the presence of organizing pneumonia on day 28; D and E: Computed tomography showing pulmonary thromboembolism.

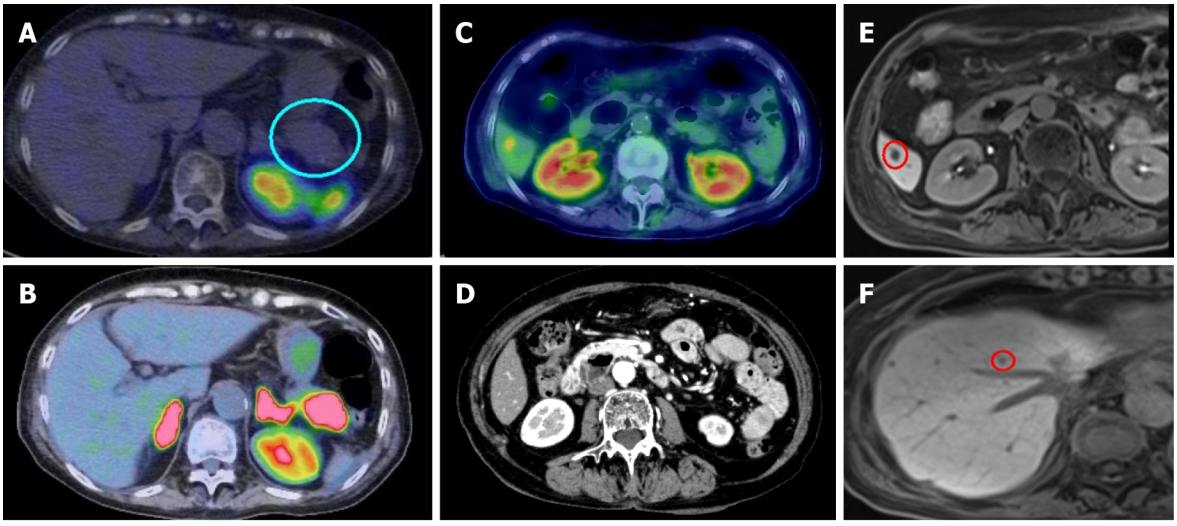

DOI: 10.12998/wjcc.v10.i17.5723 **Copyright** ©The Author(s) 2022.

Figure 4 Radioisotope studies, computed tomography, and magnetic resonance imaging. A: Somatostatin receptor scintigraphy using ^{111}In-pentetoreotide showed no uptake in the pancreatic tumor; B and C: Positron emission tomography using ^{18}F-fluorodeoxyglucose showed uptake in the pancreatic tumor and the liver; D: The computed tomography scan performed before transfer to Mie University showed no lesion; E and F: Gadolinium-ethoxybenzyl-diethylenetriamine pentaacetic acid (Gd-EOB-DTPA)-magnetic resonance imaging also revealed multiple liver tumors suggesting metastases.

The urinary tract infection was treated with meropenem (2 g/day, days 2 to 5) and ceftazidime (2 g/day, days 6 to 15). Esophageal candidiasis was treated with oral fluconazole (100 mg/day, from days 1 to 15). Cytomegalovirus hepatitis was empirically treated with foscarnet (5 g/day) from day 5 after admission. Treatment with foscarnet was stopped on day 27 because the liver enzymes improved (AST 32 U/L, ALT 66 U/L on day 9), and the C7-HRP test was negative.

The pulmonary infiltrates (Figure 3A and B) suspicious for Pneumocystis pneumoniae were treated with oral trimethoprim-sulfamethoxazole (480-2400 mg/day) for 3 wk. The β-D glucan level (10.4 pg/mL) decreased, and the respiratory status was stable on day 27. Prednisolone (25 mg/day) was added to the treatment because another radiological study disclosed organizing pneumonia on day 29

(Figure 3C). Treatment with oral trimethoprim-sulfamethoxazole (80-400 mg/day, three times a week) was also continued.

The patient's hypercoagulable states and thrombotic complications were treated with nafamostat mesylate (200 mg/day, days 1 to 9) and gabexate mesylate (1500 mg/day, days 10 to19). Due to the presence of severe thrombocytopenia, the patient received 10 units of platelet transfusion on day 6. A radiologist pointed out pulmonary embolism based on a chest CT scan taken on day 9 (Figure 3D and E). Treatment with apixaban was started from day 11 (20 mg/day for the first 7 days, 10 mg/day thereafter). Disseminated intravascular coagulation improved, and the thrombi in the pulmonary artery and deep veins completely disappeared on day 88.

OUTCOME AND FOLLOW-UP

The multiple organ infections and thromboses responded well to antimicrobial and anticoagulant therapy. However, a radioisotope study with PET disclosed a pancreatic tumor and a metastatic lesion in the liver, whereas somatostatin receptor scintigraphy showed negative findings, suggesting that the primary and metastatic tumors were poorly differentiated and rapidly progressive. Based on these findings, surgical intervention was canceled. The patient was then transferred to another institution for antitumor chemotherapy. However, she died four months later due to rapid tumor progression.

DISCUSSION

ACTH-secreting pNE tumors are rare malignant diseases with aggressive behavior[3]. Patients with this malignant disease have a poorer prognosis than patients with insulinoma, gastrinoma, or non-functioning ACTH-secreting pNE tumors[4]. However, the explanation for the tumor aggressiveness and the poor patient prognosis remains unclear. A previous study suggested that hypomethylation of the proopiomelanocortin promoter may potentiate the ACTH secretory property of the tumors[8]. A high Ki-67 index indicates poor clinical outcomes in pNE tumors[1,9]. The Ki-67 index was high in our present case. A pathological diagnosis of a poorly differentiated pNE tumor also predicts a poor prognosis[1]. Cytological study of samples taken by needle aspiration was available in our patient. However, it was difficult to determine the tumor differentiation status based only on the cytological material. Previous reports suggested that radioisotope techniques may help determine cell differentiation status.

In addition to allowing localization of the primary malignant tumor and metastatic lesion, radioisotope studies of pNE tumors may provide information on the tumor cell metabolic activity and the expression of specific receptors such as somatostatin receptors[10]. In the current case, we performed somatostatin receptor scintigraphy using ^{111}In-pentetoreotide and PET using ^{18}F-fluorodeoxyglucose. The PET study confirmed the primary pNE tumor and the presence of liver metastasis, whereas the scintigraphy disclosed no tumor uptake. The combination of positive ^{18}F-fluorodeoxyglucose uptake by PET and negative ^{111}In-pentetoreotide uptake by scintigraphy indicates poor differentiation of pNE tumor cells[11,12]. Malcolm *et al*[10] reported a sensitivity of 57% for somatostatin receptor scintigraphy using ^{111}In-pentetoreotide and 100% for ^{18}F-fluorodeoxyglucose-PET in Grade 3 pNE tumors. Another study showed that metastasis of highly differentiated pNE tumors can be detected by somatostatin receptor scintigraphy using ^{111}In-pentetoreotide but not by ^{18}F-fluorodeoxyglucose-PET[13]. In the present case, the ^{18}F-fluorodeoxyglucose-PET study showed positive radioisotope uptake in the primary pNE tumor and metastatic liver lesion, but the scintigraphy showed no radioisotope uptake, suggesting that the primary and metastatic pNE tumor was not differentiated.

In the current case, the ACTH-secreting pNE tumor was associated with multiple organ infections, including urinary tract infection, viral hepatitis, esophageal candidiasis, and bilateral pulmonary infiltrates suspicious for *Pneumocystis carinii* pneumonia. Patients with hypercortisolemia are immunocompromised[14]. Immunosuppression in patients with hypercortisolism is generally characterized by the reduced bactericidal function of neutrophils, decreased CD14- and CD16-mediated phagocytic activity of monocytes, deficient cytotoxic activity of natural killer cells, and reduced number of CD4+ T cells[14]. The current case showed a reduction in lymphocytes, including CD4+ cells, and decreased peripheral blood concentration of IgG, suggesting she was an immunocompromised host. However, infections with multiple microbes responded well to antibacterial, antifungal, and antiviral drugs. The diagnosis of *Pneumocystis carinii* pneumonia in our patient was not confirmed by microscopic observation of *P. jirovecii* or positivity by polymerase chain reaction. However, we initiated therapy for *Pneumocystis carinii* pneumonia after suspecting the disease based on lung CT findings as delayed treatment of *Pneumocystis carinii* pneumonia may be fatal in patients with ectopic ACTH syndrome[5,15,16].

In the current case, the ACTH-secreting pNE tumor was also associated with many thrombotic complications, including thrombus formation in many limb peripheral veins, pulmonary embolism, and disseminated intravascular coagulation. Patients with hypercortisolemia are in a hypercoagulable state

[17]. Hypercortisolism may cause hypercoagulability, although the precise mechanism is unclear. Alterations in the blood levels of von Willebrand factor and factor VIII have been reported[17]. Some polymorphisms appear to affect the promoter activity of the von Willebrand factor gene in response to glucocorticoids, and a high concentration of cortisol may alter the multimeric structure of von Willebrand factor[17]. Decreased physical activity during hospitalization or the perioperative period is also a contributing factor to increased risk of venous thrombosis and pulmonary embolism in patients with hypercortisolemia[18,19]. The risk of thrombosis was high in our patient because of reduced physical activity and the presence of malignancy and infectious diseases[20,21]. Our patient had a decreased number of platelets on admission. We delayed the treatment with anticoagulant therapy to prevent fatal hemorrhage. However, earlier anticoagulation therapy would have improved the thrombotic complications in the patient.

CONCLUSION

This report described the clinical course of a rapidly progressive case of ACTH-secreting pNE tumor who developed infectious complications due to many types of pathogens in multiple organs, widespread thromboses, pulmonary embolism, and disseminated intravascular coagulation. This case study shows that neuroendocrine carcinoma of the pancreas secreting ACTH has a poor immune state and that the progressive and aggressive nature of ACTH-secreting pNE tumors gives no truce for treating the disease with more effective therapeutic modalities, including surgical resection.

ACKNOWLEDGEMENTS

The authors would like to thank Dr. Tetsuya Murata from the JA Suzuka General Hospital Division of Pathology.

FOOTNOTES

Author contributions: Yoshihara A and Nishihama K were responsible for clinical treatment, follow-up of the patient, and manuscript preparation; Inoue C, Okano Y, Eguchi K, Tanaka S, and Maki K were responsible for clinical treatment, follow-up of the patient, and data interpretation; Fridman D'Alessandro V contributed to data interpretation; Takeshita A, Yasuma T, and Uemura M were responsible for radiological and pathological investigation; Yasuma T, Suzuki T, Gabazza EC, and Yano Y were responsible for data interpretation, intellectual contribution, and manuscript preparation.

Informed consent statement: Written informed consent was obtained from the patient to publish clinical details and images when she was alive.

Conflict-of-interest statement: Yutaka Yano reports receiving lecture fees from Novo Nordisk. Other authors declared no conflict of interest concerning this case report.

CARE Checklist (2016) statement: The authors have read the CARE Checklist (2016), and the manuscript was prepared and revised according to the CARE Checklist (2016).

Open-Access: This article is an open-access article that was selected by an in-house editor and fully peer-reviewed by external reviewers. It is distributed in accordance with the Creative Commons Attribution NonCommercial (CC BY-NC 4.0) license, which permits others to distribute, remix, adapt, build upon this work non-commercially, and license their derivative works on different terms, provided the original work is properly cited and the use is non-commercial. See: https://creativecommons.org/Licenses/by-nc/4.0/

Country/Territory of origin: Japan

ORCID number: Akihiro Yoshihara 0000-0001-5799-2440; Kota Nishihama 0000-0002-0471-5164; Chisa Inoue 0000-0002-7022-9156; Yuko Okano 0000-0002-8441-423X; Kazuhito Eguchi 0000-0002-4968-0217; Soichiro Tanaka 0000-0002-8240-6180; Kanako Maki 0000-0001-7061-0291; Valeria Fridman D'Alessandro 0000-0002-3719-1686; Atsuro Takeshita 0000-0002-3792-7382; Taro Yasuma 0000-0002-9117-5679; Mei Uemura 0000-0002-9140-0311; Toshinari Suzuki 0000-0003-0980-1763; Esteban C Gabazza 0000-0003-2536-898X; Yutaka Yano 0000-0003-0234-1207.

S-Editor: Ma YJ
L-Editor: Webster JR
P-Editor: Ma YJ

REFERENCES

1 **Nagtegaal ID**, Odze RD, Klimstra D, Paradis V, Rugge M, Schirmacher P, Washington KM, Carneiro F, Cree IA; WHO Classification of Tumours Editorial Board. The 2019 WHO classification of tumours of the digestive system. *Histopathology* 2020; **76**: 182-188 [PMID: 31433515 DOI: 10.1111/his.13975]

2 **Wajchenberg BL**, Mendonca BB, Liberman B, Pereira MA, Carneiro PC, Wakamatsu A, Kirschner MA. Ectopic adrenocorticotropic hormone syndrome. *Endocr Rev* 1994; **15**: 752-787 [PMID: 7705280 DOI: 10.1210/edrv-15-6-752]

3 **Falconi M**, Eriksson B, Kaltsas G, Bartsch DK, Capdevila J, Caplin M, Kos-Kudla B, Kwekkeboom D, Rindi G, Klöppel G, Reed N, Kianmanesh R, Jensen RT; Vienna Consensus Conference participants. ENETS Consensus Guidelines Update for the Management of Patients with Functional Pancreatic Neuroendocrine Tumors and Non-Functional Pancreatic Neuroendocrine Tumors. *Neuroendocrinology* 2016; **103**: 153-171 [PMID: 26742109 DOI: 10.1159/000443171]

4 **Maragliano R**, Vanoli A, Albarello L, Milione M, Basturk O, Klimstra DS, Wachtel A, Uccella S, Vicari E, Milesi M, Davì MV, Scarpa A, Sessa F, Capella C, La Rosa S. ACTH-secreting pancreatic neoplasms associated with Cushing syndrome: clinicopathologic study of 11 cases and review of the literature. *Am J Surg Pathol* 2015; **39**: 374-382 [PMID: 25353285 DOI: 10.1097/PAS.0000000000000340]

5 **Cristante J**, Lepelley M, Mallaret M, Carreau A, Chabre O. Pneumocystis pneumonia can complicate medical treatment of hypercortisolism even in outpatients with Cushing's disease. *Ann Endocrinol (Paris)* 2020; **81**: 551-560 [PMID: 33278378 DOI: 10.1016/j.ando.2020.11.002]

6 **Schernthaner-Reiter MH**, Siess C, Micko A, Zauner C, Wolfsberger S, Scheuba C, Riss P, Knosp E, Kautzky-Willer A, Luger A, Vila G. Acute and Life-threatening Complications in Cushing Syndrome: Prevalence, Predictors, and Mortality. *J Clin Endocrinol Metab* 2021; **106**: e2035-e2046 [PMID: 33517433 DOI: 10.1210/clinem/dgab058]

7 **Shayesteh S**, Fouladi DF, Fishman EK, Kawamoto S. Ectopic Cushing syndrome caused by a pancreatic neuroendocrine tumor: A case report. *Radiol Case Rep* 2020; **15**: 1014-1017 [PMID: 32547669 DOI: 10.1016/j.radcr.2020.04.009]

8 **Zhang C**, Jin J, Xie J, Ye L, Su T, Jiang L, Zhou W, Jiang Y, Wu L, Wang T, Zhong X, Ning G, Shen B, Wang W. The Clinical Features and Molecular Mechanisms of ACTH-secreting Pancreatic Neuroendocrine Tumors. *J Clin Endocrinol Metab* 2020; **105** [PMID: 32785672 DOI: 10.1210/clinem/dgaa507]

9 **Hamilton NA**, Liu TC, Cavatiao A, Mawad K, Chen L, Strasberg SS, Linehan DC, Cao D, Hawkins WG. Ki-67 predicts disease recurrence and poor prognosis in pancreatic neuroendocrine neoplasms. *Surgery* 2012; **152**: 107-113 [PMID: 22503317 DOI: 10.1016/j.surg.2012.02.011]

10 **Squires MH 3rd**, Volkan Adsay N, Schuster DM, Russell MC, Cardona K, Delman KA, Winer JH, Altinel D, Sarmiento JM, El-Rayes B, Hawk N, Staley CA 3rd, Maithel SK, Kooby DA. Octreoscan Versus FDG-PET for Neuroendocrine Tumor Staging: A Biological Approach. *Ann Surg Oncol* 2015; **22**: 2295-2301 [PMID: 25786743 DOI: 10.1245/s10434-015-4471-x]

11 **Chan DL**, Pavlakis N, Schembri GP, Bernard EJ, Hsiao E, Hayes A, Barnes T, Diakos C, Khasraw M, Samra J, Eslick E, Roach PJ, Engel A, Clarke SJ, Bailey DL. Dual Somatostatin Receptor/FDG PET/CT Imaging in Metastatic Neuroendocrine Tumours: Proposal for a Novel Grading Scheme with Prognostic Significance. *Theranostics* 2017; **7**: 1149-1158 [PMID: 28435454 DOI: 10.7150/thno.18068]

12 **Kubota K**, Okasaki M, Minamimoto R, Miyata Y, Morooka M, Nakajima K, Sato T. Lesion-based analysis of (18)F-FDG uptake and (111)In-Pentetreotide uptake by neuroendocrine tumors. *Ann Nucl Med* 2014; **28**: 1004-1010 [PMID: 25179521 DOI: 10.1007/s12149-014-0900-3]

13 **Yasuda M**, Takeda S, Lee M, Hoshi S, Hoshi T, Tanaka Y, Miyajima S, Takaya H, Kajimura K. Small Cystic Pancreatic Neuroendocrine Neoplasm with Huge Liver and Bone Metastases. *Intern Med* 2020; **59**: 3027-3032 [PMID: 33268697 DOI: 10.2169/internalmedicine.5038-20]

14 **Hasenmajer V**, Sbardella E, Sciarra F, Minnetti M, Isidori AM, Venneri MA. The Immune System in Cushing's Syndrome. *Trends Endocrinol Metab* 2020; **31**: 655-669 [PMID: 32387195 DOI: 10.1016/j.tem.2020.04.004]

15 **Colby C**, McAfee S, Sackstein R, Finkelstein D, Fishman J, Spitzer T. A prospective randomized trial comparing the toxicity and safety of atovaquone with trimethoprim/sulfamethoxazole as Pneumocystis carinii pneumonia prophylaxis following autologous peripheral blood stem cell transplantation. *Bone Marrow Transplant* 1999; **24**: 897-902 [PMID: 10516703 DOI: 10.1038/sj.bmt.1702004]

16 **Song Y**, Ren Y, Wang X, Li R. Recent Advances in the Diagnosis of Pneumocystis Pneumonia. *Med Mycol J* 2016; **57**: E111-E116 [PMID: 27904052 DOI: 10.3314/mmj.16-00019]

17 **Trementino L**, Arnaldi G, Appolloni G, Daidone V, Scaroni C, Casonato A, Boscaro M. Coagulopathy in Cushing's syndrome. *Neuroendocrinology* 2010; **92** Suppl 1: 55-59 [PMID: 20829619 DOI: 10.1159/000314349]

18 **Suarez MG**, Stack M, Hinojosa-Amaya JM, Mitchell MD, Varlamov EV, Yedinak CG, Cetas JS, Sheppard B, Fleseriu M. Hypercoagulability in Cushing Syndrome, Prevalence of Thrombotic Events: A Large, Single-Center, Retrospective Study. *J Endocr Soc* 2020; **4**: bvz033 [PMID: 32064411 DOI: 10.1210/jendso/bvz033]

19 **Wagner J**, Langlois F, Lim DST, McCartney S, Fleseriu M. Hypercoagulability and Risk of Venous Thromboembolic Events in Endogenous Cushing's Syndrome: A Systematic Meta-Analysis. *Front Endocrinol (Lausanne)* 2018; **9**: 805 [PMID: 30745894 DOI: 10.3389/fendo.2018.00805]

20 **Abdol Razak NB**, Jones G, Bhandari M, Berndt MC, Metharom P. Cancer-Associated Thrombosis: An Overview of Mechanisms, Risk Factors, and Treatment. *Cancers (Basel)* 2018; **10** [PMID: 30314362 DOI: 10.3390/cancers10100380]

21 **Mullard A**, Innes H. Venous thromboembolism in malignancy. *Clin Med (Lond)* 2014; **14**: 532-534 [PMID: 25301917 DOI: 10.7861/clinmedicine.14-5-532]

World Journal of Clinical Cases

Submit a Manuscript: https://www.f6publishing.com

World J Clin Cases 2022 June 16; 10(17): 5732-5740

DOI: 10.12998/wjcc.v10.i17.5732

ISSN 2307-8960 (online)

CASE REPORT

Management of the palato-radicular groove with a periodontal regenerative procedure and prosthodontic treatment: A case report

Dan-Hua Ling, Wei-Ping Shi, Yan-Hong Wang, Dan-Ping Lai, Yan-Zhen Zhang

Specialty type: Dentistry, oral surgery and medicine

Provenance and peer review: Unsolicited article; Externally peer reviewed.

Peer-review model: Single blind

Peer-review report's scientific quality classification

Grade A (Excellent): 0
Grade B (Very good): B
Grade C (Good): C, C
Grade D (Fair): 0
Grade E (Poor): E

P-Reviewer: Rakhshan V, Iran; Rakhshan V, Iran; Scribante A, Italy; Scribante A, Italy

Received: October 28, 2021
Peer-review started: October 28, 2021
First decision: December 27, 2021
Revised: January 9, 2022
Accepted: April 9, 2022
Article in press: April 9, 2022
Published online: June 16, 2022

Dan-Hua Ling, Wei-Ping Shi, Dan-Ping Lai, Yan-Zhen Zhang, Department of Comprehensive Dentistry, The Second Affiliated Hospital of Zhejiang University School of Medicine, Hangzhou 310052, Zhejiang Province, China

Yan-Hong Wang, Department of Comprehensive Dentistry, Jiangnan Hospital Affiliated to Zhejiang Chinese Medical University, Hangzhou 311221, Zhejiang Province, China

Corresponding author: Yan-Zhen Zhang, MA, Chief Physician, Department of Comprehensive Dentistry, The Second Affiliated Hospital of Zhejiang University School of Medicine, No. 1511 Jianghong Road, Binjiang District, Hangzhou 310052, Zhejiang Province, China.
2191004@zju.edu.cn

Abstract

BACKGROUND

Palato-radicular groove (PRG) is defined as an anomalous formation of teeth. The etiology of PRG remains unclear. The prognosis of a tooth with a PRG is unfavorable. The treatment of combined periodontal-endodontic lesions requires multidisciplinary management to control the progression of bone defects. Some researchers reported cases that had short-term observations. The management of teeth with PRGs is of great clinical significance. However, to date, no case reports have been documented on the use of bone regeneration and prosthodontic treatment for PRGs.

CASE SUMMARY

This case reported the management of a 40-year-old male patient with the chief complaint of slight mobility and abscess in the upper right anterior tooth for 15 d and was diagnosed with type II PRG of tooth 12 with combined endodontic-periodontal lesions. The accumulation of plaque and calculus caused primary periodontitis and a secondary endodontic infection. A multidisciplinary management approach was designed that included root canal therapy, groove sealing, a periodontal regenerative procedure, and prosthodontic treatment. During a 2-year follow-up period, a good prognosis was observed.

CONCLUSION

This report indicates that bone regeneration and prosthodontic treatment may contribute to the long-term favorable prognosis of teeth with PRGs.

Key Words: Palato-radicular groove; Bone regeneration treatment; Prosthodontic

treatment; Maxillary lateral incisor; Dentistry; Periodontology; Case report

©The Author(s) 2022. Published by Baishideng Publishing Group Inc. All rights reserved.

Core Tip: The prognosis of a tooth with a palato-radicular groove (PRG) is unfavorable. The treatment of combined periodontal-endodontic lesions requires multidisciplinary management to control the progression of bone defects. Some researchers reported cases that had short-term observations. However, to date, no case reports have described the use of both bone regeneration treatment and prosthodontic treatment for PRG. Herein, we report a patient with PRG who was treated with bone regeneration and prosthodontic treatments, and 2 years of follow-up showed a good prognosis. This report indicates that bone regeneration and prosthodontic treatment may contribute to the long-term favorable prognosis of teeth with PRGs.

Citation: Ling DH, Shi WP, Wang YH, Lai DP, Zhang YZ. Management of the palato-radicular groove with a periodontal regenerative procedure and prosthodontic treatment: A case report. *World J Clin Cases* 2022; 10(17): 5732-5740
URL: https://www.wjgnet.com/2307-8960/full/v10/i17/5732.htm
DOI: https://dx.doi.org/10.12998/wjcc.v10.i17.5732

INTRODUCTION

Palato-radicular groove (PRG) is defined as an anomalous formation of teeth that begins in the central fossa of the maxillary incisors, extends over the cingulum, and continues apically to varying depths and distances of the root surface[1]. The etiology of PRGs remains unclear. The most common proposals of PRG development include the following four hypotheses: (1) An abnormality in embryonic development, such as in folding of Hertwig's epithelial root sheath; (2) a variant of dens invaginatus; (3) genetic alteration; and (4) an attempt to form another root[2,3].

PRG usually occurs on the palatal side of the maxillary incisors that do not have dental caries or trauma[4,5]. The incidence of PRG ranges from 0.9% to 9.6% in extracted maxillary incisors[6,7] and from 2.8% to 10% in clinical studies[4,8]. Khan *et al*[9] reported a higher incidence of PRG in lateral incisors (13.4%) than in central incisors (7.6%). Various factors could account for this difference in prevalence rate, such as different diagnostic criteria, differences in examination methodologies, or ethnic/racial differences.

Micro-computed tomography (CT) and cone-beam CT have been widely used to observe lateral incisors with PRG. Gu[10] classified PRG into three types according to the depth and length of the radicular groove. Type I PRG has a short groove with limited length to the coronal third of the root. Type II PRG has a long groove, and its length is beyond the coronal third of the root, while its depth is often shallow. This implies that the root canal system of the tooth with a type II PRG is often simple. Type III PRG has a long and deep groove, which indicates a complex root canal system. However, this classificationn cannot be accurately applied in clinical practice because of complex cases and extremely small structures[11].

Teeth with deep grooves are more likely to show signs of periodontal disease such as bleeding, deep pocket depth, and endodontic-periodontal lesions[12]. Some researchers believe that there are multiple communication channels that exist between periodontal tissues and pulp, such as the apical foramen, accessory foramina, lateral canals, and dentin tubules[3]. Plaque and calculus accumulated in the periodontal pocket may extend into the bottom part of the deep groove with pulpal involvement[13]. The prognosis of a tooth with a PRG is unfavorable. It is influenced by several factors, such as the depth and length of the PRG, the anatomical morphology of the infected root canal system, and the severity of periodontal osseous defects[3].

Multidisciplinary management might be a better approach for treating PRG, but the current evidence is limited. To date, no case reports have observed multidisciplinary management, including endodontic treatment, bone regeneration treatment, and prosthodontic treatment, in the treatment of PRG. This study reports a patient with a type II PRG that was treated with this multidisciplinary approach and his observed prognosis during a 2-year period.

CASE PRESENTATION

Chief complaints

A 40-year-old male patient was admitted to the Department of General Dentistry, The Second Affiliated Hospital of Zhejiang University School of Medicine, with the chief complaint of slight mobility and abscess in the upper right anterior tooth for 15 d.

History of present illness

Slight mobility and abscess in the upper right anterior tooth for 15 d.

History of past illness

He experienced no pain or trauma in this region during the last 10 years.

Personal and family history

There was no personal or family history.

Physical examination

On examination, tooth 12 had an intact crown without defect or fracture, but it did not respond to electric pulp testing (DY310, Denjoy Dental, Changsha, Hunan Province, China). The mobility of tooth 12 was grade I, and it showed a sensitive response to percussion. There was a sinus tract on the buccal gingival surface close to tooth 12 (Figure 1A).

Laboratory examinations

Periodontal examination using a probe (KPC15, Shanghai Kangqiao Dental Instruments Factory, Shanghai, China) revealed a 14 mm depth on the distal side of the root (Figure 1B). The vitality test (Denjoy Dental, Changsha, Hunan Province, China) of tooth 12 was negative. A PRG emerged from the cingulum, which extended to the gingival sulcus and continued disto-apically down to the lingual aspect of the root (Figure 1C).

Imaging examinations

A cone-beam CT scan (Planmeca Romexis Viewer 4.5.0R, Planmeca Oy, Helsinki, Finland) revealed a radiolucency around the distal and palatal side of the root (Figure 1D and E). Dimensional reconstruction (Asentajankatu 6, FIN-00880, Helsinki, Finland) visualized a large bone defect and a long PRG extending up to the apical part of the tooth (Figure 1F and G).

FINAL DIAGNOSIS

Based on the patient's history and clinical and radiographic examination findings, the lesion was diagnosed as a type II PRG with combined endodontic-periodontal lesions. The PRG caused accumulation of plaque and calculus, which in turn caused primary periodontitis and a secondary endodontic infection.

TREATMENT

A multidisciplinary management plan was designed, which comprised root canal therapy, groove sealing, periodontal regenerative procedures, and prosthodontic treatment. The patient signed the informed consent form after being informed about the treatment plan and the possible long-term prognosis of tooth 12.

Periodontal nonsurgical treatment was performed to remove the localized calculus. Root canal therapy was started under the isolation of a rubber dam after 1 wk. Cleaning and shaping were performed with K-files (Mani, Tochigi, Japan) and NiTi hand files (Dentsply Maillefer, Ballaigues, Switzerland). The canal was irrigated with 1% sodium hypochlorite and 0.9% normal saline. Canal filling was completed with gutta-percha (Gapadent, Tianjin, China) and iRoot SP (Innovative BioCeramix, Vancouver, BC, Canada) using the cold lateral compaction technique. The access cavity of the crown was filled with composite resin (3 M ESPE, St. Paul, MN, United States).

Two weeks later, the sinus tract disappeared just before periodontal surgery (Figure 2A). The surgical area (labiopalatine mucosa of teeth 13-22) was disinfected with 5% povidone-iodine after gargling with 0.2% chlorhexidine for 1 min, followed by local anesthesia with 5 mL of 2% lidocaine mixed with 1:100000 epinephrine. A full-thickness mucoperiosteal flap was reflected from the distal side of tooth 13 to the mesial side of tooth 11. The granulation tissue was curetted, and the surface of the root was planned with gracey curette number 5/6 (Hu-Friedy Mfg. Co., Chicago, IL, United States). After degran-

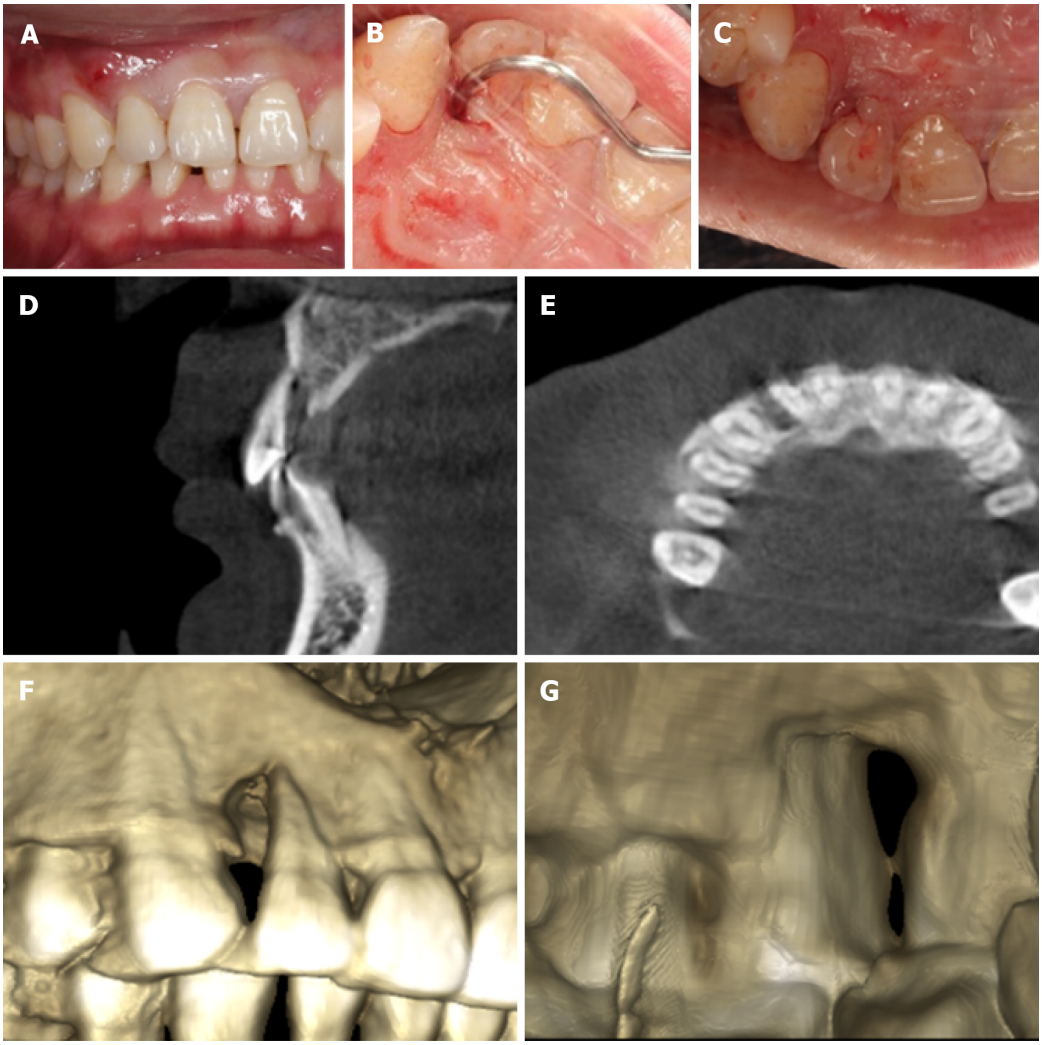

DOI: 10.12998/wjcc.v10.i17.5732 **Copyright** ©The Author(s) 2022.

Figure 1 Tooth 12 with a complex palato-radicular groove and bone defect. A: First visit photograph showed a sinus tract on the buccal gingival surface; B: Periodontal examination revealed a deep probing depth on the distal aspect of the tooth; C: Preoperative photograph showed a groove that emerged from the cingulum; D: Preoperative cone beam computed tomography showed a palatal radiolucency close to the apex of tooth 12; E: Axial view of the middle third section of tooth 12 showed radiolucency around the distal aspect of the root; F: Dimensional reconstruction showing a large bone defect around tooth 12; G: Dimensional reconstruction showed a groove starting from the cingulum and extending to the palatal aspect of the root.

ulation, a 6 mm × 14 mm pear-shaped defect was exposed (Figure 2B). A deep groove was visible extending to the apical part of the root. This groove was prepared with high-speed round diamond (Mani, Tochigi, Japan) under dental microscopy. Minocycline hydrochloride ointment was then applied for 5 min on the root to remove endotoxin. The area was isolated with a gelatin sponge (Jiangxi Xiangen Medical, Nanchang, Jiangxi Province, China) for hemostasis. The PRG was then sealed completely with iRoot BP Plus (Innovative BioCeramix, Vancouver, BC, Canada) (Figure 2C). Periodontal-guided tissue regeneration was performed using a 0.5 g bone graft (Geistlich Biomaterials, Wolhusen, Switzerland) and a 10 mm × 15 mm resorbable membrane (Geistlich Biomaterials, Wolhusen, Switzerland). The flap was sutured with a 3-0 black silk suture (Huawei Medical, Hangzhou, Zhejiang Province, China), and a periodontal dressing was placed (PULPDENT Corporation, Watertown, MA, United States) (Figure 2D). Postoperative panoramic radiography was performed after 2 h (Figure 2E). Cefuroxime axetil (500 mg twice a day for 3 d) and acetaminophen (325 mg twice a day for 1 d) were prescribed after surgery. The patient had no symptoms or discomfort, and sutures were removed after 8 d (Figure 2F).

OUTCOME AND FOLLOW-UP

The patient was re-examined at 6 wk, 3 mo, and 1 year, and 2 years after surgery. The healing was uneventful. At 1 year, there was a reduction in the pocket depth from 13 mm to 3 mm without bleeding. To prevent food impaction, veneer preparation was performed for tooth 12, and a lithium disilicate veneer (Ivoclar Vivadent, Schaan, Liechtenstein) was made to close the space between tooth 12 and

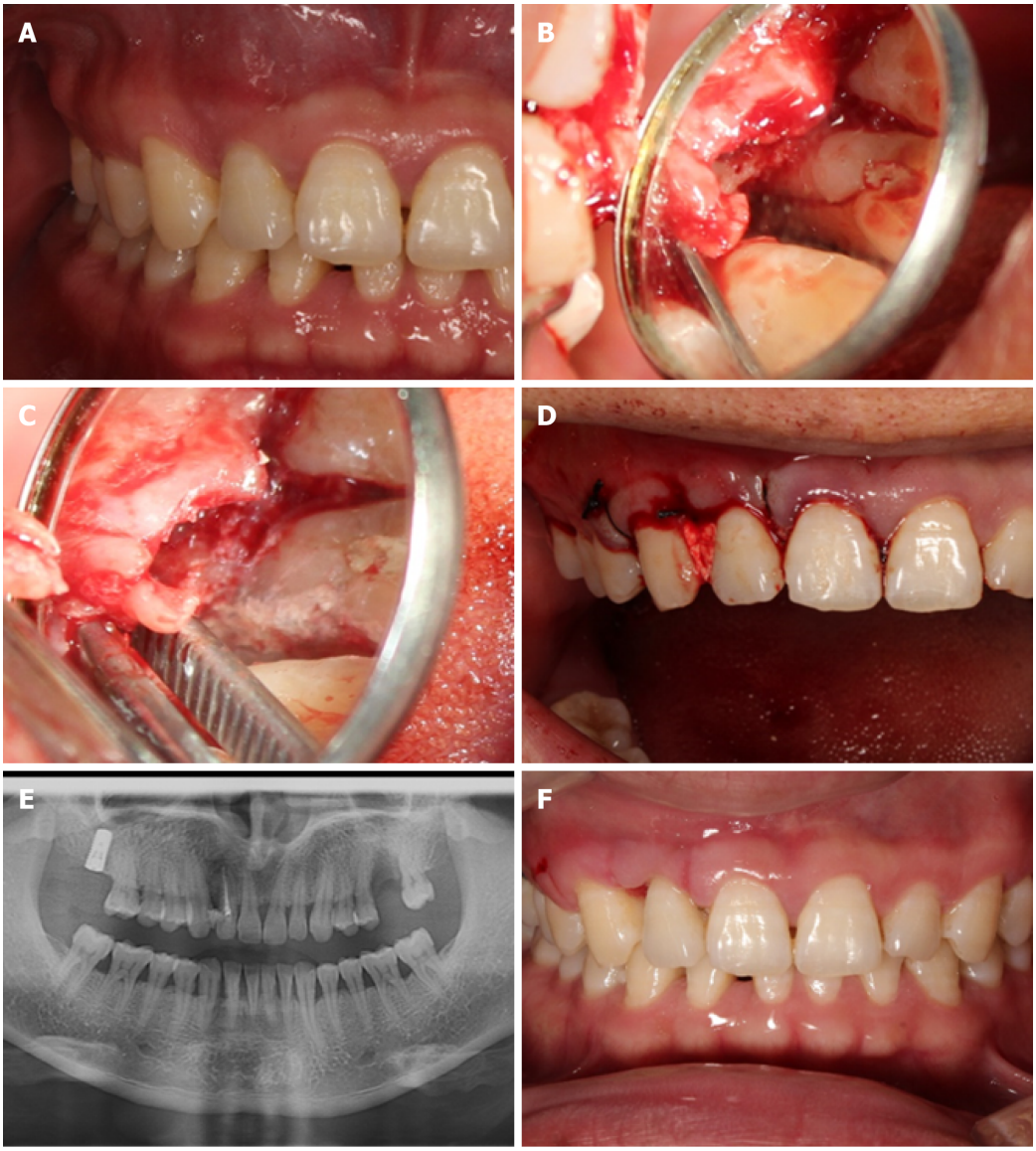

DOI: 10.12998/wjcc.v10.i17.5732 **Copyright** ©The Author(s) 2022.

Figure 2 Multidisciplinary management of tooth 12. (A) The sinus tract disappeared after root canal treatment; (B) A teardrop-shaped defect and a deep groove; (C) Palato-radicular groove sealed with iRoot BP Plus; (D) Suturing; (E) Postoperative panoramic radiography; (F) Image after removing sutures.

tooth 13 (Figure 3A and B). Postoperative cone-beam CT at 1 year showed significant bone formation around the tooth under dimensional reconstruction, and the PRG disappeared (Figure 3C and D). Dimensional reconstruction showed that the bone defect around tooth 12 disappeared. The sealing material was stable, and the groove became flat (Figure 3E and F). At 2 years, tooth 12 showed mild inflammation with dental calculus. However, the periapical radiograph confirmed that the alveolar bone around tooth 12 was stable (Figure 3G). Periodontal nonsurgical treatment was performed immediately.

DISCUSSION

Early diagnosis and treatment of a PRG may significantly improve its prognosis. Without periodontal disease and pulp impairment, conservative treatment, such as sealing the groove, can prevent complications[14]. Based on preoperative imaging findings, the patient was diagnosed with a type II PRG. Usually, shallow grooves are less likely to cause endodontic-periodontal lesions because the communication between the dental pulp and the periodontium is blocked. However, in the present case, the groove of tooth 12 was close to the apical part of the root. The apical foramen and accessory foramina may act as possible communication channels between periodontal infection and the pulp. Interdisciplinary approaches are recommended for managing such situations, such as degranulation of the defect, groove sealing, endodontic treatment, bone regeneration treatment, and prosthodontic

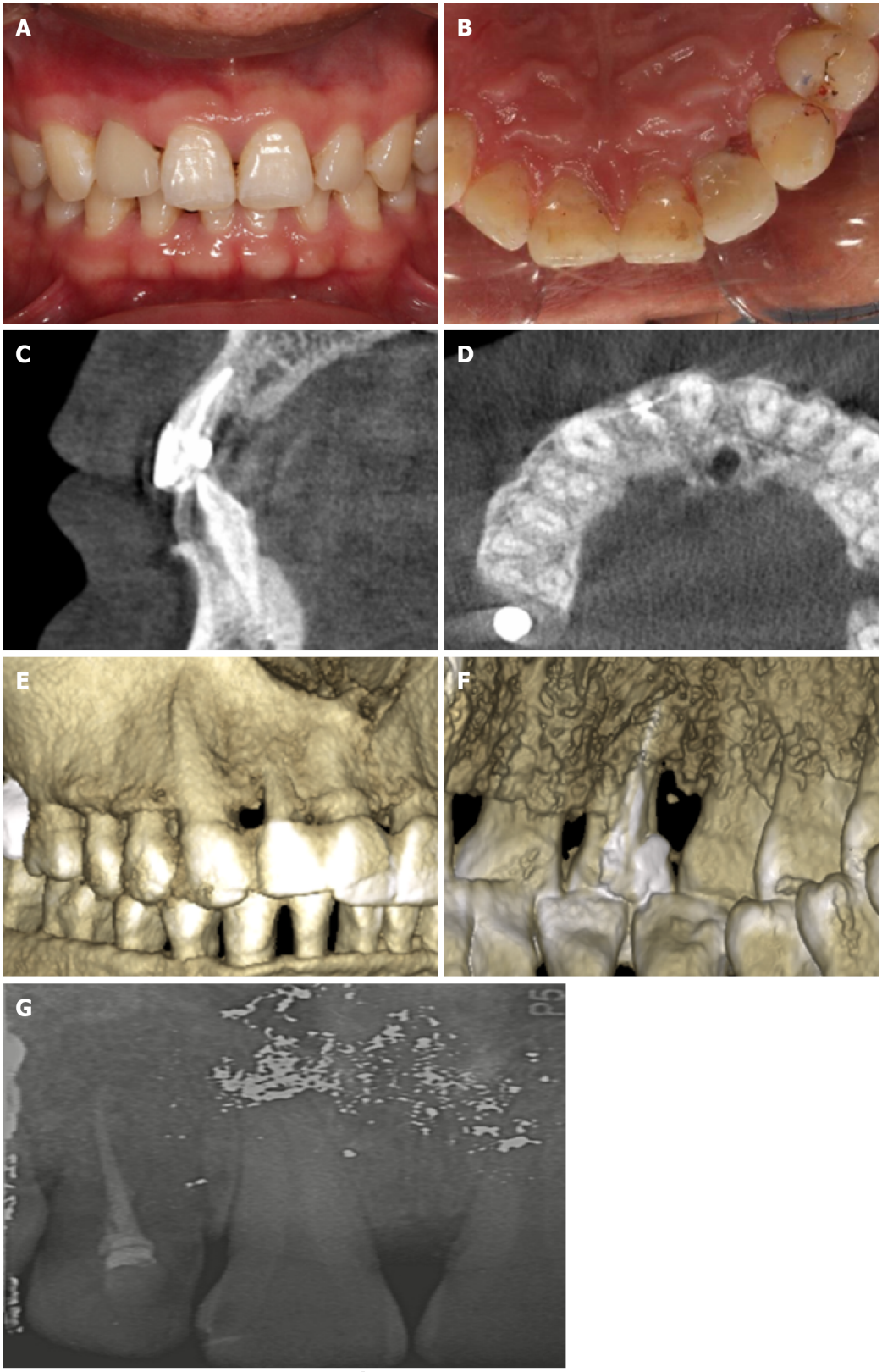

DOI: 10.12998/wjcc.v10.i17.5732 **Copyright** ©The Author(s) 2022.

Figure 3 Two-year follow-up after surgery. A: Buccal view of the clinical photograph after veneer preparation; B: Palatal view of the clinical photograph after veneer preparation; C: Postoperative cone beam computed tomography at 1 year showed the disappearance of diffuse radiolucency; D: Axial view of the middle third section of tooth 12 showed the filling of the bone defect around the distal aspect of the root; E: Dimensional reconstruction showed disappearance of the bone defect around tooth 12; F: Dimensional reconstruction showed that the groove was sealed; G: Periapical radiograph at the 2-year recall.

treatment[15]. Some unknown variables can significantly influence the oral environment. The use of probiotics[16] and natural compounds[17] can modify clinical and microbiological parameters in periodontal patients. They might also alter the outcomes of the technique described in the present

report. All these variables should be considered in future clinical trials. Although sealing the groove in type II PRGs remain controversial, some studies insist that root planning can achieve attachment[14,18]. The final goal of all treatments to make the root surface flat and smooth prevents the formation of plaque and calculus, which could lead to periodontal involvement[19]. There are various therapeutic options available, but the clinical cases are complex and need further exploration.

Many materials have been used for sealing grooves, such as amalgam, composite resin, glass ionomer cement, mineral trioxide aggregate, and iRoot BP plus. Glass ionomer cement has been widely used in the past 10 years, and its advantages include an antibacterial effect, chemical bonding ability, fluoride release property, and ability to attach to epithelial tissue[14,20]. Mineral trioxide aggregates show better biocompatibility. It exhibits lower microleakage when applied to seal the root canal and the periapical tissues[21]. However, the mean setting time of mineral trioxide aggregate is 165.5 min. This implies that mineral trioxide aggregate is unstable and may be washed away during setting[22]. iRoot BP Plus is a convenient and premixed hydraulic bioceramic putty that is newly developed for root canal repair and surgical applications. It shows a shorter setting time and better sealing ability than mineral trioxide aggregates[23]. iRoot BP Plus was also proven to trigger the osteogenic capacity of bone marrow mesenchymal stem cells[24]. Hence, we chose iRoot BP Plus as the sealing material. The healing of the tooth was uneventful, and the bone around the defect was stable after 2 years. To date, no studies have reported the results of iRoot BP Plus used in sealing PRGs. The present case may provide a clinical basis for a new application of this material. Additionally, laser[25] and ozone[26] therapies have been proposed for periodontal health, showing promising results. Future reports are required to test these therapies for PRG.

Restoration with porcelain veneers is the most conservative treatment according to the concept of minimally invasive dentistry. The final goals of this restorative treatment are to save tooth structure and restore function and esthetics. However, the aim of restoring the tooth with a veneer in the present case was to close the space between tooth 12 and tooth 13. Consequently, both food impaction and secondary periodontal problems were prevented. After 2 years of follow-up, the color of the veneer and alveolar bone was found to be stable. This suggests that prosthodontic treatment is necessary for the multidisciplinary management of PRG.

Multidisciplinary management might be a better option for optimal clinical outcomes for complex cases. However, when patients have an extensive groove area and severe complications, even a multidisciplinary approach with the combination of conservative treatment and local surgery cannot result in a favorable prognosis. Intentional extraction of a problematic tooth and subsequent reimplantation might be an alternative option for these patients[27]. On the other hand, this case report still deserves further investigation to confirm the actual role of the present multidisciplinary treatment considering the limited sample size.

CONCLUSION

We report a patient with a type II PRG who was treated with multidisciplinary treatment, including endodontic treatment, bone regeneration treatment, and prosthodontic treatment. The results of a 2-year follow-up indicate that bone regeneration and prosthodontic treatment may contribute to the long-term favorable prognosis of teeth with PRGs, which deserves further investigation.

FOOTNOTES

Author contributions: Ling DH and Zhang YZ contributed to the conception of the study; Shi WP designed the work; Wang YH and Lai DP contributed to the acquisition of the case; Zhang YZ revised the manuscript critically for important intellectual content; all authors have read the manuscript and gave their final approval of the version to be published.

Supported by the Young Innovative Talents of Zhejiang Province, No. 2022RC158.

Informed consent statement: Informed written consent was obtained from the patient for publication of this report and any accompanying images.

Conflict-of-interest statement: The authors declare that they have no conflict of interest.

CARE Checklist (2016) statement: The authors have read the CARE Checklist (2016), and the manuscript was prepared and revised according to the CARE Checklist (2016).

Open-Access: This article is an open-access article that was selected by an in-house editor and fully peer-reviewed by external reviewers. It is distributed in accordance with the Creative Commons Attribution NonCommercial (CC BY-NC 4.0) license, which permits others to distribute, remix, adapt, build upon this work non-commercially, and license their derivative works on different terms, provided the original work is properly cited and the use is non-

commercial. See: https://creativecommons.org/Licenses/by-nc/4.0/

Country/Territory of origin: China

ORCID number: Dan-Hua Ling 0000-0002-6961-9237; Wei-Ping Shi 0000-0003-3441-0959; Yan-Hong Wang 0000-0002-7383-2866; Dan-Ping Lai 0000-0001-7248-8955; Yan-Zhen Zhang 0000-0001-7890-6281.

S-Editor: Guo XR
L-Editor: Filipodia
P-Editor: Guo XR

REFERENCES

1 **Gadagi JS**, Elavarasu S, Ananda D, Murugan T. Successful treatment of osseous lesion associated with palatoradicular groove using local drug delivery and guided tissue regeneration: A report of two cases. *J Pharm Bioallied Sci* 2012; **4**: S157-S160 [PMID: 23066240 DOI: 10.4103/0975-7406.100258]
2 **Ennes JP**, Lara VS. Comparative morphological analysis of the root developmental groove with the palato-gingival groove. *Oral Dis* 2004; **10**: 378-382 [PMID: 15533215 DOI: 10.1111/j.1601-0825.2004.01009.x]
3 **Kim HJ**, Choi Y, Yu MK, Lee KW, Min KS. Recognition and management of palatogingival groove for tooth survival: a literature review. *Restor Dent Endod* 2017; **42**: 77-86 [PMID: 28503472 DOI: 10.5395/rde.2017.42.2.77]
4 **Kishan KV**, Hegde V, Ponnappa KC, Girish TN, Ponappa MC. Management of palato radicular groove in a maxillary lateral incisor. *J Nat Sci Biol Med* 2014; **5**: 178-181 [PMID: 24678222 DOI: 10.4103/0976-9668.127322]
5 **Hungund S**, Kumar M. Palato-radicular groove and localized periodontitis: a series of case reports. *J Contemp Dent Pract* 2010; **11**: 056-062 [PMID: 20978725 DOI: 10.5005/jcdp-11-5-56]
6 **Aksoy U**, Kermeoğlu F, Kalender A, Eren H, Kolsuz ME, Orhan K. Cone-beam computed tomography evaluation of palatogingival grooves: A retrospective study with literature review. *Oral Radiol* 2017; **33**: 193-198 [DOI: 10.1007/s11282-017-0288-6]
7 **Storrer CM**, Sanchez PL, Romito GA, Pustiglioni FE. Morphometric study of length and grooves of maxillary lateral incisor roots. *Arch Oral Biol* 2006; **51**: 649-654 [PMID: 16615990 DOI: 10.1016/j.archoralbio.2006.02.008]
8 **Iqbal N**, Tirmazi SM, Majeed HA, Munir MB. Prevalence of palato gingival groove in maxillary lateral incisors. *Pak Oral Dent J* 2011; **31**: 424-426
9 **Khan AM**, Shah SA, Alam F, Ullah A, Humayun A, Nisar S, Mian FM. Frequency of palatogingival groove in maxillary incisors. *Pak Oral Dent J* 2019; **39**: 82-84
10 **Gu YC**. A micro-computed tomographic analysis of maxillary lateral incisors with radicular grooves. *J Endod* 2011; **37**: 789-792 [PMID: 21787490 DOI: 10.1016/j.joen.2011.03.002]
11 **Tan X**, Zhang L, Zhou W, Li Y, Ning J, Chen X, Song D, Zhou X, Huang D. Palatal Radicular Groove Morphology of the Maxillary Incisors: A Case Series Report. *J Endod* 2017; **43**: 827-833 [PMID: 28343927 DOI: 10.1016/j.joen.2016.12.025]
12 **Gandhi A**, Kathuria A, Gandhi T. Endodontic-periodontal management of two rooted maxillary lateral incisor associated with complex radicular lingual groove by using spiral computed tomography as a diagnostic aid: a case report. *Int Endod J* 2011; **44**: 574-582 [PMID: 21342210 DOI: 10.1111/j.1365-2591.2011.01868.x]
13 **Katwal D**, Fiorica JK, Bleuel J, Clark SJ. Successful Multidisciplinary Management of an Endodontic-Periodontal Lesion Associated With a Palato-Radicular Groove: A Case Report. *Clin Adv Periodontics* 2020; **10**: 88-93 [PMID: 31562681 DOI: 10.1002/cap.10079]
14 **Corr A-Faria P**, Alcântara CE, Santos CR, Marques LS, Ramos-Jorge ML. Palatal radicular groove: clinical implications of early diagnosis and surgical sealing. *J Indian Soc Pedod Prev Dent* 2011; **29**: S92-S94 [PMID: 22169847 DOI: 10.4103/0970-4388.90753]
15 **Miao H**, Chen M, Otgonbayar T, Zhang SS, Hou MH, Wu Z, Wang YL, Wu LG. Papillary reconstruction and guided tissue regeneration for combined periodontal-endodontic lesions caused by palatogingival groove and additional root: a case report. *Clin Case Rep* 2015; **3**: 1042-1049 [PMID: 26734143 DOI: 10.1002/ccr3.441]
16 **Butera A**, Gallo S, Maiorani C, Molino D, Chiesa A, Preda C, Esposito F, Scribante A. Probiotic Alternative to Chlorhexidine in Periodontal Therapy: Evaluation of Clinical and Microbiological Parameters. *Microorganisms* 2020; **9** [PMID: 33383903 DOI: 10.3390/microorganisms9010069]
17 **Costa-Pinto AR**, Lemos AL, Tavaria FK, Pintado M. Chitosan and Hydroxyapatite Based Biomaterials to Circumvent Periprosthetic Joint Infections. *Materials (Basel)* 2021; **14** [PMID: 33567675 DOI: 10.3390/ma14040804]
18 **Schäfer E**, Cankay R, Ott K. Malformations in maxillary incisors: case report of radicular palatal groove. *Endod Dent Traumatol* 2000; **16**: 132-137 [PMID: 11202870 DOI: 10.1034/j.1600-9657.2000.016003132.x]
19 **Mahmood A**, Sajid M, Jamil M, Tahir MW. Palato Gingival Groove. *Prof Med J* 2019; **26**: 559-562 [DOI: 10.29309/TPMJ/2019.26.04.3351]
20 **Antonson SA**, Antonson DE, Brener S, Crutchfield J, Larumbe J, Michaud C, Yazici AR, Hardigan PC, Alempour S, Evans D, Ocanto R. Twenty-four month clinical evaluation of fissure sealants on partially erupted permanent first molars: glass ionomer versus resin-based sealant. *J Am Dent Assoc* 2012; **143**: 115-122 [PMID: 22298552 DOI: 10.14219/jada.archive.2012.0121]
21 **Patro S**, MohaPatra S, MiShra SJJoC, Research D. Comparative evaluation of apical microleakage of retrograde cavities filled with glass ionomer cement, light-cured composite, mineral trioxide aggregate and biodentine. *J Clin Diag Res* 2019; **13**: 18-22 [DOI: 10.7860/JCDR/2019/32601.12609]
22 **Goel M**, Bala S, Sachdeva G. Comperative evaluation of MTA, calcium hydroxide and portland cement as a root end filling

materials: a comprehensive review. *Indian J Dent Sci* 2011; **3**: 83-88

23 **Aydemir S**, Cimilli H, Gerni PM, Bozkurt A, URUCOGLU H, Chandler N, Kartal N. Comparison of the sealing ability of biodentine, iRoot BP plus and mineral trioxide aggregate. *Cumhur Dent J* 2016; **19**: 166-171

24 **Lu J**, Li Z, Wu X, Chen Y, Yan M, Ge X, Yu J. iRoot BP Plus promotes osteo/odontogenic differentiation of bone marrow mesenchymal stem cells *via* MAPK pathways and autophagy. *Stem Cell Res Ther* 2019; **10**: 222 [PMID: 31358050 DOI: 10.1186/s13287-019-1345-3]

25 **Tualzik T**, Chopra R, Gupta SJ, Sharma N, Khare M, Gulati L. Effects of ozonated olive oil and photobiomodulation using diode laser on gingival depigmented wound: A randomized clinical study. *J Indian Soc Periodontol* 2021; **25**: 422-426 [PMID: 34667386 DOI: 10.4103/jisp.jisp_655_20]

26 **Butera A**, Gallo S, Pascadopoli M, Luraghi G, Scribante A. Ozonized Water Administration in Peri-Implant Mucositis Sites: A Randomized Clinical Trial. *Appl Sci* 2021; **11**: 7812 [DOI: 10.3390/app11177812]

27 **Forero-López J**, Gamboa-Martínez L, Pico-Porras L, Niño-Barrera JL. Surgical management with intentional replantation on a tooth with palato-radicular groove. *Restor Dent Endod* 2015; **40**: 166-171 [PMID: 25984480 DOI: 10.5395/rde.2015.40.2.166]

World Journal of Clinical Cases

Submit a Manuscript: https://www.f6publishing.com

World J Clin Cases 2022 June 16; 10(17): 5741-5747

DOI: 10.12998/wjcc.v10.i17.5741

ISSN 2307-8960 (online)

CASE REPORT

Combined thoracic paravertebral block and interscalene brachial plexus block for modified radical mastectomy: A case report

Zhou-Ting Hu, Guang Sun, Shen-Tong Wang, Kai Li

Specialty type: Anesthesiology

Provenance and peer review: Unsolicited article; Externally peer reviewed.

Peer-review model: Single blind

Peer-review report's scientific quality classification

Grade A (Excellent): 0
Grade B (Very good): 0
Grade C (Good): C
Grade D (Fair): D
Grade E (Poor): 0

P-Reviewer: Amornyotin S, Thailand; Spataru A, Canada

Received: October 28, 2021
Peer-review started: October 28, 2021
First decision: December 27, 2021
Revised: January 14, 2022
Accepted: April 4, 2022
Article in press: April 4, 2022
Published online: June 16, 2022

Zhou-Ting Hu, Shen-Tong Wang, Kai Li, Department of Anesthesia, China-Japan Union Hospital of Jilin University, Changchun 130033, Jilin Province, China

Guang Sun, Department of Breast Surgery, China-Japan Union Hospital of Jilin University, Changchun 130033, Jilin Province, China

Corresponding author: Kai Li, MD, Assistant Professor, Doctor, Department of Anesthesia, China-Japan Union Hospital of Jilin University, No. 126 Xiantai Avenue, Changchun 130033, Jilin Province, China. likai@jlu.edu.cn

Abstract

BACKGROUND

Modified radical mastectomy (MRM) is the most common surgical treatment for breast cancer. General anesthesia poses a challenge in fragile MRM patients, including cardiovascular instability, insufficient postoperative pain control, nausea and vomiting. Thoracic paravertebral block (TPVB) is adequate for simple mastectomy, but its combination with interscalene brachial plexus block (IBPB) has not yet been proved to be an effective anesthesia method for MRM.

CASE SUMMARY

We describe our experience of anesthesia and pain management in 10 patients with multiple comorbidities. An ultrasound-guided TPVB was placed at T2-T3 and T5-T6, and combined with IBPB, with administration of 10, 15 and 5 mL of 0.5% ropivacaine, respectively. A satisfactory anesthetic effect was proved by the absence of ipsilateral tactile sensation within 30 min. Propofol 3 mg/kg/h and oxygen supplementation *via* a nasal cannula were administered during surgery. None of the patients required additional narcotics, vasopressors, or conversion to general anesthesia. The maximum pain score was 2 on an 11-point numerical rating scale. Two patients required one dose of celecoxib 8 h postoperatively and none reported nausea or emesis.

CONCLUSION

This case series demonstrated that combined two-site TPVB and small-volume IBPB with sedation can be used as an alternative anesthetic modality for MRM, providing good postoperative analgesia.

Key Words: Modified radical mastectomy; Paravertebral block; Brachial plexus block; Sedation; Case report

©The Author(s) 2022. Published by Baishideng Publishing Group Inc. All rights reserved.

Core Tip: Thoracic paravertebral block (TPVB) has been proved to be adequate for simple mastectomy. However, TPVB combined with interscalene brachial plexus block (IBPB) has not yet been proved to be an effective anesthesia method for modified radical mastectomy (MRM). This case series demonstrated that combined two-site TPVB and small-volume IBPB with sedation can be used as an alternative anesthetic modality for MRM, which avoids the potential risks of general anesthesia and phrenic nerve paralysis especially in frail patients with multiple comorbidities, and provides extended postoperative analgesia.

Citation: Hu ZT, Sun G, Wang ST, Li K. Combined thoracic paravertebral block and interscalene brachial plexus block for modified radical mastectomy: A case report. *World J Clin Cases* 2022; 10(17): 5741-5747
URL: https://www.wjgnet.com/2307-8960/full/v10/i17/5741.htm
DOI: https://dx.doi.org/10.12998/wjcc.v10.i17.5741

INTRODUCTION

The National Breast Cancer Foundation has confirmed that breast cancer is the second most common cancer in women, with 3.8 million women diagnosed in the United States as of January 1, 2019[1]. Modified radical mastectomy (MRM) is the most common surgical treatment for breast cancer[2]. Modified radical mastectomy is frequently performed under general anesthesia. However, general anesthesia may pose challenges especially in elderly and frail patients with comorbidities. Furthermore, some components of general anesthesia are associated with chronic pain, vomiting and impaired respiratory function[3,4]. On the other hand, regional anesthesia is commonly believed to decrease cardiovascular, respiratory and gastrointestinal adverse events in high-risk patients[5,6], and attenuate immune suppression[7]. Accordingly, there is growing interest in loco-regional anesthesia as an alternative to general anesthesia for MRM.

Thoracic epidural anesthesia combined with interscalene brachial plexus block (IBPB) has been reported to be an adequate anesthesia technique for MRM[8]. Thoracic paravertebral block (TPVB) is efficacious for simple mastectomy surgery[9], but the efficacy of TPVB combined with IBPB has not yet been studied for MRM.

In this case series, we describe our experience of intraoperative anesthesia and postoperative pain management in ten elderly and fragile MRM patients who underwent ultrasound-guided two-site TPVB and small-volume IBPB combined with sedation.

CASE PRESENTATION

Chief complaints

Ten patients scheduled for elective MRM were anesthetized by the same expert in ultrasound-guided loco-regional anesthesia in our facility between January 2019 and March 2019.

History of present illness

All patients were identified as suitable candidates for loco-regional anesthesia using current anticoagulation recommendations.

History of past illness

Patient characteristics are shown in Table 1.

Imaging examinations

All of the ten cases were diagnosed as breast neoplasm by preoperative imaging examinations either by unltrasoud or computerized tomography, suspected to be malignant.

FINAL DIAGNOSIS

All patients were identified as suitable candidates for loco-regional anesthesia using current anticoagulation recommendations.

Table 1 Patients' characteristics

Case	Sex	Age	BMI, kg/m²	Comorbidities	Surgical procedure	Oncology state
Patient 1	Female	65	21.1	HT, COPD	M + LND	T1N1M0
Patient 2	Female	72	21.4	HT	M + SNB	T2N1M0
Patient 3	Female	65	24.4	HT, COPD	M + LND	T2N3M0
Patient 4	Female	78	24.2	DM, AS	M	-
Patient 5	Female	73	20.2	HT, DM, CI	M + LND	T2N1M0
Patient 6	Female	73	30.4	HT, DM, MI	M	-
Patient 7	Female	65	24.2	HT, AS, MI	M	-
Patient 8	Female	68	21.9	HT, MI	M + SNB	T1N0M0
Patient 9	Female	65	33.6	HT, DM	M + SNB	T2N0M0
Patient 10	Female	79	24.5	DM, MI, CI	M + SNB	T1N1M0

AS: Arteriosclerosis; CI: Cerebral infarction; COPD: Chronic obstructive pulmonary disease; DM: Diabetes mellitus; HT: Hypertension; MI: Myocardial infarction; M: Mastectomy; SNB: Sentinel lymph node biopsy; LND: Lymph node dissection.

TREATMENT

On arrival in the preoperative area, standard monitoring was conducted and the patients were placed in the lateral decubitus position and received intravenous sedation with midazolam. TPVB was then initiated. A 10 MHz linear array transducer was vertically placed in the sagittal, paramedian plane, approximately 2-2.5 cm lateral to the spinous process at the predetermined level, and the following structures were identified: transverse process, parietal pleura, superior costotransverse ligament and the desired paravertebral space. Following infiltration of the skin with 2% lidocaine, a 22-G × 50-mm needle was advanced using the out-of-plane technique. Eventually, a "pop" was felt as the needle tip penetrated the anterior border of the superior costotransverse ligament. Hydro dissection with normal saline was used to confirm correct placement of the needle tip by anterior displacement of the parietal pleura (Figure 1). Ten and 15 mL of 0.5% ropivacaine were injected at two thoracic (T) levels: T2-T3 and T5-T6, respectively[10,11]. TPVB was supplemented with ipsilateral IBPB using the in-plane technique at C6 Level with an injection of 5 mL ropivacaine (0.5%). Sensory blockade was assessed by pin prick testing using a 22-G short bevel needle. A satisfactory anesthetic effect was defined as the absence of ipsilateral tactile sensation covering the region between the clavicle and T7 dermatome, and from the ipsilateral parasternal area to the axilla within 30 min after local anesthetic administration. The time required to perform the blocks ranged from 5 to 10 min.

Patients were sedated with a continuous infusion of propofol 3 mg/kg/h, and oxygen supplementation *via* a nasal cannula during surgery. A bolus of 1 μg/kg fentanyl was available for intraoperative breakthrough pain. Conversion to general anesthesia was considered if required. The patients were offered 200 mg celecoxib orally as needed for moderate postoperative pain, and an intravenous bolus of 3 mg morphine for severe pain.

OUTCOME AND FOLLOW-UP

The average duration of surgery was 115 (± 21.7) min. None of the patients required intraoperative narcotics, or conversion to general anesthesia. The patients were hemodynamically stable and did not require vasopressors. No complications due to local anesthesia, such as allergic reaction, paresthesia, vascular injury and toxicity were observed. All patients were transferred to a regular nursing ward shortly after surgery.

Postoperative pain was well controlled. Eight patients reported a maximum pain score of 2 out of 10 points and did not require additional analgesics during a 12-h-interval follow-up in the first three postoperative days. Two patients needed one dose of celecoxib 8 h after surgery. None of the patients required morphine. All patients were satisfied with their anesthesia and pain management. All patients resumed normal food intake within 4 h and were able to use the surgical-side hand within 24 h. The recovery period was uneventful, with no reports of postoperative nausea and vomiting (PONV). Timeline of all cases are shown in Table 2.

Table 2 Timeline of the case series

Case series	Ten elderly and fragile patients with multiple comorbidities scheduled for modified radical mastectomy
Interventions	Standard monitoring and sedation with midazolam in lateral decubitus position before regional anesthesia. 10 and 15 mL of 0.5% ropivacaine injected at T2-T3 and T5-T6 as thoracic paravertebral block by ultrasound-guided using the out-of-plane technique.5 mL of 0.5% ropivacaine injected as interscalene brachial plexus block using the in-plane technique
Results	Sensory blockade assessed by pin prick testing, covering the region between the clavicle and T7 dermatome, and from the ipsilateral parasternal area to the axilla. Only sedated with propofol and oxygen supplementation *via* a nasal cannula during surgery. Vasopressors, narcotics or general anesthesia was not applied but considered if required for surgery
Follow-up	Postoperative pain was well controlled as a 2 out of 10 points pain score without celecoxib or morphine. Normal food intake was resumed within 4 h and surgical-side hand were able to use within 24 h. Recovery period was uneventful, without complications or postoperative nausea and vomiting

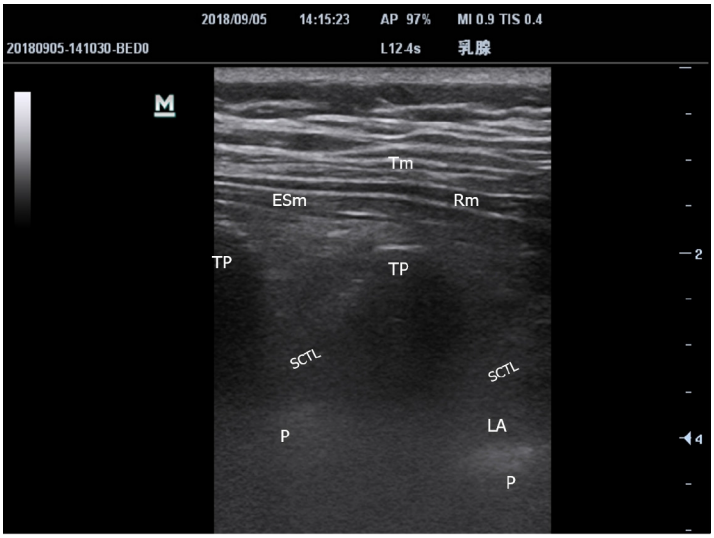

DOI: 10.12998/wjcc.v10.i17.5741 **Copyright** ©The Author(s) 2022.

Figure 1 Ultrasound image of the paravertebral block. Tm: Trapezius muscle; Rm: Rhomboideus muscle; ESm: Erector spinal muscle; TP: Transverse process; SCTL: Superior costotransverse ligament; LA: Local anesthesia agency; P: Pleura.

DISCUSSION

To the best of our knowledge, compared to single cases using TPVB for awake mastectomy[9], there are no previous reports on the combination of two-sites TPVB with IBPB as the sole anesthetic technique for MRM. In our 10 elderly patients with multiple comorbidities, this technique provided potent alternative anesthesia with extended postoperative analgesia, and avoided the use of opioids, vasopressors, neuromuscular blocking agents and mechanical ventilation. In addition, PONV, cardiovascular and pulmonary complications were not observed. A similar observation was confirmed by a single case report[12]. Also, thoracic epidural anesthesia combined with IBPB[8] provided similar anesthesia and analgesia compared to ultrasound-guided TPVB; however, the latter is a safer option. Although our technique requires expertise in ultrasound-guided loco-regional blocks and might not replace general anesthesia as routine for MRM, it remains a reliable alternative when general anesthesia is deemed undesirable or poses unacceptable risks.

With the assistance of real-time ultrasound, many high-risk regional blocks, such as TPVB, have become more popular and are safer. TPVB involves the injection of local anesthetics in the vicinity of spinal nerves emerging from the intervertebral foramina resulting in ipsilateral somatic and sympathetic nerve blockade in multiple contiguous dermatomes above and below the site of injection [13]. Although four or five site blocks provide reliable analgesia[14], this is not practical for MRM. One study showed that contrast dye spread to 4.5 dermatome segments vertically after a single paravertebral injection compared to 6 segments after double-level injections[13]. An improved analgesic effect was demonstrated with double-level TPVB compared to single-level[11]. Based on these previous reports, we decided to use two-level TPVB. Effective anesthesia of the axilla and pectoral major muscle are essential for MRM, and is not achieved by TPVB alone. This area is innervated by the lateral and medial pectoral nerves, long thoracic nerve and thoracodorsal nerve, all originating from the brachial plexus [15]. Accordingly, IBPB is an essential complement for TPVB in MRM.

Vigilance and continuous monitoring are mandatory, regarding potential complications such as inadvertent vascular puncture, epidural or intrathecal spread, pneumothorax, serious bradycardia, contralateral Harlequin syndrome and Horner's syndrome[16]. Even though there is less possibility of spreading to the intervertebral foramen and phrenic nerve and extensive intramuscular deposition with 5 mL IBPB than with 20 mL[17], it is also much better to administer nasal oxygen for 12 h. Despite the aforementioned potential complications, regional anesthesia and analgesia enhance postoperative oral intake, ambulation and rehabilitation[5], and potentially increase patient tolerance to early chemotherapy as compared with general anesthesia.

Other superficial facial blocks have been reported in case reports of MRM despite the uncertainty of local anesthetic diffusion and patchy coverage. In order to ensure the anesthesia effect, serratus anterior plane block was often combined with remifentanil infusion and 3 supplementary subcutaneous infiltrations of the intercostobrachial nerve, medial branches of the intercostal nerve and superficial cervical plexus[18], or 30 mg ketamine[19]. It was confirmed that the erector spinae plane at T4 was feasible for MRM, however fentanyl supplementation was required in all cases[20]. The Pecs II nerve block with high volume and perfect diffusion may be an alternative to the combination of two-site TPVB and small-volume IBPB for further avoidance of respiratory depression[21]. Pecs II nerve block is aimed to block at least the pectoral nerves, the intercostobrachial, intercostals III-IV-V-VI and the long thoracic nerve. These nerves need to be blocked to provide complete analgesia during breast surgery, and it is an alternative or a rescue block if paravertebral blocks and thoracic epidurals failed, with the indications such as tumorectomies, extensive excisions, and axillary clearances.

The reliable impeccable anesthesia effect and simple and convenient operation associated with ultrasound-guided two-spot TPVB combined with small-volume IBPB has been highlighted and initially proved by the present ten cases. Regarding the thoracic dermatotome and breast MRM, ultrasound-guided TPVB provide thorough anesthetic effect similar to thoracic epidural anesthesia, with better visualization and higher successful rate. Two-sites TPVB guarantee more extensive anesthesia scope than single-site, especially for intercostobrachial nerve, avoiding neither tedious process nor puncture-related pain required by 3-5 sites injection. Because axillary dermatotome, pectoral major and minor muscles are dominated by nerve roots of bronchial plexus, IBPB is more straightforward, impeccable and efficient than terminal branch block and superficial plane block, such as serratus anterior plane block, Pecs II nerve block, medial bronchial cutaneous nerve block, which facilitate puncture operation and local anesthetics dosing. The fearful anxiety of phrenic nerve paralysis associated with IBPB, is also evitable when using 5 mL rather than routine volume of 20 mL, with equivalent effect. With the better visualization and higher successful rate provided by ultrasound-guided intervention technique, the method might be also feasible in the morbid obesity population.

Our observation was performed in a single site and restricted to 10 Chinese patients. Both efficacy and safety outcomes were highly related with anesthetist's manipulation capability of ultrasound-guided regional anesthesia. Further multi-center randomized control trial with enough sample size is needed to finally determine the feasibility, efficiency and safety of the novel combinations. For further improvement, subcutaneous infiltration of the supraclavicular nerve might be supplemented for the dermatomal area around the clavicle, pectoralis major, and deltoid[12]. Further decrease of either concentration or volume of ropivacaine is worth of investigation with regard to the equivalent and safe alternative approach. Diaphragmatic activity monitoring by ultrasound, or pulmonary function test should be performed during perioperative period to provide authentic proof in terms of pulmonary function.

CONCLUSION

Two-spot TPVB combined with small-volume IBPB is considered a reliable and safe alternative anesthetic technique for MRM, which avoids the potential risks of general anesthesia especially in frail patients with multiple comorbidities, and provides extended postoperative analgesia.

FOOTNOTES

Author contributions: Li K was the patients' anesthetist; Sun G was the patients' surgeon; Li K reviewed the literature and contributed to study conception and design, acquisition, analysis and interpretation of data, drafting the article, revising it critically for important intellectual content; Hu ZT and Wang ST were contributed to follow-up, acquisition, revising the article critically for important intellectual content; all authors have read and approved the final manuscript, and agreed to be accountable for all aspects of the work.

Informed consent statement: Informed written consent was obtained from the patient for publication of this report and any accompanying images.

Conflict-of-interest statement: The authors declare that they have no conflict of interest.

CARE Checklist (2016) statement: The authors have read the CARE Checklist (2016), and the manuscript was prepared and revised according to the CARE Checklist (2016).

Open-Access: This article is an open-access article that was selected by an in-house editor and fully peer-reviewed by external reviewers. It is distributed in accordance with the Creative Commons Attribution NonCommercial (CC BY-NC 4.0) license, which permits others to distribute, remix, adapt, build upon this work non-commercially, and license their derivative works on different terms, provided the original work is properly cited and the use is non-commercial. See: https://creativecommons.org/Licenses/by-nc/4.0/

Country/Territory of origin: China

ORCID number: Zhou-Ting Hu 0000-0002-3440-7621; Guang Sun 0000-0001-5174-9829; Shen-Tong Wang 0000-0003-0296-2636; Kai Li 0000-0002-9342-8836.

S-Editor: Liu JH
L-Editor: A
P-Editor: Liu JH

REFERENCES

1 **DeSantis CE**, Ma J, Gaudet MM, Newman LA, Miller KD, Goding Sauer A, Jemal A, Siegel RL. Breast cancer statistics, 2019. *CA Cancer J Clin* 2019; **69**: 438-451 [PMID: 31577379 DOI: 10.3322/caac.21583]
2 **Jones C**, Lancaster R. Evolution of Operative Technique for Mastectomy. *Surg Clin North Am* 2018; **98**: 835-844 [PMID: 30005777 DOI: 10.1016/j.suc.2018.04.003]
3 **Shirakami G**, Teratani Y, Segawa H, Matsuura S, Shichino T, Fukuda K. Omission of fentanyl during sevoflurane anesthesia decreases the incidences of postoperative nausea and vomiting and accelerates postanesthesia recovery in major breast cancer surgery. *J Anesth* 2006; **20**: 188-195 [PMID: 16897238 DOI: 10.1007/s00540-006-0413-x]
4 **Sessler DI**, Pei L, Huang Y, Fleischmann E, Marhofer P, Kurz A, Mayers DB, Meyer-Treschan TA, Grady M, Tan EY, Ayad S, Mascha EJ, Buggy DJ; Breast Cancer Recurrence Collaboration. Recurrence of breast cancer after regional or general anaesthesia: a randomised controlled trial. *Lancet* 2019; **394**: 1807-1815 [PMID: 31645288 DOI: 10.1016/S0140-6736(19)32313-X]
5 **Malik OS**, Brovman EY, Urman RD. The Use of Regional or Local Anesthesia for Carotid Endarterectomies May Reduce Blood Loss and Pulmonary Complications. *J Cardiothorac Vasc Anesth* 2019; **33**: 935-942 [PMID: 30243870 DOI: 10.1053/j.jvca.2018.08.195]
6 **Ahn EJ**, Kim HJ, Kim KW, Choi HR, Kang H, Bang SR. Comparison of general anaesthesia and regional anaesthesia in terms of mortality and complications in elderly patients with hip fracture: a nationwide population-based study. *BMJ Open* 2019; **9**: e029245 [PMID: 31501111 DOI: 10.1136/bmjopen-2019-029245]
7 **Wall T**, Sherwin A, Ma D, Buggy DJ. Influence of perioperative anaesthetic and analgesic interventions on oncological outcomes: a narrative review. *Br J Anaesth* 2019; **123**: 135-150 [PMID: 31255291 DOI: 10.1016/j.bja.2019.04.062]
8 **Sundarathiti P**, Pasutharnchat K, Kongdan Y, Suranutkarin PE. Thoracic epidural anesthesia (TEA) with 0.2% ropivacaine in combination with ipsilateral brachial plexus block (BPB) for modified radical mastectomy (MRM). *J Med Assoc Thai* 2005; **88**: 513-520 [PMID: 16146257]
9 **Santonastaso DP**, de Chiara A, Piccioni F, Tognù A, Agnoletti V. Awake mastectomy under ultrasound guided thoracic paravertebral block in elderly patients. *J Clin Anesth* 2018; **47**: 50-51 [PMID: 29574286 DOI: 10.1016/j.jclinane.2018.03.014]
10 **Abdallah FW**, Morgan PJ, Cil T, McNaught A, Escallon JM, Semple JL, Wu W, Chan VW. Ultrasound-guided multilevel paravertebral blocks and total intravenous anesthesia improve the quality of recovery after ambulatory breast tumor resection. *Anesthesiology* 2014; **120**: 703-713 [PMID: 24071616 DOI: 10.1097/ALN.0000436117.52143.bc]
11 **Kasimahanti R**, Arora S, Bhatia N, Singh G. Ultrasound-guided single- vs double-level thoracic paravertebral block for postoperative analgesia in total mastectomy with axillary clearance. *J Clin Anesth* 2016; **33**: 414-421 [PMID: 27555203 DOI: 10.1016/j.jclinane.2016.01.027]
12 **Nirmal CP**, Gowrishankar C. Thoracic Paravertebral Block and Interscalene Brachial Plexus Block Superficial Cervical Plexus Block for Breast Surgery in A Patient with Ischemic Heart Disease. *BLOOD PRESSURE* 2019; **130**: 80
13 **Hara K**, Sakura S, Nomura T, Saito Y. Ultrasound guided thoracic paravertebral block in breast surgery. *Anaesthesia* 2009; **64**: 223-225 [PMID: 19143711 DOI: 10.1111/j.1365-2044.2008.05843.x]
14 **Naja ZM**, El-Rajab M, Al-Tannir MA, Ziade FM, Tayara K, Younes F, Lönnqvist PA. Thoracic paravertebral block: influence of the number of injections. *Reg Anesth Pain Med* 2006; **31**: 196-201 [PMID: 16701182 DOI: 10.1016/j.rapm.2005.12.004]
15 **Kaya M**, Oğuz G, Şenel G, Kadıoğulları N. Postoperative analgesia after modified radical mastectomy: the efficacy of interscalene brachial plexus block. *J Anesth* 2013; **27**: 862-867 [PMID: 23736824 DOI: 10.1007/s00540-013-1647-z]
16 **Batra RK**, Krishnan K, Agarwal A. Paravertebral block. *J Anaesthesiol Clin Pharmacol* 2011; **27**: 5-11 [PMID: 21804697]
17 **Stundner O**, Meissnitzer M, Brummett CM, Moser S, Forstner R, Koköfer A, Danninger T, Gerner P, Kirchmair L, Fritsch G. Comparison of tissue distribution, phrenic nerve involvement, and epidural spread in standard- vs low-volume ultrasound-guided interscalene plexus block using contrast magnetic resonance imaging: a randomized, controlled trial. *Br J Anaesth* 2016; **116**: 405-412 [PMID: 26865133 DOI: 10.1093/bja/aev550]

18 **Sanllorente-Sebastián R**, de Vicente-Lorenzo JM, Mediavilla-Herrera FJ, Gutiérrez-García S, Alario-Poza IS, Bustinza-Beaskoetxea Z. Case report: serratus intercostal plane block/BRILMA and sedation for mastectomy in a high risk patient. *Rev Esp Anestesiol Reanim (Engl Ed)* 2019; **66**: 46-48 [PMID: 30115502 DOI: 10.1016/j.redar.2018.06.009]

19 **Pedrosa FP**, Cravo H. Serratus Anterior Plane Block for Awake Breast Surgery: A Case Report. *A A Pract* 2020; **14**: e01354 [PMID: 33295745 DOI: 10.1213/XAA.0000000000001354]

20 **Malawat A**, Verma K, Jethava D, Jethava DD. Erector spinae plane block for complete surgical anaesthesia and postoperative analgesia for breast surgeries: A prospective feasibility study of 30 cases. *Indian J Anaesth* 2020; **64**: 118-124 [PMID: 32139929 DOI: 10.4103/ija.IJA_639_19]

21 **Blanco R**, Fajardo M, Parras Maldonado T. Ultrasound description of Pecs II (modified Pecs I): a novel approach to breast surgery. *Rev Esp Anestesiol Reanim* 2012; **59**: 470-475 [PMID: 22939099 DOI: 10.1016/j.redar.2012.07.003]

World Journal of Clinical Cases

Submit a Manuscript: https://www.f6publishing.com

World J Clin Cases 2022 June 16; 10(17): 5748-5755

DOI: 10.12998/wjcc.v10.i17.5748

ISSN 2307-8960 (online)

CASE REPORT

Chondromyxoid fibroma of the cervical spine: A case report

Cheng Li, Sen Li, Wei Hu

Specialty type: Oncology

Provenance and peer review: Unsolicited article; Externally peer reviewed.

Peer-review model: Single blind

Peer-review report's scientific quality classification

Grade A (Excellent): 0
Grade B (Very good): 0
Grade C (Good): C
Grade D (Fair): 0
Grade E (Poor): 0

P-Reviewer: Muthu S, India

Received: October 30, 2021
Peer-review started: October 30, 2021
First decision: March 3, 2022
Revised: March 14, 2022
Accepted: April 4, 2022
Article in press: April 4, 2022
Published online: June 16, 2022

Cheng Li, Sen Li, Wei Hu, Fifth Clinical Medical College, Guilin Medical University, Guilin 541002, Guangxi Zhuang Autonomous Region, China

Corresponding author: Wei Hu, MD, Chief Doctor, Fifth Clinical Medical College, Guilin Medical University, Wenming Road, Guilin 541002, Guangxi Zhuang Autonomous Region, China. howie189@126.com

Abstract

BACKGROUND

Chondromyxoid fibroma (CMF) is an unusual benign tumour of cartilaginous tissues that may be confused with other malignant tumours. It is rarely seen in the cervical spine.

CASE SUMMARY

A 24-year-old young woman was admitted to the hospital because of neck and shoulder pain. Computed tomography, magnetic resonance imaging, X-ray and other imaging examinations of the cervical spine and laboratory-related indicators combined with intraoperative pathology revealed that the patient had cervical CMF. We performed total resection of the vertebral body and intervertebral disc, and internal fixation was performed to simultaneously maintain the stability of the entire spine. The clinical results from extensive resection were satisfactory. At the 2-year follow-up, the patient's symptoms had not recurred.

CONCLUSION

CMF is a benign primary bone tumour that is rarely located in the vertebral bone. Accurate initial diagnosis of these tumours is important for appropriate treatment. *En bloc* surgical resection of the tumour is the cornerstone of treatment.

Key Words: Chondromyxoid fibroma; Benign cartilaginous tumour; Cervical tumour; Case report

©The Author(s) 2022. Published by Baishideng Publishing Group Inc. All rights reserved.

Core Tip: The case was diagnosed and operated independently by our hospital, and the patient had a good prognosis. Because of the rarity of the case itself and the rare location of tumor growth and infiltration in the case, we not only introduced the case itself in detail, but also made a retrospective study of a series of related literatures.

Citation: Li C, Li S, Hu W. Chondromyxoid fibroma of the cervical spine: A case report. *World J Clin Cases* 2022; 10(17): 5748-5755
URL: https://www.wjgnet.com/2307-8960/full/v10/i17/5748.htm
DOI: https://dx.doi.org/10.12998/wjcc.v10.i17.5748

INTRODUCTION

Chondromyxoid fibroma (CMF) is a rare benign tumour of cartilaginous origin. It accounts for less than 0.5% of bone tumours and less than 2% of benign bone tumours[1]. CMF was first reported in 1948 by Jaffe and Lichtenstien[2], and it was defined by the World Health Organization as "a benign tumour characterized by lobules of spindle-shaped or stellate cells with abundant myxoid or chondroid intercellular material separated by zones of more cellular tissue rich in spindle-shaped or round cells with varying number of multinucleated giant cells of different sizes". The morbidity rate is higher in male patients than female patients, and the male-to-female ratio is approximately 1.28:1[3]. Karyotype analysis of CMF tumour cells has demonstrated that all the cells contain clonal rearrangements of chromosome 6 and 6q13, which are not related to other types of bone and soft tissue tumours. Inv (6) (p25q13) was seen only in CMF. The persistent occurrence of 6q13 rearrangements suggests a specific oncogenic mechanism in CMFs that most likely involves the activation of oncogenes. CMF of the cervical spine is rare, but cases have been reported in various parts of the human body[4]. One case of CMF of the C7 vertebral body has been treated surgically. The operative procedure was successful, and the postoperative follow-up was satisfactory.

CASE PRESENTATION

Chief complaints

A 24-year-old young woman was admitted to the hospital because of "neck and shoulder pain for more than one month, aggravated with activity limitation for one day".

History of present illness

One month earlier, neck and shoulder pain began without obvious inducement, alternating on both sides, which was aggravated after fatigue and slightly relieved after rest. There was no sign of radiation pain, numbness or weakness of the upper limbs. One day before admission, the distending pain in the neck and shoulder was aggravated again, accompanied by limitation of neck movement.

History of past illness

The patient had been healthy in the past.

Personal and family history

The patient, who had a daughter, with no family history of heredity.

Physical examination

Physical examination showed tenderness and percussion pain of the cervical spinous process. No radiating nerve pain was detected, and other related pathological signs were negative.

Laboratory examinations

After admission, no obvious abnormalities were found in relevant laboratory examinations, female breast colour Doppler ultrasound, genitourinary system colour Doppler ultrasound or lung computed tomography (CT). A Tuberculosis(TB) test was also negative.

Imaging examinations

Cervical CT (Figure 1) showed that the bone structure of each cervical vertebral body was complete. The C7 vertebral body and C7/T1 intervertebral disc showed irregular high-density shadows with clear boundaries, and other bone density shadows showed no obvious abnormalities. Magnetic resonance imaging (MRI) (Figure 2) of the cervical vertebrae showed patchy abnormal signals at C7, low signals on T1-weighted images (T1WI), high and low mixed signals in T2WI and fat suppression images, swelling of adjacent soft tissue and inhomogeneous enhancement after enhancement. No abnormal signal was found in the C3/4-C6/7 intervertebral discs. The signal of the cervical spinal cord was normal.

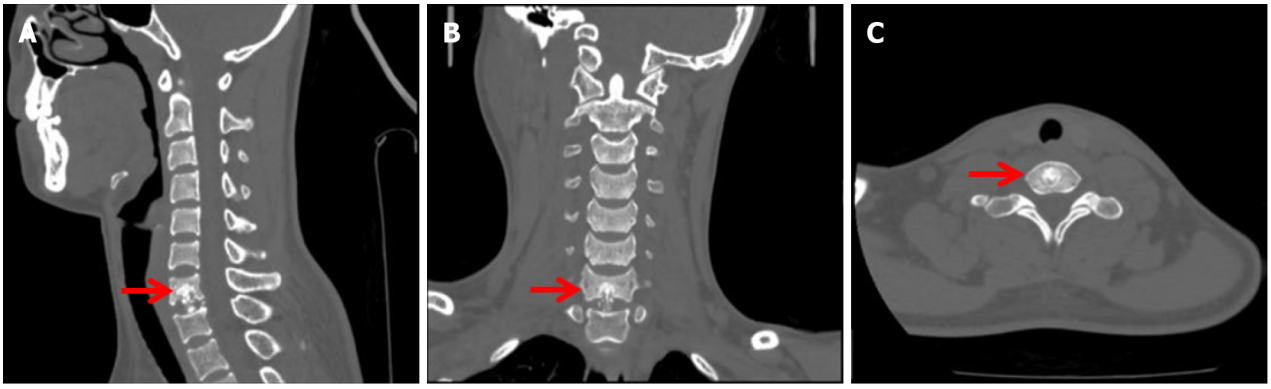

DOI: 10.12998/wjcc.v10.i17.5748 **Copyright** ©The Author(s) 2022.

Figure 1 Preoperative computed tomography of the cervical spine shows lesions of the C7 vertebral body and C7/T1 intervertebral disc. A: Three-dimensional computed tomography (CT) sagittal C7 vertebral lesions; B: Three-dimensional CT coronal C7 vertebral lesions; C: Three-dimensional CT axial C7 vertebral lesions.

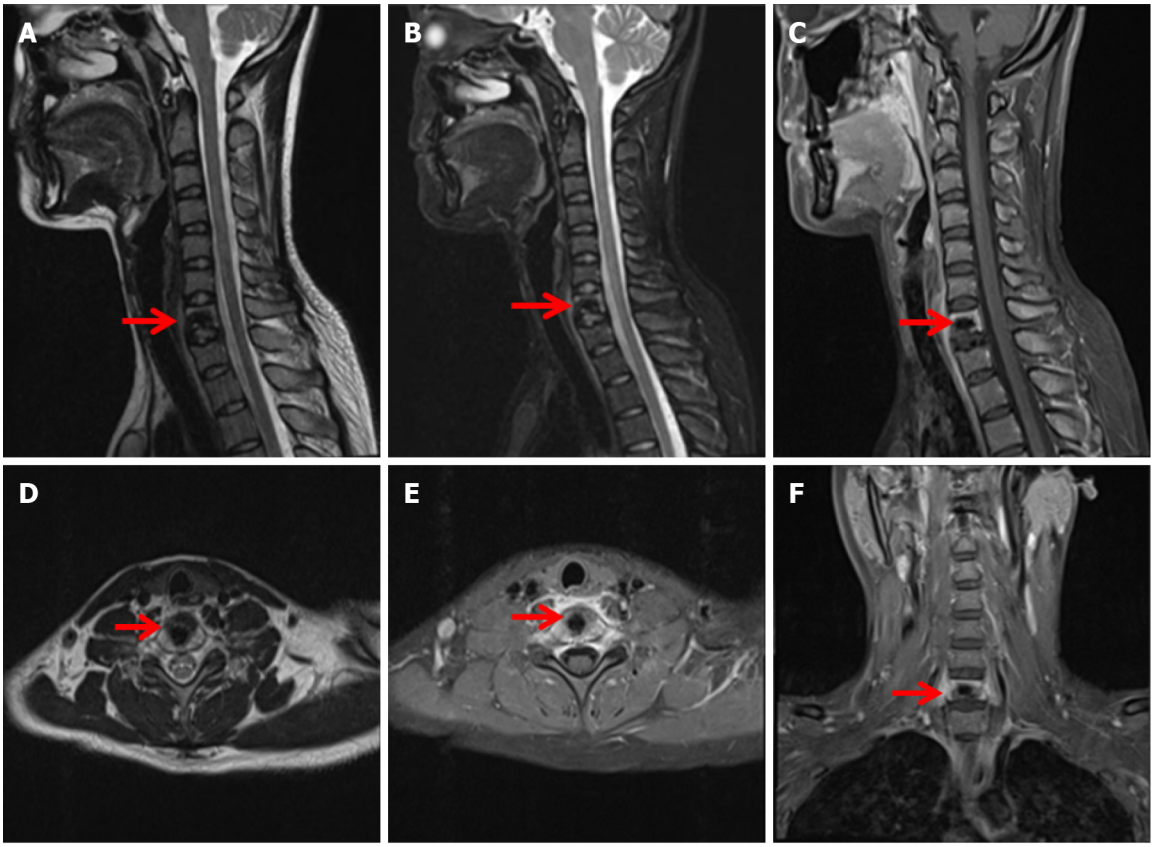

DOI: 10.12998/wjcc.v10.i17.5748 **Copyright** ©The Author(s) 2022.

Figure 2 Magnetic resonance imaging of the cervical vertebra shows a patchy, abnormal signal shadow of the C7 vertebral body, swelling of adjacent soft tissue, uneven enhancement after enhancement, and no abnormal signal of the cervical spinal cord. A, D: T1-weighted images; B: T2-weighted images; C, E and F: Fat suppression images.

FINAL DIAGNOSIS

The patient was diagnosed with cervical CMF.

TREATMENT

Under general anaesthesia with the patient in the supine position, We performed an anterior cervical surgery on the patient. C-arm fluoroscopy was used to locate the intervertebral space with a locating

needle, and a distractor was placed in the centre of the front of the C6/7 and C7/T1 vertebral bodies to expand them. And subtotal resection of the C7 vertebral body was performed with a bone rongeur. A large amount of white chyle focus tissue in the vertebral body had eroded most of the bone in the vertebral body, and specimens were obtained for pathological examination (Figure 3). The cervical canal and nerve root canal were decompressed, and the adhesion of the spinal cord and bilateral nerve roots was released. The length from the lower edge of the C6 vertebral body to the upper edge of the T1 vertebral body was measured. A titanium cage of appropriate length was selected, and autogenous iliac bone was implanted into the titanium cage between C6 and T1. A hole was drilled in front of the C6 and T1 vertebral bodies, and titanium plate screws were installed. Before the end of the operation, C-arm fluoroscopy showed that the positions of the titanium plate and screw remained acceptable.

OUTCOME AND FOLLOW-UP

After the operation, the patient's symptoms were significantly alleviated, and the patient could walk independently. The neck was fixed with a common neck brace for 6 wk. At the 2-year follow-up, the patient's symptoms had not recurred.

DISCUSSION

Retrospective study of this case revealed no obvious abnormalities in the body from the preoperative screening of patients, with the exception of the cervical spine. Laboratory tests showed that relevant tumour markers and inflammatory markers were not significantly increased. The diagnosis was confirmed according to the comprehensive judgement of imaging examinations and intraoperative pathology. The diagnosis of CMF is difficult because of its overlapping features with other bony lesions. Pathology reveals that CMF has mucinous and fibrous components[5]. The tumour cells were primarily arranged in lobules characterised by sparse cells in the centre, dense cells in the periphery, and more cells (primarily spindle cells, multinucleated giant cells and chondroblasts) between the lobules. Tumour cells were arranged in a fusiform or stellate pattern in a myxoid stroma. Calcification occurred in more than one-third of these cases but rarely became prominent. Hyaline cartilage and chondroblastoma-like areas were not uncommon. Approximately 18% of the tumours showed odd nuclei, and trabecular perforations were rare. Immunohistochemically (IHC), the tumour was positive for S100, which suggests that it was a chondroid tumour. Diseases that may be differentiated from CMF include low grade chondrosarcoma, enchondroma, chondromyxoid fifibroma-like osteosarcoma, chondroblastoma, and giant cell tumor of bone[6].

The differential diagnosis between CMF and chondrosarcoma is crucial. CMF also presents as a low-grade malignancy with histological nuclear atypia similar to chondrosarcoma[7]. The treatment and prognosis of CMF and chondrosarcoma vary greatly. Approximately 22% of CMFs are misdiagnosed as chondrosarcoma, which is a common malignant tumour in many bone tumour diseases. Chondrosarcoma morbidity peaks in the sixth and seventh decades of life, whereas CMF occurs in the second and third decades of life. Chondrosarcomas have specific demographic and radiographic features. CMF is often misdiagnosed as chondroblastoma. However, chondroid matrix, chondrocyte-like and multinucleated giant cell hyaline cartilage are predominantly absent in chondroblastoma, whereas CMF has myxochondroid matrix lobules with spindle and stem-like cells. Similarly, enchondroma has pathologically well-defined lobules with "bony encasement" and lacks atypia and myxoid areas, which is significantly different from the pathological appearance of CMF. Patients with CMF may be misdiagnosed with giant cell tumor (GCT) in the early stage, but the age of GCT patients is relatively older than that of CMF patients, and the cellular and imaging features of GCT are different from those of CMF. GCT usually originates from the metaphysis and is accompanied by epiphyseal extension. Multinucleated giant cells with the same background nuclei as interstitial cells are the main defining histological feature of GCT, whereas CMF shows only a few giant cells located close to the periphery. GCT shows neither myxoid nor cartilaginous components.

Another disease that can be confused with CMF is osteosarcoma. There are rare low-grade osteosarcomas. Chondromyxoid fibromatoid osteosarcoma (CMF-OS) was first reported in 1989, which presented with the histological and biological behaviours of low malignancy. Microscopically, it had a CMF-like appearance that consisted of loosely packed cellular gates in a highly mucoid stroma background and lobulated by fibrovessels. The most salient feature in differentiating CMF from CMF-OS should be careful study of whether the bone is neoplastic, especially in lesions with malignant radiological features. IHC staining of vimentin-positive and S100-negative cells might be helpful in distinguishing CMF from CMF-OS. Zhong *et al*[8] summarised the differences between CMF-OS and CMF using age of morbidity, tumour location, imaging examination, medical history, IHC and genetic characteristics from a series of case reviews. Finally, based on the above differences, combined with the imaging and pathological features of our case, we concluded that the nature of the patient's tumor was cervical CMF.

Table 1 Chondromyxoid fibroma of the cervical spine: presentation, management and outcomes from 1990 to 2020

Ref.	Age and sex	Involved site	Clinical symptoms	Mode of treatment	Results and follow-up
Rivierez *et al*[11], 1991	41/F	Complex of part C5 vertebral body and posterior longitudinal ligament	Torticollis, upper limb pain	Stage 2 operation	No recurrence was found in 10 months of follow-up
Lopez *et al* [12], 2002	20/M	C2 vertebral body and transverse foramen	Intermittent pain in the neck after a fall; tenderness in the back muscles of the neck; limited neck rotation and lateral bending	Transoropharyngeal approach, C2 vertebra resection, fusion of the occipital to C4 vertebrae	Relieved pain and instability and had no recurrence within two years
Bala *et al* [13], 2006	36/M	C2 vertebral body with right posterior longitudinal ligament complex	Occasional, chronic neck pain	Under CT guidance, the tumour of the C2 vertebra was resected through a transoropharyngeal approach, and the right iliac bone was harvested and implanted	At 18 months of follow-up, the patient was pain-free. Imaging revealed a residual tumour volume surrounding the graft and the right vertebral artery
Jonatha *et al* [14], 2008	35/M	C7 vertebral body and left pedicle	Neck pain with limited movement; numbness and pain in the ulnar side of the left upper limb	C7 vertebra resection and autogenous iliac bone implantation	At eight years of follow-up, the patient had no neurological symptoms. Plain films and CT scans showed no progression of the tumour
Subach *et al* [15], 2010	27/F	C6 lamina and right pedicle, extending to the foraminal location	There was paraesthesia, pain, numbness in the right neck and radiation to the right upper limb. It has worsened over the past six months	The C6 lamina and the right pedicle were completely resected, and posterolateral C5-C7 fusion and posterior intersegmental fixation were performed	The numbness and tenderness of the right upper extremity had subsided by 9 months postoperatively; a solid bony fusion showed no evidence of tumour recurrence
Taghipour *et al*[10], 2015	36/F	Encapsulated mass involving the soft tissue of the posterior margin of C3 and C4 spinous processes and partially invading the bone of the C5 spinous process	Neck pain with radiating pain in the right upper extremity for 1 yr	Surgical treatment (details unknown)	Follow-up for 2 yr, no recurrence
Our case	24/F	Involvement of the C7 vertebral body and C7/T1 intervertebral disc	Swelling and pain in the neck and shoulder with limitation of movement	Total C7 and C7/T1 discectomy with autogenous iliac bone graft	Follow-up for 14 months showed no recurrence.

CT: Computed tomography.

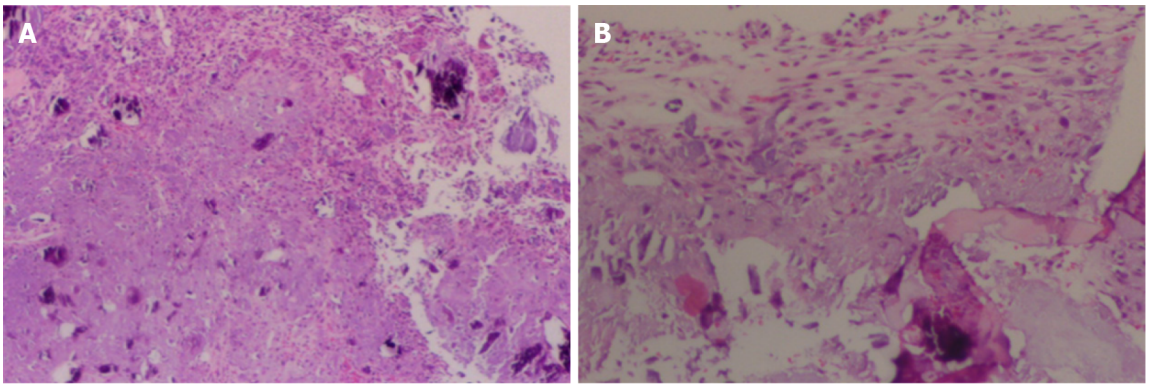

DOI: 10.12998/wjcc.v10.i17.5748 **Copyright** ©The Author(s) 2022.

Figure 3 Visible under the microscope: Medullary bone and bone trabeculae, part of the nucleus pulposus and abundant bone marrow were observed. Cartilaginous myxoid stroma, multifocal proliferating fusiform fibrous tissue with considerable calcium deposition and multinucleated giant cells are on the side. A, B: Hematoxylin and eosin (HE) staining, original magnification × 10.

Controversy about the imaging characteristics of CMF also exist. However, the literature suggests a multidisciplinary approach for distinguishing CMF from chondrosarcoma and concludes that CMF has some characteristic radiological characteristics in typical sites[9]. Tumours showing oval osteolytic lesions generally occur in the long or flat bones of young people. CMFs are isointense on T1WI and have

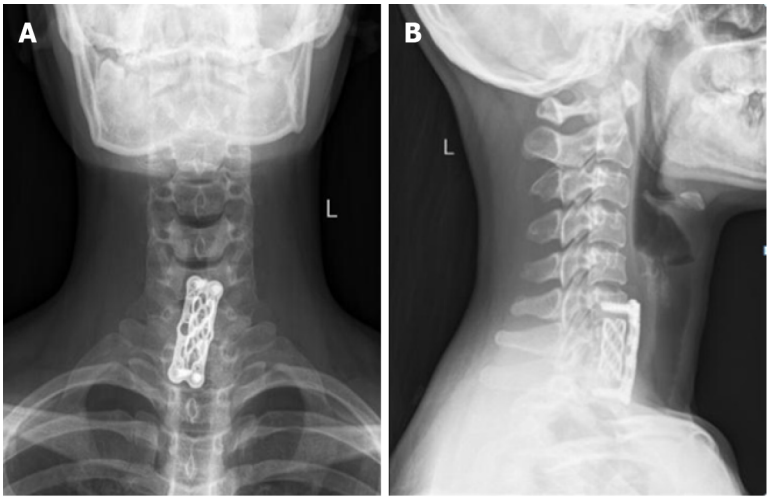

DOI: 10.12998/wjcc.v10.i17.5748 **Copyright** ©The Author(s) 2022.

Figure 4 Postoperative X-ray of cervical vertebra. A, B: Nine months after the surgery, the cervical spine was re-examined in the anteroposterior and lateral positions and showed that the internal fixation position was good.

moderate-to-high signal intensity or contrast peripheral enhancement on T2STIR/T2FS. Traditional "bite" features, low signal intensity margins on all MRI sequences, and the absence of or minimal bone marrow or soft tissue oedema might also be useful features.

CMF is generally a slow-growing asymptomatic lesion. Most CMFs are located in the metaphyseal region of the long bones, approximately one-third of which formed in the tibia, foot tubular bones, distal femur, and pelvis. Although CMF has a predilection site, most of the reported cases have been atypical. Therefore, we cannot avoid CMF in the differential diagnosis of bone tumours in various parts of the human body. The clinical manifestations vary according to the size, location and extent of the lesion. The common symptoms of CMF in cervical spine are neck and shoulder pain, limitation of movement, numbness and radiating pain of upper limbs after nerve root damage. Although CMF is a relatively rare benign tumour, vertebral CMF only accounts for 8% of all CMFs, and cervical CMF is even rarer, with fewer than 12 cases reported[10]. The features of vertebral CMF include the erosion of cortical bone, even beyond the extent of the periosteum into the surrounding soft tissue or spinal canal, and this feature indicates more serious destruction, which may indicate the malignant transformation of tumours. All cervical CMFs reported in the English literature over a 30-year period from 1991 to 2021 (Table 1) were retrieved and are summarized below.

CMF was reported in upper and lower cervical vertebrae, and the tumour invades all parts of the vertebral body, transverse foramen and posterior soft tissue. The tumour had only caused obvious disc erosion in our case. We resected all of the tumours of the vertebral body and intervertebral disc *via* surgery and performed iliac bone implantation and anterior fusion. The occipital bone and atlas maintain 50% of the flexion and extension range of motion of the cervical spine, and the atlas and axis maintain 50% of the rotation range of motion of the vertebral body. The age of the patient was fully considered in the preoperative strategy. Anterior fusion of the two segments of the lower cervical spine was performed. Therefore, it would not have a significant impact on the patient's quality of life in the future. The internal fixation position of the patient was good, and no discomfort, such as neck movement or dysphagia, was shown (Figure 4).

An epidemiological survey of primary spinal tumours in Chinese patients showed that the proportion of benign tumours is larger than that of malignant tumours, and the proportion of male patients is larger than that of female patients. Benign tumours are more likely to occur at the age of 21 to 40 years old, and malignant tumours are more likely to occur at the age of 41 to 60 years old. The distribution of primary spinal tumours in the cervical, thoracic, lumbar and sacral segments is roughly the same, with most benign tumours occurring in cervical vertebrae and most malignant tumours appearing in sacral vertebrae. The age of morbidity and the location of the tumour in our case were consistent with the characteristics of primary spinal tumours in Chinese patients. Simple curettage, without filling the defect, leads to approximately 20% to 80% tumour recurrence[16]. This recurrence might result from incomplete tumour excision and leave pseudopod processes extending from the main tumour to the cavernous body (sutures) after simple curettage. Curettage plus bone grafting or cement fixation has a much lower recurrence rate of approximately 7%[17]. To prevent tumour recurrence, we performed total resection of the vertebral body and intervertebral disc, and internal fixation was performed to simultaneously maintain the stability of the entire spine.

CONCLUSION

CMF is a benign tumor that may be associated with active growth of cartilage at the predilection site. At present, active surgical treatment, such as resection or curettage, is recommended for such tumors. Regardless of which treatment is adopted, the tumor should be totally removed as far as possible, because the residual tumor will lead to recurrence of the lesion. To prevent spinal instability after tumor resection, internal fixation should be performed at the same time to maintain spinal stability. It has been reported in the literature that there remains a certain proportion of recurrence after total resection of the lesion, and the longest recurrence time is 30 years; therefore, long-term follow-up is recommended. In this case, the lesion was located in the cervical vertebra, the lesion was completely resected, and autogenous bone was transplanted at the same time. There was no tumor recurrence after more than two years of follow-up, but close follow-up should be continued.

FOOTNOTES

Author contributions: Li C, Li S and Hu W contributed to study conception and design; Li C and Hu W collected and analyzed the clinical data and wrote the manuscript; Li C, Li S and Hu W submitted and revised the manuscript; and All authors read and approved the final version of manuscript.

Informed consent statement: Informed written consent was obtained from the patient for publication of this report and any accompanying images.

Conflict-of-interest statement: The authors declare that there is no conflict of interest.

CARE Checklist (2016) statement: The authors have read the CARE Checklist (2016), and the manuscript was prepared and revised according to the CARE Checklist (2016).

Open-Access: This article is an open-access article that was selected by an in-house editor and fully peer-reviewed by external reviewers. It is distributed in accordance with the Creative Commons Attribution NonCommercial (CC BY-NC 4.0) license, which permits others to distribute, remix, adapt, build upon this work non-commercially, and license their derivative works on different terms, provided the original work is properly cited and the use is non-commercial. See: https://creativecommons.org/Licenses/by-nc/4.0/

Country/Territory of origin: China

ORCID number: Cheng Li 0000-0002-1173-9148; Sen Li 0000-0003-2837-4808; Wei Hu 0000-0002-8110-9969.

S-Editor: Ma YJ
L-Editor: A
P-Editor: Ma YJ

REFERENCES

1 **Soni R**, Kapoor C, Shah M, Turakhiya J, Golwala P. Chondromyxoid Fibroma: A Rare Case Report and Review of Literature. *Cureus* 2016; **8**: e803 [PMID: 27833828 DOI: 10.7759/cureus.803]
2 **JAFFE HL**, LICHTENSTEIN L. Chondromyxoid fibroma of bone; a distinctive benign tumor likely to be mistaken especially for chondrosarcoma. *Arch Pathol (Chic)* 1948; **45**: 541-551 [PMID: 18891025]
3 **Douis H**, Saifuddin A. The imaging of cartilaginous bone tumours. II. Chondrosarcoma. *Skeletal Radiol* 2013; **42**: 611-626 [PMID: 23053201 DOI: 10.1007/s00256-012-1521-3]
4 **Yasuda T**, Nishio J, Sumegi J, Kapels KM, Althof PA, Sawyer JR, Reith JD, Bridge JA. Aberrations of 6q13 mapped to the COL12A1 locus in chondromyxoid fibroma. *Mod Pathol* 2009; **22**: 1499-1506 [PMID: 19648885 DOI: 10.1038/modpathol.2009.101]
5 **HemanthaKumar G**, Sathish M. Diagnosis and Literature Review of Chondromyxoid Fibroma - A Pathological Puzzle. *J Orthop Case Rep* 2019; **9**: 101-105 [PMID: 32405500 DOI: 10.13107/jocr.2019.v09.i04.1500]
6 **Wangsiricharoen S**, Wakely PE Jr, Siddiqui MT, Ali SZ. Cytopathology of chondromyxoid fibroma: a case series and review of the literature. *J Am Soc Cytopathol* 2021; **10**: 366-381 [PMID: 33958292 DOI: 10.1016/j.jasc.2021.04.001]
7 **Vasudeva N**, Shyam Kumar C, Ayyappa Naidu CR. Chondromyxoid Fibroma of Distal Phalanx of the Great Toe: A Rare Clinical Entity. *Cureus* 2020; **12**: e7133 [PMID: 32257678 DOI: 10.7759/cureus.7133]
8 **Zhong J**, Si L, Geng J, Xing Y, Hu Y, Jiao Q, Zhang H, Yao W. Chondromyxoid fibroma-like osteosarcoma: a case series and literature review. *BMC Musculoskelet Disord* 2020; **21**: 53 [PMID: 31996205 DOI: 10.1186/s12891-020-3063-5]
9 **Cappelle S**, Pans S, Sciot R. Imaging features of chondromyxoid fibroma: report of 15 cases and literature review. *Br J Radiol* 2016; **89**: 20160088 [PMID: 27226218 DOI: 10.1259/bjr.20160088]
10 **Taghipour Zahir S**, Sefidrokh Sharahjin N, Sadlu Parizi F, Rahmani K. Chondromyxoid Fibroma of Two Cervical Vertebrae with Involvement of Surrounding Soft Tissue: Radiologic Diagnostic Dilemma. *Iran J Radiol* 2015; **12**: e19273

[PMID: 26587204 DOI: 10.5812/iranjradiol.19273]

11 **Rivierez M**, Richard S, Pradat P, Devred C. [Chondromyxoid fibroma of the cervical spine. Apropos of a case treated by partial vertebrectomy]. *Neurochirurgie* 1991; **37**: 264-268 [PMID: 1922638]

12 **Lopez-Ben R**, Siegal GP, Hadley MN. Chondromyxoid fibroma of the cervical spine: case report. *Neurosurgery* 2002; **50**: 409-411 [PMID: 11844279 DOI: 10.1097/00006123-200202000-00034]

13 **Bala A**, Robbins P, Knuckey N, Wong G, Lee G. Spinal chondromyxoid fibroma of C2. *J Clin Neurosci* 2006; **13**: 140-146 [PMID: 16410218 DOI: 10.1016/j.jocn.2005.03.022]

14 **Jonathan A**, Rajshekhar V, Chacko G. Chondromyxoid fibroma of the seventh cervical vertebra. *Neurol India* 2008; **56**: 84-87 [PMID: 18310848 DOI: 10.4103/0028-3886.39323]

15 **Subach BR**, Copay AG, Martin MM, Schuler TC, Romero-Gutierrez M. An unusual occurrence of chondromyxoid fibroma with secondary aneurysmal bone cyst in the cervical spine. *Spine J* 2010; **10**: e5-e9 [PMID: 20036621 DOI: 10.1016/j.spinee.2009.11.016]

16 **Zillmer DA**, Dorfman HD. Chondromyxoid fibroma of bone: thirty-six cases with clinicopathologic correlation. *Hum Pathol* 1989; **20**: 952-964 [PMID: 2793160 DOI: 10.1016/0046-8177(89)90267-0]

17 **Basak B**, Haragan A, Shackcloth M, Thekkudan J. Chondromyxoid Fibroma of the Rib: A Rare Benign Tumor With Potential for Local Recurrence. *Cureus* 2021; **13**: e19172 [PMID: 34873515 DOI: 10.7759/cureus.19172]

World Journal of Clinical Cases

Submit a Manuscript: https://www.f6publishing.com

World J Clin Cases 2022 June 16; 10(17): 5756-5763

DOI: 10.12998/wjcc.v10.i17.5756

ISSN 2307-8960 (online)

CASE REPORT

Preterm neonate with a large congenital hemangioma on maxillofacial site causing thrombocytopenia and heart failure: A case report

Neng Ren, Chun-Shun Jin, Xiao-Qi Zhao, Wen-Hui Gao, Yu-Xian Gao, Yuan Wang, Yun-Feng Zhang

Specialty type: Pediatrics

Provenance and peer review: Unsolicited article; Externally peer reviewed.

Peer-review model: Single blind

Peer-review report's scientific quality classification

Grade A (Excellent): A, A
Grade B (Very good): 0
Grade C (Good): C
Grade D (Fair): 0
Grade E (Poor): 0

P-Reviewer: Bairwa DBL, India; Shekouhi R, Iran; Yarso KY, Indonesia

Received: November 9, 2021
Peer-review started: November 9, 2021
First decision: December 27, 2021
Revised: January 4, 2022
Accepted: April 9, 2022
Article in press: April 9, 2022
Published online: June 16, 2022

Neng Ren, Xiao-Qi Zhao, Wen-Hui Gao, Yu-Xian Gao, Yuan Wang, Department of Neonatology, The Second Hospital of Jilin University, Changchun 130041, Jilin Province, China

Chun-Shun Jin, Department of Otolaryngology, Head and Neck Surgery, The Second Affiliated Hospital of Jilin University, Changchun 130041, Jilin Province, China

Yun-Feng Zhang, Department of Pediatrics, The Second Hospital of Jilin University, Changchun 130041, Jilin Province, China

Corresponding author: Yun-Feng Zhang, DPhil, MD, PhD, Chief Doctor, Full Professor, Department of Pediatrics, The Second Hospital of Jilin University, No. 218 Ziqiang Street, Changchun 130041, Jilin Province, China. zhangyunf@jlu.edu.cn

Abstract

BACKGROUND

We report a rare case of a large congenital hemangioma (CH) in the maxillofacial region in a female neonate that caused thrombocytopenia and heart failure. With close multidisciplinary collaboration, the congenital hemangioma was successfully resected with good results.

CASE SUMMARY

The patient was delivered at gestational age of 36 wk by cesarean section due to cephalopelvic disproportion and lack of onset of labor (birth weight: 2630 g). A right-sided facial tumor was detected in the fetus during routine antenatal ultrasound examination of the mother at 32 wk of gestation. Physical examination revealed a 7 cm × 7 cm × 3 cm hard, dull purple-colored mass on the right maxillofacial region. The mass was tense and had prominent surface telangiectasias. Laboratory investigations revealed reduced hemoglobin and platelet count, and increased activated partial thromboplastin time, prothrombin time, and thrombin time. International normalized ratio, fibrin degradation products, and D-Dimer levels were significantly increased. Thromboelastography showed increased alpha angle, mean amplitude, and the clot formation speed. Thyroid-stimulating hormone level was significantly elevated. The patient was administered prednisone, propranolol, euthyrox, vitamin K1, milrinone, and digoxin. After operation, cefepime was administered for anti-infection and propranolol was prescribed at discharge.

CONCLUSION
We report a rare case of CH in the right maxillofacial region causing thrombocytopenia and heart failure.

Key Words: Congenital hemangioma; Maxillofacial site; Thrombocytopenia; Heart failure; Case report

©The Author(s) 2022. Published by Baishideng Publishing Group Inc. All rights reserved.

Core Tip: The present report highlights the management strategy for congenital hemangiomas, *i.e.*, protection of hemangioma before surgical resection, appropriate use of propranolol to contain the size and tension of the hemangioma, correction of anemia and thrombocytopenia, and improvement of congestive heart failure. Multidisciplinary collaboration is vital to achieve good outcomes.

Citation: Ren N, Jin CS, Zhao XQ, Gao WH, Gao YX, Wang Y, Zhang YF. Preterm neonate with a large congenital hemangioma on maxillofacial site causing thrombocytopenia and heart failure: A case report. *World J Clin Cases* 2022; 10(17): 5756-5763
URL: https://www.wjgnet.com/2307-8960/full/v10/i17/5756.htm
DOI: https://dx.doi.org/10.12998/wjcc.v10.i17.5756

INTRODUCTION

Hemangiomas occurring in the neonatal period are typically benign and the underlying pathogenetic mechanisms are not well characterized[1]. Congenital hemangiomas (CHs) are uncommon entities[2] accounting for < 3% of all hemangiomas. CHs have a predilection for occurring in the cranio-maxillo-facial region and lower limbs, while suboccipital neck, elbow, and knees are the other reported sites of occurrence[3]. CH typically present within the first month of life, and exhibit an accelerated growth phase followed by involution[1]. CHs develop *in utero*, are fully grown at birth, and do not show continual growth after birth[1]. Thrombocytopenia, coagulation dysfunction, heart failure, and hemorrhage are some of the complications of CH[4]. According to the 2019 guidelines for the diagnosis and treatment of hemangiomas and vascular malformations, CHs are classified into three types: Rapidly involuting CH (RICH), noninvoluting CH (NICH), and partially involuting CH (PICH)[5,6]. NICH is rarer than RICH. Surgery is often required for NICH as conservative treatment may not yield a satisfactory outcome[3]. In this work, we report a rare case of CH in the right maxillofacial region causing thrombocytopenia and heart failure. With close multidisciplinary collaboration, the CH was successfully resected with good results.

CASE PRESENTATION

Chief complaints

A female neonate was brought to the Department of Neonatology at our hospital immediately after birth with the chief complaint of a facial tumor.

History of present illness

The gestational age of the fetus at the time of delivery was 36 wk and the mother of the patient had a cesarean scar pregnancy. The patient was delivered by cesarean section due to cephalopelvic disproportion and noninitiation of labor. Apgar scores at 1 min and 5 min were 9 and 10, respectively. The birthweight was 2630 g. Routine antenatal imaging examination performed at the gestational age of 32 wk revealed a maxillofacial tumor on the right side; the cardiothoracic area ratio of the fetus was 0.39; the superior vena cava was dilated with tricuspid regurgitation; and umbilical artery pulsatility index was 1.25. At the time of admission to our department, the neonate had not been breastfed, and had not passed meconium or urine after birth.

History of past illness

The past medical history of the mother was unremarkable.

Personal and family history

There was no significant family history.

Physical examination

At admission, the general state of the neonate was poor with skin cyanosis. The anterior fontanelle was flat (approximately 2.5 cm × 2.5 cm) with no tension. Physical examination revealed a 7 cm × 7 cm × 3 cm hard, tense, dull purple-colored mass at the right maxillofacial region with prominent surface telangiectasias (Figure 1A-C). The mass was warm to the touch and had a palpable thrill. The boundary of the mass was well defined and the color did not fade on application of pressure. The respiratory rate was 40 breaths/min, and the three concave sign was negative. On chest auscultation, the breath sounds were harsh with no rales or rhonchi. Apical impulse was not palpable over the precordial region. The heart rate was 149 beats/min and there were no murmurs. Abdominal wall was soft with no peristaltic wave. There was no splenomegaly or hepatomegaly and the bowel sounds were decreased. Hypomyotonia was found in four extremities, and the primitive reflexes were attenuated. The estimated gestation age was 36 wk.

Laboratory examinations

Blood parameters at admission were as follows: Hemoglobin (Hb) 120 g/L (normal range 170-210 g/L); platelet count (PLT) 34 × 10^9/L (normal range 220× 10^9-360 × 10^9/L); prothrombin time (PT) 17.0 s (normal range 10.1-15.9 s); thrombin time (TT) 24 s (normal range 11-17 s); fibrin degradation products (FDPs) 66.5 μg/mL (normal range 0.0-5.0 μg/mL); international normalized ratio (INR) 1.48 (normal range 0.8-1.2); D-Dimer 29.74 μg/mL (normal range 0-1 μg/mL); andthyroid-stimulating hormone (TSH) 17.7 mIU/L (normal range 0.72-13.10 mIU/L). Thromboelastography findings were as follows: Alpha angle 37.2 (normal range 53–72); the clot formation speed (K) 6.5 min (normal range 1.0-3.0 min); and maximum amplitude (MA) 35.5 mm (normal range 50-70 mm). The above results showed decreased levels of Hb and PLT and increased levels of PT and TT beyond the normal range. In addition, there was significant increase in INR, FDP, and D-Dimer levels. Alpha angle, MA, and K were also elevated above the normal range. TSH level was significantly increased. On the second day of admission, the total bilirubin levels were increased beyond the normal range, mainly indirect bilirubin.

Imaging examinations

Tumor mass ultrasound showed a huge cystic-solid mixed echo mass on the right maxillofacial region and the right neck subcutaneously. The size of the lesion was approximately 7.1 cm × 5.3 cm × 3.1 cm. The interior of the mass was filled with dense point-like low echo, and abundant blood flow signals were visible inside and around the lesion. There was no obvious abnormality in thyroid ultrasonography.

Cardiac ultrasound showed an echo separation at the oval fossa of the atrial septum approximately 2.4 mm; tricuspid regurgitation signal was detected, the area was approximately 0.9 cm^2, the maximum reflux velocity was 389 cm/s, pressure gradient (Pg) was 61 mmHg, and the estimated pulmonary artery pressure was 71 mmHg. The findings suggested patent foramen ovale, which needed to be differentiated from atrial septal defect, large tricuspid regurgitation, and pulmonary hypertension (severe). X-ray film indicated that the cardiac shape was full and the cardiothoracic area ratio was 0.52.

FINAL DIAGNOSIS

The patient was diagnosed with CH, prematurity, anemia, thrombocytopenia, abnormal coagulation function, atrial septal defect, pulmonary hypertension, hypothyroidism, neonatal hyperbilirubinemia, and congestive heart failure.

TREATMENT

Management of the tumor on the maxillofacial region

The temperature of the tumor was monitored and compared with that of the surrounding skin. If a temperature difference was identified, the attending physician would be informed of the situation. The position of the patient was changed every 2 h. The tumor was thoroughly examined and the presence of redness, swelling, or corrosion was evaluated; the intensity of the fluctuation of the tumor surface was carefully palpated. Since the tumor was large and close to the neck, and the neck of the newborn is short, the tumor and the neck of the patient were separated by oil gauze or silver sulfadiazine dressing. Oil gauze or silver sulfadiazine was placed over the skin around the tumor, and sterile gauze was placed on the side of the intact skin.

The bed sheets that were in contact with the skin of the patient were replaced once a day.

Specific treatment

Owing to the detection of anemia, thrombocytopenia, and abnormal coagulation function, 40 mL cell suspension was administered within 4 h, 40 mL platelet was administered within 1 h, and 40 mL plasma

DOI: 10.12998/wjcc.v10.i17.5756 **Copyright** ©The Author(s) 2022.

Figure 1 The large hemangioma (7 cm × 7 cm × 3 cm) on the right maxillofacial region and after removal of tumor. A: Seen from the top of the tumor; B: Seen from the right shoulder; C: Seen from the front of the tumor; D: After the tumor was removed.

was administered within 4 h. Besides, oral prednisone was administered (4 mg/kg/d, divided into two equal doses) and the intended use was for 6 wk; propranolol was also administered (2 mg/kg/d, divided into two equal doses) and was adjusted based on the changes of CH. Levothyroxine was administered (7 μg/kg/d, once a day) and the dose was adjusted based on the level of TSH. Vitamin K1 was administered at 1 mg/time. Milrinone was administered *via* intravenous infusion (0.5 μg/kg/min for 24 h). In addition, the tumor was closely monitored for any change in the tension in order to avoid rupture.

Repeat blood tests performed on day 2 of admission showed no increase in PLT; thus, 40 mL platelet and 40 mL plasma were administered along with vitamin K1, 1 mg STAT. At the same time, phototherapy (intermittent blue light radiation) was administered to reduce jaundice.

On day 3 of admission, PLT had further decreased, and 40 mL platelets was administered within 1 h.

On day 7 of admission, the patient developed shortness of breath and hypouresis. Physical examination revealed increased heart rate and bilateral pitting edema in the lower extremity; in addition, liver was palpable approximately 4 cm below the rib. Therefore, digoxin (0.01 mg/kg/d, divided into two equal doses), milrinone (0.5 μg/kg/min for 24 h), and furosemide (0.5 mg/kg/time, once or twice a day) were administered.

On day 14 of admission, the patient showed stable breathing, normal volume of urine, heart rate within normal range, and no lower extremity edema; thus, digoxin and milrinone were withdrawn.

On day 29 of admission, Hb level was 95 g/L and PLT was 19 × 10^9/L; therefore, 60 mL platelets was administered within 1 h, and 45 mL red blood cell suspension was administered within 4 h.

On day 34 of admission, there was no further decrease in PLT, and the brain natriuretic peptide level was improved. TSH level was further decreased, but still higher than the normal range. Echocardiography displayed left heart enlargement, mild tricuspid insufficiency, and patent foramen ovale. Cardiac function was within the lower limit of normal range. An operation was scheduled for the next day.

On day 35 of admission, the parents of the patient consented for surgical resection of the tumor. The patient was placed in the supine position. After tracheal intubation, a pillow was placed under the shoulders and the right side of the face and neck were disinfected with strong iodine and a surgical drape was placed. A giant purple–red hemangioma was seen on the right side of the face, approximately 8 cm in diameter. The skin surrounding the hemangioma showed tortuous blood vessels. There

was local surface rupture and slight visible oozing. An incision was made at 2 cm from the lower margin of the tumor. There was ejection of dark red blood and a compress was used to stop bleeding. The tumor was separated along its lower margin, dissociated from the right facial artery and vein (the main blood supply vessel), ligated and disconnected. A subcutaneous incision was made 2 cm away from the edge of the tumor and the tumor was quickly removed. The bleeding was fully stopped after washing the operating cavity. The area was scraped and trimmed of facial skin and a Y-shaped suture was done. The subcutaneous tissue and skin were sutured layer by layer. A drainage tube was placed and pressure bandages were applied. The volume of intraoperative bleeding was approximately 350 mL, and 360 mL blood was transfused. The patient was safely returned to the ward after the operation. Respiratory support was provided, along with transfusion of red blood cell suspension, platelets, cold precipitation, and plasma to prevent infection. Symptomatic treatment was administered as necessary.

On postoperative day 1, the patient presented with coarse breath sounds and bubbling sounds in both lungs, along with worsening of lower extremity edema. Therefore, fluid intake was restricted; plus human hemoglobin was administered at 5 mL/kg once; furosemide 0.5 mg/kg/time, twice; and cefepime 30 mg/kg/time, Q12H. In addition: (1) The patient was closely monitored for blood oozing from the surgical wound and signs of impaired circulation at the surrounding skin site of the compression bandage; the color and volume of the drainage fluid was also monitored; (2) the dressing was changed every day and a compression bandage was applied; and (3) 12 d after the operation, the surgical sutures were intermittently removed and 16 d after the operation, the surgical sutures were completely removed. The wound had recovered (Figure 1D).

On day 44 of admission, C-reactive protein levels were within the normal range, and cefepime was withdrawn. On day 51 of admission, the laboratory indices were within the normal range; the patient had recovered and was discharged. The following treatment was prescribed at discharge: (1) Propranolol was divided into two equal doses (1.5 mg/kg/d); (2) regular monitoring of biochemical parameters, serum blood glucose levels, myocardial enzymes levels, electrocardiogram, and echocardiography; and (3) withdrawal of drugs: When the clinical evidence showed that the tumor disappeared and local B ultrasound showed tumor regression and no blood supply, gradual drug withdrawal to complete withdrawal can be considered within 1 mo (Table 1).

OUTCOME AND FOLLOW-UP

At 4 mo of follow-up, the patient showed good prognosis. There were no adverse drug effects and no signs of recurrence after drug withdrawal. The patient showed quick recovery and her growth and development were within the normal range.

DISCUSSION

CH is rarely encountered in clinical practice. Correct diagnosis requires detailed obstetric history and antenatal color Doppler ultrasound. The intrauterine growth of the tumor should be monitored. A key characteristic of CH is that the tumor grows *in utero*, and the growth is completed after birth, which is different from common hemangiomas. It is possible to determine the blood flow and blood supply in the tumor by combining imaging with ultrasound findings. CHs need to be differentiated from teratomas, granulomas, and Kaposi-like hemangioendothelioma.

According to the 2020 diagnosis and treatment advances of CH, NICH presents as a mass with prominent round-to-ovoid shape, in variable shades of pink to purple. The lesions are well delineated and show prominent telangiectasias and central and peripheral pallor[1]. The lesions are warm on palpation[4]. The clinical findings of our patient are similar to those of NICH. It is important to differentiate NICH from early RICH since the treatment focus for these two hemangiomas is different. RICH is frequently treated by conservative treatment with a good prognosis (almost 100% cure)[7]. RICH can also be treated by surgical resection if the patient develops complications such as thrombocytopenia, coagulation disfunction, or heart failure[8].

It is reported that NICH can be treated with propranolol alone with no significant side effects[2]; however, conservative treatment did not work for our patient[1].

The patient was diagnosed with CH accompanied with thrombocytopenia and coagulation dysfunction. Considering the large size of the tumor and presence of aberrant vessels inside the tumor, there was a risk of intravascular coagulation or local microthrombosis. Platelets were consumed after the formation of thrombus, resulting in abnormal coagulation function[4]. In this setting, the conventional treatment strategy for thrombocytopenia cannot be followed. There is a need to treat the primary disease and monitor concurrent hemorrhagic diseases[8,9].

Congestive heart failure resulted from the changes in intratumoral hemodynamics and high-output heart failure was caused by an arteriovenous shunt and excessive cardiac load. Cardiac failure can occur in infants with hemangiomas > 7 cm[4,10]. Our case confirms this point. In patients with congestive heart failure, due attention should be paid to fluid management. Our patient falls into the NICH type of

Table 1 Timelines for the findings and treatment

Timeline	Findings	Treatment
Day 1: Admission	(1) A 7.1 cm × 5.3 cm × 3.1 cm tumor was located at the right maxillofacial region; (2) the laboratory test revealed that the level of Hb and PLT was reduced, the APPT, PT, and TT were extended and INR, FDP, and D-Dimer were increased; alpha angle, MA, and K were elevated. TSH level was significantly elevated; and (3) atrial septal defect, pulmonary hypertension (severe)	(1) Appropriate limit the intake of fluid to reduce the preload of heart; (2) stepwise infusion of 40 mL cells suspension (4 h); platelet infusion of 40 mL (1 h); plasma infusion of 40 mL (4 h); prednisone tablets (4 mg/kg/d, evenly divided two times daily); intended use for 6 wk; propranolol (2mg/kg/d, evenly divided two times daily); levothyroxine (7 μg/kg/d, once a day); the dose was adjusted based on the level of TSH; vitamin K1 (1 mg/time); milrinone (0.5 μg/kg/min for 24 h); and (3) protect the tumor by paying attention to the tension change, avoiding rupture bleeding
Day 2: Continuing attempt to elevate the platelet level	(1) The laboratory test showed that the level of Hb and PLT was not significantly increased, and the level of PT and TT was not improved; however, the level of FDR and D-Dimer were increased; alpha angle, MA, and K were elevated; and (2) total bilirubin level was increased (mainly indirect bilirubin)	Additional diagnosis: Neonatal hyperbilirubinemia; platelet infusion of 40 mL (1 h); plasma infusion of 40m L (4 h); vitamin K1 (1 mg/time); blue light irradiation
Day 3: Further workup	(1) Neck enhanced CT suggested that it was a subcutaneous tumor in right maxillofacial region, tortuous and thickened vascular shadow of right neck, considered as round vascular lesion, atypical hemangioma; (2) PLT continually decreased compared with previous day; we attributed the decrease to the consumption by the hemangioma; and (3) there was no change for TT, and FDP and D-Dimer were still higher	Platelet infusion of 40 mL (1 h)
Day 4: Blood test	PLT was slightly increased; MA was significantly decreased	No adjustment of therapy strategy
Day 7: Blood test and echocardiography	(1) PLT level was still low, however, not worsened; (2) BNP was increased; (3) bilirubin was slightly decreased; and (4) symmetrical lower extremity edema; the major pulmonary artery diameter was about 10 mm, the size of the right atrium was about 21 mm × 21 mm, the heart was enlarged, mainly the right heart. The echo separation at the oval fossa was 2.0 mm; atrial level left to right shunt, tricuspid regurgitation signal, area of 0.5 cm^2, the maximum reflux velocity of 395 cm/s, Pg 62 mmHg, which suggests of the whole heart enlargement (right heart), patent foramen ovale, moderate tricuspid incompetence, and pulmonary hypertension (moderate to severe)	(1) Additional diagnosis: congestive heart failure; and (2) digoxin (0.01 mg/kg/d, evenly divided two times daily); milrinone (0.5 μg/kg/min for 24 h); furosemide (0.5 mg/kg/time, one or twice a day)
Day 10: Blood test and physical examination	PLT was in normal range; BNP was further decreased; low extremity edema improved	Continued previous treatment
Day 14: Blood test and echocardiography	(1) PLT was not further decreased; (2) BNP was further decreased, but still higher than normal; (3) TSH fell into the normal range; (4) measurement showed the tumor was 7 cm × 6.5 cm × 3 cm; and (5) echocardiography showed that the left heart was full; the tricuspid regurgitation signal was detected with area of 0.5 cm^2, the maximum reflux velocity of 301 cm/s, Pg 36 mmHg, pulmonary artery pressure 41 mmHg, which suggests patent foramen ovale, moderate tricuspid incompetence, and pulmonary hypertension (mild)	Withdrawal of digoxin and milrinone
Day 21: Blood test	(1) PLT was increased, though not as high as normal; (2) BNP was not in normal range; and (3) echocardiography: Left heart was enlarged, mild tricuspid insufficiency and patent foramen ovale were identified	No adjustment of treatment strategy
Day 25: Blood test	There was fluctuation of Hb and PLT	No adjustment of treatment strategy
Day 29: Blood test	(1) The level of Hb and PLT was still decreased; and (2) echocardiography: left heart was enlarged, mild tricuspid insufficiency, patent foramen ovale, cardiac function was within the lower limit of normal function	(1) Platelet infusion of 60 mL (1 h); red cell suspension infusion of 45 mL (4 h); and (2) pay attention to anemia and bleeding
Day 30: Blood test	The level of Hb was in normal range; PLT was increased	Continue current treatment
Day 34: Blood test and measurement of the tumor	(1) PLT was not further decreased; (2) BNP was improved; (3) TSH was further decreased, but still higher than normal; (4) echocardiography: Left heart was enlarged, mild tricuspid insufficiency and patent foramen ovale were identified, cardiac function was within lower limit of normal range; and (5) size of tumor was 6.5 cm × 6 cm × 3 cm	Surgical resection scheduled for next day
Day 35: Operation	-	(1) Volume of bleeding was about 350 mL, blood transfusion was about 360 mL; (2) the patient was safely returned to the ward after the operation; respiratory support was offered, transfusion of red blood cell suspension, platelets, cold

		precipitation, plasma was performed to prevent infection; and (3) symptomatic treatment was conducted when necessary
Day 36: Blood test, pathological examination and determination of myocardial enzymes	(1) Hb returned to normal and PLT was increased; (2) CRP increased; and (3) pathological examination showed that it was CH with massive hemorrhage; local extramedullary hematopoietic and fibrous tissue hyperplasia were seen	(1) Limited intake of liquid with precondition of maintaining normal circulation; (2) human serum albumin: 5 mL/kg/time, once; furosemide: 0.5 mg/kg/time, twice; record of intake and output of the patient; cefepime: 30mg/kg/time, Q12H; and (3) compression bandage and care for surgical wound and disinfection
Day 40: Blood test	BNP and TSH returned to normal	No adjustment of treatment strategy
Day 44: Blood test	Monitor PLT, and CRP; indicators of liver function and myocardial enzymes stayed in the normal range	Cefepime was withdrawn
Day 51: Blood test and echocardiography	PLT, indicators of coagulation function, BNP, FT3, FT4 and TSH were in normal range	The patient was discharged

Hb: Hemoglobin; PLT: Platelet count; Pg: Pressure gradient; APPT: Activated thromboplastin time; PT: Prothrombin time; MA: Maximum amplitude; TT: Thrombin time; INR: International normalized ratio; FDP: Fibrin degradation product; TSH: Thyroid-stimulating hormone; K: The clot formation speed; CT: Computed tomography; BNP: Brain natriuretic peptide; CRP: C-reactive protein; FT3: Free triiodothyronine.

CH. Conservative treatment did not work in our patient and she developed heart failure; therefore, we decided to perform surgical resection. The postoperative clinical course and echocardiography findings indicated good results. Before surgical resection, we had considered topical application of ethanol to induce necrosis of local vessels in order to reduce local blood supply and cause tumor shrinkage; this would also have reduced the blood loss during surgical resection. However, local application of ethanol may cause severe side effects in neonates. There are no available reports on the application of local ethanol for the reduction of hemangioma and its effectiveness needs further data.

Close multidisciplinary collaboration was instrumental in the successful surgical resection of the large hemangioma in this patient. There was sizable intraoperative blood loss given the small blood volume of preterm neonates. Supplementing the neonate with blood products does not correct the hypovolemia; on the contrary, it is likely to cause cardiac dysfunction or renal dysfunction. Therefore, it is important for the surgeon to identify the major blood vessels after the surgeon opens the skin, in order to maintain the vitals and remove the tumor as quickly as possible. Close collaboration among experienced head and neck surgeons, experienced nurses from the Department of Neonatology, and an expert anesthesiologist can help prevent complications such as hypovolemic shock, acute renal damage or failure, and/or cerebral hypoperfusion.

CONCLUSION

CHs are significantly different from typical hemangiomas in terms of the clinical manifestations, staging, pathology, and imaging findings. CHs are of different types, NICH, RICH, and PICH. The treatment strategies, incidence of complications, and long-term prognosis are also different. Therefore, it is crucial to determine the type of CH based on the clinical characteristics, color Doppler ultrasonography, and imaging. The treatment strategy should be guided by the specific type. Common complications of CH include intralesional hemorrhage, thrombocytopenia, abnormal coagulation function, and congestive heart failure. In our patient, we focused on limiting the liquid intake, inhibiting further growth of the hemangioma, alleviating the congestive heart failure, improving heart function, supplementing Hb, preventing bleeding, and selecting the timing for the surgery. Furthermore, close multidisciplinary collaboration, meticulous care of the tumor, surgical planning, and postoperative care were instrumental in averting postoperative complications.

FOOTNOTES

Author contributions: Ren N was the doctor who was in charge of the patient and contributed to the manuscript drafting; Jin CS was the surgeon of the patient and contributed to the manuscript drafting; Zhao XQ and Gao WH analyzed and interpreted the imaging findings and contributed to the manuscript drafting; Gao YX was in charge of the care of the patient and contributed to the manuscript drafting; Wang Y participated in the process of treatment and contributed to the manuscript drafting; Zhang YF was the consultant of the patient and revised and reviewed the manuscript; all authors issued final approval for the version to be submitted.

Informed consent statement: Informed written consent was obtained from the patients for the publication of this report and any accompanying images.

Conflict-of-interest statement: The authors declare that they have no conflict of interest.

CARE Checklist (2016) statement: The authors have read the CARE Checklist (2016), and the manuscript was prepared and revised according to the CARE Checklist (2016).

Open-Access: This article is an open-access article that was selected by an in-house editor and fully peer-reviewed by external reviewers. It is distributed in accordance with the Creative Commons Attribution NonCommercial (CC BY-NC 4.0) license, which permits others to distribute, remix, adapt, build upon this work non-commercially, and license their derivative works on different terms, provided the original work is properly cited and the use is non-commercial. See: https://creativecommons.org/Licenses/by-nc/4.0/

Country/Territory of origin: China

ORCID number: Neng Ren 0000-0002-7298-6740; Chun-Shun Jin 0000-0002-7947-5820; Xiao-Qi Zhao 0000-0002-8308-0194; Wen-Hui Gao 0000-0001-9953-6099; Yu-Xian Gao 0000-0002-7759-6055; Yuan Wang 0000-0002-3773-7220; Yun-Feng Zhang 0000-0002-7889-3967.

S-Editor: Chen YL
L-Editor: Kerr C
P-Editor: Chen YL

REFERENCES

1 **Zhang C**, Mai HM. Diagnosis and treatment advances in congenital heman-giomas. *J Oral Maxil Surg* 2020; **18** (1): 82-86
2 **Fomchenko EI**, Duran D, Jin SC, Dong W, Erson-Omay EZ, Antwi P, Allocco A, Gaillard JR, Huttner A, Gunel M, DiLuna ML, Kahle KT. De novo *MYH9* mutation in congenital scalp hemangioma. *Cold Spring Harb Mol Case Stud* 2018; 4 [PMID: 29903892 DOI: 10.1101/mcs.a002998]
3 **Li P**. Congenital Hemangioma: Clinical Manifestations and Treatment. *Pifukexue Tongbao* 2018; **35** (5): 518-526
4 **Wu XY**, Yang B. Research Progress on Congenital Hemangioma. *Yixue Zongshu* 2015; **21** (11): 2010-2012
5 **Hemangioma and vascular malformation group**, Plastic Surgery Branch; Chinese Medi-cal Association. Diagnostic and therapeutic guidelines for hemangioma and vascular mal-formation. *Zuzhi Gongcheng Yu Chongjian Waike* 2019; **15** (5): 277-304
6 **Li L**, Ma L. Progress in Classification of Hemangioma and Vascular Malformation. *Zhongguo Pifubing Zazhi* 2020; **53** (7): 569-572
7 **Tan MJ**, Yuan H, Zou Y. Compression therapy and surgical treatment of 1 case of special non-involuting congenital hemangioma. *Jiangxi Yiyao Zazhi* 2016; **51** (4): 326-327
8 **Lewis D**, Hachey K, Fitzgerald S, Vaidya R. Rapidly involuting congenital haemangioma of the liver. *BMJ Case Rep* 2018; **2018** [PMID: 29871961 DOI: 10.1136/bcr-2018-224337]
9 **Wang RQ**, Zhen YJ, Za XX. Ultrasonic diagnosis of fetal facial congenital giant hemangioma : one case report. *Zhongguo Chaosheng Yixue Zazhi* 2019; **35** (1): 17-19
10 **Shah SS**, Snelling BM, Sur S, Ramnath AR, Bandstra ES, Yavagal DR. Scalp congenital hemangioma with associated high-output cardiac failure in a premature infant: Case report and review of literature. *Interv Neuroradiol* 2017; **23**: 102-106 [PMID: 27789620 DOI: 10.1177/1591019916669089]

World Journal of Clinical Cases

Submit a Manuscript: https://www.f6publishing.com

World J Clin Cases 2022 June 16; 10(17): 5764-5769

DOI: 10.12998/wjcc.v10.i17.5764

ISSN 2307-8960 (online)

CASE REPORT

Simultaneous multiple primary malignancies diagnosed by endoscopic ultrasound-guided fine-needle aspiration: A case report

Jian Yang, Yan Zeng, Jun-Wen Zhang

Specialty type: Medicine, research and experimental

Provenance and peer review: Unsolicited article; Externally peer reviewed.

Peer-review model: Single blind

Peer-review report's scientific quality classification

Grade A (Excellent): A
Grade B (Very good): 0
Grade C (Good): 0
Grade D (Fair): D
Grade E (Poor): 0

P-Reviewer: Corvino A, Kalayarasan R

Received: November 8, 2021
Peer-review started: November 8, 2021
First decision: January 11, 2022
Revised: January 13, 2022
Accepted: April 21, 2022
Article in press: April 21, 2022
Published online: June 16, 2022

Jian Yang, Jun-Wen Zhang, Department of Gastroenterology, The First Affiliated Hospital of Chongqing Medical University, Chongqing 400016, China

Yan Zeng, Department of Psychology, The Second Affiliated Hospital of Chongqing Medical University, Chongqing 400010, China

Corresponding author: Jun-Wen Zhang, MD, Chief Doctor, Professor, Department of Gastroenterology, The First Affiliated Hospital of Chongqing Medical University, No. 1 Youyi Road, Yuzhong District, Chongqing 400016, China. 959308413@qq.com

Abstract

BACKGROUND

Multiple primary malignancies (MPMs) refer to more than one primary malignancy in the same or separate organs of the same patient, and MPMs are considered when different histological characteristics are detected in epidemiological studies. Herein, we report a case presumed to be primary pancreatic cancer with multiple liver metastases by positron-emission tomography/computed tomography (PET/CT) and confirmed to be synchronous liver and pancreatic MPMs by endoscopic ultrasound-guided fine-needle aspiration (EUS-FNA).

CASE SUMMARY

A 50-year-old man was referred to our hospital due to abdominal discomfort for 2 mo. Abdominal CT at a local hospital revealed a pancreatic mass with multiple liver nodules. After being transferred to our hospital, PET/CT confirmed all these lesions to have elevated metabolic activity, and therefore primary pancreatic cancer with multiple liver metastases was considered. EUS-guided liver aspiration unexpectedly found signet-ring cells with a high Ki-67 positive rate (20%), while EUS-guided pancreatic aspiration detected pancreatic neuroendocrine cells with a relatively low Ki-67 positive rate (1%). The final diagnosis from the multidisciplinary team was simultaneous liver and pancreatic MPMs. The patient returned to his local hospital for neoadjuvant chemotherapy and surgery, and he is still alive during the 6-mo postoperative follow-up.

CONCLUSION

Although rare, MPMs should be considered when treating pancreatic mass with suspected metastatic lesions, and EUS-FNA has proved minimally invasive and accurate.

Key Words: Multiple primary malignancies; Endoscopic ultrasound; Fine-needle aspiration; Pancreatic cancer; Liver cancer; Case report

©The Author(s) 2022. Published by Baishideng Publishing Group Inc. All rights reserved.

Core Tip: We report a rare case of synchronous multiple primary liver and pancreatic malignancies confirmed by endoscopic ultrasound-guided fine-needle aspiration (EUS-FNA), although this patient was first diagnosed as having primary pancreatic cancer with multiple liver metastases by computed tomography and positron-emission tomography/computed tomography. Although rare, multiple primary malignancies should be considered in patients with pancreatic mass and suspected metastatic lesions, and EUS-FNA has proven to be a minimally invasive and accurate preoperative diagnosis method.

Citation: Yang J, Zeng Y, Zhang JW. Simultaneous multiple primary malignancies diagnosed by endoscopic ultrasound-guided fine-needle aspiration: A case report. *World J Clin Cases* 2022; 10(17): 5764-5769
URL: https://www.wjgnet.com/2307-8960/full/v10/i17/5764.htm
DOI: https://dx.doi.org/10.12998/wjcc.v10.i17.5764

INTRODUCTION

Multiple primary malignancies (MPMs) refer to more than one primary malignancy in the same or separate organs of the same patient, and MPMs are considered when different histological characteristics are detected[1]. Simultaneous malignancies are defined as malignancies that are diagnosed at the same time or during the staging of the first malignancy, while synchronous and metachronous malignancies were usually distinguished by a 2-mo or 6-mo time point in different databases[2,3]. In patients with digestive system MPMs, it is infrequent for liver or pancreatic cancer patients to have both primary malignancies detected simultaneously[4]. Treatment strategies and associated prognoses of patients with digestive system MPMs are significantly different from those patients with primary digestive cancer and distant metastasis.

Preoperative endoscopic ultrasound-guided fine-needle aspiration (EUS-FNA) is an essential breakthrough in the endoscopic field and a substantial procedure to evaluate benign and malignant gastrointestinal tract lesions and nearby organs[5]. Taking pancreatic cancer as an example, the overall survival of the preoperative EUS-FNA group was significantly higher than that of the non-FNA group, and there was no remarkable difference in the tumor recurrence rate or peritoneal implantation rate between the two groups[6].

Herein, we report a case presumed to be primary pancreatic cancer with multiple liver metastases by positron-emission tomography/computed tomography (PET/CT) and confirmed to be synchronous liver and pancreatic MPMs by EUS-FNA.

CASE PRESENTATION

Chief complaints

A 50-year-old Chinese man was referred to our hospital due to abdominal discomfort for approximately 2 mo.

History of present illness

Approximately 1 mo previously, this patient was admitted to a local hospital due to elevated blood amylase. He denied jaundice, vomiting, and gastrointestinal bleeding. He was diagnosed with acute pancreatitis, but CT revealed an enlarged pancreatic head and suspected liver metastases. Thus, he was referred to our hospital for further management.

History of past illness

The patient had no remarkable medical history.

Personal and family history

This patient had a 30-year smoking history (half a pack per day) and has not quit smoking. He denied any family history of cancer.

Physical examination

After admission, the patient's physical examination revealed no abnormality.

Laboratory examinations

Blood analysis revealed elevated CA19-9 [106 U/mL (0-27 U/mL)], amylase [450 U/L (0-110 U/L)], and lipase [3795 U/L (0-300 U/L)]. Alpha-fetoprotein was within normal limits.

Imaging examinations

After admission, PET/CT detected increased soft tissues with elevated metabolic activity in the pancreatic head (Figure 1) and multiple liver nodules with increased metabolic activity (Figure 2), and therefore the initial diagnosis was primary pancreatic cancer with multiple liver metastases.

EUS confirmed an enlarged hypoechoic pancreatic head (Figure 3A) and multiple hypoechoic liver masses (Figure 3B). A linear Pentax echoendoscope (Hoya Co., Tokyo, Japan) and color Doppler flow imaging were employed to determine the puncture site. No malignant cells were detected in the fluid inside the peripancreatic cystic lesion extracted by EUS-FNA. EUS-FNA biopsy was performed with two 19-gauge needles (Boston Scientific Co., Natick, United States). EUS-guided liver aspiration unexpectedly revealed signet-ring cells (Figure 4A) with a high Ki-67 positive rate (20%), while EUS-guided pancreatic aspiration with another aspiration needle detected pancreatic neuroendocrine cells (Figure 4B) with a relatively low Ki-67 positive rate (1%). Three senior pathologists at our medical university confirmed that the considerable differences in immunohistochemical results indicated that the pancreatic mass and multiple liver nodules were not metastatic lesions from the other.

The gastric mucosa punctured by the EUS-guided liver aspiration needle was further inspected by magnifying endoscopy. No abnormal microsurface or microvessel was identified, and no malignant cells were found in deep excavation biopsies. The possibility of gastric signet-ring cell carcinoma was excluded. The patient's colonoscopy was negative.

FINAL DIAGNOSIS

A multi-disciplinary team of pathologists, radiologists, and clinicians was convened. The final diagnoses were listed as follows: (1) Simultaneous liver and pancreatic MPMs (hepatic signet ring cell adenocarcinoma and pancreatic neuroendocrine tumor); and (2) Pancreatic pseudocyst.

TREATMENT

The patient returned to his local hospital for neoadjuvant chemotherapy (apatinib, 500 mg, once per day) and left liver resection, and postoperative pathological results confirmed the diagnoses of hepatic signet ring cell adenocarcinoma, pancreatic neuroendocrine tumor, and post-necrotic pancreatic pseudocyst.

OUTCOME AND FOLLOW-UP

The patient is still alive at the 6-mo postoperative follow-up.

DISCUSSION

To the best of our knowledge, this is the first report of simultaneous liver and pancreatic MPMs preoperatively diagnosed by EUS-FNA in Asian patients. This case will help prompt clinicians to consider other possibilities besides primary pancreatic cancer with liver metastasis when dealing with similar issues and raise their attention to routinely perform preoperative EUS-FNA in patients with presumed malignancies.

With the continuous progress of medical techniques and the extension of life expectancy, the incidence of MPMs has increased gradually. Most patients with MPMs were male and elderly patients (> 50 years old), and the leading location in all MPMTs was the digestive system[7]. Compared with all other MPMs, liver malignancies revealed the fewest MPMs occurrences[8], and it is rarer to confirm both liver and pancreatic malignancies by EUS-FNA simultaneously. Lai *et al*[9] reported a 56-year-old Caucasian woman with a pancreatic mass and a single liver nodule. Her EUS-FNA cytology revealed pancreatic ductal adenocarcinoma, while she underwent a liver core biopsy and was confirmed to have hepatocellular carcinoma. The absence of EUS-FNA for liver biopsy may be due to the location of her liver lesion. In addition, Zhang *et al*[10] reported a 70-year-old man with pathologically confirmed

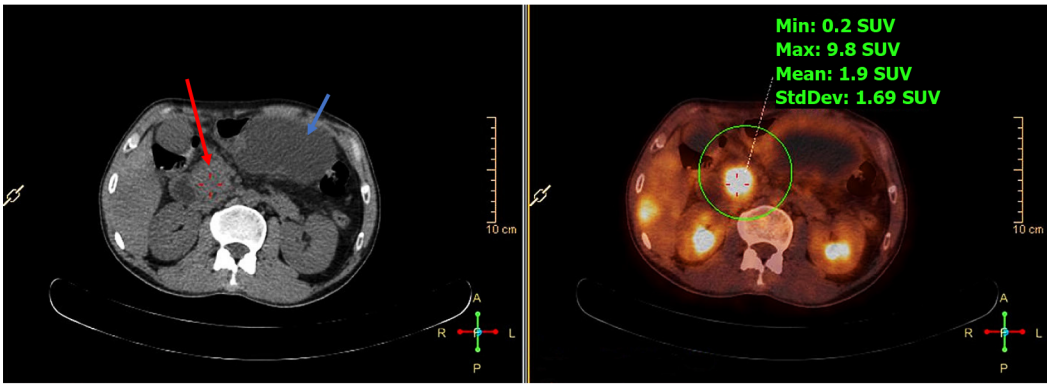

DOI: 10.12998/wjcc.v10.i17.5764 **Copyright** ©The Author(s) 2022.

Figure 1 Positron-emission tomography/computed tomography images. Positron-emission tomography/computed tomography confirmed increased soft tissues in the pancreatic head (red arrow) with elevated metabolic activity (green circle) and pancreatic pseudocyst (blue arrow) without an increase in metabolic activity.

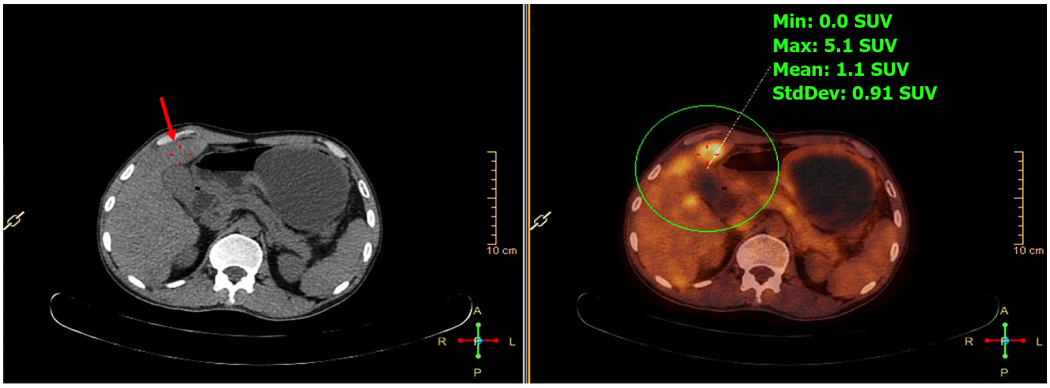

DOI: 10.12998/wjcc.v10.i17.5764 **Copyright** ©The Author(s) 2022.

Figure 2 Positron-emission tomography/computed tomography images. Positron-emission tomography/computed tomography confirmed multiple liver masses (red arrow) with elevated metabolic activity (green circle).

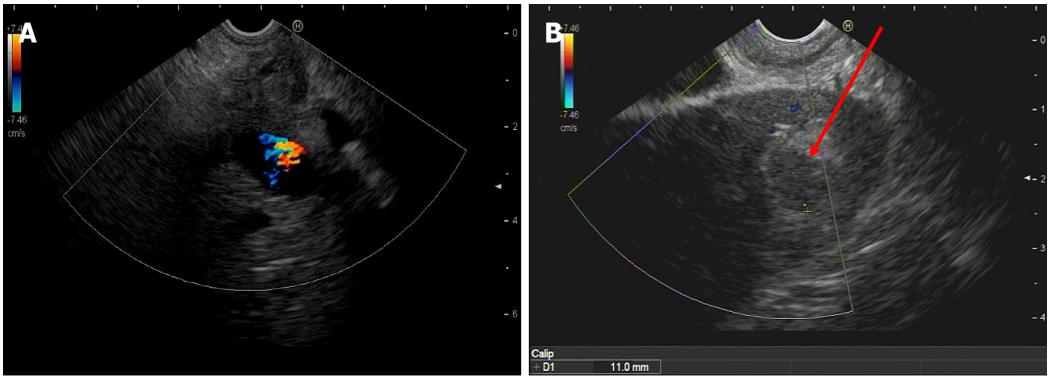

DOI: 10.12998/wjcc.v10.i17.5764 **Copyright** ©The Author(s) 2022.

Figure 3 Endoscopic ultrasound images. A: An enlarged hypoechoic pancreatic head; B: Multiple hypoechoic liver masses (red arrow).

pancreatic metastasis of hepatocellular carcinoma. Therefore, in patients with pancreatic masses and multiple liver nodules, clinicians should consider the following three possibilities: Primary pancreatic cancer with liver metastasis, primary liver cancer with pancreatic metastasis, and MPMs.

Correct diagnosis is the first and essential step in treating patients with malignancies. PET/CT, one of the sophisticated imaging methods that have been increasingly used in recent years, is playing a considerable role in the diagnosis of MPMs[11]. Compared with the inability to obtain specimens from PET/CT, the accuracy and safety advantages have been proven in the process of securing cell and tissue specimens *via* EUS-FNA[12-14]. EUS-FNA and associated procedures are expected to play an

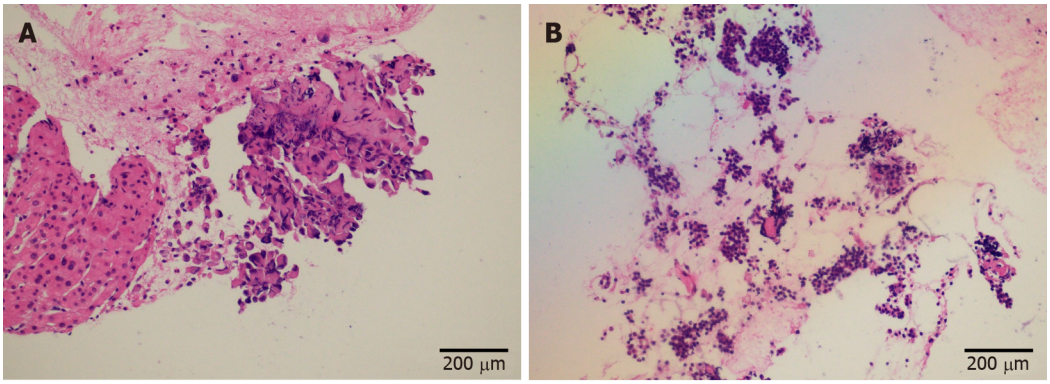

DOI: 10.12998/wjcc.v10.i17.5764 **Copyright** ©The Author(s) 2022.

Figure 4 Histopathological images. A and B: Endoscopic ultrasound-guided fine-needle aspiration biopsy revealed histologies of endoscopic ultrasound-guided liver aspiration (A) and endoscopic ultrasound-guided pancreatic aspiration (B).

increasingly important role in the preoperative diagnosis of MPMs and other suspected malignancies.

This male patient in the present case had a smoking history of up to 30 years. Males and patients with a smoking history were considered to have a higher risk of developing multiple MPMs[1,15]. Therefore, these patients need to be consciously inspected for the possibility of MPMs. Liver lesions are more often considered metastases than primary tumors[16], and thus the presumed diagnosis of this patient was primary pancreatic cancer with multiple liver metastases. However, the pathological results of EUS-guided liver and pancreatic aspiration unexpectedly confirmed a rare case of MPMs. This case also reminds us that a pathological biopsy should always be the final and definite diagnosis in patients with suspected malignancies[17].

CONCLUSION

A rare case of simultaneous liver and pancreatic MPMs has been confirmed by pathological biopsies of EUS-guided liver and pancreatic aspiration. MPMs should be considered in patients with pancreatic mass and suspected metastatic lesions, and EUS-FNA is a minimally invasive and accurate diagnostic method.

FOOTNOTES

Author contributions: Yang J, Zeng Y and Zhang JW designed and performed the research; Yang J and Zhang JW performed EUS-FNA; Yang J and Zeng Y analyzed the data and wrote the manuscript; all authors have read and approved the final manuscript.

Informed consent statement: Informed consent was obtained from the patient for publication of this report and any accompanying images.

Conflict-of-interest statement: No conflict of interest exists in the submission of this manuscript.

CARE Checklist (2016) statement: The authors have read the CARE Checklist (2016), and the manuscript was prepared and revised according to the CARE Checklist (2016).

Open-Access: This article is an open-access article that was selected by an in-house editor and fully peer-reviewed by external reviewers. It is distributed in accordance with the Creative Commons Attribution NonCommercial (CC BY-NC 4.0) license, which permits others to distribute, remix, adapt, build upon this work non-commercially, and license their derivative works on different terms, provided the original work is properly cited and the use is non-commercial. See: https://creativecommons.org/Licenses/by-nc/4.0/

Country/Territory of origin: China

ORCID number: Jian Yang 0000-0001-8170-0727; Yan Zeng 0000-0003-4935-1306; Jun-Wen Zhang 0000-0003-2911-598X.

Corresponding Author's Membership in Professional Societies: Chinese Society of Gastroenterology.

S-Editor: Gao CC
L-Editor: Wang TQ

P-Editor: Gao CC

REFERENCES

1 **Vogt A**, Schmid S, Heinimann K, Frick H, Herrmann C, Cerny T, Omlin A. Multiple primary tumours: challenges and approaches, a review. *ESMO Open* 2017; **2**: e000172 [PMID: 28761745 DOI: 10.1136/esmoopen-2017-000172]

2 **Friedrich RE**. Primary and second primary cancer in 649 patients with malignancies of the maxillofacial region. *Anticancer Res* 2007; **27**: 1805-1818 [PMID: 17649777]

3 **Xiong J**, Su Y, Bing Z, Zhao B. Survival between synchronous and non-synchronous multiple primary cutaneous melanomas-a SEER database analysis. *PeerJ* 2020; **8**: e8316 [PMID: 31915586 DOI: 10.7717/peerj.8316]

4 **Ikubo A**, Matsufuji S, Morifuji Y, Koga H, Kobarai T, Kouya N, Sakai M, Samejima R, Kojima K, Tabuchi M, Yunotani S. Clinical Features, Prognosis, Diagnostic Approaches and Treatment of Multiple Primary Malignancies in the Digestive System. *Anticancer Res* 2019; **39**: 6863-6870 [PMID: 31810954 DOI: 10.21873/anticanres.13904]

5 **Cazacu IM**, Luzuriaga Chavez AA, Saftoiu A, Vilmann P, Bhutani MS. A quarter century of EUS-FNA: Progress, milestones, and future directions. *Endosc Ultrasound* 2018; **7**: 141-160 [PMID: 29941723 DOI: 10.4103/eus.eus_19_18]

6 **Alghamdi A**, Palmieri V, Alotaibi N, Martel M, Barkun AN, Zogopoulos G, Chaudhury P, Chen YI. Sa1468 Preoperative EUS-guided FNA is associated with better overall survival in resectable pancreatic cancer when compared to upfront surgery without preoperative tissue acquisition: a systematic review and meta-analysis. *Gastrointestinal Endoscopy* 2020; **91**: AB204 [DOI: 10.1016/j.gie.2020.03.1264]

7 **Lv M**, Zhang X, Shen Y, Wang F, Yang J, Wang B, Chen Z, Li P, Li S. Clinical analysis and prognosis of synchronous and metachronous multiple primary malignant tumors. *Medicine (Baltimore)* 2017; **96**: e6799 [PMID: 28445321 DOI: 10.1097/MD.0000000000006799]

8 **Hayat MJ**, Howlader N, Reichman ME, Edwards BK. Cancer statistics, trends, and multiple primary cancer analyses from the Surveillance, Epidemiology, and End Results (SEER) Program. *Oncologist* 2007; **12**: 20-37 [PMID: 17227898 DOI: 10.1634/theoncologist.12-1-20]

9 **Lai JZ**, Zhou Y, Cao D. Synchronous Pancreatic Ductal Adenocarcinoma and Hepatocellular Carcinoma: Report of a Case and Review of the Literature. *Anticancer Res* 2018; **38**: 3009-3012 [PMID: 29715132 DOI: 10.21873/anticanres.12554]

10 **Zhang Y**, Han T, Wang D, Li G, Zhang Y, Yang X, Chen T, Zheng Z. Hepatocellular carcinoma with pancreatic mass as the first symptom: a case report and literature review. *Ann Palliat Med* 2019; **8**: 740-745 [PMID: 31865733 DOI: 10.21037/apm.2019.11.14]

11 **Pang L**, Liu G, Shi H, Hu P, Li B, Cheng D. Nineteen cases with synchronous multiple primary cancers studied by ^{18}F-FDG PET/CT. *Hell J Nucl Med* 2017; **20**: 36-40 [PMID: 28315906]

12 **Yoshinaga S**, Itoi T, Yamao K, Yasuda I, Irisawa A, Imaoka H, Tsuchiya T, Doi S, Yamabe A, Murakami Y, Ishikawa H, Saito Y. Safety and efficacy of endoscopic ultrasound-guided fine needle aspiration for pancreatic masses: A prospective multicenter study. *Dig Endosc* 2020; **32**: 114-126 [PMID: 31166046 DOI: 10.1111/den.13457]

13 **Ichim VA**, Chira RI, Mircea PA, Nagy GA, Crisan D, Socaciu MA. Accuracy of endoscopic ultrasound-guided biopsy of focal liver lesions. *Med Ultrason* 2020; **22**: 20-25 [PMID: 32096783 DOI: 10.11152/mu-2078]

14 **Matsumoto K**, Takeda Y, Onoyama T, Kawata S, Kurumi H, Koda H, Yamashita T, Isomoto H. Endoscopic ultrasound-guided fine-needle aspiration biopsy - Recent topics and technical tips. *World J Clin Cases* 2019; **7**: 1775-1783 [PMID: 31417923 DOI: 10.12998/wjcc.v7.i14.1775]

15 **Amer MH**. Multiple neoplasms, single primaries, and patient survival. *Cancer Manag Res* 2014; **6**: 119-134 [PMID: 24623992 DOI: 10.2147/CMAR.S57378]

16 **Corvino A**, Corvino F, Radice L, Catalano O. Synchronous mucinous colonic adenocarcinoma and multiple small intestinal adenocarcinomas: report of a case and review of literature. *Clin Imaging* 2015; **39**: 538-542 [PMID: 25744428 DOI: 10.1016/j.clinimag.2014.12.019]

17 **Matsubayashi H**, Sasaki K, Ono S, Abe M, Ishiwatari H, Fukutomi A, Uesaka K, Ono H. Pathological and Molecular Aspects to Improve Endoscopic Ultrasonography-Guided Fine-Needle Aspiration From Solid Pancreatic Lesions. *Pancreas* 2018; **47**: 163-172 [PMID: 29346217 DOI: 10.1097/MPA.0000000000000986]

World Journal of Clinical Cases

Submit a Manuscript: https://www.f6publishing.com

World J Clin Cases 2022 June 16; 10(17): 5770-5775

DOI: 10.12998/wjcc.v10.i17.5770

ISSN 2307-8960 (online)

CASE REPORT

Neuroendocrine tumour of the descending part of the duodenum complicated with schwannoma: A case report

Lu Zhang, Chi Zhang, Shu-Yan Feng, Pan-Pan Ma, Shuo Zhang, Qian-Qian Wang

Specialty type: Gastroenterology and hepatology

Provenance and peer review: Unsolicited article; Externally peer reviewed.

Peer-review model: Single blind

Peer-review report's scientific quality classification

Grade A (Excellent): 0
Grade B (Very good): 0
Grade C (Good): 0
Grade D (Fair): D, D, D
Grade E (Poor): 0

P-Reviewer: Cerwenka H; Austria, Endo S; Japan, Symeonidis N; Greece

Received: November 21, 2021
Peer-review started: November 21, 2021
First decision: December 26, 2021
Revised: January 6, 2022
Accepted: April 4, 2022
Article in press: April 4, 2022
Published online: June 16, 2022

Lu Zhang, Chi Zhang, Shu-Yan Feng, Pan-Pan Ma, Shuo Zhang, Qian-Qian Wang, Department of Gastroenterology, The First Affiliated Hospital, Zhejiang Chinese Medical University, Hangzhou 310006, Zhejiang Province, China

Corresponding author: Qian-Qian Wang, Doctor, Department of Gastroenterology, The First Affiliated Hospital, Zhejiang Chinese Medical University, No. 54 Youdian Road, Shangcheng District, Hangzhou 310006, Zhejiang Province, China. w18072348608@163.com

Abstract

BACKGROUND

No known case of neuroendocrine tumour (NET) with schwannoma has been reported.

CASE SUMMARY

A 63-year-old female presented to our hospital with nausea and vomiting. Upper gastrointestinal endoscopy revealed a mass in the descending part of the duodenum. Using ultrasound gastroscopy, we found that the tumour originated from the submucosa and showed low echo. We removed the tumour by electrocoagulation and sent it for pathological biopsy.

CONCLUSION

Immunohistochemical results showed that the mass was a rare NET with neurilemmoma.

Key Words: Neuroendocrine tumour; Schwannoma; Duodenum; Endoscopy; Immunohistochemistry; Trap with current; Case report

©The Author(s) 2022. Published by Baishideng Publishing Group Inc. All rights reserved.

Core Tip: Neuroendocrine tumours (NETs) and schwannomas of the duodenum are quite rare and few clinical cases have been reported. To the best of our knowledge, this is the first publication of a NET of descending duodenum complicated with schwannoma. Through a review of relevant literature, we can deepen the understanding of this type of tumour.

Citation: Zhang L, Zhang C, Feng SY, Ma PP, Zhang S, Wang QQ. Neuroendocrine tumour of the descending part of the duodenum complicated with schwannoma: A case report. *World J Clin Cases* 2022; 10(17): 5770-5775
URL: https://www.wjgnet.com/2307-8960/full/v10/i17/5770.htm
DOI: https://dx.doi.org/10.12998/wjcc.v10.i17.5770

INTRODUCTION

Neuroendocrine tumours (NETs) are rare tumours originating from neuroendocrine cells that account for approximately 2% of all malignant tumours, and approximately 50.6% of NETs are found in the digestive system; duodenal NETs are extremely rare, accounting for only 2%-3% of gastrointestinal NETs[1]. Schwannoma is a benign tumour originating from the nerve fibre sheath, accounting for approximately 5% of all soft tissue tumours; it is mostly located in the body surface and auditory nerve, less often in the digestive tract, and even more rarely in the duodenum[2].

CASE PRESENTATION

Chief complaints

One month of nausea and vomiting.

History of present illness

A 63-year-old female underwent upper gastrointestinal endoscopy at a local, grassroots hospital due to 1 mo of nausea and vomiting, and a large nipple was found in the descending part of the duodenum. The patient's faecal occult blood test was positive. The patient had obvious symptoms of nausea and vomiting, often vomiting with no stomach contents and had lost 2 kg of weight within a month. Before the operation, we administered symptomatic treatment, such as replenishing gastric protective fluid. After excluding relevant surgical contraindications, endoscopic examination was performed on the patient in our hospital, and we found a protuberant mass above the nipple of the descending duodenum, with a smooth surface and a diameter of approximately 0.5 cm. A 12 MHz ultrasound probe showed that the tumour originated from the submucosa and showed low echo. We used a nylon noose to trap the tumour, cut the bottom of the base by snaring with an electrocurrent, and clamped the wound with a titanium clip to stop the bleeding (Figure 1). To confirm the diagnosis, the excised specimens were sent for pathological examination and immunohistochemistry. One week after the operation, the patient recovered smoothly and was discharged from the hospital. The pathological results showed that the tumour in the descending part of the duodenum was a NET (grade 1) with schwannoma, and the cutting edge was negative (Figure 2). The results of immunohistochemical staining indicated that the tumour cells were positive for antigen KI-67, broad-spectrum cytokeratin, CD56, synaptophysin (Syn), chromogranin A (CgA), S-100, nerve specific enolase, CD68, CD163, and myoglobin and were negative for CD34, succinate dehydrogenase B, CD117, DOG-1, smooth muscle actin, desmin, cytokeratin (CK) 7, CK20, and myogenic differentiation 1 (Figures 3 and 4).

History of past illness

The patient has a history of infection with tuberculosis 40 years ago. The history of surgical trauma was bronchiectasis in 2015, hysterectomy and minimally invasive hysteroptosis in 2020.

Personal and family history

Parents have a history of hypertension.

Physical examination

Mild tenderness in the abdomen, no rebound pain.

Laboratory examinations

Immunohistochemical results showed that the mass was a rare NET with neurilemmoma.

Imaging examinations

Mediastinal computed tomography (CT) showed no tumour metastasis.

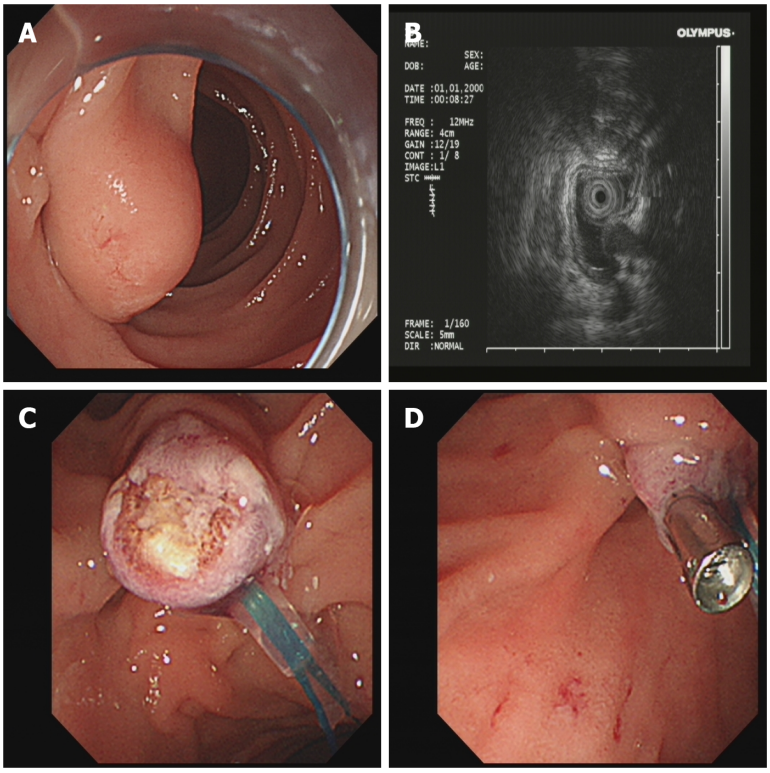

DOI: 10.12998/wjcc.v10.i17.5770 **Copyright** ©The Author(s) 2022.

Figure 1 Endoscopic resection of the tumour. A: Tumour in the descending part of the duodenum in the natural state; B: Using endoscopic ultrasonography to explore the tumour; C: Endoscopic electrocoagulation for resection of the tumour; D: A titanium clip was used to clamp the wound to stop the bleeding.

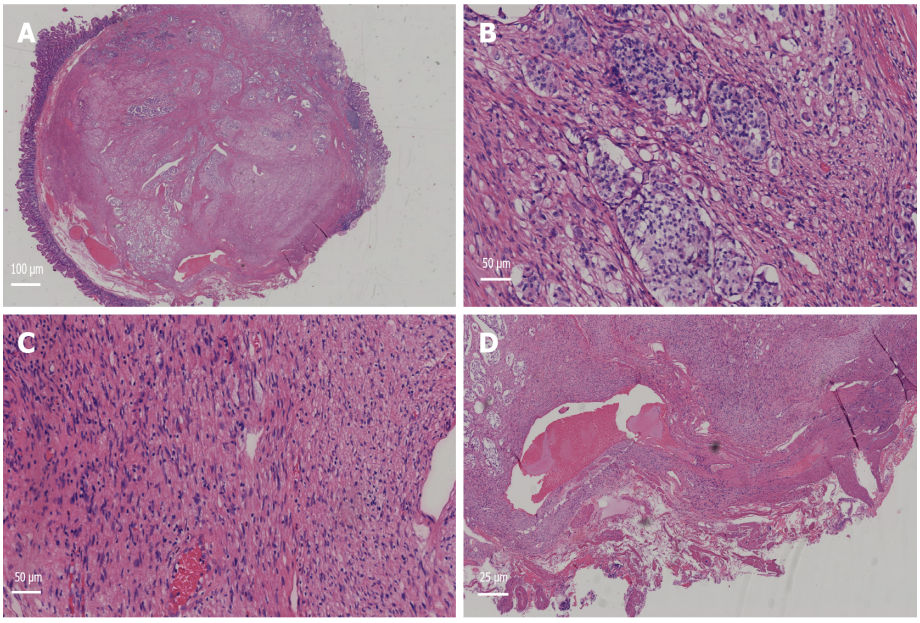

DOI: 10.12998/wjcc.v10.i17.5770 **Copyright** ©The Author(s) 2022.

Figure 2 Pathological manifestation of the tumour under a light microscope. A: Pathological tissue (Magnification: 100 ×). The lower right corner is the nesting tissue of the schwannoma, and the rest is the vesicle-like tissue of the neuroendocrine tumour; B: Neuroendocrine tumour tissue (Magnification: 200 ×); C: Schwannoma tissue (Magnification: 200 ×); D: The vertical incisal margin was negative, and there was no lymphatic vascular invasion (Magnification: 400 ×).

MULTIDISCIPLINARY EXPERT CONSULTATION

Because this patient does not have other systemic diseases, multidisciplinary experts were not invited to discuss it.

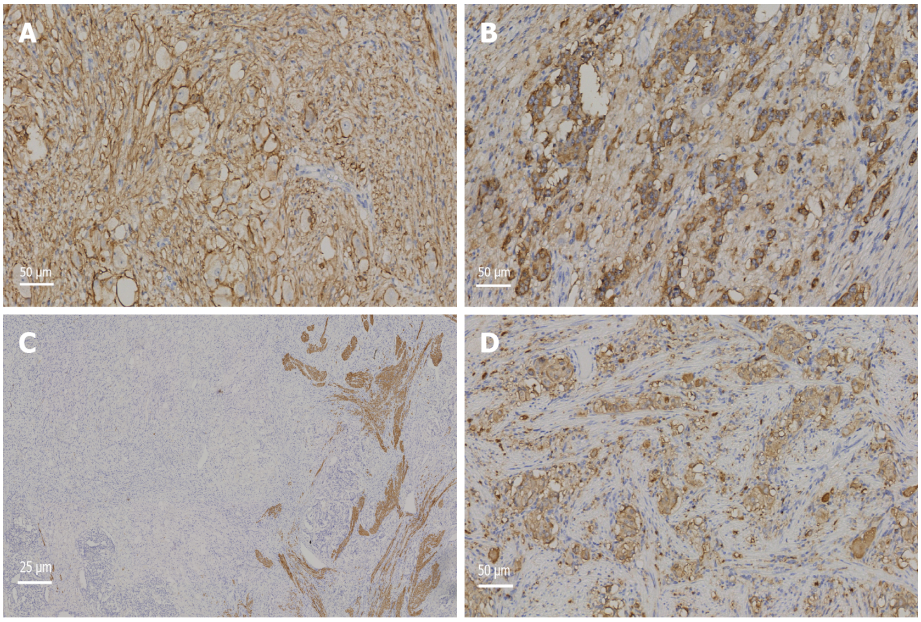

DOI: 10.12998/wjcc.v10.i17.5770 **Copyright** ©The Author(s) 2022.

Figure 3 Immunohistochemical neuroendocrine tumour results. A: CD56^{+} (Magnification: 200 ×); B: Chromogranin A+ (Magnification: 200 ×); C: Desmin+ (Magnification: 400 ×); D: Synaptophysin+ (Magnification: 200 ×).

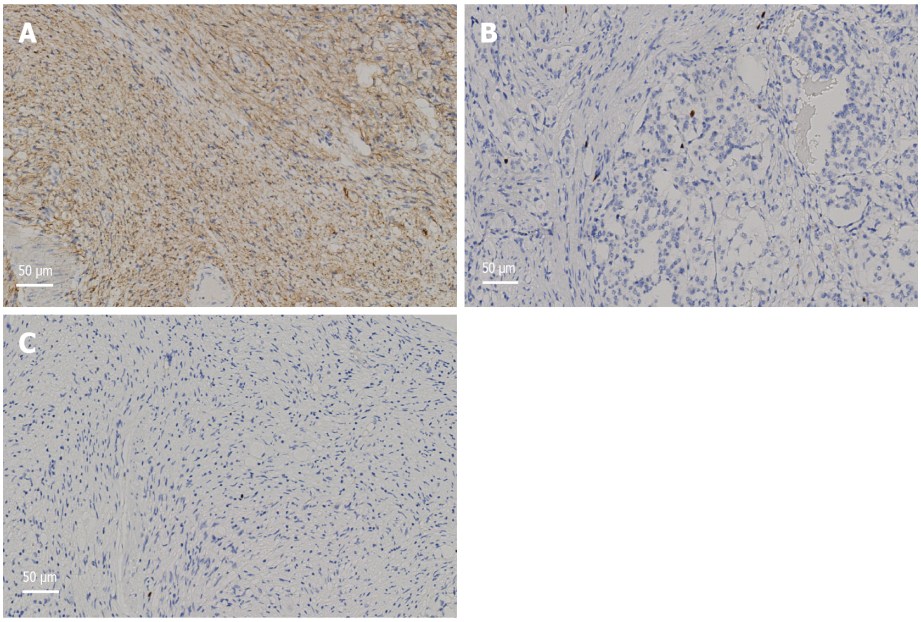

DOI: 10.12998/wjcc.v10.i17.5770 **Copyright** ©The Author(s) 2022.

Figure 4 Immunohistochemical results. A: S100+ expression in schwannoma (Magnification: 200 ×); B: The antigen KI-67 index of the neuroendocrine tumour was approximately 1% (Magnification: 200 ×); C: The KI-67 index of the schwannoma was approximately 1% (Magnification: 200 ×).

FINAL DIAGNOSIS

NET of the descending part of the duodenum complicated with schwannoma.

TREATMENT

We removed the tumour by electrocoagulation and gave the patient some other symptomatic treatment to help stopping vomiting and protect the stomach.

OUTCOME AND FOLLOW-UP

Mediastinal CT showed no tumour metastasis, and the prognosis of the patient is good.

DISCUSSION

There may be rare cases of NETs with schwannoma in the descending part of the duodenum worldwide, but there are no clinical reports. To the best of our knowledge, this is the first clinical case report of a duodenal NET complicated with schwannoma, which has high clinical value. Endoscopic NETs and schwannomas of the duodenum do not have specific features and are often mistaken for enlarged duodenal papilla, resulting in missed diagnosis and worsening of the disease. Endoscopic ultrasonography (EUS) is of high value in the diagnosis of these two kinds of tumours. Under EUS, most of the lesions are hypoechoic lesions originating from the submucosa, with clear boundaries and homogeneous internal echoes, which is consistent with our ultrasound results[3]. Duodenal schwannoma is extremely rare in gastrointestinal mesenchymal tumours, and only a few cases have been reported thus far. Duodenal neurilemmoma is often found by accident and is difficult to diagnose before surgery. There was no typical duodenal schwannoma under ordinary endoscopy. Due to the rare nature of duodenal schwannoma, no typical endoscopic ultrasonographic features have been reported [4]. The immunohistochemical results of the specimen remain the gold standard for diagnosis. NET cells are often positive for CgA, CD56, CK, and Syn, while schwannoma cells are often positive for S-100[5], which is consistent with our immunohistochemical results. Endoscopic treatment is usually the first choice for gastrointestinal NETs or schwannomas with diameters less than 1 cm, as it does not invade the lamina propria and because endoscopic treatment has the characteristics of less trauma, less cost, good prognosis, and easy follow-up after the operation[6]. It has been reported that snare polypectomy has a very high complete resection rate of gastrointestinal NETs (93.8%), and this rate may be high for several reasons. First, decoy polypectomy is more commonly used in smaller tumours (< 5.2 mm), and the appearance of polyps is more likely to be limited to the mucosa. The second reason is that electrosurgical devices, such as argon plasma coagulators, damage a larger field of vision during treatment. Therefore, for some small gastrointestinal NETs with specific shapes, the use of decoy electrocoagulation is completely effective[7]. In this case, we used EUS to determine the lesion level and endoscopic electrocoagulation for R0 resection, suggesting the feasibility and broad prospect of early endoscopic diagnosis and treatment of the tumour. The KI-67 index of the specimen was approximately 1%, suggesting that the NET phase was G1. In addition, we examined the vertical edge of the specimen with a high-power microscope. The vertical edge was negative, and there was no lymphatic invasion, which proved that we successfully removed the tumour completely. Mediastinal CT showed no tumour metastasis, and the prognosis of the patient is good.

CONCLUSION

To the best of our knowledge, this is the first publication of a neuroendocrine tumour of descending duodenum complicated with schwannoma. We removed the tumour by electrocoagulation completely and the patient recovered and was discharged.

FOOTNOTES

Author contributions: Zhang L and Zhang S were involved in the conception of the study; Zhang L and Zhang C were involved in writing the article; Zhang L, Ma PP, Feng SY, Wang QQ and Zhang S critically revised the manuscript; all authors read and approved the final manuscript.

Supported by the National Natural Science Foundation of China, No. 82074214; and the Research Fund Project of Zhejiang Chinese Medical University, No. 2019ZY02.

Informed consent statement: Informed written consent was obtained from the patient for publication of this report and any accompanying images.

Conflict-of-interest statement: The authors declare that they have no conflict of interest.

CARE Checklist (2016) statement: The authors have read the CARE Checklist (2016), and the manuscript was prepared and revised according to the CARE Checklist (2016).

Open-Access: This article is an open-access article that was selected by an in-house editor and fully peer-reviewed by external reviewers. It is distributed in accordance with the Creative Commons Attribution NonCommercial (CC BY-

NC 4.0) license, which permits others to distribute, remix, adapt, build upon this work non-commercially, and license their derivative works on different terms, provided the original work is properly cited and the use is non-commercial. See: https://creativecommons.org/Licenses/by-nc/4.0/

Country/Territory of origin: China

ORCID number: Lu Zhang 0000-0001-7726-4846; Chi Zhang 0000-0002-8983-206X; Shu-Yan Feng 0000-0003-4787-2765; Pan pan Ma 0000-0003-1193-9454; Shuo Zhang 0000-0003-1120-5872; Qian-Qian Wang 0000-0002-5889-5316.

S-Editor: Guo XR
L-Editor: Filipodia
P-Editor: Guo XR

REFERENCES

1 **Oronsky B**, Ma PC, Morgensztern D, Carter CA. Nothing But NET: A Review of Neuroendocrine Tumors and Carcinomas. *Neoplasia* 2017; **19**: 991-1002 [PMID: 29091800 DOI: 10.1016/j.neo.2017.09.002]
2 **Madero Velázquez L**, Uceda F, Buendía L. Duodenal schwannoma, an infrequent entity. *Rev Esp Enferm Dig* 2021; **113**: 548-549 [PMID: 33244978 DOI: 10.17235/reed.2020.7371/2020]
3 **De Angelis C**, Manfrè SF, Bruno M, Pellicano R. Hegemony and cost-effectiveness of endoscopic ultrasound (EUS) in the field of gastroenteropancreatic-neuroendocrine tumors (GEP-NETs). *Minerva Med* 2014; **105**: 363-370 [PMID: 25325565]
4 **Mori Y**, Kurita A, Yazumi S. Gastrointestinal: Schwannoma of the duodenum. *J Gastroenterol Hepatol* 2020; **35**: 1855 [PMID: 32390278 DOI: 10.1111/jgh.15075]
5 **Bellizzi AM**. Immunohistochemistry in the diagnosis and classification of neuroendocrine neoplasms: what can brown do for you? *Hum Pathol* 2020; **96**: 8-33 [PMID: 31857137 DOI: 10.1016/j.humpath.2019.12.002]
6 **Scherübl H**, Cadiot G. Early Gastroenteropancreatic Neuroendocrine Tumors: Endoscopic Therapy and Surveillance. *Visc Med* 2017; **33**: 332-338 [PMID: 29177161 DOI: 10.1159/000459404]
7 **Sun W**, Wu S, Han X, Yang C. Effectiveness of Endoscopic Treatment for Gastrointestinal Neuroendocrine Tumors: A Retrospective Study. *Medicine (Baltimore)* 2016; **95**: e3308 [PMID: 27082572 DOI: 10.1097/MD.0000000000003308]

World Journal of Clinical Cases

Submit a Manuscript: https://www.f6publishing.com

World J Clin Cases 2022 June 16; 10(17): 5776-5782

DOI: 10.12998/wjcc.v10.i17.5776

ISSN 2307-8960 (online)

CASE REPORT

Massive hemothorax following internal jugular vein catheterization under ultrasound guidance: A case report

Hyun Kang, Soo Young Cho, Eun Ha Suk, Wan Ju, Joon Yong Choi

Specialty type: Anesthesiology

Provenance and peer review: Unsolicited article; Externally peer reviewed.

Peer-review model: Single blind

Peer-review report's scientific quality classification

Grade A (Excellent): 0
Grade B (Very good): B, B, B
Grade C (Good): 0
Grade D (Fair): 0
Grade E (Poor): E

P-Reviewer: Sparchez Z, Romania; Tokumine J, Japan

Received: November 11, 2021
Peer-review started: November 11, 2021
First decision: December 10, 2021
Revised: December 22, 2021
Accepted: April 4, 2022
Article in press: April 4, 2022
Published online: June 16, 2022

Hyun Kang, Soo Young Cho, Eun Ha Suk, Wan Ju, Joon Yong Choi, Department of Anesthesiology and Pain Medicine, Kwangju Christian Hospital, Gwangju 61661, South Korea

Corresponding author: Soo Young Cho, MD, PhD, Professor, Anesthesiology and Pain Medicine, Kwangju Christian Hospital, Kwangju Christian Hospital, 37 Yangnim-ro, Nam-gu, Gwangju 61661, South Korea. tndud2584@gmail.com

Abstract

BACKGROUND

Hemothorax is a rare but life-threatening complication of central venous catheterization. Recent reports suggest that ultrasound guidance may reduce complications however, it does not guarantee safety

CASE SUMMARY

A 75-year-old male patient was admitted for laparoscopic radical nephrectomy. Under ultrasound guidance, right internal jugular vein catheterization was successfully achieved after failure to aspirate blood from the catheter in the first attempt. Sudden hypotension developed after surgical positioning and persisted until the end of the operation, lasting for about 4 h. In the recovery room, a massive hemothorax was identified on chest radiography and computed tomography. The patient recovered following chest tube drainage of 1.6 L blood.

CONCLUSION

Hemothorax must be suspected when unexplained hemodynamic instability develops after central venous catheterization despite ultrasound guidance. So the proper use of ultrasound is important

Key Words: Central venous catheterization; Hemothorax; Ultrasound guidance; Internal jugular vein; Case report

©The Author(s) 2022. Published by Baishideng Publishing Group Inc. All rights reserved.

Core Tip: During central venous catheterization *via* internal jugular vein, physicians should be aware of the possibility of hemothorax, even during ultrasound-guided procedures due to difficulty achieving real-time visualization of the dilator or catheter tip into the thorax. Confirmation of the guidewire within the brachiocephalic vein is recommended to prevent guidewire malposition, one of the reasons for dilator-induced hemothorax. In hemothorax caused by intrathoracic venous injury, the development of hemodynamic compromise can be delayed and managed with supportive care, obscuring prompt diagnosis during anesthesia. Clinical suspicion and timely diagnostic evaluations are needed for early diagnosis and treatment.

Citation: Kang H, Cho SY, Suk EH, Ju W, Choi JY. Massive hemothorax following internal jugular vein catheterization under ultrasound guidance: A case report. *World J Clin Cases* 2022; 10(17): 5776-5782
URL: https://www.wjgnet.com/2307-8960/full/v10/i17/5776.htm
DOI: https://dx.doi.org/10.12998/wjcc.v10.i17.5776

INTRODUCTION

Central venous catheterization (CVC) is a basic invasive procedure in anesthetic and critically ill patients management; however, it may be associated with various complications, vascular injury being the most common. Extrathoracic vascular injuries, such as common carotid artery puncture, can be easily detected and managed with manual compression. However, intrathoracic vascular injuries may be challenging to diagnose because of its invisibility, and external compression is impossible, which can lead serious results.

Ultrasound (US) guidance has markedly improved success rates, with fewer complications than the anatomic landmark method in CVC[1]. Nevertheless, it does not guarantee safety because real-time observations of the guidewire, dilator, and catheter tips are difficult. Hemothorax is a rare complication of CVC but potentially fatal if not promptly managed. The mortality rate is reported up to 93% in a closed claims analysis for hemothorax after CVC[2].

We present a case of massive hemothorax after right internal jugular vein (IJV) catheterization under US guidance and describe proper methods of US guidance and matters that require attention for the prevention of intrathoracic vascular injury causing hemothorax.

CASE PRESENTATION

Chief complaints

A 75-year-old male (ASA class II: weight, 57 kg; height, 160 cm) patient presented massive hemothorax after IJV catheterization under US guidance.

History of present illness

The patient was diagnosed with left renal cell carcinoma on computed tomography (CT) scan performed one month ago.

History of past illness

The patient was on 5 mg of amlodipine (calcium channel blocker) for hypertension for about 10 years.

Personal and family history

The patient had a free personal and family history.

Physical examination

Upon arrival in the operating room, his vital signs were as follows: Blood pressure (BP), 155/92 mmHg; heart rate (HR), 61 beats/min; SpO_2, 99%. There was no problem with the auscultation of both lungs.

Laboratory examinations

Preoperative examination showed that blood test was normal.

Imaging examinations

In the recovery room, portable chest radiography showed increased opacity of the right whole lung (Figure 1). Immediately performed chest CT showed a large amount of hemothorax in the right hemithorax. However, extravasation of contrast media was not observed, and the tip of the catheter was

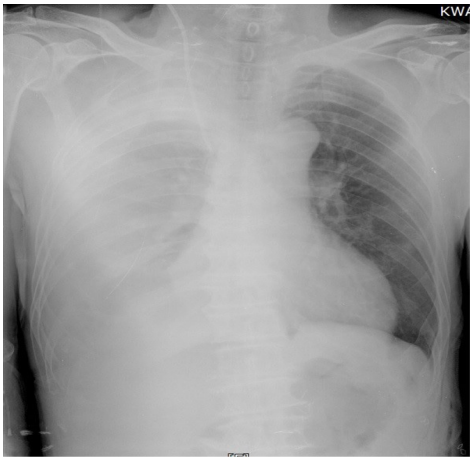

DOI: 10.12998/wjcc.v10.i17.5776 **Copyright** ©The Author(s) 2022.

Figure 1 Chest radiography in the recovery room showing increased opacity of right whole lung.

well-placed in the superior vena cava (SVC), not in the pleural space (Figure 2).

Preoperative management

Preoperative examination showed that the chest radiography, electrocardiogram, and vital signs were normal. A pulmonary function test showed mild obstructive pulmonary disease, and echocardiography showed normal cardiac function. The patient was premedicated with intramuscular glycopyrrolate 0.2 mg.

Intraoperative management

General anesthesia was induced with 40 mg lidocaine, 120 mg propofol, 50 mcg fentanyl, and 50 mg rocuronium. After tracheal intubation, anesthesia was maintained with oxygen-air-sevoflurane-remifentanil. For continuous arterial pressure measurement, a 20G catheter was placed in the left radial artery. CVC was performed on the right IJV for fluid management and central venous pressure measurement.

For CVC, the patient was placed in the Trendelenburg position, and we found that he had a relatively short neck. Right IJV catheterization was performed under US guidance. The L12-3 transducer (Philips Electronics, Tokyo, Japan) of the Philips HD15 US machine was used for confirming the right IJV in the short-axis view using the out-of-plane technique. An 18G introducer needle was inserted at the angle formed by the sternal head and the clavicular head of the sternocleidomastoid muscle under real-time US guidance, and dark nonpulsatile blood was aspirated. The J-tip guidewire was inserted through the needle smoothly and positioned in the IJV in the short-axis view of the US (Figure 3A). A dilator was advanced over the guidewire, and an 8.5 F catheter (Edwards Lifesciences, Edwards Oximetry Central Venous Catheter, triple lumen, 20 cm) was inserted over the guidewire without difficulty. However, no blood was aspirated from all three catheter lumens. The catheter was removed immediately, and the same procedure was performed again with the same technique. Before the second attempt, we examined the IJV and surrounding structures above the clavicle using US but did not detect any problems, such as hematoma. The second attempt was successful in aspiration from all three catheter lumens, and the catheter was fixed at a depth of 15 cm. There were no features of arterial puncture or air aspiration during the two attempts.

After surgical positioning to the right lateral decubitus, the BP suddenly dropped to 75/50 mmHg and SpO_2 88%. It was considered a temporary hemodynamic reaction due to hypovolemia, and 300 mL of crystalloid was rapidly injected through the central venous catheter. Subsequently, the BP and SpO_2 recovered to 110/75 mmHg and 99%. On auscultation of the right lung, there was no apparent reduction in lung sound. At that time, the arterial blood gas analysis (ABGA) results at FiO_2 0.4 were pH 7.396, PCO_2 33.6 mmHg, PO_2 148 mmHg, HCO_3^- 21.0 mEq/L, BE –2.1 mmol/L/L, SaO_2 99%, and Hb 10.6 g/dL. The central venous pressure waveform was adequate, and the patient's vital signs were stable; hence, we proceeded with the surgery.

After the initiation of surgery, the BP dropped to 90/55 mmHg again. The BP remained unstable despite sufficient fluid supply and several intravenous administrations of 0.1 mg of phenylephrine. The BP deteriorated to 80/45 mmHg 1 h later. Norepinephrine infusion was started at 0.03 to 0.06 mcg/kg/min to maintain the BP at 100–110/60–65 mmHg and SpO_2 95%-98% until the end of surgery. The total anesthetic time was 4 h and 15 minutes, and the operation time was 3 h. A total of 3500 mL fluid with 2900 mL of crystalloid and 600 mL of colloid was administered. Estimated blood loss was 500 mL, and total urine output was 400 mL. After extubation, the patient was transferred to the recovery room with norepinephrine infusion.

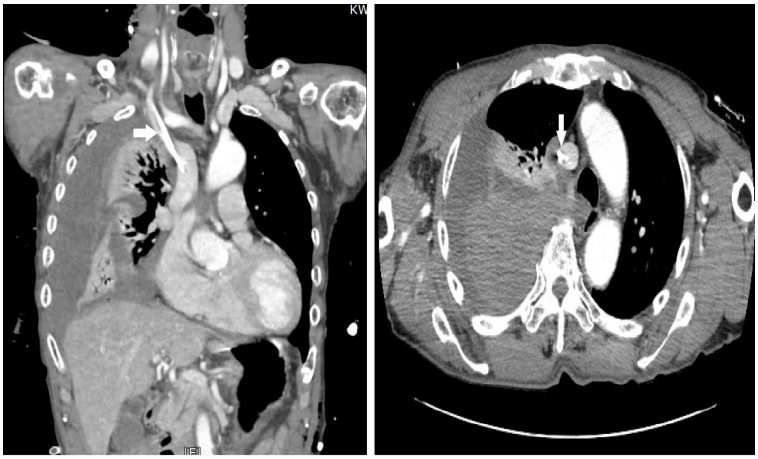

DOI: 10.12998/wjcc.v10.i17.5776 **Copyright** ©The Author(s) 2022.

Figure 2 Postoperative chest computed tomography taken upon arrival in the recovery room. There is large amount of hemothorax in the right hemithorax with no evidence of extravasation of contrast media. The central catheter (arrows) is located within the superior vena cava

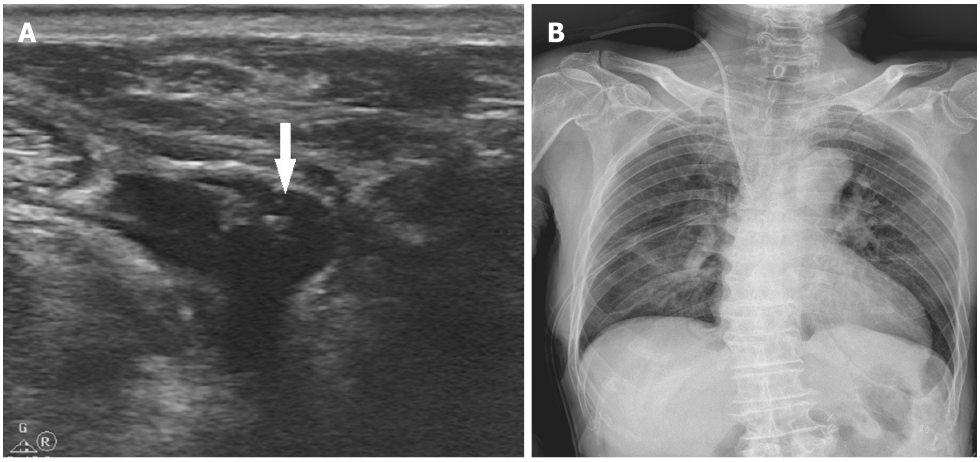

DOI: 10.12998/wjcc.v10.i17.5776 **Copyright** ©The Author(s) 2022.

Figure 3 Computed tomography imaging. A: The guidewire (arrow) placed in the internal jugular vein on a short-axis image with the out-of-plane technique; B: On postoperative day 1, hemothorax is not seen any more. The right central line and a chest tube are inserted state.

Postoperative period

In the recovery room, his vital signs were as follows: BP, 105/70 mmHg; HR, 82 beats/min; SpO_2 89%. He complained of slight difficulty in breathing. On auscultation of the lung, the right lung sound was significantly reduced.

FINAL DIAGNOSIS

CT revealed a massive hemothorax in the right hemithorax.

TREATMENT

The thoracic surgeon inserted a chest tube and drained 1.6 L of dark reddish blood. Following stabilization of vital signs with fluid replacement, he was transferred to the intensive care unit after stopping norepinephrine infusion.

OUTCOME AND FOLLOW-UP

On the next day, the chest radiography showed no more hemothorax findings (Figure 3B). About 50 mL of blood drained through the chest tube on postoperative day (POD) 1, and no blood drained on POD 2. The central venous catheter and chest tube were removed safely on POD 3, and the patient was discharged on POD 7 without any problems.

DISCUSSION

Hemothorax occurs when an intrathoracic artery or vein is perforated by the dilator or catheter during CVC insertion. Anatomically, the neck and the thoracic inlet consist of a complex network of major vessels, and prompt identification of bleeding vessels causing hemothorax can be challenging.

During CVC, the operator predicts the proper entry of the needle and catheter into the central vein by slightly pulling on the syringe and the catheter and checking for aspiration of venous blood. However, aspiration of blood does not always guarantee proper catheter positioning, and some ports of the catheter might fail to function even when the catheter is well-positioned, depending on the location of the catheter tip. When all ports do not function and blood cannot be aspirated, it is reasonable to assume that the catheter is placed outside the central vein[3]. In this patient, blood could not be aspirated from any port of the catheter after the first attempt of CVC, suggestive of inappropriate catheter location.

The first and most important sign of hemothorax is sudden unexpected hypotension. Close observation is required while performing CVC under general anesthesia, as hypotension can be caused by multiple reasons during anesthesia and may result in delayed diagnosis of hemothorax. In this case, the diagnosis of hemothorax was not prompt. One of the several reasons for this diagnostic delay was the timing of hypotension, as the hemodynamic instability did not occur immediately after IJV catheterization. The first hypotension developed when the patient was positioned in the right lateral decubitus position for surgery and briefly treated with fluid replacement. At that time, there was no obvious abnormality in ABGA and chest auscultation enough to consider hemothorax. Accordingly, we proceeded with surgery without the impression of hemothorax because various factors can cause transient hypotension during anesthesia. The second hypotension event developed and sustained after the start of surgery. During the operation, the patient was in the right lateral decubitus position and covered with surgical drapes and laparoscopic instruments, creating difficulties in right lung examination with ultrasound or chest radiography. Fortunately, we maintained hemodynamic stability with fluid and norepinephrine infusion and planned to evaluate the patient after surgery to identify the cause. Early diagnosis of hemothorax requires frequent checking of lung sound and aggressive imaging modalities when hemothorax is suspected. We should have performed portable chest radiography or lung US scan before starting surgery because there was negative blood aspiration from the first inserted catheter. Recent studies show that using bedside lung US enables a faster diagnosis of hemothorax than chest radiography. Pleural effusions that suggest hemothorax on US are seen as hypoechoic areas between the parietal pleura and visceral pleura at the posterior axillary line in the 8th to 11th intercostal space level[4].

During CVC *via* IJV, US guidance can adjust the insertion point and depth to avoid vessel injury to a certain degree, but it is less helpful in preventing intrathoracic vessel injury due to dilator or catheter insertion into the thorax. A study involving 450 patients showed that the incidence of hemothorax was 0% under US guidance compared with 1.7% with the landmark technique [1]. However, there have been reports of hemothorax shortly after catheter insertion despite US guidance with CVC *via* IJV, with reported injured vessels being the right subclavian artery and the right and left brachiocephalic vein (BCV)[5-7]. It is known that when a dilator or catheter with a diameter greater than 7Fr is inserted into an artery, bleeding control through compression is rarely successful. When a hemothorax is caused by arterial damage during CVC, rapid deterioration of vital signs can cause sudden death of the patient, and the hemothorax is only manageable through urgent surgical or interventional repair[5,8,9]. However, most vein injuries that cause hemothorax can be managed with direct compression or venous wall reconstruction by surgical approach, balloon catheter placement, or endovascular repair using endoprosthesis, with some reports even suggesting spontaneous coagulation[6,7]. Kainuma *et al*[6] reported a case of massive hemothorax due to a perforated right BCV during CVC *via* right IJV. Thoracoscopic surgery was performed to remove the intrathoracic hematoma. Videothoracoscopic image revealed that the perforation on the right BCV was no longer bleeding. Wetzel *et al*[7] reported a case of massive hemothorax due to left BCV perforation during left IJV catheterization; a series of contrast venograms revealed a gradual decrease in extravasating contrast media from the BCV to the left pleural cavity. These reports suggest that bleeding from vein injury can be controlled spontaneously, probably by compression from adjacent tissues and positive pressure ventilation during general anesthesia.

In our patient, we could not determine the exact location of the intrathoracic vessel injury, but some of our findings suggest that the hemothorax could result from vein injury. First, although our patient showed a decrease in BP for about 4 h during surgery, this change was not rapid and vital signs were

sustained with fluid replacement and vasopressors. If the hemothorax occurred due to an arterial injury, the patient's vital signs would have shown rapid deterioration and not stabilized during surgery. Second, the blood from thoracentesis was a dark red color, and a postoperative chest CT showed no leakage of contrast media, suggesting spontaneous control of vein injury bleeding. The methods to identify an injured vein when a vein perforation-induced hemothorax is suspected include direct observation through videothoracoscopy, chest CT with contrast leakage, or findings of contrast extension into the pleural cavity during venogram[6,7,10]. In most cases, the site of venous injury leading to immediate hemothorax during CVC through the right IJV is the right BCV[6,11].

Right BCV injury can cause hemothorax through two possible mechanisms. First, despite proper positioning of the guidewire in the right BCV, a strong and deep insertion of the dilator can cause direct injury to the BCV[11]. Therefore, the dilator should not be advanced further than the subcutaneous tissue and should not cross the clavicle. In this case, the patient had a short neck and was positioned in the Trendelenburg position during the CVC procedure, increasing the risk of deeper dilator insertion and direct BCV injury. Another mechanism of injury is that the guidewire from the right IJV can advance into the wrong vessels, such as the right SCV, left BCV, or the azygos vein, leading to injury to the right BCV during dilator insertion[6]. Therefore, it is crucial to ensure proper positioning of the guidewire to prevent dilator-induced vein injury. In the present case, we used US just for directing the introducer needle and identify the guidewire in the IJV. Although the proximal part of the guidewire is located within the IJV, it does not ensure that the distal portion is in the proper position in the thorax. Tampo[12] suggested a three-step procedure for a safe CVC *via* IJV using US guidance. The first and second steps are the real-time guidance of puncture needle insertion into the IJV in the short-axis and the long-axis views to prevent injury to surrounding structures and avoid penetration into the posterior wall of the IJV. The next step is to verify the guidewire in the BCV using a short-axis and coronal image. This image can be obtained using the following technique: After locating the guidewire in the IJV with a short-axis view, slide the probe down towards the supraclavicular fossa following the guidewire. Once the probe reaches the superior margin of the clavicle, it is angled caudally to obtain the images of the BCV and the subclavian vein on one screen. Fortunately, US facilitates successful visualization of the BCV in 99% of patients, and no sign of guidewire in the BCV suggests malposition of the guidewire in the intrathoracic region[13]. This last view-imaging BCV would help detect guidewire malposition in the thorax. Other options include confirming guidewire or catheter placement with transesophageal echocardiogram or transthoracic echocardiogram, if available[14]. Weekes *et al*[15] revealed that bedside transthoracic echocardiography using saline flush could predict optimal catheter tip position after CVC.

CONCLUSION

During IJV catheterization, the possibility of hemothorax persists even in US-guided procedures, especially in the event of negative blood aspiration from the inserted catheter. Proper US use is important in real-time guidance and requires adequate knowledge of technique. In addition to guidewire identification in the IJV, confirmation of the guidewire within the BCV using US is recommended to avoid guidewire malposition, one of the reasons for dilator-induced hemothorax. The physicians should also be aware that hemothorax caused by intrathoracic venous injury cannot be associated with immediate hemodynamic instability. Hypotension induced by venous bleeding can develop after a time lag and be managed with fluid and vasopressor therapy. During anesthesia and surgery, many factors causing hemodynamic compromise can obscure the prompt diagnosis of hemothorax. Therefore, clinical suspicion and timely diagnostic evaluations are necessary for early diagnosis and treatment.

FOOTNOTES

Author contributions: Kang H and Choi JY cared for the patient, conceived, and designed the case report, and wrote the manuscript; Wan JU, Cho SY and Suk EH edited the manuscript; Cho SY and Suk EH supervised the work; all authors read and approved the final manuscript.

Informed consent statement: Informed written consent was obtained from the patient for publication of this report and any accompanying images.

Conflict-of-interest statement: The authors declare that they have no conflicts of interest.

CARE Checklist (2016) statement: The authors have read the CARE Checklist (2016), and the manuscript was prepared and revised according to the CARE Checklist (2016).

Open-Access: This article is an open-access article that was selected by an in-house editor and fully peer-reviewed by external reviewers. It is distributed in accordance with the Creative Commons Attribution NonCommercial (CC BY-

NC 4.0) license, which permits others to distribute, remix, adapt, build upon this work non-commercially, and license their derivative works on different terms, provided the original work is properly cited and the use is non-commercial. See: https://creativecommons.org/Licenses/by-nc/4.0/

Country/Territory of origin: South Korea

ORCID number: Hyun Kang 0000-0003-1625-1245; Soo Young Cho 0000-0002-1709-7537; Eun Ha Suk 0000-0003-0644-3411; Wan Ju 0000-0002-6700-2436; Joon Yong Choi 0000-0003-2576-2493.

S-Editor: Xing YX
L-Editor: A
P-Editor: Xing YX

REFERENCES

1 **Karakitsos D**, Labropoulos N, De Groot E, Patrianakos AP, Kouraklis G, Poularas J, Samonis G, Tsoutsos DA, Konstadoulakis MM, Karabinis A. Real-time ultrasound-guided catheterisation of the internal jugular vein: a prospective comparison with the landmark technique in critical care patients. *Crit Care* 2006; **10**: R162 [PMID: 17112371 DOI: 10.1186/cc5101]
2 **Domino KB**, Bowdle TA, Posner KL, Spitellie PH, Lee LA, Cheney FW. Injuries and liability related to central vascular catheters: a closed claims analysis. *Anesthesiology* 2004; **100**: 1411-1418 [PMID: 15166560 DOI: 10.1097/00000542-200406000-00013]
3 **Ki S**, Kim M-h, Lee W, Cho H. Tension hydrothorax induced by malposition of central venous catheter: A case report. Anesth Pain Med. 2017;12(2):151-4 DOI:10.17085/apm.2017.12.2.151 [DOI: 10.17085/apm.2017.12.2.151]
4 **Kim YI**, Ryu JH, Min MK, Park MR, Park SC, Yeom SR, Han SK, Park SW, Lee SH. Usefulness of ultrasonography for the evaluation of catheter misplacement and complications after central venous catheterization. *Clin Exp Emerg Med* 2018; **5**: 71-75 [PMID: 29973031 DOI: 10.15441/ceem.16.189]
5 **Kim JH**, Kim YJ, Jang JS, Hwang SM. [Endovascular repair of subclavian artery injury secondary to internal jugular vein catheterization: case report]. *Braz J Anesthesiol* 2019; **69**: 413-416 [PMID: 31353065 DOI: 10.1016/j.bjan]
6 **Kainuma A**, Oshima K, Ota C, Okubo Y, Fukunaga N, Suh SH. Brachiocephalic Vein Perforation During Cannulation of Internal Jugular Vein: A Case Report. *A A Case Rep* 2017; **9**: 258-261 [PMID: 28622147 DOI: 10.1213/XAA.0000000000000585]
7 **Wetzel LR**, Patel PR, Pesa NL. Central Venous Catheter Placement in the Left Internal Jugular Vein Complicated by Perforation of the Left Brachiocephalic Vein and Massive Hemothorax: A Case Report. *A A Case Rep* 2017; **9**: 16-19 [PMID: 28410259 DOI: 10.1213/XAA.0000000000000511]
8 **Tam JK**, Atasha A, Tan AK. Video-assisted thoracic surgery repair of subclavian artery injury following central venous catheterization: a new approach. *Interact Cardiovasc Thorac Surg* 2013; **17**: 13-15 [PMID: 23518293 DOI: 10.1093/icvts/ivt109]
9 **Lee DJ**, Yun JC, Choi HR, Im UJ, Woo SH. Subclavian artery perforation and hemothorax after right internal jugular vein catheterization. *Korean J Anesthesiol* 2013; **64**: 558-559 [PMID: 23814663 DOI: 10.4097/kjae.2013.64.6.558]
10 **Park JH**, Song J, Oh PW. Massive hemothorax after central venous catheter insertion in a patient with multiple trauma. *J Dent Anesth Pain Med* 2021; **21**: 81-85 [PMID: 33585687 DOI: 10.17245/jdapm.2021.21.1.81]
11 **Innami Y**, Oyaizu T, Ouchi T, Umemura N, Koitabashi T. Life-threatening hemothorax resulting from right brachiocephalic vein perforation during right internal jugular vein catheterization. *J Anesth* 2009; **23**: 135-138 [PMID: 19234840 DOI: 10.1007/s00540-008-0696-1]
12 **Tampo A**. Three-step procedure for safe internal jugular vein catheterization under ultrasound guidance. *J Med Ultrason (2001)* 2018; **45**: 671-673 [PMID: 29948474 DOI: 10.1007/s10396-018-0885-y]
13 **Bowdle A**, Jelacic S, Togashi K, Ferreira R. Ultrasound Identification of the Guidewire in the Brachiocephalic Vein for the Prevention of Inadvertent Arterial Catheterization During Internal Jugular Central Venous Catheter Placement. *Anesth Analg* 2016; **123**: 896-900 [PMID: 27509224 DOI: 10.1213/ANE.0000000000001446]
14 **Smit JM**, Raadsen R, Blans MJ, Petjak M, Van de Ven PM, Tuinman PR. Bedside ultrasound to detect central venous catheter misplacement and associated iatrogenic complications: a systematic review and meta-analysis. *Crit Care* 2018; **22**: 65 [PMID: 29534732 DOI: 10.1186/s13054-018-1989-x]
15 **Weekes AJ**, Johnson DA, Keller SM, Efune B, Carey C, Rozario NL, Norton HJ. Central vascular catheter placement evaluation using saline flush and bedside echocardiography. *Acad Emerg Med* 2014; **21**: 65-72 [PMID: 24552526 DOI: 10.1111/acem.12283]

World Journal of Clinical Cases

Submit a Manuscript: https://www.f6publishing.com

World J Clin Cases 2022 June 16; 10(17): 5783-5788

DOI: 10.12998/wjcc.v10.i17.5783

ISSN 2307-8960 (online)

CASE REPORT

Unilateral adrenal tuberculosis whose computed tomography imaging characteristics mimic a malignant tumor: A case report

Hui Liu, Tian-Jiao Tang, Zhen-Mei An, Ye-Rong Yu

Specialty type: Endocrinology and metabolism

Provenance and peer review: Unsolicited article; Externally peer reviewed.

Peer-review model: Single blind

Peer-review report's scientific quality classification
Grade A (Excellent): 0
Grade B (Very good): B
Grade C (Good): 0
Grade D (Fair): D
Grade E (Poor): 0

P-Reviewer: Huei TJ, Malaysia; Piltcher-da-Silva R, Brazil

Received: November 13, 2021
Peer-review started: November 13, 2021
First decision: December 10, 2021
Revised: December 18, 2021
Accepted: April 4, 2022
Article in press: April 4, 2022
Published online: June 16, 2022

Hui Liu, Department of General Practice, West China Hospital of Sichuan University, Chengdu 610041, Sichuan, China

Tian-Jiao Tang, The Center of Gerontology and Geriatrics, West China Hospital of Sichuan University, Chengdu 610041, Sichuan Province, China

Zhen-Mei An, Ye-Rong Yu, Department of Endocrinology and Metabolism, West China Hospital of Sichuan University, Chengdu 610041, Sichuan Province, China

Corresponding author: Ye-Rong Yu, MD, Chief Doctor, Professor, Endocrinology and Metabolism, West China Hospital of Sichuan University, No. 37 Guoxue Alley, Wuhou District, Chengdu 610041, Sichuan Province, China. yerongyu@scu.edu.cn

Abstract

BACKGROUND

Adrenal tuberculosis usually presents with bilateral involvement. It has special characteristics in computed tomography (CT) images, such as small size, low attenuation in the center, and peripheral rim enhancement, which differ from those of primary tumors.

CASE SUMMARY

A 42-year-old female presented to the hospital with low back pain. She had been diagnosed with hypertension as well as pulmonary and cerebral tuberculosis but denied having any fever, fatigue, anorexia, night sweats, cough, or weight loss. Abdominal CT revealed an irregular 6.0 cm × 4.5 cm mass with uneven density in the right adrenal gland, while the left adrenal gland was normal. No abnormalities were observed in plasma total cortisol (8 am), adrenocorticotropic hormone, aldosterone/renin ratio, blood catecholamines, or urine catecholamines. A fine-needle aspiration biopsy of the right adrenal gland provided evidence of tuberculosis. After three years of anti-tuberculosis treatments, the large mass in the right adrenal gland was reduced to a slight enlargement.

CONCLUSION

This is a case of unilateral adrenal tuberculosis with CT imaging characteristics mimicking those of a malignant tumor. Extended anti-tuberculosis therapy is recommended in such cases.

Key Words: Adrenal incidentaloma; Adrenal tuberculosis; Fine-needle aspiration biopsy;

Anti-tuberculosis therapy; Case report

©The Author(s) 2022. Published by Baishideng Publishing Group Inc. All rights reserved.

Core Tip: In this report, we report a female patient with unilateral adrenal tuberculosis whose CT image characteristics mimic those of a malignant tumor. After a long-term anti-tuberculosis regimen, the large mass in the right adrenal gland was reduced.

Citation: Liu H, Tang TJ, An ZM, Yu YR. Unilateral adrenal tuberculosis whose computed tomography imaging characteristics mimic a malignant tumor: A case report. *World J Clin Cases* 2022; 10(17): 5783-5788
URL: https://www.wjgnet.com/2307-8960/full/v10/i17/5783.htm
DOI: https://dx.doi.org/10.12998/wjcc.v10.i17.5783

INTRODUCTION

Tuberculosis (TB) is known to present with varied clinical features, but involvement of the adrenal glands in TB is rare[1]. Isolated adrenal TB accounts for under 2% of adrenal incidentalomas[2], while 75%-100% of patients with adrenal TB have bilateral involvement[3-5]. As a result, unilateral adrenal TB is considered a rare clinical entity. The computed tomography (CT) imaging characteristics of adrenal TB are significantly different from those of primary tumors, such as small size, low attenuation in the center, and peripheral rim enhancement[3,6,7]. Herein, we report an unusual case of unilateral adrenal TB whose imaging characteristics were extremely atypical and suggested a high likelihood of a malignant tumor. Fine-needle aspiration biopsy (FNAB) was used to confirm TB, and prolonged anti-TB treatment was given to stabilize her condition.

CASE PRESENTATION

Chief complaints

A 42-year-old female was admitted to our department after presenting with a half-year history of osphyalgia.

History of present illness

A 42-year-old female had low back pain for a half year, which was exaggerated when taking a deep breath or lying flat and relieved when standing. She denied frequent micturition, painful urination, fever, hematuria, or pyuria.

History of past illness

The patient had a remote history of hypertension. She had been diagnosed with pulmonary and cerebral TB four months before presentation, and she had started a regimen of anti-TB drugs (isoniazid 0.3 g QD, rifampicin 0.45 g QD, ethambutol 0.75 g QD, and ofloxacin 0.5 g QD) upon diagnosis.

Personal and family history

Her personal and family history were insignificant.

Physical examination

Physical examination showed nothing special despite percussive pain in the right kidney area.

Laboratory examinations

Laboratory tests yielded the following results: plasma total cortisol (8 am), 594.6 nmol/L (reference, 147.3-609.3 nmol/L); adrenocorticotropic hormone, 48.30 ng/L (reference, 5.0-78 ng/L); and aldosterone/renin ratio, 16.92 ng/dL per ng/mL/h. No abnormalities were observed in the blood and urine catecholamines. Routine blood tests, routine urine tests, and biochemical tests were roughly in the normal range. CT-guided Fine needle aspiration biopsy (FNAB) of the right adrenal gland was performed, and pathological examination detected granulomas and necrosis (Figure 1A and B).

Imaging examinations

Four months prior to presentation, the patient had undergone an abdominal CT scan, which revealed a

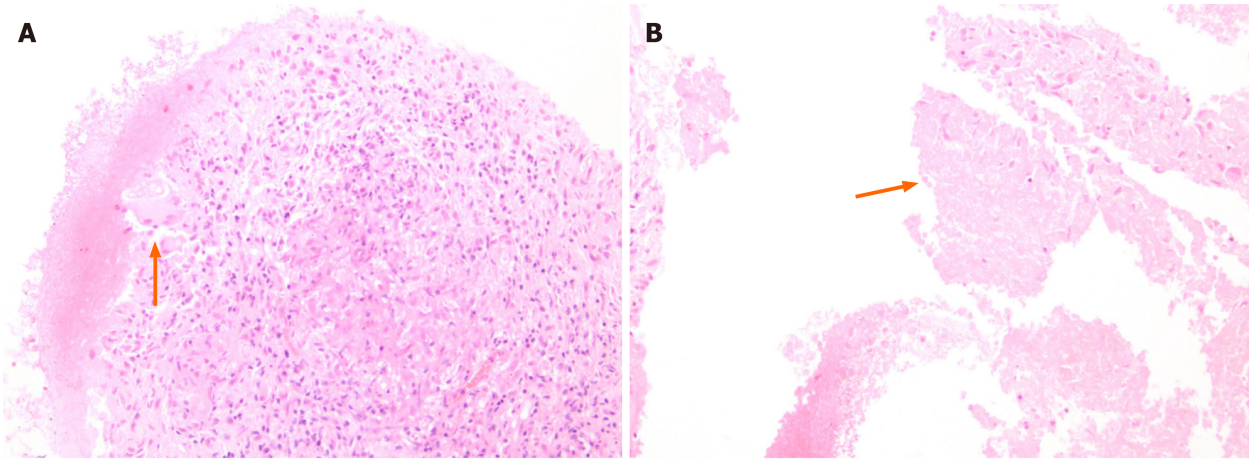

DOI: 10.12998/wjcc.v10.i17.5783 **Copyright** ©The Author(s) 2022.

Figure 1 Microscopic examination of fine needle aspiration biopsy of the right adrenal gland showed Langerhans cells. A: Epithelioid cells; B: Necrosis; which were suggestive of tuberculosis infection.

1.5 cm isointense mass in the right adrenal gland (Figure 2A). On presentation to our department, she underwent another abdominal CT scan, which revealed a 6.0 cm × 4.5 cm irregular mass with uneven density in the right adrenal gland, while the left adrenal gland was normal (Figure 2B).

FINAL DIAGNOSIS

Unilateral adrenal tuberculosis.

TREATMENT

Treatment with 4 anti-TB drugs was continued.

OUTCOME AND FOLLOW-UP

The patient's low back pain was relieved, and abdominal CT (Figure 2C) demonstrated a significant reduction of the mass in the right adrenal gland (2.7 cm × 2.4 cm) after 15 mo of anti-TB therapy. Three years later, abdominal CT (Figure 2D) showed a slight enlargement of the right adrenal gland.

DISCUSSION

Extrapulmonary TB constitutes about 15%-20% of all TB patients[8]. The most frequent sites of extrapulmonary TB include the lymph nodes (19%), pleural cavity (7%), gastrointestinal tract (4%), bone (6%), central nervous system (3%), and genitourinary system (1%)[9]. Of the 370 reports of extrapulmonary TB in a systematic review spanning 10 years[1], only one case was shown to involve the adrenal gland, which demonstrated adrenal TB as a rare clinical entity. Bilateral involvement usually occurs because of hematogenous and lymph spread from the site of the primary mycobacterial infection to both adrenal glands, which are equally susceptible[10]. In our case, adrenal TB (lesions of 1.5 cm to 5 cm) was aggravated while the anti-TB regimen was continued. It is necessary to distinguish adrenal masses from adrenal tumors. Adrenal incidentalomas, adenomas, metastases, adrenocortical carcinomas, myelolipomas, and pheochromocytomas accounted for 41%, 19%, 10%, 9%, and 8%, respectively. The etiologies of these partly depend on the size, such that larger tumors are more likely to be malignant. Adrenal carcinomas and metastases comprise 25% and 18% of lesions and are larger than 6 cm, while adenomas account for only 18%[11]. For tumors smaller than 4 cm, adrenal carcinomas comprise 2% and adenomas comprise 65%[11]. Untreated TB lesions were smaller than primary tumors (2.8 cm ± 1.3 cm *vs* 3.5 cm ± 2.4 cm)[6], while the diameters of benign, malignant pheochromocytoma and adrenocortical carcinoma were 5.7 cm ± 2.3 cm, 8.3 cm ± 4.1 cm[12] and 11 cm ± 4 cm[13], respectively. It is difficult to provide evidence with regard to TB based on size (6.0 cm × 4.5 cm) in this case. The CT value, attenuation measurement, and reduced central area (7 ± 4 HU) compared to the peripheral area (32 ± 14 HU) were

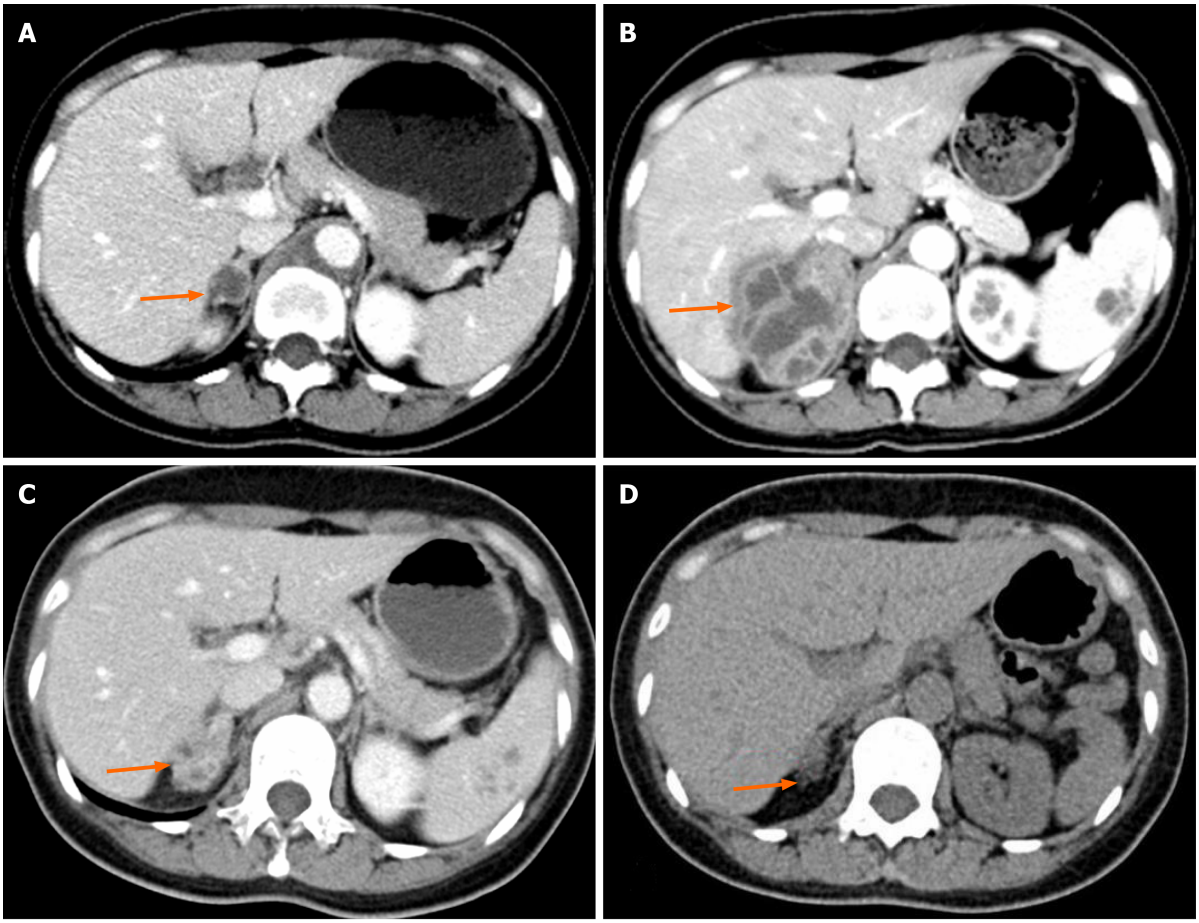

DOI: 10.12998/wjcc.v10.i17.5783 **Copyright** ©The Author(s) 2022.

Figure 2 These were contrast-enhanced axial computed tomography images of the abdomen. A: Showed an isointense mass of 1.5 cm in the right adrenal gland; B: Showed an irregular mass of 6.0 cm × 4.5 cm with uneven density (20-30 HU in the central and 80-90 HU in the peripheral) in the right adrenal gland, while the left one was normal; C: Showed that the mass became smaller (2.7 cm × 2.4 cm) after anti-TB therapy for a total of 15 mo; D: Showed a slight enlargement of the right adrenal gland after about three years' anti-TB therapy.

observed between unenhanced and contrast-enhanced scans in adrenal TB[3]. This characteristic of central necrosis surrounded by fibrous and granulomatous inflammatory tissue is much less common in primary adrenal tumors[6], owing to sufficient blood supply in the central area. Pheochromocytoma always has a high enhancement of > 110 HU in the arterial phase[14], while adrenocortical carcinoma is less likely to show an enhancement of >100 HU. In the present case, evidence from images could not rule out a malignant tumor in the adrenal gland. In addition, calcification preferentially occurred in the later stages of adrenal TB than in adrenal tumors (59% *vs* 8%), which helped with a proper diagnosis[6].

In addition to the ineffectiveness of FNAB in distinguishing adrenal adenoma from adenocarcinoma [11], it is considered advantageous due to its ease, cost-effectiveness, reduced time consumption, low complication rates, and high accuracy[15-17]. It is often used for suspected nonfunctional and nonneoplastic adrenal gland lesions, but not employed for pheochromocytomas[11,17] due to the risk of hemodynamic instability. In the present case, blood pressure was well controlled and had no abnormalities in blood and urine catecholamines, indicating a lower possibility of pheochromocytoma. Therefore, FNAB was performed to obtain histological evidence, which subsequently provides clear evidence regarding targeted therapy.

Patients with adrenal TB are usually treated with standard quadruple antitubercular treatment (such as isoniazid, rifampicin, pyrazinamide, and ethambutol)[18-20] for nearly 12 mo or longer. Adverse reactions to anti-TB drugs and their interactions with corticosteroids that are administered for replacement therapy remain challenging[21,22]. Firstly, rifampicin increases cortisol catabolism while isoniazid produces increased levels of cortisol *via* an opposite effect on the enzyme activity 6-Bhydroxylase; secondly, hepatitis, induced by isoniazid and worsened by rifampicin, leads to failure of 11-B-oxo-reductase, which converts cortisone to cortisol; and finally, tuberculous Addison's disease might require increased amounts of hydrocortisone due to rifampicin administration[23]. Up to 70% of patients with active TB have subclinical adrenal insufficiency[24]. Anti-TB treatment might cause adrenal crisis[18], and patients should be closely monitored when starting this treatment. Most of the cases demonstrated a good response to anti-TB treatment. Early diagnosis and no delay in treatment initiation contributed to minimizing the high mortality rate[22,25]. Addison's disease usually occurs

when more than 90% of adrenal tissue has been destroyed[26]. Only a few patients with tuberculous Addison's disease showed recovery of adrenal function[27].

CONCLUSION

Unilateral adrenal tuberculous infection, although rare, should be considered in patients with unilateral adrenal mass but without Cushing syndrome, primary aldosteronism, or pheochromocytoma. FNAB assists in diagnosing TB, and early initiation and longer duration of anti-TB therapy are crucial to treating patients with unilateral adrenal tuberculous infection.

FOOTNOTES

Author contributions: Yu YR and An ZM contributed to the conceptualization; Liu H and Tang TJ collected the information; Liu H wrote the original draft; Yu YR reviewed and edited the manuscript; all authors issued final approval for the version to be submitted.

Informed consent statement: Informed written consent was obtained from the patient for publication of this report and any accompanying images.

Conflict-of-interest statement: The authors declare that they have no conflict of interest.

CARE Checklist (2016) statement: The authors have read the CARE Checklist (2016), and the manuscript was prepared and revised according to the CARE Checklist (2016).

Open-Access: This article is an open-access article that was selected by an in-house editor and fully peer-reviewed by external reviewers. It is distributed in accordance with the Creative Commons Attribution NonCommercial (CC BY-NC 4.0) license, which permits others to distribute, remix, adapt, build upon this work non-commercially, and license their derivative works on different terms, provided the original work is properly cited and the use is non-commercial. See: https://creativecommons.org/Licenses/by-nc/4.0/

Country/Territory of origin: China

ORCID number: Hui Liu 0000-0002-9352-3358; Tian-Jiao Tang 0000-0002-4817-2907; Zhen-Mei An 0000-0003-1435-8209; Ye-Rong Yu 0000-0003-0103-0087.

S-Editor: Xing YX
L-Editor: A
P-Editor: Xing YX

REFERENCES

1 **Edlin GP**. Active tuberculosis unrecognised until necropsy. *Lancet* 1978; **1**: 650-652 [PMID: 76179 DOI: 10.1016/s0140-6736(78)91149-2]
2 **Lam KY**, Lo CY. A critical examination of adrenal tuberculosis and a 28-year autopsy experience of active tuberculosis. *Clin Endocrinol (Oxf)* 2001; **54**: 633-639 [PMID: 11380494 DOI: 10.1046/j.1365-2265.2001.01266.x]
3 **Ma ES**, Yang ZG, Li Y, Guo YK, Deng YP, Zhang XC. Tuberculous Addison's disease: morphological and quantitative evaluation with multidetector-row CT. *Eur J Radiol* 2007; **62**: 352-358 [PMID: 17466476 DOI: 10.1016/j.ejrad.2006.12.012]
4 **Gupta P**, Bhalla A, Sharma R. Bilateral adrenal lesions. *J Med Imaging Radiat Oncol* 2012; **56**: 636-645 [PMID: 23210583 DOI: 10.1111/j.1754-9485.2012.02435.x]
5 **Guo YK**, Yang ZG, Li Y, Ma ES, Deng YP, Min PQ, Yin LL, Hu J, Zhang XC, Chen TW. Addison's disease due to adrenal tuberculosis: contrast-enhanced CT features and clinical duration correlation. *Eur J Radiol* 2007; **62**: 126-131 [PMID: 17182208 DOI: 10.1016/j.ejrad.2006.11.025]
6 **Yang ZG**, Guo YK, Li Y, Min PQ, Yu JQ, Ma ES. Differentiation between tuberculosis and primary tumors in the adrenal gland: evaluation with contrast-enhanced CT. *Eur Radiol* 2006; **16**: 2031-2036 [PMID: 16435135 DOI: 10.1007/s00330-005-0096-y]
7 **Alshahrani MA**, Bin Saeedan M, Alkhunaizan T, Aljohani IM, Azzumeea FM. Bilateral adrenal abnormalities: imaging review of different entities. *Abdom Radiol (NY)* 2019; **44**: 154-179 [PMID: 29938331 DOI: 10.1007/s00261-018-1670-5]
8 **Sharma SK**, Mohan A, Kohli M. Extrapulmonary tuberculosis. *Expert Rev Respir Med* 2021; **15**: 931-948 [PMID: 33966561 DOI: 10.1080/17476348.2021.1927718]
9 **Houston A**, Macallan DC. Extrapulmonary tuberculosis. *Medicine* 2014; **42**: 18-22
10 **Kissane**, John M. Anderson's Pathology. 1985
11 **Aron D**, Terzolo M, Cawood TJ. Adrenal incidentalomas. *Best Pract Res Clin Endocrinol Metab* 2012; **26**: 69-82 [PMID:

22305453 DOI: 10.1016/j.beem.2011.06.012]
12 **Khadilkar K**, Sarathi V, Kasaliwal R, Pandit R, Goroshi M, Malhotra G, Dalvi A, Bakshi G, Bhansali A, Rajput R, Shivane V, Lila A, Bandgar T, Shah NS. Predictors of malignancy in patients with pheochromocytomas/paragangliomas: Asian Indian experience. *Endocr Connect* 2016; **5**: 89-97 [PMID: 27852633 DOI: 10.1530/EC-16-0086]
13 **Zhang HM**, Perrier ND, Grubbs EG, Sircar K, Ye ZX, Lee JE, Ng CS. CT features and quantification of the characteristics of adrenocortical carcinomas on unenhanced and contrast-enhanced studies. *Clin Radiol* 2012; **67**: 38-46 [PMID: 21783181 DOI: 10.1016/j.crad.2011.03.023]
14 **Northcutt BG**, Raman SP, Long C, Oshmyansky AR, Siegelman SS, Fishman EK, Johnson PT. MDCT of adrenal masses: Can dual-phase enhancement patterns be used to differentiate adenoma and pheochromocytoma? *AJR Am J Roentgenol* 2013; **201**: 834-839 [PMID: 24059372 DOI: 10.2214/AJR.12.9753]
15 **Patel S**, Jinjuvadia R, Devara A, Naylor PH, Anees M, Jinjuvadia K, Al-Haddad M. Performance characteristics of EUS-FNA biopsy for adrenal lesions: A meta-analysis. *Endosc Ultrasound* 2019; **8**: 180-187 [PMID: 30880721 DOI: 10.4103/eus.eus_42_18]
16 **Kerimaa P**, Marttila A, Hyvönen P, Ojala R, Lappi-Blanco E, Tervonen O, Blanco Sequeiros R. MRI-guided biopsy and fine needle aspiration biopsy (FNAB) in the diagnosis of musculoskeletal lesions. *Eur J Radiol* 2013; **82**: 2328-2333 [PMID: 24099641 DOI: 10.1016/j.ejrad.2013.09.005]
17 **Patil R**, Ona MA, Papafragkakis C, Duddempudi S, Anand S, Jamil LH. Endoscopic ultrasound-guided fine-needle aspiration in the diagnosis of adrenal lesions. *Ann Gastroenterol* 2016; **29**: 307-311 [PMID: 27366030 DOI: 10.20524/aog.2016.0047]
18 **Denny N**, Raghunath S, Bhatia P, Abdelaziz M. Rifampicin-induced adrenal crisis in a patient with tuberculosis: a therapeutic challenge. *BMJ Case Rep* 2016; **2016** [PMID: 27899384 DOI: 10.1136/bcr-2016-216302]
19 **Shrestha B**, Omran A, Rong P, Wang W. Successfully treated unusual case of primary adrenal and spinal tuberculosis with three years follow up. *Pan Afr Med J* 2014; **17**: 108 [PMID: 25018843 DOI: 10.11604/pamj.2014.17.108.2575]
20 **Manso MC**, Rodeia SC, Rodrigues S, Domingos R. Synchronous presentation of two rare forms of extrapulmonary tuberculosis. *BMJ Case Rep* 2016; **2016**: 10.1136/bcr-2015 [PMID: 27090536 DOI: 10.1136/bcr-2015-212917]
21 **Thijs E**, Wierckx K, Vandecasteele S, Van den Bruel A. Adrenal insufficiency, be aware of drug interactions! *Endocrinol Diabetes Metab Case Rep* 2019; **2019** [PMID: 31581123 DOI: 10.1530/EDM-19-0062]
22 **Shah M**, Reed C. Complications of tuberculosis. *Curr Opin Infect Dis* 2014; **27**: 403-410 [PMID: 25028786 DOI: 10.1097/QCO.0000000000000090]
23 **Kusuki K**, Watanabe S, Mizuno Y. Tuberculous Addison's disease with increased hydrocortisone requirements due to administration of rifampicin. *BMJ Case Rep* 2019; **12** [PMID: 30872343 DOI: 10.1136/bcr-2018-228293]
24 **Sarin BC**, Sibia K, Kukreja S. Study of adrenal function in patients with tuberculosis. *Indian J Tuberc* 2018; **65**: 241-245 [PMID: 29933867 DOI: 10.1016/j.ijtb.2017.08.033]
25 **Zhao N**, Gao Y, Ni C, Zhang D, Zhao X, Li Y, Sun B. An autopsy case of unexpected death due to Addison's disease caused by adrenal tuberculosis. *Eur J Med Res* 2021; **26**: 137 [PMID: 34863306 DOI: 10.1186/s40001-021-00611-w]
26 **Alevritis EM**, Sarubbi FA, Jordan RM, Peiris AN. Infectious causes of adrenal insufficiency. *South Med J* 2003; **96**: 888-890 [PMID: 14513986 DOI: 10.1097/01.SMJ.0000073269.49575.DF]
27 **Penrice J**, Nussey SS. Recovery of adrenocortical function following treatment of tuberculous Addison's disease. *Postgrad Med J* 1992; **68**: 204-205 [PMID: 1589379 DOI: 10.1136/pgmj.68.797.204]

World Journal of Clinical Cases

Submit a Manuscript: https://www.f6publishing.com

World J Clin Cases 2022 June 16; 10(17): 5789-5797

DOI: 10.12998/wjcc.v10.i17.5789

ISSN 2307-8960 (online)

CASE REPORT

Modified membrane fixation technique in a severe continuous horizontal bone defect: A case report

Lin-Hong Wang, Yan Ruan, Wen-Yan Zhao, Jian-Ping Chen, Fan Yang

Specialty type: Dentistry, oral surgery and medicine

Provenance and peer review: Unsolicited article; Externally peer reviewed.

Peer-review model: Single blind

Peer-review report's scientific quality classification

Grade A (Excellent): 0
Grade B (Very good): B, B
Grade C (Good): 0
Grade D (Fair): 0
Grade E (Poor): E

P-Reviewer: Agrawal AA, India; Oji C, Nigeria; Rakhshan V, Iran

Received: November 16, 2021
Peer-review started: November 16, 2021
First decision: February 14, 2022
Revised: February 26, 2022
Accepted: April 3, 2022
Article in press: April 3, 2022
Published online: June 16, 2022

Lin-Hong Wang, Jian-Ping Chen, Fan Yang, Center for Plastic and Reconstructive Surgery, Department of Stomatology, Zhejiang Provincial People's Hospital (Affiliated People's Hospital, Hangzhou Medical College), Hangzhou 310014, Zhejiang Province, China

Yan Ruan, Graduate Department, Bengbu Medical College, Bengbu 233030, Anhui Province, China

Wen-Yan Zhao, Department of Stomatology, The First People's Hospital of Hangzhou Lin'an District, Hangzhou 311399, Zhejiang Province, China

Corresponding author: Fan Yang, DDS, PhD, Professor, Center for Plastic and Reconstructive Surgery, Department of Stomatology, Zhejiang Provincial People's Hospital (Affiliated People's Hospital, Hangzhou Medical College), No. 158 Shangtang Road, Hangzhou 310014, Zhejiang Province, China. yangfan@hmc.edu.cn

Abstract

BACKGROUND

Continuous severe horizontal bone defect is common in the aesthetic maxillary anterior area, and presents a major challenge in implant dentistry and requires predictable bone augmentation to increase the width of the alveolar bone.

CASE SUMMARY

A 24-year-old man, with a history of well-controlled IgA nephropathy, presented to the Dentistry Department of our hospital complaining of missing his right maxillary anterior teeth 1 mo ago. Severe horizontal alveolar bone defects at sites of teeth 12, 13 and 14 were diagnosed. A modified guided bone regeneration surgical approach stabilizing the absorbable collagen membrane and particulate graft materials by periosteal diagonal mattress suture (PDMS) combined with four corner pins was used for this severe continuous horizontal bone defect. The outcome revealed that the newly formed alveolar ridge dimension increased from 0.72 mm to 11.55 mm horizontally 10 mo postoperatively, with no adverse events. The implant surgery was successfully performed.

CONCLUSION

This case highlights that PDMS combined with four corner pins is feasible to maintain the space and stabilize the graft and membranes in severe continuous horizontal bone defect.

Key Words: Horizontal bone defect; Guided bone regeneration; Periosteal diagonal

mattress suture; Pin; Case report

©The Author(s) 2022. Published by Baishideng Publishing Group Inc. All rights reserved.

Core Tip: We report a 24-year-old man with severe horizontal alveolar bone defects in the maxillary anterior teeth area. A modified guided bone regeneration surgical approach stabilizing the absorbable collagen membrane and particulate graft materials by periosteal diagonal mattress sutures (PDMS) combined with four corner pins was used for this severe continuous horizontal bone defect. The outcome revealed that the newly formed alveolar ridge dimension increased approximately 10 mm horizontally at 10 mo postoperatively. The technique PDMS combined with four corner pins may provide an alternative to traditional methods to obtain better bone regeneration.

Citation: Wang LH, Ruan Y, Zhao WY, Chen JP, Yang F. Modified membrane fixation technique in a severe continuous horizontal bone defect: A case report. *World J Clin Cases* 2022; 10(17): 5789-5797
URL: https://www.wjgnet.com/2307-8960/full/v10/i17/5789.htm
DOI: https://dx.doi.org/10.12998/wjcc.v10.i17.5789

INTRODUCTION

Horizontal bone defect is common in the aesthetic maxillary anterior area, and presents a major challenge in implant dentistry and often requires bone augmentation to increase the width of the alveolar bone[1,2]. Various horizontal ridge reconstruction methods have been developed[3], including guided bone regeneration (GBR), onlay bone block graft, ridge splitting and expansion, distraction osteogenesis, and sandwich osteoplasty[4]. According to the decision tree of horizontal bone augmentation[5], when the ridge width is less than 3.5 mm, onlay bone grafting with the use of an autogenic or allogenic block is the first choice for horizontal bone augmentation[6]. However, this treatment also has some complications, such as extended surgical time, cost, discomfort to patients, nerve damage or morbidity, and unavoidable bone resorption[7]. An average resorption rate is 35%-51%, and 10 years of follow-up showed the range was between 20% and 92%[8].

GBR for alveolar bone reconstruction is effective and less invasive than block grafting. Advances in biomaterials and clinical techniques have led to the incorporation of GBR as a potential alternative in these challenging cases[9]. GBR with particulate graft materials and absorbable collagen membranes is an effective technique for horizontal alveolar ridge augmentation, and additional techniques like membrane fixation and decortication may be beneficial[10]. However, GBR for large horizontal and vertical ridge defects is still a technically sensitive procedure. External pressure from the flap or the occlusal forces may displace the graft and membrane laterally and apically, resulting in deficient bone. The "PASS" principle of GBR requires the use of absorbable or nonabsorbable membranes for the creation of a stable space for the particulate graft above the bone defect and under the periosteum[11].

Membrane fixation may have beneficial implications for GBR[12,13]. Several membrane fixation techniques have been reported despite them having several clinical challenges[13-18]. Application of titanium minipins for fixation of the nonabsorbable barrier membranes could limit movement of the membrane, surrounding bone and soft tissue flap[16]. The sausage technique using a membrane fixed with titanium pins has been developed to stabilize the particle grafts and membrane[18]. However, several potential risks have been documented: Damage of the adjacent roots and underlying anatomical vital structures, and the need for an extensive reopening procedure to retrieve the nonresorbable pins [19,20]. Therefore, a technique utilizing periosteal vertical mattress suture (PVMS) for the fixation of grafts and membranes has been proposed for single implant sites, and this technique can avoid potential complications of using fixation pins[13]. Similar to PVMS, continuous periosteal strapping sutures (CPSS) have been used to fix the grafts and absorbable membranes for buccal ridge augmentation and minimize the risks and comorbidities[17]. However, all this suture techniques are all limited by the tensile strength and the resorption rate of the sutures, the time of fixation is also limited by the biodegradation period of the absorbable suture material. Another limitation is that the linear-guided suture may result in possible migration of the particulate graft material in an apicocoronal direction. Moreover, the PVMS technique may not provide enough stability for grafts in large defects, and for large ridge defects the use of pins is still recommended. In the case of large bone defects with continuous multi-tooth positions, it is still recommended to use a large number of pins to fix the membrane and grafts, which is still the first choice currently, even if it has high technical sensitivity and costly.

So far, there are still no literatures about the combination use of suture technique and titanium pins to fix the membrane and grafts. Here, we present a case using a modified membrane fixation technique for stabilizing the absorbable membrane and underlying particulate grafts in a continuous severe horizontal bone defect with an average width of only approximately 1 mm. We used GBR with the graft composed of a 1:1 mixture of autogenous bone and anorganic bovine bone mineral (ABBM), covered by bilayer absorbable membranes, fixed by periosteal diagonal mattress suture (PDMS) and four corner titanium pins.

CASE PRESENTATION

Chief complaints

A 24-year-old male patient was referred to the Dentistry Department of Zhejiang Provincial People's Hospital complaining of spontaneous loss of his right maxillary anterior tooth 1 mo previously.

History of present illness

The patient lost his right maxillary anterior tooth 1 mo prior to referral due to excessive loosening, and now he felt that it affected his appearance and required repair.

History of past illness

The patient had IgA nephropathy and hypertension, which were well controlled after treatment, and the conditions have been stable for > 5 years.

Personal and family history

The patient had no other personal or family history.

Physical examination

His vital sign was stable, with blood pressure of 120/82 mmHg, heart rate of 75 beats per minute and body temperature of 36.7°C. Oral examination showed tooth 12 deficiency, and deciduous tooth 53 retention with a mobility degree of II, the root of tooth 14 was exposed and the buccal alveolar bone completely absorbed, poor oral hygiene with dental calculus and bleeding on probing (Figure 1A).

Laboratory examinations

Blood analysis and other laboratory findings were normal.

Imaging examinations

Cone beam computed tomography (CBCT) scanning revealed the vertical height of alveolar bone was sufficient (19.2-21.3 mm) but the horizontal width of alveolar crest was merely 0.6-2.5 mm.

FINAL DIAGNOSIS

The final diagnosis of the presented case was deficiency of tooth 12, and deciduous tooth 53 retention, severe periodontitis of tooth 14, severe continuous horizontal alveolar bone defects at sites of teeth 12, 13 and 14, and chronic gingivitis.

TREATMENT

The initial treatment was extraction of teeth 53 and 14 (Figure 1B), periodontal scaling and oral hygiene maintenance. Three weeks after teeth extraction and soft tissue healing (Figure 1C), clinical examination indicated that the bone quantity of right maxillary regions was insufficient for implant placement. CBCT scanning revealed the vertical height of alveolar bone was sufficient (19.2-21.3 mm) but the horizontal width of alveolar bone was merely 0.6-2.5 mm at the site 5 mm and 10 mm below the alveolar crest at sites 12 (Figure 2A) and 14 (Figure 2B). Horizontal bone augmentation and postponed implant placement was planned for this continuous severe horizontal bone defect. Bone augmentation was treated by GBR, with the graft composed of a 1:1 mixture of autogenous bone and ABBM, covered by bilayer absorbable membranes. The graft and membranes were fixed by PDMS combined with four corner pins. This study was approved by the Zhejiang Provincial People's Hospital Institutional Review Board (No. 2021QT267) and the participant gave signed informed consent.

Autogenous bone harvest: a vestibular incision followed by two divergent vertical incisions were made below the mucogingival border in the mandibular intercanine region under local anesthesia, and a full-thickness mucoperiostal flap was elevated to expose the bone. Autogenous bone fragments were

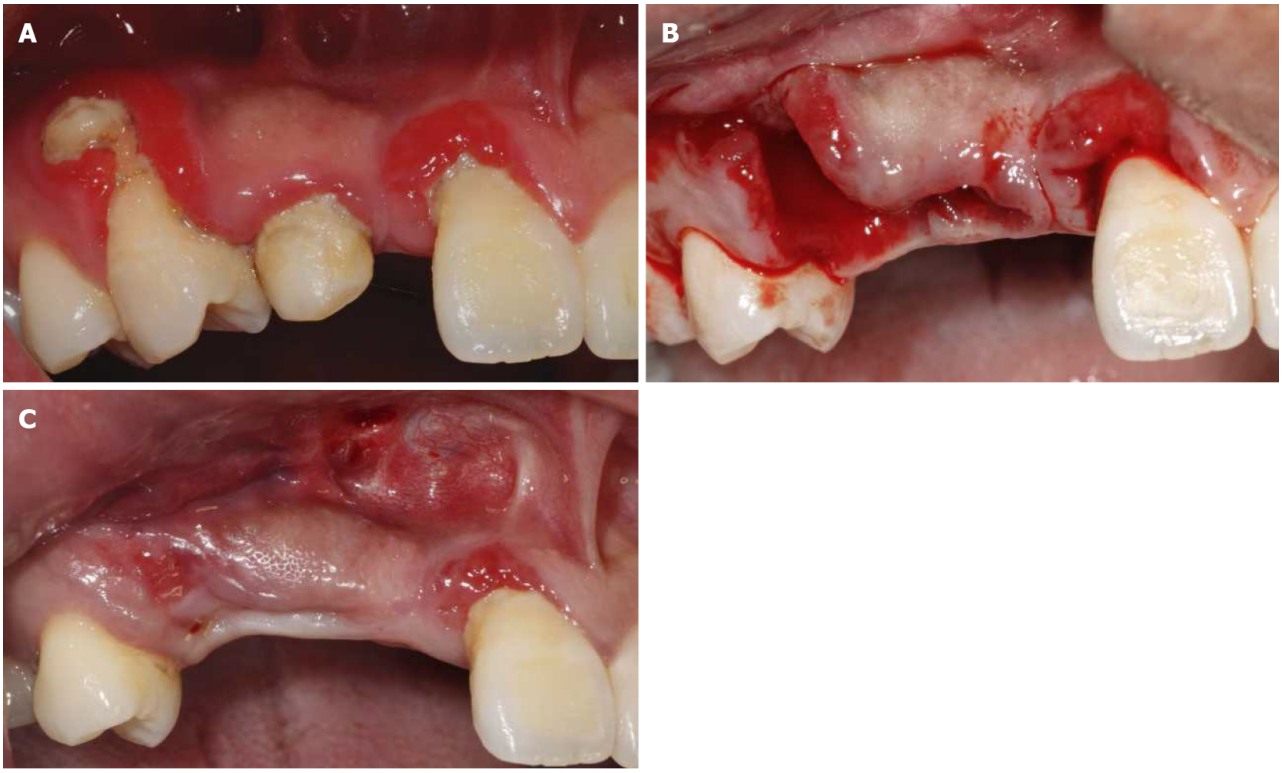

DOI: 10.12998/wjcc.v10.i17.5789 **Copyright** ©The Author(s) 2022.

Figure 1 Oral examination of the patient at initial visit, after tooth extraction and before bone grafting. A: Initial situation of the edentulous site in maxillary anterior; B: Extraction of teeth 53 and 14; C: Three weeks after teeth extraction and before bone augmentation surgery.

harvested using an autogenous bone drill (Osstem, Korea) within the safety margin to the tooth apex and the mental foramen, then mixed with particle bone graft (Bio-Oss, Geistlich, Switzerland) at a ratio of 1:1. Prior to soft tissue closure of the donor site, sharp edges were removed and a gelatin sponge was applied to the remaining defect as a hemostatic dressing. The wounds were closed with 4-0 resorbable suture (Coated VICRYL, Ethicon, United States). To minimize postoperative swelling and hematoma, an extraoral pressure dressing was applied to the donor sites and maintained for 3 d.

Recipient site preparation: after disinfection and local anesthesia, a mid-crestal incision along with an intrasulcus incision of the adjacent tooth were performed, extending into the distal of teeth 11 and 15, with two divergent vertical incisions made one tooth away from teeth 11 and 15 and a full-thickness flap was reflected. Decortication holes were prepared on the surface of the recipient region (Figure 3A). The mixed particle bone graft was adapted to the recipient sites, with the width more than 10 mm, then entirely covered by bilayer absorbable collagen membrane (Bio-Gide, Geistlich, Switzerland) (Figure 3B). Four titanium pins (Trausim, China) were used to fix the four marginal angles of the collagen membrane; two of which were located on the buccal side and two on the palatal side, avoiding the anatomical structures such as root and maxillary sinus. A periosteal release incision was made 2-3 mm beneath the planned apical position of the graft material and membrane. Incremental incisions of 1 to 3 mm into the periosteum and submucosa were made perpendicular to the base of the inner surface of the flap[21]. The flap on the palatal side was partially reflected and the buccal flap advancement was evaluated to determine if deeper incisions into the submucosa were needed to attain more advancement to make sure the soft tissue could be closed without any tension (Figure 3C)[22]. A 6-0 absorbable suture (Coated VICRYL, Ethicon, United States) was used to fix the absorbable membranes and bone graft material using PDMS (Figure 3D).

PDMS and titanium pins fixation technique: after accurate placement of the four titanium pins, the suture needle was introduced through the palatine mucosa at a point one third distal to the mesial corner pin at the palatal site. The needle was carried over the membrane and stitched through the periosteum 2-3 mm apical to the periosteal release incision at a point one third mesial to the distal buccal pin. The needle was looped back at the exterior surface of the grafts and passed through the palatine mucosa, tightening the suture, and then a knot was tied at the exterior of the palatine mucosa to stabilize the suture. The same procedure was repeated at a point one third mesial to the distal corner pin at the palatal site to a point one third distal to the mesial buccal corner pin and then knotted. The two sutures formed a figure of eight cross at the midpoint of the graft material on the buccal side (Figure 4). After tightening the suture, we checked if the bone graft and the membrane were completely immobilized and positioned correctly. Two PDMS prevented potential movement and migration of the bone graft and membranes. Finally, the mucoperiosteal flap was released to ensure a tension-free

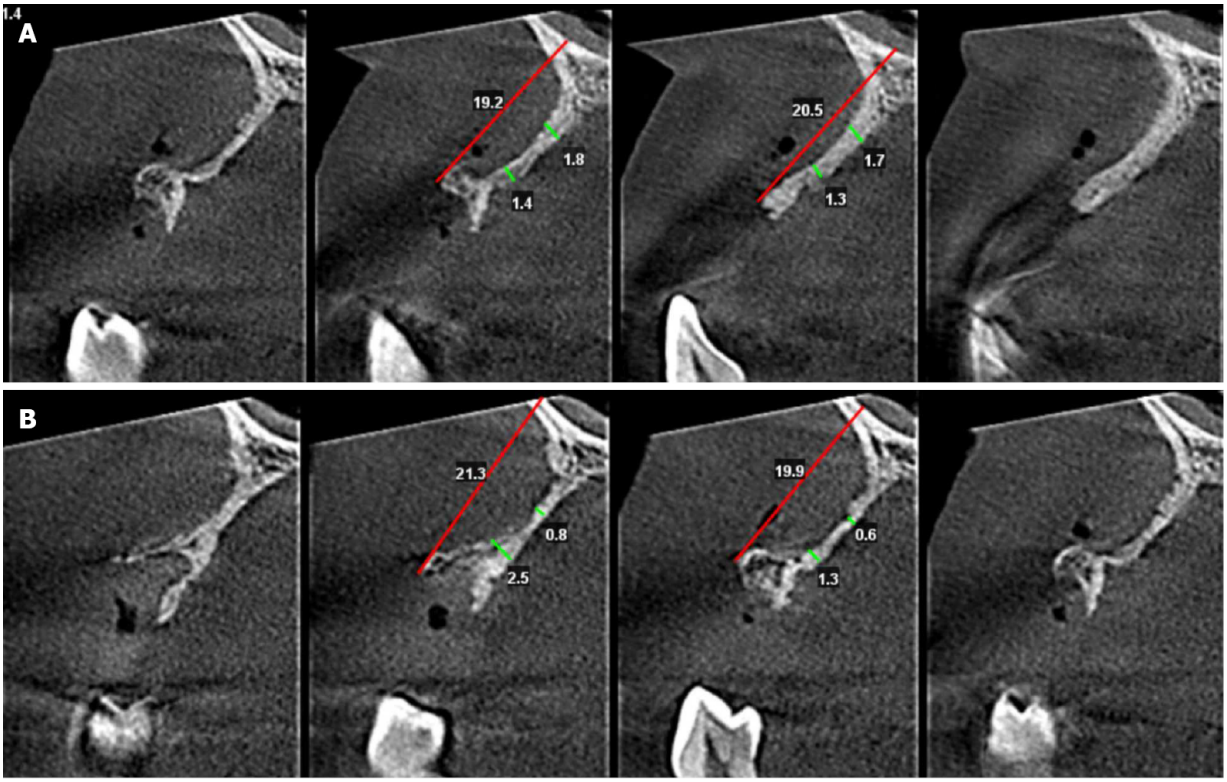

DOI: 10.12998/wjcc.v10.i17.5789 **Copyright** ©The Author(s) 2022.

Figure 2 Bone volume at the defect area before bone grafting. A: Cone beam computed tomography (CBCT) before bone augmentation surgery 5 and 10 mm below the alveolar crest at the site of missing tooth 12; B: CBCT before bone augmentation surgery 5 and 10 mm below the alveolar crest at the site of missing tooth 14.

closure and the flaps were sutured by two layers, combining horizontal mattress sutures with single interrupted sutures. Vertical incisions were closed using single interrupted sutures, which were removed 7 d after surgery, while the mattress suture remained in place until 2 wk. The patient was instructed to use antibiotics and 0.2% chlorhexidine mouth rinse twice a day for 7 d to prevent infection. Two implants (Ankylos A11; Friadent, Germany) were placed after 10 mo's healing without any bone augmentation surgery, and the final prostheses were finished at 3 mo after implant placement.

OUTCOME AND FOLLOW-UP

The cross-sections of the grafted area were measured to evaluate the width of the reconstructed alveolar ridge. CBCT imaging was performed preoperatively, immediately after bone augmentation surgery, and before and after implant placement. The CBCT images were superimposed before bone grafting and after implantation using a software system (3Shape, Denmark); the yellow line represented the alveolar ridge before bone grafting. The result showed that an average augmentation of approximately 10 mm in the alveolar ridge width was achieved at the surgical site after 10 mo' of healing. Two sites were selected to analyze the volume of bone augmentation, 5 and 10 mm below the alveolar crest. Significant bone width increment was achieved by this modified GBR technique. CBCT images showed that at the tooth 12 site, the bone width was increased from 1.83 to 8.83 mm at a point 5 mm below the crest, and from 1.70 to 9.47 mm at a point 10 mm below the crest (Figure 5A). At the tooth 14 site, the bone width was increased from 0.72 to 9.23 mm and from 4.22 to 11.55 mm at points 5 and 10 mm below the crest, respectively (Figure 5B).

DISCUSSION

Various techniques and materials have been used for bone augmentation procedures. It is difficult to choose GBR or Onlay bone blocks in cases of continuous severe horizontal alveolar bone defects. In this case, the remaining alveolar ridge width was < 2 mm at most sites and it seemed that onlay bone graft was the first choice for horizontal bone augmentation according to the decision tree of horizontal bone augmentation[5]. Moreover, bone block is reported to be more effective than GBR in maintaining the

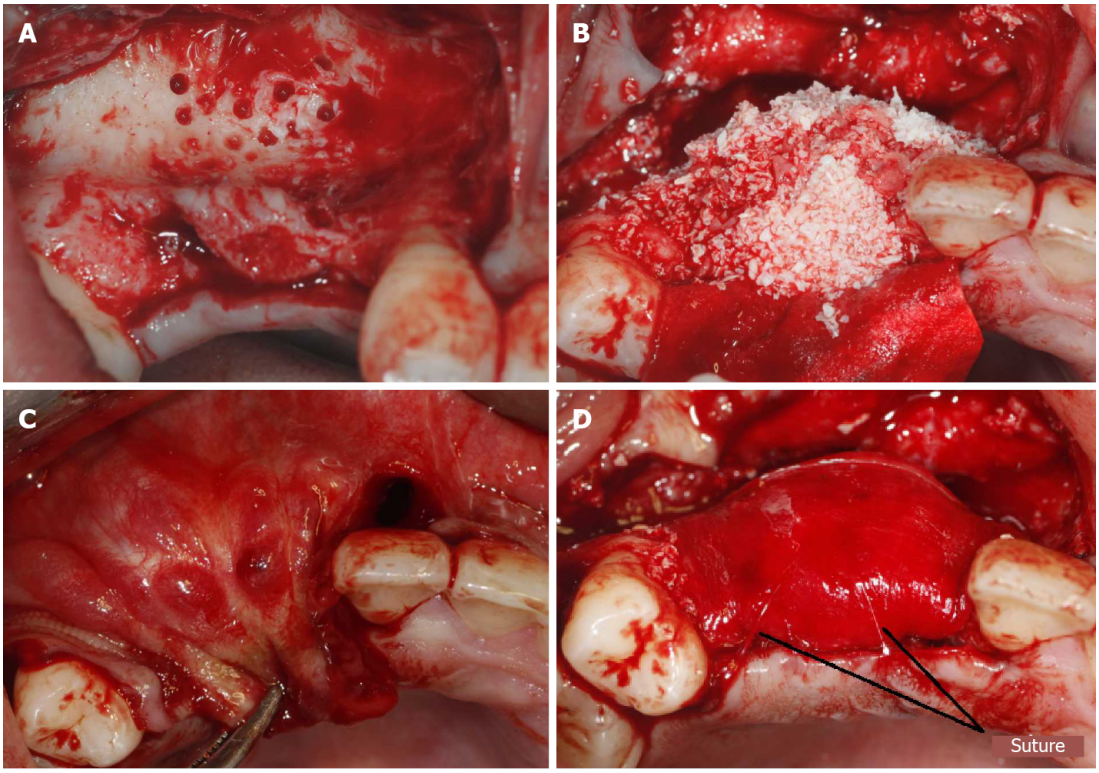

DOI: 10.12998/wjcc.v10.i17.5789 **Copyright** ©The Author(s) 2022.

Figure 3 Procedure of bone grafting. A: Decortication holes were prepared at the recipient area; B: Bone graft material was placed; C: Make sure the soft tissue could be primary closed without tension; D: The resorbable membranes and bone grafts were fixed using periosteal diagonal mattress sutures and four corner pins.

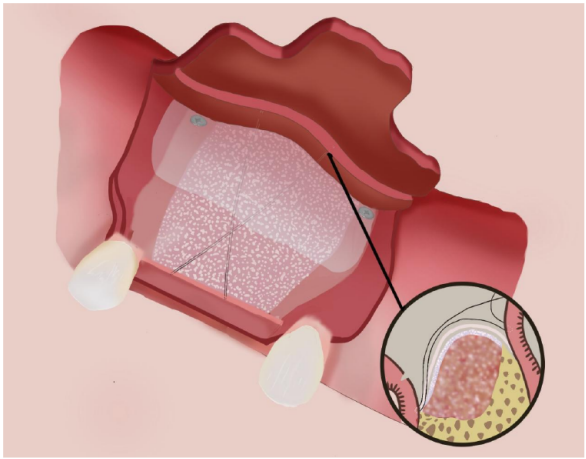

DOI: 10.12998/wjcc.v10.i17.5789 **Copyright** ©The Author(s) 2022.

Figure 4 Fixation of the membrane using periosteal diagonal mattress suture and four corner pins.

volume at the initial stages of healing, and GBR experiences more changes compared with block grafts [2]. However, in the present case, it was difficult to use bone blocks. Firstly, the residual bone of most sites was only 1 mm or less and it was too thin to be used for retention and stabilization of the graft bone bock by titanium screws. Secondly, it was difficult to obtain bone blocks of sufficient size and thickness in the mandibular intercanine region and the external oblique line due to the large area of bone defect, and the patient refused additional surgery outside the oral cavity, such as the fibula or the ilium, and he refused to use any allogenic bone. Finally, GBR might have been a good alternative choice, and an average of approximately 10 mm horizontal bone was gained by GBR to fix the absorbable collagen membranes and particulate grafts with PDMS and four corner pins after 10 mo of healing.

Bone augmentation surgery was performed 3 wk after tooth extraction and the soft tissue was healing at that time. More recently, clinicians have preferred to use non-form-stable collagen membranes to reconstruct severely thin ridges instead of titanium mesh or Poly Tetra Fluoro Ethylene membrane

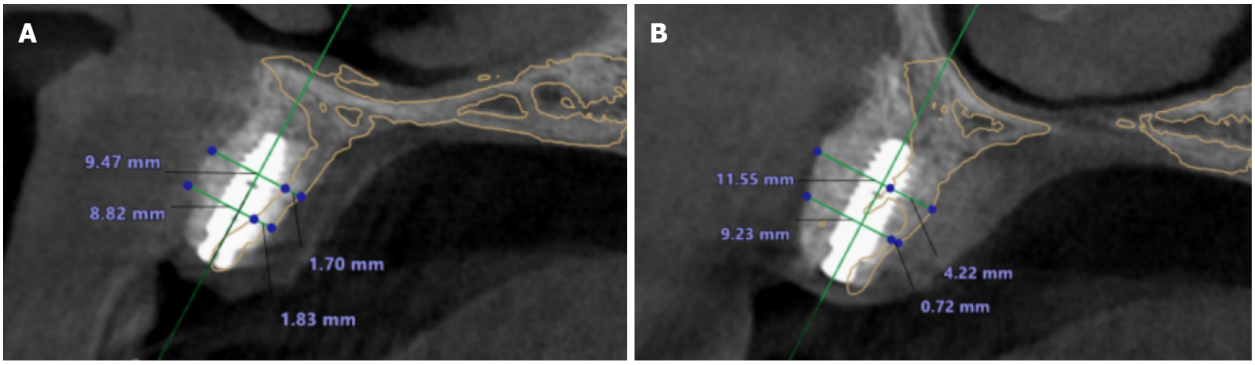

DOI: 10.12998/wjcc.v10.i17.5789 **Copyright** ©The Author(s) 2022.

Figure 5 Cone beam computed tomography superimposed images before bone grafting and after implantation. A: At site of implant 12. The yellow line represented the alveolar ridge before bone grafting. The bone width was increased from 1.83 to 8.83 mm at a point 5 mm below the crest, and from 1.70 to 9.47 mm at a point 10 mm below the crest; B: At site of implant 14. The yellow line represented the alveolar ridge before bone grafting. The bone width was increased from 0.72 to 9.23 mm at a point 5 mm below the crest, and from 4.22 to 11.55 mm at a point 10 mm below the crest.

which is a more sensitive technique, with poor angiogenesis, higher rate of soft tissue dehiscence and difficulty in secondary removal[10,23]. Moreover, significant scar tissue was found in the area of the bone defect and the soft tissue was a thin gingival biological type, therefore absorbable collagen membrane was selected for GBR.

For severe horizontal bone defect, the key factor for successful GBR is to fix the graft material and membranes at the desired position, reduce the movement, and maintain the spatial shape[24]. The stability of the bone substitute and collagen membrane can be enhanced by the application of fixation pins or by the use of block bone substitute instead of particulate bone substitute[25]. The sausage technique using a membrane fixed with titanium pins to stabilize the particle grafts has been reported [18]; however, several potential risks have been documented such as damage to the adjacent roots and underlying anatomical vital structures, and the need for an extensive reopening procedure to retrieve the nonabsorbable pins[20]. The PVMS technique may be preferable to fix the absorbable collagen membrane and particulate graft materials for single implant sites. However, a limitation to this technique is the tensile strength of the absorbable suture material, and possible migration of the particulate graft material in an apicocoronal direction[13], it is only possible to fix the membrane by means of a linear-guided suture, resulting in possible migration of the particulate graft material in an apicocoronal direction. Thus, for continuous severe horizontal bone defect, the use of pins is still recommended because PVMS may not provide sufficient graft stabilization. So far, the relationship between the new bone regeneration and the various fixation methods used is still unknown, and future research is needed to establish the optimal fixation method for adequate bone regeneration[26].

In the present case, the stability of the graft and membrane seemed unable to be provided only by the PDMS technique, thus, the use of four corner pins was still mandatory. Firstly, the four corner pins can limit the possible movement of the membrane and the particulate graft material in the apicocoronal direction. Secondly, the four corner pins might compensate the gradually decreasing strength of the suture due to degradation and absorption. According to the manufacturer, the tensile strength of the VICRYL suture is approximately 75% of its original strength after 14 d and approximately 25% after 28 d *in vivo*. All of the original tensile strength is lost by 5 wk after implantation. Absorption of the suture is essentially complete between 56 and 70 d. In contrast, the Bio-Gide membrane showed obvious tissue integration at 2 wk postimplantation, and almost complete degradation at week 4[27]. Membrane thickness decreased significantly at week 4, and at week 12, the Bio-Gide was almost absorbed and there was a significant increase in mean bone formation[28]. However, it should be kept in mind that the membrane absorption time might not be the most important, and angiogenesis of the membrane plays a crucial role in GBR[29]. The prolonged biodegradation of the membranes might be associated with decreased tissue integration, vascularization and foreign body reactions[27]. The stability of the graft and membrane, as well as vascularization of the membrane, are crucial to the success of GBR, especially in the early stage of bone regeneration. So far there is no evidence for the time required for membrane fixation, and whether the biodegradation period of the absorbable suture material affects the result of GBR is still unknown.

Titanium pins and sutures can be combined effectively and flexibly. Compared with the sausage technique using pins only, multiple pins are required, which is costly, and it is difficult to operate the pins on the lingual or palatal side, and sometimes it is also difficult to avoid hazardous sites and damage to adjacent roots during insertion. Reducing the number of titanium pins can reduce the risk of complications and the difficulty of surgery. This combined technique is flexible and is very useful in clinical practice.

CONCLUSION

For continuous severe horizontal bone defect, PDMS combined with four corner pins may provide an alternative to traditional methods to obtain better bone regeneration, and is a feasible technique to maintain the space and stabilize the graft and membranes in severe horizontal bone defect. Nevertheless, well-designed future clinical studies are needed to verify that the technique described here generates comparable and reproducible results.

FOOTNOTES

Author contributions: Wang LH conceived the study design and carried out the study, and drafted the manuscript; Ruan Y and Zhao WY participated in the literature searching, acquisition of data, analysis and interpretation of data; Chen JP supervised writing the manuscript; Yang F designed the treatment plan and performed the surgery; all authors gave final approval of the version to be published.

Informed consent statement: Written consent was obtained from the patient to participate in the study.

Conflict-of-interest statement: The authors declare that they have no conflicts of interest to disclose.

CARE Checklist (2016) statement: The authors have read the CARE Checklist (2016), and the manuscript was prepared and revised according to the CARE Checklist (2016).

Open-Access: This article is an open-access article that was selected by an in-house editor and fully peer-reviewed by external reviewers. It is distributed in accordance with the Creative Commons Attribution NonCommercial (CC BY-NC 4.0) license, which permits others to distribute, remix, adapt, build upon this work non-commercially, and license their derivative works on different terms, provided the original work is properly cited and the use is non-commercial. See: https://creativecommons.org/Licenses/by-nc/4.0/

Country/Territory of origin: China

ORCID number: Lin-Hong Wang 0000-0001-9215-3845; Yan Ruan 0000-0001-9139-9237; Wen-Yan Zhao 0000-0001-8257-2595; Jian-Ping Chen 0000-0002-5607-0601; Fan Yang 0000-0002-1308-4827.

Corresponding Author's Membership in Professional Societies: Zhejiang Stomatological Association, vice-chairman; Chinese Stomatological Association, Standing Committee member.

S-Editor: Wu YXJ
L-Editor: A
P-Editor: Wu YXJ

REFERENCES

1 **Benic GI**, Hämmerle CH. Horizontal bone augmentation by means of guided bone regeneration. *Periodontol 2000* 2014; **66**: 13-40 [PMID: 25123759 DOI: 10.1111/prd.12039]
2 **Elnayef B**, Porta C, Suárez-López Del Amo F, Mordini L, Gargallo-Albiol J, Hernández-Alfaro F. The Fate of Lateral Ridge Augmentation: A Systematic Review and Meta-Analysis. *Int J Oral Maxillofac Implants* 2018; **33**: 622-635 [PMID: 29763500 DOI: 10.11607/jomi.6290]
3 **Chiapasco M**, Casentini P. Horizontal bone-augmentation procedures in implant dentistry: prosthetically guided regeneration. *Periodontol 2000* 2018; **77**: 213-240 [PMID: 29478251 DOI: 10.1111/prd.12219]
4 **Aghaloo TL**, Moy PK. Which hard tissue augmentation techniques are the most successful in furnishing bony support for implant placement? *Int J Oral Maxillofac Implants* 2007; **22** Suppl: 49-70 [PMID: 18437791]
5 **Fu JH**, Wang HL. Horizontal bone augmentation: the decision tree. *Int J Periodontics Restorative Dent* 2011; **31**: 429-436 [PMID: 21837309]
6 **Lehmijoki M**, Holming H, Thorén H, Stoor P. Rehabilitation of the severely atrophied dentoalveolar ridge in the aesthetic region with corticocancellous grafts from the iliac crest and dental implants. *Med Oral Patol Oral Cir Bucal* 2016; **21**: e614-e620 [PMID: 27475690 DOI: 10.4317/medoral.21146]
7 **Scheerlinck LM**, Muradin MS, van der Bilt A, Meijer GJ, Koole R, Van Cann EM. Donor site complications in bone grafting: comparison of iliac crest, calvarial, and mandibular ramus bone. *Int J Oral Maxillofac Implants* 2013; **28**: 222-227 [PMID: 23377069 DOI: 10.11607/jomi.2603]
8 **Sbordone C**, Toti P, Guidetti F, Califano L, Santoro A, Sbordone L. Volume changes of iliac crest autogenous bone grafts after vertical and horizontal alveolar ridge augmentation of atrophic maxillas and mandibles: a 6-year computerized tomographic follow-up. *J Oral Maxillofac Surg* 2012; **70**: 2559-2565 [PMID: 22959878 DOI: 10.1016/j.joms.2012.07.040]
9 **Urban IA**, Monje A. Guided Bone Regeneration in Alveolar Bone Reconstruction. *Oral Maxillofac Surg Clin North Am* 2019; **31**: 331-338 [PMID: 30947850 DOI: 10.1016/j.coms.2019.01.003]

10 **Wessing B**, Lettner S, Zechner W. Guided Bone Regeneration with Collagen Membranes and Particulate Graft Materials: A Systematic Review and Meta-Analysis. *Int J Oral Maxillofac Implants* 2018; **33**: 87-100 [PMID: 28938035 DOI: 10.11607/jomi.5461]

11 **Wang HL**, Boyapati L. "PASS" principles for predictable bone regeneration. *Implant Dent* 2006; **15**: 8-17 [PMID: 16569956 DOI: 10.1097/01.id.0000204762.39826.0f]

12 **An YZ**, Strauss FJ, Park JY, Shen YQ, Thoma DS, Lee JS. Membrane fixation enhances guided bone regeneration in standardized calvarial defects: A pre-clinical study. *J Clin Periodontol* 2022; **49**: 177-187 [PMID: 34866208 DOI: 10.1111/jcpe.13583]

13 **Urban IA**, Lozada JL, Wessing B, Suárez-López del Amo F, Wang HL. Vertical Bone Grafting and Periosteal Vertical Mattress Suture for the Fixation of Resorbable Membranes and Stabilization of Particulate Grafts in Horizontal Guided Bone Regeneration to Achieve More Predictable Results: A Technical Report. *Int J Periodontics Restorative Dent* 2016; **36**: 153-159 [PMID: 26901293 DOI: 10.11607/prd.2627]

14 **Johnson TM**, Vargas SM, Wagner JC, Lincicum AR, Stancoven BW, Lancaster DD. The Triangle Suture for Membrane Fixation in Guided Bone Regeneration Procedures: A Report of two Cases. *Clin Adv Periodontics* 2022 [PMID: 34986274 DOI: 10.1002/cap.10193]

15 **Kamat SM**, Khandeparker RV, Akkara F, Dhupar V, Mysore A. SauFRa Technique for the Fixation of Resorbable Membranes in Horizontal Guided Bone Regeneration: A Technical Report. *J Oral Implantol* 2020; **46**: 609-613 [PMID: 32315438 DOI: 10.1563/aaid-joi-D-19-00265]

16 **Kirsch A**, Ackermann KL, Hurzeler MB, Durr W, Hutmacher D. Development and clinical application of titanium minipins for fixation of nonresorbable barrier membranes. *Quintessence Int* 1998; **29**: 368-381 [PMID: 9728148]

17 **Shalev TH**, Kurtzman GM, Shalev AH, Johnson DK, Kersten MEM. Continuous Periosteal Strapping Sutures for Stabilization of Osseous Grafts With Resorbable Membranes for Buccal Ridge Augmentation: A Technique Report. *J Oral Implantol* 2017; **43**: 283-290 [PMID: 28628357 DOI: 10.1563/aaid-joi-D-17-00060]

18 **Wang HL**, Misch C, Neiva RF. "Sandwich" bone augmentation technique: rationale and report of pilot cases. *Int J Periodontics Restorative Dent* 2004; **24**: 232-245 [PMID: 15227771]

19 **Siar CH**, Toh CG, Romanos G, Ng KH. Subcutaneous reactions and degradation characteristics of collagenous and noncollagenous membranes in a macaque model. *Clin Oral Implants Res* 2011; **22**: 113-120 [PMID: 20678135 DOI: 10.1111/j.1600-0501.2010.01970.x]

20 **Lorenzoni M**, Pertl C, Polansky RA, Jakse N, Wegscheider WA. Evaluation of implants placed with barrier membranes. A restrospective follow-up study up to five years. *Clin Oral Implants Res* 2002; **13**: 274-280 [PMID: 12010157 DOI: 10.1034/j.1600-0501.2002.130306.x]

21 **Zazou N**, Diab N, Bahaa S, El Arab AE, Aziz OA, El Nahass H. Clinical comparison of different flap advancement techniques to periosteal releasing incision in guided bone regeneration: A randomized controlled trial. *Clin Implant Dent Relat Res* 2021; **23**: 107-116 [PMID: 33155422 DOI: 10.1111/cid.12960]

22 **Romanos GE**. Periosteal releasing incision for successful coverage of augmented sites. A technical note. *J Oral Implantol* 2010; **36**: 25-30 [PMID: 20218867 DOI: 10.1563/AAID-JOI-D-09-00068]

23 **Atef M**, Tarek A, Shaheen M, Alarawi RM, Askar N. Horizontal ridge augmentation using native collagen membrane vs titanium mesh in atrophic maxillary ridges: Randomized clinical trial. *Clin Implant Dent Relat Res* 2020; **22**: 156-166 [PMID: 32185856 DOI: 10.1111/cid.12892]

24 **Carpio L**, Loza J, Lynch S, Genco R. Guided bone regeneration around endosseous implants with anorganic bovine bone mineral. A randomized controlled trial comparing bioabsorbable versus non-resorbable barriers. *J Periodontol* 2000; **71**: 1743-1749 [PMID: 11128923 DOI: 10.1902/jop.2000.71.11.1743]

25 **Mir-Mari J**, Wui H, Jung RE, Hämmerle CH, Benic GI. Influence of blinded wound closure on the volume stability of different GBR materials: an in vitro cone-beam computed tomographic examination. *Clin Oral Implants Res* 2016; **27**: 258-265 [PMID: 25856209 DOI: 10.1111/clr.12590]

26 **Cucchi A**, Chierico A, Fontana F, Mazzocco F, Cinquegrana C, Belleggia F, Rossetti P, Soardi CM, Todisco M, Luongo R, Signorini L, Ronda M, Pistilli R. Statements and Recommendations for Guided Bone Regeneration: Consensus Report of the Guided Bone Regeneration Symposium Held in Bologna, October 15 to 16, 2016. *Implant Dent* 2019; **28**: 388-399 [PMID: 31344018 DOI: 10.1097/ID.0000000000000909]

27 **Rothamel D**, Schwarz F, Sager M, Herten M, Sculean A, Becker J. Biodegradation of differently cross-linked collagen membranes: an experimental study in the rat. *Clin Oral Implants Res* 2005; **16**: 369-378 [PMID: 15877758 DOI: 10.1111/j.1600-0501.2005.01108.x]

28 **Hämmerle CH**, Jung RE, Yaman D, Lang NP. Ridge augmentation by applying bioresorbable membranes and deproteinized bovine bone mineral: a report of twelve consecutive cases. *Clin Oral Implants Res* 2008; **19**: 19-25 [PMID: 17956571 DOI: 10.1111/j.1600-0501.2007.01407.x]

29 **Schwarz F**, Rothamel D, Herten M, Wüstefeld M, Sager M, Ferrari D, Becker J. Immunohistochemical characterization of guided bone regeneration at a dehiscence-type defect using different barrier membranes: an experimental study in dogs. *Clin Oral Implants Res* 2008; **19**: 402-415 [PMID: 18324961 DOI: 10.1111/j.1600-0501.2007.01486.x]

World Journal of Clinical Cases

Submit a Manuscript: https://www.f6publishing.com

World J Clin Cases 2022 June 16; 10(17): 5798-5804

DOI: 10.12998/wjcc.v10.i17.5798

ISSN 2307-8960 (online)

CASE REPORT

Surgical repair of an emergent giant hepatic aneurysm with an abdominal aortic dissection: A case report

Xin Wen, Zuo-Yi Yao, Qian Zhang, Wei Wei, Xi-Yang Chen, Bin Huang

Specialty type: Surgery

Provenance and peer review: Unsolicited article; Externally peer reviewed.

Peer-review model: Single blind

Peer-review report's scientific quality classification

Grade A (Excellent): 0
Grade B (Very good): B, B
Grade C (Good): C
Grade D (Fair): 0
Grade E (Poor): 0

P-Reviewer: Baran B, Turkey; Covantsev S, Russia; Stepanyan SA, Armenia

Received: November 23, 2021
Peer-review started: November 23, 2021
First decision: February 7, 2022
Revised: February 27, 2022
Accepted: April 15, 2022
Article in press: April 15, 2022
Published online: June 16, 2022

Xin Wen, Xi-Yang Chen, Department of Vascular Surgery, West China Hospital, Chengdu 610041, Sichuan Province, China

Zuo-Yi Yao, Qian Zhang, Wei Wei, Department of General Surgery, Chengdu Fifth People's Hospital, Chengdu 611100, Sichuan Province, China

Bin Huang, Department of Vascular Surgery, West China Hospital of Sichuan University, Chengdu 610041, Sichuan Province, China

Corresponding author: Bin Huang, PhD, Professor, Department of Vascular Surgery West China Hospital of Sichuan University, No. 37 Guoxue Xiang, Chengdu 610041, Sichuan Province, China. xgwkhb@126.com

Abstract

BACKGROUND

Hepatic artery aneurysm (HAA) is the second most common visceral aneurysm. A significant number of hepatic aneurysms are found accidentally on examination. However, their natural history is characterized by their propensity to rupture, which is very serious and requires urgent treatment. An emergent giant hepatic aneurysm with an abdominal aortic dissection is less commonly reported.

CASE SUMMARY

We report the complicated case of a giant hepatic aneurysm with an abdominal aortic dissection. A 66-year-old female presented with the complaint of sudden upper abdominal pain accompanied by vomiting. Physical examination showed that her blood pressure was 214/113 mmHg. Her other vital signs were stable. Computed tomography found a giant hepatic proper aneurysm and dissection of the lower segment of the abdominal aorta. Furthermore, angiography showed a HAA with the maximum diameter of approximately 56 mm originating from the proper hepatic artery and located approximately 15 mm from the involved bifurcation of the left and right hepatic arteries with no collateral circulation. Therefore, we decided to use a stent to isolate the abdominal aortic dissection first, and then performed open repair. After the operation, the patient recovered well without complications, and her 3-month follow-up checkup did not reveal any late complications.

CONCLUSION

Open surgery is a proven method for treating giant hepatic aneurysms. If the patient's condition is complex, staged surgery is an option.

Key Words: Giant hepatic artery aneurysm; Abdominal aortic dissection; Open repair; Reconstruction; Good prognosis; Case report

©The Author(s) 2022. Published by Baishideng Publishing Group Inc. All rights reserved.

Core Tip: We report a relatively rare case of a giant hepatic aneurysm combined with abdominal aortic coarctation. The patient had an acute onset and was treated for abdominal aortic coarctation after blood pressure control, followed by a second stage open surgery to manage the hepatic aneurysm in a comprehensive manner. The patient's prognosis is good.

Citation: Wen X, Yao ZY, Zhang Q, Wei W, Chen XY, Huang B. Surgical repair of an emergent giant hepatic aneurysm with an abdominal aortic dissection: A case report. *World J Clin Cases* 2022; 10(17): 5798-5804
URL: https://www.wjgnet.com/2307-8960/full/v10/i17/5798.htm
DOI: https://dx.doi.org/10.12998/wjcc.v10.i17.5798

INTRODUCTION

Hepatic artery aneurysm (HAA) is the second most common visceral aneurysm[1]. The incidence rate of HAA in 2091965 patients who visited the Mayo Clinic between 1980 and 1986 was 0.002%[2]. A total of 77% HAAs are isolated in the proximal part of the liver, of which 20% are combined with parenchymal and extraparenchymal invasion and 3% are confined to the liver[3]. Excluding traumatic aneurysms, patients most commonly suffer from HAAs during their sixth decade of life[4]. Lesions in the hepatic circulation show a ratio of approximately 3:2 in terms of sex with male predominance[2]. Risk factors for HAA include atherosclerosis, medial degeneration, infection, trauma, and vasculitis[4]. A large majority of HAAs are diagnosed incidentally *via* computed tomography (CT) scan[3]. Most patients with symptomatic aneurysms present with one or more of Quincke's classic triad of biliary bleeding (jaundice, biliary colic, and gastrointestinal bleeding)[4]. Diagnosis can be made by ultrasound scan, CT angiography (CTA), and digital subtraction angiography. CTA is recommended as the diagnostic tool of choice in patients who are thought to have HAA[5]. Despite recent advances in therapeutic techniques and diagnostic tools, the management of a visceral artery aneurysm remains clinically challenging. Rupture is the most emergent and life-threatening situation in HAA. Lumsden *et al*[4] pointed out that the HAA-related early incidence of rupture and mortality was 9.1% and 22.7%, respectively. Fibromuscular dysplasia and polyarteritis nodosa increase the risk of HAA rupture and account for 50% of HAA ruptures[5]. The majority of these lesions rupture when they are > 2 cm in diameter[3].

The guideline, named "the Society for Vascular Surgery clinical practice guidelines on the management of visceral aneurysms", states that all hepatic artery pseudoaneurysms regardless of cause (Grade 1A) and all symptomatic HAAs regardless of size (Grade 1A) should be repaired as soon as possible; in asymptomatic patients without significant comorbidity, repair is recommended if the true HAA is > 2 cm (Grade 1A) or if the aneurysm enlarges at the rate of > 0.5 cm per year (Grade 1C); in patients with significant comorbidities, repair is recommended if the HAA is > 5.0 cm (Grade 1B); furthermore, the repair of HAA in patients with vasculopathy or vasculitis regardless of size (Grade 1C) or with positive blood cultures (Grade 1C) is recommended[5]. The clinical practice guidelines on the management of visceral aneurysms set by the Society for Vascular Surgery indicate that treatment approaches mainly include endovascular repair with covered stents, open repair, and coil embolization. The endovascular approach represents a minimally-invasive alternative with low mortality and morbidity[6]. Given the abundant collateral supply of the liver, the incidence of hepatic necrosis after disruption of the common hepatic artery is low. Percutaneous embolization is of special value in patients with intrahepatic aneurysms[5]. Endovascular therapy has become the mainstream approach. However, open repair remains a therapeutic option with definite efficacy and is mostly chosen under the conditions of HAA rupture, infeasible endovascular approach and for symptomatic patients with fibromuscular dysplasia or polyarteritis nodosa and lesions in the proper hepatic and proximal right or left hepatic branches[5].

CASE PRESENTATION

Chief complaints

A 66-year-old woman was admitted to our hospital with the chief complaint of severe abdominal pain with vomiting. Four hours before admission, the patient had a sudden onset of sharp pain in the upper

and middle abdomen with no obvious cause. The pain was unbearable and persistent without relief, which involved back pain and was accompanied by vomiting the contents of the stomach, without dizziness, headache, chest tightness, chest pain, acid reflux, heartburn, chills, fever and other symptoms.

History of present illness

The patient was found to have hypertension for more than 20 years, with the highest blood pressure reaching 220/160 mmHg. She was taking nimodipine tablets (30 mg tid) regularly, and her blood pressure was controlled at approximately 140/75 mmHg, usually without dizziness and headache.

History of past illness

The patient had no other previous illnesses.

Personal and family history

Her personal and family history was unremarkable.

Physical examination

Physical examination showed slight tenderness in the upper abdomen and no rebound pain; blood pressure of 214/139 mmHg; pulse of 64 beats/min; and temperature of 36.4°C.

Laboratory examinations

Her blood test results showed no special abnormalities.

Imaging examinations

CT revealed: (1) A giant aneurysm of the proper hepatic artery (maximum diameter approximately 56 mm); and (2) Dissection of the lower abdominal aorta (single break) (Figure 1A and B).

FINAL DIAGNOSIS

The patient was diagnosed with abdominal aortic dissection, hepatic artery aneurysm, and hypertension grade 3 (very high risk).

TREATMENT

After receiving blood pressure control, sedation and related symptomatic treatment from the coronary heart disease center of our cardiology department, the patient's symptoms disappeared and her vital signs stabilized. The patient was transferred to our department on the same day of admission due to CT findings of abdominal aortic coarctation and a hepatic aneurysm. We performed angiography, which showed that the HAA had a maximum diameter of approximately 5.6 cm and that it originated from the proper hepatic artery and was located approximately 1.5 cm from the involved bifurcation of the left and right hepatic arteries with no collaterals. Prolonged angiography revealed no communication between the HAA and superior mesenteric artery (Figure 1C). Considering the complexity of the patient's condition, the aortic dissection was repaired with a Endurant II stent graft (Medtronic, Inc.) at the first stage, and the HAA was scheduled for surgical repair at the second stage. Postoperatively, the patient was treated with antiplatelet, lipid-lowering and blood pressure control therapy.

Open repair was performed six days later. A right subcostal incision was made, and the surgical approach was *via* the small omental sac. Intraoperative findings showed the following: the proper hepatic artery, which was approximately 6 cm × 6 cm in size, was located between the medial side of the descending duodenum and the anterior of the pancreatic head and bile duct (Figure 2A). We then mobilized the inflow and outflow of the proper hepatic artery. After systemic heparinization, the inflow and outflow of the HAA was clamped, and the aneurysm was directly opened. An aneurysm break approximately 2 mm in size and slight mural thrombus (Figure 2B) were found. No collateral vessel was detected in the aneurysm. The proximal part of the proper hepatic artery was anastomosed end to end with the right hepatic artery as the adjacent orifice location, and the left hepatic artery was anastomosed end to side with the proper hepatic artery (Figure 2C). The hepatic artery clamp time was 31 min. After anastomosis, ultrasound revealed the patency of the anastomotic site and the distal hepatic artery branches. The operation was performed without difficulties.

OUTCOME AND FOLLOW-UP

Postoperatively, the patient experienced no specific discomfort. Antiplatelet, blood pressure control,

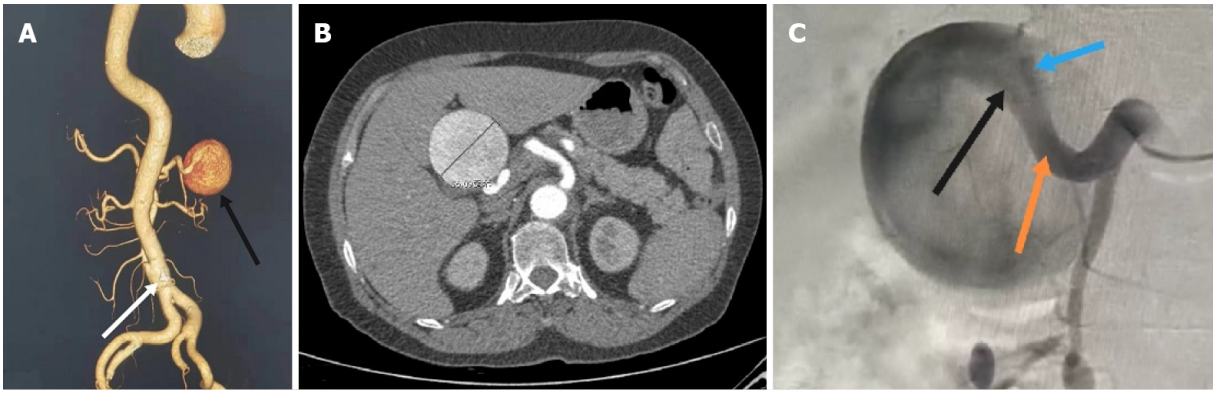

DOI: 10.12998/wjcc.v10.i17.5798 **Copyright** ©The Author(s) 2022.

Figure 1 Computed tomography scan. A: Abdominal computed tomography (CT) three-dimensional reconstruction showed a proper hepatic artery aneurysm (black arrow) and abdominal aortic dissection (white arrow); B: The patient's abdominal CT scan showed a huge proper hepatic artery aneurysm with a maximum diameter of approximately 56 mm; C: Abdominal aortography showed a huge proper hepatic aneurysm: A bit twisted, no collaterals, originated from the proper hepatic artery (orange arrow) and involving the bifurcation of the left (black arrow) and right hepatic arteries (blue arrow).

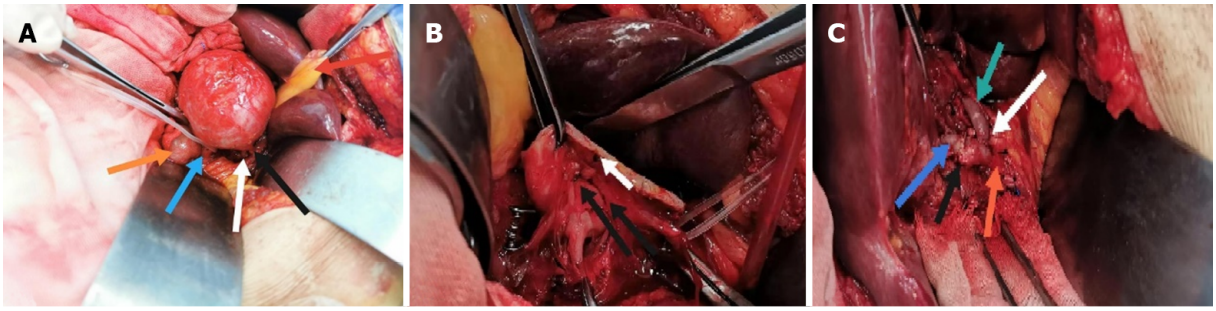

DOI: 10.12998/wjcc.v10.i17.5798 **Copyright** ©The Author(s) 2022.

Figure 2 Open repair was performed six days later. A: This is a general view of the isolated hepatic aneurysm. The red arrow indicates the gallbladder; the yellow arrow the descending duodenum; the green arrow the proper hepatic artery; the white arrow the right hepatic artery and the black arrow the left hepatic artery; B: This is a general view of the cut aneurysm. The white arrow indicates the aneurysm break and the black arrow the mural thrombus; C: The general view of the proper hepatic artery (red arrow) after suturing with the left (dark green arrow) and right hepatic arteries (light green arrow), respectively. The black arrow indicates the end-to-end anastomosis of the proper hepatic artery and the right hepatic artery while the white arrow indicates the end to side anastomosis of the proper hepatic artery and the left hepatic artery.

and lipid-lowering treatments were maintained. Eleven days later, the patient was successfully discharged without surgery-related complications. The important times and events during the patient's hospitalization are shown in Table 1. The patient's 3-mo follow-up checkup did not reveal any late complications (Figure 3). She reported no specific discomfort on review and was very satisfied with her treatment.

DISCUSSION

Visceral aneurysms, despite their rare incidence of 0.01%-0.2%, are of clinical importance, especially if we consider their natural history which is characterized by their propensity to rupture, with HAA accounting for approximately 20% of visceral aneurysms and a rupture rate of 44%[5]. They are usually asymptomatic and difficult to detect until they rupture and cause abdominal pain and hypovolemic shock. As a result, most visceral aneurysms are found incidentally. The mortality rate following ruptured visceral aneurysms remains high (30% reported in the last decade)[7].

The timing of the intervention for hepatic aneurysms has been mentioned above. The treatment of a hepatic aneurysm is mainly as follows: Covered stent, open repair, and embolization[2,3,5]. The ideal surgical option should be to remove the aneurysm while maintaining the hepatic circulation. Therefore, the primary treatment of hepatic aneurysms varies by site. The main treatments for common HAAs include open surgical ligation, endovascular embolization, resection/reconstruction, aneurysmorrhaphy, and a covered stent; those for the proper hepatic artery are resection with arterial reconstruction and endovascular repair with a covered stent; those for the proximal right or left hepatic branches are resection with arterial reconstruction and endovascular stent grafting; and finally, those for an

Table 1 Important events and dates during this patient's hospitalization

Date	Events
December 8, 2020	(1) The patient was admitted to the emergency department with acute abdominal pain and widespread pulling pain in the back with a blood pressure of 214/139 mmHg at the time of the emergency; (2) Computed tomography (CT) suggested abdominal aortic coarctation with intramural hematoma, hepatic artery aneurysm, bilateral common iliac artery and calcified plaque in the internal iliac artery; and (3) The patient was transferred to our department due to CT findings of abdominal aortic coarctation and hepatic aneurysm
December 14, 2020	Ultrasound showed no special abnormalities in the renal artery and bilateral carotid and vertebral arteries
December 23, 2020	Abdominal aortogram + endoluminal isolation of abdominal aortic coarctation (non-emergency) was performed
December 29, 2020	Hepatic intrinsic aneurysm resection+ hepatic artery reconstruction (non-emergency) was performed
January 9, 2021	The patient was successfully discharged with a good prognosis and without any associated complications

DOI: 10.12998/wjcc.v10.i17.5798 **Copyright** ©The Author(s) 2022.

Figure 3 The patient was reexamined 3 mo after surgery and showed no complications. The anastomotic end of the proper hepatic artery was unobstructed. The abdominal aortic dissection was well isolated.

intrahepatic aneurysm are endovascular embolization and resection of the lobe in which the aneurysm is located[5,8]. However, the specific choice of treatment should be based on the patient's specific circumstances.

In this case, we did not select coil embolization mainly for the following reasons: First, the endovascular repair of extrahepatic HAA depends on the collaterals and location of the HAA. Given that the maintenance of distal organ perfusion is important, embolization is usually discouraged in patients with HAAs in the proper hepatic artery due to the risk of liver ischemia[5]. Furthermore, in this case, the location of the HAA in the proper hepatic artery involved the bifurcation of the left and right hepatic arteries with no collateral circulation and thus increased the risk. Second, the HAA was so large that a large parenchymal lesion would be created if we performed embolization; this lesion might compress the biliary tract and duodenum and thus cause jaundice, gastrointestinal obstruction, and even duodenum fistula[5,9].

Another main option for HAA repair is endovascular stent grafting. The endovascular repair of visceral aneurysms with stent implantation can simultaneously enable aneurysm exclusion and vascular preservation, and therefore minimize the risk of ischemic complications[10]. Nearly all retrospective case series have shown that although the outcomes for visceral artery aneurysms after open or endovascular repair share similar long-term results, morbidity is significantly worse with open repair than with the endovascular approach[5,8]. The scope of aneurysm morphology suitable for endovascular repair is expanding with the accumulation of experience and improvements in equipment. The anatomical complexity of aneurysms is generally believed to affect the technical difficulty of repair with the development of the application of endovascular covered grafts; this belief is the main reason why we did not choose the approach of endovascular covered grafting. The main complications of

endovascular stent grafting include occlusion[9,11]. However, the patency rate of hepatic artery stenting is rarely reported. Künzle *et al*[12] reported that the 2-year patency of the endovascular stent grafting of visceral artery aneurysms is approximately 81%.

Open surgery, which is usually known as open surgical revascularization, is another common method for the treatment of HAA. Considering the possibility of central liver necrosis despite adequate collateral flow by endovascular exclusion, open repair is recommended in low-risk patients if endovascular stent graft exclusion is not possible[5]. In addition, open surgery has its unique role in aneurysm rupture.

The main methods of vascular reconstruction include direct vascular anastomosis and bypass of the artificial vascular or saphenous vein and vascular patch[11]. The main complications of open surgical revascularization are infection and occlusion. Erben *et al*[11] reported that in open surgical revascularization, the incidence of occlusion is 12%, with saphenous veins and artificial vessels sharing 6% and 6% equally, and the incidence of infection is 6%.

In this case, deploying the covered stent was difficult considering the tortuosity of the delivery route. Therefore, the proper hepatic artery was anastomosed end to end with the right hepatic artery, and the left hepatic artery was anastomosed end to side with the proper hepatic artery without an artificial blood vessel or saphenous vein. This approach was riddled with the considerations discussed above. First, we anastomosed the blood vessels directly because the ends were highly adjacent, and the tension was low after direct anastomosis with no need for the use of artificial blood vessels or saphenous veins, so that the patient could reduce the subsequent anticoagulant burden. Second, we did not first anastomose the left and right hepatic arteries and then anastomose them with the proper hepatic artery as during the operation, we found that the patient's right hepatic artery was thick and large, so that we could prevent complications in one of the left and right hepatic arteries from affecting the other artery to the greatest extent. Moreover, we did not completely isolate the whole aneurysm, thus reducing the damage to the surrounding tissue and the incidence of postoperative complications. During the entire operation, the hepatic artery occlusion time was 31 min, which reduced the probability of hepatic ischemia.

CONCLUSION

Diagnosing huge hepatic aneurysms in time and choosing the best treatment are very challenging. When other serious diseases, such as Stanford type B aortic dissection, are found at the same time, the complexity of the patient's condition and the difficulty of treatment double. Although endovascular therapy is the first choice in most cases, open surgery still has a unique role. We should not only strictly understand the indications of various surgical procedures, but also make clinical decisions in accordance with the specific conditions of patients.

FOOTNOTES

Author contributions: Wen X was responsible for collecting the information and writing the article; Yao ZY was involved in surgery and communication with the patient; Zhang Q participated in surgery and data collection; Wei W participated in surgery; Chen XY revised the article; Huang B designed the surgical plan and participated in the surgery; all authors have read and approved the final manuscript.

Informed consent statement: The patient provided informed written consent prior to study enrollment.

Conflict-of-interest statement: This article is not supported by funding and has no conflict of interest.

CARE Checklist (2016) statement: The authors have read the CARE Checklist (2016), and the manuscript was prepared and revised according to the CARE Checklist (2016).

Open-Access: This article is an open-access article that was selected by an in-house editor and fully peer-reviewed by external reviewers. It is distributed in accordance with the Creative Commons Attribution NonCommercial (CC BY-NC 4.0) license, which permits others to distribute, remix, adapt, build upon this work non-commercially, and license their derivative works on different terms, provided the original work is properly cited and the use is non-commercial. See: https://creativecommons.org/Licenses/by-nc/4.0/

Country/Territory of origin: China

ORCID number: Xi-Yang Chen 0000-0002-4108-1869; Bin Huang 0000-0003-4767-0629.

S-Editor: Wu YXJ
L-Editor: Webster JR
P-Editor: Wu YXJ

REFERENCES

1 **Pulli R**, Dorigo W, Troisi N, Pratesi G, Innocenti AA, Pratesi C. Surgical treatment of visceral artery aneurysms: A 25-year experience. *J Vasc Surg* 2008; **48**: 334-342 [PMID: 18644480 DOI: 10.1016/j.jvs.2008.03.043]

2 **Abbas MA**. Hepatic artery aneurysm: factors that predict complications. *J Vasc Surg* 2003; **38**: 41-45 [DOI: 10.1016/s0741-5214(03)00090-9]

3 **Berceli SA**. Hepatic and splenic artery aneurysms. *Semin Vasc Surg* 2005; **18**: 196-201 [PMID: 16360576 DOI: 10.1053/j.semvascsurg.2005.09.005]

4 **Lumsden AB**, Mattar SG, Allen RC, Bacha EA. Hepatic artery aneurysms: the management of 22 patients. *J Surg Res* 1996; **60**: 345-350 [PMID: 8598666 DOI: 10.1006/jsre.1996.0055]

5 **Chaer RA**, Abularrage CJ, Coleman DM, Eslami MH, Kashyap VS, Rockman C, Murad MH. The Society for Vascular Surgery clinical practice guidelines on the management of visceral aneurysms. *J Vasc Surg* 2020; **72**: 3S-39S [PMID: 32201007 DOI: 10.1016/j.jvs.2020.01.039]

6 **Perera P**, Mailhot T, Riley D, Mandavia D. The RUSH exam: Rapid Ultrasound in SHock in the evaluation of the critically lll. *Emerg Med Clin North Am* 2010; **28**: 29-56, vii [PMID: 19945597 DOI: 10.1016/j.emc.2009.09.010]

7 **Haghighatkhah H**, Sanei Taheri M, Kharazi SM, Zamini M, Rabani Khorasgani S, Jahangiri Zarkani Z. Hepatic Artery Aneurysms as a Rare but Important Cause of Abdominal Pain; a Case Series. *Arch Acad Emerg Med* 2019; **7**: e25 [PMID: 31432035]

8 **Cochennec F**, Riga CV, Allaire E, Cheshire NJ, Hamady M, Jenkins MP, Kobeiter H, Wolfe JN, Becquemin JP, Gibbs RG. Contemporary management of splanchnic and renal artery aneurysms: results of endovascular compared with open surgery from two European vascular centers. *Eur J Vasc Endovasc Surg* 2011; **42**: 340-346 [PMID: 21628100 DOI: 10.1016/j.ejvs.2011.04.033]

9 **Chen X**, Ge J, Zhao J, Yuan D, Yang Y, Huang B. Duodenal Necrosis Associated with a Threatened Ruptured Gastroduodenal Artery Pseudoaneurysm Complicated by Chronic Pancreatitis: Case Report. *Ann Vasc Surg* 2020; **68**: 571.e9-571.e13 [PMID: 32422293 DOI: 10.1016/j.avsg.2020.04.050]

10 **Venturini M**, Marra P, Colombo M, Panzeri M, Gusmini S, Sallemi C, Salvioni M, Lanza C, Agostini G, Balzano G, Tshomba Y, Melissano G, Falconi M, Chiesa R, De Cobelli F, Del Maschio A. Endovascular Repair of 40 Visceral Artery Aneurysms and Pseudoaneurysms with the Viabahn Stent-Graft: Technical Aspects, Clinical Outcome and Mid-Term Patency. *Cardiovasc Intervent Radiol* 2018; **41**: 385-397 [PMID: 29164308 DOI: 10.1007/s00270-017-1844-5]

11 **Erben Y**, De Martino RR, Bjarnason H, Duncan AA, Kalra M, Oderich GS, Bower TC, Gloviczki P. Operative management of hepatic artery aneurysms. *J Vasc Surg* 2015; **62**: 610-615 [PMID: 26094044 DOI: 10.1016/j.jvs.2015.03.077]

12 **Künzle S**, Glenck M, Puippe G, Schadde E, Mayer D, Pfammatter T. Stent-graft repairs of visceral and renal artery aneurysms are effective and result in long-term patency. *J Vasc Interv Radiol* 2013; **24**: 989-996 [PMID: 23727420 DOI: 10.1016/j.jvir.2013.03.025]

World Journal of Clinical Cases

Submit a Manuscript: https://www.f6publishing.com

World J Clin Cases 2022 June 16; 10(17): 5805-5809

DOI: 10.12998/wjcc.v10.i17.5805

ISSN 2307-8960 (online)

CASE REPORT

Heterotopic ossification beneath the upper abdominal incision after radical gastrectomy: Two case reports

Xiang Zhang, Ping-Tian Xia, Yan-Chao Ma, Yong Dai, Yan-Lei Wang

Specialty type: Surgery

Provenance and peer review: Unsolicited article; Externally peer reviewed.

Peer-review model: Single blind

Peer-review report's scientific quality classification
Grade A (Excellent): 0
Grade B (Very good): B
Grade C (Good): C
Grade D (Fair): 0
Grade E (Poor): 0

P-Reviewer: Oley MH, Indonesia; Sharfman Z, Israel

Received: November 24, 2021
Peer-review started: November 24, 2021
First decision: December 27, 2021
Revised: December 31, 2021
Accepted: April 3, 2022
Article in press: April 3, 2022
Published online: June 16, 2022

Xiang Zhang, Ping-Tian Xia, Department of Colorectal Surgery, Qilu Hospital of Shandong University, Jinan 250012, Shandong Province, China

Yan-Chao Ma, Department of Radiology, Qilu Hospital of Shandong University, Jinan 250012, Shandong Province, China

Yong Dai, Department of Colorectal and Anal Surgery, Qilu Hospital of Shandong University, Jinan 250012, Shandong Province, China

Yan-Lei Wang, Department of General Surgery, Qilu Hospital of Shandong University, Jinan 250012, Shandong Province, China

Corresponding author: Yan-Lei Wang, MD, PhD, Chief Doctor, Department of General Surgery, Qilu Hospital of Shandong University, No. 107 West Wenhua Road, Jinan 250012, Shandong Province, China. yanleiwang@hotmail.com

Abstract

BACKGROUND

Heterotopic ossification (HO) is a rare clinical phenomenon that refers to bone formation in nonossifying tissues.

CASE SUMMARY

This report presents two cases of HO beneath the upper abdominal median incision after radical gastrectomy. The first patient had postoperative pain below the incision area. There were no signs of anastomotic leakage, and the wound healed. Computed tomography (CT) findings 2 wk postoperatively were negative for HO, but the 6-wk CT showed HO beneath the incision. The patient refused reoperation, and after conservative therapy, the pain was gradually relieved after 2 wk. In the second case, postoperative recovery was uneventful, and HO was only detected on routine follow-up CT after 4 mo. An anti-adhesion membrane was applied beneath the peritoneum in both patients. Our findings suggest that HO beneath the abdominal incision might form at approximately 1 mo postoperatively. It may cause intractable pain; however, reoperation is usually not required.

CONCLUSION

In our cases, we suspect that HO may be related to the use of foreign materials beneath the peritoneum, which needs to be further investigated.

Key Words: Heterotopic ossification; Upper abdominal incision; Radical gastrectomy; Case report

©The Author(s) 2022. Published by Baishideng Publishing Group Inc. All rights reserved.

Core Tip: Heterotopic ossification (HO) beneath the upper abdominal incision is a rare clinical phenomenon that refers to bone formation in nonossifying tissues. In our cases, we suspect that HO may be related to the use of foreign materials beneath the peritoneum, which needs to be further investigated.

Citation: Zhang X, Xia PT, Ma YC, Dai Y, Wang YL. Heterotopic ossification beneath the upper abdominal incision after radical gastrectomy: Two case reports. *World J Clin Cases* 2022; 10(17): 5805-5809
URL: https://www.wjgnet.com/2307-8960/full/v10/i17/5805.htm
DOI: https://dx.doi.org/10.12998/wjcc.v10.i17.5805

INTRODUCTION

Heterotopic ossification (HO) is a rare clinical phenomenon that refers to bone formation in nonossifying tissues. This is a unique phenomenon that has rarely been reported following abdominal surgery. HO of an incisional scar was first described by Askanazy in 1901 as a subset of myositis ossificans traumatica[1,2]. Since then, more than 100 cases have been reported worldwide[2-6]. These numbers are probably an underestimate of the actual incidence, because these ossifications are usually asymptomatic[3]. HO has been described as a benign postoperative complication in most studies.

CASE PRESENTATION

Chief complaints

Case 1: The first patient was a 62-year-old man, he underwent radical gastrectomy (Billroth I anastomosis) with a midline abdominal incision. Postoperatively, the patient experienced pain below the incisional area.

Case 2: A 57-year-old man also underwent distal gastroscopy (Billroth I anastomosis) due to gastric cancer with a midline abdominal incision. The patient had no other comorbidities.

History of present illness

The two patients underwent distal gastroscopy (Billroth I anastomosis) because of gastric cancer.

History of past illness

Case 1: The patient had a history of coronary stent implantation performed 3 mo ago.

Case 2: The patients had no significant past illness.

Personal and family history

The patients had no significant personal and family history.

Physical examination

Case 1: There were no signs of anastomotic leakage, and the wound healed.

Case 2: Upon palpation, the incisional area was hard and firm.

Imaging examinations

Case 1: Computed tomography (CT) 2 wk postoperatively showed no obvious abnormality (Figure 1A), but the 6-wk CT showed calcification beneath the incision (Figure 1B-D).

Case 2: In the 4-mo follow-up CT scan, calcified tissue was noted under the upper abdominal incision, extending from the immediate subxiphoid region to the umbilical region (Figure 1E-G).

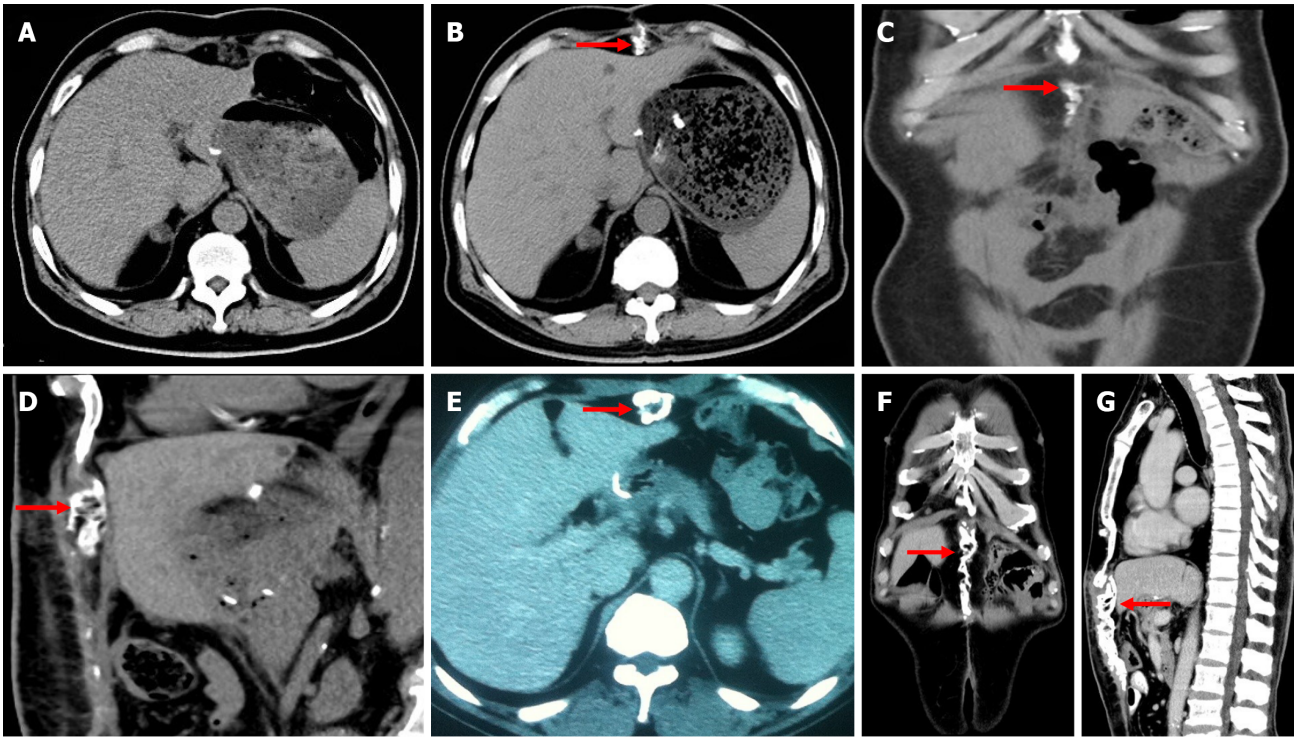

DOI: 10.12998/wjcc.v10.i17.5805 **Copyright** ©The Author(s) 2022.

Figure 1 Imaging examinations. A: Computed tomography (CT) scan 2 wk postoperatively in case 1 shows no obvious abnormality beneath the incision; B: CT scan 6 wk postoperatively in case 1 shows calcified tissue beneath the incision (arrow); C and D: Coronal and sagittal images of calcified tissue in case 1 between the incision and liver (arrow); E: CT scan 4 mo postoperatively in case 2 shows calcified tissue beneath the midline incision (arrow); F and G: Coronal and sagittal images in case 2 show extension of calcification (arrow).

FINAL DIAGNOSIS

The patients were diagnosed with ossification beneath the upper abdominal incision.

TREATMENT

The patient of case 1 refused reoperation, and after conservative therapy (non-steroidal anti-inflammatory drugs), the pain was gradually relieved after 2 wk.

OUTCOME AND FOLLOW-UP

At a 1-year follow-up, the patients of case 1 had no signs of recurrence.

DISCUSSION

The following common features of ectopic ossification have been summarized in documented cases: (1) Male patients are more susceptible to ectopic ossification, and the male-to-female ratio is as high as 10:1 [7]; (2) this pathology has mostly been reported in vertical scars; (3) the ectopic bone is generally formulated within the first year postoperatively; and (4) all cases in the literature occurred during primary healing, and neither wound complications nor changes in serum ion levels were noted. Both our cases fit all of these features. Moreover, the newly formed bone was detected in the first case 6 wk postoperatively, which is sooner than the earliest ectopic abdominal incision ossifications reported in the literature (2 mo)[1]. Our findings suggest that HO beneath the abdominal incision might form at approximately 1 mo postoperatively.

While no certain theory has yet been confirmed regarding etiology, several mechanisms have been studied to help explain this pathological process. Injury or, more specifically, surgical incision is considered a necessary trigger[4]. Three requisite components are involved in the pathogenesis[7]: (1) Inductive signaling pathways are activated by a stimulation factor released from the site of injury. These

factors, including bone morphogenic proteins, have been implicated as potential signaling vehicles[8]; (2) then, inducible mesenchymal stem cells, which are located at the injury site, differentiate into osteoblasts or chondroblasts after receiving these signals. This process has been described as osteogenic induction[1,4]; and (3) a heterotopic environment conducive to osteogenesis must exist. HO of the abdominal wall is a subtype of myositis ossificans traumatica. Pieces of the periosteum or perichondrium of the xiphisternum or symphysis pubis may "plant" into the incision wound during the operation and then grow into bone in the scar[1,4]. During laparotomy, we extended the incision to the xiphisternum in both cases, which can be regarded as proof of this theory to some extent.

Tam *et al*[9] recently reported a case of HO in a patient after hernia repair. In the ectopically formed bone, they found an acellular dermal matrix that had been placed in the primary incision. In our case, we placed a sodium hyaluronate-based bioresorbable membrane (Seprafilm) under the peritoneum of each patient to prevent adhesion. It has been postulated that this type of anti-adhesion agent can cause inflammatory reactions as a severe postoperative complication[10-12]. Whether Seprafilm was the culprit in our case needs to be further investigated.

The main symptoms of HO include local pain and swelling[7]. In suspicious cases, CT or magnetic resonance imaging should be performed for diagnosis[2]. It is also important to exclude other postoperative complications, such as anastomotic leakage and tumor recurrence. In patients with intractable abdominal pain, conservative therapy, such as analgesic administration, parenteral transfusion, and physical therapy, should be initially performed. If conservative therapy fails, then complete excision of the lesion should be considered. Asymptomatic patients need no treatment apart from observation. The first patient in our experience had sustained abdominal pain postoperatively and was readmitted to the hospital twice. After 1 mo of conservative therapy, pain was immediately relieved before surgery was considered.

CONCLUSION

Non-steroidal anti-inflammatory drug therapy, radiotherapy, and diphosphate (ethindronate disodium) administration have been proposed to decrease heterotopic bone formation[1]. However, the routine application of these methods is controversial and unnecessary.

FOOTNOTES

Author contributions: Zhang X, Dai Y and Wang YL were the patients' surgeons, reviewed the literature and drafted the manuscript; Xia PT and Ma YC contributed to the manuscript drafting; Ma YC created figures and interpreted the imaging findings; all authors approved the final version of the manuscript.

Supported by the Clinical and Practical New Technology Development Fund of Qilu Hospital of Shandong University.

Informed consent statement: Informed written consent was obtained from the patients for the publication of this report and any accompanying images.

Conflict-of-interest statement: The authors declare that they have no conflict of interest.

CARE Checklist (2016) statement: The authors have read the CARE Checklist (2016), and the manuscript was prepared and revised according to the CARE Checklist (2016).

Open-Access: This article is an open-access article that was selected by an in-house editor and fully peer-reviewed by external reviewers. It is distributed in accordance with the Creative Commons Attribution NonCommercial (CC BY-NC 4.0) license, which permits others to distribute, remix, adapt, build upon this work non-commercially, and license their derivative works on different terms, provided the original work is properly cited and the use is non-commercial. See: https://creativecommons.org/Licenses/by-nc/4.0/

Country/Territory of origin: China

ORCID number: Xiang Zhang 0000-0001-7417-6082; Ping-Tian Xia 0000-0001-8032-8871; Yan-Chao Ma 0000-0002-9157-4063; Yong Dai 0000-0001-6163-8022; Yan-Lei Wang 0000-0002-4227-0274.

S-Editor: Chen YL
L-Editor: A
P-Editor: Chen YL

REFERENCES

1 **Reardon MJ**, Tillou A, Mody DR, Reardon PR. Heterotopic calcification in abdominal wounds. *Am J Surg* 1997; **173**: 145-147 [PMID: 9074383 DOI: 10.1016/S0002-9610(96)00415-1]

2 **Jacobs JE**, Birnbaum BA, Siegelman ES. Heterotopic ossification of midline abdominal incisions: CT and MR imaging findings. *AJR Am J Roentgenol* 1996; **166**: 579-584 [PMID: 8623631 DOI: 10.2214/ajr.166.3.8623631]

3 **Fennema EM**, de Boer J, Mastboom WJ. Ossification of abdominal scar tissue: a case series with a translational review on its development. *Hernia* 2014; **18**: 825-830 [PMID: 24668529 DOI: 10.1007/s10029-014-1240-x]

4 **Hogan NM**, Caffrey E, Curran S, Sheehan M, Joyce MR. Heterotopic ossification of the abdominal wall. *Int J Surg Case Rep* 2012; **3**: 489-491 [PMID: 22858788 DOI: 10.1016/j.ijscr.2012.06.004]

5 **Ma JP**, Xian MF, Liao B, Hong GX, He YL, Zhan WH. Postoperative heterotopic mesenteric and incision ossification. *Chin Med J (Engl)* 2013; **126**: 3799-3780 [PMID: 24112190]

6 **Lai HJ**, Jao SW, Lee TY, Ou JJ, Kang JC. Heterotopic mesenteric ossification after total colectomy for bleeding diverticulosis of the colon--a rare case report. *J Formos Med Assoc* 2007; **106**: S32-S36 [PMID: 17493894 DOI: 10.1016/s0929-6646(09)60350-8]

7 **Kaplan FS**, Glaser DL, Hebela N, Shore EM. Heterotopic ossification. *J Am Acad Orthop Surg* 2004; **12**: 116-125 [PMID: 15089085 DOI: 10.5435/00124635-200403000-00007]

8 **McCarthy EF**, Sundaram M. Heterotopic ossification: a review. *Skeletal Radiol* 2005; **34**: 609-619 [PMID: 16132978 DOI: 10.1007/s00256-005-0958-z]

9 **Tam V**, Zelken J, Sacks JM. Total heterotopic ossification of an acellular dermal matrix used for abdominal wall reconstruction. *BMJ Case Rep* 2013; **2013** [PMID: 24121808 DOI: 10.1136/bcr-2013-009081]

10 **Klingler PJ**, Floch NR, Seelig MH, Branton SA, Wolfe JT, Metzger PP. Seprafilm-induced peritoneal inflammation: a previously unknown complication. Report of a case. *Dis Colon Rectum* 1999; **42**: 1639-1643 [PMID: 10613487 DOI: 10.1007/BF02236221]

11 **Remzi FH**, Oncel M, Church JM, Senagore AJ, Delaney CP, Fazio VW. An unusual complication after hyaluronate-based bioresorbable membrane (Seprafilm) application. *Am Surg* 2003; **69**: 356-357 [PMID: 12716099]

12 **Huang JC**, Yeh CC, Hsieh CH. Laparoscopic management for Seprafilm-induced sterile peritonitis with paralytic ileus: report of 2 cases. *J Minim Invasive Gynecol* 2012; **19**: 663-666 [PMID: 22935311 DOI: 10.1016/j.jmig.2012.04.006]

World Journal of Clinical Cases

Submit a Manuscript: https://www.f6publishing.com

World J Clin Cases 2022 June 16; 10(17): 5810-5815

DOI: 10.12998/wjcc.v10.i17.5810

ISSN 2307-8960 (online)

CASE REPORT

Non-alcoholic Wernicke encephalopathy in an esophageal cancer patient receiving radiotherapy: A case report

Ye Zhang, Lei Wang, Jin Jiang, Wen-Yu Chen

Specialty type: Oncology

Provenance and peer review: Unsolicited article; Externally peer reviewed.

Peer-review model: Single blind

Peer-review report's scientific quality classification

Grade A (Excellent): 0
Grade B (Very good): B
Grade C (Good): C, C
Grade D (Fair): 0
Grade E (Poor): 0

P-Reviewer: Nyamuryekung'e MK, Tanzania; Zhang X, United States

Received: December 1, 2021
Peer-review started: December 1, 2021
First decision: January 12, 2022
Revised: January 13, 2022
Accepted: April 22, 2022
Article in press: April 22, 2022
Published online: June 16, 2022

Ye Zhang, Lei Wang, Department of General Practice, The Affiliated Hospital of Jiaxing University, Jiaxing 314000, Zhejiang Province, China

Jin Jiang, Department of Oncology, The Affiliated Hospital of Jiaxing University, Jiaxing 314000, Zhejiang Province, China

Wen-Yu Chen, Department of Respiration, The Affiliated Hospital of Jiaxing University, Jiaxing 314000, Zhejiang Province, China

Corresponding author: Lei Wang, Doctor, Chief Doctor, Department of General Practice, The Affiliated Hospital of Jiaxing University, No. 1882 Zhonghuan South Road, Nanhu District, Jiaxing 314000, Zhejiang Province, China. jxdyyywlyx@163.com

Abstract

BACKGROUND

Wernicke encephalopathy is a rare but potentially fatal adverse event caused by thiamine deficiency. Reports of non-alcoholic Wernicke encephalopathy due to malignancy are scarce in the literature, with those reported mainly being on haematological cancer, followed by gastrointestinal cancer. As a result, there is considerable under-recognition and delay in the diagnosis and treatment of Wernicke encephalopathy in oncology departments. To our knowledge, there has been no report of Wernicke encephalopathy in a patient with esophageal cancer while receiving radiotherapy.

CASE SUMMARY

A 64-year-old man presented to the oncology outpatient clinic with a history of dysphagia for 2 mo, and was diagnosed with locally advanced esophageal squamous cell carcinoma (stage IIIB). Radiotherapy was initiated to alleviate dysphagia due to malignant esophageal stenosis; however, the patient exhibited consciousness disturbances starting on day 10 of radiotherapy. Brain magnetic resonance imaging indicated the development of Wernicke encephalopathy. Subsequent treatment with thiamine led to rapid improvement in the patient's neurological symptoms.

CONCLUSION

Wernicke encephalopathy may develop in non-alcoholic patients undergoing radiotherapy for esophageal cancer. Early diagnosis and sufficient thiamine supplementation during radiotherapy are essential.

Key Words: Wernicke encephalopathy; Thiamine deficiency; Esophageal cancer; Radiotherapy; Consciousness disturbance; Case report

©The Author(s) 2022. Published by Baishideng Publishing Group Inc. All rights reserved.

Core Tip: Wernicke encephalopathy is a neuropsychiatric disorder resulting from thiamine deficiency. It is frequently associated with alcoholism and is challenging to diagnose in non-alcoholic patients. Only scarce reports of Wernicke encephalopathy accompanying cancer have been reported, mainly in haematological malignancies followed by gastrointestinal malignancies. There have been no reports about Wernicke encephalopathy accompanying esophageal cancer. Here we report the first case of Wernicke encephalopathy in an esophageal cancer patient receiving radiotherapy. It is presented to emphasize that early nutritional evaluation and diagnosis are important. Prompt thiamine supplementation is the key to preventing permanent neurological damage.

Citation: Zhang Y, Wang L, Jiang J, Chen WY. Non-alcoholic Wernicke encephalopathy in an esophageal cancer patient receiving radiotherapy: A case report. *World J Clin Cases* 2022; 10(17): 5810-5815
URL: https://www.wjgnet.com/2307-8960/full/v10/i17/5810.htm
DOI: https://dx.doi.org/10.12998/wjcc.v10.i17.5810

INTRODUCTION

Wernicke encephalopathy is an acute or subacute neuropsychiatric disorder secondary to thiamine (vitamin B1) deficiency. It is characterized by the classical triad of ophthalmoplegia, gait ataxia, and altered mental status[1-3], which, however, presents in only 10%-16% of the cases[1,3,4]. Chronic alcoholism is the most common predisposing factor for thiamine deficiency, followed by malnutrition or decreased thiamine absorption secondary to hyperemesis gravidarum, gastrointestinal disease, prolonged fasting, prolonged parenteral nutrition support, hemodialysis, or malignant disease[5-9]. Compared to alcoholic Wernicke encephalopathy, non-alcoholic Wernicke encephalopathy may be prone to diagnostic delays owing to its atypical clinical presentation and the interval between symptom onset and clinical diagnosis[10]. To the best of our knowledge, there have been no reports of Wernicke encephalopathy occurring in cases of esophageal cancer. Moreover, the most common predisposing factors for non-alcoholic Wernicke encephalopathy in cancer include gastrectomy, chemotherapy, or end-stage of life; radiotherapy is rarely documented. Herein, we describe the first case of non-alcoholic Wernicke encephalopathy accompanying esophageal cancer in a patient receiving radiotherapy.

CASE PRESENTATION

Chief complaints

A 64-year-old man was admitted to our hospital with complaints of progressive difficulty in swallowing.

History of present illness

The patient's symptoms started 2 mo prior, with recurrent episodes of difficulty in swallowing. He could ingest fluids with ease, but semi-liquid foods only with difficulty. He also reported feeling fatigued.

History of past illness

There was no remarkable medical history. He had a history of smoking for 20 years, but no history of alcohol or drug consumption.

Personal and family history

The patient had a disease-free personal and family history.

Physical examination

The patient was emaciated and had a body mass index of 19.88 kg/m^2. There were no mental status changes, cerebellar symptoms, or abnormal eye movements. No clinical ophthalmoplegia or encephalopathy was detected. The other items of the physical examination were normal.

Laboratory examinations

Blood biochemistry revealed mild hypoproteinemia (36 g/L). The results of routine blood and urine tests and arterial blood gas analysis were normal.

Imaging examination

An esophagogastroscopy revealed a significant esophageal tumor located 26-33 cm from the upper incisors, and biopsy results indicated squamous cell carcinoma. Chest contrast-enhanced computed tomography (CT) revealed thickening of the middle and lower esophageal wall with luminal stenosis. The abdominal CT findings were unremarkable. As per the eighth edition of the Union for International Cancer Control staging, the final diagnosis was locally advanced esophageal squamous cell carcinoma, clinical stage cT3N2M0 (stage IIIB).

Further diagnostic work-up

The patient refused surgery or chemotherapy. In order to alleviate dysphagia due to malignant esophageal stenosis, he received 60 Gy of local radiotherapy in 30 fractions without concurrent chemotherapy. Repeated vomiting and dorsalgia occurred during radiotherapy, without diarrhea. A parenteral nutritional supplement including high glucose but no thiamine was administered. On day 8 of radiotherapy, the dysphagia status was markedly improved. From day 10 of radiotherapy, the patient gradually displayed apathy, disorientation, and passivity; was disinterested in his surroundings; and slept abundantly. On neurological examination, he was minimally responsive to verbal and painful stimuli, uncooperative for the finger-to-nose examination, had a slow pupillary response to light, and a Glasgow coma scale score of 10. This was followed by the onset of lethargy on day 12 of radiotherapy. An emergency brain CT scan performed immediately was normal. Brain magnetic resonance imaging (MRI) showed bilateral symmetrical hyperintensities in the dorsal thalamus, the periventricular region of the third ventricle, and around the cerebral aqueduct as seen on T2-weighted imaging, fluid-attenuated inversion recovery (FLAIR), and diffusion-weighted imaging (DWI) (Figure 1).

FINAL DIAGNOSIS

At first, the signs and symptoms rendered cerebrovascular disease or metastatic brain tumors as the most probable diagnosis. However, after combining the clinical manifestations and typical brain MRI findings, a final diagnosis of Wernicke encephalopathy secondary to thiamine deficiency was made.

TREATMENT

We started immediate intravenous thiamine replacement therapy at a dose of 500 mg/d for 3 d, followed by 200 mg for a week, and one tablet of 100 mg oral thiamine per day.

OUTCOME AND FOLLOW-UP

The patient regained consciousness within 3 d. After 5 d, his mental status improved, and he could understand simple commands. At discharge, the patient's neurological symptoms were improved significantly. Neurological examination at the 2-mo follow-up was normal, except for mild memory impairment.

DISCUSSION

Wernicke encephalopathy is a neurological disorder resulting from the deficiency of thiamine, and is commonly related to the chronic abuse of alcohol[1,2]. Recently, the incidence of non-alcoholic Wernicke encephalopathy has been increasing, and malignancy is one of the attributable causes. The most common type of malignancy reported with non-alcoholic Wernicke encephalopathy is haematological, followed by gastrointestinal neoplasms. There have been no studies reporting cases of Wernicke encephalopathy in patients with esophageal cancer thus far.

Thiamine cannot be synthesized in the human body, and hence is mainly derived from food. Therefore, any kind of malnutrition lasting for more than 3-4 wk depletes the thiamine reserve[11]. Esophageal cancer is often accompanied by malnutrition due to dysphagia and declined appetite. The potential for subclinical thiamine deficiency should be considered despite the absence of changes in the mental state[12].

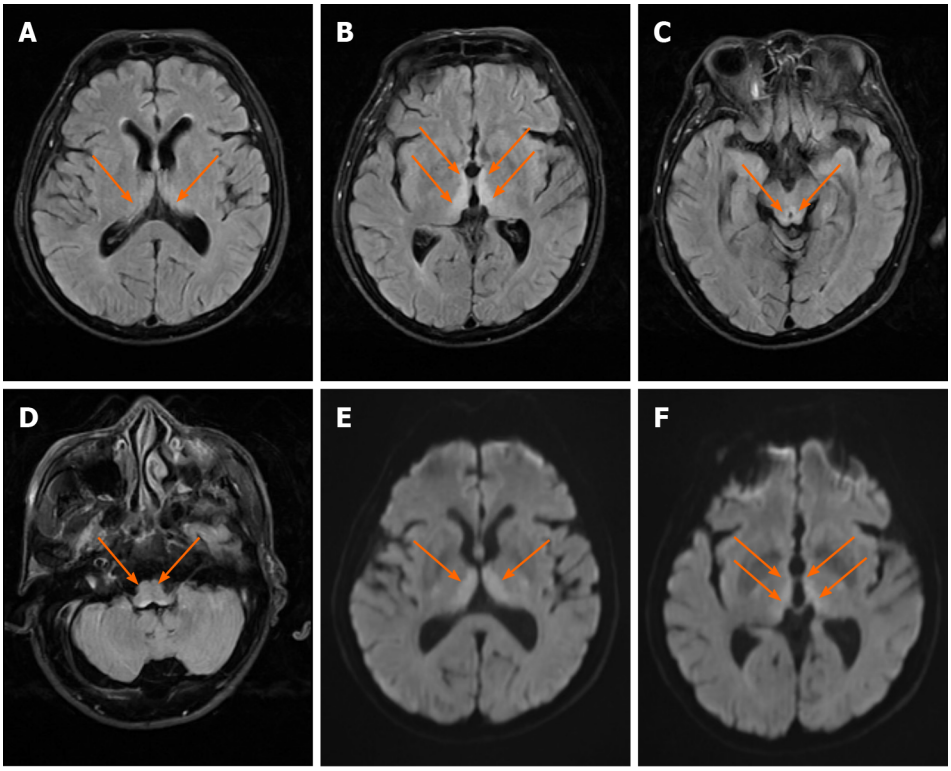

DOI: 10.12998/wjcc.v10.i17.5810 **Copyright** ©The Author(s) 2022.

Figure 1 Patient's brain magnetic resonance imaging. A-D: Axial fluid-attenuated inversion recovery images showing symmetrical high signals in bilateral dorsal thalami (A and B), around the third ventricle (B), cerebral aqueduct (C), and the fourth ventricle (D); E and F: Axial diffusion-weighted images showing symmetrical high signals in bilateral dorsal thalami (E and F) and the periventricular region of the third ventricle (F).

In patients with cancer, Wernicke encephalopathy can occur after surgery, during chemotherapy, or at the end of life. It is extremely rare in patients receiving radiotherapy based on existing reports, and there is no guidance on whether radiotherapy can accelerate thiamine deficiency. It needs to be confirmed by more studies in the future. We concluded that chronic malnutrition caused by repeated dysphagia and vomiting was the main reason for Wernicke encephalopathy in our patient. Therefore, a total nutritional evaluation and prophylactic thiamine supplementation are major preventative and therapeutic measures for impaired dietary intake in non-surgical esophageal cancer patients from the time of diagnosis, especially before radiotherapy.

The classically described clinical triad of ophthalmoplegia, ataxia, and mental disturbances is often absent in Wernicke encephalopathy. Therefore, a non-alcoholic patient presenting with atypical clinical manifestations can frequently be misdiagnosed. Day *et al*[13] reported underdiagnosis rates of 68% and 94% in alcoholic and non-alcoholic Wernicke encephalopathy, respectively. Delayed diagnosis and treatment can lead to the progression of the disease. As per recommendations, the diagnosis of Wernicke encephalopathy is made when two of the following signs are present: (1) Dietary deficiencies; (2) eye signs; (3) cerebellar dysfunction; and (4) either an altered mental state or a mild memory impairment[8]. In our patient, the clinical suspicion of Wernicke encephalopathy was delayed as the patient was a non-alcoholic, and disturbance of consciousness was the only manifestation.

MRI is currently considered the most valuable method for the diagnosis of non-alcoholic Wernicke encephalopathy, especially the FLAIR sequence which has a 93% specificity[14]. The common MRI findings for non- alcoholic Wernicke encephalopathy are hyperintense signals in the dorsal medial thalamic nuclei, periaqueductal gray area, and the third or fourth ventricles as seen on DWI, T2-weighted imaging, and FLAIR sequence[1,11,15,16]. In our patient, there were no obvious abnormalities on CT, but typical findings were detected on MRI, similar to that in current literature reports. Therefore, it is important to detect Wernicke encephalopathy in the early stages of the disease using MRI, since CT has a low sensitivity in the acute phase. Wernicke encephalopathy should be considered as one of the common differential diagnoses when patients develop unexplained altered mental status during radiotherapy while admitted to the Department of Oncology.

Thiamine plays a major role in glucose metabolism. The administration of glucose may thus accelerate the consumption of thiamine and hasten the onset of Wernicke encephalopathy. Our patient received no thiamine, but received continuous glucose solutions as a part of his parenteral nutrition supplement, which is consistent with that reported in the literature[17-19]. Therefore, glucose should be used with caution.

Once a diagnosis of Wernicke encephalopathy is suspected, it is advisable to administer thiamine as early as possible to prevent permanent neurological damage[20]. Although there are no published guidelines for the treatment of Wernicke encephalopathy in non-alcoholics patients, intravenous thiamine supplementation in the acute stage is currently recommended. Several researchers recommend that patients be treated with a high-dose thiamine regimen, consisting of 500 mg thiamine every 8 h intravenously for at least 2-3 d, followed by 250 mg thiamine once a day intravenously for 5 d[21]. In our patient, there was significant improvement in his mental state, but mild cognitive impairment remained due to the late diagnosis of the condition. Therefore, our objective in reporting this case is to emphasize the importance of early nutritional evaluation and diagnosis, so that lasting neurological sequelae can be avoided in patients with Wernicke encephalopathy.

CONCLUSION

Our case illustrates that Wernicke encephalopathy can occur in non-alcoholic patients with esophageal cancer. Clinicians should keep in mind that patients with esophageal cancer and underlying malnutrition are at a high risk of Wernicke encephalopathy. Nutritional evaluation and diagnosis are necessary at the earliest possible instance. Any clinical suspicion of Wernicke encephalopathy should be treated promptly with thiamine supplementation to prevent permanent neurological damage.

FOOTNOTES

Author contributions: Zhang Y and Jiang J were the patient's doctors, reviewed the literature, and contributed to manuscript drafting; Wang L reviewed the literature and contributed to manuscript drafting; Chen WY analyzed and interpreted the imaging findings; Zhang Y and Wang L were responsible for the revision of the manuscript for important intellectual content; all authors issued final approval for the version to be submitted.

Supported by the Scientific Technology Plan Program for Healthcare in Zhejiang Province, No. 2021KY1100; and the Key Discipline of Jiaxing General Practice Medicine Construction Project, No. 2019-fc-03.

Informed consent statement: Informed written consent was obtained from the patient for publication of this report and any accompanying images.

Conflict-of-interest statement: Dr. Zhang reports grants from Scientific Technology Plan Program for Healthcare in Zhejiang Province during the conduct of the study.

CARE Checklist (2016) statement: The authors have read the CARE Checklist (2016), and the manuscript was prepared and revised according to the CARE Checklist (2016).

Open-Access: This article is an open-access article that was selected by an in-house editor and fully peer-reviewed by external reviewers. It is distributed in accordance with the Creative Commons Attribution NonCommercial (CC BY-NC 4.0) license, which permits others to distribute, remix, adapt, build upon this work non-commercially, and license their derivative works on different terms, provided the original work is properly cited and the use is non-commercial. See: https://creativecommons.org/Licenses/by-nc/4.0/

Country/Territory of origin: China

ORCID number: Ye Zhang 0000-0001-9740-1502; Lei Wang 0000-0002-0246-1607; Jin Jiang 0000-0002-2518-0162; Wen-Yu Chen 0000-0002-4930-9530.

S-Editor: Yan JP
L-Editor: Wang TQ
P-Editor: Yan JP

REFERENCES

1 **Sinha S**, Kataria A, Kolla BP, Thusius N, Loukianova LL. Wernicke Encephalopathy-Clinical Pearls. *Mayo Clin Proc* 2019; **94**: 1065-1072 [PMID: 31171116 DOI: 10.1016/j.mayocp.2019.02.018]
2 **Vogrig A**, Zanoni T, Moretto G. Nystagmus and Lower Extremity Hyperalgesia After Colectomy. *JAMA* 2016; **316**: 1488-1489 [PMID: 27727364 DOI: 10.1001/jama.2016.13658]
3 **Harper CG**, Giles M, Finlay-Jones R. Clinical signs in the Wernicke-Korsakoff complex: a retrospective analysis of 131 cases diagnosed at necropsy. *J Neurol Neurosurg Psychiatry* 1986; **49**: 341-345 [PMID: 3701343 DOI: 10.1136/jnnp.49.4.341]

4 **Zuccoli G**, Gallucci M, Capellades J, Regnicolo L, Tumiati B, Giadás TC, Bottari W, Mandrioli J, Bertolini M. Wernicke encephalopathy: MR findings at clinical presentation in twenty-six alcoholic and nonalcoholic patients. *AJNR Am J Neuroradiol* 2007; **28**: 1328-1331 [PMID: 17698536 DOI: 10.3174/ajnr.A0544]

5 **Arita T**, Komatsu S, Kosuga T, Konishi H, Morimura R, Murayama Y, Kuriu Y, Shiozaki A, Ikoma H, Nakanishi M, Ichikawa D, Okamoto K, Otsuji E. [Laparoscopic Gastrostomy for a Patient with Wernicke's Encephalopathy after Gastrectomy--A Case Report with a Literature Review]. *Gan To Kagaku Ryoho* 2015; **42**: 2037-2039 [PMID: 26805256]

6 **D'Ettorre M**, Rosa F, Coppola A, Mele C, Alfieri S, Doglietto GB. Postoperative suspected Wernicke's encephalopathy in a rectal cancer patient: a case report. *J Palliat Care* 2012; **28**: 290-292 [PMID: 23413765]

7 **Zafar A**. Wernicke's encephalopathy following Roux en Y gastric bypass surgery. *Saudi Med J* 2015; **36**: 1493-1495 [PMID: 26620994 DOI: 10.15537/smj.2015.12.12643]

8 **Galvin R**, Bråthen G, Ivashynka A, Hillbom M, Tanasescu R, Leone MA; EFNS. EFNS guidelines for diagnosis, therapy and prevention of Wernicke encephalopathy. *Eur J Neurol* 2010; **17**: 1408-1418 [PMID: 20642790 DOI: 10.1111/j.1468-1331.2010.03153.x]

9 **Sriram K**, Manzanares W, Joseph K. Thiamine in nutrition therapy. *Nutr Clin Pract* 2012; **27**: 41-50 [PMID: 22223666 DOI: 10.1177/0884533611426149]

10 **Dhir S**, Tarasenko M, Napoli E, Giulivi C. Neurological, Psychiatric, and Biochemical Aspects of Thiamine Deficiency in Children and Adults. *Front Psychiatry* 2019; **10**: 207 [PMID: 31019473 DOI: 10.3389/fpsyt.2019.00207]

11 **Zuccoli G**, Pipitone N. Neuroimaging findings in acute Wernicke's encephalopathy: review of the literature. *AJR Am J Roentgenol* 2009; **192**: 501-508 [PMID: 19155417 DOI: 10.2214/AJR.07.3959]

12 **Yoshioka A**, Sato I, Onishi H, Ishida M. Subclinical thiamine deficiency identified by pretreatment evaluation in an esophageal cancer patient. *Eur J Clin Nutr* 2021; **75**: 564-566 [PMID: 32895510 DOI: 10.1038/s41430-020-00735-y]

13 **Day GS**, del Campo CM. Wernicke encephalopathy: a medical emergency. *CMAJ* 2014; **186**: E295 [PMID: 24016788 DOI: 10.1503/cmaj.130091]

14 **Guler A**, Alpaydin S, Sirin H, Calli C, Celebisoy N. A non-alcoholic Wernicke's encephalopathy case with atypical MRI findings: Clinic *vs* radiology. *Neuroradiol J* 2015; **28**: 474-477 [PMID: 26306933 DOI: 10.1177/1971400915598080]

15 **Manzo G**, De Gennaro A, Cozzolino A, Serino A, Fenza G, Manto A. MR imaging findings in alcoholic and nonalcoholic acute Wernicke's encephalopathy: a review. *Biomed Res Int* 2014; **2014**: 503596 [PMID: 25050351 DOI: 10.1155/2014/503596]

16 **Zuccoli G**, Santa Cruz D, Bertolini M, Rovira A, Gallucci M, Carollo C, Pipitone N. MR imaging findings in 56 patients with Wernicke encephalopathy: nonalcoholics may differ from alcoholics. *AJNR Am J Neuroradiol* 2009; **30**: 171-176 [PMID: 18945789 DOI: 10.3174/ajnr.A1280]

17 **Jin J**, Mulesa L, Carrilero Rouillet M. Trace Elements in Parenteral Nutrition: Considerations for the Prescribing Clinician. *Nutrients* 2017; **9** [PMID: 28452962 DOI: 10.3390/nu9050440]

18 **Harada D**, Nakayama M. Influence of Glucose Dosage in Parenteral Nutrition on Body Thiamine Levels in Rats. *Int J Med Sci* 2019; **16**: 1-7 [PMID: 30662322 DOI: 10.7150/ijms.28756]

19 **Gralak MA**, Dębski B, Drywień M. Thiamine deficiency affects glucose transport and β-oxidation in rats. *J Anim Physiol Anim Nutr (Berl)* 2019; **103**: 1629-1635 [PMID: 31259440 DOI: 10.1111/jpn.13146]

20 **Smith H**, McCoy M, Varughese K, Reinert JP. Thiamine Dosing for the Treatment of Alcohol-Induced Wernicke's Encephalopathy: A Review of the Literature. *J Pharm Technol* 2021; **37**: 107-113 [PMID: 34752552 DOI: 10.1177/8755122520962859]

21 **Ho PA**, York A, Rustad JK, Felde A, Stern TA. Non-Alcohol-Related Wernicke's Encephalopathy: Diagnosis and Treatment. *Prim Care Companion CNS Disord* 2021; **23** [PMID: 34651469 DOI: 10.4088/PCC.21f02968]

World Journal of Clinical Cases

Submit a Manuscript: https://www.f6publishing.com

World J Clin Cases 2022 June 16; 10(17): 5816-5824

DOI: 10.12998/wjcc.v10.i17.5816

ISSN 2307-8960 (online)

CASE REPORT

New approach for the treatment of vertical root fracture of teeth: A case report and review of literature

Xue Zhong, Ping Yan, Wei Fan

Specialty type: Medicine, research and experimental

Provenance and peer review: Unsolicited article; Externally peer reviewed.

Peer-review model: Single blind

Peer-review report's scientific quality classification

Grade A (Excellent): 0
Grade B (Very good): B
Grade C (Good): C
Grade D (Fair): 0
Grade E (Poor): 0

P-Reviewer: Garg P, India; Kukiattrakoon B, Thailand

Received: December 15, 2021
Peer-review started: December 15, 2021
First decision: January 26, 2022
Revised: January 31, 2022
Accepted: April 4, 2022
Article in press: April 4, 2022
Published online: June 16, 2022

Xue Zhong, Ping Yan, Wei Fan, School and Hospital of Stomatology, Wuhan University, Wuhan 430079, Hubei Province, China

Corresponding author: Wei Fan, PhD, Chief Physician, Reader (Associate Professor), School and Hospital of Stomatology, Wuhan University, No. 237 Luoyu Road, Wuhan 430079, Hubei Province, China. weifan@whu.edu.cn

Abstract

BACKGROUND

Vertical root fracture (VRF) is one of the most common reasons for tooth extraction, although various methods have been applied for saving teeth with VRF.

CASE SUMMARY

This case report describes a woman who had a sinus tract on the labial gingiva of the left maxillary central incisor for past two months. Periodontal probing revealed an 8–10 mm deep, narrow, isolated pocket on the palatal side of the tooth. Clinical and radiographic examination confirmed a longitudinal root fracture. A new approach using a combination of resin and iRoot BP Plus through intentional replantation was used for the treatment of the tooth. At one-year follow-up, the tooth remained asymptomatic with normal periodontal probing depth, and radiographic images showed almost normal bone and periodontal structures around the root.

CONCLUSION

This new approach may be developed as an effective method for saving teeth with VRF.

Key Words: Vertical root fracture; Intentional replantation; iRoot BP Plus; Resin; Teeth; Treatment; Case report

©The Author(s) 2022. Published by Baishideng Publishing Group Inc. All rights reserved.

Core Tip: This case report proposes a new approach for the treatment of teeth with vertical root fracture (VRF) using both resin and iRoot BP Plus through intentional replantation. This approach may be developed as an effective method to save teeth with VRF.

Citation: Zhong X, Yan P, Fan W. New approach for the treatment of vertical root fracture of teeth: A case report and review of literature. *World J Clin Cases* 2022; 10(17): 5816-5824
URL: https://www.wjgnet.com/2307-8960/full/v10/i17/5816.htm
DOI: https://dx.doi.org/10.12998/wjcc.v10.i17.5816

INTRODUCTION

Vertical root fracture (VRF) is a longitudinally oriented fracture of the root and can be classified as an incomplete or complete VRF based on the degree of separation of the fragments according to Leubke's classification[1-4]. VRF is a serious complication with poor prognosis in endodontically treated teeth. The overall prevalence of VRF reported in retrospective studies is 3%–5%, but the prevalence of VRF in endodontically treated teeth is approximately 3.69%–25%[1,3]. Even if extraction is usually the first choice of management for teeth with VRF, various other methods to preserve the teeth have also been described in many case reports, such as using adhesive composite resin[4-6], CO_2 and Nd:YAG laser[7], mineral trioxide aggregates (MTAs)[8,9] and biodentine[10,11].

Adhesive composite resin is commonly used to bond fractured segments owing to their superior adhesive strength. Intentional replantation combined with bonding of fractured segments using adhesive composite resin has been reported as a successful treatment method for preserving teeth with VRF. Despite this, owing to the poor tissue attachment to the resin surface, deep and narrow periodontal pockets along the bonded fracture could easily recur.

iRoot BP Plus is a ready-to-use calcium silicate-based bioceramic material suitable for repairing various root canal perforations or resorptions because of its ability to induce tissue attachment and mineralization[12-15]. Based on its excellent biological features, iRoot BP Plus is an ideal material for repairing VRF. However, the bond strength between iRoot BP Plus and dentin is not as strong as that of the adhesive composite resin when holding the fractured segments in position[16].

Based on these concerns, in the present case combination of adhesive composite resin and iRoot BP Plus was used to repair a VRF through intentional replantation. This new approach may be developed as an effective method for saving teeth with VRF. This case report was prepared according to the Preferred Reporting Items for Case Reports in Endodontics (PRICE) 2020[17].

CASE PRESENTATION

Chief complaints

A 27-year-old Chinese woman was referred to our department for treatment of pustules on the labial gingiva of the maxillary anterior teeth.

History of present illness

The pustule occurred two months ago, and the patient reported that tooth #9 (left maxillary central incisor) had undergone root canal treatment (RCT) and full crown restoration several years ago.

History of past illness

The patient denied any relevant past medical history.

Personal and family history

No relevant personal and family history.

Physical examination

Intraoral examination revealed that tooth #9 was restored with a full crown and that there was a sinus tract on the labial gingival mucosa near the apical area of tooth #9 (Figure 1A). The tooth was sensitive to vertical percussion and did not respond to thermal testing. Periodontal probing revealed an 8–10 mm deep narrow isolated pocket on the palatal side of the tooth (Figure 1B).

Laboratory examinations

The results of laboratory examinations were within normal range.

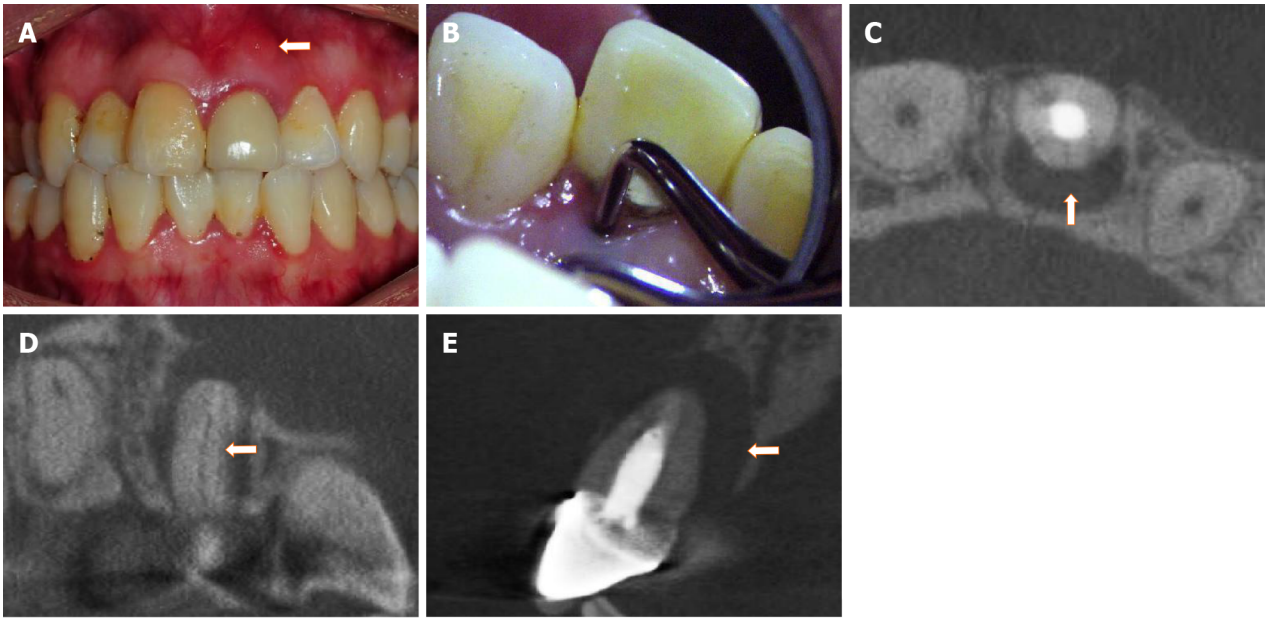

DOI: 10.12998/wjcc.v10.i17.5816 **Copyright** ©The Author(s) 2022.

Figure 1 Preoperative images. A: Sinus on the labial gingival mucosa near the apical region of tooth #9; B: Deep narrow isolated pocket on the palatal aspect of tooth #9; C: A cone beam computed tomography (CBCT) cross-sectional image showing a fracture line (arrowhead) on the palatal aspect of tooth #9; D: A CBCT coronal-section image showing a fracture line (arrowhead) from the cervical region to the apex; E: A CBCT sagittal-section image showing a large region of bone destruction (arrowhead) in the palatal and apical areas of the root.

Imaging examinations

Cone beam computed tomography (CBCT) (J Morita Corporation, Kyoto, Japan) images confirmed that the tooth had undergone RCT, and a vertical fracture line on the palatal side of the root was identified from the cervical area to the apex (Figure 1C and D). Furthermore, there was a large area of bone destruction around the apical and palatal sides of the root (Figure 1E).

FINAL DIAGNOSIS

Based on clinical and CBCT examinations, the final diagnosis of tooth #9 was VRF.

TREATMENT

After communicating with the patient, the intentional replantation method was selected for the treatment of the tooth, and informed consent was obtained. However, the prognosis of this treatment was unpredictable at the moment. The timeline of the treatment and review of this case is summarized in Table 1.

After local anesthesia, tooth #9 was extracted carefully with dental forceps only touching the crown of the tooth, and then the root of the tooth was covered with wet gauze saturated with normal saline throughout the procedure. The vertical fracture line was observed under a dental microscope (Zumax Medical Co. Ltd., Suzhou, China) after granulation tissue was carefully removed using a curette (Figure 2A). The apical 3 mm of the root was excised (Figure 2B). A 3-mm retrograde canal cavity was prepared using an ultrasonic tip and filled with iRoot BP Plus (Innovative Bioceramix Inc., Vancouver, Canada) (Figure 2C). The vertical fracture line was then evenly enlarged to approximately 1.5 mm in width using a high-speed handpiece with a fissure bur along the fracture line (Figure 2D). To enhance fixation strength, two trapezoidal retention forms were prepared on both sides of the fracture line at the coronal 1/3 and apical 1/3 of the line. The width of the outer side of the trapezoidal retention form was approximately 3 mm and the width of the inner side was approximately 2 mm. The depth of the retention form was approximately 2 mm. After applying the bonding agent, a light-cure composite resin (Ketac Molar Easymix; 3M ESPE, St Paul, MN) was filled into the fracture line and retention form (Figure 2E). After the resin was cured, the surface resin was removed to a depth of approximately 1 mm using a fissure bur, and the rest of the resin surface was covered with iRoot BP Plus (Figure 2F). The tooth was then cleaned with normal saline and replanted into the root socket using gentle pressure (Figure 2G). The tooth was splinted to the adjacent teeth using a ligation wire. The occlusion was

Table 1 The timeline for the treatments and reviews of this case

Treatment or review	Fracture treatment and intentional replantation	One-month review	Three months review	Six-months review	One-year review
Date	2020-09-17	2020-10-16	2020-12-16	2021-03-14	2021-09-15

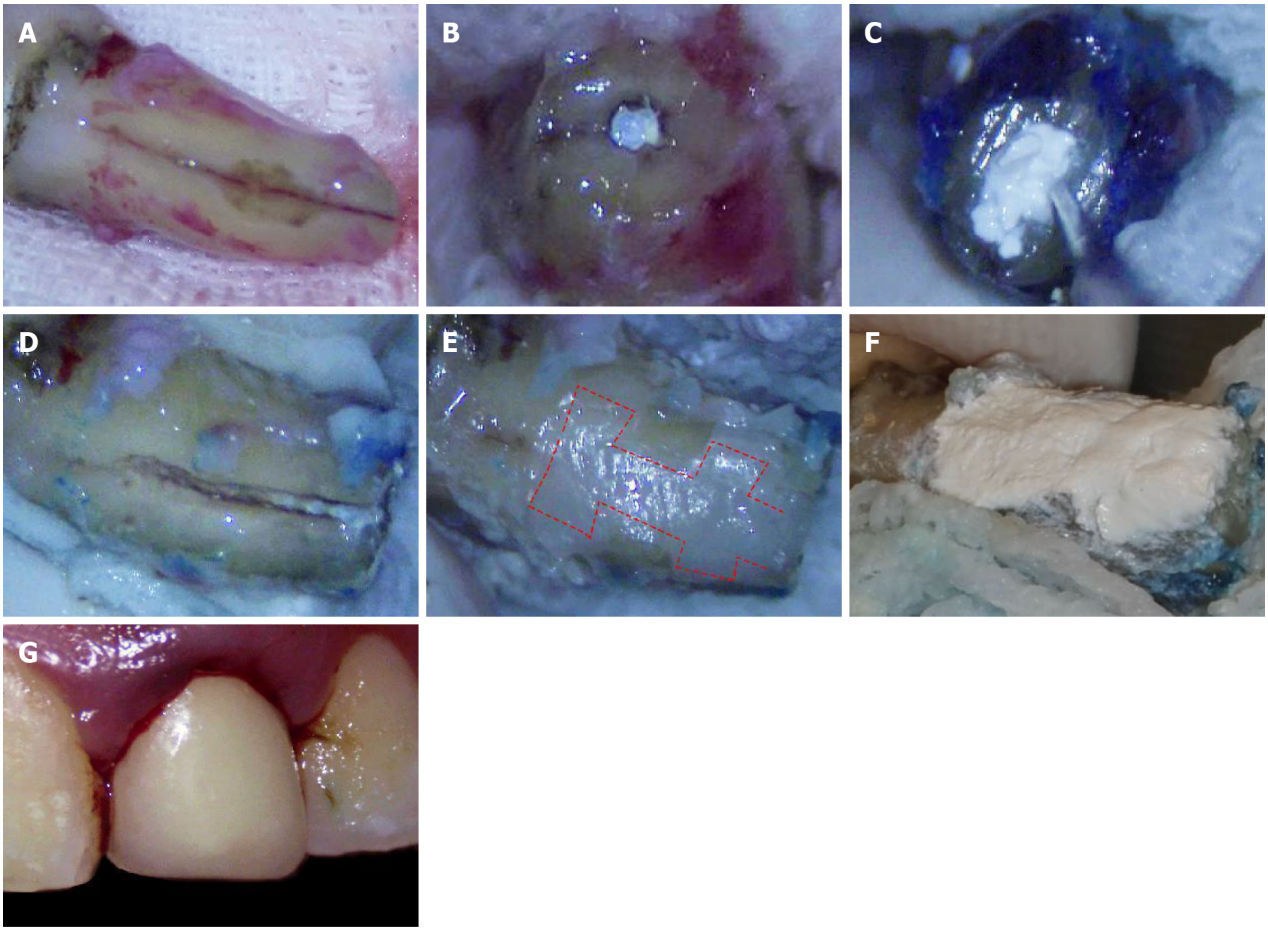

DOI: 10.12998/wjcc.v10.i17.5816 **Copyright** ©The Author(s) 2022.

Figure 2 Operative images. A: A vertical root fracture line after the granulation tissue was removed; B: Excision of the 3-mm apex; C: Filling of the retrograde canal with iRoot BP Plus after retrograde canal preparation; D: Cleaning and enlargement of the fracture line; E: Filling of the fracture and trapezoidal retention forms (shown by dotted line) with resin; F: Covering of the resin surface with iRoot BP Plus; G: Replantation of the tooth.

checked after replantation, and using occlusal adjustment, early contact in centric occlusion and lateral or protrusive movements were avoided. Posttreatment, oral hygiene instructions were provided to the patient.

OUTCOME AND FOLLOW-UP

An immediate postoperative radiograph (Kavo Focus, Tuusula, Uusima, Finland) was obtained to confirm the correct position of tooth #9 (Figure 3A). The follow-up examinations were scheduled at one month, three months, six months, and one year after the treatment. At the one-month follow-up, the mobility of tooth #9 returned to the normal range and the ligation wire was removed. The radiograph showed slightly reduced apical radiolucency (Figure 3B). At three-month recall, the radiograph revealed that the periapical and periodontal radiolucency was significantly reduced (Figure 3C). At six-month follow-up, radiography and CBCT revealed significant bone regeneration around the root (Figure 3D-F). The tooth was asymptomatic, with a normal gingival appearance, periodontal probing depth, and mobility (Figure 3G and H). At the one-year follow-up, the tooth remained asymptomatic with normal gingival appearance, periodontal probing depth, and mobility (Figure 4A and B). The radiograph, together with the CBCT image, showed almost normal bone and periodontal structures around the root (Figure 4C-E), and the patient was satisfied with the treatment outcome.

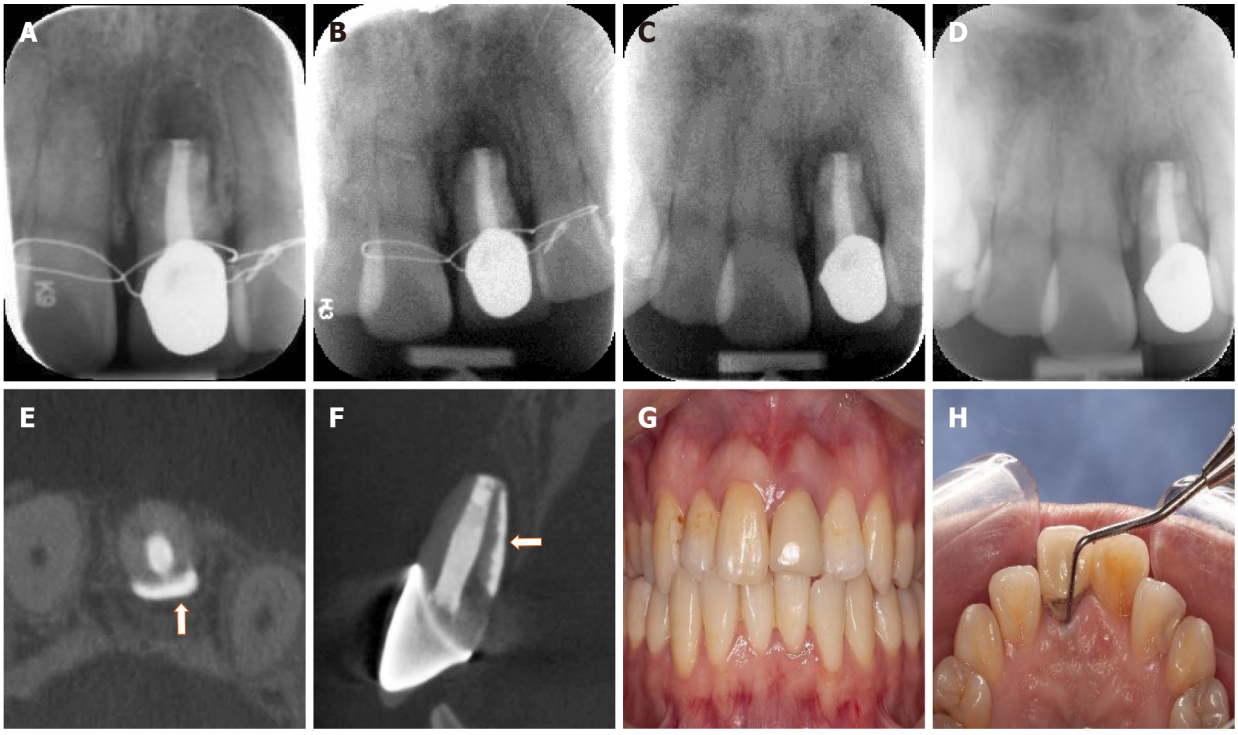

DOI: 10.12998/wjcc.v10.i17.5816 **Copyright** ©The Author(s) 2022.

Figure 3 Postoperative images within six months. A: Immediate postoperative radiograph; B: One-month review radiograph; C: Three-month review radiograph; D: Six-month review radiograph; E and F: Cone beam computed tomography cross-sectional and sagittal-section images at the six-month review showing significant bone and periodontal regeneration (arrowhead) around the root; G: Labial view of tooth #9 at the six-month review; H: Palatal periodontal probing of tooth #9 at the six-month review showing normal periodontal probing depth.

DISCUSSION

Intentional replantation is regarded as the last option for the treatment of periodontitis, pulpitis, and post-traumatic cases, and is defined as the intentional removal of a tooth and replantation into original socket, and fixation *in situ* after evaluation and treatment[18]. This procedure allows the extracted tooth to be treated extraorally, and the infected tissue to be thoroughly removed under a microscope[6]. In the present case, the left maxillary central incisor was vertically fractured and a large amount of granulation tissue was found around the fracture line and apex. To remove the infected tissue and repair the fracture more accurately, an intentional replantation method was used for the treatment. After tooth extraction, both the root apex and fracture line were cleaned and treated.

Factors that may affect the prognosis of VRF treatment include the reattachment of periodontal tissue, alveolar bone regeneration, proper sealing of the fracture line, and prevention of refracture. The use of adhesive composite resin has been widely reported in the literature for the treatment of VRF[4-6,19-23]. The ideal bonding and repair material for VRF should have the following features to allow periodontal tissue attachment: sufficient fixation strength, short setting time, easy application, hydrophilicity, bacteriostaticity, and biocompatibility[24]. Recently, 4-methacryloxyethyl trimellitate anhydride/methyl methacrylate-tri-n-butylborane (4-META/MMA-TBB) resin, a self-cure adhesive resin cement, has been primarily used for splinting mobile teeth or treating fractured teeth with successful reconstruction outcomes[6,23]. In addition to the advantages of adhesive properties to dentin, Tanaka *et al*[24] reported that 4-META/MMATBB resin adheres to cementum by inducing the formation of hybridized cementum in the short term, which can provide a good seal for bonding vertically fractured roots. However, Sugaya *et al*[25] found no cementum-like hard tissue formation on the 4-META/MMA-TBB resin surface, and it was difficult to control polymerization of the material.

In contrast, the endodontic reparation cement ProRoot MTA[8,9] and Biodentine[10,11] have also been used for the treatment of VRF. These materials showed an effective seal against dentin and cementum and could promote biological repair and regeneration of periodontal tissue. Compared with MTA, Biodentine has a shorter setting time, is resistant to hydrolysis during setting, and releases more calcium and silicon, which is beneficial for the mineralization of bone and dentin[11]. Similarly, iRoot BP Plus is a hydrophilic calcium silicate-based bioceramic material. iRoot BP Plus has excellent mechanical properties, sealing ability, and antibacterial activity[15,26]. Moreover, iRoot BP Plus exhibits outstanding biological characteristics. Mahmood *et al*[27] reported high biocompatibility and desired repair of pulpal and periodontal tissues after iRoot BP Plus treatment of lateral perforations in the roots of rat incisors. Due to the biocompatibility of iRoot BP Plus and the satisfactory bonding strength of the

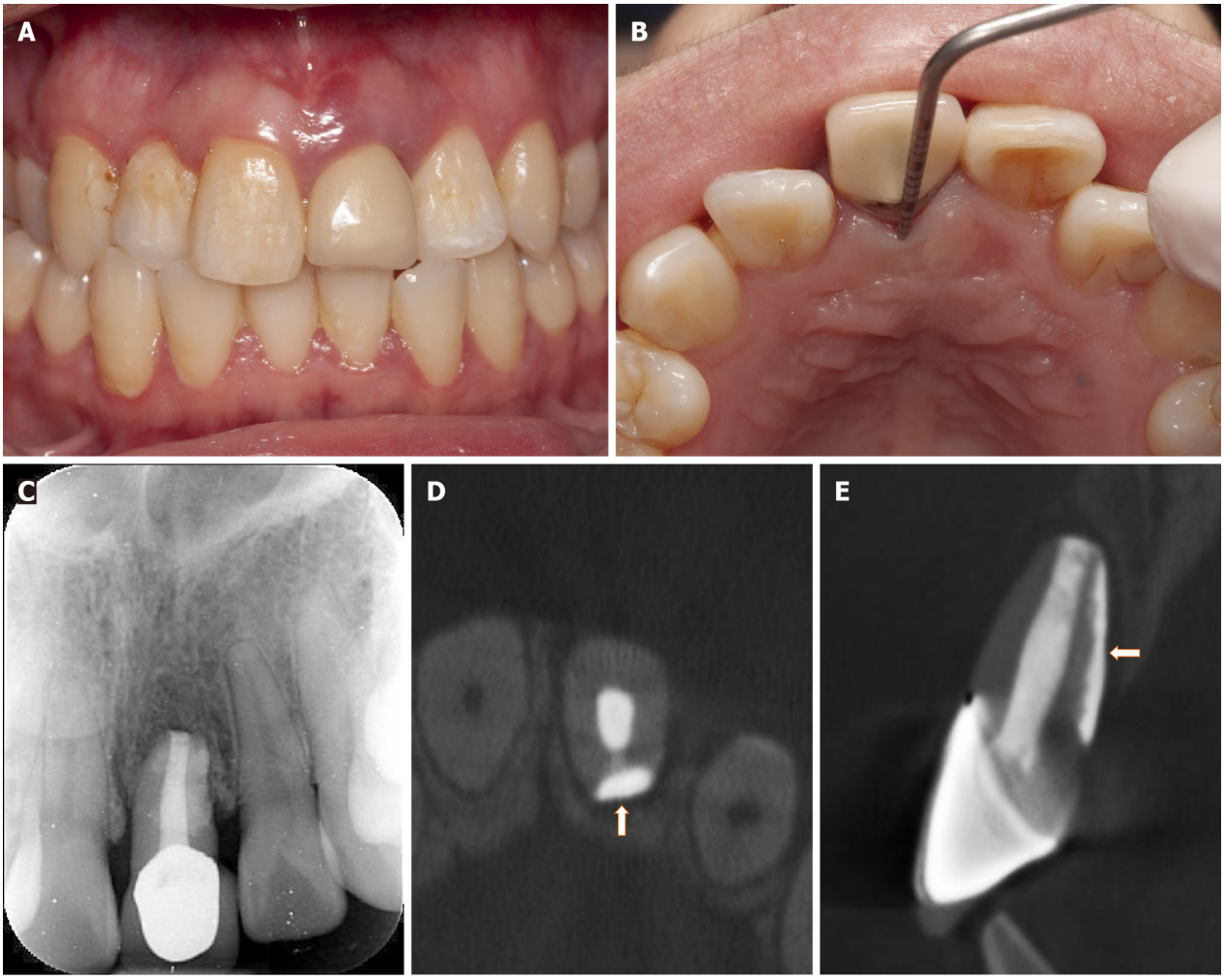

DOI: 10.12998/wjcc.v10.i17.5816 **Copyright** ©The Author(s) 2022.

Figure 4 Postoperative images at one-year review. A: Labial view of tooth #9 at one-year review; B: Palatal periodontal probing of tooth #9 at one-year review showing normal periodontal probing depth; C-E: Radiograph and cone beam computed tomography cross-sectional and sagittal-section images at one-year review showing almost normal bone and periodontal structure (arrowhead) around the root.

adhesive composite resin, this study combined these two materials to repair vertical fractures. Furthermore, repeated stress overloading can result in fatigue failure of the tooth structure. Even normal functional stresses might result in VRF in case of tooth structure with reduced mechanical properties caused by aging, pulp necrosis, and endodontic therapy[28]. It is crucial to enhance the fixation strength of the vertical fracture line during the treatment of VRF to reduce the possibility of future refracture. However, even though composite resin has a stronger bonding strength than bioceramic materials[29], fixation strength is also closely related to the shape of the defect. Studies have confirmed that the retention form is necessary to improve fixation strength, and the design of the retention form could effectively increase the contact area and enhance the retention force of the repair materials[30]. Consequently, two trapezoidal retention forms were prepared on both sides of the fracture line to obtain a higher fixation strength and reduce the possibility of future refracture (Figure 5). After the fracture line and retention form were filled with resin, a thin layer of surface resin was evenly removed, and iRoot BP Plus was applied on top of it so that both, bonding strength and a pro-osteogenic surface could be achieved. In addition, occlusal adjustment was performed to facilitate the recovery of the replanted tooth.

The difference in the follow-up period may have influenced the judgment of the treatment results. Through a follow-up study of 1000 cases treated by endodontic surgery, Rud *et al*[31] reported that a standard follow-up should be at one year after the operation because most changes take place within the first year after the operation, and very few cases that are successful at the one-year recall shift to questionable or failed treatment outcomes in subsequent follow-ups[31]. Therefore, one-year follow-up in this case might be sufficient to demonstrate the primary treatment outcome, although a longer observation period is still necessary.

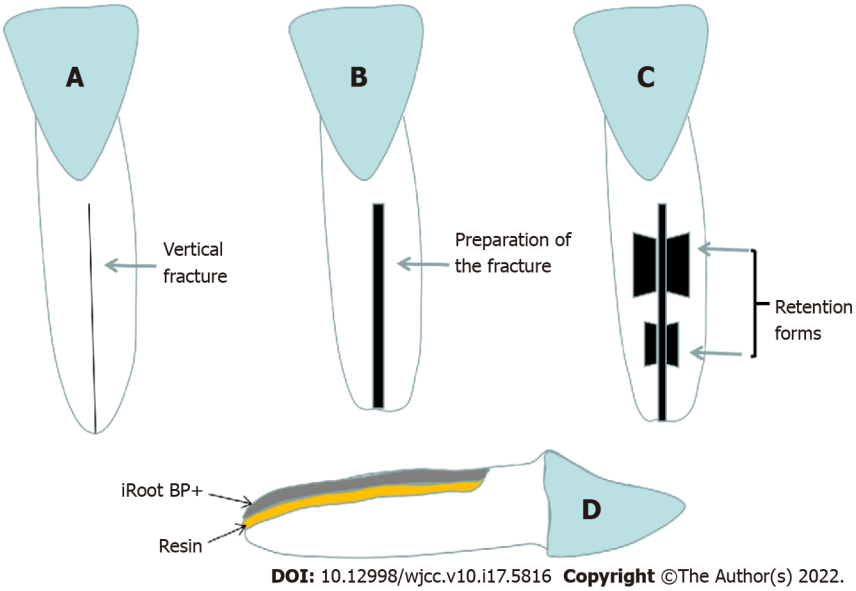

DOI: 10.12998/wjcc.v10.i17.5816 **Copyright** ©The Author(s) 2022.

Figure 5 Schematic illustration of the fracture and retention form preparation. A: Original vertical root fracture line; B: Cleaning and enlargement of the fracture line; C: Preparation of the trapezoidal retention forms along the fracture; D: Side view of the filling of the fracture and retention forms using combination of resin and iRoot BP Plus.

CONCLUSION

In summary, the new approach in this study successfully combined the resin and bioceramic material to repair VRF through a retention form on both sides of the fracture and the intentional replantation method. Additional clinical applications and longer observation times are necessary to further test the outcomes of this approach. This approach may provide a new treatment design for VRF.

FOOTNOTES

Author contributions: Zhong X collected the information, assisted in the treatment of this case, and prepared the manuscript; Fan W and Yan P designed the treatment procedure, performed the surgery, and reviewed the manuscript.

Informed consent statement: Signed informed consent has been obtained from the patient.

Conflict-of-interest statement: The authors declare no conflicts of interest.

CARE Checklist (2016) statement: The authors have read the CARE Checklist (2016), and the manuscript was prepared and revised according to the CARE Checklist (2016).

Open-Access: This article is an open-access article that was selected by an in-house editor and fully peer-reviewed by external reviewers. It is distributed in accordance with the Creative Commons Attribution NonCommercial (CC BY-NC 4.0) license, which permits others to distribute, remix, adapt, build upon this work non-commercially, and license their derivative works on different terms, provided the original work is properly cited and the use is non-commercial. See: https://creativecommons.org/Licenses/by-nc/4.0/

Country/Territory of origin: China

ORCID number: Xue Zhong 0000-0002-7933-9917; Ping Yan 0000 0002 4171 5841; Wei Fan 0000-0002-3688-1896.

Corresponding Author's Membership in Professional Societies: Chinese Stomatological Association, No. 010515.

S-Editor: Fan JR
L-Editor: A
P-Editor: Fan JR

REFERENCES

1 **Liao WC**, Chen CH, Pan YH, Chang MC, Jeng JH. Vertical Root Fracture in Non-Endodontically and Endodontically Treated Teeth: Current Understanding and Future Challenge. *J Pers Med* 2021; **11** [PMID: 34945847 DOI: 10.3390/jpm11121375]

2 **Colleagues for excellence**. Cracking the cracked tooth code: detection and treatment of various longitudinal tooth fractures. Chicago: American Association of Endodontics; 2008

3 **Dhawan A**, Gupta S, Mittal R. Vertical root fractures: An update review. *J Res Dent* 2014; **2**: 107-113 [DOI: 10.4103/2321-4619.143457]

4 **Kallel I**, Moussaoui E, Chtioui F, Douki N. Diagnosis and Managment of Maxillary Incisor with Vertical Root Fracture: A Clinical Report with Three-Year Follow-Up. *Case Rep Dent* 2018; **2018**: 4056390 [PMID: 29552361 DOI: 10.1155/2018/4056390]

5 **Kawai K**, Masaka N. Vertical root fracture treated by bonding fragments and rotational replantation. *Dent Traumatol* 2002; **18**: 42-45 [PMID: 11841465 DOI: 10.1034/j.1600-9657.2002.180106.x]

6 **Okaguchi M**, Kuo T, Ho YC. Successful treatment of vertical root fracture through intentional replantation and root fragment bonding with 4-META/MMA-TBB resin. *J Formos Med Assoc* 2019; **118**: 671-678 [PMID: 30145002 DOI: 10.1016/j.jfma.2018.08.004]

7 **Arakawa S**, Cobb CM, Rapley JW, Killoy WJ, Spencer P. Treatment of root fracture by CO2 and Nd:YAG lasers: an *in vitro* study. *J Endod* 1996; **22**: 662-667 [PMID: 9220751 DOI: 10.1016/S0099-2399(96)80060-4]

8 **Taschieri S**, Tamse A, Del Fabbro M, Rosano G, Tsesis I. A new surgical technique for preservation of endodontically treated teeth with coronally located vertical root fractures: a prospective case series. *Oral Surg Oral Med Oral Pathol Oral Radiol Endod* 2010; **110**: e45-e52 [PMID: 21112525 DOI: 10.1016/j.tripleo.2010.07.014]

9 **Taschieri S**, Bortolin M, Weinstein T, Del Fabbro M. Preservation of an injured vital tooth using ultrasonic device and mineral trioxide aggregate. *Minerva Stomatol* 2011; **60**: 467-477 [PMID: 21956353]

10 **Hadrossek PH**, Dammaschke T. New treatment option for an incomplete vertical root fracture--a preliminary case report. *Head Face Med* 2014; **10**: 9 [PMID: 24670232 DOI: 10.1186/1746-160X-10-9]

11 **Baranwal HC**, Singh N, Kumar N, Garg R, Yadav J, Tripathi R. New Approach in the Management of Vertical Root Fracture with the Help of Biodentine and CBCT. *Case Rep Dent* 2020; **2020**: 2806324 [PMID: 33005457 DOI: 10.1155/2020/2806324]

12 **Lee GW**, Yoon JH, Jang JH, Chang HS, Hwang YC, Hwang IN, Oh WM, Lee BN. Effects of newly-developed retrograde filling material on osteoblastic differentiation in vitro. *Dent Mater J* 2019; **38**: 528-533 [PMID: 30971649 DOI: 10.4012/dmj.2018-124]

13 **Yang Y**, Xia B, Xu Z, Dou G, Lei Y, Yong W. The effect of partial pulpotomy with iRoot BP Plus in traumatized immature permanent teeth: A randomized prospective controlled trial. *Dent Traumatol* 2020; **36**: 518-525 [PMID: 32348009 DOI: 10.1111/edt.12563]

14 **Mahgoub N**, Alqadasi B, Aldhorae K, Assiry A, Altawili ZM, Tao Hong. Comparison between iRoot BP Plus (EndoSequence Root Repair Material) and Mineral Trioxide Aggregate as Pulp-capping Agents: A Systematic Review. *J Int Soc Prev Community Dent* 2019; **9**: 542-552 [PMID: 32039073 DOI: 10.4103/jispcd.JISPCD_249_19]

15 **Jeevani E**, Jayaprakash T, Bolla N, Vemuri S, Sunil CR, Kalluru RS. "Evaluation of sealing ability of MM-MTA, Endosequence, and biodentine as furcation repair materials: UV spectrophotometric analysis". *J Conserv Dent* 2014; **17**: 340-343 [PMID: 25125846 DOI: 10.4103/0972-0707.136449]

16 **Hursh KA**, Kirkpatrick TC, Cardon JW, Brewster JA, Black SW, Himel VT, Sabey KA. Shear Bond Comparison between 4 Bioceramic Materials and Dual-cure Composite Resin. *J Endod* 2019; **45**: 1378-1383 [PMID: 31492579 DOI: 10.1016/j.joen.2019.07.008]

17 **Nagendrababu V**, Chong BS, McCabe P, Shah PK, Priya E, Jayaraman J, Pulikkotil SJ, Setzer FC, Sunde PT, Dummer PMH. PRICE 2020 guidelines for reporting case reports in Endodontics: a consensus-based development. *Int Endod J* 2020; **53**: 619-626 [PMID: 32090342 DOI: 10.1111/iej.13285]

18 **Wang L**, Jiang H, Bai Y, Luo Q, Wu H, Liu H. Clinical outcomes after intentional replantation of permanent teeth: A systematic review. *Bosn J Basic Med Sci* 2020; **20**: 13-20 [PMID: 30684952 DOI: 10.17305/bjbms.2019.3937]

19 **Oztürk M**, Unal GC. A successful treatment of vertical root fracture: a case report and 4-year follow-up. *Dent Traumatol* 2008; **24**: e56-e60 [PMID: 18821949 DOI: 10.1111/j.1600-9657.2008.00705.x]

20 **Moradi Majd N**, Akhtari F, Araghi S, Homayouni H. Treatment of a vertical root fracture using dual-curing resin cement: a case report. *Case Rep Dent* 2012; **2012**: 985215 [PMID: 23316397 DOI: 10.1155/2012/985215]

21 **Arikan F**, Franko M, Gürkan A. Replantation of a vertically fractured maxillary central incisor after repair with adhesive resin. *Int Endod J* 2008; **41**: 173-179 [PMID: 18042224 DOI: 10.1111/j.1365-2591.2007.01334.x]

22 **Dogan MC**, Akgun EO, Yoldas HO. Adhesive tooth fragment reattachment with intentional replantation: 36-month follow-up. *Dent Traumatol* 2013; **29**: 238-242 [DOI: 10.1111/j.1600-9657.2012.01144.x]

23 **Unver S**, Onay EO, Ungor M. Intentional re-plantation of a vertically fractured tooth repaired with an adhesive resin. *Int Endod J* 2011; **44**: 1069-1078 [PMID: 21902699 DOI: 10.1111/j.1365-2591.2011.01922.x]

24 **Tanaka S**, Sugaya T, Kawanami M, Nodasaka Y, Yamamoto T, Noguchi H, Tanaka Y, Ikeda T, Sano H, Sidhu SK. Hybrid layer seals the cementum/4-META/MMA-TBB resin interface. *J Biomed Mater Res B Appl Biomater* 2007; **80**: 140-145 [PMID: 16680694 DOI: 10.1002/jbm.b.30578]

25 **Sugaya T**, Tomita M, Motoki Y, Zaman K, Miyaji H, Kawanami M. Periodontal tissue repair after sealing of the gap in vertical root fracture. *Odontology* 2017; **105**: 202-207 [PMID: 27655624 DOI: 10.1007/s10266-016-0270-5]

26 **Elshamy FM**, Singh G, Elraih H, Gupta I, Idris FA. Antibacterial Effect of New Bioceramic Pulp Capping Material on the Main Cariogenic Bacteria. *J Contemp Dent Pract* 2016; **17**: 349-353 [PMID: 27443359 DOI: 10.5005/jp-journals-10024-1854]

27 **Mahmood Talabani R**, Taha Garib B, Masaeli R. The Response of the Pulp-Dentine Complex, PDL, and Bone to Three Calcium Silicate-Based Cements: A Histological Study in an Animal Rat Model. *Bioinorg Chem Appl* 2020; **2020**: 9582165

[PMID: 32351551 DOI: 10.1155/2020/9582165]

28 **Tang W**, Wu Y, Smales RJ. Identifying and reducing risks for potential fractures in endodontically treated teeth. *J Endod* 2010; **36**: 609-617 [PMID: 20307732 DOI: 10.1016/j.joen.2009.12.002]

29 **Kaup M**, Dammann CH, Schäfer E, Dammaschke T. Shear bond strength of Biodentine, ProRoot MTA, glass ionomer cement and composite resin on human dentine ex vivo. *Head Face Med* 2015; **11**: 14 [PMID: 25908430 DOI: 10.1186/s13005-015-0071-z]

30 **Gilboe DB**, Teteruck WR. Fundamentals of extracoronal tooth preparation. Part I. Retention and resistance form. 1974. *J Prosthet Dent* 2005; **94**: 105-107 [PMID: 16046962 DOI: 10.1016/j.prosdent.2005.02.018]

31 **Rud J**, Andreasen JO, Jensen JE. A follow-up study of 1,000 cases treated by endodontic surgery. *Int J Oral Surg* 1972; **1**: 215-228 [PMID: 4199169 DOI: 10.1016/s0300-9785(72)80014-0]

World Journal of Clinical Cases

Submit a Manuscript: https://www.f6publishing.com

World J Clin Cases 2022 June 16; 10(17): 5825-5832

DOI: 10.12998/wjcc.v10.i17.5825

ISSN 2307-8960 (online)

CASE REPORT

Ultrasound-guided microwave ablation as a palliative treatment for mycosis fungoides eyelid involvement: A case report

Yan-Wei Chen, Hai-Zhen Yang, Shuang-Shuang Zhao, Zheng Zhang, Zhe-Ming Chen, Hua-Hui Feng, Mao-Hui An, Ke-Ke Wang, Ran Duan, Bao-Ding Chen

Specialty type: Radiology, nuclear medicine and medical imaging

Provenance and peer review: Unsolicited article; Externally peer reviewed.

Peer-review model: Single blind

Peer-review report's scientific quality classification

Grade A (Excellent): 0
Grade B (Very good): B
Grade C (Good): 0
Grade D (Fair): 0
Grade E (Poor): 0

P-Reviewer: Sartori S, Italy

Received: December 6, 2021
Peer-review started: December 6, 2021
First decision: March 7, 2022
Revised: March 11, 2022
Accepted: April 3, 2022
Article in press: April 3, 2022
Published online: June 16, 2022

Yan-Wei Chen, Hai-Zhen Yang, Shuang-Shuang Zhao, Zheng Zhang, Zhe-Ming Chen, Hua-Hui Feng, Mao-Hui An, Ke-Ke Wang, Ran Duan, Bao-Ding Chen, Department of Medical Ultrasound, The Affiliated Hospital of Jiangsu University, Zhenjiang 212000, Jiangsu Province, China

Corresponding author: Bao-Ding Chen, MD, Doctor, Professor, Department of Medical Ultrasound, The Affiliated Hospital of Jiangsu University, No. 438 Jiefang Road, Zhenjiang 212000, Jiangsu Province, China. alphalife@163.com

Abstract

BACKGROUND

Mycosis fungoides (MF) is a form of lymphoma derived from heterogeneous T cells, and eyelid involvement is extremely rare. The common methods to treat eyelid involvement are radiotherapy and chemotherapy, but their efficacies are limited. Herein, we report a case of advanced-stage MF eyelid involvement, propose ultrasound (US)-guided microwave ablation (MWA) therapy and present a literature review.

CASE SUMMARY

A male patient was admitted to our hospital in June 2018 and diagnosed with MF *via* radiological and histopathological examinations. The patient's condition was not well controlled by various conventional chemotherapies. US-guided MWA was performed to relieve the patient's symptoms and improve his quality of life, showing satisfactory efficacy.

CONCLUSION

Eyelid involvement is one of the most troublesome clinical problems for advanced-stage MF patients. This is the first report on the use of US-guided MWA as a palliative therapy for MF eyelid involvement; the treatment successfully relieved the patient's clinical symptoms and reduced his anxiety behaviours. Our study sheds new light on methods for improving the clinical management of eyelid involvement in MF.

Key Words: Mycosis fungoides; Cutaneous lymphomas; Eyelid involvement; Microwave ablation; Palliative care; Case report

©The Author(s) 2022. Published by Baishideng Publishing Group Inc. All rights reserved.

Core Tip: In this case report, we propose the use of ultrasound-guided percutaneous microwave ablation for the treatment of advanced mycosis fungoides eyelid involvement. Compared with traditional surgical methods, it has less trauma, faster recovery and fewer side effects. As a palliative treatment method, it can greatly alleviate the patient's clinical symptoms and improve the quality of life.

Citation: Chen YW, Yang HZ, Zhao SS, Zhang Z, Chen ZM, Feng HH, An MH, Wang KK, Duan R, Chen BD. Ultrasound-guided microwave ablation as a palliative treatment for mycosis fungoides eyelid involvement: A case report. *World J Clin Cases* 2022; 10(17): 5825-5832
URL: https://www.wjgnet.com/2307-8960/full/v10/i17/5825.htm
DOI: https://dx.doi.org/10.12998/wjcc.v10.i17.5825

INTRODUCTION

Mycosis fungoides (MF) is the most common form of cutaneous T-cell lymphoma (CTCL), accounting for approximately 50% of all cutaneous primary lymphomas[1]. Most MF patients show a chronic course with slow progression; however, nonspecific features such as skin patches and plaques can result in misdiagnoses and rapidly progressing disease[2]. Advanced-stage MF has a worse prognosis, and only a few patients achieve long-term survival with allogeneic stem cell transplantation[3]. Ultrasound (US)-guided microwave ablation (MWA) is a novel method for inoperable tumours and has been proven to be effective for various tumours, namely, lung, prostate, breast, colon, rectum, lung and cervix cancers[4]. The main purpose of palliative MWA for malignancies is to reduce tumour burden, control tumour progression and achieve symptom relief[5]. Here, we described the case of a male patient treated with US-guided MWA for MF eyelid involvement.

CASE PRESENTATION

Chief complaints

A 52-year-old man was admitted to our hospital in March 2020 because of continuous enlargement of the left eyelid mass with swelling and pain.

History of present illness

The patient initially presented to our hospital with small hard bulges that emerged from both facial aspects after a frontofacial crash in June 2018. The rash tissue on the right side of the patient's face was biopsied and confirmed to be MF by histopathology. The patient subsequently received twelve courses of COP (cyclophosphamide 400 mg day 1-5; prednisone 100 mg day 1-5; vincristine 2 mg day 1). Chidamide was suggested after rapid disease progression, but the patient refused it initially for economic reasons. In August 2019, the patient presented with swelling of the left orbital tissue and severe skin rashes on the forehead and cheeks. CVP (cyclophosphamide 1200 mg day 1; vincristine 2 mg day 1; prednisone 100 mg day 1-5), DHAX (oxaliplatin 250 mg day 1; cytarabine 3300 mg day 2; dexamethasone 40 mg day 1-4) and CHOPE (doxorubicin 80 mg day 1; vincristine 2 mg day 1; cyclophosphamide 1200 mg day 1; prednisone 100 mg day 1-5; etoposide 100 mg day 1-3) regimens were attempted continuously, but the eyelid mass and rashes were not significantly improved.

History of past illness

The patient was diagnosed with syphilis two years prior and received treatment.

Personal and family history

There was no relevant personal or family history.

Physical examination

Physical examination revealed that the skin was scattered with rashes, and a palpable mass approximately 2 cm × 2 cm in size with tenderness was detected in the right groin. There were multiple skin masses and plaque-like rashes on the frontal face; the largest was an approximately 3 cm × 4 cm mass on the left eyelid.

Laboratory examinations

During hospitalization, the patient's leukocyte count was 13.5 × 10^9/L (reference range: 3.5-9.5 × 10^9/L), his lymphocyte ratio was 14.7% (reference range: 20%-50%), the monocyte ratio was 13.3% (reference

range: 3%-10%), his red blood count was 3.18 × 10^{12}/L (reference range: 4.3-5.8 × 10^{12}/L), and high-the sensitivity C-reactive protein (hsCRP) level was 24.2 mg/L (reference range: 0-10 mg/L). Blood smear examination showed that the mature lymphocyte ratio was 15.0% (reference range: 20%-50%). The increased white blood cell count and hsCRP level were considered complications of infection caused by bone marrow suppression after chemotherapy.

Imaging examinations

Abnormal fluorodeoxyglucose (FDG) uptake in multiple organs and lymph nodes throughout the body was identified with 18F-FDG positron-emission tomography (PET)-computed tomography (CT) (Figure 1).

Orbital CT showed swelling of the facial, periorbital and intraorbital soft tissues on the left side with mass shadows and compression of the left eyeball and extraocular muscle (Figure 2).

US images showed a mass 24.8 mm × 45.5 mm in size in the left upper eyelid. Colour Doppler flow imaging (CDFI) and contrast-enhanced ultrasound (CEUS) showed abundant blood flow signals in the mass (Figure 3).

Pathological examination of the facial skin revealed a T cell proliferative disease. Immunohistochemical staining revealed that the tumour was positive for CD3, CD4, CD5, CD8, CD45RO, CD20, CD79a, Ki67 (+ = 40%) and EMA, but negative for CD56, CD30, GR-B, and EBEV (Figure 4).

FINAL DIAGNOSIS

The patient was diagnosed with MF involving the left eyelid.

TREATMENT

The doctors ruled out radical resection due to the patient's condition. Given the unsatisfactory effect of chemotherapy, US-guided MWA was recommended in May 2020 as a palliative treatment to alleviate the symptoms of ocular compression and pain. An ECO-100A1 microwave therapeutic system (Nanjing ECO Microwave System Co., Ltd., Nanjing, China) consisting of a microwave generator, a hollow water-cooled shaft antenna (16 Guage) and a flexible coaxial cable (Figure 5A and B) was employed, and the whole ablation process was monitored by US in real-time. The optimal puncture paths were determined with the guidance of ultrasonography. Lidocaine (2%, 10 mL) was injected for topical anaesthesia, while saline (20 mL) was used to protect the surrounding tissues. The needle pin was accurately inserted into the eyelid mass under ultrasonic dynamic monitoring to initiate MWA treatment with a microwave instrument with a power output of 35 W. The echogenicity of the microwave needle was continuously enhanced with the release of microwave energy (Figure 5C), while moving-spot technology was used to ensure complete ablation. Ablation was accomplished when CDFI revealed no blood flow signal and when no distinct enhancement was detected in the mass by CEUS. The ablation procedure took 6 minutes and 10 s in total, and the patient recovered well postoperatively. The patient received 4 courses of the CVP (cyclophosphamide 300 mg day 1-5; vincristine 2 mg day 1; dexamethasone 10 mg day 1-5) chemotherapy regimen after MWA.

OUTCOME AND FOLLOW-UP

Macroscopic examination showed that the eyelid mass had decreased in size, and the patient reported significant alleviation of the compression-related symptoms after MWA (Figure 5D-F). Three months later, re-examination *via* orbital CT indicated that eyeball compression and deformation were significantly improved. Anti-PD1 monoclonal antibody or anti-CD30 monoclonal antibody therapy was recommended to prevent disease progression, but the patient refused further treatment and died in January 2021.

DISCUSSION

MF is the most frequent subtype of CTCL and belongs to a group of heterogeneous T cell-derived extranodal non-Hodgkin lymphomas[6]. Diagnosis of MF in the early stages is challenging and requires a combination of clinical, pathological and immunohistochemical analyses[7]. Although the survival time of early-stage MF patients is similar to that of the general population, those with advanced-stage MF have poor prognoses and a median survival time under five years[8]. Regrettably, many patients miss optimal opportunities for treatment due to misdiagnosis. Systemic treatments (biological and

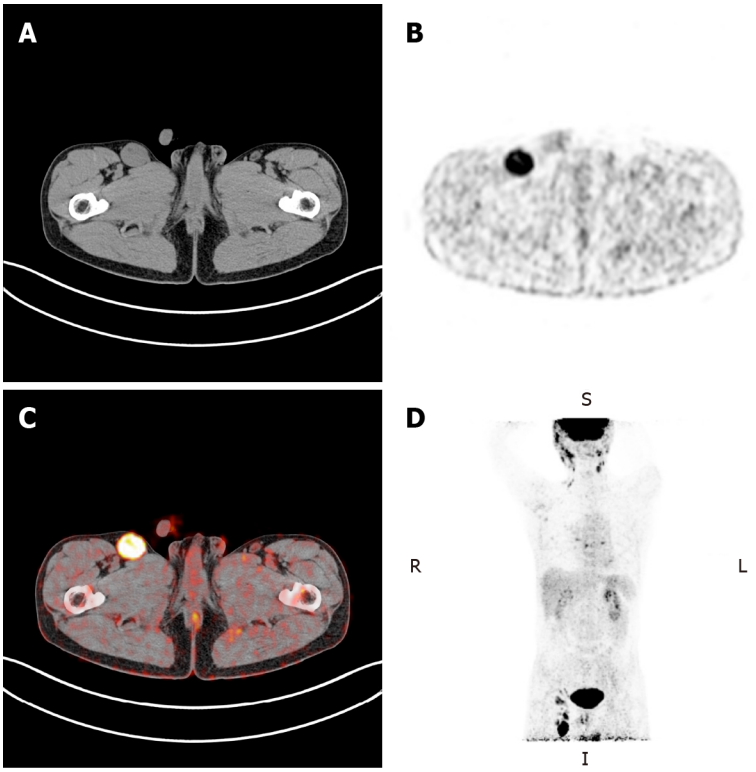

DOI: 10.12998/wjcc.v10.i17.5825 **Copyright** ©The Author(s) 2022.

Figure 1 Positron emission tomography-computed tomography examination. A: Computed tomography (CT) examination detected enlarged lymph node in the right inguinal region; B: Positron emission tomography (PET) images showed that metabolism was obviously increased in the enlarged lymph node; C: PET-CT fusion image; D: The image of PET in the coronal plane indicated abnormal fluorodeoxyglucose accumulation in the whole body.

DOI: 10.12998/wjcc.v10.i17.5825 **Copyright** ©The Author(s) 2022.

Figure 2 Orbital computed tomography. A: The orbital computed tomography (CT) image in June 2019 showed slightly swelling surrounded the eyes; B: Preoperative orbital CT in April 2020 indicated that left eyeball and extra-ocular muscle were compressed; C: Postoperative orbital CT 3 mo after microwave ablation.

targeted therapies) alone or combined with skin-directed therapies and chemotherapies are the most common interventions for advanced-stage MF. Although many patients initially respond well to treatment, the duration of this response is limited[9]. The aim of the aforementioned treatments for patients with advanced MF is to alleviate symptoms and improve quality of life; stem cell transplantation is currently the only method that provides an opportunity to achieve radical cure[10, 11]. Many patients cannot easily access systemic and standard treatments for various reasons, such as poor economic status and limited access to medical care.

In this case, concurrent involvement of the left upper eyelid was observed in a patient with advanced-stage MF. He experienced persistent mechanical ocular compression and pus discharge from the large mass. Although chemotherapy provided some relief, the mass rapidly increased after chemotherapy ended, causing the patient substantial physical and psychological stress. Surgical excision was considered risky and likely to lead to infection due to the patient's poor general condition. Percutaneous thermal ablation is a minimally invasive approach that creates a smaller wound than surgery and is easier to heal from. Percutaneous thermal or energy-based ablation for various tumours under real-time imaging guidance has been widely applied since the 1990s[12]. The most frequently used high

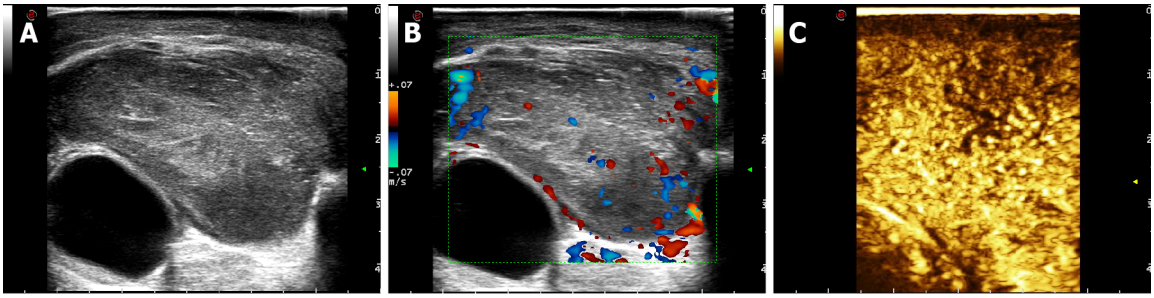

DOI: 10.12998/wjcc.v10.i17.5825 **Copyright** ©The Author(s) 2022.

Figure 3 Preoperative sonography of the eyelid mass. A: Preoperative ultrasonography of the eyelid mass; B: Colour Doppler flow imaging showed the mass was rich in blood flow signals; C: Marked contrast enhancement of the mass was observed *via* contrast-enhanced ultrasound.

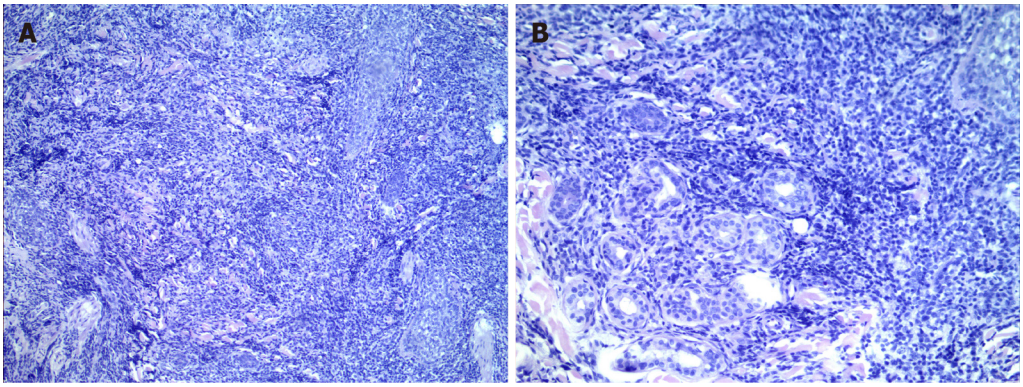

DOI: 10.12998/wjcc.v10.i17.5825 **Copyright** ©The Author(s) 2022.

Figure 4 Pathological examination of the facial skin. A: Magnification: 200 ×; B: Magnification: 400 ×.

temperature-based techniques in recent years are MWA and radiofrequency ablation. Hyperthermic injury caused by thermal ablation damages the cell membrane *via* direct or indirect mechanisms, inducing cell death and tumour destruction[13]. Compared to radiofrequency, microwave energy produces greater temperatures and covers larger areas; thus, MWA is superior for treating large tumours[14]. Furthermore, areas treated with MWA generally show clearer boundaries than those treated with other thermal therapies[15]. Consistent with our expectations, the mass rapidly reduced in size when chemotherapy was combined with MWA. Moreover, the patient's ocular compression and pus discharge symptoms markedly improved, and he regained some perception of light. While the mass increased in size again two months later, the patient reported obvious attenuation of ocular compression, which was also evidenced by a CT scan in August 2020. We considered that even though MWA failed to completely eradicate the mass, coagulation necrosis of the tissue caused by the high temperature may have prevented further intraorbital infiltration to some extent[16].

Eyelid involvement in MF is not frequently reported, and local percutaneous thermal ablation for this neoplasia has not been previously attempted. We reviewed the literature published over the past two decades (from 2000 to 2021) in PubMed (https://pubmed.ncbi.nlm.nih.gov/) and seven cases of MF eyelid involvement were retrieved (Table 1)[17-22]. Almost all the patients were male except one 33-year-old female, and the average age was 59 years. In five cases with inconsistent outcomes, overall survival times were not significantly affected by local radiotherapy, psoralen ultraviolet A therapy or non-local treatment. These findings are likely ascribable to the advanced stage of the disease and the poor overall condition of the patients; thus, the patients only survived for a number of months after diagnosis. Only one male patient with an eyelid mass as the exclusive and initial symptom survived over 13 years. Symptomatic relief was more important than a complete cure for these patients in such a context. However, multiple X-ray exposures may lead to faint erythema and moist desquamation, exacerbated in MF patients. In recent years, percutaneous MWA has been recognized as a safe and effective technique widely used in various fields of medicine. In addition to conventional locations, such as the liver, kidney and thyroid, MWA has been gradually applied to unique sites, such as the bone, lung and bile duct, achieving excellent outcomes[23]. Furthermore, MWA has unique advantages in spherical lesions and superficial locations; thus, this approach was considered suitable for the eyelid mass in this case. Under the guidance of US, operators could observe the ablation range in real-time and with a clear visual of the operation, while needle placement could be flexibly handled to ensure precision. The high temperature causes tissue charring, leading to shrinkage of the mass. Physiolo-

Table 1 Clinical characteristics of cases of advanced-stage mycosis fungoides eyelid involvement

Ref.	Gender	Age	Tumor position	Physical signs	Treatment	Survival
Jusufbegovic *et al* [17], 2015	Male	50s	Left lower eyelid	Periorbital edema	Radiotherapy, chemotherapy, and multiple facial reconstructive surgery	> 13 yr
Chokoeva *et al*[18], 2015	Male	64	Right upper eyelid	Solitary ulcerated-necrotic lesion	CHOP chemotherapy regimen	Several months
Gül *et al*[19], 2008	Female	33	Right eyelid	Infiltrative plaques and tumoral lesions	Radiotherapy	
Kiratli *et al*[20], 2006	Male	67	Left lower eyelid	Thickened skin with pigment spots	CVP chemotherapy regimen	4 mo
	Male	56	Right eyelid	Decreased vision in the right eye	PUVA therapy and CVP chemotherapy regimen	2 mo
Ing *et al*[21], 2005	Male	72	Left upper and right lower eyelids	Skin ulcerations	Ocular lubrication and radiotherapy	Several months
Game *et al*[22], 2002	Male	72	Left lower eyelid	Erythematous lesion	Electron beam therapy	

CVP: Cyclophosphamide, vincristine and prednisone; PUVA: Psoralen plus ultraviolet A; CHOP: Adriamycin, cyclophosphamide, vincristine and prednisone.

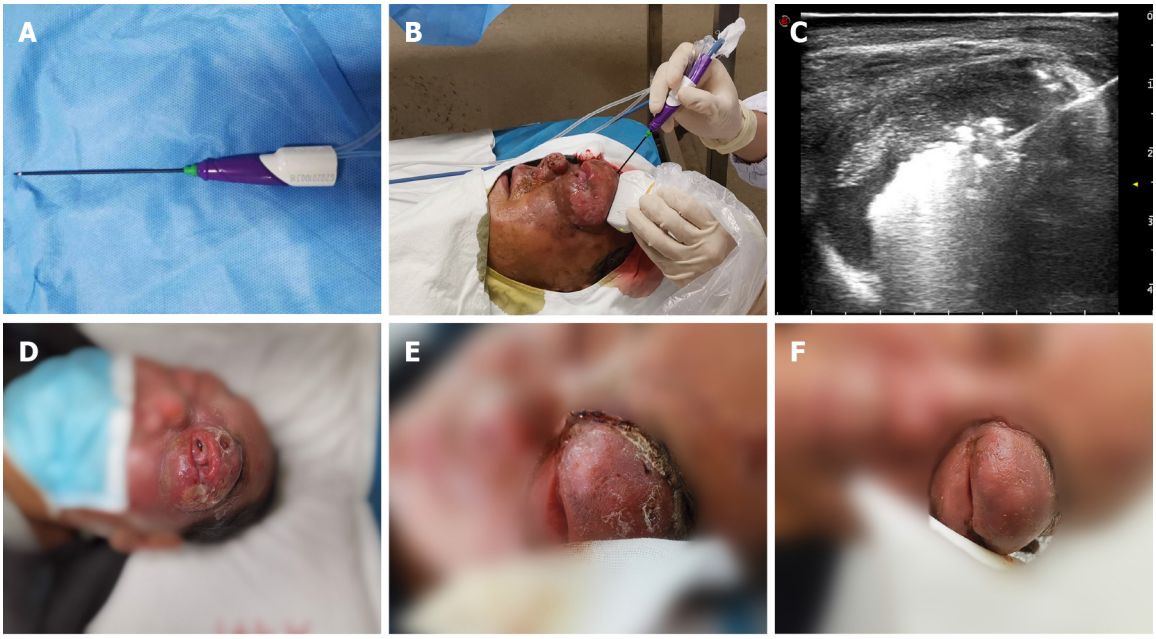

DOI: 10.12998/wjcc.v10.i17.5825 **Copyright** ©The Author(s) 2022.

Figure 5 Procedure and follow-up of microwave ablation. A: The disposable microwave therapeutic antenna; B: The microwave ablation was performed under ultrasound guidance; C: Ultrasound image showed microwave energy was being released; D: One day before microwave ablation; E: One week after microwave ablation; F: Two weeks after microwave ablation.

gically, malignant $CD4^+$ T cells play a vital role in the development of MF, while Th2 cytokines (which secrete IL-4, IL-5 and IL-10) account for the majority of lymphocytes arising from $CD4^+$ Th0 cells[24]. Dumolard *et al*[25] reported that IL-12 secretion increases and IL-4 and IL-10 secretion decreases after MWA, thus inducing an antitumour effect. Based on this finding, it was presumed that MWA plus immunotherapy combination therapy might enhance the antitumour immune response and improve the curative effect of MF. Nevertheless, the patient refused other higher-level treatment options for several reasons. Further studies remain to be conducted to investigate whether repeated MWA can improve the efficacy of immunotherapy in MF patients.

The psychological status of haematologic malignancy patients requires more attention due to the poor prognosis and need for repeated treatments. Recent research has also demonstrated that palliative treatments are feasible and acceptable, which promises improvements in patient care[26]. In this case, the patient exhibited serious symptoms of depression and anxiety during chemotherapy. He became irritated and refused to undergo continuous long-term treatment even though he was in a deteriorated

condition. After receiving MWA, his mental condition recovered gradually when he realized that the mass had shrunk. Additionally, palliative treatments such as MWA also reflect humanistic care for patients, which plays a crucial role in subsequent treatment episodes.

CONCLUSION

We described a male patient with advanced-stage MF eyelid involvement who underwent US-guided MWA. In this case, MWA was shown to be a safe and effective treatment for preventing the mass from further compressing the eyeball, and it may also play a remarkable role in dramatically alleviating patients' clinical symptoms and anxiety. Regrettably, the patient did not receive more advanced treatments, and the therapeutic value of WMA in combination with other modalities deserves further investigation.

FOOTNOTES

Author contributions: Chen YW, Wang KK and An MH contributed to collecting the data; Chen YW and Yang HZ were responsible for writing and editing the manuscript; Chen BD and Duan R performed the operation; Zhao SS, Zhang Z, Chen ZM and Feng HH reviewed the manuscript; all authors read and approved the final manuscript.

Supported by Zhenjiang Social Development Fund, No. SH2021028; Zhenjiang Social Development Fund, No. SH2018035; and the "169" Project of Zhenjiang City, No. YLJ201931.

Informed consent statement: Written informed consent was obtained from the patient for publication of this case report and accompanying images before the microwave ablation.

Conflict-of-interest statement: The authors report no conflicts of interest in this work.

CARE Checklist (2016) statement: The authors have read the CARE Checklist (2016) and the manuscript was prepared and revised according to the CARE Checklist (2016).

Open-Access: This article is an open-access article that was selected by an in-house editor and fully peer-reviewed by external reviewers. It is distributed in accordance with the Creative Commons Attribution NonCommercial (CC BY-NC 4.0) license, which permits others to distribute, remix, adapt, build upon this work non-commercially, and license their derivative works on different terms, provided the original work is properly cited and the use is non-commercial. See: https://creativecommons.org/Licenses/by-nc/4.0/

Country/Territory of origin: China

ORCID number: Yan-Wei Chen 0000-0002-1486-1755; Hai-Zhen Yang 0000-0002-5500-2922; Shuang-Shuang Zhao 0000-0001-7269-5479; Zheng Zhang 0000-0003-1702-0553; Zhe-Ming Chen 0000-0002-4245-4794; Hua-Hui Feng 0000-0003-3575-5019; Mao-Hui An 0000-0002-5282-8761; Ke-Ke Wang 0000-0003-0587-7090; Ran Duan 0000-0002-3469-2928; Bao-Ding Chen 0000-0001-9559-9199.

S-Editor: Zhang H
L-Editor: A
P-Editor: Zhang H

REFERENCES

1 **Mahalingam M**, Reddy VB. Mycosis Fungoides, Then and Now… Have We Travelled? *Adv Anat Pathol* 2015; **22**: 376-383 [PMID: 26452212 DOI: 10.1097/PAP.0000000000000092]
2 **Yeşiltaş YS**, Hoşal MB, Yüksel MK, Okçu Heper A. Severe upper eyelid mass in a patient with mycosis fungoides. *Orbit* 2020; **39**: 150-152 [PMID: 31311383 DOI: 10.1080/01676830.2019.1639772]
3 **Larocca C**, Kupper T. Mycosis Fungoides and Sézary Syndrome: An Update. *Hematol Oncol Clin North Am* 2019; **33**: 103-120 [PMID: 30497668 DOI: 10.1016/j.hoc.2018.09.001]
4 **Hernández JI**, Cepeda MF, Valdés F, Guerrero GD. Microwave ablation: state-of-the-art review. *Onco Targets Ther* 2015; **8**: 1627-1632 [PMID: 26185452 DOI: 10.2147/OTT.S81734]
5 **Vogl TJ**, Nour-Eldin NA, Hammerstingl RM, Panahi B, Naguib NNN. Microwave Ablation (MWA): Basics, Technique and Results in Primary and Metastatic Liver Neoplasms - Review Article. *Rofo* 2017; **189**: 1055-1066 [PMID: 28834968 DOI: 10.1055/s-0043-117410]
6 **Willemze R**, Jaffe ES, Burg G, Cerroni L, Berti E, Swerdlow SH, Ralfkiaer E, Chimenti S, Diaz-Perez JL, Duncan LM, Grange F, Harris NL, Kempf W, Kerl H, Kurrer M, Knobler R, Pimpinelli N, Sander C, Santucci M, Sterry W, Vermeer

MH, Wechsler J, Whittaker S, Meijer CJ. WHO-EORTC classification for cutaneous lymphomas. *Blood* 2005; **105**: 3768-3785 [PMID: 15692063 DOI: 10.1182/blood-2004-09-3502]

7 **Ahn CS**, ALSayyah A, Sangüeza OP. Mycosis fungoides: an updated review of clinicopathologic variants. *Am J Dermatopathol* 2014; **36**: 933-948 [PMID: 25415138 DOI: 10.1097/DAD.0000000000000207]

8 **Agar NS**, Wedgeworth E, Crichton S, Mitchell TJ, Cox M, Ferreira S, Robson A, Calonje E, Stefanato CM, Wain EM, Wilkins B, Fields PA, Dean A, Webb K, Scarisbrick J, Morris S, Whittaker SJ. Survival outcomes and prognostic factors in mycosis fungoides/Sézary syndrome: validation of the revised International Society for Cutaneous Lymphomas/European Organisation for Research and Treatment of Cancer staging proposal. *J Clin Oncol* 2010; **28**: 4730-4739 [PMID: 20855822 DOI: 10.1200/JCO.2009.27.7665]

9 **Kamijo H**, Miyagaki T. Mycosis Fungoides and Sézary Syndrome: Updates and Review of Current Therapy. *Curr Treat Options Oncol* 2021; **22**: 10 [PMID: 33415447 DOI: 10.1007/s11864-020-00809-w]

10 **Hughes CF**, Khot A, McCormack C, Lade S, Westerman DA, Twigger R, Buelens O, Newland K, Tam C, Dickinson M, Ryan G, Ritchie D, Wood C, Prince HM. Lack of durable disease control with chemotherapy for mycosis fungoides and Sé zary syndrome: a comparative study of systemic therapy. *Blood* 2015; **125**: 71-81 [PMID: 25336628 DOI: 10.1182/blood-2014-07-588236]

11 **Jawed SI**, Myskowski PL, Horwitz S, Moskowitz A, Querfeld C. Primary cutaneous T-cell lymphoma (mycosis fungoides and Sézary syndrome): part I. Diagnosis: clinical and histopathologic features and new molecular and biologic markers. *J Am Acad Dermatol* 2014; **70**: 205.e1-16; quiz 221 [PMID: 24438969 DOI: 10.1016/j.jaad.2013.07.049]

12 **Erridge S**, Pucher PH, Markar SR, Malietzis G, Athanasiou T, Darzi A, Sodergren MH, Jiao LR. Meta-analysis of determinants of survival following treatment of recurrent hepatocellular carcinoma. *Br J Surg* 2017; **104**: 1433-1442 [PMID: 28628947 DOI: 10.1002/bjs.10597]

13 **Nikfarjam M**, Muralidharan V, Christophi C. Mechanisms of focal heat destruction of liver tumors. *J Surg Res* 2005; **127**: 208-223 [PMID: 16083756 DOI: 10.1016/j.jss.2005.02.009]

14 **Facciorusso A**, Di Maso M, Muscatiello N. Microwave ablation versus radiofrequency ablation for the treatment of hepatocellular carcinoma: A systematic review and meta-analysis. *Int J Hyperthermia* 2016; **32**: 339-344 [PMID: 26794414 DOI: 10.3109/02656736.2015.1127434]

15 **Yi Y**, Zhang Y, Wei Q, Zhao L, Han J, Song Y, Ding Y, Lu G, Liu J, Ding H, Dai F, Tang X. Radiofrequency ablation or microwave ablation combined with transcatheter arterial chemoembolization in treatment of hepatocellular carcinoma by comparing with radiofrequency ablation alone. *Chin J Cancer Res* 2014; **26**: 112-118 [PMID: 24653633 DOI: 10.3978/j.issn.1000-9604.2014.02.09]

16 **Tian Z**, Cheng Y, Dong T, Gao X, Nan Q. Numerical Study for Lung Microwave Ablation in Different Thermal and Electrical Properties. In: Lhotska L, Sukupova L, Lacković I, Ibbott G. World Congress on Medical Physics and Biomedical Engineering 2018. Springer: Singapore, 2018: 563-566 [DOI: 10.1007/978-981-10-9035-6_104]

17 **Jusufbegovic D**, Char DH. Clinical variability of ocular involvement in mycosis fungoides. *JAMA Ophthalmol* 2015; **133**: 341-343 [PMID: 25541838 DOI: 10.1001/jamaophthalmol.2014.5223]

18 **Chokoeva AA**, Tchernev G. Mycosis Fungoides: The Multicentric Tumor D'emblee. *Mayo Clin Proc* 2015; **90**: 1746-1747 [PMID: 26653306 DOI: 10.1016/j.mayocp.2015.10.005]

19 **Gül U**, Soylu S, Aslan E, Yazar Z, Demiriz M. Uncommon presentation of mycosis fungoides: eyelid margin involvement. *J Dermatol* 2008; **35**: 581-584 [PMID: 18837703 DOI: 10.1111/j.1346-8138.2008.00526.x]

20 **Kiratli H**, Gümüs K. [Mycosis fungoides of the eyelids. Two case reports]. *J Fr Ophtalmol* 2006; **29**: 323-326 [PMID: 16557179 DOI: 10.1016/s0181-5512(06)73791-3]

21 **Ing E**, Hsieh E, Macdonald D. Cutaneous T-cell lymphoma with bilateral full-thickness eyelid ulceration. *Can J Ophthalmol* 2005; **40**: 467-468 [PMID: 16116511 DOI: 10.1016/S0008-4182(05)80007-9]

22 **Game JA**, Davies R. Mycosis fungoides causing severe lower eyelid ulceration. *Clin Exp Ophthalmol* 2002; **30**: 369-371 [PMID: 12213165 DOI: 10.1046/j.1442-9071.2002.00559.x]

23 **Vogl TJ**, Nour-Eldin NA, Albrecht MH, Kaltenbach B, Hohenforst-Schmidt W, Lin H, Panahi B, Eichler K, Gruber-Rouh T, Roman A. Thermal Ablation of Lung Tumors: Focus on Microwave Ablation. *Rofo* 2017; **189**: 828-843 [PMID: 28511267 DOI: 10.1055/s-0043-109010]

24 **Kim EJ**, Hess S, Richardson SK, Newton S, Showe LC, Benoit BM, Ubriani R, Vittorio CC, Junkins-Hopkins JM, Wysocka M, Rook AH. Immunopathogenesis and therapy of cutaneous T cell lymphoma. *J Clin Invest* 2005; **115**: 798-812 [PMID: 15841167 DOI: 10.1172/JCI24826]

25 **Dumolard L**, Ghelfi J, Roth G, Decaens T, Macek Jilkova Z. Percutaneous Ablation-Induced Immunomodulation in Hepatocellular Carcinoma. *Int J Mol Sci* 2020; **21** [PMID: 32575734 DOI: 10.3390/ijms21124398]

26 **El-Jawahri A**, Nelson AM, Gray TF, Lee SJ, LeBlanc TW. Palliative and End-of-Life Care for Patients With Hematologic Malignancies. *J Clin Oncol* 2020; **38**: 944-953 [PMID: 32023164 DOI: 10.1200/JCO.18.02386]

World Journal of Clinical Cases

Submit a Manuscript: https://www.f6publishing.com

World J Clin Cases 2022 June 16; 10(17): 5833-5840

DOI: 10.12998/wjcc.v10.i17.5833

ISSN 2307-8960 (online)

CASE REPORT

Pulp revascularization on an adult mandibular right second premolar: A case report

Ye-Qing Yang, Bu-Ling Wu, Jun-Kai Zeng, Chong Jiang, Ming Chen

Specialty type: Dentistry, oral surgery and medicine

Provenance and peer review: Unsolicited article; Externally peer reviewed.

Peer-review model: Single blind

Peer-review report's scientific quality classification

Grade A (Excellent): A
Grade B (Very good): B
Grade C (Good): 0
Grade D (Fair): 0
Grade E (Poor): 0

P-Reviewer: Capparè P, Italy; Ghaffar KA, Egypt

Received: December 13, 2021
Peer-review started: December 13, 2021
First decision: March 7, 2022
Revised: March 18, 2022
Accepted: April 3, 2022
Article in press: April 3, 2022
Published online: June 16, 2022

Ye-Qing Yang, Ming Chen, Department of Stomatology, Stomatological Hospital of Southern Medical University, Guangzhou 510280, Guangdong Province, China

Ye-Qing Yang, Jun-Kai Zeng, School of Stomatology, Southern Medical University, Guangzhou 510515, Guangdong Province, China

Bu-Ling Wu, Shenzhen Stomatology Hospital (Pingshan), Southern Medical University, Shenzhen 518118, Guangdong Province, China

Chong Jiang, Department of Stomatology, Guangdong Provincial People's Hospital; Guangdong Academy of Medical Sciences, Guangzhou 510080, Guangdong Province, China

Corresponding author: Ming Chen, MD, Attending Doctor, Department of Stomatology, Stomatological Hospital of Southern Medical University, No. 366 Jiangnan Avenue South, Haizhu District, Guangzhou 510280, Guangdong Province, China. kumiming@smu.edu.cn

Abstract

BACKGROUND

Pulp revascularization has become a new method for the treatment of periapical diseases in young permanent teeth in recent years. Through root canal flushing and disinfection, avoiding mechanical preparation, guiding apical stem cells into the root canal and promoting the continuous development of tooth roots, it has achieved good clinical curative effects. But in adult patients with chronic periapical periodontitis with immature roots and open apices, apical barrier technology is often used to treat these teeth.

CASE SUMMARY

Pulp revascularization of a 26-year-old patient's tooth was performed using cefaclor instead of minocycline and iRoot BP instead of mineral trioxide aggregate as intracanal medication. The case was followed up for 36 mo. Observations showed evidence of regression of clinical signs and symptoms, resolution of apical periodontitis and no discolouration of affected teeth.

CONCLUSION

For adult patients with chronic periapical periodontitis with immature roots and open apices, pulp revascularisation showed favourable results in treating these teeth.

Key Words: Pulp revascularization; Chronic periapical periodontitis; Immature roots; Open

apices; Abnormal central tip; Case report

©The Author(s) 2022. Published by Baishideng Publishing Group Inc. All rights reserved.

Core Tip: Pulp revascularization is especially suitable for young permanent teeth with incomplete apical development. However, few scholars have reported on adult teeth with apical periodontitis caused by an abnormal central tip being treated with dental pulp revascularization technology. The purpose of this case report was to describe the potential of using pulp revascularization to treat a permanent adult tooth.

Citation: Yang YQ, Wu BL, Zeng JK, Jiang C, Chen M. Pulp revascularization on an adult mandibular right second premolar: A case report. *World J Clin Cases* 2022; 10(17): 5833-5840
URL: https://www.wjgnet.com/2307-8960/full/v10/i17/5833.htm
DOI: https://dx.doi.org/10.12998/wjcc.v10.i17.5833

INTRODUCTION

Pulp revascularization has become a new method for the treatment of periapical diseases in young permanent teeth in recent years. Through root canal flushing and disinfection, avoiding mechanical preparation, guiding apical stem cells into the root canal and promoting the continuous development of tooth roots, it has achieved good clinical curative effects[1,2]. Initially, Holden *et al*[3] stimulated apical tissue bleeding to treat young permanent tooth periapical disease according to the mechanism of trauma healing caused by blood clots. They used the blood cells of necrotic teeth to regenerate tissue in the root canal but only formed approximately 2 mm of granulation tissue in the root tip. With the improvement of root canal disinfection and crown sealing technology, in 2001, Iwaya *et al*[4] placed antibiotics in the root canal for disinfection when treating a young permanent tooth patient with chronic periapical disease, stimulated apical bleeding and filled the root canal. Finally, the crown was tightly sealed with mineral trioxide aggregate (MTA). After 30 mo of follow-up, the root of the affected tooth continued to develop, the root canal wall thickened, the root tip closed, and an electrical activity test continued to show positive results[4]. An increasing number of clinicians have used this method and obtained similar results.

The biological mechanism of pulp revascularization is still unknown. The main process is thorough and effective root canal disinfection. Root canal disinfection and chemical irrigation are used to remove infectious materials in the root canal. Commonly used rinsing fluids include 1.5%-3% sodium hypochlorite solution and 17% EDTA solution[5]. After chemical preparation, the root canal is sealed with a triple antibacterial paste, which is generally composed of ciprofloxacin, metronidazole and minocycline[6,7]. During the treatment process, it is best to protect the residual dental pulp tissue, dental pulp stem cells and apical papillary stem cells. Studies have shown that stem cells that isolated from various problems of the oral cavity have emerged as important sources for bone and dental regulation, given stem cells plasticity, they can differentiate into specific cell lineages with a capacity of almost unlimited self-renewal and release of trophic/immunomodular factors[8-10]. These stem cells have different differentiation potentials induced by signalling molecules and the bioactive material MTA, which can form dental pulp and dentin and periodontal ligaments[11,12]. Subsequently, a regenerative scaffold based on blood clots is formed, and growth factors are provided. Some scholars have added platelet-rich plasma or platelet-rich fibrin[13]. The effect is good, but this approach involves blood product extraction and technical sensitivity. Its application prospects are still unknown. Finally, a tight crown seal is performed to provide a good environment for stem cell proliferation and differentiation, thereby promoting the continued development of tooth roots. Here we present a male adult patient with chronic periapical periodontitis with immature roots and open apices, and this tooth used pulp revascularisation to show a favourable result.

CASE PRESENTATION

Chief complaints

A 26-year-old man presented with an abscess for more than one month associated with a right mandibular posterior tooth.

History of present illness

A 26-year-old male presented for more than one month history of an abscess on the right mandibular posterior tooth. The patient did not receive any treatment for the affected tooth.

History of past illness

The patient had no history of any previous disease.

Personal and family history

The patient had no personal and family history.

Physical examination

An extraoral examination revealed no abnormalities. There were no palpable lymph nodes in the head and neck. An intraoral examination showed that the abscess was localized buccally in the periapical region of the right mandibular second premolar (Figure 1A). Pressing the abscess showed yellowish white pus discharging. The occlusal surface of the affected tooth showed an abnormal central cusp worn away, a mild response to percussion/palpation, a periodontal pocket probing depth within normal limits (3-4 mm), and no pathologic tooth mobility. The tooth did not show any response to cold and hot pulp sensitivity tests.

Imaging examinations

A radiographic examination revealed the presence of a periapical lesion associated with an immature root with an apical (Figure 1B).

FINAL DIAGNOSIS

Based on the patient's history and clinical and radiographic examinations, the right mandibular second premolar was diagnosed with chronic periapical periodontitis.

TREATMENT

Treatment options, including pulp revascularization technology and apical barrier technology, were presented to the patient. The advantages and disadvantage of the two technologies were discussed with the patient. The patient was informed that the outcome of pulp revascularization for adult permanent teeth with persistent apical periodontitis was unknown. The patient opted for pulp revascularization. The timeline of this case is presented in Table 1.

First treatment visit

Local anaesthesia with 2% lidocaine containing 1:100000 epinephrine was administered. The tooth was isolated with a rubber dam, and the pulp cavity was accessed with a carbide bur under a microscope. Pus could be seen in the root canal (Figure 1C). The root canal was rinsed with 3% sodium hypochlorite and 17% EDTA and dried with sterile paper points. Granulation tissue could be seen at the apical. The working length (WL) 0.5 mm short of the radiographic apex was determined with an electronic apex locator and periapical radiography (WL = 15 mm). Due to the large apical foramen, chemical preparation was emphasized, and mechanical preparation was assisted. Low-concentration (0.1-1.0 mg/mL) triple antibiotic paste was used to seal the root canal (Figure 1D), which was composed of ciprofloxacin, metronidazole and cefaclor (1:1:1). The access cavity was closed with a sterile cotton pellet and temporary restorative material.

Second treatment visit

Two weeks after the first treatment visit, the localized sinus had subsided, and the tooth was asymptomatic (Figure 2A). Local anaesthesia with 2% mepivacaine without a vasoconstrictor was administered. The tooth was isolated with a rubber dam, and the seal was removed with a carbide bur under a microscope. Triple antibacterial paste in the canal was removed with copious amounts of 3% sodium hypochlorite and 17% EDTA irrigation and dried with paper points. A #10 K-file was used to penetrate the periapical tissue and provoke periapical bleeding into the canal, reaching the position of the enamel-cemental junction (Figure 2B). After the bleeding became semicoagulated, an absorbable gelatine sponge was placed as a stop point (Figure 2C), and then an iRoot BP of approximately 3-mm thickness was placed over the absorbable gelatine sponge (Figure 2D). A moist cotton pellet was placed over the iRoot BP, and the access cavity was closed with temporary restorative material.

Table 1 Timeline of the case

Timeline	Events	
September 30, 2018	First treatment visit	Triple antibiotic paste was used to seal the root canal
October 15, 2018	Second treatment visit	Penetrated the periapical tissue and provoked bleeding into the canal
October 16, 2018	Third treatment visit	The access cavity was restored with light-curing composite resin
April 23, 2019	6-mo follow-up	The periapical lesion had slightly decreased in size
October 22, 2019	12-mo follow-up	The periapical lesion was smaller than before
October 14, 2020	24-mo follow-up	The periapical lesion showed further radiographic evidence of healing
October 23, 2021	36-mo follow-up	Indicating reparation of the periapical lesion

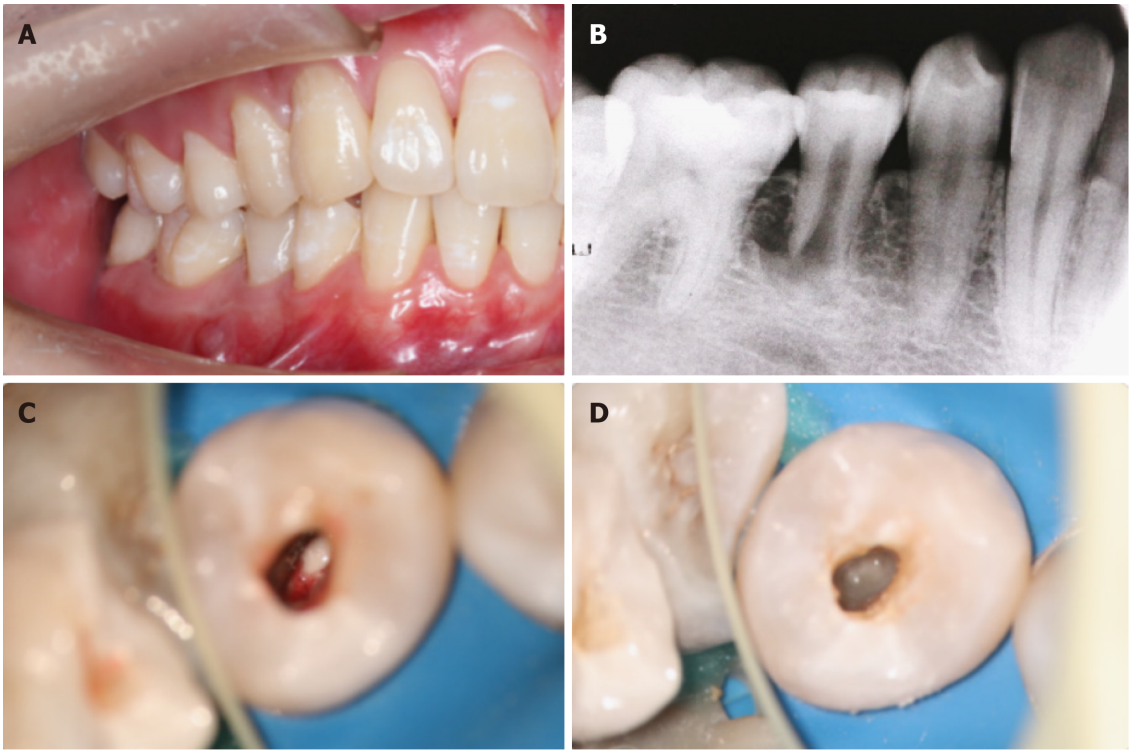

DOI: 10.12998/wjcc.v10.i17.5833 **Copyright** ©The Author(s) 2022.

Figure 1 First treatment visit. A: Preoperative view; B: A preoperative periapical radiograph; C: Pus could be seen in the root canal; D: Triple antibiotic paste was used to seal the root canal.

Third treatment visit

One day after the second treatment visit, the temporary restorative material and cotton pellet were removed from the access cavity. It was determined that the iRoot BP had completely hardened. The access cavity was restored with light-curing composite resin.

OUTCOME AND FOLLOW-UP

At the 6-mo follow-up, the periapical lesion had slightly decreased in size (Figure 3C). At the 12-mo follow-up, the periapical lesion was smaller than before (Figure 3D). At the 24-mo follow-up visit, the periapical lesion showed further radiographic evidence of healing, showing the improvement of pulp revascularization treatment (Figure 3E). The same was observed at the 36-mo follow-up visits, indicating reparation of the periapical lesion (Figure 3F). At the same time, the affected teeth did not discolouration (Figure 4A and B). However, the tooth of the canal walls did not thicken, and the apex also did not appear to have closed and did not respond to pulp tests with cold, heat, and electric pulp tests.

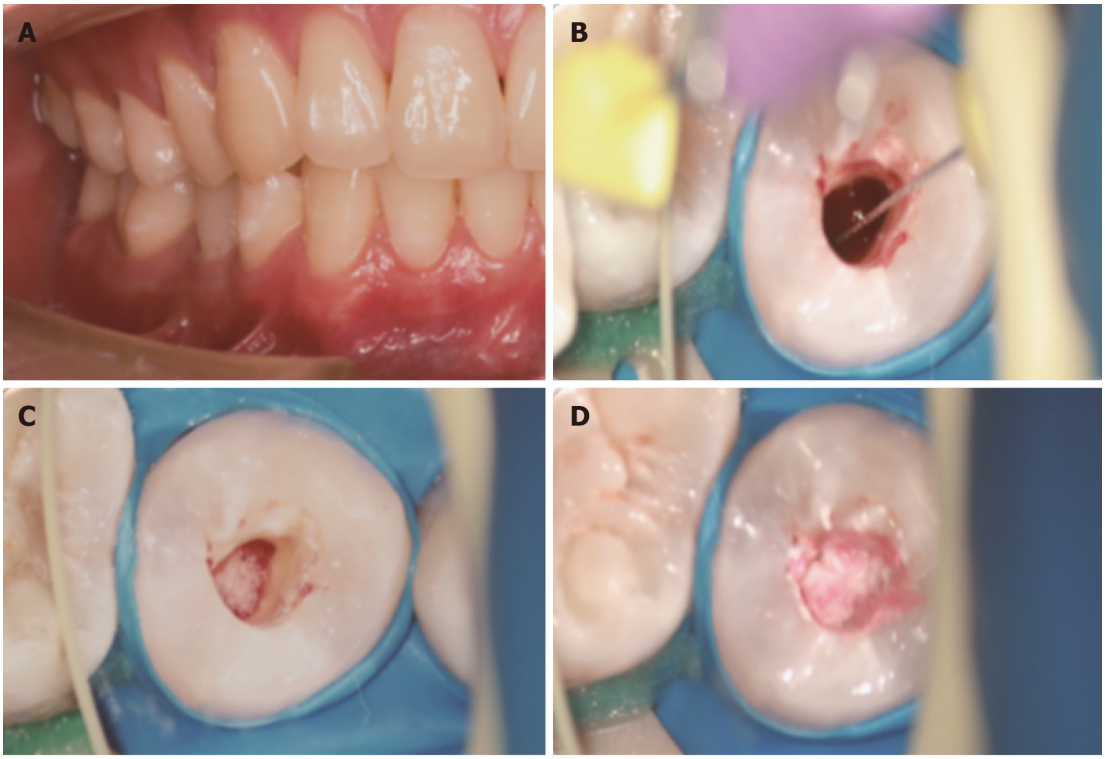

DOI: 10.12998/wjcc.v10.i17.5833 **Copyright** ©The Author(s) 2022.

Figure 2 Second treatment visit. A: Second treatment visit view; B: A #10 K-file was used to provoke periapical bleeding into the canal; C: Placed an absorbable gelatine sponge; D: Placed an iRoot BP.

DISCUSSION

In the present case report, we have described the potential of using pulp revascularization to treat adult permanent teeth with apical periodontitis. In adult patients with chronic periapical periodontitis with immature roots and open apices, apical barrier technology is often used to treat these teeth. Apical barrier technology refers to the use of MTA to form an immediate artificial barrier in the apical area for sealing[14]. However, this technology has a high cost and difficult clinical manipulation. In addition, clinical treatment and follow-up visits found that apical barrier technology caused less root development and no thickening of the root wall or extension of the root length[15]. In this case, pulp revascularization with easy clinical manipulation was used, and the final effect on affected teeth was good. However, there is inadequate literature to support that pulp revascularization has a good effect on adult patients with immature roots and open apical teeth[15].

At present, there is no consistent standard for evaluating the efficacy of pulp revascularization. The curative effect has been mainly based on clinical manifestation, pulp vitality examination and radiographic examination. According to the American Association of Endodontists guidelines, the primary goals are healing apical periodontitis and eliminating clinical symptoms. Increased thickening of the canal walls and/or continued root development as well as a positive response to cold and hot pulp sensitivity tests are desirable but not essential to determine success[16]. In this case, the periapical lesions healed, but root development stopped and remained in a static state. The reason may be the lack and low activity of stem cells in adult permanent teeth, although stem cells cannot provide the best function. Therefore, the selection and implantation of endogenous or exogenous biological scaffolds may be a very important step in the treatment of adult permanent teeth. However, at present, there is no literature citing which kind of scaffold has a better curative effect on adult permanent teeth.

A common complication of revascularization is tooth discoloration. Previous studies have suggested that tooth discoloration is related to the triple antibiotic paste. Minocycline is considered to form a chelate with calcium ions in dentinal tubules, which changes the refractive index of teeth and causes tooth discoloration[17]. Cefaclor is an antibiotic alternative to minocycline. Thibodeau *et al*[18] and Dabbagh *et al*[19] proposed replacing minocycline with cefaclor and reported successful regenerative treatment using this technique. It has also been suggested that the possible mechanism of tooth discoloration may be related to the interaction between MTA and blood and the blockade of dentinal tubules [20]. In this case, there was no obvious discoloration of the affected teeth, which may be because cefaclor was used instead of minocycline and iRoot BP was used instead of MTA. Some studies have found that iRoot BP promotes increased alkaline phosphatase activity compared with MTA, and iRoot BP has better biocompatibility and repair performance and promotes the expression of factors related to

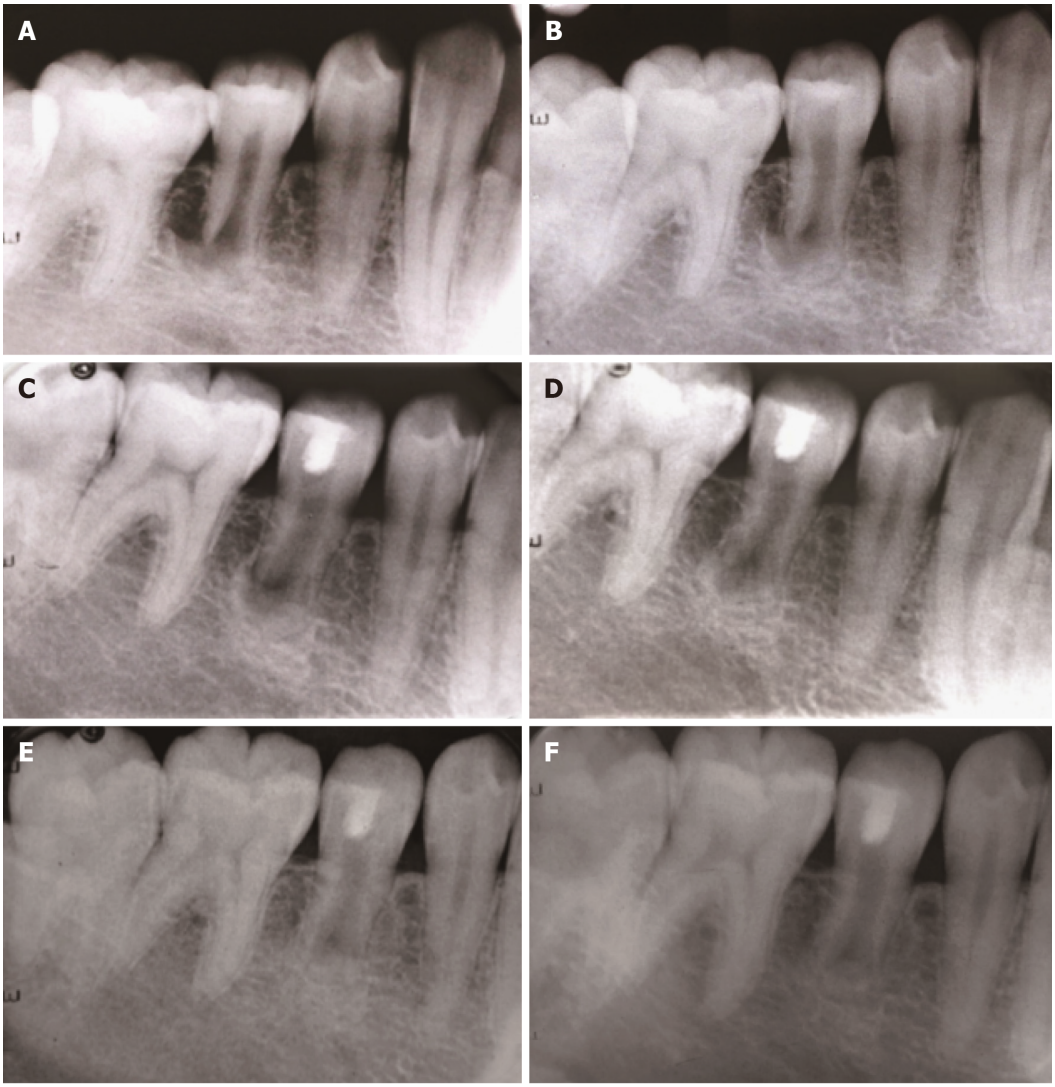

DOI: 10.12998/wjcc.v10.i17.5833 **Copyright** ©The Author(s) 2022.

Figure 3 Periapical radiographs. A: A preoperative periapical radiograph; B: An intraoperative periapical radiograph; C: At the 6-mo follow-up, a periapical radiograph; D: At the 12-mo follow-up, a periapical radiograph; E: At the 24-mo follow-up, a periapical radiograph; F: At the 36-mo follow-up, a periapical radiograph.

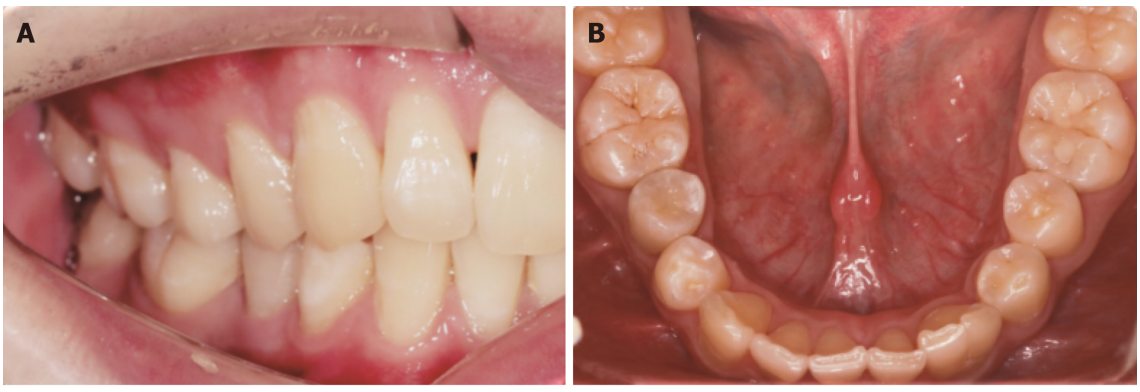

DOI: 10.12998/wjcc.v10.i17.5833 **Copyright** ©The Author(s) 2022.

Figure 4 Postoperative view. A and B: At the 36-mo follow-up, a postoperative view.

odontogenic differentiation, so it has a higher biomineralization ability and induces dentin differentiation[21]. Until a large number of reliable clinical cases prove that cefaclor and iRoot BP improve the success rate, this approach can be used according to the principle of evidence-based medicine.

CONCLUSION

In this case, it was possible to observe that pulp revascularisation in immature roots with open apical teeth was clinically and radiographically relatively successful, as was evident in the 36 mo of follow-up, with repair of the periapical lesion. Such facts demonstrate that immature roots with open apical teeth, necrotic pulp and apical periodontitis can be treated using revascularization. It may be preferable to fill the root canals with the host's own vital tissue rather than with artificial material. However, randomized, prospective clinical trials are needed to demonstrate that the treatment outcome of pulp revascularisation is better.

FOOTNOTES

Author contributions: Yang YQ wrote the main manuscript text, collected the case; Wu BL revised manuscript editing; Zeng JK and Jiang C collected data and prepared Figures; Chen M designed the study, performed critical revisions; all authors reviewed the manuscript; all authors read and approved the final manuscript.

Supported by General Program of National Natural Scientific Foundation of China, No. 81870755; Medical Scientific Research Foundation of Guangdong Province of China, No. A2022199; and Science Research Cultivation Program of Stomatological Hospital, Southern Medical University, No. PY2020018 and No. PY2021021.

Informed consent statement: Written informed consent was obtained from the patient for publication of this report and any accompanying images.

Conflict-of-interest statement: The authors declare no conflict of interest.

CARE Checklist (2016) statement: The authors have read the CARE Checklist (2016), and the manuscript was prepared and revised according to the CARE Checklist (2016).

Open-Access: This article is an open-access article that was selected by an in-house editor and fully peer-reviewed by external reviewers. It is distributed in accordance with the Creative Commons Attribution NonCommercial (CC BY-NC 4.0) license, which permits others to distribute, remix, adapt, build upon this work non-commercially, and license their derivative works on different terms, provided the original work is properly cited and the use is non-commercial. See: https://creativecommons.org/Licenses/by-nc/4.0/

Country/Territory of origin: China

ORCID number: Ye-Qing Yang 0000-0002-7931-1009; Bu-Ling Wu 0000-0001-5499-0693; Jun-Kai Zeng 0000-0003-4515-011X; Chong Jiang 0000-0001-8324-4112; Ming Chen 0000-0003-3440-0232.

S-Editor: Gong ZM
L-Editor: A
P-Editor: Gong ZM

REFERENCES

1 **Saoud TM**, Huang GT, Gibbs JL, Sigurdsson A, Lin LM. Management of Teeth with Persistent Apical Periodontitis after Root Canal Treatment Using Regenerative Endodontic Therapy. *J Endod* 2015; **41**: 1743-1748 [PMID: 26279479 DOI: 10.1016/j.joen.2015.07.004]
2 **Brogni JK**, Vitali FC, Cardoso IV, Dos Santos JD, Prado M, Alves AMH, Duque TM. A second attempt at pulp revascularisation on an immature traumatised anterior tooth: a case report with two-year follow-up. *Aust Endod J* 2021; **47**: 90-96 [PMID: 33247881 DOI: 10.1111/aej.12466]
3 **Holden T**, Nygaard-Ostby B. [Treatment of pulp necrosis developing before the root is fully formed]. *Nor Tannlaegeforen Tid* 1968; **78**: 740-743 [PMID: 5257799]
4 **Iwaya SI**, Ikawa M, Kubota M. Revascularization of an immature permanent tooth with apical periodontitis and sinus tract. *Dent Traumatol* 2001; **17**: 185-187 [PMID: 11585146 DOI: 10.1034/j.1600-9657.2001.017004185.x]
5 **Zeng Q**, Nguyen S, Zhang H, Chebrolu HP, Alzebdeh D, Badi MA, Kim JR, Ling J, Yang M. Release of Growth Factors into Root Canal by Irrigations in Regenerative Endodontics. *J Endod* 2016; **42**: 1760-1766 [PMID: 27871480 DOI: 10.1016/j.joen.2016.04.029]
6 **do Couto AM**, Espaladori MC, Leite APP, Martins CC, de Aguiar MCF, Abreu LG. A Systematic Review of Pulp Revascularization Using a Triple Antibiotic Paste. *Pediatr Dent* 2019; **41**: 341-353 [PMID: 31648664]
7 **Montero-Miralles P**, Martín-González J, Alonso-Ezpeleta O, Jiménez-Sánchez MC, Velasco-Ortega E, Segura-Egea JJ. Effectiveness and clinical implications of the use of topical antibiotics in regenerative endodontic procedures: a review. *Int Endod J* 2018; **51**: 981-988 [PMID: 29480932 DOI: 10.1111/iej.12913]
8 **Tetè G**, Capparè P, Gherlone E. New Application of Osteogenic Differentiation from HiPS Stem Cells for Evaluating the

Osteogenic Potential of Nanomaterials in Dentistry. *Int J Environ Res Public Health* 2020; **17** [PMID: 32188154 DOI: 10.3390/ijerph17061947]

9 **Capparè P**, Tetè G, Sberna MT, Panina-Bordignon P. The Emerging Role of Stem Cells in Regenerative Dentistry. *Curr Gene Ther* 2020; **20**: 259-268 [PMID: 32811413 DOI: 10.2174/1566523220999200818115803]

10 **Tetè G**, D'Orto B, Nagni M, Agostinacchio M, Polizzi E, Agliardi E. Role of induced pluripotent stem cells (IPSCS) in bone tissue regeneration in dentistry: a narrative review. *J Biol Regul Homeost Agents* 2020; **34**: 1-10 [PMID: 33386051]

11 **Kaukua N**, Shahidi MK, Konstantinidou C, Dyachuk V, Kaucka M, Furlan A, An Z, Wang L, Hultman I, Ahrlund-Richter L, Blom H, Brismar H, Lopes NA, Pachnis V, Suter U, Clevers H, Thesleff I, Sharpe P, Ernfors P, Fried K, Adameyko I. Glial origin of mesenchymal stem cells in a tooth model system. *Nature* 2014; **513**: 551-554 [PMID: 25079316 DOI: 10.1038/nature13536]

12 **Chrepa V**, Henry MA, Daniel BJ, Diogenes A. Delivery of Apical Mesenchymal Stem Cells into Root Canals of Mature Teeth. *J Dent Res* 2015; **94**: 1653-1659 [PMID: 26195498 DOI: 10.1177/0022034515596527]

13 **Ulusoy AT**, Turedi I, Cimen M, Cehreli ZC. Evaluation of Blood Clot, Platelet-rich Plasma, Platelet-rich Fibrin, and Platelet Pellet as Scaffolds in Regenerative Endodontic Treatment: A Prospective Randomized Trial. *J Endod* 2019; **45**: 560-566 [PMID: 30935618 DOI: 10.1016/j.joen.2019.02.002]

14 **Torabinejad M**, Chivian N. Clinical applications of mineral trioxide aggregate. *J Endod* 1999; **25**: 197-205 [PMID: 10321187 DOI: 10.1016/S0099-2399(99)80142-3]

15 **Kim SG**, Malek M, Sigurdsson A, Lin LM, Kahler B. Regenerative endodontics: a comprehensive review. *Int Endod J* 2018; **51**: 1367-1388 [PMID: 29777616 DOI: 10.1111/iej.12954]

16 **AAE**. Clinical Considerations for a Regenerative Procedure. 2016

17 **Akcay M**, Arslan H, Yasa B, Kavrık F, Yasa E. Spectrophotometric analysis of crown discoloration induced by various antibiotic pastes used in revascularization. *J Endod* 2014; **40**: 845-848 [PMID: 24862714 DOI: 10.1016/j.joen.2013.09.019]

18 **Thibodeau B**, Trope M. Pulp revascularization of a necrotic infected immature permanent tooth: case report and review of the literature. *Pediatr Dent* 2007; **29**: 47-50 [PMID: 18041512]

19 **Dabbagh B**, Alvaro E, Vu DD, Rizkallah J, Schwartz S. Clinical complications in the revascularization of immature necrotic permanent teeth. *Pediatr Dent* 2012; **34**: 414-417 [PMID: 23211919]

20 **Santos LGPD**, Chisini LA, Springmann CG, Souza BDM, Pappen FG, Demarco FF, Felippe MCS, Felippe WT. Alternative to Avoid Tooth Discoloration after Regenerative Endodontic Procedure: A Systematic Review. *Braz Dent J* 2018; **29**: 409-418 [PMID: 30517438 DOI: 10.1590/0103-6440201802132]

21 **Lin J**, Zeng Q, Wei X, Zhao W, Cui M, Gu J, Lu J, Yang M, Ling J. Regenerative Endodontics Versus Apexification in Immature Permanent Teeth with Apical Periodontitis: A Prospective Randomized Controlled Study. *J Endod* 2017; **43**: 1821-1827 [PMID: 28864219 DOI: 10.1016/j.joen.2017.06.023]

World Journal of Clinical Cases

Submit a Manuscript: https://www.f6publishing.com

World J Clin Cases 2022 June 16; 10(17): 5841-5845

DOI: 10.12998/wjcc.v10.i17.5841

ISSN 2307-8960 (online)

CASE REPORT

Barrett's esophagus in a patient with bulimia nervosa: A case report

Ahmed Gouda, Mohamed El-Kassas

Specialty type: Medicine, research and experimental

Provenance and peer review: Unsolicited article; Externally peer reviewed.

Peer-review model: Single blind

Peer-review report's scientific quality classification

Grade A (Excellent): 0
Grade B (Very good): B
Grade C (Good): 0
Grade D (Fair): D
Grade E (Poor): 0

P-Reviewer: Nagahara H, Japan; Sato Y, Japan

Received: December 12, 2021
Peer-review started: December 12, 2021
First decision: February 8, 2022
Revised: February 18, 2022
Accepted: April 9, 2022
Article in press: April 9, 2022
Published online: June 16, 2022

Ahmed Gouda, Department of Gastroenterology NMC, Ruwais Hospital, Abu Dhabi 14638, United Arab Emirates

Mohamed El-Kassas, Department of Endemic Medicine, Faculty of Medicine, Helwan University, Cairo 11795, Egypt

Corresponding author: Mohamed El-Kassas, MD, Full Professor, Department of Endemic Medicine, Faculty of Medicine, Helwan University, Ain Helwan, Cairo 11795, Egypt.
m_elkassas@yahoo.com

Abstract

BACKGROUND

Barrett's esophagus is a known complication of long-standing gastroesophageal reflux disease, and it is a potential risk factor of developing esophageal adenocarcinoma.

CASE SUMMARY

Here, we present a case of a 47-year-old male patient referred to the gastroenterology clinic for upper endoscopy because he has a long-standing history of heartburn and vomiting after meals. On examination, he had characteristic findings of self-induced vomiting as abrasions and callosities on the dorsum of the right hand and dental erosions. A detailed history revealed that he had 17 years of binge eating with self-induced vomiting. His upper endoscopy showed gastroesophageal reflux grade D with salmon-red mucosal projections, and the biopsy revealed intestinal mucosal metaplasia.

CONCLUSION

This case emphasized the importance of considering upper endoscopy screening for Barrett's esophagus in patients with eating disorders, especially those with self-induced vomiting, as in bulimia nervosa.

Key Words: Barrett's esophagus; Bulimia nervosa; Gastroesophageal reflux disease; Case report

©The Author(s) 2022. Published by Baishideng Publishing Group Inc. All rights reserved.

Core Tip: Barrett's esophagus is a known complication of long-standing gastroesophageal reflux disease. Here, we present a case of a 47-year-old male patient with a long-standing history of heartburn and vomiting after meals. Upper endoscopy showed gastroesophageal reflux grade D with intestinal mucosal metaplasia. This emphasized the importance of considering upper endoscopy screening for Barrett's esophagus in patients with eating disorders, especially those with self-induced vomiting, as in bulimia nervosa.

Citation: Gouda A, El-Kassas M. Barrett's esophagus in a patient with bulimia nervosa: A case report. *World J Clin Cases* 2022; 10(17): 5841-5845
URL: https://www.wjgnet.com/2307-8960/full/v10/i17/5841.htm
DOI: https://dx.doi.org/10.12998/wjcc.v10.i17.5841

INTRODUCTION

Barrett's esophagus is the condition in which metaplastic columnar epithelial cells with gastric and intestinal features replace the stratified squamous epithelium that normally lines the distal esophagus. The condition develops due to chronic gastroesophageal reflux disease (GERD) and is a significant risk factor for adenocarcinoma of the esophagus[1]. Bulimia nervosa is characterized by recurrent episodes of binge eating followed by inappropriate compensatory behavior to prevent weight gain, such as self-induced vomiting, misuse of medications such as laxatives, diuretics, insulin, or thyroid hormone[2].

Binge eating disorder represents a real health problem. Low treatment rates highlight the importance of questioning patients about eating problems even when not mentioned in their presenting complaints [3]. The complications that occur with bulimia nervosa can affect many organ systems and depend upon the method and frequency of purging (*i.e.* self-induced vomiting or misuse of laxatives, diuretics, or enemas)[4]. Gastrointestinal complications of bulimia nervosa can include GERD and Barrett's esophagus[5].

CASE PRESENTATION

Chief complaints

We present a case of a 47-year-old male patient referred for upper endoscopy for having heartburn and vomiting after meals.

History of present illness

The patient denied any history of eating or psychological disorders.

History of past illness

Upon intense history taking and after several attempts, the patient reported a 17-year history of having frequent heavy meals and drinking large amounts of carbonated drinks up to 10 cans every day, followed by self-induced vomiting using the index finger of the right hand. This condition confirms the diagnosis of bulimia nervosa. The patient also reported heavy smoking of Shisha.

Personal and family history

His body mass index was maintained throughout this period, with no significant medical history.

Physical examination

Upon physical examination, abrasions and callosities were noticed on the dorsum of the right hand (Russell's sign of self-induced vomiting, Figure 1A), and teeth erosions were observed (Figure 1B).

Laboratory examinations

Routine laboratory investigations were within the accepted ranges.

Imaging examinations

Upper endoscopic examination showed incompetent dilated cardia with GERD grade D (Los Angeles classification). The lesions started 25 cm from the incisors. Salmon-red mucosal projections into the esophageal lumen and mucosal islands were observed. Multiple biopsies were taken, which later showed metaplastic columnar epithelium typical for Barrett's esophagus without dysplasia (Figure 2).

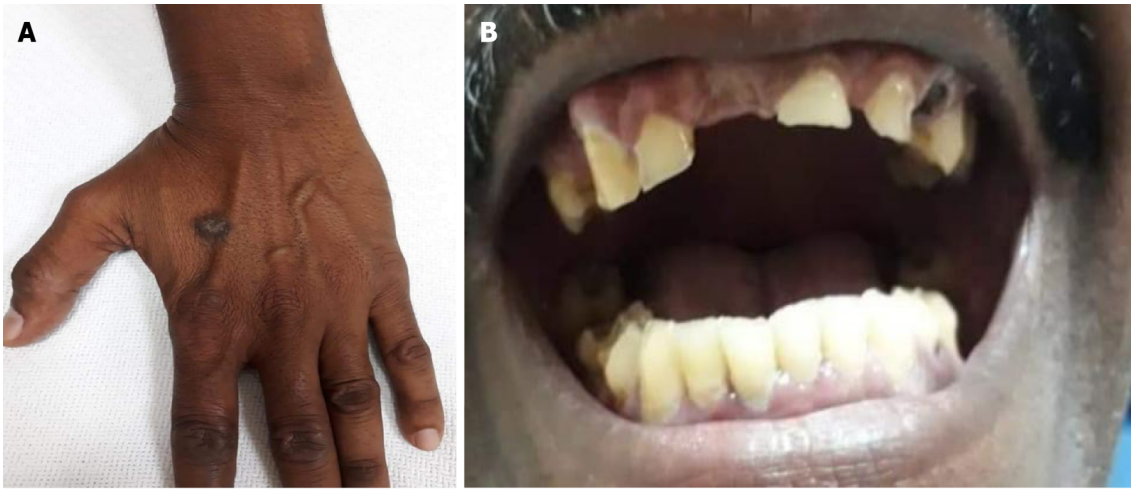

DOI: 10.12998/wjcc.v10.i17.5841 **Copyright** ©The Author(s) 2022.

Figure 1 Physical examination. A: Abrasions and callosities on the dorsum of the right hand (Russell's sign of self-induced vomiting); B: Significant teeth erosions arising from repeated vomiting.

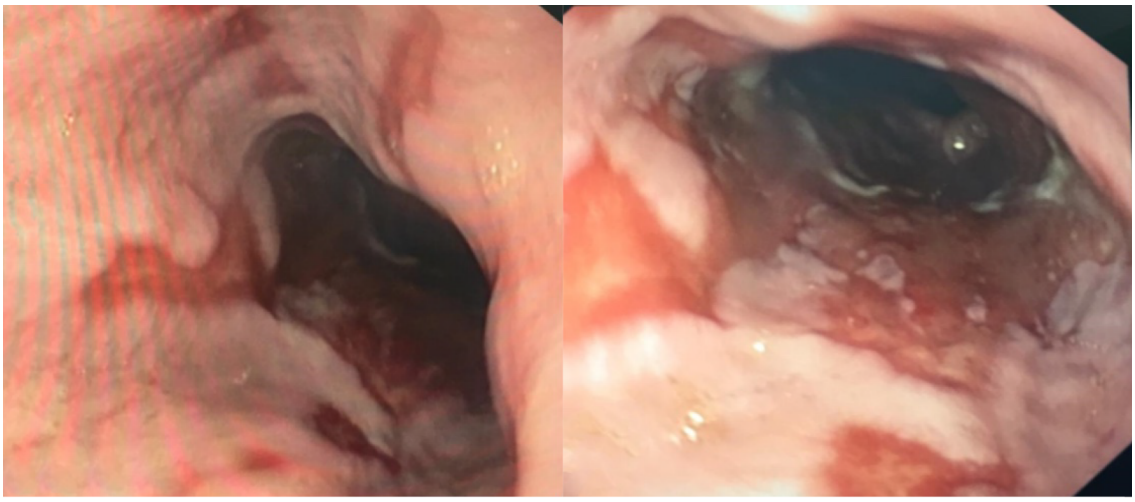

DOI: 10.12998/wjcc.v10.i17.5841 **Copyright** ©The Author(s) 2022.

Figure 2 Lower esophagus showing tongue like projections of Barrett's esophagus.

FINAL DIAGNOSIS

The patient was diagnosed with bulimia nervosa and Barrett's esophagus.

TREATMENT

Long-term acid suppression was decided as a treatment for Barrett's esophagus, in addition to the scheduling of an endoscopic surveillance program.

OUTCOME AND FOLLOW-UP

Patient was referred for psychiatric consultation.

DISCUSSION

GERD symptoms in patients with eating disorders such as bulimia nervosa are usually linked to

repeated, self-induced vomiting, but the relationship is still unclear[6]. Acid exposure is not limited to purging patients; binge eating itself, which is commonly associated with various esophageal disorders, could be a risk factor for GERD[7].

Repeated acid exposure can be associated with the development of Barrett's esophagus, whereby the esophageal squamous epithelium is replaced by metaplastic columnar epithelium, being more susceptible to malignancy[8]. Theoretically speaking, prolonged standing self-induced vomiting may be associated with the development of Barrett's esophagus, but there is no definitive conclusion can be reached due to lack of data[9]. Barrett's esophagus is associated with a 30-fold increased risk of developing esophageal adenocarcinoma over the general population[10]. Moreover, there are few case reports of patients with bulimia nervosa presenting with worsening epigastric pain and reflux who were finally diagnosed with esophageal adenocarcinoma[11].

In our case, there was a history of upper gastrointestinal problems, which was the chief presenting complaint. On the other hand, a more profound history revealed the riddle of the bulimia nervosa diagnosis that was beneath this presenting ailment. The patient had been suffering from bulimia nervosa for 17 years without a diagnosis because of his unwillingness to consult a therapist or because of the stigma possibly associated with the disease in his imagination. The patient had a history of binge eating episodes, including increased calorie intake and compensatory purging to eliminate the extra food intake. This led to the diagnosis of bulimia nervosa induced Barrett's esophagus in our case, which is a rare occurrence. Many cohort studies reported that patients with Barrett's esophagus who received maintenance therapy with proton pump inhibitors had a lower probability of developing neoplastic Barrett's esophagus than those who did not receive maintenance therapy[12]. Diagnosing Barrett's esophagus in such cases should make a difference, considering the possibility of prescribing long-term proton pump inhibitors.

CONCLUSION

A thorough understanding of the risk factors for Barrett's esophagus is required to combat the rising incidence of this precancerous lesion worldwide. The emerging risk factors for GERD and Barrett's esophagus must be updated considering the rising incidence of psychological eating disorders in today's world. Additionally, providers should consider endoscopic evaluation of patients with eating disorders who have persistent symptoms of dyspepsia or vomiting, given the potential risk of esophageal precancerous and cancerous disorders.

FOOTNOTES

Author contributions: Gouda A performed the endoscopic procedure and collected the patient's data; El-Kassas M wrote the first draft of the manuscript; Both authors reviewed and approved the final version of the manuscript.

Informed consent statement: All procedures performed in this study were in accordance with the ethical standards of the institutional and/or national research committee and with the 1964 Helsinki declaration and its later amendments or comparable ethical standards. An informed consent was obtained from the participant included in the study.

Conflict-of-interest statement: Nothing related to this work.

CARE Checklist (2016) statement: The authors have read the CARE Checklist (2016), and the manuscript was prepared and revised according to the CARE Checklist (2016).

Open-Access: This article is an open-access article that was selected by an in-house editor and fully peer-reviewed by external reviewers. It is distributed in accordance with the Creative Commons Attribution NonCommercial (CC BY-NC 4.0) license, which permits others to distribute, remix, adapt, build upon this work non-commercially, and license their derivative works on different terms, provided the original work is properly cited and the use is non-commercial. See: https://creativecommons.org/Licenses/by-nc/4.0/

Country/Territory of origin: Egypt

ORCID number: Ahmed Gouda 0000-0001-5992-6113; Mohamed El-Kassas 0000-0002-3396-6894.

S-Editor: Fan JR
L-Editor: Filipodia
P-Editor: Fan JR

REFERENCES

1 **Que J**, Garman KS, Souza RF, Spechler SJ. Pathogenesis and Cells of Origin of Barrett's Esophagus. *Gastroenterology* 2019; **157**: 349-364.e1 [PMID: 31082367 DOI: 10.1053/j.gastro.2019.03.072]

2 **Torjesen I**. Diabulimia: the world's most dangerous eating disorder. *BMJ* 2019; **364**: l982 [PMID: 30824423 DOI: 10.1136/bmj.l982]

3 **Kessler RC**, Berglund PA, Chiu WT, Deitz AC, Hudson JI, Shahly V, Aguilar-Gaxiola S, Alonso J, Angermeyer MC, Benjet C, Bruffaerts R, de Girolamo G, de Graaf R, Maria Haro J, Kovess-Masfety V, O'Neill S, Posada-Villa J, Sasu C, Scott K, Viana MC, Xavier M. The prevalence and correlates of binge eating disorder in the World Health Organization World Mental Health Surveys. *Biol Psychiatry* 2013; **73**: 904-914 [PMID: 23290497 DOI: 10.1016/j.biopsych.2012.11.020]

4 **Forney KJ**, Buchman-Schmitt JM, Keel PK, Frank GK. The medical complications associated with purging. *Int J Eat Disord* 2016; **49**: 249-259 [PMID: 26876429 DOI: 10.1002/eat.22504]

5 **Brown CA**, Mehler PS. Medical complications of self-induced vomiting. *Eat Disord* 2013; **21**: 287-294 [PMID: 23767670 DOI: 10.1080/10640266.2013.797317]

6 **Denholm M**, Jankowski J. Gastroesophageal reflux disease and bulimia nervosa--a review of the literature. *Dis Esophagus* 2011; **24**: 79-85 [PMID: 20659142 DOI: 10.1111/j.1442-2050.2010.01096.x]

7 **Peat CM**, Huang L, Thornton LM, Von Holle AF, Trace SE, Lichtenstein P, Pedersen NL, Overby DW, Bulik CM. Binge eating, body mass index, and gastrointestinal symptoms. *J Psychosom Res* 2013; **75**: 456-461 [PMID: 24182635 DOI: 10.1016/j.jpsychores.2013.08.009]

8 **Lin JA**, Woods ER, Bern EM. Common and Emergent Oral and Gastrointestinal Manifestations of Eating Disorders. *Gastroenterol Hepatol (N Y)* 2021; **17**: 157-167 [PMID: 34035776]

9 **Pacciardi B**, Cargioli C, Mauri M. Barrett's esophagus in anorexia nervosa: a case report. *Int J Eat Disord* 2015; **48**: 147-150 [PMID: 24753136 DOI: 10.1002/eat.22288]

10 **Van der Veen AH**, Dees J, Blankensteijn JD, Van Blankenstein M. Adenocarcinoma in Barrett's oesophagus: an overrated risk. *Gut* 1989; **30**: 14-18 [PMID: 2920919 DOI: 10.1136/gut.30.1.14]

11 **Shinohara ET**, Swisher-McClure S, Husson M, Sun W, Metz JM. Esophageal cancer in a young woman with bulimia nervosa: a case report. *J Med Case Rep* 2007; **1**: 160 [PMID: 18047676 DOI: 10.1186/1752-1947-1-160]

12 **Marabotto E**, Pellegatta G, Sheijani AD, Ziola S, Zentilin P, De Marzo MG, Giannini EG, Ghisa M, Barberio B, Scarpa M, Angriman I, Fassan M, Savarino V, Savarino E. Prevention Strategies for Esophageal Cancer-An Expert Review. *Cancers (Basel)* 2021; **13** [PMID: 34062788 DOI: 10.3390/cancers13092183]

World Journal of Clinical Cases

Submit a Manuscript: https://www.f6publishing.com

World J Clin Cases 2022 June 16; 10(17): 5846-5853

DOI: 10.12998/wjcc.v10.i17.5846

ISSN 2307-8960 (online)

CASE REPORT

Spontaneous gallbladder perforation and colon fistula in hypertriglyceridemia-related severe acute pancreatitis: A case report

Qi-Pu Wang, Yi-Jun Chen, Mei-Xing Sun, Jia-Yuan Dai, Jian Cao, Qiang Xu, Guan-Nan Zhang, Sheng-Yu Zhang

Specialty type: Medicine, research and experimental

Provenance and peer review: Unsolicited article; Externally peer reviewed.

Peer-review model: Single blind

Peer-review report's scientific quality classification

Grade A (Excellent): 0
Grade B (Very good): 0
Grade C (Good): C
Grade D (Fair): D
Grade E (Poor): 0

P-Reviewer: Hosoya S, Japan; Priyadarshi RN, India

Received: December 23, 2021
Peer-review started: December 23, 2021
First decision: January 27, 2022
Revised: February 2, 2022
Accepted: April 9, 2022
Article in press: April 9, 2022
Published online: June 16, 2022

Qi-Pu Wang, Yi-Jun Chen, Mei-Xing Sun, Sheng-Yu Zhang, Department of Gastroenterology, Peking Union Medical College Hospital, Beijing 100730, China

Yi-Jun Chen, School of Medicine, Tsinghua University, Beijing 100084, China

Jia-Yuan Dai, Department of Emergency Medicine, Peking Union Medical College Hospital, Beijing 100730, China

Jian Cao, Department of Radiology, Peking Union Medical College Hospital, Beijing 100730, China

Qiang Xu, Guan-Nan Zhang, Department of General Surgery, Peking Union Medical College Hospital, Beijing 100730, China

Corresponding author: Sheng-Yu Zhang, MD, Doctor, Department of Gastroenterology, Peking Union Medical College Hospital, No. 1 Shuaifuyuan, Wangfujing, Dongcheng District, Beijing 100730, China. pumchzsy@126.com

Abstract

BACKGROUND

Gallbladder perforation and gastrointestinal fistula are rare but serious complications of severe acute pancreatitis (SAP). However, neither spontaneous gallbladder perforation nor cholecysto-colonic fistula has been reported in acalculous acute pancreatitis patients.

CASE SUMMARY

A 31-year-old male presenting with epigastric pain was diagnosed with hypertriglyceridemia-related SAP. He suffered from multiorgan failure and was able to leave the intensive care unit on day 20. Three percutaneous drainage tubes were placed for profound exudation in the peripancreatic region and left paracolic sulcus. He developed spontaneous gallbladder perforation with symptoms of fever and right upper quadrant pain 1 mo after SAP onset and was stabilized by percutaneous drainage. Peripancreatic infection appeared 1 mo later and was treated with antibiotics but without satisfactory results. Then multiple colon fistulas, including a cholecysto-colonic fistula and a descending colon fistula, emerged 3 mo after the onset of SAP. Nephroscopy-assisted peripancreatic debridement and ileostomy were carried out immediately. The fistulas achieved spontaneous closure 7 mo later, and the patient recovered after cholecystectomy

and ileostomy reduction. We presume that the causes of gallbladder perforation are poor bile drainage due to external pressure, pancreatic enzyme erosion, and ischemia. The possible causes of colon fistulas are pancreatic enzymes or infected necrosis erosion, ischemia, and iatrogenic injury. According to our experience, localized gallbladder perforation can be stabilized by percutaneous drainage. Pancreatic debridement and proximal colostomy followed by cholecystectomy are feasible and valid treatment options for cholecysto-colonic fistulas.

CONCLUSION
Gallbladder perforation and cholecysto-colonic fistula should be considered in acalculous SAP patients.

Key Words: Acalculous severe acute pancreatitis; Gallbladder perforation; Cholecysto-colonic fistula; Percutaneous drainage; Cholecystectomy; Case report

©The Author(s) 2022. Published by Baishideng Publishing Group Inc. All rights reserved.

Core Tip: To the best of our knowledge, this is the first time that spontaneous gallbladder perforation and cholecysto-colonic fistula have been reported in patients with acalculous severe acute pancreatitis. Biliary obstruction due to peripancreatic effusions, pancreatic enzymes or infected necrosis erosion, ischemia, and iatrogenic injury might be related. According to our experience, localized gallbladder perforation can be stabilized by percutaneous drainage. Pancreatic debridement and proximal colostomy followed by cholecystectomy are feasible and valid treatment options for cholecysto-colonic fistulas.

Citation: Wang QP, Chen YJ, Sun MX, Dai JY, Cao J, Xu Q, Zhang GN, Zhang SY. Spontaneous gallbladder perforation and colon fistula in hypertriglyceridemia-related severe acute pancreatitis: A case report. *World J Clin Cases* 2022; 10(17): 5846-5853
URL: https://www.wjgnet.com/2307-8960/full/v10/i17/5846.htm
DOI: https://dx.doi.org/10.12998/wjcc.v10.i17.5846

INTRODUCTION

Pancreatic pseudocysts, wall-off necrosis, and peripancreatic abscess are well-known local complications of severe acute pancreatitis (SAP). There are few reports on rare complications of gallbladder perforation[1] or gastrointestinal fistula. Gallbladder perforation occurs in 2%-10% of patients with acute cholecystitis[2], usually occurs in elderly males[3], and is mostly associated with calculous cholecystitis[4]. Delays in diagnosis lead to a poor prognosis. One study reported that the morbidity and mortality of gallbladder perforation are 37.5% and 12.5%, respectively[4]. Gastrointestinal fistula most commonly occurs in the colon, with an incidence of 3.3% in acute pancreatitis (AP) and 15% in SAP[5], which can also involve the duodenum, stomach, and small intestine[6]. Compared with patients without colon complications, SAP patients with colon involvement have significantly higher morbidity and mortality (54% for colonic necrosis)[7]. However, neither gallbladder perforation nor cholecysto-colonic fistula has been recorded in acalculous AP patients. Herein, we present the first case of spontaneous gallbladder perforation and cholecysto-colonic fistula in a patient with acalculous SAP.

CASE PRESENTATION

Chief complaints

A 31-year-old male presented in the emergency room with epigastric pain for 3 d and loss of consciousness for 1 d.

History of present illness

This patient with a body mass index of 29.39 kg/m^2 was admitted to the local hospital because of epigastric pain for 1 d after a fatty meal. He described the pain as persistent, severe, and radiating to the back, accompanied by nausea and vomiting. Local laboratory examination revealed that the serum amylase level was over 500 U/L (the upper normal limit was 135 U/L), and the triglyceride concentration was 44 mmol/L. The abdominal computed tomography (CT) scan showed pancreatic edema without gallstones. Considering hypertriglyceridemia-related AP, he received lipid-lowering

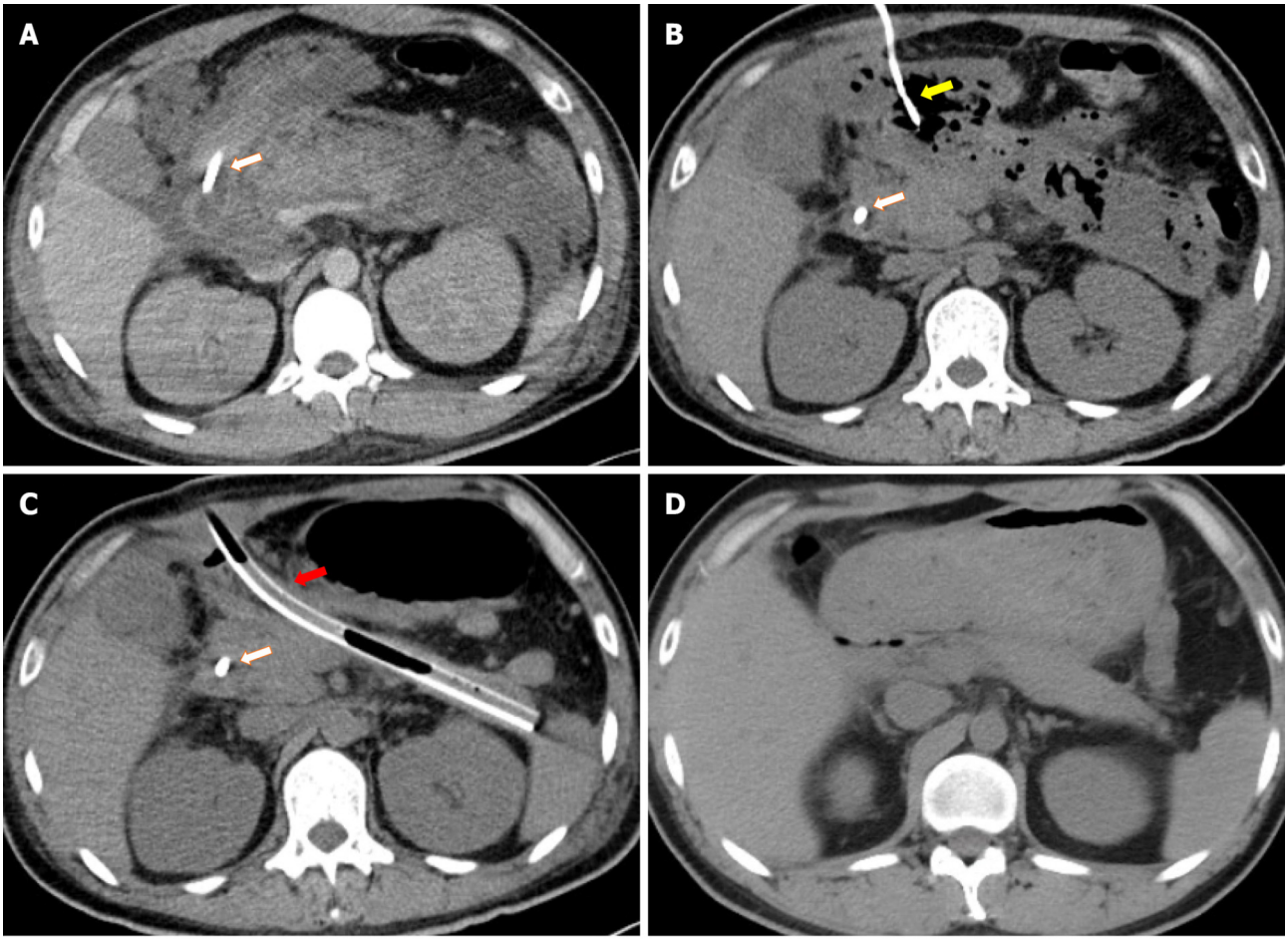

DOI: 10.12998/wjcc.v10.i17.5846 Copyright ©The Author(s) 2022.

Figure 1 Pancreatic imaging changes during the course of disease. The jejunal feeding tube is marked by a white arrow. The percutaneous drainage tube for the pancreatic head region is marked by a yellow arrow. A: Contrast-enhanced computed tomography (CT) demonstrating pancreatic edema and profound peripancreatic exudation after severe acute pancreatitis (SAP) onset; B: CT demonstrating peripancreatic infected necrosis 2 mo after SAP onset; C: CT after nephroscopy-assisted debridement of peripancreatic necrosis 3 mo after SAP onset. One of the thicker drainage tubes is marked by a red arrow; D: CT demonstrating recovery 10 mo after SAP onset.

(fenofibrate) and supportive treatment. Two days later, he was transferred to our hospital for worsened situations with loss of consciousness, anuria, and high fever.

History of past illness

The patient reported no remarkable history of past illness.

Personal and family history

The patient liked fatty food, smoked 40 cigarettes per day for 10 years, and drank 500 mL of liquor per day for 10 years. There was no family history of malignant tumors.

Physical examination

The patient's body temperature was 40 °C, heart rate was 180 beats per min, and respiratory rate was 40 breaths per min. Blood pressure and oxygen saturation could not be measured. Neurological examination revealed loss of light reflection from both pupils, and the Glasgow Coma Scale was E1V1M1. The abdomen was distended, tension was high, and bowel sounds were weak.

Laboratory examinations

The auxiliary examination results at admission are shown in Table 1.

Imaging examinations

An enhanced CT scan showed swelling of the pancreas and profound effusions in the periphery of the pancreas, omental sac, and left paracolic sulcus (Figure 1A).

Table 1 Laboratory examinations at admission

Test item	Test result	Reference range
White blood cell (× 10^9/L)	8.7	3.5-9.5
Hemoglobin (g/L)	78	120–160
Platelet (× 10^9/L)	206	100-350
Alanine aminotransferase (U/L)	230	9-50
Alkaline phosphatase (U/L)	67	45-125
Total bilirubin (μmol/L)	17.1	5.1-22.2
Conjugated bilirubin (μmol/L)	9.9	0-6.8
Potassium (mmol/L)	4.4	3.5-5.5
Serum urea (mmol/L)	19	2.78-7.14
Serum creatinine (μmol/L)	404	59-104
Creatine kinase (U/L)	42853	24-195
Myoglobin (μg/L)	88925	10-92
High-sensitivity C-reactive protein (mg/L)	> 250	< 3.0
Erythrocyte sedimentation rate (mm/h)	> 140	0-15
Procalcitonin (ng/mL)	16	< 0.25
Blood cultures	Negative	Negative

FINAL DIAGNOSIS

The patient was diagnosed with hypertriglyceridemia-related SAP with multiorgan failure, including shock, respiratory failure, acute renal failure, and rhabdomyolysis.

TREATMENT

After supportive treatment including vasoactive agents, mechanical ventilation, kidney replacement therapy, and early enteral nutrition support the patient was stabilized and admitted to the general ward after spending 20 d in the intensive care units, during which time three percutaneous drainage tubes were placed for possible infection in necrosis collection and fluid effusions in the peripancreatic region and left paracolic sulcus (Figures 1B, 2A and 2B). The drainage fluid culture was negative.

One month after the onset of SAP, the patient developed fever and right upper quadrant pain with elevated conjugated bilirubin and alkaline phosphatase levels of 37.3 μmol/L and 340 U/L, respectively. Contrast-enhanced CT (Figure 2A) and magnetic resonance cholangiopancreatography (Figure 2C) revealed a cystic lesion adjacent to and communicating to a large gallbladder (Figure 2B), and gallbladder perforation was considered. Therefore, another drainage tube was placed into the cystic lesion percutaneously (Figure 2D). The drainage fluid was bile-like with an elevated total bilirubin level of 412 μmol/L.

Two months after the onset of SAP, fever came intermittently when abdominal CT showed gas in the necrotic tissue (Figure 1B), and the peripancreatic drainage fluid gradually turned into pus, which could be readily treated by antibiotics but recurred after antibiotics were ceased. One month later, when the radiologists replaced drainage tubes, feces were withdrawn from the gallbladder fossa and left paracolic sulcus. As indirect evidence of cholecysto-colonic fistula, CT showed gas in the gallbladder lumen (Figure 2E). Then, cholecysto-colonic fistula and descending colon fistula were confirmed *via* contrast examination. The patient immediately received nephroscopy-assisted debridement of peripancreatic necrosis and ileostomy. Peripancreatic and paracolic drains were changed to larger tubes (Figure 1C), and the abdominal cavity was flushed with normal saline every day. One month after surgery, the patient's body temperature returned to normal, and he was discharged from the hospital.

OUTCOME AND FOLLOW-UP

Six months after the onset of SAP, the patient gradually resumed oral intake with good tolerance, and

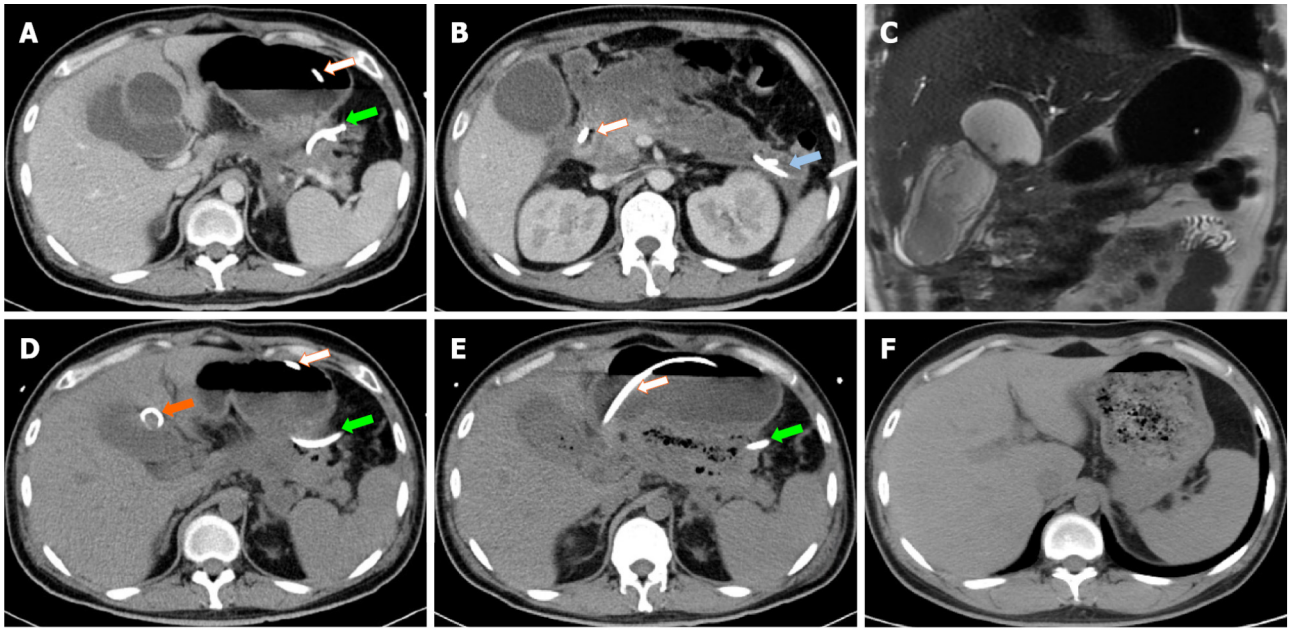

DOI: 10.12998/wjcc.v10.i17.5846 **Copyright** ©The Author(s) 2022.

Figure 2 Gallbladder perforation and cholecysto-colonic fistula during the course of disease. The jejunal feeding tube is marked by a white arrow. The percutaneous drainage tube for the pancreatic tail area is marked by a green arrow. The percutaneous drainage tube for the left paracolic sulcus is marked by a blue arrow. A: Contrast-enhanced computed tomography (CT) demonstrating a cystic lesion communicating to the gallbladder 1 mo after severe acute pancreatitis (SAP) onset; B: Contrast-enhanced CT demonstrating a large gallbladder and profound exudation in pancreatic head region 1 mo after SAP onset; C: Magnetic resonance cholangiopancreatography demonstrating a cystic lesion adjacent to the gallbladder 1 mo after SAP onset; D: CT demonstrating adequate drainage of gallbladder perforation 2 mo after SAP onset. The percutaneous drainage tube for the cystic lesion is marked by an orange arrow; E: CT demonstrating gas in the gallbladder lumen as indirect evidence of cholecysto-colonic fistula before debridement surgery; F: CT demonstrating a recovery from cholecystectomy 10 mo after SAP onset.

all drains were removed 1 mo later. Seven months after ileostomy, a colonoscopy revealed spontaneous closure of colon fistulas, and abdominal CT showed the absorption of peripancreatic infectious necrosis (Figure 1D). The patient subsequently underwent cholecystectomy (Figure 2F) and ileostomy reversal. Pathology of the gallbladder suggested chronic inflammation of fibrous connective tissue. Since then, the patient has been symptom free for 5 mo. To illustrate the patient's medical history succinctly and clearly, we briefly summarize it in Table 2.

DISCUSSION

Gallbladder perforation usually occurs days to weeks after acute cholecystitis[3]. It can cause diffuse peritonitis, or it can be surrounded by connective tissue, causing only localized peritonitis[2]. Gallbladder perforation is commonly seen in calculous cholecystitis and sometimes in cancer or trauma [8,9]. On the other hand, acalculous gallbladder perforation in AP is extremely rare. In this case, gallbladder perforation was diagnosed 1 mo after the onset of SAP. Fortunately, the bile was confined to the cystic lesion adjacent to gallbladder without causing generalized biliary peritonitis.

One of the possible mechanisms of gallbladder perforation is that poor bile drainage leads to increased pressure in the gallbladder, causing gallbladder ischemia and necrosis[10]. In this case, pancreatic edema and peripancreatic exudation might have caused biliary obstruction. Second, pancreatic enzymes can erode the adjacent gallbladder[3]. Our patient had profound effusions in the omental sac, which might contribute to damaging the integrity of the gallbladder walls. Third, hypotension will lead to insufficient blood supply to the gallbladder[10]. Our patient developed distributive shock shortly after SAP onset. Moreover, fasting after SAP onset and jejunal nutrition further increased the intraluminal pressure of the gallbladder according to animal models[11,12].

Colon complications of acute pancreatitis are uncommon and mainly include necrosis, perforation, fistula, and stricture[7,13,14]. Necrosis and perforation appear early in the course of necrotizing pancreatitis, usually within 1 mo, while fistulas and stricture usually occur several months later. In the current case, a cholecysto-colonic fistula, which has not been reported before, and a descending colon fistula were found during drain replacement 3 mo after the onset of SAP and 1 mo after peripancreatic infection.

Table 2 Time course of this case

Time since SAP onset	Clinical events
11 d	Started jejunal nutrition
1 mo	Gallbladder perforation
	Percutaneous drainage
2 mo	Peripancreatic infection
	Antibiotics and percutaneous drainage
3 mo	Cholecysto-colonic fistula and descending colon fistula
	Peripancreatic debridement and ileostomy
4 mo	Normal body temperature
	Discharged from hospital
6 mo	Started oral intake
7 mo	All drains removed
10 mo	Cholecystectomy and ileostomy reversal
15 mo	Free from the symptoms after surgery

SAP: Severe acute pancreatitis.

Similar to gallbladder perforation, erosion of pancreatic enzymes and infectious necrosis, as well as hypotension from shock, can also cause disruption of the colon wall[15,16]. Iatrogenic injury could easily injure the intestine. However, a retrospective study ruled out percutaneous drainage as a risk factor for colon complications[13]. In the present case, it was difficult to fully rule out the possibility of puncture injury.

Local inflammation is prominent when colon fistula forms. Therefore, it is best not to repair the intestinal wall in the early stage. Pancreatic debridement and proximal colostomy are feasible options [17,18], after which some fistulas can thus be cured[7]. When local inflammation subsided, ostomy reduction was performed a mean of 248.1 d after the initial surgery[13]. Currently, there is no treatment recommendation for patients with gallbladder perforation or fistula in acalculous AP. According to our experience, localized gallbladder perforation can be stabilized by percutaneous drainage instead of urgent surgery. Pancreatic debridement and proximal colostomy followed by cholecystectomy after a period of 7 mo are feasible and valid treatment options for cholecysto-colonic fistulas.

CONCLUSION

Although gallbladder perforation and gastrointestinal fistula are rare complications in acalculous SAP patients, they should be considered for their poor prognosis. Pancreatic debridement and proximal colostomy followed by cholecystectomy after the infection is relieved are feasible and valid treatment options for cholecysto-colonic fistulas.

FOOTNOTES

Author contributions: Wang QP and Chen YJ were the patient's gastroenterologists, reviewed the literature, and contributed to manuscript drafting; Sun MX was the patient's gastroenterologist; Dai JY was the patient's emergency doctor; Cao J interpreted the imaging findings and performed the percutaneous drainage; Xu Q and Zhang GN performed all surgeries; Zhang SY was the patient's gastroenterologist and was responsible for the revision of the manuscript for important intellectual content; All authors issued final approval for the version to be submitted.

Supported by Beijing Science and Technology Program, No. Z181100001618013; and Peking Union Medical College Education Reform Program, No. 2019zlgc0116.

Informed consent statement: Informed written consent was obtained from the patient for publication of this report and any accompanying images.

Conflict-of-interest statement: Dr. Zhang reports grants from Beijing Science and Technology Program, grants from

Peking Union Medical College Education Reform Program, during the conduct of the study.

CARE Checklist (2016) statement: The authors have read the CARE Checklist (2016), and the manuscript was prepared and revised according to the CARE Checklist (2016).

Open-Access: This article is an open-access article that was selected by an in-house editor and fully peer-reviewed by external reviewers. It is distributed in accordance with the Creative Commons Attribution NonCommercial (CC BY-NC 4.0) license, which permits others to distribute, remix, adapt, build upon this work non-commercially, and license their derivative works on different terms, provided the original work is properly cited and the use is non-commercial. See: https://creativecommons.org/Licenses/by-nc/4.0/

Country/Territory of origin: China

ORCID number: Qi-Pu Wang 0000-0002-4173-3169; Yi-Jun Chen 0000-0003-1329-2527; Mei-Xing Sun 0000-0003-3293-330X; Jia-Yuan Dai 0000-0002-2948-8519; Jian Cao 0000-0002-4724-7065; Qiang Xu 0000-0002-6785-7178; Guan-Nan Zhang 0000-0001-8685-5015; Sheng-Yu Zhang 0000-0001-5321-457X.

S-Editor: Fan JR
L-Editor: Filipodia
P-Editor: Fan JR

REFERENCES

1 **Perera M**, Pham T, Toshniwal S, Lennie Y, Chan S, Houli N. A case of concomitant perforated acute cholecystitis and pancreatitis. *Case Rep Surg* 2013; **2013**: 263046 [PMID: 23956917 DOI: 10.1155/2013/263046]
2 **Quiroga-Garza A**, Alvarez-Villalobos NA, Angeles-Mar HJ, Garcia-Campa M, Muñoz-Leija MA, Salinas-Alvarez Y, Elizondo-Omaña RE, Guzmán-López S. Localized gallbladder perforation: a systematic review of treatment and prognosis. *HPB (Oxford)* 2021; **23**: 1639-1646 [PMID: 34246546 DOI: 10.1016/j.hpb.2021.06.003]
3 **Başara I**, Seçil M. Spontaneous asymptomatic gallbladder perforation. *Quant Imaging Med Surg* 2014; **4**: 212-213 [PMID: 24914424 DOI: 10.3978/j.issn.2223-4292.2014.03.03]
4 **Derici H**, Kara C, Bozdag AD, Nazli O, Tansug T, Akca E. Diagnosis and treatment of gallbladder perforation. *World J Gastroenterol* 2006; **12**: 7832-7836 [PMID: 17203529 DOI: 10.3748/wjg.v12.i48.7832]
5 **Dhadlie S**, Ratnayake S. A rare case report of ascending colon perforation secondary to acute pancreatitis. *Int J Surg Case Rep* 2019; **55**: 62-65 [PMID: 30690284 DOI: 10.1016/j.ijscr.2018.12.010]
6 **Andrew D**, Shyam K, Johny J, Beaty S. Elderly male patient with gastrocolic fistula following severe acute necrotising pancreatitis. *BMJ Case Rep* 2021; **14** [PMID: 33414125 DOI: 10.1136/bcr-2020-240426]
7 **Mohamed SR**, Siriwardena AK. Understanding the colonic complications of pancreatitis. *Pancreatology* 2008; **8**: 153-158 [PMID: 18382101 DOI: 10.1159/000123607]
8 **Zhang J**, Shen G, Shi Y, Zhang C, Hong D, Jin L, Yang H, Sun W, Cai H, Hu Z, Wu W. Spontaneous acalculous gallbladder perforation in a man secondary to chemotherapy and radiation: A rare case report. *Medicine (Baltimore)* 2018; **97**: e0674 [PMID: 29742709 DOI: 10.1097/MD.0000000000010674]
9 **Katagiri T**, Irisawa A, Wakabayashi H, Tsunoda T, Tomoda H, Saito R, Kinuta S. Idiopathic perforation of acalculous gallbladder after insertion of a transpapillary pancreatic stent. *Endosc Int Open* 2016; **4**: E838-E840 [PMID: 27540570 DOI: 10.1055/s-0042-109598]
10 **Gunasekaran G**, Naik D, Gupta A, Bhandari V, Kuppusamy M, Kumar G, Chishi NS. Gallbladder perforation: a single center experience of 32 cases. *Korean J Hepatobiliary Pancreat Surg* 2015; **19**: 6-10 [PMID: 26155270 DOI: 10.14701/kjhbps.2015.19.1.6]
11 **Psáder R**, Sterczer A, Pápa K, Harnos A, Szilvási V, Pap A. Effect of enteral feeding on gallbladder function in dogs. *Acta Vet Hung* 2012; **60**: 211-222 [PMID: 22609992 DOI: 10.1556/AVet.2012.018]
12 **Ledeboer M**, Masclee AA, Biemond I, Lamers CB. Gallbladder motility and cholecystokinin secretion during continuous enteral nutrition. *Am J Gastroenterol* 1997; **92**: 2274-2279 [PMID: 9399769]
13 **Maatman TK**, Nicolas ME, Roch AM, Lewellen KA, Al-Azzawi HH, Ceppa EP, House MG, Nakeeb A, Schmidt CM, Zyromski NJ. Colon Involvement in Necrotizing Pancreatitis: Incidence, Risk Factors, and Outcomes. *Ann Surg* 2022; **275**: 568-575 [PMID: 32649468 DOI: 10.1097/SLA.0000000000004149]
14 **Gondal B**, Ogunsua AA, McIntosh L, Shaikh Y, Cave D. Perforation of the descending colon in severe acute pancreatitis: a case report and literature review. *Pancreas* 2014; **43**: 488-490 [PMID: 24622088 DOI: 10.1097/MPA.0000000000000056]
15 **Patterson M**, Bernstein CN. A Rare Complication of Pancreatitis. *Gastroenterology* 2021; **160**: 1479-1480 [PMID: 33346005 DOI: 10.1053/j.gastro.2020.12.022]
16 **Van Minnen LP**, Besselink MG, Bosscha K, Van Leeuwen MS, Schipper ME, Gooszen HG. Colonic involvement in acute pancreatitis. A retrospective study of 16 patients. *Dig Surg* 2004; **21**: 33-38; discussion 39 [PMID: 14707391 DOI: 10.1159/000075824]
17 **Yoshikawa K**, Lefor AK, Kubota T. Acute pancreatitis followed by retroperitoneal perforation of the descending colon and a duodenal fistula: Report of a case. *Int J Surg Case Rep* 2020; **72**: 599-602 [PMID: 32698297 DOI: 10.1016/j.ijscr.2020.05.095]
18 **Hozaka Y**, Kurahara H, Mataki Y, Kawasaki Y, Iino S, Sakoda M, Mori S, Maemura K, Shinchi H, Natsugoe S. Successful

treatment for severe pancreatitis with colonic perforation using video-assisted retroperitoneal debridement: A case report. *Int J Surg Case Rep* 2018; **52**: 23-27 [PMID: 30308424 DOI: 10.1016/j.ijscr.2018.09.046]

World Journal of Clinical Cases

Submit a Manuscript: https://www.f6publishing.com

World J Clin Cases 2022 June 16; 10(17): 5854-5860

DOI: 10.12998/wjcc.v10.i17.5854

ISSN 2307-8960 (online)

CASE REPORT

Beware of gastric tube in esophagectomy after gastric radiotherapy: A case report

Can Yurttas, Doerte Wichmann, Cihan Gani, Malte N Bongers, Stephan Singer, Christian Thiel, Alfred Koenigsrainer, Karolin Thiel

Specialty type: Medicine, research and experimental

Provenance and peer review: Unsolicited article; Externally peer reviewed.

Peer-review model: Single blind

Peer-review report's scientific quality classification

Grade A (Excellent): 0
Grade B (Very good): 0
Grade C (Good): C
Grade D (Fair): D
Grade E (Poor): 0

P-Reviewer: Di Meglio L, Italy; Ding X, China

Received: December 27, 2021
Peer-review started: December 27, 2021
First decision: March 10, 2022
Revised: March 11, 2022
Accepted: April 9, 2022
Article in press: April 9, 2022
Published online: June 16, 2022

Can Yurttas, Doerte Wichmann, Christian Thiel, Alfred Koenigsrainer, Karolin Thiel, Department of General, Visceral and Transplant Surgery, University Hospital of Tuebingen, Tuebingen 72076, Germany

Cihan Gani, Department of Radiooncology, University Hospital of Tuebingen, Tuebingen 72076, Germany

Malte N Bongers, Department of Diagnostic and Interventional Radiology, University Hospital of Tuebingen, Tuebingen 72076, Germany

Stephan Singer, Department of Pathology, University Hospital of Tuebingen, Tuebingen 72076, Germany

Corresponding author: Karolin Thiel, MD, Department of General, Visceral and Transplant Surgery, University Hospital of Tuebingen, Hoppe Seyler Str 3, Tuebingen 72076, Germany. karolin.thiel@med.uni-tuebingen.de

Abstract

BACKGROUND

Gastric tube formation and pull-up is the most common technique of reconstruction following esophagectomy for esophageal cancer. If previous treatment with radiotherapy for gastric mucosa-associated lymphoid tissue (MALT)-lymphoma restricts suitability of the stomach for anastomosis to the esophagus is unknown.

CASE SUMMARY

A 57-year-old man underwent sequential chemotherapy and radiotherapy for gastric MALT-lymphoma seven years prior to diagnosis of esophageal adenocarcinoma. Esophagectomy without neoadjuvant treatment was recommended by the multidisciplinary tumor board due to early tumor stage [uT1 (sm2) uN+ cM0 according to TNM-classification of malignant tumors, 8th edition] without lymph node involvement. Minimal invasive esophageal resection with esophagogastrostomy was performed. Due to gastric tube necrosis with anastomotic leakage on the twelfth postoperative day, diverting resection with construction of a cervical salivary fistula was necessary. Rapid recovery facilitated colonic interposition without any complications six months afterwards.

CONCLUSION

This case report may represent the start for further investigation to know if it is reasonable to refrain from esophagogastrostomy in patients with a long interval between gastric radiotherapy and surgery.

Key Words: Esophageal cancer; Mucosa-associated lymphoid tissue lymphoma; Esophagogastrostomy; Cervical fistula; Colonic interposition; Case report

©The Author(s) 2022. Published by Baishideng Publishing Group Inc. All rights reserved.

Core Tip: A patient with previous radiotherapy for gastric mucosa-associated lymphoid tissue lymphoma underwent esophagectomy and esophagogastrostomy for esophageal cancer more than seven years later. Gastric tube necrosis, made diversion surgery with salivary fistula necessary. Six months later, interposition of the transverse colon was performed without occurrence of any complications. The patient fully recovered with unlimited oral intake capability and remains free of tumor recurrence at date of publication. In patients with a long interval between gastric radiotherapy and surgery esophagogastrostomy should be avoided.

Citation: Yurttas C, Wichmann D, Gani C, Bongers MN, Singer S, Thiel C, Koenigsrainer A, Thiel K. Beware of gastric tube in esophagectomy after gastric radiotherapy: A case report. *World J Clin Cases* 2022; 10(17): 5854-5860
URL: https://www.wjgnet.com/2307-8960/full/v10/i17/5854.htm
DOI: https://dx.doi.org/10.12998/wjcc.v10.i17.5854

INTRODUCTION

Esophagectomy, combined with neoadjuvant chemo(radio)therapy in the locally advanced situation, is considered standard treatment with curative intention for carcinomas of the esophagus and the esophagogastric junction[1]. Most commonly, anastomosis of the remnant esophagus to a gastric tube is performed[2]. Whether prior chemoradiotherapy for gastric mucosa-associated lymphoid tissue lymphoma limits the stomach's suitability for reconstruction is unknown. With this case report we provide first evidence for pretreated stomach usage for esophagogastrostomy in esophagectomy.

CASE PRESENTATION

Chief complaints

Due to asymptomatic gastro-esophageal reflux disease with Long Segment Barrett's esophagus C9M13 according to Prague Classification, a 64-year-old patient underwent repetitive esophagogastroduodenoscopy.

History of present illness

In 2020, biopsy of the distal esophagus 34 cm from row of teeth revealed invasive moderately differentiated (G2) adenocarcinoma. Moreover, erythema and atrophy of the gastric mucosa were detected. However, the patient had no disease-specific complaints when he first presented to our department. Oral intake of standard western-diet was unrestricted and body weight was constant at a BMI of 29.1 kg/m^2.

History of past illness

In 2012, the 57-year-old man was diagnosed with diffuse large B-cell lymphoma (DLBCL) of the stomach in the course of endoscopic treatment of gastric bleeding (2a according to the Forrest Classification of gastrointestinal bleedings). Although there was no detection of *Helicobacter pylori*, eradication therapy was performed. Endosonography proved localization at the posterior gastric wall without infiltration of neighboring tissues, whereas computed tomography (CT) scan and bone marrow biopsy were without evidence of disease equivalent to stage IE according to the Ann Arbor staging system. Following four courses of rituximab, cyclophosphamide, doxorubicin hydrochloride (hydroxydaunorubicin), vincristine sulfate (Oncovin), and prednisone (R-CHOP) with curative intention percutaneous normofractionated radiotherapy of the stomach with a total of 39.6 Gray (Gy) in 20 fractions weekly was performed as consolidating therapy. Both systemic and radiation therapy were well tolerated. Due to

herpes zoster of the left thorax antiviral therapy with aciclovir was introduced.

The patient had a history of herniated vertebral disc, struma nodosa, chronic-venous insufficiency and endoscopic resection of a low-grade adenoma of the sigmoid colon and regularly took metformin, thyroxine and sitagliptin for type 2 diabetes mellitus and hypothyroidism respectively. Hepatic and renal function were not impaired. Follow-up examinations up to five years were without any peculiarities or evidence of tumor recurrence. The patient had skipped drinking and smoking after intake of 60 pack-years.

Personal and family history

Family history was unremarkable and not related to the present case.

Physical examination

The patient was in a normal general state without any evidence of disease or restriction of normal activities.

Laboratory examinations

Preoperative blood examinations were unremarkable. Tumor markers CEA, CA19-9 and CA72-4 were within reference range.

Imaging examinations

Whereas CT scan showed no signs of distant metastases or involvement of locoregional lymph nodes, endosonography described uT1 (sm2) uN+ according to TNM classification of malignant tumors, 8th edition. Positron emission tomography-CT was performed for further clarification, which ruled out involvement of locoregional lymph nodes.

Material and methods

Surgery for esophageal cancer and gastric tube necrosis: Surgery was performed in minimally invasive technique of Ivor Lewis esophagectomy. Access to the abdominal cavity and capnoperitoneum was established with the help of a Veress needle. An optic trocar was introduced under vision with a 30° camera (KARL STORZ SE & Co. KG, Tuttlingen, Germany). The abdominal cavity was inspected to rule out injuries during access and also peritoneal or hepatic metastases. Then, gastric mobilization was performed with an electrosurgical vessel sealer, left gastric artery was clipped whereas the right gastric artery as well as the right gastroepiploic arcade were preserved. Complete D2-lymphadenectomy was performed followed by stapled gastric tube formation of approximately 5 cm in diameter. Esophagectomy including mediastinal lymphadenectomy was operated thoracoscopically with four right-sided intercostal trocars. The resection was completed with formation of a stapled circular end-to-side-esophagogastrostomy.

Emergency thoracotomy was necessary for resection of the necrotic gastric tube, hemithyroidectomy and creation of the salivary glandula. A jejunal feeding tube was inserted after laparotomy. Continuous intestinal passage was reconstructed by colonic interposition. Following laparotomy, the transverse colon was prepared for retrosternal pull-up and formation of an end-to-end esophagocolostomy and an end-to-side colojejunostomy. A side-to-side ascendodescendostomy was created.

Endoscopy and endoscopic negative-pressure therapy: Endoscopy was performed with a standard gastroscope with 9.8-mm outer caliber and 3.2-mm working channel (PENTAX Medical, Tokyo, Japan). A thin open-pore film wrapped around a drain (Medicoplast, Illingen, Germany) and fixed with a suture was constructed prior to endoscopically controlled insertion and positioning of the device. Negative pressure of -125 mmHg was established with the use of a vacuum therapy system (KCI medical, Wiesbaden, Germany).

FINAL DIAGNOSIS

Moderately differentiated adenocarcinoma of the distal esophagus with infiltration of the submucosal layer without locoregional lymph node metastases [TNM: pT1b, pN0 (0/17) L0, V0, Pn0, R0, Grading: G2].

TREATMENT

The multidisciplinary tumor board consequently recommended surgical resection without neoadjuvant treatment. Thoracoscopic and laparoscopic abdominal right thoracic esophagectomy with two-field lymphadenectomy (Ivor Lewis) and stapled end-to-side esophagogastrostomy was performed. Histopathological examination confirmed the diagnosis and staging results and complete resection of a

moderately differentiated adenocarcinoma of the distal esophagus. The gastric mucosa showed signs of erosive gastritis with denuded surface epithelium, subepithelial and interstitial hemorrhage, but no recurrent lymphoma infiltrates. The initial postoperative course was regular and without any pathologic findings. Following extubation immediately after surgery, the patient was monitored at the intermediate care unit for one day without requiring cardiocirculatory or respiratory support before transfer to the general ward. Low-dose anticoagulation with unfractionated heparin was initiated six hours after surgery. Amount and quality of drain output were unsuspicious. Seven days after surgery the patient's general state was seen to deteriorate and elevated leukocytes and C-reactive protein were observed, which required endoscopic assessment of the esophagogastrostomy to rule out anastomotic leakage. The gastric interposition showed compromised perfusion without evidence of anastomotic insufficiency. Endoscopic negative-pressure therapy was therefore introduced. After vomiting with aspiration during anaesthetization the patient was transferred to the intensive care unit. Despite initiation of calculated antibiotic therapy with meropenem, vancomycin and anidulafungin there was no observable improvement. On day 12 postoperative, endoscopy revealed necrosis of the gastric interposition with a pronounced anastomotic insufficiency prompting surgical resection of the gastric tube interposition, creation of a cervical fistula and insertion of a jejunal feeding catheter (Figure 1). Histopathology confirmed ischemic necrosis of the proximal gastric tube with anastomotic leakage. There was no evidence of residual adenocarcinoma or recurrent lymphoma in the resected esophagogastrostomy or gastric tube. Postoperative pleural effusion was treated with a thoracic drain and central venous line-associated blood-stream infection, while paroxysmal tachycardia and delirium necessitated respective therapy. The patient slowly recovered until he was discharged 40 d after esophageal resection. Follow-up care was recommended by the multidisciplinary tumor board.

OUTCOME AND FOLLOW-UP

Six months later, the patient underwent colonoscopy and CT scan in preparation for colonic interposition without any contraindications or signs of tumor recurrence. Retrosternal interposition of the transverse colon creating an end-to-end esophagotransversostomy, end-to-side transversojejunostomy and a side-to-side ascendotransversostomy was performed. Postoperative course was normal. Oral intake of food and liquids was without difficulty. Supportive enteral feeding was continued. The patient was discharged home on day 12 postoperative. Nine weeks later, the patient was in an unrestricted general condition with stable body weight so that the jejunal feeding catheter was removed. Table 1 shows information from this case report organized in a time table.

DISCUSSION

When the patient first presented to our out-patient clinic, the suitability of the pretreated stomach for construction of an esophagogastrostomy was uncertain because evidence was missing. In the literature, complications of esophagogastrostomy in general are reported to occur in 12% and mortality in 4% of all cases[3]. According to the present literature, small bowel or colonic interposition may be considered alternative grafts. Compared to the colon, small bowel grafts require fewer anastomoses, are rarely affected by malignancies and have good peristalsis, but provide no reservoir function. Colonic interposition is complicated by the need for three to four anastomoses and potential metachronous development of adenoma and carcinoma. Nevertheless, longer grafts are available offering reservoir-like function and less reflux[4,5]. However, a retrospective cohort study comparing complex esophageal reconstruction including 44.7% of patients with other than gastric tube formation to non-complex esophagectomy with direct gastric pull-up reported higher morbidity and longer length of stay for patients in the complex therapy group[6]. Jejunal grafts are described as suitable primary alternatives for any scope of esophageal replacement, but are accompanied by up to 36% anastomotic leakage and 10% mortality[7]. In colonic interposition, higher overall morbidity of 45.0%-64.0% and increased risk of anastomotic leakage occurring in 13.0%-30.0% of patients is shown[8-11]. Alternatively, construction of a cervical salivary fistula with secondary gastric tube formation could be an option, but especially patients with cancer were shown to have poor outcome after primary diversion and secondary reconstruction in esophagectomy[12]. Considering our experience with gastric tubes and the lower complication rates as compared to small bowel and colonic interposition, the decision for esophagogastrostomy was therefore made together with the patient.

Despite expectable poor outcome following resection of the necrotic gastric tube with diversion[12], creation of a cervical fistula and secondary colonic interposition, our patient fully recovered, has sufficient oral intake capacity and to date remains without signs of any tumor recurrence.

Neoadjuvant radiochemotherapy prior to esophagectomy has been shown to improve overall survival compared to surgery alone with a very favourable toxicity profile. In particular, no increase in anastomotic leakage was reported in the CROSS trial[13], whereas in-field creation of anastomosis following neoadjuvant radiochemotherapy and esophagectomy was identified as a risk factor for

Table 1 Information from this case report organized in a time table

Date	Diagnosis	Intervention
September, 2012	Gastric MALT lymphoma	R-CHOP
February, 2013	Gastric MALT lymphoma	Intensity-modulated radiation therapy up to 39.6 Gy
July, 2020	Barrett's carcinoma	Endoscopic biopsy
November, 2020	Barrett's carcinoma	Abdominal right-thoracic esophagectomy with two-field lymphadenectomy (Ivor Lewis)
December, 2020	Gastric tube necrosis	Diverting resection with creation of cervical salivary fistula
June, 2021	Presence of a cervical salivary fistula	Colonic interposition and insertion of a jejunal feeding catheter
August, 2021	Needless jejunal feeding catheter	Extraction of jejunal feeding catheter

MALT: Mucosa-associated lymphoid tissue; R-CHOP: Rituximab, cyclophosphamide, doxorubicin hydrochloride (hydroxydaunorubicin), vincristine sulfate (Oncovin), and prednisone.

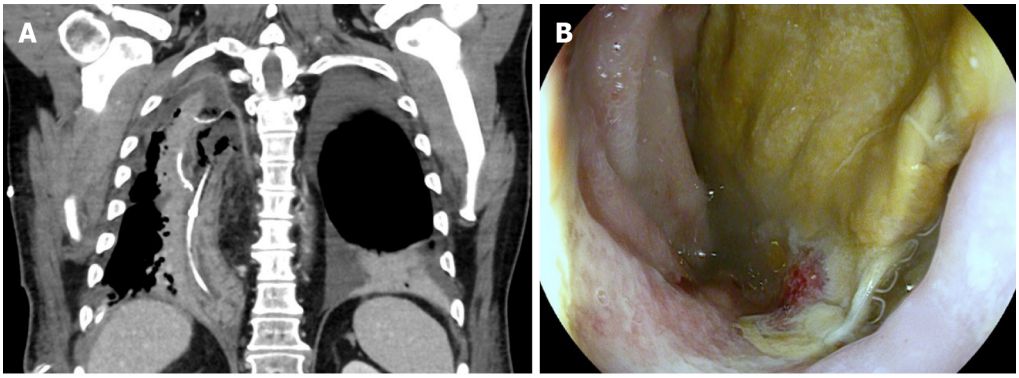

DOI: 10.12998/wjcc.v10.i17.5854 **Copyright** ©The Author(s) 2022.

Figure 1 Ischemic necrosis of the gastric interposition with anastomotic leakage. A and B: Computed tomography (A) and endoscopy (B). Computed tomography also shows left-sided pleural effusion and inserted nasogastric tube. Endoscopy also revealed the anastomotic dehiscence with cavity and the exposed staples.

anastomotic leakage in a retrospective analysis of 285 patients treated for esophageal cancer[14]. Especially in distal esophageal cancer the celiac lymph nodes and the ones at the lesser gastric curvature are frequently irradiated in the preoperative setting with doses that are comparable to the dose given in the current case presentation resulting in a considerable dose burden to the stomach without causing an excessive rate of anastomotic leakage. A major difference however between preoperative radiotherapy for esophageal cancer and the previous treatment with radiotherapy in the current case is the interval between radiotherapy and surgery. While surgery after planned neoadjuvant therapy is commonly scheduled within a couple of weeks, the interval was seven years in the present case. One can hypothesize that the tissue turned less "flexible" over the time due to fibrosis which might have contributed to anastomotic leakage. However, in the present case radiotherapy was applied to the specimen employed for reconstruction and not to the resected organ.

CONCLUSION

We therefore recommend that stomachs pretreated by radiotherapy should not be utilized for reconstruction in esophagectomy. Although this case report provides little evidence from a single patient only without proven causality, further investigations as to whether stomachs pretreated by radiotherapy in general should not be utilized for reconstruction in esophagectomy are required.

ACKNOWLEDGEMENTS

The authors thank Margreiter MH for her kind contribution to preparation of the manuscript.

FOOTNOTES

Author contributions: Yurttas C, Thiel K and Koenigsrainer A conceived and wrote the manuscript; Thiel K and Koenigsrainer A were responsible for overall treatment; Endoscopic treatment was performed by Wichmann D; Yurttas C and Bongers MN prepared the figures; Yurttas C, Thiel K, Gani C, Thiel C, Singer S and Koenigsrainer A revised the manuscript; all authors read and approved the final version of the manuscript.

Informed consent statement: For all clinical data and personal images written consent for publication was obtained from the patient.

Conflict-of-interest statement: The authors have no competing interests to declare in the context of the current case.

CARE Checklist (2016) statement: The authors have read the CARE Checklist (2016), and the manuscript was prepared and revised according to the CARE Checklist (2016).

Open-Access: This article is an open-access article that was selected by an in-house editor and fully peer-reviewed by external reviewers. It is distributed in accordance with the Creative Commons Attribution NonCommercial (CC BY-NC 4.0) license, which permits others to distribute, remix, adapt, build upon this work non-commercially, and license their derivative works on different terms, provided the original work is properly cited and the use is non-commercial. See: https://creativecommons.org/Licenses/by-nc/4.0/

Country/Territory of origin: Germany

ORCID number: Can Yurttas 0000-0001-9720-8243; Doerte Wichmann 0000-0002-8832-5031; Cihan Gani 0000-0003-0242-9428; Malte N Bongers 0000-0003-2852-0270; Stephan Singer 0000-0003-4775-6609; Christian Thiel 0000-0001-8880-4860; Alfred Koenigsrainer 0000-0002-2301-4080; Karolin Thiel 0000-0002-7328-7589.

S-Editor: Gao CC
L-Editor: A
P-Editor: Gao CC

REFERENCES

1 **Low DE**. Evolution in surgical management of esophageal cancer. *Dig Dis* 2013; **31**: 21-29 [PMID: 23797119 DOI: 10.1159/000343650]
2 **Low DE**, Kuppusamy MK, Alderson D, Cecconello I, Chang AC, Darling G, Davies A, D'Journo XB, Gisbertz SS, Griffin SM, Hardwick R, Hoelscher A, Hofstetter W, Jobe B, Kitagawa Y, Law S, Mariette C, Maynard N, Morse CR, Nafteux P, Pera M, Pramesh CS, Puig S, Reynolds JV, Schroeder W, Smithers M, Wijnhoven BPL. Benchmarking Complications Associated with Esophagectomy. *Ann Surg* 2019; **269**: 291-298 [PMID: 29206677 DOI: 10.1097/SLA.0000000000002611]
3 **Butskiy O**, Rahmanian R, White RA, Durham S, Anderson DW, Prisman E. Revisiting the gastric pull-up for pharyngoesophageal reconstruction: A systematic review and meta-analysis of mortality and morbidity. *J Surg Oncol* 2016; **114**: 907-914 [PMID: 27774626 DOI: 10.1002/jso.24477]
4 **Watanabe M**, Mine S, Nishida K, Kurogochi T, Okamura A, Imamura Y. Reconstruction after esophagectomy for esophageal cancer patients with a history of gastrectomy. *Gen Thorac Cardiovasc Surg* 2016; **64**: 457-463 [PMID: 27234222 DOI: 10.1007/s11748-016-0661-0]
5 **Sohn M**, Agha A, Trum S, Moser C, Gundling F, Hochrein A, Pratschke J, Aigner F, Ritschl P. Frequency of Polyps and Adenocarcinoma in Colon Interposition After Esophagectomy in Adulthood - A Systematic Review. *Anticancer Res* 2019; **39**: 6419-6430 [PMID: 31810906 DOI: 10.21873/anticanres.13856]
6 **Moore JM**, Hooker CM, Molena D, Mungo B, Brock MV, Battafarano RJ, Yang SC. Complex Esophageal Reconstruction Procedures Have Acceptable Outcomes Compared With Routine Esophagectomy. *Ann Thorac Surg* 2016; **102**: 215-222 [PMID: 27217296 DOI: 10.1016/j.athoracsur.2016.02.039]
7 **Gaur P**, Blackmon SH. Jejunal graft conduits after esophagectomy. *J Thorac Dis* 2014; **6** Suppl 3: S333-S340 [PMID: 24876939 DOI: 10.3978/j.issn.2072-1439.2014.05.07]
8 **Hamai Y**, Hihara J, Emi M, Aoki Y, Okada M. Esophageal reconstruction using the terminal ileum and right colon in esophageal cancer surgery. *Surg Today* 2012; **42**: 342-350 [PMID: 22200754 DOI: 10.1007/s00595-011-0103-7]
9 **Mine S**, Udagawa H, Tsutsumi K, Kinoshita Y, Ueno M, Ehara K, Haruta S. Colon interposition after esophagectomy with extended lymphadenectomy for esophageal cancer. *Ann Thorac Surg* 2009; **88**: 1647-1653 [PMID: 19853126 DOI: 10.1016/j.athoracsur.2009.05.081]
10 **Klink CD**, Binnebösel M, Schneider M, Ophoff K, Schumpelick V, Jansen M. Operative outcome of colon interposition in the treatment of esophageal cancer: a 20-year experience. *Surgery* 2010; **147**: 491-496 [PMID: 20004440 DOI: 10.1016/j.surg.2009.10.045]
11 **Davis PA**, Law S, Wong J. Colonic interposition after esophagectomy for cancer. *Arch Surg* 2003; **138**: 303-308 [PMID: 12611579 DOI: 10.1001/archsurg.138.3.303]
12 **DiPierro FV**, Rice TW, DeCamp MM, Rybicki LA, Blackstone EH. Esophagectomy and staged reconstruction. *Eur J Cardiothorac Surg* 2000; **17**: 702-709 [PMID: 10856863 DOI: 10.1016/s1010-7940(00)00408-5]
13 **van Hagen P**, Hulshof MC, van Lanschot JJ, Steyerberg EW, van Berge Henegouwen MI, Wijnhoven BP, Richel DJ,

Nieuwenhuijzen GA, Hospers GA, Bonenkamp JJ, Cuesta MA, Blaisse RJ, Busch OR, ten Kate FJ, Creemers GJ, Punt CJ, Plukker JT, Verheul HM, Spillenaar Bilgen EJ, van Dekken H, van der Sangen MJ, Rozema T, Biermann K, Beukema JC, Piet AH, van Rij CM, Reinders JG, Tilanus HW, van der Gaast A; CROSS Group. Preoperative chemoradiotherapy for esophageal or junctional cancer. *N Engl J Med* 2012; **366**: 2074-2084 [PMID: 22646630 DOI: 10.1056/NEJMoa1112088]

14 **Juloori A**, Tucker SL, Komaki R, Liao Z, Correa AM, Swisher SG, Hofstetter WL, Lin SH. Influence of preoperative radiation field on postoperative leak rates in esophageal cancer patients after trimodality therapy. *J Thorac Oncol* 2014; **9**: 534-540 [PMID: 24736077 DOI: 10.1097/JTO.0000000000000100]

World Journal of Clinical Cases

Submit a Manuscript: https://www.f6publishing.com

World J Clin Cases 2022 June 16; 10(17): 5861-5868

DOI: 10.12998/wjcc.v10.i17.5861

ISSN 2307-8960 (online)

CASE REPORT

Transition from minimal change disease to focal segmental glomerulosclerosis related to occupational exposure: A case report

Long Tang, Zhen Cai, Su-Xia Wang, Wen-Jing Zhao

Specialty type: Urology and nephrology

Provenance and peer review: Unsolicited article; Externally peer reviewed.

Peer-review model: Single blind

Peer-review report's scientific quality classification

Grade A (Excellent): 0
Grade B (Very good): B
Grade C (Good): C
Grade D (Fair): 0
Grade E (Poor): 0

P-Reviewer: Trevino S, Mexico; Yorioka N, Japan

Received: December 29, 2021
Peer-review started: December 29, 2021
First decision: February 8, 2022
Revised: February 21, 2022
Accepted: April 22, 2022
Article in press: April 22, 2022
Published online: June 16, 2022

Long Tang, Zhen Cai, Wen-Jing Zhao, Department of Nephrology, Beijing Hospital of Traditional Chinese Medicine, Capital Medical University, Beijing 100010, China

Su-Xia Wang, Laboratory of Electron Microscopy, Pathological Center, Peking University First Hospital, Peking University Institute of Nephrology, Beijing 100034, China

Corresponding author: Wen-Jing Zhao, MD, PhD, Associate Professor, Chief Physician, Department of Nephrology, Beijing Hospital of Traditional Chinese Medicine, Capital Medical University, No. 23 Meishuguanhou Street, Dongcheng District, Beijing 100010, China. wenjingz@263.net

Abstract

BACKGROUND

Although minimal change disease (MCD) and focal segmental glomerulosclerosis (FSGS) have been described as two separate forms of nephrotic syndrome (NS), they are not completely independent. We report a case of a patient transitioning from MCD to FSGS, review the literature, and explore the relationship between the two diseases.

CASE SUMMARY

A 42-year-old male welder, presenting with lower extremity edema and elevated serum creatinine, was diagnosed with NS and end-stage kidney disease (ESKD) based on laboratory test results. The patient had undergone a kidney biopsy for NS 20 years previously, which indicated MCD, and a second recent kidney biopsy suggested FSGS. The patient was an electric welder with excessive levels of cadmium and lead in his blood. Consequently, we suspect that his aggravated pathology and occurrence of ESKD were related to metal nephrotoxicity. The patient eventually received kidney replacement therapy and quit his job which involved long-term exposure to metals. During the 1-year follow-up period, the patient was negative for metal elements in the blood and urine and recovered partial kidney function.

CONCLUSION

MCD and FSGS may be different stages of the same disease. The transition from MCD to FSGS in this case indicates disease progression, which may be related to excessive metal contaminants caused by the patient's occupation.

Key Words: Minimal change disease; Focal segmental glomerulosclerosis; Occupational

exposure; Cadmium; Lead; Case report

©The Author(s) 2022. Published by Baishideng Publishing Group Inc. All rights reserved.

Core Tip: Minimal change disease (MCD) and focal segmental glomerulosclerosis (FSGS) are the two major forms of nephrotic syndrome. Although MCD and FSGS are defined as different types of primary glomerular disease, there is some overlap between them in clinical features and pathological changes. We present a rare case that highlights that MCD and FSGS are actually different histological manifestations of the same disease progression. FSGS may be MCD of advanced stage, and metal overexposure may be an important cause of disease progression.

Citation: Tang L, Cai Z, Wang SX, Zhao WJ. Transition from minimal change disease to focal segmental glomerulosclerosis related to occupational exposure: A case report. *World J Clin Cases* 2022; 10(17): 5861-5868
URL: https://www.wjgnet.com/2307-8960/full/v10/i17/5861.htm
DOI: https://dx.doi.org/10.12998/wjcc.v10.i17.5861

INTRODUCTION

Nephrotic syndrome (NS) is a common glomerulopathy characterized by nephrotic proteinuria, hypoproteinemia, edema, and hyperlipidemia. Most patients with NS have similar clinical manifestations, but their pathology can be different. Minimal change disease (MCD) and focal segmental glomerulosclerosis (FSGS) are the two major forms of NS. MCD is the most frequent glomerular disease leading to NS in childhood, accounting for 70%-90% of cases, and is an important cause of primary NS in adolescents, with the reported rates varying between 10% and 15% of NS patients[1]. Most MCD patients are responsive to corticosteroid therapy. Active treatment can achieve complete remission, and rarely result in progression to end-stage kidney disease (ESKD). Unlike MCD, more FSGS patients are resistant to corticosteroids, and NS due to FSGS can appear at any age. A failure to respond to corticosteroids in MCD patients may predict the presence of FSGS[2].

In most textbooks, MCD and FSGS are often described as two separate diseases based on their respective characteristics, histology and outcomes, but there is still considerable evidence that they are different manifestations of the same progressive disease[3]. Steroid-sensitive NS, which is associated with MCD, might progress to steroid-resistant NS, which is associated with FSGS. Some studies have proposed that they are actually different histological manifestations of the same disease progression, and some patients experience a transition from the initial state of a collapsed cytoskeleton (MCD) to the decompensated state of permanent podocyte loss and replacement with scar (FSGS)[4].

We report a patient with MCD who underwent a second kidney biopsy due to deterioration of renal function, and the result showed a change in pathological type from MCD to FSGS, which may be related to excessive metal exposure caused by the patient's occupation. To the best of our knowledge, this is the first case report to demonstrate the transition from MCD to FSGS associated with lead and cadmium exposure.

CASE PRESENTATION

Chief complaints

A 42-year-old Asian male welder, was admitted to our hospital with bilateral lower extremity edema and elevated serum creatinine for 1 wk.

History of present illness

The patient's symptoms started 1 wk ago with recurrent episodes of bilateral lower extremity edema. At the local hospital, he was found to have an elevated serum creatinine level of 1002 μmol/L, which had reached uremic levels.

History of past illness

The patient had a history of MCD dating back 20 years, but no other relevant medical history. The patient was diagnosed with NS 20 years ago, and MCD was confirmed by kidney biopsy (Figure 1). At that time, the patient was regularly treated with corticosteroids. Prednisolone 40 mg/d was initially prescribed, which was gradually reduced and then stopped within 12 mo. The clinical symptoms of NS

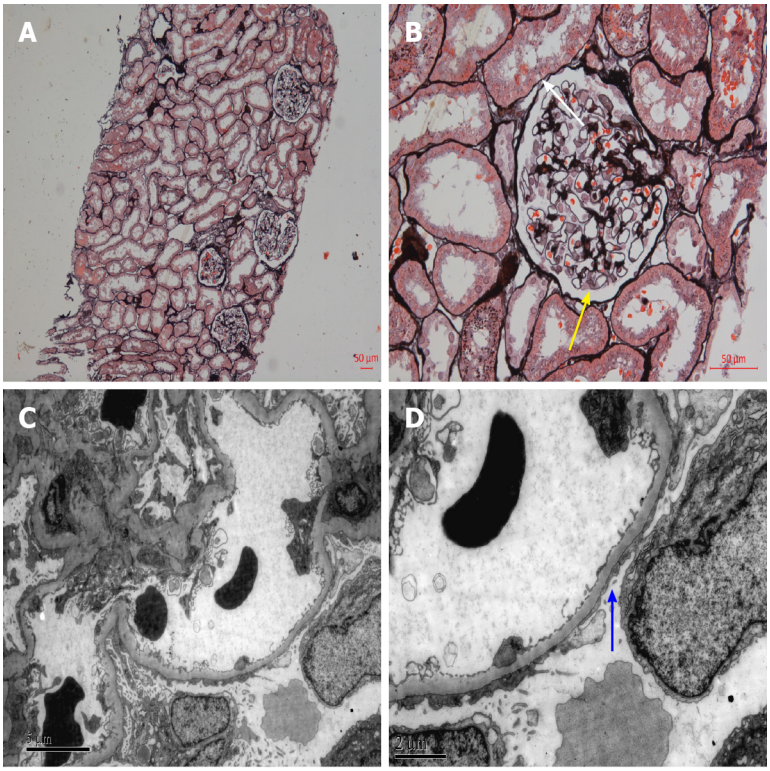

DOI: 10.12998/wjcc.v10.i17.5861 **Copyright** ©The Author(s) 2022.

Figure 1 Light microscopy and electron microscopy of histological changes of renal biopsy 20 years ago. A: Periodic acid-silver methenamine (PASM), × 100. No obvious lesions in renal interstitium and arterioles; B: PASM, × 400. Vacuolar degeneration of glomerular capillary basement membrane (yellow arrow), renal tubular epithelial cells vacuoles and granular degeneration (white arrow); C and D: Extensive fusion of foot process of glomerular visceral epithelial cells (C: × 6000; D: × 12000, blue arrow).

were completely relieved after treatment, and his proteinuria turned negative. The patient's NS did not relapse within 1 year after glucocorticoid discontinuation. Subsequently, the patient did not regularly return visit, and routine urinalysis or kidney function was not monitored.

Personal and family history

The patient had worked as a welder for about 10 years and had been frequently exposed to welding work containing cadmium and lead in the past 1 year. The patient denied having family history.

Physical examination

The patient's vital signs upon admission were as follows: temperature, 36.5 °C; heart rate, 78 bpm; respiratory rate, 17 breaths/min; blood pressure, 150/90 mmHg, and oxygen saturation in room air, 99%. No evident abnormalities were found during a physical examination except for mild edema in both his lower extremities.

Laboratory examinations

The results of laboratory tests showed urinalysis: Protein 3+, occult blood 3+, red blood cells 18-20/HP, glucose 3+, ketones -; 24-h urinary protein quantitation 10 920 mg/24 h; serum albumin 22.3 g/L; serum creatinine 1096 μmol/L; blood urea nitrogen 34.26 mmol/L; estimated glomerular filtration rate 4.4 mL/min/1.73 m^2; blood cadmium 2.8 μg/L and blood lead 32.8 μg/L. Urine metal elements, plasma complement C3, C4, serum and urine free light chain, immunofixation electrophoresis, anti-GBM antibody, ANCA, anti-nuclear antibody series, serology for HBV, HCV, HIV, and PLA2R were all negative.

Imaging examinations

Nephrosonography revealed enhanced echogenic parenchyma without any significant kidney shrinkage, and his echocardiography, kidney artery ultrasound, and chest computed tomography were normal.

Further diagnostic work-up

After obtaining consent from the patient, we performed another kidney biopsy and the results indicated FSGS (Figure 2).

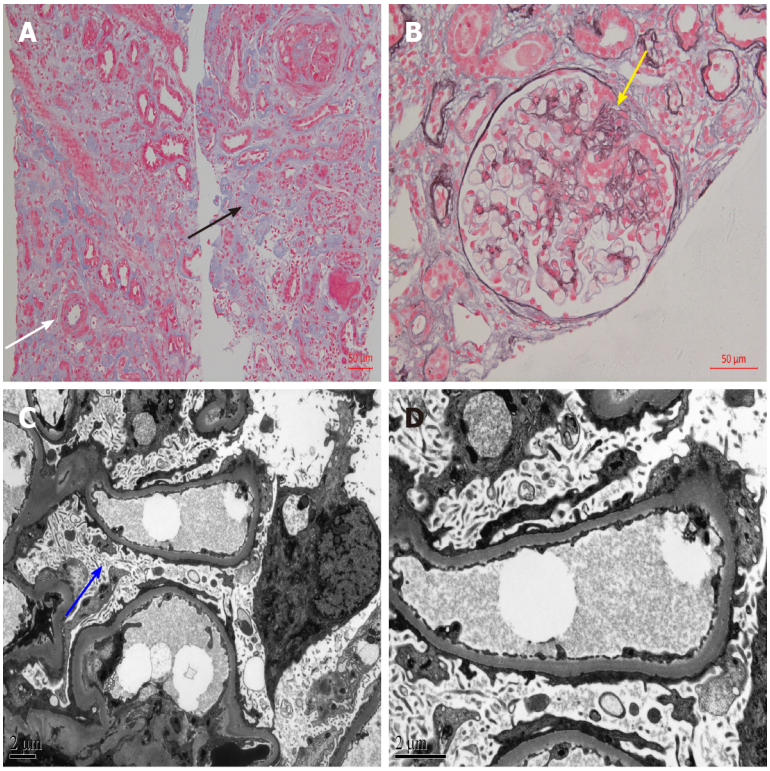

DOI: 10.12998/wjcc.v10.i17.5861 **Copyright** ©The Author(s) 2022.

Figure 2 Light microscopy and electron microscopy of histological changes of renal biopsy after 20 years. A: Masson, × 200. Multifocal and patchy atrophy of renal tubules, multifocal and patchy lymphocytic infiltration of renal interstitium with fibrosis (black arrow), and thickening of arterioles (white arrow); B: Periodic acid-silver methenamine, × 400. Mild segmental hyperplasia of glomerular mesangial cells and matrix, and segmental sclerosis (yellow arrow); C and D: Microvillous transformation of podocytes and extensive fusion of foot processes (C: × 6000, blue arrow; D: × 12000).

FINAL DIAGNOSIS

The final diagnosis of the presented case was ESKD, FSGS-induced NS, and the pathological type transitioned from MCD to FSGS.

TREATMENT

Our primary diagnosis was recurrent MCD-induced acute kidney injury (AKI). Considering that the patient had experienced an episode of worsening acute kidney failure, and the re-examination showed no recovery trend of serum creatinine, urgent hemodialysis was performed. After ward rounds and case discussions, the patient was recommended to try prednisolone acetate tablets orally at a dose of 30 mg/d. Other adjuvant therapies during dialysis included diuretics and traditional Chinese medicine. Although the use of oral prednisolone during hemodialysis is controversial, our aim was to help this patient alleviate MCD or AKI through aggressive treatment, and avoid ESKD or long-term dialysis. However, edema was relieved after 1 mo of treatment, but his kidney function did not significantly improve. The previous kidney biopsy of the patient showed MCD with a favorable prognosis, which was insufficient to explain the current ESKD. Therefore, we did another kidney biopsy and the results showed FSGS. Coupled with the kidney biopsy results, the patient eventually received continuous kidney replacement therapy with rapid corticosteroid reduction and withdrawal.

OUTCOME AND FOLLOW-UP

The patient resigned from his job after being discharged from the hospital, which discontinued his exposure to metal. During the regular 1-year follow-up period, the patient was negative for metal elements in the blood and urine and recovered partial kidney function (Table 1).

Table 1 Temporal evolution of the laboratory parameters

Parameter	Time							
	1 wk[1]				2 wk	3 wk[2]	4 wk[3]	1 yr[4]
Urinalysis								
24hUP (mg/24 h)	10920				10320	11482.8	-	3320
mALB/Cr (mg/mmol)	866.95				-	-	-	339.06
RBCs (cells/HP)	18-20				8-12	7-10	-	1-2
DysEry (%)	> 80				> 75	> 70	-	-
Biochemical test								
CR (μmol/L)	Pre-HD	1096	848.3	902.8	760	703	901.5	504.4
	Post-HD	587.7	528.6	596				
BUN (mmol/L)	Pre-HD	34.26	22.27	22.8	14.64	13.48	23.11	15.38
	Post-HD	18.1	13.82	10.88				
ALB (g/L)	22.3				21.2	22.4	22.7	36
CHO (mmol/L)	7.4				-	4.27	-	3.89
TG (mmol/L)	1.53				-	1.31	-	1.33
Blood toxicity elements test								
Pb (μg/L)	32.8				-	-	-	24.3
Cd (μg/L)	2.8				-	-	-	1.5
As (μg/L)	6.4				-	-	-	5.1
Hg (μg/L)	0.2				-	-	-	< 0.1
Tl (μg/L)	< 0.1				-	-	-	0
Al (μg/L)	48.1				-	-	-	30
Mn (μg/L)	< 0.1				-	-	-	< 0.1

[1]Time of hemodialysis (HD) and prednisolone acetate initiation. Kidney function tests pre- and post-HD were observed in the following weeks.
[2]Try stopping HD for 1 wk.
[3]Time of repeat kidney biopsy, discontinuing the prednisolone acetate, and entering maintenance HD.
[4]Laboratory examination after 1 yr of follow-up.
"-": No results; 24hUP: 24-h urinary protein; mALB/Cr: Urinary microalbumin to creatinine ratio; RBCs: Red blood cells; DysEry: Dysmorphic erythrocytes ratio; CR: Creatinine; BUN: Blood urea nitrogen; ALB: Albumin; CHO: Total cholesterol; TG: Triglyceride; Pb: Lead; Cd: Cadmium; As: Arsenic; Hg: Mercury; Tl: Thallium; Al: Aluminum; Mn: Manganese.

DISCUSSION

Our patient underwent a kidney biopsy at the time of initial diagnosis of NS, which pathologically revealed MCD. MCD is considered to be a benign disease with a favorable long-term prognosis, which rarely progresses to ESKD. There was no glomerular injury detected under light microscopy, and only the foot process of podocytes disappeared under electron microscopy, but no podocytes loss[5]. Although the proportion of adult-onset MCD patients in NS is low, unlike children, adults are less responsive to corticosteroids and more prone to AKI. Moreover, steroid-resistant MCD patients may progress to ESKD, and these patients may be the missed FSGS patients. In contrast to MCD, patients with FSGS have a higher risk of corticosteroid resistance and kidney failure. Glomerular injury caused by FSGS leads to irreversible scar formation, which has a poor prognosis and eventually develops into ESKD. Irreversible glomerular damage caused in the context of FSGS can be explained by podocyte depletion. Compensatory hypertrophy of the remaining podocytes, cell-to-cell propagation of podocyte injury, and segmental solidification of the glomerular tuft can lead to progressive focal and segmental sclerosis[6].

As far as we know, cases of transition between MCD and FSGS are not rare in clinical practice, but few cases have been reported. Some cases have appeared in observational studies without proper in-depth analysis, and most of these studies involved children or adolescents[4,7,8]. In the above literature, most scholars placed FSGS at the onset of the disease. The focal and segmental nature of FSGS leads to sample error or diagnosis error, which may result in MCD misdiagnosis, or FSGS being missed, we

agree, especially in patients with early lesions or limited glomeruli in the biopsy specimens. Early FSGS can only show the diffuse effacement of the foot process, which is consistent with MCD. There was no difference in the decrease of podocyte density labeled by WT1 between MCD and FSGS[9]. These factors sometimes result in confusion between the two diseases for clinicians. In fact, FSGS lesions may be absent in the early stages of NS, and the presence of FSGS lesions in the repeated biopsy tissue reflected the progression of MCD. The dose dependence of animal models supports the hypothesis that MCD and FSGS are two successive pathological processes of podocyte disease. Both models are based on the induction of podocyte injury and subsequent podocyte loss, and the difference depends on the degree of podocyte injury and the severity of podocyte loss. Only foot process of podocyte exfoliation similar to that in MCD is observed in the initial phase, while persistent podocyte loss results in the development of FSGS[10]. In the initial stages, this disease is steroid-sensitive. With relapses and delays, continuous proteinuria and podocyte loss lead to a decrease or loss of steroid sensitivity. When podocyte loss is more than 30%-40%, an ESKD outcome seems inevitable[3]. In this case, after MCD diagnosis, the patient was treated regularly with corticosteroid and achieved complete remission. Although there was no regular long-term follow-up, no serious relapses occurred, according to his records. A typical NS recurrence materialized 20 years later, at which time his clinical course and repeated kidney biopsy results both supported the FSGS diagnosis. In order to avoid misdiagnosis, we retrieved his kidney tissue sample (24 glomeruli) from 20 years ago for a pathological re-examination, and the results still supported the diagnosis of MCD. Therefore, we suggest that the patient progressed from MCD to FSGS, rather than FSGS being missed at the first diagnosis.

It is no coincidence that pathological changes occurred before and after the repeated kidney biopsy. FSGS is not a diagnosis of a specific disease, but a progressive glomerular pathological change caused by podocyte depletion. Most glomerular diseases eventually result in loss of renal function due to FSGS, and FSGS lesions can be described as an outcome of persistent damage in certain glomerular diseases or as a common endpoint event in some glomerular diseases[11]. MCD and FSGS are both podocyte diseases, and when FSGS is excluded from being missed or misdiagnosed as MCD, their sequential occurrence often suggests that FSGS is the progression of MCD[6]. The patient did not have regular follow-up visits when his NS was in remission, which was also a limitation of this case. Since recurrence of MCD is based on proteinuria, this patient most likely had an undetected recurrence of MCD. We hypothesized that the neglected recurrent MCD lead to persistent podocyte damage that ultimately caused FSGS, and heavy metal exposure is involved in exacerbating this process. Primary FSGS is usually caused by circulating factors, and the etiology of secondary FSGS includes infection, drugs, maladaptive responses, familial/genetic form, and variation of the *APOL1* gene[12]. The patient did not have the above background, but a possible related factor was his occupation. The patient was an electric welder with excessive levels of cadmium and lead in his blood. Consequently, we suspect that his aggravated pathology and ESKD occurrence were related to metal nephrotoxicity. Nephrotoxicity induced by excess exposure to certain metals is well known, and lithium has been shown to cause MCD and FSGS[13]. Although there is not enough literature to confirm that lead and cadmium can cause FSGS, it has been proven that both of them induce podocytotoxicity and can even induce podocyte apoptosis[14,15]. Kidney exposure to cadmium and lead mainly causes proximal renal tubule dysfunction, acute exposure can lead to Fanconi syndrome, and long-term exposure leads to a persistent decline in kidney function[16,17]. This may explain the positive urine sugar content of the patient, and it may also be the reason for the occurrence of NS and ESKD in this patient. The levels of cadmium and lead in the blood of this patient were not that high compared to the normal range, but chronic, long-term exposure to low doses of the metal can cause kidney damage. Both lead and cadmium can increase the risk of chronic kidney disease, even at low levels (Blood lead < 5 mg/dL; Blood cadmium < 0.6 mg/L)[18,19]. The kidney damage caused by lead and cadmium is long-term and chronic, and combination of the two has a more profound nephrotoxicity. We hope to provide convincing evidence for the contention that lead and cadmium cause the transition from MCD to FSGS through future in-depth research.

Although, unfortunately, the patient ultimately required kidney replacement therapy, this case is still thought-provoking. MCD and FSGS are defined as different types of primary glomerular disease, but there is some overlap between them in clinical features and pathological changes. MCD and FSGS are both podocyte diseases, clinically presenting with sudden-onset NS, characterized by the absence of immune deposits under immunofluorescence[20]. However, their treatment response and prognosis are different. The differential diagnosis of MCD and FSGS is difficult, but it is important to distinguish between the two. A positive attitude towards second, or multiple kidney biopsies is needed for uncertain or recurrent MCD patients and early stage FSGS patients. In addition to invasive kidney puncture, urinary myo-inositol, parietal epithelial cell marker staining, and IgG/albumin staining ratio in tubular protein reabsorption droplets are also potential diagnostic markers to differentiate between MCD and FSGS[21-23].

CONCLUSION

We recognize through this rare case and a literature review that FSGS could be the later stage of MCD. FSGS lesions found in a repeated kidney biopsy can often reflect disease progression, and metal overexposure may be one of the possible reasons. Patients with MCD who have a slower and less effective response to steroid hormones should be alerted by clinicians to the risk of conversion to FSGS, or the possibility of coexistence with FSGS lesions. Due to its focal and segmental nature, we propose a higher requirement for nephrologists, at least to ensure the number of glomeruli.

ACKNOWLEDGEMENTS

We gratefully thank the patient for allowing us to publish this case report. We acknowledge technical assistance from members of the Pathological Centre, Peking University First Hospital.

FOOTNOTES

Author contributions: Tang L obtained and interpreted the patient clinical data, wrote and finally submitted the manuscript; Tang L and Cai Z performed the histological examination of the kidney, participated in the analysis of patient pathological data; Zhao WJ and Wang SX critically reviewed and revised the final manuscript, and were consultants during the treatment and the final diagnosis; all authors read and approved the final manuscript.

Informed consent statement: Informed written consent was obtained from the patient for publication of this report and any accompanying images.

Conflict-of-interest statement: The authors declare that they have no conflict of interest.

CARE Checklist (2016) statement: The authors have read the CARE Checklist (2016), and the manuscript was prepared and revised according to the CARE Checklist (2016).

Open-Access: This article is an open-access article that was selected by an in-house editor and fully peer-reviewed by external reviewers. It is distributed in accordance with the Creative Commons Attribution NonCommercial (CC BY-NC 4.0) license, which permits others to distribute, remix, adapt, build upon this work non-commercially, and license their derivative works on different terms, provided the original work is properly cited and the use is non-commercial. See: https://creativecommons.org/Licenses/by-nc/4.0/

Country/Territory of origin: China

ORCID number: Long Tang 0000-0003-4609-413X; Zhen Cai 0000-0002-0600-3806; Su-Xia Wang 0000-0001-7631-6464; Wen-Jing Zhao 0000-0003-3053-3839.

S-Editor: Yan JP
L-Editor: A
P-Editor: Yan JP

REFERENCES

1 **Lionaki S**, Mantios E, Tsoumbou I, Marinaki S, Makris G, Liapis G, Vergandis C, Boletis I. Clinical Characteristics and Outcomes of Adults with Nephrotic Syndrome Due to Minimal Change Disease. *J Clin Med* 2021; **10** [PMID: 34441929 DOI: 10.3390/jcm10163632]
2 **Wang CS**, Greenbaum LA. Nephrotic Syndrome. *Pediatr Clin North Am* 2019; **66**: 73-85 [PMID: 30454752 DOI: 10.1016/j.pcl.2018.08.006]
3 **Maas RJ**, Deegens JK, Smeets B, Moeller MJ, Wetzels JF. Minimal change disease and idiopathic FSGS: manifestations of the same disease. *Nat Rev Nephrol* 2016; **12**: 768-776 [PMID: 27748392 DOI: 10.1038/nrneph.2016.147]
4 **Wieder N**, Greka A. Calcium, TRPC channels, and regulation of the actin cytoskeleton in podocytes: towards a future of targeted therapies. *Pediatr Nephrol* 2016; **31**: 1047-1054 [PMID: 26490951 DOI: 10.1007/s00467-015-3224-1]
5 **Vivarelli M**, Massella L, Ruggiero B, Emma F. Minimal Change Disease. *Clin J Am Soc Nephrol* 2017; **12**: 332-345 [PMID: 27940460 DOI: 10.2215/CJN.05000516]
6 **Rosenberg AZ**, Kopp JB. Focal Segmental Glomerulosclerosis. *Clin J Am Soc Nephrol* 2017; **12**: 502-517 [PMID: 28242845 DOI: 10.2215/CJN.05960616]
7 **Ahmad H**, Tejani A. Predictive value of repeat renal biopsies in children with nephrotic syndrome. *Nephron* 2000; **84**: 342-346 [PMID: 10754411 DOI: 10.1159/000045609]
8 **Maas RJ**, Deegens JK, Beukhof JR, Reichert LJ, Ten Dam MA, Beutler JJ, van den Wall Bake AWL, Rensma PL,

Konings CJ, Geerse DA, Feith GW, Van Kuijk WH, Wetzels JF. The Clinical Course of Minimal Change Nephrotic Syndrome With Onset in Adulthood or Late Adolescence: A Case Series. *Am J Kidney Dis* 2017; **69**: 637-646 [PMID: 28089478 DOI: 10.1053/j.ajkd.2016.10.032]

9 **da Silva CA**, Monteiro MLGDR, Araújo LS, Urzedo MG, Rocha LB, Dos Reis MA, Machado JR. In situ evaluation of podocytes in patients with focal segmental glomerulosclerosis and minimal change disease. *PLoS One* 2020; **15**: e0241745 [PMID: 33147279 DOI: 10.1371/journal.pone.0241745]

10 **Pippin JW**, Brinkkoetter PT, Cormack-Aboud FC, Durvasula RV, Hauser PV, Kowalewska J, Krofft RD, Logar CM, Marshall CB, Ohse T, Shankland SJ. Inducible rodent models of acquired podocyte diseases. *Am J Physiol Renal Physiol* 2009; **296**: F213-F229 [PMID: 18784259 DOI: 10.1152/ajprenal.90421.2008]

11 **Müller-Deile J**, Schenk H, Schiffer M. [Minimal change disease and focal segmental glomerulosclerosis]. *Internist (Berl)* 2019; **60**: 450-457 [PMID: 30887070 DOI: 10.1007/s00108-019-0590-y]

12 **Shabaka A**, Tato Ribera A, Fernández-Juárez G. Focal Segmental Glomerulosclerosis: State-of-the-Art and Clinical Perspective. *Nephron* 2020; **144**: 413-427 [PMID: 32721952 DOI: 10.1159/000508099]

13 **Łukawska E**, Frankiewicz D, Izak M, Woźniak A, Dworacki G, Niemir ZI. Lithium toxicity and the kidney with special focus on nephrotic syndrome associated with the acute kidney injury: A case-based systematic analysis. *J Appl Toxicol* 2021; **41**: 1896-1909 [PMID: 33798272 DOI: 10.1002/jat.4167]

14 **Eichler TE**, Ransom RF, Smoyer WE. Differential induction of podocyte heat shock proteins by prolonged single and combination toxic metal exposure. *Toxicol Sci* 2005; **84**: 120-128 [PMID: 15590893 DOI: 10.1093/toxsci/kfi048]

15 **Eichler T**, Ma Q, Kelly C, Mishra J, Parikh S, Ransom RF, Devarajan P, Smoyer WE. Single and combination toxic metal exposures induce apoptosis in cultured murine podocytes exclusively *via* the extrinsic caspase 8 pathway. *Toxicol Sci* 2006; **90**: 392-399 [PMID: 16421179 DOI: 10.1093/toxsci/kfj106]

16 **Satarug S**, C Gobe G, A Vesey D, Phelps KR. Cadmium and Lead Exposure, Nephrotoxicity, and Mortality. *Toxics* 2020; **8** [PMID: 33066165 DOI: 10.3390/toxics8040086]

17 **Jalili C**, Kazemi M, Cheng H, Mohammadi H, Babaei A, Taheri E, Moradi S. Associations between exposure to heavy metals and the risk of chronic kidney disease: a systematic review and meta-analysis. *Crit Rev Toxicol* 2021; **51**: 165-182 [PMID: 33960873 DOI: 10.1080/10408444.2021.1891196]

18 **Nakhaee S**, Amirabadizadeh A, Brent J, Mehrpour O. Impact of chronic lead exposure on liver and kidney function and haematologic parameters. *Basic Clin Pharmacol Toxicol* 2019; **124**: 621-628 [PMID: 30471187 DOI: 10.1111/bcpt.13179]

19 **Madrigal JM**, Ricardo AC, Persky V, Turyk M. Associations between blood cadmium concentration and kidney function in the U.S. population: Impact of sex, diabetes and hypertension. *Environ Res* 2019; **169**: 180-188 [PMID: 30466011 DOI: 10.1016/j.envres.2018.11.009]

20 **Ahn W**, Bomback AS. Approach to Diagnosis and Management of Primary Glomerular Diseases Due to Podocytopathies in Adults: Core Curriculum 2020. *Am J Kidney Dis* 2020; **75**: 955-964 [PMID: 32331832 DOI: 10.1053/j.ajkd.2019.12.019]

21 **An JN**, Hyeon JS, Jung Y, Choi YW, Kim JH, Yang SH, Oh S, Kwon S, Lee SH, Cho JH, Park SH, Ha H, Kim DK, Lee JP, Hwang GS. Urinary myo-inositol is associated with the clinical outcome in focal segmental glomerulosclerosis. *Sci Rep* 2019; **9**: 14707 [PMID: 31605028 DOI: 10.1038/s41598-019-51276-9]

22 **Suzuki T**, Kohatsu K, Han W, Watanabe S, Yahagi K, Nakata M, Ueno T, Ichikawa D, Imai N, Shirai S, Koike J, Shibagaki Y. Morphological Features of Minimal Change Disease and Focal Segmental Glomerulosclerosis Using Repeat Biopsy and Parietal Epithelial Cell Marker. *Kidney Dis (Basel)* 2020; **6**: 119-124 [PMID: 32309294 DOI: 10.1159/000505125]

23 **Bu L**, Mirocha J, Haas M. Immunoglobulin G/albumin staining in tubular protein reabsorption droplets in minimal change disease and focal segmental glomerulosclerosis. *Nephrol Dial Transplant* 2021; **36**: 1016-1022 [PMID: 32191308 DOI: 10.1093/ndt/gfaa039]

World Journal of Clinical Cases

Submit a Manuscript: https://www.f6publishing.com

World J Clin Cases 2022 June 16; 10(17): 5869-5876

DOI: 10.12998/wjcc.v10.i17.5869

ISSN 2307-8960 (online)

CASE REPORT

Lung adenocarcinoma metastasis to paranasal sinus: A case report

Wen-Jing Li, Hai-Xiang Xue, Jian-Qiang You, Chang-Jiang Chao

Specialty type: Oncology

Provenance and peer review: Unsolicited article; Externally peer reviewed.

Peer-review model: Single blind

Peer-review report's scientific quality classification

Grade A (Excellent): A
Grade B (Very good): 0
Grade C (Good): C
Grade D (Fair): 0
Grade E (Poor): 0

P-Reviewer: Nepal SP, Japan; Sezer HF, Turkey

Received: December 26, 2021
Peer-review started: December 26, 2021
First decision: January 25, 2022
Revised: February 6, 2022
Accepted: April 4, 2022
Article in press: April 4, 2022
Published online: June 16, 2022

Wen-Jing Li, Hai-Xiang Xue, Jian-Qiang You, Chang-Jiang Chao, Department of Otolaryngology Head and Neck Surgery, The Third Affiliated Hospital of Soochow University, Changzhou 213000, Jiangsu Province, China

Corresponding author: Chang-Jiang Chao, Doctor, Professor, Department of Otolaryngology Head and Neck Surgery, The Third Affiliated Hospital of Soochow University, No. 185 Juqian Street, Changzhou 213000, Jiangsu Province, China. entczyy@163.com

Abstract

BACKGROUND

Lung cancer is often metastasized to the brain, liver, kidneys, bone, bone marrow, and adrenal glands; however, metastasis of primary lung cancer to the paranasal sinuses is extremely rare.

CASE SUMMARY

In this paper, we present a case of metastatic tumors of the sinus secondary to lung adenocarcinoma. The patient was a 46-year-old woman who underwent surgical removal of lung carcinoma. Four months after the surgical removal of the lung tumor, the patient presented with epistaxis, and on investigation, the diagnosis was confirmed to be nasal sinus tumors due to metastasis of lung adenocarcinoma.

CONCLUSION

Thorough investigation of patients with epistaxis and a history of lung cancer is necessary to diagnose metastatic sinus tumors. We reviewed relevant literature and found that there are no characteristic clinical or radiologic features for metastatic sinus tumors; however, the diagnosis can be confirmed by histopathological examination of biopsied tumor sample.

Key Words: Lung adenocarcinoma; Paranasal sinus; Metastasis; Case report

©The Author(s) 2022. Published by Baishideng Publishing Group Inc. All rights reserved.

Core Tip: Lung adenocarcinoma metastasis restricted to the paranasal sinus is a rare phenomenon. In this report, we present a rare case of metastatic tumors of the sinus secondary to lung adenocarcinoma. After lung cancer surgery, the patient had no postoperative complications and was completely asymptomatic at the second-year postoperative follow-up. We reviewed relevant literature in order to identify the characteristic features observed in cases of sinus metastasis of lung adenocarcinoma.

Citation: Li WJ, Xue HX, You JQ, Chao CJ. Lung adenocarcinoma metastasis to paranasal sinus: A case report. *World J Clin Cases* 2022; 10(17): 5869-5876
URL: https://www.wjgnet.com/2307-8960/full/v10/i17/5869.htm
DOI: https://dx.doi.org/10.12998/wjcc.v10.i17.5869

INTRODUCTION

Advanced lung cancer is associated with a high incidence of distant metastasis[1,2], and metastasis to distant vital organs is an important factor contributing to the high mortality rate associated with lung cancer[3-5]. Metastasis of lung cancer occurs most commonly to the bones, liver, and brain and only rarely to the pericardial, adrenal, or subcutaneous tissues, spinal cord, kidney, and other organs[6]. Occasionally, lung cancer may metastasize to the external auditory canal, orbital ball, nasal cavity, or jejunum[7]. Other very rare sites of lung cancer metastases have also been reported in the literature. With respect to pathological type, studies have also shown that the most common type of metastasizing lung cancer is the adenocarcinoma[8]. Furthermore, reports have also indicated that lung cancer with nasal and sinus metastasis is associated with a short survival period and poor prognosis[1].

In this paper, we present a rare case of metastatic sinus tumor arising from adenocarcinoma of the lungs. In addition, we review literature on metastatic tumors of the nasal cavity and paranasal sinuses secondary to primary lung carcinoma.

CASE PRESENTATION

Chief complaints

The patient was a 45-year-old woman who was diagnosed with lung adenocarcinoma and underwent surgical resection of the tumor. Four months after the tumor removal, she presented with epistaxis and left-sided headache. however, the symptoms were considered insignificant and were not investigated further. Five months after the lung surgery, the patient developed a swelling around the left eye socket, which increased progressively and was accompanied by purulent nasal discharge, nasal obstruction, decreased sense of smell, or decreased vision.

History of present illness

Previously, the patient was found to have a right upper pulmonary mass during a routine physical examination (Figure 1). To rule out malignancy, thoracoscopy was performed, which revealed a mass (diameter approximately 3 cm) located in the posterior segment of the right upper lobe of the lung. Surgical removal of the tumor was successful, with resection of the right upper lobe and adjacent lymph nodes. The tumor was firm in consistency and oval, with an intact capsule. Postoperative pathological examination revealed that the lesion was a moderately differentiated lung adenocarcinoma, with no involvement of the incision margin of the bronchus and no metastasis to the lymph nodes.

History of past illness

The patient had no previous medical history.

Personal and family history

History taking also revealed that the patient had no other relevant medical history or family history.

Physical examination

On physical examination at presentation, the external nose was found to be normal in shape. No obstruction of the nasal passages was observed on either side, and no abnormal secretion or colonization was detected. There was no obvious tenderness over the areas of the sinuses.

Laboratory examinations

Results of serum tests for tumor markers were all negative. No abnormalities were noted in the

DOI: 10.12998/wjcc.v10.i17.5869 **Copyright** ©The Author(s) 2022.

Figure 1 Computerized tomography examination showing a mass located in the posterior segment of the right upper lobe of the lung.

coagulation indices or in the results of routine blood tests, tests for immunoglobulin light chains, thyroid hormone levels, and tests for autoimmune antibodies.

Imaging examinations

Computed tomography (CT) and magnetic resonance imaging (MRI) examination of the sinus was performed, the findings revealed left maxillary sinusitis, bilateral ethmoid sinusitis, and septal deviation, with bone destruction of the left ethmoid sinus. (Figure 2A and B).

FINAL DIAGNOSIS

On the basis of the clinical and imaging findings, the diagnosis was established as lung cancer metastasis to the nasal cavity. The tumor in the paranasal sinus was removed and subjected to pathological examination.

TREATMENT

The patient underwent surgical treatment for the removal of the sinus tumors at our hospital. During the operation, a large number of lesions with fish-meat-like appearance of the tissue were found in the ethmoid sinus; the lesions were fragile and easily bleeding. Destruction of the cribriform plate was observed, as well as tumor pressure on the orbit through the orbital fascia. Pathological examination of the biopsied tumor tissue sample revealed that the tumor was malignant. The anterior and middle groups of the ethmoidal sinuses were debrided until the cribriform roof; the frontal sinus was then opened, and a large number of lesions with fish-meat-like appearance of tissue were found in the frontal recess and frontal sinus. An incision was made on the eyebrow arch, and the subcutaneous tissue and muscle tissue were separated. Bone destruction was also observed in the anterior frontal sinus wall, along with the presence of lesions with fish-meat-like appearance, which were removed. The frontal sinus cavity was opened, and the necrotic bone tissue was removed. Finally, the eyebrow arch incision was sutured. Postoperative pathological examination revealed the presence of adenocarcinoma infiltrate between fibrous connective tissues. The results of immunohistochemical examination were as follows: CK7(+), CK20(-), Villin(-), Syn(-), CgA(-), TTF-1(+), Napsin A(+), CDX-2(-), S100(-), CK5/6(-), and P63(-). Figure 3 shows the results of the immunohistochemical examination of tissue sample obtained from the metastatic tumors of the sinus.

OUTCOME AND FOLLOW-UP

The patient had no postoperative complications and was discharged safely after 7 days. The patient did not receive further radiotherapy or chemotherapy. Follow-up was continued for 2 years, and during this period, she remained completely asymptomatic; CT scans of the lung and sinus were also normal (Figure 4A and B).

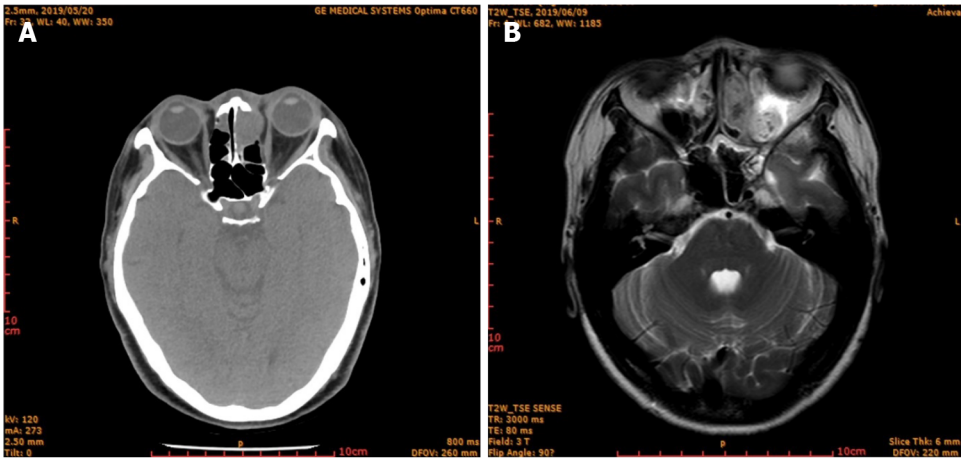

DOI: 10.12998/wjcc.v10.i17.5869 **Copyright** ©The Author(s) 2022.

Figure 2 Imaging examination. A: Computerized tomography examination showing tumor invasion of the ethmoid sinus; B: Magnetic resonance imaging showing a mass in the ethmoid sinus.

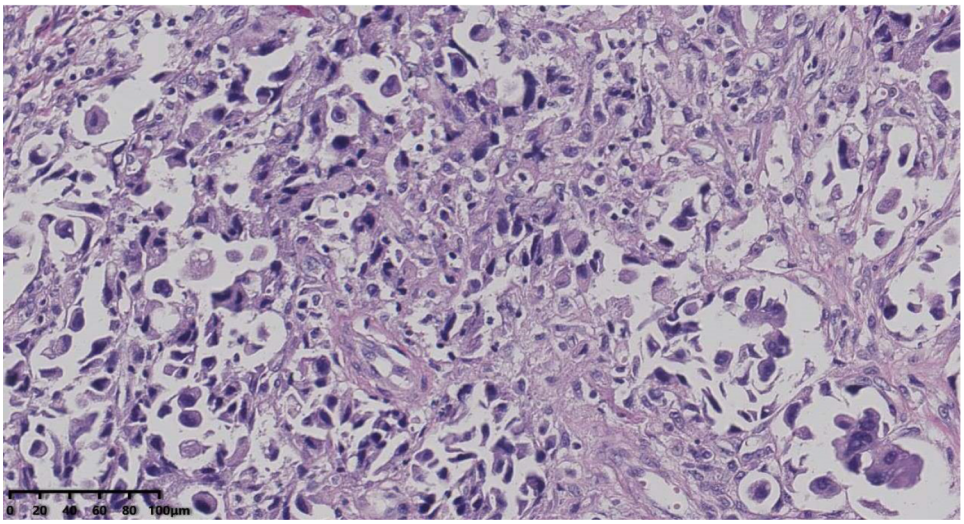

DOI: 10.12998/wjcc.v10.i17.5869 **Copyright** ©The Author(s) 2022.

Figure 3 Pathological immunohistochemistry showing adenocarcinoma infiltrates between fibrous connective tissues, indicating lung adenocarcinoma.

DISCUSSION

Malignant sinus tumors are mostly primary tumors, and only in rare cases are they caused by metastatic tumors originating elsewhere. Metastatic sinus tumors arising from primary tumors of the kidney, lungs, and liver have rarely been reported[9].

The most likely route by which the metastasis occurs to the sinuses may be hematogenous spread of tumor cells. Since the lungs have a rich blood supply, cells of lung adenocarcinoma may easily enter venous circulation. Intrapleural pressure and abdominal pressure may cause detachment of a tumor plug, whereby tumor cells enter blood circulation. The tumor plug may traverse to the large veins of the head, such as the wing plexus and cavernous sinus, eventually reaching the paranasal sinuses through retrograde movement. Since blood flow at the sinuses is sluggish, the tumor plug may easily fall off the circulation and plant itself, leading to the growth of metastatic tumors.

Distant metastasis of primary lung cancer generally occurs to the liver, adrenal glands, brain, or bone, and only rarely to the nasal cavity and paranasal sinuses. Four cases of lung cancer metastasizing to the nasal cavity and sinuses have been reported since 2001; in all of cases, the tumors were squamous-cell carcinoma and epistaxis was the initial clinical presentation. The distant metastasis of lung cancer is a complex process involving the detachment, transport, and growth of tumor cells[10]. Tumor cells break away from the primary tumor, adhere, and invade the basement membrane; thus, they come into close contact with local capillary or lymphatic capillary endothelial cells. The tumor cells pass through the walls of the blood or lymph vessels and are transported *via* the blood or lymphatic circulation; platelet

Table 1 Number of cases for different pathological type of metastatic tumors to the nasal cavity and sinuses from primary lung cancer

Pathological type	No. of cases
Adenocarcinoma	46
Squamous-cell carcinoma	39
Small-cell carcinoma	23
Adenosquamous carcinoma	3
Carcinoma gigantocellulare	2
Non-small-cell lung cancer	2
Large-cell lung cancer	2
Small-round-cell malignant tumors	1
Sarcomatoid carcinoma	1
Papillocarcinoma	1
Mucoepidermoid carcinoma	1
Neuroendocrine carcinoma	1
Germ-cell tumor	1

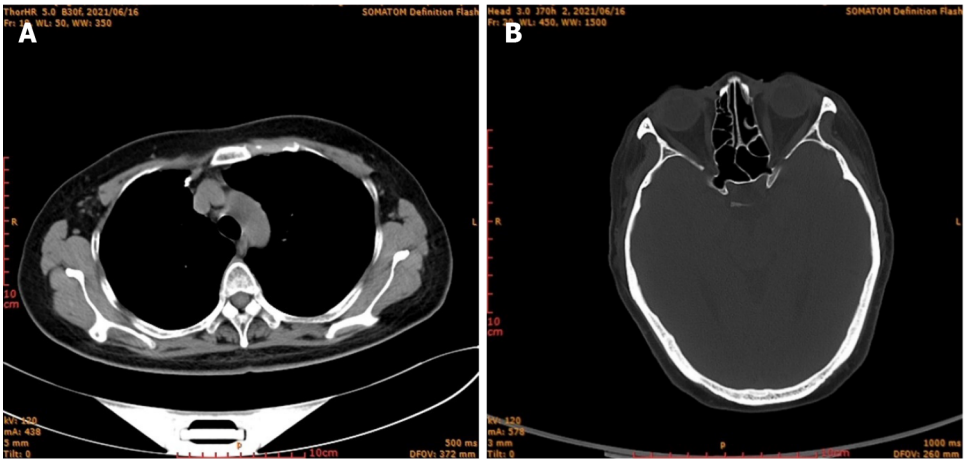

DOI: 10.12998/wjcc.v10.i17.5869 **Copyright** ©The Author(s) 2022.

Figure 4 Computed tomography images. A: Computed tomography (CT) of lung obtained two years later, showing no recurrence; B: CT of paranasal sinus obtained two years later, showing no recurrence.

agglutination may then occur, leading to the formation of a tumor thromboembolus, which reaches the target tissue to give rise to the metastatic tumor[11]. Lung cancer may metastasize though hematogenous spread, lymphatic spread, or direct invasion[12]. Adenocarcinoma and squamous-cell carcinoma of lung are mainly metastasized *via* blood circulation and lymphatic circulation, respectively; additionally, in lung cancer, metastasis to lymph nodes generally occurs earlier than other metastases [13].

We conducted a literature search of relevant literature with "lung cancer" and "metastasis" as search terms. The PubMed, Scopus, CNKI, and WANFANG MED ONLINE databases were searched for entries published since 2001, and case reports were screened out. One hundred and thirty-eight cases of lung cancer with distant metastasis were identified. The case reports included 100 males and 38 females, and the youngest patient was 17 years old, while the oldest was 97 years old. In all, 123 cases with confirmed pathological results and metastatic sites were identified; among these cases, adenocarcinoma (Table 1) was the most common pathological type and the sites of metastatic tumors were diverse (Table 2).

Metastasis of lung cancer to the sinus is rare and its presentation nonspecific. No characteristic clinical or radiologic features have been described to differentiate metastatic tumors from primary malignancy of the sinus[3]. However, nasal and sinus tumors commonly present with epistaxis, and the diagnosis can be confirmed by histopathologic examination of biopsy tissue[4].

Table 2 Metastatic sites and number of cases

Metastatic site	No. of cases	Metastatic site	No. of cases
Eyeball	12	Cerebrum	16
Choroid	11	Peripheral nerve	3
Iris	5	Bone	15
Eyelid	2	Skin	8
Retina	1	Cardioid	8
Colon	4	Marrow	6
Jejunum	3	Nasal cavity	4
Pancreas	3	Oral cavity	3
Spleen	2	Mammary gland	3
Intestine	2	Tonsil	2
Rectal	2	Inguinal glands	2
Stomach	1	Thyroid	2
Liver	1	Kidney	2
Appendix	1	Pituitary	2
Cervix	3	Greater omentum	1
Ovary	2	Abdominal wall	1
Penis	1	Abdominal cavity	1
Prostate	1	Thyroid cartilage	1
Testis	1		

Distant metastasis of lung cancer generally occurs in the middle and late stages of cancer, and the survival period for patients is less than 1 year, with poor prognosis[14]. No effective treatments have been identified thus far. The survival of the patients may be improved by surgical resection of the primary and metastatic lesions and subsequent radiotherapy and chemotherapy[4]. Currently, targeted therapy combined with radiotherapy and chemotherapy are mostly used for brain metastasis of lung cancer, while chemotherapy is mainly used for bone metastasis of lung cancer[15]. Surgery combined with radiotherapy is mostly used for eyeball metastasis of lung cancer[16,17], and there is no standard treatment plan for choroidal metastasis of lung cancer[18]. In this case report, the patient received no other treatment except surgical resection of the lesion, and no recurrence was observed during follow-up for two years. Complete spontaneous remission of metastatic non-small-cell carcinoma has also been reported, which may be related to the differentiation of malignant cells into normal phenotype and/or cell death caused by apoptosis or inflammatory necrosis[19]. However, data on the efficacy of treatment are still limited, and further investigation, including large-scale clinical trials, are warranted.

CONCLUSION

To summarize, we presented a rare case of metastatic sinus tumor secondary to primary lung adenocarcinoma. We also reviewed relevant literature and found that the findings of metastatic sinus tumors were nonspecific. Therefore, physicians should be aware of the possibility of metastatic sinus lesions in patients with a history of primary lung cancer presenting with epistaxis; investigating such patients for sinus metastasis would help early diagnosis and timely initiation of appropriate treatment measures.

FOOTNOTES

Author contributions: Li WJ contributed to formal analysis, methodology, data processing, resources, investigation, writing-original draft, writing-review and editing; Xue HX contributed to investigation, methodology, validation; You JQ contributed to methodology, validation; Chao CJ contributed to methodology, supervision, writing-review and editing.

Informed consent statement: Informed written consent was obtained from the patient for publication of this report and any accompanying images.

Conflict-of-interest statement: The authors declare that they have no conflict of interest.

CARE Checklist (2016) statement: The authors have read the CARE Checklist (2016), and the manuscript was prepared and revised according to the CARE Checklist (2016).

Open-Access: This article is an open-access article that was selected by an in-house editor and fully peer-reviewed by external reviewers. It is distributed in accordance with the Creative Commons Attribution NonCommercial (CC BY-NC 4.0) license, which permits others to distribute, remix, adapt, build upon this work non-commercially, and license their derivative works on different terms, provided the original work is properly cited and the use is non-commercial. See: https://creativecommons.org/Licenses/by-nc/4.0/

Country/Territory of origin: China

ORCID number: Wen-Jing Li 0000-0003-4915-8119; Hai-Xiang Xue 0000-0002-9349-805X; Jian-Qiang You 0000-0001-6958-0646; Chang-Jiang Chao 0000-0001-6666-7877.

S-Editor: Gong ZM
L-Editor: A
P-Editor: Gong ZM

REFERENCES

1 **Katz TS**, Mendenhall WM, Morris CG, Amdur RJ, Hinerman RW, Villaret DB. Malignant tumors of the nasal cavity and paranasal sinuses. *Head Neck* 2002; **24**: 821-829 [PMID: 12211046 DOI: 10.1002/hed.10143]
2 **Clarkson JH**, Kirkland PM, Mady S. Bronchogenic metastasis involving the frontal sinus and masquerading as a Pott's puffy tumour: a diagnostic pitfall. *Br J Oral Maxillofac Surg* 2002; **40**: 440-441 [PMID: 12379194 DOI: 10.1016/s0266-4356(02)00131-6]
3 **King AD**, Tse GM, Ahuja AT, Yuen EH, Vlantis AC, To EW, van Hasselt AC. Necrosis in metastatic neck nodes: diagnostic accuracy of CT, MR imaging, and US. *Radiology* 2004; **230**: 720-726 [PMID: 14990838 DOI: 10.1148/radiol.2303030157]
4 **Huang CT**, Hong RL. Nasion swelling as the presenting symptom of lung adenocarcinoma. *J Thorac Oncol* 2009; **4**: 555-558 [PMID: 19333075 DOI: 10.1097/JTO.0b013e3181949f30]
5 **Porceddu S**, Martin J, Shanker G, Weih L, Russell C, Rischin D, Corry J, Peters L. Paranasal sinus tumors: Peter MacCallum Cancer Institute experience. *Head Neck* 2004; **26**: 322-330 [PMID: 15054735 DOI: 10.1002/hed.10388]
6 **Chhiber SS**, Nizami FA, R. KA. Renal cell carcinoma presenting as metastasis to frontal sinus in a young male: a case report. *Neurosurg Q* 2011; **21**: 288-291 [DOI: 10.1097/WNQ.0b013e31821d0626]
7 **Orvidas LJ**, Lewis JE, Weaver AL, Bagniewski SM, Olsen KD. Adenocarcinoma of the nose and paranasal sinuses: a retrospective study of diagnosis, histologic characteristics, and outcomes in 24 patients. *Head Neck* 2005; **27**: 370-375 [PMID: 15714475 DOI: 10.1002/hed.20168]
8 **Rombaux P**, Hamoir M, Liistro G, Bertrand B. Frontal sinus tumor as the first sign of adenocarcinoma of the lung. *Otolaryngol Head Neck Surg* 2005; **132**: 816-817 [PMID: 15886645 DOI: 10.1016/j.otohns.2004.09.070]
9 **Koktekir E**, Koktekir BE, Recber F, Akdemir G. Lung adenocarcinoma metastasis to frontal sinus mimicking Pott's puffy tumor. *J Craniofac Surg* 2013; **24**: e538-e539 [PMID: 24220459 DOI: 10.1097/SCS.0b013e318285d98a]
10 **Lachhab L**, Fikri M, Aitbenhaddou EH, Arkha Y, Regragui W, Jiddane M, Benomar A, Yahyaoui M. [Atypical metastatic sites for adenocarcinoma of the lung]. *J Fr Ophtalmol* 2013; **36**: e23-e26 [PMID: 23083771 DOI: 10.1016/j.jfo.2012.03.009]
11 **Nagano H**, Yoshifuku K, Deguchi K, Kurono Y. Adenocarcinoma of the paranasal sinuses and nasal cavity with lung metastasis showing complete response to combination chemotherapy with docetaxel, cisplatin and 5-fluorouracil (TPF): a case report. *Auris Nasus Larynx* 2010; **37**: 238-243 [PMID: 19560300 DOI: 10.1016/j.anl.2009.05.007]
12 **Agrawal S**, Jayant K, Agarwal RK, Dayama KG, Arora S. An unusual case of metastatic male breast cancer to the nasopharynx-review of literature. *Ann Palliat Med* 2015; **4**: 233-238 [PMID: 26541404 DOI: 10.3978/j.issn.2224-5820.2015.08.02]
13 **Tang WF**, Wu M, Bao H, Xu Y, Lin JS, Liang Y, Zhang Y, Chu XP, Qiu ZB, Su J, Zhang JT, Zhang C, Xu FP, Chen JH, Fu R, Chen Y, Yang T, Chen QK, Wu TT, Wu X, Shao Y, Zheng JT, Xie Z, Lv ZY, Dong S, Wu YL, Zhong WZ. Timing and Origins of Local and Distant Metastases in Lung Cancer. *J Thorac Oncol* 2021; **16**: 1136-1148 [PMID: 33722707 DOI: 10.1016/j.jtho.2021.02.023]
14 **Ates I**, Yazici O, Ates H, Ozdemir N, Zengin N. Unusual metastases of lung cancer: bulbus oculi and maxillary sinus. *Exp Oncol* 2015; **37**: 231-232 [PMID: 26928715 DOI: 10.31768/2312-8852.2015.37(3):231-232].]
15 **D'Antonio C**, Passaro A, Gori B, Del Signore E, Migliorino MR, Ricciardi S, Fulvi A, de Marinis F. Bone and brain metastasis in lung cancer: recent advances in therapeutic strategies. *Ther Adv Med Oncol* 2014; **6**: 101-114 [PMID: 24790650 DOI: 10.1177/1758834014521110]
16 **De Potter P**. Ocular manifestations of cancer. *Curr Opin Ophthalmol* 1998; **9**: 100-104 [PMID: 10387328 DOI: 10.1097/00055735-199812000-00018]

17 **Chen HF**, Wang WX, Li XF, Wu LX, Zhu YC, Du KQ, Xu CW. Eye metastasis in lung adenocarcinoma mimicking anterior scleritis: A case report. *World J Clin Cases* 2020; **8**: 410-414 [PMID: 32047793 DOI: 10.12998/wjcc.v8.i2.410]

18 **Arepalli S**, Kaliki S, Shields CL. Choroidal metastases: origin, features, and therapy. *Indian J Ophthalmol* 2015; **63**: 122-127 [PMID: 25827542 DOI: 10.4103/0301-4738.154380]

19 **Kappauf H**, Gallmeier WM, Wünsch PH, Mittelmeier HO, Birkmann J, Büschel G, Kaiser G, Kraus J. Complete spontaneous remission in a patient with metastatic non-small-cell lung cancer. Case report, review of the literature, and discussion of possible biological pathways involved. *Ann Oncol* 1997; **8**: 1031-1039 [PMID: 9402178 DOI: 10.1023/a:1008209618128]

World Journal of Clinical Cases

Submit a Manuscript: https://www.f6publishing.com

World J Clin Cases 2022 June 16; 10(17): 5877-5883

DOI: 10.12998/wjcc.v10.i17.5877

ISSN 2307-8960 (online)

CASE REPORT

Follicular lymphoma presenting like marginal zone lymphoma: A case report

Hao-Yu Peng, Ying-Jie Xiu, Wei-Hong Chen, Qing-Li Gu, Xin Du

Specialty type: Pathology

Provenance and peer review: Unsolicited article; Externally peer reviewed.

Peer-review model: Single blind

Peer-review report's scientific quality classification

Grade A (Excellent): 0
Grade B (Very good): B
Grade C (Good): C
Grade D (Fair): 0
Grade E (Poor): 0

P-Reviewer: Bairwa DBL, India; Kamalabadi-Farahani M, Iran

Received: December 29, 2021
Peer-review started: December 29, 2021
First decision: March 7, 2022
Revised: March 20, 2022
Accepted: April 4, 2022
Article in press: April 4, 2022
Published online: June 16, 2022

Hao-Yu Peng, Wei-Hong Chen, Qing-Li Gu, Xin Du, Department of Hematology, Shenzhen Second People's Hospital, The First Affiliated Hospital of Shenzhen University, Shenzhen 518035, Guangdong Province, China

Ying-Jie Xiu, Department of Pathology, Shenzhen Second People's Hospital, The First Affiliated Hospital of Shenzhen University, Shenzhen 518035, Guangdong Province, China

Corresponding author: Xin Du, PhD, Chief Doctor, Department of Hematology, Shenzhen Second People's Hospital, The First Affiliated Hospital of Shenzhen University, No. 3002 Sungang West Road, Futian District, Shenzhen 518035, Guangdong Province, China. duxingz@medmail.com.cn

Abstract

BACKGROUND

Follicular lymphoma (FL), a common type of indolent lymphoma, carries markers of the germinal center, and the rearrangement of the *BCL-2* gene is regarded as an initiating event and a hallmark of the neoplasm. When FL has marginal zone differentiation, some marginal zone features are carried by the neoplasm.

CASE SUMMARY

A 54-year-old male with lymphadenopathy, splenomegaly and hyperlymphocytosis was diagnosed with FL with marginal zone differentiation. The tumor demonstrated different features in the bone marrow (BM) compared with the follicle of the lymph node (LN). Some component of the neoplasm mimicked marginal zone lymphoma, such as infiltrating the marginal zone of the LN, displaying a monocytoid shape and lacking the expression of CD10 in the BM. The diagnosis of FL was made due to the concurrent detection of *BCL-2* rearrangement in the LN and BM.

CONCLUSION

Discordant pathological features in LN and BM could mislead diagnosis. When clinical and pathological manifestations are confusing in diagnosis, typical genetic abnormalities are decisive.

Key Words: Follicular lymphoma; Marginal zone differentiation; Discordant immunophenotypes; Gene rearrangement; Case report

©The Author(s) 2022. Published by Baishideng Publishing Group Inc. All rights reserved.

Core Tip: We reported a case of follicular lymphoma presenting like marginal zone lymphoma due to its marginal zone differentiation and made the diagnosis according to the detection of the rearrangement of *BCL-2*.

Citation: Peng HY, Xiu YJ, Chen WH, Gu QL, Du X. Follicular lymphoma presenting like marginal zone lymphoma: A case report. *World J Clin Cases* 2022; 10(17): 5877-5883
URL: https://www.wjgnet.com/2307-8960/full/v10/i17/5877.htm
DOI: https://dx.doi.org/10.12998/wjcc.v10.i17.5877

INTRODUCTION

As the most common indolent lymphoma, follicular lymphoma (FL) is recognized as the neoplasm of B lymphocytes in germinal center, characterized by t (14; 18) (q32; q21)[1]. Clinically, FL is sensitive to treatments but manifests an incurable and recrudescent course. The neoplastic cells of FL are composed of small to medium-sized cleaved centrocytes and large non-cleaved centroblasts, whose proportion determines the grading system[2]. The rearrangement of chromosomes 14 and 18 leads to the fusion of the *IGH* and *BCL-2* genes, causing the overexpression of the anti-apoptotic protein BCL-2. Based on the morphology of neoplastic centrocytes and centroblasts in the follicles, as well as the typical immunophenotype of the malignant cells, the pathological diagnosis of FL is made, and the detection of *BCL-2* rearrangement makes the diagnosis overt. FL is occasionally associated with marginal zone or plasmacytic differentiation, sharing some morphologic and phenotypic features of marginal zone lymphoma (MZL) or plasmacytoma[3].

MZL is also a kind of indolent lymphoma, with different subtypes including nodal marginal zone lymphoma (NMZL), mucosa associated lymphoid tissue lymphoma and splenic marginal zone lymphoma (SMZL). The cells of MZL harbor a monocytoid shape and display a phenotype of post-germinal center B lymphocytes without the expression of CD10. The bone marrow (BM) is very likely to be involved in patients with SMZL and NMZL, and white blood cell count is often high in patients with SMZL. In this paper, we reported a case of FL with marginal zone differentiation, which showed distinct phenotypes in the lymph node (LN) and the BM and resembled the presentation of MZL.

CASE PRESENTATION

Chief complaints

The hospitalized patient, a 54-year-old male, complained about fatigue and breathlessness.

History of present illness

The patient had fatigue for 1 mo and progressive breathlessness for 1 wk.

History of past illness

The patient had no other remarkable medical histories, and there was no history of fever.

Personal and family history

The patient had no previous or family history of similar illness.

Physical examination

Swelling of cervical, axillary and inguinal LNs was discovered through physical examination.

Laboratory examinations

The patient's complete blood count showed: white blood cell count 142 × 10^9/L, lymphocyte count 133 × 10^9/L, hemoglobin 35 g/L, platelet count 298 × 10^9/L. Lactate dehydrogenase was elevated at a level of 412 U/L.

Imaging examinations

Image examination demonstrated splenomegaly and multiple lymphadenopathy of the mediastinum and the enterocoelia.

Examinations of BM

BM aspirate revealed prominent hyperplasia of lymphocytes, between small and medium size,

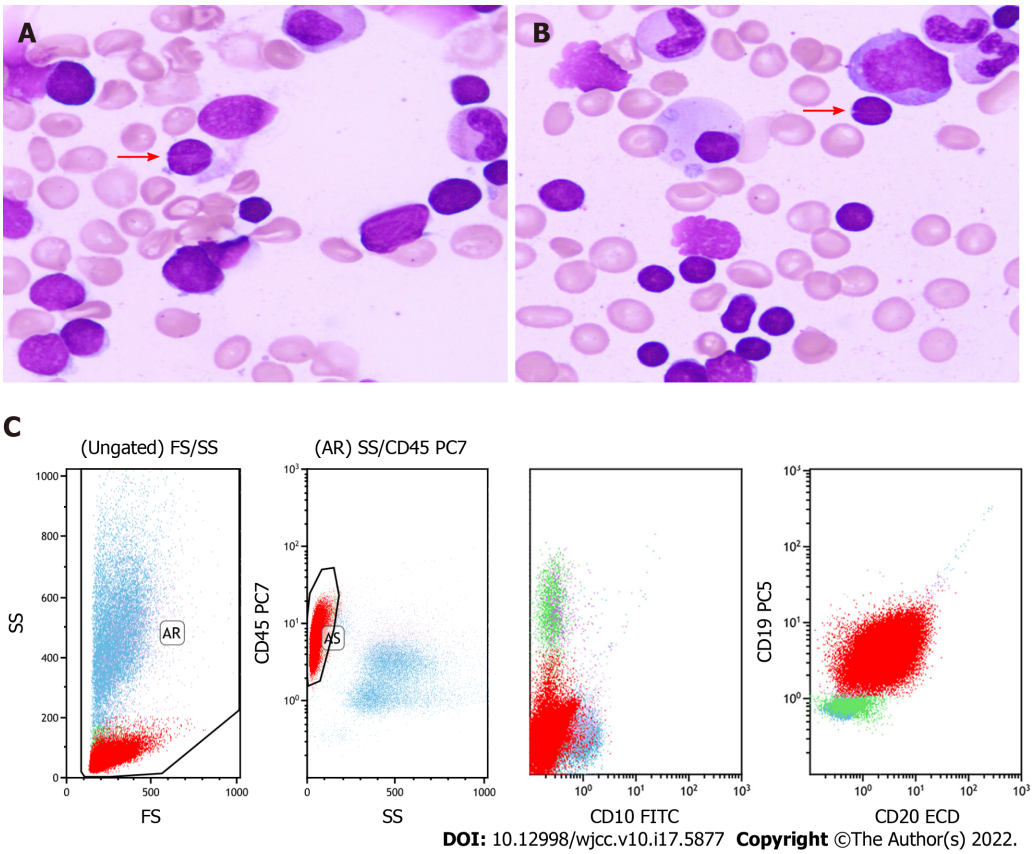

DOI: 10.12998/wjcc.v10.i17.5877 **Copyright** ©The Author(s) 2022.

Figure 1 Morphology and flow cytometry analysis of the bone marrow. A and B: The bone marrow (BM) was mainly infiltrated by monocytoid cells, accompanied with a few cells with cleaved or notched nuclei (pointed by arrows) [400 × (A) and 400 × (B)]; C: Flow cytometry revealed that the neoplastic cells (the red group) in BM were positive for CD19 and CD20 but negative for CD5 and CD10.

accounting for 85% of the nucleated cells. Most of the lymphocytes were small with a round nucleus, while a small fraction of them had cleaved or notched nuclei (Figure 1A and B). Flow cytometry analysis proved a clonal population of mature B lymphocytes, positive for CD19, CD20, CD79b and FMC7 instead of CD3, CD5 or CD10 (Figure 1C). BM biopsy confirmed the paratrabecular infiltration of the neoplastic lymphocytes and a phenotype consistent with flow cytometry analysis (Figure 2A and B). The fusion of the *BCL-2* and *IGH* genes were detected by fluorescence *in situ* hybridization of the BM (Figure 3A and B). The next generation sequencing of the BM revealed mutations of genes *TP53*, *CREBBP* (p. R1446H) and *KMT2D* (p. Q1613X).

Histological examinations

Then cervical LN biopsy was performed. Hematoxylin and eosin stain of the LN gave the information that the expanded follicles were infiltrated by large centroblasts and relatively smaller centrocytes. The number of large centroblasts in the follicles significantly increased, over 15/high power field. Numerous and serried monocytoid lymphocytes occupied the marginal zone surrounding and between the follicles, forming a dark background (Figure 2C and D). Immunohistochemical examination discovered that the overgrown follicular cells were positive for CD10 (Figure 4A and B), BCL-6, CD20 (Figure 4C and D) and Ki-67 (40%) but negative for myeloid cell nuclear differentiation antigen, a marker closely associated with NMZL. The positive CD21 confirmed a follicular dendritic cell meshwork. The neoplastic cells in the marginal zone were negative for CD10 (Figure 4A and B) but positive for CD20 (Figure 4C and D). Fluorescence *in situ* hybridization detection of the LN illustrated the *BCL-2/IGH* rearrangement in both follicles and marginal zone (Figure 3C and D).

FINAL DIAGNOSIS

In the follicles, the phenotype of the cells was different from that in the marginal zone and the BM, but the two groups of cells with distinct phenotypes should be considered as one clone for the coexistence of the rearrangement of *BCL-2*. The patient was diagnosed with follicular lymphoma with marginal zone differentiation involving the BM.

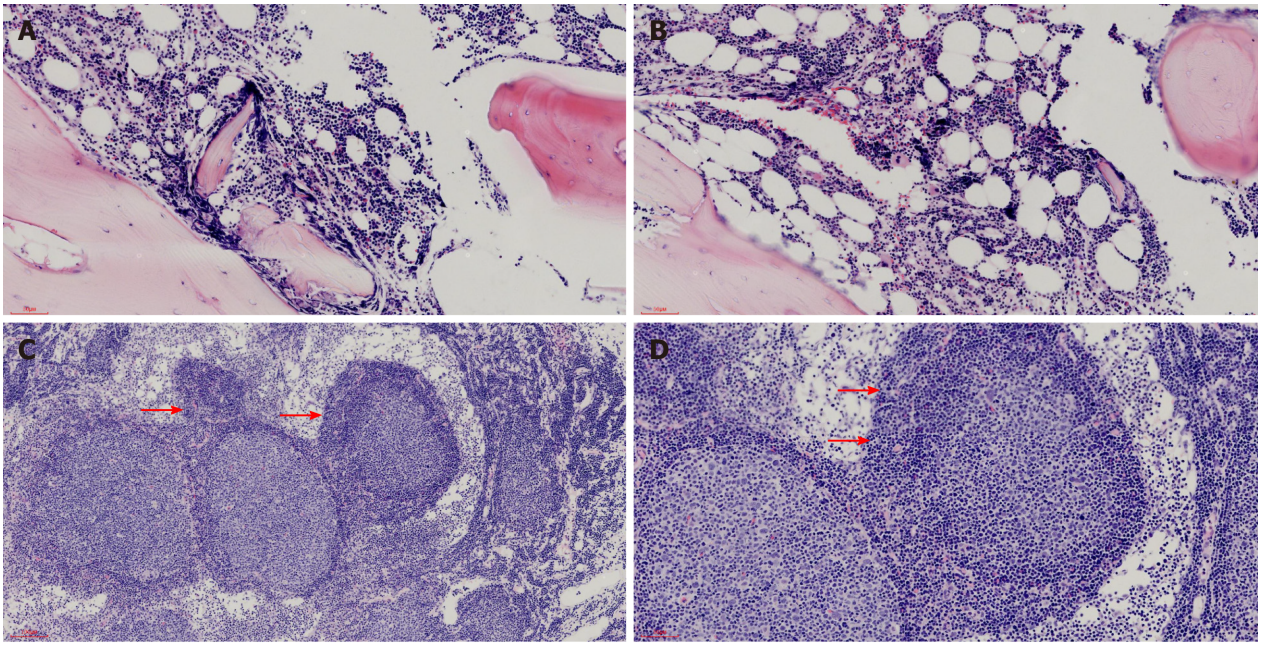

DOI: 10.12998/wjcc.v10.i17.5877 **Copyright** ©The Author(s) 2022.

Figure 2 Morphology of the bone marrow and lymph node. A and B: Hematoxylin and eosin (HE) stain displayed that the bone marrow was infiltrated by neoplastic lymphocytes in a paratrabecular pattern [100 × (A) and 200 × (B)]; C and D: HE stain showed that expanded follicles were infiltrated by neoplastic centroblasts and centrocytes, and serried monocytoid cells (arrows) [100 × (C) and 200 × (D)] surrounded them.

TREATMENT

The patient received six cycles of immune-chemotherapy of R-CHOP (rituximab, cyclophosphamide, liposomal doxorubicin, vindesine and prednisone). After that, his symptoms were markedly relieved, and the hemoglobin level and white blood cell and platelet count became normal. The whole-body computed tomography scan revealed significant shrinkage of the LNs and the spleen.

OUTCOME AND FOLLOW-UP

The patient received the maintenance therapy of rituximab every 2 mo. However, he died of relapse after 2 years.

DISCUSSION

The morphologic manifestations of FL with marginal zone differentiation have been described as neoplastic follicles that were surrounded by proliferative monocytoid B lymphocytes[4,5]. This was extensively observed in this case. The follicles were infiltrated by centroblasts and centrocytes, and the interfollicular area was occupied by vast monocytoid lymphocytes. But in this case, the phenotype of the two parts was discordant, reflecting two successive stages in B lymphocyte differentiation. The positive stain of CD20 indicated that both components were B cell-derived, while the marginal zone component was negative for CD10, which was positive in the follicles. In addition, it was reported that myeloid cell nuclear differentiation antigen was widely expressed in NMZL but scarcely in FL[6,7]. The absence of its expression could distinguish FL with concurrent NMZL.

The neoplastic cells in the germinal center and the marginal zone of this case were different in phenotype, but it was clear that they were related to genetics according to some previous studies[8,9]. The molecular analysis of immunoglobulin heavy chain gene of the two components revealed that they shared identical or nearly identical complementarity determining region III sequences[4,10], and the rearrangement of *BCL-2* was found to be a common event of them by PCR[11]. In this case, the pathological manifestation of the LN was consistent with the features of FL with marginal zone differentiation, and the rearrangement of *BCL-2* confirmed this diagnosis. The discordant phenotype in the follicle and the marginal area indicated the coexistence of two differentiation status in one neoplasm.

In BM and peripheral blood, the MZL cells have been reported to be polymorphic and predominantly monocytoid while infrequently centrocytoid or plasmacytic[12,13]. But for FL, the BM is mainly involved by centrocytoid cells, with typical "cleaved or notched" nuclei[14-16]. The MZL cells display

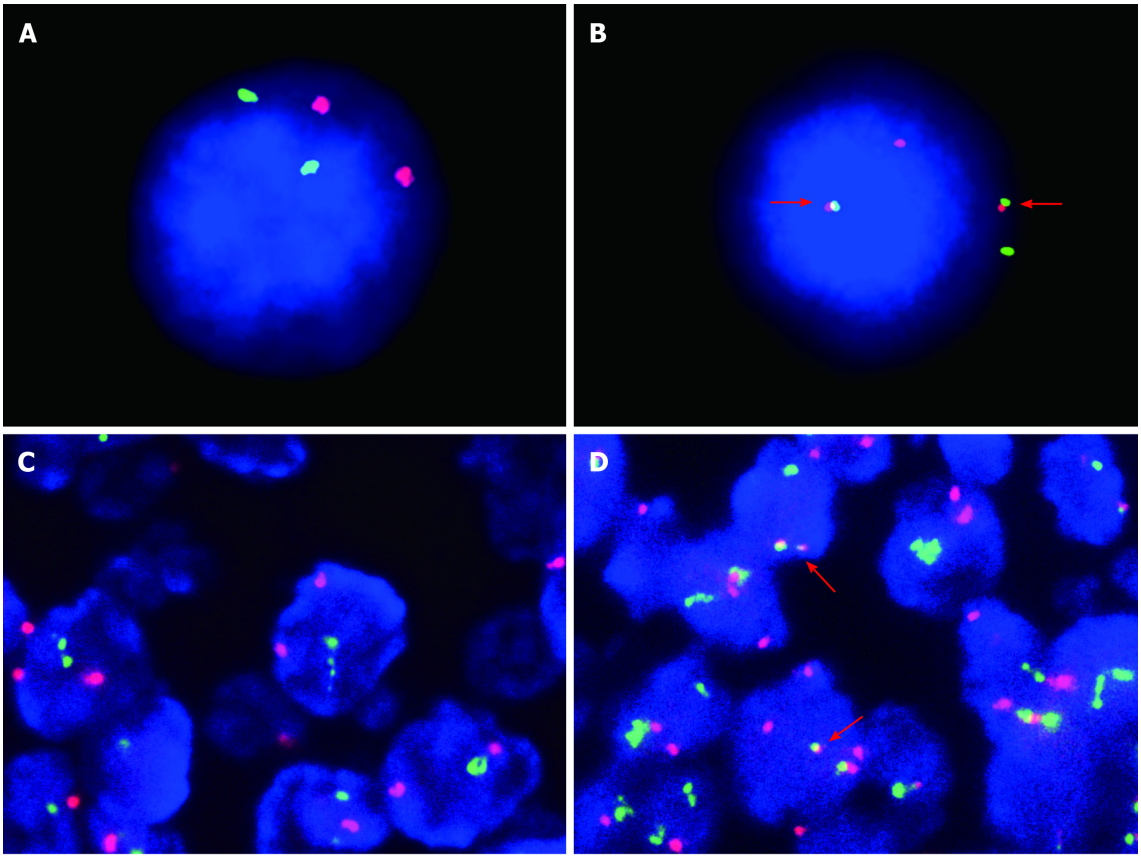

DOI: 10.12998/wjcc.v10.i17.5877 **Copyright** ©The Author(s) 2022.

Figure 3 Fluorescence *in situ* hybridization analysis of the bone marrow and lymph node. A-D: A and C were the control groups [1000 × (A) and 1000 × (B), 400 × (C) and 400 × (D)], the rearrangement of *BCL-2/IGH* (fusion of the red light and the green light) (B) was detected in the bone marrow and in the lymph node (fusion of the red light and the green light) (D) shown by fluorescence *in situ* hybridization.

markers of post-germinal center B cell and are negative for CD10, which is different from the FL cells in BM. In addition, it is a normal event of FL infiltrating the BM, but it is rare for the peripheral blood to be involved, not to mention in a hyperleukocytic pattern[14,16]. This is in contrast to MZL, especially SMZL, which usually takes on hyperlymphocytosis. In this case, the BM and the peripheral blood were mainly infiltrated by the CD10 negative monocytoid cells, with a few cleaved or notched-nuclei cells. Also, the white blood cell count massively increased, resembling the features of MZL. Nevertheless, the rearrangement of *BCL-2/IGH* was detected in both the LN and the BM, while it has been scarcely detected in MZL[17,18]. Additionally, FL is abundant in mutations of genes that encode histone modifiers, such as *KMT2D*, *EZH2* and *CREBBP*[19]. The concurrent mutations of *CREBBP* and *KMT2D*, in addition to the *BCL-2/IGH* rearrangement, strongly indicated that the neoplasm was germinal center originated instead of MZL. These genetic alterations suggested that the cells in the LN and BM were from the identical clone of FL essentially.

There were reports that FL cells occasionally lost the expression of CD10 when BM was involved, but the underlying reasons were not clarified[20]. FL cells with marginal zone differentiation tended to mimic the biological behavior and the clinical presentation of MZL, and the CD10 of the marginal zone component was usually missing[8]. Therefore, it is presumable that, in this case, the marginal zone component of the lymphoma migrated to the blood and the marrow, displaying the features of MZL (the monocytoid shape, the absence of CD10, being hyperleukocytic and splenomegaly, *etc*) but carrying the intrinsic genetic abnormalities of FL.

The patient responded to the R-CHOP regimen well, which also applies to MZL patients. However, he suffered from an early relapse, due to the dismal prognosis of the disease harboring the mutation of *TP*53.

CONCLUSION

Generally, different subtypes of B cell lymphoma represent different evolutional stages of normal lymphocytes. The primary site and the phenotype of lymphomas tend to resemble its normal counterparts. On the contrary, the morphology, the immunophenotype and the clinical presentation of

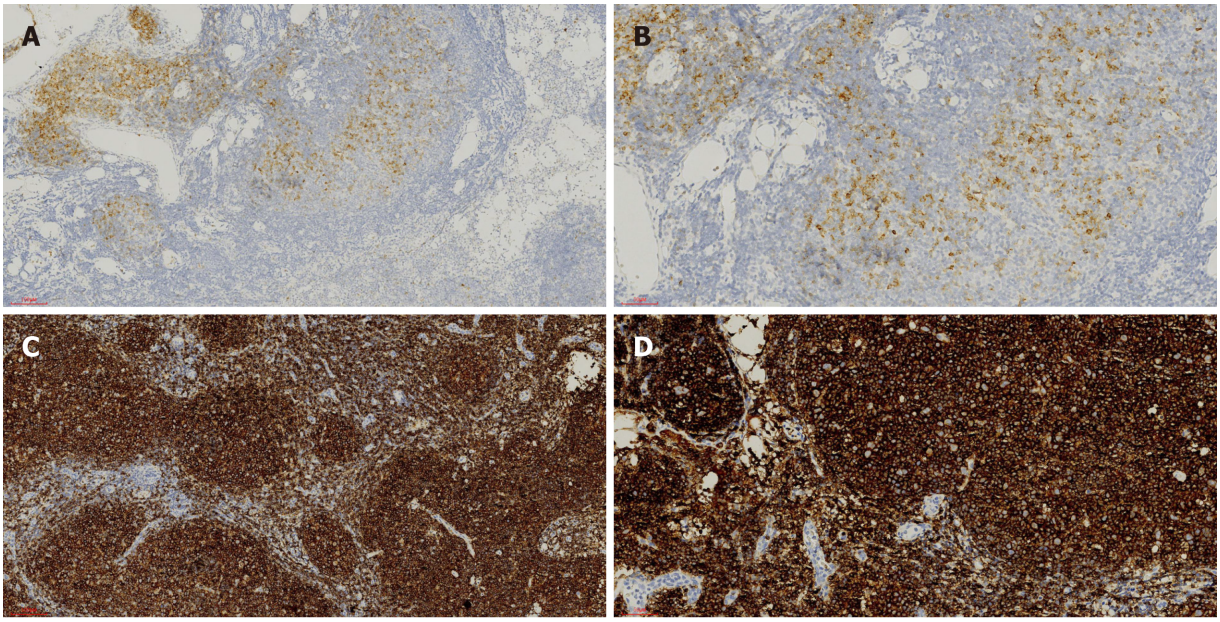

DOI: 10.12998/wjcc.v10.i17.5877 **Copyright** ©The Author(s) 2022.

Figure 4 Immunohistochemical examination of the lymph node. A-D: The follicular cells were positive for CD10 [100 × (A) and 200 × (B)] and CD20 [100 × (C) and 200 × (D)], and the proliferative marginal component was negative for CD10 (A and B) and positive for CD20 (C and D).

the disease are deceiving when it is with marginal zone differentiation. Without genetic detection, this case can be easily misdiagnosed as concurrent existence of two types of lymphoma. Therefore, it is necessary to take a deep insight into the genetic message of the neoplasm when performing diagnosis.

FOOTNOTES

Author contributions: Peng HY wrote the manuscript; Xiu YJ provided the pathological pictures and contributed to the diagnosis; Chen WH reviewed the cases and edited the manuscript; Gu QL was in charge of the follow-up; Du X designed the study; all authors issued final approval for the version to be submitted; All authors approved the manuscript for publication.

Informed consent statement: Written informed consent was obtained from the patient for publication of this report and any accompanying images.

Conflict-of-interest statement: The authors have no conflicts of interest to declare.

CARE Checklist (2016) statement: The authors have read the CARE Checklist (2016), and the manuscript was prepared and revised according to the CARE Checklist (2016).

Open-Access: This article is an open-access article that was selected by an in-house editor and fully peer-reviewed by external reviewers. It is distributed in accordance with the Creative Commons Attribution NonCommercial (CC BY-NC 4.0) license, which permits others to distribute, remix, adapt, build upon this work non-commercially, and license their derivative works on different terms, provided the original work is properly cited and the use is non-commercial. See: https://creativecommons.org/Licenses/by-nc/4.0/

Country/Territory of origin: China

ORCID number: Hao-Yu Peng 0000-0001-9743-0282; Ying-Jie Xiu 0000-0001-8154-7347; Wei-Hong Chen 0000-0002-2972-1069; Qing-Li Gu 0000-0001-6118-5852; Xin Du 0000-0002-4077-5578.

S-Editor: Gong ZM
L-Editor: Filipodia
P-Editor: Gong ZM

REFERENCES

1 **Küppers R**. Mechanisms of B-cell lymphoma pathogenesis. *Nat Rev Cancer* 2005; **5**: 251-262 [PMID: 15803153 DOI: 10.1038/nrc1589]

2 **Swerdlow SH**, Campo E, Pileri SA, Harris NL, Stein H, Siebert R, Advani R, Ghielmini M, Salles GA, Zelenetz AD, Jaffe ES. The 2016 revision of the World Health Organization classification of lymphoid neoplasms. *Blood* 2016; **127**: 2375-2390 [PMID: 26980727 DOI: 10.1182/blood-2016-01-643569]

3 **Chapman JR**, Alvarez JP, White K, Sanchez S, Khanlari M, Algashaamy K, Cassidy D, Peng JH, Fan YS, Alencar A, Alderuccio JP, Lossos IS, Vega F. Unusual Variants of Follicular Lymphoma: Case-based Review. *Am J Surg Pathol* 2020; **44**: 329-339 [PMID: 31688142 DOI: 10.1097/PAS.0000000000001399]

4 **Abou-Elella A**, Shafer MT, Wan XY, Velanker M, Weisenburger DD, Nathwani BN, Gascoyne RD, Greiner TC, Chan WC. Lymphomas with follicular and monocytoid B-cell components. Evidence for a common clonal origin from follicle center cells. *Am J Clin Pathol* 2000; **114**: 516-522 [PMID: 11026097 DOI: 10.1309/X559-FDJB-LJGD-YG7E]

5 **Schmid U**, Cogliatti SB, Diss TC, Isaacson PG. Monocytoid/marginal zone B-cell differentiation in follicle centre cell lymphoma. *Histopathology* 1996; **29**: 201-208 [PMID: 8884347 DOI: 10.1111/j.1365-2559.1996.tb01392.x]

6 **Metcalf RA**, Monabati A, Vyas M, Roncador G, Gualco G, Bacchi CE, Younes SF, Natkunam Y, Freud AG. Myeloid cell nuclear differentiation antigen is expressed in a subset of marginal zone lymphomas and is useful in the differential diagnosis with follicular lymphoma. *Hum Pathol* 2014; **45**: 1730-1736 [PMID: 24925224 DOI: 10.1016/j.humpath.2014.04.004]

7 **van den Brand M**, Mathijssen JJ, Garcia-Garcia M, Hebeda KM, Groenen PJ, Falini B, Serrano S, van Krieken JH. Immunohistochemical differentiation between follicular lymphoma and nodal marginal zone lymphoma--combined performance of multiple markers. *Haematologica* 2015; **100**: e358-e360 [PMID: 26069292 DOI: 10.3324/haematol.2014.120956]

8 **Dogan A**, Du MQ, Aiello A, Diss TC, Ye HT, Pan LX, Isaacson PG. Follicular lymphomas contain a clonally linked but phenotypically distinct neoplastic B-cell population in the interfollicular zone. *Blood* 1998; **91**: 4708-4714 [PMID: 9616169]

9 **Matsuda I**, Shimizu Y, Okamoto T, Hirota S. Follicular lymphoma mimicking marginal zone lymphoma in lymph node: a case report. *Int J Clin Exp Pathol* 2014; **7**: 7076-7081 [PMID: 25400800]

10 **Robetorye RS**, Bohling SD, Medeiros LJ, Elenitoba-Johnson KS. Follicular lymphoma with monocytoid B-cell proliferation: molecular assessment of the clonal relationship between the follicular and monocytoid B-cell components. *Lab Invest* 2000; **80**: 1593-1599 [PMID: 11045576 DOI: 10.1038/Labinvest.3780169]

11 **Yegappan S**, Schnitzer B, Hsi ED. Follicular lymphoma with marginal zone differentiation: microdissection demonstrates the t(14;18) in both the follicular and marginal zone components. *Mod Pathol* 2001; **14**: 191-196 [PMID: 11266525 DOI: 10.1038/modpathol.3880284]

12 **Mollejo M**, Camacho FI, Algara P, Ruiz-Ballesteros E, García JF, Piris MA. Nodal and splenic marginal zone B cell lymphomas. *Hematol Oncol* 2005; **23**: 108-118 [PMID: 16307458 DOI: 10.1002/hon.762]

13 **van den Brand M**, van Krieken JH. Recognizing nodal marginal zone lymphoma: recent advances and pitfalls. A systematic review. *Haematologica* 2013; **98**: 1003-1013 [PMID: 23813646 DOI: 10.3324/haematol.2012.083386]

14 **Arber DA**, George TI. Bone marrow biopsy involvement by non-Hodgkin's lymphoma: frequency of lymphoma types, patterns, blood involvement, and discordance with other sites in 450 specimens. *Am J Surg Pathol* 2005; **29**: 1549-1557 [PMID: 16327427 DOI: 10.1097/01.pas.0000182405.65041.8b]

15 **Torlakovic E**, Torlakovic G, Brunning RD. Follicular pattern of bone marrow involvement by follicular lymphoma. *Am J Clin Pathol* 2002; **118**: 780-786 [PMID: 12428800 DOI: 10.1309/EG2M-YHB9-WEFW-7H1R]

16 **Melo JV**, Robinson DS, De Oliveira MP, Thompson IW, Lampert IA, Ng JP, Galton DA, Catovsky D. Morphology and immunology of circulating cells in leukaemic phase of follicular lymphoma. *J Clin Pathol* 1988; **41**: 951-959 [PMID: 3056987 DOI: 10.1136/jcp.41.9.951]

17 **Arribas AJ**, Rinaldi A, Mensah AA, Kwee I, Cascione L, Robles EF, Martinez-Climent JA, Oscier D, Arcaini L, Baldini L, Marasca R, Thieblemont C, Briere J, Forconi F, Zamò A, Bonifacio M, Mollejo M, Facchetti F, Dirnhofer S, Ponzoni M, Bhagat G, Piris MA, Gaidano G, Zucca E, Rossi D, Bertoni F. DNA methylation profiling identifies two splenic marginal zone lymphoma subgroups with different clinical and genetic features. *Blood* 2015; **125**: 1922-1931 [PMID: 25612624 DOI: 10.1182/blood-2014-08-596247]

18 **Spina V**, Khiabanian H, Messina M, Monti S, Cascione L, Bruscaggin A, Spaccarotella E, Holmes AB, Arcaini L, Lucioni M, Tabbò F, Zairis S, Diop F, Cerri M, Chiaretti S, Marasca R, Ponzoni M, Deaglio S, Ramponi A, Tiacci E, Pasqualucci L, Paulli M, Falini B, Inghirami G, Bertoni F, Foà R, Rabadan R, Gaidano G, Rossi D. The genetics of nodal marginal zone lymphoma. *Blood* 2016; **128**: 1362-1373 [PMID: 27335277 DOI: 10.1182/blood-2016-02-696757]

19 **Morin RD**, Mendez-Lago M, Mungall AJ, Goya R, Mungall KL, Corbett RD, Johnson NA, Severson TM, Chiu R, Field M, Jackman S, Krzywinski M, Scott DW, Trinh DL, Tamura-Wells J, Li S, Firme MR, Rogic S, Griffith M, Chan S, Yakovenko O, Meyer IM, Zhao EY, Smailus D, Moksa M, Chittaranjan S, Rimsza L, Brooks-Wilson A, Spinelli JJ, Ben-Neriah S, Meissner B, Woolcock B, Boyle M, McDonald H, Tam A, Zhao Y, Delaney A, Zeng T, Tse K, Butterfield Y, Birol I, Holt R, Schein J, Horsman DE, Moore R, Jones SJ, Connors JM, Hirst M, Gascoyne RD, Marra MA. Frequent mutation of histone-modifying genes in non-Hodgkin lymphoma. *Nature* 2011; **476**: 298-303 [PMID: 21796119 DOI: 10.1038/nature10351]

20 **Maeshima AM**, Taniguchi H, Tanioka K, Kitahara H, Miyamoto K, Fukuhara S, Munakata W, Suzuki T, Maruyama D, Kobayashi Y, Tobinai K, Kushima R. Clinicopathological characteristics of follicular lymphoma with peripheral blood involvement. *Leuk Lymphoma* 2015; **56**: 2000-2004 [PMID: 25315078 DOI: 10.3109/10428194.2014.963578]

World Journal of Clinical Cases

Submit a Manuscript: https://www.f6publishing.com

World J Clin Cases 2022 June 16; 10(17): 5884-5892

DOI: 10.12998/wjcc.v10.i17.5884

ISSN 2307-8960 (online)

CASE REPORT

Primary renal small cell carcinoma: A case report

Kun Xie, Xi-Ya Li, Bang-Jie Liao, Si-Cheng Wu, Wei-Min Chen

Specialty type: Medicine, research and experimental

Provenance and peer review: Unsolicited article; Externally peer reviewed.

Peer-review model: Single blind

Peer-review report's scientific quality classification

Grade A (Excellent): 0
Grade B (Very good): B
Grade C (Good): C
Grade D (Fair): 0
Grade E (Poor): 0

P-Reviewer: Kaewput W, Thailand; Peitsidis P, Greece

Received: December 31, 2021
Peer-review started: December 31, 2021
First decision: February 21, 2022
Revised: March 15, 2022
Accepted: April 4, 2022
Article in press: April 4, 2022
Published online: June 16, 2022

Kun Xie, Xi-Ya Li, Bang-Jie Liao, Si-Cheng Wu, Wei-Min Chen, Department of Urology, The First Affiliated Hospital of Nanchang University, Nanchang 330036, Jiangxi Province, China

Corresponding author: Wei-Min Chen, Doctor, Chief Doctor, Doctor, Surgeon, Surgical Oncologist, Department of Urology, The First Affiliated Hospital of Nanchang University, No. 17 Yongwai Zhengjie, Nanchang 330036, Jiangxi Province, China. cwmncdxyfy@126.com

Abstract

BACKGROUND

Small cell carcinoma (SCC) is a malignant tumour that is frequently accompanied by extensive metastasis. Primary renal SCC has typical characteristics related to SCC and is extremely rare, with no uniform treatment standard. Clinical treatment is mainly based on the literature. Here we report the diagnosis and treatment of an interesting case of primary renal SCC.

CASE SUMMARY

We report a tortuous course of treatment for a 68-year-old man. Four years before diagnosis, the patient developed continuous gross haematuria, during which he underwent several ureteral biopsies, ureteral stricture relief, and urine exfoliated cell examinations; however, SCC was not confirmed. One month before radical resection of the renal pelvic carcinoma, the severe haematuria recurred. Computed tomography revealed transitional cell carcinoma in the right kidney and right upper ureter. A preoperative examination exluded the possibility of a pulmonary origin of the tumour, and primary renal SCC was diagnosed. The postoperative pathology findings were suggestive of SCC. The patient was treated with combined chemotherapy but died of tumour progression at 7 mo postoperative.

CONCLUSION

Our patient's disease onset in the context of a succession of regular testing and the fact that it occurred so quickly with perirenal encroachment immediately after diagnosis reveals the cruel and unforgiving side of the disease. Furthermore, patients with poor comprehensive treatment results require new treatment regimens.

Key Words: Kidney; Small cell carcinoma; Clinical features; Diagnosis; Treatment; Case report

©The Author(s) 2022. Published by Baishideng Publishing Group Inc. All rights reserved.

Core Tip: Our patient's onset in the context of a succession of regular testing, and the fact that it occurred so quickly, with perirenal encroachment immediately after diagnosis, reveals the cruel and cunning side of the disease. Futhermore, patients with poor comprehensive treatment results, proving the need to develop new treatment regimens.

Citation: Xie K, Li XY, Liao BJ, Wu SC, Chen WM. Primary renal small cell carcinoma: A case report. *World J Clin Cases* 2022; 10(17): 5884-5892
URL: https://www.wjgnet.com/2307-8960/full/v10/i17/5884.htm
DOI: https://dx.doi.org/10.12998/wjcc.v10.i17.5884

INTRODUCTION

Small cell carcinoma (SCC) usually arises from the lungs, and extrapulmonary SCC accounts for 2.5%-5% of all SCC cases[1]. SCC occurs in the urinary system is extremely rare, and most commonly occurs in the bladder[2]. Primary renal SCC is even rarer. The rarity, aggressiveness, and poor prognosis of these tumours adds to the seriousness of the disease[3]. The overall survival rate of renal SCC is worse than that of pulmonary SCC[4,5]. Given the very aggressive behaviour of renal SCC, standard treatments are required[5]. Here we report a case of primary renal SCC and discuss its rapid clinical progression, treatment, and long-term effects.

CASE PRESENTATION

Chief complaints

Right low back pain, abdominal distension and repeated gross hematuria for 2 wk.

History of present illness

The patient was a 68-year-old man admitted to The First Affiliated Hospital of Nanchang University on September 20, 2020 with a 2-wk history of right waist pain and abdominal distension with repeated gross haematuria. No special observation was noted during physical examination.

In August 2016, the patient was admitted to our hospital with repeated gross haematuria. Computed tomography (CT) showed thickening of the wall of the lower part of the right ureter suggestive of ureteral cancer, hydronephrosis of the right kidney and upper and middle ureteral segments, and right renal insufficiency. After consultation with the patient and his dependents, we decided to perform a ureteral tumour biopsy, and postoperative pathology exhibited a limited lower segment of the right ureter, suspected to be cancerous. Immunohistochemistry showed CD20 (+ mainly umbrella cells, focal whole layer +), Ki-67 (+ mainly basal cells), and p53 (-) (Figure 1A). We recommended a radical ureterectomy for this cancer; however, the patient and his family refused, and he agreed to undergo ureteral bladder replantation to treat distal ureteral strictures (right) 1 wk after the biopsy (right). Intraoperative frozen pathology and postoperative pathology of the vesicoureteral junction revealed chronic mucositis and mild atypical hyperplasia of the local urothelium (Figure 1B).

The patient's postoperative recovery was good, but irregular gross haematuria was observed during the follow-up period. Re-examination with CT in our hospital in January 2017, March 2019, and September 2019 showed postoperative changes in the lower segment of the right ureter and slight hydronephrosis in the right kidney and upper ureteral segment. A ureteral biopsy was performed again in 2019 for gross haematuria, and the postoperative pathology findings were consistent with the morphological manifestation of a right ureteral polyp (Figure 1C). Urine exfoliative cytology was performed in August 2016 and March 2019, but the results were negative. The remainder of this paper is nothing special.

History of past illness

The patient had no relevant medical history.

Personal and family history

The patient had no relevant personal or family history.

Physical examination

The patient's vital signs were normal. There is percussion pain in the right renal area, normal on the left side.

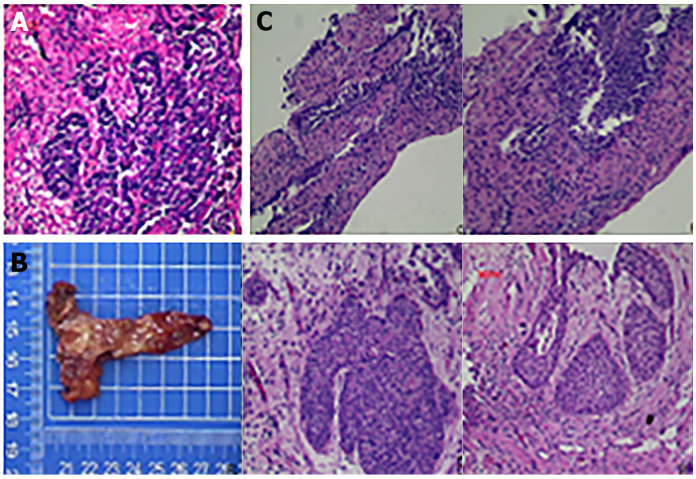

DOI: 10.12998/wjcc.v10.i17.5884 **Copyright** ©The Author(s) 2022.

Figure 1 Postoperative pathology in 2016 and 2019. A: After ureteral biopsy in 2016. Carcinoma tissue was suspected. Under the microscope, mucosal tissue was mixed with hemorrhagic necrotic tissue, and the surface of the mucosa was covered with urothelium, which showed papillary or solid nest like inverted growth. The tumor nucleus was oval, the cytoplasm was deep, mitosis was occasionally seen, and the focal area seemed to be a staggered arrangement of solid nestlike cells and proliferative stroma; B: After ureteral bladder replantation. Chronic mucositis and mild atypical hyperplasia was considered. Under the microscope, the urinary tract epithelium covered by the mucosal surface of some areas proliferated, and grew to the lamina propria to form a small nest or glandular tube-like structure, focal squamous metaplasia, partial mucosal surface necrosis, covered with a large amount of red staining without structure, and significant interstitial edema in the lamina propria; C: after ureteral biopsy in 2019. Polypoid change was showed. Under the microscope, part of the surface is lined with hyperplastic urothelial epithelium and lamina propria fibrous interstitial hyperplasia.

Laboratory examinations

The patient's creatinine level was 114.1 μmol/L and urea nitrogen level was 4.9 mmol/L. The glomerular filtration rate (GFR) of the left kidney was 31.88 mL/min, while that of the right kidney was 14.38 mL/min. The remaining participants were not special.

Imaging examinations

B-mode ultrasound showed the following: (1) Hydronephrosis of the right kidney suggestive of possible middle and lower ureteral obstructions; and (2) Benign prostatic hyperplasia with calcification. CT showed the following: (1) A soft-tissue tumour of the right kidney and right upper ureter segment suggestive of transitional cell carcinoma in addition to multiple enlarged lymph nodes in the right renal hilum suggestive of metastasis; (2) Blood perfusion and excretion function of the right kidney were significantly decreased; (3) Postoperative changes in the right ureter. The wall of the lower part of the right ureter near the entrance of the bladder was slightly thickened and enhanced. Therefore, an endoscopic examination was recommended; and (4) The presence of multiple nodes in both lungs suggested the possibility of metastasis (Figure 2).

FINAL DIAGNOSIS

The postoperative pathology showed 60% high-grade invasive papillary urothelial carcinoma with 40% SCC in the right kidney, nervous invasion, visible tumour thrombus in vessels, and invasion of the renal parenchyma. No cancer was noted in the ureteral stump or perirenal fat. Immunohistochemistry showed GATA-3 (nest group +, flake -); CK7 (nest group +, flake -); p63 (nest group +, flake -); CGA (nest group -, flake +); syn (nest group -, flake +); CD56 (nest group -, flake +); CK20 (-); NSE (-); Ki-67 (nest group 60% +, flake 90% +); and CK (nest group strong +, flake weak +). Microscopic examination of the right lower ureter revealed lumen dilation, a partial epithelial defect, partial coverage with urothelium, and severe mechanical injury to the focal epithelial cells affecting the observation. There were two right renal pedicle lymph nodes, but no cancer metastasis was found (0 take 2). Primary renal SCC of the right kidney was also considered (Figure 3).

TREATMENT

The preoperative diagnosis was renal pelvic carcinoma, and Laparoscopic radical resection of the tumour was performed in October 2020.

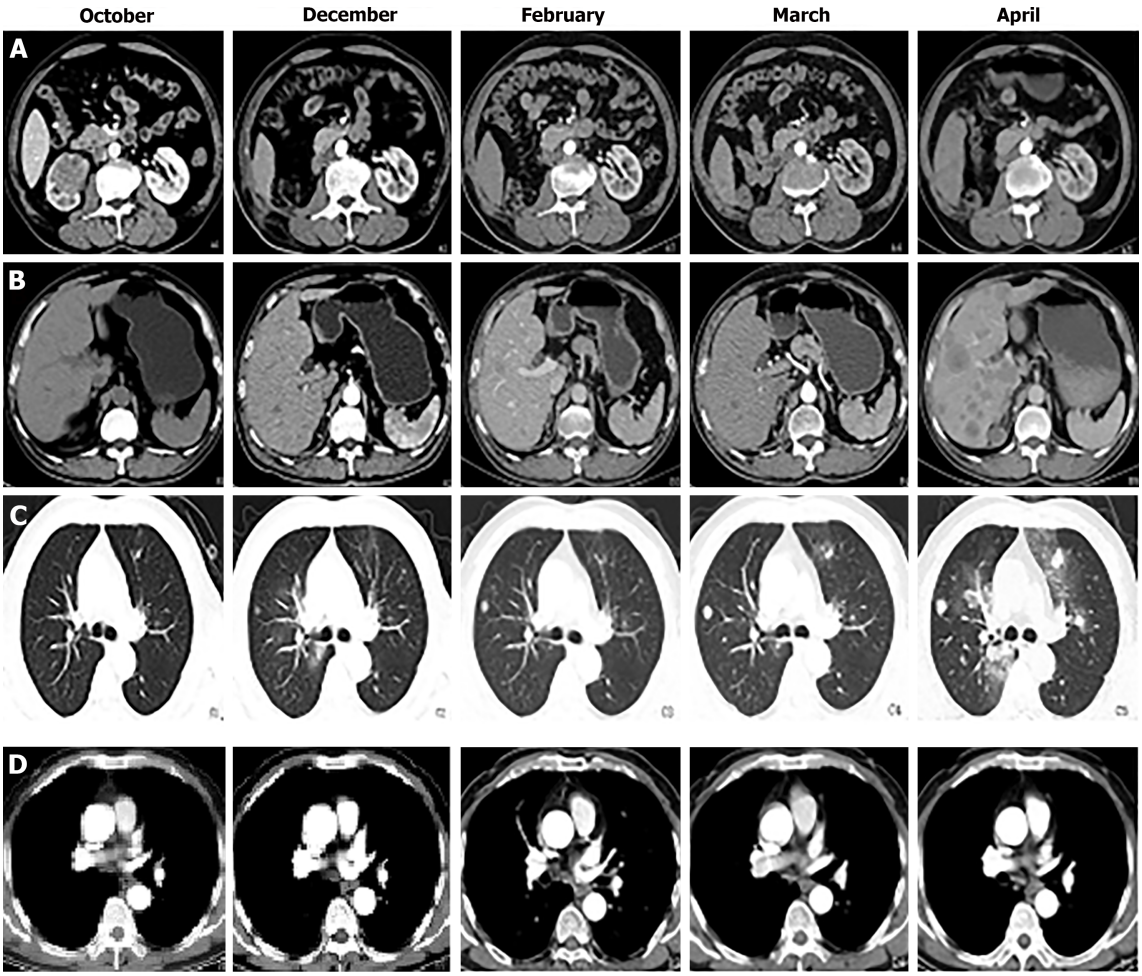

DOI: 10.12998/wjcc.v10.i17.5884 **Copyright** ©The Author(s) 2022.

Figure 2 There are the results of computed tomography examination before and after operation. There was no obvious occupation of liver, lung and mediastinum before operation, but these sites began to occupy space since December, especially the change was quite rapid between March and April, and tumor metastasis occurred at the operation site. A: Kidney; B: Liver; C: Lung; D: Mediastinum.

OUTCOME AND FOLLOW-UP

Combined with the relevant guidelines and literature recommendations, we recommended that the patient start GP chemotherapy 1 mo after surgery, such as gemcitabine 1000 mg/m^2, D1 and D8 intravenous drip, and carboplatin 80 mg/m^2 D1-3 intravenous drip as a 21-d cycle. The dosage would be adjusted after each cycle according to the change in the patient's body surface area. Moreover, a regular monthly review of CT scans enables observation of the changes in the disease (in January, CT examinations were not performed due to the serious epidemic situation of the novel coronavirus, but chemotherapy was still performed on schedule). CT showed tumour metastasis in the lungs and liver in December, and the mediastinum seemed to occupy space. From December to February, the space occupation of the lung seemed to improve, while the liver metastasis became increasingly serious and there was no significant change in the mediastinum. The examination in March showed that the occupation of the lung, liver, and mediastinum had increased, and there was a new mass in the right kidney area of the original operation. In April, metastatic tumours developed rapidly (Figure 2). Other than fatigue and emaciation, the patient did not experience any other discomfort and the chemotherapy drugs were not rejected. During this period, we suggested to the patient and his family that we change the chemotherapy method and add radiotherapy, immunotherapy, and other therapies according to the changes in his condition; however, the idea was rejected and he continued the original treatment plan. When the six cycles of chemotherapy were completed, we suggest that he receive further treatment, but he and his family refused. On May 5, he died of multiple organ failure.

DISCUSSION

The incidence of renal SCC is low, and studies and reports worldwide are rare[6]. We incompletely

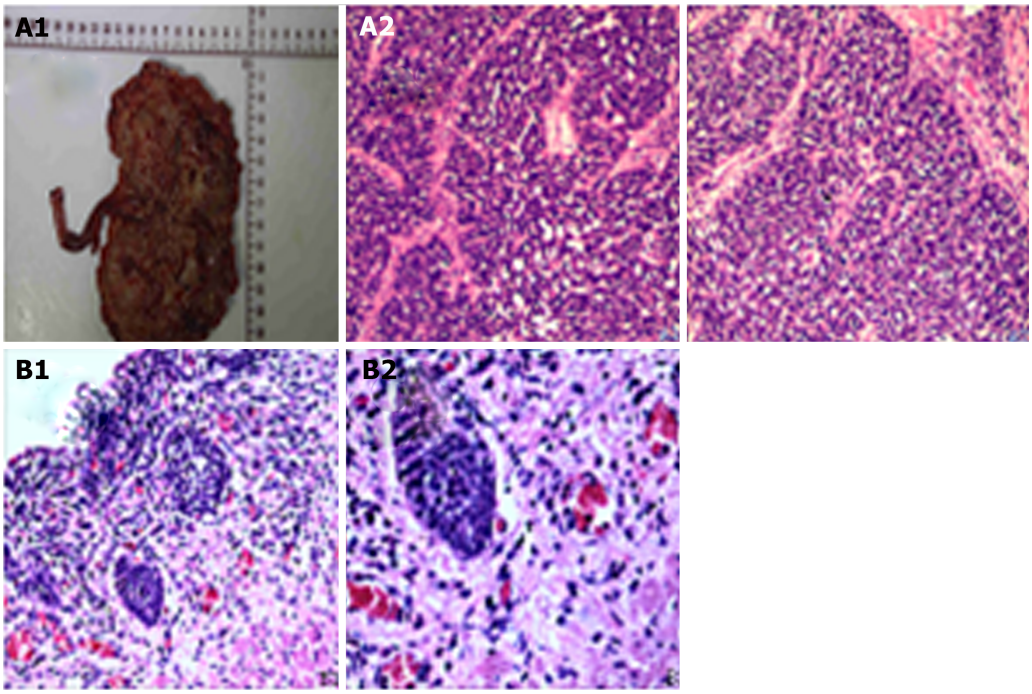

DOI: 10.12998/wjcc.v10.i17.5884 **Copyright** ©The Author(s) 2022.

Figure 3 Postoperative pathology in 2020. High-grade invasive papillary urothelial carcinoma and small cell carcinoma were suspected. A: Under the microscope, tumor cells were composed of two components: one type of cells was nest-like arrangement, with larger cell volume, abundant cytoplasm, large nuclei, deep staining and obvious atypia; the other type of cells was uniformly distributed in sheets, with medium to small cells, abundant cytoplasm or medium cytoplasm, and round nuclei. And the boundary between the two forms is clear (A1 and A2); B: There was no obvious abnormality at the broken end of the ureter (B1 and B2).

counted 92 globally published cases of renal SCC from 1984 to 2022 and summarized their clinical characteristics and treatment options (Table 1). The common clinical manifestations of renal SCC are not significantly different from those of other renal parenchymal malignant tumours and include low back pain, haematuria, abdominal mass, abdominal discomfort, weight loss, and swelling of lymph nodes on the body surface[7]. In addition, it is unrelated to paraneoplastic syndromes[8]. To date, only one case was reportedly associated with a syndrome of inappropriate antidiuretic hormone secretion[5].

The diagnosis of renal SCC relies mainly on histopathological and immunohistochemical findings[9]. Renal SCC is easily misdiagnosed as other small cell tumours, such as undifferentiated carcinoma, Ewing's sarcoma, embryonal rhabdomyosarcoma, lymphoma, and primitive neuroectodermal tumour [4]. Immunohistochemical staining and electron microscopic examinations are helpful for the identification. Besides, in the diagnosis of renal SCC, metastatic SCC, especially those originating from the lung, should be excluded[10]. The diagnosis of renal SCC must be based on the patient's clinical history and chest imaging findings. If the patient has a history of pulmonary SCC or the chest imaging examination shows lung neoplastic lesions, renal metastasis of pulmonary SCC should be considered first; however, if urothelial carcinoma is mixed with SCC, the diagnosis of primary renal SCC should be supported[11].

Histologically, renal SCC is similar to other types of SCC and is mostly mixed with other types, including urothelial carcinoma, squamous cell carcinoma, and adenocarcinoma[12]. Under a light microscope, the tumour tissue shows a solid flake or nest-like arrangement with extensive necrosis. The tumour cells are small, similar to lymphocytes, with rare cytoplasm, deep nuclear staining, unclear nucleoli, and frequent mitotic figures[4]. Immunohistochemistry can express specific neuroendocrine markers such as NSE, CD56, Syn, and CgA[13]. Among them, the Ki-67 score seems a better predictor of survival than the degree of differentiation[14]. Serum NSE levels are potentially useful in early diagnosis and treatment monitoring during chemotherapy[15], neural cell adhesion molecule (NCAM or CD56) is the most sensitive neuroendocrine marker, and chromogranin A, a protein found in neurosecretory granules, is the most specific marker[16].

Owing to the small number of primary renal SCC cases, standard treatment guidelines are lacking. Surgery and chemotherapy are currently the most widely used treatment options. Studies have found that targeted drug therapy combined with radical surgery has significant survival benefits compared to simple radical surgery, while radiotherapy is mostly used for postoperative residual lesions or distant metastases[4]. The targeted drug sunitinib is recommended for the treatment of advanced non-clear cell carcinoma[17]. The Department of Urology, Beijing Friendship Hospital Affiliated to Capital Medical University, diagnosed and treated one patient with renal cell carcinoma. The lymph nodes were fused, and the disease entered partial remission 3 mo after sunitinib treatment at 1 mo after surgery; the

Table 1 Ninety-two globally published cases of renal small cell carcinoma from 1984 to 2022 and their clinical characteristics and treatment options

Features	Classifications	Cases (%)
Age (yr)	≤ 55	38 (41.3)
	> 55	54 (58.7)
Gender	Male	50 (54.3)
	Female	42 (45.7)
Clinical presentation	Flank/abdominal pain	55 (60.0)
	Hematuria	32 (34.7)
	Lump	11 (11.9)
	Neurological symptoms	5 (5.4)
	Other nonspecific symptoms	7 (7.6)
Size (cm)	≤ 10	43 (58.9)
	> 10	30 (41.1)
Affected side	Right	40 (48.1)
	Left	43 (51.9)
pT stage	T1-T2	24 (27.6)
	T3-T4	63 (72.4)
Renal vein tumor thrombus	Yes	16 (34.8)
	No	30 (65.2)
Lymph node metastasis	Yes	41 (50.0)
	No	39 (50.0)
Distant metastasis	Yes	23 (28.3)
	No	58 (71.7)
Surgery	Yes	74 (81.3)
	No	17 (19.8)
Chemotherapy	Yes	51 (68.0)
	No	24 (32.0)
	Cisplatin	29 (56.9)
	Other	22 (43.1)

disease then progressed at 13 mo and the patient died of tumour metastasis after 24 mo. Patient survival was significantly prolonged after surgical resection of the affected kidney and postoperative adjuvant targeted therapy[18]. Although this patient benefited from targeted therapy, the maintenance time was short, and the late-stage treatment effect of this type of tumour requires verification in a large sample of cases.

Some scholars have proposed that simple chemotherapy has a better prognosis than surgery combined with chemotherapy, suggesting that chemotherapy should be the first choice and surgery should only be used to treat local symptoms[19]. Other scholars have proposed that, for patients whose tumours are confined to the kidney, early surgical treatment can enable long-term survival, and the prognosis of patients with clinical stage pT1-pT2 is significantly better than that of patients with pT3-pT4 disease, with a median survival time of 31 and 8 mo, respectively[20]. In a study of 14 cases of renal SCC, Si *et al*[21] found that one patient with SCC limited to the kidney survived tumour-free after surgery for 137 mo. However, a recent study reported no significant difference in estimated median survival across individual treatment modalities. Multimodal therapies likely merit particular investigative attention in terms of growing evidence supporting their use in treating other primary small cell malignancies of the genitourinary tract[22].

In this case, the patient's condition changed rapidly and distant metastasis occurred within 1 year. When the disease was diagnosed, the patient was already in the late stage and had missed the opportunity for early radiotherapy and chemotherapy. It is difficult to obtain suitable specimens for

relevant pathological examinations without surgery, such as when the patient's urine exfoliated cells are negative. In addition, some studies reported that the early application of platinum-based chemotherapy can improve the survival rate, and patients who received platinum-based regimens had a median survival of 20 mo *vs* 8 mo for those who received other regimens[23]. Our patient showed an improving trend with the platinum-based chemotherapy regimen. Patrick also reported an 80-mo survival of a patient who underwent nephroureterectomy plus multiple metastasectomies followed by chemotherapy with octreotide, temozolomide, and capecitabine[13]. This is the first report of the use of a somatostatin analogue in the management of primary upper urinary tract SCC. Having no fairly large series capable of allowing a randomized study, their approach requires confirmation in broader studies. Neoadjuvant chemotherapy may also be effective at reducing the pathological stages of SCC[8,24]. However, these treatments are insufficient to achieve a cure, and other strategies are needed to improve the treatment of this deadly cancer. SCRC-1 was the first cell line derived from renal SCC[25]. However, based on this cell line and its related characteristics, further studies of the immunobiology and histogenesis of this rare malignant disease are lacking. These tumours are reportedly involved in c-kit expression and platelet-derived growth factor receptor-α (PDGFRA) mutations[26], which may be potential therapeutic targets[2]; drugs targeting c-kit and/or PDGFRA may be promising topics of future research[12]. In summary, new molecular therapies and immunotherapies for these tumours are still under active exploration and research.

The reason why our patient developed the disease so rapidly is related to the fact that it was diagnosed very late. Interestingly, the patient also underwent surgery in 2019 and did not have the disease, indicating that the tumour was highly malignant. In previous studies, renal SCC had a poor prognosis with a median overall survival, and 95% confidence interval of 9.9 mo (range, 6.9-31.6 mo), and more patients died of tumour metastasis in the short term, mostly from lung, brain, liver, and other systemic metastases. Early detection of the tumour, use of cisplatin-based chemotherapy, and careful follow-up for local recurrence or frequent metastasis within 6 mo after the primary treatment could be important for improving overall survival[27].

CONCLUSION

In conclusion, primary renal SCC is an extremely rare tumour for which neuroendocrine markers are helpful for making its pathological diagnosis. Limited available data indicate that the disease has an aggressive natural history and poor prognosis. Clinical stage, tumour composition, and sex may be important factors in determining prognosis. Close follow-up within 6 mo after the initial treatment is the key to an improved overall survival, and once metastases occur, the survival time is substantially reduced. We suggest a comprehensive treatment approach, which currently involves the combination of surgery and chemotherapy, but clinical experience is limited and more data are needed to determine its optimal treatment.

FOOTNOTES

Author contributions: Wu SC and Xie K contributed equally to this work; Wu SC, Li XY, Liao BJ, Xie K and Chen WM designed the research study; Wu SC, Li XY, Xie K and Liao BJ performed the research; Wu SC and Xie K contributed new reagents and analytic tools; Li XY, Xie K and Liao BJ analyzed the data and wrote the manuscript; all authors have read and approve the final manuscript.

Informed consent statement: All study participants, or their legal guardian, provided informed written consent prior to study enrollment.

Conflict-of-interest statement: The authors declare that there is no conflict of interest statement.

CARE Checklist (2016) statement: The authors have read the CARE Checklist (2016), and the manuscript was prepared and revised according to the CARE Checklist (2016).

Open-Access: This article is an open-access article that was selected by an in-house editor and fully peer-reviewed by external reviewers. It is distributed in accordance with the Creative Commons Attribution NonCommercial (CC BY-NC 4.0) license, which permits others to distribute, remix, adapt, build upon this work non-commercially, and license their derivative works on different terms, provided the original work is properly cited and the use is non-commercial. See: https://creativecommons.org/Licenses/by-nc/4.0/

Country/Territory of origin: China

ORCID number: Kun Xie 0000-0003-0628-2128; Xi-Ya Li 0000-0002-9017-1203; Bang-Jie Liao 0000-0002-8892-0180; Si-Cheng Wu 0000-0003-3429-1849; Wei-Min Chen 0000-0001-5634-4417.

S-Editor: Gao CC
L-Editor: A
P-Editor: Cai YX

REFERENCES

1 **Howard S**, O'Regan K, Jagannathan J, Krajewski K, Giardino A, Ramaiya N. Extrapulmonary small cell carcinoma: a pictorial review. *AJR Am J Roentgenol* 2011; **197**: W392-W398 [PMID: 21862764 DOI: 10.2214/AJR.10.5757]
2 **Ping JH**, Chen ZX, Jiong Q, Han YQ, Nong X. Small cell neuroendocrine carcinoma of the ureter: A case report and literature review. *Oncol Lett* 2014; **7**: 728-730 [PMID: 24520292 DOI: 10.3892/ol.2013.1757]
3 **Tombet CA**, Aynaou M, Mhanna T, El Houmaidi A, Achraf M, Barki A. Low back pain revealing a primary small cell neuroendocrine carcinoma of the upper urinary tract: A case report and review of the literature. *Urol Case Rep* 2020; **33**: 101338 [PMID: 32835003 DOI: 10.1016/j.eucr.2020.101338]
4 **Kuroda N**, Imamura Y, Hamashima T, Ohe C, Mikami S, Nagashima Y, Inoue K, Perez-Montiel D, Petersson F, Michal M, Hes O. Review of small cell carcinoma of the kidney with focus on clinical and pathobiological aspects. *Pol J Pathol* 2014; **65**: 15-19 [PMID: 25119004 DOI: 10.5114/pjp.2014.42664]
5 **Chu C**, Hu CY, Batra R, Lin AY. Small cell carcinoma of the kidney: a case report and analysis of data from the Surveillance, Epidemiology, and End Results registry. *J Med Case Rep* 2019; **13**: 71 [PMID: 30841901 DOI: 10.1186/s13256-018-1965-8]
6 **Capella C**, Eusebi V, Rosai J. Primary oat cell carcinoma of the kidney. *Am J Surg Pathol* 1984; **8**: 855-861 [PMID: 6095693 DOI: 10.1097/00000478-198411000-00006]
7 **Jiang ZC**, Zhou Qi, Ren YY. Clinicopathological features and prognostic factors of 5 cases of primary renal small cell carcinoma. *Zhenduan Bingli Xue Zazhi* 2020; **27**: 649-652 [DOI: 10.3969/j.issn.1007-8096.2020.09.011]
8 **Rupert V**, Clifton MM, Fulmer BR, Mori RL, Williams H, Park A. Primary small cell carcinoma of the upper urinary tract: A case report. *Urol Case Rep* 2019; **27**: 100995 [PMID: 31467857 DOI: 10.1016/j.eucr.2019.100995]
9 **Xu JL**, Guo Y. Clinical characteristics and survival of extrapulmonary small cell carcinoma in 11 different primary tumor sites in the United States, 1975-2016. *Curr Med Res Opin* 2021; **37**: 71-81 [PMID: 33135938 DOI: 10.1080/03007995.2020.1846024]
10 **Uemura KI**, Nakagawa G, Chikui K, Moriya F, Nakiri M, Hayashi T, Suekane S, Matsuoka K. A useful treatment for patients with advanced mixed-type small cell neuroendocrine carcinoma of the prostate: A case report. *Oncol Lett* 2013; **5**: 793-796 [PMID: 23426029 DOI: 10.3892/ol.2013.1136]
11 **Lee JY**, Kim J. Renal Metastasis of Small Cell Lung Cancer With Urothelial Carcinoma of the Bladder Misdiagnosed as Renal Cell Carcinoma. *J Med Cases* 2019; **10**: 253-256 [PMID: 34434316 DOI: 10.14740/jmc3353]
12 **Shimasaki N**, Inoue K, Nishigawa H, Kuroda N, Shuin T. Combined small cell carcinoma and sarcomatoid squamous cell carcinoma in the renal pelvis. *Int J Urol* 2005; **12**: 686-689 [PMID: 16045564 DOI: 10.1111/j.1442-2042.2005.01134.x]
13 **Hensley PJ**, Bhalodi AA, Gupta S. Primary Upper Urinary Tract Small Cell Carcinoma: A Case Series and Literature Review. *J Endourol Case Rep* 2017; **3**: 165-168 [PMID: 29177194 DOI: 10.1089/cren.2017.0103]
14 **Faggiano A**, Mansueto G, Ferolla P, Milone F, del Basso de Caro ML, Lombardi G, Colao A, De Rosa G. Diagnostic and prognostic implications of the World Health Organization classification of neuroendocrine tumors. *J Endocrinol Invest* 2008; **31**: 216-223 [PMID: 18401203 DOI: 10.1007/BF03345593]
15 **Carranza OE**, Castañón E, Abella LE, Zudaire ME, Castillo A, Arévalo E, Fusco JP, Zudaire JJ, Carías R, Cambeiro M, Martínez-Monge R, Gil-Bazo I. Clinical management of small-cell carcinoma of the urinary tract: a 10-year single-center's experience. *Clin Genitourin Cancer* 2013; **11**: 168-174 [PMID: 23146567 DOI: 10.1016/j.clgc.2012.09.011]
16 **Berniker AV**, Abdulrahman AA, Teytelboym OM, Galindo LM, Mackey JE. Extrapulmonary small cell carcinoma: imaging features with radiologic-pathologic correlation. *Radiographics* 2015; **35**: 152-163 [PMID: 25590395 DOI: 10.1148/rg.351140050]
17 **Wang XD**, Shen HL, Yang PQ, Tian Y. A case report of sunitinib in the treatment of advanced renal small cell carcinoma. *Zhonghua Miniao Waike Zazhi* 2017; **38**: 151-152 [DOI: 10.3760/cma.j.issn.1000-6702.2017.02.022]
18 **Abdel-Rahman O**, Fouad M. Efficacy and toxicity of sunitinib for non clear cell renal cell carcinoma (RCC): a systematic review of the literature. *Crit Rev Oncol Hematol* 2015; **94**: 238-250 [PMID: 25638704 DOI: 10.1016/j.critrevonc.2015.01.006]
19 **La Rosa S**, Bernasconi B, Micello D, Finzi G, Capella C. Primary small cell neuroendocrine carcinoma of the kidney: morphological, immunohistochemical, ultrastructural, and cytogenetic study of a case and review of the literature. *Endocr Pathol* 2009; **20**: 24-34 [PMID: 19096940 DOI: 10.1007/s12022-008-9054-y]
20 **Ouzzane A**, Ghoneim TP, Udo K, Verhasselt-Crinquette M, Puech P, Betrouni N, Rouprêt M, Villers A, Leroy X, Colin P. Small cell carcinoma of the upper urinary tract (UUT-SCC): report of a rare entity and systematic review of the literature. *Cancer Treat Rev* 2011; **37**: 366-372 [PMID: 21257269 DOI: 10.1016/j.ctrv.2010.12.005]
21 **Si Q**, Dancer J, Stanton ML, Tamboli P, Ro JY, Czerniak BA, Shen SS, Guo CC. Small cell carcinoma of the kidney: a clinicopathologic study of 14 cases. *Hum Pathol* 2011; **42**: 1792-1798 [PMID: 21733553 DOI: 10.1016/j.humpath.2011.03.005]
22 **Monaghan TF**, Michelson KP, Suss NR, Agudelo CW, Rahman SN, Robins DJ, Flores VX, McNeil BK, Weiss JP, Winer AG. Primary Small Cell Carcinoma of the Kidney: Disease Characteristics and Treatment Outcomes. *Medicines (Basel)* 2021; **8** [PMID: 33477429 DOI: 10.3390/medicines8010006]
23 **Majhail NS**, Elson P, Bukowski RM. Therapy and outcome of small cell carcinoma of the kidney: report of two cases and a systematic review of the literature. *Cancer* 2003; **97**: 1436-1441 [PMID: 12627507 DOI: 10.1002/cncr.11199]
24 **Lynch SP**, Shen Y, Kamat A, Grossman HB, Shah JB, Millikan RE, Dinney CP, Siefker-Radtke A. Neoadjuvant

chemotherapy in small cell urothelial cancer improves pathologic downstaging and long-term outcomes: results from a retrospective study at the MD Anderson Cancer Center. *Eur Urol* 2013; **64**: 307-313 [PMID: 22564397 DOI: 10.1016/j.eururo.2012.04.020]

25 **Chuang CK**, Shen YC, Wu JH, Tsai LH, Liao SK. Immunobiologic, cytogenetic and drug response features of a newly established cell line (SCRC-1) from renal small cell carcinoma. *J Urol* 2000; **163**: 1016-1021 [PMID: 10688041]

26 **Terada T**. Primary small cell carcinoma of the ureter: a case report involving immunohistochemical and molecular genetic analyses of KIT and PDGFRA genes. *Pathology* 2010; **42**: 101-102 [PMID: 20025496 DOI: 10.3109/00313020903443018]

27 **Lee SY**, Hsu HH, Lin HY, Chen YC, Wong YC, Wang LJ, Ng KF, Chuang CK, Hung CC, Yang CW. Factors associated with the survival of patients with primary small cell carcinoma of the kidney. *Int J Clin Oncol* 2013; **18**: 139-147 [PMID: 22138976 DOI: 10.1007/s10147-011-0355-7]

World Journal of Clinical Cases

Submit a Manuscript: https://www.f6publishing.com

World J Clin Cases 2022 June 16; 10(17): 5893-5898

DOI: 10.12998/wjcc.v10.i17.5893

ISSN 2307-8960 (online)

CASE REPORT

Gitelman syndrome: A case report

Shi-Yuan Chen, Ning Jie

Specialty type: Medicine, research and experimental

Provenance and peer review: Unsolicited article; Externally peer reviewed.

Peer-review model: Single blind

Peer-review report's scientific quality classification

Grade A (Excellent): A
Grade B (Very good): B
Grade C (Good): C
Grade D (Fair): 0
Grade E (Poor): 0

P-Reviewer: Lambrecht NW, United States; Mittal M, India; Thongon N, Thailand

Received: January 1, 2022
Peer-review started: January 1, 2022
First decision: February 8, 2022
Revised: February 24, 2022
Accepted: April 4, 2022
Article in press: April 4, 2022
Published online: June 16, 2022

Shi-Yuan Chen, Ning Jie, Department of Endocrinology, Longhua Central Hospital, Shenzhen 518110, Guangdong Province, China

Corresponding author: Ning Jie, MD, Chief Doctor, Department of Endocrinology, Longhua Central Hospital, No. 187 Guanlan Avenue, Shenzhen 518110, Guangdong Province, China. jiening919@gmail.com

Abstract

BACKGROUND

Gitelman syndrome (GS) is an autosomal recessive salt-losing renal tubulopathy arising from mutations in the thiazide-sensitive Na-Cl cotransporter gene. Due to its low incidence and lack of awareness, GS can be easily misdiagnosed or missed in diagnosis.

CASE SUMMARY

A 24-year-old male presented with > 4 years of repeated limb weakness without any treatment. The previous day, the patient was bitten by ants and showed weakness of the lower limbs. The patient had hypokalemia (1.66-2.83 mmol/L), hypomagnesemia (0.4 mmol/L), hypocalciuria (1.51-2.46 mmol/d), metabolic alkalosis (7.47-7.54), normal blood pressure, and increased activity of aldosterone and plasma renin activity (PRA) (PRA 6.4 and 16.45 ng/mL/h and aldosterone 330.64 and 756.82 pg/mL in the supine and upright position, respectively). In addition, *SLCI2A3* gene mutation with GS was diagnosed. Oral and intravenous supplementation with potassium and magnesium was initiated. Serum magnesium returned to 0.48 mmol/L and serum potassium returned to 3.08 mmol/L, alleviating the patient's fatigue symptoms.

CONCLUSION

GS should be considered in patients with hypokalemia complicated with hypomagnesemia. Genetic testing is essential to confirm the diagnosis.

Key Words: Gitelman syndrome; Limb weakness; Hypokalemia; Hypomagnesemia; Hypocalciuria; Genetic testing; Case report

©The Author(s) 2022. Published by Baishideng Publishing Group Inc. All rights reserved.

Core Tip: Gitelman syndrome (GS) is easily misdiagnosed or missed in diagnosis due to its low incidence and lack of awareness. Herein, we present a rare case of GS in a young man with limb weakness. This case demonstrates that attention should be focused on GS in patients with hypokalemia complicated with hypomagnesemia. Genetic testing is helpful in confirming the diagnosis.

Citation: Chen SY, Jie N. Gitelman syndrome: A case report. *World J Clin Cases* 2022; 10(17): 5893-5898
URL: https://www.wjgnet.com/2307-8960/full/v10/i17/5893.htm
DOI: https://dx.doi.org/10.12998/wjcc.v10.i17.5893

INTRODUCTION

Gitelman syndrome (GS) is characterized by low blood potassium, low blood magnesium, low blood chloride, low urinary calcium, normal or low blood pressure, alkalosis, and activation of the renin-angiotensin-aldosterone system (RAAS), which are the clinical manifestations of autosomal recessive salt-losing renal tubular disease, also known as familial hypokalemia and hypomagnesemia[1]. The incidence of GS is low and is reported to be approximately 1/40000 in Europeans[2], and 10.3/10000 in Japanese[3] based on the heterozygous carrier rate, and is easily misdiagnosed or missed in diagnosis. We here report a case of GS diagnosed and treated in the Department of Endocrinology, Longhua District Central Hospital, Shenzhen, China.

CASE PRESENTATION

Chief complaints

A 24-year-old male presented with > 4 years of repeated limb weakness and a relapse of 1 d.

History of present illness

Four years ago, the patient developed limb weakness and fatigue, especially in the lower limbs, which could be relieved spontaneously after rest. He could walk and hold objects with both hands. During the period without a specific diagnosis and treatment, the above symptoms occasionally occurred without aggravation but could be relieved spontaneously after rest. One day ago, the patient was bitten by ants and showed weakness in the lower limbs. His blood potassium level was 1.66 mmol/L when examined in the Emergency Department. Following oral and intravenous potassium supplementation and intravenous magnesium supplementation, his blood potassium was reexamined and was found to be 2.22 mmol/L, and the patient was admitted to our department with hypokalemia.

History of past illness

The patient had no medical history.

Personal and family history

No member of the patient's immediate or extended family reported similar symptoms. He denied the use of any herbal medicine, diuretics, or laxatives.

Physical examination

Physical examination revealed a thin man, 156 cm in height, and 33.5 kg in weight. His temperature was 36.5 ℃, respiratory rate was 20 breaths/min, and blood pressure was 116/53 mmHg with a regular heart rate of 100 bpm. Thyroid palpation revealed that his thyroid was normal. Chest auscultation revealed that his lungs were clear and heart sounds were normal. Muscle strength of his left lower limb was grade 4, and that of the right lower and both upper limbs was grade 5.

Laboratory examinations

Laboratory investigations carried out at the time of presentation are summarized in Table 1. We confirmed the persistence of a hypokalemic state secondary to renal potassium wasting, while serum potassium levels remained at approximately 1.66–2.83 mmol/L, and urinary potassium excretion was increased from 102.43 to 120.08 mmol/d. Intriguingly, we observed hypomagnesemia (0.4 mmol/L), hypocalciuria (1.51-2.46 mmol/d), and metabolic alkalosis (7.47-7.54). Urinalysis did not show any alterations. Serum creatinine and creatinine clearance were slightly higher than normal. Glycosylated hemoglobin and plasma cortisol were within the normal range. Echocardiography and renal ultrasound did not show any abnormalities. Liver function, thyroid function, and other biochemical parameters were normal. Secondary hyperreninemic hyperaldosteronism was detected in the supine and upright

Table 1 Laboratory examinations

	Value or range	Normal range
Urinary pH	8.5	5.0-8.4
Urinary specific gravity	1.01	1.021-1.03
Urinary protein	Negative	Negative
BUN, mmol/L	4.62	3.1-8
CR, mmol/L	76.3	57-97
pH	7.47-7.54	7.35-7.45
HCO_3^-, mmol/L	24.1-27.7	22-26
Serum magnesium, mmol/L	0.4	0.7-1.0
Serum potassium, mmol/L	1.66-2.83	3.5-5.3
Serum sodium, mmol/L	132.6-139.3	137-147
Serum calcium, mmol/L	2.21-2.36	2.11-2.52
Serum phosphorus, mmol/L	0.69	0.85-1.51
Urinary potassium, mmol/d	102.43-120.08	25-100
Urinary calcium, mmol/d	1.51-2.46	130-260
Glycosylated hemoglobin, %	5.5	4-6
Parathyroid hormone, pg/mL	8.67	14.5-87.1
Cor, nmol/L (8 a.m.)	287.17	6-10 a.m.: 133-537
Cor, nmol/L (4 p.m.)	151.73	4-8 p.m.: 68.2-327
ACTH, pmol/L (8 a.m.)	12.94	8 a.m., 4 p.m.: 2-14
ACTH, pmol/L (4 p.m.)	3.5	8 a.m., 4 p.m.: 2-14

BUN: Blood urea nitrogen; CR: Complete response; Cor: Cortisone; ACTH: Adreno-cortico-tropic-hormone.

positions (PRA 6.4 and 16.45 ng/mL/h and aldosterone 330.64 and 756.82 pg/mL, respectively) (Tables 2 and 3).

Imaging examinations

Computed tomography revealed hyperplasia at the junction of the left adrenal gland and calcification of the diverticulum in the right renal pelvis. Electrocardiography showed sinus rhythm and low T wave level.

FINAL DIAGNOSIS

The patient was diagnosed with hypokalemia, hypomagnesia, hypocalciuria, alkalosis, low serum chlorine, increased renin-angiotensin-aldosterone activity, normal blood calcium, and normal blood pressure. The detection of *SLC12A3* gene mutation confirmed the diagnosis of GS.

Genetic testing

The Guangzhou KingMed Center for Clinical Laboratory tested the genes of this patient, including the exon sequence of *SLC12A3* gene. The DNA extracted from the samples was tested by gene sequencing, and possible gene mutations were identified by comparing with the reference sequence. Two pathogenic mutations related to GS (Table 3) were detected: heterozygous rs768527231 Exon1 missense mutation C.248G>A (p.Asg83Gln), which is included in the dbSNP147 database, and Exon21 nonsense mutation C.2532G>A (p.Trp844*), confirming the diagnosis of GS (Figure 1).

Table 2 Results of postural stimulation test

Position	Aldosterone/(pg/mL)	Renin/(ng/mL/h)	ARR
Clinostatism	330.64 (40.0-310.0)	6.4 (0.15-2.33)	5.36 (0-30)
Orthostatism	756.82 (10.0-160.0)	16.45 (1.31-3.95)	4.6 (0-30)

ARR: Aldosterone renin ratio.

Table 3 Genetic testing

Gene	Zone	Reference sequence	Location	cDNA level	Protein level	Status	Classification of variation
SLC12A3	16q13	NM_000339.2	Exon1	c.248G>A	p.*Arg83G1n*	Heterozygosis	Suspicious pathologically
SLC12A3	16q13	NM_000339.2	Exon21	c.2532G>A	p.*Trp844**	Heterozygosis	Pathological

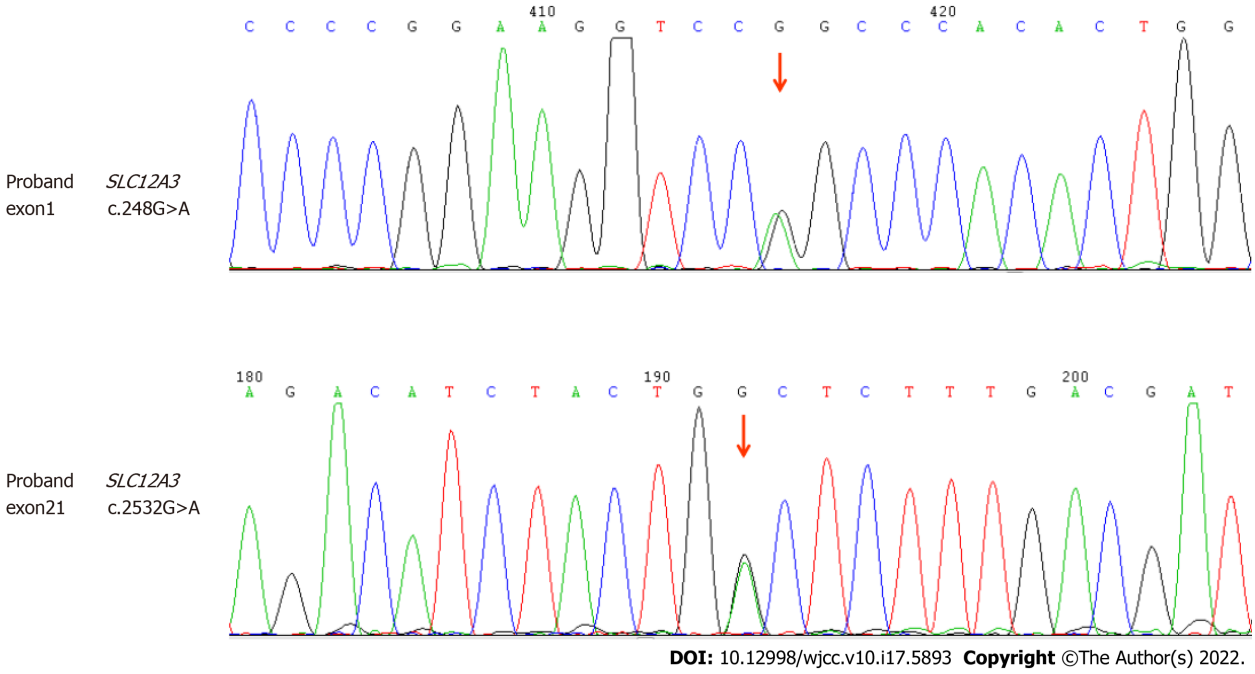

DOI: 10.12998/wjcc.v10.i17.5893 **Copyright** ©The Author(s) 2022.

Figure 1 Exon sequencing of pathogenic genes.

TREATMENT

Oral and intravenous supplementation with potassium and magnesium was initiated.

OUTCOME AND FOLLOW-UP

After treatment, the patient's serum magnesium returned to 0.48 mmol/L, and serum potassium returned to 3.08 mmol/L. As a result, his fatigue symptoms were alleviated.

DISCUSSION

Hypokalemia is a common electrolyte disorder in clinical practice. Severe hypokalemia can lead to life-threatening reactions, such as dyspnea and arrhythmia. There are several causes of hypokalemia that can lead to insignificant limb weakness symptoms and can be easily ignored by patients; therefore, the diagnosis is challenging.

According to the etiopathogenesis, potassium deficiency due to inadequate intake and increased potassium excretion, hypokalemia, metastatic hypokalemia, and dilutive hypokalemia are included. The common causes of potassium deficiency in hypokalemia are inadequate potassium intake and excessive potassium loss in the digestive tract and kidney. Metastatic hypokalemia occurs when potassium is transferred from extracellular to intracellular, resulting in hypokalemia, in which the total amount of potassium is not deficient.

The diagnosis and differential diagnosis of hypokalemia was carried out. The patient was a young male with recurrent fatigue. Repeated blood potassium (3.5 mmol/L) and synchronous 24 h urine potassium excretion increased to > 25 mmol/d, indicating renal potassium loss. The patient had a normal appetite, adequate potassium intake, no history of using diuretics or a large dosage of insulin, and no long-term nausea, vomiting, and diarrhea; therefore, gastrointestinal loss was not considered. Metastatic hypokalemia was not supported as hyperthyroidism was absent and the patient's blood glucose was normal. The patient had significantly elevated aldosterone levels, which excluded exogenous mineralocorticoid hyperplasia, Cushing syndrome, adrenal congenital 17-α/11-β hydroxylase deficiency, and Liddle syndrome. The patient's blood pressure was normal, renin activity was increased, and no renal mass was observed. Primary aldosteronism and renin tumors were excluded. The patient did not have renal artery stenosis or proteinuria, and blood gas analysis suggested metabolic alkalosis. Therefore, renal tubular acidosis, renal artery stenosis, and chronic kidney disease were not considered. The patient developed the disease as an adult and was thin and small since childhood, which was related to long-term hypokalemia, with hypomagnesia, hypochloremia, and hypocalciuria. Genetic testing suggested a heterozygous variation in the *SLC12A3* gene. Two pathogenic mutations related to GS were detected in the *SLC12A3* gene region of the patient, including heterozygous rs768527231 Exon1 missense mutation C.248G > A (p.agsg83gln), which is included in the dbSNP147 database, and the Exon21 nonsense mutation C.2532g > A (p.TP844*)[5], which was expected to change the amino acid position 844 of the encoded protein from Trp to stop codon, leading to protein translation terminated in advance. Based on these findings, the diagnosis of GS was established.

Furthermore, GS is an autosomal recessive genetic disorder, first described as an individual condition by Gitelman *et al* in 1966. GS can be attributed to structural and/or functional abnormalities of the sodium-chloride cotransporter (NCCT) due to the loss-of-function mutation in the gene *SLCI2A3*, encoding the thiazide diuretic sensitive NCCT located in the distal renal tubules[6].

Reduced sodium chloride reabsorption, blood volume, and renal salinization lower the blood pressure, activating the RAAS system and increasing aldosterone and renin levels, leading to hypokalemia and metabolic alkalosis. Decreased urinary calcium in GS patients may be associated with abnormal Na+/Cl- combined transport, weakening the intracellular Cl-superactivation, increasing CA2+ back absorption, and decreasing urinary calcium[4].

The decrease in serum magnesium level may be caused by increased Na+ reabsorption under the action of aldosterone, which results in the formation of luminal side negative potential and increases the level of urinary magnesium through increased Mg2+/Na+ exchange. This phenomenon may be related to the inactivation of transient receptor potential cation channel 6 (TRPM6) located at the apical domain of the distal convoluted tubules and brush border of the duodenal magnesium-transporter cells, resulting in decreased blood magnesium[7,8,10]. Simultaneously, hypomagnesemia can reduce the release of parathyroid hormone[7].

The mainstay of treatment for GS includes individualized lifelong administration of potassium and magnesium supplements (a strategy implemented in the present patient) combined with aldosterone antagonists and/or potassium-sparing agents, such as spironolactone, amiloride, and eplerenone to induce clinical remission.

A worldwide consensus[1,9] suggested that GS patients' blood potassium and magnesium levels should be maintained at > 3.0 mmol/L and > 0.6 mmol/L, respectively.

This patient was mainly treated with potassium chloride and magnesium sulfate. After treatment, the patient's clinical symptoms were relieved, but blood potassium did not reach the normal level; hence, regular follow-up was essential. GS is an autosomal recessive hereditary disease. Riveira-Munoz *et al* [11] suggested that the nature/position of *SLC12A3* mutation, combined with male gender, is a determining factor in the severity of GS. Therefore, investigation of the family by lineal gene testing is essential.

CONCLUSION

GS can be easily misdiagnosed or missed in diagnosis due to its low incidence and lack of awareness. Therefore, it is necessary to consider the possibility of GS in patients with clinical hypokalemia, low urinary calcium and low blood magnesium, and improve genetic screening for accurate diagnosis.

FOOTNOTES

Author contributions: Chen SY and Ning J analyzed the data and diagnosed Gitelman syndrome; Chen SY wrote the manuscript; Ning J modified this manuscript.

Informed consent statement: Informed written consent was obtained from the patient for publication of this report.

Conflict-of-interest statement: The authors declare that they have no conflict of interest.

CARE Checklist (2016) statement: The authors have read the CARE Checklist (2016), and the manuscript was prepared and revised according to the CARE Checklist (2016).

Open-Access: This article is an open-access article that was selected by an in-house editor and fully peer-reviewed by external reviewers. It is distributed in accordance with the Creative Commons Attribution NonCommercial (CC BY-NC 4.0) license, which permits others to distribute, remix, adapt, build upon this work non-commercially, and license their derivative works on different terms, provided the original work is properly cited and the use is non-commercial. See: https://creativecommons.org/Licenses/by-nc/4.0/

Country/Territory of origin: China

ORCID number: Shi-Yuan Chen 0000-0002-3709-9257; Ning Jie 0000-0001-5673-2604.

S-Editor: Wang LL
L-Editor: A
P-Editor: Wang LL

REFERENCES

1 **Knoers NV**. Gitelman syndrome. *Adv Chronic Kidney Dis* 2006; **13**: 148-154 [PMID: 16580616 DOI: 10.1053/j.ackd.2006.01.014]
2 **Melander O**, Orho-Melander M, Bengtsson K, Lindblad U, Råstam L, Groop L, Hulthén UL. Genetic variants of thiazide-sensitive NaCl-cotransporter in Gitelman's syndrome and primary hypertension. *Hypertension* 2000; **36**: 389-394 [PMID: 10988270 DOI: 10.1161/01.HYP.36.3.389]
3 **Tago N**, Kokubo Y, Inamoto N, Naraba H, Tomoike H, Iwai N. A high prevalence of Gitelman's syndrome mutations in Japanese. *Hypertens Res* 2004; **27**: 327-331 [PMID: 15198479 DOI: 10.1291/hypres.27.327]
4 **Kurtz I**. Molecular pathogenesis of Bartter's and Gitelman's syndromes. *Kidney Int* 1998; **54**: 1396-1410 [PMID: 9767561 DOI: 10.1046/j.1523-1755.1998.00124.x]
5 **Lin SH**, Shiang JC, Huang CC, Yang SS, Hsu YJ, Cheng CJ. Phenotype and genotype analysis in Chinese patients with Gitelman's syndrome. *J Clin Endocrinol Metab* 2005; **90**: 2500-2507 [PMID: 15687331 DOI: 10.1210/jc.2004-1905]
6 **Yang W**, Zhao S, Xie Y, Mo Z. A novel SLC12A3 homozygous c2039delG mutation in Gitelman syndrome with hypocalcemia. *BMC Nephrol* 2018; **19**: 362 [PMID: 30558554 DOI: 10.1186/s12882-018-1163-3]
7 **Pantanetti P**, Arnaldi G, Balercia G, Mantero F, Giacchetti G. Severe hypomagnesaemia-induced hypocalcaemia in a patient with Gitelman's syndrome. *Clin Endocrinol (Oxf)* 2002; **56**: 413-418 [PMID: 11940055 DOI: 10.1046/j.1365-2265.2002.01223.x]
8 **Blanchard A**, Bockenhauer D, Bolignano D, Calò LA, Cosyns E, Devuyst O, Ellison DH, Karet Frankl FE, Knoers NV, Konrad M, Lin SH, Vargas-Poussou R. Gitelman syndrome: consensus and guidance from a Kidney Disease: Improving Global Outcomes (KDIGO) Controversies Conference. *Kidney Int* 2017; **91**: 24-33 [PMID: 28003083 DOI: 10.1016/j.kint.2016.09.046]
9 **Gitelman Syndrome Collaborative Study Group**. Expert consensus for the diagnosis and treatment of patients with Gitelman syndrome. *Chin J Intern Med* 2017; **56**: 712-716 [DOI: 10.3760/cma.j.issn.0578-1426.2017.09.021]
10 **Jiang L**, Chen C, Yuan T, Qin Y, Hu M, Li X, Xing X, Lee X, Nie M, Chen L. Clinical severity of Gitelman syndrome determined by serum magnesium. *Am J Nephrol* 2014; **39**: 357-366 [PMID: 24776766 DOI: 10.1159/000360773]
11 **Riveira-Munoz E**, Chang Q, Godefroid N, Hoenderop JG, Bindels RJ, Dahan K, Devuyst O; Belgian Network for Study of Gitelman Syndrome. Transcriptional and functional analyses of SLC12A3 mutations: new clues for the pathogenesis of Gitelman syndrome. *J Am Soc Nephrol* 2007; **18**: 1271-1283 [PMID: 17329572 DOI: 10.1681/asn.2006101095]

World Journal of Clinical Cases

Submit a Manuscript: https://www.f6publishing.com

World J Clin Cases 2022 June 16; 10(17): 5899-5909

DOI: 10.12998/wjcc.v10.i17.5899

ISSN 2307-8960 (online)

CASE REPORT

High-frame-rate contrast-enhanced ultrasound findings of liver metastasis of duodenal gastrointestinal stromal tumor: A case report and literature review

Jia-Hui Chen, Ying Huang

Specialty type: Medicine, research and experimental

Provenance and peer review: Unsolicited article; Externally peer reviewed.

Peer-review model: Single blind

Peer-review report's scientific quality classification

Grade A (Excellent): A
Grade B (Very good): 0
Grade C (Good): 0
Grade D (Fair): D
Grade E (Poor): 0

P-Reviewer: Kim YJ, Malaysia; Madian A, Egypt

Received: January 22, 2022
Peer-review started: January 22, 2022
First decision: February 24, 2022
Revised: March 3, 2022
Accepted: April 4, 2022
Article in press: April 4, 2022
Published online: June 16, 2022

Jia-Hui Chen, Ying Huang, Department of Ultrasound, Shengjing Hospital of China Medical University, Shenyang 110004, Liaoning Province, China

Corresponding author: Ying Huang, MD, PhD, Chief Doctor, Department of Ultrasound, Shengjing Hospital of China Medical University, No. 36 Sanhao Street, Heping District, Shenyang 110004, Liaoning Province, China. huangying712@163.com

Abstract

BACKGROUND

Liver metastasis of duodenal gastrointestinal stromal tumor (GIST) is rare. Most reports mainly focus on its treatment and approaches to surgical resection, while details on its contrast-enhanced ultrasound (CEUS) findings are lacking. The diagnosis and imaging modalities for this condition remain challenging.

CASE SUMMARY

A 53-year-old Chinese man presented with mild signs and symptoms of the digestive tract. He underwent routine examinations after GIST surgery. Magnetic resonance imaging showed a 2.3 cm hepatic space-occupying lesion. All the laboratory test results were within normal limits. For further diagnostic confirmation, we conducted high frame rate CEUS (H-CEUS) and found a malignant perfusion pattern. Heterogeneous concentric hyper-enhancement, earlier wash-in than the liver parenchyma, and two irregular vessel columns could be observed at the periphery of the lesion during the arterial phase. Ultrasound-guided puncture biopsy was used to confirm the diagnosis of the lesion as liver metastasis of duodenal GIST. Imatinib was prescribed after biopsy, and the patient's clinical course was monitored.

CONCLUSION

H-CEUS is useful for detecting microcirculation differences, wash-in patterns, and vascular morphogenesis and diagnosing liver metastasis of duodenal GIST.

Key Words: High frame rate; Contrast-enhanced ultrasound; Duodenal gastrointestinal stromal tumor; Metastatic liver cancer; Case report

©The Author(s) 2022. Published by Baishideng Publishing Group Inc. All rights reserved.

Core Tip: Gastrointestinal stromal tumors (GISTs) are the most common types of gastrointestinal mesenchymal tumors. The liver is considered the most common organ target of metastasis; however, liver metastasis of duodenal GIST is extremely rare. We describe a new imaging modality, high frame rate contrast-enhanced ultrasound, for detecting microcirculation differences in the lesion, wash-in patterns during the early arterial phase, and vascular morphogenesis due to its high frame rate, during which liver metastasis of duodenal GIST can be diagnosed accurately. No complications were observed in our patient. We recommend this new technology for the diagnosis of liver metastasis of duodenal GIST.

Citation: Chen JH, Huang Y. High-frame-rate contrast-enhanced ultrasound findings of liver metastasis of duodenal gastrointestinal stromal tumor: A case report and literature review. *World J Clin Cases* 2022; 10(17): 5899-5909
URL: https://www.wjgnet.com/2307-8960/full/v10/i17/5899.htm
DOI: https://dx.doi.org/10.12998/wjcc.v10.i17.5899

INTRODUCTION

Gastrointestinal stromal tumors (GISTs) are the most common mesenchymal tumors originating from the digestive tract, and they account for 1%-3% of gastrointestinal tumors. Their clinical manifestations have not been established, and no specific tumor markers have been reported; approximately 15%-50% of GISTs are found due to liver metastasis[1]. Duodenal GISTs are rare, accounting for 12%-18% of small intestine GISTs and 1%-4% of all GISTs, and only 6 cases of liver metastasis of duodenal GISTs have been reported[2-7]. Usually, computed tomography (CT) scan, ultrasound endoscopy, and digestive tract contrast can help in the evaluation of the size, local immersion, and metastasis and location of the GIST[8]. Herein, we report a case of metastatic duodenal GIST that was initially accurately diagnosed by high frame rate contrast-enhanced ultrasound (H-CEUS). This report is intended to introduce a new imaging technology, which could not only provide important information in diagnosing rare disease liver metastasis of duodenal GIST but may also contribute to the diagnosis of many other hepatic lesions.

CASE PRESENTATION

Chief complaints

A 53-year-old Chinese man was admitted to our hospital with a progressively enlarged liver lesion for 2 years.

History of present illness

The lesion in the liver had been found during a routine re-examination after surgery two years earlier, and no significant progression was observed during subsequent annual examinations until three months earlier. The maximum diameter of the lesion had grown from 1.3 cm to 3.5 cm within a year, accompanied by mild abdominal discomfort. The patient reported to our hospital for further diagnosis.

History of past illness

The patient had a 30-year history of fatty liver but no history of hepatitis and liver cirrhosis and had undergone duodenal stromal tumor resection twice in our hospital in March 2012 and September 2016. He had no significant symptoms but slightly abdominal discomfort occasionally. His dietary was regular, but the sleep was not that well.

Personal and family history

The patient had a 30-year history of alcohol consumption. His father had a gastrointestinal-related disease, but the details are unknown.

Physical examination

The entire abdomen was soft, and there was no pressure pain, rebound pain, and muscle tension. A vertical surgery scar of approximately 15 cm was found. All the other vital signs were stable, and no positive signs were revealed.

Laboratory examinations

The results of the laboratory tests were negative, except an ALT level of 75 U/L. The tumor markers, AFP, CEA, CA19-9, had normal concentrations. The blood tests and fecal, coagulation function, and

Helicobacter pylori antibody examinations showed normal results.

Imaging examinations

Three months earlier, magnetic resonance imaging (MRI) showed a 2.3 cm occupying lesion in the left external liver lobe (Figure 1). The patient underwent an abdominal ultrasound examination using the Resona9 ultrasound system (Mindray Medical International, China) equipped with an SC6-1U (1-6 MHz) transducer. Conventional ultrasound (US) showed an uneven hypo-echo lesion with a peripheral hypoechoic halo located in the left lobe of the liver. The lesion had an approximate size of 3.5 × 2.2 × 2.4 cm^3, a round shape, and slightly clear margins. Color Doppler flow imaging (CDFI) showed the dot-linear blood flow signal within the lesion (Figure 2A and B). Given the history of duodenal GIST, the patient's doctor suggested further CEUS diagnosis and obtained patient's consent. The depth, gain, and focus were thoroughly adjusted for optimal display according to the operator's habits. After a bolus injection of 1.5 mL of Sonovue (Bracco, Italy) suspension, an ultrasound contrast agent, with 5 mL physiological saline (Italy, Bracco), the timer was activated. The target lesion and surrounding liver parenchyma were continuously observed for 5 min. Based on the accepted guidelines, the arterial, portal, and late phases were defined after 10-30 s, 30-120 s, and 121-360 s of the contrast agent injection, respectively. On CEUS, the solid nodule appeared heterogeneous, and there was hyper-enhancement during the arterial phase without a significant concentric perfusion and rim-like enhancement (Figure 2C-F). Quantitative analysis showed a peak intensity difference between the lesion and liver parenchyma (Δ PI) of 3.58 dB (Figure 3A-C). The enhancement of the lesion was washed out rapidly and gradually; a heterogeneous enhancement and hypo-enhancement were observed during the portal and late phases. During the late phase, the contrast agent was barely perfused. These features were suggestive of malignancy. To observe the process and direction of the contrast agent more precisely and better assess the liver lesion, we carried out a second H-CEUS after the patient rested for 1 h. During the arterial phase, a solid lesion that was enhanced from the periphery to the center was observed; a heterogeneous hyper-enhancement at peak was also observed. We also found two irregular branch-like vascular columns around the lesion. Rim enhancement was more significant this time (Figure 3G-J). The video showing the H-CEUS in arterial phase is displayed (Video 1). Quantitative analysis showed a peak intensity difference between the lesion and liver parenchyma (Δ PI) of 6.63 dB (Figure 3D-F). Similar to the CEUS findings, the contrast agent was washed out rapidly during the portal and late phases, and, finally, no enhancement was observed. The arterial phase of the lesion was suggestive of a malignancy, and metastasis was suspected based on the history.

Pathological findings and immunohistochemical staining

The final pathological findings were as follows: (1) Microscopic: the short and spindle cells were patchy; and (2) Immunohistochemical results: CD117, Dog-1, and Vimentin were positive, and Ki-67 was > 5% (Figure 4).

Gene mutational analysis

Molecular testing revealed *c-Kit 11* (c.1655_1699del 15 type), *c-Kit 9*, c-*Kit 13*, c-*Kit 17*, *PDGFRα12*, and *PDGFRα18* wild type mutations, which were associated with poor prognosis (Figure 5).

FINAL DIAGNOSIS

The final diagnosis of the presented case was liver metastasis of duodenal GIST.

TREATMENT

The patient currently takes 400 mg imatine per day and has no other symptoms. Although the patient had not quit drinking, he had reduced the frequency and amount of alcohol consumption to a large extent.

OUTCOME AND FOLLOW-UP

The patient remained on imatine therapy, and was followed up.

DISCUSSION

Duodenal GIST is rare, accounting for 12%-18% of small intestine GISTs and 1%-4% of all GISTs[9-11].

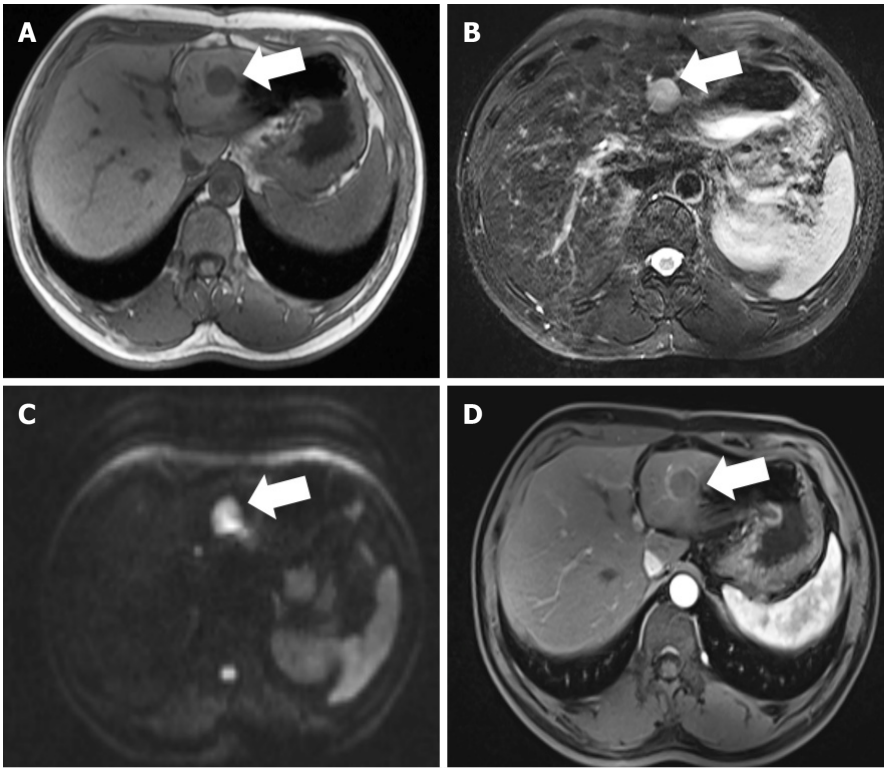

DOI: 10.12998/wjcc.v10.i17.5899 **Copyright** ©The Author(s) 2022.

Figure 1 Magnetic resonance imaging findings. The lesion is approximately 2.3 cm in the left external lobe. A: T1-weighted image of the nodule showing hypo-intensity; B T2-weighted image of the tumor showing higher intensity; C: Diffusion-weighted image of the tumor showing a higher intensity; D: The lesion presented edge enhancement after reinforcement (white arrows).

The clinical features of duodenal GIST include mild gastrointestinal bleeding, abdominal pain, and an abdominal mass[12]. The diagnosis of duodenal GIST is usually based on histopathological and imaging findings. Usually, ultrasound endoscopy, CT scan, MRI, and digestive tract contrast can help in evaluating the size, local immersion, metastasis, and location of the GIST[13-15].

Metastatic liver cancer (MLC) is one of the most common metastatic tumors, and is usually associated with a lower survival rate[16,17]. The most common type of liver metastasis derives from colorectal cancer. GISTs only account for 1%-3% of gastrointestinal tumors. Due to the higher malignancy and poor prognosis of MLCs, early detection and therapy are of great significance.

CT and MRI are the preferred imaging modalities for diagnosing MLC. Liver metastasis often shows heterogeneous hypodense lesions with progressive concentric enhancement in CT scans, with a sensitivity of up to 97%[18], while the MRI technique can detect smaller lesions[18,19]. These two imaging modalities are not used in real-time evaluation, and their scanning durations are longer. Their radiation and high cost should be taken into consideration for neonates and pregnant women. CEUS has been widely used to detect focal liver lesions (FLLs) in recent years[20,21], but there have only been 10 reports of liver metastatic lesions so far (Table 1). Herein, we collected information regarding the age, gender, clinical manifestation, MLC's originated organs, treatment, and follow-up from four cases and six clinical research studies. As shown in Table 1, MLCs mainly originated from gastrointestinal organs, except for three patients in whom the primary malignant tumors were medullary thyroid cancer[22], choroidal melanoma[23] and breast cancer[24]. MLCs usually have no specific symptoms. The US and CEUS features are depicted in Table 1. We found that MLCs often present as oval or round with irregular margins, and their echo characteristics are not specific. For MLCs from colorectal and ileal lesions, there is a central part with no echo[25,26]. They may consist of a hemorrhage and a necrotic area. It was reported that approximately 50% of all GISTs show cystic or necrotic areas[27]. CEUS is more sensitive in detecting avascular areas than US when part of the isoechoic or hypoechoic area was necrotic. Regarding the CEUS findings, the majority of these cases presented with homogeneous or heterogeneous hyper-enhancement during the arterial phase, mostly earlier than liver parenchyma. The contrast agents washed out very rapidly during the portal phase and presented hypo-enhancement until the end of the late phase. Wu *et al*[28] showed that metastatic lesion presented non-enhancement during the late phase. Zhang *et al*[29] found that lung primary lesion's MLC showed no significant enhancement in CEUS, which was contrary to other findings. We deduced that it was probably associated with the pathological type, but more supportive literature was required to make further conclusions. For this present case, CEUS showed a solid nodule that appeared heterogeneous and hyper-enhanced during the arterial phase; these were consistent with malignant liver lesion perfusion

Table 1 Case and literature reports of patients with MLC sonographic features

Ref.	Country	Age/gender	Clinical manifestation	Organs originated	US features	CEUS features	Contrast agent/dosage	Treatment	Follow-up
Zhou J *et al* [22], 2017	China	33/F	Increase in calcitonin and CEA	MTC	Hyper-and net-like; echogenicity, clear margin, well-defined shape	Hyper-enhancement during the arterial phase and hypo-enhancement in portal and parenchyma phase	Sonovue 1.2 mL	Surgery	Calcitonin and CEA remained normal
Corvino *et al* [42], 2015	Italy	41/M	No specific symptoms	Rectal melanoma	Solitary hypo-anechoic complex cystic lesion with a thin internal septum	Hyper-enhancement of the cystic wall and intra-cystic septation during the arterial phase, rapid wash-out, and hypo-enhancement during the portal and late phases	Sonovue 2.4 mL	Surgery	N/A
Toni *et al*[23], 2011	Germany	36/M	No specific symptoms	Choroidal melanoma	Iso-echogenicity	Homogeneous hyper-enhancement in arterial phase; hypo-enhancement in portal phase and punched-out enhancement defect; in late phase	Sonovue 2.0 mL	Surgery	N/A
Paulatto *et al* [25], 2020	France	74/M	N/A	NOS of colon	N/A	Central part remains hypoechoic	N/A	Surgery	N/A
Ishikawa *et al* [43], 2021	Japan	N/A	N/A	Pancreas	Round with irregular margin	Strong peripheral enhancement in the arterial phase, early washout, hypo-enhancement in the portal, and post-vascular phases	Sonazoid 0.015 mL/kg	N/A	N/A
Michima *et al* [24], 2016	Japan	N/A	N/A	Breast	Clearly round, oval, or lobulated solid focal lesions, irregular margin.	Hypoechoic defects in enhancing parenchyma in the portal venous or postvascular phase	Sonazoid 0.015 mL/kg	N/A	N/A
Yang DP *et al* [26], 2020	China	N/A	N/A	Colorectum	Hypo- or mix- echogenicity and anechoic area	Capsule enhancement, starting time of washout of > 40 s, un-enhancement area, and proportion of non-enhancement area > 50%	Sonovue 2.4 mL	N/A	N/A
Wu *et al*[28], 2020	China	N/A	N/A	Colorectum	Not mentioned	Peripheral nodular enhancement, heterogeneous hyper-enhancement, or rim-like enhancement during the arterial phase and a non-enhancement area during the late phase	Sonovue 2.0 mL	N/A	N/A
Schwarze *et al* [44], 2019	Germany	N/A	N/A	NET of ileum	Anechoic oval-shaped	Earlier wash-in, hyperenhancement during the arterial phase, and hypo-enhancement in the portal phase	Not mentioned	N/A	N/A
Schwarze *et al* [44], 2019	Germany	N/A	N/A	Pancreas	N/A	Earlier wash-in, hyperenhancement during the arterial phase, and hypo-enhancement during the portal phase	Not mentioned	N/A	N/A
Zhang GD *et al*[29], 2013	China	N/A	N/A	Stomach	Round with regular margin, iso-echo	Earlier rim-like enhancement and washed out in portal phase, non-enhancement in late phase	Sonovue 2.4 mL	N/A	N/A
Zhang GD *et al*[29], 2013	China	N/A	N/A	Lung	Oval and hypo-echo	No significant enhancement, hypo-perfusion compared with liver parenchyma	Sonovue 2.4 mL	N/A	N/A

F: Female; M: Male; MTC: Medullary thyroid cancer; CEA: Carcinoembryonic antigen; NOS: Non-otherwise specified; NET: Neuroendocrine tumor; N/A: Not available.

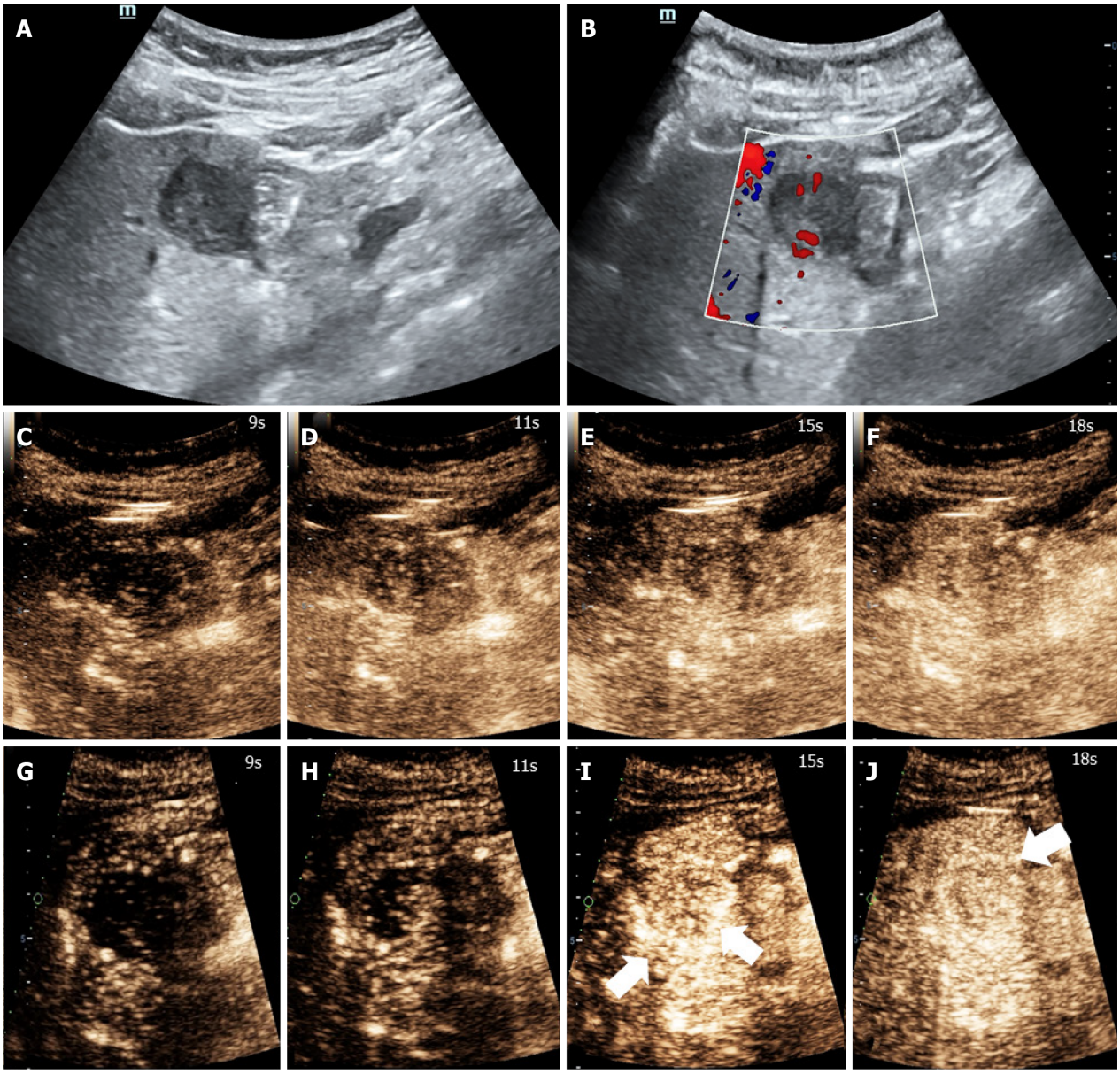

DOI: 10.12998/wjcc.v10.i17.5899 **Copyright** ©The Author(s) 2022.

Figure 2 High-frame-rate contrast-enhanced ultrasound findings. Images showing high-frame-rate contrast-enhanced ultrasound perfusion patterns corresponding to those in contrast-enhanced ultrasound images. Concentric enhancement was more obvious. Irregular vessel column and rim enhancement can be seen (white arrows). A: Conventional ultrasound showing an uneven hypo-echo lesion with an approximate size of 3.5 cm × 2.2 cm × 2.4 cm and a peripheral hypoechoic halo located in the left lobe of the liver; B: Color Doppler flow imaging showing the dot-linear blood flow signal within the lesion; C-E: Contrast-enhanced ultrasound findings; F: The lesion showed heterogeneous hyper-enhancement at peak; G-J: We could not find obvious concentric and rim enhancement on contrast-enhanced ultrasound.

patterns previously reported[20,30]. As we all know, hyper-enhancement of atypical hemangiomas during the arterial phase or non-enhancement during the portal and late phases can lead to a misleading diagnosis. Intrahepatic cholangiocellular carcinomas behave like metastases, washing out rapidly and appearing as defects during the late phase[31]. Consequently, further imaging characteristics are needed for a precise diagnosis.

The contrast agent was a pure-blood pool tracer for showing microcirculation perfusion of solid organs[21,32]. It can detect smaller (> 40 μm) blood vessels better than CDFI (> 100 μm) and is widely used in FLLs[33,34]. While it is partly affected by the frame rate, the frame frequency of CEUS is within 9-15 Hz, which is probably not adequate for detecting quick wash-in progression and the vascular architecture during the early arterial phase. H-CEUS provides a frame rate of tens of thousands of images per second to compensate for the reduced focusing of the acoustic beam and enhance the signal-to-noise ratio. H-CEUS can show microcirculation differences and wash-in patterns during the early arterial phase and vascular morphogenesis. In this case of H-CEUS technology, the enhancement appeared at the peripheral part of the lesion, and there was concentric perfusion. This may be mainly due to the increase in frame rate, which facilitated a better display of the first enhancement area, and the

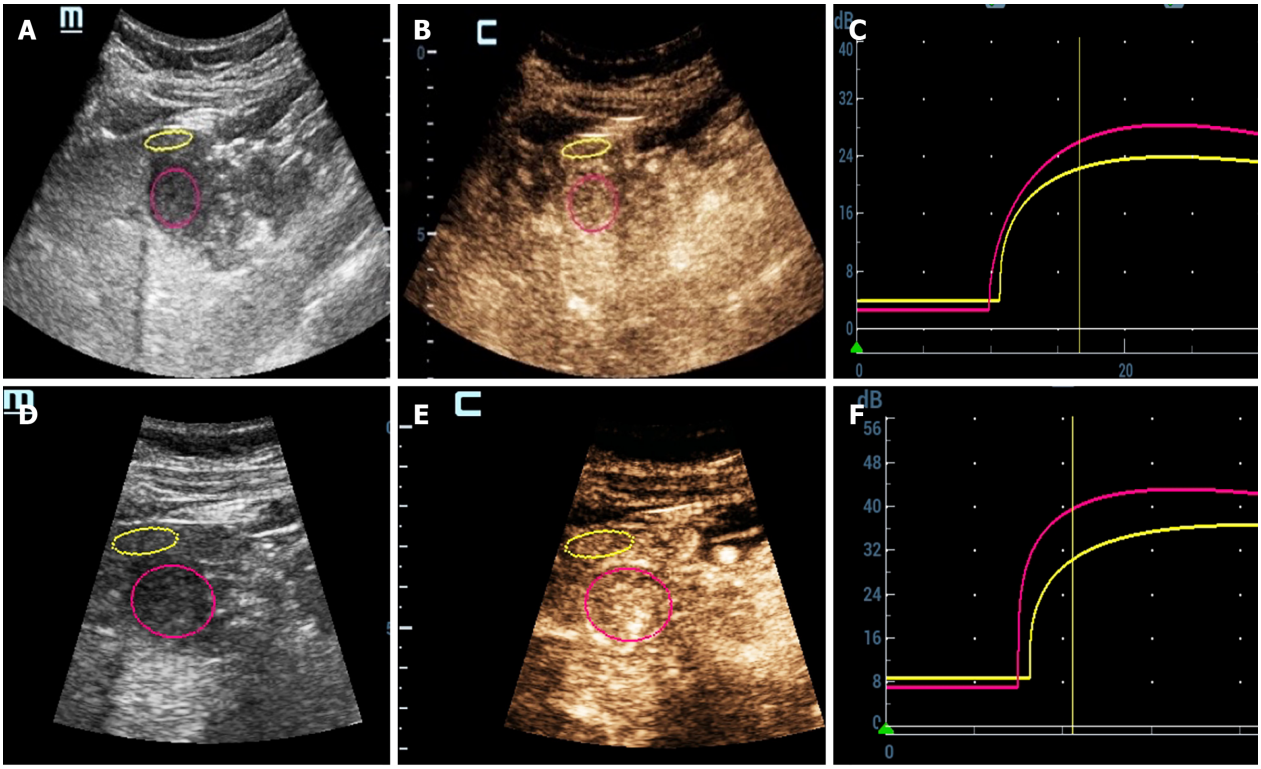

DOI: 10.12998/wjcc.v10.i17.5899 **Copyright** ©The Author(s) 2022.

Figure 3 Contrast-enhanced ultrasound quantitative analysis results. A-C: Contrast-enhanced ultrasound quantitative analysis showed △PI of 3.58 dB at peak; D-F: High-frame-rate contrast-enhanced ultrasound quantitative analysis showed △PI of 6.63 dB at peak.

site where the change in enhancement over time demonstrated the direction of contrast perfusion. Nevertheless, when the image frame rate is low, it is impossible to accurately display the contrast enhancement area, as the enhancement appears almost simultaneously in various parts of the lesion. Instead, it is presented as an entire perfusion on CEUS. Besides, vascular morphology is one of the important features for identifying and diagnosing the nature of FLL, and irregular vascular morphology is usually the main manifestation of malignant FLL[35,36]. The vascular morphology can be demonstrated by recording the path of contrast agent microbubbles, as the bubbles cannot enter the tissue gap through the vessel wall, and can only continuously move in the vessel[37-40]. The arterial phase is important for observing the vascular morphology, and rapid flow of arterial blood leads to the rapid movement of contrast agents. Therefore, only when the frame rate of contrast imaging reaches a certain threshold. In our case, we observed irregular branch-like vascular columns, which suggested the presence of malignancy; resulting in the final diagnosis of "liver metastasis of duodenal GIST." Compared with the CEUS technology, H-CEUS is more suitable for accurately detecting the movement of contrast agents to ascertain the vascular morphology of liver lesions.

The prognosis and treatment of liver metastasis of duodenal GIST have not been established due to the limited number of reported cases[2,3]. Based on our literature review, we found that distant metastases can occur years after the surgical excision of the primary duodenal lesion. Both patients reported in the two cases experienced bleeding after rupture of the liver metastatic lesion[2,3,6,41]. Given that liver metastases of duodenal GISTs are negatively correlated with disease prognosis, early detection is important. Consequently, our report is useful, as it is the first to highlight the value and utility of H-CEUS for diagnosis of patients with liver metastases of duodenal GISTs. This case reminds clinicians that the H-CEUS technology can facilitate the diagnosis of liver metastatic cancers, resulting in improved diagnosis, treatment, and outcomes.

CONCLUSION

Duodenal GISTs are relatively rare, but they usually have a poor prognosis and are associated with high incidences of metastases. The H-CEUS findings were as follows: a solid lesion enhanced from the periphery to the center with two irregular branch-like vessel columns during the early arterial phase with peak heterogeneous hyper-enhancement and rim enhancement. The contrast agent was washed out rapidly during the portal phase and showed no enhancement during the late phase. To the best of our knowledge, this report is the first to describe the H-CEUS patterns of this disease. It also highlights

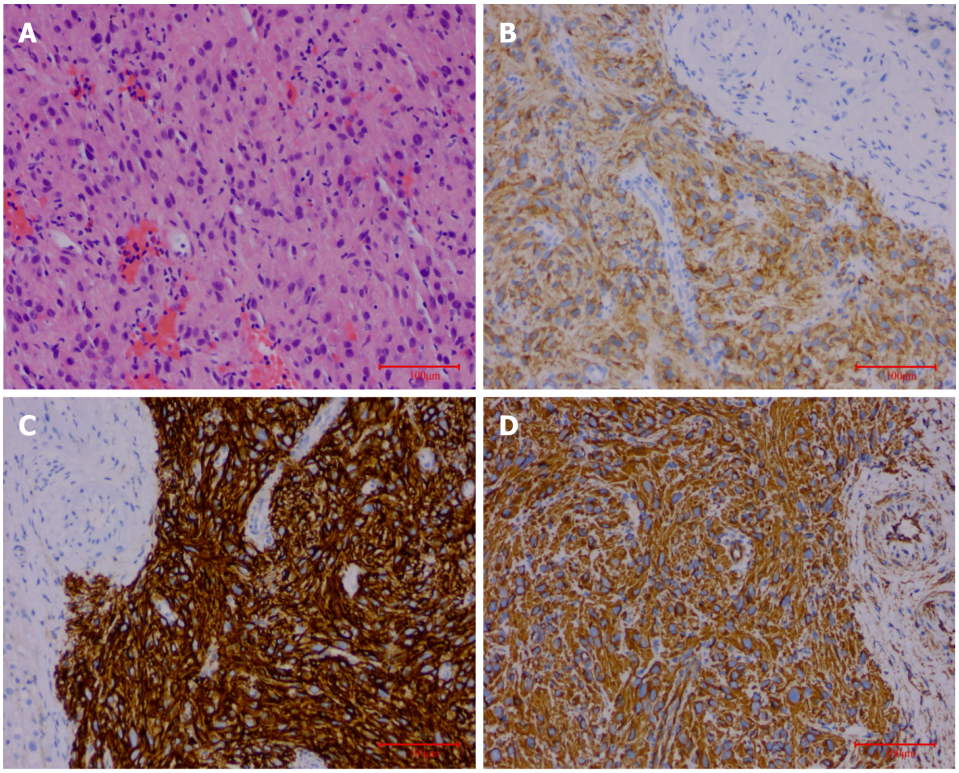

DOI: 10.12998/wjcc.v10.i17.5899 **Copyright** ©The Author(s) 2022.

Figure 4 Histopathology findings. A: Microscopy showed a patchy distribution of short and spindle cells (H&E staining, × 200); B-D: Immunohistochemical staining displayed CD117 (+), Dog-1 (+), and Vimentin (+) (H&E staining, × 200).

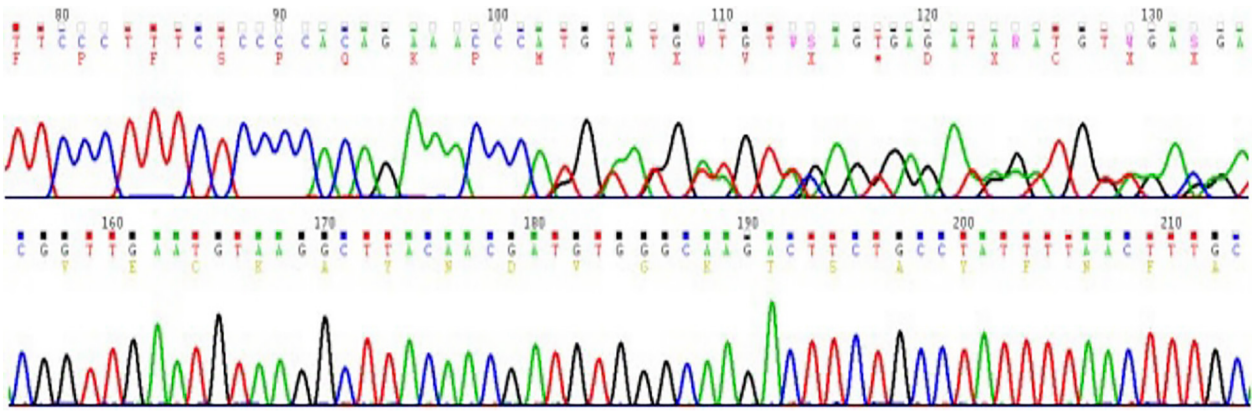

DOI: 10.12998/wjcc.v10.i17.5899 **Copyright** ©The Author(s) 2022.

Figure 5 DNA sequencing electropherograms. DNA sequencing electropherograms revealed c-Kit 11 (c.1655_1699del 15 type), c-Kit 9, c-Kit 13, c-Kit 17, PDGFRα12, and PDGFRα18 wild type mutations.

the challenges associated with the CEUS findings of metastatic hepatic cancers.

ACKNOWLEDGEMENTS

We thank Dr. Jin Y, Department of Gastroenterology, Shengjing Hospital of China Medical University for her pathological diagnosis.

FOOTNOTES

Author contributions: Chen JH and Huang Y reviewed the literature and contributed to manuscript drafting; Huang

Y performed the high frame rate contrast-enhanced ultrasound and biopsy operation; all authors issued final approval for the version to be submitted.

Supported by the Guide Project for Key Research and Development Foundation of Liaoning Province, No. 2019JH8/10300008; the 345 Talent Project; and the Liaoning Baiqianwan Talents Program.

Informed consent statement: Informed written consent was obtained from the patient for publication of this report and any accompanying images.

Conflict-of-interest statement: The authors declare that they have no conflicts of interest.

CARE Checklist (2016) statement: The authors have read the CARE Checklist (2016), and the manuscript was prepared and revised according to the CARE Checklist (2016).

Open-Access: This article is an open-access article that was selected by an in-house editor and fully peer-reviewed by external reviewers. It is distributed in accordance with the Creative Commons Attribution NonCommercial (CC BY-NC 4.0) license, which permits others to distribute, remix, adapt, build upon this work non-commercially, and license their derivative works on different terms, provided the original work is properly cited and the use is non-commercial. See: https://creativecommons.org/Licenses/by-nc/4.0/

Country/Territory of origin: China

ORCID number: Jia-Hui Chen 0000-0001-7616-7163; Ying Huang 0000-0002-3361-7184.

S-Editor: Wang LL
L-Editor: A
P-Editor: Wang LL

REFERENCES

1 **Gaitanidis A**, Alevizakos M, Tsaroucha A, Simopoulos C, Pitiakoudis M. Incidence and predictors of synchronous liver metastases in patients with gastrointestinal stromal tumors (GISTs). *Am J Surg* 2018; **216**: 492-497 [PMID: 29690997 DOI: 10.1016/j.amjsurg.2018.04.011]
2 **Mori T**, Kataoka M, Kaiho T, Yanagisawa S, Nishimura M, Kobayashi S, Okaniwa A, Ashizawa Y, Oka Y, Ohya M. [A Case of Liver Metastasis 28 Years after Resection for Gastrointestinal Stromal Tumor of Duodenum]. *Gan To Kagaku Ryoho* 2020; **47**: 1810-1812 [PMID: 33468837]
3 **Koike K**, Kubota H, Takayanagi Y, Ikeda T, Ito T. [A case of gastrointestinal stromal tumor of the duodenum with ruptured liver metastasis during administration of imatinib]. *Nihon Shokakibyo Gakkai Zasshi* 2020; **117**: 914-918 [PMID: 33041303 DOI: 10.11405/nisshoshi.117.914]
4 **Kishi Y**, Takaki S, Fukuhara T, Mori N, Okanobu H, Tsuji K, Maeda T, Fujiwara M, Nagai K, Furukawa Y. [A case of liver metastasis 11 years after resection of a gastrointestinal stromal tumor of the duodenum]. *Nihon Shokakibyo Gakkai Zasshi* 2019; **116**: 1030-1038 [PMID: 31827043 DOI: 10.11405/nisshoshi.116.1030]
5 **Stratopoulos C**, Soonawalla Z, Piris J, Friend PJ. Hepatopancreatoduodenectomy for metastatic duodenal gastrointestinal stromal tumor. *Hepatobiliary Pancreat Dis Int* 2006; **5**: 147-150 [PMID: 16481303]
6 **Sakata M**, Kaneyoshi T, Fushimi T, Watanabe J. Rare cause of cystic liver lesions: Liver metastasis of gastrointestinal stromal tumors. *JGH Open* 2021; **5**: 408-409 [PMID: 33732891 DOI: 10.1002/jgh3.12487]
7 **Inoue M**, Shishida M, Watanabe A, Kajikawa R, Kajiwara R, Sawada H, Ohmori I, Miyamoto K, Ikeda M, Toyota K, Sadamoto S, Takahashi T. A liver metastasis 7 years after resection of a low-risk duodenal gastrointestinal stromal tumor. *Clin J Gastroenterol* 2021; **14**: 1464-1469 [PMID: 34117599 DOI: 10.1007/s12328-021-01464-w]
8 **McGuirk M**, Gachabayov M, Gogna S, Da Dong X. Robotic duodenal (D3) resection with Roux-en-Y duodenojejunostomy reconstruction for large GIST tumor: Step by step with video. *Surg Oncol* 2021; **36**: 130 [PMID: 33370658 DOI: 10.1016/j.suronc.2020.12.006]
9 **Cassier PA**, Ducimetière F, Lurkin A, Ranchère-Vince D, Scoazec JY, Bringuier PP, Decouvelaere AV, Méeus P, Cellier D, Blay JY, Ray-Coquard I. A prospective epidemiological study of new incident GISTs during two consecutive years in Rhône Alpes region: incidence and molecular distribution of GIST in a European region. *Br J Cancer* 2010; **103**: 165-170 [PMID: 20588273 DOI: 10.1038/sj.bjc.6605743]
10 **Rubin BP**, Heinrich MC, Corless CL. Gastrointestinal stromal tumour. *Lancet* 2007; **369**: 1731-1741 [PMID: 17512858 DOI: 10.1016/s0140-6736(07)60780-6]
11 **Sandvik OM**, Søreide K, Kvaløy JT, Gudlaugsson E, Søreide JA. Epidemiology of gastrointestinal stromal tumours: single-institution experience and clinical presentation over three decades. *Cancer Epidemiol* 2011; **35**: 515-520 [PMID: 21489899 DOI: 10.1016/j.canep.2011.03.002]
12 **Qiu H**, Zhang P, Feng X, Chen T, Sun X, Yu J, Chen Z, Li Y, Tao K, Li G, Zhou Z. Changes of diagnosis and treatment for gastrointestinal stromal tumors during a 18-year period in four medical centers of China. *Zhonghua Weichang Waike Zazhi* 2016; **19**: 1265-1270 [PMID: 27928797]
13 **Karaca C**, Turner BG, Cizginer S, Forcione D, Brugge W. Accuracy of EUS in the evaluation of small gastric subepithelial lesions. *Gastrointest Endosc* 2010; **71**: 722-727 [PMID: 20171632 DOI: 10.1016/j.gie.2009.10.019]

14 **Park CH**, Kim EH, Jung DH, Chung H, Park JC, Shin SK, Lee YC, Kim H, Lee SK. Impact of periodic endoscopy on incidentally diagnosed gastric gastrointestinal stromal tumors: findings in surgically resected and confirmed lesions. *Ann Surg Oncol* 2015; **22**: 2933-2939 [PMID: 25808096 DOI: 10.1245/s10434-015-4517-0]

15 **Zhou Z**, Lu J, Morelli JN, Hu D, Li Z, Xiao P, Hu X, Shen Y. Utility of noncontrast MRI in the detection and risk grading of gastrointestinal stromal tumor: a comparison with contrast-enhanced CT. *Quant Imaging Med Surg* 2021; **11**: 2453-2464 [PMID: 34079715 DOI: 10.21037/qims-20-578]

16 **Obayashi J**, Kawaguchi K, Manabe S, Nagae H, Wakisaka M, Koike J, Takagi M, Kitagawa H. Prognostic factors indicating survival with native liver after Kasai procedure for biliary atresia. *Pediatr Surg Int* 2017; **33**: 1047-1052 [PMID: 28852838 DOI: 10.1007/s00383-017-4135-y]

17 **Hara Y**, Ogata Y, Shirouzu K. Early tumor growth in metastatic organs influenced by the microenvironment is an important factor which provides organ specificity of colon cancer metastasis. *J Exp Clin Cancer Res* 2000; **19**: 497-504 [PMID: 11277329]

18 **Tsili AC**, Alexiou G, Naka C, Argyropoulou MI. Imaging of colorectal cancer liver metastases using contrast-enhanced US, multidetector CT, MRI, and FDG PET/CT: a meta-analysis. *Acta Radiol* 2021; **62**: 302-312 [PMID: 32506935 DOI: 10.1177/0284185120925481]

19 **Niekel MC**, Bipat S, Stoker J. Diagnostic imaging of colorectal liver metastases with CT, MR imaging, FDG PET, and/or FDG PET/CT: a meta-analysis of prospective studies including patients who have not previously undergone treatment. *Radiology* 2010; **257**: 674-684 [PMID: 20829538 DOI: 10.1148/radiol.10100729]

20 **Wilson SR**, Feinstein SB. Introduction: 4th Guidelines and Good Clinical Practice Recommendations for Contrast Enhanced Ultrasound (CEUS) in the Liver-Update 2020 WFUMB in Cooperation with EFSUMB, AFSUMB, AIUM and FLAUS. *Ultrasound Med Biol* 2020; **46**: 3483-3484 [PMID: 32888748 DOI: 10.1016/j.ultrasmedbio.2020.08.015]

21 **Claudon M**, Dietrich CF, Choi BI, Cosgrove DO, Kudo M, Nolsøe CP, Piscaglia F, Wilson SR, Barr RG, Chammas MC, Chaubal NG, Chen MH, Clevert DA, Correas JM, Ding H, Forsberg F, Fowlkes JB, Gibson RN, Goldberg BB, Lassau N, Leen EL, Mattrey RF, Moriyasu F, Solbiati L, Weskott HP, Xu HX; World Federation for Ultrasound in Medicine; European Federation of Societies for Ultrasound. Guidelines and good clinical practice recommendations for Contrast Enhanced Ultrasound (CEUS) in the liver - update 2012: A WFUMB-EFSUMB initiative in cooperation with representatives of AFSUMB, AIUM, ASUM, FLAUS and ICUS. *Ultrasound Med Biol* 2013; **39**: 187-210 [PMID: 23137926 DOI: 10.1016/j.ultrasmedbio.2012.09.002]

22 **Zhou J**, Luo Y, Ma BY, Ling WW, Zhu XL. Contrast-enhanced ultrasound diagnosis of hepatic metastasis of concurrent medullary-papillary thyroid carcinoma: A case report. *Medicine (Baltimore)* 2017; **96**: e9065 [PMID: 29390301 DOI: 10.1097/md.0000000000009065]

23 **De Toni EN**, Gallmeier E, Auernhammer CJ, Clevert DA. Contrast-enhanced ultrasound for surveillance of choroidal carcinoma patients: features of liver metastasis arising several years after treatment of the primary tumor. *Case Rep Oncol* 2011; **4**: 336-342 [PMID: 21769292 DOI: 10.1159/000329453]

24 **Mishima M**, Toh U, Iwakuma N, Takenaka M, Furukawa M, Akagi Y. Evaluation of contrast Sonazoid-enhanced ultrasonography for the detection of hepatic metastases in breast cancer. *Breast Cancer* 2016; **23**: 231-241 [PMID: 25143060 DOI: 10.1007/s12282-014-0560-0]

25 **Paulatto L**, Dioguardi Burgio M, Sartoris R, Beaufrère A, Cauchy F, Paradis V, Vilgrain V, Ronot M. Colorectal liver metastases: radiopathological correlation. *Insights Imaging* 2020; **11**: 99 [PMID: 32844319 DOI: 10.1186/s13244-020-00904-4]

26 **Yang D**, Zhuang B, Wang W, Xie X. Differential diagnosis of liver metastases of gastrointestinal stromal tumors from colorectal cancer based on combined tumor biomarker with features of conventional ultrasound and contrast-enhanced ultrasound. *Abdom Radiol (NY)* 2020; **45**: 2717-2725 [PMID: 32458028 DOI: 10.1007/s00261-020-02592-6]

27 **Baheti AD**, Shinagare AB, O'Neill AC, Krajewski KM, Hornick JL, George S, Ramaiya NH, Tirumani SH. MDCT and clinicopathological features of small bowel gastrointestinal stromal tumours in 102 patients: a single institute experience. *Br J Radiol* 2015; **88**: 20150085 [PMID: 26111069 DOI: 10.1259/bjr.20150085]

28 **Wu XF**, Bai XM, Yang W, Sun Y, Wang H, Wu W, Chen MH, Yan K. Differentiation of atypical hepatic hemangioma from liver metastases: Diagnostic performance of a novel type of color contrast enhanced ultrasound. *World J Gastroenterol* 2020; **26**: 960-972 [PMID: 32206006 DOI: 10.3748/wjg.v26.i9.960]

29 **Zhang GD**, Zou SD, Wang H, He J, Huang D. [Contrast-enhanced ultrasound in diagnosing 55 cases of various types of liver metastatic carcinoma]. *Shijie Huaren Xiaohua Zazhi* 2013; **21**: 2849-2850 [DOI: 10.11569/wcjd.v21.i27.2849]

30 **Chammas MC**, Bordini AL. Contrast-enhanced ultrasonography for the evaluation of malignant focal liver lesions. *Ultrasonography* 2022; **41**: 4-24 [PMID: 34724777 DOI: 10.14366/usg.21001]

31 **Xu HX**, Lu MD, Liu GJ, Xie XY, Xu ZF, Zheng YL, Liang JY. Imaging of peripheral cholangiocarcinoma with low-mechanical index contrast-enhanced sonography and SonoVue: initial experience. *J Ultrasound Med* 2006; **25**: 23-33 [PMID: 16371552 DOI: 10.7863/jum.2006.25.1.23]

32 **Sidhu PS**, Cantisani V, Dietrich CF, Gilja OH, Saftoiu A, Bartels E, Bertolotto M, Calliada F, Clevert DA, Cosgrove D, Deganello A, D'Onofrio M, Drudi FM, Freeman S, Harvey C, Jenssen C, Jung EM, Klauser AS, Lassau N, Meloni MF, Leen E, Nicolau C, Nolsoe C, Piscaglia F, Prada F, Prosch H, Radzina M, Savelli L, Weskott HP, Wijkstra H. The EFSUMB Guidelines and Recommendations for the Clinical Practice of Contrast-Enhanced Ultrasound (CEUS) in Non-Hepatic Applications: Update 2017 (Long Version). *Ultraschall Med* 2018; **39**: e2-e44 [PMID: 29510439 DOI: 10.1055/a-0586-1107]

33 **Jiang Y**, Zhang M, Zhu Y, Zhu D. Diagnostic role of contrast-enhanced ultrasonography *vs* conventional B-mode ultrasonography in cirrhotic patients with early hepatocellular carcinoma: a retrospective study. *J Gastrointest Oncol* 2021; **12**: 2403-2411 [PMID: 34790401 DOI: 10.21037/jgo-21-611]

34 **Guo HL**, Lu XZ, Hu HT, Ruan SM, Zheng X, Xie XY, Lu MD, Kuang M, Shen SL, Chen LD, Wang W. Contrast-Enhanced Ultrasound-Based Nomogram: A Potential Predictor of Individually Postoperative Early Recurrence for Patients With Combined Hepatocellular-Cholangiocarcinoma. *J Ultrasound Med* 2021 [PMID: 34751450 DOI: 10.1002/jum.15869]

35 **Ferraioli G**, Meloni MF. Contrast-enhanced ultrasonography of the liver using SonoVue. *Ultrasonography* 2018; **37**: 25-35

[PMID: 28830058 DOI: 10.14366/usg.17037]

36 **Zarzour JG**, Porter KK, Tchelepi H, Robbin ML. Contrast-enhanced ultrasound of benign liver lesions. *Abdom Radiol (NY)* 2018; **43**: 848-860 [PMID: 29167944 DOI: 10.1007/s00261-017-1402-2]

37 **Kang XN**, Zhang XY, Bai J, Wang ZY, Yin WJ, Li L. Analysis of B-ultrasound and contrast-enhanced ultrasound characteristics of different hepatic neuroendocrine neoplasm. *World J Gastrointest Oncol* 2019; **11**: 436-448 [PMID: 31139313 DOI: 10.4251/wjgo.v11.i5.436]

38 **Jang HJ**, Kim TK, Burns PN, Wilson SR. CEUS: An essential component in a multimodality approach to small nodules in patients at high-risk for hepatocellular carcinoma. *Eur J Radiol* 2015; **84**: 1623-1635 [PMID: 26092406 DOI: 10.1016/j.ejrad.2015.05.020]

39 **Kitao A**, Zen Y, Matsui O, Gabata T, Nakanuma Y. Hepatocarcinogenesis: multistep changes of drainage vessels at CT during arterial portography and hepatic arteriography--radiologic-pathologic correlation. *Radiology* 2009; **252**: 605-614 [PMID: 19703890 DOI: 10.1148/radiol.2522081414]

40 **Fukukura Y**, Nakashima O, Kusaba A, Kage M, Kojiro M. Angioarchitecture and blood circulation in focal nodular hyperplasia of the liver. *J Hepatol* 1998; **29**: 470-475 [PMID: 9764996 DOI: 10.1016/s0168-8278(98)80067-6]

41 **Sakakura C**, Kumano T, Mizuta Y, Yamaoka N, Sagara Y, Hagiwara A, Otsuji E. Successful treatment of huge peritoneal metastasis from duodenal gastrointestinal stromal tumor resistant for imatinib mesylate. *Gan To Kagaku Ryoho* 2007; **34**: 2144-2146 [PMID: 18219926]

42 **Corvino A**, Catalano O, Corvino F, Petrillo A. Rectal melanoma presenting as a solitary complex cystic liver lesion: role of contrast-specific low-MI real-time ultrasound imaging. *J Ultrasound* 2016; **19**: 135-139 [PMID: 27298643 DOI: 10.1007/s40477-015-0182-1]

43 **Ishikawa T**, Ohno E, Mizutani Y, Iida T, Koya T, Sasaki Y, Ogawa H, Kinoshita F, Hirooka Y, Kawashima H. Comparison of contrast-enhanced transabdominal ultrasonography following endoscopic ultrasonography with GD-EOB-DTPA-enhanced MRI for the sequential diagnosis of liver metastasis in patients with pancreatic cancer. *J Hepatobiliary Pancreat Sci* 2021 [PMID: 34878726 DOI: 10.1002/jhbp.1097]

44 **Schwarze V**, Marschner C, Grosu S, Rübenthaler J, Knösel T, Clevert DA. [Modern sonographic imaging of abdominal neuroendocrine tumors]. *Radiologe* 2019; **59**: 1002-1009 [PMID: 31440790 DOI: 10.1007/s00117-019-00586-0]

World Journal of Clinical Cases

Submit a Manuscript: https://www.f6publishing.com

World J Clin Cases 2022 June 16; 10(17): 5910-5915

DOI: 10.12998/wjcc.v10.i17.5910

ISSN 2307-8960 (online)

CASE REPORT

Tumor-like disorder of the brachial plexus region in a patient with hemophilia: A case report

En-Qi Guo, Xiao-Dong Yang, Hong-Rui Lu

Specialty type: Medicine, research and experimental

Provenance and peer review: Unsolicited article; Externally peer reviewed.

Peer-review model: Single blind

Peer-review report's scientific quality classification

Grade A (Excellent): 0
Grade B (Very good): 0
Grade C (Good): C
Grade D (Fair): D
Grade E (Poor): 0

P-Reviewer: Gupta S, United States; Le PH, Taiwan

Received: January 16, 2022
Peer-review started: January 16, 2022
First decision: March 16, 2022
Revised: March 25, 2022
Accepted: April 9, 2022
Article in press: April 9, 2022
Published online: June 16, 2022

En-Qi Guo, Xiao-Dong Yang, Hong-Rui Lu, Center for Plastic and Reconstructive Surgery, Department of Hand and Reconstructive Surgery, Zhejiang Provincial People's Hospital, Affiliated People's Hospital, Hangzhou Medical College, Hangzhou 310014, Zhejiang Province, China

Corresponding author: Hong-Rui Lu, MD, Doctor, Center for Plastic and Reconstructive Surgery, Department of Hand and Reconstructive Surgery, Zhejiang Provincial People's Hospital, Affiliated People's Hospital, Hangzhou Medical College, No. 158 Shangtang Road, Hangzhou 310014, Zhejiang Province, China. guoenqi@hmc.edu.cn

Abstract

BACKGROUND

Various tumors and tumor-like disorders, originating from the neural sheath, as well as other types, may affect the brachial plexus region. Due to the infrequent presentation, brachial plexus palsy caused by spontaneous hematoma in patients with hemophilia might miss the treatment by early surgical decompression and progress to permanent nerve damage.

CASE SUMMARY

The case reported here was a 30-year-old man with hemophilia, as well as both sensory and motor dysfunction of the left upper extremity. A presumptive diagnosis of brachial plexus tumor was initially made, which was subsequently confirmed to be an organized chronic hematoma rather than a neoplasm. The hemophilia-induced expanding hematoma compressing the brachial plexus was considered to be the main reason for the patient's complaints. The clinical symptoms were alleviated and the involved nerves partially recovered at a follow-up of 1 year.

CONCLUSION

Early surgical intervention is crucial and it seems to be an essential precondition for recovery of nerve function in brachial plexus lesions.

Key Words: Brachial plexus lesions; Hematoma; Hemophilia; Surgical intervention; Case report

©The Author(s) 2022. Published by Baishideng Publishing Group Inc. All rights reserved.

Core Tip: Due to the infrequent presentation, brachial plexus palsy caused by spontaneous hematoma in patients with hemophilia might miss the treatment by early surgical decompression and progress to permanent nerve damage. We presented our experience with successful surgical management of a brachial plexus tumor-like disorder, which was eventually proved to be an extrinsic muscular hematoma in the vicinity of the plexus. Early surgical intervention is crucial and it seems to be an essential precondition for recovery of nerve function.

Citation: Guo EQ, Yang XD, Lu HR. Tumor-like disorder of the brachial plexus region in a patient with hemophilia: A case report. *World J Clin Cases* 2022; 10(17): 5910-5915
URL: https://www.wjgnet.com/2307-8960/full/v10/i17/5910.htm
DOI: https://dx.doi.org/10.12998/wjcc.v10.i17.5910

INTRODUCTION

Various tumors and tumor-like disorders, originating from the neural sheath, as well as other types, may affect the brachial plexus region[1,2]. In cases of brachial plexus lesions, no imaging or radiographic test that is currently available, such as angiography, computed tomography (CT), or magnetic resonance imaging (MRI), is able to reliably distinguish between benign and malignant neurogenic tumors[3]. Use of nonspecific symptoms and imaging findings for preoperative diagnosis probably leads to error.

The case reported here was a 30-year-old man with hemophilia, as well as both sensory and motor dysfunction of the left upper extremity. A presumptive diagnosis of brachial plexus tumor was initially made, which was subsequently confirmed to be an organized chronic hematoma rather than a neoplasm. Due to the infrequent presentation, brachial plexus palsy caused by spontaneous hematoma in patients with hemophilia might miss the treatment by early surgical decompression and progress to permanent nerve damage. We presented our experience with successful surgical management of a brachial plexus tumor-like disorder, which was eventually proved to be an extrinsic muscular hematoma in the vicinity of the plexus.

CASE PRESENTATION

Chief complaints

A 30-year-old man with hemophilia A had numbness and paresthesia on the entire left forearm and hand. He complained of swelling and pain in his left arm and denied a history of trauma. He described nearly complete loss of flexion of his left elbow, wrist and finger joints afterwards.

History of present illness

He missed early operation, due to the high risk of hemorrhage, probably aggravated by surgical intervention. The symptoms worsened throughout the subsequent 2 mo. He was referred to our hospital 2 mo after the onset of symptoms.

History of past illness

The patient suffered from congenital severe hemophilia A.

Personal and family history

The patient had no history of smoking, drinking, or familial tumors.

Physical examination

On physical examination, the patient was found to have moderate swelling and tenderness to palpation over the medial side of the left arm. Abundant ecchymosis from the axilla to the medial side of the left arm was noticed. He presented with a mixed sensory and motor deficit. His neurological examination revealed hypoesthesia in the distribution of the lateral antebrachial cutaneous nerve and medial antebrachial cutaneous nerve. Numbness was involved along the median and ulnar nerves of the hand. The motor function loss in his left shoulder flexion (range of motion, 0-60°) was recorded. The significantly decreased elbow flexion and extension on the same side was documented. The severe weakness in wrist flexion (2/5), as well as in flexion and opposition of all five digits was detected. He was unable to grip anything.

Laboratory examinations

Hematological examination demonstrated a normal platelet count and bleeding time but prolonged partial thromboplastin time. The coagulation factor assay showed that the activity of coagulation factor VIII was low at 0.3%. He had a normal factor IX level at 81%.

Imaging examinations

Enhanced T2-weighted magnetic resonance imaging in the sagittal and coronal planes showed a hyperintense heterogenic lesion that was adjacent to the axillary segment of the brachial plexus (Figure 1).

Electromyography (EMG) was suggestive of compression of the lateral, medial and posterior cords, which was more predominant in the lateral cord of the brachial plexus.

FINAL DIAGNOSIS

Based on the combination of history, coagulation assay, EMG and characteristic imaging findings, a presumptive diagnosis of brachial plexus tumor with congenital severe hemophilia A was made initially. However, the frozen and permanent specimens documented peripheral neovascular granular tissue, degenerated muscle fibers, fibrosis, and microscopic foci of hemosiderin consistent with an organized hematoma rather than a neoplasm (Figure 2). Definite diagnosis was muscular hematoma in the brachial plexus region, concomitant with severe hemophilia A.

TREATMENT

Preoperative factor replacement therapy

The patient was treated with recombinant factor VIII infusions and his factor VIII level increased towards 100% before surgical treatment.

Surgical procedures

After shared decision-making and informed consent, the patient underwent surgical resection of the mass. On exploration, we discovered that the brachial plexus lesion was a fibrous-encapsulated mass with organized inflammatory tissue of a brownish color. The organized hematoma and surrounding scar were found to be directly compressing the lateral, medial and posterior cords of the brachial plexus. The internal structure of the nerve was not violated or involved. There was no neuroma noted or obvious intraneural bleeding. The mass along the coracobrachialis muscle was excised and the brachial plexus was released *via* neurolysis and dissection of the brachial fascia. The cut surface of the resected specimen indicated an organized chronic hematoma instead of a neoplasm (Figure 3). Partial pectoralis major muscle was transected near its insertion but repaired in place at the end of surgery, which provided adequate access for the dissection of the axilla. The patient continued factor VIII replacement therapy for 10 d. While he was being tapered off replacement therapy, an unexpected acute hematoma occurred. Emergency surgical decompression was required. On exploration of the pectoralis major, the expanding hematoma was gently evacuated with suction and forceps. The postoperative course was uneventful, with another 21 d of an aggressive infusion program.

OUTCOME AND FOLLOW-UP

At 12 months' follow-up, there was no recurrence or other significant complaint. The clinical symptoms were alleviated and the involved nerves partially recovered when compared to the preoperative results. There was sensory improvement in the region of dermatomal hypoesthesia. The active arc of motion (flexion/extension) of his left elbow and wrist increased to 90° and 50°, respectively. The grip strength of the affected hand measured 35% of the contralateral side (Figure 4). The DASH (Disabilities of Arm, Shoulder, and Hand) score of our patient at final follow-up was 21, compared to 65 preoperatively. The patient was satisfied with the restoration of daily activities and return to the previous work as a manual laborer.

DISCUSSION

A radiologic plan is necessary to recognize soft tissue lesions with a neural origin, their association with a peripheral nerve, and whether they are a true tumor or a pseudotumor such as a neuroma, hematoma, or peripheral nerve sheath ganglion[1,4]. Accurate diagnosis of these lesions is critical for determining

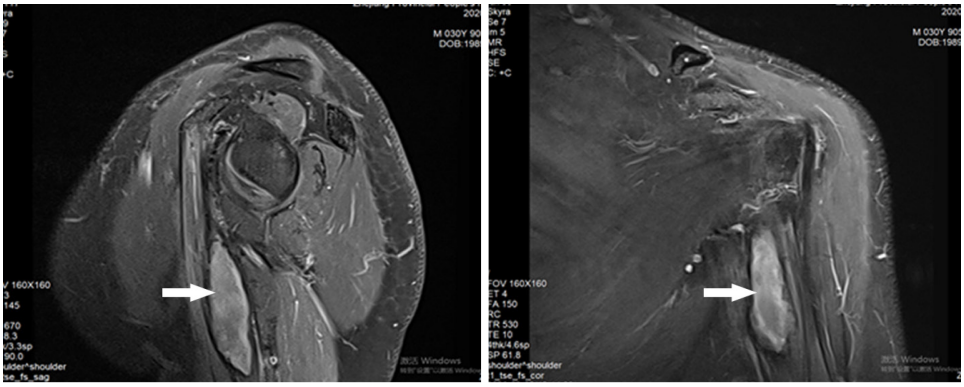

DOI: 10.12998/wjcc.v10.i17.5910 **Copyright** ©The Author(s) 2022.

Figure 1 Magnetic resonance images of the left upper limb. Sagittal and coronal views of T2-weighted images showed a focal mass on left coracobrachialis muscle (white arrow).

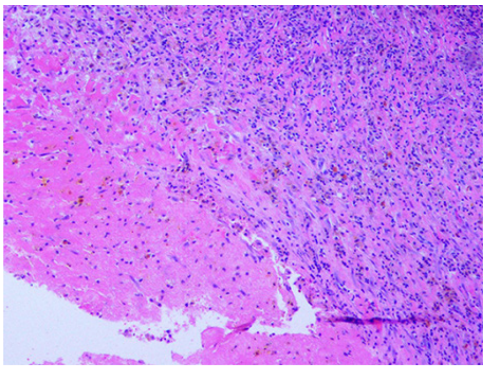

DOI: 10.12998/wjcc.v10.i17.5910 **Copyright** ©The Author(s) 2022.

Figure 2 Histopathological examination of the resected mass showed inflammatory infiltration with hemosiderin pigments and fibrosis (hematoxylin and eosin stain, × 100).

the appropriate management options. Delaying the treatment of a highly aggressive nerve sheath tumor can have devastating consequences, whereas many hematomas resolve without surgery.

Brachial plexus hematomas are rare and can mimic malignant peripheral nerve sheath tumors both radiographically and clinically[4]. The purpose of this case report is to clarify the etiology of brachial plexus lesions, review the differential diagnostic considerations, and discuss the role of imaging modalities, together with the usefulness of electrophysiological tests.

High quality CT or MRI was conducted to delineate tumor location, margins, and relationship to surrounding structures. MRI may also determine whether the contents are in liquid or in solid form[1, 3]. Nevertheless, an organized hematoma has no particular differentiating imaging features. The interest in pre-therapeutic biopsy on benign lesions is limited because the sensitivity of this procedure is moderate and the procedure could damage intact fascicles or cause hemorrhage[1].

The findings of EMG studies for this case supported the diagnosis of brachial plexus compressive neuropathy. Establishing peripheral nerve lesions in hemophiliac patients is difficult, since disability or hemarthrosis can also give rise to motor disorders, reflex disturbances and muscular atrophy. Electrodiagnostic evaluation may confirm the diagnosis, pinpoint the lesions, determine the severity of axial discontinuity, and eliminate other clinical entities from differential diagnosis[5]. Recently, the use of intraoperative electrophysiological tests has been an integral part of brachial plexus surgery.

Our patient had already been afflicted with severe hemophilia. Thus, we speculated that the hemophilia-induced expanding hematoma within the soft tissue resulted in pressure on the adjacent brachial plexus. At the site of the hematoma in this case, brachial plexus was vulnerable to get compressed between coracobrachialis muscle hematoma and its overlying fascia. Our experience suggested that surgical intervention for nerve compression with adequate factor replacement should be considered as soon as possible in cases such as this.

To the best of our knowledge, our patient was the first reported case in the literature developing brachial plexus palsy that was ascribed to severe hemophilia without any slight provocation or minor trauma/injury. Ogawa *et al*[6] discussed the management of a 42-year-old man with underlying moderate hemophilia, as well as compressive brachial plexopathy. In his study, that patient mentioned a history of lifting heavy weights, which was thought to be the cause of the following intramuscular

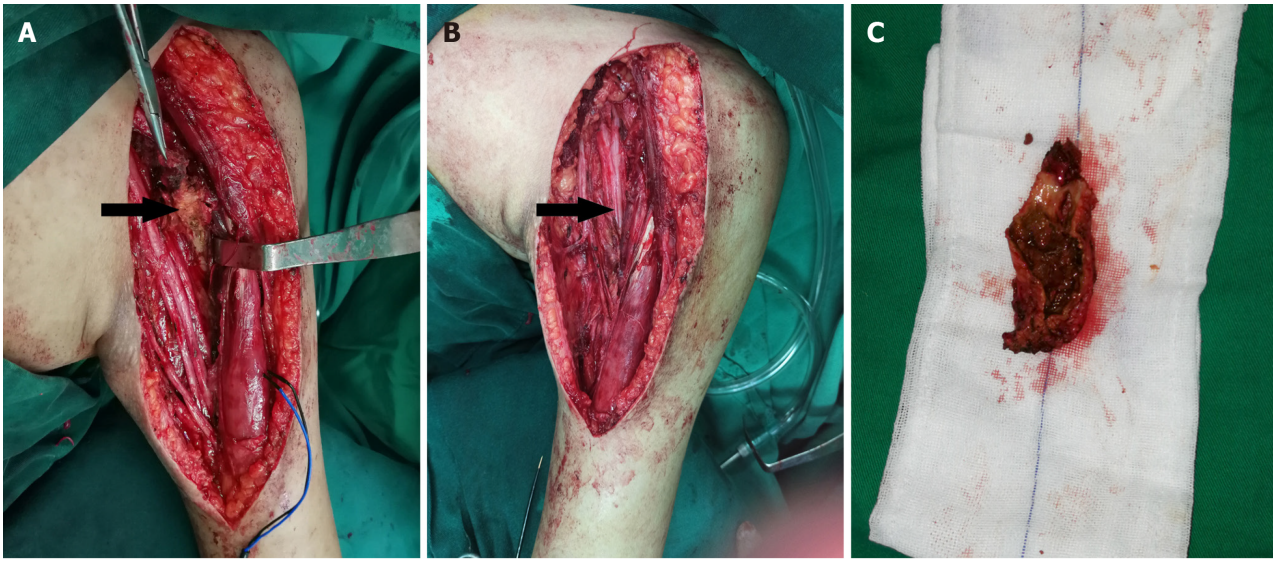

DOI: 10.12998/wjcc.v10.i17.5910 **Copyright** ©The Author(s) 2022.

Figure 3 Intraoperative findings of the patient. A: An organized mass was exposed prior to excision (black arrow); B: Brachial plexus neurolysis was performed after the mass resection; C: The cut surface of the resected specimen indicated an organized chronic hematoma rather than a neoplasm.

DOI: 10.12998/wjcc.v10.i17.5910 **Copyright** ©The Author(s) 2022.

Figure 4 A 12 mo follow-up assessment demonstrated definite improvement in the left shoulder abduction, elbow flexion and grip strength after successful surgery.

bleeding. Both the Ogawa reported case and our case achieved encouraging functional restoration, despite of the initial underestimation and misdiagnosis.

Finally, our patient experienced a recurrent acute muscle hematoma, and was subjected to an emergency operation. This patient was immobilized with his arm into a sling immediately after the first operation, which perhaps did not offer enough protection and *stability* for the shoulder joint. Once upon shoulder abduction and external rotation, an acute pectoralis major tear occurred, which eventually progressed to formation of a large hematoma. We therefore infer that strict rest and temporary splint application to the extremity is required to accelerate healing between the ends of the ruptured myofibers and formation of stable scar tissue. However, it should not be unnecessarily prolonged because early mobilization is needed for decrease of adhesion and resorption of scar tissue[7].

CONCLUSION

In summary, improvements in factor replacement safety and effectiveness have made the performance of major surgical procedures increasingly possible in recent years. Given the short window between symptomatic onset and irreversible histopathologic neural changes, early surgical intervention is crucial and it seems to be an essential precondition for recovery of nerve function. In general, a comprehensive

treatment protocol for hemophiliac patients with concomitant entrapment neuropathies, should be developed and clinically validated.

FOOTNOTES

Author contributions: Yang XD and Lu HR diagnosed the patient, provided surgical treatment, acquired clinical data, revised and reviewed the manuscript for the final publication; Guo EQ reviewed the literature, and drafted the manuscript; all authors read and approved the final manuscript.

Supported by the Foundation of Science and Technology Department of Zhejiang Province, No. LGF19H060010; and the Foundation of Health and Family Planning Commission of Zhejiang Province, No. 2021KY445.

Informed consent statement: Written informed consent was obtained from the patient for publication of this report and accompanying images.

Conflict-of-interest statement: The authors declare that they have no conflict of interest.

CARE Checklist (2016) statement: The authors have read the CARE Checklist (2016), and the manuscript was prepared and revised according to the CARE Checklist (2016).

Open-Access: This article is an open-access article that was selected by an in-house editor and fully peer-reviewed by external reviewers. It is distributed in accordance with the Creative Commons Attribution NonCommercial (CC BY-NC 4.0) license, which permits others to distribute, remix, adapt, build upon this work non-commercially, and license their derivative works on different terms, provided the original work is properly cited and the use is non-commercial. See: https://creativecommons.org/Licenses/by-nc/4.0/

Country/Territory of origin: China

ORCID number: En-Qi Guo 0000-0002-5455-5170; Xiao-Dong Yang 0000-0001-7542-624X; Hong-Rui Lu 0000-0002-4619-0693.

S-Editor: Wang LL
L-Editor: A
P-Editor: Wang LL

REFERENCES

1 **Siqueira MG**, Martins RS, Teixeira MJ. Management of brachial plexus region tumours and tumour-like conditions: relevant diagnostic and surgical features in a consecutive series of eighteen patients. *Acta Neurochir (Wien)* 2009; **151**: 1089-1098 [PMID: 19448970 DOI: 10.1007/s00701-009-0380-8]
2 **Das S**, Ganju A, Tiel RL, Kline DG. Tumors of the brachial plexus. *Neurosurg Focus* 2007; **22**: E26 [PMID: 17613218 DOI: 10.3171/foc.2007.22.6.27]
3 **Binder DK**, Smith JS, Barbaro NM. Primary brachial plexus tumors: imaging, surgical, and pathological findings in 25 patients. *Neurosurg Focus* 2004; **16**: E11 [PMID: 15174831 DOI: 10.3171/foc.2004.16.5.12]
4 **Krisht KM**, Karsy M, Shah LM, Schmidt MH, Dailey AT. Unusual brachial plexus lesion: Hematoma masquerading as a peripheral nerve sheath tumor. *Surg Neurol Int* 2016; **7**: S64-S66 [PMID: 26904368 DOI: 10.4103/2152-7806.174889]
5 **Ferrante MA**. Electrodiagnostic assessment of the brachial plexus. *Neurol Clin* 2012; **30**: 551-580 [PMID: 22361374 DOI: 10.1016/j.ncl.2011.12.005]
6 **Ogawa K**, Yoshida A, Ui M. Brachial plexus palsy presenting as an initial manifestation of hemophilia in a middle-aged man. *J Shoulder Elbow Surg* 1998; **7**: 546-548 [PMID: 9814940 DOI: 10.1016/s1058-2746(98)90212-9]
7 **Beyer R**, Ingerslev J, Sørensen B. Muscle bleeds in professional athletes--diagnosis, classification, treatment and potential impact in patients with haemophilia. *Haemophilia* 2010; **16**: 858-865 [PMID: 20491962 DOI: 10.1111/j.1365-2516.2010.02278.x]

World Journal of Clinical Cases

Submit a Manuscript: https://www.f6publishing.com

World J Clin Cases 2022 June 16; 10(17): 5916-5922

DOI: 10.12998/wjcc.v10.i17.5916

ISSN 2307-8960 (online)

CASE REPORT

Response to dacomitinib in advanced non-small-cell lung cancer harboring the rare delE709_T710insD mutation: A case report

Fei Xu, Meng-Ling Xia, Hui-Yun Pan, Jiong-Wei Pan, Yi-Hong Shen

Specialty type: Medicine, research and experimental

Provenance and peer review: Unsolicited article; Externally peer reviewed.

Peer-review model: Single blind

Peer-review report's scientific quality classification

Grade A (Excellent): A
Grade B (Very good): B
Grade C (Good): 0
Grade D (Fair): 0
Grade E (Poor): 0

P-Reviewer: Covantsev S, Russia; Suravajhala PN, India

Received: January 22, 2022
Peer-review started: January 22, 2022
First decision: March 16, 2022
Revised: March 21, 2022
Accepted: April 9, 2022
Article in press: April 9, 2022
Published online: June 16, 2022

Fei Xu, Meng-Ling Xia, Yi-Hong Shen, Department of Respiratory Diseases, The First Affiliated Hospital, Zhejiang University School of Medicine, Hangzhou 310000, Zhejiang Province, China

Hui-Yun Pan, Department of Day Care Ward, The First Affiliated Hospital, Zhejiang University School of Medicine, Hangzhou 310000, Zhejiang Province, China

Jiong-Wei Pan, Department of Respiratory Diseases, Lishui City People's Hospital, Lishui 323000, Zhejiang Province, China

Corresponding author: Yi-Hong Shen, MD, Chief Doctor, Department of Respiratory Diseases, The First Affiliated Hospital, Zhejiang University School of Medicine, No. 79 Qingchun Road, Hangzhou 310000, Zhejiang Province, China. drsyh@zju.edu.cn

Abstract

BACKGROUND

Tyrosine kinase inhibitors (TKI) have been the standard first-line therapy for advanced non-small cell lung cancer (NSCLC) of epidermal growth factor receptor (*EGFR*) sensitive mutations. Uncommon *EGFR* mutations are increasingly reported with the development of next-generation sequencing. However, their sensitivity to TKIs is variable with limited clinical evidence.

CASE SUMMARY

Here, we report a patient with the rare delE709_T710insD mutation, who showed the favorable efficacy of dacomitinib and achieved a partial response with a progression-free survival of 7.0 mo.

CONCLUSION

To our knowledge, this is the first report displaying the clinical efficacy of dacomitinib for patients with delE709_T710insD, which may help to provide alternatives in non-classical variant NSCLC patients. Further studies are warranted to make the optimal choice of *EGFR*-TKI for rare mutations.

Key Words: Next-generation sequencing; DelE709_T710insD; Non-small-cell lung cancer; Dacomitinib; Uncommon *EGFR* mutation; Case report

©The Author(s) 2022. Published by Baishideng Publishing Group Inc. All rights reserved.

Core Tip: DelE709_T710insD is an extremely rare complex in-frame deletion mutation in exon 18 and accounts for only 0.11% of epidermal growth factor receptor mutations. The development of next-generation sequencing enabled the more identification of rare variants. Our case is the first report describing the clinical efficacy of dacomitinib for delE709_T710insD and achieved a progression-free survival of 7.0 mo. More patients with the rare variants may benefit from dacomitinib targeted therapy based on our study.

Citation: Xu F, Xia ML, Pan HY, Pan JW, Shen YH. Response to dacomitinib in advanced non-small-cell lung cancer harboring the rare delE709_T710insD mutation: A case report. *World J Clin Cases* 2022; 10(17): 5916-5922
URL: https://www.wjgnet.com/2307-8960/full/v10/i17/5916.htm
DOI: https://dx.doi.org/10.12998/wjcc.v10.i17.5916

INTRODUCTION

Among non-small-cell lung cancer (NSCLC) patients with epidermal growth factor receptor (*EGFR*) mutations, the most common mutations are exon 19 deletions and exon 21 L858R point mutations, accounting for 80%-90% of all *EGFR* mutations[1]. With the development of next-generation sequencing (NGS), more rare or atypical mutations, such as *EGFR* exon 20 and exon 18, have been identified, but their responses to TKIs have been variable and less investigated.

Mutations in *EGFR* exon 18, including point mutations and deletion-insertion mutations, were observed in approximately 4% of patients with *EGFR* mutations[2]. DelE709_T710insD is a rare complex in-frame deletion mutation in exon 18 and accounts for only 0.11% of *EGFR* mutations (33/31015) according to the Catalog of Somatic Mutations in Cancer (COSMIC) v.94 database[3]. Evidence regarding its response to available *EGFR*-TKIs is limited.

Here, we present a patient with advanced lung adenocarcinoma harboring the rare *EGFR* delE709_T710insD mutation who responded well to the second-generation *EGFR* TKI dacomitinib.

CASE PRESENTATION

Chief complaints

A 56-year-old female patient presented with right chest discomfort for 3 mo.

History of present illness

Chest computed tomography (CT) revealed a 1.9 cm × 2.1 cm mass in the anterior segment of the right upper lobe and multiple nodules in the bilateral lungs, accompanied by right pleural effusion. Moreover, the right hilar, mediastinal, and paratracheal lymph nodes (LNs) were found to be enlarged.

History of past illness

The patient had no history of any other diseases.

Personal and family history

The patient was free of any known congenital disease.

Physical examination

The right supraclavicular painless lymph node was palpated in the size of a soybean.

Laboratory examinations

The laboratory test data revealed that the serum carcinoembryonic antigen level was 279.6 ng/mL.

Imaging examinations

A positron emission tomography (PET) scan showed increased fluorodeoxyglucose (FDG) uptake in the right upper lobe mass, multiple pulmonary and subpleural nodules, and right supraclavicular, mediastinal, and right hilar lymph nodes. PET also indicated hypermetabolic nodules with low density in segment 6 of the liver and anterolateral area of the liver capsule, along with multiple bone destruction changes and high FDG uptake in T7 and T8 vertebral bodies and appendages, L5 spinous processes, and bilateral iliac bones (Figure 1). Magnetic resonance imaging of the brain was negative.

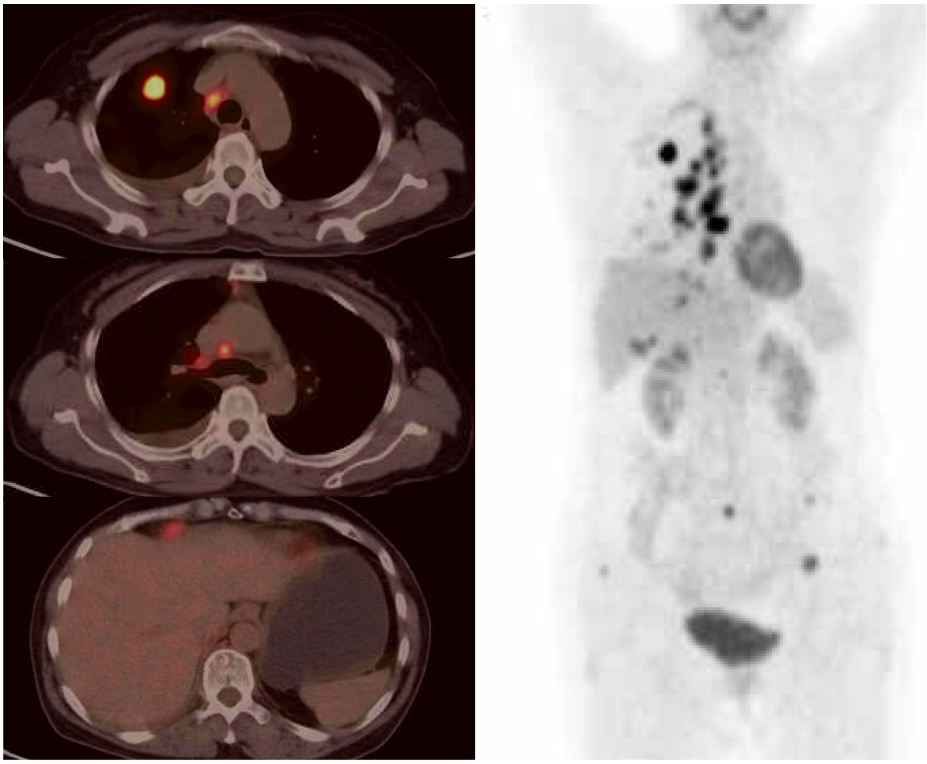

DOI: 10.12998/wjcc.v10.i17.5916 **Copyright** ©The Author(s) 2022.

Figure 1 Positron emission tomography scans at presentation.

MULTIDISCIPLINARY EXPERT CONSULTATION

She subsequently underwent ultrasound-guided needle biopsy of the right supraclavicular lymph node and right closed thoracic drainage. Endobronchial ultrasound-transbronchial needle aspiration (EBUS-TBNA) was performed on LN 7 and 11R. Cancer cells were found both in the pleural effusion and clavicular lymph nodes. Pathological results of LN 11R were identified pulmonary adenocarcinoma, with P40 (-), CK7 (+), TTF-1 (+), Napsin A (+), CK5/6 (-), ALK Ventana (-), ALK-Negative (-) through immunohistochemistry (IHC). Genetic testing was performed on cell block samples from pleural effusion by polymerase chain reaction (PCR). Routine molecular genetic testing, including mutation of *EGFR, KRAS, NRAS, BRAF, HER2, MET,* and *PIK3CA*, and fusion of *ALK, RET,* and *ROS1*, were all negative. Supplementary material listed all gene and mutation sites of the PCR diagnostic kits.

FINAL DIAGNOSIS

Based on this, the patient was identified as "driver gene-negative" right lung adenocarcinoma, cT1cN3M1c (TNM 8th Edition), stage IVB.

TREATMENT

The patient then started chemotherapy with pemetrexed plus carboplatin and bevacizumab in September 2020. A CT scan after 2 cycles showed a reduction in the mass in the right upper lobe, but disease progression was observed in February 2021. The progression-free survival1 (PFS1) is 5 mo, and the best response was reduced stable disease based on Response Evaluation Criteria in Solid Tumors (RECIST) criteria. To seek more effective and potential treatment, CT-guided transthoracic lung biopsy was taken from the right upper lobe as her family demanded. A 12-gene NGS panel (Shanghai Yikon Genomics Inc. China) for lung cancer revealed the *EGFR* Del18 (delE709_T710insD) mutation. However, there are no recommended targeted drugs for this rare mutation. Dacomitinib 30 mg/d was administered as the second-line treatment, starting in February 2021.

Table 1 Studies of epidermal growth factor receptor-tyrosine kinase inhibitors response for delE709_T710insD

Ref.	Patient No.	Gender	Age (yr)	Smoking	Stage	Histologic type	TKI used/line	Response	PFS (m)	OS (m)
Wu *et al*[7], 2011	1	F	61	No	IV	AD	Gefitinib/NA	SD	5.1	22.7
	2	M	65	Yes	IV	AD	Gefitinib/NA	PD	0.9	11.1
Ackerman *et al*[9], 2012	3	F	88	No	IV	AD	Erlotinib/1st	PR	6	NA
Kobayashi *et al*[19], 2015	4	M	63	NA	IV	AD	Erlotinib/3rd	SD	NA	NA
							Afatinib/4th	PR	NA	
Wu *et al*[6], 2016	5	F	57	No	IV	AD	Gefitinib/NA	PD	0.6	24.1
	6	M	79	Yes	IV	AD	Gefitinib/NA	SD	6.2	6.2
	7	M	68	Yes	IV	AD	Gefitinib/NA	PD	2.3	29.5
Klughammer *et al*[10], 2016	8	F	50	No	III/IV	NSCLC	Erlotinib/2nd	PD	1.3	1.7
Ibrahim *et al*[13], 2017	9	F	52	No	IV	AD	Afatinib/1st	PR	NA	NA
An *et al*[14], 2019	10	M	56	No	IV	AD	Afatinib/2nd	PR	11	More than 21
Iwamoto *et al*[15], 2019	11	F	56	No	IV	AD	Afatinib/6th	PR	7	NA
D'Haene *et al*[16], 2019	12	F	57	No	III	AD	Afatinib/2nd	PR	12	36
Martin *et al*[11], 2019	13	M	60	No	IV	AD	Erlotinib/NA	PD	1	3
Isaksson *et al*[12], 2020	14	NA	NA	NA	IV	NA	Erlotinib/1st	PD	8	NA
Sousa *et al*[8], 2020	15	F	66	Yes	IV	AD	Gefitinib/1st	PD	3	24
	16	F	46	Yes	II	AD	Erlotinib/2nd	PD	4	26
	17	F	57	No	IV	AD	Erlotinib/2nd	PD	3	18
Wei *et al*[17], 2021	18	F	70	No	II	NSCLC	Afatinib/1st	PR	23	On going
Jelli *et al*[18], 2021	19	F	57	No	IV	AD	Afatinib/1st	CR	17 (On going)	17 (On going)
Xu *et al*, 2021 (this case)	20	F	56	No	IV	AD	Dacomitinib/2nd	PR	7	On going

F: Female; M: Male; NA: Data not-available; PFS: Progression-free survival; OS: Overall survival; TKI: Tyrosine kinase inhibitor; AD: Lung adenocarcinoma; NSCLC: Non-small cell lung cancer; PR: Partial response; SD: Stable disease; PD: Progression disease.

OUTCOME AND FOLLOW-UP

A CT scan revealed that the primary lesion significantly decreased in size after 2 mo, and a partial response (PR) was achieved (Figure 2). There were no significant adverse effects of dacomitinib therapy. Nevertheless, recent CT showed that the mass of the right upper lobe grew larger, which met the RECIST criteria for progressive disease (PD) after 7.0 mo of dacomitinib treatment.

DISCUSSION

EGFR mutations are observed in up to 50% of Asian non-small-cell lung cancer (NSCLC) patients and approximately 10%-20% of non-Asian patients. *EGFR*-TKIs have become the standard first-line treatment for *EGFR* sensitizing mutations (del18 and L858R) NSCLC based on Phase III trials *vs* platinum-based doublet chemotherapy[4], which has revolutionized the management of *EGFR*-mutated NSCLC. Uncommon mutations or less frequent alterations involving exons 18 and 20 in *EGFR* account for 10-20% of all *EGFR* mutations in NSCLC. Individuals with uncommon *EGFR* mutations seem to be a

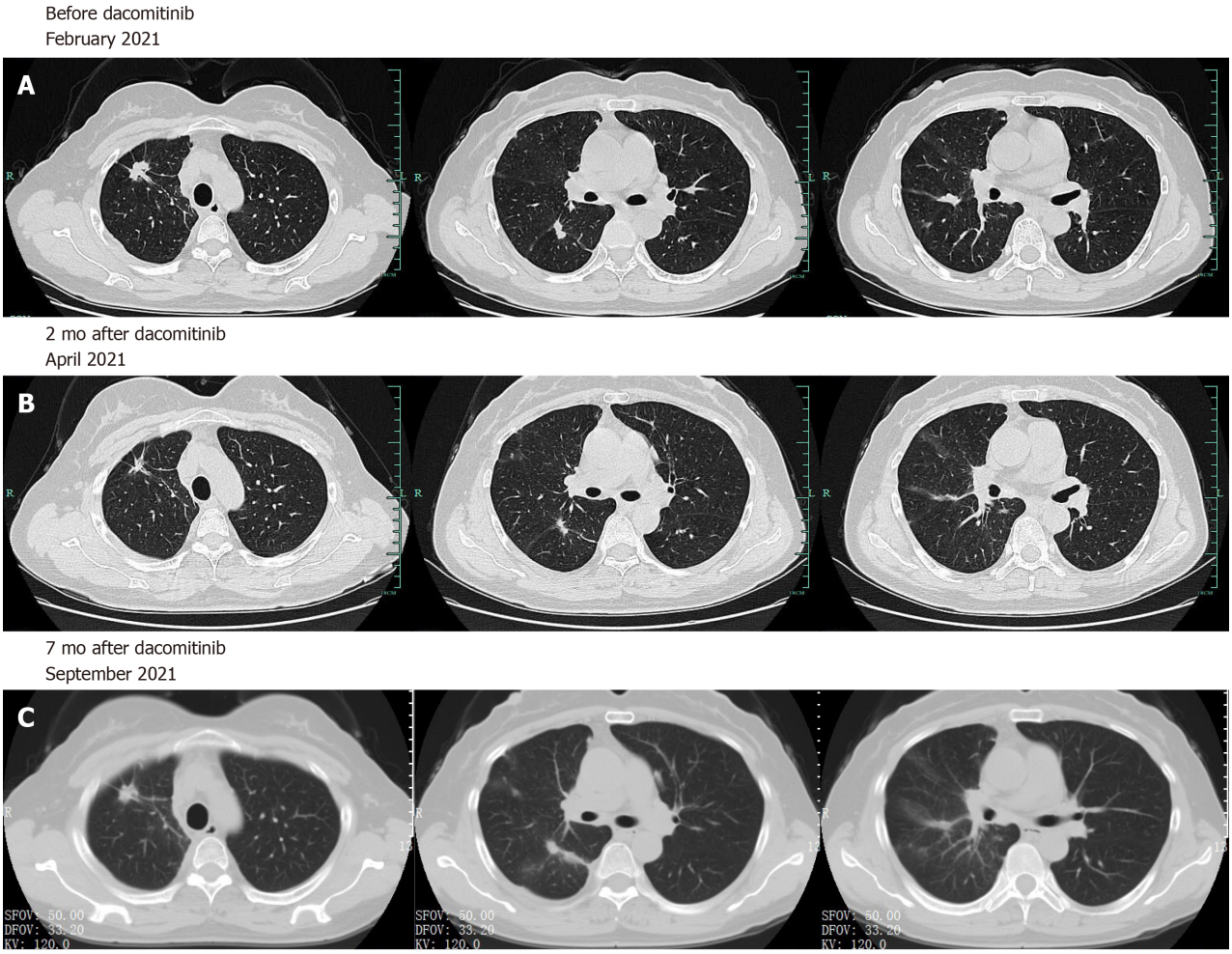

DOI: 10.12998/wjcc.v10.i17.5916 **Copyright** ©The Author(s) 2022.

Figure 2 Chest computed tomography scans. A: Chest computed tomography scans before (A) and after dacomitinib therapy; B and C: The patient achieved partial response 2 mo after the initiation of dacomitinib therapy and progressed at 7 mo later.

heterogeneous group exhibiting differential sensitivity to *EGFR* inhibitors, but clinical evidence is scarce [5].

Studies on the delE709_T710insD mutation and its response to *EGFR*-TKIs, including gefitinib, erlotinib, and afatinib, have been reported sporadically in recent years (Table 1). Wu JY *et al*[6] reported that the prevalence of delE709_T710insD is 0.16% (5/3146) in *EGFR* mutations. Six gefitinib-treated patients harboring delE709_T710insD were nonresponders, with a median PFS of 2.65 mo[6-8]. Erlotinib was administered in previous case reports[8-12], which also seemed to be a frustrated treatment for delE709_T710insD. One had a PR, 5 had PD, and the response rate was only 25% (1/6). Afatinib was proven to be effective for such rare variants[13-18]. Among the 6 patients receiving afatinib, one achieved a complete response (CR), and 5 achieved a PR. More significantly, 1 patient with E709_T710delinsD mutations showed a survival benefit of afatinib after erlotinib treatment failed[19]. The overall response rate of afatinib for delE709_T710insD was 100% (7/7). According to the analysis by Rubiera-Pebe R *et al*[20], the median PFS comparison between first-generation TKIs and afatinib for patients with delE709_T710insD is 3.1 mo *vs* 7.0 mo, respectively. *In vitro*, a study by Kobayashi Y *et al* [19] investigated the sensitivities of exon 18 mutations to various *EGFR*-TKIs and suggested that second-generation *EGFR*i have broader inhibitory profiles than other TKIs for rare mutations.

Like afatinib, dacomitinib is a second-generation pan-*HER* inhibitor that irreversibly binds to all three kinase-active members of the ErbB family (*HER1/EGFR, HER2, and HER4*), leading to more efficient *EGFR* inhibition. The efficacy of dacomitinib on patients acquiring Ex18 G719A as later-line therapy has been reported by Morita A *et al*[21]. In addition, dacomitinib *in vitro* has an IC_{50}=29 nM for Ba/F3 cells expressing exon 18 delE709_T710insD[19], indicating the potential activity of this nonclassical mutation. The results of a phase 3 trial of dacomitinib (NCT01774721, ARCHER 1050) indicated that first-line dacomitinib significantly improved PFS and OS *vs* gefitinib, and the adverse events were manageable [22]. Based on these findings, dacomitinib seemed to be a promising candidate for *EGFR*-positive advanced NSCLC, including less common mutations. However, limited clinical data have shown the effect of dacomitinib on rare mutations.

CONCLUSION

In our study, we reported that a patient with *EGFR* delE709_T710insD achieved PR after the initiation of dacomitinib, with a PFS2 of 7 mo. To the best of our knowledge, this is the first report describing the clinical efficacy of dacomitinib for *EGFR* delE709_T710insD. The efficacy of dacomitinib on rare mutations needs to be evaluated *in vivo or in vitro* by further studies. In addition, appropriate genetic diagnosis methodologies will provide patients with more opportunities for targeted therapy. Our report may help to provide new treatment options for NSCLC patients with nonclassical variants.

FOOTNOTES

Author contributions: Shen YH initiated the case report and supervised the entire study; Xu F collected patient data, performed a literature review and wrote the manuscript; Xia ML obtained and analyzed the next-generation sequencing results; Pan HY reviewed the histological pathological examination of the biopsy; Pan JW was involved in patient follow-up after discharge; all authors read and approved the final manuscript.

Informed consent statement: Informed written consent was obtained from the patient for publication of this report and any accompanying images.

Conflict-of-interest statement: The authors declare that they have no conflict of interest.

CARE Checklist (2016) statement: The authors have read the CARE Checklist (2016), and the manuscript was prepared and revised according to the CARE Checklist (2016).

Open-Access: This article is an open-access article that was selected by an in-house editor and fully peer-reviewed by external reviewers. It is distributed in accordance with the Creative Commons Attribution NonCommercial (CC BY-NC 4.0) license, which permits others to distribute, remix, adapt, build upon this work non-commercially, and license their derivative works on different terms, provided the original work is properly cited and the use is non-commercial. See: https://creativecommons.org/Licenses/by-nc/4.0/

Country/Territory of origin: China

ORCID number: Fei Xu 0000-0003-4200-1485; Meng-Ling Xia 0000-0002-0182-7400; Hui-Yun Pan 0000-0002-2536-5773; Jiong-Wei Pan 0000-0002-4077-2561; Yi-Hong Shen 0000-0002-7815-9973.

S-Editor: Wang LL
L-Editor: A
P-Editor: Wang LL

REFERENCES

1 **Han B**, Tjulandin S, Hagiwara K, Normanno N, Wulandari L, Laktionov K, Hudoyo A, He Y, Zhang YP, Wang MZ, Liu CY, Ratcliffe M, McCormack R, Reck M. *EGFR* mutation prevalence in Asia-Pacific and Russian patients with advanced NSCLC of adenocarcinoma and non-adenocarcinoma histology: The IGNITE study. *Lung Cancer* 2017; **113**: 37-44 [PMID: 29110846 DOI: 10.1016/j.lungcan.2017.08.021]

2 **Cheng C**, Wang R, Li Y, Pan Y, Zhang Y, Li H, Zheng D, Zheng S, Shen X, Sun Y, Chen H. *EGFR* Exon 18 Mutations in East Asian Patients with Lung Adenocarcinomas: A Comprehensive Investigation of Prevalence, Clinicopathologic Characteristics and Prognosis. *Sci Rep* 2015; **5**: 13959 [PMID: 26354324 DOI: 10.1038/srep13959]

3 **Atalogue of Somatic Mutations in Cancer**, release version 94. [cited 20 January 2022]. Available from: https://cancer.sanger.ac.uk/cosmic

4 **Hsu WH**, Yang JC, Mok TS, Loong HH. Overview of current systemic management of *EGFR*-mutant NSCLC. *Ann Oncol* 2018; **29**: i3-i9 [PMID: 29462253 DOI: 10.1093/annonc/mdx702]

5 **Russo A**, Franchina T, Ricciardi G, Battaglia A, Picciotto M, Adamo V. Heterogeneous Responses to Epidermal Growth Factor Receptor (*EGFR*) Tyrosine Kinase Inhibitors (TKIs) in Patients with Uncommon *EGFR* Mutations: New Insights and Future Perspectives in this Complex Clinical Scenario. *Int J Mol Sci* 2019; **20** [PMID: 30901844 DOI: 10.3390/ijms20061431]

6 **Wu JY**, Shih JY. Effectiveness of tyrosine kinase inhibitors on uncommon E709X epidermal growth factor receptor mutations in non-small-cell lung cancer. *Onco Targets Ther* 2016; **9**: 6137-6145 [PMID: 27785061 DOI: 10.2147/OTT.S118071]

7 **Wu JY**, Yu CJ, Chang YC, Yang CH, Shih JY, Yang PC. Effectiveness of tyrosine kinase inhibitors on "uncommon" epidermal growth factor receptor mutations of unknown clinical significance in non-small cell lung cancer. *Clin Cancer Res* 2011; **17**: 3812-3821 [PMID: 21531810 DOI: 10.1158/1078-0432.CCR-10-3408]

8 **Sousa AC**, Silveira C, Janeiro A, Malveiro S, Oliveira AR, Felizardo M, Nogueira F, Teixeira E, Martins J, Carmo-Fonseca M. Detection of rare and novel *EGFR* mutations in NSCLC patients: Implications for treatment-decision. *Lung Cancer*

2020; **139**: 35-40 [PMID: 31715539 DOI: 10.1016/j.lungcan.2019.10.030]

9 **Ackerman A**, Goldstein MA, Kobayashi S, Costa DB. *EGFR* delE709_T710insD: a rare but potentially *EGFR* inhibitor responsive mutation in non-small-cell lung cancer. *J Thorac Oncol* 2012; **7**: e19-e20 [PMID: 22982663 DOI: 10.1097/JTO.0b013e3182635ab4]

10 **Klughammer B**, Brugger W, Cappuzzo F, Ciuleanu T, Mok T, Reck M, Tan EH, Delmar P, Klingelschmitt G, Yin AY, Spleiss O, Wu L, Shames DS. Examining Treatment Outcomes with Erlotinib in Patients with Advanced Non-Small Cell Lung Cancer Whose Tumors Harbor Uncommon *EGFR* Mutations. *J Thorac Oncol* 2016; **11**: 545-555 [PMID: 26773740 DOI: 10.1016/j.jtho.2015.12.107]

11 **Martin J**, Lehmann A, Klauschen F, Hummel M, Lenze D, Grohé C, Tessmer A, Gottschalk J, Schmidt B, Pau HW, Witt C, Moegling S, Kromminga R, Jöhrens K. Clinical Impact of Rare and Compound Mutations of Epidermal Growth Factor Receptor in Patients With Non-Small-Cell Lung Cancer. *Clin Lung Cancer* 2019; **20**: 350-362.e4 [PMID: 31175009 DOI: 10.1016/j.cllc.2019.04.012]

12 **Isaksson S**, Hazem B, Jönsson M, Reuterswärd C, Karlsson A, Griph H, Engleson J, Oskarsdottir G, Öhman R, Holm K, Rosengren F, Annersten K, Jönsson G, Borg Å, Edsjö A, Levéen P, Brunnström H, Lindquist KE, Staaf J, Planck M. Clinical Utility of Targeted Sequencing in Lung Cancer: Experience From an Autonomous Swedish Health Care Center. *JTO Clin Res Rep* 2020; **1**: 100013 [PMID: 34589915 DOI: 10.1016/j.jtocrr.2020.100013]

13 **Ibrahim U**, Saqib A, Atallah JP. *EGFR* exon 18 delE709_T710insD mutated stage IV lung adenocarcinoma with response to afatinib. *Lung Cancer* 2017; **108**: 45-47 [PMID: 28625646 DOI: 10.1016/j.lungcan.2017.02.023]

14 **An N**, Wang H, Zhu H, Yan W, Jing W, Kong L, Zhang Y, Yu J. Great efficacy of afatinib on a patient with lung adenocarcinoma harboring uncommon *EGFR* delE709_T710insD mutations: a case report. *Onco Targets Ther* 2019; **12**: 7399-7404 [PMID: 31686847 DOI: 10.2147/OTT.S221638]

15 **Iwamoto Y**, Ichihara E, Hara N, Nakasuka T, Ando C, Umeno T, Hirabae A, Maeda Y, Kiura K. Efficacy of afatinib treatment for lung adenocarcinoma harboring exon 18 delE709_T710insD mutation. *Jpn J Clin Oncol* 2019; **49**: 786-788 [PMID: 31187861 DOI: 10.1093/jjco/hyz086]

16 **D'Haene N**, Le Mercier M, Salmon I, Mekinda Z, Remmelink M, Berghmans T. SMAD4 Mutation in Small Cell Transformation of Epidermal Growth Factor Receptor Mutated Lung Adenocarcinoma. *Oncologist* 2019; **24**: 9-13 [PMID: 30413663 DOI: 10.1634/theoncologist.2018-0016]

17 **Wei Y**, Cui Y, Guo Y, Li L, Zeng L. A Lung Adenocarcinoma Patient With a Rare *EGFR* E709_T710delinsD Mutation Showed a Good Response to Afatinib Treatment: A Case Report and Literature Review. *Front Oncol* 2021; **11**: 700345 [PMID: 34178699 DOI: 10.3389/fonc.2021.700345]

18 **Jelli B**, Taton O, D'Haene N, Remmelink M, Mekinda Z. Complete Response to Afatinib of an *EGFR* Exon 18 delE709_T710insD-Mutated Stage IV Lung Adenocarcinoma. *Eur J Case Rep Intern Med* 2021; **8**: 002749 [PMID: 34527619 DOI: 10.12890/2021_002749]

19 **Kobayashi Y**, Togashi Y, Yatabe Y, Mizuuchi H, Jangchul P, Kondo C, Shimoji M, Sato K, Suda K, Tomizawa K, Takemoto T, Hida T, Nishio K, Mitsudomi T. *EGFR* Exon 18 Mutations in Lung Cancer: Molecular Predictors of Augmented Sensitivity to Afatinib or Neratinib as Compared with First- or Third-Generation TKIs. *Clin Cancer Res* 2015; **21**: 5305-5313 [PMID: 26206867 DOI: 10.1158/1078-0432.ccr-15-1046]

20 **Rubiera-Pebe R**, Hicks JK, Tanvetyanon T. Efficacy of tyrosine kinase inhibitors against lung cancer with *EGFR* exon 18 deletion: Case report and pooled analysis. *Cancer Treat Res Commun* 2021; **28**: 100407 [PMID: 34090219 DOI: 10.1016/j.ctarc.2021.100407]

21 **Morita A**, Hosokawa S, Yamada K, Umeno T, Kano H, Kayatani H, Shiojiri M, Sakugawa M, Bessho A. Dacomitinib as a retreatment for advanced non-small cell lung cancer patient with an uncommon *EGFR* mutation. *Thorac Cancer* 2021; **12**: 1248-1251 [PMID: 33651475 DOI: 10.1111/1759-7714.13897]

22 **Wu YL**, Cheng Y, Zhou X, Lee KH, Nakagawa K, Niho S, Tsuji F, Linke R, Rosell R, Corral J, Migliorino MR, Pluzanski A, Sbar EI, Wang T, White JL, Nadanaciva S, Sandin R, Mok TS. Dacomitinib *vs* gefitinib as first-line treatment for patients with *EGFR*-mutation-positive non-small-cell lung cancer (ARCHER 1050): a randomised, open-label, phase 3 trial. *Lancet Oncol* 2017; **18**: 1454-1466 [PMID: 28958502 DOI: 10.1016/S1470-2045]

World Journal of Clinical Cases

Submit a Manuscript: https://www.f6publishing.com

World J Clin Cases 2022 June 16; 10(17): 5923-5928

DOI: 10.12998/wjcc.v10.i17.5923

ISSN 2307-8960 (online)

CASE REPORT

Loss of human epidermal receptor-2 in human epidermal receptor-2+ breast cancer after neoadjuvant treatment: A case report

Jing Yu, Nan-Lin Li

Specialty type: Medicine, research and experimental

Provenance and peer review: Unsolicited article; Externally peer reviewed.

Peer-review model: Single blind

Peer-review report's scientific quality classification

Grade A (Excellent): 0
Grade B (Very good): B, B
Grade C (Good): 0
Grade D (Fair): 0
Grade E (Poor): 0

P-Reviewer: Chia CL, Singapore; Sheikh Hassan M, Somalia

Received: January 25, 2022
Peer-review started: January 25, 2022
First decision: March 16, 2022
Revised: March 18, 2022
Accepted: April 4, 2022
Article in press: April 4, 2022
Published online: June 16, 2022

Jing Yu, Nan-Lin Li, Department of Thyroid, Breast and Vascular Surgery, Xijing Hospital, Air Force Medical University, Xi'an 710032, Shaanxi Province, China

Corresponding author: Nan-Lin Li, MD, Associate Chief Physician, Department of Thyroid, Breast and Vascular Surgery, Xijing Hospital, Air Force Medical University, No. 127 West Changle Road, Xi'an 710032, Shaanxi Province, China. yuyujing0729@163.com

Abstract

BACKGROUND

Human epidermal receptor-2 (HER-2) expression has been reported to be discordant between primary tumor and metastatic tissue.

CASE SUMMARY

We presented a case diagnosed with the HER-2+ breast cancer patient who exhibited changes in the expression of HER-2 receptors on tumour samples from surgical specimens obtained after neoadjuvant treatment (NAT) compared with initial biopsy. The patient underwent a HER-2-targeted therapy consequently, in spite of HER+ gene loss. After the surgery, the patient subsequently underwent endocrine therapy and radiotherapy.

CONCLUSION

Changes in HER-2 expression after NAT should be retested by physicians and pathologists before systemic treatment instead of avoiding further HER-2-targeted therapy, and we will perform immunohistochemical multiple-spot biopsy analyses of other important clinical issues to better define prognosis and tailor subsequent adjuvant therapy.

Key Words: Human epidermal receptor-2+ breast cancer; Human epidermal receptor-2 loss; Neoadjuvant treatment; Case report

©The Author(s) 2022. Published by Baishideng Publishing Group Inc. All rights reserved.

Core Tip: We presented a case diagnosed with the human epidermal receptor(HER)-2+ breast cancer patient who exhibited changes in the expression of HER-2 receptors on tumour samples from surgical specimens obtained after neoadjuvant treatment (NAT) compared with initial biopsy. Changes in HER-2 expression after NAT should be retested by physicians and pathologists before systemic treatment instead of avoiding further HER-2-targeted therapy. In general, the exact mechanisms of HER-2 discordance remain unknown and further investigations are needed.

Citation: Yu J, Li NL. Loss of human epidermal receptor-2 in human epidermal receptor-2+ breast cancer after neoadjuvant treatment: A case report. *World J Clin Cases* 2022; 10(17): 5923-5928
URL: https://www.wjgnet.com/2307-8960/full/v10/i17/5923.htm
DOI: https://dx.doi.org/10.12998/wjcc.v10.i17.5923

INTRODUCTION

The Human epidermal receptor-2 (HER-2) gene is over-expressed in approximately 15%-20% of primary breast cancers, and HER-2-targeted therapies are associated with significantly improved survival. Neoadjuvant treatment (NAT) is the standard of care for HER-2–positive early breast cancer, especially for positive pathologic axillary lymph nodes. However, HER-2 expression has been reported to be discordant between the primary tumour and the remaining tumour after NAT and is associated with poor prognosis and treatment. Data regarding HER-2 Loss suggest that 2.3%-43% of post-treatment tumours lose HER-2 positivity, which is associated with worse survival[1-3]. Herein, by reviewing the relevant literature, we present a case of HER-2 Loss with HER-2+ breast cancer undergoing NAT, to determine the prognostic impact of HER-2 Loss and improve disease management.

CASE PRESENTATION

Chief complaints

She complained of a mass in her left breast for several months.

History of present illness

A 55-year-old postmenopausal female patient presented to the Xi Jing Hospital of Air Force Medical University in September 2019. She complained of a mass in her left breast for several months.

History of past illness

The patient was healthy with no previous comorbidity.

Personal and family history

Her family history of cancer was negative.

Physical examination

She found two irregular nodules in the upper external quadrant of the left breast.

Laboratory examinations

All tumuor markers, including serum carcinoembryonic antigen, neuron-specific enolase, and alpha fetoprotein, were within normal ranges. Histopathology revealed invasive breast carcinoma and infiltrating ductal carcinoma in the axillary lymph nodes. Immunohistochemical (IHC) staining was positive for ER, progesterone receptor, Ki-67 30% and suspicious positive for HER-2. Because of the suspicious positivity for HER-2, the fluorescence in situ hybridization (FISH) method was strongly recommended. FISH testing was positive, as shown in Figure 1. Breast cancer and metastatic lymph nodes were identical in FISH expression. The physical and imaging examinations showed no primary lesions in either breast or in other organs.

Imaging examinations

Ultrasonographic examination showed two irregular nodules in the upper external quadrant of the left breast. The largest mass was 2.6 cm × 0.9 cm × 1.1 cm in diameter, with invasion of deeper structures. Doppler ultrasound showed a fixed, 2 cm lymph nodule.

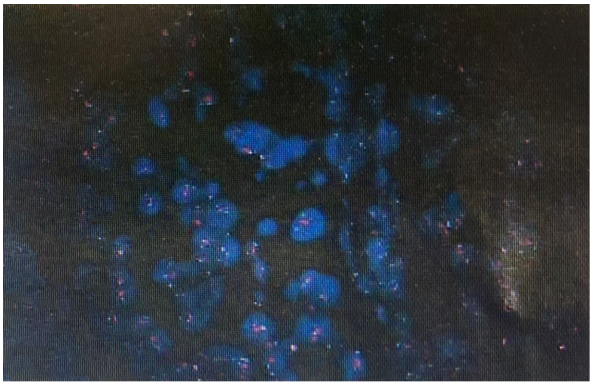

DOI: 10.12998/wjcc.v10.i17.5923 **Copyright** ©The Author(s) 2022.

Figure 1 The fluorescence in situ hybridization results before neoadjuvant treatment.

FINAL DIAGNOSIS

The patient was diagnosed with the HER-2+ early breast cancer.

TREATMENT

The multidisciplinary board of the Breast Centre recommended "neoadjuvant" chemotherapy: T(HP)-EC scheme: 4 cycles of docetaxel 90 mg/m^2, trastuzumab, and pertuzumab, followed by 4 cycles of epirubicin 90 mg/m^{2}and cyclophosphamide 600 mg/m^2, every 3 wk for 8 cycles) before total mastectomy and axillary lymph node dissection. Histopathologic analysis of these specimens showed residual ductal carcinoma disease. Histopathology revealed grade 3 invasive breast carcinoma, (RCB-II, 6 scores). Microscopically, the residual invasive breast cancer was approximately 7 mm, and 5 out of 20 dissected axillary lymph nodes showed metastasis. With all of this, the tumour was classified as ypT1bN2aM0. Immunohistochemistry was performed, and the results were as follows: 90% positivity for estrogen receptors with high intensity, 90% positivity for progesterone receptors with high intensity, and suspicious positivity for HER-2 (++). FISH testing was negative, as shown in Figure 2. We retrospectively reevaluated these results from the central laboratory FISH screening. On May 8, 2020, the patient received T-DM1 at a dose of 3.6 mg per kilogram of body weight intravenously every 3 wk for 14 cycles. Simultaneously, adjuvant radiotherapy was also recommended because of her axillary lymph node features on excisional biopsy. At the follow-up, 1 year after diagnosis and treatment initiation, the patient had no sign of local or distant recurrence. Considering the hormone sensitivity of the tumour, the guidelines decided for endocrine adjuvant therapy were as follows: (abemaciclib 150 mg twice daily + anastrozole 1mg once daily).

OUTCOME AND FOLLOW-UP

At the time of drafting the present report (January 2022), routine follow-up of the patient continued, showing no complications.

DISCUSSION

The current standard presurgical systemic treatment in HER-2-positive breast cancer patients is NAT, especially for positive pathologic axillary lymph nodes. The addition of anti-HER-2 treatment to neoadjuvant chemotherapy significantly improves the pathological complete response (pCR) rate, which is a surrogate for disease-free survival (DFS), overall survival and distant recurrence–free survival (DRFS)[4]. Mittendorf *et al*[5] found that according to FISH analysis, approximately one-third of their patients with sufficient residual disease to warrant repeat HER-2 testing had lost HER-2 gene amplification. Furthermore, patients who lose HER-2 gene amplification have significantly lower relapse-free survival than those whose tumours retain HER-2 gene amplification[6]. Notably, we found that this case exhibited changes in the expression of HER-2 receptors on tumour samples from surgical specimens obtained after NAT compared with initial biopsy. This is in agreement with early studies in which the rate of HER-2 gain and loss was observed to be 6.5% and 14.2%, respectively, and loss of HER-2 expression was more commonly observed than gain of HER-2 expression[3,7].

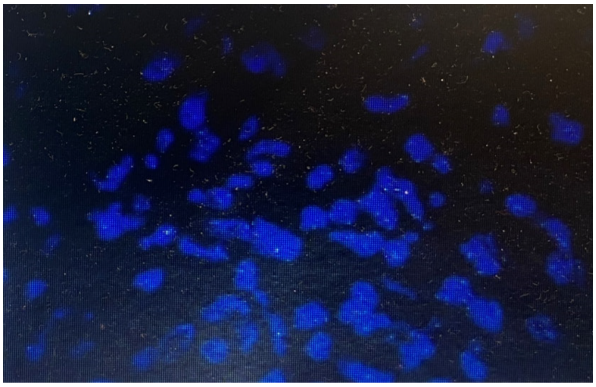

DOI: 10.12998/wjcc.v10.i17.5923 **Copyright** ©The Author(s) 2022.

Figure 2 The fluorescence in situ hybridization results after neoadjuvant treatment.

In the neoadjuvant setting, the addition of trastuzumab and, more recently, pertuzumab to chemotherapy significantly improves the pCR rate compared to chemotherapy alone[8]. The KATHERINE study showed that among patients with HER-2-positive early breast cancer who had residual invasive disease after completion of neoadjuvant therapy, the risk of recurrence of invasive breast cancer or death was 50% lower with adjuvant trastuzumab emtansine (T-DM1) than with trastuzumab alone. Further subgroup analyses showed that 8.3% of posttreatment tumours lost HER-2 positivity after NAT (n = 70); invasive-disease events occurred in 11 patients in the adjuvant trastuzumab group; and no events occurred in the T-DM1 group, reminding us that adjuvant T-DM1 remains beneficial in tumour loss in the HER-2 population[9]. This case was HR+, HER-2+ breast cancer. The ExteNET trial demonstrated that neratinib given for 1 year following trastuzumab-based therapy significantly improved invasive DFS (iDFS) in patients with HER-2+ breast cancer, with the greatest efficacy seen in patients who initiated treatment within 1 year of prior trastuzumab therapy and in those with HR+ disease[10]. Meanwhile, the most recently results showed that neratinib achieved an 11.9% iDFS benefit for the HR+ subgroup within 1 year of prior trastuzumab therapy in the 5-year analysis. In comparison with the previously reported KATHERINE trial, the iDFS benefit was 11.3% at the 3-year analysis in patients with T-DM1. However, patients in the KATHERINE trial had a substantially worse baseline prognosis than those enrolled in the ExteNET trial. The KATHERINE trial focused on higher-risk patients with residual invasive breast cancer after completion of neoadjuvant chemotherapy administered with trastuzumab-containing therapy. We considered that the patient could benefit from T-DM1 rather than neratinib, owing to adverse events, group characteristics and accessibility. Subsequently, the MonarchE study showed that there was a 25% reduction in the risk of developing an iDFS event in the abemaciclib plus endocrine therapy (ET) group relative to ET alone, as well as a 3.5% absolute improvement in 2-year IDFS rates (92.2% *vs* 88.7%).The addition of abemaciclib to ET also resulted in an improvement in DRFS (distant relapse-free survival) compared with ET alone, with 2-year DRFS rates of 93.6% in the abemaciclib arm and 90.3% in the control arm[11,12].

In general, the exact mechanisms of HER-2 discordance remain unknown and further investigations are needed. The interval between the last HER-2-targeted treatment, the time of surgical excision of the tumour after NAT, and biopsy of the metachronous metastasis or intratumoural heterogeneity of the HER-2 gene were associated with a significant change in HER-2 expression. Nevertheless, FISH testing is associated with less discordance than the IHC method[1,13]. Despite observations revealing HER-2 Loss between initial biopsy and surgical specimens, management of patients with HER-2+ breast cancer is frequently based on primary tumor characteristics. Furthermore, Several studies suggested that all subgroups of women seem to benefit from trastuzumab in exploratory subgroup analysis, regardless of changes in HER status[13-16]. In our opinion, changes in HER-2 expression after NAT should be retested by physicians and pathologists before systemic treatment instead of avoiding further HER-2-targeted therapy. Furthermore, if the HER-2 status changes between the primary tumour and the remaining tumour undergoing NAT, the actual guidelines recommend the use of HER-2 status in metastatic tissue, and the FISH method is strongly recommended. In this way, changes in HER-2 expression influenced by HER-2 internalization and degradation may be avoided. Finally, we will perform IHC multiple-spot biopsy analyses of other important clinical issues to better define prognosis and tailor subsequent adjuvant therapy.

CONCLUSION

In conclusion, our study presented a case of HER+ gene loss in a patient with the HER-2+ breast cancer after NAT and we went on to do a literature review of this phenomenon which has been shown in about

10% of patient in case series. Although HER-2 Loss after NAT is considered extremely rare, repeating HER-2 test or IHC multiple-spot biopsy analyses is required for accurate prognosis and therapy.

FOOTNOTES

Author contributions: Yu J analyzed the data and wrote the manuscript; Li NL and Yu J performed the research; all authors have read and approve the final manuscript.

Informed consent statement: Informed written consent was obtained from the patient for publication of this report and any accompanying images.

Conflict-of-interest statement: The authors declare that they have no conflict of interest.

CARE Checklist (2016) statement: The authors have read the CARE Checklist (2016), and the manuscript was prepared and revised according to the CARE Checklist (2016).

Open-Access: This article is an open-access article that was selected by an in-house editor and fully peer-reviewed by external reviewers. It is distributed in accordance with the Creative Commons Attribution NonCommercial (CC BY-NC 4.0) license, which permits others to distribute, remix, adapt, build upon this work non-commercially, and license their derivative works on different terms, provided the original work is properly cited and the use is non-commercial. See: https://creativecommons.org/Licenses/by-nc/4.0/

Country/Territory of origin: China

ORCID number: Jing Yu 0000-0001-9733-9286; Nanlin Li 0000-0002-7212-1026.

S-Editor: Wang LL
L-Editor: A
P-Editor: Wang LL

REFERENCES

1 **Ignatov T**, Gorbunow F, Eggemann H, Ortmann O, Ignatov A. Loss of HER2 after HER2-targeted treatment. *Breast Cancer Res Treat* 2019; **175**: 401-408 [PMID: 30806922 DOI: 10.1007/s10549-019-05173-4]
2 **Branco FP**, Machado D, Silva FF, André S, Catarino A, Madureira R, Pinto JM, Godinho JP, Simões PD, Brito M, Casa-Nova M, Moreira AR, Passos-Coelho JL. Loss of HER2 and disease prognosis after neoadjuvant treatment of HER2+ breast cancer. *Am J Transl Res* 2019; **11**: 6110-6116 [PMID: 31632579 DOI: 10.1016/s0959-8049(18)30510-0]
3 **Niikura N**, Tomotaki A, Miyata H, Iwamoto T, Kawai M, Anan K, Hayashi N, Aogi K, Ishida T, Masuoka H, Iijima K, Masuda S, Tsugawa K, Kinoshita T, Nakamura S, Tokuda Y. Changes in tumor expression of HER2 and hormone receptors status after neoadjuvant chemotherapy in 21,755 patients from the Japanese breast cancer registry. *Ann Oncol* 2016; **27**: 480-487 [PMID: 26704052 DOI: 10.1093/annonc/mdv611]
4 **Press MF**, Sauter G, Buyse M, Fourmanoir H, Quinaux E, Tsao-Wei DD, Eiermann W, Robert N, Pienkowski T, Crown J, Martin M, Valero V, Mackey JR, Bee V, Ma Y, Villalobos I, Campeau A, Mirlacher M, Lindsay MA, Slamon DJ. HER2 Gene Amplification Testing by Fluorescent In Situ Hybridization (FISH): Comparison of the ASCO-College of American Pathologists Guidelines With FISH Scores Used for Enrollment in Breast Cancer International Research Group Clinical Trials. *J Clin Oncol* 2016; **34**: 3518-3528 [PMID: 27573653 DOI: 10.1200/jco.2016.66.6693]
5 **Mittendorf EA**, Wu Y, Scaltriti M, Meric-Bernstam F, Hunt KK, Dawood S, Esteva FJ, Buzdar AU, Chen H, Eksambi S, Hortobagyi GN, Baselga J, Gonzalez-Angulo AM. Loss of HER2 amplification following trastuzumab-based neoadjuvant systemic therapy and survival outcomes. *Clin Cancer Res* 2009; **15**: 7381-7388 [PMID: 19920100 DOI: 10.1158/1078-0432.ccr-09-1735]
6 **Niikura N**, Liu J, Hayashi N, Mittendorf EA, Gong Y, Palla SL, Tokuda Y, Gonzalez-Angulo AM, Hortobagyi GN, Ueno NT. Loss of human epidermal growth factor receptor 2 (HER2) expression in metastatic sites of HER2-overexpressing primary breast tumors. *J Clin Oncol* 2012; **30**: 593-599 [PMID: 22124109 DOI: 10.1200/jco.2010.33.8889]
7 **Yeung C**, Hilton J, Clemons M, Mazzarello S, Hutton B, Haggar F, Addison CL, Kuchuk I, Zhu X, Gelmon K, Arnaout A. Estrogen, progesterone, and HER2/neu receptor discordance between primary and metastatic breast tumours-a review. *Cancer Metastasis Rev* 2016; **35**: 427-437 [PMID: 27405651 DOI: 10.1007/s10555-016-9631-3]
8 **Gianni L**, Pienkowski T, Im YH, Tseng LM, Liu MC, Lluch A, Starosławska E, de la Haba-Rodriguez J, Im SA, Pedrini JL, Poirier B, Morandi P, Semiglazov V, Srimuninnimit V, Bianchi GV, Magazzù D, McNally V, Douthwaite H, Ross G, Valagussa P. 5-year analysis of neoadjuvant pertuzumab and trastuzumab in patients with locally advanced, inflammatory, or early-stage HER2-positive breast cancer (NeoSphere): a multicentre, open-label, phase 2 randomised trial. *Lancet Oncol* 2016; **17**: 791-800 [PMID: 27179402 DOI: 10.1016/s1470-2045(16)00163-7]
9 **Haran JP**, Wilsterman E, Zeoli T, Goulding M, McLendon E, Clark MA. Deviating from IDSA treatment guidelines for non-purulent skin infections increases the risk of treatment failure in emergency department patients. *Epidemiol Infect* 2018; **147**: e68 [PMID: 30516120 DOI: 10.1056/nejmoa1814017]
10 **Chan A**, Moy B, Mansi J, Ejlertsen B, Holmes FA, Chia S, Iwata H, Gnant M, Loibl S, Barrios CH, Somali I, Smichkoska

S, Martinez N, Alonso MG, Link JS, Mayer IA, Cold S, Murillo SM, Senecal F, Inoue K, Ruiz-Borrego M, Hui R, Denduluri N, Patt D, Rugo HS, Johnston SRD, Bryce R, Zhang B, Xu F, Wong A, Martin M; ExteNET Study Group. Final Efficacy Results of Neratinib in HER2-positive Hormone Receptor-positive Early-stage Breast Cancer From the Phase III ExteNET Trial. *Clin Breast Cancer* 2021; **21**: 80-91.e7 [PMID: 33183970 DOI: 10.1016/s0960-9776(21)00093-x]

11 **Harbeck N**, Rastogi P, Martin M, Tolaney SM, Shao ZM, Fasching PA, Huang CS, Jaliffe GG, Tryakin A, Goetz MP, Rugo HS, Senkus E, Testa L, Andersson M, Tamura K, Del Mastro L, Steger GG, Kreipe H, Hegg R, Sohn J, Guarneri V, Cortés J, Hamilton E, André V, Wei R, Barriga S, Sherwood S, Forrester T, Munoz M, Shahir A, San Antonio B, Nabinger SC, Toi M, Johnston SRD, O'Shaughnessy J; monarchE Committee Members. Adjuvant abemaciclib combined with endocrine therapy for high-risk early breast cancer: updated efficacy and Ki-67 analysis from the monarchE study. *Ann Oncol* 2021; **32**: 1571-1581 [PMID: 34656740 DOI: 10.1200/jco.20.02514]

12 **Burstein HJ**, Somerfield MR, Barton DL, Dorris A, Fallowfield LJ, Jain D, Johnston SRD, Korde LA, Litton JK, Macrae ER, Peterson LL, Vikas P, Yung RL, Rugo HS. Endocrine Treatment and Targeted Therapy for Hormone Receptor-Positive, Human Epidermal Growth Factor Receptor 2-Negative Metastatic Breast Cancer: ASCO Guideline Update. *J Clin Oncol* 2021; **39**: 3959-3977 [PMID: 34324367 DOI: 10.1200/JCO.21.01392]

13 **Yoshida A**, Hayashi N, Suzuki K, Takimoto M, Nakamura S, Yamauchi H. Change in HER2 status after neoadjuvant chemotherapy and the prognostic impact in patients with primary breast cancer. *J Surg Oncol* 2017; **116**: 1021-1028 [PMID: 28767137 DOI: 10.1002/jso.24762]

14 **Lindström LS**, Karlsson E, Wilking UM, Johansson U, Hartman J, Lidbrink EK, Hatschek T, Skoog L, Bergh J. Clinically used breast cancer markers such as estrogen receptor, progesterone receptor, and human epidermal growth factor receptor 2 are unstable throughout tumor progression. *J Clin Oncol* 2012; **30**: 2601-2608 [PMID: 22711854 DOI: 10.1200/jco.2011.37.2482]

15 **Smith I**, Procter M, Gelber RD, Guillaume S, Feyereislova A, Dowsett M, Goldhirsch A, Untch M, Mariani G, Baselga J, Kaufmann M, Cameron D, Bell R, Bergh J, Coleman R, Wardley A, Harbeck N, Lopez RI, Mallmann P, Gelmon K, Wilcken N, Wist E, Sánchez Rovira P, Piccart-Gebhart MJ; HERA study team. 2-year follow-up of trastuzumab after adjuvant chemotherapy in HER2-positive breast cancer: a randomised controlled trial. *Lancet* 2007; **369**: 29-36 [PMID: 17208639 DOI: 10.1016/s0140-6736(07)60028-2]

16 **Gianni L**, Eiermann W, Semiglazov V, Manikhas A, Lluch A, Tjulandin S, Zambetti M, Vazquez F, Byakhow M, Lichinitser M, Climent MA, Ciruelos E, Ojeda B, Mansutti M, Bozhok A, Baronio R, Feyereislova A, Barton C, Valagussa P, Baselga J. Neoadjuvant chemotherapy with trastuzumab followed by adjuvant trastuzumab versus neoadjuvant chemotherapy alone, in patients with HER2-positive locally advanced breast cancer (the NOAH trial): a randomised controlled superiority trial with a parallel HER2-negative cohort. *Lancet* 2010; **375**: 377-384 [PMID: 20113825 DOI: 10.1016/s0140-6736(09)61964-4]

World Journal of Clinical Cases

Submit a Manuscript: https://www.f6publishing.com

World J Clin Cases 2022 June 16; 10(17): 5929-5933

DOI: 10.12998/wjcc.v10.i17.5929

ISSN 2307-8960 (online)

LETTER TO THE EDITOR

Repetitive transcranial magnetic stimulation for post-traumatic stress disorder: Lights and shadows

Carmen Concerto, Giuseppe Lanza, Francesco Fisicaro, Manuela Pennisi, Alessandro Rodolico, Giulia Torrisi, Rita Bella, Eugenio Aguglia

Specialty type: Medicine, research and experimental

Provenance and peer review: Unsolicited article; Externally peer reviewed.

Peer-review model: Single blind

Peer-review report's scientific quality classification

Grade A (Excellent): 0
Grade B (Very good): B, B
Grade C (Good): 0
Grade D (Fair): 0
Grade E (Poor): 0

P-Reviewer: Ge X, China; Kar SK, India

Received: January 2, 2022
Peer-review started: January 2, 2022
First decision: January 23, 2022
Revised: January 27, 2022
Accepted: May 12, 2022
Article in press: May 12, 2022
Published online: June 16, 2022

Carmen Concerto, Alessandro Rodolico, Giulia Torrisi, Eugenio Aguglia, Department of Clinical and Experimental Medicine, Psychiatry Unit, University of Catania, Catania 95124, Italy

Giuseppe Lanza, Department of Surgery and Medical-Surgical Specialties, University of Catania, Catania 95123, Italy

Giuseppe Lanza, Clinical Neurophysiology Research Unit, Oasi Research Institute-IRCCS, Troina 94018, Italy

Francesco Fisicaro, Manuela Pennisi, Department of Biomedical and Biotechnological Sciences, University of Catania, Catania 95123, Italy

Rita Bella, Department of Medical and Surgical Sciences and Advanced Technologies "G. F. Ingrassia", University of Catania, Catania 95123, Italy

Corresponding author: Giuseppe Lanza, MD, MSc, PhD, Associate Professor, Department of Surgery and Medical-Surgical Specialties, University of Catania, *Via* Santa Sofia, 78, Catania 95123, Italy. giuseppe.lanza1@unict.it

Abstract

We have read with interest the publication that describes the available data related to the use of neuromodulation strategies for the treatment of post-traumatic stress disorder (PTSD). Despite treatment advances, however, a substantial proportion of PTSD patients receiving psychological and/or pharmacological treatment do not reach an adequate clinical response. In their paper, the authors draw attention to the current understanding of the use of repetitive transcranial magnetic stimulation (rTMS) as a potential treatment for PTSD. Most of the previous studies indeed applied both inhibitory (1 Hz) and excitatory (> 1 Hz, up to 20 Hz) rTMS to the right and/or left dorsolateral prefrontal cortex. Despite larger therapeutic effects observed when high-frequency stimulation was applied, the question of which side and frequency of stimulation is the most successful is still debated. The authors also reported on the after-effect of rTMS related to neuroplasticity and identified the intermittent theta burst stimulation as a technique of particular interest because of it showed the most effective improvement on PTSD symptoms. However, although numerous studies have highlighted the possible beneficial use of rTMS protocols for PTSD, the exact mechanism of action remains unclear. In their conclusions, the authors stated that rTMS has been demonstrated to be effective for the treatment of PTSD symptoms.

Nevertheless, we believe that further research with homogeneous samples, standardized protocols, and objective outcome measures is needed to identify specific therapeutic targets and to better define significant changes when active and sham stimulation procedures are compared.

Key Words: Post-traumatic stress disorder; Neuromodulation; Repetitive transcranial magnetic stimulation; Translational neuroscience; Neuroplasticity; Metaplasticity

©The Author(s) 2022. Published by Baishideng Publishing Group Inc. All rights reserved.

Core Tip: The interesting publication of the basic principle, current applications, and future directions of repetitive transcranial magnetic stimulation for the non-pharmacological treatment of post-traumatic stress disorder (PTSD) have been summarized. Therapeutic effects on core PTSD symptoms, such as avoidance, hyperarousal, and intrusions, appear to be larger when high-frequency stimulation over the right dorsolateral prefrontal cortex was used. However, although the technique has demonstrated safety and efficacy, several concerns remain related to the mechanisms of action and protocols to be adopted, including the heterogeneity in the sample selection, stimulation procedures, and outcome measures.

Citation: Concerto C, Lanza G, Fisicaro F, Pennisi M, Rodolico A, Torrisi G, Bella R, Aguglia E. Repetitive transcranial magnetic stimulation for post-traumatic stress disorder: Lights and shadows. *World J Clin Cases* 2022; 10(17): 5929-5933
URL: https://www.wjgnet.com/2307-8960/full/v10/i17/5929.htm
DOI: https://dx.doi.org/10.12998/wjcc.v10.i17.5929

TO THE EDITOR

We have read with interest the recent publication by Cheng *et al*[1] summarizing the current understanding on the use of transcranial magnetic stimulation (TMS) as a potential treatment for post-traumatic stress disorder (PTSD). As known, PTSD is a mental health disorder that may occur after experiencing or witnessing a significantly traumatic event. Symptoms include flashbacks, nightmares, and severe anxiety, as well as uncontrollable thoughts about the event, affective symptoms, and negative cognition[2]. These symptoms can significantly impact personal relationships and social and work activities, thus impairing functional independence and quality of life[3,4].

Neuromodulation strategies based on non-invasive brain stimulation techniques, such as repetitive TMS (rTMS) and transcranial direct current stimulation, have been recently investigated and applied in PTSD patients who did not reach an adequate clinical response with conventional therapy[5,6]. TMS has been widely used for the treatment of other psychiatric disorders, in particular it has shown to be highly effective in adults with drug-resistant major depressive disorder[7], including long-lasting effects on depressive-associated cognitive dysfunction[8]. Regarding PTSD, the latest evidence-based guidelines on the therapeutic use of rTMS concluded that level B evidence (probable efficacy) was reached for high-frequency (excitatory) rTMS over the right dorsolateral prefrontal cortex (DLPFC)[9]. However, these recommendations are based on the differences reached in therapeutic efficacy of real *vs* sham (fictitious) stimulation replicated in a sufficient number of independent studies, but this does not mean that the benefit produced by rTMS inevitably reaches a clinical relevance[9].

In their paper, Cheng *et al*[1] suggested the role of rTMS as an effective and promising treatment for PTSD. However, the previous literature they reviewed mainly shows considerable variation regarding stimulation parameters, type of traumatic events, and sample characteristics. Regarding the stimulation area, most of the previous studies identified the DLPFC as the preferential stimulation target, although differences were observed between either the frequency or the side of stimulation. The interest in targeting the right DLPFC comes from previous evidence showing that high-frequency rTMS was able to increase neural activity and blood flow in the right hemisphere, thus improving some of the core PTSD symptoms, such as avoidance, hyperarousal, and intrusions[10]. Conversely, high-frequency rTMS over the left DLPFC has been mainly used as a neuromodulatory protocol for mood disorders[7], suggesting its application for the PTSD-related affective symptoms.

Regarding the rTMS protocols, most studies applied a stimulation intensity of 120% of the individual's resting motor threshold. Subjects who underwent 1-Hz (inhibitory) stimulation usually received 2250 pulses over 37.5 min, whereas those stimulated at 10-Hz (excitatory) received 3000 pulses over the same time period (4-s stimulation train, with 26-s intertrain interval), for 2 wk of daily treatments[11-14], although some more recent rTMS trial designs in PTSD have delivered more treatments[15-17]. However, the question of which side and frequency of stimulation is the most successful in terms of remission or response from PTSD symptoms is still debated.

Regarding the side of stimulation, it seems that rTMS could be effective over both the left and right DLPFC, as suggested by the authors themselves[1]. Of clinical relevance is also the finding of a better treatment outcome for the high-frequency rTMS applied over the right than the left DLPFC. This is in line with a recent meta-analysis by Harris and Reece[10], who discussed the effects of rTMS on episodic memory retrieval and reiteration of the traumatic event, which is responsible for the flashback symptoms. They suggested that the DLPFC might be involved in the recurrence of trauma reminiscence and, therefore, may participate in the inhibition of the trauma memory. Likewise, Cheng *et al*[1] reported of a previous work by Parson and Ressler[18] on the correlation between dysregulated response to fear and PTSD symptoms. Overall, it appears that DLPFC is involved in emotional regulation, being also thought to influence the activity between the ventral medial prefrontal cortex (vmPFC) and the amygdala[19]. Accordingly, other studies highlighted the role of the vmPFC in modulating fear responsivity[20], as well other cerebral areas, such as the temporal-insular cortex[21].

It should be also considered that an earlier study suggested that the effectiveness of rTMS might depend not only on PTSD symptoms only, but also on the patient's personality traits, such as impulsivity, risk proneness, and sensation seeking[22]. DLPFC plays indeed a key role in mood-affect and impulsivity regulation and a hyperactivity of the limbic structures has been related to behavioral instability[23]. Emotional dysregulation and disturbed impulse control are also common borderline personality traits. In this context, a previous TMS report explored the influence of comorbid borderline personality traits on treatment response to TMS in major depressed patients[24], whereas a recent study by Ward *et al*[25] reported that borderline personality traits did not affect treatment response to DLPFC-TMS in a large naturalistic dataset of patients receiving conventional clinical treatment for depression. In their conclusion, the authors stated that the antidepressant efficacy of rTMS was independent from comorbid borderline personality disorder.

Interestingly, Cheng *et al*[1] also reported on the after-effect of rTMS on neuroplasticity, and in particular on long-term potentiation and long-term depression, phenomena likely related to glutamatergic (especially to AMPA and NMDA receptor) and GABAergic activity, respectively. They further identified the intermittent theta burst stimulation (iTBS) as a technique of particular interest, because of its most effective improvement on PTSD symptoms. The authors also reported on a sham-controlled study by Philip *et al*[26]. who indicated which PTSD symptoms, including depression, improved the most after iTBS treatment and hypothesized the effects on hippocampal synaptic activity and connections.

Among the cellular and molecular mechanisms underlying distinct forms of synaptic plasticity, however, we believe that more attention should be paid to metaplasticity, which refers to the activity-dependent modulation of synaptic plasticity. This pivotal determinant of learning, memory, and other functions represents a higher order of synaptic plasticity that acts on the threshold for modifying synaptic strength[27]. Moreover, impaired synaptic plasticity, the so-called "maladaptive plasticity", has been associated with the pathogenesis and trajectory of several brain diseases, including contributions to the dysfunctional remodeling of underlying neural networks[28]. Given its role in regulating synaptic plasticity, alterations to metaplastic mechanisms are likely to represent an important element of many neurological and psychiatric disorders, including PTSD. The development of non-invasive brain stimulation techniques has allowed to induce and modulate metaplasticity in human subjects, both in normal and pathological conditions. In support of this, Thomson and Sack[29] focused on the use of iTBS to develop metaplasticity-based treatments to induce or restore the desired level of plasticity. They further identified accelerated iTBS at longer intervals (60 min) as being of particular interest, as it seems to maximize metaplasticity effects and clinical outcomes[29].

In their conclusions, the authors stated that rTMS demonstrated to be a safe and effective neurostimulation treatment for PTSD[1]. However, although several studies highlighted the beneficial use of TMS protocols for PTSD, the exact mechanism of action remains unclear. Therefore, we believe that further research with homogeneous samples, standardized protocols, and objective outcome measures is needed to better define the optimal stimulation settings (including the active and sham stimulation comparison) and to clarify whether these interventions may be applied not only to the core symptoms of PTSD but also on its cognitive and mood-affect manifestations.

FOOTNOTES

Author contributions: Concerto C and Lanza G contributed equally to this work; Concerto C, Lanza G, Fisicaro F, and Rodolico A conceived the study; Pennisi M and Torrisi G performed the literature search; Concerto C and Lanza G wrote the first draft of the manuscript; Bella R and Aguglia E revised the manuscript and supervised the research group; and all authors have read and approve the final manuscript.

Conflict-of-interest statement: The authors declared no conflict of interest.

Open-Access: This article is an open-access article that was selected by an in-house editor and fully peer-reviewed by external reviewers. It is distributed in accordance with the Creative Commons Attribution NonCommercial (CC BY-NC 4.0) license, which permits others to distribute, remix, adapt, build upon this work non-commercially, and license

their derivative works on different terms, provided the original work is properly cited and the use is non-commercial. See: https://creativecommons.org/Licenses/by-nc/4.0/

Country/Territory of origin: Italy

ORCID number: Carmen Concerto 0000-0002-7426-5250; Giuseppe Lanza 0000-0002-5659-662X; Francesco Fisicaro 0000-0002-1579-8807; Manuela Pennisi 0000-0003-0776-1411; Alessandro Rodolico 0000-0003-2196-0601; Giulia Torrisi 0000-0002-4897-9786; Rita Bella 0000-0001-8332-6863; Eugenio Aguglia 0000-0003-2146-7737.

Corresponding Author's Membership in Professional Societies: European Academy of Neurology (EAN); Italian Society of Neurology (SIN); Italian Society for Translational Research and Health Professionals (SIRTEPS); Italian Association of Sleep Medicine (AIMS); Italian Stroke Organization (ISO); International Neuromodulation Society (INS); World Sleep Society (WSS); International Parkinson and Movement Disorder Society (MDS).

S-Editor: Wang JJ
L-Editor: Filipodia
P-Editor: Wang JJ

REFERENCES

1 **Cheng P**, Zhou Y, Xu LZ, Chen YF, Hu RL, Zou YL, Li ZX, Zhang L, Shun Q, Yu X, Li LJ, Li WH. Clinical application of repetitive transcranial magnetic stimulation for post-traumatic stress disorder: A literature review. *World J Clin Cases* 2021; **9**: 8658-8665 [PMID: 34734044 DOI: 10.12998/wjcc.v9.i29.8658]
2 **American Psychiatric Association**. DSM-5 Task Force 5th ed. Washington: American Psychiatric Publishing, 2013
3 **Signorelli MS**, Costanzo MC, Cinconze M, Concerto C. What kind of diagnosis in a case of mobbing: post-traumatic stress disorder or adjustment disorder? *BMJ Case Rep* 2013; **2013** [PMID: 23761569 DOI: 10.1136/bcr-2013-010080]
4 **Rodolico A**, Vaccino N, Riso MC, Concerto C, Aguglia E, Signorelli MS. Prevalence of Post-Traumatic Stress Disorder Among Asylum Seekers in Italy: A Population-Based Survey in Sicily. *J Immigr Minor Health* 2020; **22**: 634-638 [PMID: 31863404 DOI: 10.1007/s10903-019-00948-9]
5 **Berger W**, Mendlowicz MV, Marques-Portella C, Kinrys G, Fontenelle LF, Marmar CR, Figueira I. Pharmacologic alternatives to antidepressants in posttraumatic stress disorder: a systematic review. *Prog Neuropsychopharmacol Biol Psychiatry* 2009; **33**: 169-180 [PMID: 19141307 DOI: 10.1016/j.pnpbp.2008.12.004]
6 **Gouveia FV**, Davidson B, Meng Y, Gidyk DC, Rabin JS, Ng E, Abrahao A, Lipsman N, Giacobbe P, Hamani C. Treating Post-traumatic Stress Disorder with Neuromodulation Therapies: Transcranial Magnetic Stimulation, Transcranial Direct Current Stimulation, and Deep Brain Stimulation. *Neurotherapeutics* 2020; **17**: 1747-1756 [PMID: 32468235 DOI: 10.1007/s13311-020-00871-0]
7 **Spampinato C**, Aguglia E, Concerto C, Pennisi M, Lanza G, Bella R, Cantone M, Pennisi G, Kavasidis I, Giordano D. Transcranial magnetic stimulation in the assessment of motor cortex excitability and treatment of drug-resistant major depression. *IEEE Trans Neural Syst Rehabil Eng* 2013; **21**: 391-403 [PMID: 23559064 DOI: 10.1109/TNSRE.2013.2256432]
8 **Concerto C**, Lanza G, Cantone M, Ferri R, Pennisi G, Bella R, Aguglia E. Repetitive transcranial magnetic stimulation in patients with drug-resistant major depression: A six-month clinical follow-up study. *Int J Psychiatry Clin Pract* 2015; **19**: 252-258 [PMID: 26398527 DOI: 10.3109/13651501.2015.1084329]
9 **Lefaucheur JP**, Aleman A, Baeken C, Benninger DH, Brunelin J, Di Lazzaro V, Filipović SR, Grefkes C, Hasan A, Hummel FC, Jääskeläinen SK, Langguth B, Leocani L, Londero A, Nardone R, Nguyen JP, Nyffeler T, Oliveira-Maia AJ, Oliviero A, Padberg F, Palm U, Paulus W, Poulet E, Quartarone A, Rachid F, Rektorová I, Rossi S, Sahlsten H, Schecklmann M, Szekely D, Ziemann U. Evidence-based guidelines on the therapeutic use of repetitive transcranial magnetic stimulation (rTMS): An update (2014-2018). *Clin Neurophysiol* 2020; **131**: 474-528 [PMID: 31901449 DOI: 10.1016/j.clinph.2019.11.002]
10 **Harris A**, Reece J. Transcranial magnetic stimulation as a treatment for posttraumatic stress disorder: A meta-analysis. *J Affect Disord* 2021; **289**: 55-65 [PMID: 33940319 DOI: 10.1016/j.jad.2021.04.003]
11 **Cohen H**, Kaplan Z, Kotler M, Kouperman I, Moisa R, Grisaru N. Repetitive transcranial magnetic stimulation of the right dorsolateral prefrontal cortex in posttraumatic stress disorder: a double-blind, placebo-controlled study. *Am J Psychiatry* 2004; **161**: 515-524 [PMID: 14992978 DOI: 10.1176/appi.ajp.161.3.515]
12 **Boggio PS**, Rocha M, Oliveira MO, Fecteau S, Cohen RB, Campanhã C, Ferreira-Santos E, Meleiro A, Corchs F, Zaghi S, Pascual-Leone A, Fregni F. Noninvasive brain stimulation with high-frequency and low-intensity repetitive transcranial magnetic stimulation treatment for posttraumatic stress disorder. *J Clin Psychiatry* 2010; **71**: 992-999 [PMID: 20051219 DOI: 10.4088/JCP.08m04638blu]
13 **Watts BV**, Landon B, Groft A, Young-Xu Y. A sham controlled study of repetitive transcranial magnetic stimulation for posttraumatic stress disorder. *Brain Stimul* 2012; **5**: 38-43 [PMID: 22264669 DOI: 10.1016/j.brs.2011.02.002]
14 **Leong K**, Chan P, Ong L, Zwicker A, Willan S, Lam RW, McGirr A. A Randomized Sham-controlled Trial of 1-Hz and 10-Hz Repetitive Transcranial Magnetic Stimulation (rTMS) of the Right Dorsolateral Prefrontal Cortex in Civilian Post-traumatic Stress Disorder: Un essai randomisé contrôlé simulé de stimulation magnétique transcrânienne repetitive (SMTr) de 1 Hz et 10 Hz du cortex préfrontal dorsolatéral droit dans le trouble de stress post-traumatique chez des civils. *Can J Psychiatry* 2020; **65**: 770-778 [PMID: 32379487 DOI: 10.1177/0706743720923064]
15 **Kozel FA**, Motes MA, Didehbani N, DeLaRosa B, Bass C, Schraufnagel CD, Jones P, Morgan CR, Spence JS, Kraut MA,

Hart J Jr. Repetitive TMS to augment cognitive processing therapy in combat veterans of recent conflicts with PTSD: A randomized clinical trial. *J Affect Disord* 2018; **229**: 506-514 [PMID: 29351885 DOI: 10.1016/j.jad.2017.12.046]

16 **Kozel FA**, Van Trees K, Larson V, Phillips S, Hashimie J, Gadbois B, Johnson S, Gallinati J, Barrett B, Toyinbo P, Weisman M, Centorino M, Gibson CA, Catalano G. One hertz versus ten hertz repetitive TMS treatment of PTSD: A randomized clinical trial. *Psychiatry Res* 2019; **273**: 153-162 [PMID: 30641346 DOI: 10.1016/j.psychres.2019.01.004]

17 **Koek RJ**, Roach J, Athanasiou N, van 't Wout-Frank M, Philip NS. Neuromodulatory treatments for post-traumatic stress disorder (PTSD). *Prog Neuropsychopharmacol Biol Psychiatry* 2019; **92**: 148-160 [PMID: 30641094 DOI: 10.1016/j.pnpbp.2019.01.004]

18 **Parsons RG**, Ressler KJ. Implications of memory modulation for post-traumatic stress and fear disorders. *Nat Neurosci* 2013; **16**: 146-153 [PMID: 23354388 DOI: 10.1038/nn.3296]

19 **Lyoo IK**, Kim JE, Yoon SJ, Hwang J, Bae S, Kim DJ. The neurobiological role of the dorsolateral prefrontal cortex in recovery from trauma. Longitudinal brain imaging study among survivors of the South Korean subway disaster. *Arch Gen Psychiatry* 2011; **68**: 701-713 [PMID: 21727254 DOI: 10.1001/archgenpsychiatry.2011.70]

20 **Milad MR**, Quirk GJ. Fear extinction as a model for translational neuroscience: ten years of progress. *Annu Rev Psychol* 2012; **63**: 129-151 [PMID: 22129456 DOI: 10.1146/annurev.psych.121208.131631]

21 **Cantone M**, Lanza G, Bella R, Pennisi G, Santalucia P, Bramanti P, Pennisi M. Fear and disgust: case report of two uncommon emotional disturbances evoked by visual disperceptions after a right temporal-insular stroke. *BMC Neurol* 2019; **19**: 193 [PMID: 31409291 DOI: 10.1186/s12883-019-1417-0]

22 **De Vidovich GZ**, Muffatti R, Monaco J, Caramia N, Broglia D, Caverzasi E, Barale F, D'Angelo E. Repetitive TMS on Left Cerebellum Affects Impulsivity in Borderline Personality Disorder: A Pilot Study. *Front Hum Neurosci* 2016; **10**: 582 [PMID: 27994543 DOI: 10.3389/fnhum.2016.00582]

23 **Coccaro EF**, Sripada CS, Yanowitch RN, Phan KL. Corticolimbic function in impulsive aggressive behavior. *Biol Psychiatry* 2011; **69**: 1153-1159 [PMID: 21531387 DOI: 10.1016/j.biopsych.2011.02.032]

24 **Feffer K**, Peters SK, Bhui K, Downar J, Giacobbe P. Successful dorsomedial prefrontal rTMS for major depression in borderline personality disorder: Three cases. *Brain Stimul* 2017; **10**: 716-717 [PMID: 28196679 DOI: 10.1016/j.brs.2017.01.583]

25 **Ward HB**, Yip A, Siddiqui R, Morales OG, Seiner SJ, Siddiqi SH. Borderline personality traits do not influence response to TMS. *J Affect Disord* 2021; **281**: 834-838 [PMID: 33229022 DOI: 10.1016/j.jad.2020.11.054]

26 **Philip NS**, Barredo J, Aiken E, Larson V, Jones RN, Shea MT, Greenberg BD, van 't Wout-Frank M. Theta-Burst Transcranial Magnetic Stimulation for Posttraumatic Stress Disorder. *Am J Psychiatry* 2019; **176**: 939-948 [PMID: 31230462 DOI: 10.1176/appi.ajp.2019.18101160]

27 **Müller-Dahlhaus F**, Ziemann U. Metaplasticity in human cortex. *Neuroscientist* 2015; **21**: 185-202 [PMID: 24620008 DOI: 10.1177/1073858414526645]

28 **Cantone M**, Lanza G, Ranieri F, Opie GM, Terranova C. Editorial: Non-invasive Brain Stimulation in the Study and Modulation of Metaplasticity in Neurological Disorders. *Front Neurol* 2021; **12**: 721906 [PMID: 34276553 DOI: 10.3389/fneur.2021.721906]

29 **Thomson AC**, Sack AT. How to Design Optimal Accelerated rTMS Protocols Capable of Promoting Therapeutically Beneficial Metaplasticity. *Front Neurol* 2020; **11**: 599918 [PMID: 33224103 DOI: 10.3389/fneur.2020.599918]

Published by **Baishideng Publishing Group Inc**
7041 Koll Center Parkway, Suite 160, Pleasanton, CA 94566, USA
Telephone: +1-925-3991568
E-mail: bpgoffice@wjgnet.com
Help Desk: https://www.f6publishing.com/helpdesk
https://www.wjgnet.com

© 2022 Baishideng Publishing Group Inc. All rights reserved.